

AFWAL-TR-82-3073



USAF DAMAGE TOLERANT DESIGN HANDBOOK: GUIDELINES FOR THE ANALYSIS AND DESIGN OF DAMAGE TOLERANT AIRCRAFT STRUCTURES

ADA 153141

J.P. Gallagher, F.J. Giessler, and A.P. Berens
University of Dayton Research Institute
Dayton, Ohio 45469

R.M. Engle, Jr.
Structural Integrity Branch

May 1984

Final Report for Period September 1980 to March 1984

Approved for public release; distribution unlimited.

**FLIGHT DYNAMICS LABORATORY
AIR FORCE WRIGHT AERONAUTICAL LABORATORIES
AIR FORCE SYSTEMS COMMAND
WRIGHT-PATTERSON AIR FORCE BASE, OHIO 45433**

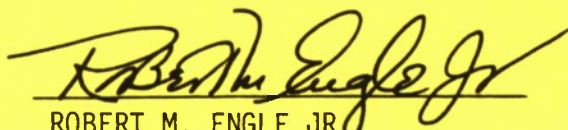
ADA 153161

NOTICE

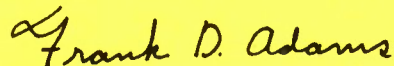
When Government drawings, specifications, or other data are used for any purpose other than in connection with a definitely related Government procurement operation, the United States Government thereby incurs no responsibility nor any obligation whatsoever; and the fact that the government may have formulated, furnished, or in any way supplied the said drawings, specifications, or other data, is not to be regarded by implication or otherwise as in any manner licensing the holder or any other person or corporation, or conveying any rights or permission to manufacture use, or sell any patented invention that may in any way be related thereto.

This report has been reviewed by the Office of Public Affairs (ASD/PA) and is releasable to the National Technical Information Service (NTIS). At NTIS, it will be available to the general public, including foreign nations.

This technical report has been reviewed and is approved for publication.

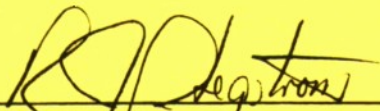


ROBERT M. ENGLE JR
Project Engineer



DR FRANK D. ADAMS, Acting Chief
Structural Integrity Branch

FOR THE COMMANDER:



ROGER J. HEGSTROM, Colonel, USAF
Chief, Structures & Dynamics Division

"If your address has changed, if you wish to be removed from our mailing list, or if the addressee is no longer employed by your organization please notify AFWAL/FIOE W-PAFB, OH 45433 to help us maintain a current mailing list".

Copies of this report should not be returned unless return is required by security considerations, contractual obligations, or notice on a specific document.



DEPARTMENT OF THE AIR FORCE
AIR FORCE WRIGHT AERONAUTICAL LABORATORIES (AFSC)
WRIGHT-PATTERSON AIR FORCE BASE, OHIO 45433-6543

22 JAN 1986

REPLY TO
ATTN OF: FIBEC

U218044

SUBJECT: Corrections to AFWAL-TR-82-3073, "USAF Damage Tolerant Design Handbook: Guidelines for the Analysis and Design of Damage Tolerant Aircraft Structures"

TO: Damage Tolerant Design Handbook Recipients

1. Due to a publishing error, the FOREWORD was inadvertently omitted from the printed copies of the subject document. The purpose of this section was to acknowledge the contributions of the previous edition of the Handbook and the work of others who supported the development of the Handbook. A copy of the omitted FOREWORD is included (Attachment 1). This page is numbered, ii, and should be inserted after the DD 1473.

2. In recognition of his contributions to the framework and the original release of the Handbook, Howard A. Wood, ASD/ENF, is being recognized as an author of the current document. A corrected TITLE page is enclosed (Attachment 2).

ROBERT M. ENGLE JR, AERO ENGR
Project Engineer, Damage Tolerant Handbook
Fatigue, Fracture & Reliability Gp
Structural Integrity Branch
Structures & Dynamics Division

2 Atch
1. FOREWORD
2. TITLE Page

RECEIVED
NAVPGSCOL

1981 FEB 2 P 1:01

FOREWORD

This report was prepared under Contract F33615-80-C-3229 by the University of Dayton Research Institute under the direction of Mr Robert M. Engle, Jr for the Structural Integrity Branch, Structures and Dynamics Division, Flight Dynamics Laboratory of the Air Force Wright Aeronautical Laboratories. The work was performed under Work Unit 24010143, Damage Tolerant Design Handbook Revision. Chapter 6, Damage Tolerance Analysis, was written in-house by Mr Engle under Work Unit 24010179, Life Analysis Methods for Aerospace Structures. Chapter 10, Analysis of Repaired Structures, was added after completion of the contract but prior to final publication.

This document represents an update, revision, and completion of AFFDL-TR-79-3021 also titled "Damaged Tolerant Design Handbook: Guidelines for the Analysis and Design of Damage Tolerant Aircraft Structures," which was released in March 1979. This original partial release of the handbook was written by Howard A. Wood and Robert M. Engle, Jr of the Flight Dynamics Laboratory. It contained only chapters two, four, and five plus appendix A. Major portions of the original chapters four and five were developed by D. Broek and S. H. Smith of Battelle Columbus Laboratory under contract F33615-75-C-3101. That contract was administered by Mr Engle.

This report covers work accomplished during the period September 1980 through March 1984.

This report was released for publication in May 1984.

AFWAL-TR-82-3073



USAF DAMAGE TOLERANT DESIGN HANDBOOK: GUIDELINES FOR THE ANALYSIS AND DESIGN OF DAMAGE TOLERANT AIRCRAFT STRUCTURES

**J.P. Gallagher, F.J. Giessler, and A.P. Berens
University of Dayton Research Institute
Dayton, Ohio 45469**

**R.M. Engle, Jr.
Structural Integrity Branch**

**H.A. Wood
Directorate of Flight Systems Engineering**

May 1984

Final Report for Period September 1980 to March 1984

Approved for public release; distribution unlimited.

**FLIGHT DYNAMICS LABORATORY
AIR FORCE WRIGHT AERONAUTICAL LABORATORIES
AIR FORCE SYSTEMS COMMAND
WRIGHT-PATTERSON AIR FORCE BASE, OHIO 45433**

UNCLASSIFIED

SECURITY CLASSIFICATION OF THIS PAGE (When Data Entered)

REPORT DOCUMENTATION PAGE		READ INSTRUCTIONS BEFORE COMPLETING FORM										
1. REPORT NUMBER AFWAL-TR-82-3073	2. GOVT ACCESSION NO.	3. RECIPIENT'S CATALOG NUMBER										
4. TITLE (and Subtitle) USAF DAMAGE TOLERANT DESIGN HANDBOOK: GUIDELINES FOR THE ANALYSIS AND DESIGN OF DAMAGE TOLERANT AIRCRAFT STRUCTURES		5. TYPE OF REPORT & PERIOD COVERED Final Report from Sept. 1980 to March 1984										
		6. PERFORMING ORG. REPORT NUMBER										
7. AUTHOR(s) J. P. Gallagher, F. J. Giessler, A. P. Berens and R. M. Engle, Jr.		8. CONTRACT OR GRANT NUMBER(s) F33615-80-C-3229										
9. PERFORMING ORGANIZATION NAME AND ADDRESS University of Dayton Research Institute Dayton, Ohio 45469		10. PROGRAM ELEMENT, PROJECT, TASK AREA & WORK UNIT NUMBERS Project: 2401 Task: 01 Work Unit: 43										
11. CONTROLLING OFFICE NAME AND ADDRESS Flight Dynamics Laboratory (AFWAL/FIBEC) Air Force Wright Aeronautical Laboratories (AFSC) Wright-Patterson Air Force Base, Ohio 45433		12. REPORT DATE May 1984										
		13. NUMBER OF PAGES										
14. MONITORING AGENCY NAME & ADDRESS (if different from Controlling Office)		15. SECURITY CLASS. (of this report) UNCLASSIFIED										
		15a. DECLASSIFICATION/DOWNGRADING SCHEDULE										
16. DISTRIBUTION STATEMENT (of this Report) Approved for public release; distribution unlimited.												
17. DISTRIBUTION STATEMENT (of the abstract entered in Block 20, if different from Report)												
18. SUPPLEMENTARY NOTES												
19. KEY WORDS (Continue on reverse side if necessary and identify by block number) <table border="0"> <tr> <td>Damage Tolerance Requirements</td> <td>Damage Size Considerations</td> </tr> <tr> <td>Fracture Mechanics</td> <td>Damage Tolerance Testing</td> </tr> <tr> <td>Residual Strength</td> <td>Fracture Control Guidelines</td> </tr> <tr> <td>Crack Growth Predictions</td> <td>Individual Airplane Tracking</td> </tr> <tr> <td>Design Guidelines</td> <td></td> </tr> </table>			Damage Tolerance Requirements	Damage Size Considerations	Fracture Mechanics	Damage Tolerance Testing	Residual Strength	Fracture Control Guidelines	Crack Growth Predictions	Individual Airplane Tracking	Design Guidelines	
Damage Tolerance Requirements	Damage Size Considerations											
Fracture Mechanics	Damage Tolerance Testing											
Residual Strength	Fracture Control Guidelines											
Crack Growth Predictions	Individual Airplane Tracking											
Design Guidelines												
20. ABSTRACT (Continue on reverse side if necessary and identify by block number) <p>This handbook supports the USAF Airplane Damage Tolerance Requirements contained in MIL-A-83444. The handbook provides specific background data and justification for the detailed requirements of MIL-A-83444 and provides guidelines and state-of-the-art analysis methods to assist contractor and USAF personnel in complying with the intent of the specification and in solving cracking problems, in general, for metallic aircraft structures. The material contained in this document is general enough to be useful in the evaluation</p>												

20. ABSTRACT (cont'd)

of the damage tolerance of in-service aircraft designed and qualified prior to the issuance of MIL-A-83444. The handbook has been structured to provide a clear and concise summary of the specification, MIL-A-83444, as well as supporting analysis methods, test techniques, and nondestructive inspection (NDI) methods are provided as state-of-the-art along with suggested and/or recommended practices, limitations, etc. For the convenience of the user, copies of appropriate USAF structural specifications are contained as an appendix to this handbook.

COMMENT FORM

TITLE: USAF Damage Tolerant Design Handbook: Guidelines for the
Analysis and Design of Damage Tolerant Aircraft Structures

PUBLICATION: AFWAL-TR-82-3073 REVISION: B (Complete Handbook)

1. USAF solicits your comments concerning this handbook so that its usefulness may be improved in later editions. Send any comments to the following address:

AFWAL/FIBE
ATTN: R.M. Engle, Jr.
WPAFB, OH 45433

2. Comments are solicited in the following areas:

- a. Is the handbook adequate?
- b. What improvements would make the handbook more adequate?
- c. Are there any general comments concerning the handbook?

3. Please note any specific errors which have been discovered. Include the page number for reference.

[illegible]

TABLE OF CONTENTS

<u>CHAPTER</u>		<u>PAGE</u>
1.0	INTRODUCTION AND METHODOLOGY FUNDAMENTALS	1.1.1
2.0	SUMMARY OF REQUIREMENTS	2.0.1
3.0	DAMAGE SIZE CHARACTERIZATIONS	3.0.1
4.0	RESIDUAL STRENGTH	4.0.1
5.0	ANALYSIS OF DAMAGE GROWTH	5.0.1
6.0	EXAMPLE DAMAGE TOLERANT ANALYSES	6.0.1
7.0	DAMAGE TOLERANCE TESTING	7.0.1
8.0	INDIVIDUAL AIRCRAFT TRACKING	8.0.1
9.0	GUIDELINES FOR DAMAGE TOLERANCE DESIGN AND FRACTURE CONTROL PLANNING	9.0.1
10.0	ANALYSIS OF STRUCTURAL REPAIRS	10.0.1
APPENDIX A - AIR FORCE SPECIFICATIONS AND STANDARDS		A-1
APPENDIX B - ASTM STANDARDS		B-1

1.0 INTRODUCTION AND METHODOLOGY FUNDAMENTALS

<u>SECTION</u>	<u>PAGE</u>
1.1 GENERAL	1.1.1
1.1.1 <u>Background</u>	1.1.1
1.1.2 <u>Objective</u>	1.1.3
1.1.3 <u>Content</u>	1.1.3
1.1.4 <u>Damage Tolerant Design (Data) Handbook</u>	1.1.6
1.2 INTRODUCTION TO DAMAGE CONCEPTS AND BEHAVIOR	1.2.1
1.2.1 <u>Damage Growth Concepts</u>	1.2.1
1.2.2 <u>Damage Growth Behavior/Effects</u>	1.2.4
1.2.2.1 Initial Crack Size - A Measure of Quality	1.2.5
1.2.2.2 Stress History - A Measure of Usage and Location	1.2.5
1.2.2.3 Material Properties - A Measure of Material Resistant to Cracking	1.2.6
1.2.2.4 Structural Properties - A Measure of Geometry	1.2.7
1.2.2.5 Summary of Effects	1.2.8
1.3 FRACTURE MECHANICS FUNDAMENTALS	1.3.1
1.3.1 <u>Background</u>	1.3.1
1.3.2 <u>Stress Intensity Factor - What It Is</u>	1.3.2
1.3.3 <u>Application to Fracture</u>	1.3.6
1.3.4 <u>Fracture Toughness - A Material Property</u>	1.3.8
1.3.5 <u>Crack Tip Plastic Zone Size</u>	1.3.9
1.3.6 <u>Application to Subcritical Crack Growth</u>	1.3.10
1.4 LIFE PREDICTION METHODOLOGY	1.4.1
1.4.1 <u>Crack Growth Damage Integration Package - Summary</u>	1.4.1
1.4.2 <u>Initial Flaw Distribution</u>	1.4.2
1.4.3 <u>Usage</u>	1.4.3
1.4.4 <u>Material Properties</u>	1.4.5
1.4.5 <u>Crack Tip Stress Intensity Factor Analysis</u>	1.4.6
1.4.6 <u>Damage Integration Models</u>	1.4.7
1.4.7 <u>Failure Criteria</u>	1.4.9
1.5 ACHIEVING CONFIDENCE IN THE LIFE PREDICTION METHODOLOGY	1.5.1
1.5.1 <u>Summary</u>	1.5.1
1.5.2 <u>Methods for Comparing Predictability</u>	1.5.2

INTRODUCTION AND METHODOLOGY FUNDAMENTALS
(Cont'd)

<u>SECTION</u>	<u>PAGE</u>
1.6 SCHEMES FOR DETERMINING STRESS INTENSITY FACTORS	1.6.1
1.6.1 <u>General</u>	1.6.1
1.6.1.1 Principle of Superposition	1.6.2
1.6.1.2 Advanced Uses of the Principle of Superposition	1.6.4
1.6.2 <u>Handbook Solutions</u>	1.6.8
1.6.2.1 Handbook of Table of Contents	1.6.8
1.6.2.2 Typical Solution Formats	1.6.15
1.6.3 <u>Developing Stress-Intensity Factor Solutions</u>	1.6.17
1.6.3.1 Green's Function Technique	1.6.18
1.6.3.2 The Weight Function Technique	1.6.22
1.6.4 <u>Finite Element Methods</u>	1.6.26
1.6.4.1 Direct Methods	1.6.30
1.6.4.2 Indirect Methods	1.6.32
1.6.4.3 Cracked Element Methods	1.6.35
1.7 SELECTED STRESS-INTENSITY FACTOR CASES	1.7.1
1.7.1 <u>Through-Thickness-Internally Cracked Type Geometries</u>	1.7.1
1.7.2 <u>Through-Thickness-Edge-Crack Type Geometries</u>	1.7.6
1.7.3 <u>Through-Thickness Cracks Growing From Circular Holes</u>	1.7.6
1.7.3.1 Remotely Loaded, Radially Cracked Hole	1.7.10
1.7.3.2 Remotely Loaded, Diametrically Cracked Hole	1.7.11
1.7.3.3 Pin Loaded Holes	1.7.11
1.7.4 <u>Internal Flaws</u>	1.7.19
1.7.5 <u>Part-Through Cracks</u>	1.7.20
1.7.6 <u>Corner Cracks At The Edge of a Plate</u>	1.7.23
1.7.7 <u>Corner Cracks at the Edge of a Hole</u>	1.7.29
1.7.7.1 Radial Corner Cracks	1.7.29
1.7.7.2 Diametrical Corner Cracks	1.7.32
1.7.8 <u>Semi-Elliptical Surface Crack at a Hole</u>	1.7.39
1.7.9 <u>Lug Crack Geometries</u>	1.7.39
1.8 APPROXIMATE SOLUTIONS FOR STRESS-INTENSITY FACTORS	1.8.1
1.8.1 <u>Effect of Stress Concentration</u>	1.8.2
1.8.2 <u>Effect of Finite Width</u>	1.8.7
1.8.3 <u>Effect of Crack Shape Changes</u>	1.8.15

INTRODUCTION AND METHODOLOGY FUNDAMENTALS
(Conc'd)

<u>SECTION</u>	<u>PAGE</u>
1.9 ALTERNATE FRACTURE MECHANICS ANALYSIS METHODS	1.9.1
1.9.1 <u>Strain Energy Release Rate, G</u>	1.9.3
1.9.1.1 The Griffith-Irwin Energy Balance	1.9.5
1.9.1.2 The Relationship Between G, Compliance, and Elastic Strain Energy	1.9.7
1.9.2 <u>The J-Integral, J</u>	1.9.10
1.9.2.1 J-Integral Calculations	1.9.11
1.9.2.2 Engineering Estimates of J	1.9.14
1.9.3 <u>Crack Opening Displacement (COD)</u>	1.9.21
1.10 LIST OF REFERENCES	1.10.1

LIST OF FIGURES

<u>FIGURE</u>		<u>PAGE</u>
1.2.1	Schematic of Observed Crack Growth Behavior for a Typical Structural Cracking Problem.	1.2.9
1.2.2	Schematic of Relationship Between Failure Strength and Crack Length for a Typical Single Element Type Structure.	1.2.9
1.2.3	Residual Strength Diagram Relationship Between Residual Strength Capacity and Elapsed Time. Note that when the Residual Strength Capacity Degrades to the Level of the Applied Stress, Failure Occurs.	1.2.10
1.2.4	Description of Baseline Conditions for Observed Crack Growth Behavior.	1.2.11
1.2.5	Schematic Summary of the Effects of Quality, Usage, Material and Geometry on Both the Crack Growth and Residual Strength Curves.	1.2.12
1.2.6	Summary of Schemes Which Illustrate the Sensitivity of Life to Various Structural Parameters.	1.2.13
1.3.1	The Three Modes of Crack Extension.	1.3.16
1.3.2	Infinite Plate with a Flaw That Extends Through Thickness.	1.3.16
1.3.3	Results of a Wide Plate Fracture Study Compared with a Fracture Toughness Curve Calculated Using the Finite Width Plate Stress Intensity Factor Equation, Equation 1.3.4 Data from Reference 7.	1.3.16
1.3.4	Yield Zones Observed on the Surface and Cross Section of a Cracked Sheet Under Uniaxial Tensile Loading in: A-Plane Stress, 45 Degree Shear Type; B-Plane Strain, Hinge Type ⁽⁸⁾ .	1.3.17
1.3.5	Small-Scale Yield Model for Restricted Crack Tip Plastic Deformation.	1.3.17

LIST OF FIGURES (Cont'd)

<u>FIGURE</u>		<u>PAGE</u>
1.3.6	Parameters that Define Constant Amplitude Load Histories for Fatigue Crack Growth. The Figure also Illustrates the Transformation Between Stress History Loading and Stress-Intensity-Factor Loading at One Crack Length Position.	1.3.18
1.3.7	Description of Crack Growth Behavior Observed for Two Very Much Different Structural Geometries.	1.3.19
1.3.8	Comparison of Crack Growth Rate Results for the Two Structural Geometries. The Coincidence of the Data Shows that the Hypothesis (Equation 1.3.6) is Correct.	1.3.19
1.3.9	Schematic Illustration of the Fatigue Crack Growth Rate as a Function of Stress Intensity Range.	1.3.20
1.4.1	Distribution of Initial Crack Size for a Given Type of Crack (e.g., Radial Cracks Growing from Fastener Holes).	1.4.12
1.4.2	Certification of NDI Capability.	1.4.12
1.4.3	Determining Initial Quality by Back Calculation.	1.4.13
1.4.4	Initial Flaw Distribution for F-4 Based on Back Calculation.	1.4.13
1.4.5	Typical Load Factor Exceedance Information Indicating Usage.	1.4.14
1.4.6	Load Factor to Stress History Transformation.	1.4.14
1.4.7	Stress-Intensity Factors - Cyclic Loading.	1.4.15
1.4.8.	Constant Amplitude Crack Growth Rate Data for 7075-T6 Aluminum.	1.4.15
1.4.9	Stress-Intensity-Factor Coefficients Showing Influence of Hole on K.	1.4.16
1.4.10	Influence of Hole on Geometric Correction Factor, β .	1.4.16

LIST OF FIGURES (Cont'd)

<u>FIGURE</u>		<u>PAGE</u>
1.4.11	Complex Crack Geometries.	1.4.17
1.4.12	Sequence of Steps Required to Calculate Crack Growth Increment.	1.4.18
1.4.13	Effect of Critical Crack Size on Life.	1.4.19
1.4.14	Economic Final Crack Size.	1.4.19
1.5.1	Single Overload Correlation with Modified Wheeler Retardation Model.	1.5.4
1.5.2	Spectrum Correlation Using the AFWAL Willenborg-Retardation-Model (Damage Integration Package).	1.5.5
1.5.3	Prediction Capability of Damage Integration Package (Based on 21 Laboratory Tests Conducted at AFWAL/FIB).	1.5.5
1.6.1	Edge Crack Geometry Loaded With Axial and Bending Loads.	1.6.37
1.6.2	Crack at Rivet in a Riveted Skin-Stringer Panel (No Crack Buckling).	1.6.38
1.6.3	Superposition of Stress Intensities for Uniform Tension and Concentrated Force.	1.6.39
1.6.4	Internally Pressurized Center Crack.	1.6.40
1.6.5	Principle of Superposition Illustrated for Center Cracked Geometry.	1.6.41
1.6.6a	Uniform Stresses Along Dotted Line Generated by Remote Loading.	1.6.42
1.6.6b	Opposing Stresses Applied Along the Dotted Line.	1.6.42
1.6.7	Illustration of Superposition Principle.	1.6.43
1.6.8	Application of Superposition Principle.	1.6.43
1.6.9	Stress Intensity Factor for Pin-Loaded Hole (Bearing By-pass Problem) Obtained by Superposition.	1.6.44

LIST OF FIGURES (Cont'd)

<u>FIGURE</u>		<u>PAGE</u>
1.6.10	Example Stress-Intensity Factor Solution Taken From Sih Handbook.	1.6.45
1.6.11	Example Stress-Intensity Factor Solution from the Tada, et al. Handbook.	1.6.48
1.6.12	Example Stress-Intensity Factor Solution from the Rooke-Cartwright Handbook.	1.6.49
1.6.13	Point Load (P) Applied to the Crack Faces for a Central Crack Located in an Infinite Plate.	1.6.51
1.6.14	Distributed Loading Applied to Crack Faces of the Central Crack.	1.6.51
1.6.15	Diametrically Cracked Hole With Symmetrically Located Point Focus.	1.6.52
1.6.16	Green's Function for Geometry and Loading Described in Figure 1.6.15 (References 38, 41, and 42).	1.6.52
1.6.17	Stress-Intensity Factor Calibration for a Cold Worked Hole ⁽⁴⁵⁾ .	1.6.53
1.6.18	Finite-Element Nodes Near Crack Tip.	1.6.54
1.7.1	Finite Width Correction Factors for Crack Tip "A".	1.7.50
1.7.2	Finite Width Correction Factors for Crack Tip "B".	1.7.51
1.7.3	Bowie β Factors for Through-Thickness Cracks at Remotely Loaded Circular Holes.	1.7.52
1.7.4	Beta Factor for a Through Crack Growing From a Hole, Loaded by a Close Tolerance Fastener (Reference 64).	1.7.53
1.7.5	Beta Factor for a Diametrical Through Crack Growing From a Hole, Loaded by a Close Tolerance Fastener (Reference 64).	1.7.54
1.7.6	Embedded Elliptical Crack Geometry.	1.7.55

LIST OF FIGURES (Cont'd)

<u>FIGURE</u>		<u>PAGE</u>
1.7.7	Shape Parameter Curves for Surface and Internal Flaws.	1.7.56
1.7.8	A Small Semi-Elliptical Crack in Uniformly Stressed Thick Structure.	1.7.57
1.7.9	Stress-Intensity Factors at the Point of Maximum Crack Depth for Surface Flaws Subjected to Bending Stresses (Reference 64).	1.7.58
1.7.10	Stress-Intensity Factors at Plate Surface Flaws for Surface Flaws Subjected to Bending Stresses (Reference 64).	1.7.59
1.7.11	Comparison of Boundary-Correction Factors for Quarter-Circular Corner Crack in a Plate Subjected to Tension ($a/c = 1$; $a/B = 0.2$). (Reference 72.)	1.7.60
1.7.12	Corner Crack Geometry for Solution by Liu (Reference 73).	1.7.61
1.7.13	Empirical Curves to Determine the Effective Size of a Corner Crack at a Hole (Reference 68).	1.7.61
1.7.14	Normalized Stress-Intensity Factors for Single Crack Emanating from Straight Attachment Lugs (Reference 88).	1.7.62
1.7.15	Normalized Stress-Intensity Factors for Single Crack Emanating from Tapered Attachment Lugs Subjected to a Pin Loading Applied to 0° Loading (Reference 88).	1.7.63
1.8.1	A Small Edge Crack Located at Stress Concentration.	1.8.19
1.8.2	Distribution of Stresses Normal to the Crack Path for a Radial Crack Growing from an Uniaxially Loaded Hole in a Wide Plate.	1.8.20
1.8.3	Radial Crack at Hole Growing Toward Splice Joint.	1.8.21
1.8.4	Model Crack for Example 1.8.3.	1.8.22
1.8.5	Comparison of Stress-Intensity Factor Relationships for the Crack Geometry Described in Figure 1.8.3.	1.8.22

LIST OF FIGURES (Conc'd)

<u>FIGURE</u>		<u>PAGE</u>
1.8.6	Finite Width Strip Containing A Diametrically Cracked Hole.	1.8.23
1.8.7	Plan Views of the Fracture Surfaces of Several Three-Dimensional Crack Problems.	1.8.23
1.8.8	Corner Crack Transitioning to a Thru-Thickness Crack.	1.8.24
1.8.9	Log-Log Plot of Equations 1.8.22 and 1.8.23 Showing the Development of the Transition Power Law Equation 1.8.24.	1.8.25
1.8.10	Stress-Intensity Factor for Transitioning Crack Shown in Figure 1.8.8.	1.8.25
1.9.1	Finite Width, Center Cracked Panel, Loaded in Tension with Load P.	1.9.25
1.9.2	Griffith Crack and Loading Configuration, Uniformly Loaded, Infinite Plate with a Center Crack of Length $2a$.	1.9.26
1.9.3	Load-Displacement Diagrams for the Structure Illustrated in Figure 1.9.1. The Diagram Shows the Changes that Occur in the Elastic Strain Energy as a Crack Grows Under the Two Defined Conditions.	1.9.27
1.9.4	J-Integral Parameters Illustrated.	1.9.28
1.9.5	Rectangular Path for J Calculation.	1.9.29
1.9.6	Description of Model Used to Establish the CTOD Under Elastic Conditions.	1.9.30
1.9.7	Dugdale Type Strip Yield Zone Analysis.	1.9.31
1.9.8	Definition of the Crack Tip Opening Displacement (CTOD) Per Rice, Shih, and Coworkers.	1.9.32

LIST OF TABLES

<u>TABLE</u>		<u>PAGE</u>
1.3.1	STRESS INTENSITY FACTORS FOR BASIC CRACK GEOMETRIES	1.3.5
1.6.1	ABBREVIATED TABLE OF CONTENTS FOR HANDBOOK OF STRESS-INTENSITY FACTORS	1.6.9
1.6.2	ABBREVIATED TABLE OF CONTENTS FOR "THE STRESS ANALYSIS OF CRACKS HANDBOOK"	1.6.11
1.6.3	ABBREVIATED TABLE OF CONTENTS FOR "COMPENDIUM OF STRESS INTENSITY FACTORS"	1.6.13
1.6.4	GREEN'S FUNCTION FOR A DOUBLE CRACK EMANATING FROM AN OPEN HOLE IN AN INFINITE PLATE (REF. 42)	1.6.21
1.6.5	LEAST SQUARES FIT OF FINITE ELEMENT DATA FOR CRACK MOUTH DISPLACEMENT (REF. 45)	1.6.27
1.7.1	STRESS INTENSITY FACTORS FOR INTERNALLY CRACKED STRUCTURES WITH THROUGH-THICKNESS CRACKS	1.7.2
1.7.2	STRESS-INTENSITY FACTORS FOR CRACKS STARTING AT THE EDGE OF A STRUCTURE	1.7.7
1.7.3	STRESS-INTENSITY FACTORS FOR CIRCULAR HOLES WITH THROUGH-THICKNESS HOLES	1.7.15
1.7.3A	COMPARISON OF β FACTORS FOR THROUGH-THICKNESS, RADially CRACKED AND REMOTELY LOADED HOLE CRACKS	1.7.17
1.7.3B	COMPARISON OF β FACTORS FOR THROUGH-THICKNESS, DIAMETRICALLY CRACKED AND REMOTELY LOADED HOLE CRACKS	1.7.17
1.7.3C	RADially CRACKED-PIN LOADED HOLE ($W=\infty$)	1.7.18
1.7.3D	DIAMETRICALLY CRACKED-PIN LOADED HOLE ($W=\infty$)	1.7.18
1.7.4	STRESS-INTENSITY FACTORS FOR EMBEDDED CRACKS	1.7.21
1.7.5	STRESS-INTENSITY FACTOR SOLUTIONS FOR SURFACE (SEMI-ELLIPTICAL) CRACK GEOMETRIES	1.7.24

LIST OF TABLES (Cont'd)

<u>TABLE</u>		<u>PAGE</u>
1.7.5A	STRESS INTENSITY CHARACTERISTIC FOR SURFACE (SEMI-ELLIPTICAL) FLAW IN SEMI-INFINITE PLATE	1.7.26
1.7.5B	BACK SURFACE CORRECTION FACTOR ^(70,71)	1.7.27
1.7.5C	NEWMAN AND RAJU ⁽⁷²⁾ SOLUTION (1981) FOR SURFACE FLAW CASE 1.7.5.3	1.7.28
1.7.6	QUARTER-ELLIPTICAL STRESS-INTENSITY FACTOR SOLUTIONS SUBJECTED TO TENSILE LOADING	1.7.30
1.7.6A	PARAMETERS OF QUARTER-ELLIPTICAL STRESS-INTENSITY FACTOR SOLUTION PRESENTED	1.7.31
1.7.7	STRESS-INTENSITY FACTORS FOR CORNER CRACKS AT HOLES	1.7.35
1.7.7A	NEWMAN AND RAJU SOLUTION FOR RADIAL CORNER CRACK (REFERENCE 72)	1.7.36
1.7.7B	NEWMAN AND RAJU SOLUTION FOR DIAMETRICAL CORNER CRACKS	1.7.38
1.7.8	SEMI-ELLIPTICAL SURFACE CRACKS AT A HOLE	1.7.40
1.7.9	STRESS-INTENSITY FACTOR SOLUTIONS FOR LUG-TYPE GEOMETRIES	1.7.42
1.7.9A	STRESS-INTENSITY FACTORS FOR STRAIGHT SHANK LUG AS A FUNCTION OF OUTER TO INNER RADIUS (r_o/r_i)	1.7.44
1.7.9B	NORMALIZED STRESS-INTENSITY FACTORS FOR SINGLE CORNER CRACKS AT STRAIGHT ATTACHMENT LUGS OBTAINED USING COMPOUNDING METHOD (B/R = 1/3) PER REFERENCE 88	1.7.45
1.7.9C	NORMALIZED STRESS-INTENSITY FACTORS FOR SINGLE CORNER CRACKS AT STRAIGHT ATTACHMENT LUGS OBTAINED USING COMPOUNDING METHOD (B/R = 2/3) PER REFERENCE 88	1.7.46
1.7.9D	GREEN FUNCTIONS FOR W/D = 1.500 (MODIFIED FOR PIN LOADING) PER REFERENCE 88	1.7.47
1.7.9E	GREEN FUNCTIONS FOR W/D = 2.250 (MODIFIED FOR PIN LOADING) PER REFERENCE 88	1.7.48

LIST OF TABLES (Conc'd)

<u>TABLE</u>		<u>PAGE</u>
1.7.9F	GREEN FUNCTIONS FOR $W/D = 3.000$ (MODIFIED FOR PIN LOADING) PER REFERENCE 88	1.7.49
1.8.1	COMPARISON OF β FACTORS BASED ON REPRESENTATIVE STRESSES FOR SINGLE EDGE RADIAL CRACK PROBLEMS	1.8.6
1.8.2	VARIOUS WIDTH BETA (β_w) FACTORS	1.8.11
1.8.3	STRESS-INTENSITY FACTOR ANALYSIS FOR EXAMPLE 1.8.3	1.8.13
1.8.4	β VALUES FOR STRESS-INTENSITY FACTOR COMPONENTS IN PROBLEM 1.8.4	1.8.16
1.9.1a	h_1 , h_2 and h_3 FOR THE PLANE STRAIN CCP IN TENSION (REFERENCES 103, 104, 111)	1.9.19
1.9.1b	h_1 , h_2 and h_3 FOR THE PLANE STRESS CCP IN TENSION (REFERENCES 103, 104, 111)	1.9.20

DEFINITION OF TERMS

1. Deterministic Analysis Methods/Approaches - Methods which predict life, level of damage (i.e., crack size) by considering all input data as discrete items. For a given set of data the prediction is a single value.
2. Probabilistic Analysis Methods/Approaches - Methods which predict distributions of lives or levels of damage (i.e., crack size population) by considering the statistical nature of one or more of the input variables. For a given set of data the result is presented in terms of probability of equaling or exceeding a given value.
3. Reliability (Structural) - The probability that a structure will perform its specified mission without failure when subjected to loads or other adverse environments.
4. Risk (Structural) - The probability that a structure will not perform its specified mission without failure when subjected to loads or other adverse environments.
5. Safety - The assurance that safety of flight structure of each aircraft will achieve and maintain a specified residual strength level (in the presence of undetected damage) throughout the anticipated service life.
6. Durability - The assurance that the force can operate effectively with a minimum of structural maintenance, inspection and downtime, costly retrofit, repair and replacement of major structure due to the degrading influence of general cracking, corrosion, wear, etc.
7. Damage - Flaws, cracks, voids, delaminations, etc. which may be present in structures as a result of manufacturing operations or service. In this report damage is considered as a sharp crack.
8. Damage Tolerance - The ability of a structure to successfully contain damage over a specified life increment without adversely affecting safety of flight.
9. Residual Strength (Required) - The minimum internal member load, P_{xx} , which the structure is required to sustain with damage present without endangering safety of flight.
10. Life (Force) Management - The actions required to maintain safety and durability throughout the service life of the force.

LIST OF SYMBOLS

a	crack size/length
a_{cr}	critical crack size/length
a_o	initial crack size/length
K	stress intensity factor
K_c	fracture toughness
ΔK	stress intensity factor range
K_{max}	maximum stress intensity factor
K_{min}	minimum stress intensity factor
P_{xx}	residual strength (load)
N	flights, blocks, cycles
N_e	economic life
N_f	life, number of flights, blocks, cycles to failure
N_z	load factor
R	stress ratio
t	elapsed time
t_f	life/elapsed time to failure
β	geometric correction factor
σ	stress
σ_{res}	residual strength (stress)

1.0 INTRODUCTION AND METHODOLOGY FUNDAMENTALS

1.1 GENERAL

1.1.1 Background

In 1970, the USAF started to develop a Damage Tolerance Philosophy in order to eliminate the type of structural failures and cracking problems encountered on various military aircraft. These failures and cracking problems contributed to overcost, behind schedule airframe developments, unacceptably high in-service maintenance and repair costs, excessive downtimes, and, in some cases, loss of life. Air Force reviews of these problems have led to the conclusion that fatigue, stress corrosion, and corrosion-fatigue are the primary mechanisms of crack growth. In addition, it has been found that pre-existing manufacturing quality deficiencies (e.g. scratches, flaws, burrs, cracks, etc.) or service induced damage (e.g. corrosion pits), are very often the basic cause of the cracking problems. The effect of these flaws on the safety of the aircraft is dependent on their initial sizes, the rates of growth with service usage, the critical flaw sizes, the inspectability of the structure, and the fracture containment capabilities of the basic structural design.

From the standpoint of flight safety, it is found prudent to assume that new airframe structures can and very often do contain such initial damage. Likewise, for older systems and those structures which have

experienced service cracking, it is essential that safety of flight be provided through the consideration of an "initial flaw" model in which some size of initial damage is assumed to exist consistent with the inspection capability either in the field or during manufacture. The critical assumed initial damage shall be considered to be that damage just smaller than can be detected by the appropriate NDI methods.

In 1975, the USAF issued its Airplane Damage Tolerant Requirements in the form of a military specification (MIL-A-83444); these requirements remained intact during the change of structural specifications to the structures MIL PRIME specification. The intent of the USAF Airplane Damage Tolerant Requirements is to ensure that the maximum possible initial damage will not grow to a size which would endanger flight safety during the service life of the aircraft. When properly interpreted and applied, the specification requirements should accomplish this intent through:

- a. Proper material selection and control
- b. Control of stress levels
- c. Use of fracture resistant design concepts
- d. Manufacturing process control
- e. Use of qualified inspection procedures

While it is expected that compliance with the requirements will also tend to lead to improved structural durability, this is not their primary purpose. Requirements directed towards minimizing and delaying

crack initiation and structural deterioration due to fatigue and corrosion, i.e. durability, are contained in MIL-A-8866B.

1.1.2 Objective

The primary purpose of this handbook document is to provide guidelines and state-of-the-art analysis methods that should assist engineering personnel comply with the intent of the USAF Airplane Damage Tolerant Requirements for metallic structures. A secondary purpose is to provide specific background data and justification for the detailed requirements specified.

1.1.3 Content

This handbook has been structured to provide a clear and concise summary of the Damage Tolerant Requirements as well as supporting data and rationale behind the critical assumptions. Where appropriate, analysis methods, test techniques, and NDI methods are provided as state-of-the-art with suggested and/or recommended practices, limitations, etc., so stated.

In the subsequent sections of Chapter 1, the basic elements of the methodology for damage tolerant analysis are presented. By presenting the common methodology in this chapter with the introductory material, subsequent chapters can concentrate on developing those methodology details specific to each damage tolerant requirement. Chapters 2 through 10 address the following topics:

Chapter 2.0 - Summary of Requirements contains a review of MIL-A-83444 including examples for clarity, data to support specific requirements, and assumptions and rationale where limited data exists.

Chapter 3.0 - Damage Size Considerations discusses appropriate NDI practice, state-of-the-art procedures, demonstration programs to qualify NDI, in service NDI practice and specific examples illustrating how damage is assumed to exist in structures.

Chapter 4.0 - Determination of Residual Strength summarizes theory, methods, assumptions, material data, test verification, and gives examples for estimating the final fracture strength or crack arrest potential of cracked structures.

Chapter 5.0 - Analysis of Damage Growth describes current practice for estimating the rate of crack growth as a function of time, cyclic and sustained load occurrence; gives examples indicating limitations of methods, use of material data and suggested testing to support predictions and establish confidence.

Chapter 6.0 - Damage Tolerance Analysis - Sample Problems - provides detailed analysis of typical structural examples illustrating methodology and assumptions required.

Chapter 7.0 - Damage Tolerance Testing describes methods and recommended tests to verify methods, full-scale testing to verify residual strength and slow crack growth rates.

Chapter 8.0 - Individual Airplane Tracking describes current methods available to account for usage variations for individual force aircraft based on a crack growth model.

Chapter 9.0 - Guidelines for Damage Tolerant Design and Fracture Control Planning describes methods and procedures for development and implementation of a damage tolerance control plan as required in MIL-STD-1530A (5.1.3.1).

Chapter 10.0 - Repair Guidelines describes the factors which should be considered when designing a repair, in order to ensure that the basic damage tolerance present in the original structure is not degraded by the repair.

For the convenience of the user, copies of appropriate USAF structural specifications are contained as an appendix to this handbook. Any conflict or discrepancy in information contained in this handbook and/or the MIL PRIME structures specification is unintentional and in all cases, the governing document is the current version of the specification.

Throughout the handbook references to the specifications will be given by using paragraph numbers in parentheses, e.g. (3.1.1.2) refer to paragraph 3.1.1.2 Continuing damage on page 4 of MIL-A-83444.

1.1.4 Damage Tolerant Design (Data) Handbook

Damage tolerance analyses require supporting fracture mechanics materials data. A primary source of such data is MCIC-HB-01[†] and the Damage Tolerant Design (Data) Handbook which was first issued in 1972 and revised in 1975 and 1983. The 1983 revision of this data handbook contains data on (a) critical plane-strain stress-intensity factors (K_{Ic}), (b) critical plane-stress intensity factors (K_{Ic}), (c) crack growth resistance curve behavior (K_R vs Δa), (d) sustained load threshold stress-intensity factors in corrosive media (K_{Isc}), (e) sustained load crack growth rates in corrosive media (da/dt vs K_I) and (f) fatigue crack growth rates (da/dN vs ΔK). The reader will find that many examples of the data formats from the Damage Tolerant Design (Data) Handbook presented in Chapters 4 and 5 along with descriptions of how the data can be employed for various damage tolerance analyses.

[†]Available from: Metals and Ceramics Information Center, Battelle Laboratories, Columbus, Ohio.

1.2 INTRODUCTION TO DAMAGE CONCEPTS AND BEHAVIOR

1.2.1 Damage Growth Concepts

Past experience with tests of structures under simulated flight loading has indicated that the time to initiation of cracks from most structural details such as sharp corners or holes is relatively short and that the majority of the life (i.e., 95%) is spent growing the resultant cracks to failure. Likewise, analyses of in-service fractures, cracking instances, etc. have indicated that a major source of cracks is the occurrence of initial manufacturing defects such as sharp corners, tool marks and the like. Thus, it is now common practice to consider the damage accumulation process as entirely crack growth, with zero time to initiate the crack. Although this assumption may seem unduly severe, recent studies have shown the approach feasible, of minimal detriment to weight, cost, etc., but most important, the consideration of initial damage in the form of cracks or equivalent damage is absolutely necessary to ensure structural safety.

This subsection will detail the fundamentals of life prediction based on crack growth. The crack length will be the measure of damage and the crack growth rate will define the rate of damage accumulation. Figure 1.2.1 shows the type of information that defines the parameters basic to a life prediction.

Figure 1.2.1 presents a schematic of typical growth behavior for a crack being observed in a structural element as it moves from an initial damage size to a damage size that causes structural failure (loss of structural safety). Note that the abscissa (x-axis) measures either the elapsed time (t) during which loading is applied or the number of loading events (N) applied, and the ordinate (y-axis) measures the corresponding length of crack observed in the structure. Typically, the elapsed time is given in operational flight hours and the number of loading events is counted (grossly) by the number of the aircraft's flights.

The crack grows in response to the cyclic loading applied to the structure. Any crack (a) will grow a given increment (Δa) when subjected to a given number of cycles (ΔN), the rate being measured by $\Delta a / \Delta N$. When the crack length reaches a critical value (a_{cr}), the growth becomes unstable, thereby inducing failure.

When the crack (a) reaches the critical length, the measure of loading (t or N) reaches the structural life limit (t_f or N_f). The structural life limit is a measure of the maximum allowable service time (or number of accumulated service events) associated with driving the crack from its initial length (a_o) to the critical length (a_{cr}). It is the objective of the Damage Tolerant Requirements to ensure that cracks do not reach levels that could impair the safety of the aircraft during the expected

lifetime (t_s or N_s) of the aircraft, i.e. $t_f(N_f)$ must be greater than $t_s(N_s)$.

As can be noted from Figure 1.2.1, when the crack is small, it grows very slowly. As the crack gets longer, the rate of growth increases until the crack reaches the critical size a_{cr} , whereupon fracture of the structural element ensues. While the subcritical crack growth process occurring for $a \leq a_{cr}$ may take twenty to thirty years of service, the fracture process is almost instantaneous. Studies of the failure process indicate a very close relationship between the length of crack at failure and the load or stress that induces the onset of rapid fracture.

Typically, this relationship between crack length and failure strength level is as shown in Figure 1.2.2. The cracked element strength is referred to as the residual strength (σ_{res}) since this represents the remaining strength of a damaged structure. By considering the basic elements of Figures 1.2.1 and 1.2.2 collectively, a residual strength diagram can be developed as a function of elapsed time (or loading events).

A residual strength diagram is presented in Figure 1.2.3; this diagram shows that while the structure is young ($t \ll t_f$) the residual strength capacity is basically unimpaired because the crack is both small and doesn't grow much with time. As the structure starts to age, the

residual strength capacity is shown to decrease and just prior to failure, the rate of decrease in residual strength capacity is accelerating because now the crack is rapidly becoming very large. When the residual strength capacity equals the level of the maximum stress in the operational history, failure occurs.

As implied by the residual strength diagram, a ten to twenty percent change in the maximum applied stress in the operational history would not normally affect the allowable structural life significantly, assuming that the subcritical crack growth process (Figure 1.2.1) was unaffected. Normally, when the loads in the operational history change, the subcritical crack growth process changes its pattern of growth and this in turn affects the residual strength diagram and the allowable structural life.

1.2.2 Damage Growth Behavior/Effects

As discussed in subsection 1.2.1, the crack length a_0 will grow to a_{cr} in some life t_f , and as the crack grows the residual strength capability decreases. Experiments have shown that several parameters affect the crack growth life; the most important of these being (a) the initial crack size, a_0 , (b) the load history, (c) the material properties, and (d) the structural properties. The isolated effect of each parameter on the crack growth behavior and the residual strength curves will be discussed in turn using the baseline conditions identified in Figure 1.2.4. The interrelation of these parameters will be developed in the discussion of life prediction methodology (Section 1.4).

1.2.2.1 Initial Crack Size - A Measure of Quality

The effect of initial crack size is significant.

Given a configuration and loading, the smaller the initial crack size, the longer the life and the higher the residual strength capacity at any time. These observations are displayed in Figure 1.2.5 parts a and b, respectively. Note that the shape of the crack growth curve (for a given configuration and loading) remains essentially constant for any given crack growth increment.

Thus, given the crack growth curve for the smaller initial crack, it is possible to construct the crack growth curve for the baseline condition. This can be accomplished by shifting the crack growth curve with a smaller initial crack horizontally to the left until the curve intersects the vertical axis at the baseline initial crack size. Also, note that the residual strength curve for the baseline condition can be constructed from the curve obtained for the smaller initial crack size.

1.2.2.2 Stress History - A Measure of Usage and Location

As an aircraft flies different missions and different maneuvers, it experiences different loadings. The magnitude and sequence of aircraft loadings are noted to have a significant effect on the rate at which cracks grow. The stress history describes the magnitude and sequence of stresses at one location that results from the sequence of missions or maneuvers which an aircraft flies. Figure 1.2.5 parts c and d illustrate the effect that stress history (usage)

can have on the crack growth behavior and residual strength capacity, respectively. While it was not shown, a change in stress history will normally also change the applied stress level at which fracture occurs.

The stress history experienced at each location on the aircraft will also differ due to changes in bending moment, twisting moment, shear loading, etc., given a particular crack configuration (e.g., a crack growing from a fastener hole on a wing). The loading spectra for a lower surface location is typically more severe than a corresponding upper surface location; and, therefore, the life for the lower surface will be significantly shorter than that of the upper surface all other conditions being equal.

1.2.2.3 Material Properties - A Measure of Material Resistant to Cracking

Experimentally, it has been shown that for the same loading condition (i.e., the same number and amplitude of stress cycles) cracks will grow faster in certain alloys than in others. The crack growth rate ($\Delta a/\Delta N$) can be derived experimentally for each material. Given the same load and geometric conditions, the alloy having the slower growth rate characteristics (i.e. 2024-T3) will have a longer life (t_f) as shown in Figure 1.2.5 part e.

The material also has some inherent resistance to fracture. The higher this inherent resistance, the higher the residual strength capacity for any crack length. This effect is described in Figure 1.2.5 part f.

If the cracks are so small that the fracture process is controlled by gross yielding, then the residual strength curve is controlled by a net section failure criterion rather than a fracture criterion. In this case, the material with the highest yield strength would have the highest residual strength in the region of the curve controlled by the behavior of the small cracks.

1.2.2.4 Structural Properties - A Measure of Geometry

The most complex of the parameters affecting crack growth behavior are the structural properties. The structural properties involve such things as crack configuration, load transfer through fasteners, fastener hole size, part thickness, etc. A substantial amount of experimental work has been performed to characterize the geometrical effects on life. The effect of a change of hole radius on the crack growth behavior and on the residual strength capacity is shown in Figure 1.2.5 parts g and h. The structure with the smaller hole, and thus the smaller stress concentration is noted to have the longer life and higher residual strength.

1.2.2.5 Summary of Effects

As discussed above, there are four major parameters which affect the crack growth life and residual strength capacity of structures. These parameters are in the realm of quality (initial crack size), usage (loading history), material (material properties), and geometry (structural properties). Figure 1.2.6 has been prepared to summarize the parameters' effect on life and to illustrate various presentation schemes that might be employed to compare effects.

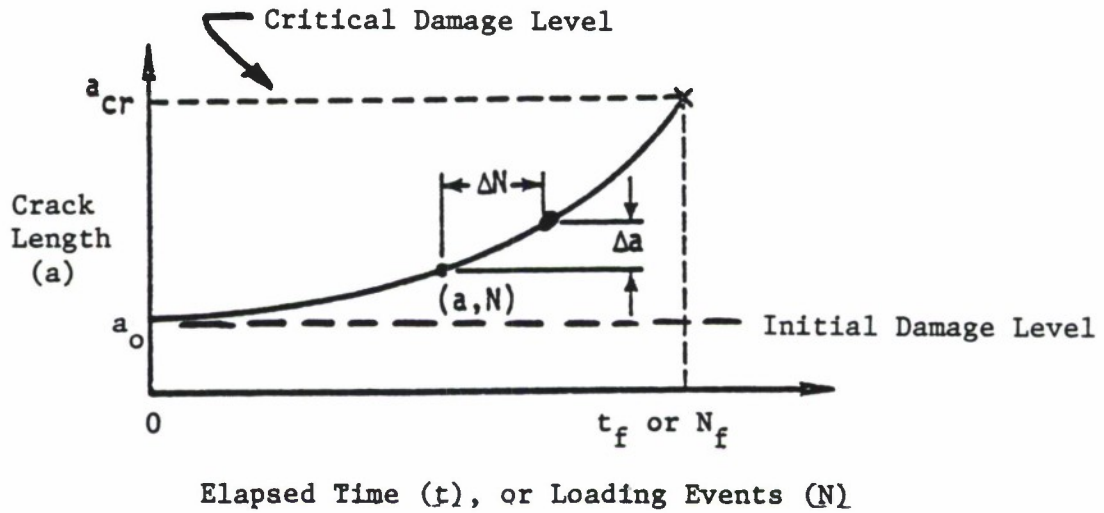


Figure 1.2.1. Schematic of Observed Crack Growth Behavior for a Typical Structural Cracking Problem.

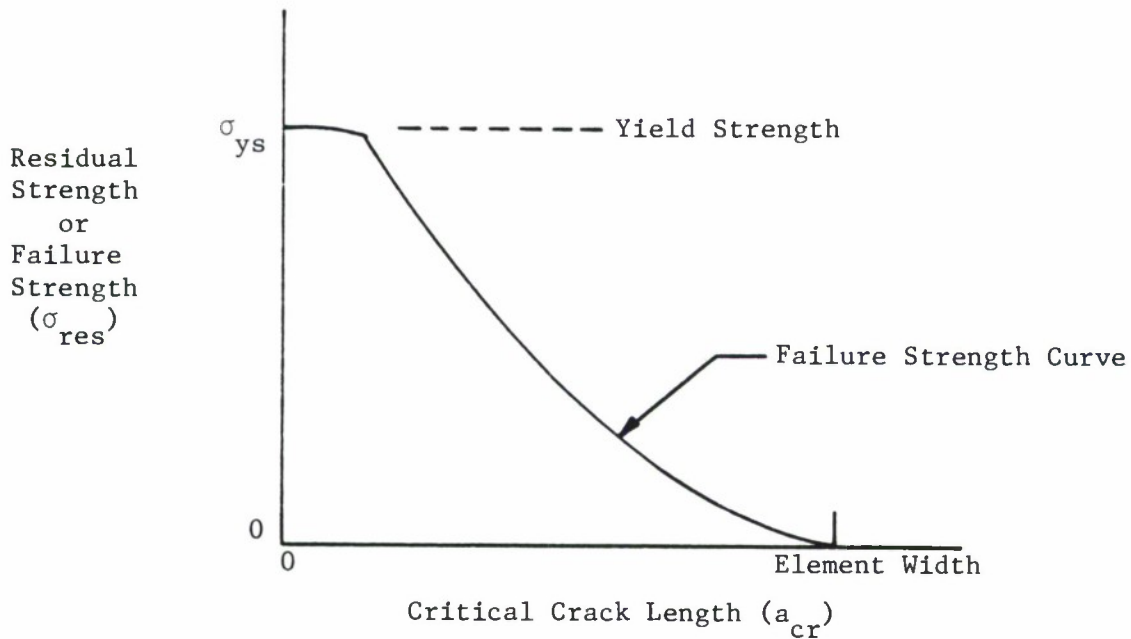


Figure 1.2.2. Schematic of Relationship Between Failure Strength and Crack Length for a Typical Single Element Type Structure.

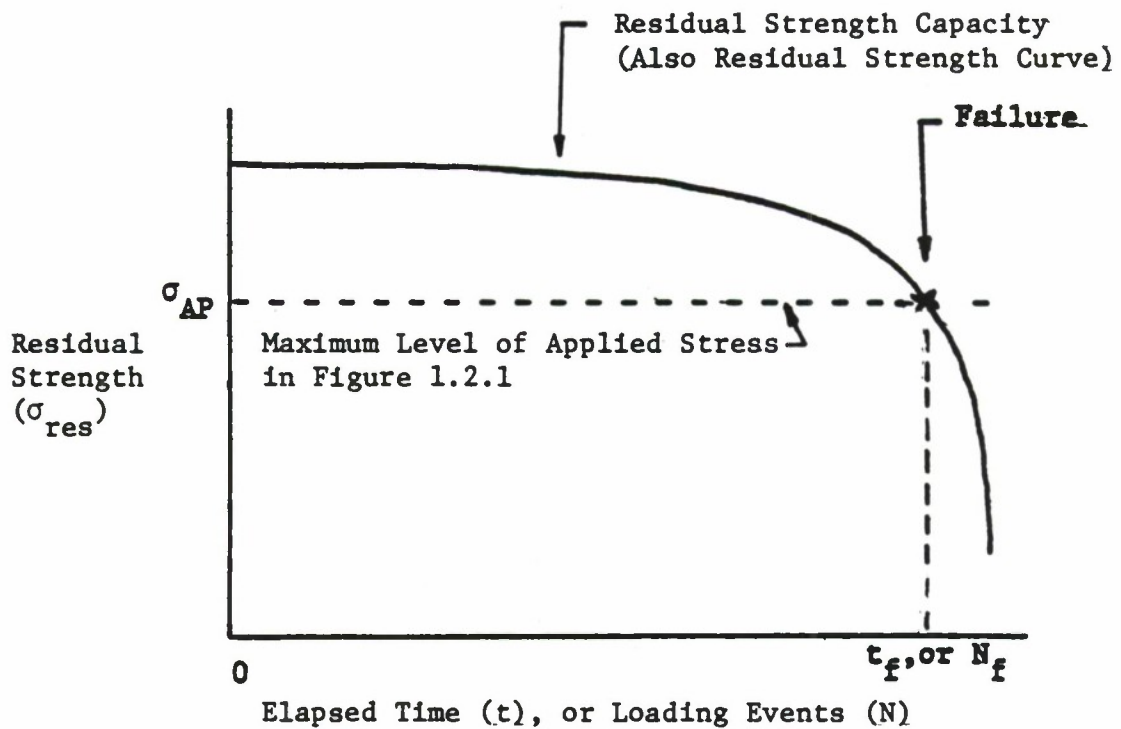


Figure 1.2.3. Residual Strength Diagram Relationship Between Residual Strength Capacity and Elapsed Time. Note that when the Residual Strength Capacity Degrades to the Level of the Applied Stress, Failure Occurs.

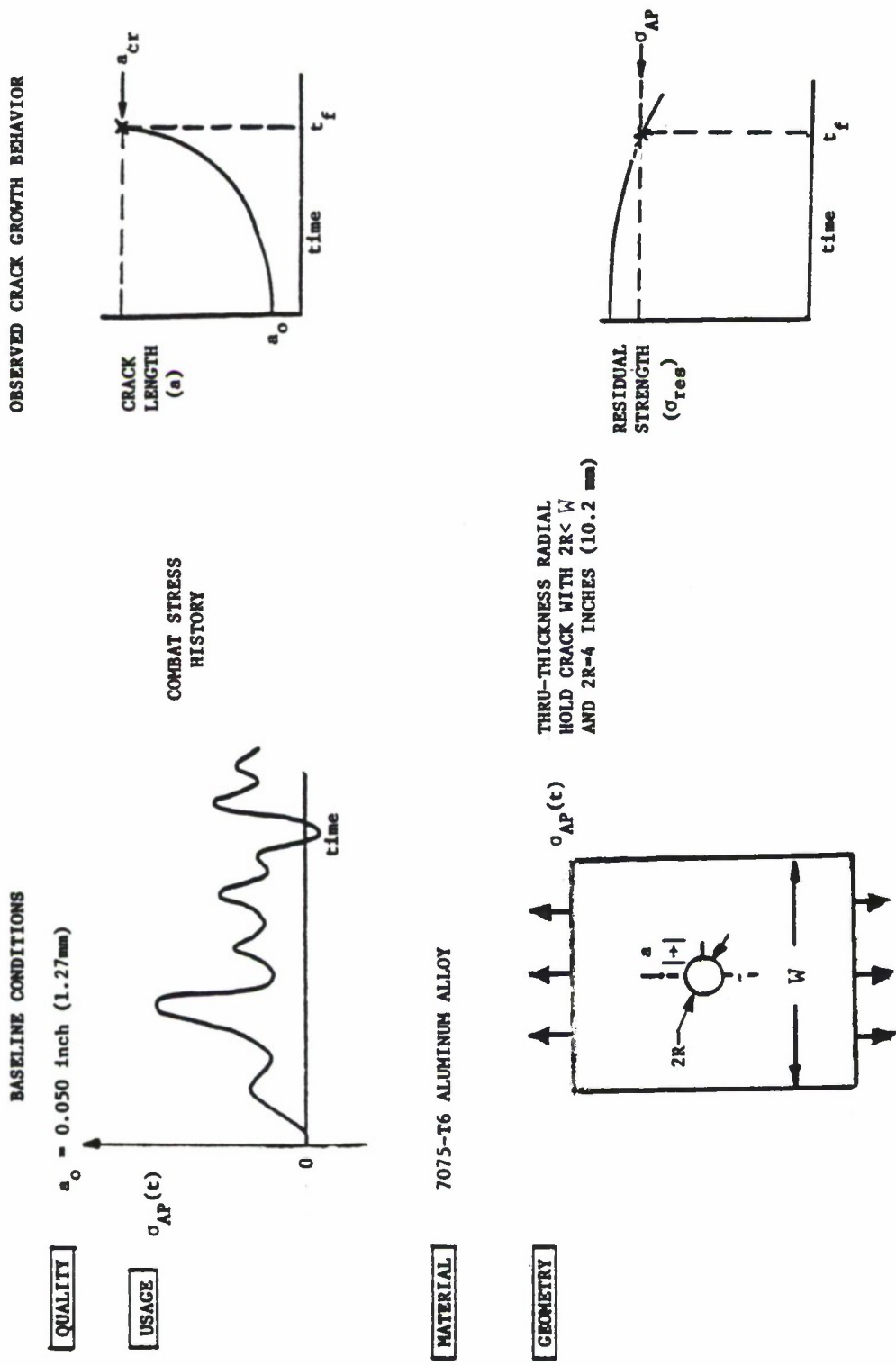


Figure 1.2.4. Description of Baseline Conditions for Observed Crack Growth Behavior.

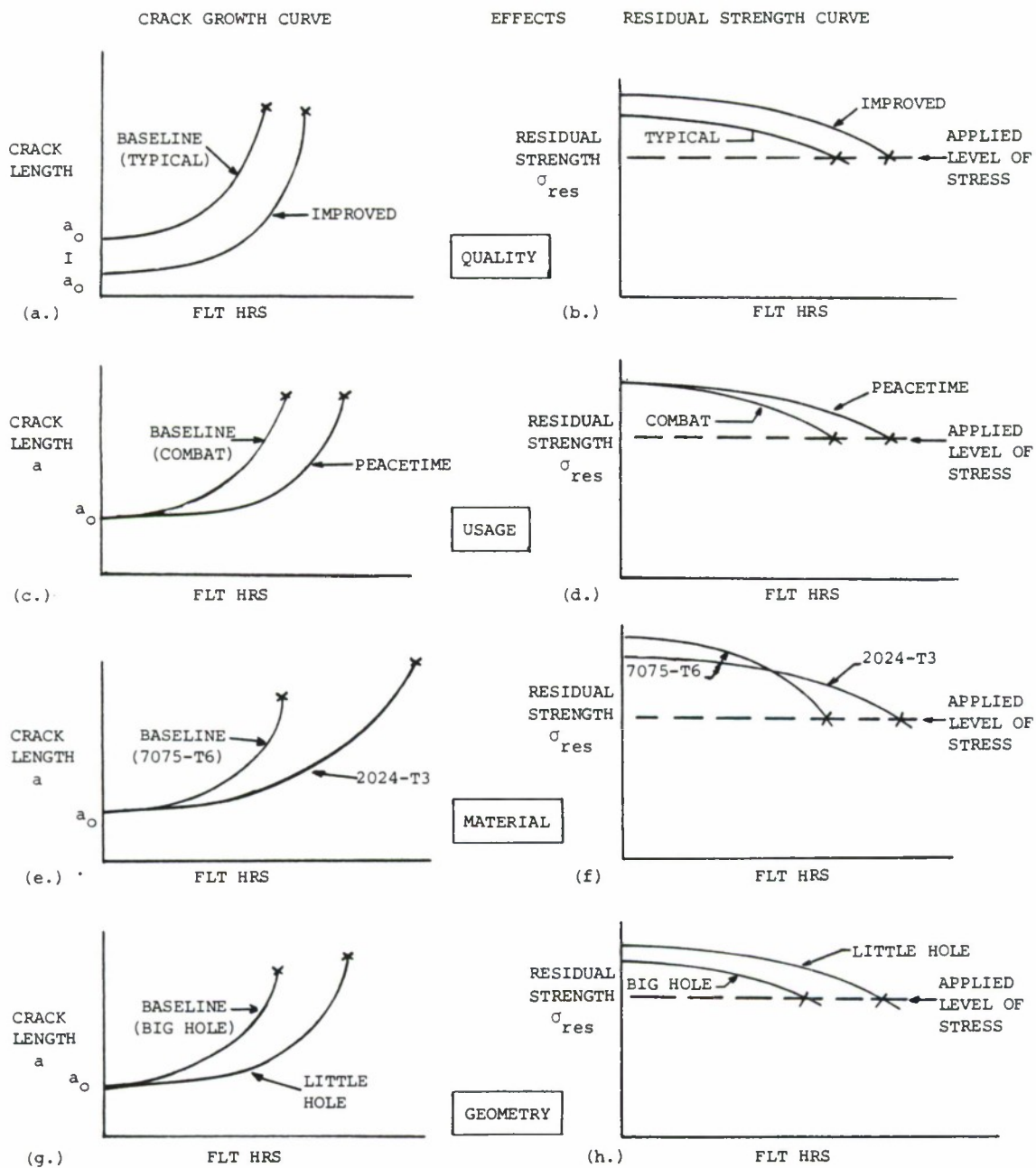
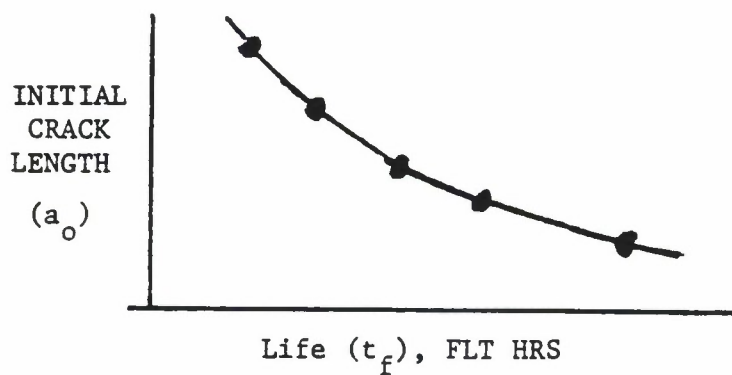
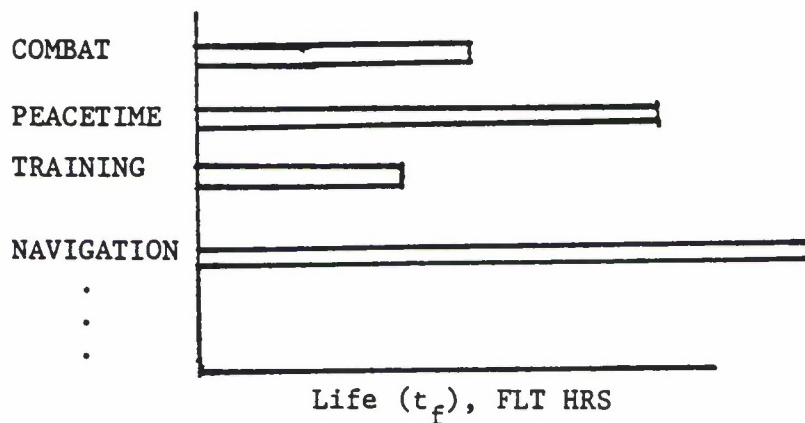


Figure 1.2.5. Schematic Summary of the Effects of Quality, Usage, Material and Geometry on Both the Crack Growth and Residual Strength Curves.

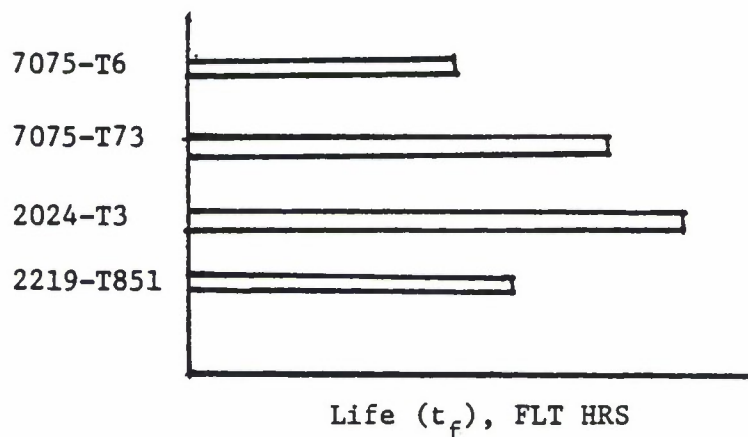
QUALITY



USAGE



MATERIAL



GEOMETRY

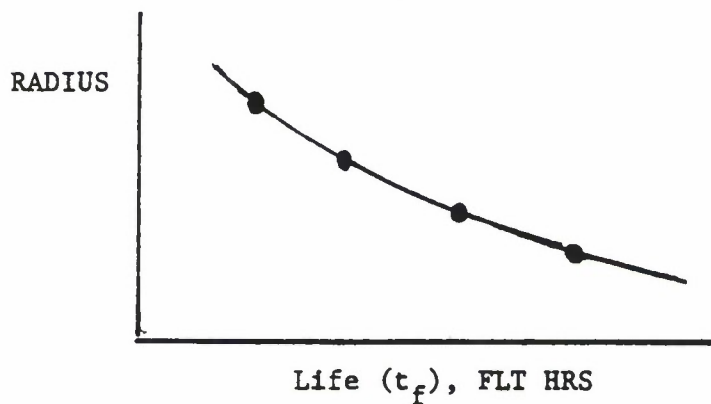


Figure 1.2.6. Summary of Schemes Which Illustrate the Sensitivity of Life to Various Structural Parameters.

1.3 FRACTURE MECHANICS FUNDAMENTALS

1.3.1 Background

Fracture Mechanics is that technology concerned with the modeling of cracking phenomena. Bulk (smooth specimen) properties are not normally useful in design for determining a material's tolerance to cracks or crack-like defects, because material tolerance to flaws resides in a material's ability to deform locally. Since the source of fractures can be identified with the lack of material tolerance to cracks, it seems only natural that attention should be focused on the crack tip region where the material must resist crack extension. This subsection will introduce the principal features of a mechanical model that characterizes crack movement in structural components fabricated from materials having low tolerance to flaws.

This subsection will present basic information that a designer should be familiar with prior to the utilization of remaining sections and chapters of this handbook. This subsection will define the meaning and use of the fracture mechanics model for the control of fracture and subcritical crack growth processes.

The application of a fracture mechanics model to solve crack problems came about through the following realization: component fractures that result from the extension of small crack-like defects are failures that depend on localized phenomena. Consider the three independent modes of

crack extension that are illustrated in Figure 1.3.1. The tensile opening mode, Mode 1, represents the principal action observed and this is the type of separation that we design against. While fractures induced by shear stresses can occur, these fractures are rather infrequent. There are hypotheses available for describing the combined influence of two (or three) modes of crack extension but these will not be discussed until Chapter 4. In general, since improvement of a material's Mode 1 fracture resistance will also improve the resistance to the combined mode action, the development of concepts throughout the Handbook will emphasize Mode 1 crack extension behavior.

A linear elastic analysis of a cracked body provides a good first approximation to the localized stress state in materials that fracture at gross section stresses below the yield strength. No additional refinements in the analysis are necessary if the gross section stresses at failure are below $0.7\sigma_{ys}$. The elastic analysis when modified to account for restricted amounts of stress relaxation due to crack tip plastic deformation provides an adequate description of fractures that occur above $0.7\sigma_{ys}$.

1.3.2 Stress Intensity Factor - What It Is

The model referred to above is called the linear elastic fracture mechanics model and has found wide acceptance as a method for determining the resistance of a material to below-yield strength fractures. The model is based on the use of linear elastic stress

analysis; therefore, in using the model one implicitly assumes that at the initiation of fracture any localized plastic deformation is small and contained within the surrounding elastic stress field. Application of linear elastic stress analysis tools to cracks of the type shown in Figure 1.3.2 shows that the local stress field (within $r < a/10$) is given by (1-4)*.

$$\begin{aligned}\sigma_x &= \frac{K}{\sqrt{2\pi r}} \cos \frac{\theta}{2} \left[1 - \sin \frac{\theta}{2} \sin \frac{3\theta}{2} \right] \\ \sigma_y &= \frac{K}{\sqrt{2\pi r}} \cos \frac{\theta}{2} \left[1 + \sin \frac{\theta}{2} \sin \frac{3\theta}{2} \right] \\ \sigma_{xy} &= \frac{K}{\sqrt{2\pi r}} \sin \frac{\theta}{2} \left[\cos \frac{\theta}{2} \cos \frac{3\theta}{2} \right]\end{aligned}\tag{1.3.1}$$

The stresses in the third direction are given by $\sigma_z = \sigma_{xz} = \sigma_{yz} = 0$ for the plane stress problem, and when the third directional strains are zero (plane strain problem), the out of plane stresses become $\sigma_{xz} = \sigma_{yz} = 0$ and $\sigma_z = \nu (\sigma_x + \sigma_y)$. While the geometry and loading of a component may change, as long as the crack opens in a direction normal to the crack path, the crack tip stresses are found to be as given by Equations 1.3.1. Thus, the Equations 1.3.1 only represent the crack tip stress field for the Mode I crack extension described by Figure 1.3.2.

Three variables appear in the stress field equation: the crack tip polar coordinates r and θ and the parameter K . The functions of the

* Superscript numbers in parentheses refer to literature cited in the List of References for Chapter 1.

coordinates determine how the stresses vary with distance from the right hand crack tip (point B) and with angular displacement from the x-axis. As the stress element is moved closer to the crack tip, the stresses are seen to become infinite. Mathematically speaking, the stresses are said to have a square root singularity in r . Because most cracks have the same geometrical shape at their tip, the square root singularity in r is a general feature of most crack problem solutions.

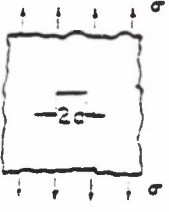
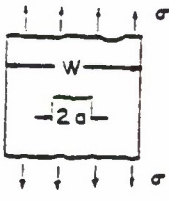
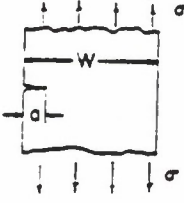
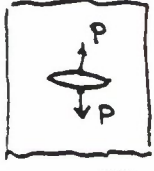
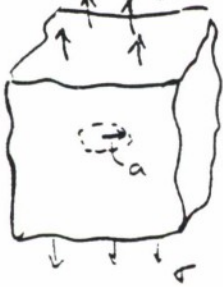
The parameter K , which occurs in all three stresses, is called the stress intensity factor because its magnitude determines the intensity or magnitude of the stresses in the crack tip region. The influence of external variables, i.e. magnitude and method of loading and the geometry of the cracked body, is sensed in the crack tip region only through the stress intensity factor. Because the dependence of the stresses (Equation 1.3.1) on the coordinate variables remain the same for different types of cracks and shaped bodies, the stress intensity factor is a single parameter characterization of the crack tip stress field.

Table 1.3.1 provides several stress intensity factors for some geometries of basic interest. As seen from the equations, the stress intensity factors for each of the geometries can be described using the general form:

$$K = \sigma \beta \sqrt{\pi a} \quad (1.3.2)$$

where the factor β is used to relate gross geometrical features to the

TABLE 1.3.1
STRESS INTENSITY FACTORS FOR BASIC CRACK GEOMETRIES

GEOMETRY	DESCRIPTION	STRESS INTENSITY FACTOR (K)	STRESS INTENSITY FACTOR COEFFICIENT (K/ σ)
	Infinite Plate, Center Cracked, Remote Loading.	$\sigma\sqrt{\pi a}$	$\sqrt{\pi a}$
	Finite Width, Center Cracked, Remote Loading.	$\sigma\left[\pi a \sec \frac{\pi a}{W}\right]^{1/2}$	$\sqrt{\pi a \sec \frac{\pi a}{W}}$
	Edge Crack, Remote Loading	$1.1\sigma\sqrt{\pi a}$ $a \ll W$	$1.1\sqrt{\pi a}$
	Finite Width, Center Cracked Wedge Loading	$\frac{P/B}{\sqrt{\pi a}} \cdot \sqrt{\frac{1}{\frac{W}{2\pi a} \sin \frac{2\pi a}{W}}}$	$\sqrt{\pi a} \cdot \left[\frac{2W}{\pi a} \cdot \frac{1}{\sin \frac{2\pi a}{W}} \right]^{1/2}$
	Imbedded Penny Shaped Crack of Radius "a"	$\sigma\left(\frac{2}{\pi}\right)\sqrt{\pi a}$	$\sqrt{\pi a} \cdot \left(\frac{2}{\pi}\right)$

stress intensity factors. Note that β can be a function of crack length (a) as well as of other geometrical features.

It is seen from Equation 1.3.1 that the intensity of the stress field and hence the stresses in the crack tip region are linearly proportional to the remotely applied stress and proportional to the square root of the half crack length.

A structural analyst should be able to determine either analytically, numerically, or experimentally the stress-intensity factor relationship for almost any conceivable cracked body geometry and loading. The analysis for stress-intensity factors, however, is not always straightforward and information for determining this important structural property will be presented subsequently in Section 1.6. A mini-handbook of stress-intensity factors is provided in Section 1.7 and some methods for approximating stress-intensity factors are presented in Section 1.8.

1.3.3 Application to Fracture

Can the magnitude or intensity of this crack tip pattern be used to characterize the material instability at fracture? The formulation of such a hypothesis for measuring a material's resistance to fracture was developed by G. R. Irwin and his co-workers at the Naval Research Laboratories in the 1950's (1,5,6).

The hypothesis can be stated: if the level of crack tip stress intensity factor exceeds a critical value, unstable fracture will occur. The concept is analogous to the criterion of stress at a point reaching a

critical value such as the yield strength. The value of the stress-intensity factor at which unstable crack propagation occurs is called the fracture toughness and is given the symbol K_c . In equation form, the hypothesis states:

$$\text{if} \quad K = K_c \quad (1.3.3)$$

then catastrophic crack extension (fracture) occurs.

To verify the usefulness of the proposed hypothesis, consider the results of a wide plate fracture study given in Figure 1.3.3⁽⁷⁾. These data represent values of half crack length and gross section stress at fracture. The stress-intensity factor for the uniformly-loaded center-cracked finite-width panel is given by:

$$K = \sigma \left[\pi a \sec \frac{\pi a}{W} \right]^{\frac{1}{2}} \quad (1.3.4)$$

where W is the panel width. Application of Equation 1.3.4 given in Figure 1.3.3 followed by averaging the calculated fracture toughness values (except for those at the two smallest crack lengths) gives the average fracture toughness curve shown. This example illustrates that the fracture toughness concept can be used to adequately describe fractures that initiate at gross sectional stresses below 70% of the yield strength.

Note that since plastic deformation is assumed negligible in the linear elastic analysis, Equation 1.3.3 is not expected to yield an accurate

approximation where the zone of plastic deformation is large compared to the crack length and specimen dimensions. Figure 1.3.3 shows that the relationship derived on the basis of the Equation 1.3.3 hypothesis does not describe the crack growth behavior for small cracks in plastic stress fields.

1.3.4 Fracture Toughness - A Material Property

Fracture toughness (K_{IC}) is a mechanical property that measures a material's resistance to fracture. This parameter characterizes the intensity of stress field in the material local to the crack tip when rapid crack extension takes place. Similar to other microstructurally sensitive material properties, fracture toughness can vary as a function of temperature and strain rate. But, unlike the yield strength, K_{IC} will be strongly dependent on the amount of crack tip constraint due to component thickness. The reason why thickness has to be considered in fracture analysis is due to its influence on the pattern of crack tip plastic deformation. The two thickness limiting crack tip plastic deformation patterns are shown in Figure 1.3.4. For "thin" plane stress type components, a 45 degree through the thickness yielding pattern develops; while in "thicker" plane strain components of the same material the hinge-type plastic deformation pattern predominates (8). Chapters 4 and 7 discuss the effect of thickness and other factors on fracture toughness.

The linear elastic fracture mechanics approach can only be expected to characterize fracture when the region in which plastic deformation occurs is contained within the elastic crack tip stress field. When the crack tip plastic deformation is unrestricted by elastic material around the crack, the engineer must resort to using elastoplastic techniques to predict the critical crack size at fracture (see Section 1.9). Presently, it is not possible to say if these techniques will lead to the same type of single parameter characterization of fracture discussed above.

1.3.5 Crack Tip Plastic Zone Size

It is recognized that plastic deformation will occur at the crack tip as a result of the high stresses that are generated by the sharp stress concentration. To estimate the extent of this plastic deformation, Irwin equated the yield strength to the y-direction stress along the x-axis and solved for the radius. The radius value determined was the distance along the x-axis where the stress perpendicular to the crack direction would equal the yield strength; thus, Irwin found that the extent of plastic deformation was

$$r_y = \frac{1}{2\pi} \left(\frac{K}{\sigma_{ys}} \right)^2 \quad (1.3.5)$$

Subsequent investigations have shown that the stresses within the crack tip region are lower than the elastic stresses and that the size of the plastic deformation zone in advance of the crack is between r_y and $2r_y$.

Models of an elastic, perfectly plastic material have shown that the material outside the plastic zone is stressed as if the crack were centered

in the plastic zone. Figure 1.3.5 describes a schematic model of the plastic zone and the stresses ahead of the crack tip. Note that the real crack is blunted as a result of plastic deformation.

If the extent of the plastic zone as estimated by Equation 1.3.5 is small with respect to features of the structural geometry and to the physical length of the crack, linear elastic fracture mechanics analyses apply. Sometimes, the concept of contained yielding as illustrated in Figure 1.3.5 is referred to as small scale yielding. Most structural problems of interest to the aerospace community can be characterized by linear elastic fracture mechanics parameters because the extent of yielding is contained within a small region around the crack tip.

1.3.6 Application to Subcritical Crack Growth

The only quantifiable measure of subcritical damage is a crack. Cracks impair the load-carrying characteristics of a structure. As described above, a crack can be characterized for length and configuration using a structural parameter termed the stress intensity factor (K). This structural parameter was shown to interrelate the local stresses in the region of the crack with (a) crack geometry, (b) structural geometry, and (c) level of load on the structure. In a manner similar to Irwin, who utilized the stress intensity factor for fracture studies, Paris and his colleagues at Lehigh University and at the Boeing Company developed a crack mechanics approach to solve subcritical crack growth problems^(9,10,11).

The concepts that Paris and his colleagues developed were based upon a similitude hypothesis: if the crack tip stress state and its waveform are the same in a given time period for two separate geometry and loading conditions, then the crack growth rate behavior observed by the two cracks should be the same for that time period. This hypothesis is a direct extension of Equation 1.3.3 to the problem of subcritical crack growth. The equation representing the subcritical crack growth hypothesis is simply:

$$\frac{\Delta a}{\Delta t} = f(K(t))$$

or

(1.3.6)

$$\frac{\Delta a}{\Delta N} = f(K(t))$$

That is, a material's rate of crack growth is a function of the stress intensity factor. The stress intensity factor is shown to explicitly depend on time in order to indicate the influence of its waveform on the crack growth rate. The value of the hypothesis stated by Equation 1.3.6 is that the material behavior can be characterized in the laboratory and then utilized to solve structural cracking problems when the structure's loading conditions match the laboratory loading conditions. A general description of the procedure utilized will be presented in Section 1.4. Chapter 5 is devoted to a complete description of the detailed methodology available to a designer for estimating the crack growth life of a structural component using a material's crack growth rate properties.

A verification of Paris' Hypothesis was first conducted using fatigue crack growth data generated under constant amplitude type repeated loading. The parameters that pertain to constant amplitude type loading are presented in Figure 1.3.6. Figure 1.3.6a describes a repeating constant amplitude cycle with a maximum stress of σ_{\max} , a minimum stress of σ_{\min} , and a stress range of $\Delta\sigma$. The stress ratio (R) is given by the ratio of the minimum stress to the maximum stress. In describing constant amplitude stress histories, it is only necessary to define two of the above four parameters; typically $\Delta\sigma$ and R or σ_{\max} and R are used. A stress history is converted into a stress-intensity factor history by multiplying the stresses by the stress-intensity-factor coefficient (K/σ). As can be noted from the figure, the coefficient is evaluated at the current crack length a_i and the stress-intensity-factor history is shown to be a repeating cyclic history in Figure 1.3.6b. The terms K_{\max} , K_{\min} and ΔK define the maximum, the minimum and range of stress-intensity factor, respectively. Strictly speaking, the stress-intensity factor history given in Figure 1.3.6b should not be shown constant but reflective of the changes in the stress-intensity-factor coefficient as the crack grows. For small changes in crack length, however, the stress-intensity factor coefficient does not change much, so the portrayal in Figure 1.3.6b is reasonably accurate for the number of cycles shown.

The fatigue crack growth rate behaviors exhibited by a plate structure subjected to two extreme loading conditions (but at the same nominal stress level) are compared in Figure 1.3.7 ^(10,12). These loading

conditions are referred to as wedge loading and remote loading. In the remote loaded structure, the rate of crack length change accelerates as the crack grows (also see Figure 1.2.1). An opposite growth rate behavior is exhibited by the wedge loaded structure. These two extreme loading conditions provide a good test for the application of the fracture mechanics approach to the study of fatigue crack growth rates. If the approach can be used to describe these opposite growth rate behaviors, then it should be generally applicable to any other type of structure or loading.

Paris, et al. ⁽⁹⁾, suggested that the appropriate stress intensity parameter for fatigue crack propagation should be the difference between the maximum and minimum stress-intensity factors in a cycle of fatigue loading. This difference in the stress-intensity factors is the stress-intensity range (ΔK) and it measures the alternating intensity of the crack tip stress field responsible for inducing reversed plastic deformation. The stress-intensity range as a function of crack length is obtained from the static stress-intensity-factor formulas where the range in stress (load) replaces the static stress (load). Section 1.4 provides a more extensive description of the calculation procedures for stress-intensity-factor parameters that are used to describe subcritical crack growth. The stress-intensity-factor expressions for the remote and wedge loaded structures (finite width) can be found in Table 1.3.1.

Approximate expressions for the small crack in a wide plate are shown in Figure 1.3.7. The reader will note that the stress-intensity factor for the remotely loaded wide plate increases with crack length while just the reverse is observed to occur for the wedge loaded wide plate.

Drawing tangents to the cyclic crack length curves given in Figure 1.3.7 provides estimates of the cyclic (fatigue) crack growth rates at various crack lengths ($\frac{da}{dN} \doteq \frac{\Delta a}{\Delta N}$). Calculation of corresponding stress-intensity ranges for these same crack lengths provides the data plotted in Figure 1.3.8 ^(10,12). Note that at the same stress-intensity range (ΔK), the same crack growth rate (da/dN) is observed, even though both the form of the stress-intensity equations and the cycle-crack length curves are very different.

The general fatigue cracking behavior pattern exhibited by most structural materials is shown in Figure 1.3.9. The shape of the curve is sigmoidal with no crack growth being observed below a given threshold level of stress-intensity range and rapid crack propagation occurring when the maximum stress-intensity-factor in the fatigue cycle approaches the fracture toughness of the material. In the subcritical growth region, numerous investigators have indicated that the rate of cyclic growth (da/dN) can be described using a power law relation

$$\frac{da}{dN} = C (\Delta K)^p \quad (1.3.7)$$

where C and p are experimentally developed constants. Fatigue crack propagation data of the type shown in Figure 1.3.9 can be conveniently

collected using the conventional specimen geometries where load is controlled and the crack length is measured optically (20x) as a function of applied cycles. The details of the methodology employed to generate such curves are covered in Chapter 7.

The application of subcritical crack growth curves to the design of a potentially cracked structure only requires that the differentiation process be reversed. In other words, given crack growth rate data of the type shown in Figure 1.3.9, the designer integrates the crack growth rate as a function of the stress-intensity factor for the structure through the crack growth interval of interest.

Other investigations have demonstrated that subcritical crack growth processes that result from variable amplitude loading, stress corrosion cracking, hydrogen embrittlement and liquid metal embrittlement can in general be described using Equation 1.3.6. The subcritical cracking of structural materials has been successfully modeled with fracture mechanics tools primarily because the plastic deformation processes accompanying cracking are localized and thereby controlled by the surrounding stress field. As suspected, the magnitude in the elastic crack tip stress field is found to correlate well with the rate of subcritical crack advance.

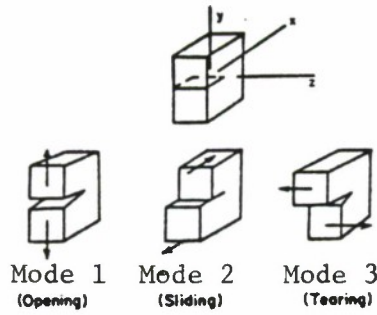


Figure 1.3.1 The Three Modes of Crack Extension.

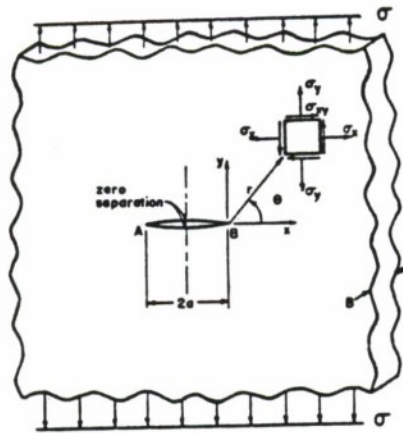


Figure 1.3.2 Infinite Plate with a Flaw That Extends Through Thickness.

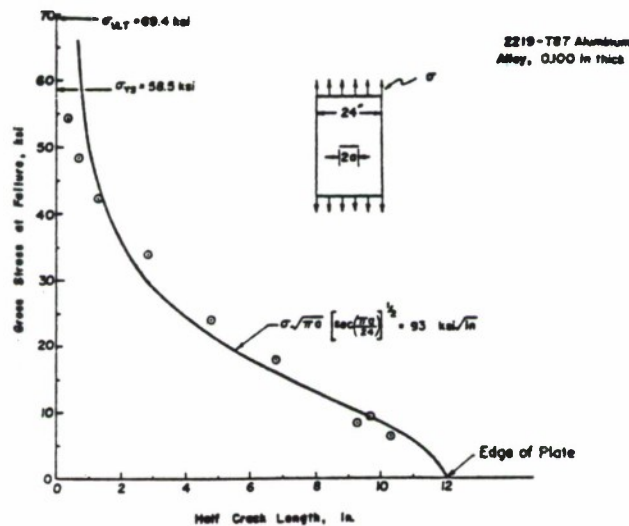


Figure 1.3.3 Results of a Wide Plate Fracture Study Compared with a Fracture Toughness Curve Calculated Using the Finite Width Plate Stress Intensity Factor Equation, Equation 1.3.4 Data from Reference 7.

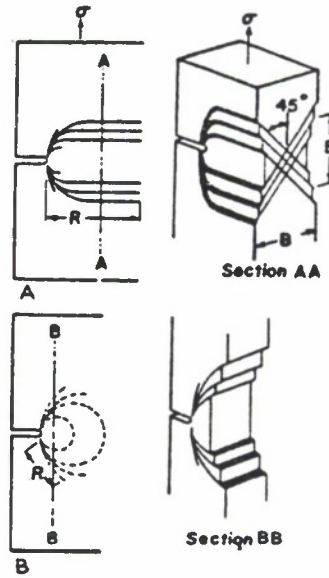


Figure 1.3.4 Yield Zones Observed on the Surface and Cross Section of a Cracked Sheet Under Uniaxial Tensile Loading in: A-Plane Stress, 45 degree Shear Type; B-Plane Strain, Hinge Type⁽⁸⁾.

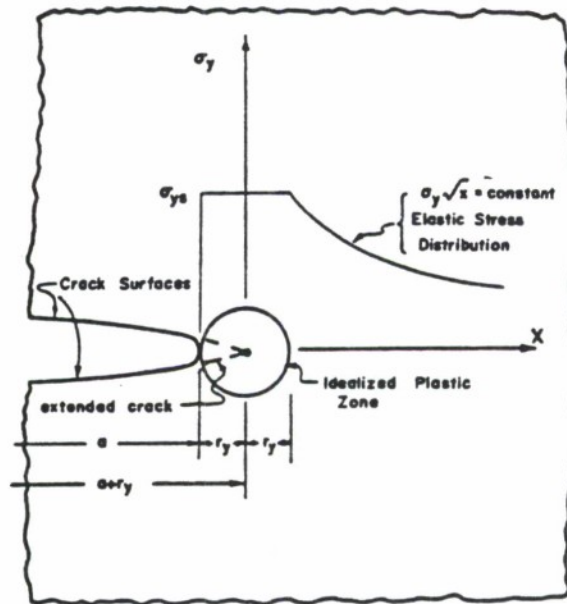
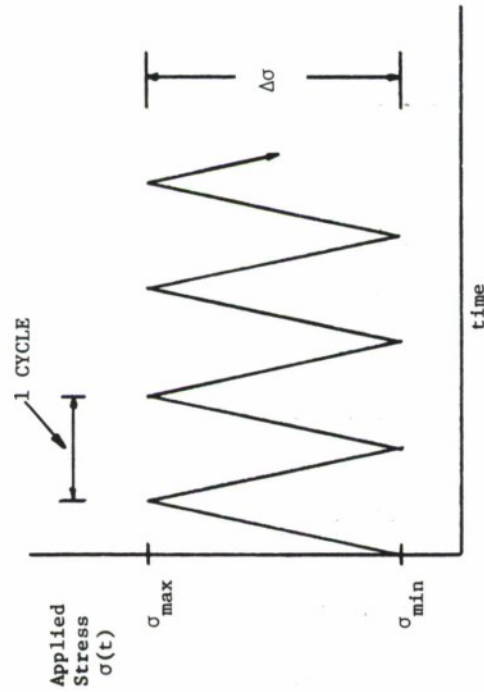


Figure 1.3.5 Small-Scale Yield Model for Restricted Crack Tip Plastic Deformation.

$$R = \frac{\sigma_{\min}}{\sigma_{\max}}$$

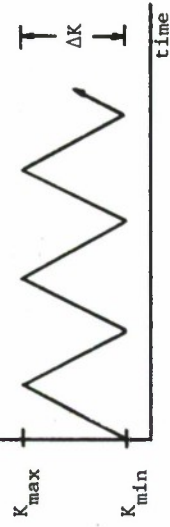


1.3.6a The Constant Amplitude Stress Cycle

crack length
is approximately
constant.

STRESS
INTENSITY
FACTOR
 $K(t)$

$$\times \frac{K}{\sigma} \bigg|_{a=a_f} =$$



1.3.6b The Corresponding Constant Amplitude Stress Intensity Factor Cycle

Figure 1.3.6. Parameters that Define Constant Amplitude Load Histories for Fatigue Crack Growth. The Figure also Illustrates the Transformation between Stress History Loading and Stress-Intensity-Factor Loading at One Crack Length Position.

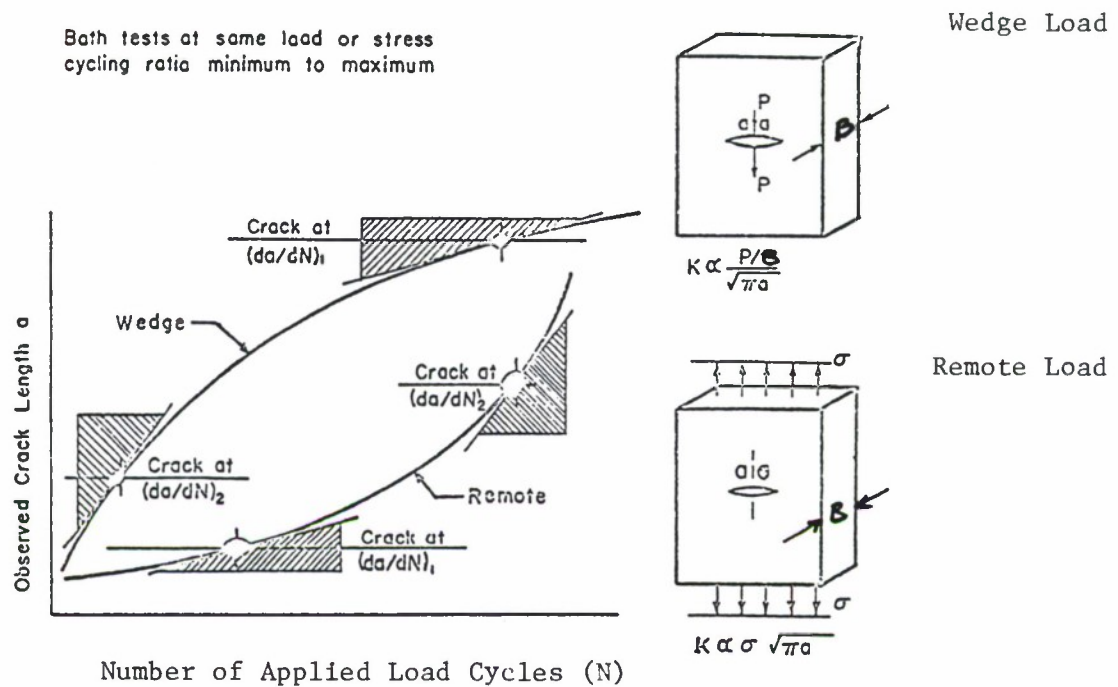


Figure 1.3.7 Description of Crack Growth Behavior Observed for Two Very Much Different Structural Geometries.

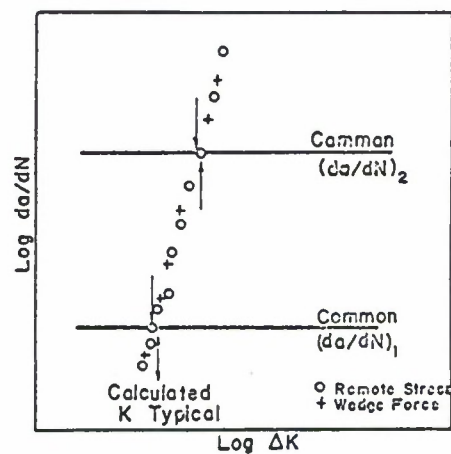


Figure 1.3.8 Comparison of Crack Growth Rate Results for the Two Structural Geometries. The Coincidence of the Data Shows that the Hypothesis (Equation 1.3.6) is Correct.

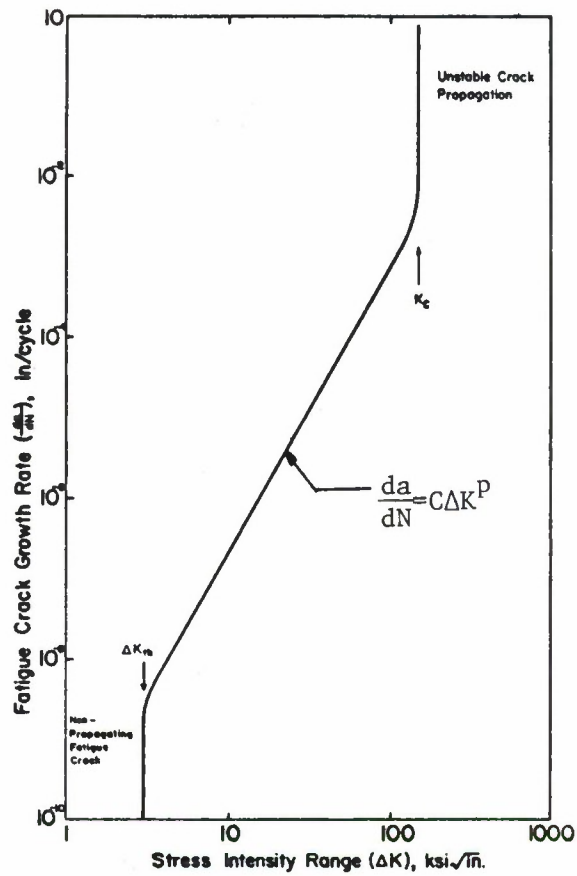


Figure 1.3.9 Schematic Illustration of the Fatigue Crack Growth Rate as a Function of Stress Intensity Range.

1.4 LIFE PREDICTION METHODOLOGY

1.4.1 Crack Growth Damage Integration Package - Summary

Currently, within the Air Force, airframe life predictions are based on a crack growth damage integration package that uses a data base and analysis to interrelate the following six elements:

- a) The initial flaw distribution which accounts for size variations and location of cracks in a given structure;
- b) aircraft usage describing the load spectra data base;
- c) constant amplitude crack growth rate material properties accounting for stress ratio and environmental effects;
- d) crack tip stress intensity factor analyses which account for crack size, shape, and structural interactions;
- e) damage integrator model which assigns a level of crack growth for each applied stress application and accounts for load history interactions; and
- f) the fracture or life limiting criterion which establishes the end point of the life calculation.

Prior to describing each of the above itemized elements in separate subsections, the damage integrating equation will be introduced to show how the various elements interact. As expressed in a numerical form, the damage integrating equation is

$$a_{cr} = a_o + \sum_{j=1}^{t_f} \Delta a_j \quad (1.4.1)$$

where Δa_j is the growth increment associated with the j^{th} time increment. The purpose of Equation 1.4.1 is to determine the life t_f . The various elements affect the quantities in Equation 1.4.1 in the following manner:

1. a_{cr} is determined interrelating elements b, d, and f.
2. a_o is determined using element a.
3. Δa_j is determined by interrelating elements a, b, c, d, and e.

1.4.2 Initial Flaw Distribution

A measure of initial quality in a component of service hardware is given by the distribution of initial crack sizes as illustrated in Figure 1.4.1. For predictions of safety limits, the initial cracks larger than the nondestructive inspection (NDI) detectability limit are of principal concern. Current specifications detail NDI limits and require verification/certification of contractor capability to detect cracks smaller than the specified NDI limits. Normally, such certification is demonstrated with curves of the type shown in Figure 1.4.2. The program of certification for a contractor's quality control inspector/inspection techniques allows the USAF to assess the probability and confidence limits associated with detecting a given crack. Chapter 3 will present a state-of-the-art summary of the technology and equipment that supports the establishment of initial flaws via nondestructive tools.

Recent results generated by the F-4 Independent Review Team (IRT) provided a method of characterizing the initial flaw population (apparent initial quality) based on full-scale fatigue test-induced cracking behavior⁽¹³⁾. Given the measurable flaw distribution in a structure at some time subsequent to test startup, the initial flaw population can be backtracked by analysis. The "back" extrapolation of the flaw population is conducted using the damage integration package. The process is schematically illustrated in Figure 1.4.3. Subsequently, the initial flaw distribution established as illustrated in Figure 1.4.3 can be used to estimate influence of load factors, mission profiles, and usage changes on the life of service hardware. The F-4 IRT study also provided an evaluation of statistical methods for describing the large crack length extremes for initial flaw distributions established in this manner. The resulting distribution of F-4 initial cracks is shown in Figure 1.4.4^(13,14).

1.4.3 Usage

The sum of the load levels that a structure is expected to experience is determined by a projection of the amount of usage expected over the life in the various possible missions; e.g., hours in training, air-to-air combat, reconnaissance, weapons delivery, etc. The mission mix includes the relative amounts of time spent in each mission. The most basic information needed is the load factor exceedances at the center of gravity (CG) of the aircraft. This information is illustrated

in Figure 1.4.5. For new designs, this data is derived from actual measured exceedances from operational aircraft flying similar missions. The USAF specifications contain such data. The new Air Force Guidelines Handbook for developing Load/Environmental Design Spectra summarizes the techniques that are currently being utilized to develop the loading and environmental spectra based on these data for various types of structures.

The specific sequence of loads applied to the structure is necessary to the crack growth damage accumulation analysis. Current practice is to simulate the overall life on a flight-by-flight basis. Each flight in the design, analysis, or test load spectrum consists of a series of cycles that combine the deterministic and probabilistic events describing the type of mission. The deterministic events include takeoff and landing and certain basic maneuver loads during each flight. Probabilistic events such as gusts or rough field taxiing occur periodically. Although it is possible to estimate the number of times these events occur, their position in the load sequences is determined in a probabilistic manner.

In developing the load spectrum for crack growth damage analysis, it is necessary to determine the stress history for each critical area on the airframe. This is accomplished by determining the relationship between the load history derived above and the stress response. Figure 1.4.6 schematically illustrates the load factor to stress history transformation.

Differences in crack growth resulting from mission mix can be significant. A fighter aircraft that is used primarily for air-combat or air-combat training typically accumulates more damage than one that is used for the same number of hours on a reconnaissance-type mission.

1.4.4 Material Properties

The material properties enter the damage integration package in the form of constant amplitude crack growth rate data. Crack growth data are generated in the laboratory under constant cyclic loading on simple specimens with accepted characterizing stress intensity factors. Crack growth rate data are developed and correlated on the basis of growth rate (da/dN) as a function of stress intensity factor range, ΔK , ($\Delta K = K_{\max} - K_{\min}$), as defined in Figure 1.4.7. The ASTM defines $K_{\min} = 0$ and thus $\Delta K = K_{\max}$ whenever $R < 0$ ($R = \sigma_{\min}/\sigma_{\max}$), see Section 5.1 for additional discussion.

For a given ΔK , the crack growth rate increases with increasing stress ratio, R for $R > 0$. Hence, the constant amplitude crack growth rate properties for a given material or alloy consist of a family of curves as illustrated in Figure 1.4.8. The crack mechanics approach described in Section 1.3 considers that for a given ΔK , R combination, there is a da/dN that is independent of geometry. Thus, the damage integration package has available a growth rate for each ΔK determined for the given crack configuration and loading.

When necessary, thermal or chemical environment and time (frequency of loading) effects are also included in the crack growth rate data generated for use with the damage integration package.

Chapter 7 presents a summary of the currently available procedures and techniques which are used to establish crack growth rate data.

1.4.5

1.4.5 Crack Tip Stress Intensity Factor Analysis

The crack tip stress intensity factor (K) interrelates the crack geometry, the structural geometry, and the load on the structure with the local stresses in the region of the crack tip. The stress intensity factor takes the form

$$K = \beta \sigma \sqrt{\pi a} \quad (1.4.2)$$

where

- β = geometric term for structural configuration, can be
a function of crack length
- σ = stress applied to the structure
- a = crack length

It can be seen that any number of combinations of the parameters β , a , and σ can give rise to the same K. The crack growth analysis rests on the experimentally verified proposition that a given K gives rise to a certain crack growth rate, regardless of the way in which the parameters were combined to generate that K.

A considerable body of data exists which defines experimental and mathematical solutions for stress intensity factors for various structural configurations. A review of the procedures for obtaining stress intensity factors is covered by Section 1.6 and the K solutions for a number of practical structural geometries are presented in Section 1.7.

1.4.6

Since stress enters Equation 1.4.2 in a linear sense it is appropriate to express the geometrical part of the stress intensity factor by using the stress intensity factor coefficient, K/σ . Figure 1.4.9 illustrates two typical solutions expressed in this manner. For a through-the-thickness crack in a plate of infinite extent, the value of β is unity and K becomes

$$K = \sigma \sqrt{\pi a} \quad (1.4.2a)$$

Equation 1.4.2a provides one way of normalizing more complex K solutions in terms of the infinite plate solution. Figure 1.4.10 depicts a typical solution of this type.

Through-the-thickness cracks are handled quite well analytically. However, for corner cracks and semielliptical part-through cracks, such as illustrated in Figure 1.4.11, K varies from point to point around the crack perimeter. This variation allows the crack shape to change as it grows, which leads to a very complex three-dimensional problem. In the last five years, the determination of β and K/σ for these complex cases have received a substantial amount of attention (see Section 1.7).

1.4.6 Damage Integration Models

Rewriting Equation 1.4.1 such that the integration is conducted between the initial crack length (a_0) and any intermediate crack length (a_K) between a_0 and the critical crack length results in

$$a_K = a_o + \sum_{j=1}^t \Delta a_j \quad (1.4.3)$$

where t (N) is the elapsed time (number of load cycles) corresponding to growing the crack a_o to the intermediate crack length a_K . The next cycle of the applied stress (the $N + 1$ cycle) induces a crack length growth increment Δa_{N+1} . The damage integration model provides the analysis capability to determine this crack length growth increment. The growth increment Δa_{N+1} is equated to the constant amplitude crack growth rate, which in turn is determined from a function of stress intensity factor range (ΔK) and stress ratio (R), i.e.,

$$\Delta a_{N+1} = \left. \frac{da}{dN} \right|_{N+1} = f(\Delta K_{N+1}, R_{N+1}) \quad (1.4.4)$$

The stress intensity factor range and stress ratio in Equation 1.4.4 are determined by using the maximum and minimum stresses in the $N+1$ cycle of the given stress history and evaluating the stress intensity factor coefficients associated with the given structural geometry at the crack length a_K . Subsequent to the direct calculation of the two crack tip parameters ΔK and R , and prior to their insertion in Equation 1.4.4 ΔK and R are modified to account for the effect of prior load history using retardation models. Retardation models account for high-to-low load interaction effects, i.e., the phenomena whereby the growth of a crack is slowed by application of a high load in the spectrum. Failure to account for high-to-low load interaction via a retardation model leads

to conservative (~ 2 to 5 times shorter) life. There are numerous functional forms of Equation 1.4.4 and numerous models describing retardation. Figure 1.4.12 and the following list describe the general scheme of the crack growth calculation.

Step 1 - Knowing crack length a_K , determines the stress intensity factor coefficient, K/σ .

Step 2 - For the given stress cycle, $\Delta\sigma$, and the coefficient K/σ , determine the stress intensity factor cycle, ΔK , and stress ratio R .

Step 3 - Utilizing the retardation model, modify the stress-intensity cycle ΔK and R to account for previous load history.

Step 4 - Determine the growth rate for the stress-intensity factor cycle to establish the crack growth increment.

Chapter 5 provides a current state-of-the-art summary of the procedures and techniques which are used in damage integration models.

1.4.7 Failure Criteria

The interrelationship between critical crack length, loading, and residual strength of a structure was first discussed in Section 1.2 using Figure 1.2.3. Based on the information presented in Section 1.3, the residual strength (σ_{res}), the load-carrying capacity of the cracked structure, can be shown to monotonically* decrease with increasing crack

* monotonic implies that the rate of change does not change sign.

length in the following manner:

$$\sigma_{\text{res}} = K_c / f(a) \quad (1.4.5)$$

where

K_c = the material resistance to fracture, termed fracture toughness,

and

$f(a) = \beta(a) \sqrt{\pi a}$, the structural property, termed the stress intensity factor coefficient

When the residual strength decays to the level of the maximum stress in the service load history, fracture of the structure occurs. The crack length associated with fracture (i.e., a_{cr}) is normally determined by solving Equation 1.4.5 for crack length, assuming that the residual strength equals the maximum stress in the stress history. The reader should note that the rate of growth of a crack is directly related to the rate of loss of residual strength through Equation 1.4.5 thus justifying the selection of the crack to quantify structural fatigue damage.

The critical crack length (a_{cr}) is thus a function of material, structural geometry, and loading. As shown in Figure 1.4.13, the relative effect of a_{cr} on life is typically small (i.e., when $a_{\text{cr}}/a_o \geq 5$). The primary advantage of designing for a large critical crack length is the increased inspectability it provides. A large critical crack length increases the probability of locating the crack before it becomes critical, thereby enhancing aircraft safety.

Determination of the critical crack size via Equation 1.4.5 would ordinarily be sufficient for safety limits; however, durability considerations often dictate that the final crack size, a_f , be chosen smaller than a_{cr} to represent rework or repair limits. A choice of a_f along these lines is shown in Figure 1.4.14.

Chapter 4 provides a summary of available residual strength estimating techniques and procedures which are generally applicable to all different types of structures and materials. Chapter 7 presents the experimental methods and procedures used to generate toughness data and residual strength data.

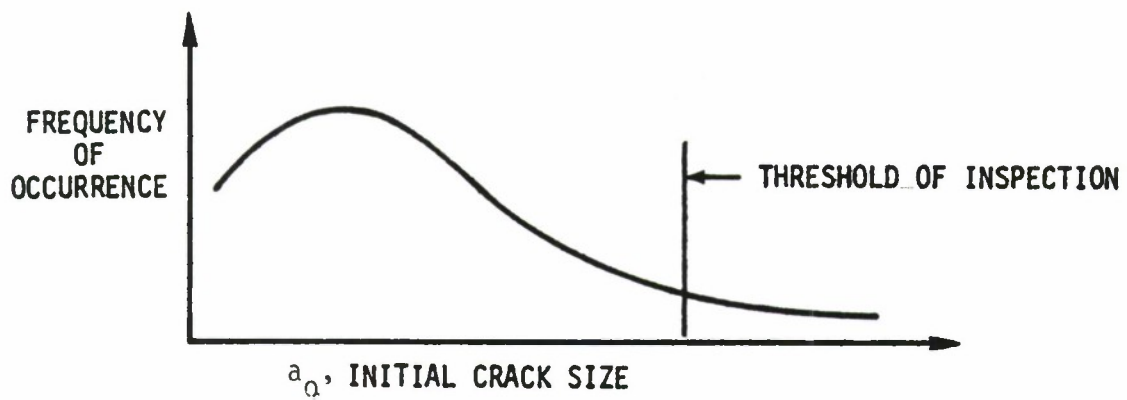


Figure 1.4.1. Distribution of Initial Crack Size for a Given Type of Crack (e.g., Radial Cracks Growing from Fastener Holes).

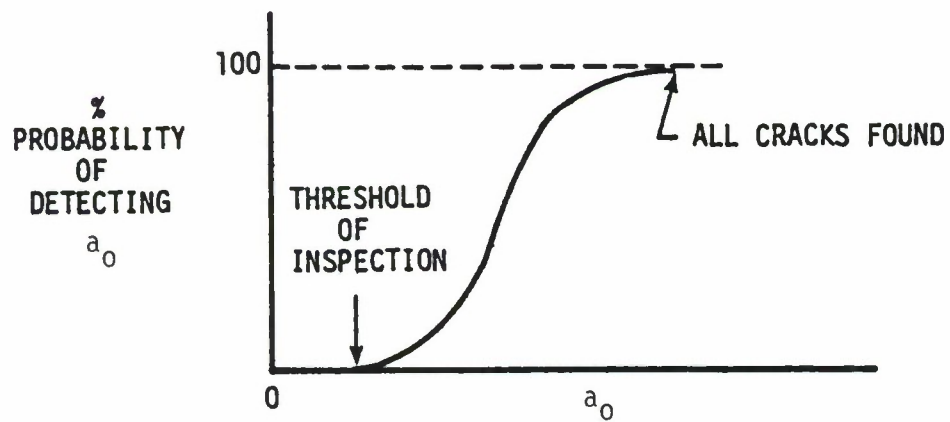
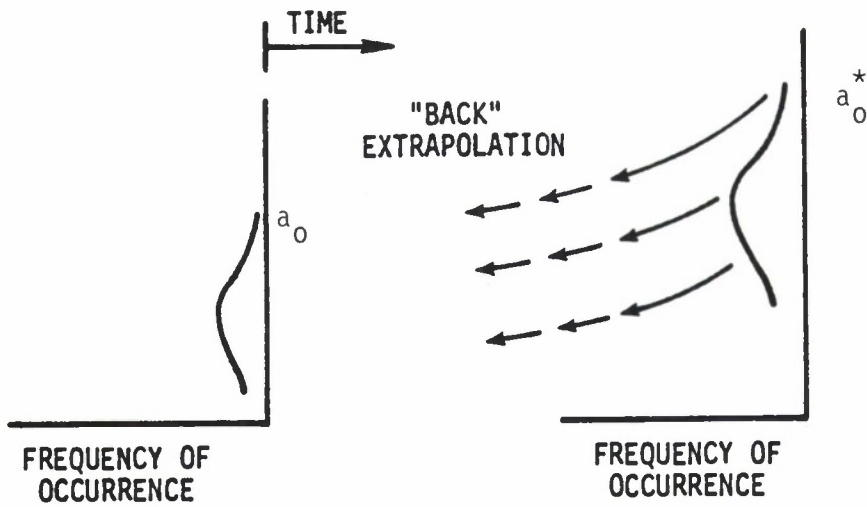


Figure 1.4.2. Certification of NDI Capability.



a) INITIAL FLAW DISTRIBUTION

b) FLAW DISTRIBUTION FOUND AFTER FATIGUE TEST

Figure 1.4.3. Determining Initial Quality by Back Calculation.

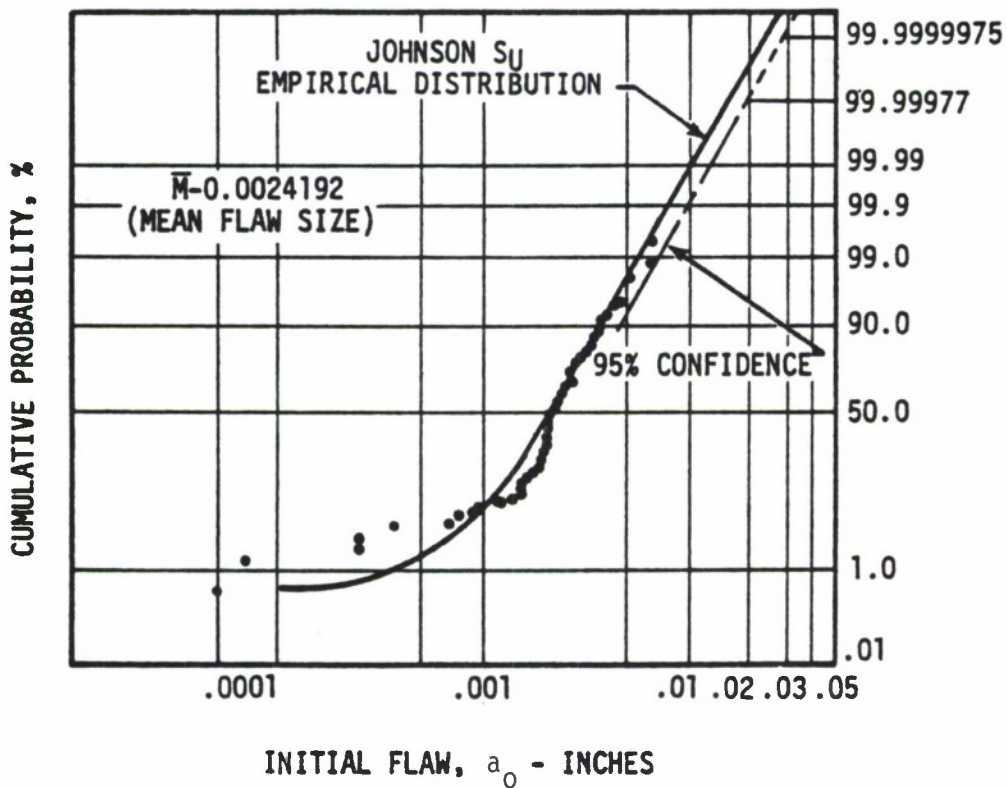


Figure 1.4.4. Initial Flaw Distribution for F-4 Based on Back Calculation.

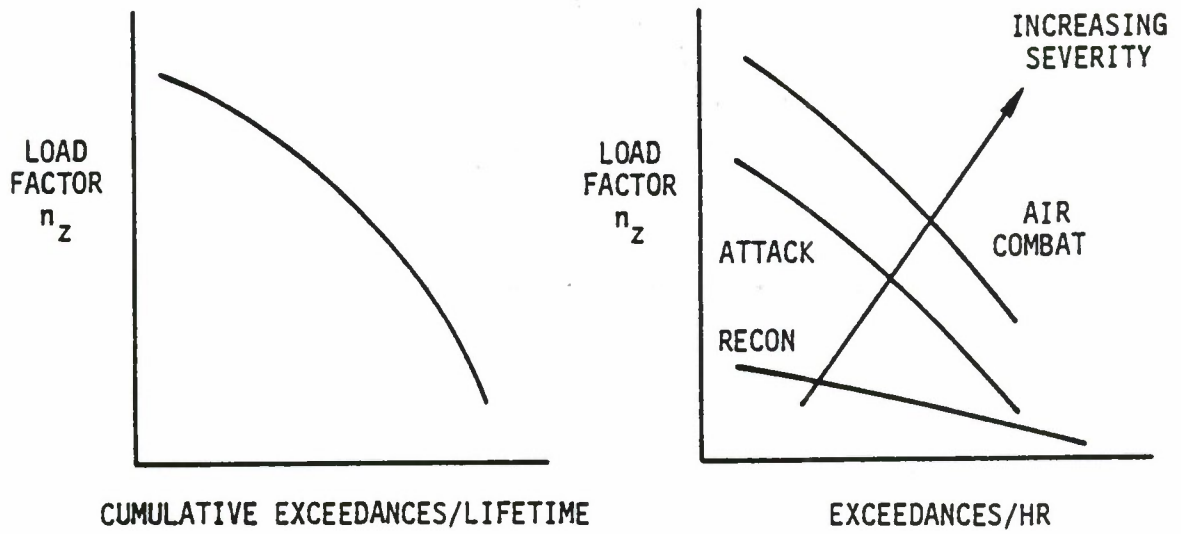


Figure 1.4.5. Typical Load Factor Exceedance Information Indicating Usage.

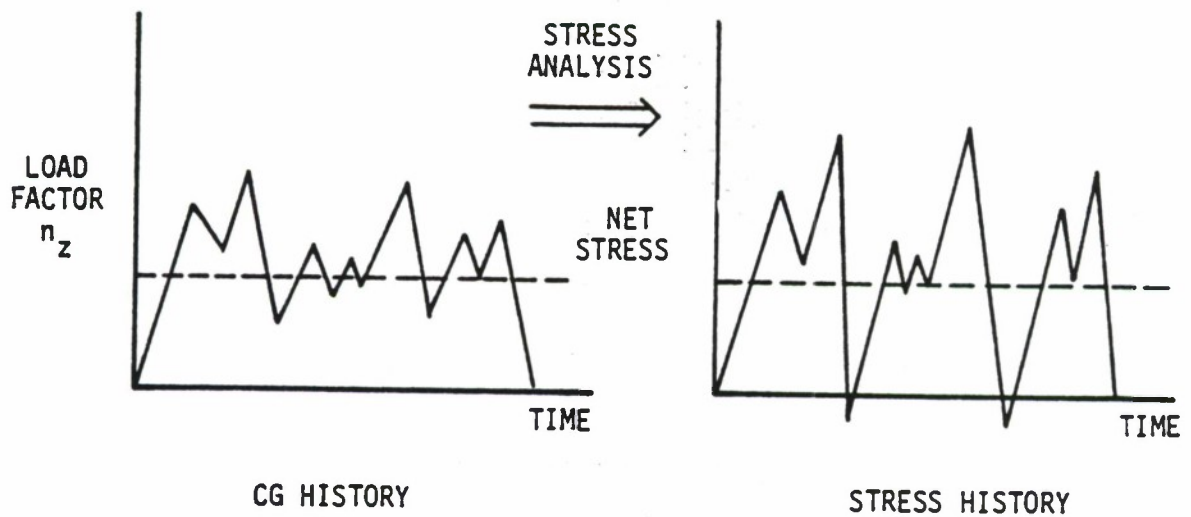


Figure 1.4.6. Load Factor to Stress History Transformation.

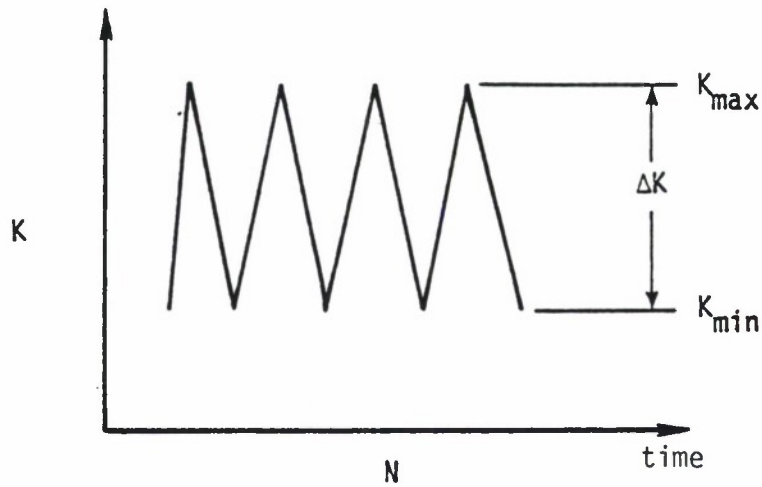


Figure 1.4.7. Stress-Intensity Factors - Cyclic Loading.

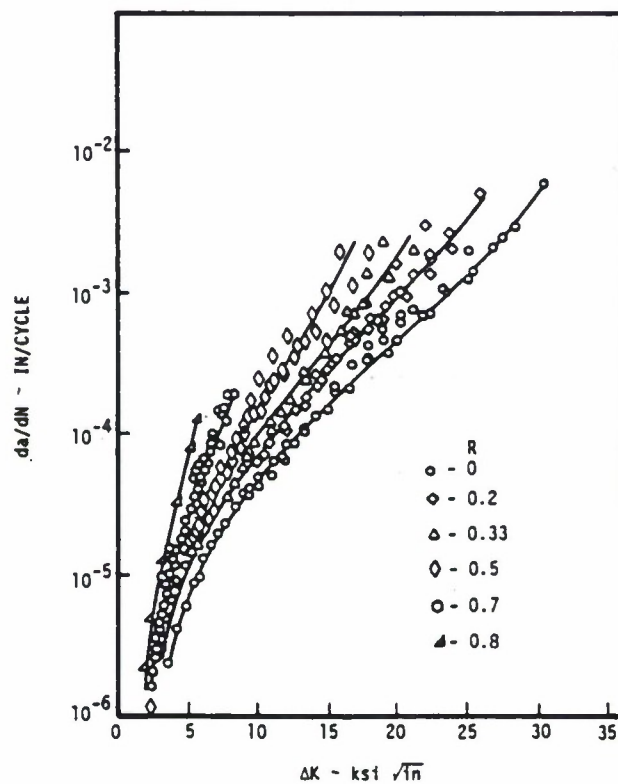


Figure 1.4.8. Constant Amplitude Crack Growth Rate Data for 7075-T6 Aluminum.

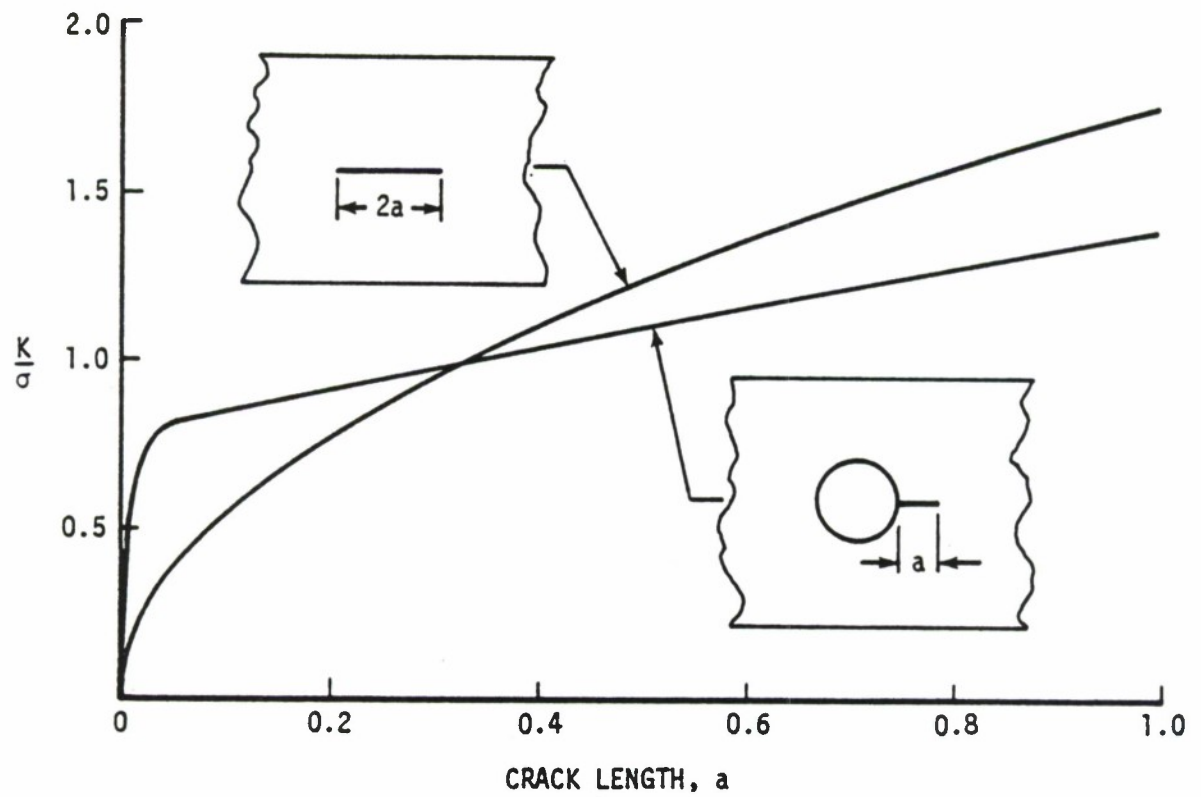


Figure 1.4.9. Stress-Intensity-Factor Coefficients Showing Influence of Hole on K .

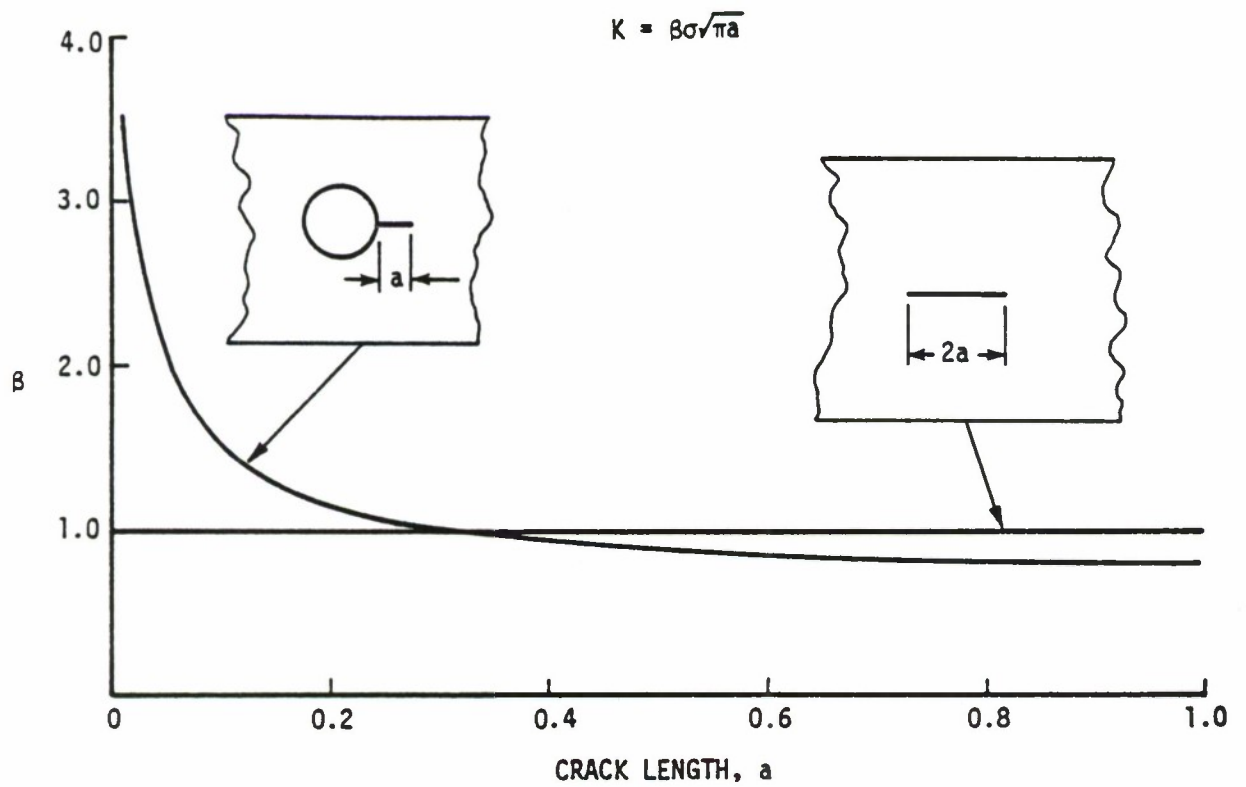


Figure 1.4.10. Influence of Hole on Geometric Correction Factor, β .

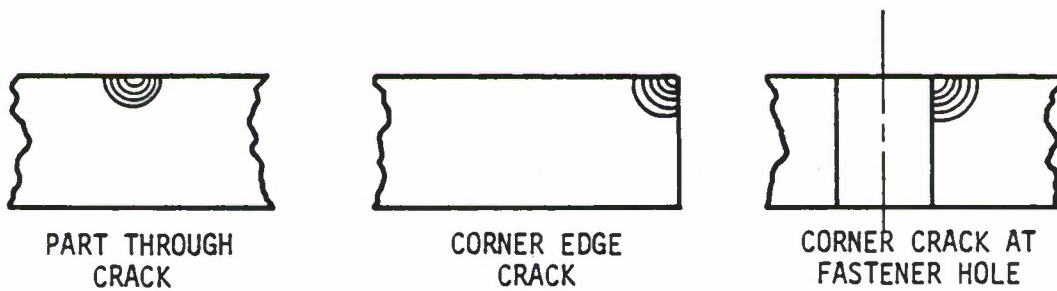
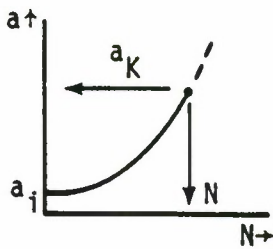
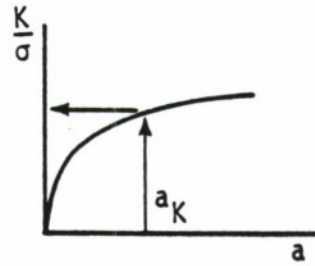


Figure 1.4.11. Complex Crack Geometries.

STEP 1



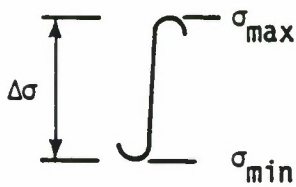
CRACK LENGTH POSITION



STRESS INTENSITY FACTOR COEFFICIENT



STEP 2

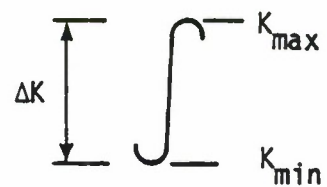


N+1 SPECTRUM
STRESS CYCLE

x

WITH $\frac{K}{\sigma} \bigg|_{a_K}$

=



and R

GIVES N+1 STRESS INTENSITY
FACTOR CYCLE

STEP 3

$$\Delta K_{N+1} = g_1 (\Delta K, \sigma(N - N_0))$$

$$R_{N+1} = g_2 (R, \sigma(N - N_0))$$

STEP 4

$$\frac{da}{dN} \bigg|_{N+1} = f(\Delta K_{N+1}, R_{N+1})$$

WHERE f MAY HAVE, FOR EXAMPLE
THE FORM

$$f(\Delta K, R) = \frac{5 \times 10^{-7} \times \Delta K^3}{68 \times (1 - R) - \Delta K}$$

Figure 1.4.12. Sequence of Steps Required to Calculate Crack Growth Increment.

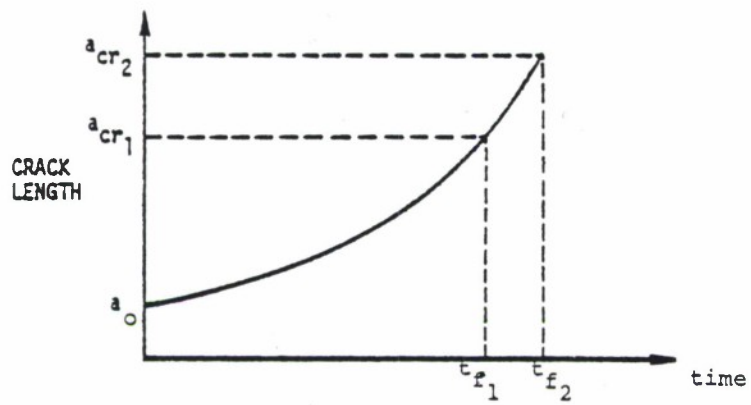


Figure 1.4.13. Effect of Critical Crack Size on Life.

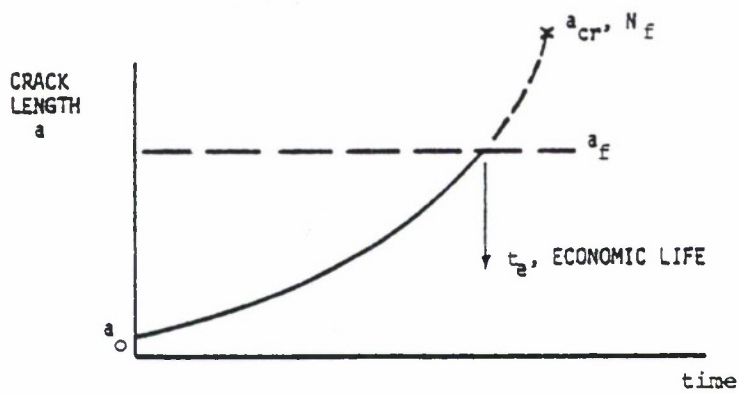


Figure 1.4.14. Economic Final Crack Size.

1.5 ACHIEVING CONFIDENCE IN THE LIFE PREDICTION METHODOLOGY

1.5.1 Summary

As discussed in Section 1.4, airframe life predictions are based on a crack growth damage package that interrelates the following six elements: (a) initial flaw distributions, (b) aircraft usage, (c) basic crack growth material properties, (d) crack/structural properties, (e) damage model, and (f) fracture or life limiting criteria.

Since life predictions for service hardware are based on the crack growth damage integration package, the confidence in a life prediction value must be based on a measure of the ability for a given package to predict measured phenomena. To support evaluation of the damage integration package, laboratory tests are conducted which simulate the basic features of cracked hardware. Predictions are then compared to measured crack growth behavior. The confidence normally associated with life predictions using a damage integration package is derived from the ability of the package to predict the laboratory generated crack growth behavior.

Verification of the package is normally conducted in steps progressing from predictions of laboratory-generated fatigue crack growth data (for which all test conditions are reasonably well characterized and documented) to predictions of service-experienced cracking behavior.

Verifying the package in steps allows for immediate deletion of

inaccurate or erroneous assumptions made in developing or improving a given element of the package. Since the package will be used to make life predictions where unknowns (e.g., spectra, structural load interactions) prevail, it is essential that confidence be established for each level of prediction capability that has been achieved.

A change of any fundamental element within the package (e.g., retardation model) generally requires a resubstantiation of this confidence for the revised package. An extension of capability, i.e., more complex geometry, would require only a substantiation for that level of complexity. This approach must be taken because of the substantiated influence of each of the variables associated with the individual elements.

Only when cracking is evident from service inspections can there be the necessary information to verify that the damage integration package is performing satisfactorily. The difficulty of assessing the confidence level associated with the life prediction derived from the damage integration package results from extrapolating the use of the package from a simple data base to the more complex service hardware case.

1.5.2 Methods for Comparing Predictability

Figures 1.5.1 through 1.5.3 are provided as examples to show how elements within a package are verified. All figures show the correlation between predicted and measured life. Figure 1.5.1 provides an evaluation of a new retardation model in which the data base was a

measure of the cyclic delay subsequent to an overload. Figure 1.5.2 compares the predictions developed with the AFWAL-Willenborg-retardation model (damage integration package to laboratory test data) which show the influences of spectra and crack geometry changes. Figure 1.5.3 shows the evaluation of a AFWAL modified damage integration package which accounts specifically for C-5A spectra changes on life observed when the crack geometry is a radial corner crack growing from an open or plugged hole.

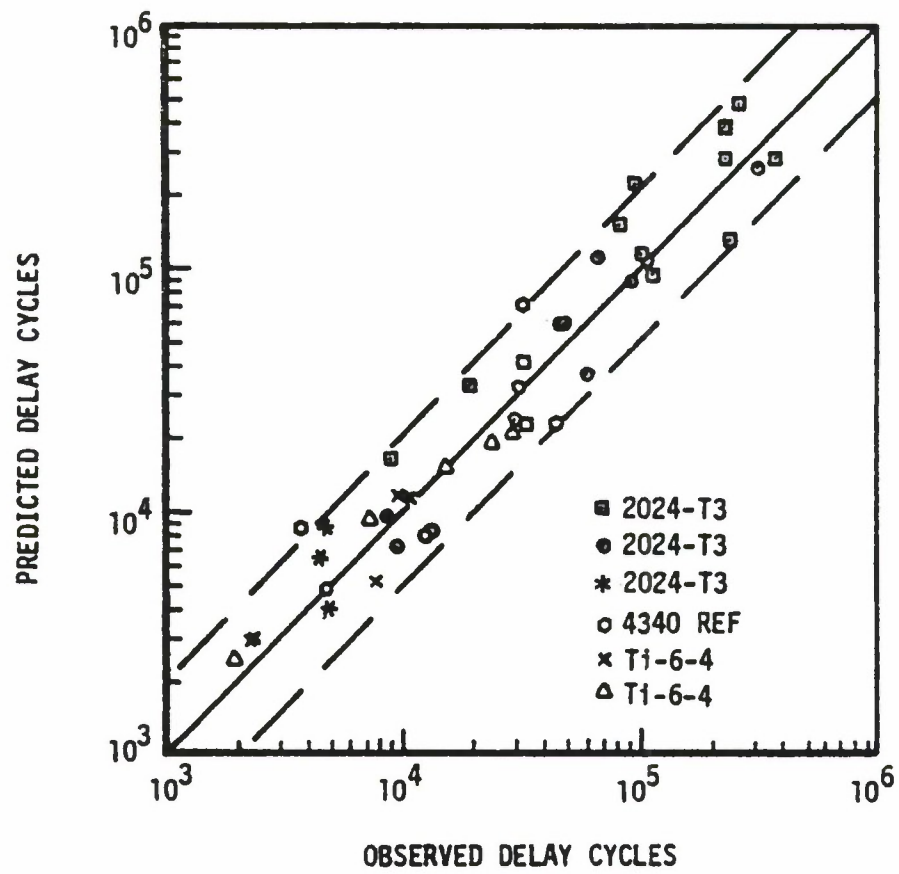


Figure 1.5.1. Single Overload Correlation with Modified Wheeler Retardation Model.

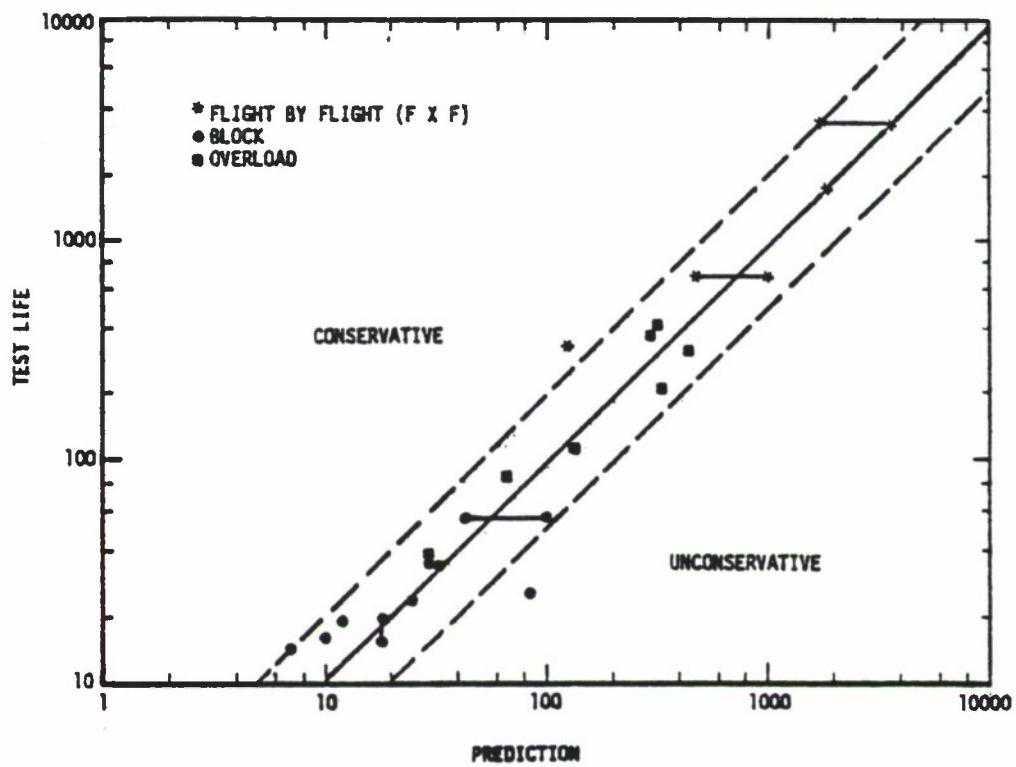


Figure 1.5.2. Spectrum Correlation Using the AFWAL Willenborg-Retardation-Model (Damage Integration Package).

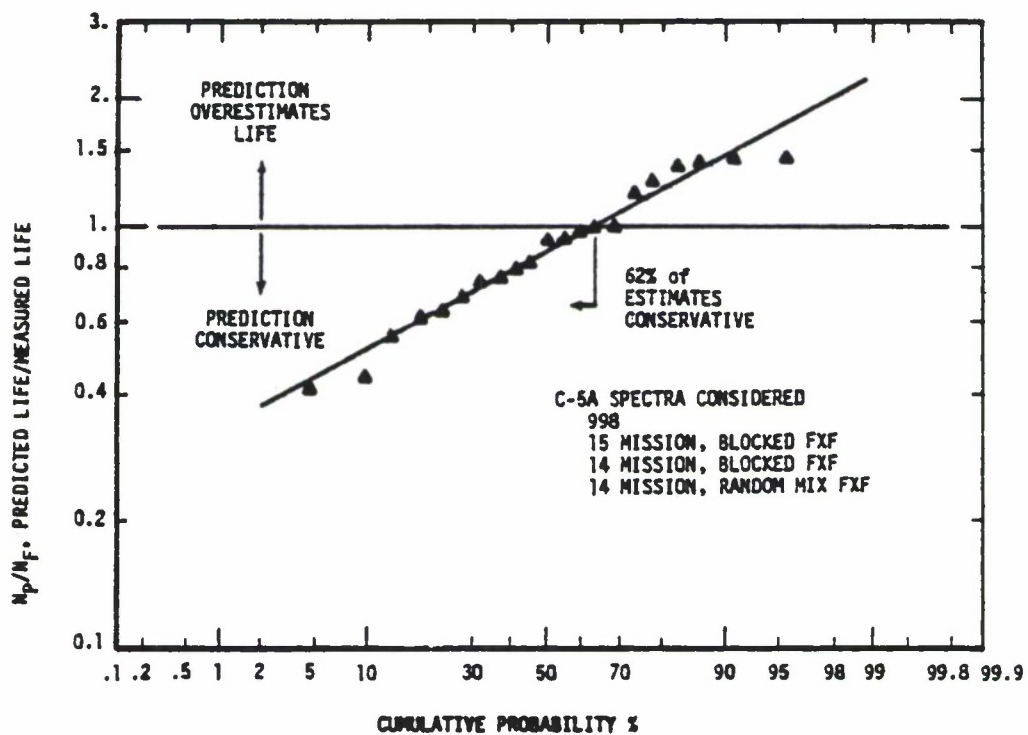


Figure 1.5.3. Prediction Capability of Damage Integration Package (Based on 21 Laboratory Tests Conducted at AFWAL/FIB).

1.6 SCHEMES FOR DETERMINING STRESS INTENSITY FACTORS

1.6.1 General

The linear elastic fracture mechanics approach to the analysis of cracked structures depends on the calculation of stress-intensity factors (K) for the typical crack geometries of interest. Various solutions have been compiled in reference works and handbooks, see for example references 15, 16, 17, and 18. Section 1.7 also contains a summary of frequently used stress-intensity factor solutions.

The handbook solutions, which are typically fundamental, may be extended to more complex cases through the principle of superposition or by compound analysis. The handbook solutions are also quite useful for bounding exact solutions as discussed in Section 1.8. When the structural geometry and loading system is fairly complicated, engineers normally resort to numerical analysis procedures (e.g., finite element analysis) which have been proven for their accuracy in establishing stress-intensity factors.

The stress-intensity factor can always be expressed as

$$K_I = \beta \sigma \sqrt{\pi a} \quad (1.6.1)$$

where σ is the nominal stress remote from the crack and a is the crack size. The factor β is a function of crack geometry and of structural geometry. Since the dimension of K is ksi $\sqrt{\text{in.}}$ or equivalent, β must be dimensionless. For a central crack of length, $2a$, in an infinite sheet, the stress-intensity factor may be written

$$K_I = \sigma \sqrt{\pi a} \quad (1.6.2)$$

Comparison with Equation 1.6.1 shows that for an infinite sheet β is unity. Thus, β may be considered as a correction factor relating the actual stress-intensity factor to the central crack in an infinite sheet. The correction factors for various geometrical conditions under a given load condition may be combined in the form of a product to account for the increase or decrease in the stress-intensity factor. In some cases (e.g., wedge/fastener loading), Equation 1.6.1 is not a convenient form for the stress-intensity factor. These cases will be discussed on an individual basis as they arise.

1.6.1.1 Principle of Superposition

Because the linear elastic fracture mechanics approach is based on elasticity, one can determine the effects of more than one type of loading on the crack tip stress field by linearly adding the stress-intensity factor due to each type of loading. The process of adding stress-intensity factor solutions for the same geometry is sometimes referred to as the principle of superposition. The only constraint on the summation process is that the stress-intensity factors must be associated with the same structural geometry (including crack geometry). Thus, stress-intensity factors associated with edge crack problems cannot be added to that of a crack growing radially from a hole. An example will illustrate the conditions under which one might linearly add stress-intensity factors.

EXAMPLE 1.6.1 - Axial and Bending Loads Combined

An edge crack of length a is subjected to a combination of axial and bending loads as shown in Figure 1.6.1. The stress-intensity factor for the edge crack geometry subjected to the tensile load (P) is given by

$$K_P = \frac{P}{B \cdot W} (\sqrt{\pi a}) \cdot [1.12 - 0.23(\frac{a}{W}) + 10.6(\frac{a}{W})^2 - 21.7(\frac{a}{W})^3 + 30.4(\frac{a}{W})^4]$$

while that due to the bending moment (M) is given by

$$K_M = \frac{6(M/B)}{W^2} \sqrt{\pi a} \cdot [1.12 - 1.39(\frac{a}{W}) + 7.32(\frac{a}{W})^2 - 13.1(\frac{a}{W})^3 + 14.0(\frac{a}{W})^4]$$

The stress intensity factor resulting from the combination of tensile and bending loads is given by the sum of K_P and K_M , so that

$$K_{TOTAL} = K_P + K_M$$

As shown by Example 1.6.1, if the geometry of the structure is described, the effect of each loading condition can be separately determined and the effect of all the loading conditions can be obtained by summing the individual conditions, i.e.,

$$K_{TOTAL} = K_1 + K_2 + K_3 + \dots \quad (1.6.3)$$

This particular property is quite useful in the analysis of complex structures. Example 1.6.2 further illustrates the principle of superposition.

EXAMPLE 1.6.2 - Remote Loading and Concentrated Forces Combined (Reference 19)

Many times in a particular aircraft design a part may develop cracks at rivet holes where the skin is attached to the frame or stringer. This situation is depicted in Figure 1.6.2 and will be analyzed as a simple case in which the sheet is in uniaxial tension and the rivets above and below the crack are influential in keeping the crack closed. (Tests of panels with concentrated forces superimposed on the uniform tension loading simulate crack growth behavior.

in the presence of rivets.) The insert of Figure 1.6.2 shows the local parameters necessary for determining the stress-intensity factors.

Assuming that a crack grows from the rivet hole, the total stress-intensity factor for this geometry is obtained using the linear superposition of stress intensity factors. Closer examination of Figure 1.6.2 indicates that the loading can be decomposed as shown in Figure 1.6.3, and thus the total stress-intensity factor is the sum of the remote loading and concentrated load induced stress-intensity factors. Note: The concentrated force induced stress-intensity factor solution presented is only applicable if the concentrated forces are applied along the centerline of the sheet and at a distance greater than 3 or 4 times the hole diameter. Inasmuch as the concentrated forces are in an opposite direction to the uniform stress, and tend to close the crack, this stress-intensity is subtracted from the uniform extensional stress-intensity factor.

With knowledge of the stress-intensity solution for this geometry, it is possible to determine what effect the rivet closure forces have on the local stress field for similar problems .

Methods do exist to analyze riveted, cracked structure when boundary forces are known. These will be demonstrated later in Chapter 4.

1.6.1.2 Advanced Uses of the Principle of Superposition

In some cases, the additive property of the stress-intensity factor can be used to derive solutions for loading conditions that are not readily available. The process of deriving the stress-intensity factor for a center crack geometry, which is uniformly loaded with a pressure

(p), see Figure 1.6.4, illustrates this feature. Figure 1.6.5 describes the process whereby the remotely loaded center crack geometry is decomposed into a set of two center crack geometries which have loading conditions, that when added, result in the cancelling of the crack line loadings. The stress-intensity factor (K_1) for the plate loaded with the remote stress condition (σ) and the crack closing stresses (also equal to σ) is zero, i.e. $K_1 = 0$, because the crack is clamped closed under such conditions. Thus, the equation for addition of stress-intensity factors

$$K_{\text{TOTAL}} = K_1 + K_2 \quad (1.6.4)$$

reduces to

$$K_{\text{TOTAL}} = 0 + K_2 \quad (1.6.5)$$

so that the stress-intensity factor for a pressurized center crack with pressure (p) equal to σ is the same as that associated with remote loading, i.e.,

$$K_2 = \sigma \sqrt{\pi a} = K_{\text{TOTAL}} \quad (1.6.6)$$

Sometimes, it is difficult to visualize how one arrives at the values of the crack closing stresses. Consider the uncracked body with the uniformly applied remote loading as shown in Figure 1.6.6a. Determination of the stresses along the dotted line lead to the observation that the stresses here are equal to the remote stress (σ). To obtain a stress-free condition along the dotted line, and thus simulate a cracked structural configuration, one must apply opposing stresses of magnitude σ along the length of the dotted line as shown in Figure 1.6.6b. The stresses along the dotted

line generated by the applied remote stresses are the opening stresses (Figure 1.6.6a). The equal but opposite stresses are the crack closing stresses. The reader should note that the stresses on the dotted line that are generated by the remote loading lead to the crack opening condition; these opening stresses lead to non-zero values for the stress-intensity factor (See Figure 1.6.5).

Figure 1.6.7 presents the concept of linear superposition of elastic solutions in a slightly different way so that the reader has a full appreciation of the procedure. The structural element B is noted to be exactly the same as element A; the crack closing stresses exactly balance the effect of the remote stresses along the line so the structural element B still experiences uniform tension throughout. Structural element B is further decomposed into elements D and E. Note that the crack loading stresses shown on the structural element E are crack closing stresses and therefore result in a stress-intensity factor which is the negative of the remotely applied loading case, i.e. $K_E = -K_D$.

Since K_D is known ($=\sigma\sqrt{\pi a}$), it follows that $K_E = -\sigma\sqrt{\pi a}$. As we noted before, if the direction of stress in element E is reversed (becomes crack opening) then the stress-intensity factor is $K = \sigma\sqrt{\pi a}$.

The loading on structural element A in Figure 1.6.8 can be decomposed into the series of loadings shown. The stress-intensity factor for element A is obtained from the superposition of the three other loadings:

$$K_A = K_B + K_D - K_E \quad (1.6.7)$$

Since it is obvious that the loadings in elements A and E will result in the same stress-intensity factor, i.e. $K_A = K_E$, the stress-intensity factor for element A becomes

$$K_A = \frac{1}{2} [K_B + K_D] \quad (1.6.8)$$

The stress-intensity factors for elements B and D are known, i.e.,

$$K_B = \sigma \sqrt{\pi a} \text{ and } K_D = \left[\frac{W}{2a} \right] \sigma \sqrt{\pi a} \text{ and therefore,}$$

$$K_A = \frac{1}{2} \left[1 + \frac{W}{2a} \right] \sigma \sqrt{\pi a} \quad (1.6.9)$$

Now a more complex example is presented using the principle of superposition applied in a two-step process. Shown in Figure 1.6.9 is a structural element (F) in which intermediate values of load transfer occur through a pin loaded hole. As shown, Step 1 consists of decomposing element F into two parts, such that in one part the pin reacts its entire load and the other part is remotely loaded. The stress-intensity factor for element F is the sum of those generated by the decomposed elements, i.e.,

$K_F = K_A + K_B^{\sigma_2}$ where the superscript denotes the loading. Step 2 involves the determination of K_A . The pin reactive loading on element A is decomposed into the loading shown in Figure 1.6.9; via the logic previously illustrated in Figure 1.6.8, K_A is determined as $0.5 (K_B^{\sigma} + K_D^P)$. The stress-intensity factor for the loading on element F is

$$K_F = 0.5 (K_B^{\sigma} + K_D^P) + K_B^{\sigma_2} \quad (1.6.10)$$

Note that while the stress-intensity factor solution formula for element B is the same in Steps 1 and 2, the stresses used in each calculation are different (as indicated by the superscripts).

1.6.2 Handbook Solutions

As the linear elastic fracture mechanics approach to engineering problems became a typical design approach, a widespread need for stress-intensity factor solutions for typical geometries arose. This need was met by a series of handbooks (References 16, 17, and 18) which presented available solutions in a compact format. This subsection of the Damage Tolerant Design Handbook summarizes these current stress-intensity factor handbooks by presenting an abbreviated table of contents for each handbook. In addition, this subsection also presents a stress-intensity factor solution from each handbook using the format utilized in that handbook. By evaluating both an abbreviated table of contents and a sample solution, the reader will be able to better determine if these stress-intensity factor handbooks satisfy his individual needs.

1.6.2.1 Handbook Table of Contents

The abbreviated tables of contents for references 16, 17 and 18 are found in Tables 1.6.1, 1.6.2, and 1.6.3, respectively. Table 1.6.1 indicates that the "Sih" handbook is a two-volume handbook; but actually, this handbook is completely bound in a single three-ring notebook (approximately 2.5 inches thick). The Sih handbook is also noted to contain references at the end of each section. The basic theory

TABLE 1.6.1
ABBREVIATED TABLE OF CONTENTS FOR
HANDBOOK OF STRESS-INTENSITY FACTORS

G. C. Sih
Lehigh University
(1973)
VOLUME I

	<u>NO. OF PAGES</u>
INTRODUCTORY SECTION - CLASSICAL CONCEPTS AND STRAIN ENERGY DENSITY THEORY	34
SECTION 1 PLANE EXTENSION CRACK PROBLEMS	
1.1 INTRODUCTION ON METHODS OF ANALYSIS	42
1.2 INFINITE BOUNDARIES	65
1.2.1 Central Crack	
1.2.2 Multiple Central Cracks	
1.2.3 Hypocycloid	
1.2.4 Circular Arc Crack	
1.2.5 Collinear Cracks	
1.2.6 Parallel Cracks	
1.2.7 A Pair of Inclined Cracks	
1.2.8 Crack Emanating or Approaching Cutouts	
1.2.9 Semi-Infinite Crack	
1.2.10 Two Collinear Semi-Infinite Cracks	
1.3 SEMI-INFINITE BOUNDARIES	9
1.3.1 Edge Crack	
1.3.2 Semi-Infinite Crack	
1.4 FINITE WIDTH STRIP	22
1.5 RECTANGULAR PANEL	11
1.5.1 Edge Crack	
1.5.2 Central Crack	
1.5.3 Cracks Emanating From Cutouts	
1.6 CIRCULAR DISK	2
1.7 BEAMS	1
1.8 BI-MATERIAL PLANES (<i>Interface Type Cracks</i>)	11
1.9 REFERENCES	4
SECTION 2 ANTI-PLANE CRACK PROBLEMS	84
2.1 BASIC EQUATIONS AND SOLUTION METHODS	
2.2 INFINITE BOUNDARIES	
2.3 SEMI-INFINITE BOUNDARIES	

TABLE 1.6.1 (CONCLUDED)

		<u>NO. OF PAGES</u>
	2.4 FINITE WIDTH STRIP	
	2.5 BEAMS	
	2.6 REFERENCES	
SECTION 3	THREE-DIMENSIONAL CRACKS	70
	3.1 THREE-DIMENSIONAL STRESS DISTRIBUTION	
	3.2 INFINITE BOUNDARIES	
	3.3 BEAMS AND BARS	
	3.4 REFERENCES	
SECTION 4	THERMOELASTIC CRACK PROBLEMS	29
	4.1 THERMOELASTIC EQUATIONS	
	4.2 INFINITE BOUNDARIES	
	4.3 REFERENCES	
	VOLUME II	
SECTION 5	ANISOTROPY AND NONHOMOGENEITY	130
	5.1 THEORETICAL CONSIDERATIONS	
	5.2 POLARLY ORTHOTROPIC MATERIAL	
	5.3 TRANSVERSELY ISOTROPIC MEDIUM	
	5.4 ORTHOTROPIC MATERIAL	
	5.5 NONHOMOGENEOUS MEDIUM	
	5.6 REFERENCES	
SECTION 6	BENDING AND STRETCHING OF FLAT PLATES	73
	6.1 THEORIES OF FLAT PLATES	
	6.2 CLASSICAL THEORY (Poisson, Kirchhoff)	
	6.3 REISSNER'S PLATE THEORY	
	6.4 GOLDENWEIZER'S PLATE HISTORY	
	6.5 HARTRANFT AND SIH'S PLATE THEORY	
	6.6 STIFFENED PLATES	
	6.7 REFERENCES	
SECTION 7	CRACKS IN SHELLS	44
	7.1 SHELL THEORIES	
	7.2 CLASSICAL THEORY	
	7.3 SHEAR DEFORMATION THEORY	
	7.4 REFERENCES	
SECTION 8	DYNAMIC CRACK PROPAGATION	141
	8.1 CRACK PROBLEMS IN ELASTODYNAMICS	
	8.2 MOVING CRACKS UNDER STATIC LOADING	
	8.3 STATIONARY CRACK SUBJECTED TO ELASTIC WAVES	
	8.4 MOVING CRACK SUBJECTED TO ELASTIC WAVES	
	8.5 STATIONARY CRACK SUBJECTED TO IMPACT LOAD	
	8.6 REFERENCES	

TABLE 1.6.2

ABBREVIATED TABLE OF CONTENTS FOR
"THE STRESS ANALYSIS OF CRACKS HANDBOOK"

By
H. Tada, P. C. Paris, and G. R. Irwin
Del Research Corporation
(1973/1978)

	<u>PAGE</u>
<u>Part I - Introductory Information (Detailed)</u>	
Introduction	1.1
Crack-tip stress fields for linear elastic bodies	1.1
Slender notches and stress concentrations from stress intensity factors	1.6
Energy rate analysis of crack extension	1.10
Relationships between G and K	1.11
Superposition of G and K results	1.12
The meaning of plane stress and plane strain for fracture mechanics problems	1.13
Effects of small scale yielding on linear-elastic fracture mechanics	1.17
Introduction to stress function methods	1.19
Additivity of crack stress fields and K values	1.25
Boundary collocation method	1.27
Successive boundary stress correction method	1.28
K -estimates from finite element methods	1.30
<u>Part II - Stress Analysis Results for Common Test Specimen Configurations (Detailed)</u>	
The centrally cracked strip	2.1
The double edge notched strip	2.6
The single edge notched strip	2.10
Pure bending (of an edge notched rectangular beam)	2.13
The three point bend specimen	2.16

TABLE 1.6.2 (CONCLUDED)

	<u>PAGE</u>
The compact tension specimen	2.19
Additional results for these common specimen configurations including double cantilever beams	2.22 to 2.36
Part III - Two-Dimensional Stress Solutions for Various Configurations with Cracks	
<u>A. Cracks Along a Single Line</u>	3.1 to 11.15
<u>B. Parallel Cracks</u>	12.1 to 18.4
<u>C. Cracks and Holes (Detailed)</u>	
Infinite planes with crack(s) emanating from a hole	19.1 to 19.13
Infinite planes with a finite crack near hole(s)	20.1 to 20.5
<u>D. Curve, Angled or Branched Cracks</u>	21.1 to 21.6
<u>E. Reinforced Plates</u>	22.1 to 22.2
<u>Part IV - Three-Dimensional Cracked Configurations</u>	23.1 to 28.3
<u>Part V - Slender Rods by Energy Rate Analysis</u>	29.1 to 29.10
<u>Part VI - Strip Yield Model Solutions</u>	20.1 to 32.6
<u>Appendices (Detailed)</u>	
A. Compliance Calibration Methods	A.1 to A.13
B. A Method for Computing Certain Displacements Relevant to Crack Problems	B.1 to B.5
C. The Weight Function Method for Determining Stress- Intensity Factors	C.1 to C.20
D. Anisotropic Linear-Elastic Crack Tip Stress Fields	D.1 to D.3
J. Table of Elliptical Integrals	J.1
K. A Table of Gamma Functions	K.1 to K.3
R. References	R.1 to R.22
Additional References	R.23 to R.24
X. Corrections	X.1 to X.4

TABLE 1.6.3
ABBREVIATED TABLE OF CONTENTS FOR
"COMPENDIUM OF STRESS INTENSITY FACTORS"

By

D. P. Rooke, Royal Aircraft Establishment
D. J. Cartwright, University of Southampton
(1976)

	<u>PAGE</u>
GENERAL INTRODUCTION	1
1 Flat Sheets	7
Introduction	
1.1 Single cracks	9
1.2 Multiple cracks	10
1.3 Cracks near stress concentrations	158
2 Stiffened Sheets (Detailed)	185
Introduction	187
2.1 Continuously attached stiffeners	
2.1.1 Central crack in a finite width sheet with stiffened edges: uniaxial tensile stress	188
2.1.2 Crack symmetrical about a stiffener in a sheet: uniaxial tensile stress	191
2.1.3 Crack near a stiffener in a sheet: uniaxial tensile stress	193
2.1.4 Crack near a junction of two sheets: uniaxial tensile stress	195
2.1.5 Equally spaced collinear cracks in a periodically stiffened sheet: uniaxial tensile stress	198
2.2 Discretely attached stiffeners	
2.2.1 Crack symmetrical about a stiffener in a sheet: uniaxial tensile stress	200
2.2.2 Crack near a stiffener in a sheet: uniaxial tensile stress	203
2.2.3 Crack in a sheet with periodically spaced stiffeners: uniaxial tensile stress	205
References	216

TABLE 1.6.3 (CONCLUDED)

	<u>PAGE</u>
3 Discs, Tubes and Bars	217
Introduction	
3.1 Discs	
3.2 Tubes	
3.3 Bars	
4 Three Dimensions	267
Introduction	
4.1 Circular cracks	
4.2 Elliptical cracks	
4.3 Junctions	
5 Plates and Shells	311
Introduction	
5.1 Plates	
5.2 Shells	

associated with obtaining the solutions presented in each section is also covered in that section.

Table 1.6.2 describes the contents of the "Tada" handbook. The table shows that the Tada handbook has a substantially different organization scheme than the Sih handbook. The Tada handbook presents theory and background through its Part I and the Appendices, its references are presented at the back of the book, and generally it concentrates on summarizing solutions in Parts II through VI. This handbook is contained in a three-ring notebook (approximately 1 inch thick).

Table 1.6.3 presents the contents of the "Rooke-Cartwright" handbook. This handbook focuses on stress-intensity factor solutions in each of its five chapters. References are presented at the end of each chapter and introductory remarks are made about the approach utilized to obtain the various stress-intensity factor solutions. The Rooke-Cartwright handbook comes in a hardback book bound volume.

1.6.2.2 Typical Solution Formats

Described in Figure 1.6.10 is the "Sih" handbook presentation of the "Isida" solution for the eccentrically located crack in an uniformly loaded, infinitely long, finite width strip. The first page of the figure describes the geometry and relevant equations; the next two present the numerical values of the function $F(\delta, \lambda)$ which describes the effect of finite width and eccentricity. The $F(\delta, \lambda)$ function is normally presented in graphically formats which are difficult to read and interpolate. The "Sih" tabular presentation format shown makes it easy

for the engineer to construct stress-intensity factor solutions for cases where the crack center (f) is fixed and the crack length (a) is increasing. Figure 1.6.11 describes a stress-intensity factor found in the Tada handbook for a crack growing from an elliptical notch. The top right-hand portion of the figure presents a sketch of the geometry. As can be noted from Figure 1.6.11, all information necessary for the solution is found on one page. The equations are found at the top of the page and the numerical solutions of the functions $F(s, \frac{c}{b})$ and $f(\frac{c}{b})$ are presented graphically in the center of the page. The bottom of the page presents data on method of solution, accuracy and references. The reader should note that the function $F(s, \frac{c}{b})$ is the stress-intensity factor function β given in Equation 1.6.1.

In Figure 1.6.12, the reader will find the solution presented by the Rooke-Cartwright handbook for a crack near a stiffener in a sheet subjected to uniaxial tensile stress. The first page of the figure describes the problem, defines the original reference work, and gives an estimate of solution accuracy. Note that the second page of Figure 1.6.12 presents the solution graphically along with an inserted sketch which illustrates the geometry and loading under consideration. The ordinate of page 2 of Figure 1.6.12, i.e. (K_I/K_0) , is the stress-intensity factor function β given in Equation 1.6.1.

1.6.3 Developing Stress-Intensity Factor Solutions

There are a number of methods that are available for developing stress-intensity factor solutions to crack body problems. References 3, 4 and 15-23 provide review articles and textbook chapters that summarize these methods. The basic solutions for simple geometries can be derived by means of classical methods of elasticity which employ complex stress functions (3,4,24,25).

For finite size bodies containing cracks, the boundary conditions usually prohibit a closed form solution. In such cases, numerical solutions can be obtained using methods such as the finite element method (See Subsection 1.6.4), the boundary collocation technique (26,27), or the boundary integral method (28,29). Solutions for multiple load path geometries can sometimes be obtained from basic stress field solutions combined with displacement compatibility requirements for all the structural members involved (30). Chapter 4 describes this method and provides an example based on the displacement compatibility method.

There are also several experimental methods that have been used to obtain (or verify) the stress-intensity factor for cracked structural members. These experimental methods include: The compliance method (See Section 1.9), the photoelastic method (31,32), the fatigue crack growth (inverse) method (33,34,35), and the Interferometric method (36,37).

While a general knowledge of each stress-intensity factor solution method might be useful for attacking specific problems, detailed knowledge is required before any method can be applied to solve a given problem. Beyond what is described elsewhere in these guidelines, an engineer can also utilize two separate solution techniques to solve any two-dimensional structural geometry or loading situation without access to a damage tolerant specialist. One solution technique involves the generation of the stress for an uncracked body along the expected path of crack propagation. (The finite element method provides a powerful tool for generating stress at any point in an uncracked body). The second solution technique involves the generation of the stress-intensity factor solution via an integral calculation that employs the stresses obtained for the case of the uncracked body along the expected path of the crack. Two integral calculation technique types are available: The Green's Function technique⁽³⁸⁻⁴²⁾ and the Weight Function technique^(39,40,43-45). These two crack-line loading techniques are reviewed in paragraphs 1.6.3.1 and 1.6.3.2, respectively.

1.6.3.1 Green's Function Technique

This technique takes advantage of the additive property of the stress-intensity factor and is based on generalized point load solutions of crack problems. For example, the point load solution for the central crack problem described in Figure 1.6.13 is given by:

$$K = \frac{P}{B} \frac{1}{\sqrt{\pi a}} \sqrt{\frac{a+x}{a-x}} \quad (1.6.11)$$

This solution can be used to obtain the stress-intensity factor for stresses distributed over the crack faces by noting that the point load per unit thickness (P/B) in Equation 1.6.11 can be replaced by the product of the pressure stress ($\sigma(x)$) and the distance over which it acts (dx). Thus, the stress-intensity factor for the distributed stresses applied to the crack (See Figure 1.6.14) becomes:

$$K = \int_{-a}^{+a} \frac{\sigma dx}{\sqrt{\pi a}} \frac{a+x}{\sqrt{a^2-x^2}} \quad (1.6.12)$$

The stress-intensity factor for the case of uniform opening stresses applied to the crack, i.e. $\sigma = \text{constant}$, is determined to be $K = \sigma\sqrt{\pi a}$, as was expected from the discussion of the method of superposition described in Subsection 1.6.1.

Given a point force solution for a geometry of concern, it is then possible to define the summation process that would integrate the effects of stress loading over the crack faces. Integral equations such as that defined by Equation 1.6.12 utilize the stress solutions from the uncracked body problem. A number of point force stress-intensity factor solutions are presented in the tables given in Section 1.7 and an extensive review of the availability and application of Green's Functions can be found in Reference 38. Other reviews can be found in References 39 and 40.

One of the cases reviewed by Cartwright and Rooke ⁽³⁸⁾ is of particular interest to structural engineers. They presented the work by Hsu and Rudd ⁽⁴¹⁾ on the development of a Green's Function for a diametrically

cracked hole. The Hsu and Rudd Green's Function was based on a series of finite-element determined stress-intensity factor solutions for a symmetrical set of point forces of the type shown in Figure 1.6.15. The finite-element point force solutions were developed as a function of position for $X(=x/a) < 0.9$ and a limiting expression was given for $X > 0.9$. The Hsu and Rudd Green's Function is shown in Figure 1.6.16 for several values of a/R ; also shown are Green's Functions for an edge crack and for a central crack. Note that all the Green's Functions tend to infinity as X approaches 1. It should also be noted that the Green's Functions presented are based on the following format

$$K = \frac{1}{\sqrt{\pi a}} \int_0^a \sigma(x) \cdot G(x,a) dx \quad (1.6.13)$$

which has been widely used. Hsu and Rudd based their presentation of the Green's Function on an approach taken by Hsu et al. ⁽⁴²⁾, wherein the Green's Function $G(x,a)$ in Equation 1.6.13 is obtained by multiplying the Hsu et al. value G^H by π , i.e.

$$G(x,a) = \pi G^H(x,a) \quad (1.6.14)$$

The complete table of $G^H(x,a)$ derived by Hsu et al. can be found in Table 1.6.4. Other work by Hsu and co-workers on Lug-type problems can be found in Section 1.7.

TABLE 1.6.4

GREEN'S FUNCTION FOR A DOUBLE CRACK EMANATING FROM AN OPEN HOLE IN AN INFINITE PLATE
(REF. 42)

$\frac{a/r}{x/a}$.20	.30	.40	.50	.60	.70	.80	.90	1.00	1.40	1.60	2.00	2.40	3.00
.00	.664	.629	.603	.595	.568	.575	.572	.554	.548	.571	.582	.594	.600	.611
.10	.676	.639	.615	.604	.582	.583	.586	.569	.563	.587	.596	.603	.603	.615
.20	.688	.645	.628	.617	.599	.596	.600	.589	.578	.604	.612	.613	.609	.624
.30	.699	.658	.646	.633	.621	.613	.623	.610	.598	.627	.630	.625	.619	.639
.40	.718	.679	.671	.656	.651	.639	.655	.639	.624	.656	.653	.642	.635	.664
.45	.740	.691	.689	.671	.673	.657	.674	.658	.643	.674	.665	.654	.647	.680
.50	.760	.708	.712	.689	.698	.681	.701	.682	.668	.692	.678	.670	.662	.699
.55	.781	.732	.739	.712	.730	.711	.733	.708	.699	.709	.695	.692	.679	.723
.60	.802	.764	.762	.746	.770	.752	.766	.739	.737	.730	.725	.721	.702	.753
.65	.840	.811	.793	.790	.814	.803	.808	.781	.786	.766	.760	.760	.729	.793
.70	.889	.868	.837	.838	.865	.867	.850	.827	.847	.819	.801	.811	.760	.842
.75	.960	.946	.907	.911	.913	.960	.912	.911	.929	.888	.859	.884	.817	.905
.80	1.071	1.089	1.044	1.030	.989	1.056	1.018	.995	1.021	.985	.955	.979	.904	.977
.85	1.234	1.254	1.245	1.211	1.141	1.252	1.177	1.187	1.192	1.130	1.130	1.120	1.042	1.101
* .90	1.429	1.432	1.434	1.436	1.437	1.438	1.440	1.441	1.442	1.445	1.446	1.448	1.449	1.451

$$* \text{ For } x/a > 0.9, G^H(a/r, x/a) = \frac{1}{\pi} \left[\frac{4(1+r/a)}{(1-x/a)(1+x/a+2r/a)} \right]^{1/2}$$

There are two cautionary remarks that must be made about the use of Green's Function techniques for solving crack problems. First, if all the loading across the crack tip is not tensile, and if the stress-intensity factor is positive at the crack tip of interest, the crack faces at some distance away from the crack tip may have (mathematically) merged in a nonphysical overlapping manner and the estimated stress-intensity factor might be unconservatively low. Accordingly, one should check to determine if the crack displacements all along the crack are positive and thus non-overlapping to ensure validity of the solution. Second, it is important in displacement boundary value problems to derive a Green's Function that accounts for the requirement that there be zero displacement on those boundaries where displacement conditions are applied when estimating the stress-intensity factor from the uncracked geometry solution. Typically, neglecting this requirement for displacement boundary value problems produces a stress-intensity factor that is conservatively high. These two cautions apply equally well to the Weight Function Technique.

1.6.3.2 The Weight Function Technique

This particular technique (20,40,43,44) can be derived using the definition of the strain energy release rate (See Section 1.9). The stress-intensity factor is obtained from the difference between the strain energy of a cracked structure and of the identical structure without a crack, and is given by:

$$K_I = \int_a \sigma(x) m(x,a) dx \quad (1.6.15)$$

where the function $m(x,a)$ is the Bueckner Weight Function, a function which is unique for the given geometry and is independent of the loading from which it was derived. The Weight Function is defined as a function of (1) material properties, (2) a known stress-intensity factor (K^*) for the given geometry under a defined loading and (3) the crack opening $v^*(x,a)$ corresponding to K^* :

$$m(x,a) = \frac{H}{2K^*} \frac{\partial v^*}{\partial a}(x,a) \quad (1.6.16)$$

H is a material constant that is given by:

$$H = \frac{8\mu}{1+\kappa} = \begin{cases} E & \text{for plane stress, or} \\ E/(1-\nu^2) & \text{for plane strain} \end{cases} \quad (1.6.17)$$

with μ = shear modulus and κ is defined as a function of the stress state and Poisson's ratio (ν)

$$\kappa = \begin{cases} \frac{3-\nu}{1+\nu} & \text{for plane stress} \\ 3-4\nu & \text{for plane strain} \end{cases} \quad (1.6.18)$$

For the infinite plate center crack problem K^* , v^* , $\frac{\partial v^*}{\partial a}$, and m are given by the following equations:

$$K^* = \sigma\sqrt{\pi a} \quad (1.6.19)$$

$$v^*(x,a) = \left(\frac{1+\kappa}{4\mu}\right) \sigma\sqrt{a^2 - x^2} \text{ for } -a \leq x \leq a \quad (1.6.20)$$

$$\frac{\partial v^*}{\partial a} = \left(\frac{1 + \kappa}{4 \mu} \right) \sigma a \frac{1}{\sqrt{a^2 - x^2}} \quad (1.6.21)$$

and

$$m(x, a) = \sqrt{\frac{a}{\pi}} \frac{1}{\sqrt{a^2 - x^2}} \quad (1.6.22)$$

The stress-intensity factor associated with a symmetrical pressure loading of $\sigma(x)$ on the central crack faces is then given by

$$K = \sqrt{\frac{a}{\pi}} \int_{-a}^{+a} \frac{\sigma(x)}{\sqrt{a^2 - x^2}} dx \quad (1.6.23)$$

The reader is cautioned to note that Equations 1.6.23 and 1.6.12 differ. However, both equations yield exactly the same stress-intensity factor solution when the pressure stress σ is a symmetrical function, i.e., the stress at $x = x_0$ is equal to the stress at $x = -x_0$ ($0 \leq x_0 \leq a$). The reason that Equations 1.6.23 and 1.6.12 differ is that the Bueckner Function in Equation 1.6.21 was derived for a symmetrical loading whereas the Green's Function was derived for the more general case of unsymmetrical loading. Thus, when deriving the Weight Function one should seek to locate stress-intensity factor (K^*) and crack displacement (v^*) solutions which are representative of the loading symmetry associated with the problems that are to be solved.

A Weight Function for radially and diametrically cracked holes was developed by Grandt ⁽⁴⁵⁾ for through-thickness type cracks. His solution is given by

$$K = \frac{H}{K_B} \int_0^a \sigma(x) \frac{\partial \eta}{\partial a} dx \quad (1.6.24)$$

where K_B represents the appropriate (radial or diametrical) Bowie stress-intensity factor (See Table 1.7.3, Cases 1.7.3.1 and 1.7.3.2) and the crack opening displacement η was obtained from finite-element solutions. The displacements η were described by the conic section equation:

$$\left(\frac{\eta}{\eta_0} \right)^2 = \frac{2}{2+m} \left(\frac{a-x}{a} \right) + \frac{m}{2+m} \left(\frac{a-x}{a} \right)^2 \quad (1.6.25)$$

Here η_0 is the displacement at the crack mouth ($x=0$) and m is the conic section coefficient found from

$$m = \pi \left[\frac{H\eta_0}{2\sigma a Y} \right]^2 - 2 \quad (1.6.26)$$

In this instance, Y is the Bowie geometric factor

$$Y = \frac{K_B}{\sigma \sqrt{a}} \quad (1.6.27)$$

The finite-element results for the crack mouth displacement η_0 were closely represented by the least squares expression

$$\eta_0 = R \sum_{i=0}^6 D_i (a/R)^i \quad (1.6.28)$$

where the coefficients D_i are given in Table 1.6.5.

Grandt has applied the Weight Function technique to a number of fastener-type cracked hole problems. Using finite-element descriptions of the stress along the expected crack path for a hole that has been cold-worked (loaded) to a 0.006 inch radial expansion and then unloaded, Grandt was able to derive the stress-intensity factor shown in Figure 1.6.17 for a remote stress loading of 40 Ksi. Figure 1.6.17 also provides the stress-intensity factor solution for a remote stress loading of 40 Ksi applied to a radially cracked hole without cold-working. The dramatic difference in stress-intensity factors from the two cases has been shown to translate itself into orders of magnitude difference in crack growth rate behavior.

1.6.4 Finite Element Methods

In all cases where an expression for the stress-intensity factor cannot be obtained from existing solutions, finite-element analysis can be used to determine K (46-50). Certain aircraft structural configurations have to be analyzed by finite-element techniques because of the influence of complex geometrical boundary conditions or complex load transfer situations. In the case of load transfer, the magnitude and distribution of loadings may be unknown. With the application of finite-

TABLE 1.6.5

LEAST SQUARES FIT OF FINITE ELEMENT DATA FOR
CRACK MOUTH DISPLACEMENT (REF. 45)

$$\eta_o/R = \sum_{i=0}^6 D_i (a/R)^i$$

Coefficient	Single Crack	Double Crack
D_0	-1.567×10^{-6}	1.548×10^{-5}
D_1	6.269×10^{-4}	5.888×10^{-4}
D_2	-6.500×10^{-4}	-4.497×10^{-4}
D_3	4.466×10^{-4}	3.101×10^{-4}
D_4	-1.725×10^{-4}	-1.162×10^{-4}
D_5	3.485×10^{-5}	2.228×10^{-5}
D_6	-2.900×10^{-6}	-1.694×10^{-6}

element methods, the required boundary conditions and applied loadings must be imposed on the model.

Complex structural configurations and multicomponent structures present special problems for finite-element modeling. These problems are associated with the structural complexity. When they can be solved, the stress-intensity factor is determined in the same way as in the case of a simpler geometry. This subsection deals with the principles and procedures that permit the determination of the stress-intensity factor from a finite-element solution.

Usually quadrilateral, triangular, or rectangular constant-strain elements are used, depending on the particular finite-element structural analysis computer program being used. For problems involving holes or other stress concentrations, a fine-grid network is required to accurately model the hole boundary and properly define the stress and strain gradients around the hole or stress concentration.

Within the finite-element grid system of the structural problem, the crack surface and length must be simulated. Usually, the location and direction of crack propagation is perpendicular to the maximum principal stress direction. If the maximum principal stress direction is unknown, then an uncracked stress analysis of the finite-element model should be conducted to establish the location of the crack and the direction of propagation.

The crack surfaces and lengths are often simulated by double-node coupling of elements along the crack line. Progressive crack extension is then simulated by progressively "unzipping" the coupled nodes along the crack line. Because standard finite-element formulations do not treat singular stress behavior in the vicinity of the ends of cracks, special procedures must be utilized to determine the stress-intensity factor. Three basic approaches to obtain stress-intensity factors from finite-element solutions have been rather extensively studied. These approaches are as follows:

a) Direct Method. The numerical results of stress, displacement, or crack-opening displacement are fitted to analytical forms of crack-tip-stress-displacement fields to obtain stress-intensity factors.

b) Indirect Method. The stress-intensity follows from its relation to other quantities such as compliance, elastic energy, or work energy for crack closure.

c) Cracked Element. A hybrid-cracked element allowing a stress singularity is incorporated in the finite-element grid system and stress-intensity factors are determined from nodal point displacements along the periphery of the cracked element.

These approaches can be applied to determine both Mode 1 and Mode 2 stress-intensity factors. Application of methods has been limited to two-dimensional planar problems. The state-of-the-art for treating three-dimensional structural crack problems is still a research area.

1.6.4.1 Direct Methods

The direct methods use the results of the general elastic solutions to the crack-tip stress and displacement fields. For the Mode I, the crack tip stresses can always be described by the equations

$$\begin{aligned}\sigma_x &= \frac{K_1}{\sqrt{2\pi r}} \cos \frac{\theta}{2} \left[1 - \sin \frac{\theta}{2} \sin \frac{3\theta}{2} \right], \\ \sigma_y &= \frac{K_1}{\sqrt{2\pi r}} \cos \frac{\theta}{2} \left[1 + \sin \frac{\theta}{2} \sin \frac{3\theta}{2} \right],\end{aligned}\tag{1.6.29}$$

$$\sigma_z = 0 \text{ (plane stress) or } \sigma_z = \nu(\sigma_x + \sigma_y) \text{ (plane strain) ,}$$

$$\tau_{xy} = \frac{K_1}{\sqrt{2\pi r}} \sin \frac{\theta}{2} \cos \frac{\theta}{2} \cos \frac{3\theta}{2} ,$$

and

$$\tau_{xz} = \tau_{yz} = 0 ,$$

where r and θ are polar coordinates originating at the crack tip, and where x is the direction of the crack, y is perpendicular to the crack in the plane of the plate, and z is perpendicular to the plate surface.

If the stresses around the crack tip are calculated by means of finite-element analysis, the stress-intensity factor can be determined as

$$K_1 = \sigma_{ij} \frac{\sqrt{2\pi r}}{f_{ij}(\theta)} ,\tag{1.6.30}$$

where i and j are used to represent various permutations of x and y .

By taking the stress calculated for an element not too far from the crack tip, the stress-intensity follows from a substitution of this stress and the r and θ of the element into Equation 1.6.30. This can be done for any element in the crack tip vicinity.

Ideally, the same value of K should result from each substitution; however, the stress field equations are only valid in an area very close to the crack tip. Also at some distance from the crack tip, nonsingular terms should be taken into account. Consequently, the calculated K differs from the actual K . The result can be improved ⁽⁴⁶⁾ by refining the finite-element mesh or by plotting the calculated K as a function of the distance of the element to the crack tip. The resulting line should be extrapolated to the crack tip, since the crack tip equations are exact for $r = 0$. Usually, the element at the crack tip should be discarded. Since it is too close to the singularity, the calculated stresses are largely in error. As a result, Equation 1.6.30 yields a K value that is more in error than those for more remote elements, despite the neglect of the nonsingular terms.

Instead of the stresses, one can also use the displacements for the determination of K . In general, the displacements of the crack edge (crack-opening displacements) are employed. The Mode 1 and Mode 2 plane strain displacement equations are given by

$$u_1 = \frac{2K_1(1+\nu)}{E} \left[\frac{r}{2\pi} \right]^{\frac{1}{2}} \cos \frac{\theta}{2} (1 - 2\nu + \sin^2 \frac{\theta}{2}),$$

and

(1.6.31)

$$v_1 = \frac{2K_1(1+\nu)}{E} \left[\frac{r}{2\pi} \right]^{\frac{1}{2}} \sin \frac{\theta}{2} (2 - 2\nu - \cos^2 \frac{\theta}{2}),$$

and by

$$u_2 = \frac{2K_2(1+\nu)}{E} \left[\frac{r}{2\pi} \right]^{\frac{1}{2}} \sin \frac{\theta}{2} (2 - 2\nu + \cos^2 \frac{\theta}{2}),$$

and

(1.6.32)

$$v_2 = \frac{2K_2(1+\nu)}{E} \left[\frac{r}{2\pi} \right]^{\frac{1}{2}} \cos \frac{\theta}{2} (2\nu - 1 + \sin^2 \frac{\theta}{2}),$$

respectively. The functions u and v represent the displacements in the x and y direction, respectively. The crack tip polar coordinates r and θ are chosen to coincide with the nodal points in the finite element mesh where displacements are desired. Since the above elastic field equations are only valid in an area near the tip of the crack, the application should be restricted to that area.

1.6.4.2 Indirect Methods

The indirect methods use relationships that exist between the stress-intensity factor (K) and the elastic-energy content (U) of the cracked structure. These relationships are developed in Section 1.9 along with a full discussion of the strain energy release rate (G) and compliance (C), i.e. the inverse stiffness of the system. The stress-intensity factor is related to these parameters by the following:

$$K^2 = G\bar{E} \quad (1.6.33)$$

$$K^2 = \frac{\partial U}{\partial a} \cdot \frac{\bar{E}}{B} \quad (1.6.34)$$

and

$$K^2 = \frac{P^2}{2B} \cdot \frac{\partial C}{\partial a} \cdot \bar{E} \quad (1.6.35)$$

where B is the plate thickness and \bar{E} is the elastic modulus E in plane stress and is $E/(1-\nu^2)$ in plane strain.

The elastic energy content and the compliance of cracked structures are obtained for a range of crack sizes either by solving the problem for different crack sizes or by unzipping nodes. Differentiation with respect to crack size gives K from the above equations. The advantage of the elastic-energy content and compliance methods is that a fine mesh is not necessary, since accuracy of crack-tip stresses is not required. A disadvantage is that differentiation procedures can introduce errors.

The strain energy release rate relationship (Equation 1.6.33) was derived based on the use of the crack tip stress field and displacement equations to calculate the work done by the forces required to close the crack tip. The crack tip closing work can be calculated by uncoupling the next nodal point in front of the crack tip and by calculating the work done by the nodal forces to close the crack to its original size.

The concept is that if a crack were to extend by a small amount, Δa , the energy absorbed in the process is equal to the work required to close the crack to its original length. The general integral equations for strain energy release rates for Modes 1 and 2 deformations are

$$G_1 = \lim_{\Delta a \rightarrow 0} \frac{1}{2\Delta a} \int_0^{\Delta a} \sigma_y (\Delta a - r, 0) v(r, \pi) dr, \quad (1.6.36)$$

$$G_2 = \lim_{\Delta a \rightarrow 0} \frac{1}{2\Delta a} \int_0^{\Delta a} \tau_{xy} (\Delta a - r, 0) u(r, \pi) dr .$$

The significance of this approach is that it permits an evaluation of both K_1 and K_2 from the results of a single analysis.

In finite-element analysis, the displacements have a linear variation over the elements and the stiffness matrix is written in terms of forces and displacements at the element corners or nodes. Therefore, to be consistent with finite-element representation, the approach for evaluating G_1 and G_2 is based on the nodal-point forces and displacements. An explanation of application of this work-energy method is given with reference to Figure 1.6.18. The crack and surrounding elements are a small segment from a much larger finite-element model of a structure. In terms of the finite-element representation, the amount of work required to close the crack, Δa , is one-half the product of the forces at nodes c and d and the distance $(v_c - v_d)$ which are required to close these nodes. The expressions for strain energy release rates in terms of nodal-point displacements and forces are (see Figure 1.6.18 for notations)

$$G_1 = \lim_{\Delta a \rightarrow 0} \frac{1}{2\Delta a} \bar{F}_c (v_c - v_d) ,$$

(1.6.37)

$$G_2 = \lim_{\Delta a \rightarrow 0} \frac{1}{2\Delta a} \bar{T}_c (u_c - u_d) .$$

1.6.4.3 Cracked Element Methods

This approach involves the use of a hybrid-cracked element which is incorporated into a finite-element structural analysis program. To date, only two dimensional crack problems can be solved with the cracked-element approach. Elements have been developed⁽⁴⁷⁻⁵³⁾ that allow a stress singularity to occur at the crack tip.

The cracked element consists of boundary nodal points around the geometrical boundary of the element. The element is either contained within the complete finite-element model or is solved separately using the results of finite-element analysis. In either case, the crack surface is simulated by unzipping a double-noded line along the line of expected crack extension. This builds into the structural model the proper stiffness due to the presence of the crack. The variation of stress-intensity factors (K_1 and K_2) with crack length is determined by progressively unzipping the sets of coupled nodes.

Studies have been conducted on the variation of stress-intensity factors with cracked-element size and location (51,52). These results define some definite guidelines in using cracked-element models. First, the distance from the crack tip to the cracked-element nodal points should be as constant as possible. Secondly, for long edge-cracks or cracks emanating from holes, the cracked element should only contain an area very near the crack tip.

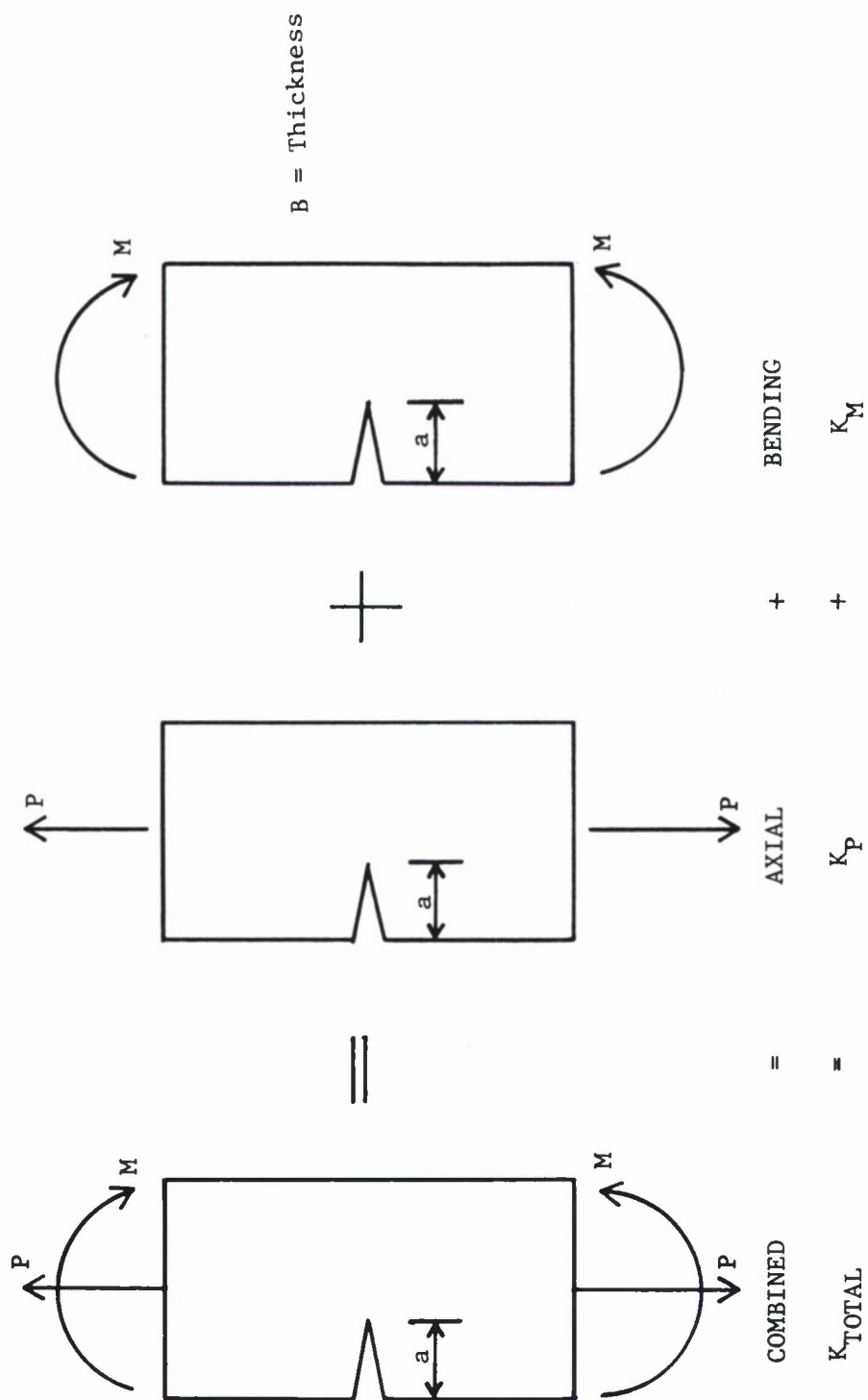


Figure 1.6.1.1. Edge Crack Geometry Loaded With Axial and Bending Loads.

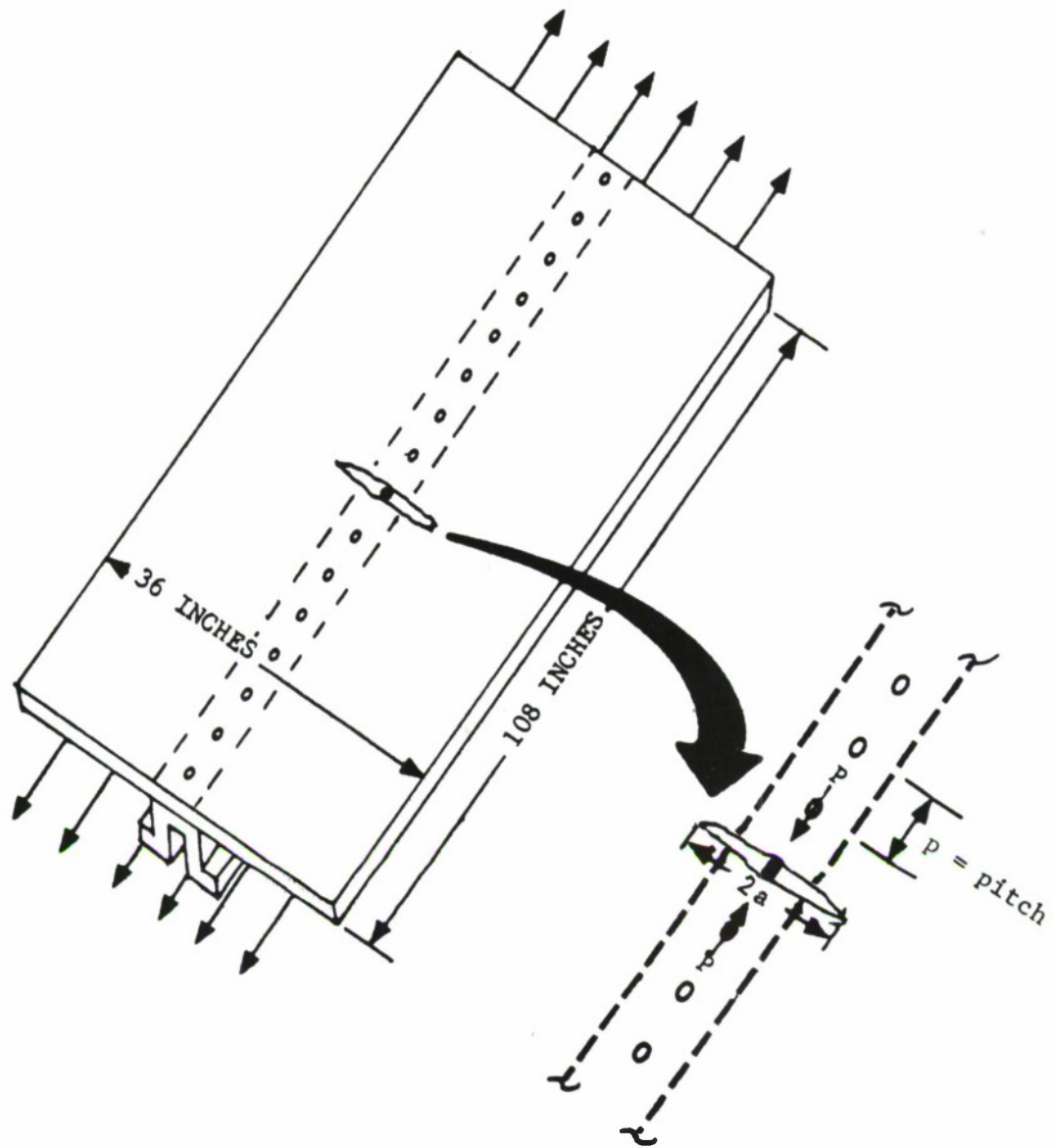
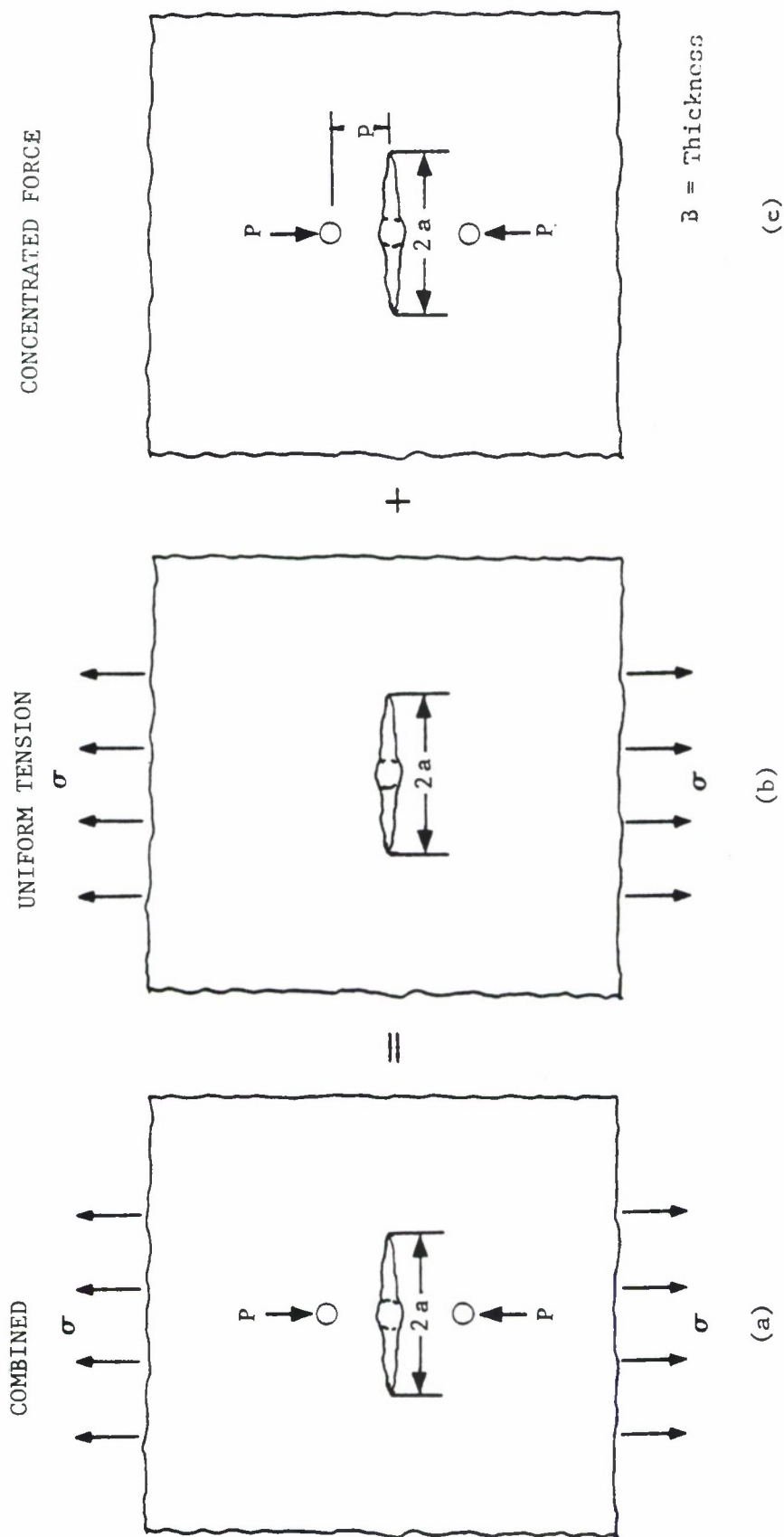
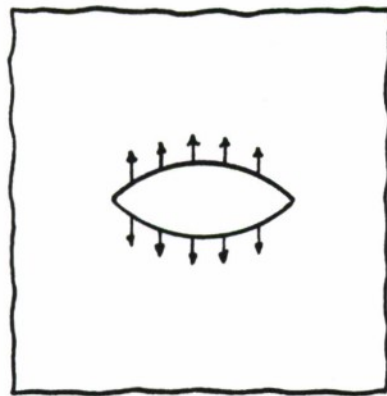


Figure 1.6.2. Crack At Rivet In a Riveted Skin-Stringer Panel
(No Crack Buckling).



$$K_{\text{TOTAL}} = K \left(= \sqrt{\pi a} \right) + K_p \left(= \frac{-P\sqrt{\pi a}}{2\pi B} \frac{(3 + \nu)p^2 + 2a^2}{(a^2 + p^2)^{3/2}} \right)$$

Figure 1.6.3. Superposition of Stress Intensities for Uniform Tension and Concentrated Force.



pressure = p

Figure 1.6.4. Internally Pressurized Center Crack.

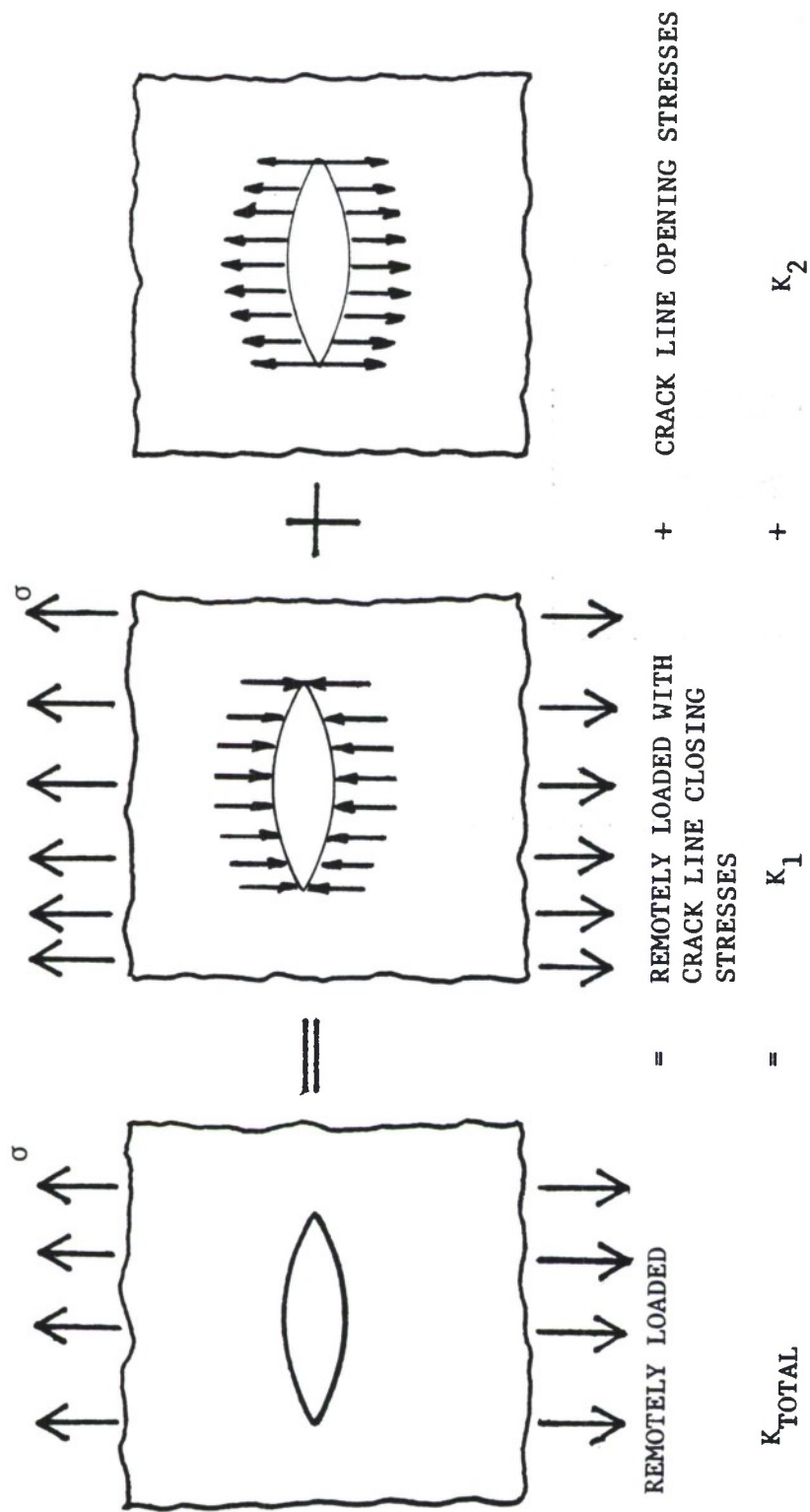


Figure 1.6.5. Principle of Superposition Illustrated for Center Cracked Geometry.

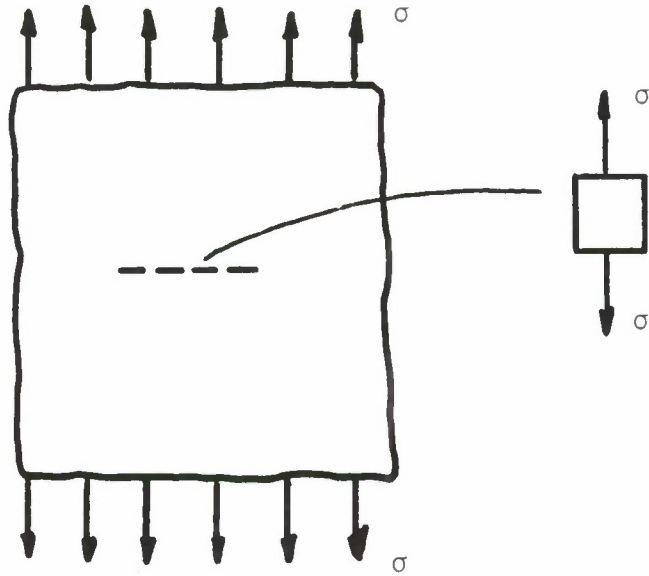


Figure 1.6.6a. Uniform Stresses Along Dotted Line Generated by Remote Loading.

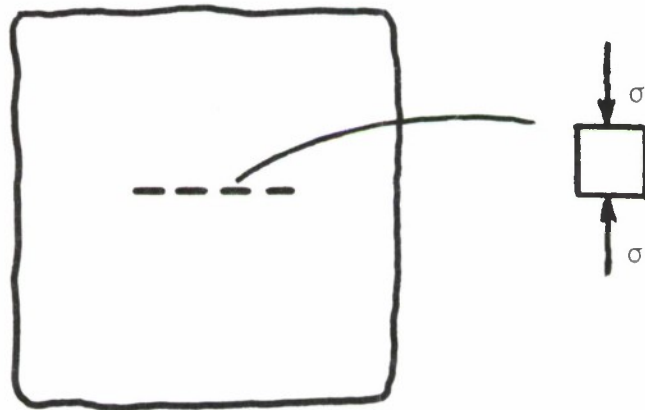


Figure 1.6.6b. Opposing Stresses Applied Along the Dotted Line.

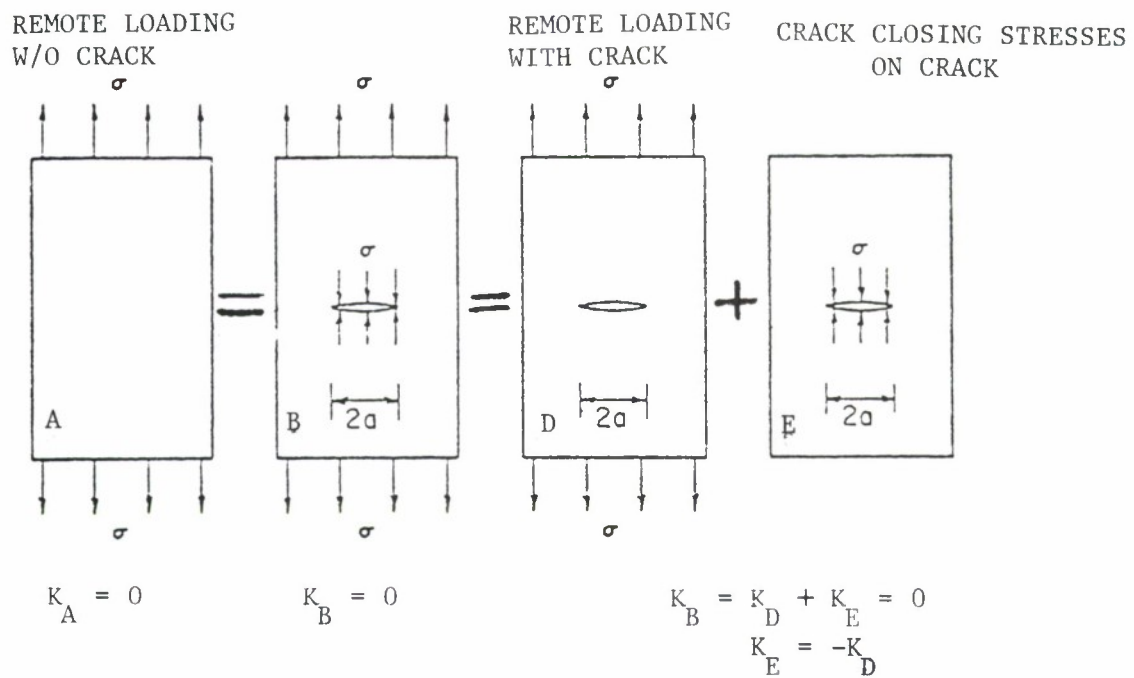


Figure 1.6.7. Illustration of Superposition Principle.

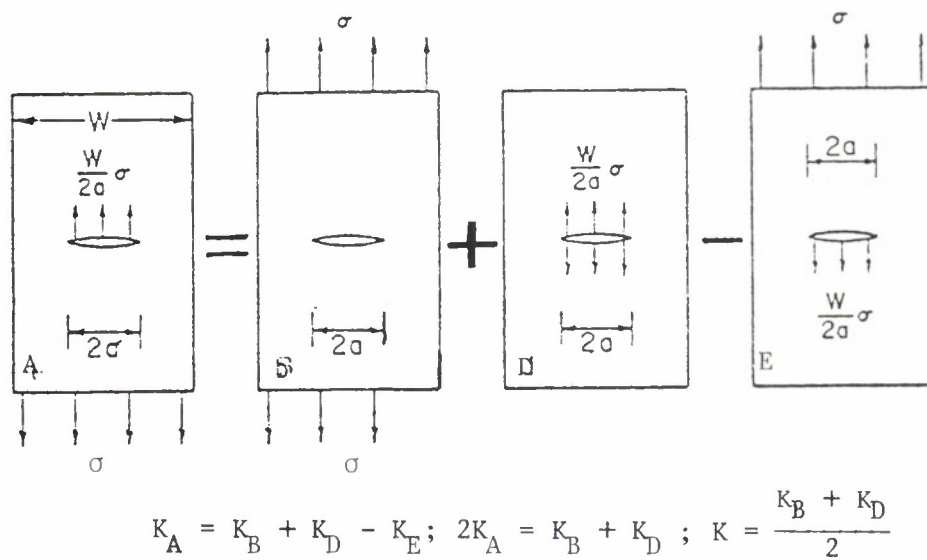
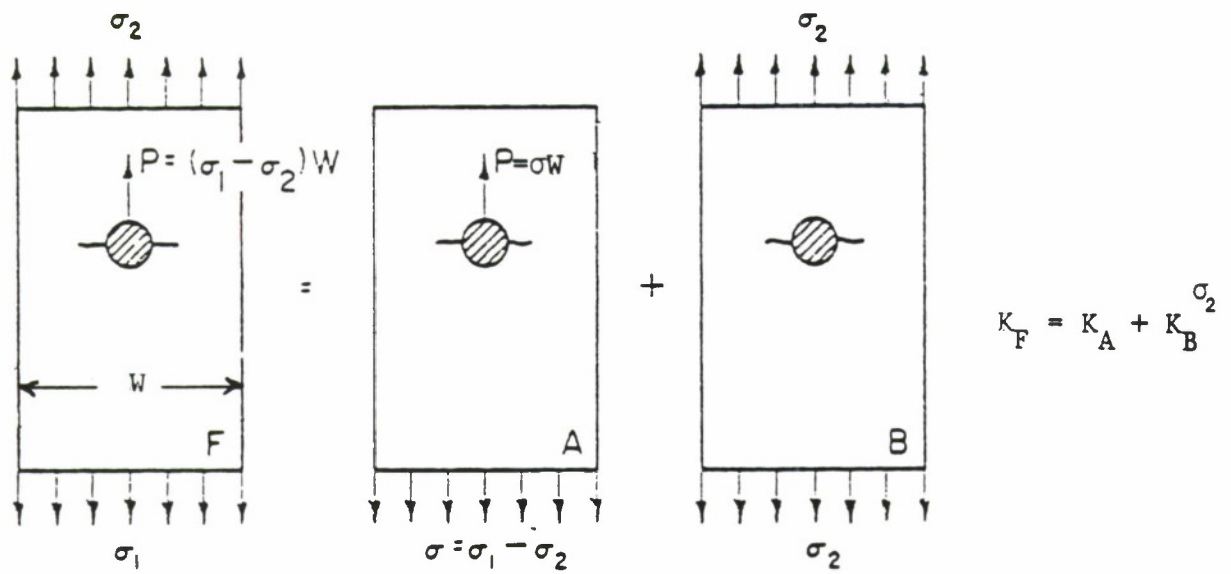
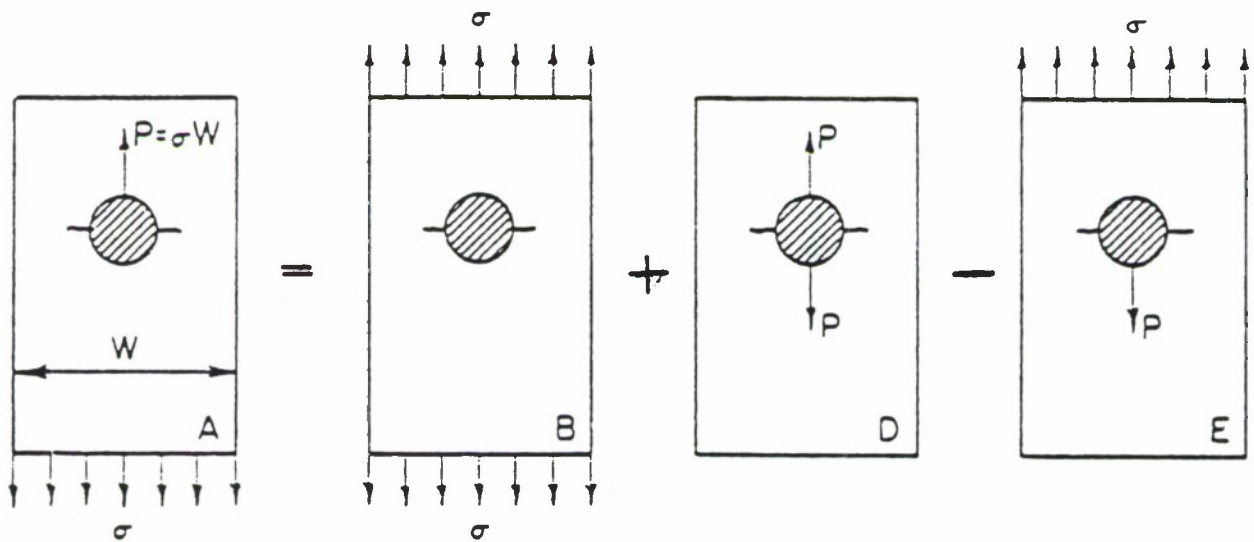


Figure 1.6.8. Application of Superposition Principle.



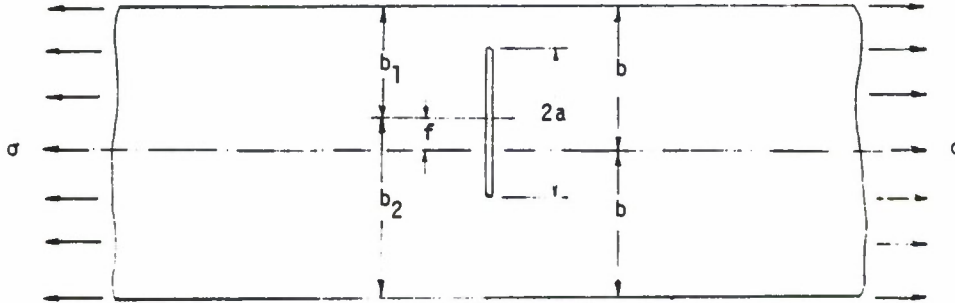
Step 1: Decompose loading so that pin reacts its entire load.



Step 2: Decompose pin reactive loading. $K_A = \frac{K_B^{\sigma_2} + K_D^P}{2}$

Figure 1.6.9. Stress Intensity Factor for Pin-Loaded Hole (Bearing Bypass Problem) Obtained by Superposition.

Infinite Strip with an Eccentric Crack (Isida [1973])



Consider an eccentrically cracked infinite strip subjected to uniform tensile stress σ at infinity. The stress intensity factors can be written in terms of the geometric parameters ($\delta = \frac{f}{b}$, $\lambda = \frac{a}{b_1}$) as

$$k_1 = F(\delta, \lambda) \sigma \sqrt{a} \quad (\text{see}^* \text{note below})$$

$$k_2 = 0$$

Numerical values of the function $F(\delta, \lambda)$ are given in the following tables for various geometric parameters.

* Damage Tolerant Handbook Users Note:

The Mathematician's Definition of Stress Intensity Factor is Employed, i.e., $K = k \sqrt{\pi}$ so that $F(\delta, \lambda)$ does not contain the factor $\sqrt{\pi}$.

Figure 1.6.10. Example Stress-Intensity Factor Solution Taken from Sih Handbook (page 1 of 3).

Values of $F(\delta, \lambda)$ for Upper Crack Tip

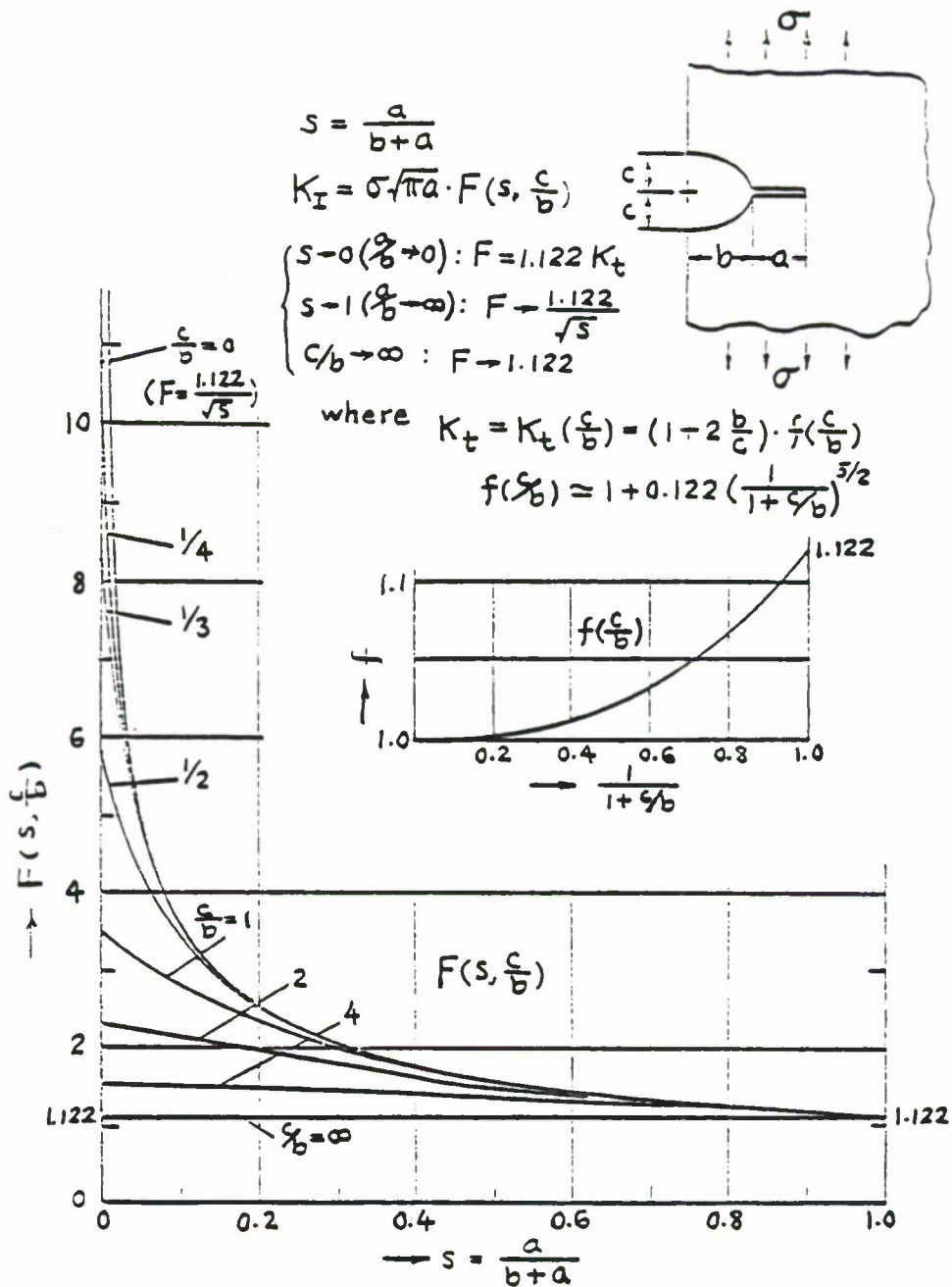
δ	λ	0.1	0.2	0.3	0.4	0.5	0.6	0.7	0.8	0.9
0		1.0060	1.0246	1.0577	1.1094	1.1867	1.3033	1.4881	1.811	2.47
0.02		1.0058	1.0239	1.0564	1.1073	1.1837	1.2994	1.4832	1.806	2.47
0.04		1.0056	1.0234	1.0553	1.1056	1.1814	1.2965	1.4799	1.804	2.48
0.06		1.0055	1.0229	1.0544	1.1042	1.1795	1.2943	1.4777	1.803	2.49
0.08		1.0054	1.0225	1.0537	1.1031	1.1781	1.2927	1.4764	1.804	2.50
0.1		1.0053	1.0222	1.0530	1.1022	1.1770	1.2916	1.4758	1.805	2.51
0.2		1.0050	1.0212	1.0513	1.0999	1.1745	1.2898	1.4765	1.814	2.54
0.3		1.0049	1.0208	1.0507	1.0989	1.1732	1.2881	1.4743	1.810	2.54
0.4		1.0048	1.0205	1.0497	1.0969	1.1695	1.2812	1.4614	1.784	2.47
0.5		1.0046	1.0197	1.0476	1.0926	1.1613	1.2664	1.4344	1.732	2.36
0.6		1.0043	1.0183	1.0442	1.0855	1.1483	1.2436	1.3943	1.657	2.20
0.7		1.0039	1.0164	1.0395	1.0762	1.1316	1.2152	1.3460	1.572	2.03
0.8		1.0034	1.0142	1.0341	1.0659	1.1136	1.1854	1.2972	1.489	1.88
0.9		1.0029	1.0122	1.0295	1.0569	1.0985	1.1608	1.2583	1.426	1.77
1		1.0026	1.0112	1.0272	1.0528	1.0915	1.1497	1.2407	1.397	1.72

1.4.3-4

Values of $F(\delta, \lambda)$ for Lower Crack Tip

δ	λ	0.1	0.2	0.3	0.4	0.5	0.6	0.7	0.8	0.9
0		1.0060	1.0246	1.0577	1.1094	1.1867	1.3033	1.4881	1.811	2.47
0.02		1.0057	1.0234	1.0544	1.1021	1.1724	1.2759	1.4342	1.695	2.18
0.04		1.0055	1.0223	1.0516	1.0959	1.1602	1.2531	1.3910	1.608	1.98
0.06		1.0053	1.0214	1.0491	1.0906	1.1500	1.2341	1.3562	1.542	1.85
0.08		1.0052	1.0206	1.0470	1.0861	1.1413	1.2184	1.3280	1.490	1.75
0.1		1.0050	1.0199	1.0452	1.0823	1.1340	1.2053	1.3051	1.450	1.67
0.2		1.0046	1.0179	1.0399	1.0709	1.1127	1.1680	1.2426	1.348	1.51
0.3		1.0045	1.0172	1.0380	1.0672	1.1058	1.1565	1.2249	1.324	1.48
0.4		1.0044	1.0170	1.0374	1.0660	1.1040	1.1540	1.2218	1.321	1.48
0.5		1.0042	1.0165	1.0364	1.0645	1.1018	1.1510	1.2177	1.315	1.47
0.6		1.0040	1.0155	1.0343	1.0608	1.0960	1.1424	1.2047	1.294	1.44
0.7		1.0036	1.0139	1.0309	1.0546	1.0860	1.1269	1.1813	1.258	1.38
0.8		1.0031	1.0120	1.0264	1.0465	1.0729	1.1068	1.1511	1.212	1.31
0.9		1.0026	1.0101	1.0222	1.0388	1.0603	1.0876	1.1227	1.170	1.24
1		1.0024	1.0092	1.0201	1.0349	1.0540	1.0779	1.1084	1.149	1.21

Figure 1.6.10. (page 3 of 3).



Methods: Stress Relaxation (Superposition) (Nishitani; $c/b = 1/2, 1, 2$ and $0.2 \leq a/b \leq 1$)

Estimated by interpolation (Tada)

Accuracy: Better than 2 %

References: Nishitani 1973, Tada 1973

Figure 1.6.11. Example Stress-Intensity Factor Solution from the Tada, et al. Handbook.

Crack near a stiffener in a sheet: uniaxial tensile stress

A sheet of thickness t , with a stiffener of area A continuously attached along a line, contains a crack of length $2a$ which is along a line perpendicular to the stiffener; the centre of the crack is a distance b from the stiffener. A uniform uniaxial tensile stress σ is applied to the sheet, remote from the crack, in a direction perpendicular to the crack (see Fig.126). To satisfy strain compatibility between the stiffener and the sheet the stress applied to the stiffener, remote from the crack, is $E_2\sigma/E_1$. E_1 and E_2 are the Young's moduli of the sheet and the stiffener respectively. The in-plane bending stiffness of the stiffener is assumed to be zero. Greif and Sanders⁴ used complex stress functions to study this configuration and from their work the opening mode stress intensity factor can be determined, to an accuracy of much better than 1%, as a function of an extensional stiffness parameter λ given by

$$\lambda = \frac{2E_1at}{AE_2} . \quad (1)$$

The results for plane stress conditions with Poisson's ratio = 1/3 are shown as curves of K_I/K_0 vs. λ in Fig.126 for both tip B (farther from the stiffener) and tip C (nearer the stiffener). K_0 is the stress intensity factor at both tips in the absence ($b = \infty$) of the stiffener and is given by

$$K_0 = \sigma \sqrt{\pi a} . \quad (2)$$

page no. 193

Figure 1.6.12. Example Stress-Intensity Factor Solution from the Rooke-Cartwright Handbook (page 1 of 2).

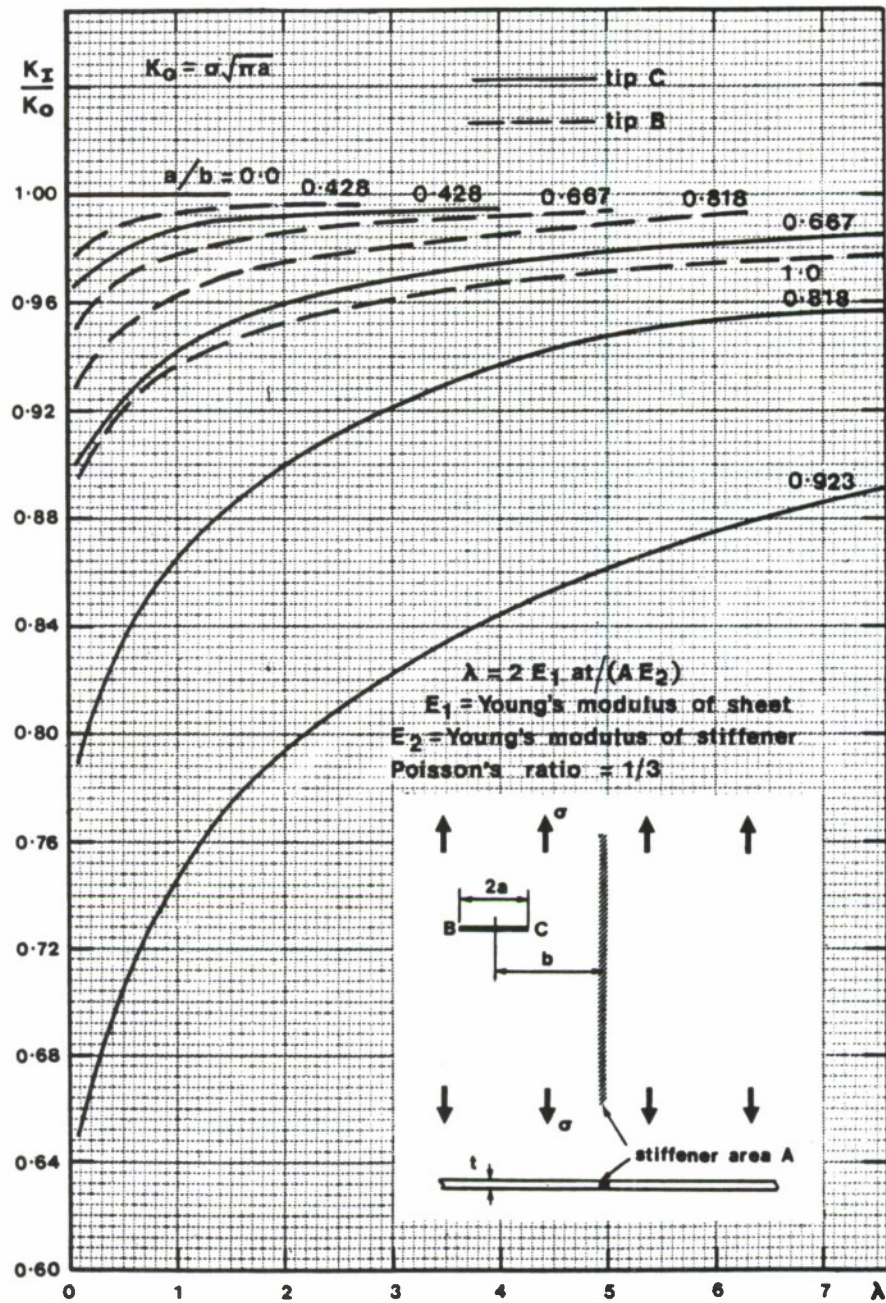


Fig.126 K_I for a crack near a stiffener in a sheet subjected to a uniaxial tensile stress

Figure 1.6.12. (page 2 of 2),

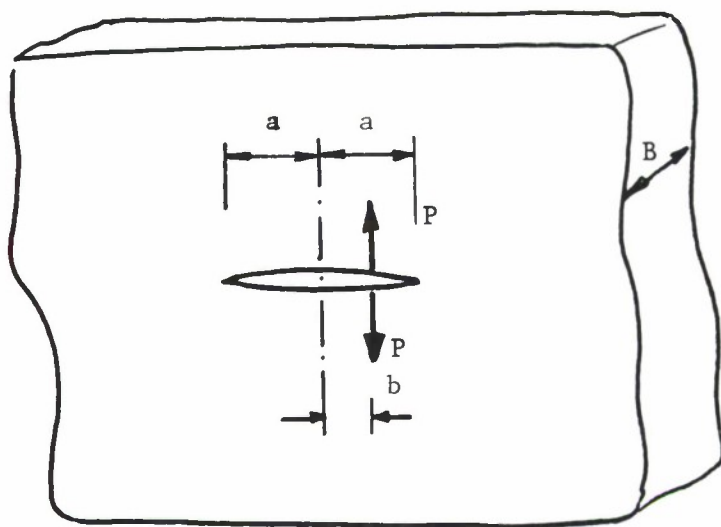


Figure 1.6.13 Point Load (P) Applied to the Crack Faces for a Central Crack Located in an Infinite Plate.

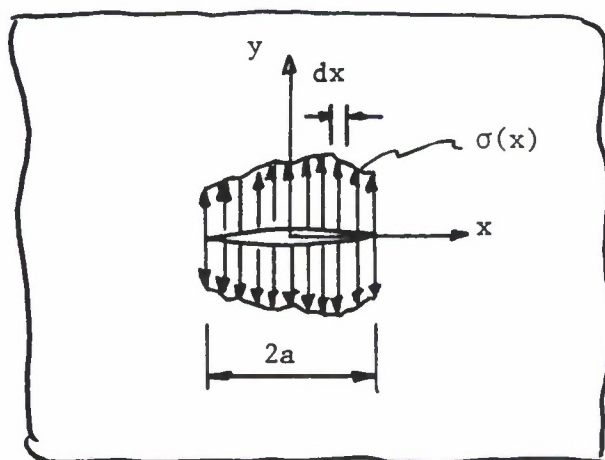


Figure 1.6.14 Distributed Loading Applied to Crack Faces of the Central Crack.

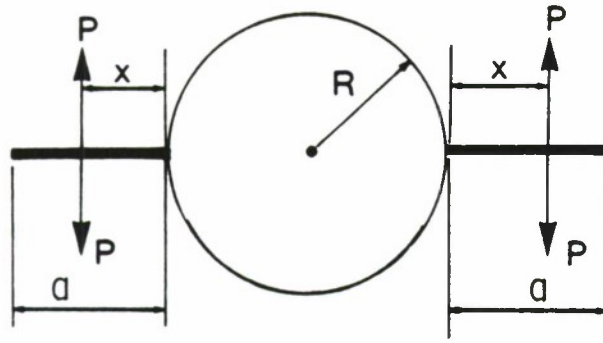


Figure 1.6.15 Diametrically Cracked Hole With Symmetrically Located Point Focus.

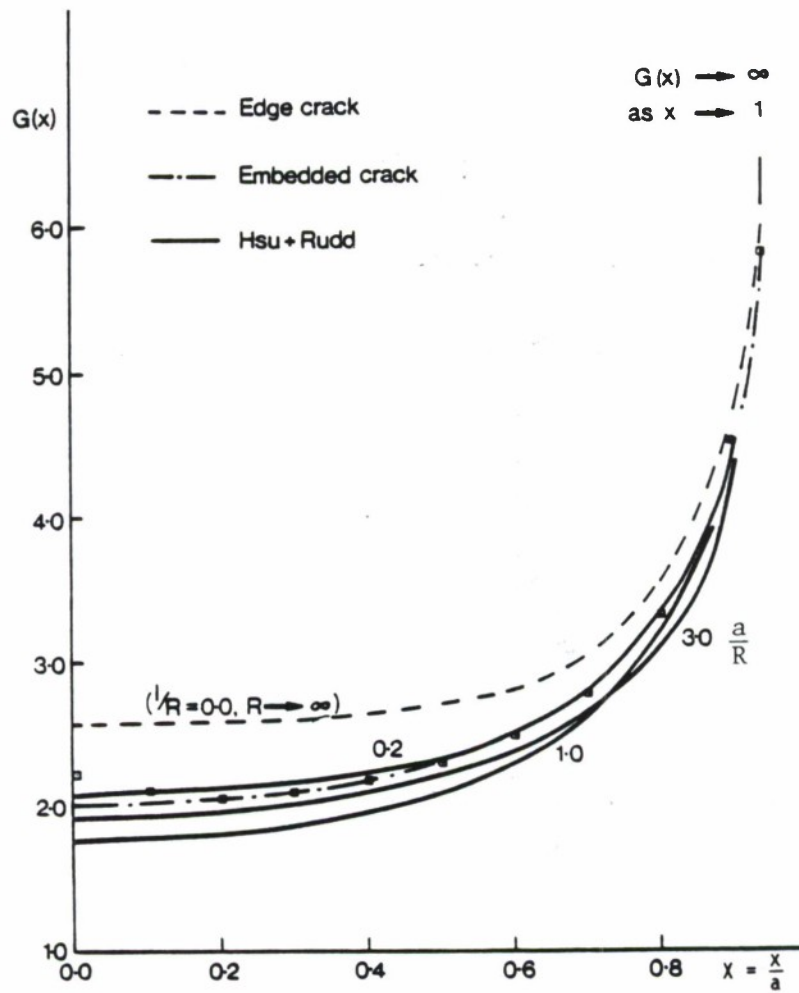


Figure 1.6.16 Green's Function for Geometry and Loading Described in Figure 1.6.15 (References 38, 41 and 42).

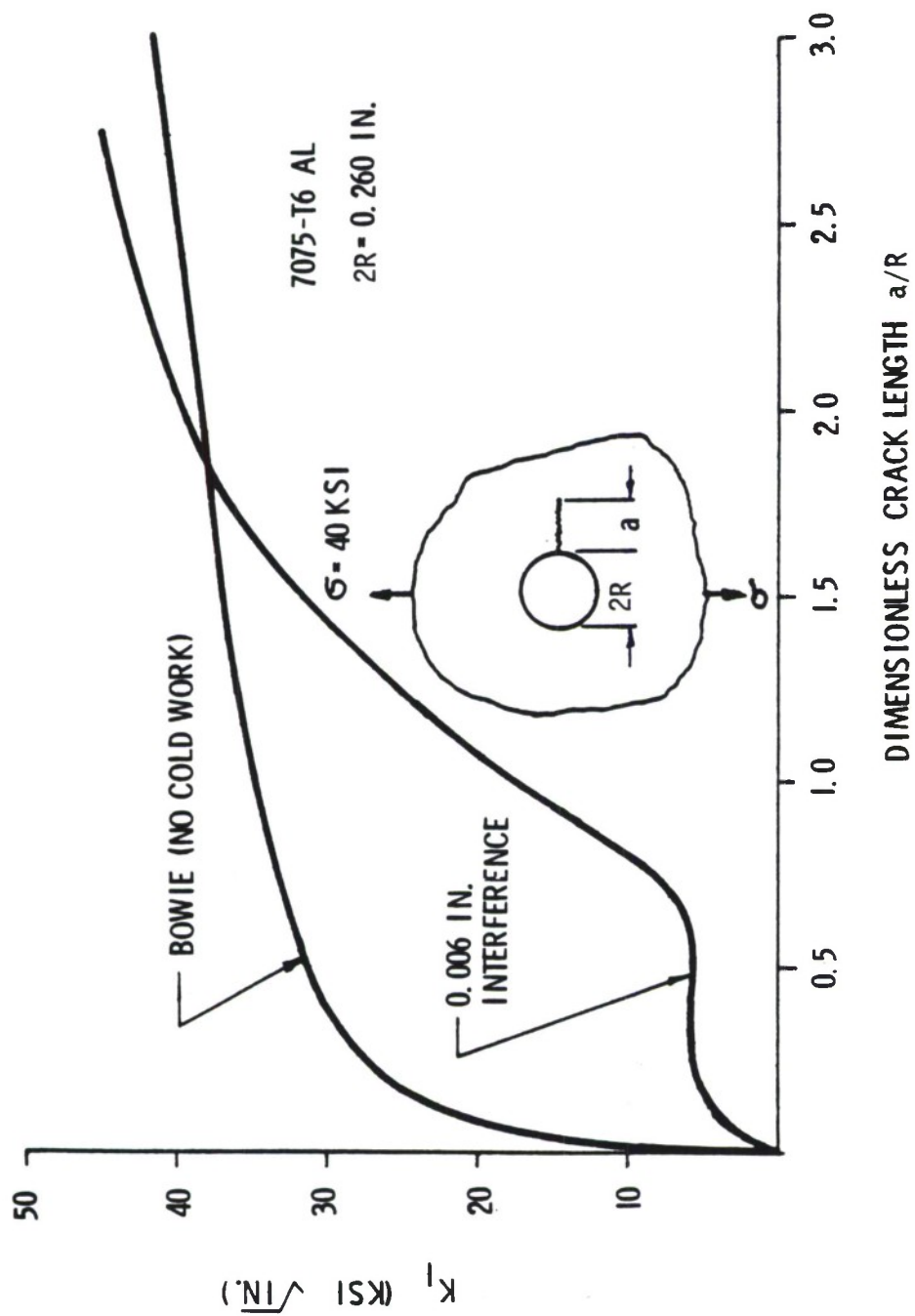


Figure 1.6.17 Stress-Intensity Factor Calibration for a Cold Worked Hole (45).

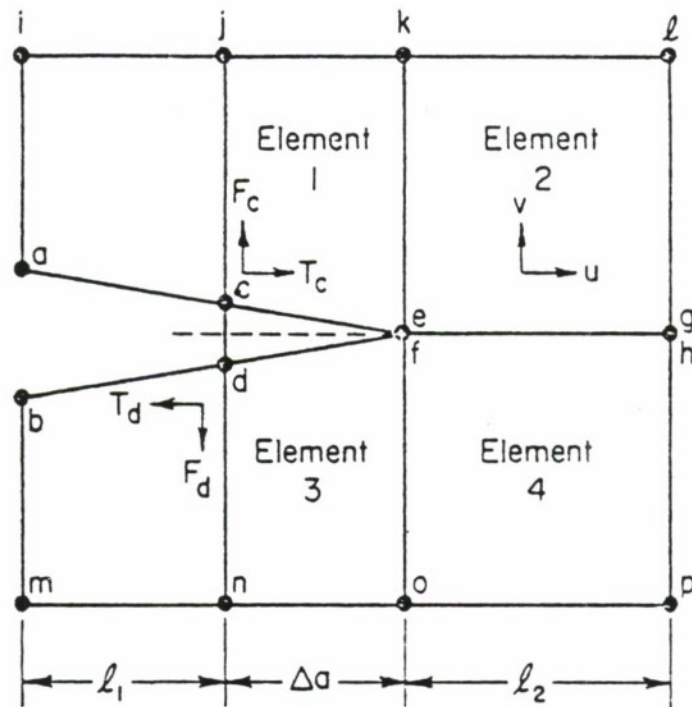


Figure 1.6.18 Finite-Element Nodes Near Crack Tip.

1.7 SELECTED STRESS-INTENSITY FACTOR CASES

This section will present a catalog of stress-intensity factor solutions for relatively simple crack geometries in plates. The remote loading solutions are typically presented in the form

$$K = \beta \sigma \sqrt{\pi a} \quad (1.7.1)$$

where the coefficient β is expressed as a function of geometry. Other solution forms also include

$$K = \frac{P}{BW} f(a) \quad (1.7.2)$$

for wedge force loading. Some of the cases considered can be used to develop more complex solutions through the methods of superposition and compounding. Many of the solutions are directly useful for obtaining approximate solutions to isolate local effects.

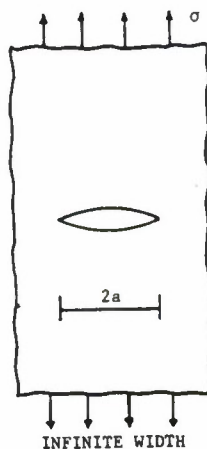
1.7.1 Through-Thickness-Internally Cracked Type Geometries

Table 1.7.1 presents a series of twelve solutions which are primarily of the center cracked geometry configuration. The table first presents the remotely loaded cases and then the wedge and point loaded cases. Each geometry and loading condition in Table 1.7.1 is graphically defined and given a case number, e.g. Case 1.7.1.10 is the case where the point loading is applied off the crack face along the perpendicular bisector of the crack.

TABLE 1.7.1
STRESS INTENSITY FACTORS FOR INTERNALLY CRACKED
STRUCTURES WITH THROUGH-THICKNESS CRACKS

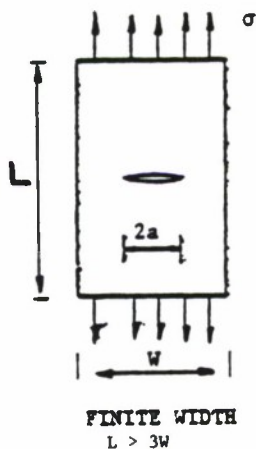
CASE NO.	REMOTELY LOADED AND CENTER AND ECCENTRICALLY CRACKED GEOMETRIES	STRESS INTENSITY FACTOR
----------	---	-------------------------

1.7.1.1



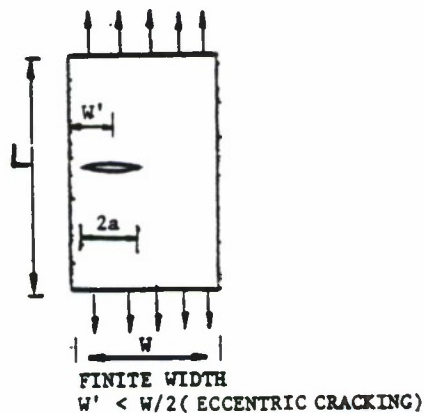
$$K = \sigma\sqrt{\pi a}$$

1.7.1.2



$$K = \sigma\left[\pi a \sec \frac{\pi a}{W}\right]^{1/2}$$

1.7.1.3



See Figures 1.6.10,
1.7.1 and 1.7.2,
References 16-18, 54.

1.7.2

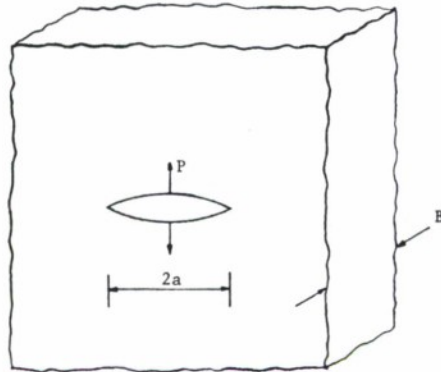
TABLE 1.7.1 (Continued)

CASE NO.

WEDGE LOADED CENTER
CRACKED GEOMETRIES

STRESS-INTENSITY FACTOR

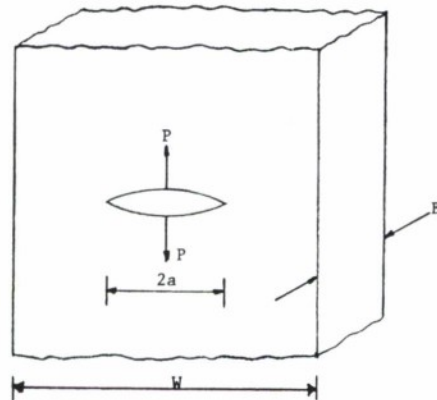
1.7.1.4



INFINITE WIDTH-LOAD AT
CENTER OF CRACK

$$K = \frac{(P/B)}{\sqrt{\pi a}}$$

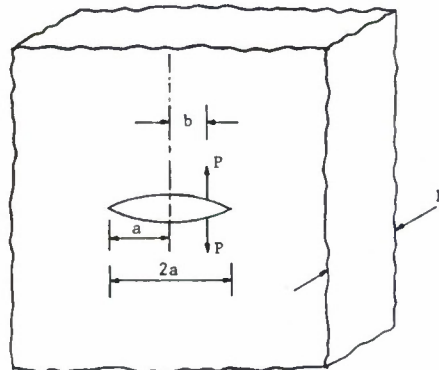
1.7.1.5



FINITE WIDTH-LOAD AT
CENTER OF CRACK

$$K = \frac{(P/B)}{\sqrt{\pi a}} \sqrt{\frac{1}{\frac{W}{2\pi a} \sin \frac{2\pi a}{W}}}$$

1.7.1.6



INFINITE WIDTH-LOAD OFFSET
FROM CRACK CENTER

$$K = \frac{(P/B)}{\sqrt{\pi a}} \sqrt{\frac{a+b}{a-b}}$$

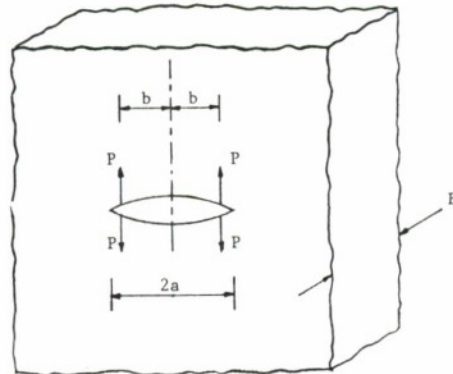
TABLE 1.7.1 (Continued)

CASE NO.

WEDGE AND POINT LOADED
CENTER CRACKED GEOMETRIES

STRESS-INTENSITY FACTOR

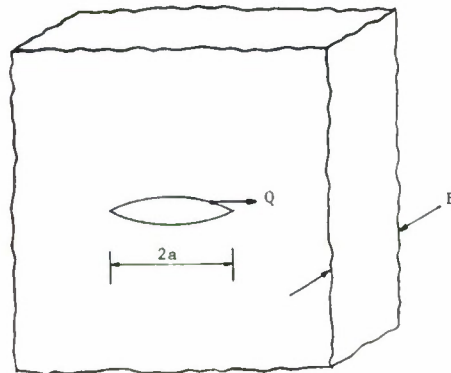
1.7.1.7



INFINITE WIDTH-LOAD PAIRS
OFFSET FROM CENTER

$$K = 2(P/B) \frac{a}{\pi} \cdot \frac{1}{\sqrt{a^2 - b^2}}$$

1.7.1.8



INFINITE WIDTH, CRACK
LOADED WITH HORIZONTAL LOAD

$$K = \frac{Q}{2\sqrt{\pi a}} \left(\frac{\kappa - 1}{\kappa + 1} \right)$$

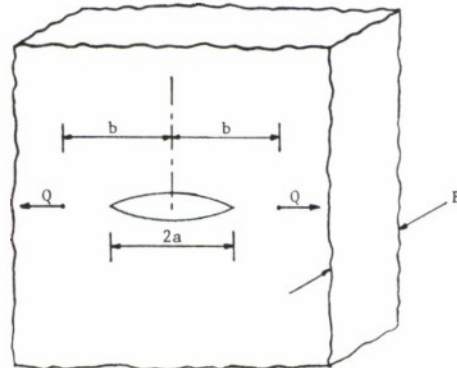
Where

$\kappa = 3 - 4\nu$ Plane Strain

$$\kappa = \frac{3 - \nu}{1 + \nu}$$

and ν = Poisson's ratio
Reference 55

1.7.1.9



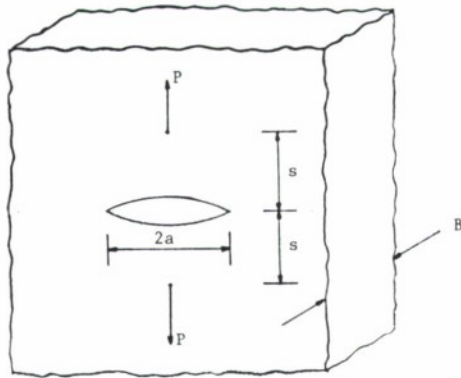
INFINITE WIDTH-LOADS
APPLIED IN LINE WITH CRACK

$$K \begin{cases} = 0 & \text{if } b < a \\ \text{or} \\ = \frac{-Q (\kappa - 1) \sqrt{a}}{\sqrt{\pi} (\kappa + 1) \sqrt{b^2 - a^2}} \end{cases}$$

κ defined for case 1.7.1.8
Reference 55

TABLE 1.7.1 (Concluded)

1.7.1.10

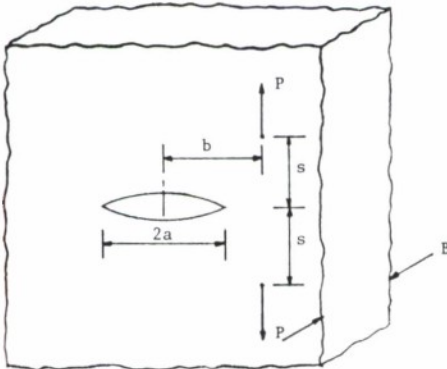


INFINITE WIDTH-LOAD TO
CRACK, ALONG OF CRACK

$$K = \frac{(P/B)}{2} \sqrt{\frac{a}{\pi}} \cdot \frac{(3+\nu)s^2 + 2a^2}{(a^2 + s^2)^{3/2}}$$

Reference 56

1.7.1.11



INFINITE WIDTH, LOAD TO
CRACK, AND OFFSET FROM

$$K = \frac{(P/B)}{2\sqrt{\pi a}} \left[\frac{\gamma}{\omega} - \frac{\alpha s^2 [\omega^2 (\omega - \nu) - 4ab(a-b)]}{\gamma \nu \omega^3} \right]$$

$$u = a^2 - b^2 + s^2$$

$$\nu = \sqrt{(a+b)^2 + s^2}$$

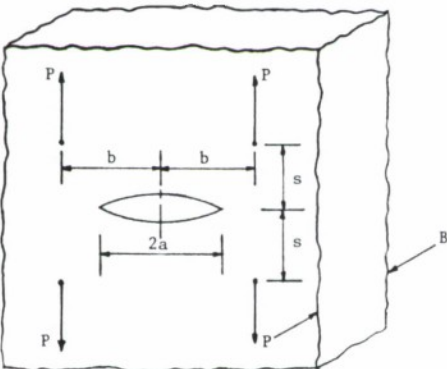
$$\omega = \sqrt{(a-b)^2 + s^2}$$

$$\gamma = \sqrt{2} \sqrt{u + \nu \omega}$$

$$\alpha = \frac{1+\nu}{2} \quad \text{Plane Stress}$$

Reference 17

1.7.1.12



INFINITE WIDTH, LOAD TO
CRACK SYMMETRICAL ABOUT

$$K = P/B \cdot \sqrt{\frac{a}{\pi}} \left[(3+\nu) I_1 - (1+\nu) I_2 \right]$$

$$I_1 = \beta / I_3$$

$$I_2 = \frac{(a^2 + b^2) s^2 + (a^2 - b^2)^2 \beta^2 + b^2 s^2 \cdot (s^2 - a^2 + b^2)}{\beta I_3^3}$$

$$I_3 = \sqrt{(s^2 + a^2 - b^2) + 4b^2 s^2}$$

$$\beta^2 = \frac{1}{2} [(s^2 + a^2 - b^2) + I_3]$$

Plane Strain Solution

Reference 56, 57, 17

1.7.2 Through-Thickness-Edge Crack Type Geometries

Table 1.7.2 presents five solutions which describe several edge cracked geometries subjected to remote and wedge type loading conditions. The geometrical configurations include both finite and semi-infinite configurations. A comparison of the three remotely loaded cases will show the reader that the solutions for the small crack in a finite width plate reduce to the form

$$K = (1.12) \sigma_{\text{LOCAL}} \sqrt{\pi a} \quad (1.7.3)$$

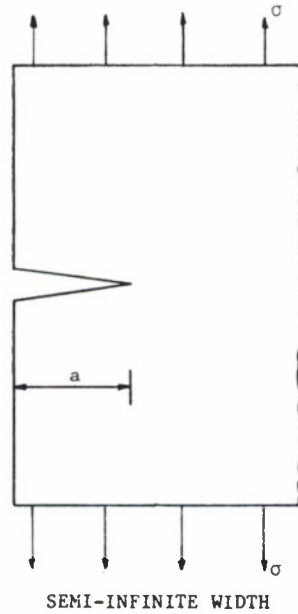
1.7.3 Through-Thickness Cracks Growing From Circular Holes

One of the more important crack geometries for an aircraft designer's point of view has received extensive study. One of the first studies was conducted by Bowie⁽⁶⁰⁾; his results are presented in Figure 1.7.3 for the cases dealing with uniaxial and biaxial remote loading of radially and diametrically cracked circular holes. The tabular results in the figure represent the values of the β factors for the various cases as a function of the crack length (a) to radius (r) ratio. Note that for the radial crack $\beta = F_1(a/r)$, while for the diametrical crack, $\beta = F_2(a/r)$. Tweed and Rooke⁽⁶¹⁾ conducted a later study that improved the accuracy of the solution in the small crack region. Others, such as Brussat⁽⁶²⁾, Newman⁽⁶³⁾, Hall et al.⁽⁶⁴⁾, Shah⁽⁶⁵⁾ and Grandt⁽⁴⁵⁾ have considered cracked circular hole problems associated with pin loading and cold-working effects. The solutions to the geometrical configurations and loading conditions considered are summarized in Table 1.7.3. The text below further defines the solutions presented in this table.

TABLE 1.7.2
STRESS-INTENSITY FACTORS FOR CRACKS STARTING
AT THE EDGE OF A STRUCTURE

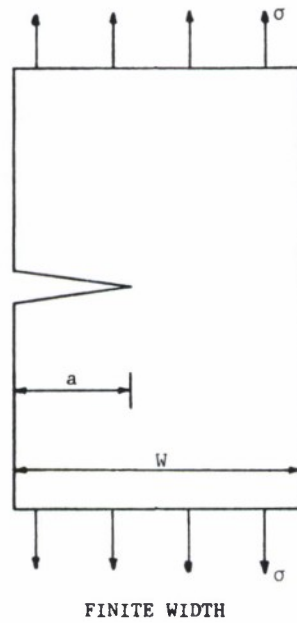
CASE NO.	REMOTELY LOADED AND EDGE CRACKED GEOMETRIES	STRESS-INTENSITY FACTOR
----------	--	-------------------------

1.7.2.1



$$K = 1.12 \sigma \sqrt{\pi a}$$

1.7.2.2



$$K = \sigma \beta \sqrt{\pi a}$$

$$\beta = 1.12 - 0.23 \left(\frac{a}{W}\right) + 10.6 \left(\frac{a}{W}\right)^2$$

$$- 21.7 \left(\frac{a}{W}\right)^3 + 30.4 \left(\frac{a}{W}\right)^4$$

$$\frac{a}{W} \leq 0.6$$

Reference 58

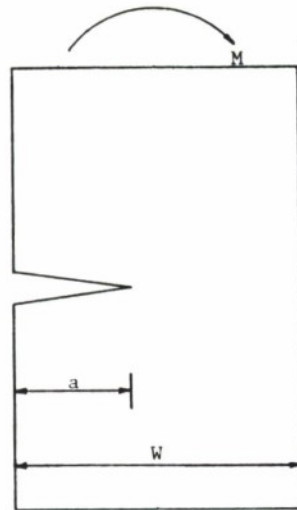
TABLE 1.7.2 (Continued)

CASE NO.

EDGE CRACKED GEOMETRY
AND LOADING

STRESS-INTENSITY FACTOR

1.7.2.3



FINITE-WIDTH IN BENDING

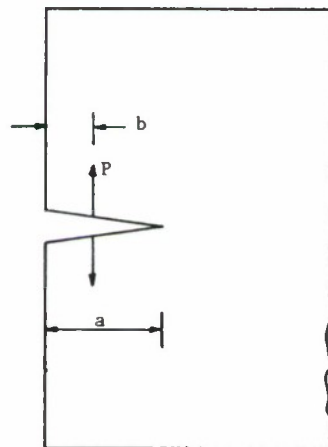
$$K = \frac{6(M/B)\sqrt{\pi a}}{W^2} \cdot \beta$$

$$\beta = 1.12 - 1.39 \left(\frac{a}{W}\right) + 7.32 \left(\frac{a}{W}\right)^2 \\ - 13.1 \left(\frac{a}{W}\right)^3 + 14.0 \left(\frac{a}{W}\right)^4;$$

$$\frac{a}{W} \leq 0.6$$

Reference 58

1.7.2.4



POINT LOADING ON EDGE CRACK
IN SEMI-INFINITE PLATE

$$K = \frac{2}{\pi} \frac{1+F\left(\frac{b}{a}\right)}{\sqrt{a^2-b^2}} \frac{P\sqrt{\pi a}}{B}$$

$$F\left(\frac{b}{a}\right) = \left(1 - \left(\frac{b}{a}\right)^2\right) \left[0.2945 - 0.3912 \left(\frac{b}{a}\right)^2 \right. \\ \left. + 0.7685 \left(\frac{b}{a}\right)^4 - 0.9942 \left(\frac{b}{a}\right)^6 \right. \\ \left. + 0.5094 \left(\frac{b}{a}\right)^8 \right]$$

References 59, 16

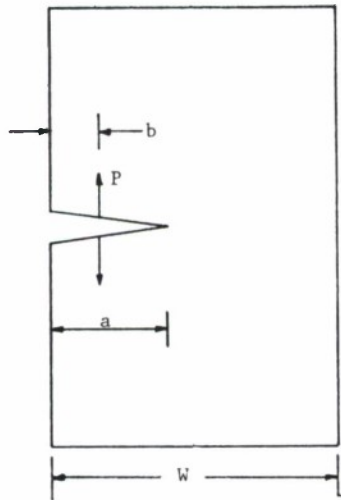
$$K = \frac{P}{B} \cdot \sqrt{\frac{2}{\pi(a-b)}} \cdot \left[1 + 0.6147 \left(1 - \frac{b}{a}\right) \right. \\ \left. + 0.2502 \left(1 - \frac{b}{a}\right)^2 \right]$$

Reference 20

TABLE 1.7.2 (Concluded)

CASE NO.	EDGE CRACKED GEOMETRY AND LOADING	STRESS-INTENSITY FACTOR
----------	--------------------------------------	-------------------------

1.7.2.5



POINT LOADING ON EDGE CRACK
IN FINITE WIDTH PLATE

$$K = \frac{P}{B} \cdot \sqrt{\frac{2}{\pi(a-b)}} \left[1 + m_1 \left(1 - \frac{b}{a}\right) + m_2 \left(1 - \frac{b}{a}\right)^2 \right]$$

Where $a < 0.5W$ and

$$m_1 = 0.6147 + 17.1844 \left(\frac{a}{W}\right)^2 + 8.7822 \left(\frac{a}{W}\right)^6$$

$$m_2 = 0.2502 + 3.2899 \left(\frac{a}{W}\right)^2 + 70.0444 \left(\frac{a}{W}\right)^6$$

Reference 43

1.7.3.1 Remotely Loaded, Radially Cracked Hole

At least three regression equations have been developed to describe the results from the Bowie or Tweed and Rooke studies for the remotely and uniaxially loaded hole with a radial crack. These results are presented below in the format of Table 1.7.3, Case 1.7.3.1. Grandt's approximation⁽⁴⁵⁾ of the Bowie solution is given by

$$F_1\left(\frac{a}{r}\right) = \frac{0.8734}{(0.3246 + \frac{a}{r})} + 0.6762 \quad (1.7.4)$$

Newman's approximation⁽⁶³⁾ of the Bowie solution is given by

$$F_1\left(\frac{a}{r}\right) = 0.707 - 0.18\lambda + 6.55\lambda^2 - 10.54\lambda^3 + 6.85\lambda^4 \quad (1.7.5a)$$

where

$$\lambda = \frac{1}{1 + \left(\frac{a}{r}\right)} \quad (1.7.5b)$$

Brussat's approximation⁽⁶²⁾ which agrees with the Tweed and Rooke solution to within one percent is given by

$$F_1\left(\frac{a}{r}\right) = \exp \left(1.2133 - 2.205 \left(\frac{a}{a+r} \right) + 0.6451 \left(\frac{a}{a+r} \right)^2 \right) \quad (1.7.6)$$

These three β factors are compared to the corresponding Bowie factor in Table 1.7.3A. It can be noted that all the results presented are close to one another (Equations 1.7.4 and 1.7.6 differ by less than two percent over the (a/r) range from 0.1 to 10).

1.7.3.2 Remotely Loaded, Diametrically Cracked Hole

Two regression equations have been developed to describe the Bowie solution for the remotely and axially loaded hole with diametric type cracks. These results are presented below in the format of Table 1.7.3, Case 1.7.3.2.

Grandt's approximation⁽⁴⁵⁾ of the Bowie solution is given by

$$F_2\left(\frac{a}{r}\right) = \frac{0.6866}{(0.2772 + \frac{a}{r})} + 0.9439 \quad (1.7.7)$$

and Newman's approximation of the same solution is given by

$$F_2\left(\frac{a}{r}\right) = 1 - 0.15\lambda + 3.46\lambda^2 - 4.47\lambda^3 + 3.52\lambda^4 \quad (1.7.8a)$$

where

$$\lambda = \frac{1}{1 + \left(\frac{a}{r}\right)} \quad (1.7.8b)$$

These two solutions are compared to the corresponding Bowie factor in Table 1.7.3B. Again the results are noted to be close to one another.

1.7.3.3 Pin Loaded Holes

For cracks at pin loaded holes, Hall et al.⁽⁶⁴⁾ Shah⁽⁶⁵⁾, Newman⁽⁶³⁾, and Brussat⁽⁶²⁾ have provided several solutions that describe the impact of the localized load on the stress intensity factor as the crack(s) grow from the edge of the hole. The fully loaded hole with a radial crack type as described by Case 1.7.3.3 was analyzed by Brussat⁽⁶²⁾. The results are presented in Table 1.7.3.

For the radially cracked, pin loaded hole with a balancing remote stress (Case 1.7.3.4), Shah provided a solution for an infinitely wide structure; his results are presented in the form of bearing stress (load ÷ thickness and hole diameter), i.e.,

$$K = \frac{P}{2rB} \sqrt{\pi a} \beta_{PR} \left(\frac{a}{r}\right) \quad (1.7.9)$$

where β_{PR} is given in Figure 1.7.4. Newman utilized the method of superposition approach described in paragraph 1.6.2 as applied to the problem in Figure 1.6.9, and obtained a solution for the finite width plate:

$$K = \frac{P}{2rB} \sqrt{\pi a} \cdot f_w \cdot F_1 \cdot f_h \cdot G_1 \quad (1.7.10)$$

where F_1 was given by Equation 1.7.5, where

$$f_w = \sqrt{\sec\left(\frac{\pi}{2} \cdot \frac{2r+a}{W-a}\right)} , \quad (1.7.11a)$$

$$f_h = \sqrt{\sec \frac{\pi r}{W}} , \text{ and} \quad (1.7.11b)$$

$$G_1 = \frac{r}{W} + \frac{1}{\pi} \left[\frac{r}{r + \frac{a}{2}} \right] \sqrt{\frac{1}{1 + \frac{a}{r}}} \quad (1.7.11c)$$

and where through comparison with Equations 1.7.9 and 1.7.10 β_{PR} is found to be

$$\beta_{PR} = f_w \cdot F_1 \cdot f_h \cdot G_1 \quad (1.7.12)$$

For the case of a wide plate ($W \rightarrow \infty$), f_w and f_h are approximately 1.0 and β_{PR} is then

$$\beta_{PR} \cong F_1 \cdot \left[\frac{1}{\pi} \left(\frac{r}{r + \frac{a}{2}} \right) \sqrt{\frac{1}{1 + \frac{a}{r}}} \right] \quad (1.7.13)$$

Using Brussat's results given for Case 1.7.3.2 and the method of superposition, an alternate stress-intensity factor solution for the radially cracked hole with pin loading can be derived for the wide plate. The resulting β_{PR} is given by

$$\beta_{PR} = \frac{r}{\pi \sqrt{a(r + \frac{a}{2})}} \sqrt{\frac{1}{1 + \frac{a}{r}}} \cdot F_1 \cdot \phi_2 \quad (1.7.14)$$

where F_1 is given by Equation 1.7.6 and ϕ_2 is given by

$$\phi_2 = \exp \left(0.15 \left(\left(\frac{a}{a + r} \right)^2 - 1 \right) \right) \quad (1.7.15)$$

The β_{PR} factors from Figure 1.7.4 and from Equations 1.7.13 and 1.7.14 are compared in Table 1.7.3C. It appears that the Newman method of superposition and the Shah results are similar for short cracks and that both method of superposition type solutions underestimate the Shah results for long cracks.

For the pin loaded holes that are diametrically cracked (Case 1.7.3.5) there are two known solutions. The Shah numerical solution is presented in the form of the bearing stress (load ÷ thickness and diameter), i.e.,

$$K = \frac{P}{2rB} \sqrt{\pi a} \cdot \beta_{PD} \left(\frac{a}{r} \right) \quad (1.7.16)$$

where $\beta_{PD} \left(\frac{a}{r}\right)$ is given in Figure 1.7.5. The Newman solution based on the method of superposition is

$$K = \frac{P}{2rB} \sqrt{\pi a} [f_w \cdot F_2 \cdot f_h \cdot G_2] \quad (1.7.17)$$

where F_2 was given by Equation 1.7.8, where

$$f_w = \sqrt{\sec\left(\pi \cdot \left(\frac{r+a}{W}\right)\right)}, \quad (1.7.18a)$$

$$f_h = \sqrt{\sec \frac{\pi r}{W}}, \text{ and} \quad (1.7.18b)$$

$$G_2 = \frac{r}{W} + \frac{1}{\pi} \left[\frac{1}{1 + \frac{a}{r}} \right] \quad (1.7.18c)$$

and where comparison between Equations 1.7.16 and 1.7.17 shows that

$$\beta_{PD} = f_w \cdot F_2 \cdot f_h \cdot G_2 \quad (1.7.19)$$

For the case of the wide plate ($W \rightarrow \infty$), the Newman solution is seen to reduce to

$$\beta_{PD} = F_2 \left(\frac{1}{\pi} \frac{1}{\left(1 + \frac{a}{r}\right)} \right) \quad (1.7.20)$$

The β factors given in Figure 1.7.5 and by Equation 1.7.20 are compared in Table 1.7.3D. The two factors are reasonably close for small crack lengths; the Newman solution underestimates the Shah solution for long crack lengths.

TABLE 1.7.3

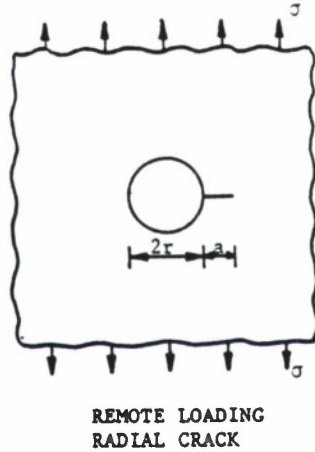
STRESS-INTENSITY FACTORS FOR CIRCULAR HOLES
WITH THROUGH-THICKNESS HOLES

CASE NO.

GEOMETRY AND LOADING

STRESS-INTENSITY FACTOR

1.7.3.1

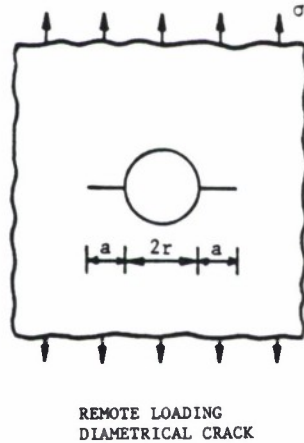


$$K = \sigma \sqrt{\pi a \beta}$$

where

$\beta = F_1 \left(\frac{a}{r} \right)$ as defined by Equations 1.7.4, 1.7.5, or 1.7.6 which are compared in Table 1.7.3A to the Bowie $F_1 \left(\frac{a}{r} \right)$

1.7.3.2

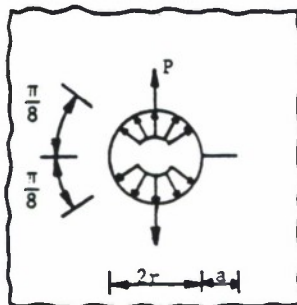


$$K = \sigma \sqrt{\pi a \beta}$$

where

$\beta = F_2 \left(\frac{a}{r} \right)$ as defined by Equations 1.7.7 or 1.7.8 which are compared in Table 1.7.3B to the Bowie $F_2 \left(\frac{a}{r} \right)$

1.7.3.3



$$K = \frac{P}{B \sqrt{\pi \left(r + \frac{a}{r} \right)}} \sqrt{\frac{1}{1 + \frac{a}{r}}} \cdot F_1 \cdot \phi_2$$

where $F_1 \left(\frac{a}{r} \right)$ is given by Equation 1.7.6

and

$$\phi_2 = \exp \left(0.15 \left(\left(\frac{a}{a+r} \right)^2 - 1 \right) \right)$$

and B = thickness

Reference 62

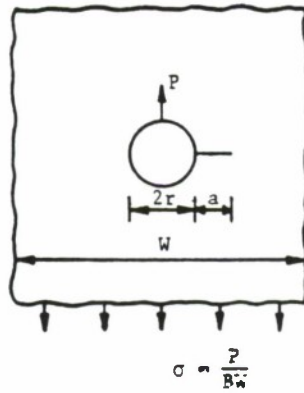
TABLE 1.7.3 (Concluded)

CASE NO.

GEOMETRY AND LOADING

STRESS-INTENSITY FACTOR

1.7.3.4



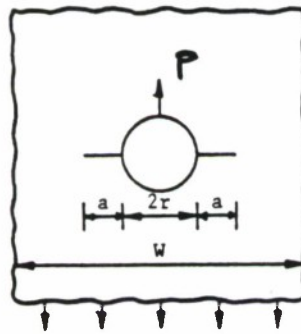
PIN LOADING
RADIAL CRACK

$$K = \frac{P}{2rB} \sqrt{\pi a} \beta$$

where

$\beta = \beta_{PR} \left(\frac{a}{r} \right)$ as defined by Figure 1.7.4, Equation 1.7.12, or Equation 1.7.14, which are compared in Table 1.7.3C for $W \rightarrow \infty$.

1.7.3.5



PIN LOADING
DIAMETRICAL CRACK

$$K = \frac{P}{2rB} \sqrt{\pi a} \beta$$

where

$\beta = \beta_{PD} \left(\frac{a}{r} \right)$ as defined by Figure 1.7.5 or Equation 1.7.19 which are compared in Table 1.7.3D for $W \rightarrow \infty$.

TABLE 1.7.3A
COMPARISON OF β FACTORS FOR THROUGH-THICKNESS,
RADIALY CRACKED AND REMOTELY LOADED HOLE CRACKS

$\frac{a}{r}$	β_{BOWIE}	β_{GRANDT}	β_{BRUSSAT}	β_{NEWMAN}
0.0	3.39	3.367	3.365	3.387
0.1	2.73	2.733	2.768	2.716
0.2	2.30	2.341	2.372	2.310
0.3	2.04	2.074	2.093	2.045
0.4	1.86	1.882	1.889	1.862
0.5	1.73	1.735	1.733	1.728
0.6	1.64	1.621	1.611	1.625
0.8	1.47	1.453	1.434	1.474
1.0	1.37	1.336	1.313	1.365
1.5	1.18	1.155	1.130	1.1838
2.0	1.06	1.052	1.030	1.069
3.0	0.94	0.939	0.925	0.933
5.0	0.81	0.840	0.838	0.815
10.0	0.75	0.761	0.772	0.737
∞	0.707	0.6762	0.707	0.707

TABLE 1.7.3B
COMPARISON OF β FACTORS FOR THROUGH-THICKNESS,
DIAMETRICALLY CRACKED AND REMOTELY LOADED HOLE CRACKS

$\frac{a}{r}$	β_{BOWIE}	β_{GRANDT}	β_{NEWMAN}
0.0	3.39	3.421	3.36
0.1	2.73	2.764	2.769
0.2	2.41	2.383	2.389
0.3	2.15	2.133	2.130
0.4	1.96	1.958	1.945
0.5	1.83	1.827	1.809
0.6	1.71	1.727	1.704
0.8	1.58	1.581	1.553
1.0	1.45	1.481	1.451
1.5	1.29	1.330	1.298
2.0	1.21	1.245	1.212
3.0	1.14	1.153	1.123
5.0	1.07	1.074	1.053
10.0	1.03	1.011	1.012
∞	1.00	0.9439	1.00

TABLE 1.7.3C
RADIALLY CRACKED-PIN LOADED HOLE ($W=\infty$)

$$K_I = \sigma_b \sqrt{\pi a} \beta_{PR} \left(\frac{a}{r} \right)$$

$\frac{a}{r}$	$\beta_{PR} \left(\frac{a}{r} \right)$ SHAH	$\beta_{PR} \left(\frac{a}{r} \right)$ NEWMAN	$\beta_{PR} \left(\frac{a}{r} \right)$ BRUSSAT
0	>1	1.078	∞
0.25	0.58	0.547	1.032
0.50	0.43	0.359	0.498
0.75	0.34	0.264	0.309
1.00	0.28	0.205	0.216
2.00	0.17	0.098	0.087
4.00	0.11	0.041	0.034

TABLE 1.7.3D
DIAMETRICALLY CRACKED-PIN LOADED HOLE ($W=\infty$)

$$K_I = \sigma_b \sqrt{\pi a} \beta_{PD} \left(\frac{a}{r} \right)$$

$\frac{a}{r}$	$\beta_{PR} \left(\frac{a}{r} \right)$ SHAH	$\beta_{PR} \left(\frac{a}{r} \right)$ NEWMAN
0	>1	1.069
0.25	0.58	0.573
0.50	0.45	0.384
0.75	0.38	0.288
1.00	0.33	0.231
2.00	0.22	0.128
4.00	0.15	0.069

1.7.4 Internal Flaws

The development of stress-intensity factors for surface flaw geometries followed the generation of the solutions for three dimensional structures containing internal cracks. For background, continuity, and potential application, the two more important cases are covered. Since the "penny shaped" or circular crack solution can be derived from the elliptical crack case, only the details of the elliptical crack solution are presented. The two cases and their results are summarized in Table 1.7.4.

Irwin⁽⁶⁶⁾ derived an exact expression for the Mode I stress-intensity factor around an elliptical crack in an infinite elastic solid subjected to uniform tension (see Figure 1.7.6 for geometry and loading). The stress-intensity factor at any point (say P) along the boundary of the elliptical crack was given by

$$K = \frac{\sigma\sqrt{\pi a}}{\Phi} \left(\left(\frac{a}{c}\right)^2 \cos^2\theta + \sin^2\theta \right)^{\frac{1}{4}} \quad (1.7.21)$$

where Φ is the complete elliptical integral of the second kind and is given by

$$\Phi = \int_0^{\pi} \sqrt{1 - \left(1 - \left(\frac{a}{c}\right)^2\right) \sin^2\phi}^{\frac{1}{2}} d\phi \quad (1.7.22)$$

Note from Figure 1.7.6 that the angle θ locates the coordinates of the point P. Rawe⁽⁶⁷⁾ and Newman⁽⁶⁸⁾ have developed some very useful empirical expressions for Φ ; these are

$$\phi^2 = \begin{cases} 1. + 1.464 \left(\frac{a}{c}\right)^{1.65} & \text{for } \frac{a}{c} \leq 1 \\ \text{or} \\ 1. + 1.464 \left(\frac{c}{a}\right)^{1.65} & \text{for } \frac{a}{c} > 1 \end{cases} \quad (1.7.23)$$

The maximum error in ϕ^2 for all values of a/c was about 0.13 percent.

For $c > a$, the maximum stress-intensity factor is at $\theta = \pi/2$ is given by

$$K = \frac{\sigma \sqrt{\pi a}}{\phi} \quad (1.7.24)$$

Later modifications to Equation 1.7.21 included the development of a plasticity correction factor which became combined with the elliptical integral ϕ . For this reason, the combined plasticity/elliptical integral factor became known as the "flaw shape" factor and was given the symbol Q . The flaw shape factor is defined by

$$Q = \phi^2 - 0.212(\sigma/\sigma_{ys})^2 \quad (1.7.25)$$

Figure 1.7.7 presents Q as a function of $a/2c$ and σ/σ_{ys} . Typically then, one finds the stress-intensity factor for an embedded elliptical flaw expressed as

$$K = \sigma \sqrt{\frac{\pi a}{Q}} \cdot \left[\left(\frac{a}{c}\right)^2 \cos^2 \theta + \sin^2 \theta \right]^{1/4} \quad (1.7.26)$$

1.7.5 Part-Through Cracks

In practice, cracks usually start as semielliptical surface flaws or as quarter-elliptical surface flaws. Therefore, stress-intensity solutions are required to deal with such flaw geometries because the damage assumptions in MIL-A-83444 concern elliptical flaws.

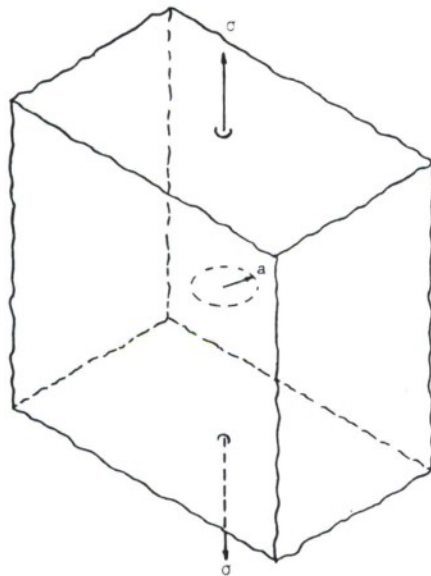
TABLE 1.7.4
STRESS-INTENSITY FACTORS FOR EMBEDDED CRACKS

CASE NO.

GEOMETRY

STRESS-INTENSITY FACTOR

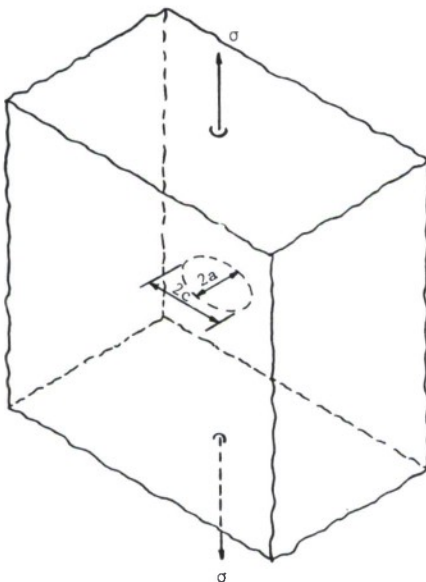
1.7.4.1



Uniformly Loaded Penny Shaped Crack

$$K = \sigma \left(\frac{2}{\pi} \right) \sqrt{\pi a}$$

1.7.4.2



Uniformly Loaded Elliptically Shaped Crack

$$K = \frac{\sigma \sqrt{\pi a}}{\phi} \cdot \left[\left(\frac{a}{c} \right)^2 \cos^2 \theta + \sin^2 \theta \right]^{\frac{1}{4}}$$

Elliptical flaws, corner flaws, and part-through flaws at stress concentration sites are difficult to analyze because the stress problem is three-dimensional in nature. The stress-intensity factor solutions presented are approximate solutions. Different solutions of the same problems may show significantly different results.

Almost all stress-intensity factor solutions for part-through cracks, whether surface flaws or corner flaws are based (or compared) on Irwin's solution⁽⁶⁶⁾ for a flat elliptical flaw in a plate in tension (see Figure 1.7.8 for geometry and loading). The solution for the stress-intensity factor at any point P on the crack boundary is given by

$$K = 1.1\sigma\sqrt{\pi a/Q} \cdot \left(\left(\frac{a}{c}\right)^2 \cos^2\theta + \sin^2\theta\right)^{\frac{1}{4}} \quad (1.7.27)$$

where Q is given by Equation 1.7.25 and the factor, 1.1, is an assumed correction for the front-free surface. Irwin's derivation assumes that the major axis of the ellipse lies along the free surface which requires $\frac{a}{c} \leq 1$. It is obvious from Equation 1.7.27 that a semi-circular surface flaw ($\frac{a}{c} = 1$) has a constant stress-intensity factor around the crack front. The maximum stress intensity occurs at the end of the minor axis ($\theta = 90^\circ$) and the minimum occurs at the end of the major axis ($\theta = 0^\circ$). Strictly speaking the equation is invalid due to localized edge effects at $\theta = 0^\circ$. Equation 1.7.27 will form the basis for presenting a number of the part-through crack stress-intensity factors.

It is also possible to derive a β such that Equation 1.7.27 may be written in the form of Equation 1.7.1. It is more common, however, to use the form

$$K = \sigma \sqrt{\frac{\pi a}{Q}} M_1 \left[\left(\frac{a}{c}\right)^2 \cos^2 \theta + \sin^2 \theta \right]^{\frac{1}{2}} \quad (1.7.28)$$

where M_1 are various correction factors for geometry and loadings. These correction factors typically multiply in the same manner as the β factors. Table 1.7.5 provides some useful stress intensity factor cases.

1.7.6 Corner Cracks At The Edge of a Plate

A corner crack can be considered as a quarter-elliptical crack and its stress intensity can be described using an equation somewhat similar to Equation 1.7.28. A number of investigators have considered the case where the crack is quarter circular in shape, i.e., $a = c$ (see References 72 through 76). The results from several solutions are compared in Figure 1.7.11 as a function of the angle θ . As can be seen from the available solutions, the maximum stress intensity factor occurs at the free edges. Newman and Rajus⁽⁷²⁾ solution for the more general case of a quarter elliptical crack geometry is given in Table 1.7.6 by

$$K = \frac{\sigma \sqrt{\pi a}}{\sqrt{2}} \cdot F_c \left(\frac{a}{c}, \frac{a}{B}, \theta \right) \quad (1.7.29)$$

The authors developed the solution from finite element results that considered the ranges $0.2 \leq a/c \leq 2$, $a/B < 1$, and $0 \leq \theta \leq 90^\circ$ for

TABLE 1.7.5
STRESS-INTENSITY FACTOR SOLUTIONS FOR SURFACE
(SEMI-ELLIPTICAL) CRACK GEOMETRIES

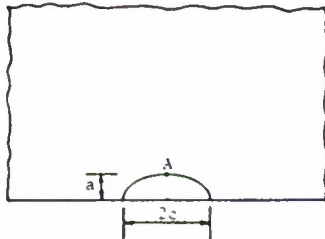
CASE NO.

GEOMETRY

STRESS-INTENSITY FACTOR

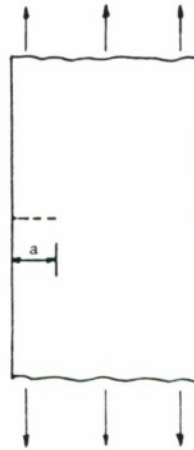
1.7.5.1

Cross-Section



SEMI-ELLIPTICAL CRACK IN SEMI-INFINITE PLATE

Side View
& Loading

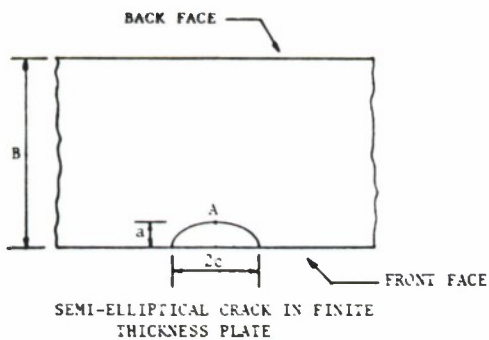


UNIFORM
UNIAXIAL
TENSION

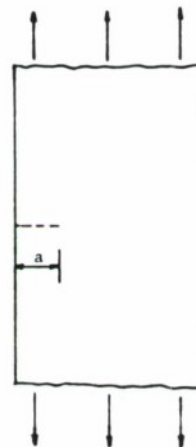
$$K_A = 1.1 \sigma \sqrt{\frac{\pi a}{Q}}$$

See Table 1.7.5A for cases of different $a/2c$ ratios.

1.7.5.2



SEMI-ELLIPTICAL CRACK IN FINITE THICKNESS PLATE



UNIFORM
UNIAXIAL
TENSION

$$K_A = \sigma \sqrt{\frac{\pi a}{Q}} \cdot M_F \cdot M_K$$

where the front face correction M_F is

$$M_F = 1.0 + 0.12 \left(1 - \frac{a}{2c}\right)^2$$

Reference 69, and the back face correction M_K is presented in Table 1.7.5B

References 70, 71

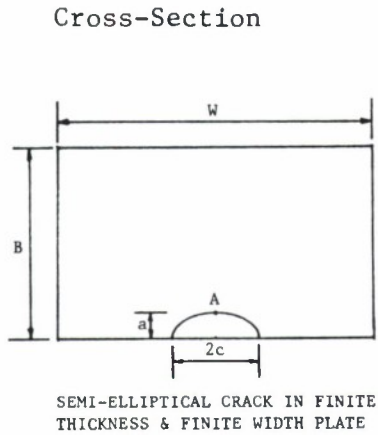
TABLE 1.7.5 (Concluded)

CASE NO.

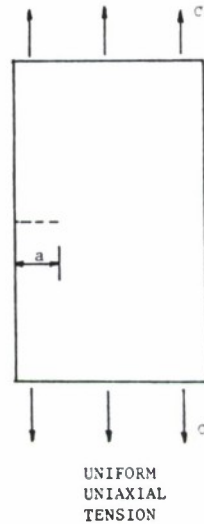
GEOMETRY

STRESS-INTENSITY FACTOR

1.7.5.3



Side View
& Loading



$$K_A = \sigma \sqrt{\frac{\pi a}{Q}} \cdot M_F \cdot M_K \cdot M_W$$

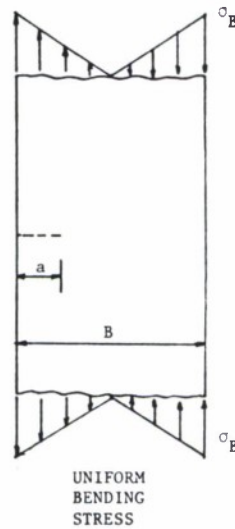
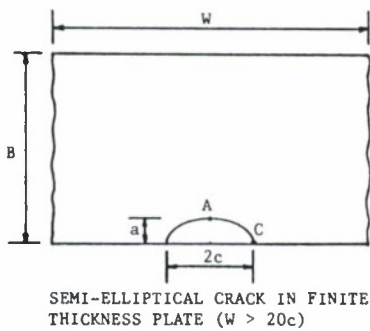
where M_F and M_K are as defined in Case 1.7.5.2 and M_W is

$$M_W = \sqrt{\sec \frac{\pi c}{W}}$$

Also see Table 1.7.5C

Reference 72

1.7.5.4



$$K_A = \sigma_B \sqrt{\frac{\pi a}{Q}} \cdot M_{B0}$$

$$K_C = \sigma_B \sqrt{\frac{\pi a}{Q}} \cdot M_{B90}$$

where

$$\sigma_B = \frac{MB}{2I} = \frac{6M}{WB^2}$$

M_{B0} is presented in Figure 1.7.9, and M_{B90} is presented in Figure 1.7.10.

M_{B0} and M_{B90} include the effect of thickness

Reference 64

TABLE 1.7.5A
STRESS INTENSITY CHARACTERISTIC FOR SURFACE (SEMI-ELLIPTICAL)
FLAW IN SEMI-INFINITE PLATE

DEPTH/SURFACE LENGTH (a/2c)	GEOMETRY	STRESS-INTENSITY FACTOR
0.0 (long, shallow)		$K_I = 1.1 \sigma \sqrt{\pi a}$
0.125		$K_I = 1.03 \sigma \sqrt{\pi a}$
0.25		$K_I = 0.91 \sigma \sqrt{\pi a}$
0.375		$K_I = 0.80 \sigma \sqrt{\pi a}$
0.5 (semi-circular)		$K_I = 0.70 \sigma \sqrt{\pi a}$

TABLE 1.7.5B
BACK SURFACE CORRECTION FACTOR (70,71)

a/B	a/2c					
	0.05	0.10	0.20	0.30	0.40	0.50
	M_K					
0.0	1.00	1.00	1.00	1.00	1.00	1.00
0.1	1.01	1.01	1.01	1.01	1.01	1.00
0.2	1.03	1.03	1.02	1.02	1.01	1.00
0.3	1.06	1.06	1.04	1.03	1.02	1.00
0.4	1.12	1.12	1.08	1.05	1.02	1.00
0.5	1.22	1.18	1.14	1.08	1.03	1.01
0.6	1.34	1.30	1.22	1.13	1.06	1.01
0.7	1.48	1.42	1.31	1.20	1.08	1.02
0.8	1.64	1.57	1.41	1.26	1.13	1.04
0.9	1.77	1.68	1.50	1.32	1.18	1.08
1.0	1.84	1.75	1.59	1.38	1.22	1.10

TABLE 1.7.5C
NEWMAN AND RAJU⁽⁷²⁾ SOLUTION (1981) FOR SURFACE FLAW CASE 1.7.5.3

$$K_I = \frac{\sigma\sqrt{\pi a}}{\Phi} F_S \left(\frac{a}{c}, \frac{a}{B}, \frac{c}{W}, \theta \right)$$

valid within the ranges of:

$$0 \leq \frac{a}{c} \leq 2, \frac{c}{W} < \frac{1}{4}, 0 \leq \theta \leq \pi, \text{ and}$$

$$\frac{a}{B} \leq 1.25 \left(\frac{a}{c} + 0.6 \right) \text{ for } 0 \leq \frac{a}{c} \leq 0.2$$

$$\frac{a}{B} < 1 \quad \text{for } 0.2 \leq \frac{a}{c} \leq \infty$$

Φ is defined by Equation 1.7.23 and

$$F_S \left(\frac{a}{c}, \frac{a}{B}, \frac{c}{W}, \theta \right) = \left[M_1 + M_2 \left(\frac{a}{B} \right)^2 + M_3 \left(\frac{a}{B} \right)^4 \right] \cdot g \cdot f_\phi \cdot f_w$$

where $f_w = \sqrt{\sec \left(\frac{\pi c}{W} \sqrt{\frac{a}{B}} \right)}$ and the other factors are defined as a function of $\frac{a}{c}$ below

	for $a/c \leq 1$	for $a/c > 1$
M_1	$1.13 - 0.09 \left(\frac{a}{c} \right)$	$\sqrt{\frac{c}{a}} (1 + 0.04 \frac{c}{a})$
M_2	$-0.54 + \frac{0.89}{(0.2 + \frac{a}{c})}$	$0.2 \left(\frac{c}{a} \right)^4$
M_3	$0.5 - \frac{1}{0.65 + \frac{a}{c}} + 14 \left(1 - \frac{a}{c} \right)^{24}$	$-0.11 \left(\frac{c}{a} \right)^4$
g	$1 + \left[0.1 + 0.35 \left(\frac{a}{B} \right)^2 \right] (1 - \sin \theta)^2$	$1 + \left[0.1 + 0.35 \left(\frac{c}{a} \right) \left(\frac{a}{B} \right)^2 \right] (1 - \sin \theta)^2$
f_ϕ	$\left[\left(\frac{a}{c} \right)^2 \cos^2 \theta + \sin^2 \theta \right]^{\frac{1}{4}}$	$\left[\left(\frac{c}{a} \right)^2 \sin^2 \theta + \cos^2 \theta \right]^{\frac{1}{4}}$

$c/B < 0.2$. The function F_c was chosen as

$$F_c = [M_1 + M_2 \left(\frac{a}{B}\right)^2 + M_3 \left(\frac{a}{B}\right)^4] g_1 g_2 f_\theta \quad (1.7.30)$$

The parameters M_1 , M_2 , M_3 , g_1 , g_2 , and f_θ are presented in Table 1.7.6A for $a/c \leq 1$ and $a/c > 1$.

1.7.7 Corner Cracks at the Edge of a Hole

The military specifications require that a designer shall assume that a quarter-circular crack exists at the edge of all holes in a safety-of-flight critical structure. For primary damage sites, the crack size is 0.050 inch (for safe crack growth structure), while for secondary damage sites, the crack size is 0.005 inch. As a result of this fundamental assumption, a great deal of attention has been given to developing solutions for corner cracks at the edge of a hole.

1.7.7.1 Radial Corner Cracks

One of the simplest solutions for the corner crack problem described by Figure 1.7.12 was developed by Liu⁽⁷³⁾; he derived his equation based on a compounding analysis of a quarter-circular crack, i.e., $a = c$

$$K = 1.12 \times \frac{2\sigma}{\pi} \sqrt{\pi a} \cdot f_B \left(\frac{a_e}{r}\right) \quad (1.7.31)$$

where $a_e = a/\sqrt{2}$, and $f_B \left(\frac{a}{r}\right)$ was given by Equation 1.7.4. Hall and Finger⁽⁷⁷⁾ derived an empirical expression based on an analysis of

TABLE 1.7.6

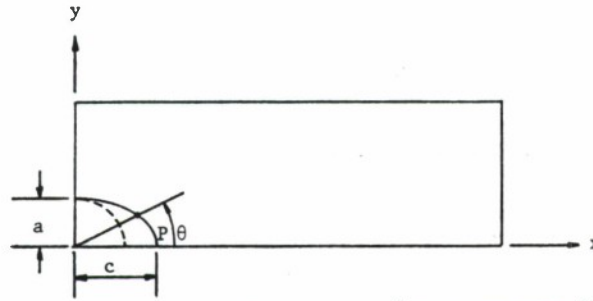
QUARTER-ELLIPTICAL STRESS-INTENSITY FACTOR
SOLUTIONS SUBJECTED TO TENSILE LOADING

CASE NO.

GEOMETRY

SOLUTION

1.7.6.1

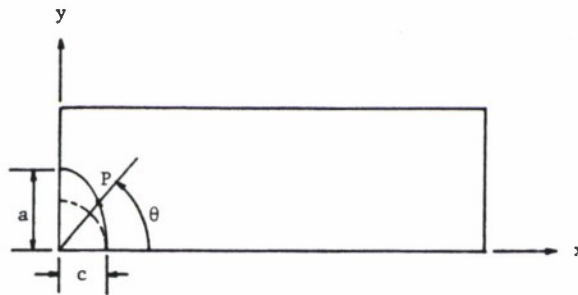


$$\frac{a}{c} \leq 1 \quad P \begin{cases} x = c \cos \theta \\ y = a \sin \theta \end{cases}$$

$$K_p = \frac{\sigma \sqrt{\pi a}}{\phi} \cdot F_c$$

where F_c is given
by Equation
1.7.30 and
Table 1.7.6A.

1.7.6.2



$$\frac{a}{c} > 1 \quad P \begin{cases} x = c \cos \theta \\ y = a \sin \theta \end{cases}$$

$$K_p = \frac{\sigma \sqrt{\pi a}}{\phi} \cdot F_c$$

where F_c is given
by Equation
1.7.30 and
Table 1.7.6A.

TABLE 1.7.6A
PARAMETERS OF QUARTER-ELLIPTICAL STRESS-INTENSITY
FACTOR SOLUTION PRESENTED

$$F_c = \left[M_1 + M_2 \left(\frac{a}{B} \right)^2 + M_3 \left(\frac{a}{B} \right)^4 \right] g_1 \cdot g_2 \cdot f_\phi$$

Parameter	$\frac{a}{c} \leq 1$	$\frac{a}{c} > 1$
M_1	$1.08 - 0.03 \left(\frac{a}{c} \right)$	$\sqrt{\frac{c}{a}} (1.08 - 0.03 \left(\frac{c}{a} \right))$
M_2	$-0.44 + \frac{1.06}{0.3 + \frac{a}{c}}$	$0.375 \left(\frac{c}{a} \right)^2$
M_3	$-0.5 + 0.25 \left(\frac{a}{c} \right) + 14.8 \left(1 - \frac{a}{c} \right)^{15}$	$-0.25 \left(\frac{c}{a} \right)^2$
g_1	$1 + \left[0.08 + 0.4 \left(\frac{a}{B} \right)^2 \right] (1 - \sin \theta)^3$	$1 + \left[0.08 + 0.4 \left(\frac{c}{B} \right)^2 \right] \cdot (1 - \sin \theta)^3$
g_2	$1 + \left[0.08 + 0.15 \left(\frac{a}{B} \right)^2 \right] (1 - \cos \theta)^3$	$1 + \left[0.08 + 0.15 \left(\frac{c}{B} \right)^2 \right] \cdot (1 - \cos \theta)^3$
f_ϕ	$\left[\left(\frac{a}{c} \right)^2 \cos^2 \theta + \sin^2 \theta \right]^{\frac{1}{4}}$	$\left[\left(\frac{c}{a} \right)^2 \sin^2 \theta + \cos^2 \theta \right]^{\frac{1}{4}}$

residual strength data collected using quarter-circular cracked hole specimens:

$$K = 0.87 \sigma \sqrt{\pi a_e^*} \cdot f_B \left(\frac{a_e^*}{B} \right) \quad (1.7.32)$$

In Equation 1.7.32, a_e^* represents an effective crack size that can be found from the empirical curves given in Figure 1.7.13.

Additional work on the quarter elliptical radial (corner) crack has been conducted by a number of other investigators: Hall et al.⁽⁶⁴⁾, Shah⁽⁶⁵⁾, Hsu and Liu⁽⁷⁸⁾, Hsu and Rudd⁽⁴¹⁾, Smith and Kullgren⁽⁷⁹⁾, Fujimoto⁽⁸⁰⁾, Rudd et al.⁽⁸¹⁾, Newman and Raju⁽⁷²⁾, and Grandt and Kullgren^(82,83). Because none of the results are exact and the solutions give stress intensity factors within 10 percent of each other, the Newman and Raju solution will be presented since it is the easiest to develop (see Table 1.7.7). Results developed by Fujimoto⁽⁸⁰⁾ who used the slice synthesis model to obtain solutions for radial corner and embedded bore type cracks are presented in Chapter 4 (see Example 4.3.2).

1.7.7.2 Diametrical Corner Cracks

A number of investigators have given attention to the crack problem where a hole contains corner cracks on diametrically opposite sides of the hole. These investigators include Hall et al.⁽⁶⁴⁾, Shah⁽⁶⁵⁾, Grandt and Kullgren^(82,83), Rudd et al.⁽⁸¹⁾, and Newman and Raju⁽⁷²⁾. Because, like the radial hole crack solutions, there is no

exact solution, only Newman and Rajus'⁽⁷²⁾ solution will be presented. (See Table 1.7.7.) Some observations by Shah and coworkers and by Rudd et al. are also worth mentioning.

Shah specifically noted that one could derive the stress-intensity factor for diametrically corner cracked holes using an approach that employed (1) a Green's Function based on a through-thickness, wedge force loading of a center-cracked geometry and (2) correction factors associated with solutions for semi-elliptical crack geometries. The Green's Function technique was utilized to evaluate the influence of various loading conditions through the analysis of the stresses associated with the individual loadings applied to the uncracked structure. Through his analysis, Shah determined that the results obtained from the Green's Function technique could be applied independent of the semi-elliptical crack geometry, i.e., the a/c ratio. The implication of Shah's work is that the stress-intensity factor (K_{DCC}) for the diametrical corner crack can be given by:

$$K_{DCC} = F_5 \cdot \sigma \sqrt{\pi a/Q} [\cos^2 \beta + (\frac{a}{c})^2 \sin^2 \beta]^{1/4} \text{ if } a/c \leq 1.0 \quad (1.7.33)$$

$$K_{DCC} = F_5 \cdot \sigma \sqrt{\pi a/Q} [\sin^2 \beta + (\frac{c}{a})^2 \cos^2 \beta]^{1/4} \text{ if } a/c > 1.0$$

where F_5 is the function that describes the effects of hole geometry, crack length, and loading conditions, but not crack geometry, i.e., not a/c . Shah's assumption facilitates the development of additional

stress-intensity factors for corner crack geometries. The method of approach is to use a known corner crack solution (say K_{DCC}^*) with its associated through-thickness crack solution (say K_S^*) and a through thickness crack solution for any other loading (say K_{other}) to generate the corner crack solution for this type of loading:

$$K_{DCC} = K_{other} \cdot \frac{K_{DCC}^*}{K_S^*} \quad (1.7.34)$$

Rudd et. al. used a similar approach to that taken by Shah; they utilized a more accurate Green's Function which accounted for the hole geometry.

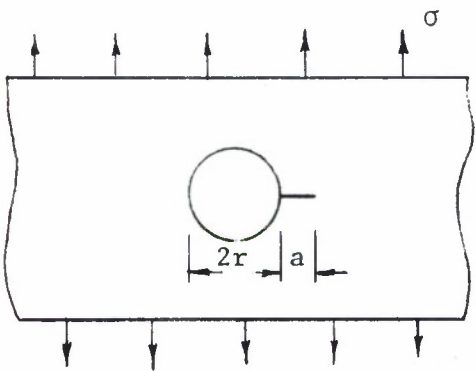
The other important observation that Shah and coworkers made is related to generating stress-intensity factor solutions for radial crack geometries from solutions for diametrical crack geometries. The expression for relating these two hole crack geometry solutions for a hole with radius r is:

$$K \Big|_{\substack{\text{one} \\ \text{crack}}} = \sqrt{\frac{2r + a}{2r + 2a}} \cdot K \Big|_{\substack{\text{two} \\ \text{cracks}}} \quad (1.7.35)$$

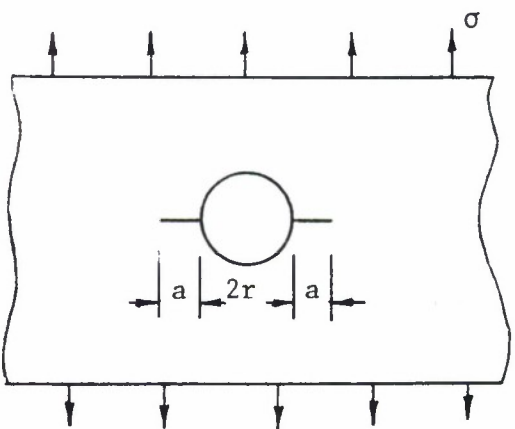
When the comparison was based on the Bowie solutions to the hole problems, Equation 1.7.35 was shown to produce estimates that were within 2 percent for $0.05 \leq a/r \leq \infty$.

TABLE 1.7.7
STRESS-INTENSITY FACTORS FOR
CORNER CRACKS AT HOLES

CASE NO.	CRACK GEOMETRY AND LOADING	STRESS-INTENSITY FACTOR
----------	-------------------------------	----------------------------

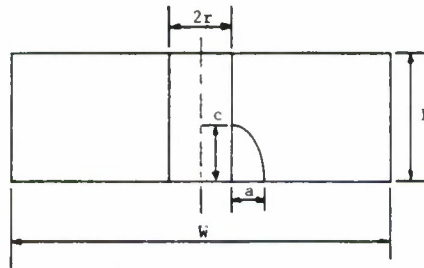
1.7.7.1	 <p>The diagram shows a rectangular plate with wavy edges. In the center is a circular hole with a horizontal line extending to the right, representing a crack. Below the hole, dimension lines indicate the hole's diameter as $2r$ and the crack's length as a. Above the plate, five upward-pointing arrows are shown, and below the plate, five downward-pointing arrows are shown, representing uniform remote loading σ.</p>	SEE TABLE 1.7.7A
---------	--	------------------

RADIALLY CORNER CRACKED
HOLE UNDER UNIFORM REMOTE
LOADING

1.7.7.2	 <p>The diagram shows a rectangular plate with wavy edges. In the center is a circular hole with a horizontal line passing through its center, representing a diametrically corner crack. Below the hole, dimension lines indicate the hole's diameter as $2r$ and the crack's length on each side as a. Above the plate, five upward-pointing arrows are shown, and below the plate, five downward-pointing arrows are shown, representing uniform remote loading σ.</p>	SEE TABLE 1.7.7B
---------	--	------------------

DIAMETRICALLY CORNER CRACKED
HOLE UNDER UNIFORM REMOTE
LOADING

TABLE 1.7.7A
NEWMAN AND RAJU SOLUTION FOR
RADIAL CORNER CRACK
(Reference 72)



$$K = \frac{\sigma \sqrt{\pi c}}{\phi} \cdot [M_1 + M_2 \left(\frac{c}{B}\right)^2 + M_3 \left(\frac{c}{B}\right)^4] g_1 \cdot g_2 \cdot g_3 \cdot f_\theta \cdot f_W \cdot f_c$$

for $0.2 \leq c/a \leq 2$, $c/B < 1$, $0.5 \leq r/B \leq 1$, $2(r + a)/W < 0.5$
and $0 \leq \theta \leq 90^\circ$ [W = 2b]

$$f_c = \sqrt{\frac{4 + \frac{\pi a c}{2 B r}}{4 + \frac{\pi a c}{B r}}}$$

$$f_W = \left[\sec \left(\frac{\pi r}{W} \right) \sec \left(\frac{\pi (2r + a)}{4 (0.5 W - a) + 2a} \sqrt{\frac{c}{B}} \right) \right]^{1/2}$$

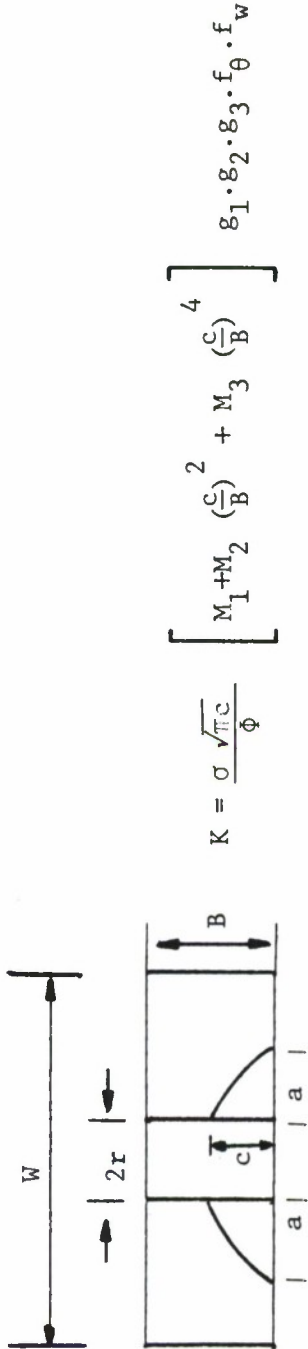
Parameter	$c/a \leq 1$	$c/a > 1$
M_1	$1.13 - 0.09 \left(\frac{c}{a}\right)$	$\sqrt{\frac{a}{c}} (1 + 0.04 \frac{a}{c})$
M_2	$-0.54 + \frac{0.89}{(0.2 + c/a)}$	$0.2 \left(\frac{a}{c}\right)^4$
M_3	$0.5 - \frac{1}{0.65 + c/a} + 14(1 - \frac{c}{a})^{24}$	$-0.11 \left(\frac{a}{c}\right)^4$

TABLE 1.7.7A (Concluded)

PARAMETER	$\frac{c}{a} < 1$	$\frac{c}{a} > 1$
g_1	$1 + [0.1 + 0.35 (\frac{c}{B})^2] (1 - \sin \theta)^2$	$1 + [0.1 + 0.35 (\frac{a}{c}) (\frac{c}{B})^2] (1 - \sin \theta)^2$
g_2	$\frac{1 - 0.15 \lambda + 3.46 \lambda^2 - 4.47 \lambda^3 + 3.52 \lambda^4}{1 + 0.13 \lambda^2}$	Same as $\frac{c}{a} \leq 1$
λ	$\frac{1}{1 + \frac{a}{r} \cos (0.85 \theta)}$	Same as $\frac{c}{a} \leq 1$
g_3	$g_4 \cdot g_5$	$g_4 \cdot g_5$
g_4	$1 + 0.04 \frac{c}{a}$	$1.13 - 0.09 \frac{a}{c}$
g_5	$[1 + 0.1 (1 - \cos \theta)^2] \cdot [0.8 + 0.2 (\frac{c}{B})^{\frac{1}{4}}]$	Same as $\frac{c}{a} \leq 1$
f_θ	$[(\frac{c}{a})^2 \cos^2 \theta + \sin^2 \theta]^{\frac{1}{4}}$	$[(\frac{a}{c})^2 \sin^2 \theta + \cos^2 \theta]^{\frac{1}{4}}$

TABLE 1.7.7B

NEWMAN AND RAJU SOLUTION FOR
DIAMETRICAL CORNER CRACKS



for $0.2 \leq c/a \leq 2$, $c/B < 1$, $0.5 \leq r/B \leq 1$ ($2(r+a)/w < 0.5$ and $0 < \theta < 90^\circ$)

$$f_w = \left[\sec \left(\frac{\pi r}{w} \right) \sec \left(\frac{\pi(2r + 2a)}{4(0.5 w - a) + 4a} \cdot \sqrt{\frac{c}{B}} \right) \right]^{\frac{1}{2}}$$

Parameter	$\frac{c}{a} \leq 1$	$\frac{c}{a} > 1$
M_1, M_2, M_3	SEE TABLE 1.7.7A	SEE TABLE 1.7.7A
g_1, g_2, g_3	SEE TABLE 1.7.7A	SEE TABLE 1.7.7A
f_θ	SEE TABLE 1.7.7A	SEE TABLE 1.7.7A

1.7.8 Semi-Elliptical Surface Crack at a Hole

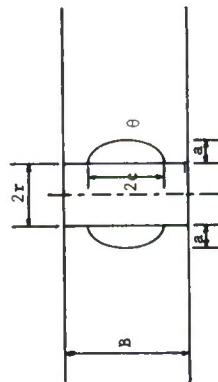
The Newman and Raju⁽⁷²⁾ solution for two symmetrical, semi-elliptical, surface cracks in the barrel of an open hole in a finite plate is presented in Table 1.7.8 for the case of uniform remote tensile loading. The solution can be used in conjunction with Equation 1.7.35 to create solutions for radial semi-elliptical surface crack type geometries and with Equation 1.7.34 to generate solutions for alternate types of loadings.

1.7.9 Lug Crack Geometries

In the recent past, an increasing amount of attention has been given to the damage tolerance design of lug type geometries. Several investigations^(35,84-88) have reported stress-intensity factor solutions for thru and corner crack geometries in straight lugs. Hsu and Brussat⁽⁸⁸⁾ have devoted particular attention to tapered lug geometries. Only those cases where (1) the loads are applied axially with respect to the lug shaft and (2) the cracks propagate perpendicular to the axis of the shaft are considered here. Off-axis loading complicates the analysis substantially since the direction of cracking is not always perpendicular to the loading direction. Table 1.7.9 presents the solutions for available lug type geometries. Note that Case 1.7.9.3 presents solutions for corner crack geometries that are controlled to grow at a crack depth (c) to crack length (a) ratio of 1.33. Also note that the Green's Functions are presented in Case 1.7.9.4 for the radial crack growing perpendicular to the axis of the lug shaft.

TABLE 1.7.8

SEMI-ELLIPTICAL SURFACE CRACKS
AT A HOLE



$$K = \sigma \sqrt{\frac{\pi c}{Q}} \left[M_1 + M_2 \left(\frac{2c}{B} \right)^2 + M_3 \left(\frac{2c}{B} \right)^4 \right] g_1 \cdot g_2 \cdot f_{\theta} \cdot f_W$$

for $0.2 \leq c/a \leq 2$, $2c/B < 1$, $0.5 \leq 2r/B \leq 2$,

$(2r + 2a)/W < 0.5$ and $-\frac{\pi}{2} \leq \theta \leq \frac{\pi}{2}$

$$f_W = \left[\sec \left(\frac{\pi r}{W} \right) \sec \left(\frac{\pi (2r + 2a)}{2(W - 2a) + 4a} - \sqrt{\frac{2c}{W}} \right) \right]^{\frac{1}{2}}$$

TABLE 1.7.8 (Concluded)

Parameter	$c/a \leq 1$	$c/a > 1$
M_1	1	$\frac{a}{c}$
M_2	$0.05/(0.11 + (c/a)^{3/2})$	Same as $c/a \leq 1$
M_3	$0.29/(0.23 + (c/a)^{3/2})$	Same as $c/a \leq 1$
g_1	$\cos \theta (1 - (2c/B)^4 / (1 + 4(2c/B)))$	Same as $c/a \leq 1$
g_2	$\frac{1 - 0.15 \lambda + 3.46 \lambda^2 - 4.47 \lambda^3 + 3.52 \lambda^4}{1 + 0.08 \lambda^2}$	Same as $c/a \leq 1$
λ	$1/(1 + \frac{a}{r} \cos (0.9\theta))$	Same as $c/a \leq 1$
f_θ	$[(\frac{c}{a})^2 \cos^2 \theta + \sin^2 \theta]^{1/4}$	$[(\frac{a}{c})^2 \sin^2 \theta + \cos^2 \theta]^{1/4}$

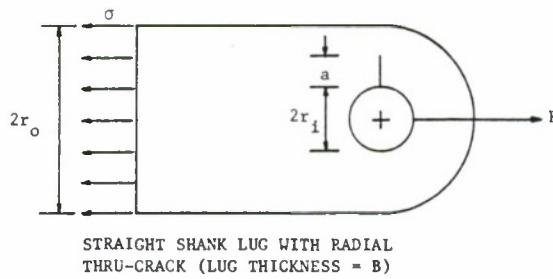
TABLE 1.7.9
STRESS-INTENSITY FACTOR SOLUTIONS FOR
LUG-TYPE GEOMETRIES

CASE NO.

GEOMETRY

STRESS-INTENSITY FACTOR

1.7.9.1

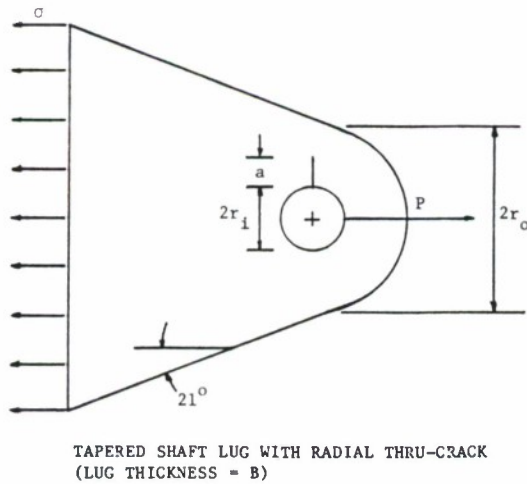


$$K = \beta \sigma_{br} \sqrt{\pi a}$$

where $\sigma_{br} = \frac{P}{2r_i B}$

See Table 1.7.9A for a comparison of β analyses and Figure 1.7.14 for β solutions as a function of $\frac{r_o}{r_i}$

1.7.9.2



$$K = \beta \sigma_{br} \sqrt{\pi a}$$

where $\sigma_{br} = \frac{P}{2r_i B}$

See Figure 1.7.15 for β solutions as a function of $\frac{r_o}{r_i}$

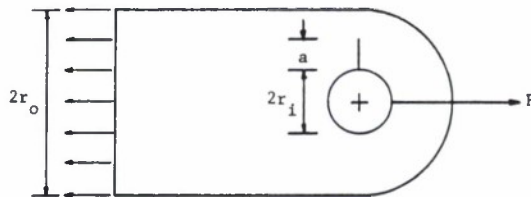
TABLE 1.7.9 (Concluded)

CASE NO.

GEOMETRY

STRESS-INTENSITY FACTOR

1.7.9.3



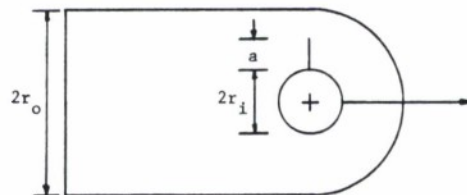
STRAIGHT SHANK LUG WITH RADIAL CORNER
CRACK (DEPTH=C) (LUG THICKNESS = B)

$$K = \beta \sigma_{br} \sqrt{\pi a}$$

$$\text{where } \sigma_{br} = \frac{P}{2r_i B}$$

See Tables 1.7.9 B,C for β
for effect of $2r_i/B$, with
 $c/a = 1.33$

1.7.9.4



STRAIGHT SHANK LUG WITH RADIAL
THRU-CRACK AND INTERFERENCE

$$K = \frac{\pi}{a} \int_0^a \sigma(x) G^H(a,x) dx$$

Based on the Green's function
 $G^H(a,x)$ described in Tables
1.7.9 D, E, F for r_o/r_i equal
to 1.5, 2.25, and 3, respectively.

TABLE 1.7.9A

STRESS-INTENSITY FACTORS FOR STRAIGHT SHANK LUG
AS A FUNCTION OF OUTER TO INNER RADIUS (r_o/r_i)

$\beta = \frac{K}{\sigma_{br}\sqrt{\pi a}}$, where																								
$\frac{r_o}{r_i}$	$\frac{r_o}{r_i} = 1.5$				$\frac{r_o}{r_i} = 1.8$		$\frac{r_o}{r_i} = 2.0$				$\frac{r_o}{r_i} = 2.25$		$\frac{r_o}{r_i} = 2.37$		$\frac{r_o}{r_i} = 2.5$				$\frac{r_o}{r_i} = 3.0$				$\frac{r_o}{r_i} = 4$	
	Hsu	Z	Or _{cos}	Or _{unif}	Z		Hsu	Or _{cos}	Or _{unif}		Im & Rich	Hsu	Z	Or _{cos}	Or _{unif}	Hsu	Or _{cos}	Or _{unif}	Hsu	Or _{cos}	Or _{unif}	Z		
0.0	5.15	4.7	---	---	3.3		3.1	---	---	2.65		2.38	2.42	2.4	---	---	2.05	---	---	---	---	1.75		
0.05	3.85	---	5.5	3.8	---		---	2.93	2.07	---		---	---	---	2.04	1.41	---	---	---	1.67	1.15	---		
0.1	3.45	3.3	5.1	3.7	2.3		2.32	2.67	1.97	2.05		1.77	1.85	1.5	1.95	1.44	1.55	1.59	1.17	---	---	1.25		
0.2	3.08	3.3	4.5	3.55	2.05		1.80	2.21	1.71	1.55		1.48	1.45	1.3	1.65	1.29	1.22	1.32	1.04	---	---	0.99		
0.3	3.05	3.6			1.94		1.60			1.34		---	1.22	1.2	1.45	1.17	1.05	1.15	0.94	---	---	0.78		
0.4	3.45	4.0			1.94		1.50			1.21		1.20	1.10	1.1	1.30	1.08	0.90	1.01	0.84	---	---	0.67		
0.5					1.94		1.48			1.15		---	1.03	1.04			0.80			---	---	0.62		
0.6					2.05		1.47			1.10		1.05	0.96	1.0			0.75			---	---	0.57		
0.7					2.2							---								---	---	0.52		
0.8					---							1.01								---	---	0.50		
0.9					---															---	---	0.47		
1.0					---															---	---	0.45		

Hsu = Ref. 88

Z = Ref. 87

Or_{cos} = Ref. 85 (cos sine loading)Or_{unif} = Ref. 85 (uniform loading)

Im + Rich = Ref. 86

TABLE 1.7.9B

NORMALIZED STRESS-INTENSITY FACTORS FOR
 SINGLE CORNER CRACKS AT STRAIGHT ATTACHMENT
 LUGS OBTAINED USING COMPOUNDING METHOD ($B/R = 1/3$)
 PER REFERENCE 88

$\frac{a}{R}$	$\beta = K/\sigma_{br} \sqrt{\pi a}$		
	$\frac{W}{D} = 1.50$	$\frac{W}{D} = 2.25$	$\frac{W}{D} = 3.00$
0.001	3.176	1.620	1.250
0.005	3.155	1.605	1.237
0.007	3.145	1.597	1.231
0.010	3.131	1.587	1.222
0.015	3.110	1.570	1.208
0.020	3.091	1.555	1.195
0.030	3.062	1.529	1.173
0.040	3.041	1.507	1.153
0.050	3.029	1.488	1.137
0.070	3.023	1.461	1.112
0.100	3.045	1.433	1.083
0.120	3.072	1.418	1.067
0.140	3.103	1.403	1.051
0.160	3.138	1.388	1.035
0.180	3.175	1.372	1.018
0.200	3.216	1.355	1.001
0.220	3.262	1.337	0.982
0.250	3.345	1.309	0.955
0.300	3.541	1.263	0.909
0.350	3.873	1.220	0.866
0.400	4.498	1.182	0.825
0.450	6.044	1.149	0.789
0.500	-	1.122	0.756
0.600	-	1.085	0.702
0.700	-	1.073	0.659
0.800	-	1.089	0.627
0.900	-	1.143	0.603
1.000	-	1.262	0.586
1.200	-	2.486	0.574
1.400	-	-	0.591
1.600	-	-	0.656
1.800	-	-	0.849

TABLE 1.7.9C
 NORMALIZED STRESS-INTENSITY FACTORS FOR
 SINGLE CORNER CRACKS AT STRAIGHT ATTACHMENT
 LUGS OBTAINED USING COMPOUNDING METHOD (B/R = 2/3)
 PER REFERENCE 88

$\frac{a}{R}$	$\beta = K/\sigma_{br}\sqrt{\pi a}$		
	$\frac{W}{D} = 1.50$	$\frac{W}{D} = 2.25$	$\frac{W}{D} = 3.00$
0.001	3.176	1.620	1.250
0.005	3.154	1.604	1.237
0.007	3.143	1.596	1.231
0.010	3.128	1.585	1.221
0.015	3.103	1.567	1.206
0.020	3.079	1.549	1.191
0.030	3.036	1.516	1.163
0.040	2.998	1.485	1.137
0.050	2.964	1.457	1.113
0.070	2.910	1.406	1.070
0.100	2.857	1.344	1.016
0.120	2.838	1.310	0.986
0.140	2.832	1.280	0.959
0.160	2.836	1.255	0.936
0.180	2.852	1.232	0.914
0.200	2.877	1.212	0.895
0.220	2.913	1.194	0.877
0.250	2.989	1.170	0.853
0.300	3.184	1.136	0.817
0.350	3.514	1.107	0.785
0.400	4.122	1.083	0.756
0.450	5.592	1.063	0.730
0.500	-	1.047	0.706
0.600	-	1.028	0.665
0.700	-	1.028	0.632
0.800	-	1.052	0.605
0.900	-	1.111	0.586
1.000	-	1.232	0.573
1.200	-	2.444	0.564
1.400	-	-	0.584
1.600	-	-	0.649
1.800	-	-	0.842

TABLE 1.7.9D
GREEN FUNCTIONS FOR $W/D = 1.500$
(MODIFIED FOR PIN LOADING)
PER REFERENCE 88

$a/(R_0 - R_1)$ x/a	.0100	.0500	.1000	.2000	.4000	.5000	.6000	.7000	.8000	.9000
.0000	.8341	.7366	.6768	.7388	.8909	.9981	1.1199	1.2895	1.5063	1.9234
.1000	.8329	.7296	.6692	.7179	.8709	.9703	1.0833	1.2426	1.4538	1.8916
.2000	.8349	.7253	.6641	.7107	.8527	.9414	1.0439	1.1970	1.4064	1.8609
.3000	.8424	.7293	.6635	.7025	.8403	.9188	1.0107	1.1558	1.3623	1.8388
.4000	.8579	.7433	.6738	.6996	.8308	.9012	.9846	1.1213	1.3235	1.8161
.5000	.8850	.7690	.7001	.7100	.8199	.8846	.9630	1.0924	1.2906	1.7978
.6000	.9303	.8110	.7454	.7372	.8081	.8686	.9445	1.0669	1.2614	1.7843
.7000	1.0081	.8828	.8152	.7844	.8087	.8639	.9361	1.0473	1.2327	1.7628
.8000	1.1564	1.0248	.9400	.8787	.8662	.9117	.9732	1.0551	1.2159	1.7592
.8250	1.2158	1.0835	.9915	.9212	.9026	.9447	1.0017	1.0702	1.2210	1.7793
.8500	1.2912	1.1593	1.0590	.9792	.9561	.9943	1.0458	1.0968	1.2357	1.8201
.8750	1.3906	1.2604	1.1513	1.0617	1.0358	1.0696	1.1146	1.1428	1.2674	1.8948
.9000	1.5282	1.4021	1.2845	1.1851	1.1585	1.1875	1.2247	1.2230	1.3307	2.0259
.9250	1.7343	1.6158	1.4916	1.3837	1.3591	1.3831	1.4116	1.3701	1.4577	2.2577
.9500	2.0872	1.9823	1.8574	1.7453	1.7277	1.7479	1.7673	1.6739	1.7379	2.6937
.9750	2.8999	2.8208	2.7119	2.6107	2.6119	2.6338	2.6490	2.5017	2.5437	3.6803
.9900	4.5359	4.4870	4.4118	4.3439	4.3735	4.4074	4.4346	4.3048	4.3578	5.4679

TABLE 1.7.9E
GREEN FUNCTIONS FOR $W/D = 2.250$
(MODIFIED FOR PIN LOADING)
PER REFERENCE 88

$\frac{a}{x} (R_o - R_f)$.0100	.0500	.1000	.2000	.4000	.5000	.6000	.7000	.8000	.9000
.0000	.8341	.7325	.6916	.6721	.7112	.7750	.8548	.9833	1.1491	1.4638
.1000	.8329	.7186	.6822	.6646	.7043	.7704	.8528	.9818	1.1531	1.4897
.2000	.8349	.7173	.6802	.6623	.7116	.7723	.8495	.9822	1.1621	1.5365
.3000	.8424	.7239	.6816	.6621	.7249	.7802	.8518	.9868	1.1748	1.5816
.4000	.8579	.7370	.6920	.6701	.7387	.7923	.8627	.9985	1.1923	1.6251
.5000	.8850	.7583	.7172	.6919	.7513	.8073	.8805	1.0176	1.2156	1.6719
.6000	.9303	.7947	.7609	.7301	.7673	.8272	.9059	1.0432	1.2446	1.7232
.7000	1.0081	.8629	.8288	.7882	.8027	.8629	.9432	1.0779	1.2782	1.7661
.8000	1.1564	1.0059	.9507	.8946	.9023	.9533	1.0228	1.1384	1.3269	1.8474
.8250	1.2158	1.0657	1.0013	.9403	.9506	.9972	1.0610	1.1649	1.3484	1.9041
.8500	1.2912	1.1430	1.0678	1.0017	1.0165	1.0576	1.1144	1.2012	1.3794	1.9977
.8750	1.3906	1.2461	1.1590	1.0878	1.1093	1.1441	1.1922	1.2545	1.4276	2.1530
.9000	1.5282	1.3901	1.2910	1.2149	1.2455	1.2731	1.3111	1.3377	1.5075	2.4157
.9250	1.7343	1.6064	1.4969	1.4170	1.4596	1.4797	1.5062	1.4803	1.6523	2.8752
.9500	2.0872	1.9759	1.8613	1.7814	1.8393	1.8529	1.8682	1.7659	1.9520	3.7044
.9750	2.8999	2.8174	2.7142	2.6461	2.7229	2.7367	2.7474	2.5661	2.7736	5.1196
.9900	4.5359	4.4854	4.4130	4.3718	4.4614	4.4882	4.5127	4.3692	4.5652	6.6282

TABLE 1.7.9F
GREEN FUNCTIONS FOR $W/D = 3.000$
(MODIFIED FOR PIN LOADING)
PER REFERENCE 88

$\frac{a}{x}/(R_o - R_1)$.0100	.0500	.1000	.2000	.4000	.5000	.6000	.7000	.8000	.9000
.0000	.8341	.6943	.6263	.5991	.6054	.6500	.7084	.8045	.9371	1.2235
.1000	.8329	.6896	.6225	.5932	.6113	.6600	.7227	.8231	.9653	1.2890
.2000	.8349	.6850	.6223	.5947	.6290	.6759	.7369	.8437	.9983	1.3580
.3000	.8424	.6884	.6264	.5994	.6523	.6074	.7565	.8689	1.0348	1.4301
.4000	.8579	.7024	.6409	.6121	.6770	.7233	.7838	.9002	1.0752	1.5041
.5000	.8850	.7281	.6708	.6386	.7010	.7525	.8189	.9384	1.1205	1.5789
.6000	.9303	.7693	.7193	.6827	.7279	.7860	.8607	.9828	1.1707	1.6548
.7000	1.0081	.8388	.7921	.7497	.7726	.8335	.9125	1.0342	1.2252	1.7330
.8000	1.1564	.9770	.9191	.8674	.8793	.9323	1.0027	1.1114	1.2939	1.8196
.8250	1.2158	1.0347	.9709	.9161	.9288	.9775	1.0426	1.1439	1.3199	1.8459
.8500	1.2912	1.1097	1.0387	.9804	.9960	1.0392	1.0975	1.1887	1.3552	1.8774
.8750	1.3906	1.2104	1.1313	1.0692	1.0899	1.1265	1.1763	1.2543	1.4074	1.9188
.9000	1.5282	1.3522	1.2647	1.1990	1.2272	1.2563	1.2959	1.3568	1.4910	1.9805
.9250	1.7343	1.5672	1.4722	1.4038	1.4424	1.4635	1.4914	1.5309	1.6391	2.0876
.9500	2.0872	1.9373	1.8390	1.7708	1.8236	1.8375	1.8537	1.8685	1.9418	2.3156
.9750	2.8999	2.7843	2.6962	2.6386	2.7100	2.7233	2.7341	2.7310	2.7661	3.0091
.9900	4.5359	4.4618	4.4005	4.3670	4.4523	4.4783	4.5025	4.5198	4.5601	4.7246

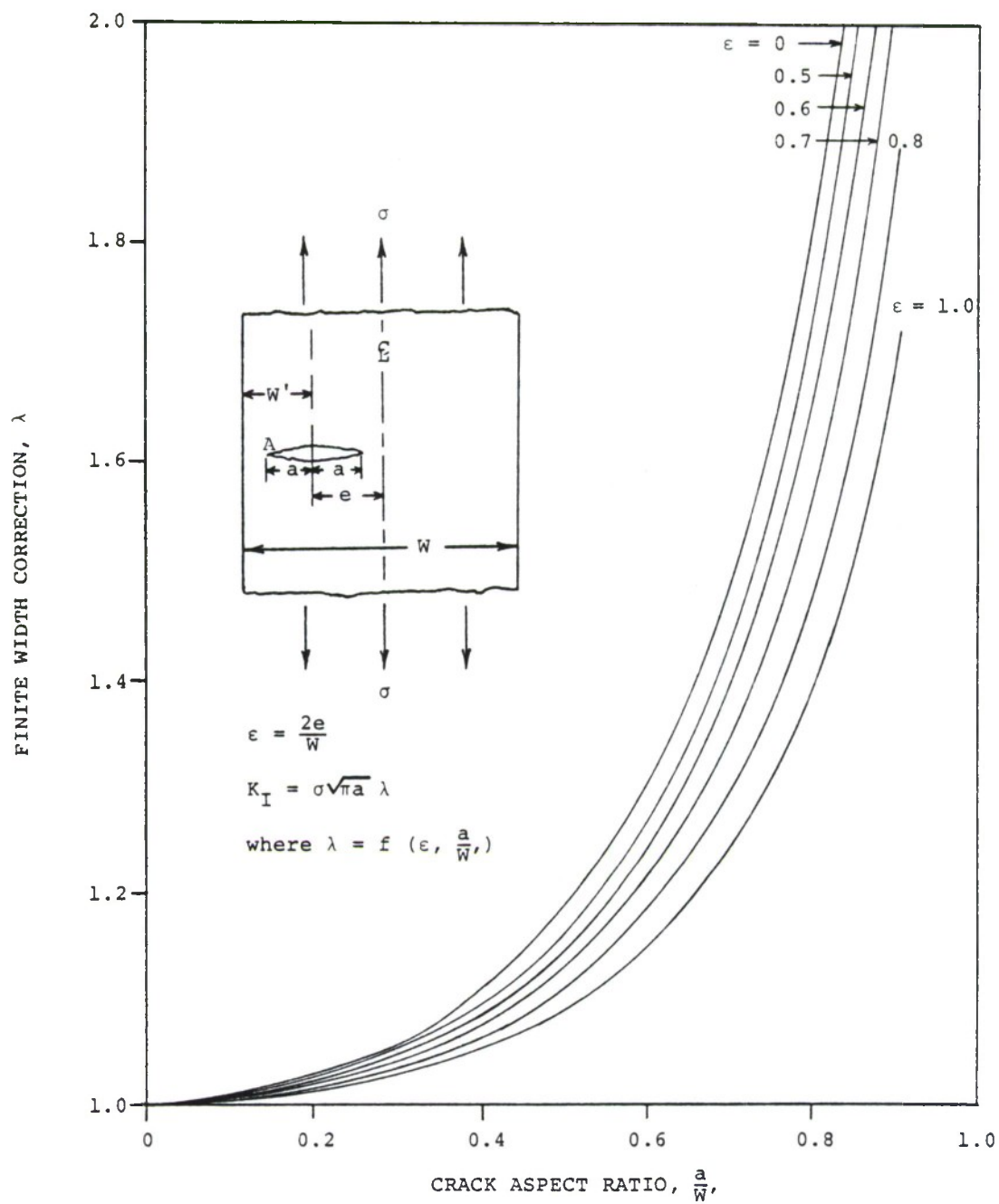


Figure 1.7.1 Finite Width Correction Factors for Crack Tip "A"

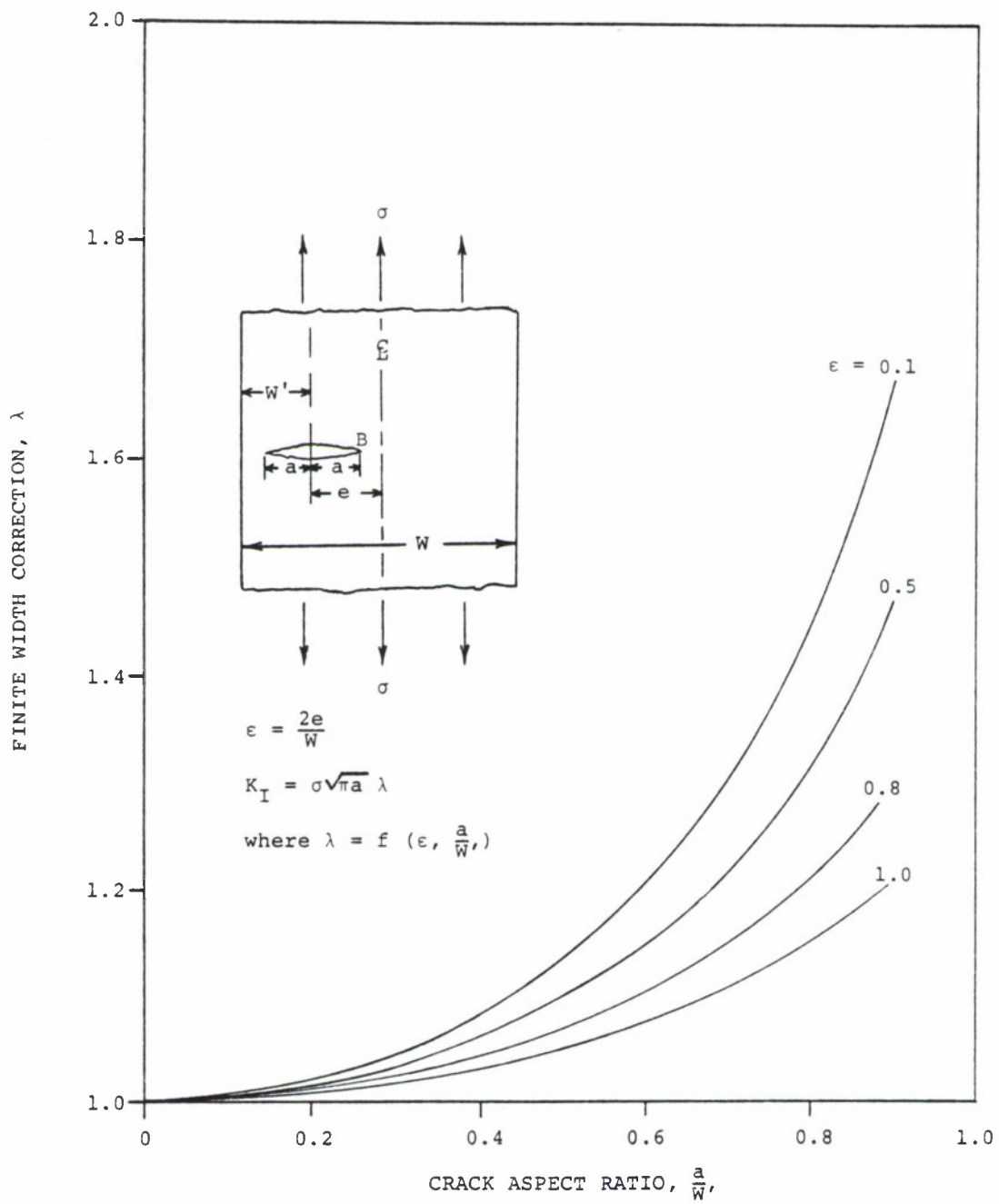
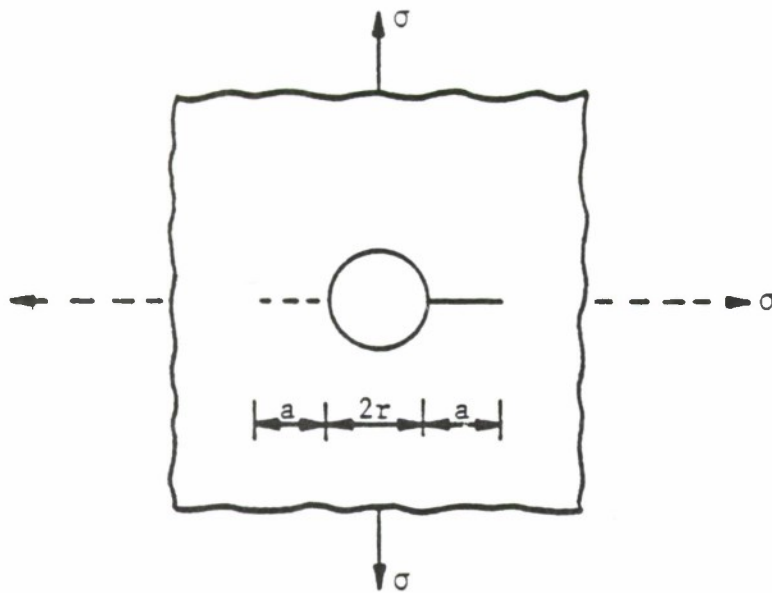


Figure 1.7.2 Finite Width Correction Factors for Crack Tip "B"



$$K = \sigma \sqrt{\pi a \beta}$$

$$\beta = F_i \left(\frac{a}{r} \right)$$

$\frac{a}{r}$	$F_1 \left(\frac{a}{r} \right), \beta$ Factor For Radially Cracked Hole		$F_2 \left(\frac{a}{r} \right), \beta$ Factor For Diametrically Cracked Hole	
	Uniaxial Loading Case 1.7.3.1	Equal Biaxial Loading	Uniaxial Loading Case 1.7.3.2	Equal Biaxial Loading
0.0	3.39	2.26	3.39	2.26
0.1	2.73	1.98	2.73	1.98
0.2	2.30	1.82	2.41	1.83
0.3	2.04	1.67	2.15	1.70
0.4	1.86	1.58	1.96	1.61
0.5	1.73	1.49	1.83	1.57
0.6	1.64	1.42	1.71	1.52
0.8	1.47	1.32	1.58	1.43
1.0	1.37	1.22	1.45	1.38
1.5	1.18	1.06	1.29	1.26
2.0	1.06	1.01	1.21	1.20
3.0	0.94	0.93	1.14	1.13
5.0	0.81	0.81	1.07	1.06
10.0	0.75	0.75	1.03	1.03
∞	0.707	0.707	1.00	1.00

Figure 1.7.3. Bowie β Factors for Through-Thickness Cracks at Remotely Loaded Circular Holes.

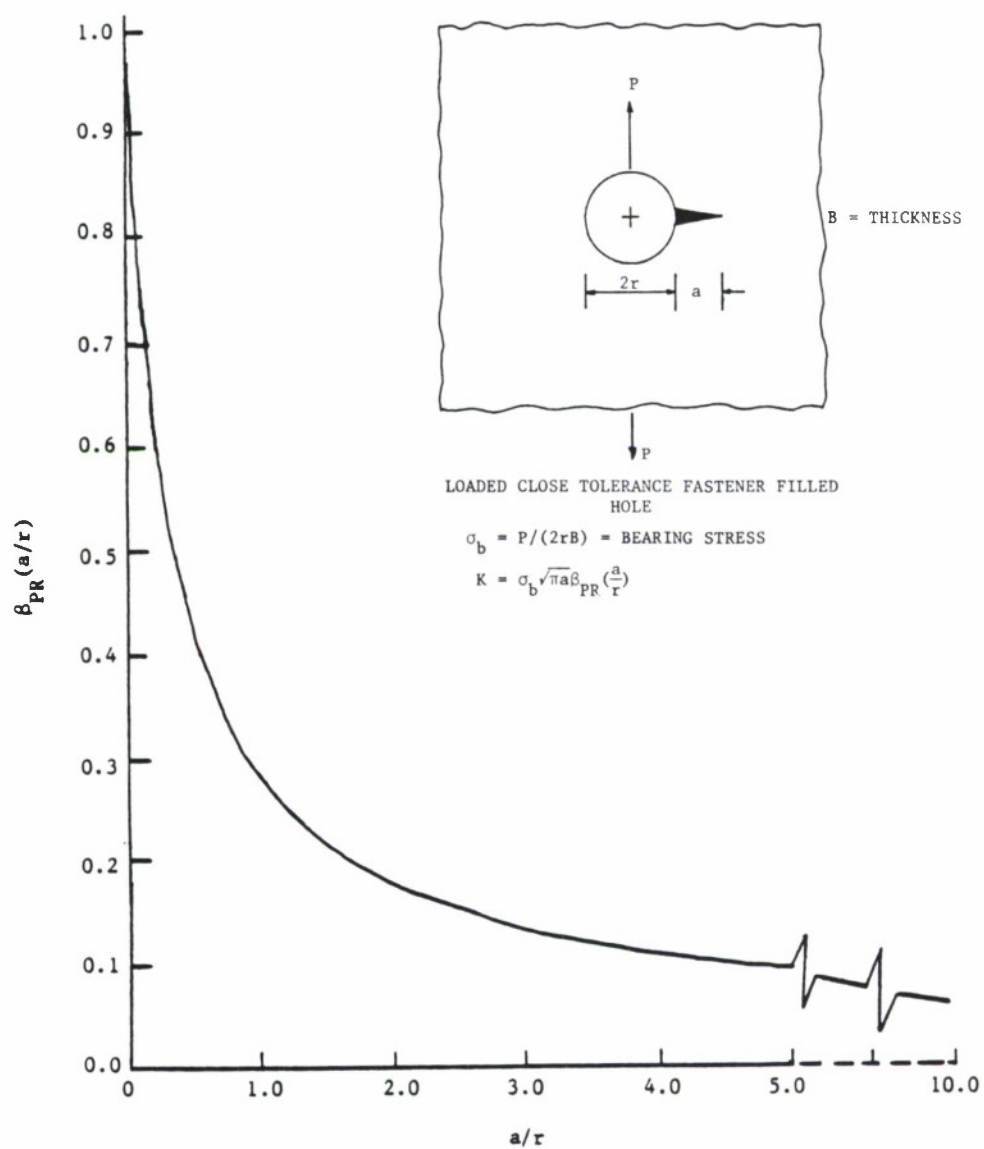


Figure 1.7.4. Beta Factor for a Through Crack Growing from a Hole, Loaded by a Close Tolerance Fastener (Reference 64).

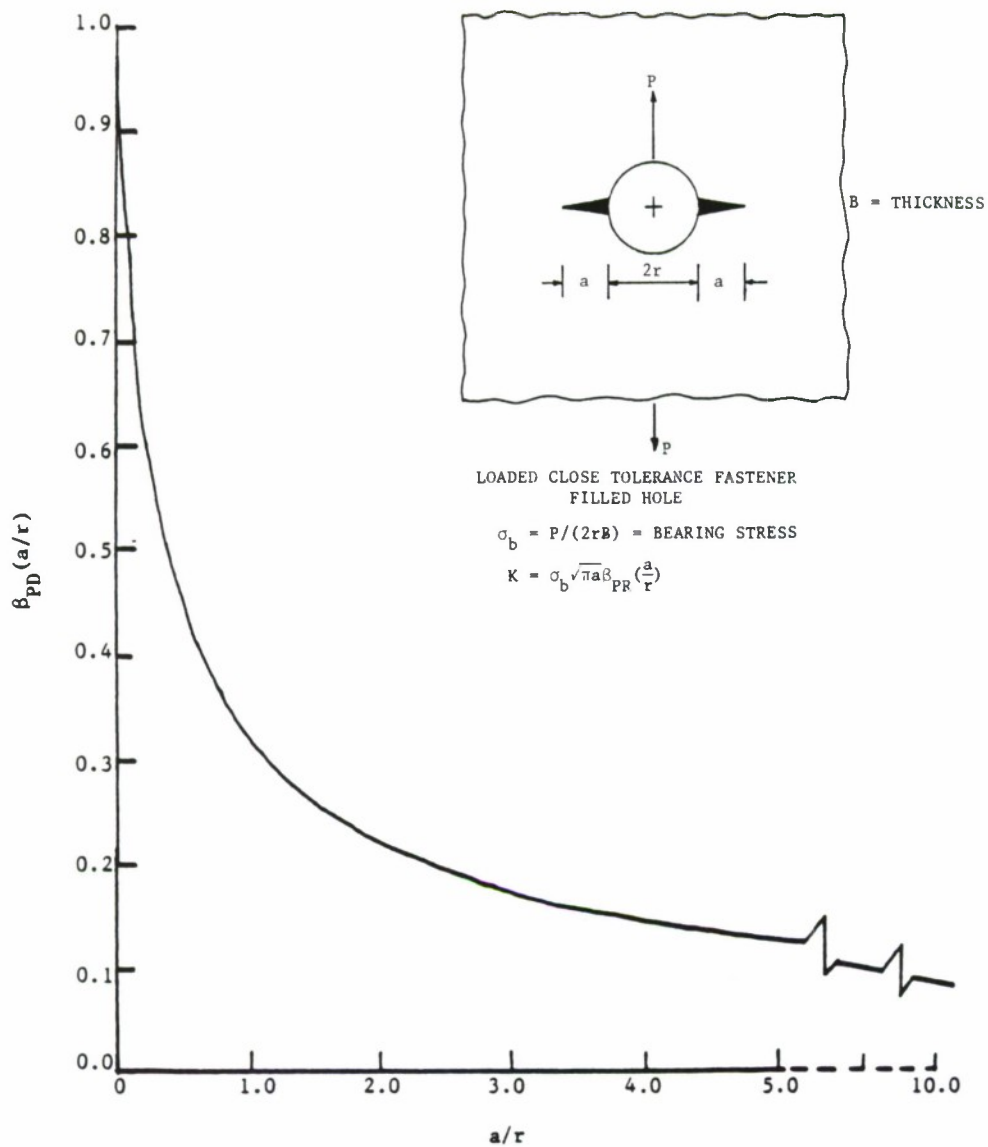
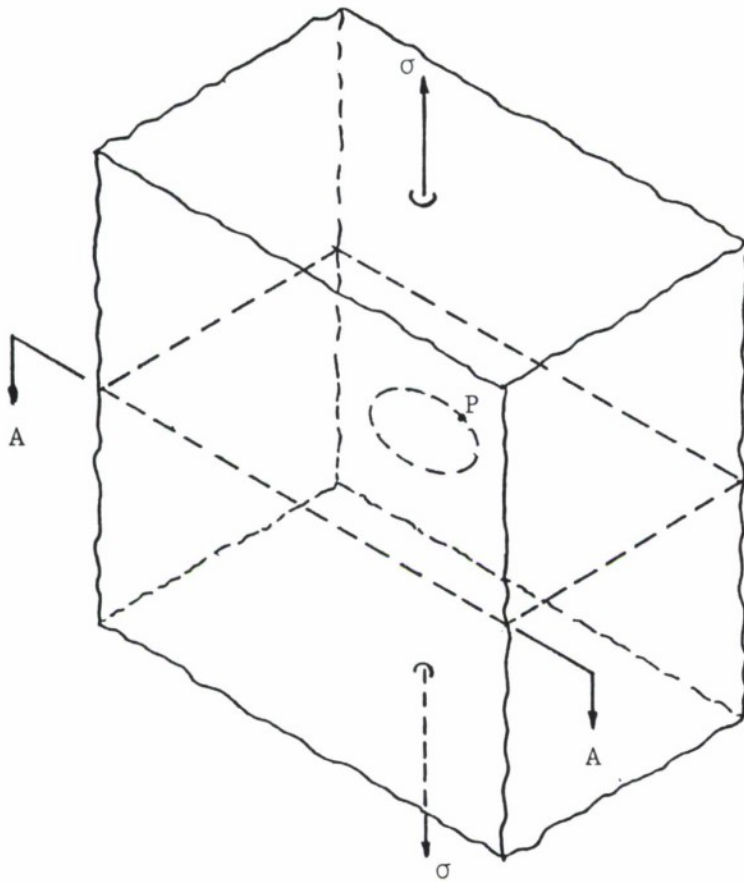
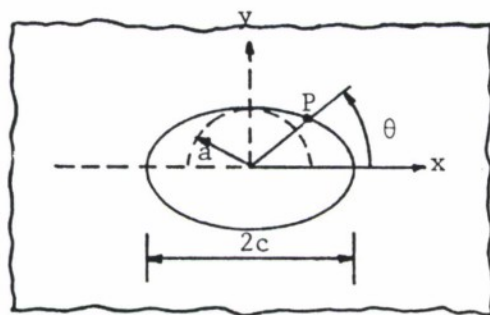


Figure 1.7.5. Beta Factor for a Diametrical Through Crack Growing from a Hole, Loaded by a Close Tolerance Fastener (Reference 64).



Coordinates of Point P
 $x = c \cos \theta$
 $y = a \sin \theta$



SECTION A-A

Figure 1.7.6. Embedded Elliptical Crack Geometry.

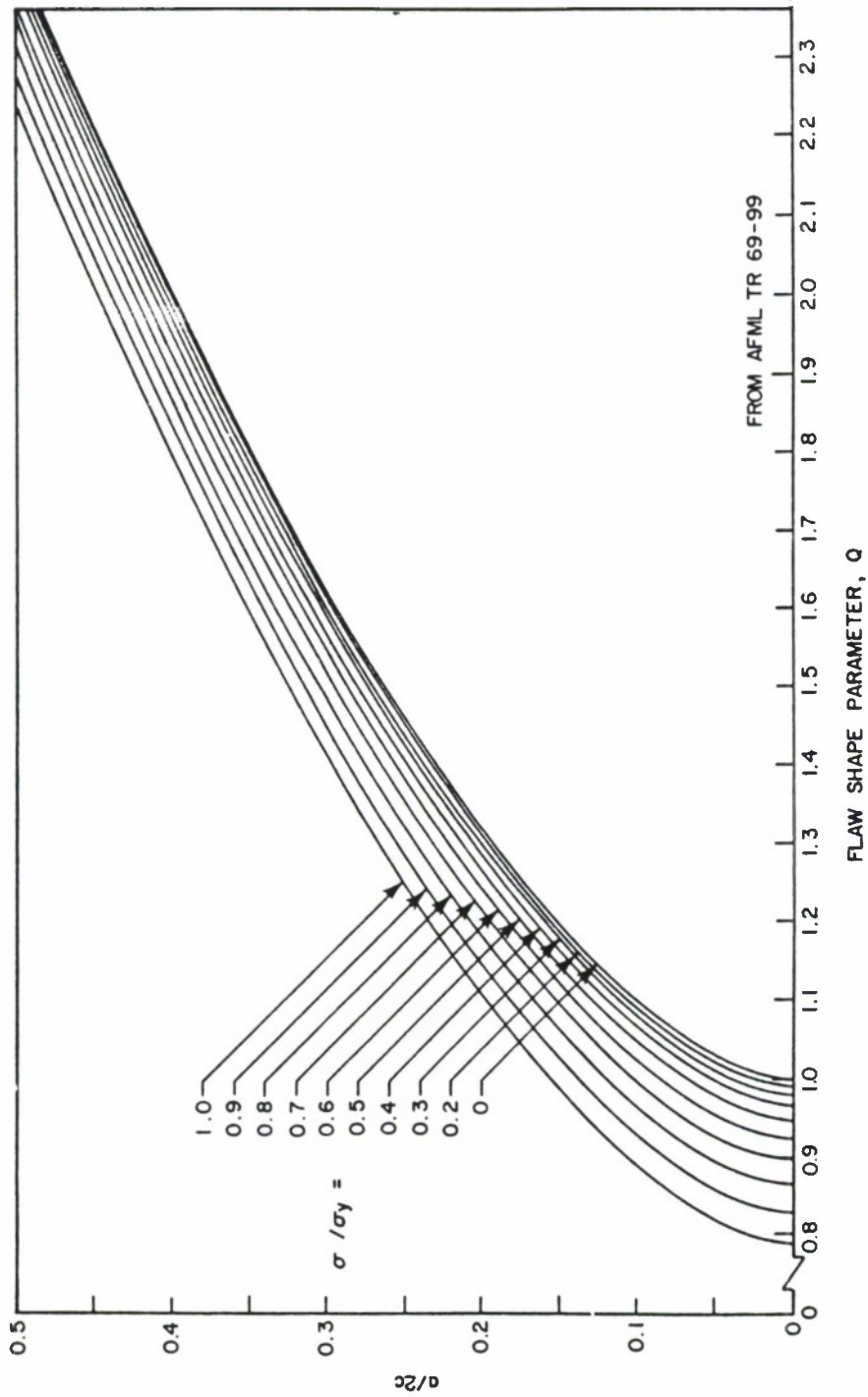
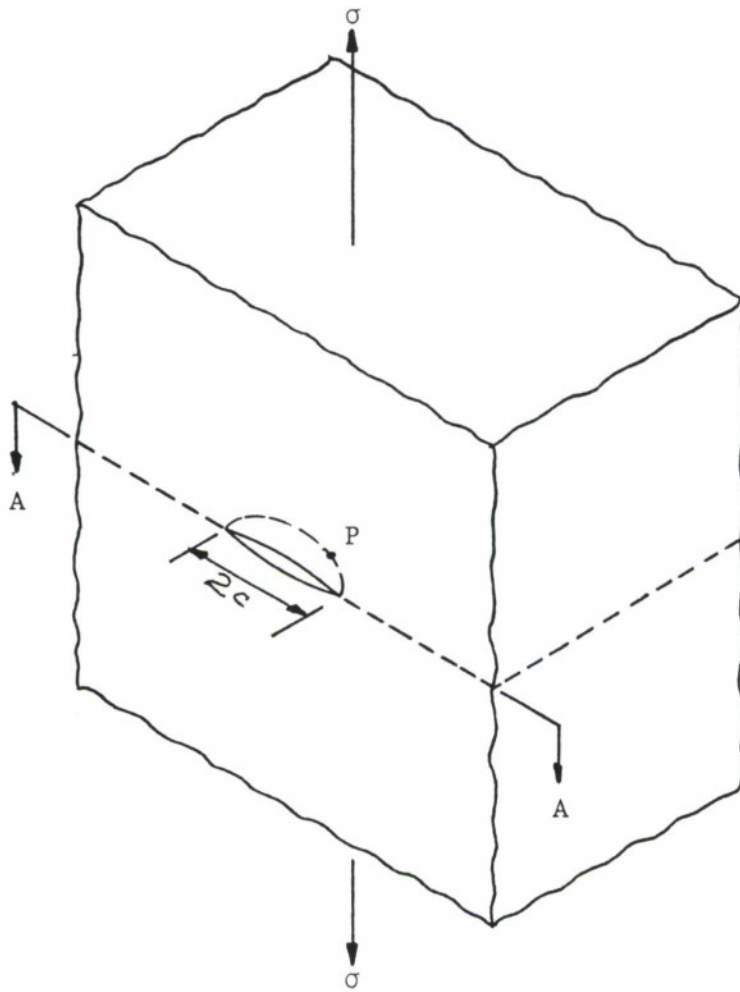


Figure 1.7.7. Shape Parameter Curves for Surface and Internal Flaws.



Coordinates of point P
 $x = c \cos \theta$
 $y = a \sin \theta$

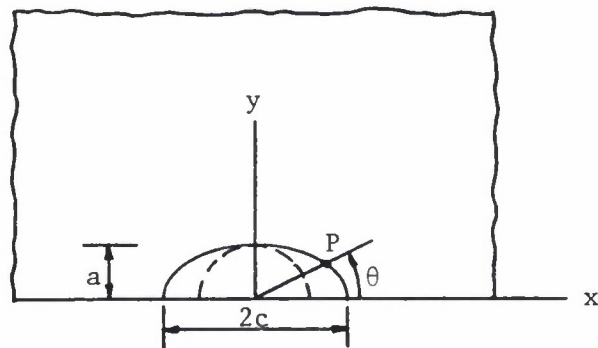


Figure 1.7.8. A Small Semi-Elliptical Crack in Uniformly Stressed Thick Structure.

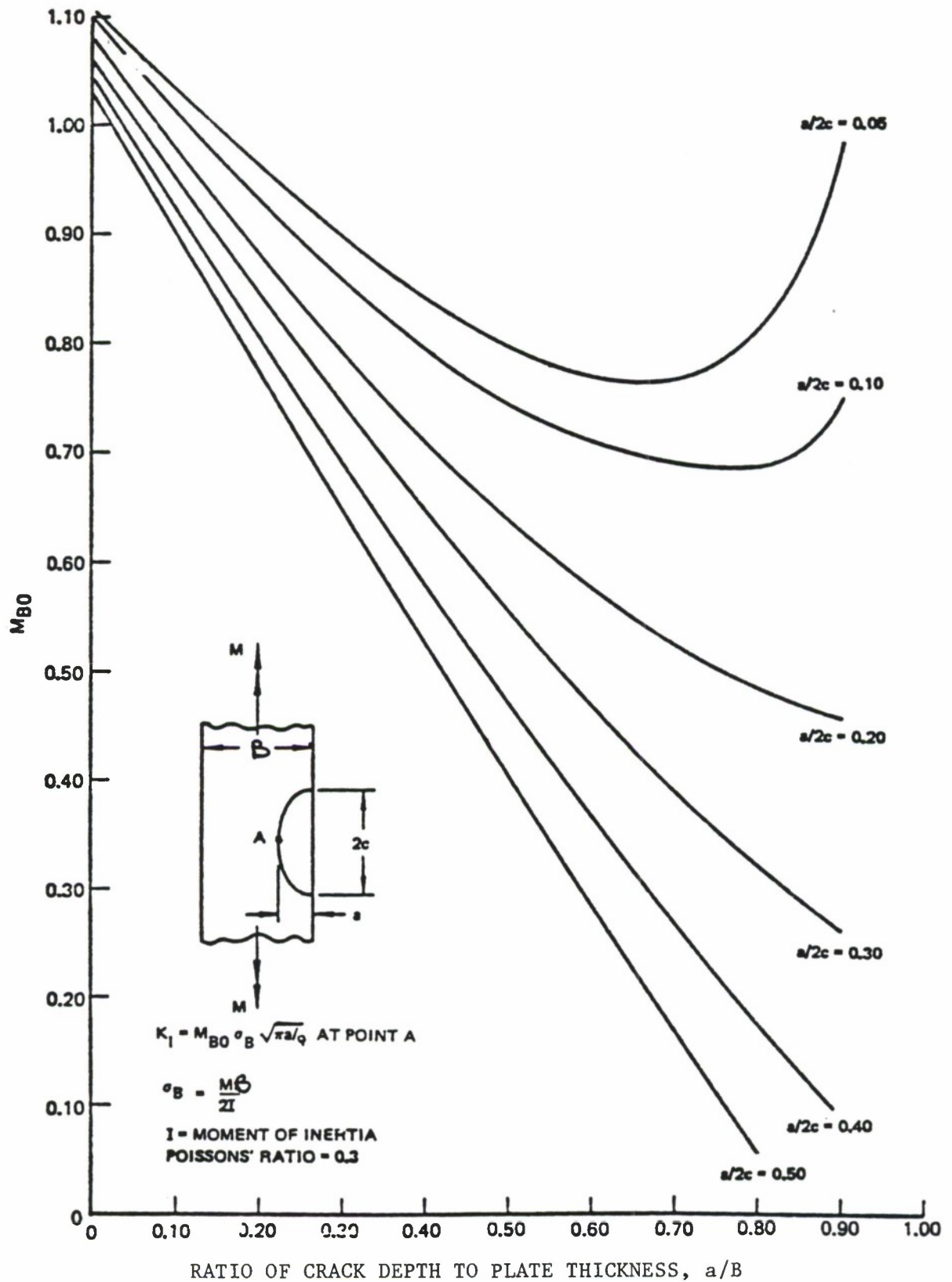


Figure 1.7.9. Stress-Intensity Factors at the Point of Maximum Crack Depth for Surface Flaws Subjected to Bending Stresses (Reference 64).

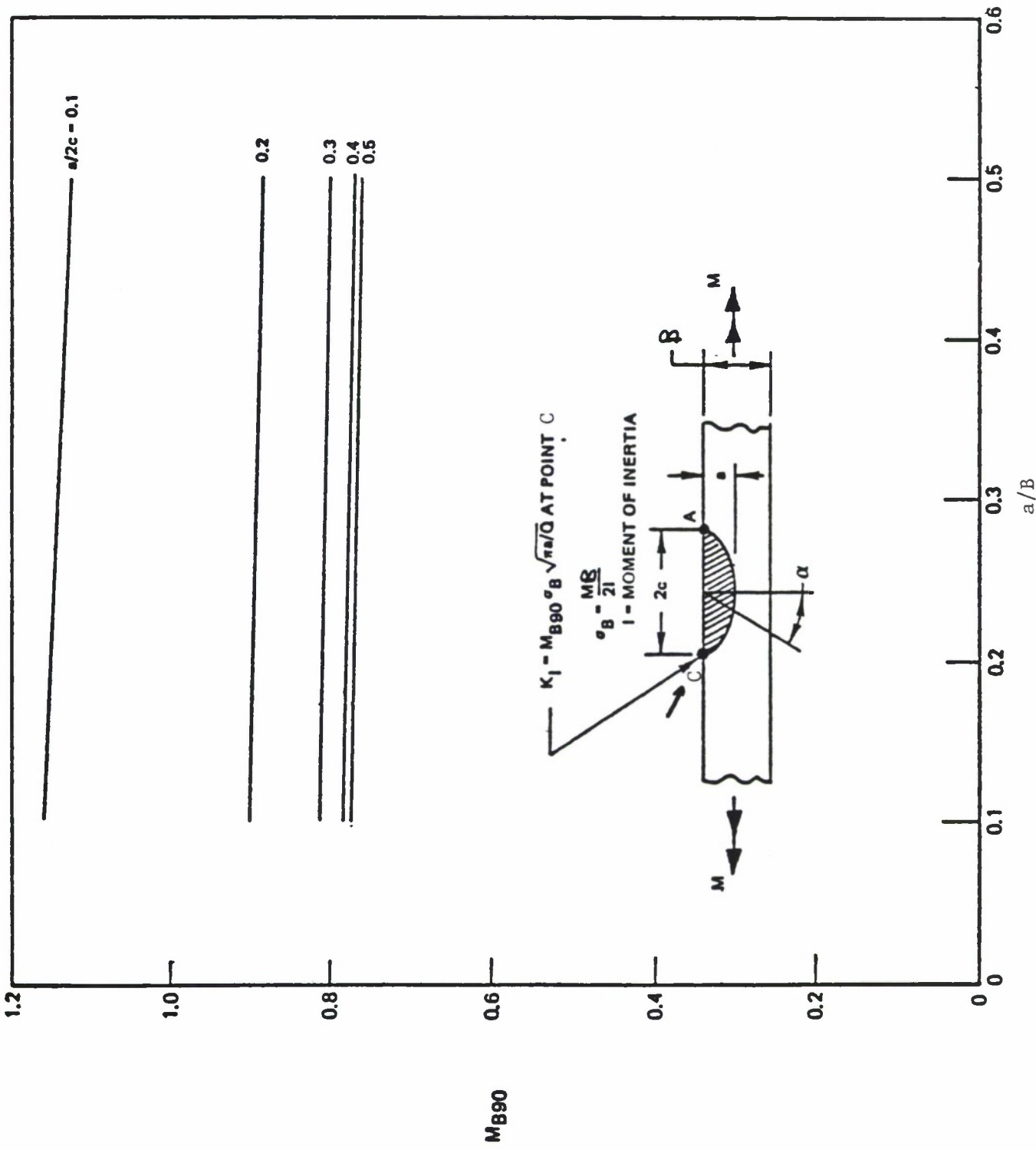


Figure 1.7.10. Stress-Intensity Factors at Plate Surface Flaws for Surface Flaws Subjected to Bending Stresses (Reference 64).

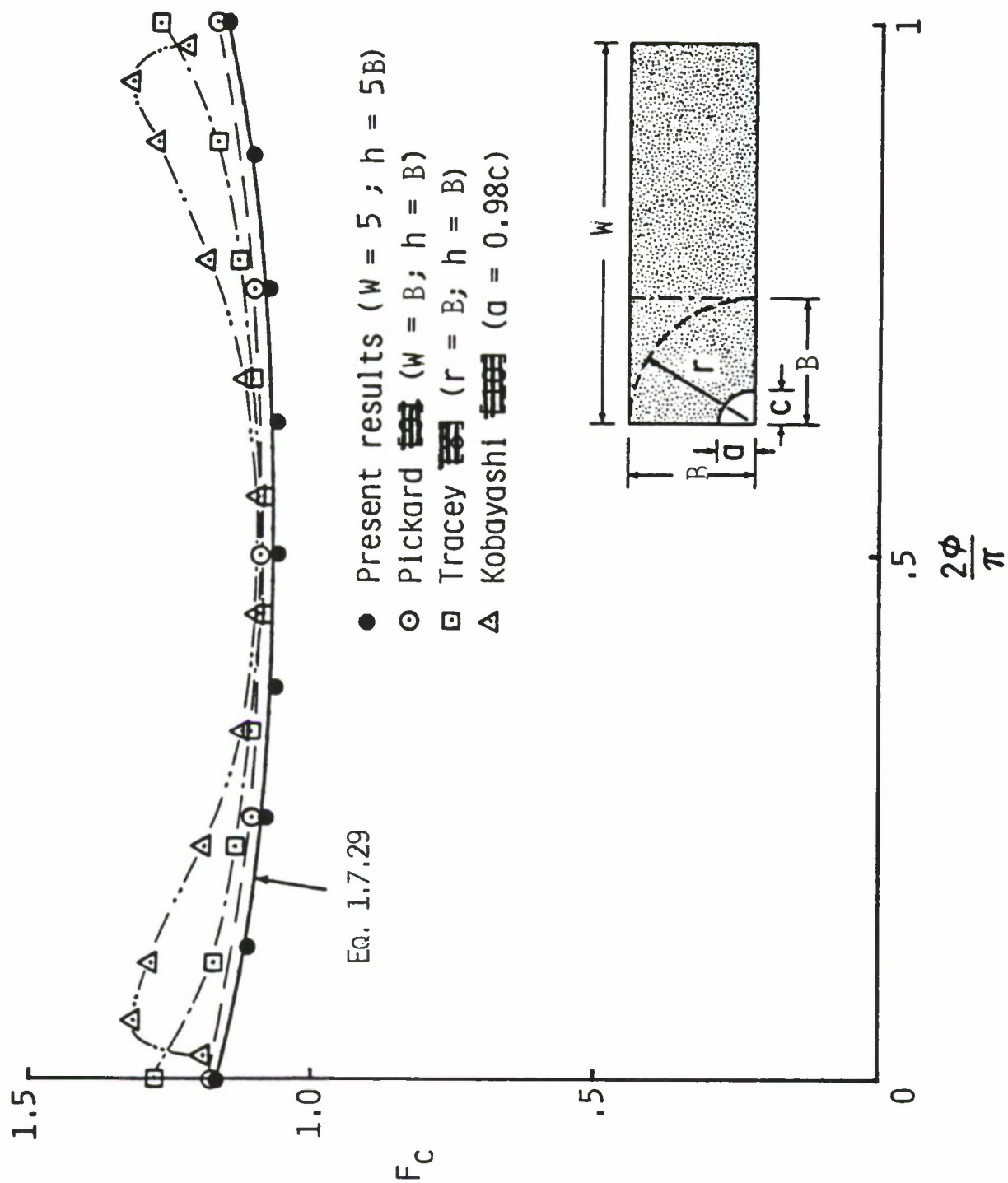


Figure 1.7.11. Comparison of Boundary-Correction Factors for Quarter-Circular Corner Crack in a Plate Subjected to Tension ($a/c = 1$; $a/B = 0.2$). (Reference 72.)

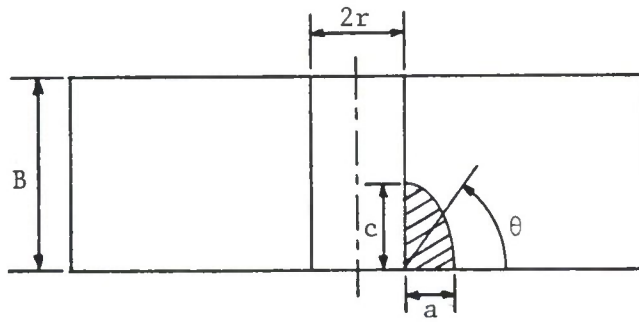


Figure 1.7.12. Corner Crack Geometry for Solution by Liu (Reference 73).

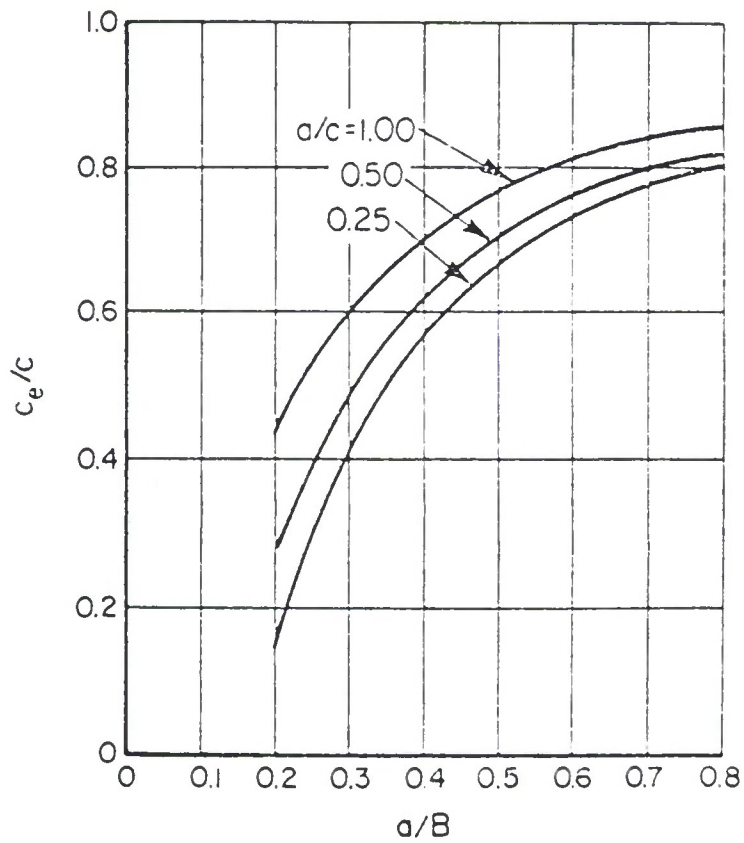


Figure 1.7.13. Empirical Curves to Determine the Effective Size of a Corner Crack at a Hole (Reference 68).

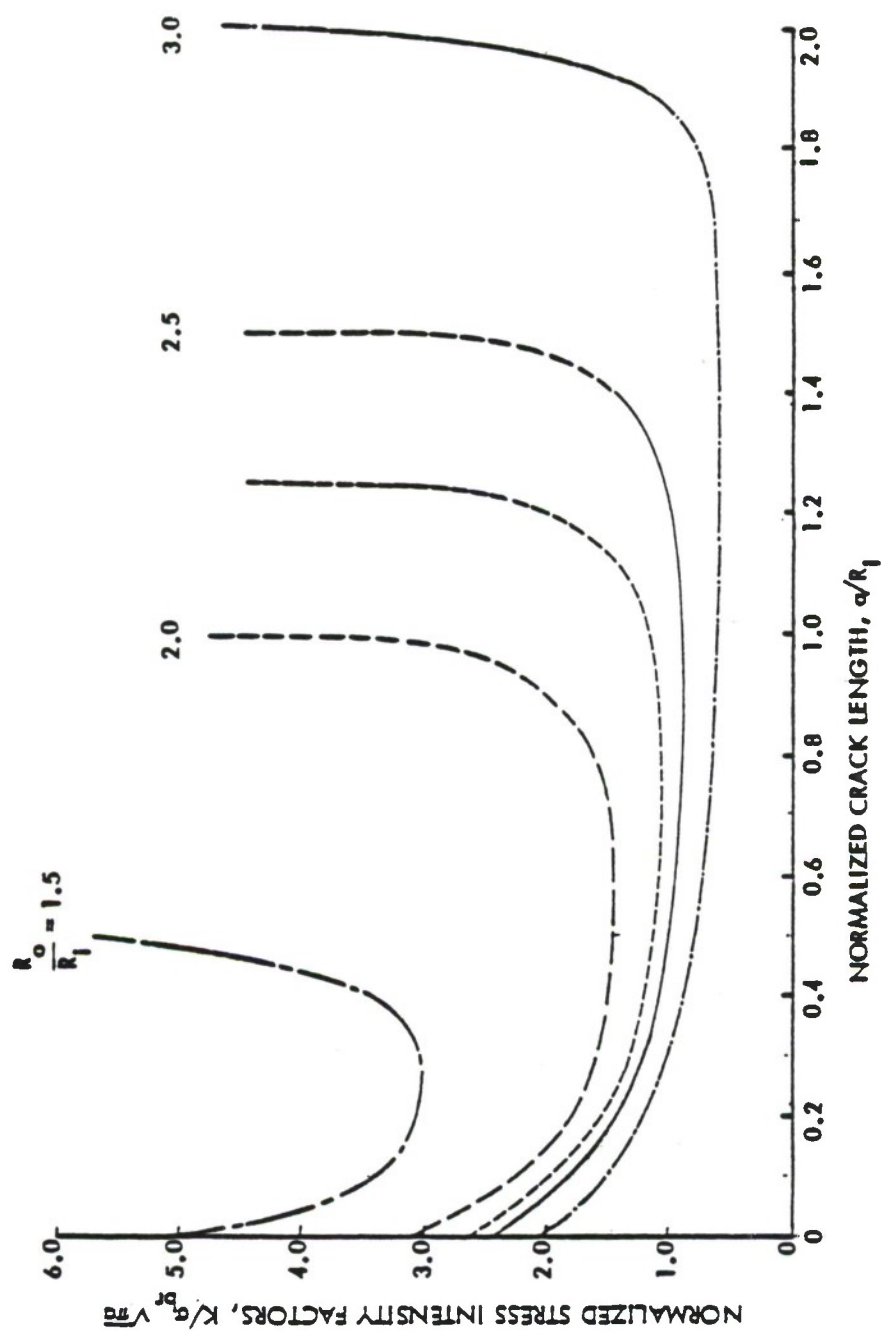


Figure 1.7.14. Normalized Stress-Intensity Factors for Single Crack Emanating from Straight Attachment Lugs (Reference 88).

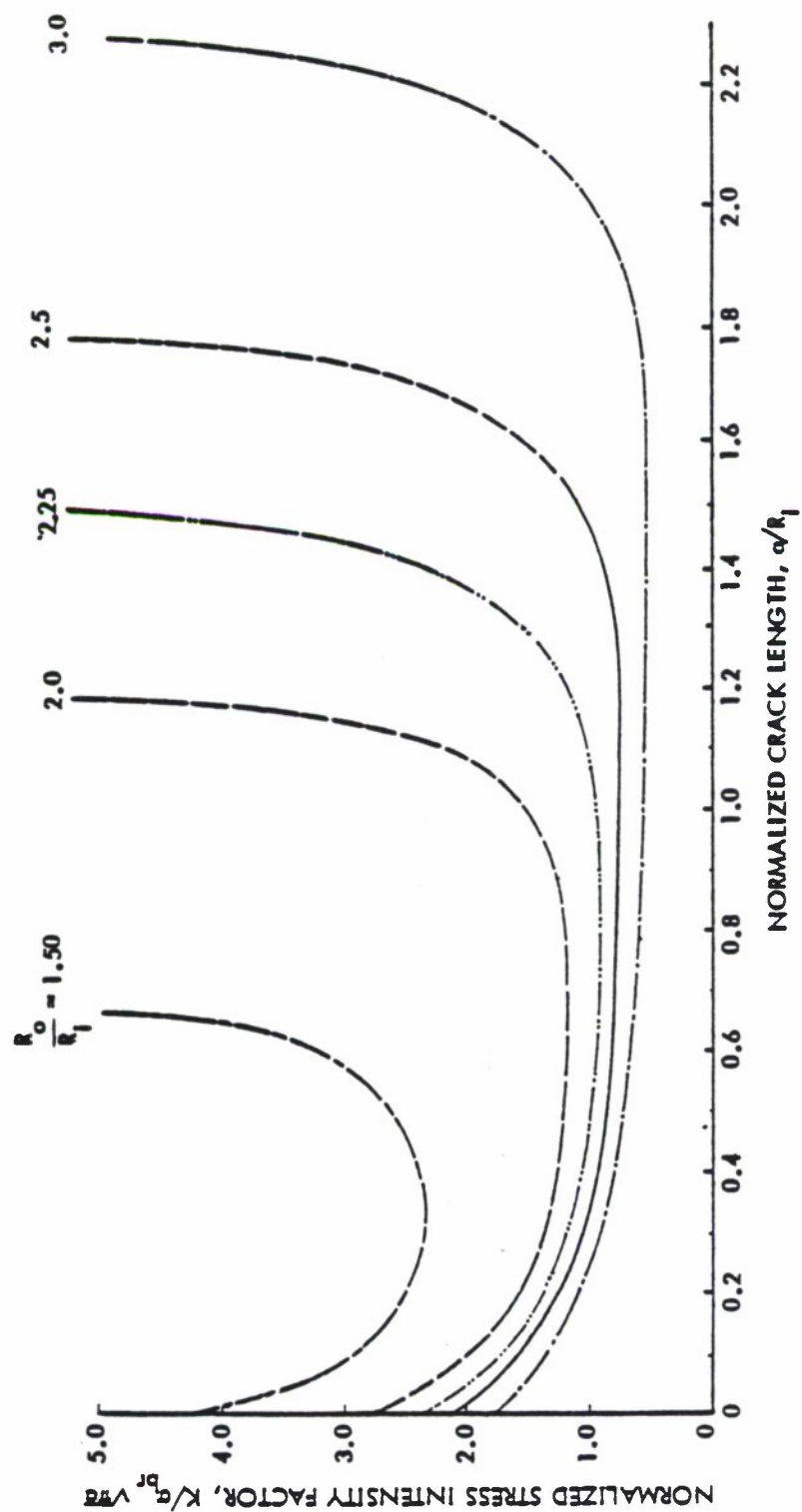


Figure 1.7.15. Normalized Stress-Intensity Factors for Single Crack Emanating from Tapered Attachment Lugs Subjected to a Pin Loading Applied in 0° Loading (Reference 88).

1.8 APPROXIMATE SOLUTIONS FOR STRESS-INTENSITY FACTORS

This subsection will discuss the procedures that one can use to obtain approximate stress-intensity solutions for complicated crack problems. Approximate solutions should only be used when the objective of the damage tolerant analysis is to bound the answer and when due care has been taken to understand all aspects of the cracking behavior. Most typically, the approximate solutions are derived using known (handbook) solutions that individually account for the effects of crack geometry, global geometry and loading. As noted in subsection 1.6.1, stress-intensity factors can be added for different types of loadings when the global and crack geometries are the same. This section will concentrate on those cases where the analyst must take existing solutions for several different geometries and estimate the stress-intensity factor for the geometry of interest. In those cases where the individual geometric effects can be accounted for by multiplication of factors, the analysis is referred to as compound analysis.

There are three geometric factors that normally must be accounted for in an approximate damage tolerant analysis: stress concentration, finite width and crack shape. The effects of all three factors on the stress-intensity factor can be established exactly using careful numerical analysis procedures. However, the solution of damage tolerant problems requires more than the accurate development of the stress-intensity factor. Frequently, the growth process causes the crack to constantly change its shape which significantly complicates the crack growth life analysis.

1.8.1

In order to describe how the three geometrical effects can be estimated, a series of examples are presented. In each case, the approximate solutions are based on known solutions. If the actual solution is available, it is compared to the approximate solution.

1.8.1 Effect of Stress Concentration

The effect of stress concentration is fairly easy to estimate for small cracks because the stress-intensity factor for an elementary crack problem can be multiplied by the elastic stress concentration factor (K_t). Example 1.8.1 illustrates this point. For longer cracks initiating at stress concentrations, the crack will be propagating through the stress field created by the stress concentration and the influence of stress gradient should be taken into account. Example 1.8.2 discusses an approximate method for estimating the stress intensity factor for a crack moving through a stress field generated by a stress concentration.

EXAMPLE 1.8.1 - A Small Edge Crack at a Stress Concentration Site

A geometrical description of the physical problem is provided in Figure 1.8.1 where a small edge crack is shown growing from the edge of a wing cutout. The stress-intensity factor for an edge crack (small with respect to the element width) is found in Section 1.7 (see Table 1.7.2, case 1.7.2.1) and is given by

$$K = 1.12 \sigma \sqrt{\pi a} \quad (1.8.1)$$

The stress term (σ) in Equation 1.8.1 typically represents the remote stress in the uniformly loaded edge cracked plate. This stress is also

the stress that would exist along the line of crack propagation if no crack were present. As indicated by Figure 1.8.1, the stress along the line of crack propagation (assuming no crack for a moment) for the given structural configuration is the product of the remote stress and the stress concentration factor (K_t) associated with the cutout, i.e., the local stress (σ_{LOCAL}) is:

$$\sigma_{\text{LOCAL}} = \sigma \times K_t \quad (1.8.2)$$

For the given structural configuration, the stresses along the line of crack propagation more closely represent the type of loading that the small edge crack would experience if it were in a uniformly loaded edge cracked plate subjected to the higher stresses given by Equation 1.8.2. It is therefore suggested that the stress-intensity factor for the structural configuration given in Figure 1.8.1 would be close to

$$K = 1.12 \sigma \times K_t \sqrt{\pi a} \quad (1.8.3)$$

In general, as long as one is dealing with small edge cracks in which the width or other geometrical effects are not important, Equation 1.8.3 provides a reasonable approximation to the stress-intensity factor for an edge crack in the vicinity of a stress concentration. See Example 1.8.2 for a discussion of stress gradient effects.

EXAMPLE 1.8.2 - An Edge Crack Growing from a Stress Concentration Site

One difficulty in utilizing Equation 1.8.3 for cracks that emanate from a stress concentration site is that the stress concentration normally generates its own stress field. The stress concentration stress field typically exhibits the highest stresses in the vicinity of the concentration ($\sigma_{\text{LOCAL}} = \sigma \times K_t$) and these high stresses decay as a function of distance from the stress concentration site. The question that needs to be answered is: If the stresses along the crack propagation path are not constant, as in the case of a uniformly loaded edge cracked plate, what stresses should be used to estimate the stress-intensity factor?

Shown in Figure 1.8.2 is the stress distribution associated with an uncracked hole in a wide plate. As can be seen from the figure, the (normal) stress drops off rapidly as a function of distance from the edge of the hole. An evaluation of the normal stress right at the edge of the hole, i.e., the local stress, leads one to the fact that

$$\sigma_{\text{LOCAL}} = \sigma \times 3 \quad (1.8.4)$$

(which is obtained by letting $R/X = 1$ in the equation given in Figure 1.8.2). Thus, K_T for the uniaxially loaded hole problem is three, i.e., $K_T = 3$ (see Equation 1.8.2) and the stress-intensity factor for a very small crack of length a at the edge of the hole is

$$K = 1.12 \times (3 \times \sigma) \sqrt{\pi a} = 3.36 \sigma \sqrt{\pi a} \quad (1.8.5)$$

A comparison between Equations 1.6.1 and 1.8.5 shows that $\beta = 3.36$, a constant. One estimate of the stress-intensity factor for a longer crack

would be given by Equation 1.8.5; but, this estimate would be high since the stresses along the crack propagation path are noted to be dropping.

In a manner similar to that presented in Example 1.8.1, a representative uniform stress can be created which would act along the crack propagation path between the crack tip and the edge of the hole (stress concentration) and thus simulate the uniformly loaded edge cracked plate geometry. Two estimates of this representative uniform stress level are made: estimate ① takes the normal stress at the half crack length point, i.e., the stress at $X = (a/2)+R$, whereas estimate ② assumes that the normal stress at the crack tip is the representative stress, i.e., the stress at $X = a+R$. A summary of the representative stress values and the β factor (= representative stress $\times 1.12$) is presented in Table 1.8.1 along with the value of the β factor for the radially cracked hole (see Case 1.7.3.1 in Section 1.7). As can be determined from the Table, estimate ② leads to representative stresses which when multiplied by the single edge crack β factor (i.e., 1.12) more closely approximate the β factor for the radially cracked hole. Estimate ① is seen to overestimate the correct β factor by a large amount. One justification for using the (no crack) normal stress level at the current crack length for estimating purposes comes from the fact that the major contribution to the stress-intensity factor is derived from the near crack tip stresses.

TABLE 1.8.1
COMPARISON OF β FACTORS BASED ON REPRESENTATIVE STRESSES
FOR SINGLE EDGE RADIAL CRACK PROBLEMS

	Estimate ①, Mid Crack		Estimate ②, Crack Tip		Actual
$\frac{a}{R}$	$\frac{R}{x} = \frac{R}{R + \frac{a}{2}}$	Stress ① $\frac{\sigma_{REP}}{\sigma}$	$\frac{R}{x} = \frac{R}{R+a}$	Stress ② $\frac{\sigma_{REP}}{\sigma}$	β [case 1.7.3.1] Equation 1.7.4
0	1	3	1	3	3.37
0.1	0.952	2.69	0.909	2.44	2.733
0.2	0.909	2.44	0.833	2.07	2.341
0.3	0.869	2.23	0.769	1.82	2.074
0.4	0.833	2.07	0.714	1.64	1.882
0.5	0.8	1.93	0.667	1.52	1.735

Several additional comments on stress concentration effects that will further guide the reader in the choice of fundamental stress-intensity factor solutions are made in some of the other examples presented in subsections 1.8.2 and 1.8.3.

1.8.2 Effect of Finite Width

As a crack tip approaches a free edge, its stress-intensity factor rapidly increases and tends to become infinite. One can look at the width contribution as a separate (multiplicative) β factor in the same way that the width contribution affects the solution of the center-crack remotely loaded geometry.

Recall that the stress-intensity factor for a loaded panel of finite width W is given by (see Section 1.7, Table 1.7.1, Case 1.7.1.2)

$$K = \sigma \sqrt{\pi a} \left(\sec \frac{\pi a}{W} \right)^{\frac{1}{2}} \quad (1.8.6)$$

which leads one to conclude that the (multiplicative) width effect β factor required to convert the infinite plate solution to the finite width solution is

$$\beta_W = \left(\sec \frac{\pi a}{W} \right)^{\frac{1}{2}} \quad (1.8.7)$$

Other geometries yield similar results. Two examples are presented to illustrate how one might develop a finite width β factor for more complicated geometries.

EXAMPLE 1.8.3 - Crack Growing Radially from Hole and Toward a Edge

Shown in Figure 1.8.3 is a crack geometry that frequently appears in aircraft structure. For this example, the crack is assumed to be a thru-thickness crack (the crack front is the same length as measured from the hole throughout the skin thickness). From an analysis point of view, two structural effects must be accounted for in the determination of the stress-intensity factor. These are: (a) the effect of the hole on the crack and (b) the effect of the free edge as the crack approaches it. A description of the influence of the hole on the stress-intensity factor was covered in the discussion of Example 1.8.2. An approximate description of K for the thru-thickness crack growing radially from a hole in a wide plate is (see Table 1.7.3, Case 1.7.3.1)

$$K = \sigma \sqrt{\pi a} \left\{ \frac{0.8734}{0.3246 + a/R} + 0.6762 \right\} \quad (1.8.8)$$

which is within a couple of percent of the exact solution (see Table 1.7.3A, Case 1.7.3.1).

Determining the effect that the finite boundary has on the stress-intensity factor for the crack described in Figure 1.8.3 requires some ingenuity if one does not wish to conduct a finite-element analysis (or other numerical analysis) study of this geometry. It is normally proposed that the stress-intensity factor effect for width (or for a free edge) is a multiplicative effect; i.e., if K^∞ represents the solution for infinite width and if K^W represents the finite width solution, then

$$K^W = K^\infty * \beta_W \quad (1.8.9)$$

where β_W is the modifying factor that accounts for width. The modifying factor for the wide center-crack panel is given by Equation 1.8.7. If one attempts to account for the finite width effect using a similar equation, i.e.

$$\beta_W = \sqrt{\sec \left(\frac{\pi a}{W} \right)} \quad (1.8.10)$$

there is some difficulty in determining what the width W should be. As suggested by Kaplan and Reiman [89], one could take the width as twice the distance from the center of the hole to the edge of the plate. This approach is equivalent to locating the hole in the center of a finite strip with a width (W) equal to 1.10 inch. If it is also now assumed that the hole does not exist and the crack has a center-crack geometry, the width modification would be expressed as

$$\beta_W^{(1)} = \sqrt{\sec \left(\frac{\pi * (a + R)}{1.10} \right)} \quad (1.8.11)$$

The term $(a+R)$ comes from the fact that crack is measured from the center of the hole.

Alternately, one could assume that the cracked edge of the hole is located in the center of the plate and the crack geometry is of the center-cracked configuration so that the width modification is given by

$$\beta_W^{(2)} = \sqrt{\sec \left(\frac{\pi * a}{0.850} \right)} \quad (1.8.12)$$

One difficulty in using either Equation 1.8.11 or 1.8.12 might be immediately obvious, and that is that a very wide plate (16.0 inch) has been replaced

with a very narrow strip. Thus, the actual geometrical constraints associated with the eccentric crack configuration we have in this problem have not been accounted for. As it will be subsequently shown, Equations 1.8.11 and 1.8.12 represent conservative upper-bound solutions to the width modification factor.

Kaplan and Reiman also suggested an approach based on the Isida width correction factor for eccentrically cracked structure. Shown in Figure 1.8.4 is a model crack configuration that could be used to estimate the influence of the free edge on the stress-intensity factor. The form of the Isida solution that will be used is

$$\beta_W = F(\delta, \lambda) \quad (1.8.13)$$

with the functional results obtained from Figure 1.6.10. The parameters δ and λ are defined in Figure 1.8.4. As shown by the figure, $\delta \approx 1$ and λ is a variable that depends on crack length in the following way:

$$\lambda = \frac{a^*}{b_1} = \frac{(a + 0.25)/2}{0.55 - a/2} \quad (1.8.14)$$

Table 1.8.2 presents a summary of the width modifications derived by the three equations presented. As previously suggested, the width modifications given by Equations 1.8.11 and 1.8.12 are much higher than 1.8.13. Column (6) was subsequently derived using Equation 1.8.5

$$\beta_W = F(\delta, \lambda) \cong 1 + \text{factor} * \left(\sqrt{\sec \left(\frac{\pi \lambda}{2} \right)} - 1 \right) \quad (1.8.15)$$

which closely represents the behavior of column (5) data.

TABLE 1.8.2
VARIOUS WIDTH BETA (β_w) FACTORS

Radial Crack Length a inch	Secant Width Effect $\sqrt{\sec \left(\frac{\pi a + 0.125}{1.1} \right)}$	Secant Width Effect $\sqrt{\sec \left(\frac{\pi a}{0.850} \right)}$	Model Crack Ratio $\lambda = a^*/b_1$	Isida Width Effect $F(1, \lambda)$	Equation 1.8.15
0	1.033	1.00	0.227	1.016	1.016
0.062	1.078	1.01	0.3	1.027	1.027
0.136	1.167	1.07	0.4	1.053	1.053
0.200	1.292	1.16	0.5	1.092	1.089
0.256	1.467	1.31	0.6	1.150	1.143
0.305	1.725	1.53	0.7	1.241	1.228
0.350	2.169	1.91	0.8	1.397	1.376
0.389	3.121	2.74	0.9	1.720	1.720

The factor for the model geometry shown in Figure 1.8.4 is 0.471; in general, this factor depends on the eccentricity ratio δ .

The stress-intensity factor for the crack geometry given in Figure 1.8.3 is then a combination of hole effects and width effects and could be expressed as:

$$K = \sigma \sqrt{\pi a} \beta_{\text{HOLE}} \beta_{\text{WIDTH}} \quad (1.8.16)$$

Table 1.8.3 presents the various functions that make up the stress-intensity factor where the width effect is estimated from the Isida solution as given by column ⑤ in Table 1.8.2. It is believed that this width correction solution is also conservative. Figure 1.8.5 presents the comparison graphically so that one can directly assess the individual contributions by the hole and the plate edge.

EXAMPLE 1.8.4 - Diametrically Cracked Hole in Strip

Shown in Figure 1.8.6 is another frequently occurring crack geometry that is seen in aircraft structures. An alternate structural geometry for the diametrically cracked hole is that of a lug. For this example, the crack is assumed to be a thru-thickness crack. Two structural effects must be considered; the effect of the hole and the effect of the finite width. The effects are assumed multiplication so that the stress-intensity factor is again given by

$$K = \sigma \sqrt{\pi a} \beta_{\text{HOLE}} \beta_{\text{WIDTH}} \quad (1.8.17)$$

TABLE 1.8.3

STRESS-INTENSITY FACTOR ANALYSIS FOR EXAMPLE 1.8.3

Crack Length (a) inch	Ratio $\frac{a}{R}$	$\sqrt{\pi a}$ $\sqrt{\text{inch}}$	Hole Factor β_{Hole} [Case 1.7.3.1]	$\frac{K_I}{\sigma} \sqrt{\text{Hole}}$ $\sqrt{\text{inch}}$	Width Factor β_{Width} [From Table 1.8.2-Isida Soln]	$\frac{K_I}{\sigma} \sqrt{\text{Width}}$ $\sqrt{\text{inch}}$	$\frac{K_I}{\sigma} = \frac{\beta_{\text{Hole}} \beta_{\text{Width}} \sqrt{\pi a}}{\sqrt{\text{inch}}}$
0	0	0	3.367	0	1.016	0	0
0.062	0.496	0.441	1.740	0.768	1.027	0.453	0.789
0.136	1.088	0.654	1.290	0.843	1.053	0.688	0.888
0.200	1.600	0.793	1.130	0.896	1.092	0.866	0.978
0.256	2.048	0.897	1.044	0.936	1.150	1.031	1.076
0.305	2.440	0.979	0.992	0.971	1.240	1.214	1.200
0.350	2.800	1.048	0.956	1.002	1.397	1.465	1.400
0.389	3.112	1.105	0.930	1.028	1.720	1.901	1.769

The β_{HOLE} for the thru-thickness diametrically cracked hole located in a wide plate is given by

$$\beta_{\text{HOLE}} = \frac{0.6866}{0.2772 + (\frac{a}{R})} + 0.9439 \quad (1.8.18)$$

(See Subsection 1.7.3, Case 1.7.3.2). The β_{WIDTH} correction factor is made up of two parts; the first part would be associated with the finite width factor associated with the center-crack configuration:

$$\beta_{\text{WIDTH}} = \sqrt{\sec \left(\frac{\pi a^*}{W} \right)}, \quad a^* = a + R \quad (1.8.19)$$

The second part of the width correction factor assumes that the initial geometry without the crack gives a stress field in the finite width strip that is higher than the remotely applied (gross) stress which raises the stress concentration effect at the hole. In fact, the stress suggested is the net stress through the section with the hole so that the stress used in the stress-intensity factor formula is the net stress given by

$$\sigma_{\text{net}} = \sigma * \left[\frac{W}{W-D} \right] \quad (1.8.20)$$

Thus, the approximate stress-intensity factor is given by

$$K = \sigma \sqrt{\pi a} \left[\frac{W}{W-D} \right] * \left[\frac{0.6866}{0.2772 + (\frac{a}{R})} + 0.9439 \right] * \sqrt{\sec \left(\frac{\pi a^*}{W} \right)} \quad (1.8.21)$$

In Table 1.8.4, the approximate stress-intensity factor result given by Equation 1.8.21 is compared to a solution developed by Tada (see Reference 17, page 19.9). Note that the Tada solution is upper-bounded by Equation 1.8.21. Also note that if the $(W/W-D)$ term is eliminated from Equation 1.8.21, the Tada solution is lower-bounded by this new expression.

1.8.3 Effect of Crack Shape Changes

The typical crack problem in most structures is that of the three-dimensional crack. Several crack geometries of interest are shown in Figure 1.8.7. Inherent in the analysis of each three-dimensional crack problem is accounting for the effect of the size and shape of the crack. As indicated in Section 1.7, there are a number of stress-intensity factor solutions already available that might be used to obtain bounds on the solution to more complicated structural crack problems. While it is difficult to obtain accurate stress-intensity factor solutions for three-dimensional crack geometries, the most difficult part of the analysis for such crack geometries is to determine the crack shape as a function of crack size. Three-dimensional cracks tend to grow such that the cracks change their shape into the most favorable shape for ease (and increased speed) of crack propagation. The rate of crack growth along the crack front varies as a function of the driving force at that location; the rate of growth is controlled by global geometry, stress state, crack size as well as the shape of the crack edge. There are some useful analytical methods for estimating the shape of a three-dimensional crack as it grows (see for example References 28 and 90);

TABLE 1.8.4

 β VALUES FOR STRESS-INTENSITY FACTOR COMPONENTS IN PROBLEM 1.8.4

Crack Length a inch	Ratio $(\frac{a}{R})$	β_{Hole} (Equation 1.8.18)	Crack Length a^* inch	Ratio $(\frac{a^*}{W})$	β_{Width} (Equation 1.8.19)	$\frac{\sigma_{net}}{\sigma}$	$\beta_{Hole} \cdot \beta_{Width}$	β_{Tada}^+	$\beta_{Hole} \cdot \beta_{Width}$
0	0	3.42	0.25	0.125	1.04		4.56	3.65	3.56
0.025	0.2	2.383	0.275	0.1375	1.05		3.34	2.94	2.50
0.050	0.4	1.960	0.30	0.150	1.06		2.77	2.69	2.06
0.100	0.8	1.581	0.35	0.175	1.08		2.27	2.17	1.71
0.200	1.6	1.310	0.45	0.225	1.15		2.01	1.96	1.51
0.300	2.4	1.200	0.55	0.275	1.24		1.98	1.91	1.49
0.400	3.2	1.141	0.65	0.325	1.38		2.09	1.86	1.57
0.500	4.0	1.104	0.75	0.375	1.62		2.38	2.10	1.78
0.600	4.8	1.079	0.85	0.425	2.07		2.97	2.58	2.23

$$+ \beta_{Tada} = \sqrt{1 - \frac{a^*}{(\frac{W}{2})}} \cdot F \left(\frac{c}{(\frac{W}{2})}, \frac{2a^*}{W} \right), \text{ Reference 17, page 19.9}$$

however, one of the surest methods for determining the shape of the growing crack is to observe the fracture surfaces of service loaded structures or structural element tests. Once confidence has been established in the shape of the propagating crack, then bounding techniques such as described in Example 1.8.5 can be used to present the growth process as a function of a single parameter. Example 1.8.5 can be used to present the growth process as a function of a single parameter.

EXAMPLE 1.8.5 - Radial Corner Crack Transitioning to a Thru-Crack

For the crack geometry illustrated in Figure 1.8.8, the corner crack is seen to start as a quarter-circular crack and grow to a thru-thickness crack. The transition between corner crack and thru-crack appears to be complete when the crack length (a in the figure) reaches a size equal to the thickness of the structure. The two bounding solutions for this crack geometry are given by the thru-thickness radial hole crack solution (see subsection 1.7.3, Case 1.7.3.1):

$$K = \sigma \sqrt{\pi a} \beta_{\text{HOLE}} = \sigma \sqrt{\pi a} \left[\frac{0.8734}{0.3246 + \left(\frac{a}{R}\right)} + 0.6762 \right] \quad (1.8.22)$$

and by the corner circular radial hole crack solution (see Subsection 1.7.5 case 1.7.5.1)

$$K = 1.12 \sigma \sqrt{\pi a} \left(\frac{2}{\pi}\right) \beta_{\text{HOLE}}^* = 1.12 \sigma \sqrt{\pi a} \left(\frac{2}{\pi}\right) \left[\frac{0.8734}{0.3246 + \left(\frac{a}{\sqrt{2R}}\right)} + 0.6762 \right] \quad (1.8.23)$$

Both Equations (1.8.22 and 1.8.23 in a K/σ format) are shown plotted on log-log coordinates in Figure 1.8.9. A transitioning curve has been fared in between the two curves so that the transition starts at 0.050 inch and is complete at a crack length of 0.250 inch. The equation of this curve is given by the power law:

$$\frac{K}{\sigma} = 1.376 a^{0.2783} \quad (1.8.24)$$

Figure 1.8.10 now describes the stress-intensity factor for the crack geometry in the usually presentation format (a linear-linear diagram). It is seen from Figure 1.8.10 that the power law curve provides a smooth transition between the two bounding stress-intensity factor solutions. An intermediate solution for a crack length of 0.100 inch has been developed using the analysis of Newman (63) for a crack length (a) to depth (c) ratio of 0.50 and it is also shown in Figure 1.8.10. It appears on the basis of the bounding solutions and the Newman result that the power law method gives reasonable estimates of the stress-intensity factor for this problem. The value in obtaining a single parameter characterization of the stress-intensity factor for a three-dimensional crack is that crack growth analysis is substantially easier to perform to determine life.

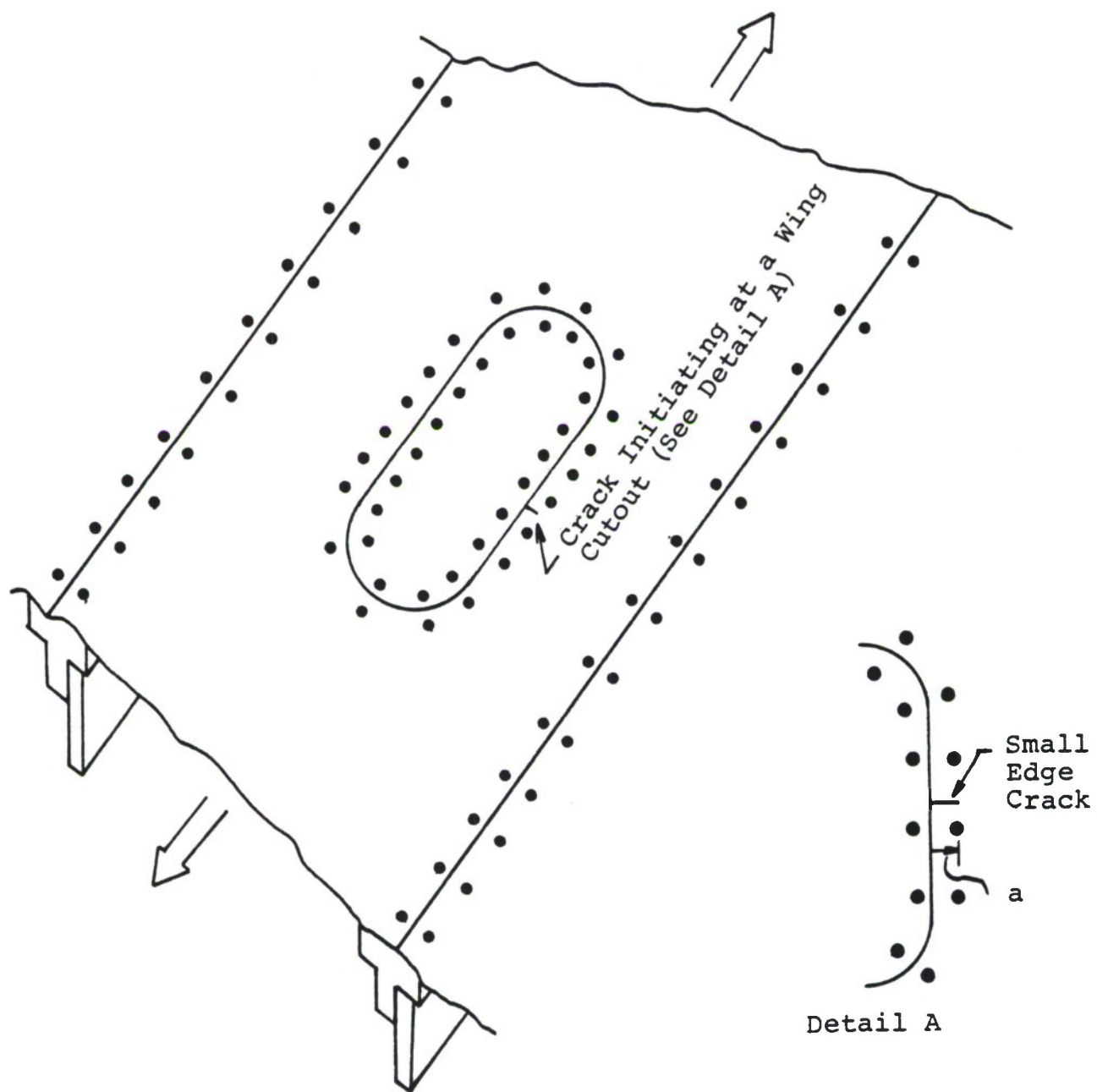


Figure 1.8.1. A Small Edge Crack Located at Stress Concentration.

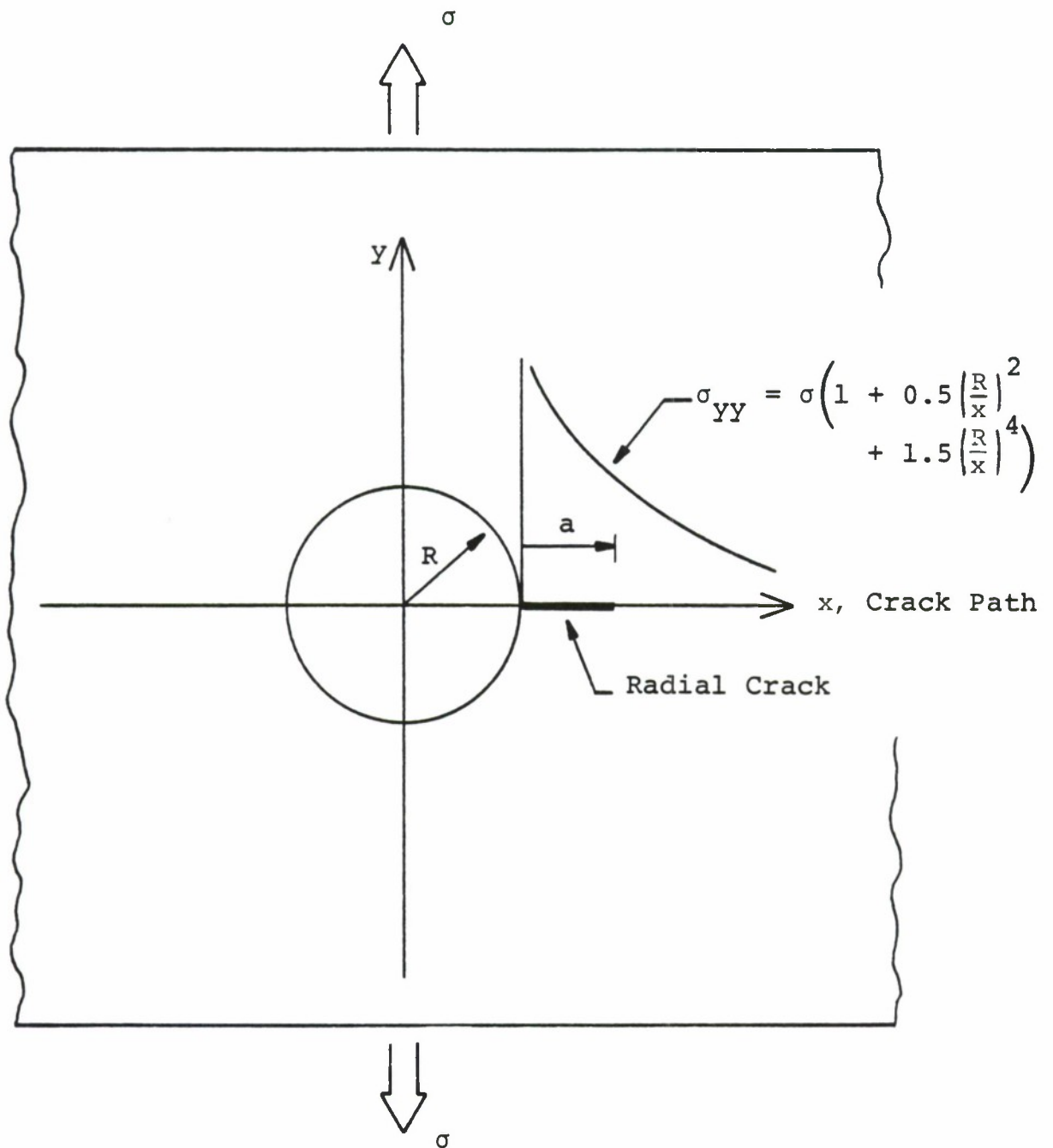
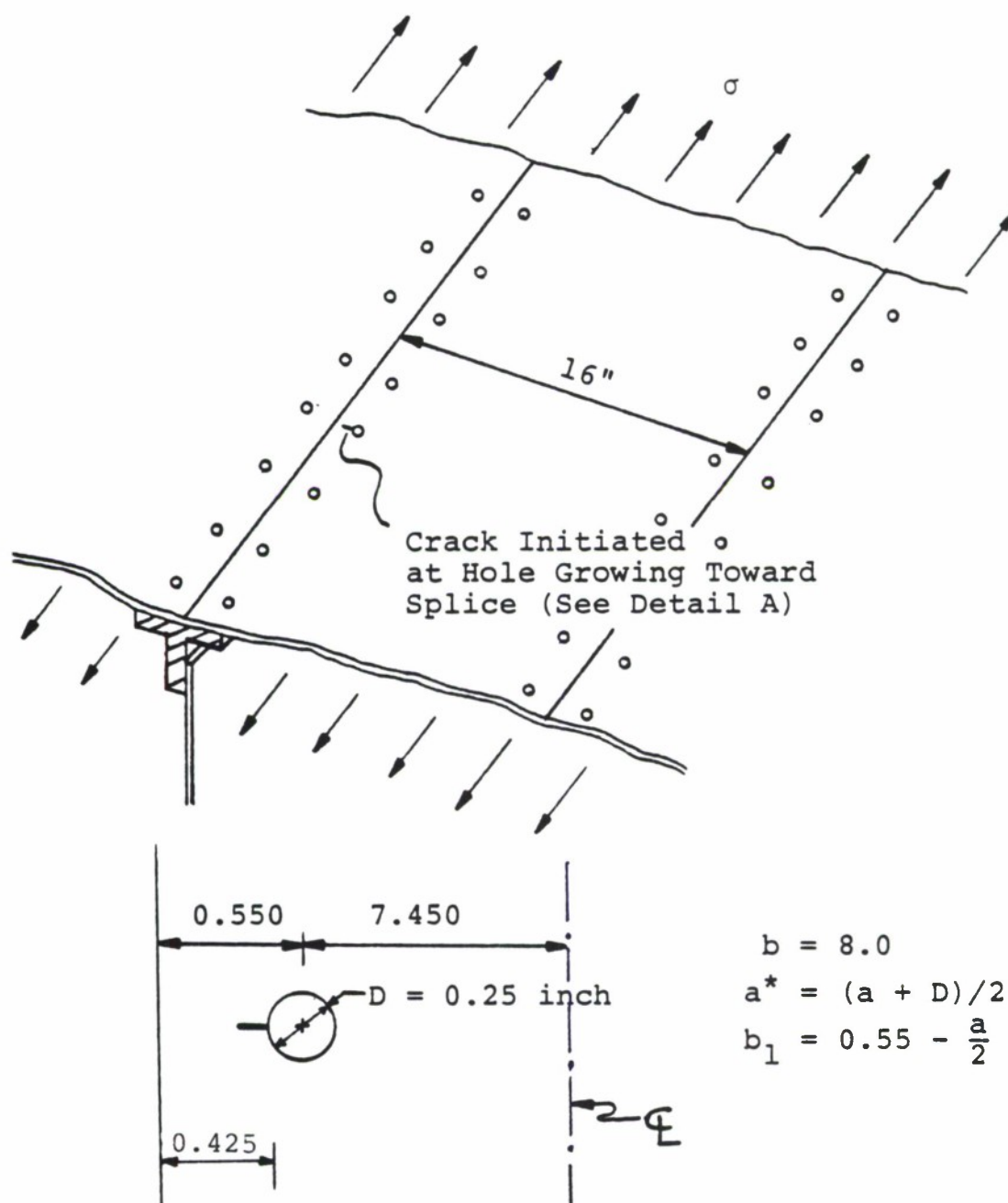


Figure 1.8.2. Distribution of Stresses Normal to the Crack Path for a Radial Crack Growing from an Uniaxially Loaded Hole in a Wide Plate.



Detail A

Figure 1.8.3. Radial Crack at Hole Growing Toward Splice Joint.

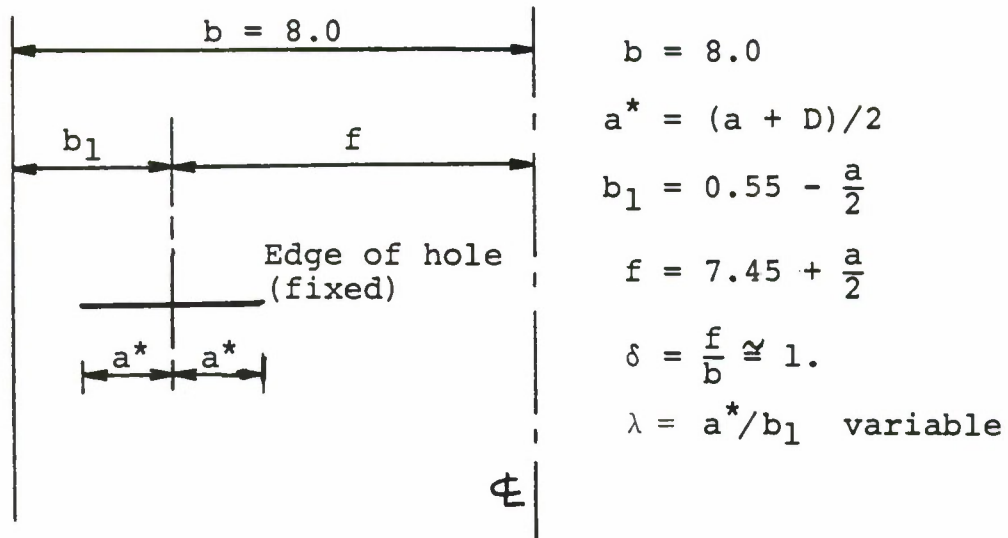


Figure 1.8.4. Model Crack for Example 1.8.3.

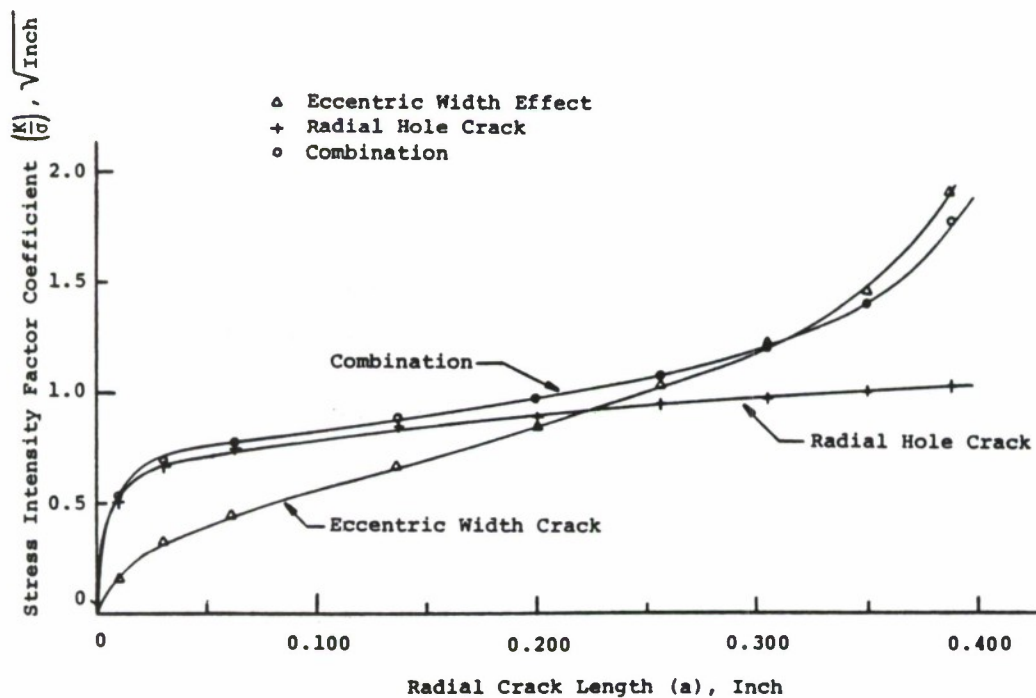


Figure 1.8.5. Comparison of Stress-Intensity Factor Relationships for the Crack Geometry Described in Figure 1.8.3.

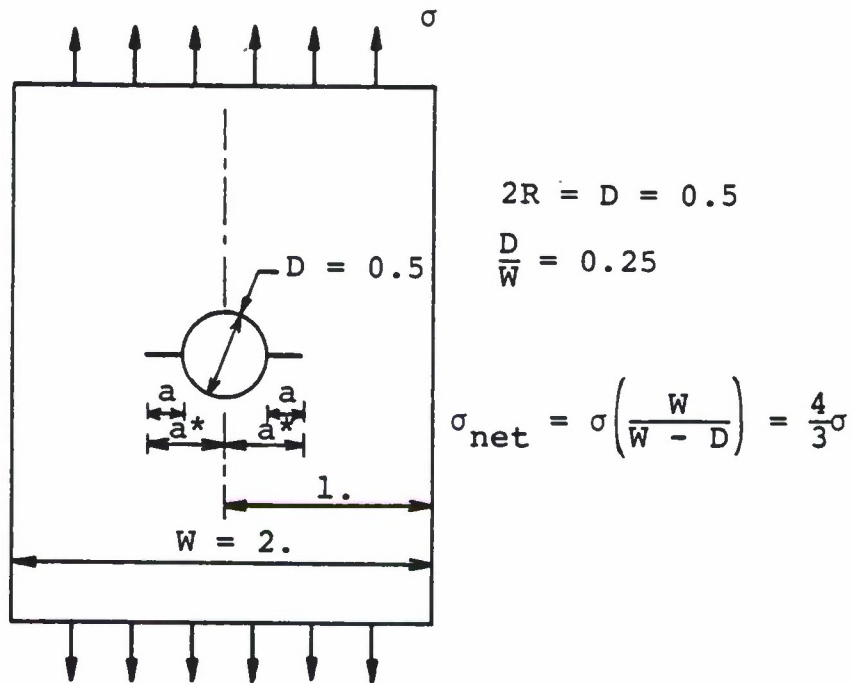


Figure 1.8.6. Finite Width Strip Containing a Diametrically Cracked Hole.

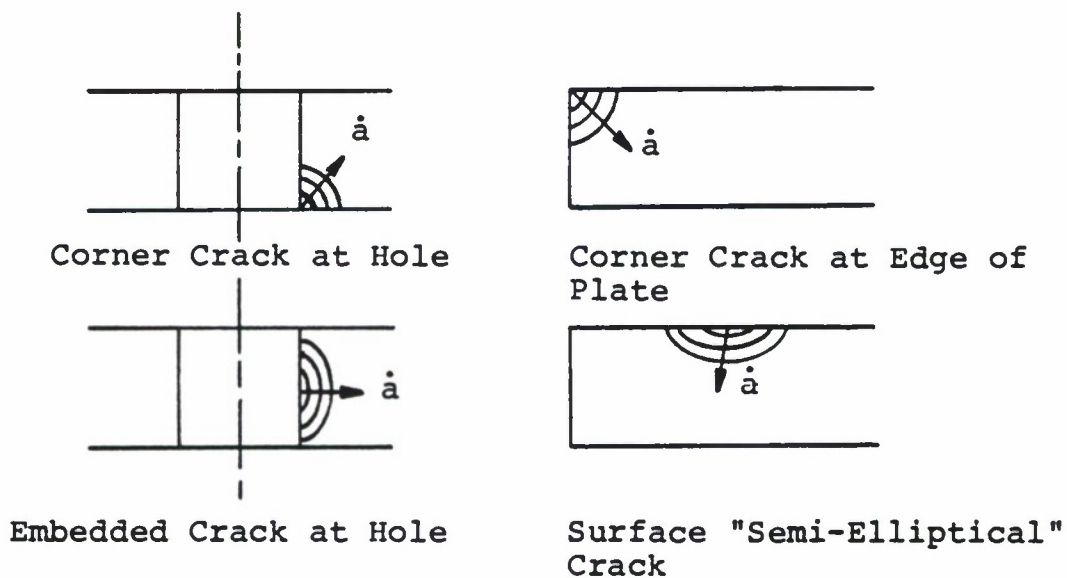


Figure 1.8.7. Plan Views of the Fracture Surfaces of Several Three-Dimensional Crack Problems.

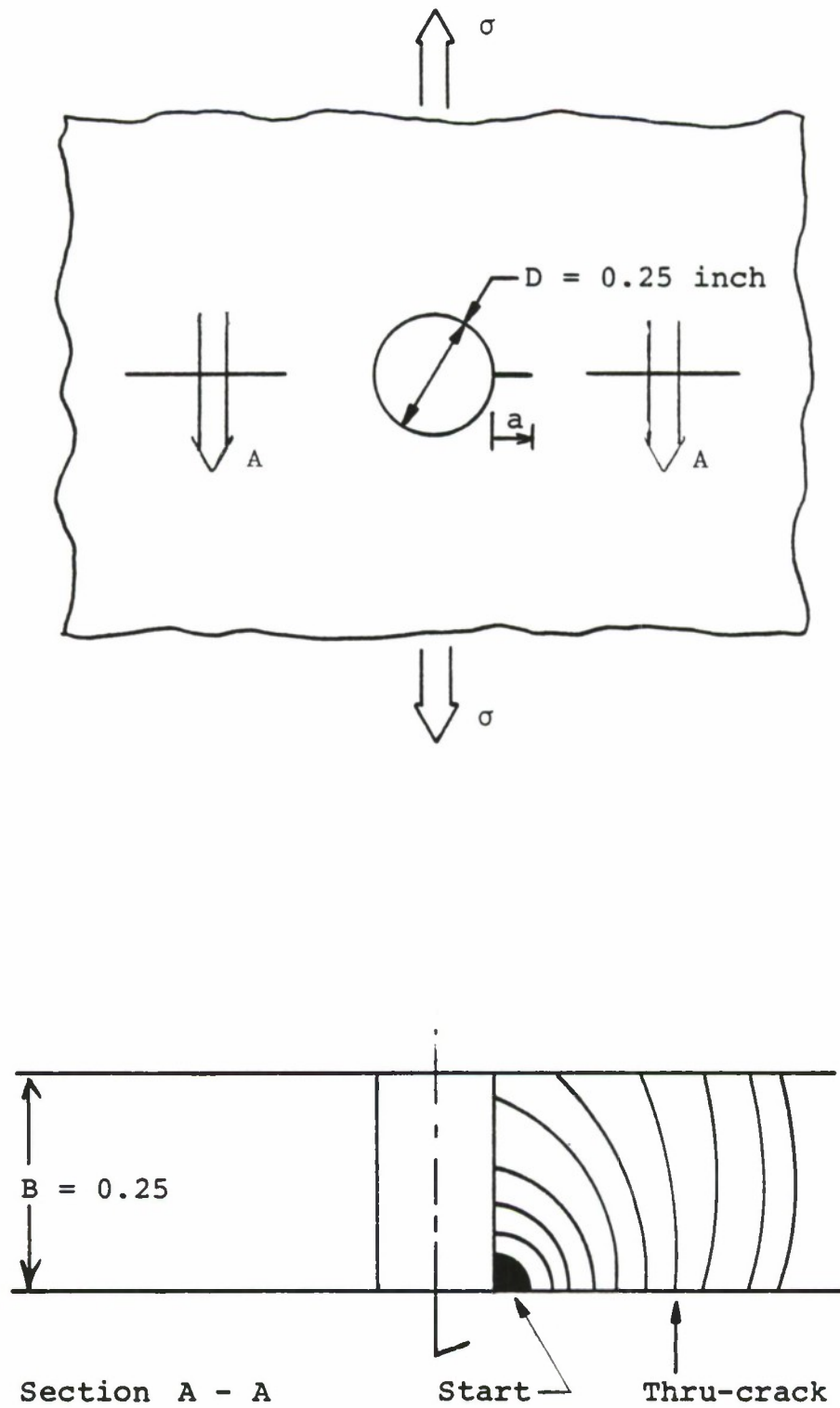


Figure 1.8.8. Corner Crack Transitioning to a Thru-Thickness Crack.

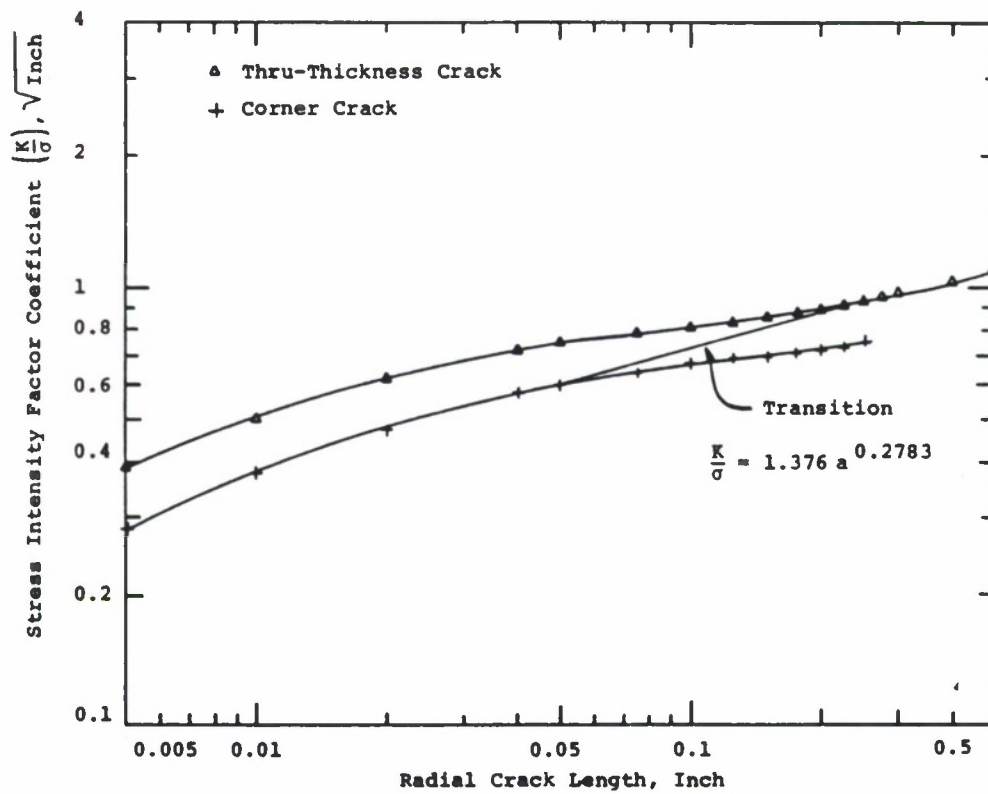


Figure 1.8.9. Log-Log Plot of Equations 1.8.22 and 1.8.23 Showing the Development of the Transition Power Law Equation 1.8.24.

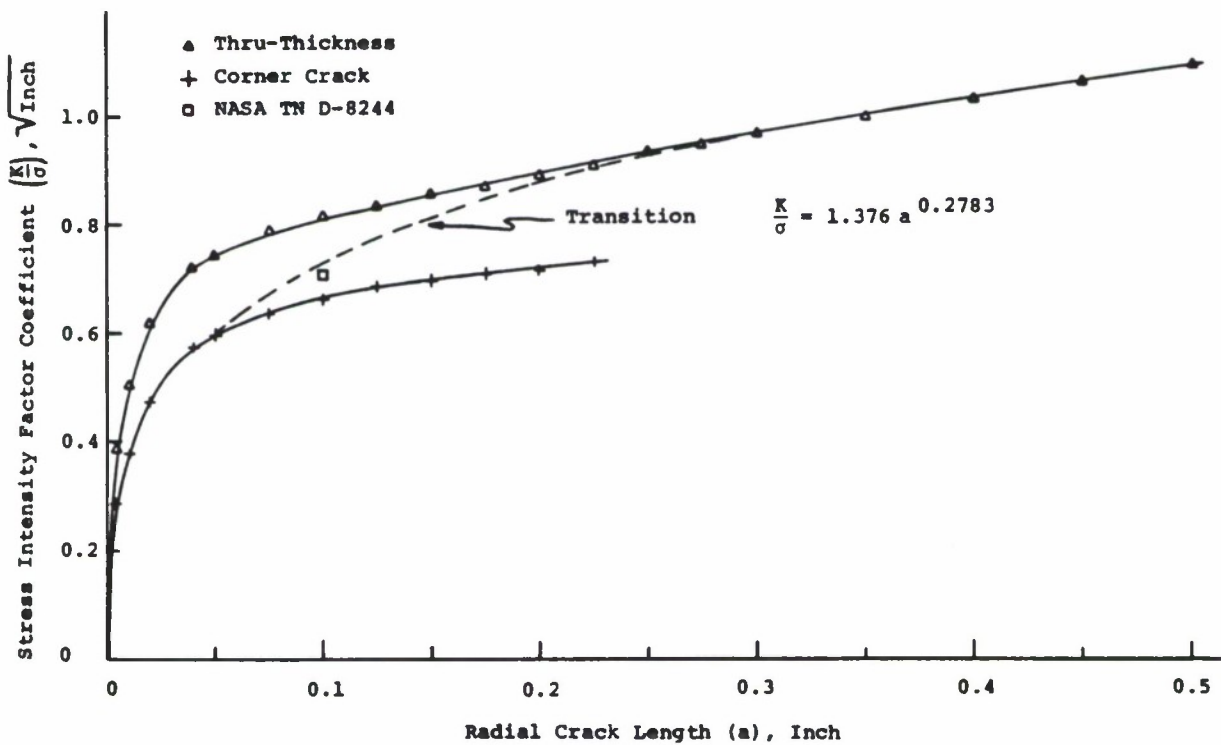


Figure 1.8.10. Stress-Intensity Factor for Transitioning Crack Shown in Figure 1.8.8.

1.9 ALTERNATE FRACTURE MECHANICS ANALYSIS METHODS

In the other sections of Chapter 1, the emphasis has been on developments of linear elastic fracture mechanics (LEFM) specifically based on the crack tip characterizing parameter K , the stress-intensity factor. This parameter has provided the major damage tolerance design tool for aerospace engineers since the early sixties. It was discovered and justified for its universal capability for describing the magnitude of the crack tip stress field by Irwin ^(1,91), and by Williams ⁽²⁾ in 1957. Irwin discovered this relationship through his studies of the energy balance equation associated with fracture. Prior to 1957, fracture research concentrated on extending the original energy balance equation given by Griffith ⁽⁹²⁾. In 1957, Irwin ⁽⁹¹⁾ linked the "driving force", G , in the energy balance equation to the stress-intensity factor, K , and suggested how the stress-intensity factor could be used as the driving force for crack tip behavior. Subsequent to Irwin's initial stress-intensity factor analysis, and as a result of the success of the LEFM approach for solving major fracture problems, interest in the energy approach to fracture waned. In the late sixties, Rice ⁽⁹³⁾ published a paper that again heightened the interest in the energy approach. Rice's specific contribution was to develop an integral, the J-integral, which could be used to account for observed non-linear behavior during the fracture process. This integral also has the useful property that it reduces to the elastic "driving force", G , when the localized plastic deformation is well contained by the elastic crack tip stress field. Because many of the materials utilized in aerospace structures have exhibited typical LEFM behavior, aerospace engineers have not assumed a leadership role in the development of the J-integral technology.

1.9.1

Engineers interested in the damage tolerance analysis of more ductile pressure vessels and welded steel structures have provided the major developments here. Aerospace applications are being recognized each day, however, for this technology, e.g., residual strength analysis of tough materials and subcritical crack growth behavior of aircraft gas turbine engine structures.

Another analysis approach for characterizing the level of the local stress-strain behavior at the tip of a crack was initiated in Britain in the early sixties. Wells ⁽⁹⁴⁾ suggested that the localized behavior at the tip of the crack was controlled by the amount of crack opening, which was referred to as the crack opening displacement, COD. The value of the technology built on the COD concept, like that of the J-Integral technology, is that it allows for the coupling of the LEFM analysis and its results to the solution of problems in which the behavior approaches unconstrained yielding. Generally speaking, the methods of COD analysis have not been extensively explored by American engineers outside the research environment.

The subsections below further describe the analysis methodologies based on the three fracture mechanics parameters: the strain energy release rate (driving force - G), the J-Integral (J), and the crack opening displacement (COD), respectively. Each subsection outlines the analytical basis for the parameter and provides the principal equations that tie the parameter to the LEFM parameter K . Further information on these parameters can be obtained by the references cited in the text.

1.9.1 Strain Energy Release Rate, G

Paris ⁽⁵⁶⁾ gave one of the better descriptions of the fracture energy balance equation associated with the stability of a cracking process in a set of notes prepared for a short course given to the Boeing Company in 1960. Paris simply described the process of determining if a crack would extend as a comparison between the Rate of Energy Input and the Rate at which Energy was absorbed or dissipated. This comparison is similar to performing an analysis based on the Principle of virtual work. In equation form, Paris indicated

$$\begin{array}{|c|} \hline \text{Rate of} \\ \text{Energy Input, } G \\ \text{(to drive crack)} \\ \hline \end{array} \longleftrightarrow \begin{array}{|c|} \hline \text{Rate of Energy} \\ \text{Dissipated, } R \\ \text{(as crack moves)} \\ \hline \end{array} \quad (1.9.1)$$

where the left hand side of Equation 1.9.1 represents the input rate (as a function of crack area A) and the right hand side represents the dissipation rate. If the input rate, the driving force G , is equal to the dissipation rate, the resistance R , then the crack is in an equilibrium (stable) position, i.e., it is ready to grow but doesn't. If the driving force exceeds the resistance, then the crack grows, an unstable position. Since a crack will not heal itself, if the resistance is greater than the driving force, then the crack is also stable.

The basis for Equation 1.9.1 was further described ⁽⁵⁶⁾ so that the components are identified as:

$$G = \frac{dX}{dA} + \frac{dG}{dA} \begin{array}{l} \leq \frac{dS}{dA} + \frac{dQ}{dA} = R \\ > \end{array} \quad (1.9.2)$$

where $<$ and $=$ imply stability while $>$ implies instability.

1.9.3

The driving force (input work rate, G) components are:

$\frac{dX}{dA}$ = The work done by external forces on the body per unit increase in crack area, dA .

$\frac{dG}{dA}$ = The elastic strain energy released per unit increase in dA .

And the resistance (rate of dissipation, R) components are:

$\frac{dS}{dA}$ = The surface energy absorbed in creating a new surface area, dA .

$\frac{dQ}{dA}$ = The plastic work dissipated throughout the body during an increase in surface area, dA .

While Equation 1.9.2 is most general and covers fractures that initiate in either brittle or ductile materials, it is not always possible to estimate the individual component terms. For linear elastic materials, the terms can be estimated; and in fact, this was accomplished by Griffith⁽⁹²⁾ forty years before Paris presented the above general work rate analysis in 1960. Before any further discussion of the work preceeding that of Paris, however, several additional points need to be made about Equation 1.9.2. First, the component terms of the input energy rate will be defined relative to a specific structural geometry and loading configuration: the uniaxially loaded, center cracked panel shown in Figure 1.9.1. Then the input energy rate (G) will be related to the elastic strain energy.

The two components of the energy input rate (G) are given by

$$\frac{dX}{dA} = \frac{PdL}{dA} \quad (1.9.3)$$

the boundary force per increment of crack extension; and by

$$\frac{dG}{dA} = \frac{-dV}{dA} \quad (1.9.4)$$

the decrease in the total elastic strain energy of the plate.

With these additional definitions, it can be seen that G is equal to the negative of the rate of change in the potential energy of deformation (U_{σ}), i.e.,

$$G = \frac{-dU_{\sigma}}{dA} \quad (1.9.5)$$

1.9.1.1 The Griffith-Irwin Energy Balance

The earliest analysis along the above lines was conducted by Griffith ⁽⁹²⁾ in 1920. Griffith used the crack geometry and loading configuration shown in Figure 1.9.2 and assumed that the stress would be constant during any incremental growth of the crack. Griffith also neglected the plastic work term in Equation 1.9.2 since he was trying to test his fracture hypothesis with a brittle material, glass. Griffith's analysis showed that the input work rate (G) was equal to the negative of the derivative of potential energy of deformation (U_{σ}) as shown by Equation 1.9.5, and the resistance (R) was equal to the rate of increase in potential energy due to surface energy (U_T) during crack extension:

$$R = \frac{dS}{dA} = \frac{dU_T}{dA} \quad (1.9.6)$$

The potential energy of deformation (U_{σ}) was found to be

$$U_{\sigma} = \frac{-\pi \sigma^2 a^2 B}{E} \quad (1.9.7)$$

while the potential energy due to surface tension (U_T) was given by

$$U_T = 4aTB \quad (1.9.8)$$

with surface tension T , and for plate thickness B

The crack area A is given by

$$A = 2aB \quad (1.9.9)$$

So the energy balance equation becomes

$$G = \frac{-dU}{dA} = \frac{\sigma^2 \pi a}{E'} = 2T = \frac{dS}{dA} = R \quad (1.9.10)$$

where E' is dependent on the stress state in the following way

$$E' = \begin{array}{ll} \text{or} & E/(1 - \nu^2), \text{ for plane strain} \\ & E, \text{ for plane stress} \end{array} \quad (1.9.11)$$

Solving Equation 1.9.10 for the critical stress (σ_{cr}) associated with the point at which the crack (a) would grow, one finds

$$\sigma_{cr} = \sqrt{\frac{2TE'}{\pi a}} \quad (1.9.12)$$

Later, Irwin (95) and Orowan (96) incorporated the effects of crack tip plasticity into the analysis by taking the plastic dissipation term in Equation 1.9.2 as a constant, i.e. they assumed that

$$\frac{dQ}{dA} = q \quad (1.9.13)$$

so that the resistance in Equation 1.9.10 was defined as the combination of surface energy absorbed and plastic work dissipated. Thus, the Griffith-Irwin-Orowan energy balance equation became

$$G = \frac{\sigma^2 \pi a}{E'} = 2T + q = R \quad (1.9.14)$$

and the critical stress was

$$\sigma_{cr} = \sqrt{\frac{(2T + q)E'}{\pi a}} \quad (1.9.15)$$

Both Irwin and Orowan noted that the plastic dissipation rate for metals was at least a factor of 1000 greater than the surface energy absorption rate so that Equation 1.9.15 could be approximated by

$$\sigma_{cr} = \sqrt{\frac{qE'}{\pi a}} \quad (1.9.16)$$

Irwin also noted that the driving force or input energy rate G was directly related to the square of the magnitude of the crack tip stress field for the Griffith center crack geometry (Figure 1.9.2), i.e., that

$$G = \frac{\sigma^2 \pi a}{E'} = \frac{K^2}{E'} \quad (1.9.17)$$

Later, Irwin ⁽⁹²⁾ reported this result to be general for any cracked elastic body based upon a virtual work analysis of the stresses and displacements associated with crack tip behavior during an infinitesimal crack extension.

1.9.1.2 The Relationship between G , Compliance, and Elastic Strain Energy

If one defines the relationship between the force (P) applied to the structure shown in Figure 1.9.1 and the deformation it induces in the direction of load as

$$\Delta L = C \cdot P \quad (1.9.18)$$

where

$$C = C(A) \quad (1.9.18a)$$

is the compliance, the inverse structural stiffness, which varies as a function of crack length (area). With the definitions given by Equation 1.9.18, the elastic strain energy (V) can be written as

$$V = \frac{P \cdot \Delta L}{2} = \frac{CP^2}{2} \quad (1.9.19)$$

The change in V simultaneous to dA and dP is:

$$dV = \left. \frac{\partial V}{\partial A} \right|_P dA + \left. \frac{\partial V}{\partial P} \right|_A dP \quad (1.9.20)$$

which leads to

$$dV = \frac{P^2}{2} \frac{\partial C}{\partial A} dA + CPdP \quad (1.9.21)$$

Similar operations on changes in dL (= d(ΔL)) lead to

$$PdL = P^2 \frac{\partial C}{\partial A} dA + PCdP \quad (1.9.21)$$

So that the input energy rate (G) based on Equation 1.9.2 becomes

$$G = \frac{dX}{dA} + \frac{dG}{dA} = \frac{P^2}{2} \cdot \frac{\partial C}{\partial A} + (0) \cdot \frac{dF}{dA} \quad (1.9.22)$$

Showing that the input energy rate is independent of the variation of force during any incremental crack extension. Thus, Equation 1.9.22 reduces to

$$G = \frac{P^2}{2} \frac{\partial C}{\partial A} \equiv \left. \frac{\partial V}{\partial A} \right|_P = \text{constant} \quad (1.9.23)$$

Equation 1.9.23 provides the basis for experimentally evaluating the crack driving force using compliance measurements and clearly shows that the rate of energy input is identically equal to the change in elastic strain energy considering the loading force constant. When one conducts a similar analysis with the displacement (ΔL) and crack area (A) as independent variables, one finds that

$$G = - \left. \frac{\partial V}{\partial A} \right|_{\Delta L} = \text{constant} \quad (1.9.24)$$

which means that the input energy rate is the negative of the areal derivative of elastic strain energy considering the displacement constant during crack extension. This is the so-called fixed displacement condition. The term strain

energy release rate was assigned to G , the input energy rate, when it was realized that for cracked elastic bodies Equations 1.9.23 and 1.9.24 were generally applicable.

Figure 1.9.3 describes the change in elastic strain energy which occurs when a crack grows under (a) fixed load and (b) fixed displacement conditions. It can be noted that the difference between the change in elastic strain energy for the two cases is the infinitesimal area $\frac{1}{2}(dP) \cdot d(\Delta L)$, shown cross-hatched in Figure 1.9.3a. For the case of the fixed load condition (Figure 1.9.3a), the elastic strain energy is seen to increase as the crack grows; the gain in elastic strain energy is greater than the indicated loss (by a factor of 2). For the case of the fixed displacement condition (Figure 1.9.3b), the elastic strain energy is seen to decrease as the crack grows; only a loss is indicated.

Some important observations presented in the subsection are: (a) the general form of Equation 1.9.17 can be utilized to relate G and K ; (b) G is equal to the negative rate of change in the potential energy of deformation (Equation 1.9.5); and, (c) G is related to the areal rate of change in compliance (Equation 1.9.23). Note that by combining Equations 1.9.17 and 1.9.5 or 1.9.23 the analyst and/or experimentalist has energy-based methods for obtaining estimates of the stress-intensity factor. These combinations are discussed in Section 1.6.4 (See, for example, Equation 1.6.35).

1.9.2 The J-Integral, J

In 1968, Rice⁽⁹³⁾ published a paper describing a path independent integral (J) which was noted to be equal to the negative of the change in potential energy of deformation occurring during the infinitesimal growth of a crack in a nonlinear elastic material, i.e. he showed that

$$J = - \frac{\partial U_G}{\partial A} \quad (1.9.25)$$

Rice's path independent integral J was defined by^(4,93)

$$J = \int_{\Gamma} \left(W \, dy - \vec{T} \cdot \frac{\partial \vec{u}}{\partial x} \, ds \right) \quad (1.9.26)$$

where Γ is any contour surrounding the crack tip, traversing in a counter clockwise direction (See Figure 1.9.4), W is the strain energy density, \vec{T} is the traction on Γ , and \vec{u} is the displacement on an element along arc s . Before elaborating on a detailed description of the parameters involved in the calculation of the J-Integral, it is useful to note that Equation 1.9.25 is the nonlinear elastic equivalent of Equation 1.9.5. Thus, for linear elastic materials, J reduces to the value of the strain energy release rate, G , i.e.

$$J = G \quad (1.9.27)$$

and the J-integral is related to the stress-intensity factor through the

expression

$$J = \frac{K^2}{E'} \quad (1.9.28)$$

where E' is given by Equation 1.9.11.

Equations 1.9.27 and 1.9.28 are noted to be valid only when the material is behaving in a linear elastic fashion. When values of the J-Integral are determined via Equation 1.9.26 using finite element methods applied to linear elastic cracked structures, Equation 1.9.28 provides the engineer with a simple energy-based method for obtaining stress-intensity factors as a function of crack length, see subsection 1.6.4.

In the first subsection below, the calculations associated with developing the J-Integral for an elastic-plastic material are detailed. In the second subsection, some engineering approximation methods for calculating the J-Integral are outlined.

1.9.2.1 J-Integral Calculations

This subsection outlines the calculation of parameters involved in the J-Integral. Consideration is given to W , \vec{T} , \vec{u} , and Γ as well as the choice of material stress-strain behavior.

The strain energy density W in Equation 1.9.26 is given by

$$W = \int [\sigma_{xx} d\epsilon_{xx} + \sigma_{xy} d\gamma_{xy} + \sigma_{xz} d\gamma_{xz} + \sigma_{yy} d\epsilon_{yy} + \sigma_{yz} d\gamma_{yz} + \sigma_{zz} d\epsilon_{zz}] \quad (1.9.29)$$

and for generalized plane stress

$$W = \int [\sigma_{xx} d\epsilon_{xx} + \sigma_{xy} d\gamma_{xy} + \sigma_{yy} d\epsilon_{yy}] \quad (1.9.30)$$

In Equation 1.9.26, the second integral involves the scalar product of the traction stress vector \vec{T} and the vector $\frac{\partial \vec{u}}{\partial x}$ whose components are the rate of change of displacement with respect to x. The traction vector is given by

$$\vec{T} = T_x \hat{i} + T_y \hat{j} = (\sigma_{xx} \cdot n_x + \sigma_{xy} \cdot n_y) \hat{i} + (\sigma_{yx} \cdot n_x + \sigma_{yy} \cdot n_y) \hat{j} \quad (1.9.31)$$

and the displacement rate vector is given by

$$\frac{\partial \vec{u}}{\partial x} = \frac{\partial u}{\partial x} \hat{i} + \frac{\partial v}{\partial x} \hat{j} \quad (1.9.32)$$

where u and v are the displacements in the x and y directions, respectively.

Typically, when evaluating the J-Integral value via computer, rectangular paths such as the one illustrated in Figure 1.9.5 are chosen. Noted on Figure K 1.9.5 are the values of the outward unit normal components and the ds path segment for the four straightline segments. For loading symmetry about the crack axis (x-axis), the results of the integration on paths 0-1, 1-2, and 2-3 are equal to the integrations on paths 6-7, 5-6, and 4-5, respectively. Thus, for such loading symmetry, one can write

$$J = 2 \left\{ \int_6^7 [W - \sigma_{xx} \frac{\partial u}{\partial x} - \sigma_{xy} \frac{\partial v}{\partial x}] dy + \int_5^6 [\sigma_{xy} \frac{\partial u}{\partial x} + \sigma_{yy} \frac{\partial v}{\partial x}] dx + \int_4^5 [W - \sigma_{xx} \frac{\partial u}{\partial x} - \sigma_{xy} \frac{\partial v}{\partial x}] dy \right\} \quad (1.9.33)$$

For paths of the type shown in Figure 1.9.5, the J-Integral can be evaluated by the integrations indicated in Equation 1.9.33. The strain energy density W , appearing in Equation 1.9.33, is given by Equation 1.9.29, or by Equation 1.9.30 for plane stress conditions. To integrate according to Equations 1.9.29 or 1.9.30, a relationship between stresses and strains is required. For material exhibiting plastic deformations, the Prandtl-Reuss equations provide a satisfactory relationship. For the case of plane stress, when the Prandtl-Reuss relations are introduced into Equation 1.9.30, Equation 1.9.30 becomes

$$W = \frac{1}{2E} [\sigma_{xx}^2 + \sigma_{yy}^2] + \frac{(1-\nu)}{E} [\sigma_{xy}^2 - \sigma_{xy} \sigma_{yy}] + \int \bar{\sigma} d\bar{\epsilon}_p \quad (1.9.34)$$

where $\bar{\sigma}$ and $\bar{\epsilon}_p$ are the equivalent stress and equivalent plastic strain, respectively. The strain energy density will have a unique value only if unloading is not permitted. If loading into the plastic range followed by unloading is permitted, then W becomes multivalued. It follows that J is also multivalued for this occurrence.

The statements made in the preceding paragraph would appear to seriously limit the use of J as a fracture criterion since the case of loading into the plastic range followed by unloading (i.e., the case for which J is multivalued) occurs when crack extension takes place. On the basis of a number of examples, Hayes⁽⁹⁷⁾ deduced that monotonic loading conditions prevail throughout a cracked body under steadily increasing load applied to the boundaries, provided that crack extension does not occur. Thus, valid J calculations can be performed for this case.

1.9.2.2 Engineering Estimates of J

While the J-Integral was developed for nonlinear elastic material behavior, it has been extensively studied for its direct application to describing elastic-plastic material behavior⁽⁹⁸⁻¹⁰²⁾.

Its nonlinear elastic foundation has provided engineers with some techniques which allow them to focus on the combination of linear-elastic and plastic-strain hardening behavior and then to separate these two components for further study of the plastic behavior. The J-Integral for an elastic-plastic material is taken as the sum of two component parts: the linear elastic part (J_{el}) and the plastic-strain hardening part (J_{pl}), i.e.,

$$J = J_{el} + J_{pl} \quad (1.9.35)$$

which when used in conjunction with Equation 1.9.28 becomes

$$J = \frac{K^2}{E'} + J_{pl} \quad (1.9.36)$$

Engineering estimates of J then focus on the development of the plastic-strain hardening part J_{pl} . Recently, Shih and coworkers⁽¹⁰³⁻¹⁰⁶⁾ have published a series of reports and technical papers detailing how the J_{pl} term can be calculated from a series of finite element models that consider changes in material properties for the same structural geometry. The following briefly describes the Shih and coworkers method for estimating J_{pl} .

First, the material is assumed to behave according to a power hardening constitutive (σ - ϵ) law of the form

$$\frac{\epsilon}{\epsilon_0} = \alpha \left(\frac{\sigma}{\sigma_0} \right)^n \quad (1.9.37)$$

where α is a dimensionless constant, σ_0 and ϵ_0 are reference (yield) stresses and strains related by $\sigma_0 = E\epsilon_0$, and n is the hardening exponent.

For $n = 1$, the material behaves as a linearly elastic material; as n approaches infinity, the material behaves more and more like a perfectly plastic material. For a generalization of Equation 1.9.37 to multiaxial states via the J_2 deformation theory of plasticity, Ilyushin⁽¹⁰⁷⁾ showed that the stress at each point in the body varies linearly with a single load such as σ , the remotely applied stress, under certain conditions.

Ilyushin's analysis allowed Shih and Hutchinson⁽¹⁰⁸⁾ to use the relationship for crack tip stresses under contained plasticity, i.e. to use⁽¹⁰⁹⁻¹¹⁰⁾

$$\sigma_{xx} = \sigma_0 \left(\frac{J_{p1}}{r\sigma_0\epsilon_0} \right)^{\frac{1}{1+n}} \tilde{\sigma}_{xx} \left(\theta, \frac{1}{n} \right) \quad (1.9.38)$$

and similar equations for σ_{yy} , σ_{xy} , etc., to relate the crack tip parameters uniquely to the remotely applied load. Note that J_{p1} term in Equation 1.9.38 acts as a (plastic) stress field magnification factor similar to that of the stress-intensity factor in the elastic case. The form of the relationship that Shih and Hutchinson postulated is given by

$$\frac{J_{p1}}{\sigma_0\epsilon_0 a} = \left(\frac{\sigma}{\sigma_0} \right)^{n+1} \cdot \hat{J} \left(\frac{a}{b}, n \right) \quad (1.9.39)$$

where \hat{J} is a function only of relative width (a/b) and n . An alternate form of Equation 1.9.39 that has been previously used in computer codes (104, 106, 111) is

$$J_{pl} = \alpha \sigma_o \epsilon_o a \cdot f_1\left(\frac{a}{b}\right) \cdot h_1\left(\frac{a}{b}, n\right) \cdot \left(\frac{P}{P_o^T}\right)^{n+1} \quad (1.9.40)$$

where P is the applied load (per unit thickness), P_o^T is the theoretical limit load (per unit thickness), f_1 is a function only of geometry and crack length, while h_1 depends on geometry, crack length, and the strain hardening exponent n . Shih and co-workers (104, 106) have tabulated the functions for a number of geometries for conditions of plane stress and plane strain. From the reference tabulated data (also see Reference 111), these functions can be obtained by interpolation for any value within the $\frac{a}{b}$ and n limits given; thus, the plastic (strain hardening) component of Equation 1.9.36 can be computed for any given applied load P from Equation 1.9.40.

EXAMPLE 1.9.1 - J Estimated for Center Crack Panel

Figure 1.9.1 describes the geometry for this example wherein the width W is set equal to $2b$ and the load P is expressed per unit thickness. Repeating Equation 1.9.36 to describe the relationship between the elastic and plastic components, we have

$$J = \frac{K^2}{E'} + J_{pl} \quad (1.9.36R)$$

From elastic analysis, the stress-intensity factor is known to be (see subsection 1.7.1):

$$K = \left(\frac{P}{2b}\right) \sqrt{\pi a \sec \left(\frac{\pi a}{2b}\right)} \quad (1.9.41)$$

For the strain hardening analysis, Equation 1.9.40 is employed, i.e., we use

$$J_{p1} = \alpha_{\sigma_0 \epsilon_0} a \cdot f_1\left(\frac{a}{b}\right) \cdot h_1\left(\frac{a}{b}, n\right) \cdot \left(\frac{P}{P_o^T}\right)^{n+1} \quad (1.9.40R)$$

For a center crack panel, the function f_1 is given by (104, 106)

$$f_1\left(\frac{a}{b}\right) = \frac{(2b - 2a)}{2b} \quad (1.9.42)$$

and the limit load (per unit thickness) is given by either

$$P_o^T = \frac{4}{\sqrt{3}} \sigma_0 (b - a) \quad (1.9.43a)$$

for plane strain or by

$$P_o^T = 2\sigma (b - a) \quad (1.9.43b)$$

for plane stress. The supporting data for calculating the function h_1 is supplied by Table 1.9.1a for plane strain conditions and by Table 1.9.1b for plane stress conditions. The other functions (h_2 and h_3) contained in these tables support displacement calculations. As indicated above, data are available for estimating the J-integral according to this approach for a number of additional (simple) geometries. See Reference 106 and 111 for further examples.

In the application of Equation 1.9.36 to structural material problems, it has been found ⁽¹¹²⁾ that better correlation with experimental results is obtained if one uses the plasticity enhanced, effective crack length (a_e) in place of the physical crack length (a) in the elastic component expressions. The effective crack length utilized by Bucci, et al. ⁽¹¹²⁾ was based on the Irwin plastic zone size correction, i.e. the effective crack length was given by

$$a_e = a + r_y \quad (1.9.44)$$

where

$$r_y = \frac{1}{x\pi} \left(\frac{K}{\sigma_0} \right)^2 \quad (1.9.45)$$

with $x = 2$ for plane stress and $x = 6$ for plane strain. The stress-intensity factor is represented by K .

TABLE 1.9.1a

 h_1, h_2 and h_3 FOR THE PLANE STRAIN CCP IN TENSION (REFERENCES 103, 104, 111)

	$n = 1$	$n = 2$	$n = 3$	$n = 5$	$n = 7$	$n = 10$	$n = 13$	$n = 16$	$n = 20$
$\left. \begin{matrix} h_1 \\ h_2 \\ h_3 \end{matrix} \right\} \begin{matrix} a/b = 1/4 \end{matrix}$	2.535 2.680 0.536	3.009 2.989 0.911	3.212 3.014 1.217	3.289 2.847 1.639	3.181 2.610 1.844	2.915 2.618 1.554	2.625 1.971 1.802	2.340 1.712 1.637	2.028 1.450 1.426
$\left. \begin{matrix} h_1 \\ h_2 \\ h_3 \end{matrix} \right\} \begin{matrix} a/b = 3/8 \end{matrix}$	2.344 2.347 0.699	2.616 2.391 1.059	2.648 2.230 1.275	2.507 1.876 1.440	2.281 1.580 1.396	1.969 1.276 1.227	1.709 1.065 1.050	1.457 0.890 0.888	1.193 0.715 0.719
$\left. \begin{matrix} h_1 \\ h_2 \\ h_3 \end{matrix} \right\} \begin{matrix} a/b = 1/2 \end{matrix}$	2.206 2.028 0.803	2.291 1.856 1.067	2.204 1.600 1.155	1.968 1.230 1.101	1.759 1.002 0.968	1.522 0.799 0.796	1.323 0.664 0.665	1.155 0.564 0.565	0.978 0.466 0.469
$\left. \begin{matrix} h_1 \\ h_2 \\ h_3 \end{matrix} \right\} \begin{matrix} a/b = 5/8 \end{matrix}$	2.115 1.705 0.844	1.960 1.322 0.937	1.763 1.035 0.879	1.616 0.696 0.691	1.169 0.524 0.522	0.863 0.358 0.361	0.628 0.250 0.251	0.458 0.178 0.178	0.300 0.114 0.115
$\left. \begin{matrix} h_1 \\ h_2 \\ h_3 \end{matrix} \right\} \begin{matrix} a/b = 3/4 \end{matrix}$	2.072 1.345 0.805	1.732 0.857 0.700	1.471 0.596 0.555	1.108 0.361 0.359	0.895 0.254 0.254	0.642 0.167 0.168	0.461 0.114 0.114	0.337 0.081 0.081	0.216 0.051 0.052

TABLE 1.9.1b

 h_1 , h_2 and h_3 FOR THE PLANE STRESS CCP IN TENSION (REFERENCES 103, 104, 111)

	$n = 1$	$n = 2$	$n = 3$	$n = 5$	$n = 7$	$n = 10$	$n = 13$	$n = 16$	$n = 20$
$\left. \begin{matrix} h_1 \\ h_2 \\ h_3 \end{matrix} \right\} \begin{matrix} a/b = 1/4 \end{matrix}$	2.544 3.116 0.611	2.972 3.286 1.010	3.140 3.304 1.352	3.195 3.151 1.830	3.106 2.926 2.083	2.896 2.595 2.191	2.647 2.288 2.122	2.467 2.081 2.009	2.196 1.814 1.792
$\left. \begin{matrix} h_1 \\ h_2 \\ h_3 \end{matrix} \right\} \begin{matrix} a/b = 3/8 \end{matrix}$	2.344 2.710 0.807	2.533 2.621 1.195	2.515 2.414 1.427	2.346 2.032 1.594	2.173 1.753 1.570	1.953 1.473 1.425	1.766 1.279 1.267	1.608 1.134 1.133	1.431 0.988 0.994
$\left. \begin{matrix} h_1 \\ h_2 \\ h_3 \end{matrix} \right\} \begin{matrix} a/b = 1/2 \end{matrix}$	2.206 2.342 0.927	2.195 2.014 1.186	2.057 1.703 1.256	1.809 1.299 1.178	1.632 1.071 1.040	1.433 0.871 0.867	1.300 0.757 0.758	1.174 0.666 0.668	1.000 0.557 0.560
$\left. \begin{matrix} h_1 \\ h_2 \\ h_3 \end{matrix} \right\} \begin{matrix} a/b = 5/8 \end{matrix}$	2.115 1.968 0.975	1.912 1.458 1.053	1.690 1.126 0.970	1.407 0.785 0.763	1.221 0.617 0.620	1.012 0.474 0.478	0.853 0.383 0.386	0.712 0.313 0.318	0.573 0.256 0.273
$\left. \begin{matrix} h_1 \\ h_2 \\ h_3 \end{matrix} \right\} \begin{matrix} a/b = 3/4 \end{matrix}$	2.073 1.611 0.933	1.708 0.970 0.802	1.458 0.685 0.642	1.208 0.452 0.450	1.082 0.361 0.361	0.956 0.292 0.292	0.745 0.216 0.216	0.646 0.183 0.183	0.532 0.148 0.149

1.9.3 Crack Opening Displacement (COD)

The crack opening displacement (COD) parameter was proposed to provide a more physical explanation for crack extension processes.^(94, 113) The philosophy was based on a crack tip strain based model of cracking that would allow for the occurrence of elastic-plastic material behavior. The initial modeling, however, was based on elasticity solutions of crack tip displacements. Equation 1.9.46 describes the x and y displacements (u and v, respectively) in the crack tip region of an elastic material:

$$u = \frac{K}{2G} \left(\frac{r}{2\pi} \right)^{\frac{1}{2}} \cos \frac{\theta}{2} [\kappa - 1 + 2\sin^2 \frac{\theta}{2}] \quad (1.9.46a)$$

$$v = \frac{K}{2G} \left(\frac{r}{2\pi} \right)^{\frac{1}{2}} \sin \frac{\theta}{2} [\kappa + 1 - 2\cos^2 \frac{\theta}{2}] \quad (1.9.46b)$$

where $\kappa = 3 - 4\nu$ for plane strain and $\kappa = (3 - \nu)/(1 + \nu)$ for plane stress, and where G is the shear modulus ($G = 0.5E/(1 + \nu)$). If the angle θ is chosen to be 180° (π), the displacements are those associated with crack sliding (u component) or opening (v component). Under mode I (symmetrical) loading, the case covered by Equation 1.9.46, the sliding displacement term is noted to be identically zero; and all displacement is perpendicular to the crack, i.e. only opening is observed. Based on Equations 1.9.46 and 1.9.11 and the definition of shear modulus (G), the displacement of the crack relative to its longitudinal axis (x axis) is

$$v = \frac{4K}{E'} \left(\frac{r}{2\pi} \right)^{\frac{1}{2}} \quad (1.9.47)$$

The relative movement of the crack faces is the COD and it is twice the value obtained by Equation 1.9.47, i.e.

$$\text{COD} = 2v \quad (1.9.48)$$

One immediate observation is that COD will vary as a function of position along

the crack, and that the COD at the crack tip, i.e. at $r = 0$, is zero. In the quasi-elastic-plastic analysis performed by Wells, the crack was allowed to extend to an effective length (a_e), one plastic zone radius larger than the physical crack length (a); the crack opening displacement was then determined at the location of the physical crack tip. Figure 1.9.6 describes the model used to define the crack tip opening displacement (CTOD). The Wells modeling approach leads one to

$$CTOD = 8 \frac{K}{E'} \left(\frac{r_y}{2\pi} \right)^{1/2} \quad (1.9.49)$$

which after some simplification gives the CTOD as

$$CTOD = \frac{4}{\pi} \frac{K^2}{E' \sigma_o} \quad (1.9.50)$$

It is immediately seen that the CTOD is directly related to the stress-intensity factor for elastic materials; thus, for elastic materials, fracture criteria based on CTOD are as viable as those based on the stress-intensity factor parameter. The other relationships developed between K and G or J in this section allow one to directly relate G and J to the CTOD in the elastic case.

In the late 1960's, Dugdale ⁽¹¹⁴⁾ conducted an elasticity analysis of a crack problem in which a zone of yielding was postulated to occur in a strip directly ahead of the crack tip. The material in the strip was assumed to behave in a perfect plastic manner. The extent of yielding was determined such that the singularity at the imaginary crack tip (see Figure 1.9.7) was canceled due to the balancing of the remote positive stress-intensity factor with the local yielding negative stress-intensity factor. The Dugdale quasi-elastic-plastic analysis provided an estimate of the relative displacement of the crack surfaces for a center crack (crack length = $2a$) in an

infinite plate subjected to a remote tensile stress (σ) and having a yield strength equal to σ_o , the CTOD is

$$\text{CTOD} = \frac{8a\sigma_o}{\pi E'} \ln\left(\sec\left(\frac{\pi\sigma}{2\sigma_o}\right)\right) \quad (1.9.51)$$

at the tip of the physical crack tip (a) and the extent of the plasticity ahead of the crack is

$$\omega = a\left[\sec\left(\frac{\pi\sigma}{2\sigma_o}\right) - 1\right] \quad (1.9.52)$$

For the case of small scale yielding, i.e., when $\frac{\sigma}{\sigma_o}$ is low, the CTOD and extent of plasticity (ω) reduce to

$$\text{CTOD} \approx \frac{\sigma^2 \pi a}{E' \sigma_o} = \frac{K^2}{E' \sigma_o} \quad (1.9.53)$$

and

$$\omega \approx \frac{\pi}{8} \frac{K^2}{\sigma_o} \quad (1.9.54)$$

It can first be noted that the extent of the plasticity (ω) is only about 20% higher than would be predicted using the Irwin estimate of the plastic zone diameter ($2r_y$). The level of CTOD estimated by Equation 1.9.53 also compares favorably with that given by Equation 1.9.50; Equation 1.9.53 gives an estimate that is about 30 percent lower than Equation 1.9.50. Numerous other studies have shown that the CTOD is related to the stress-intensity factor under conditions of small scale yielding through

$$\text{CTOD} = \alpha \frac{K^2}{E' \sigma_o} \quad (1.9.55)$$

where the constant α ranges from about 1 to 1.5. Experimental measurements^(115, 116)

have indicated that α is close to 1.0, although there is substantial disagreement about the location where CTOD should be measured.

One difficulty with elastic analyses is that the crack actually remains stationary and thus one must reposition the crack through a quasi-static crack extension so that the CTOD for the actual crack can be assessed. During loading, cracks in ductile materials tend to extend through a slow tearing mode of cracking prior to reaching the fracture load level. In these cases, the amount of opening that occurs at the initial crack tip represents one measure of the crack tip strain; but, this parameter depends not only on load, initial crack length and material properties, it also depends on the amount of crack extension from the initial crack tip. Rice and co-workers^(93, 117) attempted to provide an alternate choice of locating the position where CTOD would be measured. They found that when the CTOD was determined for the position shown in Figure 1.9.8, the CTOD and J integral were related (for ideally plastic materials) by

$$\text{CTOD} = d_n \frac{J}{\sigma_o} \quad (1.9.56)$$

For the case of plane stress behavior, d_n is unity and for plane strain behavior, d_n is about 0.78.

For strain hardening materials controlled by Equation 1.9.37, Shih and co-workers^(103, 118) have shown that Equation 1.9.56 relates J and CTOD if the constant d_n is replaced with a function that is strongly dependent on the strain hardening exponent and mildly dependent on the ratio σ_o/E . Thus, there is a direct relationship between CTOD and J throughout the region of applicability of the J-Integral and CTOD can likewise be considered a measure of the magnitude of the crack tip stress-strain field.

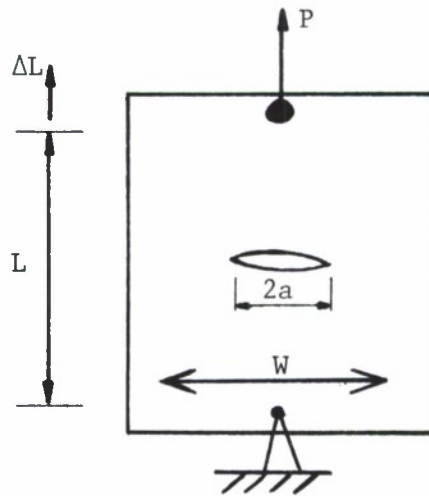


Figure 1.9.1 Finite Width, Center Cracked Panel, Loaded in Tension with Load P .

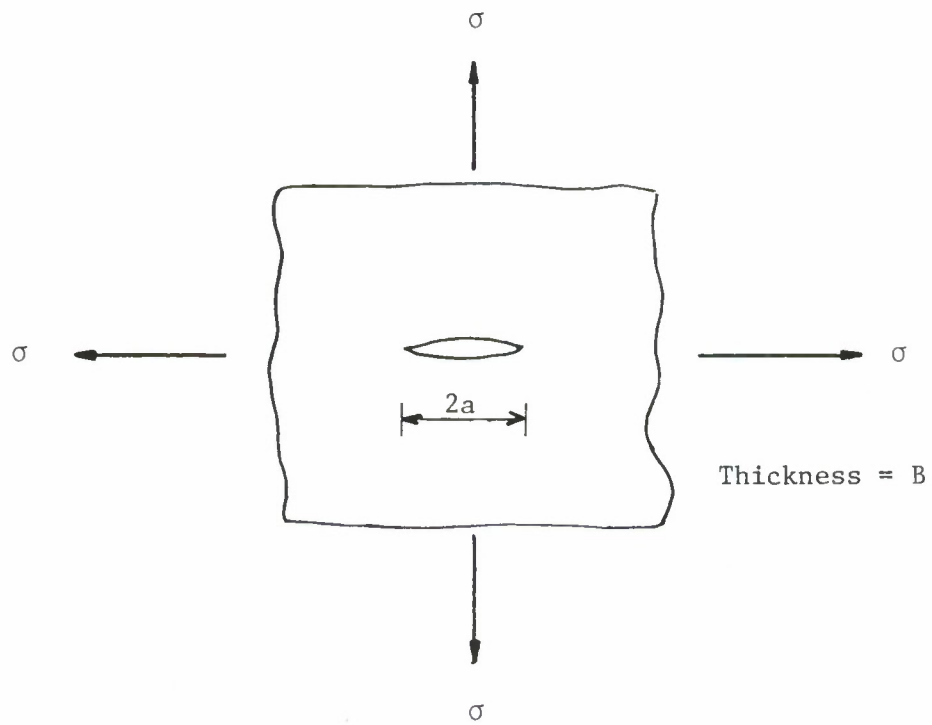
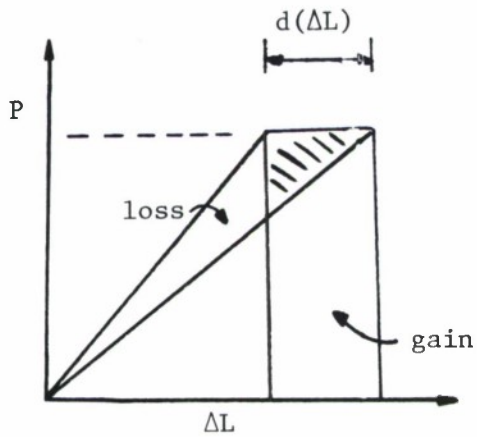
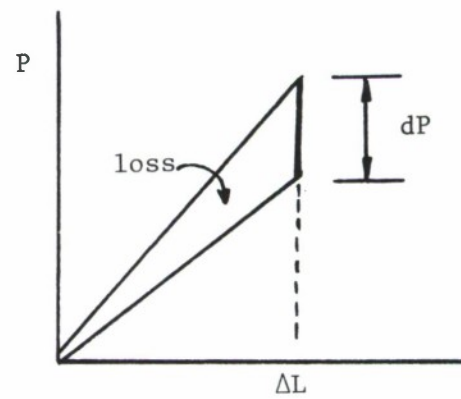


Figure 1.9.2 Griffith Crack and Loading Configuration, Uniformly Loaded, Infinite Plate with a Center Crack of Length $2a$.



(a) Fixed Load Condition



(b) Fixed Displacement Condition

Figure 1.9.3 Load-Displacement Diagrams for the Structure Illustrated in Figure 1.9.1. The Diagram Shows the Changes that Occur in the Elastic Strain Energy as a Crack Grows Under the Two Defined Conditions.

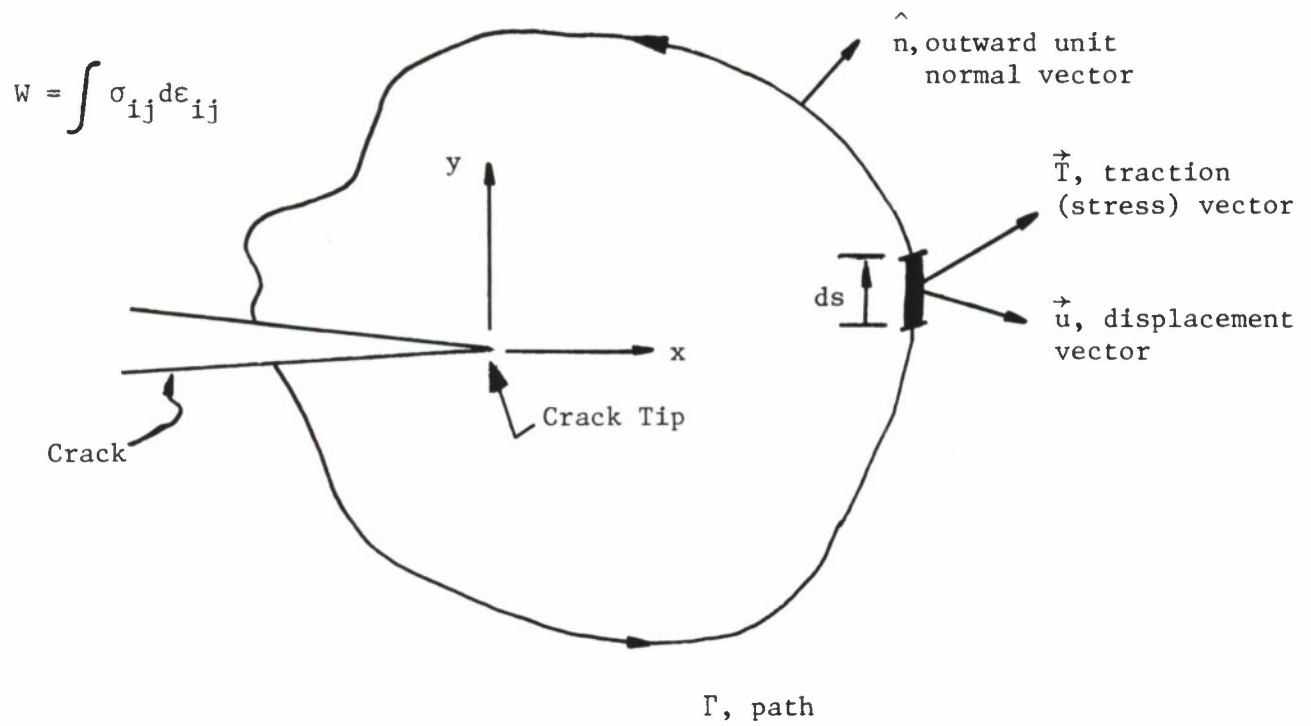


Figure 1.9.4 J-Integral Parameters Illustrated.

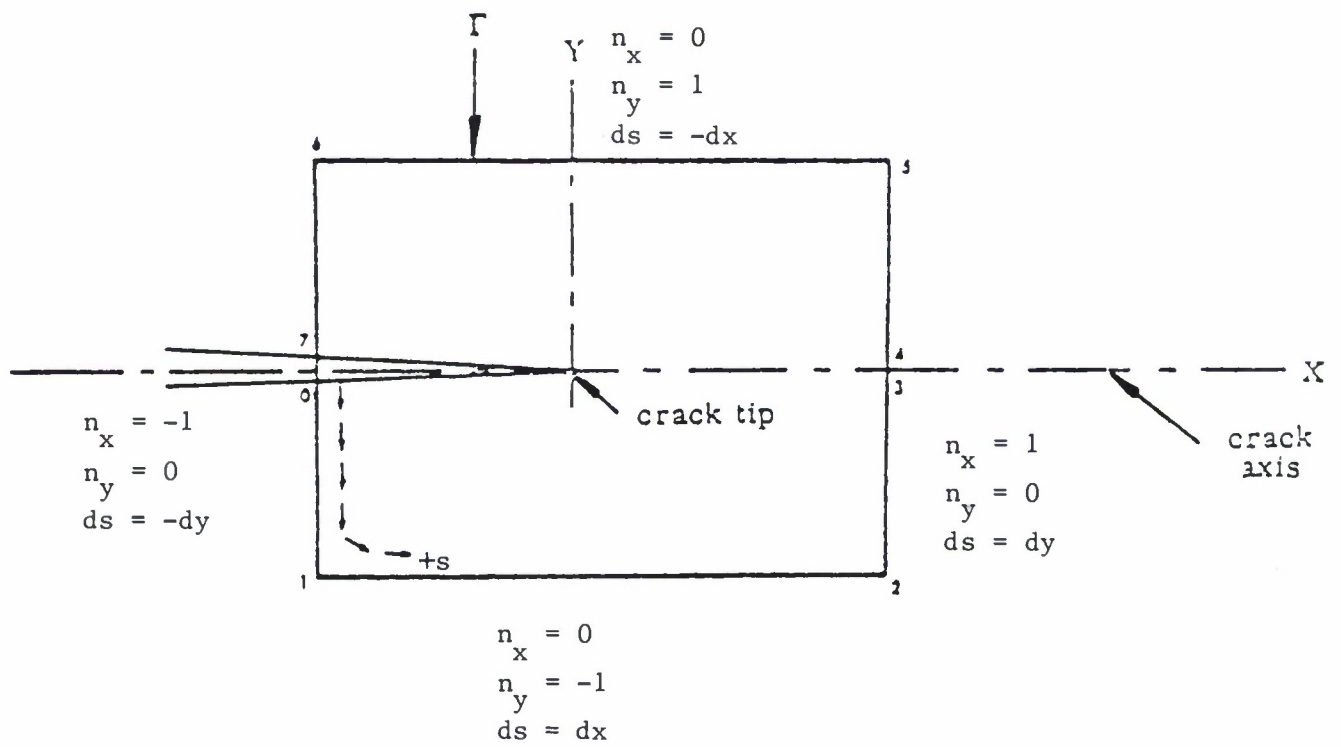


Figure 1.9.5 Rectangular Path for J Calculation.

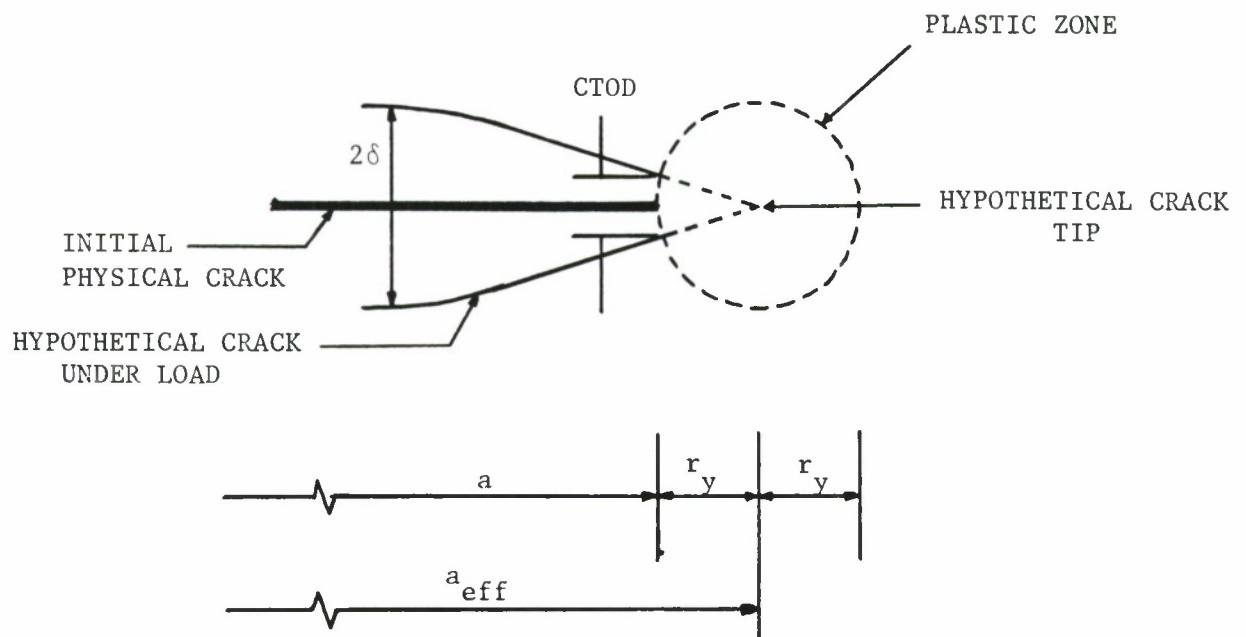


Figure 1.9.6. Description of Model Used to Establish the CTOD Under Elastic Conditions.

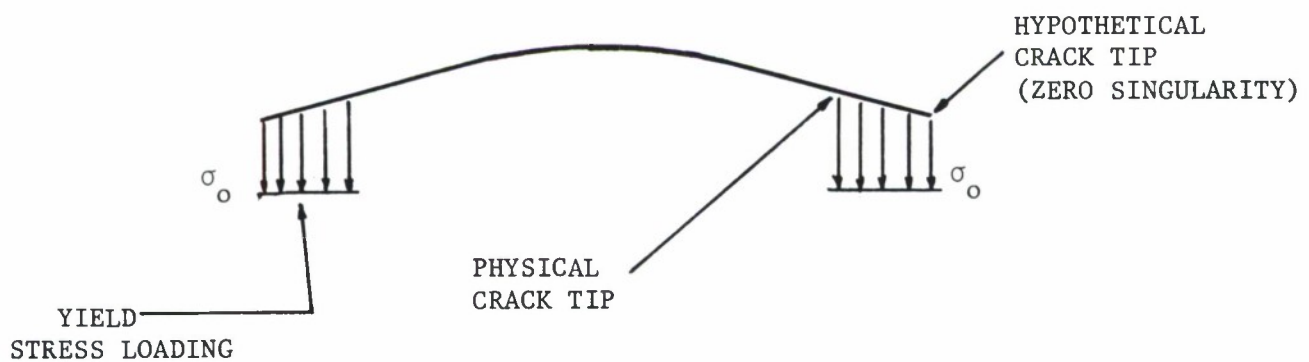
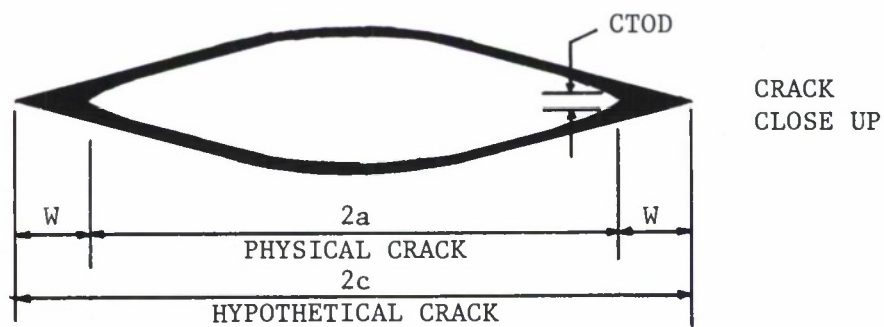
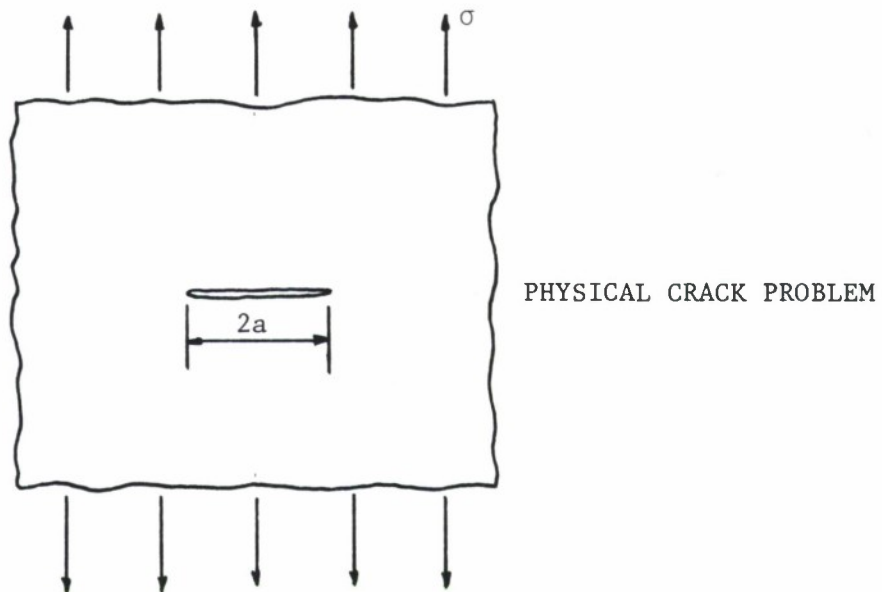


Figure 1.9.7. Dugdale Type Strip Yield Zone Analysis.

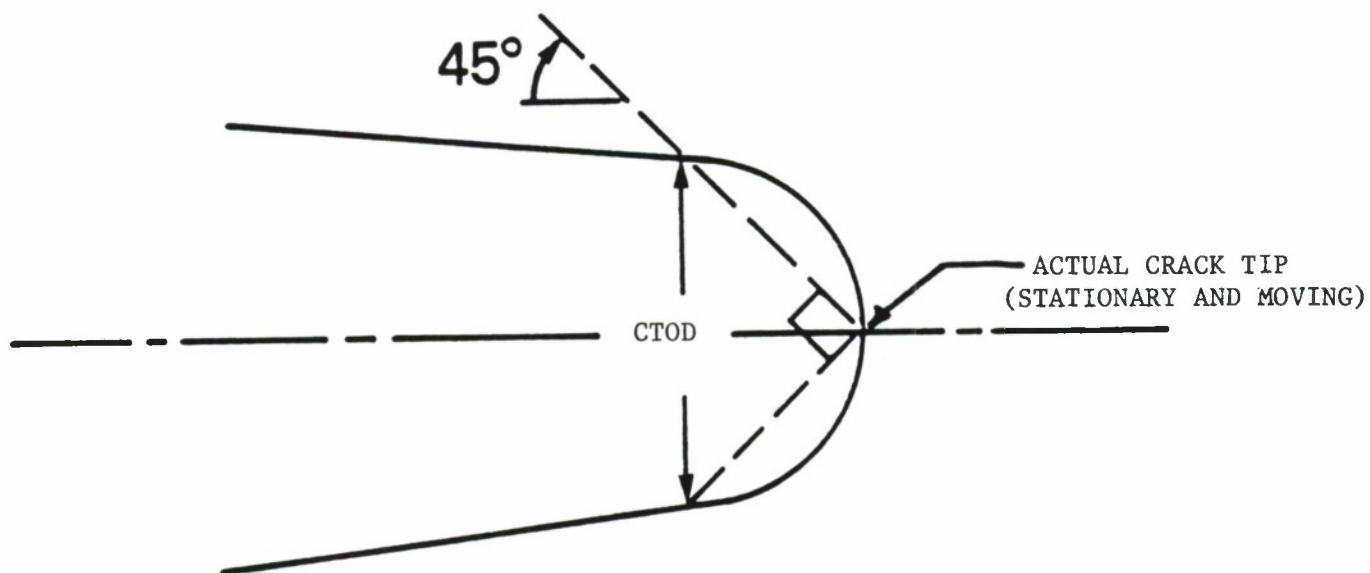


Figure 1.9.8. Definition of the Crack Tip Opening Displacement (CTOD)
Per Rice, Shih, and Coworkers.

SECTION 1.10

LIST OF REFERENCES

1. G. R. Irwin, "Analysis of Stresses and Strains Near the End of a Crack Traversing a Plate," Trans. ASME, J. Applied Mechanics, Vol. 24 (1957), p. 361.
2. M. L. Williams, "Stress Distribution at the Base of a Stationary Crack," Trans. ASME, J. Applied Mechanics, Vol. 24 (1957), p. 109.
3. I. N. Sneddon and M. Lowengrub, Crack Problems in the Classical Theory of Elasticity, New York: John Wiley and Sons, Inc., (1969).
4. J. R. Rice, "Mathematical Analysis in the Mechanics of Fracture," Ed. H. Liebowitz, Fracture, Vol. II, New York: Academic Press, (1968), pp. 191-308.
5. G. R. Irwin and J. A. Kies, "Critical Energy Rate Analysis of Fracture Strength," Welding Journal (Research Supplement), Vol. 33, (1954), p. 193s.
6. G. R. Irwin, J. A. Kies, and H. L. Smith, "Fracture Strengths Relative to Onset and Arrest of Crack Propagation," Proc. ASTM, Vol. 58, (1958), p. 640.
7. "Fracture Resistance Data Summary," Boeing Co., D2-20947 (June 1962).
8. G. T. Hahn and A. R. Rosenfield, "Local Yielding and Extension of a Crack Under Plane Stress," Acta Metallurgical, Vol. 13, No. 3, (1965), p. 293.
9. P. C. Paris, M. P. Gomez, and W. E. Anderson, "A Rational Analytic Theory of Fatigue," The Trend in Engineering, University of Washington, Vol. 13, No. 1, (Jan. 1961), p. 9.
10. D. R. Donaldson and W. E. Anderson, "Crack Propagation Behavior of Some Airframe Materials," Proceedings of the Crack Propagation Symposium, Vol. II, Cranfield, England, September 1961, p. 375.
11. P. C. Paris, "The Fracture Mechanics Approach to Fatigue," Fatigue--and Interdisciplinary Approach, Proceedings, Tenth Sagamore Conference, Syracuse, N.Y.: Syracuse University Press, (1964), p. 107.

12. W. E. Anderson and L. E. James, "Estimating Cracking Behavior of Metallic Structure," Journal of the Structural Division, Proc., Am. Soc. Civil Engineers, Vol. 96, No. 4, (April 1970), p. 773.
13. R. J. Lozano, G. S. Parker, and R. J. Werdes, "F-4 Fatigue and Damage Tolerance Assessment Program - Vol. 1" MCAIR MDC A2883, McDonnell Douglas, St. Louis, Missouri, June 28, 1974.
14. R. E. Pinchert, "Damage Tolerant Assessment of F-4 Aircraft," Presented at the American Institute of Aeronautic and Astronautics Aircraft Systems and Technology Meeting, Dallas, Texas, 27-29 September 1976.
15. P. C. Paris and G. C. Sih, "Stress Analysis of Cracks," ASTM STP 381, (1965), pp. 30-81.
16. G. C. Sih, Handbook of Stress Intensity Factors, Inst. of Fract. and Solid Mechanics, Lehigh University, (1973).
17. H. Tada, P. C. Paris, and G. R. Irwin, The Stress Analysis of Cracks Handbook, Del Research Corporation, (1973).
18. D. P. Rooke and D. J. Cartwright, Compendium of Stress Intensity Factors, Her Majesty's Stationary Office, London, (1976).
19. D. P. Wilhem, "Fracture Mechanics Guidelines for Aircraft Structural Applications," AFFDL-TR-69-111, Feb. 1970.
20. A. P. Parker, The Mechanics of Fracture and Fatigue, an Introduction, E. & F.N. Spon, Ltd., London, England, (1981).
21. G. C. Sih, Methods of Analysis and Solutions of Crack Problems, Noordhoff, (1973).
22. D. Broek, Elementary Engineering Fracture Mechanics, Noordhoff, (1974).
23. J. N. Goodier, "Mathematical Theory of Equilibrium of Cracks," Fracture II, Liebowitz, ed., Academic Press, (1969), pp. 2-67.
24. J. M. Westergaard, "Bearing Pressures and Cracks," Journal Appl. Mech. 61, (1939), pp. A49-53.

25. N. I. Mushkelishvili, Some Basic Problems of the Mathematical Theory of Elasticity, (1933), English translation, Noordhoff (1953).
26. B. Gross, J. E. Srawley, and W. F. Brown, "Stress-Intensity Factors for Single-Edge Notch Tension Specimen by Boundary Collocation of a Stress Function," NASA TN-D-2395 (1964).
27. J. C. Newman, Jr., "An Improved Method of Collocation for the Stress Analysis of Cracked Plates with Various Shaped Boundaries," NASA-TN-D-6376 (1971).
28. T. A. Cruse, "Numerical Evaluation of Elastic Stress Intensity Factors by the Boundary-Integral Equation Method," The Surface Crack: Physical Properties and Computational Solutions, ed. J. L. Swedlow, ASME, New York, (1972) pp. 153-170.
29. T. A. Cruse and P. M. Besuner, "Residual Life Prediction for Surface Cracks in Complex Structural Details," J. of Aircraft, Vol. 12, No. 4, April 1975, pp. 369-375.
30. T. Swift and D. Y. Wang, "Damage Tolerant Design Analysis Methods and Test Verification of Fuselage Structure," Air Force Conf. on Fatigue and Fracture (1969), AFFDL-TR-70-144, pp. 653-683.
31. C. W. Smith, "Use of Three-Dimensional Photoelasticity and Progress in Related Areas," Experimental Techniques in Fracture Mechanics, 2, Ed. A. S. Kobayashi, Society of Experimental Stress Analysis, Monograph 2, (1975), pp. 3-58.
32. A. S. Kobayashi, "Photoelastic Techniques," Experimental Techniques in Fracture Mechanics, 1, Ed. A. S. Kobayashi, Society of Experimental Stress Analysis Monograph 1, (1973), pp. 126-145.
33. L. A. James and W. E. Anderson, "A Simple Experimental Procedure for Stress Intensity Factor Calibration," Engineering Fracture Mechanics, Vol. 1, (1969), pp. 565-568.
34. A. F. Grandt, Jr., and T. D. Hinnericks, "Stress Intensity Factor Measurements for Flawed Fastener Holes," Proceedings of the Army Symposium on Solid Mechanics, Cape Code, MA, 10-12 Sept. 1974.
35. J. P. Gallagher, H. D. Stalnaker, and J. L. Rudd, "A Spectrum Truncation and Damage Tolerance Study Associated with the C-5A Outboard Pylon Truss Lugs," AFFDL-TR-74-5, May 1974.

36. P. F. Packman, "The Role of Interferometry in Fracture Studies," Chapter 2 in Experimental Techniques in Fracture Mechanics, 2, Ed. A. S. Kobayashi, SESA, (1975), pp.59-87.
37. F. J. Pitoniak, A. F. Grandt, L. T. Montulli, and P. F. Packman, "Fatigue Crack Retardation and Closure in Polymethyl Methacrylate," Engineering Fracture Mechanics, Vol. 5, (1974), pp.
38. D. J. Cartwright and D. P. Rooke, "Green's Functions in Fracture Mechanics," Fracture Mechanics - Current Status and Future Prospects, Ed., R. A. Smith, Pergamon, (1979), pp. 91-123.
39. D. J. Cartwright and D. P. Rooke, "Evaluation of Stress-Intensity Factors," Chapter 5 in A General Introduction to Fracture Mechanics, Mechanical Engineering Publications Ltd., London, (1978), p. 54.
40. D. J. Cartwright, "Stress-Intensity Factor Determination," Chapter 2 in Developments in Fracture Mechanics, Ed. G. G. Chell, Applied Science Publishers Ltd., London (1979), p. 29.
41. T. M. Hsu and J. L. Rudd, "Green's Function for Thru-Crack Emanating From Fastener Holes," Fracture 1977, ed. D.M.R. Taplin, Vol. 3A, Pergamon Press, (1978), p. 139.
42. T. M. Hsu, W. M. McGee, and J. A. Aberson, "Extended Study of Flaw Growth at Fastener Holes," AFFDL-TR-77-83, Vol. 1, April 1978.
43. H. F. Bueckner, "Weight Functions for the Notched Bar," Z. Angew Math. Mech., Vol. 51, (1971), pp. 97-109.
44. J. R. Rice, "Some Remarks on Elastic Crack-Tip Stress Fields," Int. Journal of Solids and Structures, Vol. 8, (1972), pp. 751-758.
45. A. F. Grandt, Jr., "Stress Intensity Factors for Some Through-Cracked Fastener Holes," Int. Journal of Fracture, Vol. 11, No. 2, (April 1975), pp. 283-294.
46. S. K. Chan, I. S. Tuba, and W. K. Wilson, "On the Finite-Element Method in Linear Fracture Mechanics," Eng. Fracture Mechanics., 2 (1970), pp. 1-12.
47. E. Byskov, "The Calculation of Stress-Intensity Factors Using the Finite-Element Method with Cracked Elements," Int. J. Fract. Mech., 6 (1970), pp. 159-167.

48. D. M. Tracey, "Finite Elements for Determination of Crack-Tip Elastic Stress-Intensity Factors," Eng. Fract. Mech., 3 (1971), pp. 255-265.
49. P. F. Walsh, "The Computation of Stress-Intensity Factors by a Special Finite-Element Technique," J. Solids and Struct., 7 (1971), pp. 1333-1392.
50. R. H. Gallagher, "A Review of Finite Element Techniques in Fracture Mechanics," Proc. First Int. Conf. on Numerical Methods in Fracture Mechanics, Ed. A. R. Luxmoore and D. R. J. Owen, University College, Swansea, UK, (1978).
51. S. Jordon, J. Padlog, A. T. Hopper, E. F. Rybicki, L. E. Hulbert, and M. F. Kanninen, "Development and Application of Improved Analytical Techniques for Fracture Analysis Using MAGIC III," AFFDL-TR-73-61 (June 1973).
52. S. N. Atluri, A. S. Kobayashi, and M. Nakagaki, "Application of an Assumed Displacement Hybrid Finite-Element Procedure to Two-Dimensional Problems in Fracture Mechanics," AIAA Paper 74-390 (April 1974).
53. T. K. Hellen, "Numerical Methods in Fracture Mechanics," Chapter 5 in Developments in Fracture Mechanics - 1, Ed. G. G. Chell, Applied Science Publishers Ltd., London, (1979), pp. 145-181.
54. M. Isida, "Crack Tip Stress-Intensity Factors for the Tension of an Eccentrically Cracked Strip," J. of Applied Mechanics, Trans ASME, Vol. 33, September 1966, pp. 674-675.
55. G. Sih, P. Paris, and F. Erdogan, "Application of Muskhelishvili's Methods to the Analysis of Crack Tip Stress-Intensity Factors for Plane Problems - Part II, Interim Report issued to Boeing Airplane Co. by Institute of Research, Lehigh University, 7 January 1961.
56. P. C. Paris, A Short Course in Fracture Mechanics, The Boeing Airplane Company, March 1960.
57. C. C. Poe, Jr., "The Effect of Riveted and Uniformly Spaced Stringers on the Stress-Intensity Factor of a Cracked Sheet," Proc. of the Air Force Conf. on Fatigue and Fracture of Aircraft Structures and Materials, AFFDL TR 70-144, Sept. 1970, pp. 207-215.

58. W. F. Brown, Jr. and J. Srawley, Plane Strain Fracture Toughness of High Strength Metallic Materials, ASTM STP 410, Am. Society for Testing and Materials, (1966).
59. R. J. Hartranft and G. C. Sih, "Alternating Method Applied to Edge and Surface Crack Problems," Methods of Analysis and Solutions of Crack Problems, ed. G. C. Sih, Noordhoff, (1973), pp. 197-238.
60. O. L. Bowie, "Analysis of an Infinite Plate Containing Radial Cracks Originating at the Boundary of an Internal Circular Hole," J. Math and Phys., 35, (1956), pp. 60-71.
61. J. Tweed, and D. P. Rooke, "The Distribution of Stress Near the Tip of a Radial Crack at the Edge of a Circular Hole," Int. J. Engng Sci., 1973, Vol. II, pp. 1185-1195.
62. T. R. Brussat, "Mode I Stress Intensity for a Radial Crack at a Hole with Arbitrary Pressure Distribution," Engineering Fracture Mechanics, Vol. 14, No. 1, (1981), pp. 233-235.
63. J. C. Newman, Jr., "Predicting Failure of Specimens with Either Surface Cracks or Corner Cracks at Holes," NASA TN D-8244, NASA Langley Research Center, June 1976.
64. L. R. Hall, R. C. Shah, and W. L. Engstrom, "Fracture and Fatigue-Crack-Growth Behavior of Surface Flaws and Flaws Originating at Fastener Holes, AFFDL-TR-74-47, (1974).
65. R. C. Shah, "Stress-Intensity Factors for Through and Part-Through Cracks Originating at Fastener Holes," Mechanics of Crack Growth, ASTM STP 590, Am. Society for Testing and Materials, (1976), pp. 429-459.
66. G. R. Irwin, "Crack Extension Force for a Part-Through Crack in a Plate," J. Appl. Mech., December 1962, pp. 651-654.
67. J. G. Merkle, "A Review of Some of the Existing Stress Intensity Factor Solutions for Part-Through Surface Crack," ORNL-TM-3983, Oak Ridge National Laboratory, Jan. 1973.
68. J. C. Newman, Jr. "Fracture Analysis of Surface - and Through-Cracked Sheets and Plates," Engineering Fracture Mechanics, Vol. 5, No. 3, Sept. 1973, pp. 667-684.

69. A. S. Kobayashi and W. L. Moss, "Stress-Intensity Magnification Factors for Surface-Flawed Tension Plate and Notched Round Tension Bar," Proc. of the 2nd Int'l Conf. on Fracture, Brighton, England, 1969.
70. R. C. Shah and A. S. Kobayashi, "Stress-Intensity Factors for an Elliptical Crack Approaching the Surface of Semi-Infinite Solid," Int. J. Fract., 9, (1975), pp. 133-146.
71. R. M. Engle, Jr., "Aspect Ratio Variability in Part-Through Crack Life Prediction, ASTM STP 687, Am. Society for Testing and Materials, (1979), pp. 74-88.
72. J. C. Newman, Jr. and I. S. Raju, "Stress-Intensity Factor Equations for Cracks in Three- Dimensional Finite Bodies," NASA TM 83200, NASA Langley Research Center, Aug. 1981.
73. A. F. Liu, "Stress-Intensity Factor for a Corner Flaw," Eng. Fract. Mech., 4, (1972), pp. 175-179.
74. A. S. Kobayashi and A. N. Enetaya, "Stress-Intensity Factor of a Corner Crack," Mechanics of Crack Growth, ASTM STP 590, Am. Society for Testing and Materials, (1976), pp. 429-459.
75. D. M. Tracey, "3D Elastic Singularity Element for Evaluation of K Along an Arbitrary Crack Front," Int. J. of Fracture, Vol. 9, 1973, pp. 340-343.
76. J. C. Newman, Jr., "A Review and Assessment of the Stress-Intensity Factor for Surface Cracks," Part-Through Crack Fatigue Life Prediction, ASTM STP 687, Am. Society for Testing and Materials, (1979), pp. 16-42.
77. L. R. Hall and R. W. Finger, "Fracture and Fatigue Growth of Partially Embedded Flaws," Air Force Conf. on Fatigue and Fracture, AFFDL-TR-70-144, (1970), pp. 235-262.
78. T. M. Hsu and A. F. Liu, "Stress Intensity Factors for Truncated Elliptical Cracks," presented at the 7th National Symposium on Fracture Mechanics, College Park, MD, 27-29 Aug. 1973.
79. F. W. Smith and T. E. Kullgren, "Theoretical and Experimental Analysis of Surface Cracks Emanating from Fastener Holes," AFFDL-TR-76-104, Air Force Flight Dynamics Laboratory, Feb. 1977.

80. W. T. Fujimoto, "Determination of Crack Growth and Fracture Toughness Parameters for Surface Flaws Emanating from Fastener Holes," Proceedings of AIAA/ASME/SAE 17th Structures, Structural Dynamics, and Materials Conference, King of Prussia, PA, 5-7 May 1976.
81. J. L. Rudd, T. M. Hsu, and H. A. Wood, "Part-Through Crack Problems in Aircraft Structures," Part-Through Crack Fatigue Life Predictions, ASTM STP 687, Am. Society for Testing and Materials, (1979), pp. 168-194.
82. A. F. Grandt, Jr. and T. E. Kullgren, "Stress Intensity Factors for Corner Cracked Holes Under General Loading Conditions," J. of Engr. Materials and Technology, ASME Transactions, Vol. 103, No. 2, April 1981, pp. 171-176.
83. A. F. Grandt, Jr., and T. E. Kullgren, "A Compilation of Stress Intensity Factor Solutions for Flawed Fastener Holes," AFWAL-TR-81-4112, Air Force Wright Aeronautical Laboratories, Nov. 1981.
84. O. Orringer, "Fracture Mechanics Analysis of an Attachment Lug," AFFDL-TR-75-51, Air Force Flight Dynamics Laboratory, Jan. 1976.
85. T. H. H. Pian, O. Orringer, G. Stalk, and J. W. Mar, "Numerical Computation of Stress Intensity Factors for Aircraft Structural Details by the Finite Element Method," AFFDL-TR-76-12, Air Force Flight Dynamics Laboratory, May 1976.
86. L. F. Impellizzeri and D. L. Rich, "Spectrum Fatigue Crack Growth in Lugs," Fatigue Crack Growth Under Spectrum Loads, ASTM STP 595, Am. Society for Testing and Materials, 1976, pp. 320-336.
87. I. J. Zatz, H. L. Eidinoff, and H. Armen, Jr., "An Application of the Energy Release Rate Concept to Crack Growth in Attachment Lugs," AIAA/ASME/ASCE/AHS 22nd Structure, Structural Dynamics, and Materials Conference, Part 1, Paper no. 81-0491, (1981), pp. 402-
88. T. M. Hsu and T. R. Brussat, "Advanced Life Analysis Methods," A series of QTR progress reports on USAF Contract F33615-80-C-3211, Jan, April, July, Oct. 1981 and Jan. 1982.
89. M. P. Kaplan and J. A. Reiman, "Use of Fracture Mechanics in Estimating Structural Life and Inspection Intervals," J. Of Aircraft, Vol. 13, No. 2, Feb. 1976, pp. 99-103.

90. J. B. Chang, Editor, Part-Through Crack Fatigue Life Prediction, ASTM STP 687, Am. Society for Testing and Materials, 1979.
91. G. R. Irwin, "Fracture Mechanics," Structural Mechanics, J. N. Goodier and N. J. Hoff, eds., Pergamon Press, (1960), pp. 557-594.
92. A. A. Griffith, "The Phenomena of Rupture and Flow in Solids," Phil. Trans. Roy. Soc. London, A221, (1921), pp. 163-197.
93. J. R. Rice, "A Path Independent Integral and the Approximate Analyses of Strain Concentration by Notches and Cracks," J. Appl. Mech., ASME, 35, (June 1968), pp. 379-386.
94. A. A. Wells, "Unstable Crack Propagation in Metals - Cleavage and Fast Fracture," Proceedings of the Cranfield Crack Propagation Symposium, 1, (Sept. 1961), pp. 210-230.
95. G. R. Irwin, "Fracture Dynamics," Fracturing of Metals, ASM, (1948), pp. 147-166.
96. E. Orowan, "Fracture and Strength of Solids," Rep. Prog. Physics, Vol. 12, (1949), pp. 185-232.
97. D. J. Hayes, "Some Applications of Elastic-Plastic Analysis to Fracture Mechanics," Ph.D. Thesis, Imperial College (1970).
98. J. A. Begley and J. D. Landes, "The J-Integral as a Fracture Criterion," Fracture Toughness, ASTM STP 514, (1972), pp. 1-20.
99. Verette, R., and Wilhem, D. P., "Development & Evaluation of Methods of Plane Stress Fracture Analysis, Review and Evaluation of Structural Residual Strength Prediction Techniques," AFFDL-TR-73-42, May 1973.
100. J. D. Landes, J. A. Begley, and G. A. Clarke, eds., Elastic-Plastic Fracture, ASTM STP 668, Am. Soc. for Testing and Mat'ls, (1979).
101. P. C. Paris, ed., Fracture Mechanics: Twelfth Conference, ASTM STP 700, Am. Soc. for Testing and Mat'ls, (1980).
102. R. Roberts, ed., Fracture Mechanics: Thirteenth Conference, ASTM STP 743, Am. Soc. for Testing and Mat'ls, (1981).
103. C. F. Shih and V. Kumar, "Estimation Techniques for the Prediction of Elastic-Plastic Fracture of Structural Components of Nuclear Systems," First Semiannual Report, July 1978-January 1979 for EPRI Contract RP 1237-1, General Electric Co., Schenectady, N.Y., June 1 1979.

104. V. Kumar, M. D. German, and C. F. Shih, "Estimation Technique for the Prediction of Elastic-Plastic Fracture of Structural Components of Nuclear Systems," Combined Second and Third Semiannual Report, Feb. 1979 to Jan. 1980 for EPRI, General Electric Company, SRD-80-094.
105. C. F. Shih, "J-Integral Estimates for Strain Hardening Materials in Antiplane Shear Using Fully Plastic Solutions," Mechanics of Crack Growth, ASTM STP 590, Am. Soc. for Testing and Mat'ls, (1976), pp. 3-22.
106. V. Kumar, M. D. German, and C. F. Shih, "An Engineering Approach for Elastic-Plastic Fracture Analysis," EPRI-NP-1931, Electric Power Research Institute, July 1981.
107. A. A. Ilyushin, "The Theory of Small Elastic-Plastic Deformations," Prikladnaia Matematika i Mekhanika, P.M.M., Vol. 13, (1946), p. 347.
108. C. F. Shih and J. S. Hutchinson, "Fully Plastic Solutions and Large Scale Yielding Estimates for Plane Stress Crack Problems," J. of Engineering and Materials and Technology, (1976), Vol. 98, pp. 289-295.
109. J. W. Hutchinson, "Plastic Stress and Strain Fields at the Crack Tip," J. of Mechanics and Physics of Solids, (1968), pp. 13-31; pp. 337-347.
110. J. R. Rice and G. F. Rosengren, "Plane Strain Deformation Near a Crack Tip in Power-Law Hardening Material," J. of Mechanics and Physics and Solids, (1968), pp. 1-12.
111. T. Weerasooriya and J. P. Gallagher, "Determining Crack Tip Field Parameters for Elastic-Plastic Materials via an Estimation Scheme," AFWAL-TR-81-4044, Air Force Wright Aeronautical Laboratories, July 1981.
112. R. J. Bucci, P. C. Paris, J. D. Landes, and J. R. Rice, "J-Integral Estimation Procedures," Fracture Toughness, ASTM STP 514, (1972), pp. 40-69.
113. F. M. Burdekin and D. E. W. Stone, "The Crack-Opening-Displacement Approach to Fracture Mechanics in Yielding," J. Strain Analysis, (1966), pp. 145-153.
114. D. S. Dugdale, "Yielding of Steel Sheets Containing Slits," J. Of Mechanics and Physics of Solids, Vol. 8, (1960), pp. 100-104.

115. C. Q. Bowles, "Strain Distribution and Deformation at the Crack Tip in Low Cycle Fatigue," AMMRC-CR-70-23, Army Mat'l and Mech. Research Center, Watertown, MA, (1970).
116. J. N. Roberson and A. S. Tetelman, "The Critical Crack-Tip Opening Displacement and Microscopic and Macroscopic Fracture Criteria for Metals, UCLA RE 7360, University of California, Los Angeles, CA, (1973).
117. J. R. Rice and D. M. Tracey, "Computational Fracture Mechanics," Numerical and Computer Methods in Structural Mechanics (Ed. S. J. Fenves et al.), Academic Press, N.Y., (1973), pp. 585-623.
118. C. F. Shih, "Relationship Between the J-Integral and the Crack Opening Displacement for Stationary and Extending Cracks," General Electric Co. TIS Report No. 79CRD075, April 1979.

2.0 SUMMARY OF REQUIREMENTS

<u>SECTION</u>	<u>PAGE</u>
2.1 GENERAL	2.1.1
2.2 DESIGN CATEGORY	2.2.1
2.3 INSPECTION CATEGORIES AND INSPECTION INTERVALS	2.3.1
2.4 INITIAL DAMAGE ASSUMPTIONS	2.4.1
2.4.1 <u>Intact Structure Primary Damage Assumption</u>	2.4.1
2.4.2 <u>Intact Structure - Marginal Hole Quality</u>	2.4.3
2.4.2.1 Continuing Damage	2.4.4
2.4.2.2 Fastener Policy	2.4.6
2.4.3 <u>In-Service Inspection Damage Assumptions</u> <u>(Minimum Assumed)</u>	2.4.8
2.4.4 <u>Demonstration of Primary Flaw Sizes Smaller</u> <u>Than Those Specified</u>	2.4.10
2.5 RESIDUAL STRENGTH REQUIREMENTS	2.5.1
2.5.1 <u>General</u>	2.5.1
2.5.2 <u>Residual Strength Requirement for Fail-Safe</u> <u>Structure at the Time of Load Path Failure</u> <u>P_{yy} (Single Load Path Failure Load)</u>	2.5.3
2.5.3 <u>Determining the Residual Strength Load, P_{xx},</u> <u>for Fail Safe Structure Subsequent to Load</u> <u>Path Failure</u>	2.5.4
2.6 REQUIRED PERIODS OF SAFE DAMAGE GROWTH (PERIOD OF UNREPAIRED SERVICE USAGE)	2.6.1
2.6.1 <u>Slow Crack Growth, Non-Inspectable Structure</u>	2.6.1
2.6.2 <u>Slow Crack Growth, Depot Level Inspectable</u> <u>Structure</u>	2.6.1
2.6.3 <u>Fail Safe Structure - Intact Requirements</u>	2.6.1
2.6.4 <u>Remaining Structure - Fail Safe Categories</u>	2.6.2
2.7 ILLUSTRATIVE EXAMPLE OF THE APPLICATION OF MIL-A-83444 TO FAIL SAFE STRUCTURE	2.7.1
2.7.1 <u>Structural Design</u>	2.7.1
2.7.2 <u>Design Service Life</u>	2.7.1
2.7.3 <u>Choice of Structural Design Concept</u>	2.7.1

SUMMARY OF REQUIREMENTS
(Cont'd)

<u>SECTION</u>		<u>PAGE</u>
2.7.4	<u>In-Service Inspection Considerations</u>	2.7.2
2.7.5	<u>Initial Flaw Considerations</u>	2.7.2
2.7.6	<u>In-Service Flaw Assumptions Following Inspection</u>	2.7.3
2.7.7	<u>Remaining Structure Damage Following the Failure of the Major Load Path</u>	2.7.4
2.7.8	<u>Analysis of Intact Structure - Residual Strength Requirements and Damage Growth Limits (3.2.2.2.1)</u>	2.7.4
2.7.9	<u>Analysis of Intact Structure (Alternate Requirement)</u>	2.7.5
2.7.10	<u>Discussion of Intact Structure Analysis</u>	2.7.5
2.7.11	<u>Analysis of Remaining Structure Subsequent to Load Path Failure</u>	2.7.6
2.7.12	<u>Derivation of Residual Strength Load P_{yy}</u>	2.7.6
2.7.13	<u>Incremental Damage Growth Δa</u>	2.7.8
2.7.14	<u>Alternative-Analysis of Remaining Structure Subsequent to Load Path Failure</u>	2.7.9
2.7.15	<u>Summary and Comments</u>	2.7.10
2.8	ILLUSTRATIVE EXAMPLE OF APPLICATION OF MIL-A-8344 TO SLOW CRACK GROWTH STRUCTURE	2.8.1
2.8.1	<u>Structural Design</u>	2.8.1
2.8.2	<u>Initial Flaw Sizes Assumed to Result from Manufacturing</u>	2.8.1
2.8.3	<u>Choice of Inspection Category</u>	2.8.2
2.8.4	<u>Choice of an In-Service Non-Inspectable Category</u>	2.8.2
	2.8.4.1 Residual Strength Load, P_{xx}	2.8.2
	2.8.4.2 Analysis Requirements	2.8.3
2.8.5	<u>Choice of Depot Level Inspectable Category</u>	2.8.3
	2.8.5.1 Residual Strength Load, P_{xx}	2.8.3
	2.8.5.2 Analysis Requirements	2.8.4

LIST OF FIGURES

<u>FIGURE</u>		<u>PAGE</u>
2.1.1	Residual-Strength and Damage-Growth Requirements.	2.1.8
2.1.2	Essential Elements of MIL-A-83444.	2.1.9
2.2.1	Damage-Tolerance Structural Design Categories	2.2.4
2.2.2	Lug Example (Slow Crack Growth).	2.2.5
2.2.3	Wing Box Example.	2.2.6
2.4.1	Examples of Fastener Holes-Preparation and Assembly Damage.	2.4.12
2.4.2	Summary of Initial-Flaw Assumption for Intact Structure.	2.4.13
2.4.3	Schematic Representation of Rationale for Selecting Initial-Damage Sizes.	2.4.14
2.4.4	Reliability of Eddy Current Inspection for Detecting Cracks at Fastener Holes.	2.4.15
2.4.5	Reliability of Manufacturing Inspection for Detecting Surface Flaws.	2.4.16
2.4.6	Illustration of Thickness Criteria for Assuming Initial Flaws (Slow Crack Growth Structure).	2.4.17
2.4.7	Representation of Marginal Hole Quality.	2.4.18
2.4.8	Example of Continuing Damage Slow-Crack Growth Structure Growth of Damage Terminated at Free Edge, and Terminated by Failure of Member.	2.4.19
2.4.9	Example of Continuing Damage Types and Locations Assumed when Primary Damage Terminated Due to Element Failure.	2.4.20
2.4.10	Continuing Crack Assumed at Opposite Side of Hole when Primary Crack Terminates at Hole.	2.4.21
2.4.11	Summary of Initial-Flaw Sizes for Structure Qualified as In-Service-Inspectable.	2.4.22
2.4.12	Development of Minimum NDI Detection for Visual Inspection.	2.4.23
2.5.1	Residual Strength Diagram.	2.5.8
2.5.2	Schematic Residual Strength Requirements for a Structural Element Prior to Failure and for Transfer of its Load to Remaining Structure at and Subsequent to Failure.	2.5.8

LIST OF FIGURES
(Cont'd)

<u>FIGURE</u>		<u>PAGE</u>
2.5.3	Illustration of Procedure to Derive M Factor to Apply to Exceedance Curve.	2.5.9
2.5.4	Example of the Derivation of P_{XX} from Exceedance Curve for Non-Inspectible Structure.	2.5.10
2.7.1	Structural Example - Lower Wing Skin.	2.7.11
2.7.2	Initial-Flaw Assumptions for Example Case Qualified as Fail Safe.	2.7.12
2.7.3	Illustration of Primary Damage Following a Depot-Level Penetrant or Ultrasonic Inspection.	2.7.13
2.7.4	Illustration of Primary Damage Assumptions Following the Failure of Major Load Path (Panel 2).	2.7.14
2.7.5	Illustration of Damage-Growth Limits and Residual-Strength; Intact Structure Following Depot or Base-Level Inspection for Less-Than-Failed Load Path.	2.7.15
2.7.6	Illustration of Damage-Growth Limits and Residual Strength; Intact Structure for when Depot Inspection Cannot Detect Less-Than-Failed Load Path.	2.7.16
2.7.7	Illustration of Damage-Growth Limits and Strength Requirements; Remaining Structure Subsequent to Load-Path Failure.	2.7.17
2.7.8	Illustration of Redistributed Panel Load $P_{\textcircled{2}}$ to Adjacent Structure.	2.7.18
2.7.9	Development of Increment of Growth Δa_2 Used in the Analysis of Damage Growth - Remaining Structure Damage - Walk-Around-Visual Inspectible. Worst Case Analysis.	2.7.18
2.7.10	Development of Increment of Growth Δa_2 Used in Analysis of Damage Growth - Remaining Structure Damage - Depot-Level-Inspectible.	2.7.19
2.7.11	Illustration of Damage Growth and Residual-Strength Requirements - Remaining Structure - Depot Level - Inspectible.	2.7.20
2.8.1	Illustration of Initial Flaws for Structure Qualified as Fail-Safe Multiple Load Path.	2.8.5

LIST OF FIGURES
(Cont'd)

<u>FIGURE</u>		<u>PAGE</u>
2.8.2	Illustration of Damage-Growth and Residual-Strength Requirements for Example Problem Qualified as Slow Crack Growth Non-Inspectable.	2.8.6
2.8.3	Illustration of Damage-Growth and Residual Strength Requirements for Example Problem Qualified as Depot-Level-Inspectable.	2.8.7

LIST OF TABLES

<u>TABLE</u>		<u>PAGE</u>
2.1.1	SLOW-CRACK-GROWTH STRUCTURE REQUIREMENTS	2.1.6
2.1.2	FAIL-SAFE STRUCTURE REQUIREMENTS	2.1.7
2.3.1	SUMMARY OF IN-SERVICE INSPECTION	2.3.2
2.5.1	INSPECTION INTERVAL MAGNIFICATION FACTORS	2.5.6
2.6.1	REQUIRED PERIODS OF SAFE CRACK GROWTH - REMAINING STRUCTURE FAIL SAFE CATEGORIES	2.6.3

Definitions

Minimum Assumed Initial Damage Size (Section 2.4) - The minimum assumed initial damage size is the smallest crack-like defect which shall be used as a starting point for analyzing residual strength and crack growth characteristics of the structure.

Minimum Assumed In-Service Damage Size (Section 2.5) - The minimum assumed in-service damage size is the smallest damage which shall be assumed to exist in the structure after completion of an in-service inspection.

Minimum Period of Unrepaired Service Usage (Section 2.7) - The minimum period of unrepaired service usage is that period of service time during which the appropriate level of damage (assumed initial or in-service) is presumed to remain unrepaired and allowed to grow within the structure.

Minimum Required Residual Strength Load (Section 2.6) - The minimum required residual strength is specified as the smallest internal member load which the aircraft must be able to sustain with damage present and without endangering safety of flight or degrading the performance of the aircraft for the specified minimum period of unrepaired service usage.

Damage Size Growth Limit - The damage size growth limit is the maximum size to which initial or in-service size damage is allowed to grow without degrading the residual strength level below its required level.

2.1 GENERAL

USAF damage tolerance design requirements as specified in MIL-A-83444 apply to all safety of flight structure, i.e., structure whose failure could cause direct loss of the aircraft, or whose failure, if it remained undetected, could result in the loss of aircraft. The requirements stipulate that damage is assumed to exist in each element of new structure in a conservative fashion (i.e., critical orientation with respect to stress field and in a region of highest stress). The structure must successfully contain the growth of the initial assumed damage for a specified period of service while maintaining a minimum level of residual static strength, both during and at the end of this period. Figure 2.1.1 illustrates these requirements in a diagrammatic form. Since residual static strength generally decreases with increased damage size, the residual strength and growth requirements are coupled through the maximum allowable damage size, i.e. the damage size growth limit established by the minimum-required residual strength load. The safe growth period (period of unrepaired service usage) is coupled to either the design life requirement for the air vehicle or to the scheduled in-service inspection intervals. While the specific requirements of MIL-A-83444 may seem more complex than described in Figure 2.1.1, all essential elements are as illustrated. The remainder of Chapter 2 will describe these individual elements.

A structure can be qualified under one of two categories of defined damage tolerance (referred to as Design Concepts in MIL-A-83444).

These are:

Slow Crack Growth - In this category, structures are designed such that initial damage will grow at a stable, slow rate under service environment and not achieve a size large enough to cause rapid unstable propagation.

Fail Safe - In this category, structures are designed such that propagating damage is safely contained by failing a major load path or by other damage arrestment features.

In Slow Crack Growth qualified structure, damage tolerance (and thus safety) is assured only by the maintenance of a slow rate of growth of damage, a residual strength capacity and the assurance that subcritical damage will either be detected at the depot or will not reach unstable dimensions within several design life times. In Fail Safe qualified structure, damage tolerance (and thus safety) is assured by the allowance of partial structural failure, the ability to detect this failure prior to total loss of the structure, the ability to operate safely with the partial failure prior to inspection and the maintenance of specified static residual strength throughout this period.

MIL-A-83444 requirements have been developed with the intention of providing approximately the same level of damage tolerance for the

Slow Crack Growth and Fail Safe categories. As will be discussed in Section 2.4, this is accomplished mainly by varying the assumed initial flaw sizes.

Each structure must qualify within one of the designated categories of in-service inspectability (referred to as "The Degree of Inspectability" in MIL-A-83444), including the option to designate Slow Crack Growth qualified structure as "in-service non-inspectable." The various degrees of inspectability refer to methods, equipment, and other techniques for conducting in-service inspections as well as accessibility and the location of the inspection (i.e., field or depot) and are defined in Section 6.2 of MIL-A-83444.

In the specification, the detailed requirements are grouped according to the particular design category:

Slow Crack Growth: Section 3.2.1

Fail Safe: multiple load path - Section 3.2.2

Fail Safe: crack arrest - Section 3.2.3

The selection of the most appropriate damage tolerance category under which to qualify the structure is the choice of the designer/analyst. The choice of degree of in-service inspectability is somewhat limited, however, to those described in MIL-A-83444. The inspection requirements have been developed based upon past and present experiences and are felt to be reasonable estimates of future practice.

It is the intent of the specification to provide for at-least design limit load residual strength capability for all intact structure (i.e., for subcritical damage sizes in slow crack growth structure and damage sizes less than a failed load path in fail safe qualified designs). This requirement allows for full limit load design capability and thus unrestricted aircraft usage. The imposition of the requirement constrains structure qualified as Slow Crack Growth to either depot level inspectable or in-service non-inspectable.

To help in understanding the steps required to utilize MIL-A-83444, the essential elements and the corresponding paragraphs required for the Slow Crack Growth and Fail Safe categories are indicated in Figure 2.1.2. Each vertical path describes the sequence to be followed to check a structure for the appropriate category. As described in Section 2.2, fail safe structure must meet both the intact structure and remaining structure requirements. Slow crack growth structure will meet either the depot level inspectable or the non-inspectable structure requirements. For each structure, evaluation of the following parameters are required:

- a. Design Category - Optional Choice of Designer
- b. Degree of In-Service Inspectability - Types of Inspection defined - selection of category is program option.

- c. Inspection Intervals - Values specified for various categories - should be used in design but may be altered for specific design based on individual system needs.
- d. Initial Damage - In-Service Damage and Continuing Damage Assumptions - Values specified - alternate values allowed if justified and demonstrated (See Section 2.4.4).
- e. Minimum Required Residual Strength - Means of obtaining value specified in terms of inspection categories and inspection intervals - no options provided.
- f. Damage Size Growth Limits - Defined
- g. Periods of Unrepaired Service Usage - Specified
- h. Remaining Structure Damage Sizes - Defined

A summary of the MIL-A-83444 requirements for Slow Crack Growth Structure and for Fail Safe Structure have been provided in Tables 2.1.1 and 2.1.2, respectively. Note that Table 2.1.2 applies equally well to multiple load path and to crack arrest types of Fail Safe Structure.

TABLE 2.1.1
SLOW-CRACK-GROWTH STRUCTURE REQUIREMENTS

INSPECTABILITY	SAFE CRACK GROWTH INTERVAL	RESIDUAL STRENGTH, P_{xx}
DEPOT OR BASE LEVEL	1/2 LIFETIME	MAXIMUM LOAD IN 5 LIFETIMES
NON-INSPECTABLE	2 LIFETIMES	MAXIMUM LOAD IN 20 LIFETIMES

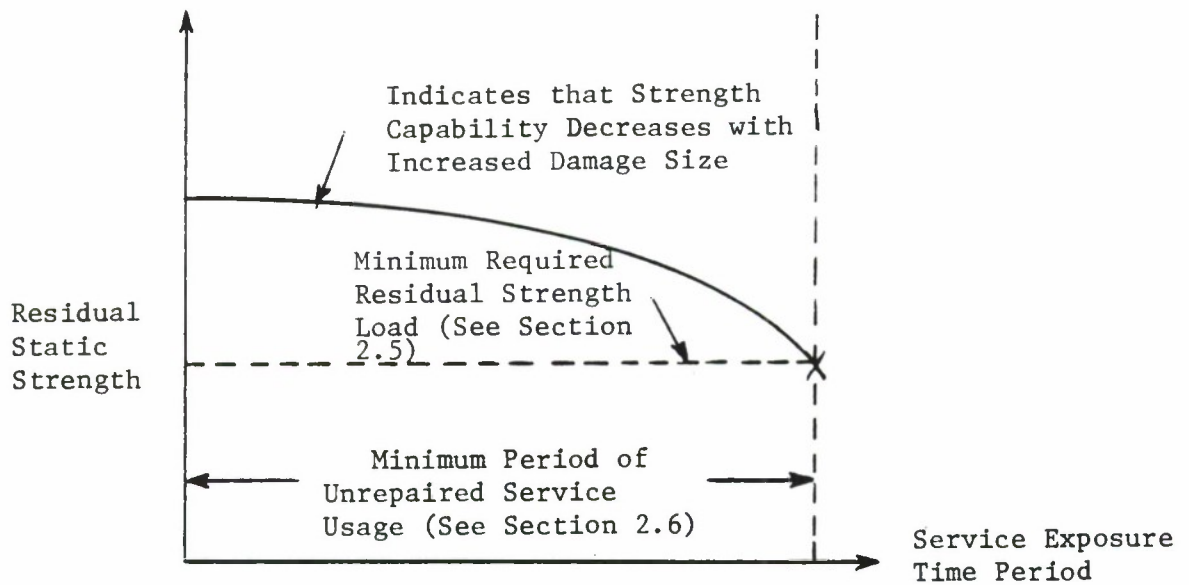
● DESIGN LIMIT LOAD $\leq P_{xx} \leq 1.2 \times$ MAXIMUM LOAD IN LIFETIME

TABLE 2.1.1.2

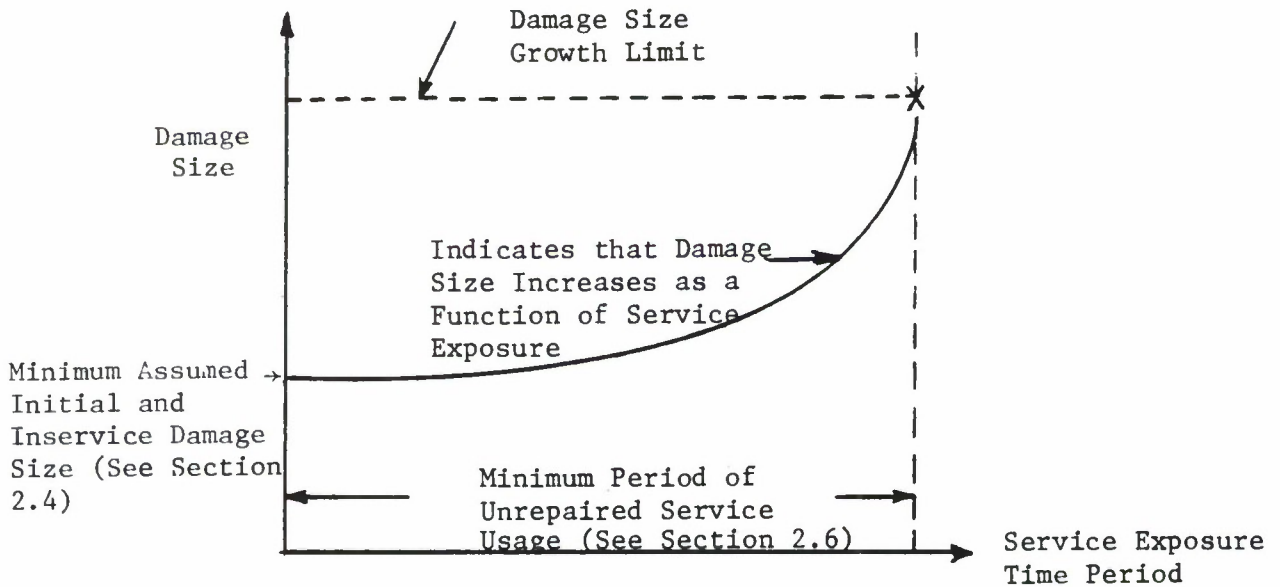
FAIL-SAFE STRUCTURE REQUIREMENTS

INSPECTABILITY	INTACT STRUCTURE		REMAINING STRUCTURE	
	SAFE CRACK GROWTH INTERVAL	RESIDUAL STRENGTH, P_{xx}	SAFE CRACK GROWTH INTERVAL	RESIDUAL STRENGTH, P_{xx}
IN-FLIGHT EVIDENT	ONE LIFETIME	MAXIMUM LOAD IN 20 LIFETIMES	RETURN TO BASE	MAXIMUM LOAD IN 100 FLIGHTS
GROUND EVIDENT			ONE FLIGHT	MAXIMUM LOAD IN 100 FLIGHTS
WALK-AROUND VISUAL			50 FLIGHTS	MAXIMUM LOAD IN 1000 FLIGHTS
SPECIAL VISUAL			2 YEARS	MAXIMUM LOAD IN 50 YEARS
DEPOT OR BASE LEVEL	1/4 LIFETIME	MAXIMUM LOAD IN 5 LIFETIMES	1/2 LIFETIME	MAXIMUM LOAD IN 5 LIFETIMES

- $P_{xx} \geq$ DESIGN LIMIT LOAD FOR ALL INTACT STRUCTURE & DEPOT OR BASE LEVEL INSPECTABLE REMAINING STRUCTURE
- $P_{xx} \leq 1.2 \times$ MAXIMUM LOAD IN LIFETIME FOR ALL STRUCTURE
- AT TIME OF FAILURE OR ARREST, $P_{yy} = 1.15 \times P_{xx}$



(a) Residual Strength Diagram



(b) Damage Growth Diagram

Figure 2.1.1. Residual-Strength and Damage-Growth Requirements.

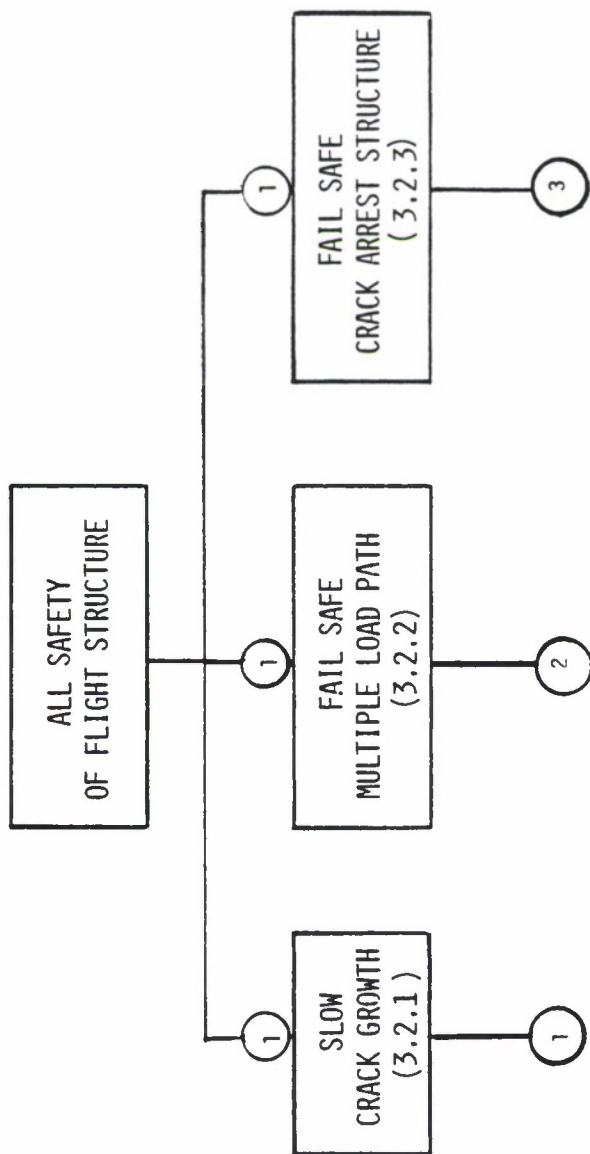


Figure 2.1.1.2 Essential Elements of MIL-A-83444.

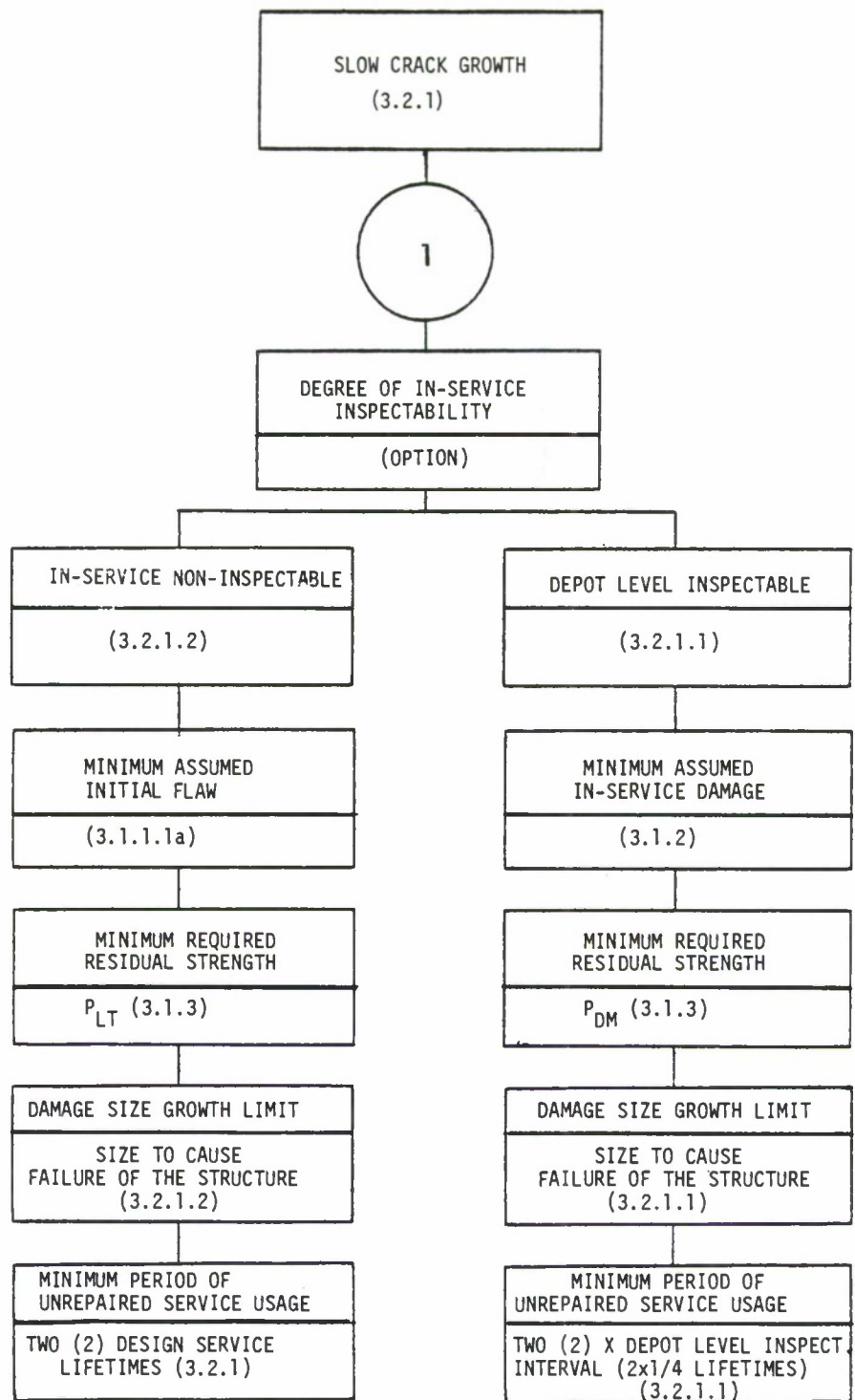


Figure 2.1.2. (Continued).

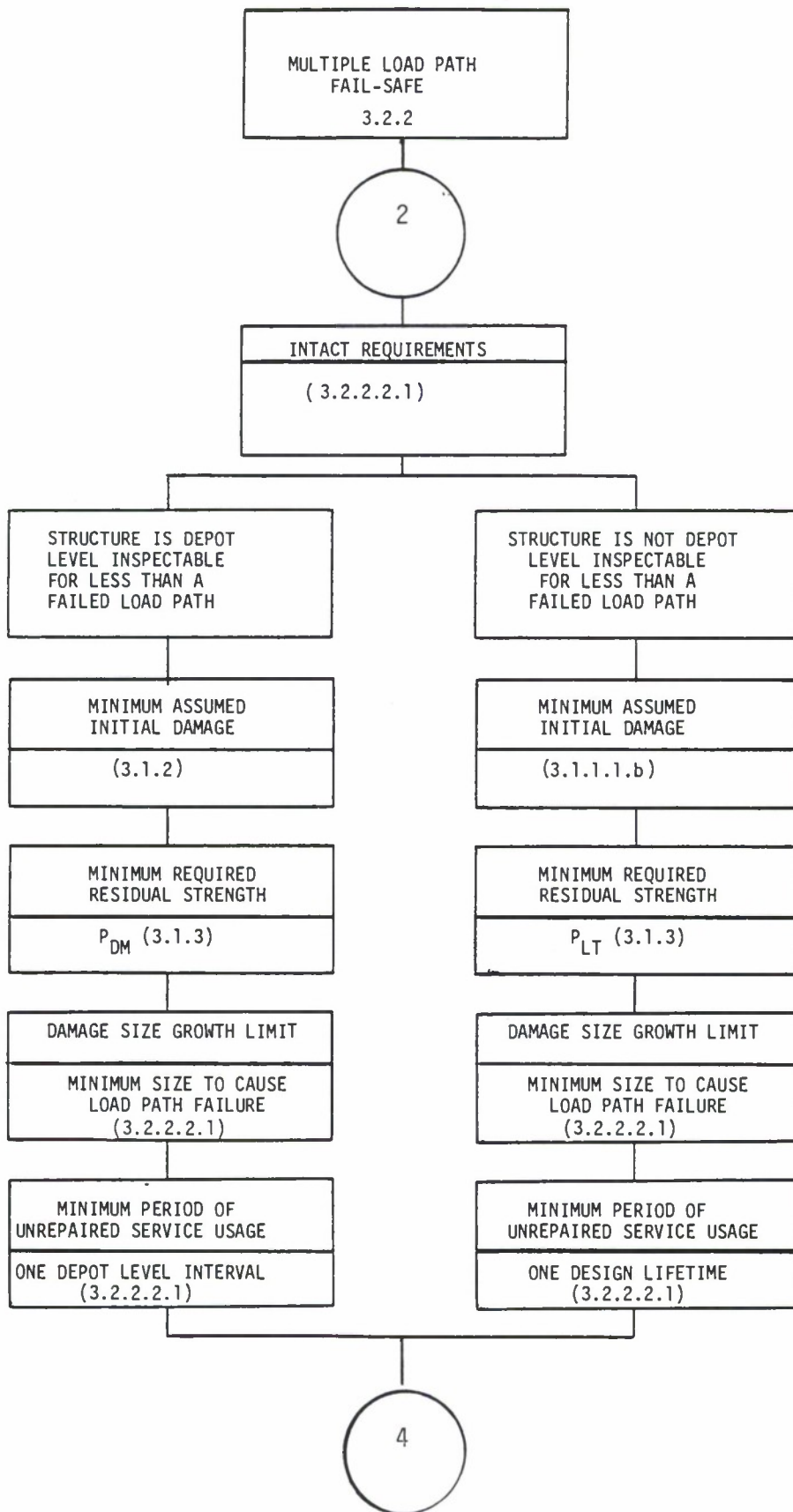


Figure 2.1.2. (Continued)

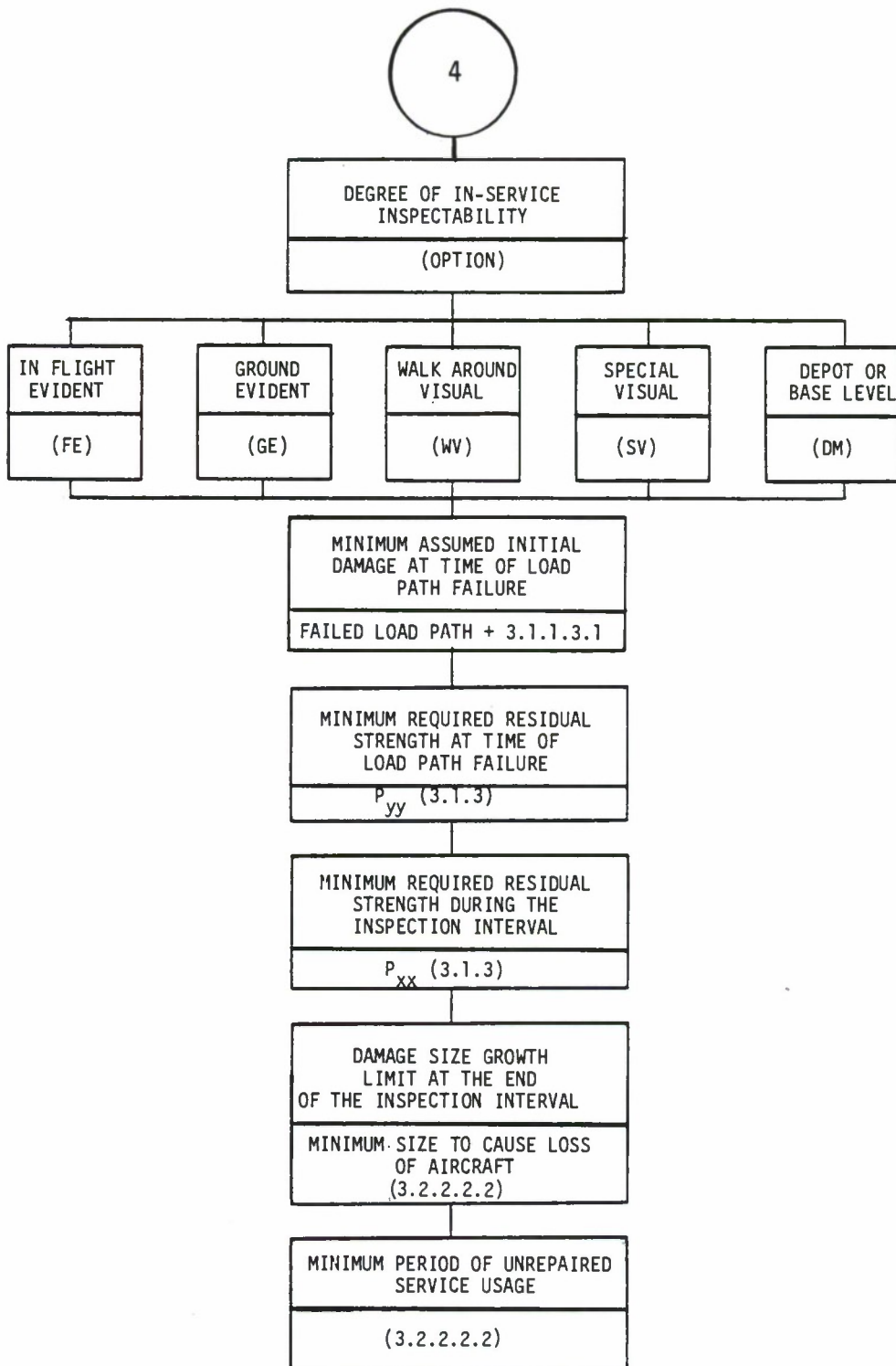
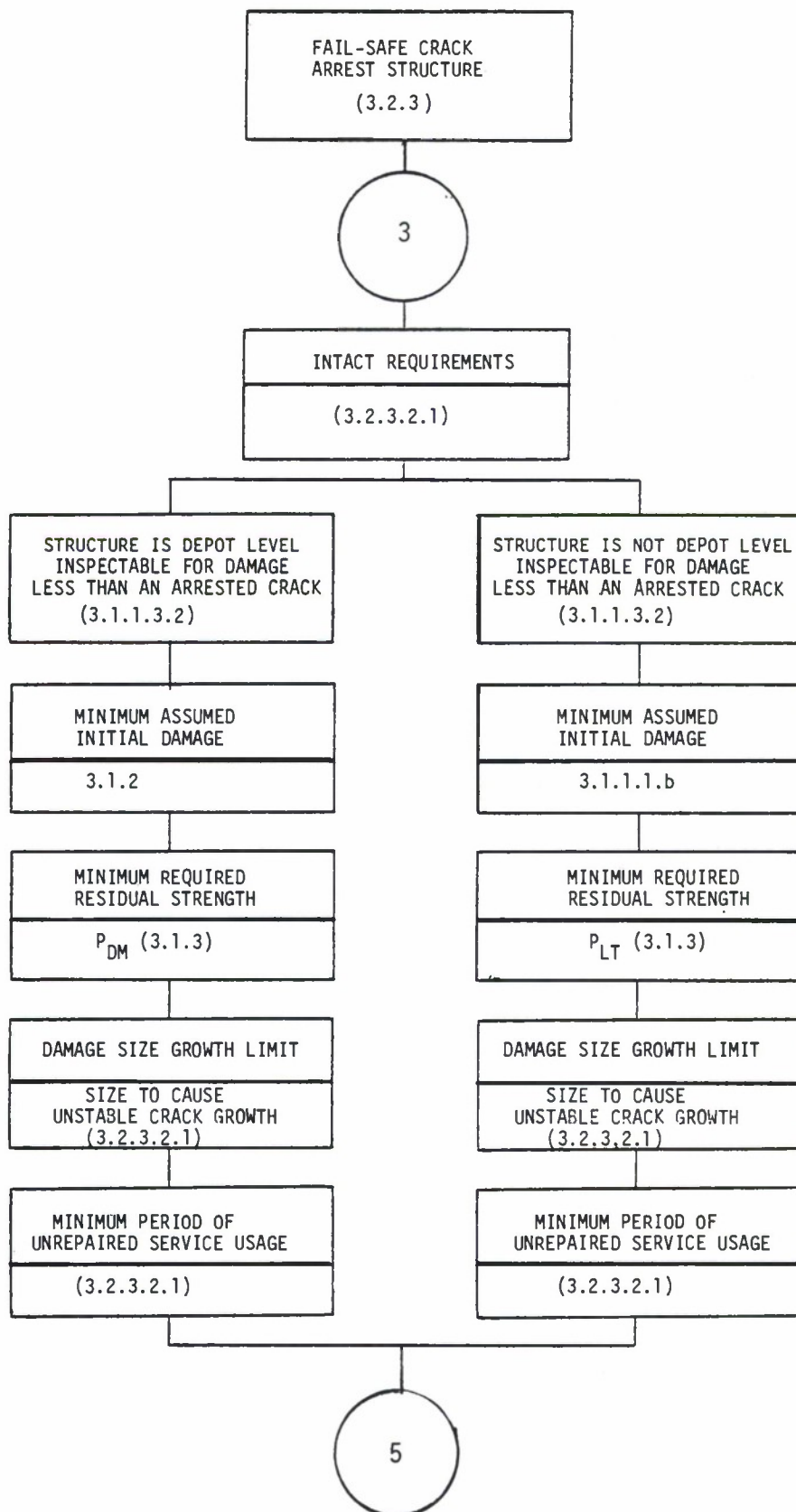


Figure 2.1.2. (Continued).



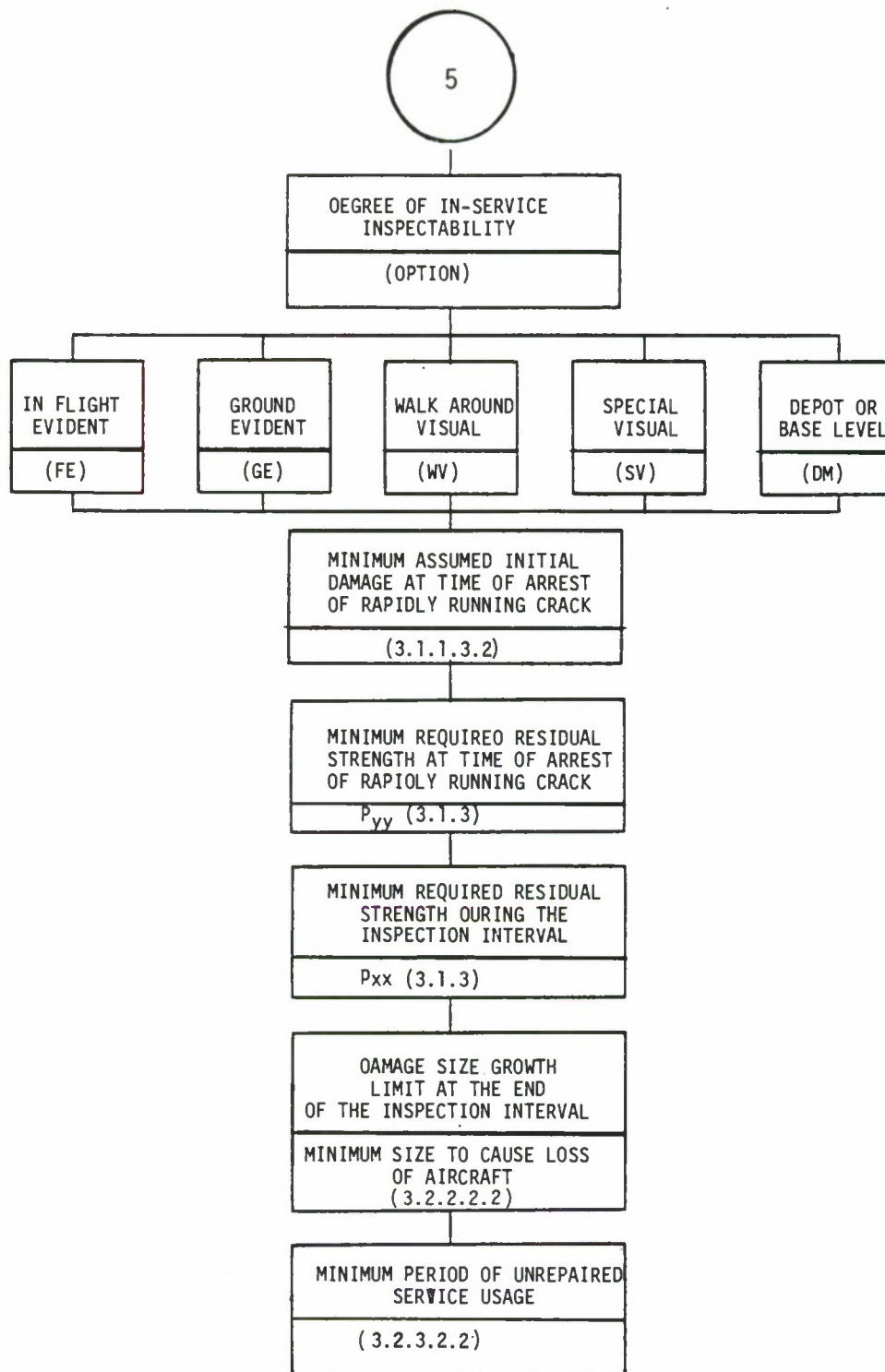


Figure 2.1.2. (Concluded)

2.2 DESIGN CATEGORY

Selection of the appropriate design category (e.g. Fail Safe or Slow Crack Growth) (Figure 2.2.1) is the initial step in applying MIL-A-83444.

In the development of the specification, it was recognized that multiple load path and crack arrest type structure have inherent potential for tolerating damage by virtue of geometric design features. On the other hand, it is often not possible to avoid primary structure with only one major load path and some provisions are necessary to ensure that these situations can be designed to be damage tolerant. It is the intent of the specification to encourage the exploration of the potentials for damage tolerance in each type of structure. Single load path or monolithic structures must rely on the slow rate of growth of damage for safety and thus, the design stress level and material selection become the controlling factors.

While single load path "monolithic" structures must be qualified as Slow Crack Growth, the designer has the choice of category for qualification of multiple load path cases. The decision may be made to qualify multiple load path structure as Slow Crack Growth for various reasons. The two reasons most frequently given are (1) the difficulty in meeting portions of the Fail Safe structural requirement (e.g., Remaining Structural Damage Growth, or Residual Strength), and (2) conducting an analysis for Slow Crack Growth Structure is less complex. Therefore, the method of construction may not agree with the design

category selected, i.e. all multiple load path structure is not fail safe. The specification allows this flexibility. The most important factor to consider when deciding on the design category option is that once a design category is chosen, the structure must meet all the requirements in the specification that cover that category.

The mere fact that a structure has alternate load paths (local redundancy) in some locations does not necessarily qualify it as Fail Safe. Some examples are helpful in illustrating this point:

EXAMPLE 2.2.1 - Identifying Non-Redundant Structure

The fitting illustrated in Figure 2.2.2 has multiple lug ends at the pinned connection. Failure or partial failure of one of the lugs (A) would allow the load to be redistributed to the remaining sound structure. Localized redundancy is often beneficial and in this case is good design practice. However, the fitting cannot be qualified as Fail Safe multiple Load Path structure since the occurrence and growth of damage at a typical location (B) would render the structure inoperative. The only means of protecting the safety of this structural element would be to qualify it as Slow Crack Growth.

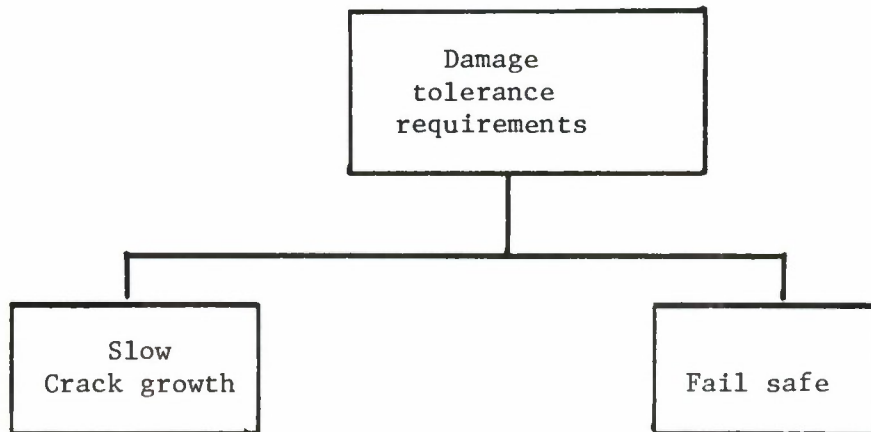
EXAMPLE 2.2.2 - Choice Options for Redundant Structure

As shown in Figure 2.2.3, a wing box is attached to the fuselage carry through structure by multiple fittings. The upper and lower skin are one piece for manufacturing and cost reduction. The substructure consists of multiple spars spaced to attach to the individual attachment fittings.

A case could be made to qualify this structure as Fail Safe Multiple Load Path. Depending upon the amount of bending carried by the spars, it would be possible to design the structure such that damage in the skin would be arrested at a spar prior to becoming critical. The design might also tolerate failure of one spar cap and a portion of the skin, prior to catastrophic failure. The attachment system could be designed to satisfy Fail Safe requirements with one fitting failed.

On the other hand, if the skin was the major bending member with a design stress of sufficient magnitude to result in a relatively short critical crack length, then the skin and spar structure could only be qualified as Slow Crack Growth structure.

Examples 2.2.1 and 2.2.2 illustrate the fact that a structure is often locally redundant (usually good design practice), but in an overall sense may have some restriction such that one is not able to take advantage of the localized redundancy in order to qualify the structure as Fail Safe. Considerable judgement is required for the selection of potential initial damage locations for the assessment of damage growth patterns and the selection of major load paths. The qualification as Fail Safe is thus a complex procedure entailing judgment and analysis. Because of this, the choice is often made to qualify the design as Slow Crack Growth regardless of the type of construction.



This category includes all types of structures, single and multiple load path which are designed such that initial damage will grow at a stable, slow rate and not achieve a size large enough to fail the structure for a specified slow crack growth period. Safety is assured by the slow rate of growth.

Usually structure comprised of multiple elements or load paths such that damage can be safely contained by failing a load path or by the arrestment of a rapidly running crack at a tear strap or other deliberate design feature. Fail safe structure must meet specific residual strength requirements following the failure of the load path or the arrestment of a running crack, safety is assured by the allowance of a partial failure of the structure, the residual strength and a period of usage during which the partial failure will be found.

Figure 2.2.1. Damage-Tolerance Structural Design Categories.

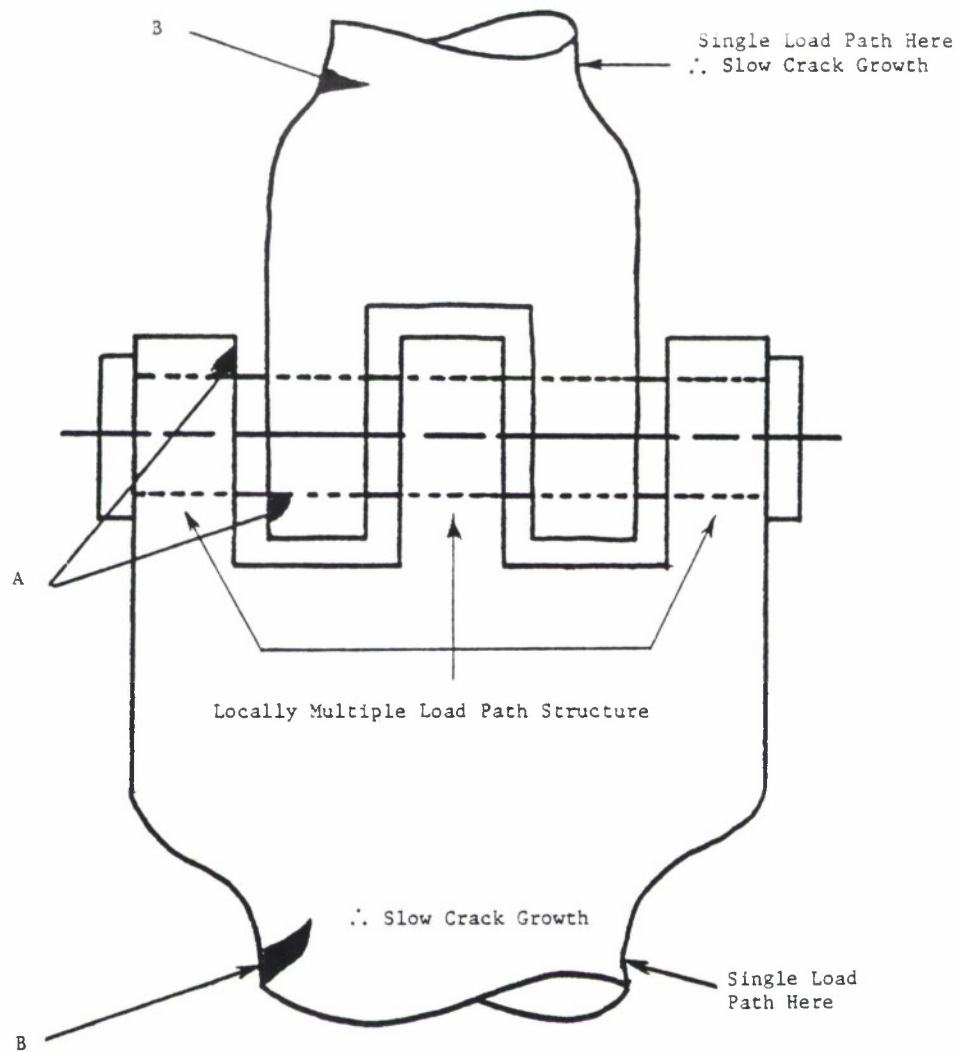


Figure 2.2.2 Lug Example (Slow Crack Growth).

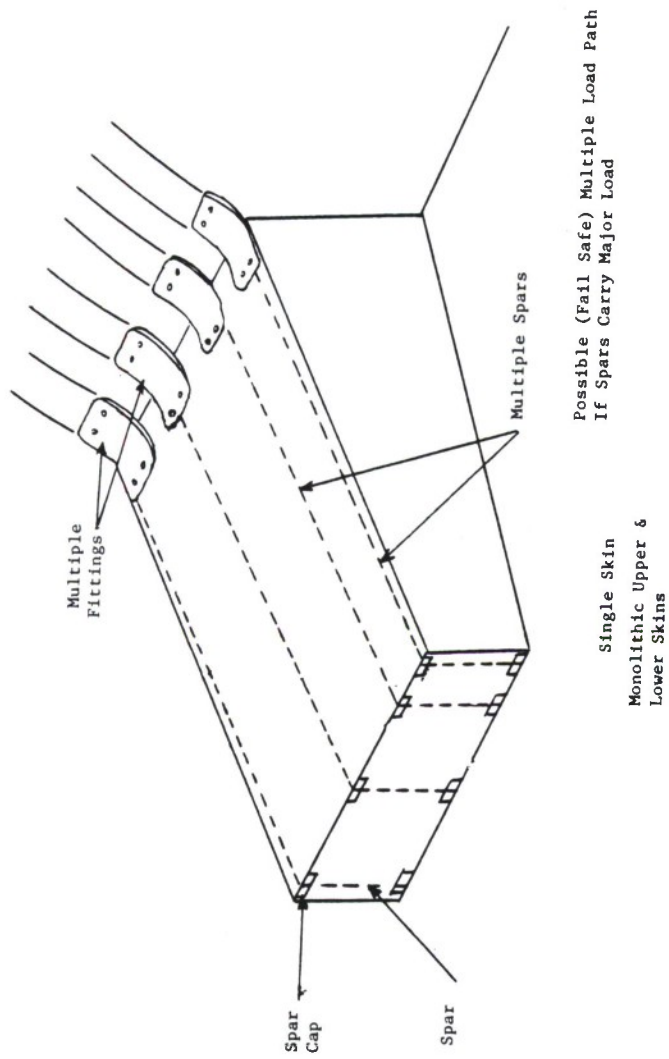


Figure 2.2.3 Wing Box Example.

2.3 INSPECTION CATEGORIES AND INSPECTION INTERVALS

Specifications for degree of inspectability are contained in Section 6.2.1 of MIL-A-83444. This information is reproduced in Table 2.3.1. For each individual aircraft system, the Air Force is obligated to specify the planned major depot and base level inspection intervals to be used in the design of the aircraft. Typically, these intervals will be approximately 1/4 of the design service life. The types and extent of inspection (i.e., equipment, accessibility, necessity for part removal, etc.) required at each of these major inspections is dependent upon the specific aircraft design and modifications resulting from development and full-scale tests or service experience. The Air Force wants its contractors to design a damage tolerant structure which will minimize the need for extensive non-destructive depot or base level inspections. Primary emphasis should therefore be placed on obtaining designs for which significant damage sizes can readily be found by visual inspection. However, where periodic inspections are required to satisfy the damage tolerance requirements, the contractor must recognize that the USAF will probably conduct the inspections. The in-service damage sizes associated with the inspection categories of MIL-A-83444 reflect the estimated capability of the Air Force to find damage.

The design of some aircraft components for intermediate special visual inspections (6.2.1.4), typically once per year, may be advanta-

TABLE 2.3.1

Summary of In-Service Inspection

<u>Degree of Inspectability</u>	<u>Typical Inspection Interval</u>
<p><u>In-Flight evident inspectable.</u> Structure is in-flight evident inspectable if the nature and extent of damage occurring in flight will result directly in characteristics which make the flight crew immediately and unmistakably aware that significant damage has occurred and that the mission should not be continued.</p>	One Flight
<p><u>Ground evident inspectable.</u> Structure is ground evident inspectable if the nature and extent of damage will be readily and unmistakably obvious to ground personnel without specifically inspecting the structure for damage.</p>	One Flight
<p><u>Walkaround inspectable.</u> Structure is walkaround inspectable if the nature and extent of damage is unlikely to be overlooked by personnel conducting a visual inspection of the structure. This inspection normally shall be a visual look at the exterior of the structure from ground level without removal of access panels or doors without special inspection aids.</p>	Ten Flights
<p><u>Special visual inspectable.</u> Structure is special visual inspectable if the nature and extent of damage is unlikely to be overlooked by personnel conducting a detailed visual inspection of the aircraft for the purpose of finding damaged structure. The procedure may include removal of access panels and doors, and may permit simple visual aids such as mirrors and magnifying glasses. Removal of paint, sealant, etc., and use of NDI techniques such as penetrant, X-ray, etc. are not part of a special visual inspection.</p>	One Year

TABLE 2.3.1

Summary of In-Service Inspection (Continued)

<p><u>Depot or base level inspection.</u> Structure is depot or base level inspectable if the nature and extent of damage will be detected utilizing one or more selected nondestructive inspection procedures. The inspection procedures may include NDI techniques such as penetrant, X-ray, ultrasonic, etc. Accessibility considerations may include removal of those components designed for removal.</p>	<p>1/4 Design Service Lifetime</p>
<p><u>In-Service non-inspectable structure.</u> Structure is in-service non-inspectable if either damage size or accessibility preclude detection during one or more of the above inspections.</p>	<p>One Design Service Lifetime</p>

geous from a performance or cost standpoint and may be used by the contractor in satisfying the requirements. Normally, special visual inspections will not be specified by the Air Force in the design and development stage but may be dictated, subsequent to design, by the results of testing or service experience.

Other visual inspectability levels include the categories of walk-around (6.2.1.3), ground evident (6.2.1.2), and in-flight evident (6.2.1.1) inspectable.

The assumed Air Force depot or base level inspection capabilities depend on the type of inspection performed. In special cases where potential benefits justify it, the contractor may recommend to the Air Force that specific components be removed from the aircraft and inspected during scheduled depot or base level inspections. If approval is given, the recommendations may be incorporated during design. In these cases, the assumed initial damage sizes subsequent to the inspection shall be the same as those in the original design providing the same inspection procedures are used and certified inspection personnel^{*} perform the inspection.

Conventional NDI procedures such as X-ray, penetrant, magnetic particle, ultrasonic, and eddy current are generally available for depot or base level inspections. Such inspection procedures will be performed as

* Certified inspection personnel must meet all requirements imposed by the manufacturer on those who initially inspected the given safety-of-flight critical structure during production.

dictated by the specific aircraft design inspection requirements, or as modified because of subsequent tests and service experience. In establishing the design inspection requirements, the contractor should attempt to minimize the need for such NDI. He should not plan on (nor design for) general fastener pulling inspections.

The specified frequency of inspections for each of the inspectability levels is indicated in 3.2.2.1 of MIL-A-83444 and Table 2.3.1 and is based on estimates of typical inspection intervals. As previously mentioned, the typical depot or base level frequency is once every one quarter of the design lifetime but may be otherwise specified in the appropriate contractual document. Special visual inspectable requires Air Force approval before being considered as a design constraint but, if approved, shall not be required more frequently than once per year. The justification for this restriction is cost and maintenance schedule requirements.

2.4 INITIAL DAMAGE ASSUMPTIONS

2.4.1 Intact Structure Primary Damage Assumption

The basic premise in arriving at the initial damage sizes is the assumption that the as-fabricated structure contains flaws of a size just smaller than the maximum undetectable flaw size found with the NDI procedures used on the production line. Typical types of manufacturing damage which have been seen on past military aircraft programs are shown in Figure 2.4.1. These flaw size shapes which are intended to be covered by the initial flaw size assumptions include radial tears, drilling burrs, and rifle marks at fastener holes as well as forging defects, welding defects, heat treatment cracks, forming cracks, and machining damage at locations other than fastener holes.

Figure 2.4.2 summarizes the initial damage assumptions for intact structure as specified in MIL-A-83444. These assumptions - relative to the size, shape and location - were based on a review of existing NDI data. The crack length values given in Figure 2.4.2 were selected as most appropriate for the types of cracks considered and for the two design categories.

The difference in crack sizes specified for the two design categories was dictated in part by the reliability of the NDI procedures and in part by the desire to achieve a high level of damage tolerance in Slow Crack Growth (single load path) structure. For any NDI procedure/material/structure combination, the maximum undetectable flaw size can only be specified in

a meaningful manner if the probability of detecting that flaw and the confidence level associated with that probability are also specified. The intact structure initial damage assumptions in MIL-A-83444 assume that the probability of detection (POD) and confidence levels are 90% and 95%, respectively, for the Slow Crack Growth category and 90% and 50%, respectively, for the Fail Safe category (see Figure 2.4.3). The 90%-95% values were selected as being economically practical from the standpoint of performing a non-destructive test demonstration program (see also Chapter 3.0). The 90% is also the basis for MIL-HDBK-5 for "B" allowable values. The same probability of detection value (i.e., 90%) is specified for the Fail Safe category as for the Slow Crack Growth category since NDI capability is not category dependent in the sense specified in MIL-A-83444. Because of the fracture containment capabilities and required in-service inspectability of the Fail Safe category, it appeared reasonable to accept a lower confidence level on detectability. A somewhat lower arbitrary value of 50% was accepted. This, in effect, resulted in a smaller value of required initial flaw size assumption for the intact structure requirement of the Fail Safe category than for the Slow Crack Growth category. The specified probability and confidence levels may be changed in future revisions to MIL-A-83444 as planned studies add more data.

The Slow Crack Growth initial damage sizes are based on NDI probability of detection (POD) data (90 percent probability of detection with 95 percent confidence). The 0.050 inch crack size for holes and cutouts is based on POD data obtained in the lab using eddy current inspection with fastener removed. (See, for example, Figure 2.4.4). The surface flaw size, 0.250 inch long by 0.125 inch deep, was obtained from Air Force sponsored inspection reliability programs where several techniques were used including ultrasonic, dye penetrant and magnetic particle (Figure 2.4.5). In these programs, most techniques were found to be sensitive to both surface length and flaw depth and thus the NDI capability must be judged in terms of the flaw shape rather than simply surface length or crack depth.

Obviously, for parts where thickness is less than or equal to the specified depths of surface or corner flaws, provisions must be made to handle the analysis of the deep flaw case. The specification stipulates that a through-the-thickness flaw is assumed for thickness less than the specified depth of cracks (Figure 2.4.6).

2.4.2 Intact Structure - Marginal Hole Quality

As a means of assessing the quality of fastener holes in military aircraft, regression analyses of crack growth tests have been conducted. The results of these studies indicate that estimates of initial quality for fastener holes can be assigned in terms of an apparent analytical initial flaw and thus degrees of quality can be

expressed in terms of the apparent initial flaw size, (i.e., the larger the apparent initial crack, the worse the quality) (Figure 2.4.7).

The results of the F-4 Durability and Damage Tolerance Analysis studies indicate that marginal quality holes (i.e., holes containing minor discrepancies of various types) can be characterized as having initial damage equivalent to a small corner crack of the order of 0.002-0.010 inch in radius. Accordingly, MIL-A-83444 assumes that any fastener hole in the structure can be marginal and can have an initial damage equivalent to a 0.005 inch radius corner flaw. Thus, the specification requires assuming that this flaw exists at each fastener hole within the structure at the time of manufacture. Since the 0.005 inch size is based on limited data, the contractor may provide data representing his own manufacturing quality and negotiate with the Air Force for a smaller size of the apparent initial flaw to represent marginal hole quality.

The 0.005 inch corner flaw representing marginal quality holes is the basis for the fastener policy, continuing damage, and remaining structure damage requirements.

2.4.2.1 Continuing Damage

In applying MIL-A-83444 to a built-up structure, it is noted that cyclic growth behavior of primary damage may be influenced by the geometry of the structure or the arrangement of the elements. In order to provide an orderly and progressive path for the crack that

eventually causes the structure to fail, the continuing damage assumptions were incorporated. There are three cases where the continuing damage assumptions are made in order to keep the crack moving; these cases are described with examples.

Figure 2.4.8 describes a skin-stringer construction where equivalent initial (primary) damage is assumed to exist in both elements of the hole marked A. According to MIL-A-83444 paragraph 3.1.1, all other holes are secondary cracking sites (marked B) and contain the small imperfections equivalent to the 0.005 inch radius corner flaw. As the primary damage progresses in both the skin and stringer eventually the radial crack in the stringer will extend to the edge of the stringer (Figure 2.4.8 - cracking sequence (ii)). At this time, a new crack, equivalent to the 0.005 inch radial crack flaw, is assumed to exist on the diametrically opposite side of the failed hole (Figure 2.4.8 - cracking sequence (iii)) so that the growth process can continue until the complete stringer fails (Figure 2.4.8 - cracking sequence (iv)).

Under the condition that the primary damage terminates due to a member or element failure, such as was illustrated in Figure 2.4.8, the designer is required to assume that continuing damage is present. The continuing damage is assumed to be present at the most critical location in the remaining element or structure. The continuing damage is a crack that starts from an initial small imperfection and grows at this secondary site until the element failure occurs at the primary site. Figure 2.4.9

illustrates several choices for potential critical locations where continuing damage might be assumed subsequent to the failure of the stringer. Site 1 is assumed to be an adjacent hole and the crack growth is in the skin and opposite in direction to the primary skin crack. Such a situation would eventually result in a stepwise shift in the crack growth path. Most logically, this type of damage could be assumed to exist at the primary damage site in the skin on the diametrically opposite side of the hole once the stiffener fails. Site 2 is located in the skin and would provide a path for link-up with the primary crack. Site 3 is located in a parallel stringer - skin hole and would also allow for possible link-up with the primary crack.

Figure 2.4.10 describes the type of continuing damage assumption that the designer must make when the assumed primary damage enters into and terminates at a fastener hole. The continuing damage in this case is a crack on the opposite side of the hole entered by the primary crack. The continuing damage crack is taken as the crack which has grown from an initial small imperfection (0.005 inch radial corner crack) through the time period that it takes the primary damage to terminate at the hole.

2.4.2.2 Fastener Policy

In practice, the growth of flaws from fastener holes can be retarded by the use of interference fit fasteners, special hole preparation (e.g. cold work), and, to some degree, by joint assembly procedures (e.g. friction due to joint clamp-up). Because these procedures

delay flaw growth, the slow crack growth lives (or intervals) can be significantly longer than those obtained from structure containing conventional low torque clearance fasteners (Note: In practice, it may be possible to permanently delay growth at a flawed hole with certain types of fastener systems).

It is the intent of the fastener policy to encourage contractors to enhance the safety and durability of the structure through the use of these flaw growth retarding fastener/hole preparation systems. Experience has shown that to achieve the beneficial effects of these techniques consistently, exceptionally high quality process control is required during manufacture. However, this is not always obtained. As a result, it is thought unwise to consider all interference or hole preparation systems effective in retarding crack growth. On the other hand, there is generally a low probability of having an ineffective interference fastener or no cold work in a hole containing the primary damage (i.e., those specified in Section 3.1.1.1 (a,b) of MIL-A-83444) and it would be unnecessarily conservative to assume this were the case. Accordingly, the policy set forth (3.1.1.1c of MIL-A-83444) assumes that any given fastener/hole preparation may be ineffective in retarding flaw growth; however, the assumed initial damage in the hole is equivalent to that associated with a marginal quality hole (0.005 inch) rather than the capabilities of non-destructive inspection.

2.4.3 In-Service Inspection Damage Assumptions (Minimum Assumed)

The basic rationale used to write assumed sizes following an in-service inspection is essentially the same as for the case of intact structure. Once it is established that reliance on in-service inspection is required (as opposed to desired) to ensure safety, the damage size assumed to exist after an in-service inspection is that associated with the appropriate level of NDI capability as opposed to that associated with initial manufacturing inspection capability. In special cases where specific part removal at the depot is economically warranted, the contractor may recommend that this action be taken. In this case, the assumed damage subsequent to part removal and inspection may be smaller than that associated with in-service inspection capabilities. It may in fact be the same as in the original design, providing the same inspection procedures as used in production are used and certified inspection personnel^{*} perform the inspection.

Figure 2.4.11 summarizes the in-service post inspection damage sizes as a function of conditions and thickness. With fasteners installed and sufficient accessibility to the location, the maximum undetectable damage size is 0.25 inch of uncovered length at fastener holes. Depending upon part thickness, this damage may be a through or part-through flaw. The

* Certified inspection personnel must meet all requirements imposed by the manufacturer on those who initially inspected the given safety-of-flight critical structure during production.

flaw size was established based on limited available inspection reliability data where the inspection was performed on the assembled aircraft as opposed to the part level inspection performed during production fabrication (Figure 2.4.4). These assumptions are considered to be applicable for penetrant, magnetic particle, and ultrasonics. Because of lack of sensitivity, X-ray is not considered appropriate for determining tight fatigue cracks and thus is not applicable to these flaw size assumptions.

At locations other than holes or cutouts, a flaw size of surface length 0.50 inch is assumed to be representative of depot level capability, although this value has not been substantiated by inspection reliability data. Where visual inspection is performed on the assembled aircraft, the minimum assumed damage is an open through the thickness crack having an uncovered length of 2 inches. This value was established based on visual inspection reliability data derived from inspection of large transport type aircraft during fatigue testing and subsequent teardown inspection (See Figure 2.4.12).

The data base for establishing values for in-service inspection is limited and in most cases the values are estimates. The maximum undetectable flaw sizes stated in this subsection are the result of data collected through approximately 1974. Current and future planned studies will extend the flaw size data base to substantiate or revise the current MIL-A-83444 post-inspection flaw sizes.

2.4.4 Demonstration of Primary Flaw Sizes Smaller Than Those Specified

For the Slow Crack Growth category, an allowance is made so that the contractor can select primary crack sizes smaller than specified in MIL-A-83444. At the current time, the contractor does not have the freedom to select smaller initial damage sizes for the Fail Safe category because the choices of damage here were initially selected to be a factor of 2.5 smaller than the Slow Crack Growth category and were deemed to be at the state-of-the-art.

The choice of initial smaller primary damage for the Slow Crack Growth category must be justified either through (a) an NDI demonstration or (b) a proof test:

- a. NDI Demonstration Program - As described in paragraph 3.1.1.1 of MIL-A-83444, the program must be formulated by the contractor and approved by the Air Force and must verify that, for the particular set of production and inspection conditions, flaws will be detected to the 90% probability level with 95% confidence.
- b. Proof Test - Where no other means of NDI is available or where it is indicated to be cost effective, the proof test can be an effective means of screening structure for flaws. Proof testing generally has been successful for the more brittle materials which exhibit plane strain fracture behavior (e.g. high strength steels)

and for small structural components. The application of proof testing to complete airframe structure in the USAF has been somewhat limited; and in general, proof testing has only been used on major airframe components as a last resort to allow operation (usually restricted) until extensive modifications are made to the structure (e.g. wing reskin modification of the B-52D). In deriving estimates of the initial flaw size associated with the proof test conditions, approved upper-bound fracture toughness values shall be used for the materials under proof test conditions. Chapter 3 also presents more information on the proof test concept.

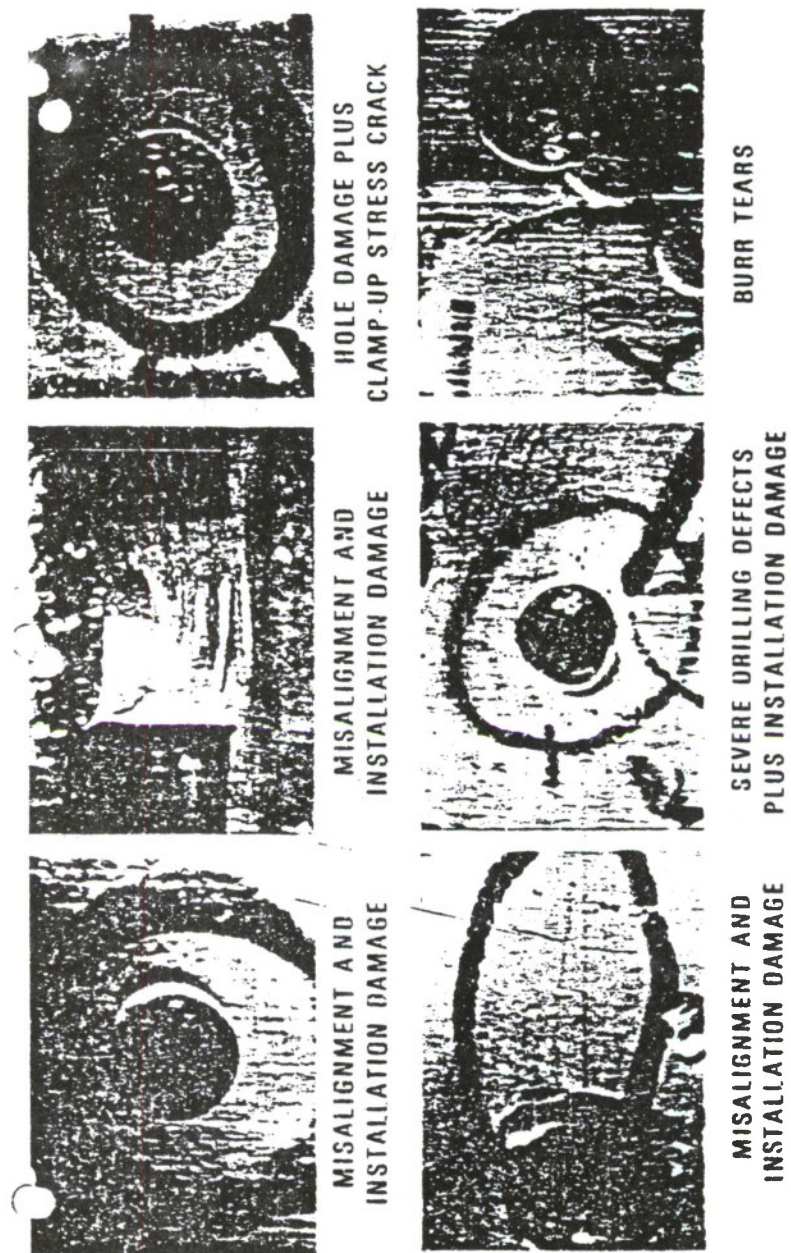


Figure 2.4.1 Examples of Fastener Holes - Preparation and Assembly Damage.

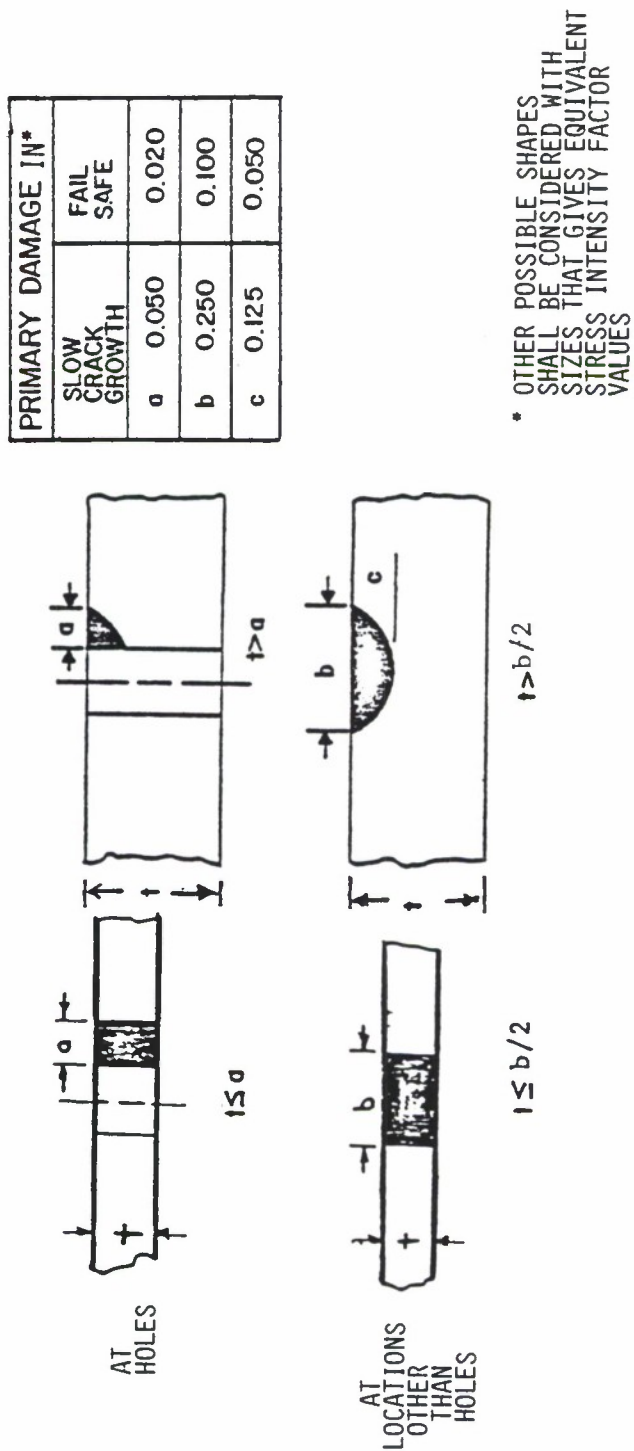


Figure 2.4.2 Summary of Initial-Flaw Assumption for Intact Structure.

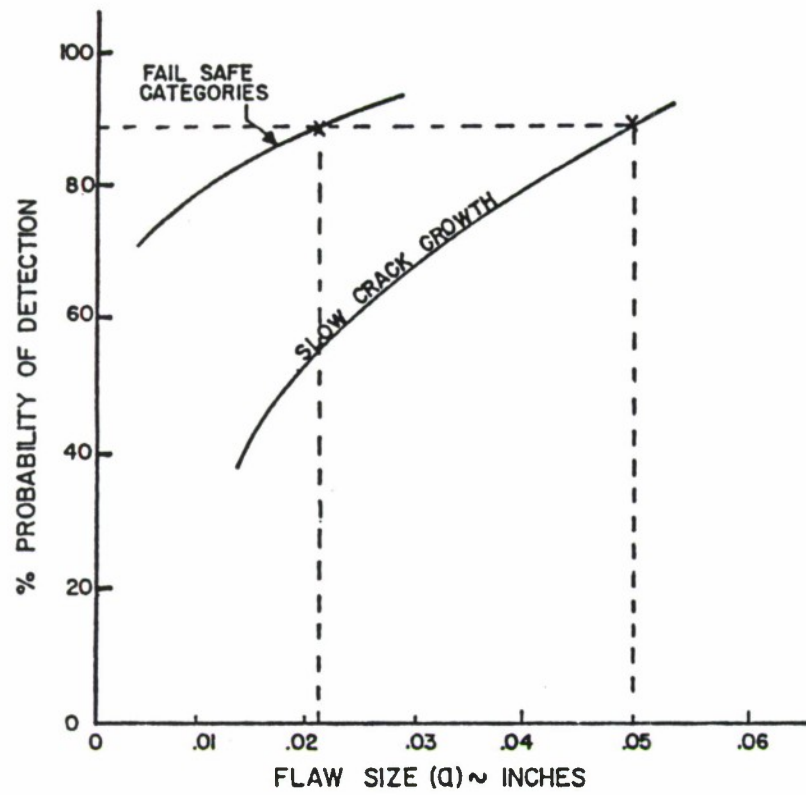
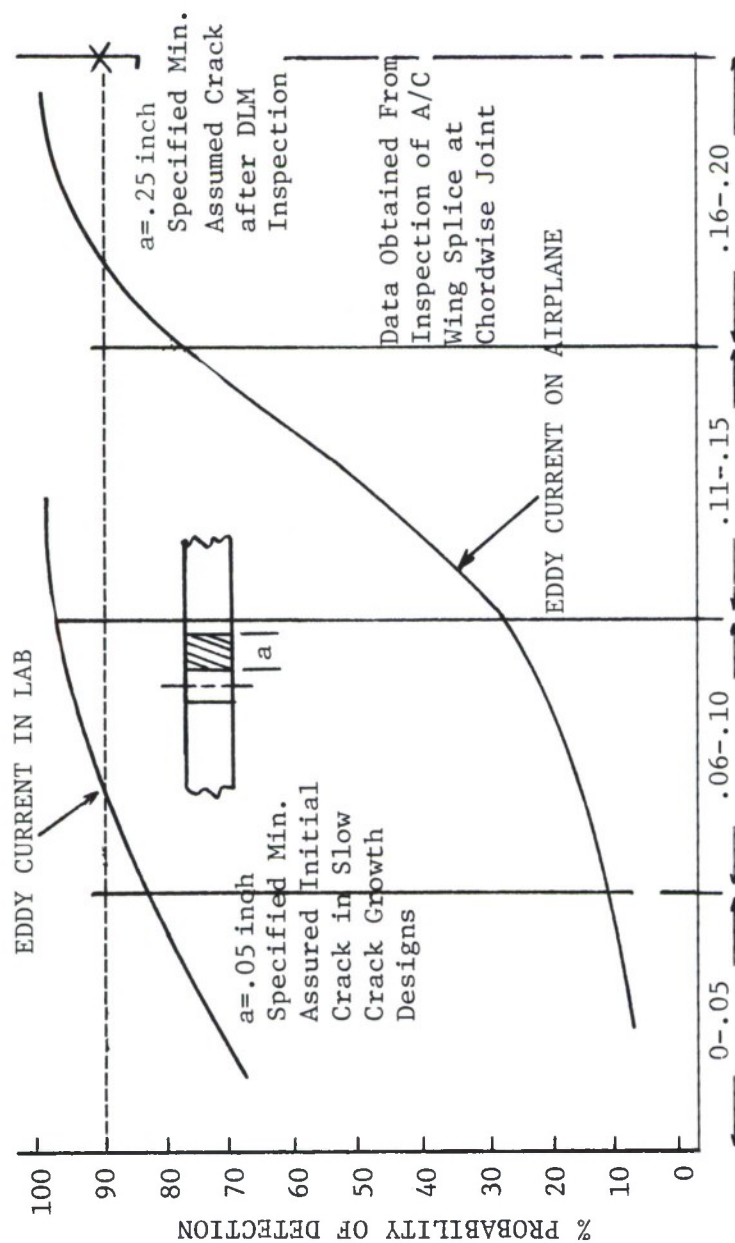


Figure 2.4.3 Schematic Representation of Rationale for Selecting Initial-Damage Sizes.



Crack Length - a Inches

Reference: B-52 Full Reference Available

Figure 2.4.4. Reliability of Eddy Current Inspection for Detecting Cracks at Fastener Holes.

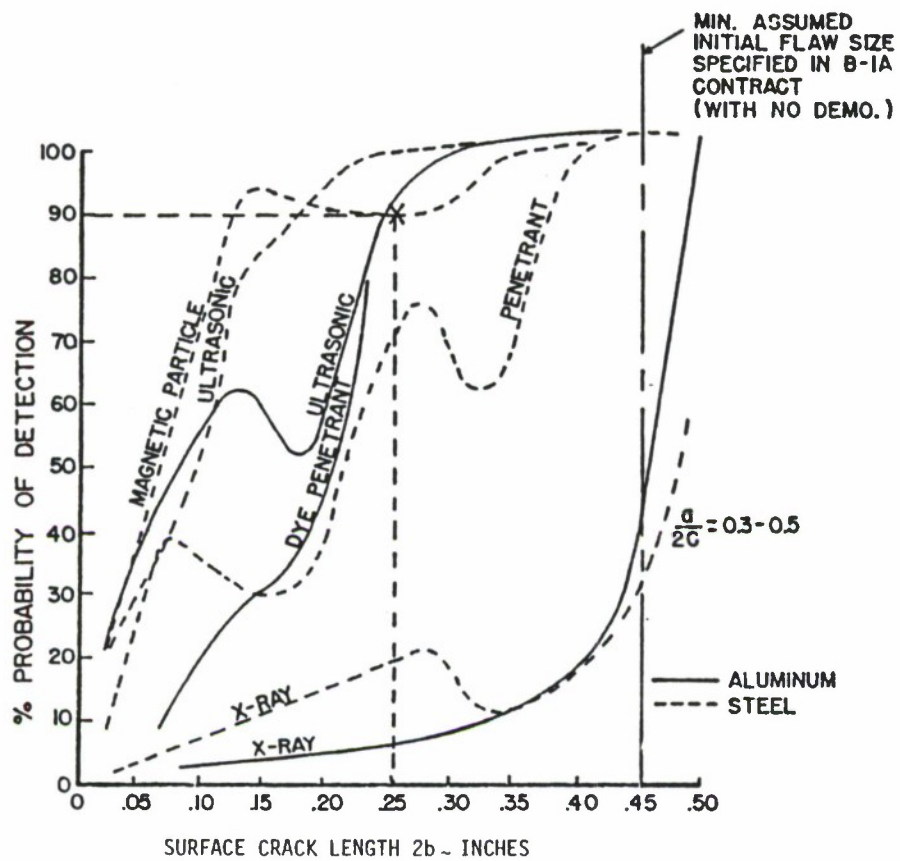


Figure 2.4.5 Reliability of Manufacturing Inspection for Detecting Surface Flaws.

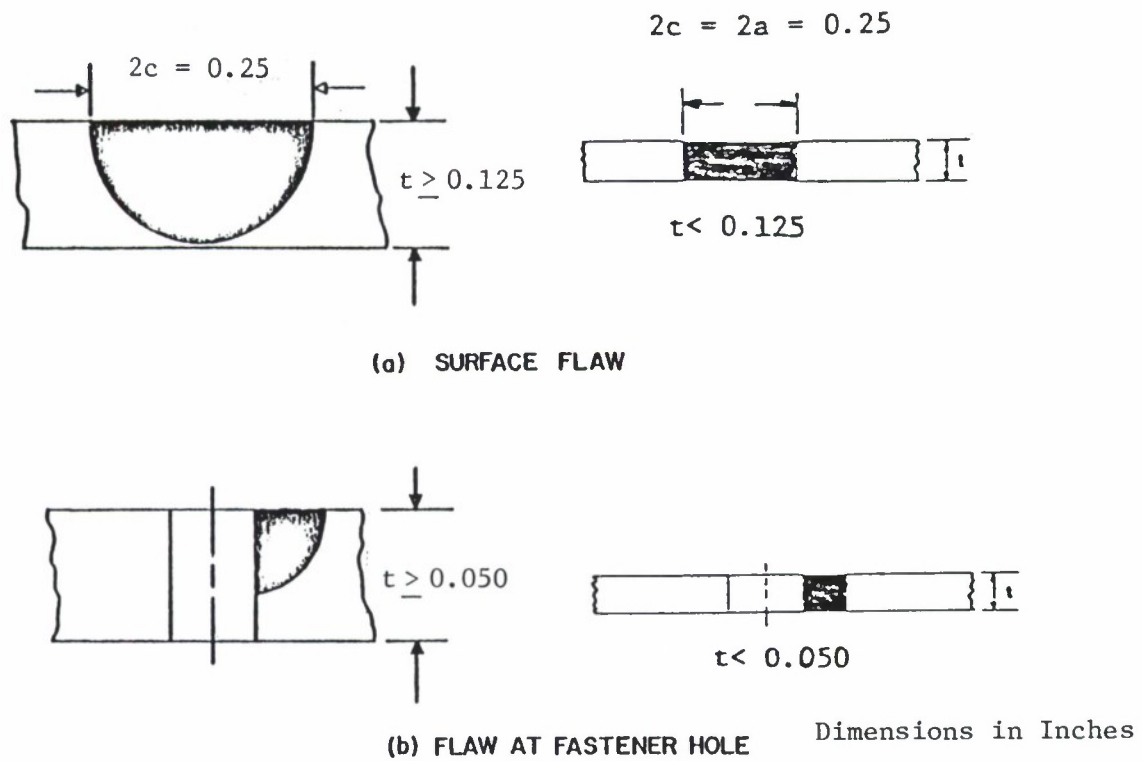


Figure 2.4.6 Illustration of Thickness Criteria for Assuming Initial Flaws (Slow Crack Growth Structure).

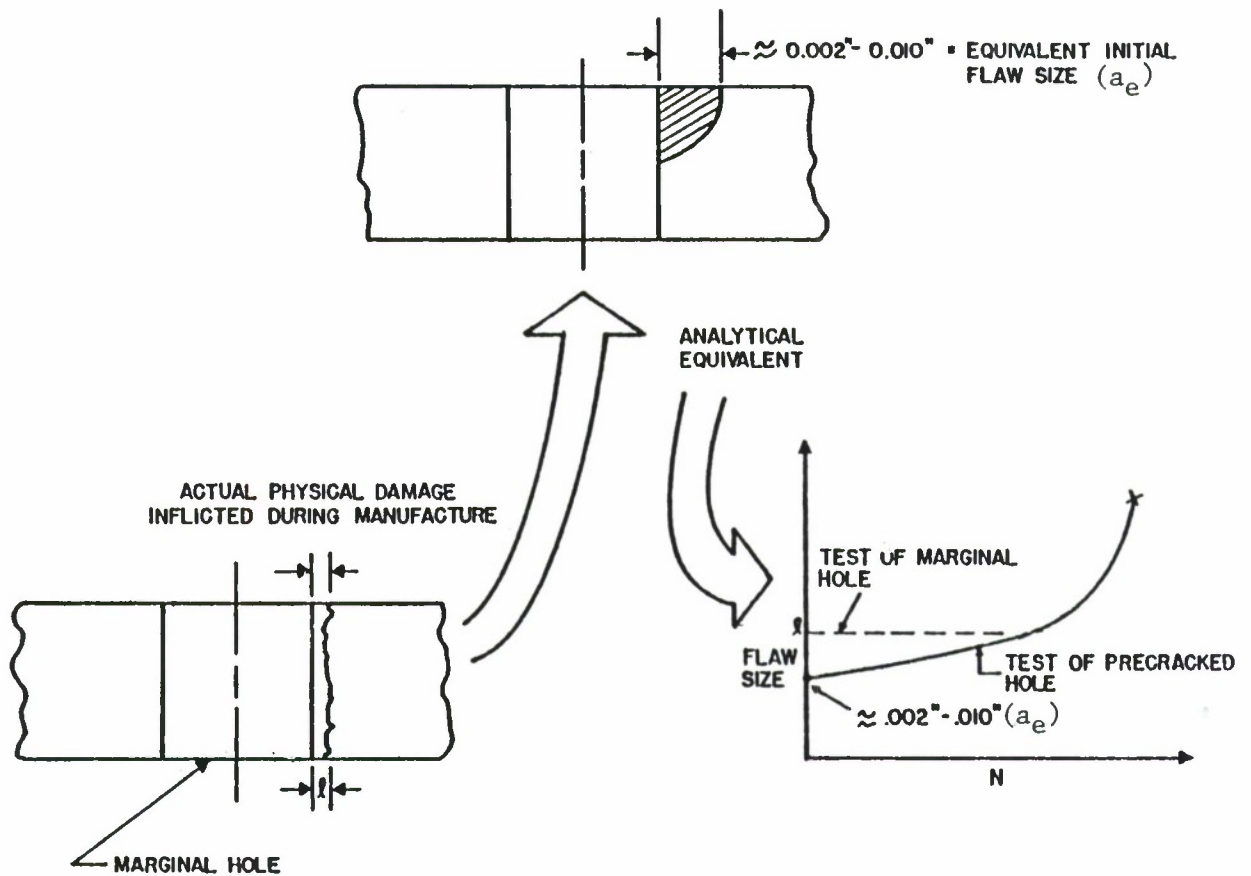


Figure 2.4.7 Representation of Marginal Hole Quality.

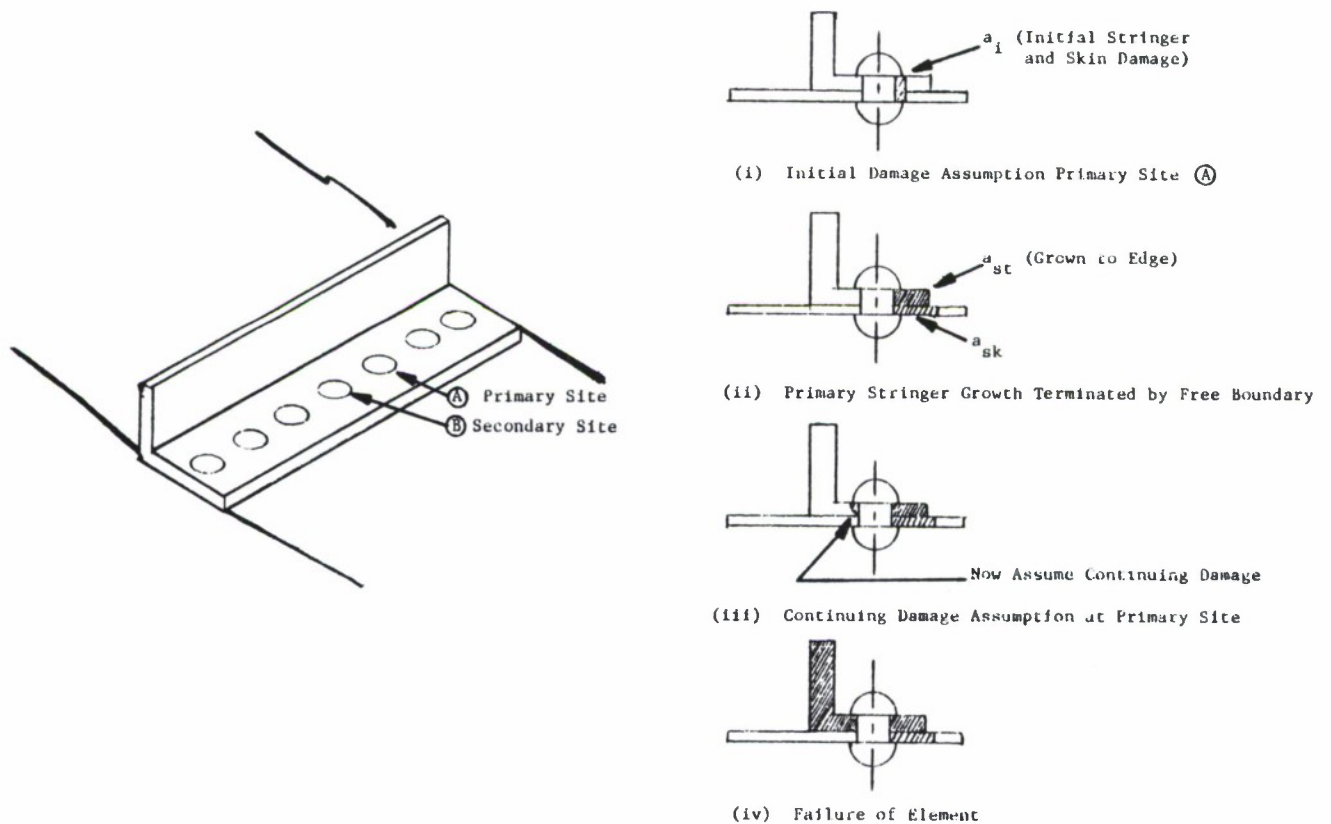


Figure 2.4.8 Example of Continuing Damage Slow-Crack-Growth Structure Growth of Damage Terminated at Free Edge, and Terminated by Failure of Member.

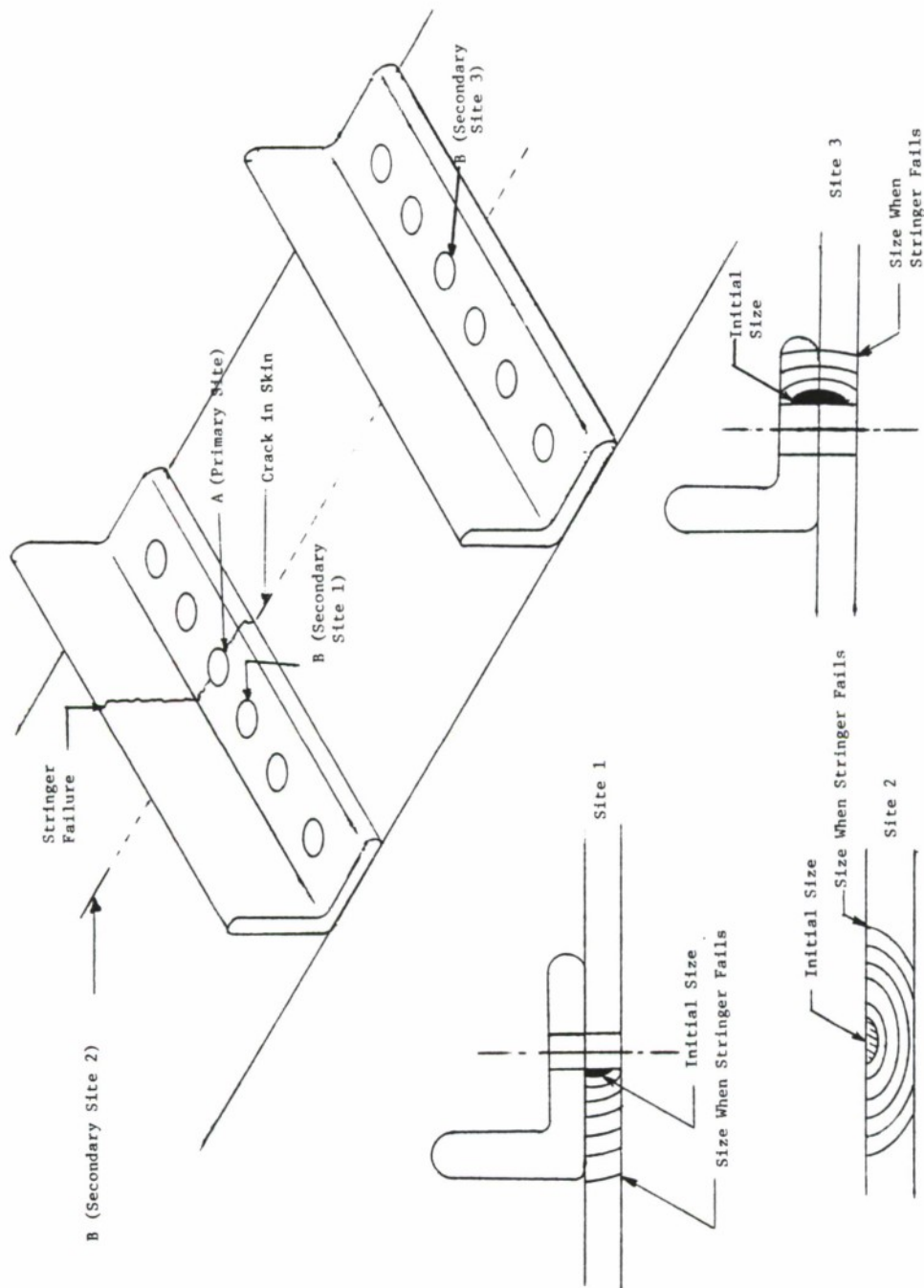


Figure 2.4.9 Example of Continuing Damage Types and Locations Assumed When Primary Damage Terminated Due to Element Failure.

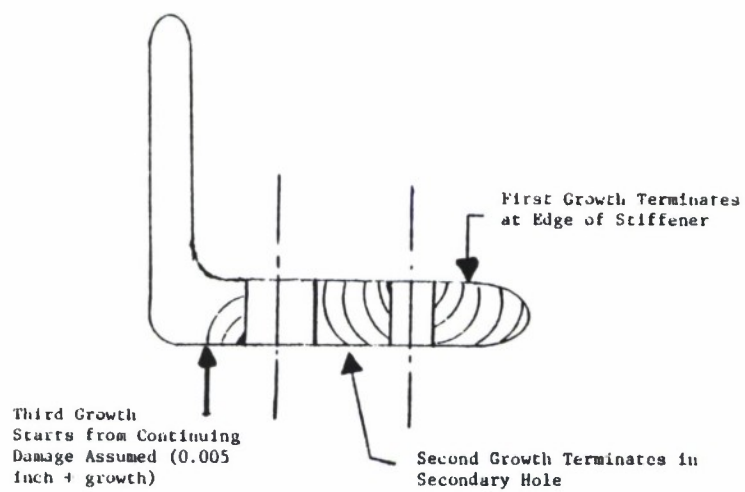
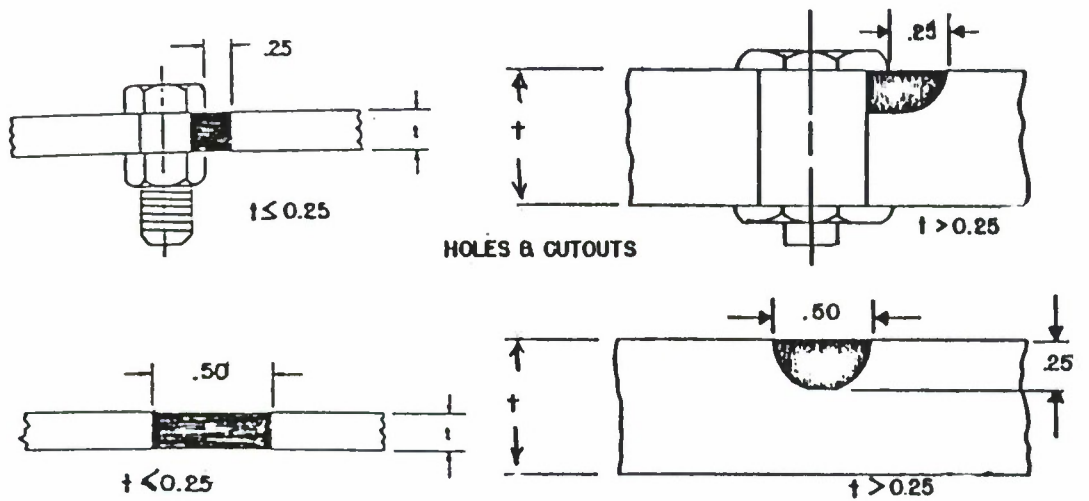
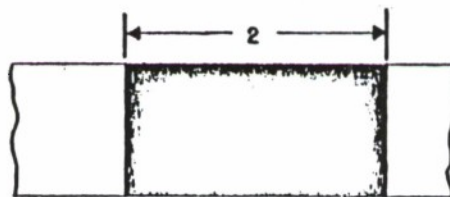


Figure 2.4.10 Continuing Crack Assumed at Opposite Side of Hole When Primary Crack Terminates at Hole.

CONDITION: PENETRANT, MAG. PART, ULTRASONIC, BUT NO PART REMOVED..... 3.1.2



CONDITION: VISUAL INSPECTION



ALL DIMENSIONS IN INCHES

Figure 2.4.11 Summary of Initial-Flaw Sizes for Structure Qualified as In-Service-Inspectable.

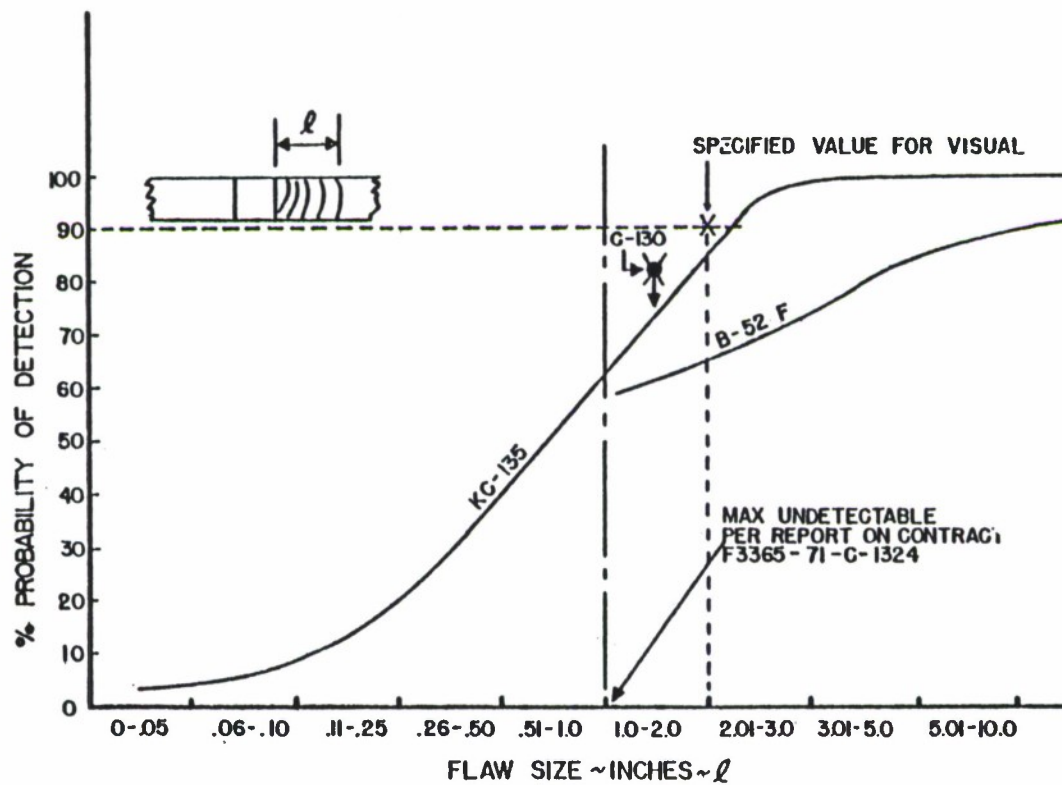


Figure 2.4.12 Development of Minimum NDI Detection for Visual Inspection.

2.5 RESIDUAL STRENGTH REQUIREMENTS

2.5.1 General

The residual strength capability is defined as the amount of static strength available at any time during the service exposure period considering that damage is initially present and grows as a function of service exposure time. Figure 2.5.1 indicates that strength degrades with increased damage size. The intent of MIL-A-83444 is to provide residual strength capability for intact structure of at-least design limit load at all times throughout the service life of the structure. The requirement to maintain limit load capability is considered necessary to allow unrestricted operational usage.

The residual strength requirements are specified in terms of the minimum internal member load P_{xx} which must be sustained.

The magnitude of P_{xx} depends upon the service exposure time of the structure between inspections and the overall capability of the inspection. The load P_{xx} is intended to represent the maximum load that the aircraft might encounter during the time interval between inspections. The required P_{xx} is at-least design limit load for all intact structure whether the structure is being qualified as Slow Crack Growth or Fail Safe. The required P_{xx} is also at least design limit load when the only planned safety inspections are at the depot (i.e., the depot or base-level inspection category).

The goal to allow unrestricted operational capability for all intact structures, has established that for all Slow Crack Growth Structure, the load P_{xx} be, at-least, limit load. This requirement is especially important for Slow Crack Growth non-inspectable structure.

In addition, all Fail Safe Structure must be designed to be at-least depot level inspectable and P_{xx} over this interval must be at-least limit load. This restriction is obvious since the only means to protect the safety is not to allow damage growth to degrade the strength of the structure to less than design limit load. Where partial failure is allowed and subsequent detection of failed load path is required, the limit load requirement on intact structure has two benefits. First, it is the only way that the operational force can be maintained with unrestricted capability; and second, when coupled with the intact structure damage growth requirements, it provides assurance that, under normal situations, early nuisance cracking will not occur as a result of lower stress. For Fail-Safe Multiple-Load-Path Structure, the levels of residual strength must be maintained for the structure at the time of and subsequent to load path failure (see Table 2.5.1, MIL-A-83444).

2.5.2 Residual Strength Requirement for Fail-Safe Structure at the Time of Load Path Failure, P_{yy} (Single Load Path Failure Load)

For Fail Safe Structure, there is the additional requirement that the remaining structure (at the time of a single load path

failure) must be capable of withstanding at least the load which causes the load path failure, plus an additional increment to account for the dynamic conditions of the breaking member (P_{yy}). While most data and analyses indicate that the dynamic magnification factor associated with the member failure is probably very small, the current specification requires that a 1.15 dynamic factor (D.F.) be applied to the amount of load distributed to the remaining structure as the result of a single load path failure. Figure 2.5.2 illustrates the change in residual strength requirements as a result of a load path failure. Note that the amount transferred from the broken member is P_{yy} .

Since the intact structure requirements for Fail Safe Structure demand that any individual load path be capable of withstanding $P_{LIMIT} \leq P_{xx} \leq 1.2 P_{LIFETIME}$, P_{yy} will always be equal to P_{xx} (Intact) times the dynamic factor. Although the specification states that P_{yy} is to be the greater of D.F. times P_{LIMIT} or D.F. times P_{xx} (Intact), the latter will always be the larger because the minimum intact structure residual strength must be at least design limit load.

2.5.3 Determining the Residual Strength Load, P_{xx} , for Fail Safe Structure Subsequent to Load Path Failure

The magnitude of the residual strength load required depends upon the exposure time in service (i.e., the longer the exposure time, the greater the probability of encountering a high load). Accordingly, the

value of required P_{xx} load increases with increase in the inspection interval or period of unrepaired service usage (allowable crack growth period). For the short service exposure times between inspections for the In-Flight Evident, Ground Evident and Walk Around Visual categories, the probability of encountering limit load conditions is low and thus the required P_{xx} may be significantly below design limit load. For the longer exposure times, this is not the case and, as stated previously, the minimum required P_{xx} for structure qualified under the non-inspectable or depot level inspectable categories must be at-least limit load.

The value of P_{xx} is established from load spectra data derived from a mission analysis of the particular aircraft considering average usage within each mission segment. Unless otherwise stated, MIL-A-008866B is the basic source of load factor data for the various classes of aircraft. Since safe operation depends upon the residual strength capability and since any individual aircraft may encounter loads in excess of the average expected during the particular exposure time, the P_{xx} load required is larger than the average derived value. One way to determine the level of P_{xx} required is to hypothetically increase the service exposure time for the aircraft between inspections by a factor M. This is the method used in MIL-A-83444. The values of M, as specified in Table I of MIL-A-83444, are summarized in Table 2.5.1. For example, under the depot level inspectability category, the P_{xx} load is the maximum value expected to occur in 20 times a typical inspection interval.

TABLE 2.5.1

Inspection Interval Magnification Factors

P_{XX}^*	Degree of Inspectability	Typical Inspection Interval	Magnification Factor, M
P_{FE}	In-Flight Evident	One Flight	100
P_{GE}	Ground Evident	One Flight	100
P_{WV}	Walk-Around Visual	Ten Flights	100
P_{SV}	Special Visual	One Year	50
P_{DM}	Depot or Base Level	1/4 Lifetime	20
P_{LT}	Non-Inspectable	One Lifetime	20

* P_{XX} = Maximum average internal member load that will occur once in M times the inspection interval. Where P_{DM} or P_{LT} is determined to be less than the design limit load, the design limit load shall be the required residual strength load level. P_{XX} need not be greater than 1.2 times the maximum load in one lifetime if greater than design limit load.

The basis for the specified M values is somewhat arbitrary although it is felt that the loads derived by this method are not unreasonably conservative. The basis for $M = 100$ is exceedance data for transport type aircraft where it has been observed that shifting exceedances by approximately two decades (i.e., $M = 100$) magnifies the value of load factor (or stress) by approximately 1.5 (Figure 2.5.3). It was recognized that for fighter data, exceedances approaching or exceeding design limit values are probable but that extrapolation of the basic exceedance curve very far beyond limit load factor (n_z) is often meaningless and unwarranted due to physical limitations of the vehicle and crew. Furthermore, in most cases actual service data is somewhat sparse for this region of the curve. Therefore, (1) an upper limit was required on P_{xx} for fighter aircraft and (2) the value of M should be less for longer inspection intervals in order that unreasonable factors would not be imposed should the actual derived P_{xx} be less than the specified upper limit. The values of M equal to 20 and 50 are arbitrary but probably not unreasonable (see Figure 2.5.3). Where the derived P_{xx} is larger than that associated with the design limit conditions, P_{xx} can be taken as 1.2 times the maximum load expected to occur in one design lifetime.

EXAMPLE 2.5.1 - Obtaining P_{xx} From Exceedance Data

The procedure for obtaining P_{xx} is illustrated using Figure 2.5.4. This figure presents the average exceedance data for one design lifetime. The point A represents the Max load expected in one lifetime; and is

shown to be larger than limit load (Point E). For the core of a non-inspectable structure, the twenty lifetime (M_x inspection interval) exceedance curve is obtained by shifting the exceedance curve from point A to point B and extrapolating to point C. The twenty lifetime exceedance curve, yields P_{xx} (derived) at C. The required load P_{xx} then is either the value derived at C or $1.2 \times$ (load at point A) i.e., the load at point D whichever is smaller. In this case, $P_{xx} = P_{LT}$ is the load at point C.

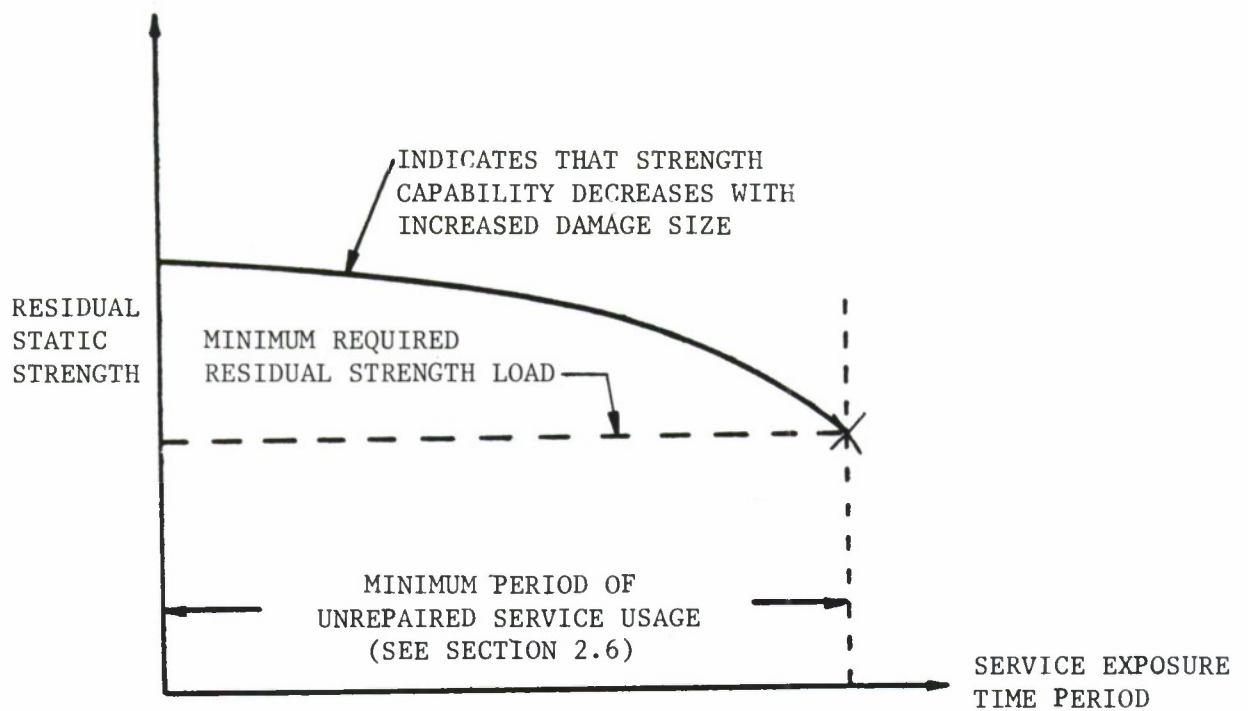


Figure 2.5.1. Residual Strength Diagram.

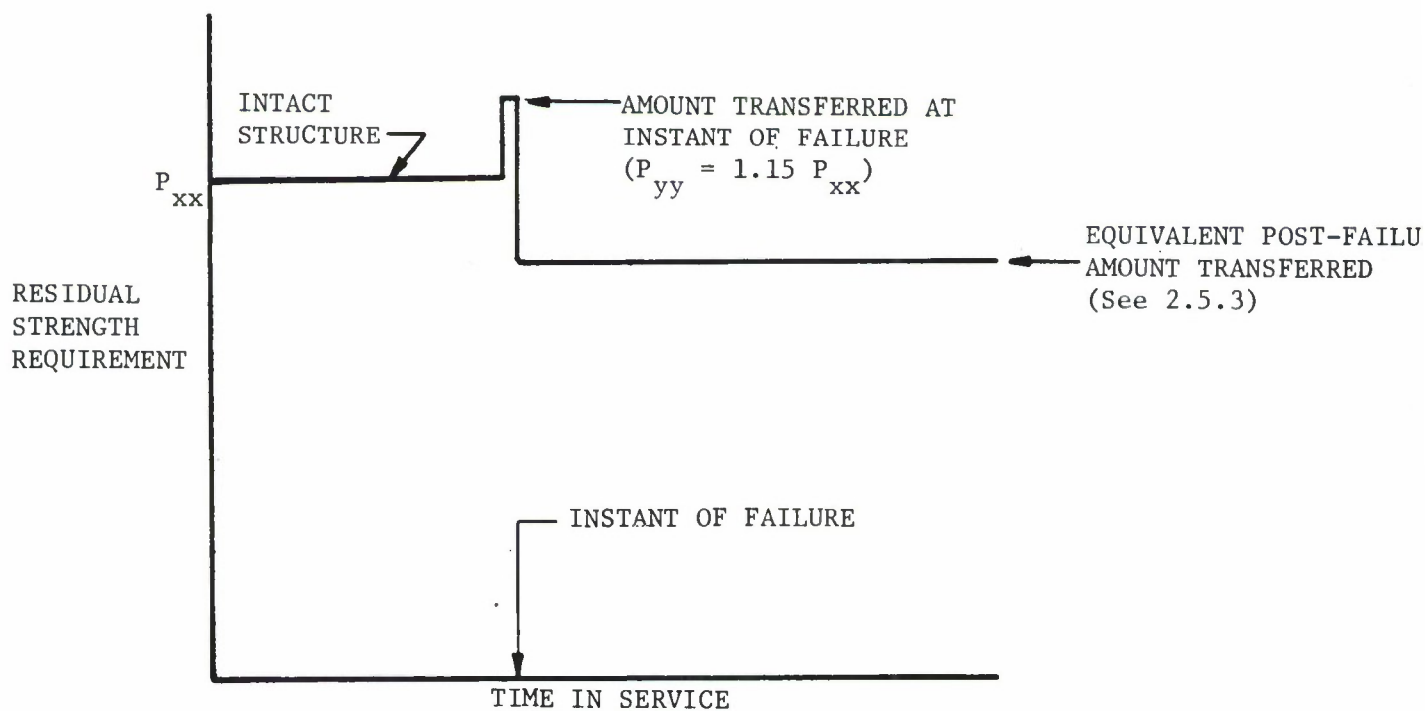


Figure 2.5.2. Schematic Residual Strength Requirements for a Structural Element Prior to Failure and for Transfer of Its Load to Remaining Structure at and Subsequent to Failure.

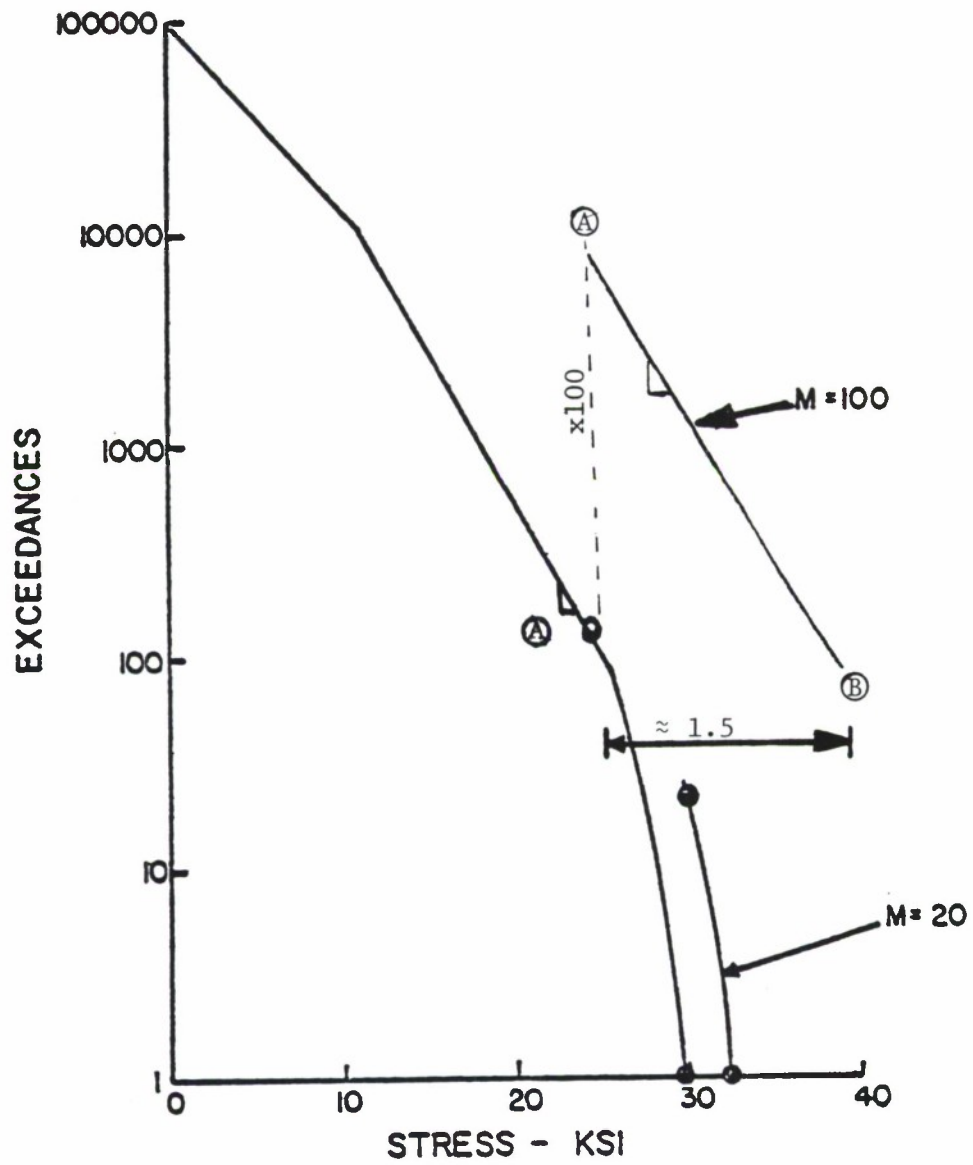


Figure 2.5.3. Illustration of Procedure to Derive M Factor to Apply To Exceedance Curve.

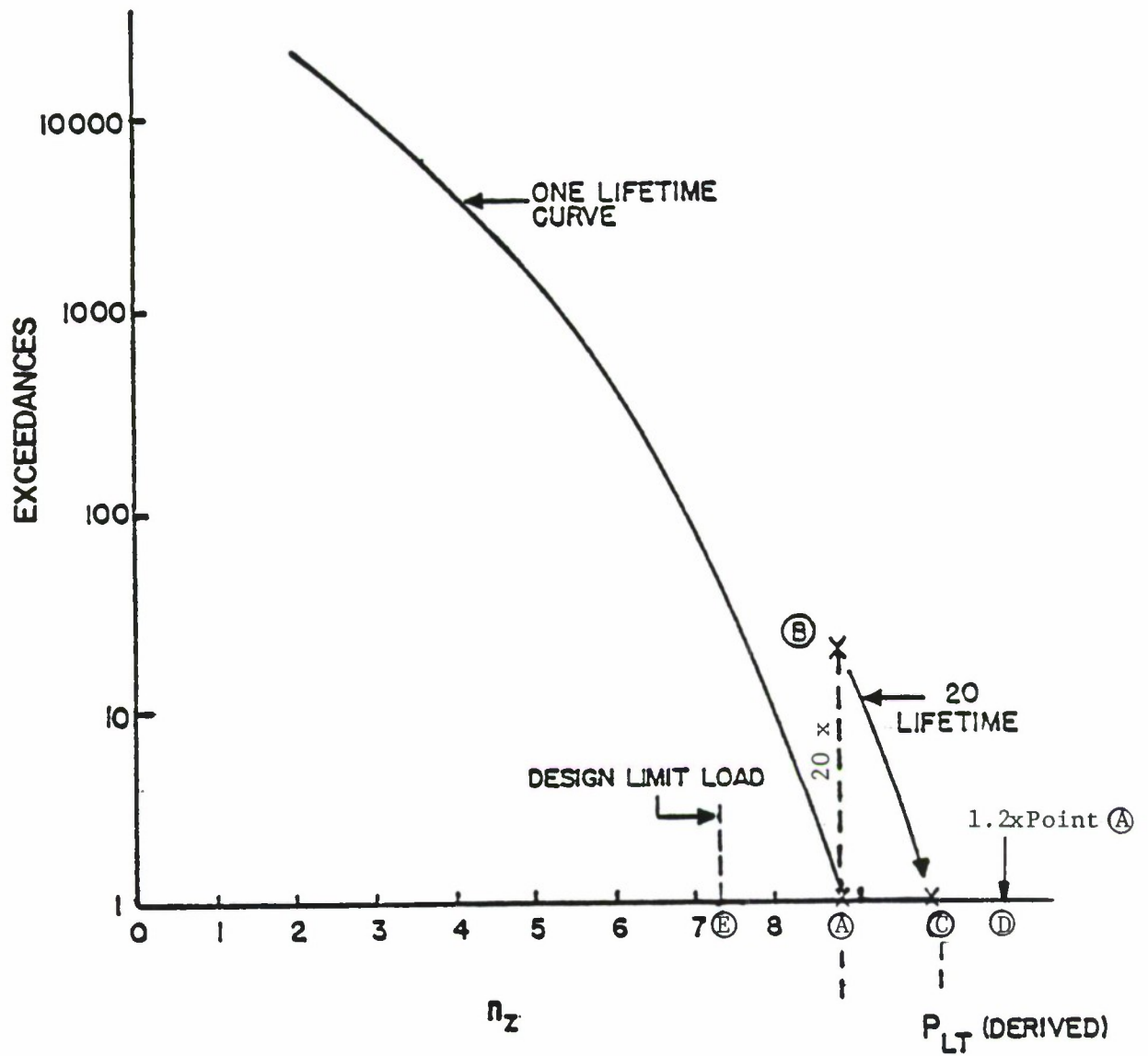


Figure 2.5.4. Example of the Derivation of P_{xx} from Exceedance Curve For Non-Inspectable Structure.

2.6 REQUIRED PERIODS OF SAFE DAMAGE GROWTH (PERIOD OF UNREPAIRED SERVICE USAGE)

The required periods of safe damage growth are specified in terms of either the design service lifetime or the scheduled inspection interval.

2.6.1 Slow Crack Growth, Non-Inspectable Structure

The required period is two times the design lifetime. A factor of two is applied to cover various uncertainties associated with crack growth during service usage that may not be adequately accounted for in analyses or laboratory test.

2.6.2 Slow Crack Growth, Depot Level Inspectable Structure

The required period is two times the depot level inspection interval. A factor of two is applied to allow for one missed inspection and still enable flaw detection and repair prior to failure.

2.6.3 Fail Safe Structure - Intact Requirements

The required period is either one design lifetime if a major load path must fail for damage to be found or one depot level inspection interval if damage can be found before a major load path fails. As previously mentioned, these requirements are not for safety, specifically, but have been imposed to help prevent adverse durability problems in multiple load path construction which could jeopardize unrestricted operational capability of the aircraft. A factor of one appears appropriate since safety is not involved and because separate

durability requirements (as contained in MIL-A-008866B) must be met by all structures.

2.6.4 Remaining Structure - Fail Safe Categories

The period (referred to as the "period of unrepaired service usage") depends upon the inspectability level.

For structure where the damage is classified as In Flight Evident inspectable, this period is the time required to return to base. For structure classified as Ground Evident inspectable, this period is a single flight. For these two cases, a factor of one is applied. This is justified on the basis that in order for the structure to be categorized in these inspectability levels, damage detection must be a certainty. For Walk Around Visual inspections, detection of failed load paths, arrested cracks and or large subcritical cracks is not a certainty during any single inspection. Accordingly, an arbitrary factor of 5 is applied to the inspection interval. For a Special Visual inspection, this factor is reduced to 2 because of the more detailed nature of such inspections and the resulting improved confidence in detection. The specified periods are contained in paragraph 3.2.2.2.2 of MIL-A-83444 and are repeated in Table 2.6.1.

TABLE 2.6.1

Required Periods of Safe Crack Growth -
Remaining Structure Fail Safe Categories

Degree of Inspectability	Minimum Period of Unrepaired Service Usage
In-Flight Evident	Return to base
Ground Evident	One Flight
Walk-Around Visual	5 x Inspection Interval - 5 x 10 Flights
Special Visual	2 x Inspection Interval - 2 x One Year
Depot or Base Level	2 x Inspection Interval - 2 x One Quarter Lifetimes

2.7 ILLUSTRATIVE EXAMPLE OF THE APPLICATION OF MIL-A-83444 TO FAIL SAFE STRUCTURE

2.7.1 Structural Design

The example will be based on the lower wing structure shown in Figure 2.7.1; the structure is comprised of multiple skin and stringer elements. The skin panels 1-5 are considered the major load paths. At each spanwise splice, a major splicing stringer is located and the construction is such that the load paths are independent, i.e., no common manufacturing tie exists between the skin panels.

2.7.2 Design Service Life - Assume the design service life is 40,000 hours.

2.7.3 Choice of Structural Design Concept

In this example, the structure will be assumed to be a Fail Safe Multiple Load Path Structure and the steps required to satisfy this requirement will be outlined. Later in Section 2.8, the same structure will be examined assuming that it is a Slow Crack Growth qualified design. The structure will be designed to be Fail Safe by virtue of being able to sustain the failure of one major load path or skin panel and still maintain the residual strength and remaining structural requirements. For illustration purposes, panel (2) was chosen to be the critical load path. Although the loss of panel (2) is critical from a remaining structure point of view, every panel must be designed to meet the intact requirements.

2.7.4 In-Service Inspection Considerations

Since the design is intended to satisfy the Fail Safe Multiple Load Path category, an in-service inspection plan is required. Assume that the lower surface will be periodically inspected in the field by a walk-around-visual-type examination, generally unaided. The frequency of these inspections is approximately every ten flights. In addition, the structure will undergo a depot level inspection at approximately 1/4 design lifetime intervals or every 10,000 hours. During manufacture, conventional inspection methods will be conducted and a fracture control program will be instituted.

2.7.5 Initial Flaw Considerations

Flaws assumed to result from manufacturing and/or material conditions are specified in 3.1.1.1 of MIL-A-83444 for Fail Safe Structure. The primary damage at a fastener hole (Figure 2.7.2) is an 0.020 inch corner flaw and since the drilling operation is common to the skin and splicing stringer, the 0.020 inch flaw must be assumed in both members. Panel ② is considered for this example because it was previously chosen to be the critical load path.* Note that only one primary damage site is assumed for each load path (e.g. along the path of expected damage, along a wing station). Also, it is not necessary to consider the interaction of

* The intact structure requirements must be checked for each major load path independently. Only panel ② is considered here.

flaws from adjacent primary sites. Each analysis of primary damage is conducted independently. At each hole other than the assumed primary site, an 0.005 inch radius corner flaw is assumed to represent average or typical manufacturing quality. The effect of interactions between the 0.005 inch flaws and the primary flaws must be considered when conducting the analysis.

2.7.6 In-Service Flaw Assumptions Following Inspection

The capability of inspection in the field is generally less than at the depot. The sizes of damage assumed to exist following inspection are specified in 3.1.2 of MIL-A-83444. For this example, assume that penetrant or ultrasonics will be used at the depot both exterior and interior to the lower surface. If this type of inspection is conducted, the damage likely to be found will be much smaller than the failed skin panel. From 3.1.2 (b) of MIL-A-83444 the minimum damage size to be assumed is a through crack of 0.25 inch uncovered length. The locations of the 0.25 inch length both in the skin and in the splicing stringer should be selected on the basis of inspectability but should be the location most critical to subsequent growth. Assume for purposes of illustration, that the damage is as indicated in Figure 2.7.3. The 0.005 inch flaw away from the primary damage site represents the initial manufacturing type damage as specified in Para. 3.1.1 of MIL-A-83444.

2.7.7 Remaining Structure Damage Following the Failure of the Major Load Path

Figure 2.7.4 illustrates the condition of the structure following the complete failure of the primary load path (skin panel (2)) represented by the cross hatched area. The condition of the remaining structure is as specified in 3.1.1.3.1 (b) of MIL-A-83444 since this is an example of independent structure. Each fastener hole in the structure is assumed to contain the 0.005 inch typical manufacturing hole quality flaw. The Δa_2 increment is the growth of these typical flaws from the time of manufacture until the point at which the load path is assumed to have failed. The increment Δa_2 will be discussed later.

2.7.8 Analysis of Intact Structure - Residual Strength Requirements and Damage Growth Limits (3.2.2.2.1)

The specific set of requirements for intact structure depends upon the capability of the depot level inspection. Since this example has assumed the situation where the normal inspection can detect less than a failed load path, this case will be examined first.

The intact requirement is that the in-service damage, assumed to be present following the depot level inspection (Figure 2.7.3), shall not grow and cause failure of the major load path (panel (2)) before the next opportunity to discover the damage, i.e., the next inspection.

Since this is merely a one-time design requirement, not specifically intended for safety, it is not necessary to account for prior service

at the time at which the requirement is imposed. Thus, the structure is considered as "new" and no incremental growth Δa due to prior service is computed. Figure 2.7.5 illustrates schematically the residual strength and growth requirements that must be met for the intact structure.

2.7.9 Analysis of Intact Structure (Alternate Requirement)

If it were determined that the depot level inspection was incapable of finding damage less than a failed load path, then the requirement for intact structure is:

Initial manufacturing damage (3.1.1.1 b) shall not grow to the size required to cause load path failure due to the application of P_{LT} in one design lifetime. The initial damage assumption for this case is illustrated in Figure 2.7.2. The schematic of the growth and residual strength requirements are illustrated in Figure 2.7.6.

2.7.10 Discussion of Intact Structure Analysis

Although the structure in the example was assumed to be depot level inspectable for less than a failed load path, the intact structure requirement associated with this set of conditions might have been more difficult to meet than would be the case if the structure were not inspectable for less than a failed load path. In the latter case, it would be satisfactory for the designer to qualified this structure under the alternate requirement described in Section 2.7.9. As is often the case, the designer may choose to qualify the structure in the easiest (analysis) manner.

2.7.11 Analysis of Remaining Structure Subsequent to Load Path Failure

The fail safe characteristics of this structure, i.e., the ability to fail panel (2) and fly safely until the failed panel is detected, depends upon the residual strength capability at the time of and subsequent to load path failure and the capability of and frequency of in-service inspections. The remaining structure requirements are specified in 3.2.2.2.2 of MIL-A-83444. As stated earlier, the fail safety will be supported by walk-around-visual inspections for damage sizes on the order of a failed load path. Generally, the walk-around-visual inspection can be aided by detectable signs such as fuel leakage. At any rate, the minimum inspection capability for this example will be considered to be a failed load path.

Thus, the damage as illustrated in Figure 2.7.4 shall not grow to a size such as to cause loss of the wing due to the application of P_{WV} in 5 times the inspection interval (10 flights), i.e. in 50 flights. This is illustrated in Figure 2.7.7. The load $P_{xx} = P_{WV}$ will generally be less than the design limit condition and P_{yy} (as discussed in Section 2.5) will always be equal to or greater than that associated with the design limit condition.

2.7.12 Derivation of Residual Strength Load P_{yy}

In the analysis of the intact structure, the critical damage limit was failure of the skin panel (2). The mode of failure was slow

growth of either depot level inspection type damage or initial manufacturing damage (Figure 2.7.5 and 2.7.6, respectively). In each case, the damage is assumed to grow in a stable manner until the critical damage size in the skin panel is reached. The critical damage size for this case would be that size at $P_{xx} = P_{DM}$ or $P_{xx} = P_{LT}$ where P_{xx} is bounded by

$$P_{LIMIT} \leq P_{xx} \leq 1.2 P_{ONE LIFETIME}$$

For a balanced fail safe design, the remaining structure must be capable of withstanding the effects of the major load path failing, including the redistribution of load to adjacent members at the time of load path failure. This is the basis for the requirement that the remaining structure must support the P_{yy} residual strength load. The load P_{yy} is dependent upon the design allowable for the first panel (Panel ② in this case). Assume for example that the P_{xx} allowable for first panel failure is exactly P_{LIMIT} . The remaining structure must be capable of supporting P_{LIMIT} , with adjacent panels carrying the increment or that portion originally carried in panel ② at P_{LIMIT} . This is illustrated in Figure 2.7.8 where the amount of load in panel ② at the limit design condition, i.e. P_2 is redistributed after it is multiplied by 1.15 to account for dynamic effects ($\Delta P_1 + \Delta P_3 + \Delta P_4 + \Delta P_5$). The total redistributed increment then is

$$1.15 P_2 = (\Delta P_1 + \Delta P_3 + \Delta P_4 + \Delta P_5)$$

The residual strength capability of the remaining structure is then checked against this condition; the P_{yy} requirement for panel ③ is

$$P_{yy}^3 = P_{yy}^3 + \Delta P_3.$$

2.7.13 Incremental Damage Growth Δa

The remaining structure analysis of damage growth and residual strength considers damage in the adjacent structure at the time of load path failure which has grown an amount Δa from the time of manufacture (Figure 2.7.6). Since the structure must meet the single design lifetime requirement, it becomes necessary to establish at what point during the lifetime the failure of the load path is assumed to take place so that the proper amount of growth Δa can be computed to represent growth during this time segment. Figure 2.7.9 illustrates the growth of the 0.005 inch manufacturing type damage from time zero for one design lifetime. In this example, the walk-around-visual inspection is used to detect the failure of the major load path and the inspection interval is 10 flights. MIL-A-83444 requires a factor of 5 on this interval and thus the damage growth life requirement is 50 flights. Therefore, the maximum amount of Δa and the condition to be met would be growth for one design lifetime minus 50 flights. For any other in-service inspection interval the amount Δa would be computed in a similar manner. For example, if the walk-around-visual inspection was not conducted and fail safety was dependent upon discovery of damage at the scheduled 10,000 hour depot level inspection, then the increment

of growth Δa_2 would be one design lifetime minus 2X (10,000 hrs.) as in Figure 2.7.10.

2.7.14 Alternative-Analysis of Remaining Structure Subsequent to Load Path Failure

As indicated in 2.7.13, the designer may choose to depend upon the depot level inspection instead of the walk-around visual. This would be a satisfactory alternative and for this situation the assumption would be made that the major load path failed between depot level inspections and that the aircraft would be designed to operate safely with the failed load path until the next depot inspection. Figure 2.7.11 illustrates this case.

2.7.15 Summary and Comments

This example has illustrated the steps required to qualify the structure under the category of Fail Safe Multiple Load Path Structure. For this category, an intact structure requirement (prior to load path failure), a residual strength requirement at the time of load path failure, and a remaining structure damage growth and residual strength requirement had to be met. The requirement to qualify the structure generally requires a complex set of analyses, and in the early design stage may be impractical. The design could be made to satisfy Slow Crack Growth Structure requirements, either non-inspectable or depot level inspectable, while still maintaining some level of fail safety (but not necessarily meeting the requirements specifically). This approach would generally be satisfactory and usually requires a lesser amount of analysis, particularly for computing residual strength and the growth increment. (See Section 2.8 for an example based on Slow Crack Growth Structure).

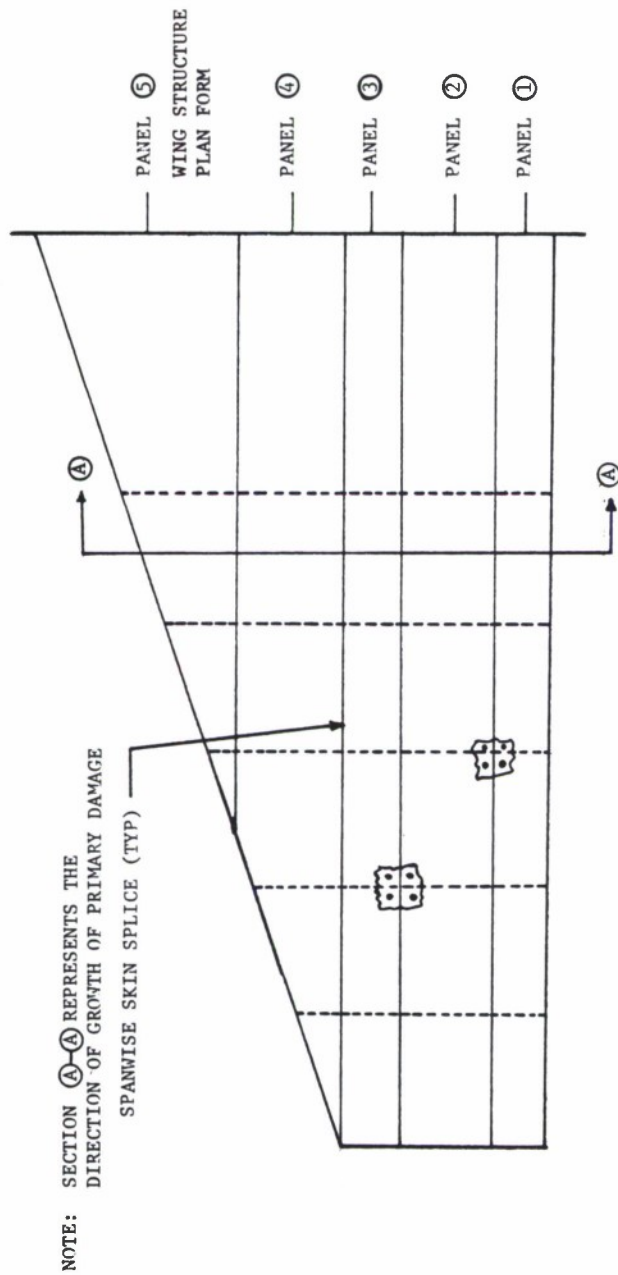


Figure 2.7.1. Structural Example - Lower Wing Skin.

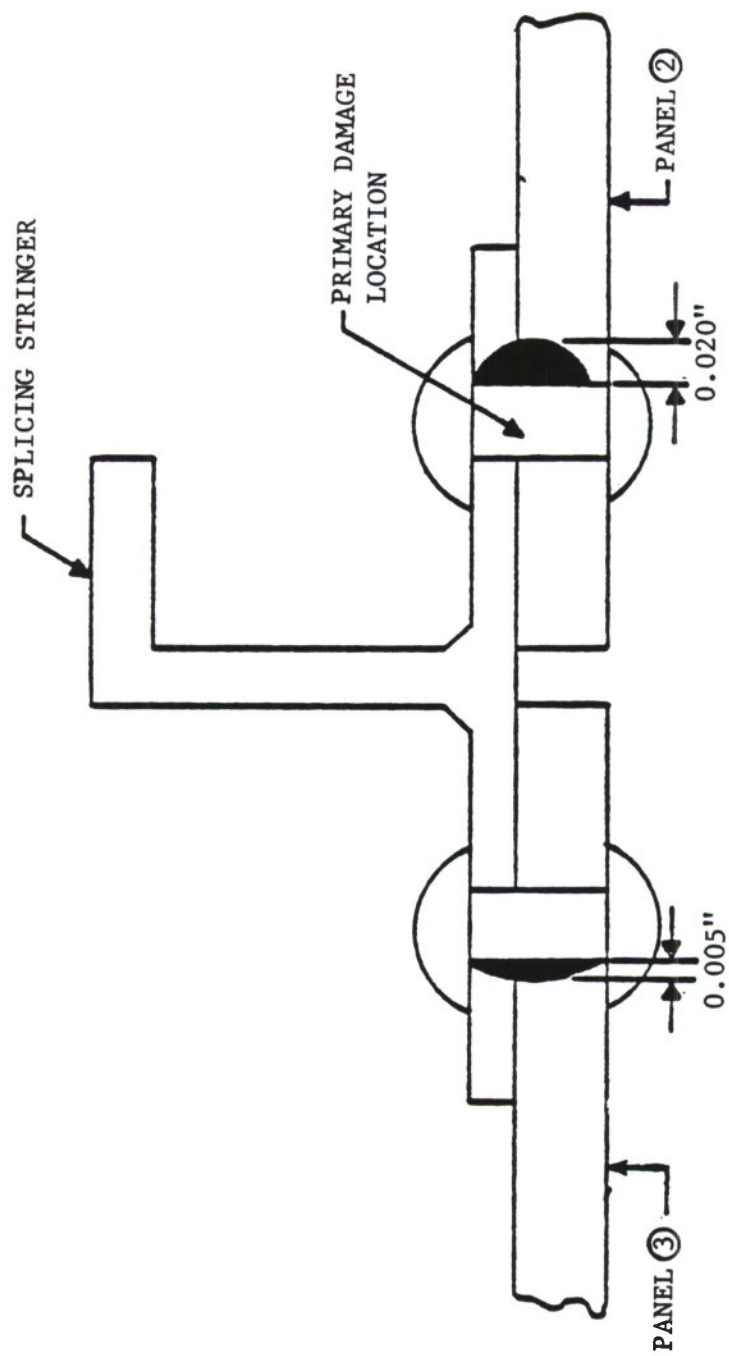
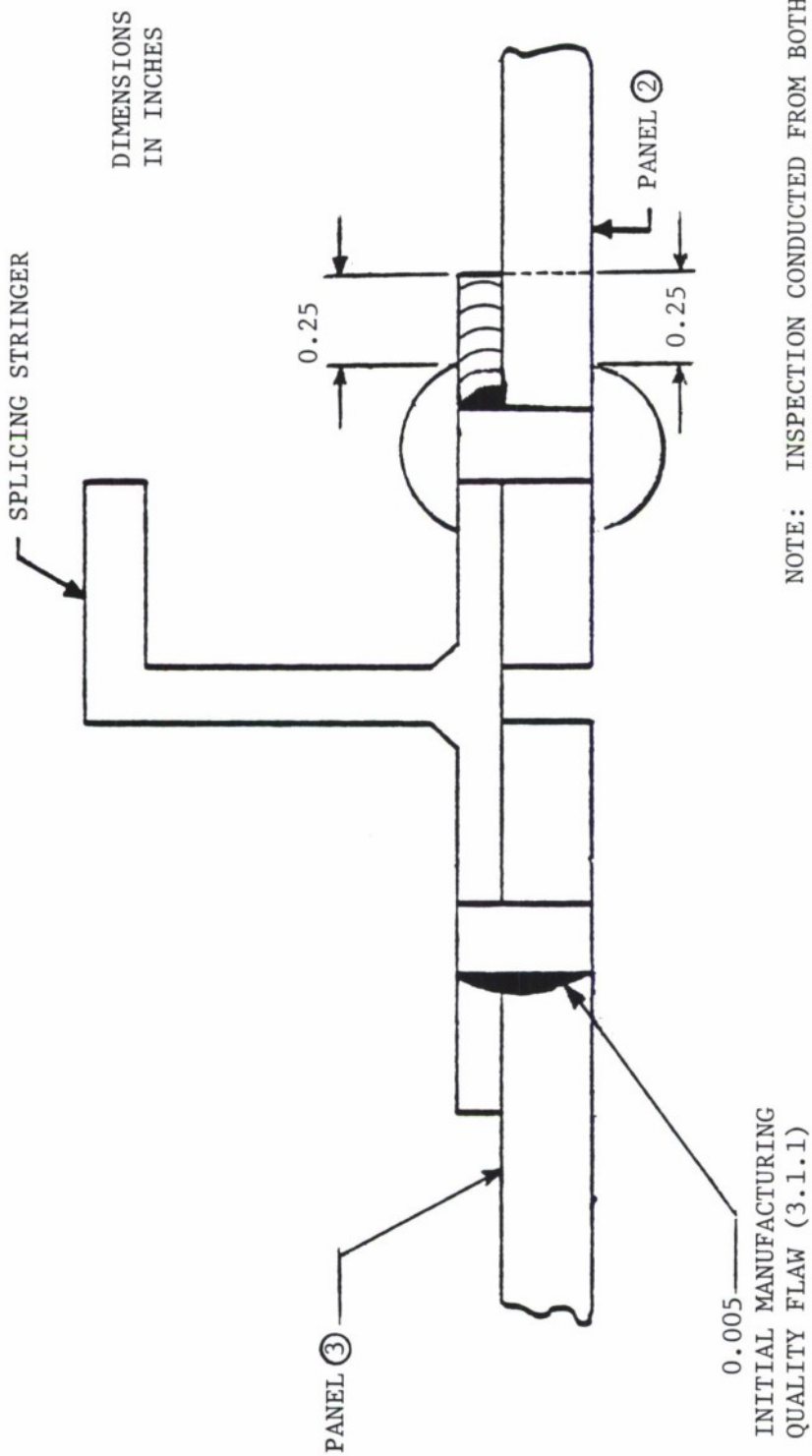


Figure 2.7.2. Initial-Flaw Assumptions for Example Case Qualified as Fail Safe.



NOTE: INSPECTION CONDUCTED FROM BOTH SIDES. NOTE THAT AFTER THE INSPECTION CRACKS ARE PLACED IN THE MOST UNFAVORABLE LOCATIONS.

Figure 2.7.3. Illustration of Primary Damage Following a Depot-Level Penetrant or Ultrasonic Inspection.

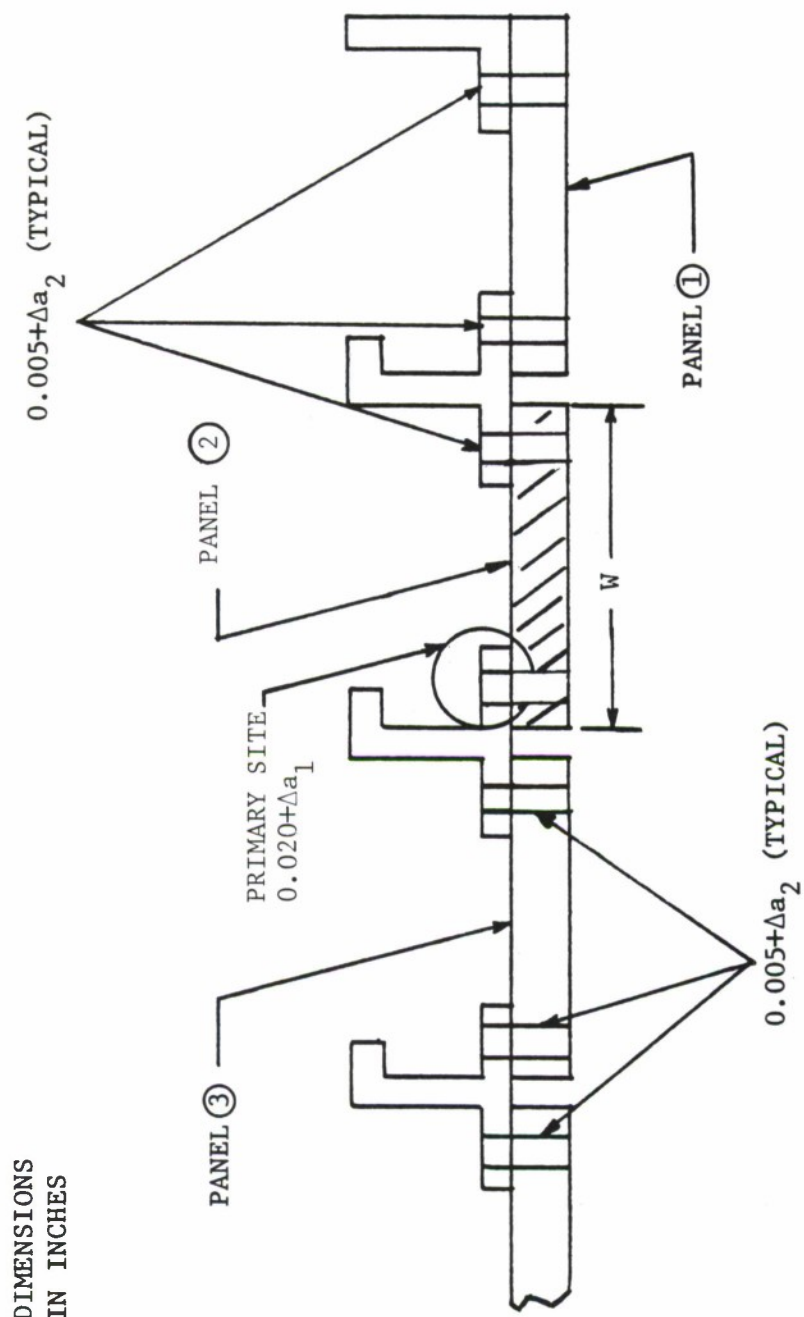


Figure 2.7.4. Illustration of Primary Damage Assumptions Following the Failure of Major Load Path (Panel 2).

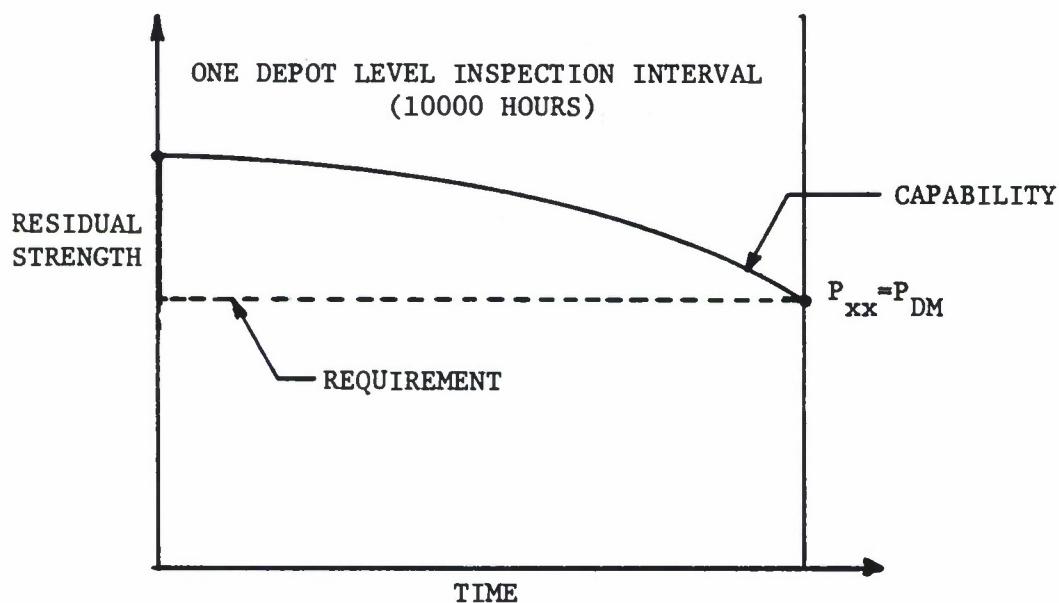
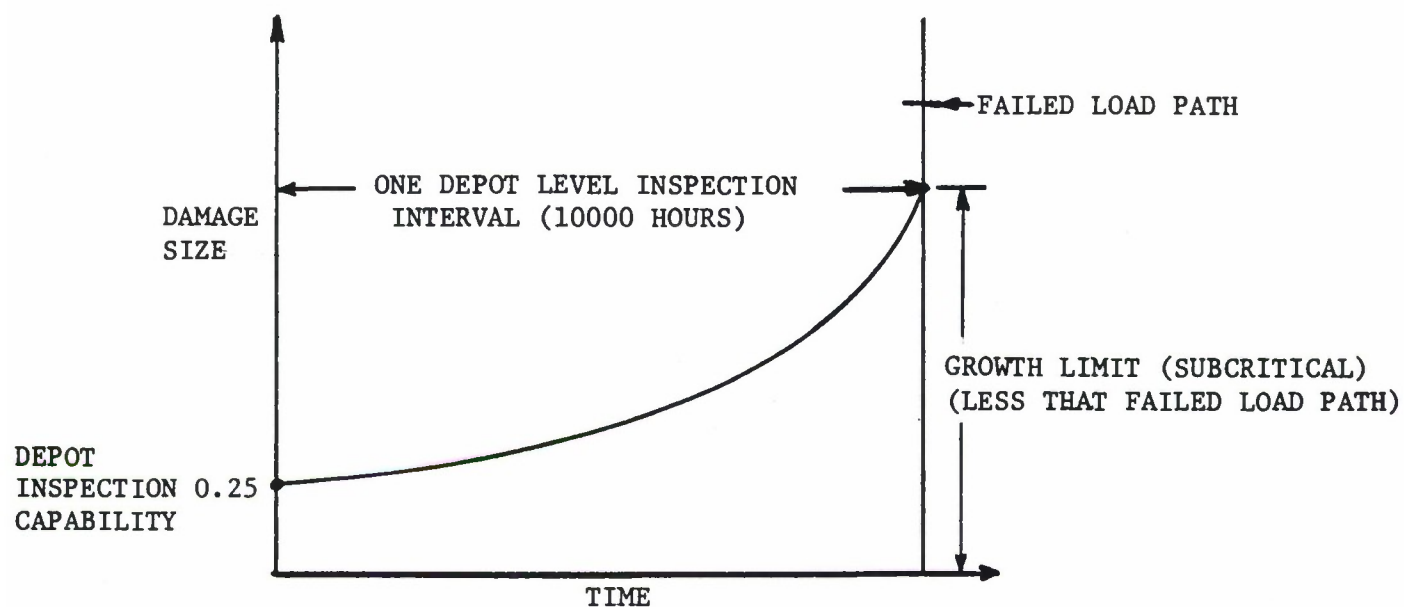


Figure 2.7.5. Illustration of Damage-Growth Limits and Residual-Strength; Intact Structure Following Depot or Base-Level Inspection for Less-Than-Failed Load Path.

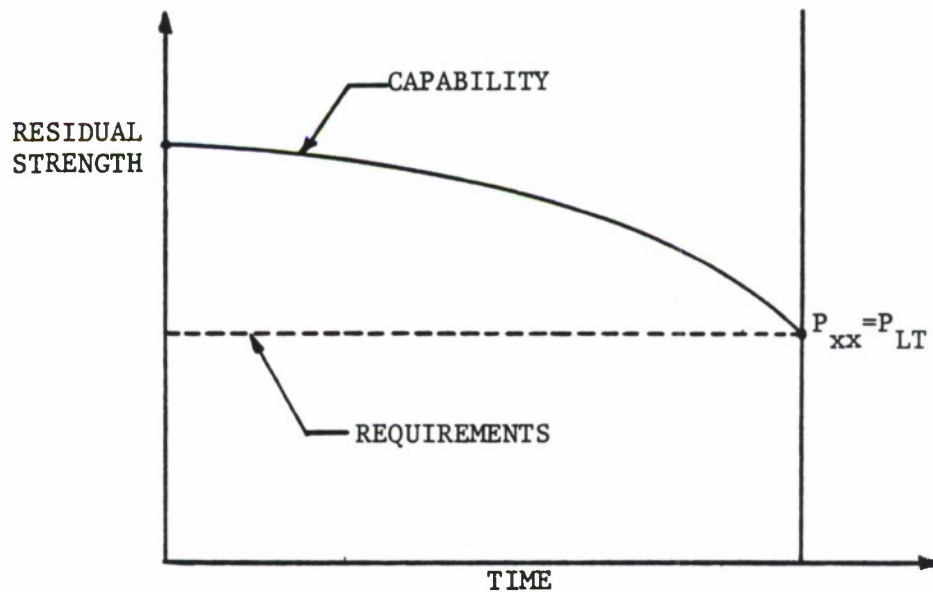
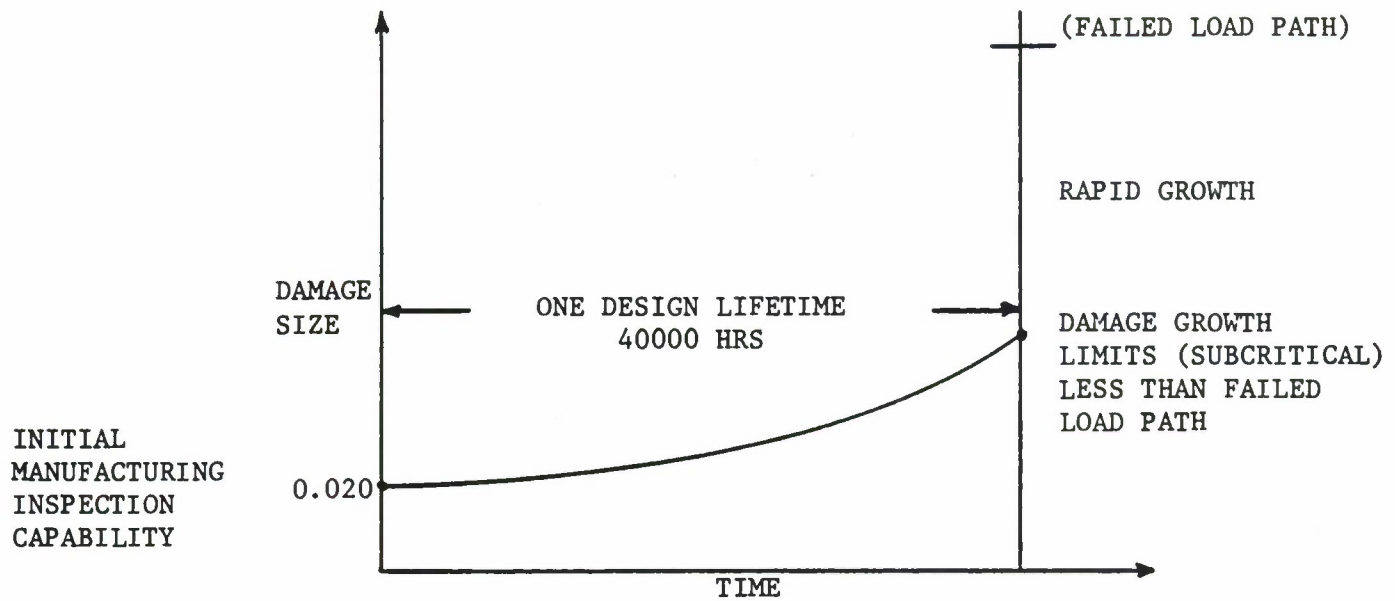


Figure 2.7.6. Illustration of Damage-Growth Limits and Residual Strength; Intact Structure for When Depot Inspection Cannot Detect Less-Than-Failed Load Path.

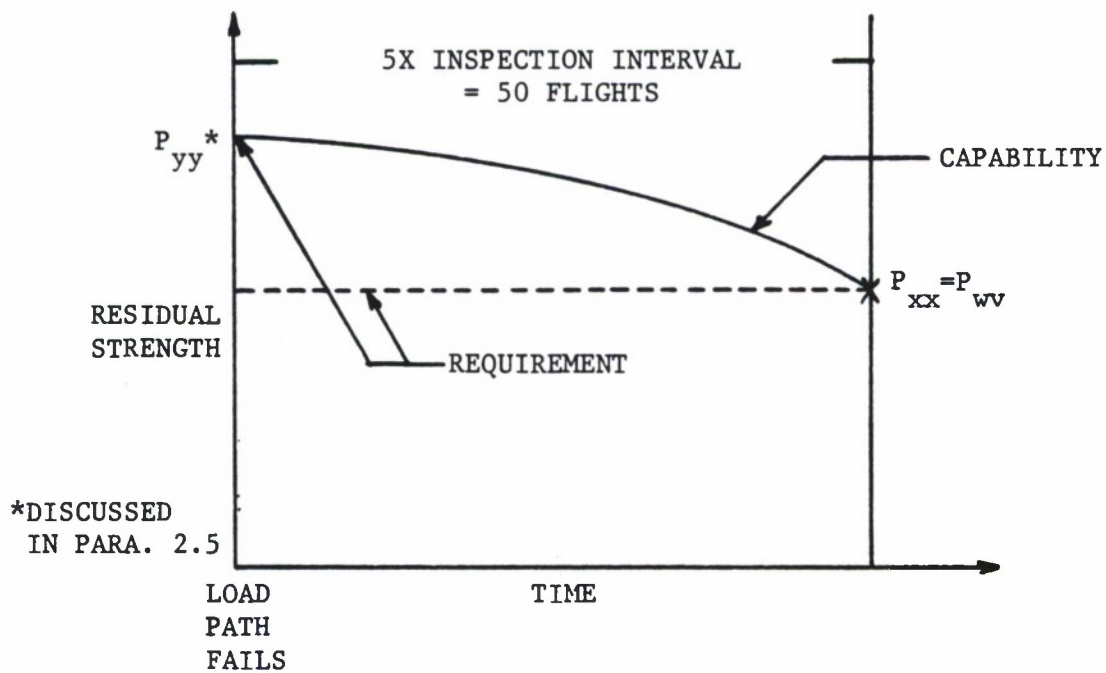
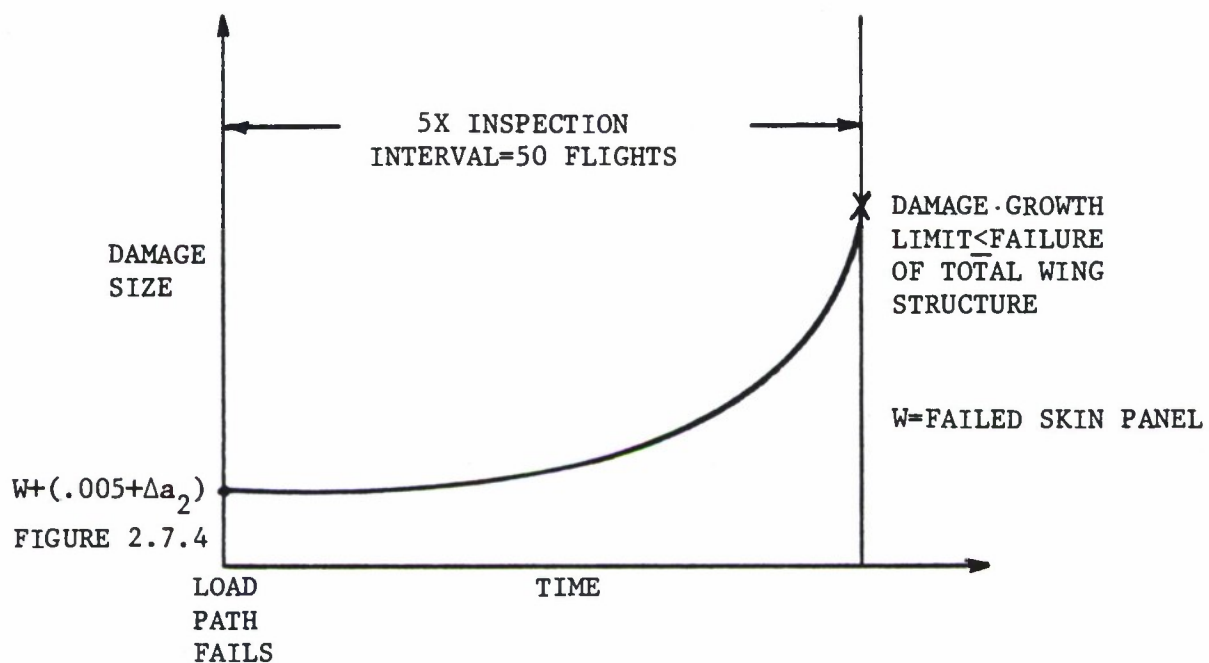


Figure 2.7.7. Illustration of Damage-Growth Limits and Strength Requirements; Remaining Structure Subsequent to Load-Path Failure.

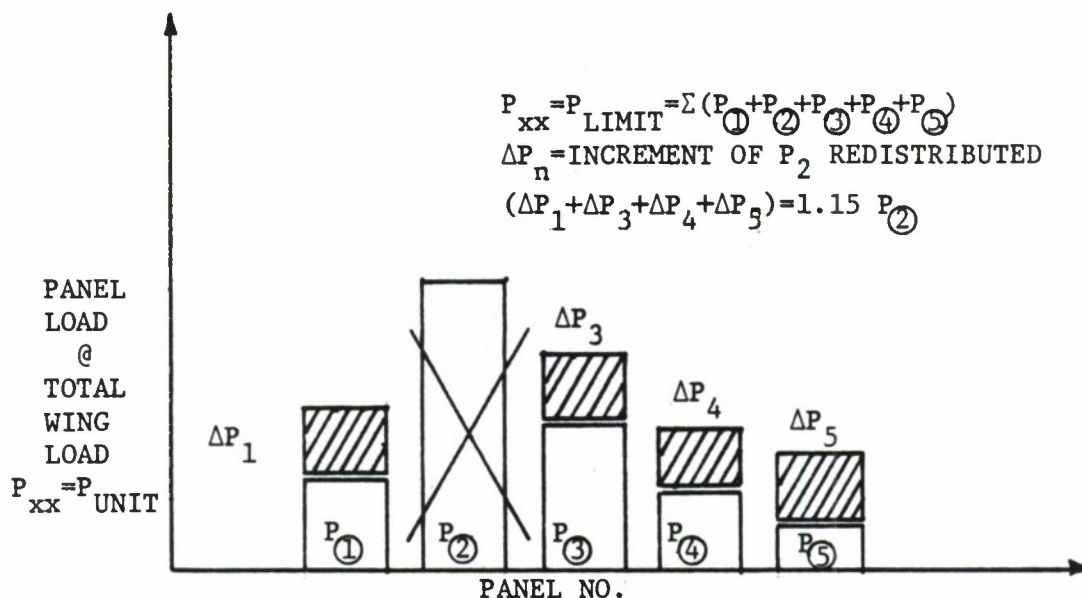


Figure 2.7.8. Illustration of Redistributed Panel Load P_2 to Adjacent Structure.

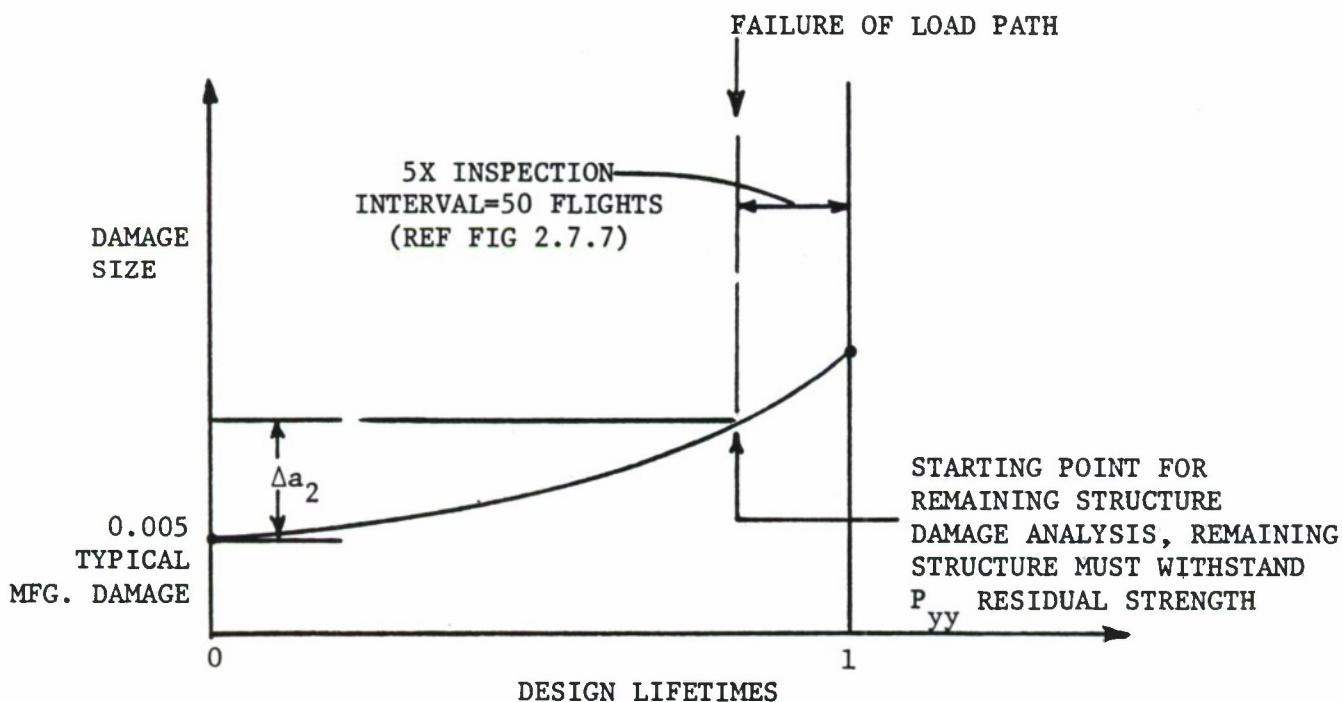


Figure 2.7.9. Development of Increment of Growth Δa_2 Used in the Analysis of Damage Growth - Remaining Structure Damage - Walk-Around-Visual Inspectable. Worst Case Analysis.

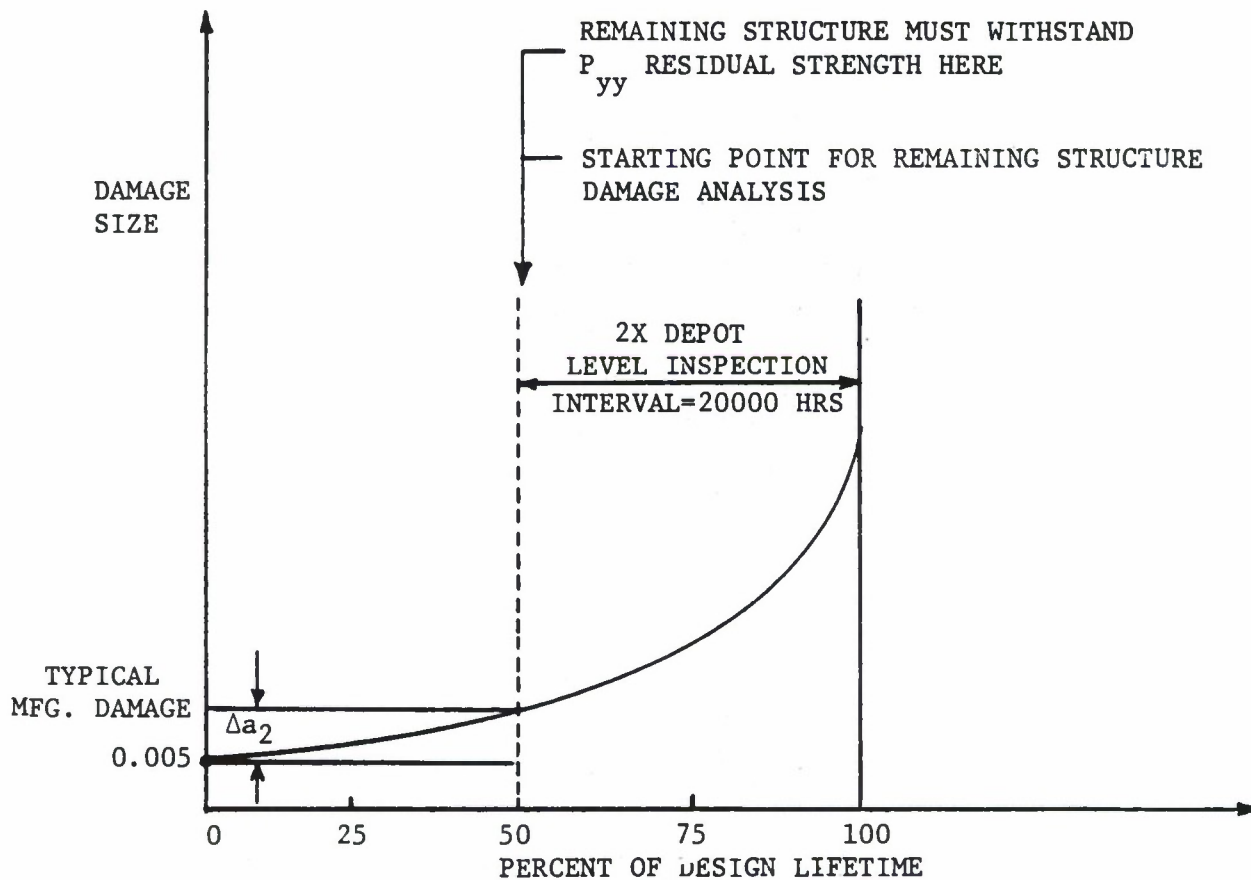
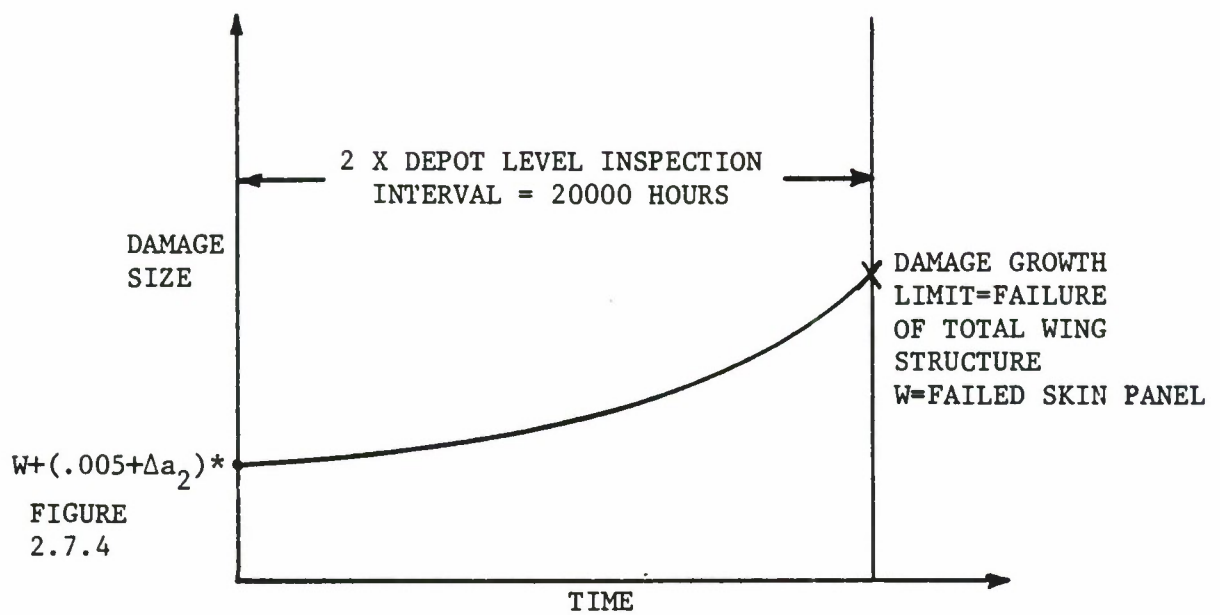


Figure 2.7.10. Development of Increment of Growth Δa_2 Used in Analysis of Damage Growth - Remaining Structure Damage - Depot-Level-Inspectable.



*NOTE: Δa_2 COMPUTED FROM TIME ZERO. SEE FIGURE 2.7.10.

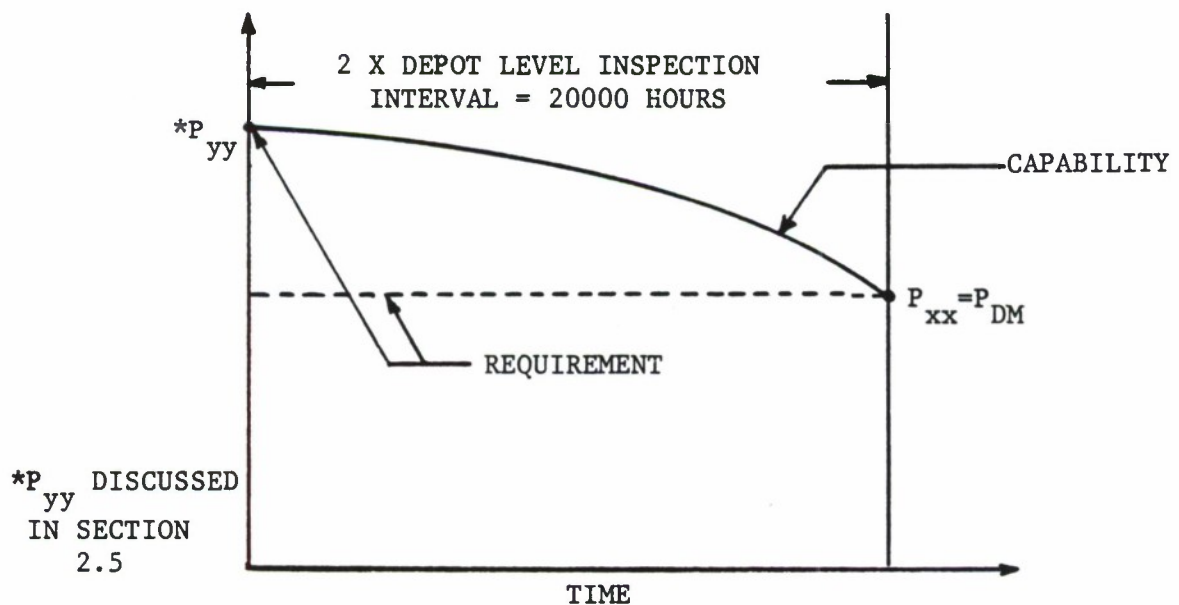


Figure 2.7.11. Illustration of Damage Growth and Residual-Strength Requirements - Remaining Structure - Depot Level - Inspectable.

2.8 ILLUSTRATIVE EXAMPLE OF APPLICATION OF MIL-A-83444 TO SLOW CRACK GROWTH STRUCTURE

2.8.1 Structural Design

This example is based on the lower wing structure shown in Figure 2.7.1 and described in paragraphs 2.7.1 and 2.7.2. The choice of structural design concept here will be Slow Crack Growth Structure and the steps required to satisfy this requirement will be outlined. Again for illustration purposes, panel ② is chosen to be the critical load path.

2.8.2 Initial Flaw Sizes Assumed to Result from Manufacturing

Flaws assumed are specified in 3.1.1.1 of MIL-A-83444 for the slow crack growth type structure. Thus, an 0.050 inch corner flaw is assumed to exist at the critical fastener hole joining panel ② and splicing stringer as shown in Figure 2.8.1. Because it was assumed that a common drilling operation was employed to prepare the hole with the primary damage, the same size crack is assumed in both elements. Also per 3.1.1 of MIL-A-83444, initial flaws equivalent (in stress-intensity factor level) to an 0.005 inch radius corner flaw shall be assumed to exist in each hole of each element in the structure such as shown in Figure 2.8.1.

2.8.3 Choice of Inspection Category

There are only two inspection categories which are available to the designer for Slow Crack Growth Structure: in-service non-inspectable and depot level inspectable. The choice of inspection category directly impacts the requirements for residual strength and for damage growth limits. For purposes of discussion, both categories are presented.

2.8.4 Choice of the In-Service Non-Inspectable Category

For this example case, no special in-service and no depot level inspections will be specifically required to protect the integrity of the lower wing structure shown in Figure 2.7.1. The implication is that no inspections are desired; however, there are cases in which the flaw size at failure is so small that such a flaw size might easily be overlooked during an inspection. Thus, the in-service non-inspectable category covers those cases where inspections are neither desirable nor practical.

2.8.4.1 Residual Strength Load, P_{xx}

The required level of residual strength for non-inspectable structure is P_{LT} , the maximum load that could occur in one lifetime. This is defined by Table I of MIL-A-83444 (Refer to Table 2.5.1). Example 2.5.1 describes the method for establishing this particular load level.

2.8.4.2 Analysis Requirements

The slow crack growth and residual strength requirements for this category are illustrated in Figure 2.8.2. Figure 2.8.2 specifically shows that the initial manufacturing damage is restricted from growing to critical size and causing failure of the structure due to the application of P_{LT} in two (2) design service lifetimes. Note that the damage limit is the ultimate failure of the wing. Engineering judgement may dictate that a more reasonable limit and, perhaps, an easier situation to adhere to would be to establish the limit at some intermediate point such as the failure of one primary load path such as panel (2). This might be accomplished in design at very little expense to overall weight.

2.8.5 Choice of Depot Level Inspectable Category

For this example case, the damage which can be presumed to exist in the structure after completion of a depot or base level inspection shall be that specified in 3.1.2 of MIL-A-83444. A description of this type of damage can be found in paragraph 2.7.6 and in Figure 2.7.3.

2.8.5.1 Residual Strength Load, P_{xx}

The required level of residual strength for the depot or base level inspection category is P_{DM} , the maximum load that would occur in the planned 1/4 lifetime or 10,000 hour inspection interval. This level is defined by Table I of MIL-A-83444 (Refer to Table 2.5.1). The method for establishing this particular load level follows that outlined

in Example 2.5.1 where the one life time exceedance curve is multiplied by a factor of 5 rather than 20.

2.8.5.2 Analysis Requirements

The slow crack growth and residual strength requirements for this category established by 3.2.1.1 of MIL-A-83444 are illustrated in Figure 2.8.3. Figure 2.8.3 specifically shows that the post-inspection damage is restricted from growing a crack to critical size and thereby causing failure of the structure due to the application of P_{DM} in two times the inspection interval (1/2 lifetime, 20,000 flight hours).

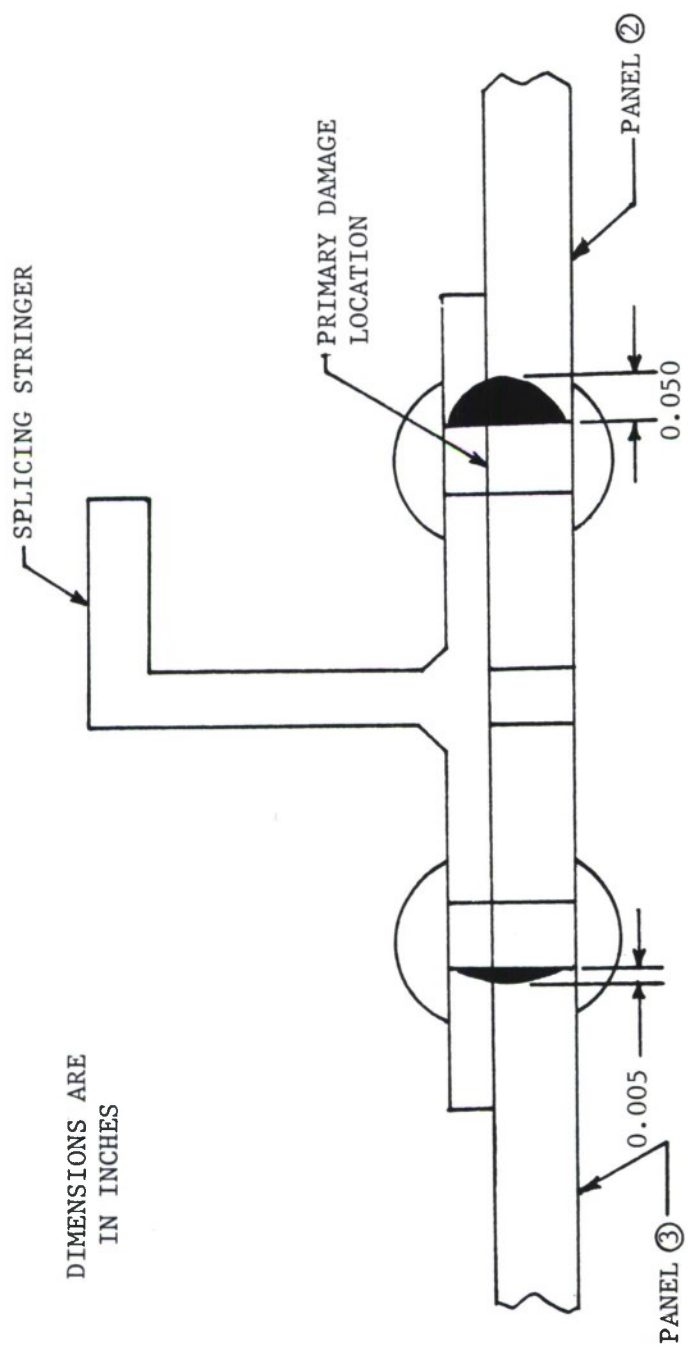


Figure 2.8.1. Illustration of Initial Flaws for Structure Qualified as Fail-Safe Multiple Load Path.

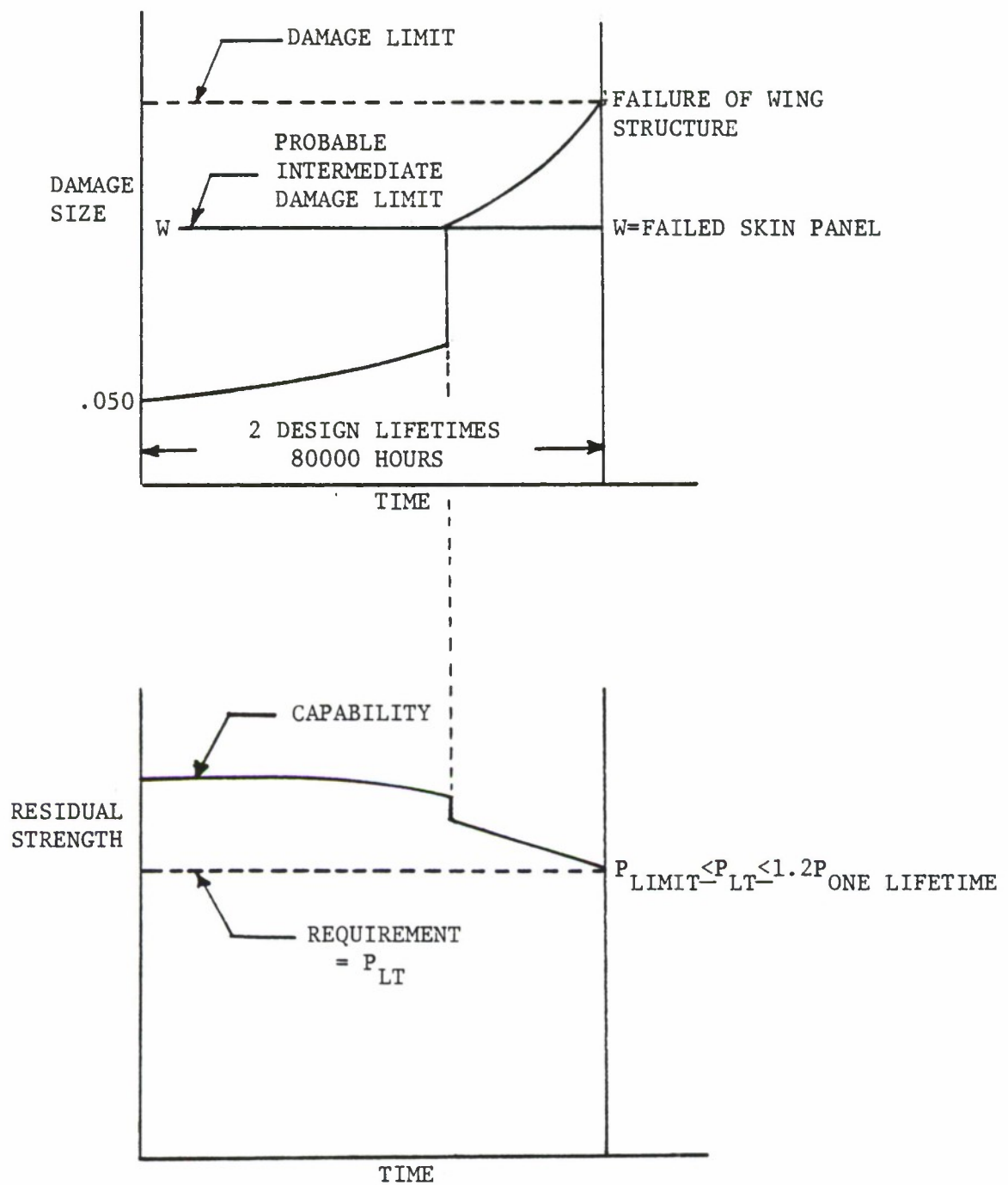


Figure 2.8.2. Illustration of Damage-Growth and Residual-Strength Requirements for Example Problem Qualified as Slow Crack Growth Noninspectable.

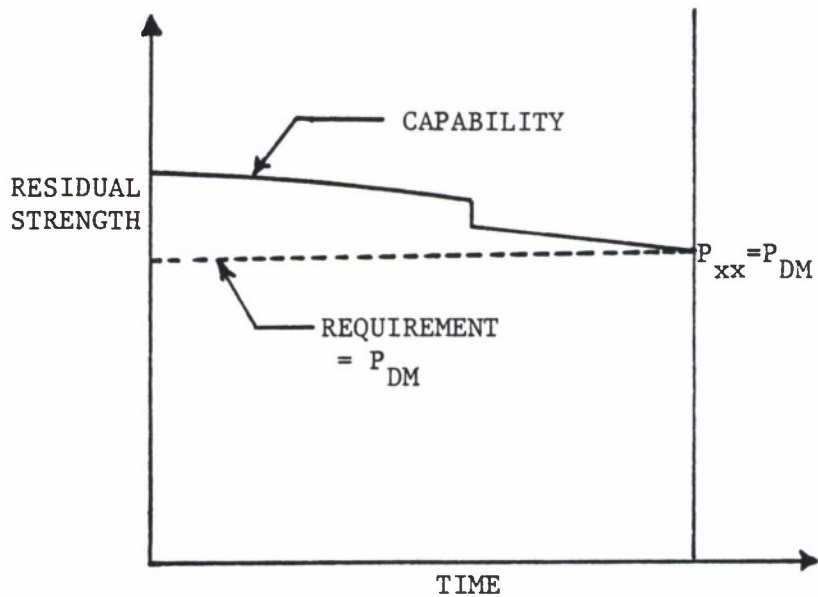
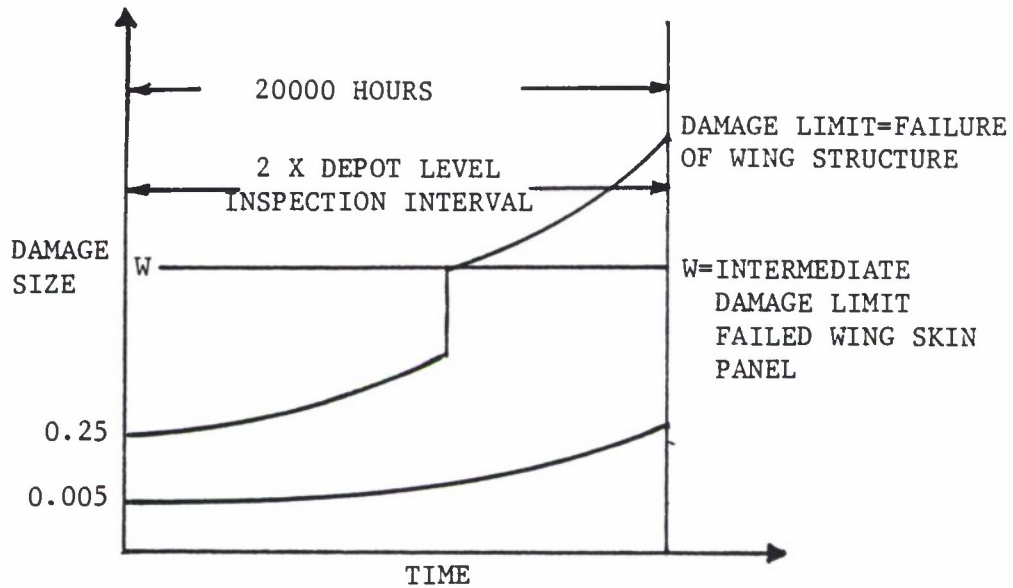


Figure 2.8.3. Illustration of Damage-Growth and Residual Strength Requirements for Example Problem Qualified as Depot-Level-Inspectable.

3.0 DAMAGE SIZE CHARACTERIZATIONS

<u>SECTION</u>		<u>PAGE</u>
3.1	INTRODUCTION	3.1.1
3.2	NDI DEMONSTRATION OF CRACK DETECTION CAPABILITY	3.2.1
3.2.1	<u>NDI Methods</u>	
3.2.1.1	Liquid Penetrant Inspection	3.2.1
3.2.1.2	Ultrasonic Inspection	3.2.2
3.2.1.3	Eddy Current Inspections	3.2.4
3.2.1.4	Magnetic Particle Inspection	3.2.5
3.2.1.5	Radiographic Inspection	3.2.6
3.2.2	<u>NDI Capability Evaluation</u>	3.2.8
3.2.2.1	Design of NDI Capability Experiments	3.2.11
3.2.2.2	Analysis Methods	
3.2.2.2.1	Category 1: NDE Capability at One Crack Length	3.2.12
3.2.2.2.2	Category 2: Estimation of the POD Function with One Observation per Crack	3.2.15
3.2.2.2.3	Category 3: Estimation of the POD Function with Multiple Observations per Crack	3.2.18
3.2.3	<u>Comparison of NDI Methods</u>	3.2.20
3.3	PROOF TEST DETERMINATIONS	3.3.1
3.3.1	<u>Description of the Proof Test Method</u>	3.3.3
3.3.2	<u>Examples</u>	3.3.6
3.4	EQUIVALENT INITIAL QUALITY (EIQ)	3.4.1
3.4.1	<u>Description of Equivalent Initial Quality Method</u>	3.4.1
3.4.2	<u>Example Application of Equivalent Initial Quality Method</u>	3.4.3
3.5	LIST OF REFERENCES	3.5.1

LIST OF FIGURES

<u>FIGURE</u>		<u>PAGE</u>
3.1.1	The Effect of Defects Distribution in Structural Integrity Planning. (Reference 3.1.)	3.1.4
3.1.2	Crack Growth-Life Curve at Second Inspection.	3.1.4
3.1.3	Various Qualification Processes.	3.1.5
3.2.1	Range Interval Method as Applied to Eddy Current Inspections of Aluminum Plates-1 Inspection Per Crack (Reference 13).	3.2.33
3.2.2	Optimized Probability Method as Applied to Eddy Current Inspections of Aluminum Plates-1 Inspection Per Crack (Reference 13).	3.2.34
3.2.3	Regression Method as Applied to Eddy Current Inspection of Fastener Holes-60 Inspections Per Crack (Reference 8).	3.2.35
3.2.4	Summary and Comparison of Nondestructive Testing Methods (Reference 1).	3.2.36
3.3.1	Fracture Critical Curve Defining Relationship Between Stress and Crack Length Associated with Fracture.	3.3.19
3.3.2	Schematic Illustrating the Relationship Between the Proof Test Diagram, the Residual Strength Capability and Crack Growth Life Interval.	3.3.20
3.3.3	Fracture Toughness Varies as a Function of (a) Thickness, (b) Yield Strength, (c) Temperature, and (d) Loading Rate.	3.3.21
3.3.4	Using a Material's Low Temperature Fracture Sensitivity to Decrease Initial Crack Size and thus Increase the Minimum Safe Crack Growth Interval for a Given Proof Stressing Condition.	3.3.22
3.3.5	Influence of Fracture Toughness Variation on the Maximum Allowable Crack Size.	3.3.22

LIST OF FIGURES (Cont'd)

<u>FIGURE</u>		<u>PAGE</u>
3.3.6	Description of Procedure Used to Establish Initial Crack Size and the Minimum Safe Crack Growth Interval According to MIL-A-83444 (3.1.1.1).	3.3.23
3.3.7	Table of Fracture Toughness Data Taken from MIL-HDBK-5 (Reference 25).	3.3.24
3.3.8	Data Required for EXAMPLE 3.3.1.	3.3.25
3.3.9	Pressure Vessel Structure with Semicircular Surface Crack. For Loading, See Figure 3.3.10, and for Material Properties, See Figure 3.3.11.	3.3.26
3.3.10	Pressure Loading for Structure Illustrated in Figure 3.3.9.	3.3.27
3.3.11	Material Properties for Steel Pressure Vessel Illustrated in Figure 3.3.9.	3.3.28
3.3.12	Change in Crack Geometry to Through-Thickness Crack After the Semicircular Crack Grows to the Inside Wall.	3.3.29
3.3.13	Graphical Procedure for Interpreting Crack Length.	3.3.30
3.4.1	Parameters that Affect Fastener-Hole Initial Quality (Reference 27).	3.4.8
3.4.2	Definition of Equivalent Initial Quality (Reference 27).	3.4.8
3.4.3	A-7A Wing Fatigue Test Fracture Surface (Reference 27).	3.4.8
3.4.4	Equivalent Initial Quality Results for A-7A Wing Fatigue Test (Reference 27).	3.4.9
3.4.5	A-7D Quality-Assessment Specimen Locations (Reference 27).	3.4.9
3.4.6	A-7D Flaws Origins (Reference 27).	3.4.9

LIST OF FIGURES (Con't)

<u>FIGURE</u>		<u>PAGE</u>
3.4.7	Fracture Surfaces for Countersunk (left) and Straight-Shank (right) Holes (Reference 27).	3.4.10
3.4.8	Probability Density of Occurrence of A-7D Equivalent Initial Quality (Reference 27).	3.4.11
3.4.9	Cumulative Probability of Occurrence of A-7D Equivalent Initial Quality (Reference 27).	3.4.11

LIST OF TABLES

<u>TABLE</u>	<u>PAGE</u>
3.2.1 MINIMUM NUMBER OF DETECTIONS REQUIRED TO CONCLUDE THE POD \geq 90% WITH 95% CONFIDENCE	3.2.14
3.2.2 SUMMARY OF NDE DATA STATISTICALLY ANALYZED (REFERENCE 13)*	3.2.23
3.2.3 THRESHOLD CRACK LENGTHS (90/95 LIMITS IN INCHES) FOR FATIGUE CRACKS IN FLAT PLATE (REFERENCE 13)	3.2.29
3.2.4 THRESHOLD CRACK LENGTHS (90/95 LIMITS IN INCHES) FOR ALUMINUM, FORGE CLOSED DEFECT TYPE (REFERENCE 13)	3.2.30
3.2.5 THRESHOLD CRACK LENGTHS (90/95 LIMITS IN INCHES) FOR 4340 M STEEL, FORGE CLOSED DEFECT TYPES (REFERENCE 13)	3.2.31
3.3.1 PROOF TESTING OF AIRCRAFT STRUCTURES	3.3.2
3.3.2 TRIAL AND ERROR SOLUTION OF EQUATION 3.3.4a	3.3.9
3.3.3 CRACK INTERVAL TABLE FOR EQUATION 3.3.6	3.3.13
3.3.4 FATIGUE CRACK GROWTH RATE CONTRIBUTION	3.3.15
3.3.5 STRESS-CORROSION CRACKING RATE CONTRIBUTION	3.3.15
3.3.6 ESTIMATING THE TIME TO GROWTH THROUGH SUCCESSIVE INTERVALS	3.3.17
3.4.1 GEOMETRIC DETAILS OF A-7D QUALITY ASSESSMENT SPECIMENS (REFERENCE 27)	3.4.7
3.4.2 A-7D QUALITY ASSESSMENT TEST RESULTS (REFERENCE 27)	3.4.7

3.0 DAMAGE SIZE CHARACTERIZATIONS

3.1 INTRODUCTION

The damage tolerance approach to structural integrity assumes that cracks are present in all critical locations and demonstrates that these cracks will not grow undetected to a critical length during a period of service usage. Since the rate of crack growth depends on the crack length, the structural service lives or periods between inspections are greatly influenced by the crack lengths assumed at the beginning of a usage period. From the safety viewpoint, these initial crack lengths must be longer than any equivalent damage that could be present in the structure after passing quality inspections. From a practical viewpoint, however, the degree of conservatism introduced by assuming long cracks must be limited to reach realistic usage lives or periods of operation without inspections. This trade-off results in great emphasis being placed on quantifying the damage sizes that may be present in the structure at the beginning of an operational period.

The distribution of crack lengths in any given structure can be considered to consist of the composite of the several distributions shown in Figure 3.1.1. The material as received from the vendor will contain very small flaws or defects such as inclusions, cracks, porosity and surface pits, scratches, and machine marks. These inherent material flaws are considerably below the detection capability of the non-destructive inspection (NDI) and should be sufficiently small to not grow appreciably in service. These small flaws form the basis of the continuing damage crack size assumption and are

characterized by a single crack length, a_1 , which is assumed to be an upper-bound on the distribution.

A distribution of larger defects can exist as a result of the fabrication process or as large inherent flaws. The production quality control process is designed to detect and eliminate as many of these cracks as possible but those which are not detected will propagate due to fatigue mechanisms during service. The largest crack size that could remain undetected in the newly fabricated structure after the final inspection is designated as a_0 . This crack length provides the starting point for the crack growth projections which demonstrate adequate service life or the necessity for an in-service inspection.

Cracks smaller than a_0 will propagate in service operations and others, due to fatigue crack initiation, corrosion, and foreign object damage, will be initiated. If any of these cracks can propagate to critical size, a_{cr} , before the end of the service life, they must be detected and repaired at scheduled maintenance intervals. The largest crack size that can remain undetected after an inspection is designated as a_{NDI} and becomes the initial crack size for the next usage period. Figure 3.1.2 is a schematic of the projected crack growth of the critical crack lengths and illustrates the resetting of the potential crack to a_{NDI} after the inspection. In this figure, the inspection was scheduled at one-half the usage time required for the initial crack (a_0 or a_{NDI}) to grow to critical.

MIL-A-83444 specifies the type and size of cracks that must be assumed during design. These are summarized in Chapter 2. The assumed crack sizes depend on: (1) the design concept (slow crack growth or fail safe); (2) inspectability level (inspectable or non-inspectable) with and without component removal; and (3) continuing damage after initial primary damage. In the current version of the specification, smaller initial crack sizes (a_0) may be assumed for slow crack growth structures based on the contractors demonstrated capability to eliminate all cracks greater than the smaller value. This demonstration may be based on an NDI system or on a proof test. These qualification processes are shown schematically in Figure 3.1.3(a) and 3.1.3(b).

The continuing damage crack size assumption can also be reduced if the contractor can demonstrate an improved manufacturing quality. One method for such a demonstration is based on the determination of the distribution of equivalent initial flaws as shown schematically in Figure 3.1.3(c).

Since NDI, proof testing, and the equivalent initial quality method can be applied under the current airplane damage tolerance requirements and may receive greater emphasis in future specifications, they will be reviewed in the following subsections. Section 3.2 describes the major NDI methods currently in use, discusses the statistically based demonstration program for measuring NDI capability and compares the current methods. Sections 3.3 and 3.4 describe and give examples of the proof test and equivalent initial quality methods, respectively.

3.1.3

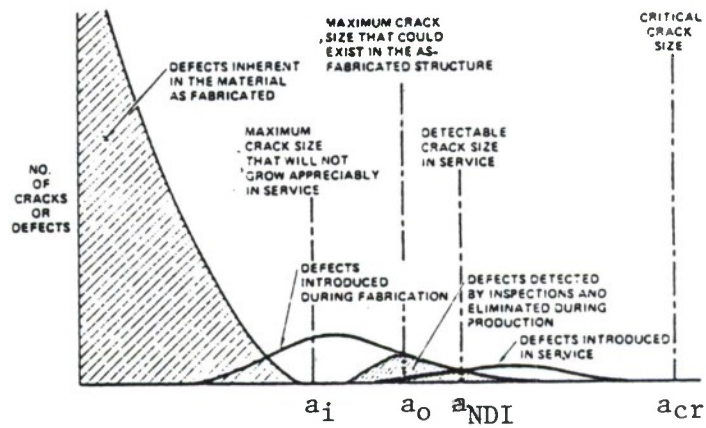


Figure 3.1.1. The Effect of Defects Distribution in Structural Integrity Planning. (Reference 3.1).

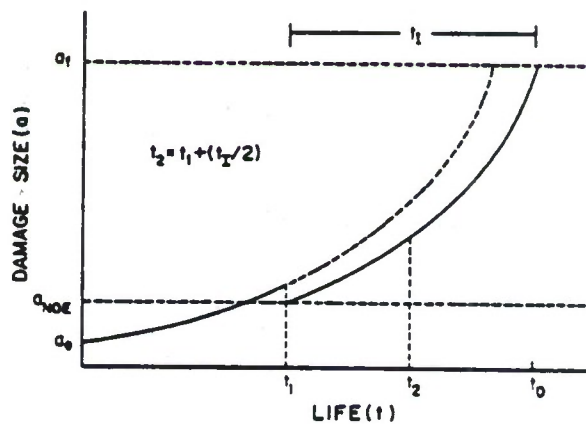
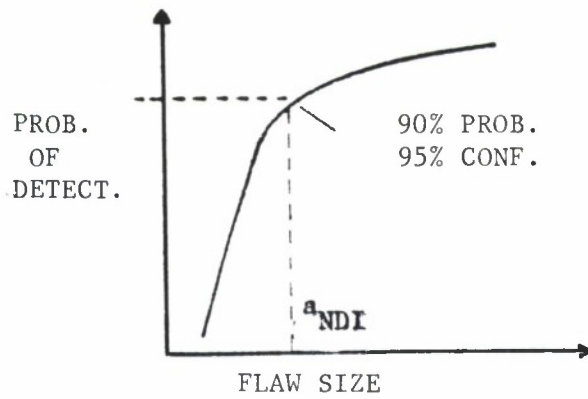
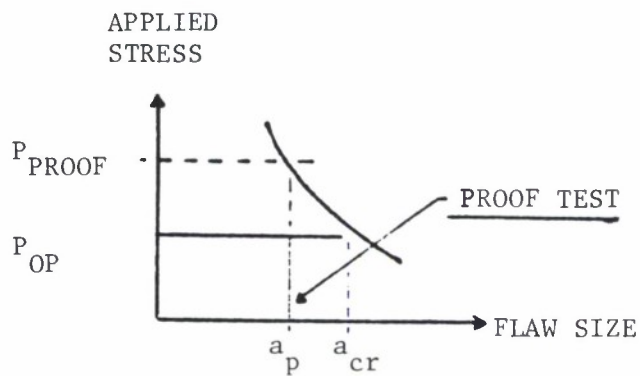


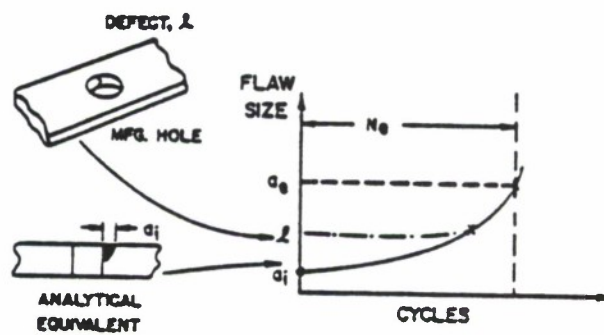
Figure 3.1.2. Crack Growth-Life Curve at Second Inspection.



a. Inspection: NDE Demonstration



b. Structure: Proof Test



c. Manufacturing: Equivalent Initial Quality

Figure 3.1.3. Various Qualification Processes.

3.2 NDI DEMONSTRATION OF CRACK DETECTION CAPABILITY

Nondestructive inspection (NDI) methods are commonly used to determine the condition of a structure during production and at in-service inspections. Detailed descriptions of the principles and use of these methods are available in many journals and references (e.g. references 1-6) and will not be repeated here. Rather, the objective of this subsection is to briefly describe and compare the common NDI methods and to discuss the statistically based demonstration programs which are required to quantify the crack detection capability of an NDI system.

3.2.1 NDI Methods

There are five commonly used NDI techniques: liquid penetrant, ultrasonic, eddy current, magnetic particle, and radiography. Each of these is discussed in the following paragraphs.

3.2.1.1 Liquid Penetrant Inspection

Liquid penetrant inspection is a non-destructive method for finding discontinuities that are open to the surface of parts fabricated from essentially nonporous materials. After cleaning the surface, the penetrant is applied and will seep or be drawn into various types of minute surface openings. The excess penetrant is removed and a developer is applied which highlights the flaws under ultraviolet light. The process is well suited for the detection of all types of surface cracks, laps, porosity, shrinkage area, laminations, and similar discontinuities.

Indications of flaws can be found regardless of size, configuration, internal structure, or chemical composition of the workpiece being inspected and regardless of the orientation of the flaw to the workpiece. Liquid penetrant inspections are relatively simple and inexpensive (as compared to the other NDI methods) and can be applied to a broad range of materials. Very small flaws can be found. However, they can only detect surface flaws and their effectiveness can be adversely influenced by surface coatings and surface roughness or porosity. Extreme care is required in pre- and post-inspection cleaning and, in some cases, etching may be required prior to inspection.

3.2.1.2 Ultrasonic Inspection

Ultrasonic inspection uses high frequency sound waves as a probing medium to detect subsurface as well as surface flaws. The sound waves travel through the part with attendant energy loss and are reflected at material-flaw interfaces. Ultrasonic inspection devices detect flaws by monitoring one or more of the following: (a) reflection of energy from interfaces or discontinuities within the metal; (b) time of transit of a sound wave through the test piece; and, (c) attenuation of the beams by absorption and scattering within the test piece.

Ultrasonic inspection is one of the most widely used NDI methods. Cracks, laminations, shrinkage cavities, bursts, flakes, pores, bonding faults and other discontinuities that act as metal-gas interfaces can be detected. Inclusions and other inhomogeneities in the metal being inspected can also

be detected by causing partial reflection or scattering of the wave even though they may not act as a metal-gas interface. Although the primary application of ultrasonic inspection in metals is the detection and characterization of internal flaws, it is also used to detect surface flaws, to define bond characteristics, to measure extent of corrosion and, (much less frequently) to determine physical properties such as structure, grain size, and elastic constants. The penetrating power of ultrasound waves allows the detection of flaws deep within a part. Due to the sensitivity of the instruments, very small flaws can be detected but, if the gain is set too high, at the expense of many false indications. Ultrasonic methods provide greater accuracy than other NDI methods in determining the position of internal flaws, estimating their size, and characterizing their orientation, shape and nature. The limitations of ultrasonic methods are governed by the requirement for experienced technicians, the difficulty in developing inspection procedures, the need for reference standards for equipment calibration, and the physical limitations of the hardware. Since couplants (light oil or water) are needed to provide effective transfer of ultrasonic wave energy between transducers and material, parts that are rough or irregular in shape are difficult to inspect. Similarly, parts which are very small are difficult to inspect. Finally, since discontinuities in a shallow layer immediately below the surface may not be detectable, inspection results of very thin components are questionable.

3.2.1.3 Eddy Current Inspections

The principles of electromagnetic induction are used in eddy current inspections to detect surface and near surface flaws in electrically conductive metals. When an electrically conductive material is subjected to an alternating magnetic field, small circulating electric currents are generated in the material. Since these eddy currents are affected by variations in conductivity, magnetic permeability, mass, and material homogeneity, the conditions which affect these characteristics can be sensed by measuring the eddy current response of the material. In practice, eddy currents are induced in the part to be inspected with a coil carrying an alternating current. The induced eddy currents generate their own magnetic field which interacts with the magnetic field of the exciting coil and changes the impedance of the exciting coil. By measuring the impedance of the exciting coil, or a separate indicating coil, the inspector can infer the presence of flaws in the material.

An important use of the eddy current NDI method has been in the detection of fatigue or stress corrosion cracks around fastener holes after the cracks have grown beyond the fastener head. Special bolt hole probes have also been devised for use after the fastener has been removed for locating cracks emanating from the wall of the fastener hole. This inspection process has been automated to remove operator influence, speed inspections, and produce a permanent inspection record.

Eddy current methods do not require contact with the specimen, do not require clean up, and are generally faster than liquid penetrant and radiographic methods. Although eddy current methods can detect both surface and subsurface flaws, the depth of inspection below the material surface is limited (approximately 0.25 in.). Since eddy currents are influenced by many material variables, masked or false indications can easily be caused by sensitivity to part geometry, lift-off, edge effects and permeability variations. Finally, eddy current methods require well trained operators to man the test instruments and reference standards are necessary.

3.2.1.4 Magnetic Particle Inspection

Magnetic particle inspection is effective in the detection of surface and near surface flaws in ferromagnetic parts. The inspection is accomplished by inducing a magnetic field in the part and applying either a dry magnetic powder or a liquid suspension of iron particles to the surface being inspected. Defects in the part cause local bipolar perturbations in the magnetic field which attract the magnetic particles, producing visible indications by color contrast or by fluorescence under "black light." The magnetically held particles form the outline of the discontinuity and generally indicate its location, size, shape, and extent to an experienced inspector.

The magnetic particle method is a relatively fast and inexpensive method for locating small and shallow surface cracks in ferromagnetic materials. Discontinuities that do not break the surface are detectable but deeper flaws must be larger to be found. Elaborate pre-cleaning is not necessary but thin coatings of paint or other non-magnetic coverings, such as plating, adversely affect the sensitivity of this inspection technique. Following the inspection, the material must often be de-magnetized and post-cleaning to remove the clinging magnetic particles is usually necessary. This NDI method can be used only on ferromagnetic materials which include most of the iron, nickel and cobalt alloys. Many of the precipitation-hardening steels, such as 17-4PH, 17-7PH, and 15-4PH stainless steels, are magnetic after aging. Non-ferromagnetic materials which cannot be inspected by this method include aluminum, magnesium, copper, and titanium alloys and austenitic stainless steels.

3.2.1.5 Radiographic Inspection

Radiographic NDI is based on the differential absorption of penetrating radiation by the structure being inspected. In conventional radiography, the object is bombarded by a beam of X-rays and the portion of the radiation that is not absorbed by the object impinges on a sheet of film. The unabsorbed radiation exposes the film emulsion similar to the way light exposes film in photography. Development of the film produces an image that is a two-dimensional "shadow picture" of the entire volume of the object. Variations in density, thickness, and composition of the object being inspected cause variations in the intensity

of the unabsorbed radiation and appear as variations in shades of gray in the developed film. Evaluation of the radiograph is based on a comparison of the differences in photographic density with known characteristics of the object or with standards derived from radiographs of similar objects of acceptable quality.

Radiographic inspection provides the capability to probe the internal characteristics of materials and components. It can disclose structural weaknesses, assembly errors, and mechanical malfunctions as well as revealing voids, long cracks, and other material anomalies. Radiography is, however, expensive, slow, and not sensitive to detecting certain types of flaws. Cracks cannot be detected unless they are parallel to the radiation beam. Tight cracks in thick sections cannot usually be detected even when properly oriented. Laminations are almost always non-detectable. Minute discontinuities such as inclusions in wrought material, flakes, microporosity and microfissures cannot be detected unless they are sufficiently segregated to produce a detectable gross effect. Finally, due to the hazards of exposure to X-rays, strict controls are required to prevent biological damage to the inspectors.

3.2.2 NDI Capability Evaluation

While all of the NDI systems are capable of finding "small" cracks, damage tolerance analyses are focused on the longest crack that could be missed at an inspection. But NDI techniques do not always produce a correct indication when applied by inspectors to cracks of the same "size". The ability and attitude of the operator, the geometry and material of the structure, the environment in which the inspection takes place, and the location, orientation and size of the crack all influence the chances of detection. When considering the efficacy of an NDI system as a function of only crack length, uncertainty is introduced as a result of ignoring the other factors and the uncertainty is quantified in terms of the probability of detection (POD) of cracks of a fixed length. The POD for all cracks of a given length is defined as the proportion of cracks that will be detected by the NDI system when applied by representative inspectors to the population of structural elements in a defined environment. Therefore, evaluating the capability of an NDI system requires a carefully controlled demonstration experiment with a valid statistical analysis of the resulting data.

The statistically based characterization of NDI capability has two significant ramifications. First, for a given NDI application, the true probability of detection as a function of crack length (or for a single crack length) will never be known exactly. The capability of an NDI system can only be demonstrated through an experiment in which representative structures with known crack lengths are inspected and the true POD is estimated by the observed percentage of correct positive indications. The estimated POD is

subject to statistical variation that results from all uncontrolled factors that can lead to nonrepeatable positive indications for cracks of a particular length. However, statistical methods (which depend on the experimental procedure) are available which yield confidence limits on the true probability. Protection against making a wrong decision on the basis of a set of non-typical results is provided by the confidence limits but an unknown element of risk will always be present.

Second, in the real world structural integrity problem, no inspection procedure will provide 100 percent assurance that all cracks greater than some useful length will be detected. The current capabilities and the uncertainty resulting from the NDI demonstration process at the short crack lengths of interest in aircraft applications dictate that the detectable crack size must be specified in terms of a high confidence that a high percentage of all cracks greater than the detectable flaw size will be found. For example, MIL-A-83444 states that a smaller initial crack can be used by the manufacturers for slow crack growth structures if it can be shown that there is 95 percent confidence that at least 90 percent of all cracks of the smaller size will be detected by the manufacturers' NDI system.

To date, characterizations of NDI capabilities have been expressed as the crack sizes for which there is at least a given POD at a defined level of confidence (the POD/CL limit). Such characterizations provide a stand-alone measure of the NDI system which is valid for applications represented by the experimental test conditions. However, there are three major problems associated with the POD/CL type characterization.

First, the choice of particular POD and confidence limits has been made on a rather arbitrary basis. For example, 90/95 values were selected for the MIL-A-83444 crack sizes even though there is no real interest in a crack length which is detected only 90 percent of the time. Rather, 90/95 limits were selected because higher POD or confidence limit values would have required much larger sample sizes in the demonstration programs for the analysis methods being used. The 95 percent confidence limit is assumed to provide the required degree of conservatism.

Second, a POD/CL limit is not a single, uniquely defined number but, rather, is a statistical or random quantity. Any particular POD/CL estimate is only one realization from a conceptually large number of repeats of the demonstration program. Berens and Hovey (8) showed there can be a large degree of scatter in these POD/CL estimates and the scatter depends on the POD function, analysis method, POD value, confidence level and number of cracks in the demonstration program.

Third, the POD/CL characterization is not related to the size of cracks that may be present in the structure after an inspection. To calculate the probability of missing a large crack requires knowledge of the entire POD function and the sizes of the cracks being inspected.

Research is currently being conducted to resolve these problems and this research may lead to a different type of characterization of NDI capability. However, after a brief description of the design of NDI capability experiments, the following paragraphs present the approaches that have been used to calculate the POD/CL limits that are stated in the current literature.

3.2.2.1 Design of NDI Capability Experiments

In an NDI capability demonstration program, sample parts known to contain cracks are mixed with crack free parts and the entire lot is inspected by a standardized procedure that essentially duplicates the proposed production inspection. The validity of the results is entirely dependent on the degree to which the experimental conditions match the real world application. This includes not only well designed specimens with appropriate sized flaws, but also the use of a representative group of inspectors.

Although several NDI demonstration programs have been conducted (2, 9, 10, 11, 12) and the problem studied (13, 14, 15), no standard demonstration program has been defined. The cited references describe program details and list recommendations. The following items from Packman, et al. (2) list some of the items which must be considered in designing the demonstration program:

- a) Specimen design - representative size, shape, and surface finish. Flaw characteristic to be evaluated. Flaw type, location, and orientation. Method for producing desired flaws.
- b) Sample size considerations - analysis method. Number of specimens with flaws of appropriate sizes. Multiple inspections of each crack.
- c) Inspection procedure - complete detailed instructions to be followed by each inspector.
- d) Specimen production - flawed and unflawed specimens, at least as many unflawed as flawed. Appropriate specimen identification.

e) Inspection - representative inspectors in anticipated usage environment with no knowledge inspection capability evaluation being conducted, if possible.

f) Analysis - determine crack sizes destructively, if necessary, and analyze results.

3.2.2.2 Analysis Methods

There are three categories of demonstration programs or experiments which have been used to evaluate the reliability of NDI systems: (1) demonstration of a capability at one crack length; (2) estimation of the POD function and confidence bounds through single inspections of cracks covering a range of lengths; and (3) estimation of the POD function and confidence bounds through multiple inspections of cracks covering a range of lengths. Analysis of data from category 1 and 2 experiments have generally been based only on binomial distribution theory. Category 3 data have been analyzed by regression analyses. Details of the three types of experiments and the analysis methods used to date are presented in References 2, 8, 11 and 13. The following paragraphs summarize pertinent features of each current experiment/analysis combination.

3.2.2.2.1 Category 1: NDE Capability at One Crack Length

This category of experiments can be viewed as a method for demonstrating that an NDE system can detect at least a given percentage of cracks of a specified length with a specified confidence limit. For example, this approach could be used to show that there is 95% confidence that at least 90% of all cracks of length 0.25 in. will be found

by a particular system. This category of experiments also serves as an introduction to the use of the binomial distribution for the analysis of NDE reliability data.

Assume that the reliability demonstration program will be conducted by inspecting a large number of specimens of which exactly n have a crack of length "a" and the results of the inspections are statistically independent. If p represents the true (but unknown) probability of detecting a crack of length "a", then the number, r , of cracked specimens that will be detected has a binomial distribution and the probability of exactly r detections is given by

$$P(r) = \frac{n!}{(n-r)!r!} p^r (1-p)^{n-r} \quad (3.2.1)$$

The unbiased, maximum likelihood estimate of p is

$$\hat{p} = r/n \quad (3.2.2)$$

However, it is extremely unlikely that \hat{p} will exactly equal p so that a lower confidence interval estimate is calculated which yields a range of p values which are consistent with the observed number of detections. The width of the interval estimate depends on the desired confidence level, $100(1-\gamma)$, the sample size, n , and the number of detections, r . In particular, the lower $100(1-\gamma)$ percent confidence bound on the estimate of p is obtained as the solution, \underline{p} , to the equation

$$\gamma = \sum_{i=r}^n \frac{n!}{(n-i)!i!} p^i (1-p)^{n-i} \quad (3.2.3)$$

The interpretation of \underline{p} as a lower confidence limit should be made as follows. If the experiment was repeated a large number of times, 100 (1 - γ) percent of the calculated values of \underline{p} would be less than the true value of p . Therefore, there is 100 (1 - γ) percent confidence that the \underline{p} from a single experiment will be less than the true value.

Solutions to Equation 3.2.3 are tabulated in Reference 16 for confidence limits of 90, 95, 99 percent. General solutions expressed in terms of the incomplete beta function and the normal approximation to the binomial distribution can be found in Reference 17 (as well as in many other statistical references). Minimum values of n and r which yield predefined values of \underline{p} and confidence level, 100 (1 - γ), are often quoted and selected values can be found in Reference 2.

For example, consider an experiment to demonstrate that there is 95 percent confidence that at least 90 percent of all cracks of a fixed length will be detected by the NDI system. To achieve the desired level of confidence and POD would require experimental results as given in Table 3.2.1 for $n \leq 103$.

TABLE 3.2.1
MINIMUM NUMBER OF DETECTIONS REQUIRED TO CONCLUDE
THE $\text{POD} \geq 90\%$ WITH 95% CONFIDENCE

<u>Number of Cracked Specimens</u>	<u>Number of Cracked Specimens Detected</u>
29	29
46	45
61	59
75	72
89	85
103	98

If there were 28 cracked specimens in an experiment and all 28 were detected, the lower 95 percent confidence bound on the POD would be 0.899 (and if less than 28 were detected, the lower confidence bound would be even less). Therefore, to obtain a 90 percent POD with 95 percent confidence requires a minimum of 29 specimens with cracks of the fixed length and all of the cracks would have to be detected in the real inspection environment.

In general, given the number of cracked specimens tested and the number of cracked specimens found a lower confidence level for p can be constructed. If the lower confidence limit is sufficiently high (as defined prior to the experiment, e.g., $p \geq 0.90$) the demonstration is complete. If the lower confidence level for p is below the targeted value, the NDI system has failed the demonstration at that crack length. This category of experiment provides information only at the crack length inspected. A complete discussion of the experiment and analysis method can be found in Reference 2.

3.2.2.2.2 Category 2: Estimation of the POD Function with One Observation per Crack

In the second category of experiments many specimens covering a range of crack sizes are inspected once and the results are used to estimate the POD as a function of crack length with confidence limits. Different analysis methods have been used on the results of these experiments but they are all based on binominal distribution theory. Since, in general, there are not a large number of specimens with cracks of the same length, the specimens are grouped into intervals of crack length. It is assumed that all cracks within a specified interval have approximately the same POD. The number of detections in each group is modeled by the

binominal distribution, analyzed as described in subsection 3.2.2.2.1, and the lower confidence bound for the POD is usually assigned to the crack length at the upper end of the interval.

The essential differences in the methods of analyzing the data from this category of experiments has been in the methods by which the crack length intervals are formed or combined. In the range interval method the crack length intervals are defined with equal lengths across the range of data and, hence, there are different numbers of observations in each interval. This method can produce an extremely erratic estimate of the confidence limit on the POD function. Figure 3.2.1 presents the results of a range interval method analysis of inspection results for eddy current inspections of etched fatigue cracks in 2219-T87 aluminum flat plates (reference 13, page D-63). The individual data points are the percentages of cracks identified in each interval while the solid line segments connect the lower 95 percent confidence boundary for each POD estimate. The extremely erratic behavior of the confidence limits resulted from small sample sizes in some of the intervals and not from different observed percentages of detection.

To avoid the problems resulting from the variable sample sizes in each interval, various methods of varying the length of the intervals to maintain constant sample size have been devised. These are the non-overlapping constant sample size, the overlapping constant sample size, and optimized probability methods. Yee, et al. ⁽¹³⁾ recommends the use of the optimized probability method over the other two and only this method is summarized here.

The optimized probability method (OPM) for analyzing category 2 experimental data is an algorithm for grouping the inspection results to achieve the highest possible lower confidence bounds. Initially, groups are formed as in the range interval method giving rise to m intervals. For convenience, these intervals will be labeled 1 through m . The first OPM interval is selected as follows. The lower confidence bound on the POD is calculated for the data in interval 1, then for the data in intervals 1 and 2 together, then for intervals 1, 2 and 3 and so forth until a lower confidence bound for the POD is calculated for the whole data set (intervals 1 through m combined). The group of intervals that gives rise to the highest value of lower confidence bound is used as the first interval in the optimized probability method. Interval 1 data is then eliminated and the set of intervals 2 through m are analyzed in a similar manner to create the second OPM interval. This process continues until confidence bounds for all m intervals are found. Figure 3.2.2 shows the result of this procedure for the same data that was used in Figure 3.2.1.

Confidence bounds obtained by the optimized probability method are better behaved than those of the other methods. However, this behavior is obtained at the expense of unknown statistical validity of the POD function across all ranges of crack length. The overlapping of intervals requires inspection results for a particular crack to be analyzed more than once. Any crack that falls in an overlap area is used in calculating the confidence bounds for all the intervals involved. Thus, there is a correlation between confidence bounds that share data and the influence of this correlation on the POD as a function of crack length is unknown.

In general, the various "interval" methods have three major deficiencies. First, since they are based on the binomial distribution, the confidence bounds are greatly influenced by the method for assigning cracks to interval. The confidence bounds are as much influenced by the analysis method as they are by the data. Second, the confidence bounds do not approach unity and, depending on the sizes of the cracks in the test specimen, may not reach the required 0.90 POD level. The entire experiment may fail to provide the desired result. Third, they provide limited inferences on the entire POD function if this function is required for further studies such as risk of failure analyses.

3.2.2.2.3 Category 3: Estimation of the POD
Function with Multiple Observations
per Crack

This category of experiment resulted from a large NDI reliability program performed for the Air Force as described in Reference 11. Sections of retired aircraft and other specimens were transported to Air Force depots and inspected for cracks by representative personnel, using various NDI systems in a typical environment. At the completion of the travel phase of the program, the structures were destructively inspected to verify the existence and lengths of the cracks. This experiment has often been called the "Have-Cracks-Will-Travel Program".

This method of collecting data yielded an estimate of a detection probability for each individual crack. For example, Figure 3.2.3, using data of Reference 11, displays the inspection results of individual cracks emanating from fastener holes in a skin and stringer wing assembly as inspected by eddy current surface scans. Each data point in the figure represents the proportion of times the crack was found when subjected to 60 independent inspections. These data clearly illustrated that not all cracks of the same length have the same detection probability and demonstrate the need for an analysis method other than those based on the binomial distribution.

Berens and Hovey ⁽⁸⁾ demonstrated that the mean of the detection probabilities at a crack length is the POD. Thus, the POD function with confidence limits can be estimated by regression analysis. Berens and Hovey ⁽¹¹⁾ fit the data of Figure 3.2.3 with the log linear logistics (or log-odds) model given by

$$POD(a) = \frac{\alpha a^{\beta}}{1 + \alpha a^{\beta}} \quad (3.2.4)$$

To perform the regression analysis, the data are transformed

$$\begin{aligned} Y_i &= \ln (p_i / 1 - p_i) \\ X_i &= \ln a_i \end{aligned} \quad (3.2.5)$$

where p_i is the observed percent of detections of crack i which has length a_i .

The simple regression model

$$Y_i = \alpha + \beta X_i + \epsilon_{ij} \quad (3.2.6)$$

is fit to the transformed data points to estimate α and β and to calculate

the lower confidence limit on the POD function.

The solid curve of Figure 3.3.3 is the estimate of the POD function using the log odds model and the dashed line is the lower 95 percent confident limit curve for the POD function.

Different POD models may be required (or acceptable) for different applications. Lewis, et al.⁽¹¹⁾ used a modified Weibull type of model to fit the POD function. This model is given by

$$\text{POD}(a) = \exp [- \alpha a^{\beta}] \quad (3.2.7)$$

and again the parameters α and β were estimated from regression analysis of transformed (a_i, p_i) data pairs.

Given a particular model, Parameters can be estimated by methods other than regression. Berens and Hovey⁽⁸⁾ also derived maximum likelihood estimates of α and β in the log-odds model for the category 2 type experiment. Development of these methods is continuing.

3.2.3 Comparison of NDI Methods

The selection of an NDI method for a particular application will be governed primarily by the type and geometry of material, type of defect, test environment and size and location of possible flaws. Figure 3.2.4 presents a comparative summary of the major features of each of the five NDI methods discussed in subsection 3.2.1. Further details can be found in References 3-7.

Although several NDI capability evaluation experiments have been conducted and reported in the literature ⁽⁹⁻¹²⁾, there are not simple quantitative characterizations of the NDI methods which are generally accepted. Test specimens, conditions, and NDI procedures are significantly variable so as to make results from different experiments at least somewhat incomparable. The incompatibility of results is further enhanced by the analysis methods used to quantify the NDI capability and the statistical variation that naturally results in the estimation of, for example, the crack length for which there is 95 percent confidence that at least 90 percent of all cracks will be detected (i.e. the 90/95 limit). However, to provide an indication of the crack sizes that are detectable by the five NDI methods, summary data from the study of Yee, et al. ⁽¹³⁾ are contained in Table 3.2.2.

In the study of Reference 13 conducted for the National Aeronautics and Space Administration, Yee, et al. compiled all available test results from NDI capability demonstration experiments. These data were screened by comparing the experimental test conditions to a set of criteria which would ensure an acceptable degree of validity. The data which passed the criteria were reduced and analyzed by the same techniques. Seven of 20 data sets were accepted for analysis. Since all seven were subjected to the same analysis procedures, the results are compatible and provide at least a gross indication of the capabilities of the five NDI methods.

Table 3.2.2 reproduces the data summary of Reference 13. The threshold crack lengths listed in the table are the lowest 90/95 limits achieved by each data set as calculated from either the optimized probability method or the

overlapping 60 point method. A dash in the 90/95 column indicates that the 95 percent confidence limit on the POD function failed to reach the 0.9 level, i.e., the experiment failed to produce a 90/95 limit.

Due to the many possible experimental conditions in the individual sets, comparisons among the NDI methods are difficult. Table 3.2.3 is a composite summary of the 90/95 limits for the specimens described as fatigue cracks in flat plates. Missing values indicate no tests for the material-NDI system combination. Similarly, Tables 3.2.4 and 3.2.5 present comparisons of NDI methods for aluminum and steel under laboratory and production conditions for different specimen designs.

These data indicate that, in general, the radiographic NDI method has larger 90/95 limits than do the other methods. No other such general statements can be made and, in fact, the statistical variability in the estimates of the 90/95 limits should be accounted for before concluding one method is significantly superior to another with respect to 90/95 limits.

TABLE 3.2.2
SUMMARY OF NDE DATA STATISTICALLY ANALYZED (REFERENCE 13)*

DATA SUB-SET	DATA SOURCE	MATERIAL TYPE	DEFECT TYPE	SPECIMEN GEOMETRY	NDE METHOD	PERTINENT PARAMETERS	90/95 CRACK LENGTH (IN.)
1	Martin Marietta	2219-T87 Al	Fatigue Cracks	Flat Plates	Ultrasonic- Surface Wave	Before Etch; and with 3 Ops; 10 MHz	0.136
2					Liquid Penetrant	Same as above, Uresco P151, K410, D499C	0.262
3					Eddy Current	Same as above; NDT-3; 100 KHz	0.108
4					X-ray	Same as above	
5					Ultrasonic- Surface Wave	After Etch; and with 3 Ops.	0.083
6					Liquid Penetrant	Same as above	0.108
7					Eddy Current	Same as above	--
8					X-ray	Same as above	0.262
9	Rockwell Inter. Space Div. (NAS9- 14000); Martin Marietta, and GD Convair	2219-T87 Al	Fatigue Cracks	Flat Plates	Ultrasonic- Shear Wave (Surface Wave) $f = 2.25$ MHz for RI-SD $f = 10$ MHz for GD Convair	After Etch, and by Operator O	0.290
10						Operator P	0.087
11						Operator Q	0.275
12						Operator R	0.275
13						Operator S	0.141
14					Liquid Penetrant	After Etch, and by	
15					P-133, D495A for RI-SD	Operator H	0.111
16						Operator I	0.290
17						Operator J	0.290
18						Operator K	0.131
19						Operator L	0.290
20						Operator M	0.134
21						Operator N	0.535
					Eddy Current	After Etch, and by	
22					Defectometer	Operator T	0.262
23					Model 2.154 $f = 2$ MHz	Operator U	0.079
24					for RI-SD	Operator V	--
						Operator W	0.131
25						Operator X	0.126

* CAUTION: The crack lengths in the POD90(CL95) column are not intended to be used for design purposes unless the user demonstrates a similar capability.

TABLE 3.2.2 SUMMARY OF NDE DATA STATISTICALLY ANALYZED (Continued)

DATA SUB-SET	DATA SOURCE	MATERIAL TYPE	DEFECT TYPE	SPECIMEN GEOMETRY	NDE METHOD	PERTINENT PARAMETERS	90/95 CRACK LENGTH (IN.)
26					X-ray	After Etch and by Operator A	--
						Operator B	--
						Operator C	--
						Operator D	--
						Operator E	0.290
						Operator F	--
						Operator G	--
33	RI-SD, Martin Marietta, & GDC	2219-T87 Al	Fatigue Cracks	Flat Plate	Ultrasonics	After Etch and Merged Results of 5 Operators	0.079
34					Liquid Penetrant	After Etch and Merged Results of 7 Operators	0.093
35					Eddy Current	After Etch and Merged Results of 5 Operators	0.111
36	RI-BI Division (TFD-72-925)	Ti-6Al-4V	Fatigue Cracks	Flat Plate	Liquid Penetrant	Used P5F-1 Penetrant	0.072
37	(TFD-72-1005)					Used P5F-2	0.067
38	(TFD-72-1515)					Used P5F-2 and D100 Developer	0.070
39	(TFD-72-793)					Used P5F-2.5	0.050
40	(TFD-72-767)					Used P5F-2.5	0.068
41	(TFD-73-532)	7075-T6511 Al	Fatigue Cracks	Flat Plates		Used P5F-2.5, NQ-1	0.080
42	(TFD-73-532)					Used P5F-2.5, D100	
43	(TFD-73-496)						
44	(TFD-73-371)	Ti-6Al-4V	Fatigue Cracks Corroded	Welded Flat Plates	Ultrasonic, Shear Wave		0.068
45	(TFD-73-372)	4330V St.				Simulate Welded Flaws	0.083
46	(TFD-73-140)	PH17-4 St.				Simulate Flaws in Wrought St.	0.087
47	(TFD-72-768)	PH17-4 St.	Fatigue Cracks	Flat Plates			
48	RI-SD, MM, GDC, and RI-BI	2219-T87 and 7075-T6511 Al	Fatigue Cracks	Flat Plates	Liquid Penetrant	Merged Results from the Four Data Source on Al	0.095

TABLE 3.2.2 SUMMARY OF NDE DATA STATISTICALLY ANALYZED (Continued)

DATA SUB-SET	DATA SOURCE	MATERIAL TYPE	DEFECT TYPE	SPECIMEN GEOMETRY	NDE METHOD	PERTINENT PARAMETERS	90/95 CRACK LENGTH (IN.)
49	Lockheed, GA (TR-68-32)	4330V St.	Fatigue Cracks	Cylindrical	Liquid Penetrant	Laboratory Condition	--
50				Shell	Magniflux ZL-2, ZE-3, and ZP-4	Production Condition	--
51		7075-T6511 Al		7.62 cm in dia.		Laboratory Condition	--
52		4330V St.		0.64 cm thick	Mag. Particle	Laboratory Condition	--
53		4330V St.			Ultrasonic Shear Wave 5 MHz	Laboratory Condition	--
54		7075-T6511 Al			Ultrasonic Shear Wave	Laboratory Condition	--
55		7075-T6511 Al			X-ray	Laboratory Condition	--
56		4330V St.			X-ray	Laboratory Condition	--
57	Boeing, W. Kan.	7178-T651 Al	Fatigue Cracks	KC-135 Wings	Eddy Current	Laboratory Condition	--
					Hand Held E. C. Probe at Tear Dorn Insp. at Depot Level		
58					Results of Team 2 (Atypical of 3 more teams)		--
59					Results of Team 4 (Atypical)		--
60	Boeing Comm.	2024-T6 Al	Forge Closed	Tandem T	Liquid Penetrant	Production Insp.	--
61	Airplane Co.	4340 M St.	Forge Closed	Solid Cyl., Threaded	ZL-2A and 30A	Production Insp.	--
62	(TR-74-241)	4340 M St.	Forge Closed	Hollow Cyl., Filletted	ZE-4B;	Production Insp.	--
63		4340 M St.	Forge Closed	Hollow Cyl.,	ZP-9B	Production Insp.	--
64		4340 M ST	Forge Closed	Solid Cyl.	Plus Others	Production Insp.	--
65		2074-T6 Al	Forge Closed	Tandem T	Liquid Penetrant	Laboratory Insp.	0.070

TABLE 3.2.2 SUMMARY OF NDE DATA STATISTICALLY ANALYZED (Continued)

DATA SUB-SET	DATA SOURCE	MATERIAL TYPE	DEFECT TYPE	SPECIMEN GEOMETRY	NDE METHOD	PERTINENT PARAMETERS	90/95 CRACK LENGTH (IN.)
66		4340 M St.	Forged Closed	Solid Cyl., Threaded	ZL-2A and 30A;	Laboratory Insp.	0.230
67		4340 M St.	EDM Slots	Hollow Cyl., Filletted	ZE-4B;	Laboratory Insp.	0.310
68		4340 M St.	"	Hollow Cyl., ZP-9B;		--	--
69		4340 M St.	"	Solid Cyl., Filletted	Plus Others	0.090	0.090
70		4340 M St.	"	Solid Cyl., Filletted		0.160	0.160
71		2024-T6 Al	"	Tandem T	Ultrasonics	Production Insp.	0.210
72		4340 M St.	"	Solid Cyl., Threaded	5 and 10 MHz		
73		4340 M St.	"	Hollow Cyl. Filletted	Shear and Surface	--	--
74		4340 M St.	"	Hollow Cyl.	Wave	--	--
75		4340 M St.	"	Solid Cyl., Filletted		0.070	0.070
76		4340 M St.	"	Solid Cyl., Filletted		0.140	0.140
77		4340 M St.	"	Solid Cyl.	Ultrasonics	Laboratory Insp.	0.140
78		4340 M St.	"	Solid Cyl., Filletted	7 and 10 MHz	0.080	0.080
79		4340 M St.	"	Hollow Cyl., Filletted	Shear Surface Wave	0.100	0.100
80		4340 M St.	"	Hollow Cyl., Filletted	Wave	0.130	0.130
81		2024-T6 Al	"	Tandem T		0.170	0.170
82		4340 M St.	"	Solid Cyl., Filletted	X-ray	Production Insp.	--
83			"	Solid Cyl., Filletted		--	--
84			"	Hollow Cyl., Filletted		--	--

TABLE 3.2.2 SUMMARY OF NDE DATA STATISTICALLY ANALYZED (Continued)

DATA SUB-SET	DATA SOURCE	MATERIAL TYPE	DEFECT TYPE	SPECIMEN GEOMETRY	NDE METHOD	PERTINENT PARAMETERS	90/95 CRACK LENGTH (IN.)
85		2024-T6 Al	EDM Slots	Hollow Cyl., Filletted			--
86			"	Solid Cyl., Threaded			--
87		2024-T6 Al	"	Tandem T			--
88		4340 M St.	"	Solid Cyl.	X-ray	Laboratory Insp.	--
89		4340 M St.	"	Hollow Cyl., Filletted			--
90		4340 M St.		Solid Cyl., Filletted			--
91		4340 M St.		Hollow Cyl., Filletted			--
92		2024-T6 Al		Tandem T			0.110
93		4340 M St.	Forge Closed	Solid Cyl., Filletted	Mag. Particle	Production Insp.	0.120
94		4340 M St.	Forge Closed	Solid Cyl., Filletted			0.130
95		4340 M St.	EDM Slots	Hollow Cyl., Filletted			--
96		4340 M St.	"	Hollow Cyl., Filletted			--
97		4340 M St.	"	Solid Cyl., Threaded			--
98		4340 M St.	"	Solid Cyl., Threaded	Mag. Particle	Laboratory Insp.	0.120
99		4340 M St.	"	Hollow Cyl., Filletted			0.130
100		4340 M St.	"	Solid Cyl., Threaded			--
101		4340 M St.	"	Solid Cyl., Filletted			0.020
102		4340 M St.	"	Hollow Cyl., Filletted			0.100

TABLE 3.2.2 SUMMARY OF NDE DATA STATISTICALLY ANALYZED (Concluded)

DATA SUB-SET	DATA SOURCE	MATERIAL TYPE	DEFECT TYPE	SPECIMEN GEOMETRY	NDE METHOD	PERTINENT PARAMETERS	90/95 CRACK LENGTH (IN.)
103		4340 M St.	EDM Slots	Solid Cyl., Filletted	Eddy Current	Production Insp.	0.160
104		4340 M St.	"	Solid Cyl., Filletted	ED400 and 520 at f=100 KHz		0.300
105		4340 M St.	"	Hollow Cyl., Filletted			--
106		4340 M St.	"	Hollow Cyl., Filletted			--
107		2024-T6 Al	"	Tandem T			0.130
108		2024-T6 Al	"	Tandem T	Eddy Current	Laboratory Insp.	0.180
109		4340 M St.	"	Solid Cyl.	ED400 and 520 at f=100 KHz		0.200
110		4340 M St.	"	Hollow Cyl., Filletted			0.140
111		4340 M St.	"	Solid Cyl., Filletted			0.230
112		4340 M St.	"	Hollow Cyl.			--

TABLE 3.2.3
THRESHOLD CRACK LENGTHS (90/95 LIMITS IN
INCHES) FOR FATIGUE CRACKS IN FLAT PLATE
(REFERENCE 13)

	MATERIAL			
	2219-T87 Aluminum		7075-T6511 Aluminum	Ti-6Al-4V
	Before Etch	After Etch	0.070	0.070
Liquid Penetrant	0.262	0.095		
Ultrasonics	0.136	0.079		
Eddy Current	0.108	0.111		
Radiography	(1)	(1)		

(1) 90/95 limit not achieved.

TABLE 3.2.4
THRESHOLD CRACK LENGTHS (90/95 LIMITS IN INCHES) FOR
ALUMINUM, FORGE CLOSED DEFECT TYPE (REFERENCE 13)

	LABORATORY CONDITION	PRODUCTION CONDITION
Liquid Penetrant	0.02	(1)
Ultrasonic	0.17	0.21
Eddy Current	0.18	0.13
X-Ray	0.11	(1)

(1) 90/95 limit not achieved.

TABLE 3.2.5
THRESHOLD CRACK LENGTHS (90/95 LIMITS IN INCHES) FOR
4340 M STEEL, FORGE CLOSED DEFECT TYPES (REFERENCE 13)

		Solid Cylinder			Hollow Cylinder	
		Straight	Filletted	Threshold	Straight	Filletted
Liquid Penetrant	Laboratory Production	0.16 (1)	0.09	0.23 (1)	(1) (1)	0.31 (1)
Ultrasonic	Laboratory Production	0.14 0.14	0.09 0.07	(1)	0.10 (1)	0.13 0.13
Eddy Current	Laboratory Production	0.20 0.16	0.23 0.30		(1) (1)	0.14 (1)
Magnetic Particle	Laboratory Production	0.12 0.12	0.07 0.13	(1) (1)	0.10 (1)	0.13 (1)
X-Ray	Laboratory Production	(1) (1)	(1) (1)	(1)	(1) (1)	(1) (1)

(1) 90/95 limit not achieved

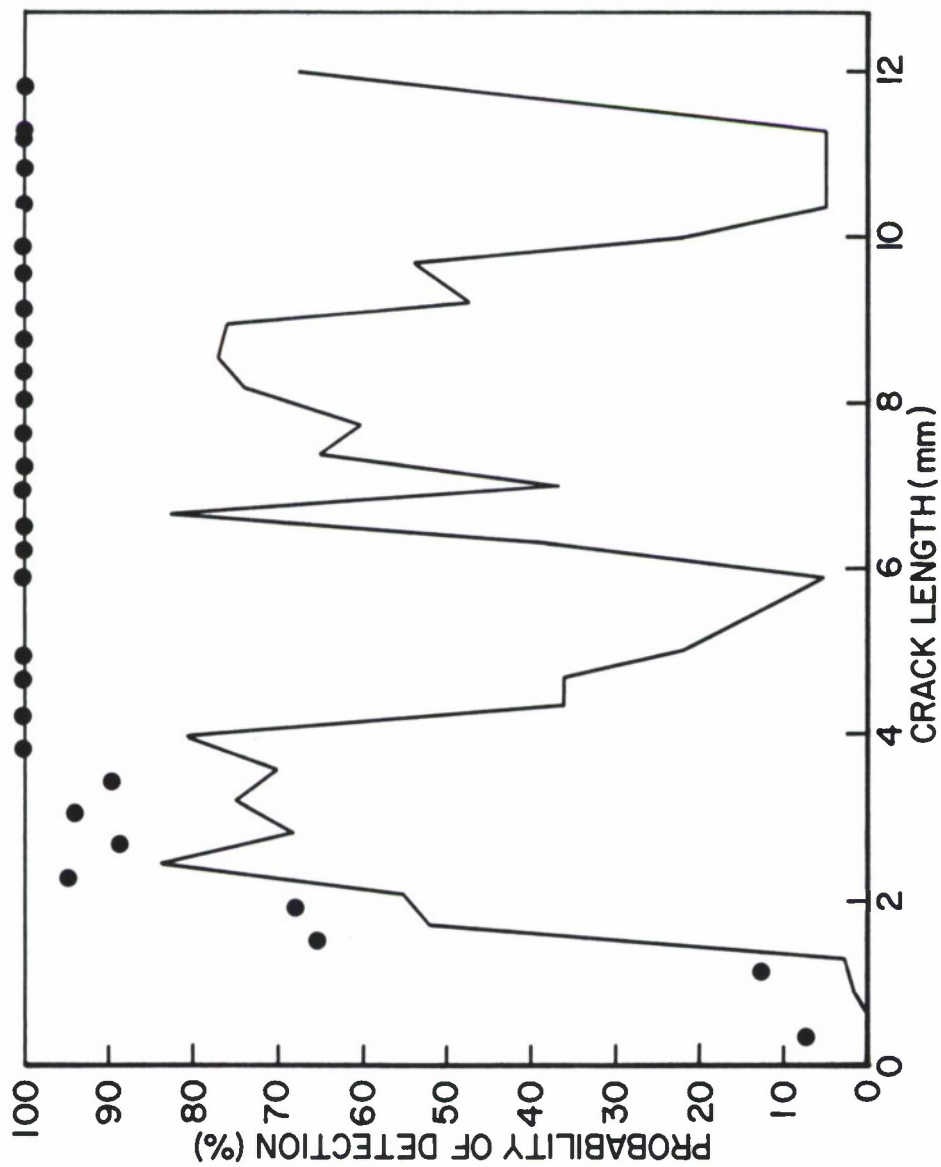


Figure 3.2.1. Range Interval Method as Applied to Eddy Current Inspections of Aluminum Plates-1 Inspection Per Crack (Reference 13).

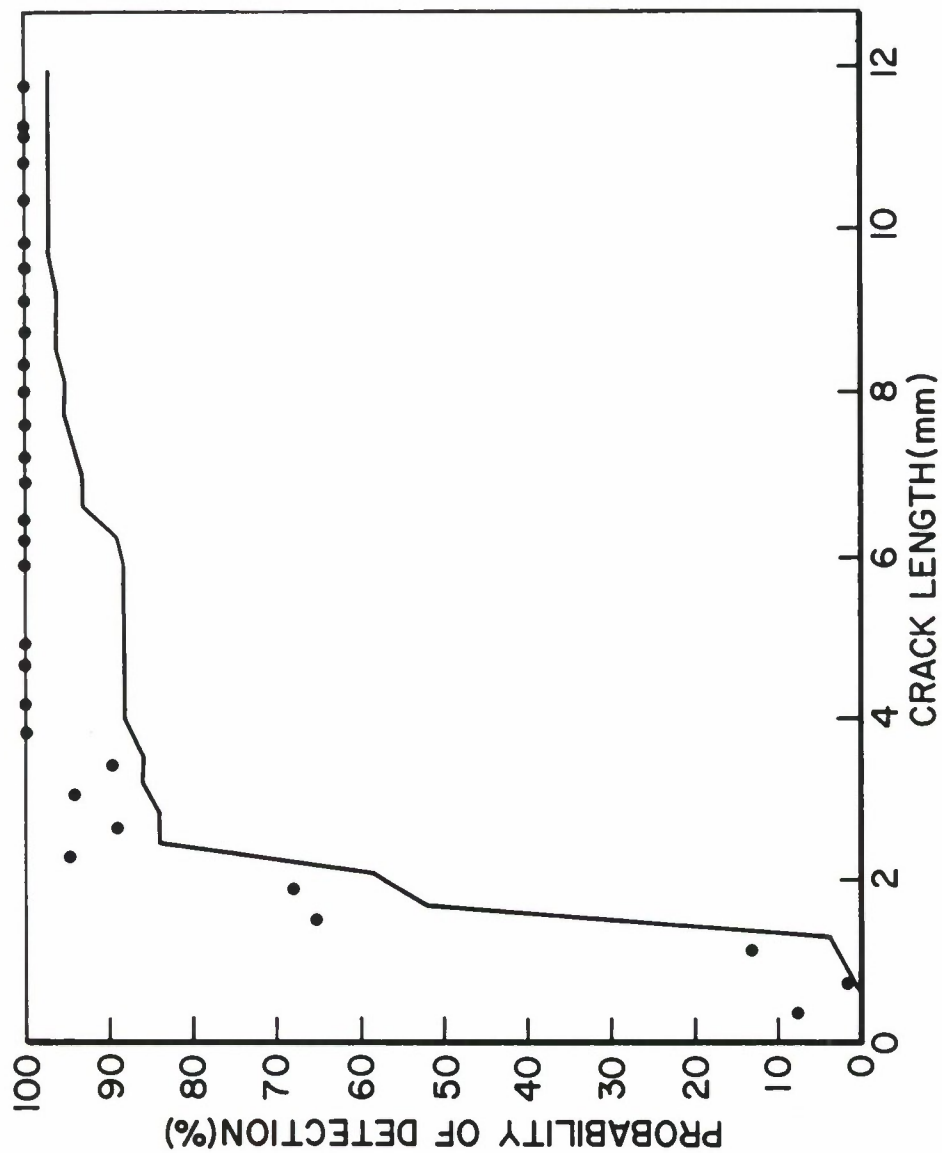


Figure 3.2.2. Optimized Probability Method as Applied to Eddy Current Inspections of Aluminum Plates- 1 Inspection Per Crack (Reference 13).

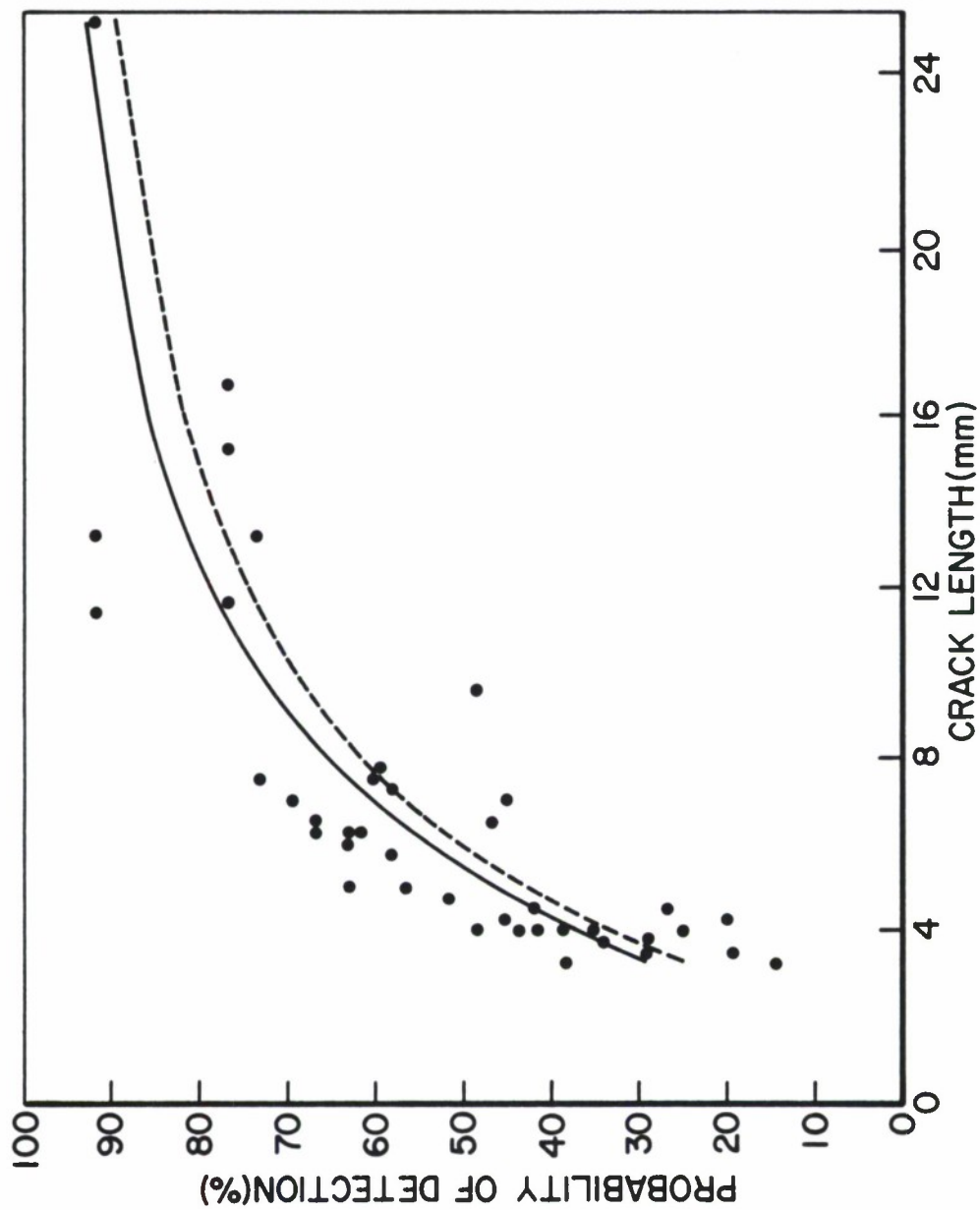


Figure 3.2.3. Regression Method as Applied to Eddy Current Inspection of Fastener Holes- 60 Inspections Per Crack (Reference 8).

METHOD	MEASURES OR DEFECTS	APPLICATIONS	ADVANTAGES	LIMITATIONS
Magnetic particles	Surface and slightly subsurface defects; cracks, seams, porosity, inclusions Permeability variations Extremely sensitive for locating small, tight cracks	Ferromagnetic materials, bar, forgings, weldments, extrusions, etc.	Advantage over penetrant in that it indicates subsurface defects, particularly inclusions Relatively fast and low cost May be portable	Alignment of magnetic field is critical Demagnetization of parts required after tests Parts must be cleaned before and after inspection Masking by surface coatings
Liquid Penetrant	Defects open to surface of parts; cracks, porosity, seams, laps, etc. Through-wall leaks	All parts with non-absorbing surfaces (forgings, weldments, castings, etc.). Note: Bleed-out from porous surfaces can mask indications of defects	Low cost Portable Indications may be further examined visually Results easily interpreted	Surface films, such as coatings, scale, and smeared metal may prevent detection of defects Parts must be cleaned before and after inspection Defect must be open to surface
Ultrasonic (0.125 MHz)	Internal defects and variations; cracks, lack of fusion, porosity, inclusions, delaminations, lack of bond, texturing Thickness or velocity Poisson's ratio, elastic modulus	Wrought metals Welds Brazed joints Adhesive-bonded joints Nonmetals In-service parts	Most sensitive to cracks Test results known immediately Automating and permanent record capability Portable High penetration	Couplant required Small, thin, complex parts may be difficult to check Reference standards required Trained operators for manual inspection Special probes
Eddy Current (200 Hz to 6 MHz)	Surface and sub-surface cracks and seams Alloy content Heat treatment variations Wall thickness, coating thickness Crack depth Conductivity Permeability	Tubing Wire Ball bearings "Spot checks" on all types of surfaces Proximity gage Metal detector Metal sorting Measure conductivity in % IACS	No special operator skills required High speed, low cost Automation possible for symmetrical parts Permanent record capability for symmetrical parts No couplant or probe contact required	Conductive materials Shallow depth of penetration (thin walls only) Masked or false indications caused by sensitivity to variation, such as part geometry, lift-off Reference standards required Permeability variations
Radiography (X-rays-film)	Internal defects and variations; porosity; inclusions; cracks; lack of fusion; geometry variations; corrosion thinning Density variations Thickness, gap and position Misassembly Misalignment	Castings Electrical assemblies Weldments Small, thin, complex wrought products Nonmetals Solid propellant rocket motors Composites	Permanent records; film Adjustable energy levels (5 kv-25 mev) High sensitivity to density changes No couplant required Geometry variations do not effect direction of X-ray beam	High initial costs Orientation of linear defects in part may not be favorable Radiation hazard Depth of defect not indicated Sensitivity decreases with increase in scattered radiation

Figure 3.2.4. Summary and Comparison of Nondestructive Testing Methods (Reference 1).

3.3 PROOF TEST DETERMINATIONS

Tiffany and Masters ⁽¹⁸⁾ first suggested that the conventional structural proof test could be used to inspect for crack damage that would eventually lead to catastrophic failure. Air Force acceptance of this proof test philosophy has been stimulated by the inability of alternate non-destructive inspection tools to reliably detect cracks of near-critical size. The Air Force in the recent past has employed the proof test as a means of determining the maximum possible initial flaw that could exist in the structural subsystems identified in Table 3.3.1. Note that almost all of the examples cited represent the application of the proof stress techniques as an In-service Inspection. References 19 through 23 document the Table 3.3.1 and other Air Force uses of the crack-inspection proof test. Reference 24 documents the recent Navy proof test of an A-7 arresting hook; this proof test is periodically repeated to ensure the continuing structural integrity of the component.

The proof test concept for all applications has been to size or eliminate the life degrading damage so that the structure would maintain its required level of structural integrity throughout a defined period of usage. However, due to substantially different technical requirements, the proof testing techniques employed in each case were different. The technical requirements which establish the type of tests conducted have been structural geometry, material properties, type of crack damage present in the structure, as well as the crack growth mechanism.

3.3.1

TABLE 3.3.1

PROOF TESTING OF AIRCRAFT STRUCTURES

SYSTEM	SUBSYSTEM	DAMAGE	SPECIAL TECHNIQUES
F-111	Lower surface of inner wings and pivot fittings	Potential forging defects propagated due to fatigue in D6AC steel	Upwing bending at 40°F after every 1,000 hours of flight
B-1A	F-101 (Development) Engine Combustor Case	Pores and inclusion stringers in circumferential butt welds in Inconel 901 alloy	Internal pressure to 200% Operating Pressure
B-52D	Center and inner wing structure	Fatigue and stress corrosion cracks nucleated during South East Asia service in 7075-T6 and 7079-T6 aluminum alloy structure	Down and up-wing bending at ambient temperature
C-141	Main Landing Gear (Cylinder)	Hydrogen entrapped during refurbishment	500 hours of continuous static loading to initiate and propagate cracks to failure
A-7	Carrier arresting hook (Navy)	Fatigue cracking initiated during service	Repeat periodically

3.3.1 Description of the Proof Test Method

Tiffany and Masters ⁽¹⁸⁾ utilized the proof test as a means of guaranteeing that a potentially cracked structure would not fail during a defined period of operation. This guarantee results from the fact that all the cracks remaining in a proof-loaded structure must be smaller than those cracks which would have failed the structure during the proof test. Since proof test loadings are typically larger than the maximum operating conditions, the post proof-tested structure's cracks are also expected to be substantially smaller than the cracks which would cause failure under operating loads.

Figure 3.3.1 schematically illustrates a stress-crack length diagram which defines the levels of loading (proof stress and operational maximum stress) and the corresponding crack lengths associated with structural failure by fracture. It can be noted from Figure 3.3.1 that all cracks larger than a_1 will cause the structure to fail during the proof test loading, thus guaranteeing a "minimum" safe crack growth interval between a_1 and the crack size (a_{op}) at which the operating conditions will cause failure. The interval established is the minimum safe interval because the structure may initially have cracks that are substantially smaller than the guaranteed initial size (a_1).

Tiffany and Masters ⁽¹⁸⁾ designed the proof test conditions so that all cracks initially present in the structure and of sufficient size that they could grow to failure during the planned service operating period would fail the structure during the proof test. If the operating conditions and the crack growth

mechanisms are known, then a crack growth life calculation can be performed to establish the minimum safe crack growth interval during which failure will not occur during service. The minimum safe crack growth interval extends from the largest allowable initial crack size (a_i^*) and the crack size (a_{op}).

Figure 3.3.2 describes the interrelationship between the crack growth life and residual strength behavior of a structure and the stress-crack size diagram. As indicated in Figure 3.3.2 (right-hand side), the life limit associated with the crack growth process and the decay of the residual strength capability is lower than the service life requirement. An increase in the proof stress is required, therefore, to decrease the corresponding crack size (a_i) to the maximum allowable crack size (a_i^*) and thus ensure a safe period of operation. Note that the stress-crack size diagram indicates that all cracks greater than a_i , present at the time of the proof test, will cause structure failure. Thus, the proof test ensures that when the structure enters service, its initial cracks will be no larger than the size associated with the proof test conditions.

The levels of proof test stress and the material's fracture toughness combine to establish the maximum initial crack size guaranteed by the proof test. Because material and stress variations will exist throughout any proof loaded structure, the designer of a proof test must be aware of several important material variations which could significantly affect the post-proof test crack size distribution. These important material variations are caused by changes in temperature, loading rate, thickness, and yield strength.

Figure 3.3.3 schematically describes how fracture toughness varies as a

function of these parameters. Note that temperature and loading rate can affect some materials (some steels and titanium alloys are particularly susceptible) while other materials are unaffected. Aluminum alloys and many nickel-base alloys exhibit almost no variation in fracture toughness as a function of temperature and strain rate.)

Figure 3.3.4 provides an example of how a material's response to external stimuli can be utilized to increase the minimum safe crack growth interval. In Figure 3.3.4, a material's known response to temperature is utilized to select a low temperature condition for conducting the proof test. The lower fracture toughness exhibited at the low temperature is shown to extend the minimum safe crack growth interval substantially beyond what would have been expected for the same proof stress at the operating temperature conditions.

As stated by MIL-A-83444 (3.1.1.1), "the minimum assumed initial flaw size shall be the calculated critical size at the proof test stress level and temperature using procuring activity approved upper-bound of the material fracture toughness data." The concept of using an approved upper-bound for the fracture toughness ensures a worst case assumption for the maximum allowable initial crack size (see Figure 3.3.5) and the minimum safe crack growth interval (See Figure 3.3.6). Figure 3.3.6 summarizes the MIL-A-83444 requirements for establishing the minimum safe crack growth interval for the NDE proof test conditions.

Consider the data provided in Figure 3.3.7 which defines the plane strain fracture toughness for a number of aluminum alloys (Reference 25). The fracture toughness values presented are representative averages as well as minimum and maximum values obtained from test data collected for the individual alloys and heat temperature conditions shown. From the data presented in Figure 3.3.7, it does not appear that there is that much variation between the minimum, the average and the maximum values of fracture toughness. However, the supporting text in Reference 25 notes that the fracture toughness values given do not have the statistical reliability of the typical mechanical properties (yield strength, elastic modulus, etc.) given in MIL-HDBK-5C. The lack of precision in defining the fracture toughness upper-bound required by MIL-A-83444 might be overcome if the upper-bound is estimated with a statistical definition that is agreed to by the procuring agency.

3.3.2 Examples

Two examples are now presented to illustrate how the proof test might be used. The first example describes how a proof stress condition might be chosen to find specific crack sizes. The second example describes a typical situation whereby the proof test must be designed to guarantee a service life interval.

EXAMPLE 3.3.1 Proof Test Stress-Crack Length Relationships

For the radially-through-thickness cracked structure illustrated in Figure 3.3.8, answer the following questions:

(a) What proof stress (σ_p) is required at room temperature to guarantee that the maximum crack size is less than 0.05 inches. Also define the ratio of proof to operating stress conditions ($\alpha = \sigma_p / \sigma_{op}$).

(b) For a proof test conducted at -40°F , define the proof stress and proof stress ratio associated with finding a crack with length 0.05 in.

(c) If the proof test ratio is 1.5, what is the minimum flaw size that will be detected at room temperature?

SOLUTION:

The equation that governs the solution to all three questions is the Irwin fracture criterion, i.e.,

$$K = K_{IC} \quad (3.3.1)$$

where

$$K = \sigma \sqrt{\pi a} \cdot F(a/r) \quad (3.3.2)$$

with $F(a/r)$ and the material properties defined in Figure 3.3.8.

To address the questions, parts a and b, Equations 3.3.1 and 3.3.2 are solved for the proof stress σ_p , i.e.

$$\sigma_p = \frac{K_{IC}}{\sqrt{\pi a} \cdot F(a/r)} \quad (3.3.3)$$

for the given K_{IC} conditions at temperature and for a 0.05 inch long crack, i.e. "a" in Equation 3.3.3 is 0.05 inch. So for room temperature, the proof

stress is

$$\sigma_p = \frac{40}{\sqrt{\pi(0.05)} \cdot (2.34)} = 43.1 \text{ ksi} \quad (3.3.3a)$$

and for -40°F the proof stress is

$$\sigma_p = \frac{35}{\sqrt{\pi(0.05)} \cdot (2.34)} = 37.7 \text{ ksi} \quad (3.3.3b)$$

In both cases, the proof stress is well below the yield strength; however, it might be noted that localized yielding at stress concentrations could occur at these levels. The proof stress ratios (α) are 1.23 and 1.08 for the room temperature and -40°F proof test conditions, respectively. To address the third part of the question, it is necessary to solve Equation 3.3.3 for crack length (a), i.e.

$$a = \frac{1}{\pi} \left(\frac{K_{IC}}{\sigma_p} \right)^2 \left[\frac{1}{F(a/r)} \right]^2 \quad (3.3.4)$$

Because Equation 3.3.4 involves crack length in the function F in a complicated fashion, the equation is solved iteratively for the given material and stress conditions, i.e. $K_{IC} = 40 \text{ ksi } \sqrt{\text{in}}$ and $\sigma_p = 1.50 \times (35) = 52.5 \text{ ksi}$. Thus,

$$a = \frac{1}{\pi} \left(\frac{40}{52.5} \right)^2 \left[\frac{1}{F\left(\frac{a}{r}\right)} \right]^2 \quad (3.3.4a)$$

A series of several trials are shown in Table 3.3.2 where a match of the right and left side of Equation 3.3.4a is achieved when $a \approx 0.0245$ inches. Thus, 0.0245 inch long cracks can be found for a proof test ratio of 1.50.

TABLE 3.3.2
TRIAL AND ERROR SOLUTION OF EQUATION 3.3.4a

a (left-hand side) (inch)	a/r	F(a/r)	a(right-hand side) (inch)
0.020	0.08	2.835	0.0230
0.025	0.10	2.733	0.0247
0.030	0.12	2.641	0.0265
0.0255	0.102	2.723	0.0249
0.0245	0.098	2.743	0.0246

In the above solutions, it is seen that in some cases the proof stress is sufficiently large such that yielding can be expected at the edge of the hole and other stress concentration sites. The reader is cautioned that linear elastic fracture mechanics (LEFM) techniques such as applied in Equation 3.3.1-3.3.4 should not be utilized when extensive local yielding occurs except to obtain first-order estimates of the crack length. From a proof test standpoint, the LEFM estimates of the minimum crack length will be actually larger than those screened by loading the structure to the proof condition, assuming load control conditions, and thus conservative.

EXAMPLE 3.3.2 Proof Test Conditions to Guarantee Life

The pressure vessel shown in Figure 3.3.9 has a semicircular surface crack of unknown size located in the longitudinal direction. This vessel is subjected to an on-off pressure loading condition of the type illustrated in Figure 3.3.10 and is made of a structural steel with the mechanical properties shown in Figure 3.3.11.

For economic purposes, it has been decided that the structure will only be inspected yearly and the inspection procedure has been chosen to be a proof test. You have been asked to select the proof pressure level that will guarantee that this vessel will not fail during the interval between proof test inspections subject to the crack/loading/material property assumptions.

SOLUTION:

It is first necessary to calculate the gross stress in the section of the structure where the crack is located. From any standard strength of materials text, it is determined that for a pressure (p) of 2,000 psi the maximum operating stress (σ) for the vessel with an outside diameter of 40 inch and a thickness (B) of 0.4 inch is given by

$$\sigma_{\max} = \frac{p D}{2 B} = \frac{(2000) (40)}{2 (0.4)} = 100,000 \text{ psi} \quad (3.3.5)$$

or 100 ksi, and the range of stress is

$$\Delta\sigma = 0.75 \sigma_{\max} = 75 \text{ ksi} \quad (3.3.6)$$

For the semicircular crack partly through the vessel wall, the stress-intensity factor is given by

$$K = 1.12 \left(\frac{2}{\pi}\right) \sigma \sqrt{\pi a} \quad (3.3.7)$$

neglecting the back surface correction factor. Assume for illustrative purposes that Equation 3.3.7 can be considered a reasonable estimate of the true stress-intensity factor at all depths through the thickness. As a first step, determine if the structure will leak before it breaks by calculating the stress-intensity factor for the condition where the crack depth is equal to the thickness. Thus, with Equation 3.3.7 and $\sigma = 100$ ksi and $a = 0.4$ in.,

$$\begin{aligned} K &= 1.12 \left(\frac{2}{\pi}\right) (100) \sqrt{\pi(0.4)} \\ &= 79.9 \text{ ksi } \sqrt{\text{in}} \end{aligned} \quad (3.3.7a)$$

which is less than $K_{IC} = 90 \text{ ksi } \sqrt{\text{in}}$ and thus the vessel might leak before fracturing. Consider, however, the potential cracking situation that occurs if the semicircular crack penetrates the wall and immediately transitions to a through thickness crack as shown in Figure 3.3.12. An analysis indicates that $K \approx 112 \text{ ksi } \sqrt{\text{in}}$ which is greater than K_{IC} . Thus, given this situation, the vessel will fail catastrophically.

To establish the crack size associated with the proof test, one must conduct a life analysis which works from the final crack size ($a = 0.4$ inch) backwards until the one-year life interval (a two-year life interval with the factor of two life margin) is guaranteed. The life analysis that is conducted illustrates an incremental crack length method that uses the iterative equation

$$\text{Life} = \sum_{i=1}^n \left[\frac{\Delta a_i}{\left| \frac{da}{dt} \right|_i} \right] \text{ (days)} \quad (3.3.8)$$

where the increments of crack length (Δa_i) and crack growth rate values

$(da/dt|_i)$ are chosen to be compatible.

On the basis of the materials data described in Figure 3.3.11, one must assume that both a fatigue and a stress-corrosion cracking mechanism are active (see Chapter 5 for discussion on these mechanisms). The fatigue crack growth rate behavior can be described using the power law

$$\frac{da}{dN} = 3.3 \times 10^{-10} \Delta K^{2.959} \text{ (in/cycle)} \quad (3.3.9)$$

On the basis of the data in Figure 3.3.11, Equation 3.3.9 is restricted to the range $10 \leq \Delta K \leq 90 \text{ ksi } \sqrt{\text{in}}$, and to the stress ratio (R) of 0.25 which is compatible with the loading cycle given in Figure 3.3.10. The stress-corrosion cracking rate data in Figure 3.3.11 can be described with the power law

$$\left. \frac{da}{dt} \right|_{\text{cor}} = 9.24 \times 10^{-15} K_{\text{max}}^{5.798} \text{ (in/day)} \quad (3.3.10)$$

which is valid for sustained loading conditions when K_{max} is between the threshold of stress corrosion cracking ($K_{\text{Isc}} = 65 \text{ ksi } \sqrt{\text{in}}$) and the fracture toughness level ($K_{\text{IC}} = 90 \text{ ksi } \sqrt{\text{in}}$).

As a first approximation of the effect of combined stress corrosion action and fatigue crack growth, the linear summation hypothesis of Wei-Landes is suggested (See Chapter 5):

$$\left. \frac{da}{dt} \right|_{\text{total}} = \left. \frac{da}{dt} \right|_{\text{cor}} + \left. \frac{da}{dt} \right|_{\text{fat}} \quad (3.3.11)$$

where the time based fatigue crack growth rate is obtained from

$$\left. \frac{da}{dt} \right|_{\text{fat}} = f \cdot \frac{da}{dN} \quad (3.3.12)$$

whereby the cycle-dependent component from Equation 3.3.9 is multiplied by the cyclic frequency (f). It is also to be noted that the stress-corrosion cracking rate contribution for a day in service is one-half that established by Equation 3.3.10 since the vessel is only loaded to the maximum pressure only half the time.

There are a number of ways that Equation 3.3.8 can be used to establish the crack length-life relationship. The method for this example will be to choose equal increments of K_{\max} between the crack size at failure and the other crack lengths established to obtain the Δa_i values. Table 3.3.3 describes the relationships between the maximum stress-intensity factor and the crack length, the crack length increment, the average values of the maximum stress-intensity factor (\bar{K}_{\max}) and stress-intensity factor range ($\overline{\Delta K}$).

TABLE 3.3.3
CRACK INTERVAL TABLE FOR EQUATION 3.3.6

K_{\max} (ksi $\sqrt{\text{in.}}$)	55	60	65	70	75	80
a (inch)	0.189	0.225	0.264	0.307	0.352	0.400
Δa (inch)		0.036	0.039	0.043	0.045	0.048
\bar{K}_{\max}^* (ksi $\sqrt{\text{in.}}$)		57.5	62.5	67.5	72.5	77.5
$\overline{\Delta K}^*$ (ksi $\sqrt{\text{in.}}$)		43.1	46.9	50.6	54.4	58.1

* Average values for the interval

The calculations of crack length a in Table 3.3.3 are directly related to K_{\max} through the equation

$$a = \left[\frac{K_{\max}}{1.12 \left(\frac{2}{\pi}\right) \sigma_{\max} \sqrt{\pi}} \right]^2 \quad (3.3.13)$$

which when solved for a typical value of K_{\max} , say 55 Ksi $\sqrt{\text{in}}$, the crack length becomes

$$a = \left[\frac{55}{1.12 \left(\frac{2}{\pi}\right) 100 \sqrt{\pi}} \right]^2 = 0.189 \text{ inch} \quad (3.3.13a)$$

The difference in crack lengths (Δa) comes from subtracting the two corresponding crack lengths. The values of \bar{K}_{\max} are computed by averaging the two corresponding K_{\max} values, e.g. 62.5 Ksi $\sqrt{\text{in}} = 0.5 (60 + 65)$. The values of $\bar{\Delta K}$ are computed from the relationship $\Delta K = (1-R) K_{\max}$ where R is the stress ratio (0.75).

Table 3.3.4 presents the fatigue crack growth rate contribution to Equation 3.3.11 and Table 3.3.5 presents the stress corrosion cracking contribution. The growth rate data are based on Equations 3.3.9 and 3.3.10, respectively.

TABLE 3.3.4
FATIGUE CRACK GROWTH RATE CONTRIBUTION

$\overline{\Delta K}$ (ksi $\sqrt{\text{in}}$)	$\frac{da}{dN}$ (in/cycle)	$\frac{da}{dt} _{\text{fat}} = \frac{5 \text{ cycles}}{\text{day}} \times \frac{da}{dN}$ (in/day)
43.1	2.26×10^{-5}	1.13×10^{-4}
46.9	2.91×10^{-5}	1.46×10^{-4}
50.6	3.64×10^{-5}	1.82×10^{-4}
54.4	4.51×10^{-5}	2.25×10^{-4}
58.1	5.48×10^{-5}	2.74×10^{-4}

TABLE 3.3.5
STRESS-CORROSION CRACKING RATE CONTRIBUTION

$\overline{K}_{\text{max}}$ (ksi $\sqrt{\text{in}}$)	$\frac{da}{dt}$ (in/day)	$\frac{da}{dt} _{\text{cor}}$ (in/day)
57.5	0*	0
62.5	0*	0
67.5	3.73×10^{-4}	1.86×10^{-4}
72.5	5.65×10^{-4}	2.82×10^{-4}
77.5	8.3×10^{-4}	4.16×10^{-4}

* $\overline{K}_{\text{max}}$ is below K_{Isc} and therefore no growth occurs

Sample calculations for Tables 3.3.4 and 3.3.5 are not presented. In Table 3.3.4, the $\bar{\Delta}K$ values are taken from Table 3.3.3 and cover each of the consecutive intervals of crack length. From Equation 3.3.9, the crack growth fatigue rate for a stress-intensity range of 43.1 is

$$\frac{da}{dN} = 3.3 \times 10^{-10} (43.1)^{2.959} = 2.26 \times 10^{-5} \frac{\text{in}}{\text{cycle}} \quad (3.3.9a)$$

The calculations of $\frac{da}{dt}|_{\text{fat}}$ follow directly from multiplying the fatigue crack growth rates by the frequency of load application (5 cycles/day).

In Table 3.3.5, the \bar{K}_{max} values are taken from Table 3.3.3 and cover each of the consecutive intervals of crack length. From Equation 3.3.10, the sustained load stress corrosion cracking growth rate is

$$\frac{da}{dN} = 9.24 \times 10^{-15} (67.5)^{5.798} = 3.73 \times 10^{-4} \text{ in/day} \quad (3.3.10a)$$

The calculations of the corrosion contribution to Equation 3.3.11 are given in the table. These come directly from the fact that the structure is only loaded into the range where stress corrosion cracking occurs for one-half of the time (on-off cycling) so the $da/dt|_{\text{cor}}$ numbers are one-half those given in the middle column.

The total contribution to cracking behavior is calculated from Equation 3.3.11, and the individual crack increments in Equation 3.3.8 are used to establish the time that it takes to grow the crack through the successive intervals. The appropriate calculations are reported in Table 3.3.6

TABLE 3.3.6
ESTIMATING THE TIME TO GROWTH THROUGH SUCCESSIVE INTERVALS

Δa (inch)	$\frac{da}{dt} _{\text{total}}$ (in/day)	Δt (days)	a (inch)	$t = \sum \Delta t$ (days)
0.036	1.13×10^{-4}	318.6	0.189	861.1
0.039	1.46×10^{-4}	267.8	0.225	542.5
0.042	3.68×10^{-4}	114.9	0.264	274.7
0.045	5.07×10^{-4}	89.5	0.307	159.8
0.048	6.9×10^{-4}	70.3	0.352	70.3
			0.400	0

The crack length increment (Δa) and the crack length (a) values given in Table 3.3.6 come from Table 3.3.3. The total crack growth rate ($da/dt|_{\text{total}}$) values come from Equation 3.3.11 where the individual contributions to Equation 3.3.11 come from Tables 3.3.4 and 3.3.5, e.g.

$$\frac{da}{dt}|_{\text{total}} = 5.07 \times 10^{-4} \frac{\text{in}}{\text{day}} = 2.25 \times 10^{-4} + 2.82 \times 10^{-4} \quad (3.3.11a)$$

for $\Delta a = 0.045$ inch and a between 0.307 and 0.352 inch. The increment of time required to propagate the crack through this interval is obtained from

$$\Delta t = \frac{\Delta a}{\frac{da}{dt} \Big|_{\text{total}}} = \frac{0.045 \text{ in}}{5.07 \times 10^{-4} \frac{\text{in}}{\text{day}}} = 89 \text{ days} \quad (3.3.14)$$

The total time that it takes to grow through successive intervals is obtained by summing the results from Equation 3.3.14 for each interval using Equation 3.3.14 for each interval using Equation 3.3.8.

The data from Table 3.3.6 that relates crack length (a) to the total time (t) to failure shows that the proof test must find a crack length between 0.189 and 0.225 inch to guarantee the integrity of the vessel with a factor of two life margin. The crack length versus total time to failure data have been graphically displayed in Figure 3.3.13, where it can be seen that for one year of growth the crack length is 0.245 inch (and for a factor of two life margin the crack length is 0.20 inch). The required proof stress for the 0.20 inch long crack length is obtained from the Irwin criterion:

$$\sigma_p = \frac{K_{IC}}{1.12 \left(\frac{2}{\pi} \right) \sqrt{\pi a}} = \frac{90}{1.264 \sqrt{(0.2)}} \quad (3.3.13)$$

which is about 80 percent of the yield strength and therefore, the proof pressure (p_p) must be at least

$$\begin{aligned} p_p &= \frac{2\sigma_p B}{D} = \frac{2(159,200)(0.4)}{40} \\ &= 3185 \text{ psi} \end{aligned} \quad (3.3.14)$$

to ensure that all semicircular cracks longer than 0.2 inch are removed from the center section of the vessel prior to operation.

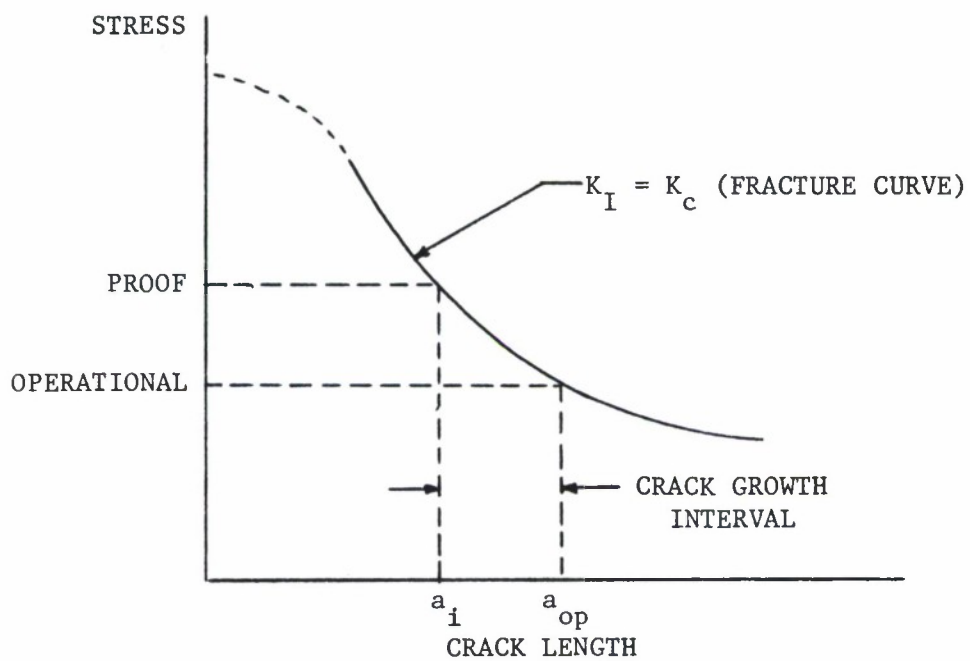


Figure 3.3.1. Fracture Critical Curve Defining Relationship Between Stress and Crack Length Associated with Fracture.

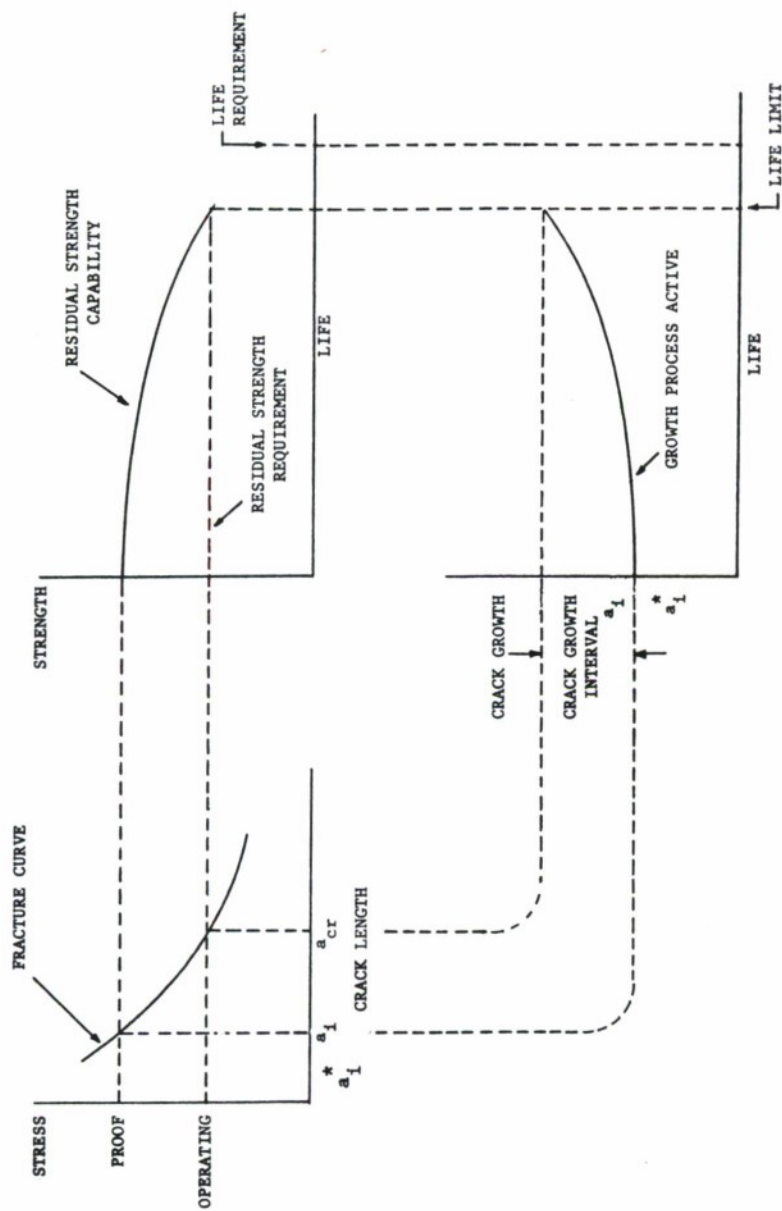


Figure 3.3.2. Schematic Illustrating the Relationship Between the Proof Test Diagram, the Residual Strength Capability and Crack Growth Life Interval.

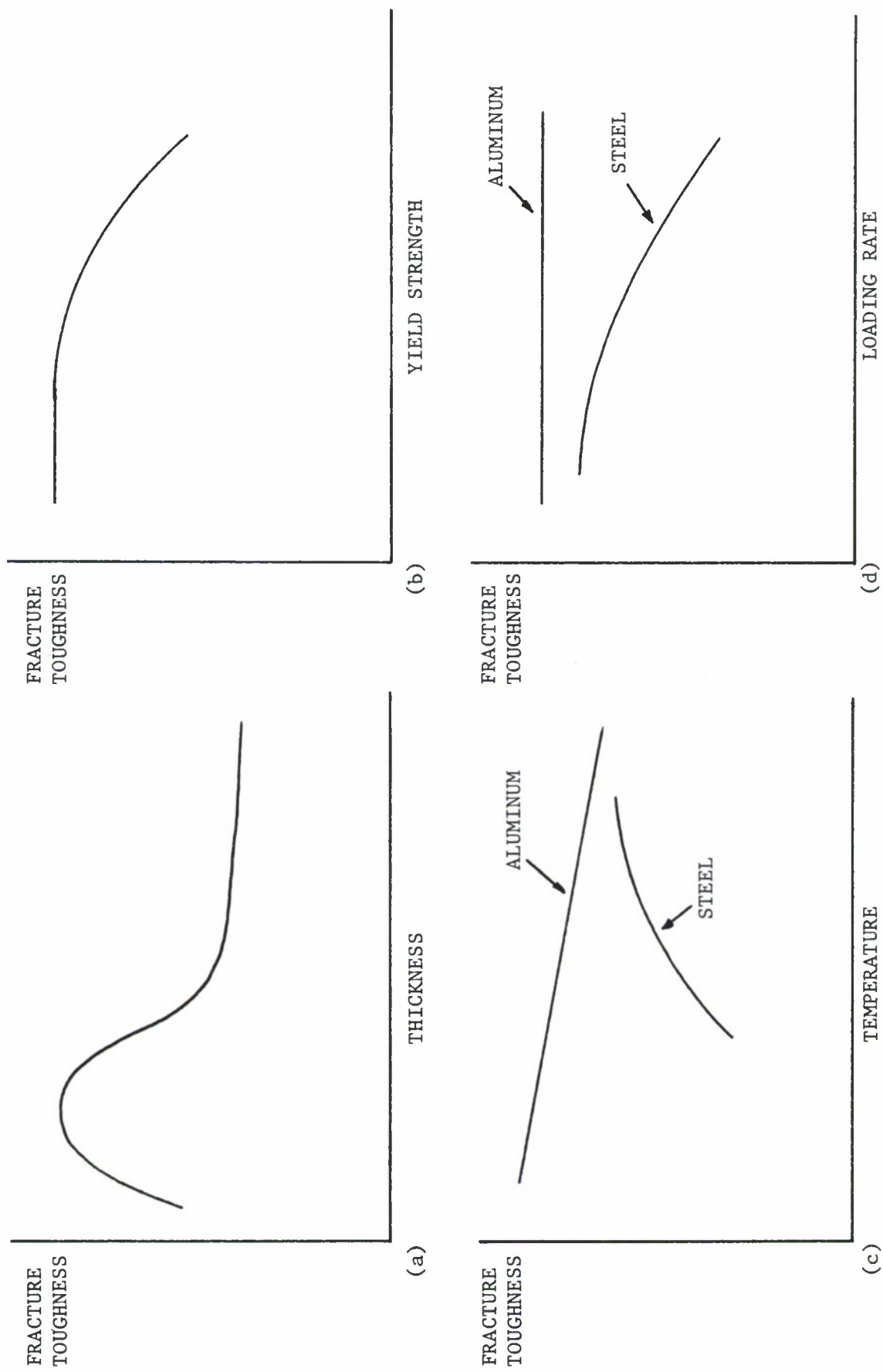


Figure 3.3.3. Fracture Toughness Varies as a Function of (a) Thickness, (b) Yield Strength, (c) Temperature, and (d) Loading Rate.

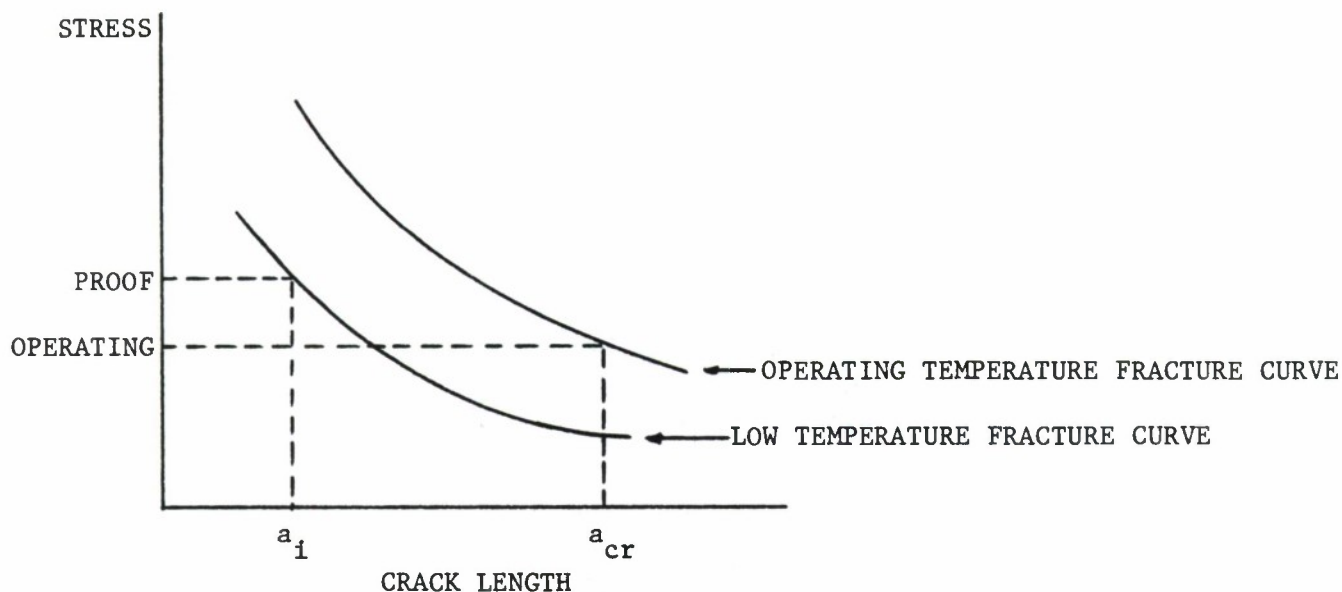


Figure 3.3.4. Using a Material's Low Temperature Fracture Sensitivity to Decrease Initial Crack Size and thus Increase the Minimum Safe Crack Growth Interval for a Given Proof Stressing Condition.

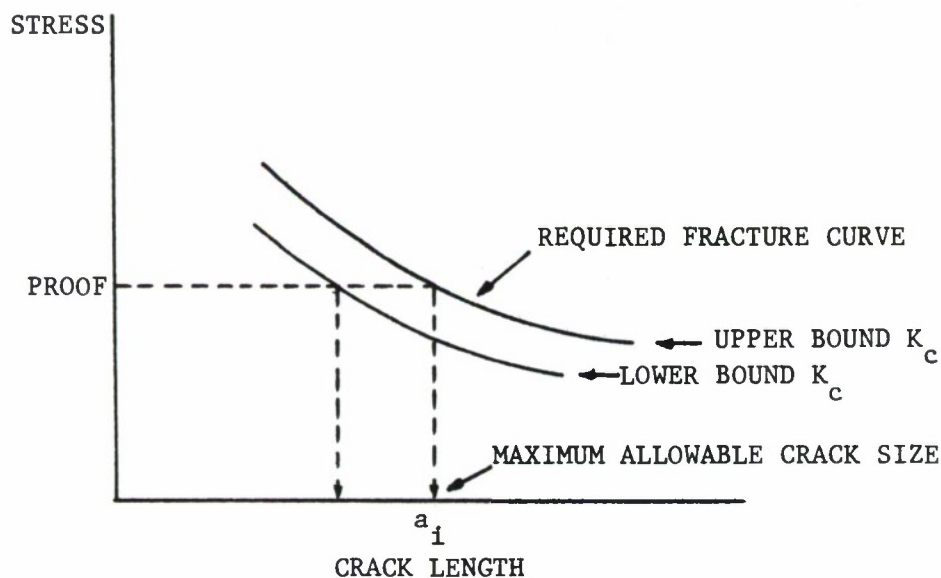


Figure 3.3.5. Influence of Fracture Toughness Variation on the Maximum Allowable Crack Size.

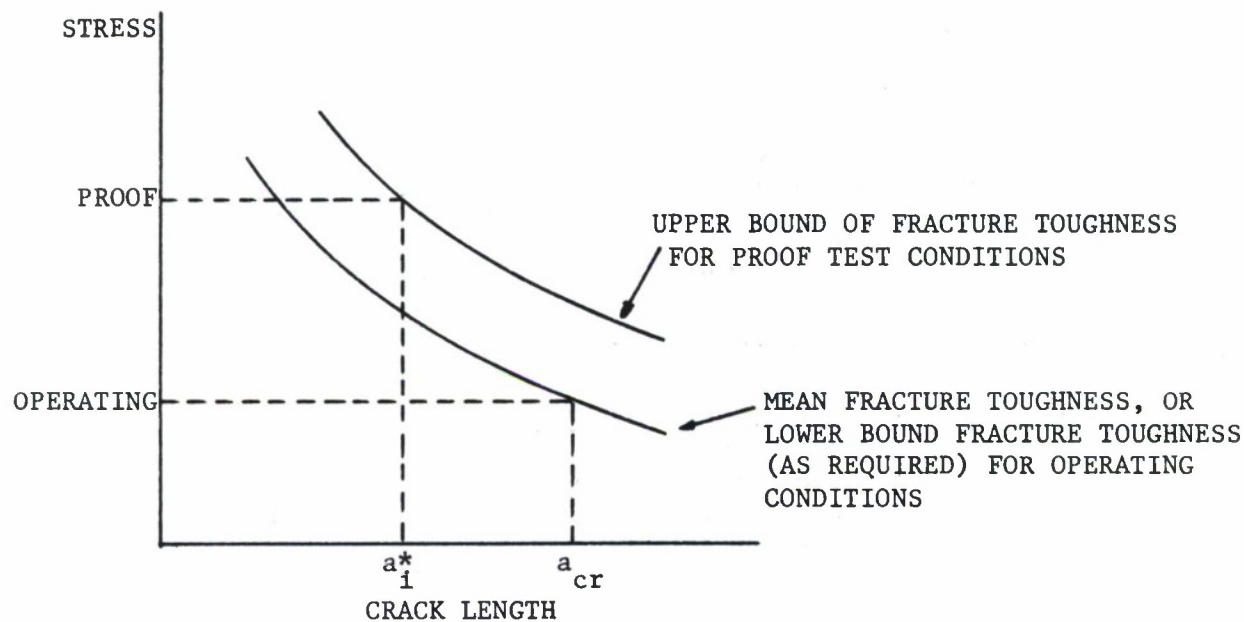


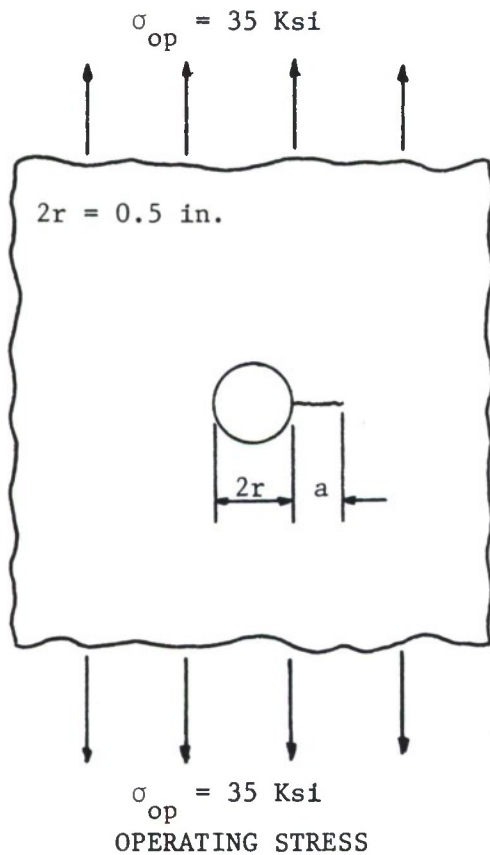
Figure 3.3.6. Description of Procedure Used to Establish Initial Crack Size and the Minimum Safe Crack Growth Interval According to MIL-A-83444 (3.1.1.1).

TABLE 3.1.2.1.6 Typical Values of Room Temperature Plane-Strain Fracture Toughness of Aluminum Alloys^a

Alloy Product		Temper	Product Thickness Range ^b , inch	K _{IC} , ksi-in. ^{1/2}									
				L - T			T - L			S - L			
				No. Specimen of Thickness ^c , Lots	inch	Min. Avg. Max.	No. Specimen of Thickness ^c , Lots	inch	Min. Avg. Max.	No. Specimen of Thickness ^c , Lots	inch	Min. Avg. Max.	
2014 Plate	T651	1 - 2	3	1	22 22 24	4	1	16 21 22	1	1/4	.. 18 ..		
	T652	2 - 6	4	3/4	25 29 24	4	3/4	19 22 30	2	1/4	15 16 16		
2024 Plate	T351	1-1/4	..	1-1/4	2	1	20 23 26		
	T3510,1	1-1/4 - 2	2	1-1/4	.. 46		
Plate	T851	1 - 2	4	1-1/4	23 22 25	2	1-1/4	28 30 20	1	1	.. 17 ..		
	T8510,1	1/4 - 4	6	3/4	22 26 22	4	3/4	16 17 16		
	T852	2 - 6	6	3/4	23 28 30	4	3/4	17 16 20	2	1/4	16 16 17		
2219 Plate	T851	1 - 2	3	1-1/4	21 22 26	2	1	29 30 30	1	3/4	.. 20 ..		
	T87	1/4 - 1	3	3/4	20 27 28	1	1/4	.. 20 ..		
7075 Plate	T651	1/4 - 2	6	1/4	25 26 27	4	1/4	20 22 23	2	1/4	15 16 18		
	T6510,1	1/4 - 4	16	1/4	26 28 22	16	1/4	16 22 28	4	1/4	16 19 22		
	T652	2 - 6	2	1/4	24 26 28	1	1/4	.. 23 ..	1	1/4	.. 17 ..		
Plate	T7351	1-1/4	1	1-1/4	.. 30 ..	2	1	25 29 33	2	1/4	19 20 21		
	T73510,1	1/4 - 4	2	3/4	21 22 24	6	1/4	23 24 28	1	1	.. 20 ..		
	T7352	1 - 5	8	3/4	27 21 35	2	3/4	22 25 20	2	1/4	16 21 25		
7079 Plate	T651	1 - 3	2	1	27 29 30	2	1	24 24 24	1	1/4	.. 16 ..		
	T652	2 - 6	2	3/4	28 30 21	2	3/4	21 23 25	2	1/4	17 18 16		
7175 Plate	T651	1/4 - 2	2	1	22 22 26	4	1/4	16 21 23	1	1/4	.. 15 ..		
	T6510,1	1/4 - 1-1/4	1	1	.. 25 11	4	1/4	16 16 20	1	1	.. 14 ..		
Plate	T7671	1/4 - 2	2	1/4	26 29 30	2	1/4	22 22 23	1	1/4	.. 17 ..		
	T7650,1	1/4 - 2	8	1/4	26 29 21	2	1/4	18 22 28	1	1/4	.. 16 ..		

^aThese values are for information only.^bIn the case of K_{IC} values for the S-L orientation, the minimum product thickness evaluated was at least 1.0 inch.^cMinimum thickness of specimen on which these values were obtained.

Figure 3.3.7. Table of Fracture Toughness Data Taken from MIL-HDBK-5 (Reference 25).



MATERIAL PROPERTIES

$$\sigma_{YS} = 70 \text{ Ksi}$$

$$K_{IC} = 40 \text{ Ksi } \sqrt{\text{in}} \text{ at } 75^\circ\text{F}$$

$$K_{IC} = 35 \text{ Ksi } \sqrt{\text{in}} \text{ at } -40^\circ\text{F}$$

STRESS INTENSITY FACTOR SOLUTION

$$K = \sigma \sqrt{\pi a} F(a/r)$$

$$\text{where } F(a/r) = \frac{0.8734}{(0.3246 + \frac{a}{r})} + 0.6762$$

Figure 3.3.8. Data Required for EXAMPLE 3.3.1.

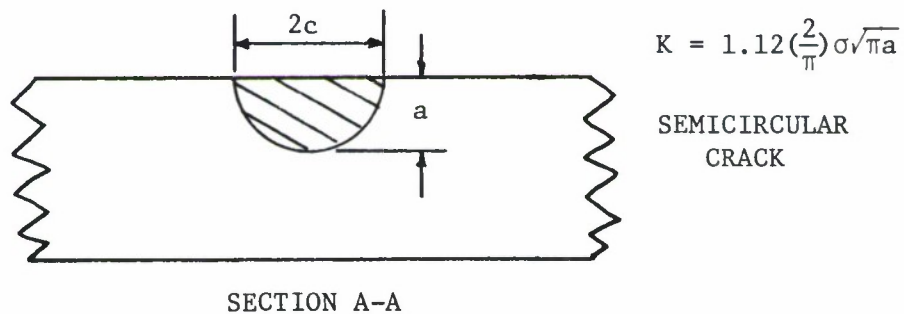
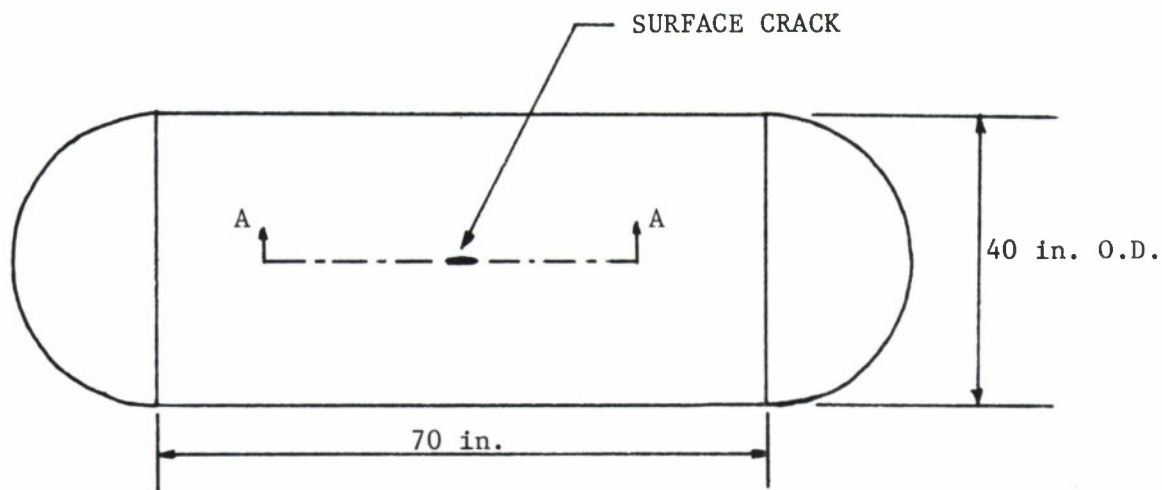


Figure 3.3.9. Pressure Vessel Structure with Semicircular Surface Crack. For Loading, See Figure 3.3.10, and for Material Properties, See Figure 3.3.11.

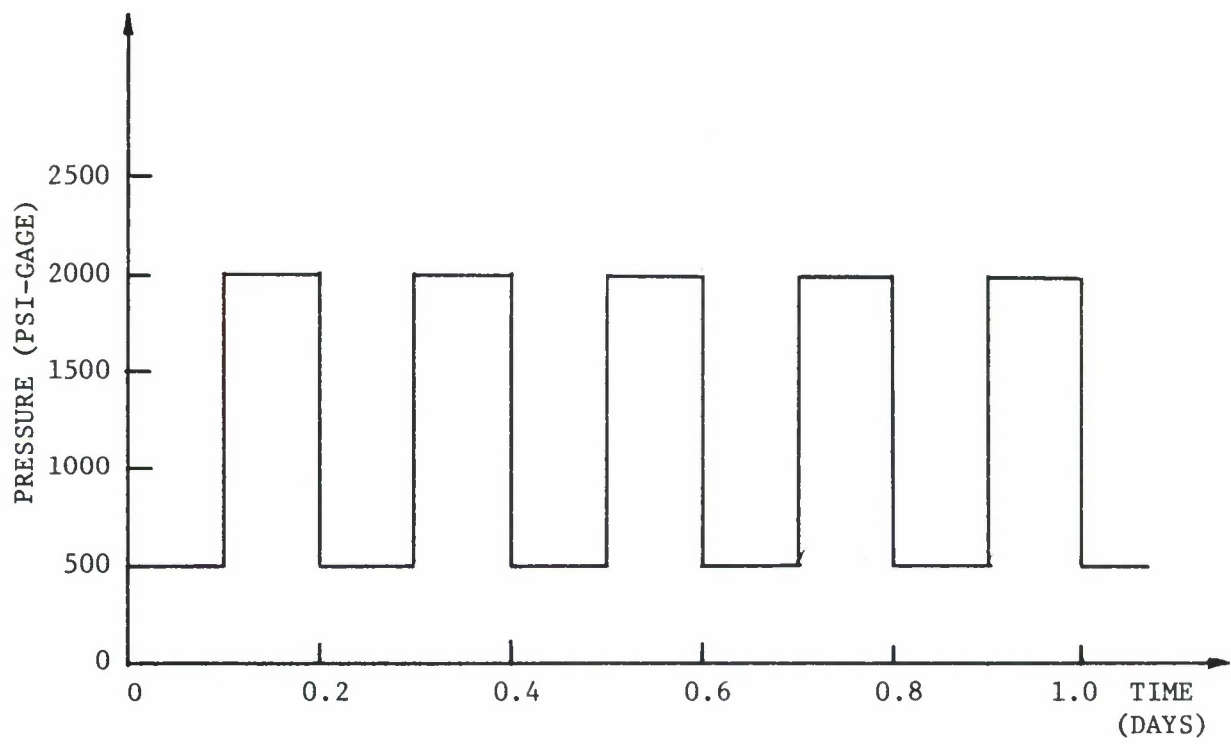


Figure 3.3.10. Pressure Loading for Structure Illustrated in Figure 3.3.9.

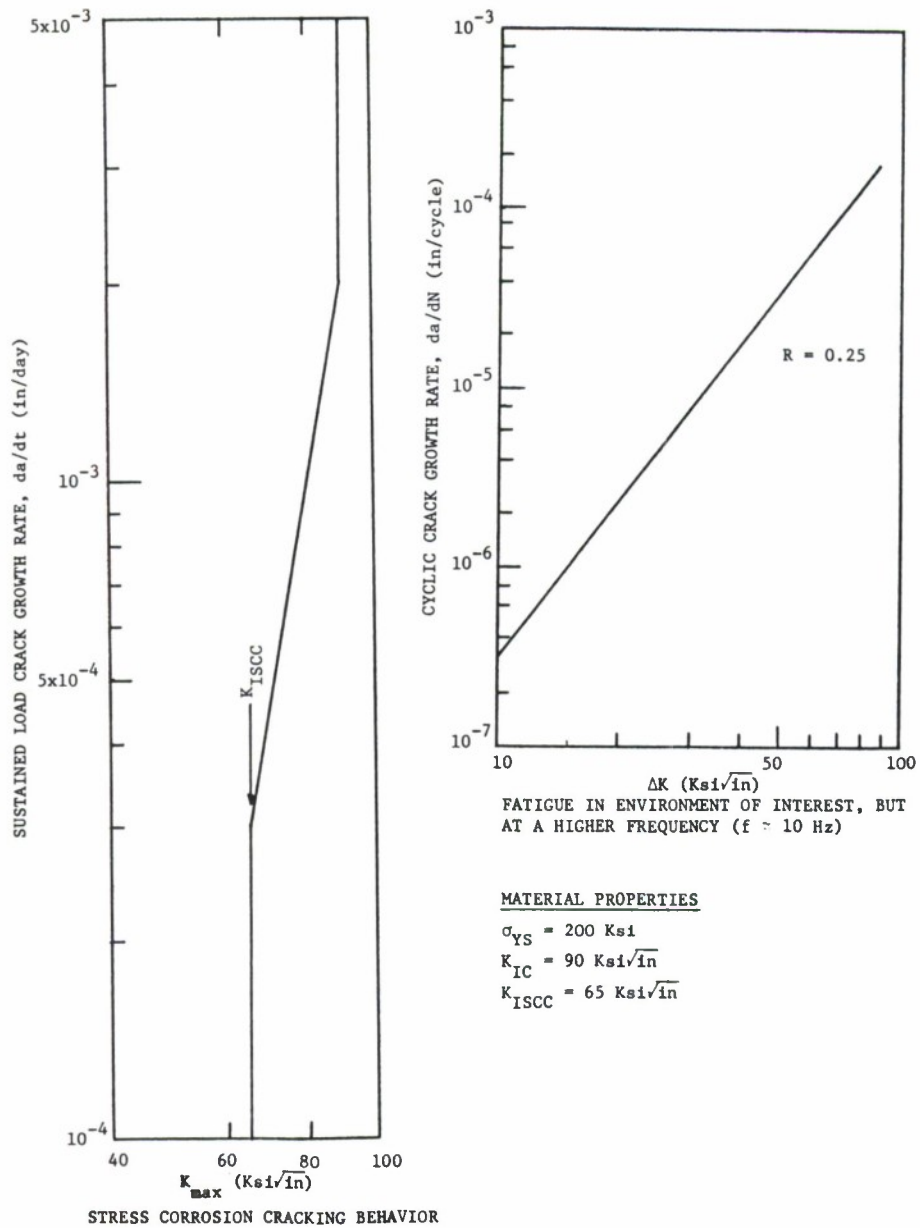


Figure 3.3.11. Material Properties for Steel Pressure Vessel Illustrated in Figure 3.3.9.

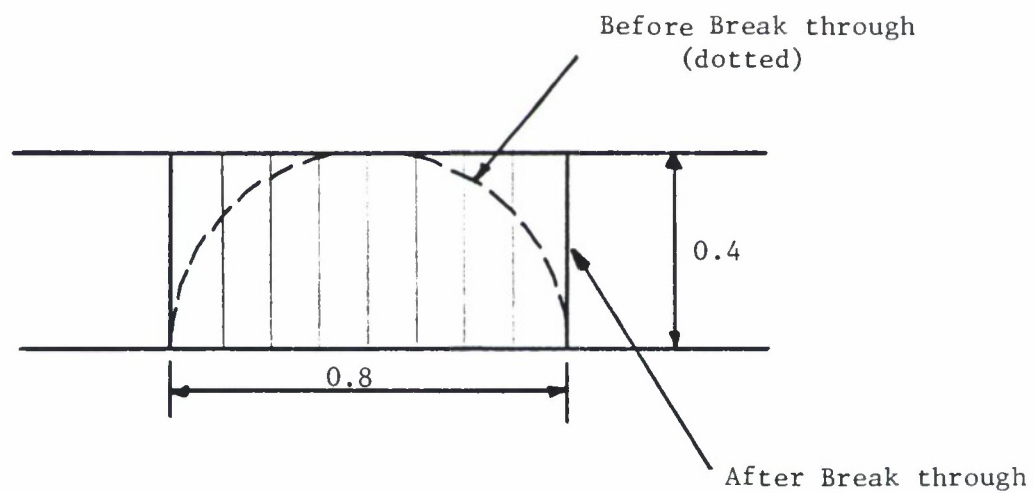


Figure 3.3.12. Change in Crack Geometry to Through-Thickness Crack After the Semicircular Crack Grows to the Inside Wall.

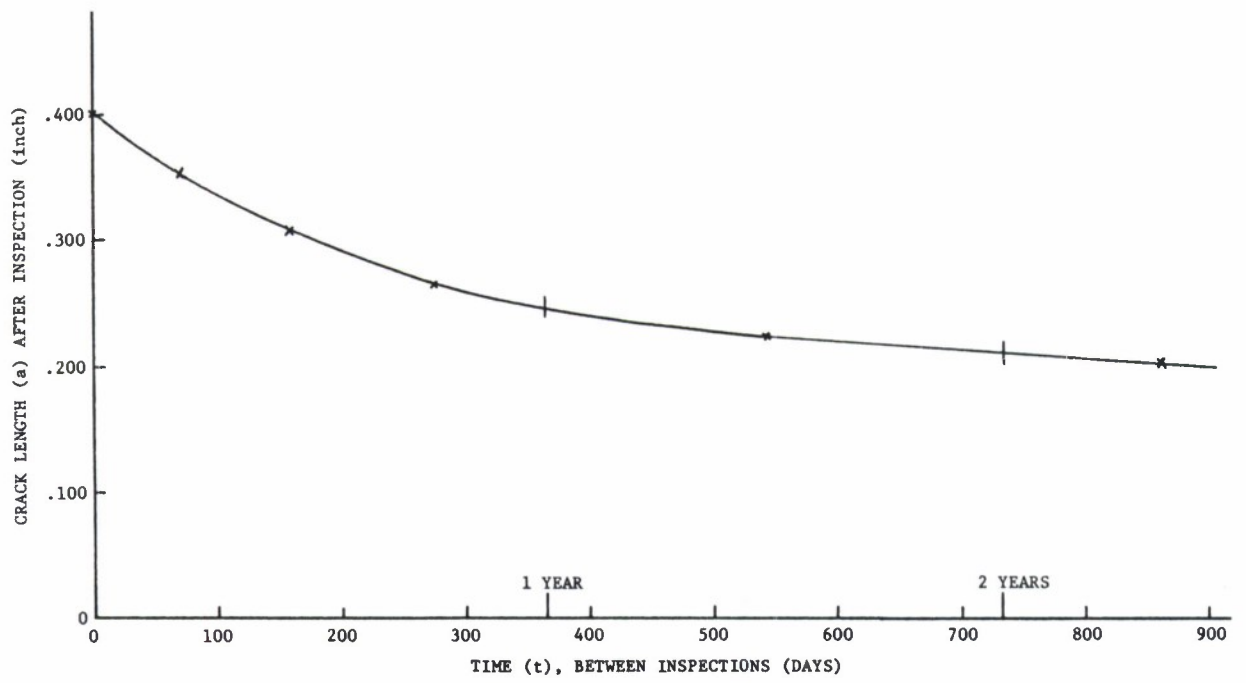


Figure 3.3.13. Graphical Procedure for Interpreting Crack Length.

3.4 EQUIVALENT INITIAL QUALITY (EIQ)

MIL-A-83444, USAF Airplane Damage Tolerance Requirements, specify that initial flaws shall be assumed to exist as a result of manufacturing and processing operations. Small imperfections, equivalent to a 0.005 in. radius corner crack, resulting from these operations shall be assumed to exist in each hole of each element in the structure. These assumed cracks provide the basis for the fastener policy requirements as well as the continuing damage and remaining damage assumptions. However, if the contractor has developed initial quality data on fastener holes, these data may be submitted to the procuring activity for review and serve as a basis for negotiating a different size than the specified 0.005-in. radius corner flaw.

One method of accounting for the initial quality is to represent the quality in terms of an equivalent fatigue crack of a particular size and shape. Such a method of quantifying the initial quality is the Equivalent Initial Quality Method⁽²⁶⁻³⁰⁾ described in the following subsection.

3.4.1 Description of Equivalent Initial Quality Method

The Equivalent Initial Quality Method is presented for fastener holes since this is the most prevalent source of cracking in aircraft structures⁽²⁷⁾. Quality may be defined as a measure of the condition of the structure relative to imperfections, flaws, defects, or discrepancies that are either inherent in the material or introduced during manufacturing of the structure. The approach is to quantify these imperfections by representing them with fatigue cracks of a particular size

and shape, such as the corner cracks illustrated in Figure 3.4.1. Also illustrated in Figure 3.4.1 are some of the parameters that can contribute to the initial quality of fastener holes. If an initial quality representation is performed for each of a number of fastener holes, an equivalent initial quality statistical distribution can be used to quantify the quality of the fastener holes produced by certain manufacturing and processing procedures⁽³⁰⁾.

The initial quality representation, defined as the equivalent initial quality, can be obtained in the following manner. Consider a piece of structure with a fastener hole containing the defect of characteristic dimension ℓ (Figure 3.4.2). This defect results in fatigue crack initiation and propagation when subjected to some known load history. Upon failure of the structure, a fractographic examination of the fracture surface is performed to obtain as much of the crack growth curve as possible. Analytical crack propagation analyses are performed until there is good agreement between the analytical prediction and the fractographic test data. The initial crack length (crack length when the load history is first applied), a_i , of the analytical crack growth curve that correlates best with the fractographic test data is defined as the equivalent initial quality. Hence, a_i is said to be the analytical equivalent of the actual defect of characteristic dimension, ℓ , if each results in a crack size a_e after N_e cycles of the same load history have been applied. Hence, fastener holes that contain actual crack lengths less than a_e after N_e cycles have been applied are of better quality than those that contain actual crack lengths equal to or greater than a_e after N_e cycles.

3.4.2 Example Application of Equivalent Initial Quality Method

Although Equivalent Initial Quality Method studies have been conducted on the F-4C/D⁽²⁸⁾, F-4E(S)⁽²⁸⁾, and A-7D⁽²⁹⁾, only a summary of a recent quality assessment program by Rudd and Gray⁽²⁷⁾ on the A-7D will be reviewed here. The following paragraphs are taken directly from Reference 27.

The purpose of the A-7D quality assessment was to establish the manufacturing quality (a_i) of the A-7D aircraft. This was accomplished using the Equivalent Initial Quality Method. The method was applied to a sample problem involving an A-7A wing fatigue test failure. Next, specimens were cut from an A-7D production aircraft and tested to failure under a selected block loading. The fracture surfaces were then fractographically examined and the equivalent initial quality was established.

A photograph of the failure area of a full-scale fatigue test of an A-7A wing was used as a sample problem to check out the Equivalent Initial Quality Method. The wing had been subjected to a 10-level, blocked, low-high stress spectrum. Fractographic measurements were taken from the photograph (Figure 3.4.3), making it possible to generate a large portion of the crack growth curve. Crack propagation analyses were performed using the computer routine EFFGRO and the Wheeler Retardation Model until the analytical crack growth curve correlated well with the fractographic test data. This correlation is presented in Figure 3.4.4, which indicates that the manufacturing quality of the test hardware at the failure location was equivalent to an initial crack of length $a_i = 0.00109$ in. This excellent correlation of the analytical crack growth prediction with the fractographic test supported the validity

of the Equivalent Initial Quality Method for this particular problem.

The Equivalent Initial Quality Method was next used to establish the A-7D quality assessment. This assessment was accomplished using test specimens cut from the lower wing skin of an A-7D production aircraft that had been used as a gunfire target. Because this particular aircraft had low flight time (691.9h), the probability of cracking in the wings was very low. The location of each specimen in the lower wing skin is illustrated in Figure 3.4.5. Each specimen was made of 7075-T6 aluminum and contained multiple holes. The geometric details for each specimen are presented in Table 3.4.1, indicating that the thickness ranged from approximately 3/16 in. to 1/4 in. and the nominal values of the width and hole diameter were 3 in. and 1/4 in., respectively. The specimens contained two types of holes--countersunk holes (wet-wing region) and straight-shank holes (dry-wing region).

The test specimens were subjected to a fatigue stress spectrum consisting of 5,000 cycles with a maximum stress of 20 ksi and a stress ratio of 0.1 followed by 100 cycles with a maximum stress of 30 ksi and a stress ratio of 0.1. The block spectrum was chosen because it produced test lives of reasonable length (less than 20 blocks) and fracture surfaces that were readily readable.

Table 3.4.2 contains a summary of the number of fastener holes involved, the number of flaws detected, the number of flaws fractographically examined, the crack length range at the time of specimen failure (a_f), and the range of the equivalent initial quality (a_i). All but 2 of the 44 holes contained double flaws. One of these two holes contained one crack, while no crack was detected in the other hole. This resulted in a total of 85 flaws, of which

44 were examined fractographically. The flaws were arbitrarily chosen for fractographic examination at magnifications ranging from 30x to 400x using a universal measuring microscope. The equivalent initial quality range for all the holes was found to be 0.00015-0.0022 in. A statistical distribution of the A-7D equivalent initial quality was obtained.

The fractographic examinations revealed the origins of the flaws for both the straight-shank holes and the countersunk holes as illustrated in Figure 3.4.6. There is equal possibility of flaw occurrence along the bore of the hole for the straight-shank hole, while the most frequently occurring flaw location for the countersunk hole is at the inside radius of the small-diameter portion of the hole. Typical flaw origins for each type of hole are shown on the fracture surfaces of Figure 3.4.7. Also illustrated in Figure 3.4.7 is the readability of the fracture surfaces for the selected stress spectrum, with the dark marking bands resulting from the application of the high-load (maximum stress of 30 ksi) portion of the specimen.

Metallurgical investigations of the A-7D flaw origins revealed that the flaws were the result of two different sources-anodize pitting and mechanical sources. The majority of the flaws (86.4%) initiated from anodize pits in the following manner. Insoluble microconstituents were exposed along the bore of the hole during the hole-drilling operation. The anodizing ate away the microconstituents and caused pitting. The exposed pits were then filled with aluminum oxide, resulting in flaw initiation. The remaining flaws (13.6%) were due to the mechanical damage. Although anodizing provided corrosion protection, it also resulted in the majority of the fatigue cracks.

All but two of the holes contained double flaws, of which none were through-the-thickness flaws. The selected stress spectrum marked the fracture surfaces extremely well, making it possible to determine the crack length within each loading block. Hence, it was possible to fractographically determine the equivalent initial quality for each flaw examined.

Figure 3.4.8 presents the probability density of occurrence versus the equivalent initial quality for the A-7D aircraft. It should be noted that the A-7D equivalent initial quality was determined by fractography alone, since it was possible to measure the crack length during the application of the first block of loading.

The probability density of occurrence (Figure 3.4.8) was used to determine the cumulative probability of occurrence for the A-7D aircraft. Figure 3.4.9 presents the cumulative probability of occurrence versus the equivalent initial quality for the A-7D and F-4 C/D aircraft. Also presented in Figure 3.4.9 is the cumulative probability of occurrence with 95% confidence for each aircraft. For example, Figure 3.4.9 indicates that with 95% confidence, 99.9% of the A-7D flaws have an equivalent length less than 0.007 in. This means that one out of a thousand flaws have an equivalent length greater than 0.007 in.

TABLE 3.4.1
Geometric Details of A-7D Quality
Assessment Specimens (Reference 27)

Specimen	Thickness ^a	Width ^a	Hole diameter
101	0.226	2.93	0.253 ^b
201	0.226	2.93	0.253 ^b
301	0.217	3.00	0.253 ^b
401	0.231	3.00	0.253 ^b
501	0.183	2.9	0.253 ^c
502	0.176	3.00	0.253 ^c
601	0.263	3.00	0.253 ^c
602	0.264	3.00	0.253 ^c

^a Dimensions in inches.

^b Countersunk hole.

^c Straight-shank hole.

TABLE 3.4.2
A-7D Quality Assessment Test Results
(Reference 27)

Specimen	No. holes	No. flaws	a_f^a range	Flaws tracked	a_i^a range
101	7	14	0.05-0.75	14	0.0004-0.0022
201	6	12	<0.01-1.10	12	0.0004-0.0012
301	4	8	0.01-0.65	1	0.0003
401	3	6	0.02-0.50	6	0.0002-0.0014
501	8	14	0.00-0.60	1	0.0007
502	8	16	<0.01-0.62	1	0.0006
601	4	8	0.02-0.50	8	0.00015-0.0009
602	4	7	0.00-1.05	1	0.0006
Total	44	85		44	

^a Dimensions in in.

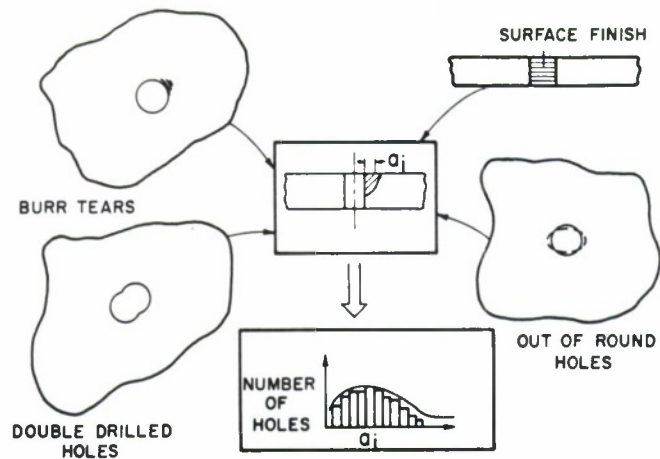


Figure 3.4.1. Parameters that Affect Fastener-Hole Initial Quality (Reference 27).

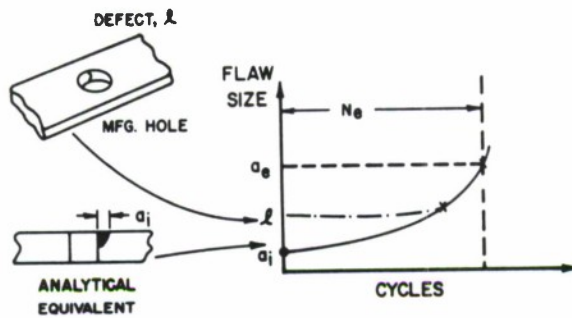


Figure 3.4.2. Definition of Equivalent Initial Quality (Reference 27).

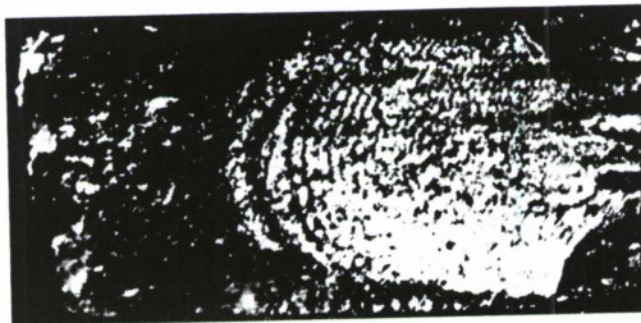


Figure 3.4.3. A-7A Wing Fatigue Test Fracture Surface (Reference 27).

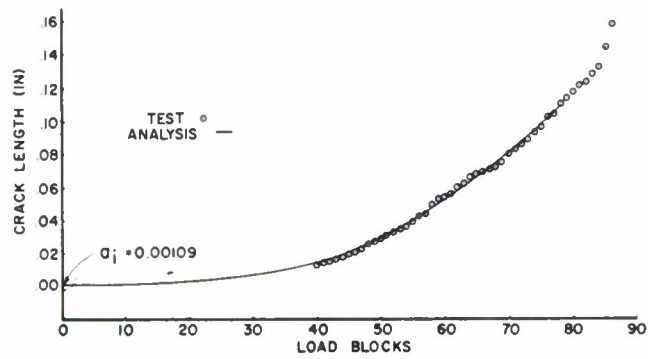


Figure 3.4.4. Equivalent Initial Quality Results for A-7A Wing Fatigue Test (Reference 27).

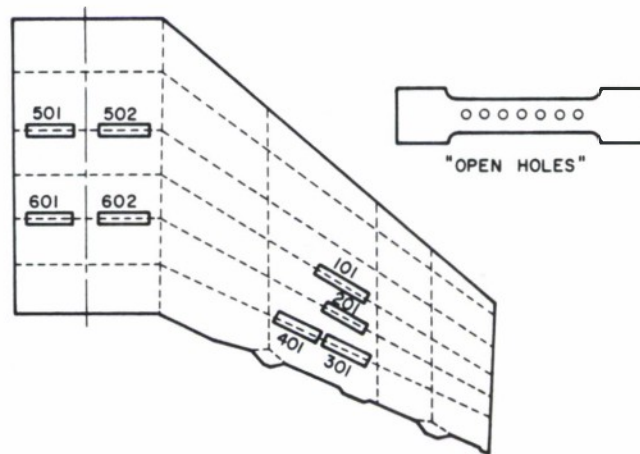


Figure 3.4.5. A-7D Quality-Assessment Specimen Locations (Reference 27).

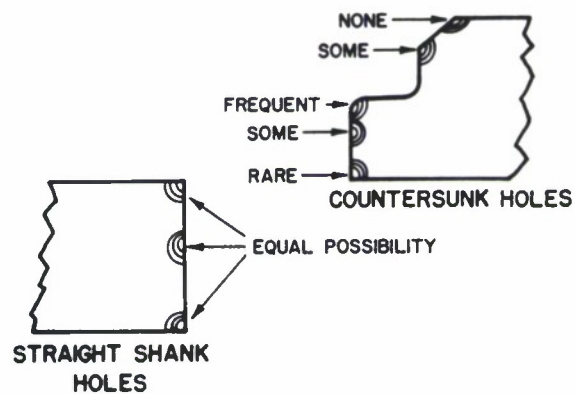


Figure 3.4.6. A-7D Flaws Origins (Reference 27).

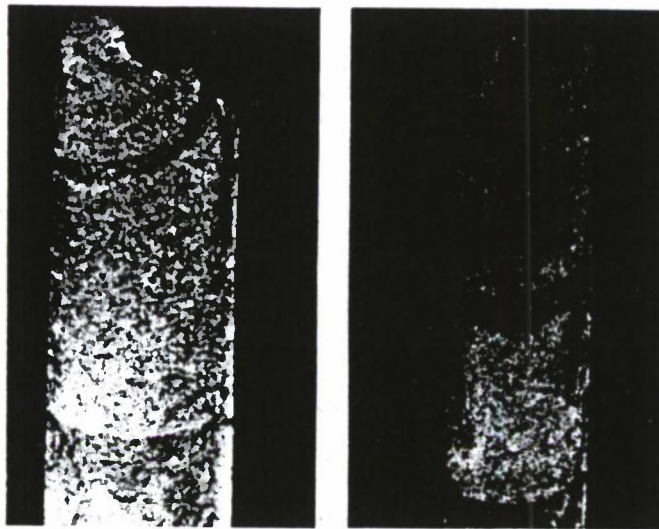


Figure 3.4.7. Fracture Surfaces for Countersunk (left) and Straight-shank (right) holes. (Reference 27).

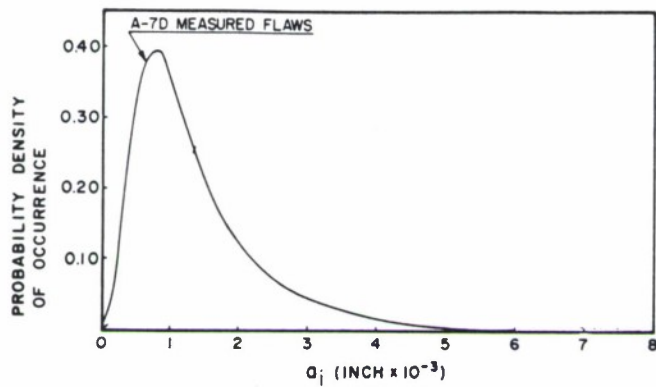


Figure 3.4.8. Probability Density of Occurrence of A-7D Equivalent Initial Quality (Reference 27).

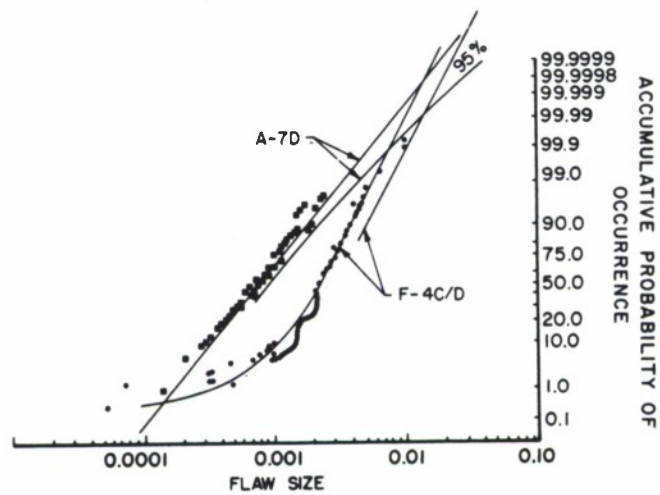


Figure 3.4.9. Cumulative Probability of Occurrence of A-7D Equivalent Initial Quality (Reference 27).

SECTION 3.5
LIST OF REFERENCES

1. Walker, E. K., Ekvall, J. C. and Rhodes, J. E., "Design for Continuing Structural Integrity," Structural Integrity Technology, A.S.M.E., N.Y., (1979).
2. Packman, P. F., Klima, S. J., Davies, R., Malpani, J., Moyzis, J., Walker, W., Yee, B. G. W. and Johnson, D. P., "Reliability of Flaw Detection by Nondestructive Inspection," ASM Metal Handbook, Vol. 11, 8th Edition, Metals Park, Ohio, (1976), pp. 214-224.
3. McGonnagle, W. J., Nondestructive Testing, McGraw-Hill, N.Y., (1961).
4. McMaster, R. C., Nondestructive Testing Handbook, Ronal Press Co., N.Y., (1959).
5. Corlin, B., Ultrasonics, McGraw-Hill, N.Y., (1960).
6. Betz, C. E., Principles of Penetrants, Magnaflux Corp., (1963).
7. Schaffer, G., "Nondestructive Testing," Special Report 692, American Mechanist, (1976).
8. Berens, A. P. and Hovey, P. W., "Evaluation of NDE Reliability Characterization," AFWAL-TR-81-4160, Air Force Wright Aeronautical Laboratories, Wright-Patterson Air Force Base, Ohio, Nov., 1981.
9. Southworth, H. L., Steel, N. W., and Torelli, P. P., "Practical Sensitivity Limits of Production Nondestructive Testing Methods in Aluminum and Steel," AFML-TR-74-241, (1974).
10. Rummel, W. O., Rathke, R. A., Jr., Todd, P. H., Tedrow, T. L. and Mullen, S. J., "Detection of Tightly Closed Flaws by Nondestructive Testing (NDT) Methods in Steel and Titanium," NAS9-14653, (1976).
11. Lewis, W. H., Dodd, B. D., Sproat, W. H., and Hamilton, J. M., "Reliability of Nondestructive Inspections - Final Report," Report No. SA-ALC/MEE 76-6-38-1, United States Air Force, San Antonio Air Logistics Center, Kelly Air Force Base, Texas, (1978).
12. Smith, D. K., "Improved Penetrant Process Evaluation Criteria," Pratt and Whitney Aircraft Report Number FR-15223, October 1981.

13. Yee, B. G. W., Chang, F. H., Couchman, J. C., Lemon, G. H., and Packman, P. F., "Assessment of NDE Reliability Data," NASA CR-134991, National Aeronautics and Space Administration, Lewis Research Center, Cleveland, Ohio, (1976).
14. Chang, F. H., Bell, J. R., Walker, T. C., Norton, J. M., Packman, P. F., and Gilstrap, L. O., "Methods for the Determination of the Sensitivity of NDE Techniques," AFML-TR-76-246, Air Force Materials Laboratory, Wright-Patterson Air Force Base, Ohio, December 1976.
15. Cargill, J. S., "Retirement for Cause Inspection System Design," Presented at AF/DARPA Review of Progress in Quantitative NDE, Boulder, Colorado, August, 1981.
16. Natrella, M. G., Experimental Statistics, Handbook 91, National Bureau of Standards, (1963).
17. Mood, A. M., Introduction to the Theory of Statistics, McGraw-Hill Book Company, Inc., New York, (1950).
18. Tiffany, C. F., and Masters, J. N., "Applied Fracture Mechanics," Fracture Toughness Testing and Its Applications," ASTM STP 381, American Society for Testing and Materials, Baltimore, MD, (1965), pp. 249-277.
19. Buntin, W. D., "Concept and Conduct of Proof Test of F-111 Production Aircraft," paper presented to the Royal Aeronautical Society, 27 Oct. 1971, London, England.
20. Cowie, W. D., "Turbine Engine Structural Integrity Program (ENSIP)," AIAA, J. of Aircraft, Vol. 12, No. 4, Special Issue (April 1975), pp. 366-369.
21. Horsley, J. J., Bryan, D. F., and Fuller, J. E., "B-52D Proof Load Program, Laboratory Crack Growth Tests," The Boeing Company, Wichita Division, Document No. D3-9700, Feb. 1976, (Restricted Publication).
22. Gunderson, A. W., "Fracture Mechanics Tests and Analyses of the AEDC APTU Storage Vessel Material," AFML-TR-74-133, Air Force Materials Laboratory, October 1974.
23. Albrectsen, U. and Aitken-Cade, P., Briefing Charts on C-141 Loading Gear Proof Test Conditions, Ogden Air Logistics Center/MMIRCL, Hill Air Force Base, March 1976.
24. White, et al., "Fatigue Life Evaluation of the A-7E Arresting Gear Hool Shank," Vought Report No. 2-30400/9R-52133, Vought Corporation, Dallas, Texas, May 1979.

25. MIL-HDBK-5C, Military Standardization Handbook, Metallic Materials and Elements for Aerospace Vehicle Structures, Vol. 1, 15 September 1976, pp. 3-8.
26. Rudd, J. L. and Gray, T. D., "Equivalent Initial Quality Method," Air Force Flight Dynamics Laboratory, AFFDL-TM-76-83-FBE, Sept. 1976.
27. Rudd, J. L. and Gray, T. D., "Quantification of Fastener-Hole Quality," Journal of Aircraft, Vol. 15, No. 3, (1978), pp. 143-147.
28. Pinckert, R. E., "Damage Tolerance Assessment of F-4 Aircraft," AIAA-76-904, presented at AIAA Aircraft Systems & Technology Meeting, Dallas, Texas, 26-27 September 1976.
29. Dumesnil, C. E., Aratki, S. D., Wilson, R. P., Martin, C. P., White, D. J., and Hooks, O. L., "A-7D ASIP Part I, Damage Tolerance and Fatigue Assessment Program," Vought Corp., Report No. 2-53440/7R-5928, Vol. I, Jan. 1977.
30. Potter, J. M., "Advances in Fastener Hole Quality Through the Application of Solid Mechanics," Proceedings of the Army Symposium on Solid Mechanics, (1978) - Case Studies on Structural Integrity and Reliability, AMMRC-MS 78-3, Watertown, MA, (1978).

4.0 RESIDUAL STRENGTH

SECTION		PAGE
4.1	INTRODUCTION	4.1.1
4.1.1	<u>Slow Crack Growth Structure</u>	4.1.3
4.1.2	<u>Fail-Safe Structure</u>	4.1.4
4.2	FAILURE CRITERIA	4.2.1
4.2.1	<u>Ultimate Strength</u>	4.2.2
4.2.2	<u>Fracture Toughness - Abrupt Fracture</u>	4.2.3
4.2.3	<u>Crack Growth Resistance - Tearing Fracture</u>	4.2.5
	4.2.3.1 The Apparent Fracture Toughness Approach	4.2.6
	4.2.3.2 The Resistance (R) Curve Approach	4.2.7
	4.2.3.3 The J-Integral Resistance Curve Approach	4.2.9
4.3	RESIDUAL STRENGTH CAPABILITY	4.3.1
4.3.1	<u>Single Load Path Residual Strength Diagrams</u>	4.3.2
4.3.2	<u>Built-Up Structure Residual Strength Diagrams</u>	4.3.9
4.4	SINGLE LOAD PATH STRUCTURE	4.4.1
4.4.1	<u>Abrupt Fracture</u>	4.4.1
4.4.2	<u>Tearing Fracture</u>	4.4.8
4.5	BUILT-UP STRUCTURES	4.5.1
4.5.1	<u>Edge Stiffened Panel with a Central Crack</u>	4.5.2
4.5.2	<u>Centrally and Edge Stiffened Panel with a Central Crack</u>	4.5.6
4.5.3	<u>Analytical Methods</u>	4.5.8
4.5.4	<u>Stiffener Failure</u>	4.5.13
4.5.5	<u>Fastener Failure</u>	4.5.17
4.5.6	<u>Methodology Basis for Stiffened Panel Example Problem</u>	4.5.19
4.5.7	<u>Example Residual Strength Analysis of Stiffened Panel</u>	4.5.22
4.5.8	<u>Tearing Failure Analysis</u>	4.5.26
4.5.9	<u>Summary</u>	4.5.30
4.6	LIST OF REFERENCES	4.6.1

LIST OF FIGURES

<u>FIGURE</u>		<u>PAGE</u>
4.1.1	The Structural Configuration or Degree of Inspectability Controls the Subsequent Choices of Design Concept and Inspection Level.	4.1.5
4.1.2	Relationship Between the Life Expended and Residual Strength Capability Showing Monotonic Decrease in Load Carrying Capacity Due to Increased Structural Damage. Failure Occurs when the Residual Strength Capability Curve Intersects the Required Residual Strength Level.	4.1.6
4.1.3	Relationship Between Crack Length and Life Expended Showing a Monotonic Increase in Crack Length Up Until Failure. Shown are the Various Technology and Specification Requirements Needed to Define the Crack Growth Curve Which, in Turn, Establishes the Life Limit.	4.1.7
4.1.4	Strength Criteria for Periodically Inspected Damage Tolerant Structure.	4.1.8
4.2.1	Description of Crack Geometry and Residual Strength Results.	4.2.12
4.2.2	Fracture Data Described as a Function of Crack Length.	4.2.13
4.2.3	The Fracture Mechanics Basis for Establishing Residual Strength.	4.2.14
4.2.4	Plane-Strain Fracture Toughness (K_{IC}) Data for 7075 Aluminum in the format of Reference 1.	4.2.15
4.2.5	Plane-Stress Fracture Toughness (K_C) Data for 7075 Aluminum in the Format of Reference 1.	4.2.16
4.2.6	Fracture Toughness Behavior as a Function of Thickness.	4.2.17
4.2.7	Schematic Illustration of Tearing Fracture Behavior and the Development of a Crack Growth Resistance Curve (R-Curve).	4.2.18

LIST OF FIGURES
(Con't)

<u>FIGURE</u>		<u>PAGE</u>
4.2.8	K_R Curves from 7475 Alloy, 16 Inch Wide Panels, 0.5 Inch Thickness (Reference 2).	4.2.19
4.2.9	Schematic Illustration of Tearing Fracture Behavior Which Further Defines the Change in Critical Level of Fracture Toughness as a Function of Crack Length (Also see Figure 4.2.7).	4.2.20
4.2.10	Description of the Three Fracture Toughness Criteria that are Utilized to Estimate Residual Strength Under Tearing Fracture Conditions.	4.2.21
4.2.11	Schematic Illustration of the Individual and Collective Parts of A K_R Fracture Analysis.	4.2.22
4.2.12	Schematic Illustration of the Individual and Collective Parts of a $\sqrt{J_R}$ Fracture Analysis.	4.2.23
4.3.1	Residual Strength Diagram for Abrupt Failure of a Single Load Path Structure.	4.3.17
4.3.2	Structural Geometry and Material Properties for Example 4.3.1.	4.3.18
4.3.3	Description of Procedures that One Might Follow to Obtain the Residual Strength Diagram Graphically.	4.3.19
4.3.4	Crack Geometries Considered for a Radial Crack Growing from a Hole for Example 4.3.2.	4.3.20
4.3.5	Stress-Intensity Factor Relationships at Points A and B for the Radial Quarter Circular Crack Geometry.	4.3.21
4.3.6	Stress-Intensity Factor Relationships at Points A and B for the Radial Embedded Semi-Circular Crack Geometry.	4.3.21
4.3.7	Residual Strength Diagram for Points A and B Located on the Radial Quarter Circular Crack Geometry Shown in Figure 4.3.4.	4.3.22
4.3.8	Residual Strength Diagram for Points A and B Located on the Embedded Semi-Circular Crack Geometry Shown in Figure 4.3.4.	4.3.22

LIST OF FIGURES
(Con't)

<u>FIGURE</u>		<u>PAGE</u>
4.3.9	Multiple Load Path (Built-Up) Structure with a Crack in the Central Member.	4.3.23
4.3.10	Reduction of Residual Strength During Successive Failure of Members in the Structure Shown in Figure 4.3.9.	4.3.24
4.3.11	Crack Growth Curve for Multiple Load Path Structure Shown in Figure 4.3.9.	4.3.25
4.3.12	Skin-Stringer Built-Up Structure.	4.3.26
4.3.13	Variation of β and L with Crack Length in Stiffened Panel with a Crack Between the Stiffeners.	4.3.27
4.3.14	Residual Strength of the Cracked Panel as a Function of Crack Length for Built-Up Skin-Stiffened Structure Compared with Unstiffened Panels. Abrupt Failure Criterion Used to Determine Residual Strength.	4.3.28
4.3.15	Residual Strength of a Cracked Panel as a Function of Crack Length for Built-Up Skin-Stiffened Structure. Only Skin Failure Mode Considered. Abrupt Failure Criterion Used to Determine Residual Strength.	4.3.29
4.3.16	Load-Crack Length Behavior Observed in Skin-Stiffened Construction with Arrest Features.	4.3.30
4.3.17	Residual Strength of Cracked Panel as a Function of Crack Length for Built-Up Skin-Stringer Structure. Tearing Failure Criterion Used to Determine Residual Strength.	4.3.31
4.4.1	Residual Strength Diagram Showing Defining Crack and Residual Strength Parameters.	4.4.12
4.4.2	Center Crack Panel and Materials Properties for Example 4.4.1.	4.4.13
4.4.3	Residual Strength Diagram Determining Critical Crack Size at 20 Ksi Operating Level.	4.4.14

LIST OF FIGURES
(Con't)

<u>FIGURE</u>		<u>PAGE</u>
4.4.4	Excentrically Cracked Panel Associated with Examples 4.4.2 and 4.4.3.	4.4.15
4.4.5	Finite-Width Correction-Eccentric Crack (Tension) (Reference 15).	4.4.16
4.4.6	Residual Strength Diagram for Panel with Eccentric Crack Given in Figure 4.4.4. Crack with Lowest Fracture Resistance Curve Extends First.	4.4.17
4.4.7	Finite Width Correction-Single Edge Crack, After the Eccentric Crack Extends from Tip A.	4.4.18
4.4.8	Residual Strength Diagram Used to Consider Arrest Features as Crack Tip A Reaches the Edge of the Plate.	4.4.19
4.4.9	Diagrams Showing Onset of Unstable Crack Growth for Conditions of Limited or Extensive Crack Extension.	4.4.20
4.4.10	Steps Associated with Calculating Residual Strength of Cracked Structures with Tearing Fractures.	4.4.21
4.4.11	Structural Geometry Associated with Example 4.4.4.	4.4.22
4.4.12	Stress-Intensity Factor Relationship for Various Values of Applied Stress.	4.4.23
4.4.13	Resistance Curve for 7075-T73 Aluminum for a Thickness of 0.063 Inches.	4.4.24
4.4.14	Matching the R-Curve and Stress-Intensity Factor Curves.	4.4.25
4.4.15	Residual Strength Diagram Obtained for Structure Shown in Figure 4.4.11 (Example 4.4.4).	4.4.26
4.5.1	Elements of Residual Strength Diagram.	4.5.31
4.5.2	Residual Strength Diagram for a Stiffened Panel.	4.5.32
4.5.3	Panel Configuration with Heavy Stringers; Skin-Critical Case.	4.5.33

LIST OF FIGURES
(Con't)

<u>FIGURE</u>		<u>PAGE</u>
4.5.4	Criterion for Fastener Failure	4.5.34
4.5.5	Residual Strength Diagram for a Panel with Three Stiffeners and a Central Crack Emanating from a Rivet Hole.	4.5.35
4.5.6	Analysis of Stiffened Panel.	4.5.36
4.5.7	Effect of Number of Fasteners Included in Analysis on Calculated Stress-Intensity Factor.	4.5.37
4.5.8	Skin-Stress-Reduction β and Stringer-Load-Concentration L as Affected by Fastener Flexibility and Stiffener Bending.	4.5.38
4.5.9	Bonded Fastener Divided into Discrete Segments.	4.5.39
4.5.10	Residual Strength Diagram Comparing Riveted and Bonded Structures.	4.5.40
4.5.11	Residual Strength Diagram for Stiffener.	4.5.41
4.5.12	Comparison of L_S and K/σ_S for Riveted and Bonded Structures.	4.5.42
4.5.13	Comparison of Residual Strength for Riveted and Bonded Stiffeners.	4.5.43
4.5.14	Residual Strength Diagram for the Fasteners in a Built-Up Structure.	4.5.44
4.5.15	Gross Stress and Critical Stress Diagram for Adhesively Bonded Stringer.	4.5.45
4.5.16	Riveted Panel with a Central Crack Between Two Stringers.	4.5.46
4.5.17	Stiffened Structure Broken into Components.	4.5.47
4.5.18	Geometrical and Displacement Parameters Relative to the Crack Tip.	4.5.48
4.5.19	Normalized Panel Displacement Function (f_{σ}/p) Due to Applied Stress Vs. Normalized Crack Length (a/p) for Various Stringer Spacings ($\bar{S} = S/p$).	4.5.49

LIST OF FIGURES
(Con't)

<u>FIGURE</u>		<u>PAGE</u>
4.5.20	Panel Displacement Function Due to Fastener Force Vs. Normalized Rivet Diameter (d/p) for All Stiffener Spacings.	4.5.50
4.5.21	Normalized Panel Displacement Function (f_p/p) Due to Distributed Pressure Along Crack Vs. Normalized Crack Length ($a/;$) for Various Stringer Spacings ($\bar{s} = s/p$).	4.5.51
4.5.22	Stringer Displacement Function Vs. Normalized Rivet Diameter (d/p) for Various Half Stringer Widths.	4.5.52
4.5.23	Parameter λ_1 Vs. Normalized Crack Length (a/p) for Various Normalized Stringer Spacings (s/p).	4.5.53
4.5.24	Structural Geometry and Material Properties for Example of Subsection 4.5.7.	4.5.54
4.5.25	Stress-Intensity Factor Diagram for Panel and Riveted Stringers.	4.5.55
4.5.26	Residual Strength Diagram for Panel and Riveted Stringers (Light Stringers).	4.5.56
4.5.27	Residual Strength Diagram for Panel and Riveted Stringers (Heavy Stringers).	4.5.57
4.5.28	Square Root of J_R Resistance Curve.	4.5.58
4.5.29	Failure Analysis Based on $J_{Critical}$ Curve.	4.5.59

CHAPTER 4

RESIDUAL STRENGTH

4.1 INTRODUCTION

The strength of a structure can be significantly affected by the presence of a crack and is usually substantially lower than the strength of the undamaged structure. To prevent catastrophic failure, one must evaluate the load carrying capacity that will exist in the potentially cracked structure throughout its expected service life. The load carrying capacity of a cracked structure is the residual strength of that structure and it is a function of material toughness, crack size, crack geometry and structural configuration.

The basic concept in damage tolerance design is to ensure the safety of the structure throughout the expected service life. To provide the required safety, a structure must be designed to withstand service loads even when cracks are present or when part of the structure has already failed; i.e., the structure has to be damage tolerant. The overriding philosophy is to maintain a minimum required residual strength so that catastrophic failure of the structure is prevented.

Figure 4.1.1 identifies the major sequence of events that ultimately define the residual strength requirements. As can be noted from the figure, once a safety-of-flight-critical element is identified, either its structural configuration or its degree of inspectability will

establish the allowable structural design concept and the inspection level categories. Every safety-of-flight-critical element must be qualified in at least one design concept category and in one inspection category. Each allowable combination of design concept and inspection category is coupled in MIL-A-83444 to a residual strength requirement, a service life requirement, and a requirement to assume a level of initial damage.

Figure 4.1.2 illustrates the residual strength and the service life interval requirements as well as a residual strength capability curve. The residual strength capability curve defines the level of load that the structure can withstand without failing in the presence of a growing crack. To account for the change in residual strength capacity as a function of time, it is necessary to determine the crack size as a function of time. The crack-growth-life curve and its various properties are shown schematically in Figure 4.1.3.

As can be seen from Figure 4.1.2, when the residual strength of the structure falls below the maximum stress in the service load history, failure can be expected. To avoid such a failure, a thorough understanding of the problem is essential. Significant advances have been made in recent years in procedures for analyzing damaged structures. Assessments now consider residual strength, damage growth, interactive multiple damage sites and quantitative structural maintenance and in-service evaluations.

The application of existing fracture mechanics solution techniques has yielded effective methods for analyzing the residual strength of the cracked structure. The necessary theories and methods for determining the residual strength capability of cracked structures are presented in this chapter. Prior to presenting this information in the following sections, a few remarks are made about the residual strength requirements for the two damage tolerant design categories: slow crack growth structure and fail-safe structure.

4.1.1 Slow Crack Growth Structure

In a slow crack growth structure, the damage tolerance must be assured by the maintenance of a slow rate of crack growth, a residual strength capacity, and the assurance that subcritical damage will either be detected at the depot⁺ or will not reach unstable dimensions within the design lifetime of the structure. The residual strength curve for a structure which is inspected periodically is schematically shown in Figure 4.1.4. As a result of the inspections, the initially assumed cracks do not grow to a critical size and the structure is restored to its original load carrying capability when an inspection capability equal to that of the manufacturer's is employed.

Single-load-path "monolithic" structure must be qualified in this category; the residual strength estimation procedure for this type of

⁺depot level inspections have been eliminated as a design option by ASD for new slow crack growth structure in airframes.

structure is fairly straightforward. Built-up (multiple-load-path) structure can be qualified either in this category or in the fail-safe category.

4.1.2 Fail-Safe Structure

The residual strength requirement of a fail-safe structure is to assure damage tolerance following a partial failure of the structure. Damage tolerance is maintained through detection of this failure prior to total loss of the structure and sufficient residual strength capability for operating safely with the partial failure prior to inspection. The fail-safe structure is typically a built-up structure with multiple load paths or crack arrest features in its design. In the event of failure of a structural member, its load must be transferred to and withstood by the remainder of the structure, which also contains crack damage, without causing the loss of whole structure. The residual strength of the built-up structure must be determined under such critical circumstances so that the fail-safe design requirements are met.

The analysis of residual strength capability for built-up structure requires the estimation of the critical stress level at which the partial failure occurs, as well as an understanding of the capability of the total structure to withstand this partial failure at and subsequent to the time of failure. The required load associated with the time subsequent to failure is based on the inspection category; and, the partially failed structure must be able to maintain this load until the time of inspection.

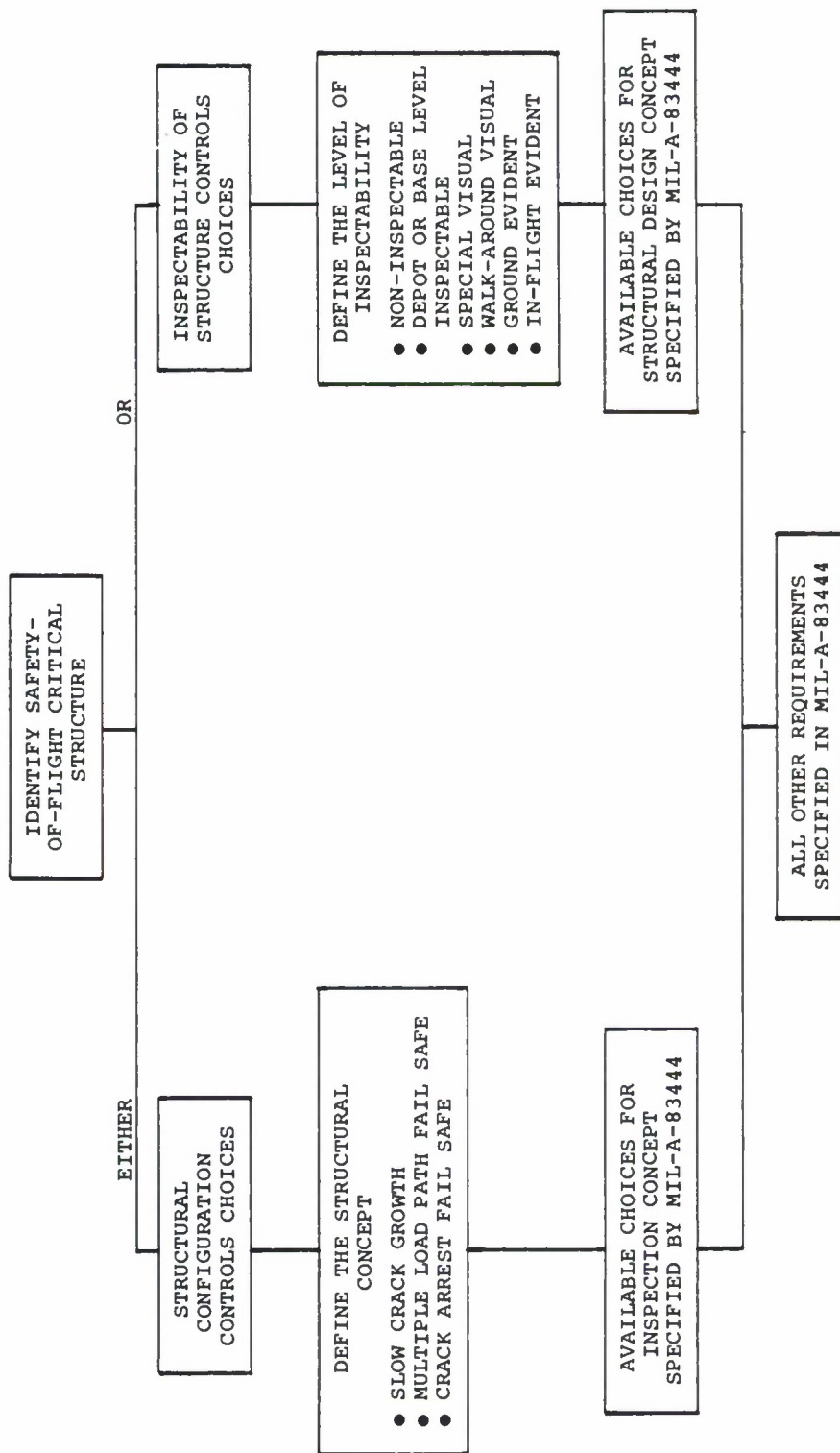


Figure 4.1.1.1. The Structural Configuration or Degree of Inspectability Controls the Subsequent Choices of Design Concept and Inspection Level.

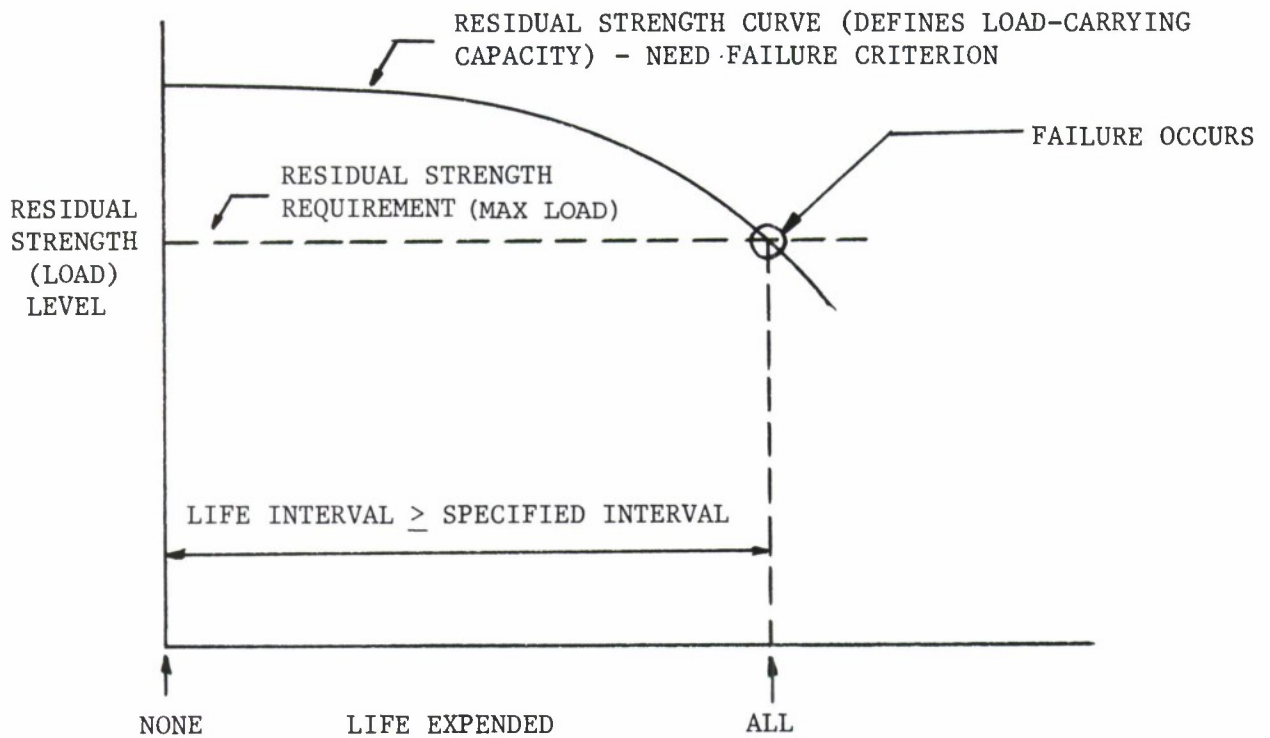


Figure 4.1.2. Relationship Between the Life Expended and Residual Strength Capability Showing a Monotonic Decrease in Load Carrying Capacity Due to Increased Structural Damage. Failure Occurs When the Residual Strength Capability Curve Intersects the Required Residual Strength Level.

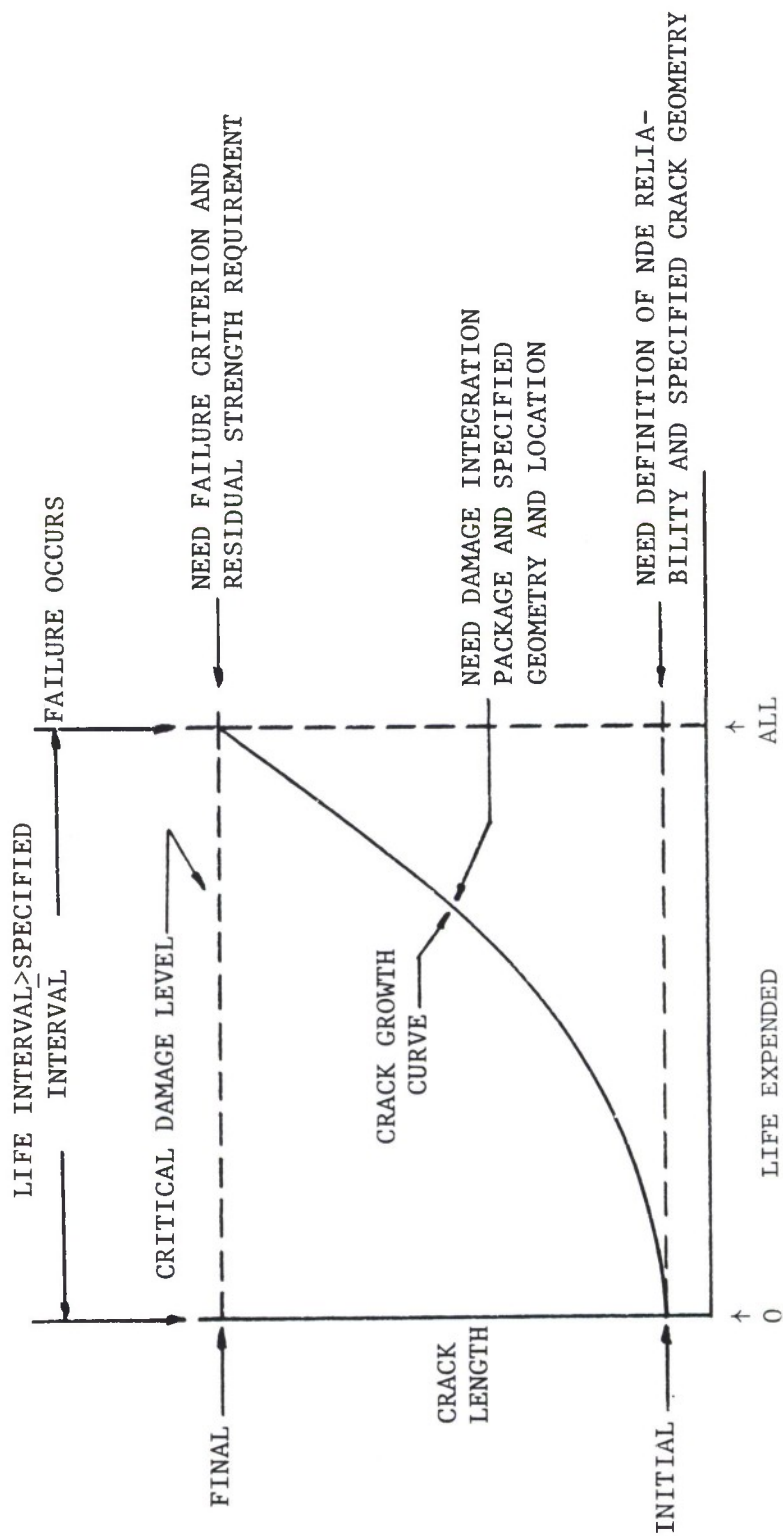


Figure 4.1.3. Relationship Between Crack Length and Life Expended Showing a Monotonic Increase in Crack Length Up Until Failure. Shown are the Various Technology and Specification Requirements Needed to Define the Crack Growth Curve Which, in Turn, Establishes the Life Limit.

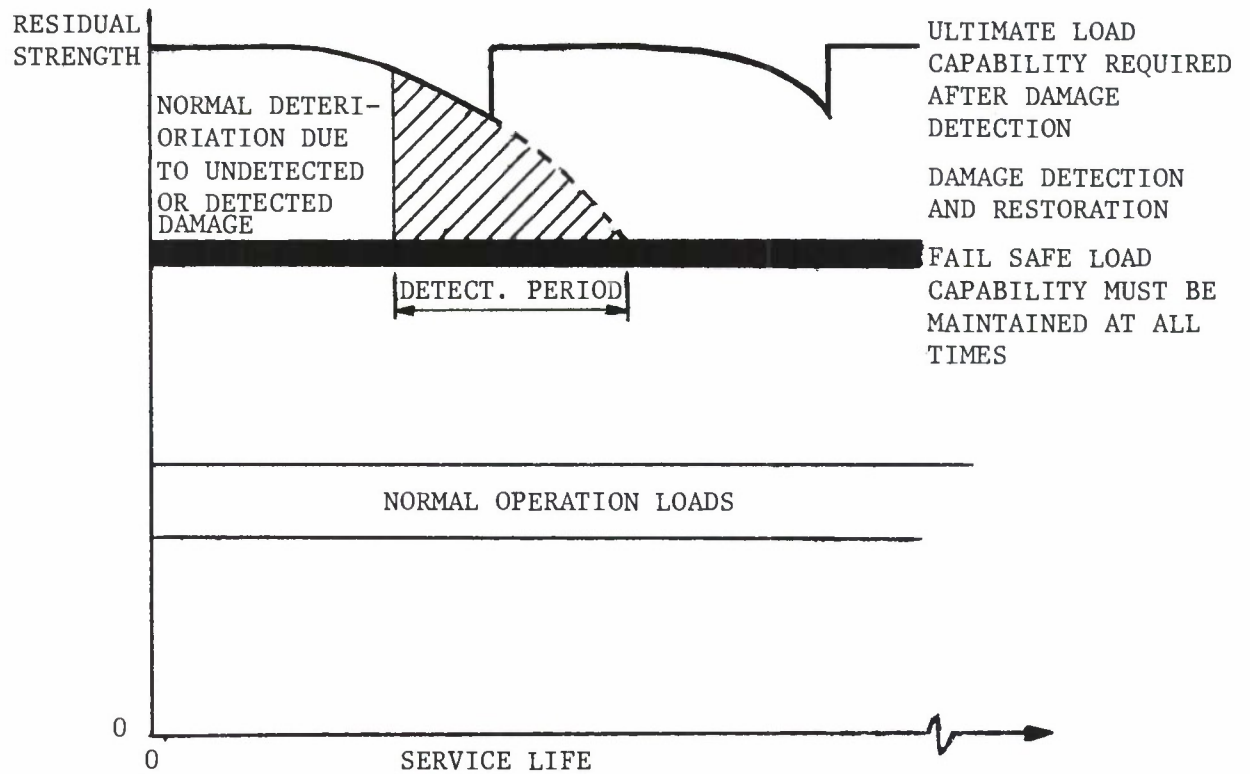


Figure 4.1.4. Strength Criteria for Periodically Inspected Damage Tolerant Structure.

4.2 FAILURE CRITERIA

The determination of residual strength for uncracked structures is straightforward because the ultimate strength of the material is the residual strength; whereas, a crack in a structure causes a high stress concentration resulting in a reduced residual strength. When the load on the structure exceeds a certain limit, the crack will extend. The crack extension may become immediately unstable and the crack may propagate in a fast uncontrollable manner causing complete fracture of the component.

Figure 4.2.1 illustrates the results obtained from a series of tests conducted on a lug geometry containing a crack. The lug geometry shown in Figure 4.2.1a is a single-load-path structure. Figure 4.2.1b indicates that the cracks in each of the three tests extended abruptly at a critical level of load which is noted to be a function of crack length. The crack length-critical load level data shown in Figure 4.2.1b provide the basis for establishing the residual strength capability curve (See Figure 4.1.2). The locus of critical load levels as a function of crack length is shown in Figure 4.2.1c where the residual strength capability of the lug structure is shown to decrease with increasing crack length.

Considering the preceding in terms of applied stress (σ) rather than load gives the σ versus a and σ_c versus a_c plots as shown in Figure 4.2.2

parts a and b. Schematically, the plots exhibit the same abrupt fracture behavior as the curves presented in Figure 4.2.1. As also shown in Figure 4.2.2 parts c and d, crack extension can first occur at a load level that is well below the fracture critical level. The point A' corresponds to the start of slow and stable extension of the crack. The unstable rapid extension leading to total failure occurs at Point A. This kind of behavior is observed typically in thin metal sheets or in tough materials. When different crack lengths are considered, the σ_c versus a_c plot will contain two distinct curves as shown in Figure 4.2.2d. The curve A'B'C' corresponds to the start of slow and stable crack extension and the curve ABC corresponds to failure.

In general, unstable crack propagation results in fracture of the component. Hence, unstable crack growth is what determines the residual strength. In order to estimate the residual strength of a structure, a thorough understanding of the crack growth behavior is needed. Also, the point at which the crack growth becomes unstable must be defined and this necessitates the need for a failure criterion. There are several criteria available; these criteria are tailored to represent the ability of a material to resist failure.

4.2.1 Ultimate Strength

The simplest failure criterion assumes that failure occurs at the ultimate (or yield) strength of the material. Thus, the failure

criterion becomes simply

$$\sigma_f = F_{tu}, \quad (4.2.1)$$

where σ_f is the fracture stress and F_{tu} is the ultimate strength. This criterion is applicable primarily to uncracked structures and is included here for completeness. In past analyses of failure of built-up structure, the residual strength of stiffeners was based upon this criterion. When the main panel between the stiffeners fails due to catastrophic crack growth, the panel loads are transferred to the stringers (or stiffeners). The transferred loads may increase the stress level in the stringer high enough to reach the value of σ_f , causing stiffener failure.

4.2.2 Fracture Toughness - Abrupt Fracture

In a cracked structure, as discussed in Chapter 1, the stress intensity factor (K) interrelates the local stresses in the region of the crack tip with: crack geometry, structural geometry, and the level of load on the structure. When the applied load level increases, the K value also increases and reaches a critical value at which time the crack growth becomes unstable as shown in Figure 4.2.3. This critical level of K, which is independent of the crack length, is a material property called fracture toughness. The fracture toughness is a measure of the material's resistance to unstable cracking. Several test procedures are available to evaluate the fracture toughness. Also, various theoretical and numerical solution techniques are available as discussed in Chapter 1, which can be used to estimate the (applied) stress intensity factor, K, for a given structure.

4.2.3

The failure criterion (Irwin's Criterion) states that abrupt fracture occurs when the crack-tip stress-intensity factor reaches or exceeds the fracture toughness of the material. The corresponding applied stress at failure is called the fracture strength. The failure criterion becomes simply

$$K \geq K_{cr} \quad (4.2.2)$$

where K_{cr} is the material's fracture toughness.

The critical K_{cr} for abrupt fracture mode is denoted as K_{Ic} for plane strain conditions and K_{Ic} for plane stress conditions; and the conditions for plane stress or plane strain are determined by experiment. The test requirements necessary for generating K_{Ic} and K_{Ic} are discussed in Chapter 7.

The Damage Tolerant Design (Data) Handbook⁽¹⁾ contains a large quantity of fracture toughness data. Examples of the formats associated with individual test data for 7075 aluminum alloy are shown in Figures 4.2.4 and 4.2.5 for plane strain and plane stress fracture toughness values, respectively. In general, a material's toughness depends on thickness as shown in Figure 4.2.6. When the thickness is such that the crack tip plastic zone size is on the order of the plate thickness, the toughness reaches a maximum value, $K_{Ic(max)}$. With increasing thickness of the plate, the plastic zone size reduces and thus the toughness gradually decreases, from $K_{Ic(max)}$ to K_{Ic} . When the thickness is large enough that the crack tip deformation is not affected by the thickness, plane strain conditions prevail at the crack tip. The toughness in the plane strain regime is

virtually independent of thickness. For increasing thickness, the toughness asymptotically approaches the plane strain fracture toughness, K_{Ic} .

4.2.3 Crack Growth Resistance - Tearing Fracture

As illustrated in Figures 4.2.2c and d, when the crack extends by a tearing mode of fracture, which typically occurs in thin metal sheets or in tough materials, the crack extension is essentially slow and stable. The failure condition for tearing fractures depends on the crack growth resistance (K_R) behavior of the material and the applied stress-intensity factor K , which in turn depends on the crack and structural configurations. Figure 4.2.7 describes the observations that lead to the development of the crack growth resistance curve (K_R vs. Δa). Figure 4.2.7 parts a and b present the tearing behavior as a function of applied stress and the corresponding stress-intensity factor, respectively. Figure 4.2.7c presents the crack growth resistance curve which is a composite of the three stress-intensity factor curves shown in Figure 4.2.7b. Note that the composite was created by using the amount of physical crack movement observed in each case as the independent variable. As implied by the data points on the crack growth resistance curve in Figure 4.2.7c, the stress-intensity factor level associated with material failure is not necessarily constant.

Shown in Figure 4.2.8 is a resistance curve for a 7475 aluminum alloy described as a function effective crack length (Ref. 2). The effective

crack length is the sum of the physical crack length and the plastic zone size corresponding to the current crack length and loading conditions.

Indeed, while the shape of the resistance curve is basically independent of crack length or other geometrical effects, the fracture level is a function of crack length (See Figure 4.7.9). To account for this variation in fracture critical level, a two parameter failure criterion was required. However, before introducing the two parameter criteria that are used for more accurate estimates, approximate single parameter criteria for tearing failures are presented.

4.2.3.1 The Apparent Fracture Toughness Approach

Due to the complexity of the two parameter fracture criteria for tearing fracture behavior, engineers sometimes obtain preliminary estimates of the residual strength using a single parameter fracture toughness criterion. Figure 4.2.10 describes the stress-crack length levels associated with the onset of cracking ($K = K_{\text{ONSET}}$) and fast fracture ($K = K_{\text{cr}}$) conditions for a tearing material. Intermediate between the two curves established from material observations is a third curve referred to as the apparent fracture curve. The apparent fracture toughness (K_{APP}) is established from the same data employed to derived K_{ONSET} and K_{cr} . The calculation procedure uses the onset (or initial) crack length (a_i) and the final recorded stress level (σ_{cr}) for the tests conducted. Thus, K_{APP} represents a fracture toughness level bounded by the onset and fast fracture levels.

For lower bound estimates of the residual strength for fast fracture of a tearing material, one could equate the level of applied stress-intensity factor (K) to the apparent fracture toughness (K_{APP}), i.e., assume that fracture occurs when

$$K = K_{APP} \quad (4.2.3)$$

in order to determine the critical level of stress. Equation 4.2.3 is an abrupt failure criterion for a tearing fracture.

4.2.3.2 The Resistance (R) Curve Approach

If the crack tip plastic zone size is estimated to be on the order of the structural thickness but substantially smaller than other geometrical variables (crack length, ligament size, height, etc.), a linear elastic fracture mechanics analysis can still be sensibly used to predict the catastrophic cracking event. The failure criterion for tearing type fractures under these conditions states that fracture will occur when (1) the stress-intensity factor K reaches or exceeds the material's fracture resistance K_R and (2) the rate of change of K (with respect to crack length) reaches or exceeds the rate of change of K_R (with respect to crack length). Physically, the criterion means that at failure, the energy available to extend the crack equals or exceeds the material resistance to crack growth. The failure criterion becomes simply,

$$K \geq K_R; \quad \frac{\partial K}{\partial a} \geq \frac{\partial K_R}{\partial a} \quad (4.2.4)$$

The corresponding applied stress, σ_f , at this point is defined as the fracture stress which determines the residual strength of the cracked structure. The criterion presented in Equation 4.2.4 is noted to be a two parameter criterion rather than the single parameter criteria that was presented in paragraph 4.2.3.1. To interpret the meaning of this criterion, first consider the structural parameters that are a function of the geometry and stress, i.e. K and $\frac{\partial K}{\partial a}$.

In general, the estimation of K involves the relationship $K = \sigma\sqrt{\pi a}$ as given in Chapter 1; using this equation, the variation of K with respect to crack length (a) can be obtained for various values of stress (σ) as shown in Figure 4.2.11a. Shown in Figure 4.2.11b is the variation of K_R with respect to the crack extension (Δa) that was developed for the given material using the procedures outlined in Figure 4.2.7. Since this R-curve is assumed to be independent of the initial crack length, it can be superimposed on the plot of K versus a as shown in Figure 4.2.11c. The tangency point between the applied stress intensity factor curve (K vs. a) and the R-curve (K_R vs. Δa) determines the commencement of unstable crack propagation. In general, the accurate method of determining the tangency point involves the numerical solution based on the experimentally obtained R-curve. Using a least squares determined polynomial expression for R-curve and knowing an expression for K in terms of crack length, the common tangent point can be obtained by equating the functional values ($K = K_R$) and also the first derivatives with respect to the crack length ($\frac{dK}{da} = \frac{dK_R}{da}$) of these two expressions.

The slow stable tear is dependent on a structural configuration in which the plastic zone at the crack tip is no longer negligible but not enormous. References 3, 4 and 5 explain the dependence of the R-curve on structural configuration as well as with test procedures used to evaluate the R-curve. See Chapter 7 for additional information on test procedures and the Damage Tolerant Design (Data) Handbook⁽¹⁾ for a summary of available data.

4.2.3.3 The J-Integral Resistance Curve Approach

The crack growth resistance curve (K_R) has shown good promise for materials where limited (small-scale) yielding occurs in front of the crack tip. Difficulties in estimating crack tip plasticity under large-scale yielding conditions, led Wilhem⁽⁶⁾ to an alternate failure criterion based on the J-integral⁽⁷⁾. For a basic introduction to the J-integral see Section 1.9.

Wilhem's J-integral criterion is similar to the K_R - curve criterion; it states that failure will occur when the following conditions are met:

$$\sqrt{J} \geq \sqrt{J_R} ; \frac{d\sqrt{J}}{da} \geq \frac{\partial \sqrt{J_R}}{\partial a} \quad (4.2.5)$$

where J is the value of the applied J-integral and J_R is the value of the J-integral representing the material resistance to fracture. The applied stress (σ_f) corresponding to Equation 4.2.5 is defined as the fracture stress. Since the effect of large-scale yielding can be appropriately incorporated through a suitable elastic-plastic model in the estimation of J-integral, it becomes an effective parameter for predicting failure

under plane stress conditions where the plastic zone size is significantly large.

The crack resistance curve for the tearing failure is now represented by $\sqrt{J_R}$ vs. Δa curve instead of K_R vs. Δa curve. The use of $\sqrt{J_R}$ rather than J_R is justified by the fact that \sqrt{J} is directly related to the stress-intensity factor for elastic behavior through the equation

$$J = K^2/E' \quad (4.2.6)$$

where E' is the elastic modulus (E) for plane stress conditions and $E/(1-\nu^2)$ for plane strain conditions.

For different levels of applied load, the J-integral can be computed using finite element techniques for the structure of interest for a series of different crack sizes; the \sqrt{J} versus crack length curve is illustrated in Figure 4.2.12a for a constant level of applied stress. It is noted that this curve will incorporate the influence of material properties (yield strength and strain hardening exponent) through the finite element analysis. In a manner similar to the stress-intensity factor type resistance curve, i.e. the K_R curve, the resistance curve based on $\sqrt{J_R}$ can be experimentally obtained^(8,9). A $\sqrt{J_R}$ versus crack movement (Δa) curve, i.e. the J-integral resistance curve, is schematically illustrated in Figure 4.2.12b. The failure criterion is also based on the tangency conditions between the \sqrt{J} versus crack length curve and the $\sqrt{J_R}$ versus crack movement curve. To obtain this condition, the $\sqrt{J_R}$ vs. Δa curve can be superimposed on the plot of \sqrt{J} vs. a curve such

that at some crack length these two curves are tangent to each other as shown in Figure 4.2.12c. The corresponding crack length then defines the critical crack size of the structure for the fracture stress, σ_f .

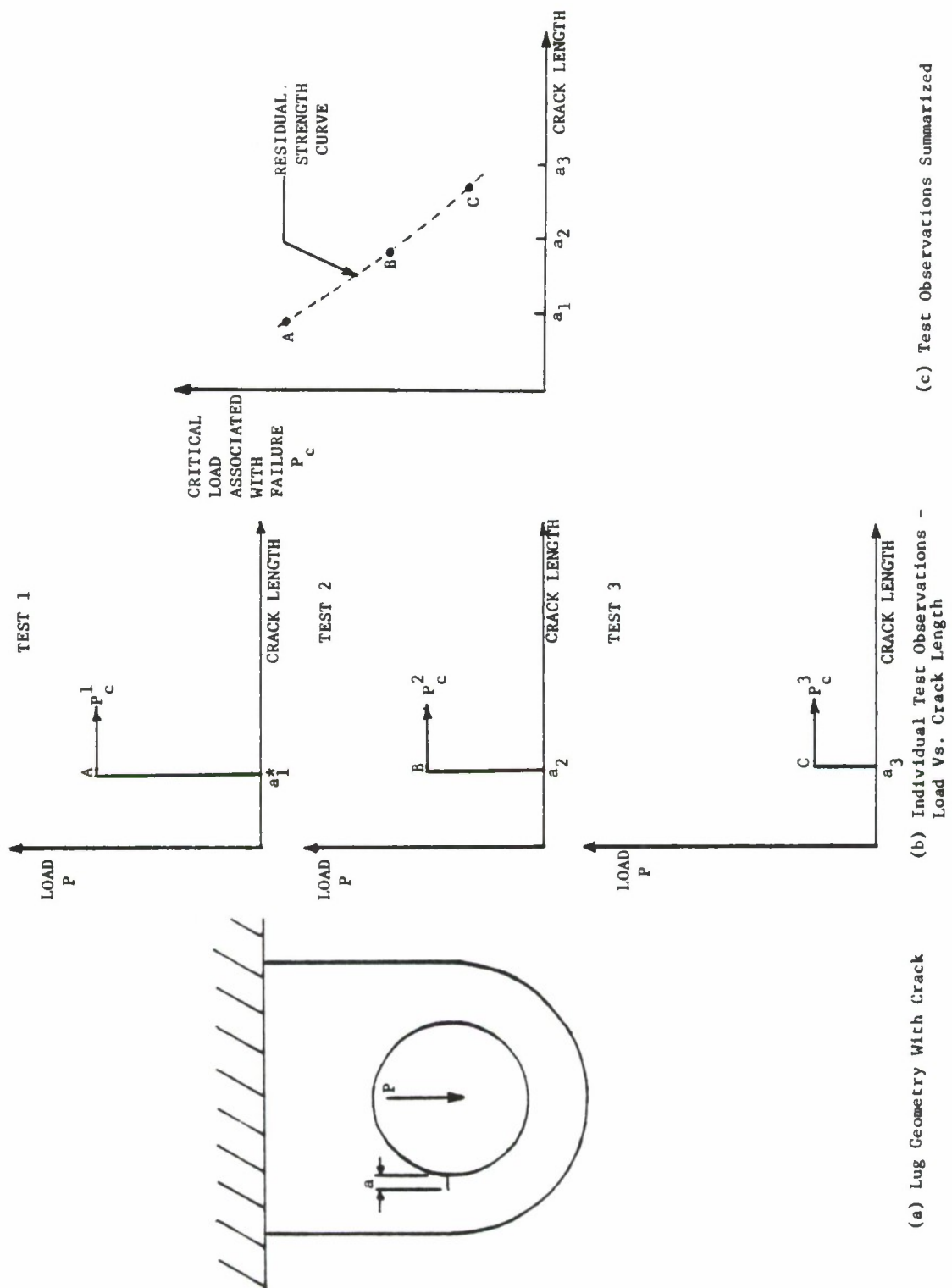
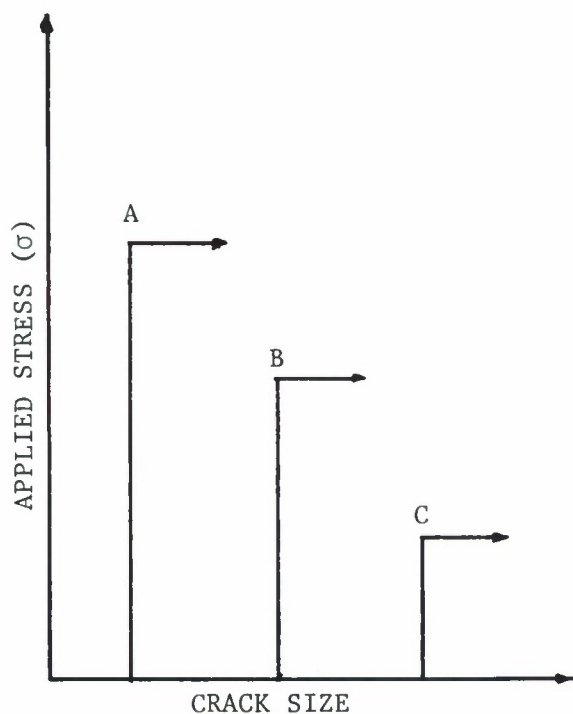
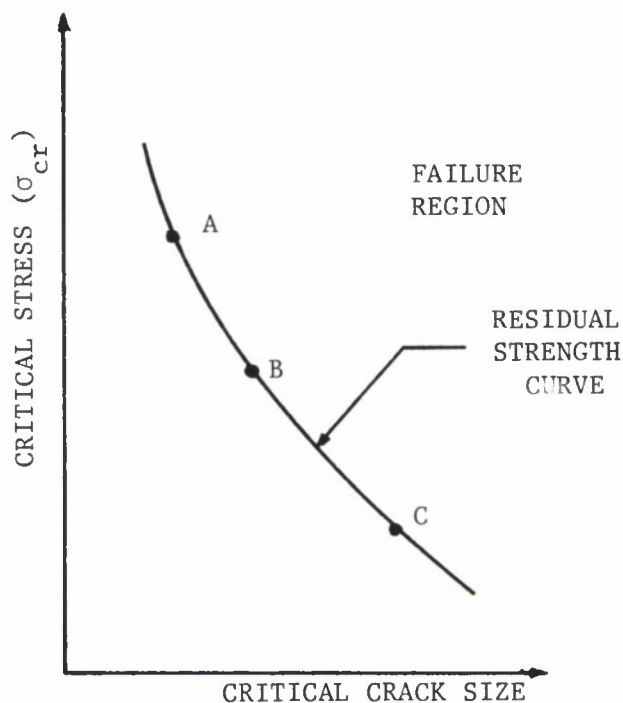


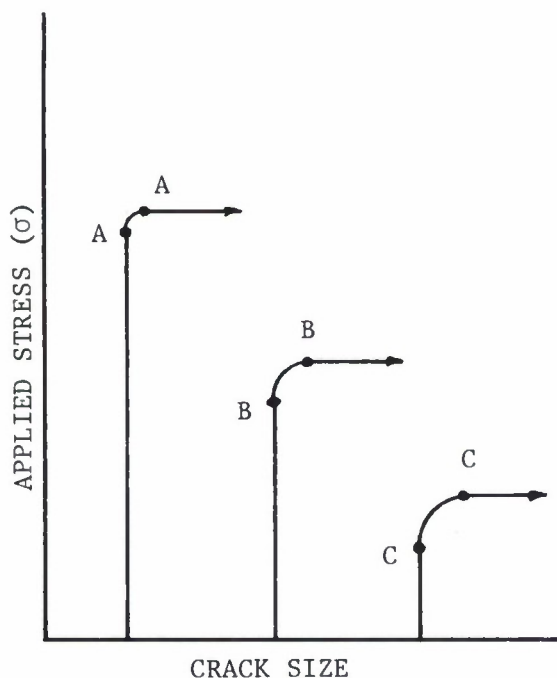
Figure 4.2.1.1. Description of Crack Geometry and Residual Strength Results.



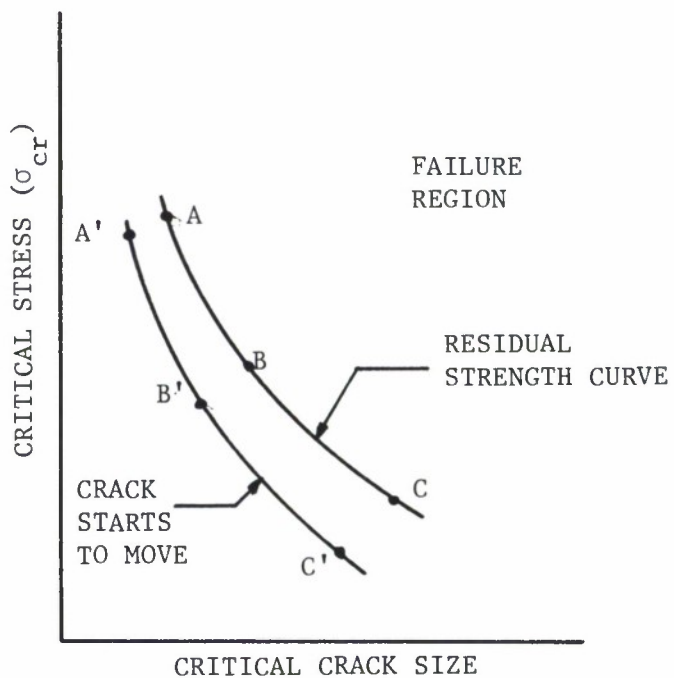
(a) Individual Test Data-
Abrupt Failure



(b) Critical Stress Data Summarized-
Abrupt Failure

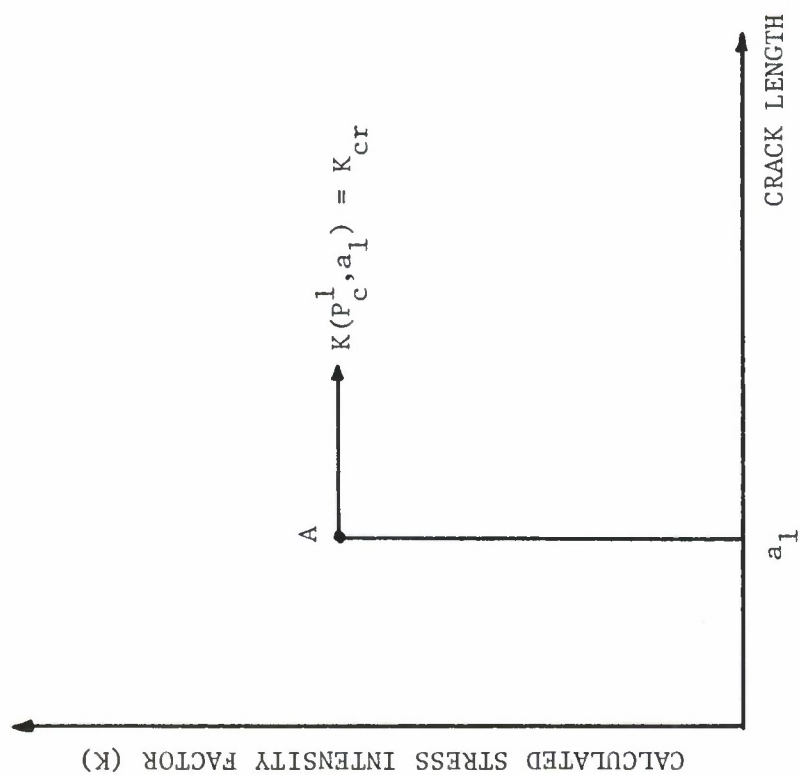


(c) Individual Test Data-
Tearing Failure

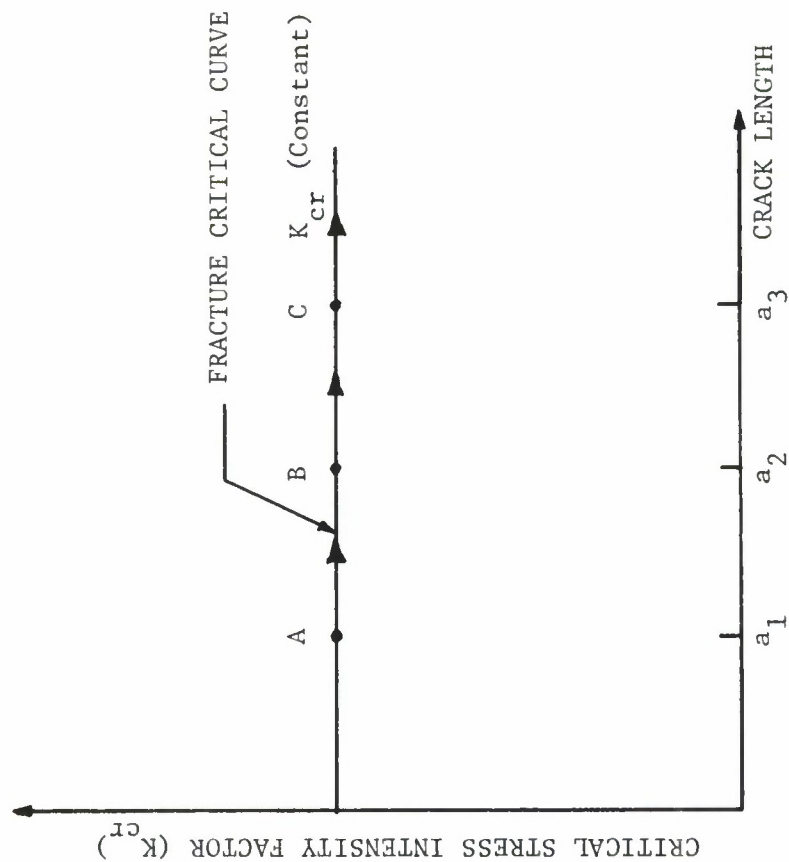


(d) Critical Stress Data Summarized-
Tearing Failure

Figure 4.2.2. Fracture Data Described as a Function of Crack Length.



(a) Stress Intensity Factor Calculated as a Function of Load and Crack Length.



(b) Critical Stress Intensity Factor Levels Described as a Function of Crack Length.

Figure 4.2.3. The Fracture Mechanics Basis for Establishing Residual Strength.

CONDITION	ALUMINUM 7075										K(C)				STAN												
	--PRODUCT--		TEST SPEC		YIELD		---SPECIMEN---		CRACK		LENGTH		---STRESS---		MAX		K(APP)		MEAN DEV		K(C)		MEAN DEV		DATE REF		
	FORM		THICK		OR		WIDTH		THICK		INIT		FINAL		ONSET		K(SI)		K(SI*SGRT IN)		K(C)		K(SI*SGRT IN)		K(C)		
	(IN)		(F)		(KSI)		(IN)		(IN)		A(D)		A(F)		S(D)		S(MAX)										
BUCKLING OF CRACK EDGES NOT RESTRAINED																											
T6	S	0.06	R. T.	T-L	75.5	4.500	0.063	1.130	1.130	1.130	1.130	1.130	1.130	---	40.00	55.46	55.46	55.46	55.46	55.46	55.46	55.46	55.46	55.46	55.46	1966 86734	
		0.06			75.5	4.500	0.063	1.130	1.130	1.130	1.130	1.130	1.130	---	40.00	55.46	55.46	55.46	55.46	55.46	55.46	55.46	55.46	55.46	55.46	1966 86734	
T6	S	0.06	R. T.	T-L	75.5	6.000	0.063	1.500	1.500	1.500	1.500	1.500	1.500	---	35.20	56.21	56.21	56.21	56.21	56.21	56.21	56.21	56.21	56.21	56.21	1966 86734	
T6	S	0.06	R. T.	T-L	75.5	10.000	0.064	2.250	2.250	2.250	2.250	2.250	2.250	---	30.10	58.42	58.42	58.42	58.42	58.42	58.42	58.42	58.42	58.42	58.42	1966 86734	
T6	S	0.06	R. T.	T-L	75.5	12.000	0.063	3.000	3.000	3.000	3.000	3.000	3.000	---	24.10	54.43	54.43	54.43	54.43	54.43	54.43	54.43	54.43	54.43	54.43	1966 86734	
T6	S	0.06	R. T.	T-L	75.5	15.000	0.063	3.750	3.750	3.750	3.750	3.750	3.750	---	21.80	55.05	55.05	55.05	55.05	55.05	55.05	55.05	55.05	55.05	55.05	1966 86734	
		0.06			72.9	15.810	0.063	5.980	5.980	5.980	5.980	5.980	5.980	---	15.80	53.20	53.20	53.20	53.20	53.20	53.20	53.20	53.20	53.20	53.20	1973 86213	
		0.06			72.9	15.810	0.063	3.010	3.010	3.010	3.010	3.010	3.010	---	25.40	56.50	56.50	56.50	56.50	56.50	56.50	56.50	56.50	56.50	56.50	1973 86213	
		0.06			72.9	15.810	0.063	3.010	3.010	3.010	3.010	3.010	3.010	---	25.70	57.17	57.17	57.17	57.17	57.17	57.17	57.17	57.17	57.17	57.17	1973 86213	
		0.06			72.9	15.820	0.063	1.000	1.000	1.000	1.000	1.000	1.000	---	42.90	53.90	53.90	53.90	53.90	53.90	53.90	53.90	53.90	53.90	53.90	1973 86213	
		0.06			72.9	15.820	0.063	4.000	4.000	4.000	4.000	4.000	4.000	---	20.40	53.25	53.25	53.25	53.25	53.25	53.25	53.25	53.25	53.25	53.25	1973 86213	
T6	S	0.06	R. T.	T-L	75.5	18.000	0.064	4.500	4.500	4.500	4.500	4.500	4.500	---	19.60	54.21	54.21	54.21	54.21	54.21	54.21	54.21	54.21	54.21	54.21	1966 86734	
T6	S	0.06	R. T.	T-L	75.5	21.000	0.064	5.250	5.250	5.250	5.250	5.250	5.250	---	19.60	58.56	58.56	58.56	58.56	58.56	58.56	58.56	58.56	58.56	58.56	1966 86734	
T6	S	0.06	R. T.	T-L	69.0	24.000	0.063	8.000	8.000	8.000	8.000	8.000	8.000	---	11.40	43.43	43.43	43.43	43.43	43.43	43.43	43.43	43.43	43.43	43.43	1966 86734	
		0.06			69.0	24.000	0.063	8.000	8.000	8.000	8.000	8.000	8.000	---	11.30	43.04	43.04	43.04	43.04	43.04	43.04	43.04	43.04	43.04	43.04	1966 86734	
		0.06			69.0	24.000	0.063	8.000	8.000	8.000	8.000	8.000	8.000	---	10.90	41.52	41.52	41.52	41.52	41.52	41.52	41.52	41.52	41.52	41.52	1966 86734	
		0.06			69.0	24.000	0.063	8.000	8.000	8.000	8.000	8.000	8.000	---	11.25	42.85	42.85	42.85	42.85	42.85	42.85	42.85	42.85	42.85	42.85	1966 86734	
		0.06			69.0	24.000	0.063	8.000	8.000	8.000	8.000	8.000	8.000	---	11.40	43.43	43.43	43.43	43.43	43.43	43.43	43.43	43.43	43.43	43.43	1966 86734	
		0.06			75.5	24.000	0.064	6.000	6.000	6.000	6.000	6.000	6.000	---	16.71	53.37	53.37	53.37	53.37	53.37	53.37	53.37	53.37	53.37	53.37	1966 86734	
		0.06			75.5	24.000	0.064	6.000	6.000	6.000	6.000	6.000	6.000	---	17.00	54.30	54.30	54.30	54.30	54.30	54.30	54.30	54.30	54.30	54.30	1966 86734	
T6	S	0.08	R. T.	T-L	73.3	29.990	0.081	15.000	15.000	15.000	15.000	15.000	15.000	---	9.70	56.00	56.00	56.00	56.00	56.00	56.00	56.00	56.00	56.00	56.00	1966 86734	

Figure 4.2.5. Plane-Stress Fracture Toughness (K_C) Data for 7075 Aluminum in the Format of Reference 1.

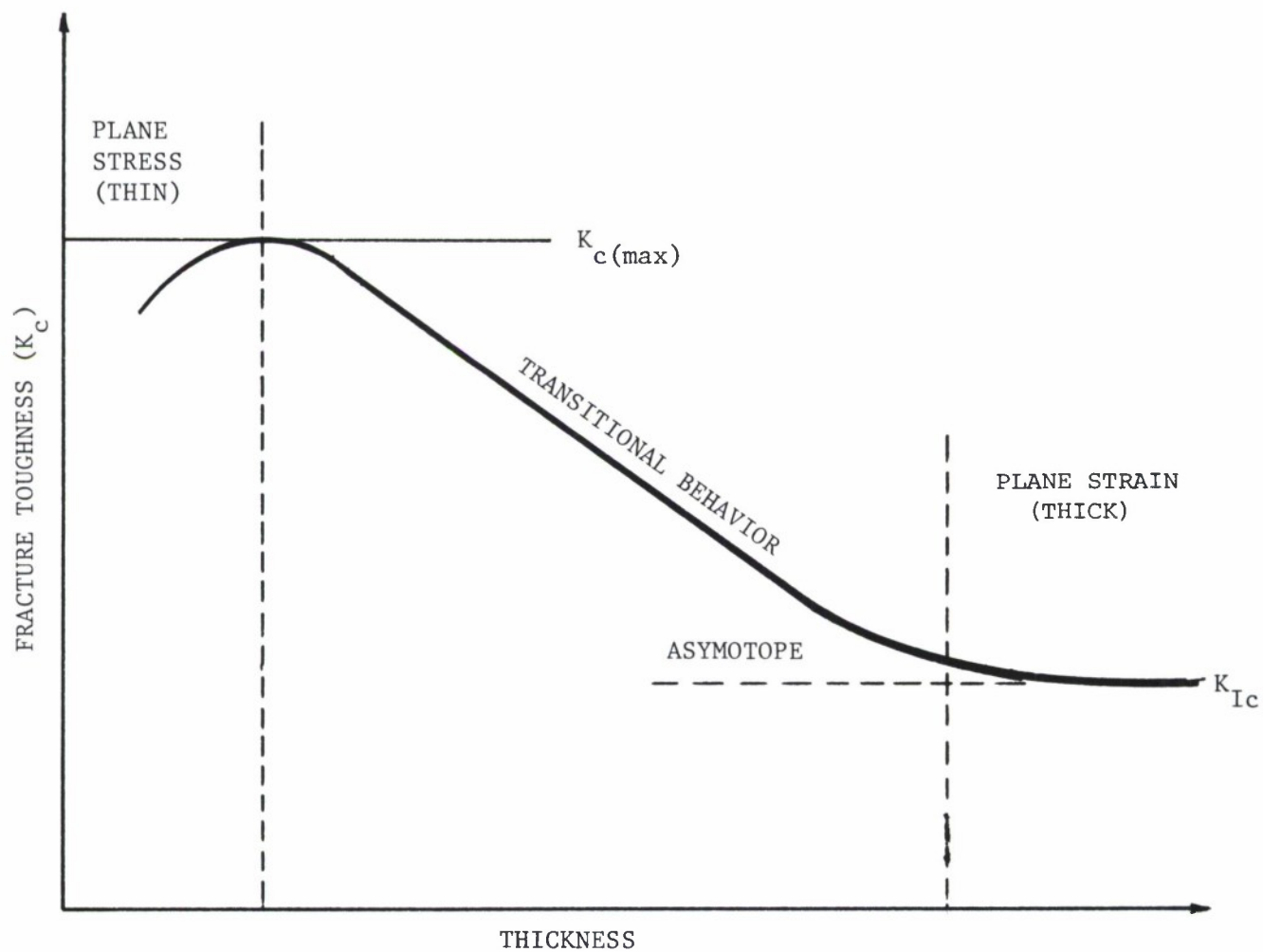


Figure 4.2.6. Fracture Toughness Behavior as a Function of Thickness.

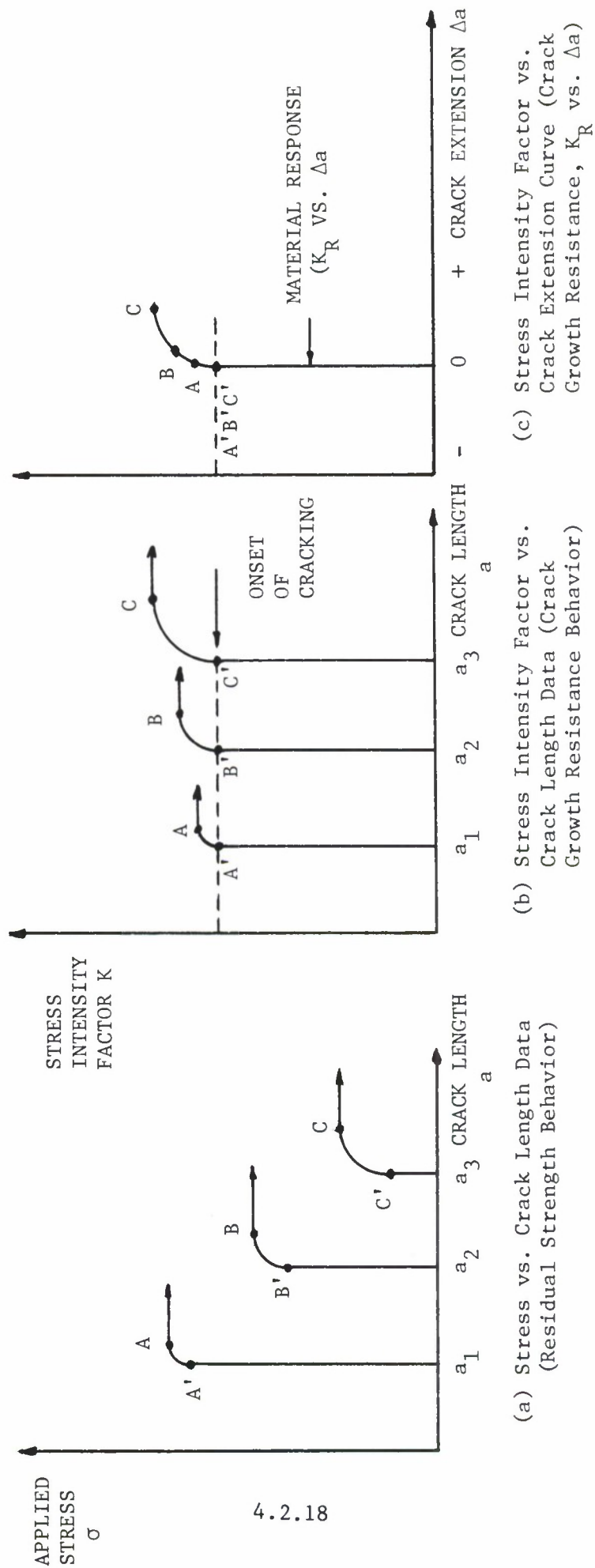


Figure 4.2.7. Schematic Illustration of Tearing Fracture Behavior and the Development of a Crack Growth Resistance Curve (R-Curve).

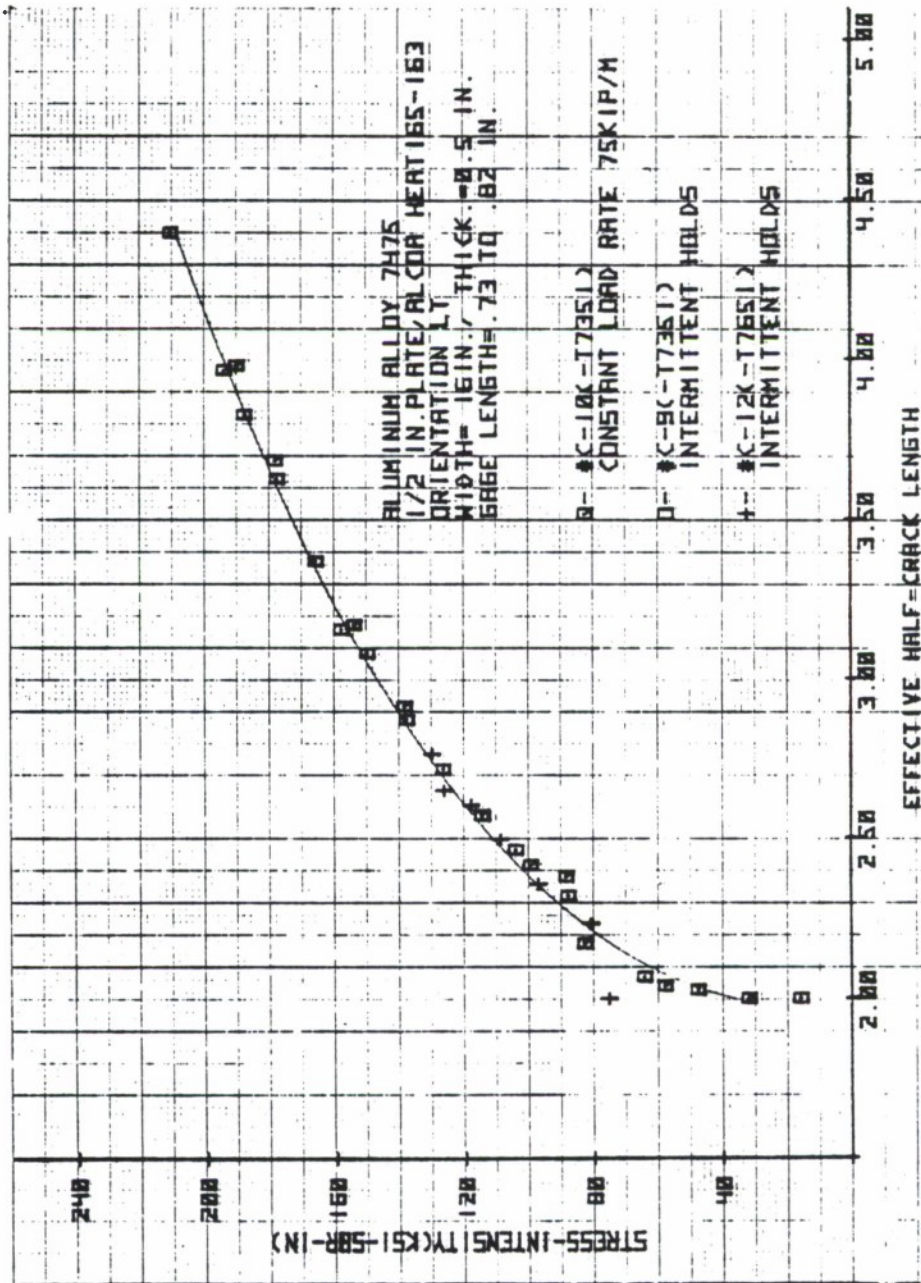


Figure 4.2.8. K_R Curves from 7475 Alloy, 16 Inch Wide Panels, 0.5 Inch Thickness (Reference 2).

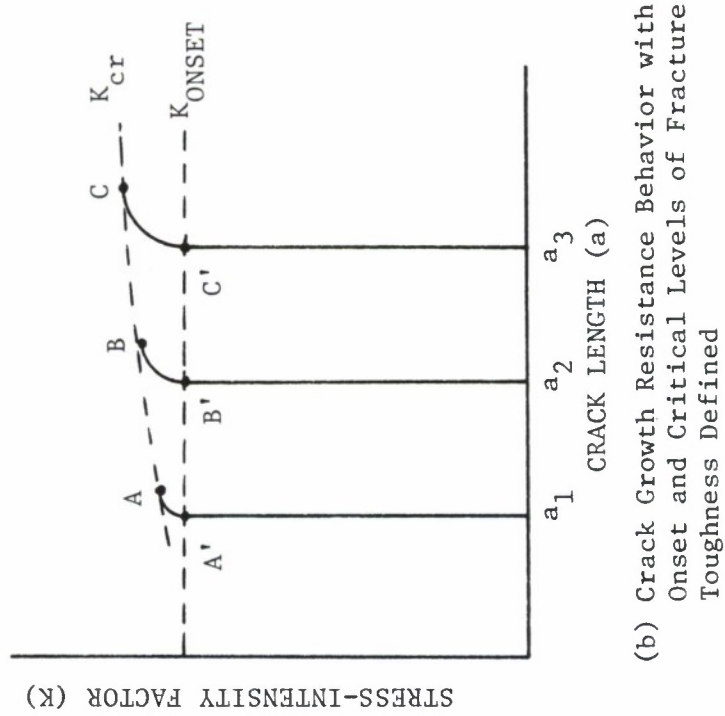
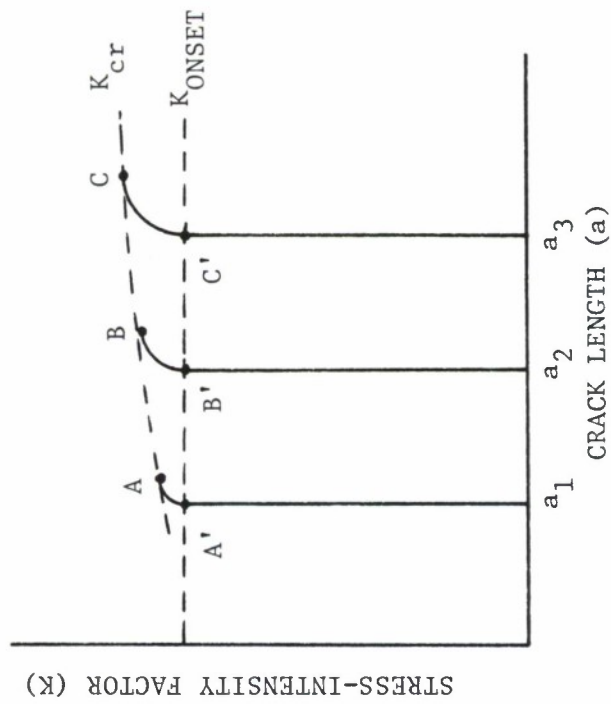


Figure 4.2.9. Schematic Illustration of Tearing Fracture Behavior Which Further Defines the Change in Critical Level of Fracture Toughness as a Function of Crack Length (Also See Figure 4.2.7).

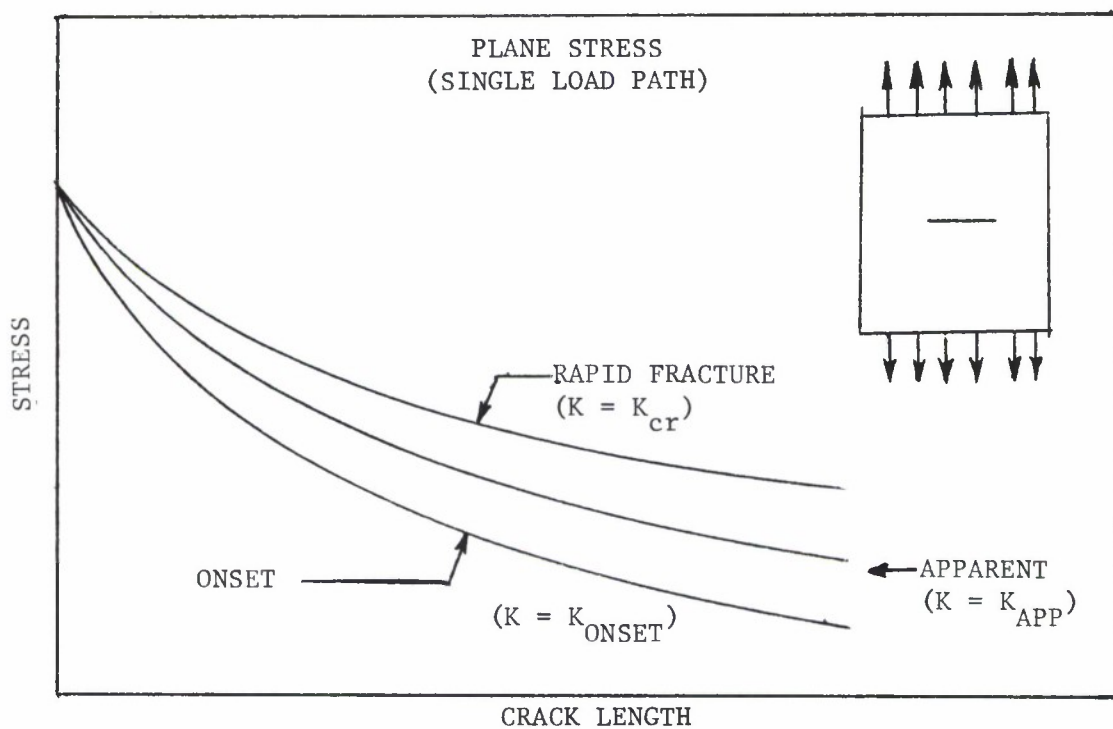
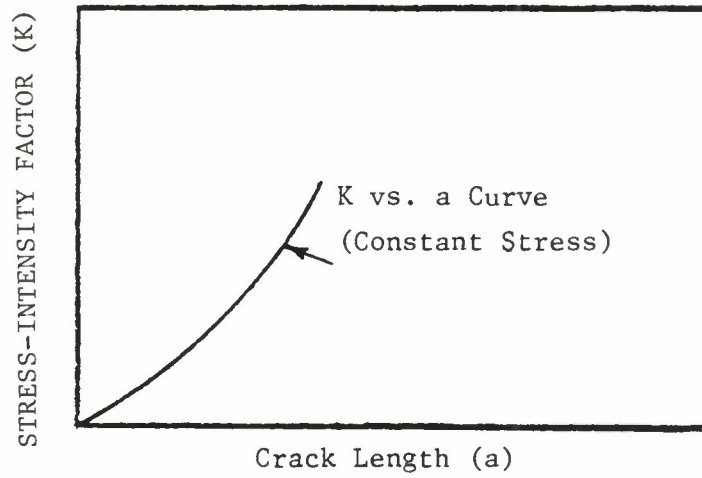
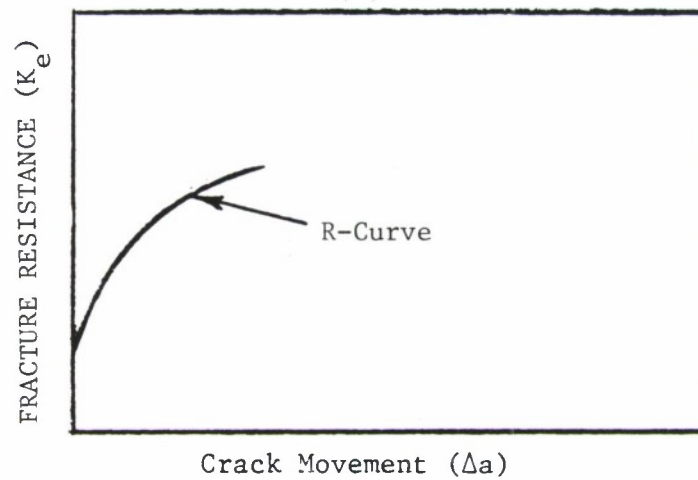


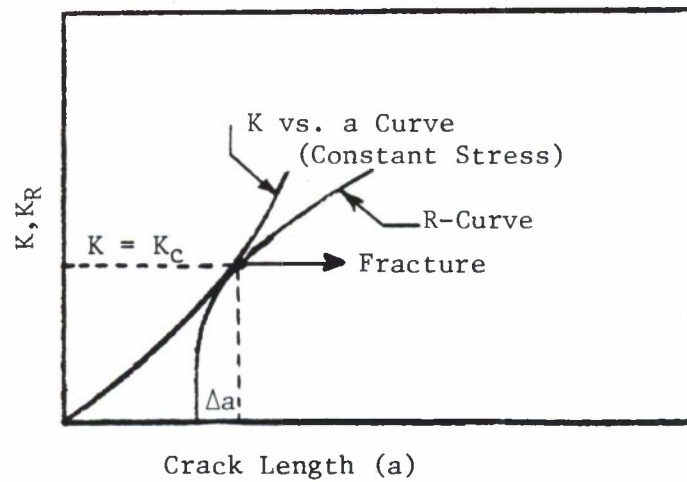
Figure 4.2.10. Description of the Three Fracture Toughness Criteria that are Utilized to Estimate Residual Strength Under Tearing Fracture Conditions.



(a) Driving Force

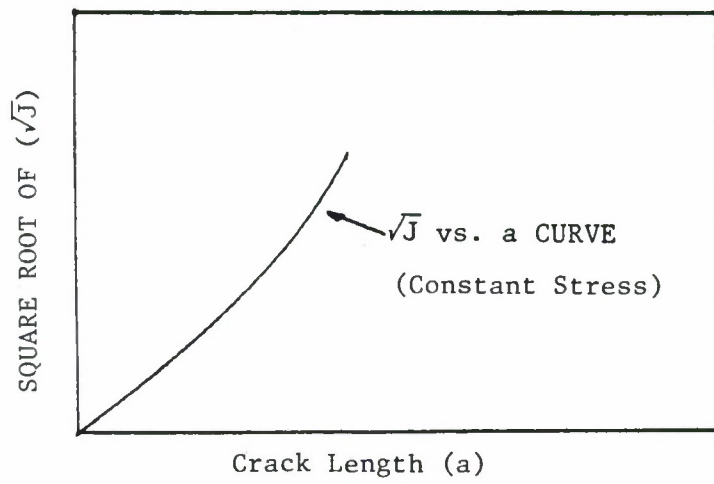


(b) Resistance to Crack Growth

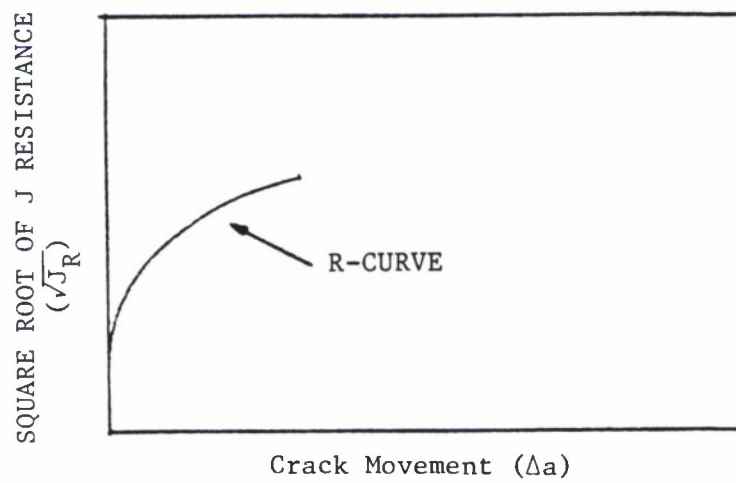


(c) Establishment of Critical Conditions

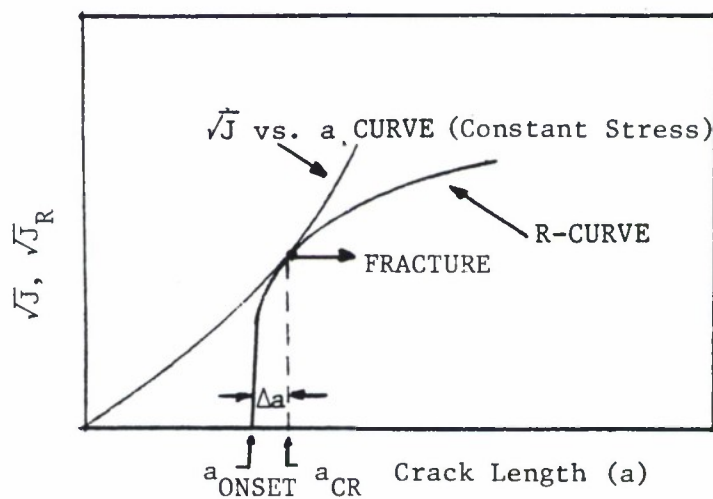
Figure 4.2.11. Schematic Illustration of the Individual and Collective Parts of A K_R Fracture Analysis.



a. Driving Force



b. Resistance to Crack Growth



c. Establishment of Critical Conditions

Figure 4.2.12. Schematic Illustration of the Individual and Collective Parts of a $\sqrt{J_R}$ Fracture Analysis.

4.3 RESIDUAL STRENGTH CAPABILITY

To establish the residual strength capability of a given structure under certain loading conditions, prediction techniques must be developed with a thorough understanding of the complexities involved in evaluating the residual strength. For monolithic or single load path structures which must be classified as slow crack growth structures, the estimation of residual strength capability is straightforward. In multiple load path (built-up) structures, whether classified as slow crack growth or fail-safe structures, the strength analysis can become complicated, due to the complex geometric construction of the built-up components. In general, the prediction techniques are based on the critical value of the stress-intensity factor for a given geometry and loading. Using fracture toughness failure criteria as explained earlier, the decay in critical stress can be obtained in terms of crack size.

As described by Figure 4.1.2, the residual strength capability is a function of service time for a given structure. This is because the residual strength capability depends on the size of the crack in the structure and the crack grows as a function of time. Thus to obtain a residual strength capability curve (Figure 4.1.2), one needs two types of data: (a) the relationship between crack length and time and (b) the relationship between fracture strength (σ_f) and crack length. Chapter 5 is devoted to obtaining the crack length-time relationship and the remainder of this chapter is devoted to presenting methods and procedures

4.3.1

for obtaining the fracture strength-crack length (σ_f vs. a) relationship. It is to be noted that the σ_f vs. a relationship is independent of time and has been referred to in the general literature as the residual strength diagram. This section presents useful information about residual strength diagrams for single load path and for multiple load path structures.

4.3.1 Single Load Path Residual Strength Diagrams

For a single load path structure, such as an unstiffened panel, the residual strength diagram under plane strain conditions, consists of a single curve as shown in Figure 4.3.1. The procedure for developing the residual strength diagram involves the calculation of the critical stress σ_f , for the critical crack length a_c , using the relationship $K_{cr} = \sigma_f \beta \sqrt{\pi a_c}$ where K_{cr} is the known value of fracture toughness of the material. (K_{cr} may be equal to K_{Ic} or K_c depending on the problem.) The plot of σ_f vs a_c then provides the necessary residual strength diagram required in design analysis for the simple configuration.

The available fracture mechanics solution techniques, as given in Chapter 1, can be employed in the calculation of the crack-tip stress-intensity factor K to construct the residual strength diagram. Depending on the complexity of the structure, K can be calculated either numerically or through closed form solutions. These techniques, in conjunction with an appropriate failure criterion, can then be used to determine the residual strength capabilities of a given structure.

4.3.2

In general, the construction of a residual strength diagram involves three steps:

- (a) The development of the relationship between the applied stress σ , the crack length parameter a , and the applied stress-intensity factor K for the given structural configuration (See Section 1.6).
- (b) The selection of an appropriate failure criterion based for the expected material behavior at the crack tip (See Section 4.2).
- (c) The fracture strength (σ_f) values for critical crack sizes (a_c) are obtained utilizing the results of the first two steps and residual strength diagram (σ_f vs a_c) for the given structural configuration is plotted.

To understand these three steps for constructing a residual strength diagram, the following two examples are considered. The first example considers a wide thin panel with a central crack which has a simple relationship for the stress intensity factor. The second example considers corner and embedded cracks emanating from a hole; the second configuration does not have a simple relationship for the stress-intensity factor. These two examples will illustrate the importance of the stress-intensity factor for constructing the residual strength diagram.

EXAMPLE 4.3.1 Unstiffened Center Crack Panel

Construct the residual strength diagram for the wide unstiffened panel shown in Figure 4.3.2, assuming that the structure is made from 7075-T6 aluminum sheet material, with a fracture toughness of $40 \text{ ksi}\sqrt{\text{in}}$.

SOLUTION:

Following the three step process, the first step that must be taken is to define the stress-intensity factor relationship. From Table 1.7.1, the stress intensity factor for a wide unstiffened, center crack panel is given by

$$K = \sigma\sqrt{\pi a} \quad (4.3.1)$$

The second step is to define the failure criterion. For this problem, it is assumed that an abrupt fracture occurs and the condition that defines the fracture is

$$K = K_{cr} = K_c = 40 \text{ ksi}\sqrt{\text{in}} \quad (4.3.2)$$

The third and final step is to utilize the results of the first two steps to derive a relationship between fracture strength (σ_f) and critical crack size (a_c) from Equations 4.3.1 and 4.3.2, the σ_f vs a_c relationship is given by

$$\sigma_f\sqrt{a_c} = 40/\sqrt{\pi} \quad (4.3.3)$$

For a half crack size (a_c) of 2.0 inch, the fracture strength (σ_f) is about 16. ksi. Other (σ_f vs a_c) values can be similarly obtained. Once a sufficient number of values are available, the residual strength diagram can be developed.

One could also attack the problem in the graphic manner which will now be explained using Figure 4.3.3. The three steps are identified in Figure 4.3.3a.

The first step is to construct a plot of K vs a using Equation 4.3.1 for

various values of stress. The second step requires that one superimpose the horizontal line $K = K_{cr} = 40 \text{ Ksi}\sqrt{\text{in}}$ on the diagram. This line represents the critical stress intensity, i.e., fracture toughness, for this material and is independent of crack length. Step 3 utilizes the intersection points of the horizontal line with curves where the failure criterion is satisfied, i.e. where $K_{cr} = \sigma_f \sqrt{\pi a_c}$. The values of the respective stresses and the crack sizes at these points are termed to be the failure stresses and the critical crack sizes for the given structure, i.e., the unstiffened panel. In Figure 4.3.2b, the residual strength diagram is finally constructed by plotting the σ_f vs a_c curve.

EXAMPLE 4.3.2 Cracked Fastener Hole

Construct the residual strength diagrams for the radially cracked structure shown in Figure 4.3.4. Consider the two radial crack geometries separately, i.e., construct one residual strength diagram for the corner cracked hole and one residual strength diagram for the embedded (bore type) cracked hole illustrated in Figure 4.3.4b. For purposes of this example, the crack geometry is assumed to maintain the same crack shape (a/b ratio) as the crack grows. Also assume the fastener hole is unloaded and the plate is subjected to remote uniform stress along the edge as shown in Figure 4.3.4.

SOLUTION:

The first step in the construction of the residual strength diagram

is to obtain the stress-intensity factor relationships ($K = \sigma\beta\sqrt{\pi a}$) for the structural configuration. The estimation of β may involve closed form solutions or numerical solutions, depending on the complexities of the structural geometry. Fujimoto⁽¹⁰⁾ has presented one method for obtaining the stress intensity factors at points A and B shown in Figure 4.3.4b for the given geometry (See Section 1.7 for other solutions). The required stress intensity factor relationship has the following form⁽¹⁰⁾,

$$K_A = \beta_A \sigma\sqrt{\pi a} \quad (4.3.4)$$

and

$$K_B = \beta_B \sigma\sqrt{\pi b} \quad (4.3.5)$$

where

$$\beta_A = \sum_{i=0}^4 A_i \left(\frac{R}{R+a}\right)^i \quad (4.3.6)$$

and

$$\beta_B = \sum_{i=0}^4 B_i \left(\frac{R}{R+a}\right)^i \quad (4.3.7)$$

The coefficients A_i and B_i are evaluated by:

$$A_i = \sum_{j=0}^2 \sum_{k=0}^3 A_{ijk} \left(\frac{a}{b}\right)^j \left(\frac{b}{B}\right)^k \quad (4.3.8)$$

and

$$B_i = \sum_{j=0}^2 \sum_{k=0}^3 B_{ijk} \left(\frac{a}{b}\right)^j \left(\frac{b}{B}\right)^k \quad (4.3.9)$$

The constants A_{ijk} and B_{ijk} for the various configurations are summarized in Table 4.3.1⁽¹⁰⁾. The solutions presented by Equations 4.3.4 through 4.3.9 are suggested to be accurate to within $\pm 7\%$ for $0.5 \leq a/b \leq 2$, $a/R \leq 3$ and $b/B \leq 0.8$ (corner crack) and $b/B \leq 0.95$ (embedded flaw). For

TABLE 4.3.1

COEFFICIENTS FOR CORNER (A_{ijk}) AND EMBEDDED (B_{ijk}) FLAWS

Table I

Aijk Coefficients				
Aijk	Open Hole Corner Flaw	Loaded Hole Corner Flaw	Open Hole Embedded Flaw	Loaded Hole Embedded Flaw
A000	-1.73913	-0.44699	-1.26736	-0.27428
A001	2.18447	-0.41009	0.22793	-0.37981
A002	-12.31660	-0.17500	-0.31572	1.06466
A003	12.28036	-0.28705	0.27700	-0.70431
A010	2.03400	0.49602	1.46408	0.22855
A011	-5.54602	-1.17354	-0.51878	0.80844
A012	26.30347	0.05565	0.60348	-2.20899
A013	-28.83108	0.52655	-0.64122	1.42081
A020	-0.62550	-0.15949	-0.42884	-0.04803
A021	2.04171	0.52542	0.59595	-0.31512
A022	-10.08710	-0.15182	-1.10433	0.82786
A023	11.28916	-0.12493	0.82250	-0.51180
A100	20.44604	3.62963	16.35029	2.04350
A101	-12.98692	-3.42947	-1.36796	3.18371
A102	79.06818	1.25362	0.90021	-8.85802
A103	-81.39789	2.58161	-1.10382	5.83154
A110	-19.15893	-4.24345	-14.44464	-1.80365
A111	32.54240	9.71349	3.18175	-6.91026
A112	-153.17228	0.99495	-0.90493	18.66301
A113	183.89616	-5.61054	2.48066	-11.94847
A120	5.63804	1.38285	3.97690	0.38262
A121	-11.48757	-4.33299	-4.73213	2.70521
A122	57.78026	0.50822	8.12799	-7.01695
A123	-71.50791	1.70251	-6.10715	4.30908
A200	-54.07142	-8.73901	-40.03081	-3.66265
A201	26.28259	10.12695	1.69908	-9.40318
A202	-173.61978	-2.81193	5.31024	26.26181
A203	186.67485	-8.39172	-2.33583	-17.22762
A210	55.38509	12.06427	37.64427	4.07100
A211	-65.48530	-28.54288	-4.94141	20.73286
A212	310.31737	-4.71604	-11.78825	-55.81962
A213	-414.90592	18.60957	3.89408	35.80193
A220	-16.99852	-4.10506	-10.77498	-0.88681
A221	21.87818	12.64776	12.74285	-8.14196
A222	-113.03797	-0.10892	-19.73785	21.00805
A223	159.51377	-6.34499	14.67313	-12.89406
A300	63.91046	9.86487	44.09282	3.18017
A301	-21.34684	-12.58513	1.30029	11.71907
A302	155.66256	2.41823	-17.28515	-32.85878
A303	-177.54153	11.37710	10.22270	21.47714
A310	-69.55437	-14.91176	-42.79166	-4.23316
A311	53.27534	35.32007	-0.41580	-26.09328
A312	-239.17594	9.64735	34.36822	70.23733
A313	382.87850	-26.68173	-19.03715	-45.03193
A320	21.97211	5.18043	12.56399	0.94129
A321	-16.45864	-15.54508	-13.63744	10.23302
A322	81.63436	-2.04295	18.05169	-26.34017
A323	-144.56350	9.86170	-13.65703	16.12578
A400	-25.48746	-3.45644	-15.57989	-0.32568
A401	6.07411	5.63847	-2.29626	-5.26245
A402	-47.33858	-0.47231	12.79822	14.81260
A403	58.83734	-5.58817	-7.87547	-9.62040
A410	30.61973	6.33835	16.18676	1.20944
A411	-15.30575	-15.72380	3.64549	11.77369
A412	56.77733	-5.25457	-24.86827	-31.67043
A413	-123.39537	13.06793	15.10964	20.30113
A420	-10.04444	-2.28421	-4.93434	-0.27841
A421	4.18466	6.85458	4.68604	-4.60124
A422	-16.39237	1.58956	-4.47318	11.81074
A423	45.39223	-5.06460	3.68566	-7.22032

Table II

Bijk Coefficients				
Bijk	Open Hole Corner Flaw	Loaded Hole Corner Flaw	Open Hole Embedded Flaw	Loaded Hole Embedded Flaw
B000	0.54048	0.15717	-0.14090	-0.04578
B001	-8.13585	-0.18905	-0.19118	0.23456
B002	38.74291	0.36964	-1.42513	-1.03245
B003	-36.61072	-0.55842	2.70092	1.04606
B010	-0.51374	-0.34371	0.24126	0.02019
B011	20.70229	0.67188	-0.06062	-0.68745
B012	-96.53400	-1.02481	3.50309	2.60507
B013	94.56232	2.24038	-5.56386	-2.53181
B020	0.23259	0.13161	-0.03900	-0.01654
B021	-8.10325	-0.24870	0.14748	0.39027
B022	37.49696	0.15076	-1.79208	-1.40898
B023	-36.02049	-0.43639	2.62247	1.30659
B100	-3.93066	-1.40838	1.51775	0.39092
B101	54.54817	3.05268	2.95869	-1.89716
B102	-267.23920	-5.58993	6.91519	8.31125
B103	257.44638	5.83453	-18.34105	-8.38878
B110	10.54763	4.21388	2.99000	0.49356
B111	-137.75080	-8.95923	1.42239	5.83529
B112	658.29611	13.40329	-33.45103	-22.27612
B113	-664.66240	-20.77969	51.72551	21.67629
B120	-3.12356	-1.39814	-0.63004	0.03033
B121	53.58138	3.40310	-0.68160	-3.10127
B122	-250.42133	-2.82250	12.97239	11.27094
B123	246.15655	3.95030	-20.04903	-10.45358
B200	12.31339	4.73501	-4.21283	-1.00774
B201	-130.01489	-13.23293	-14.43670	4.85151
B202	652.54759	23.67186	1.64581	-21.38737
B203	-639.45674	-20.29833	33.74666	21.56301
B210	-25.20873	-11.55251	-4.32532	-0.24067
B211	329.32411	36.63884	8.63271	-14.25572
B212	-1601.55759	-56.47692	47.76155	54.50932
B213	1664.84801	69.79620	-103.79259	-53.08007
B220	8.01373	4.12442	1.06179	-0.25385
B221	-126.43281	-13.84244	-2.78214	7.75229
B222	602.66553	14.96288	-18.70448	-28.10606
B223	-608.02169	-15.00235	40.49219	26.14542
B300	-14.68582	-6.15314	5.54863	1.21024
B301	130.65565	21.26107	23.96607	-5.08309
B302	-678.54260	-39.04345	-27.28160	22.36259
B303	680.29731	30.88059	-18.01680	-22.53679
B310	32.19384	15.42347	6.56869	0.72364
B311	-329.36748	-56.34595	-20.61094	15.16998
B312	1648.82514	89.92427	-16.75978	-57.78589
B313	-1780.81402	-99.14050	88.27022	56.49131
B320	-10.69055	-5.64651	-2.00699	0.07354
B321	124.22248	21.24180	8.57289	-7.89956
B322	-605.34757	-24.65551	1.19613	28.37763
B323	632.49290	21.54101	-28.78621	-26.44062
B400	6.62558	2.93506	-2.17015	-0.40455
B401	-47.11327	-11.40477	-12.23145	1.91775
B402	252.80634	20.97539	19.85932	-8.33485
B403	-260.05599	-15.75597	-0.06542	8.32499
B410	-15.12721	-7.31732	-3.18803	-0.37767
B411	118.27654	29.53266	12.75632	-5.49372
B412	-604.94418	-46.78340	-9.48745	20.67719
B413	681.55676	47.49374	-21.42362	-20.07632
B420	5.12997	2.70455	0.99823	-0.00082
B421	-43.91149	-11.21255	-5.70704	2.73978
B422	217.00926	13.56194	8.16120	-9.63864
B423	-234.55121	-10.63665	3.75003	8.91080

the detailed solution procedures involved in obtaining these expressions, refer to the paper by Fujimoto⁽¹⁰⁾ who also presents solutions for the condition where the fastener is loaded.

Subjected to the conditions when the crack size ratio (a/b) is equal to 1.0, the stress-intensity factor solutions for points A and B are given in Figure 4.3.5 for the quarter-circular corner crack and in Figure 4.3.6 for the embedded semicircular crack. The K_A and K_B curves in these two figures were obtained from Equations 4.3.4 through 4.3.9 with the appropriate coefficients taken from Table 4.3.1.

Having established a relationship for the applied stress intensity factors K_A and K_B , the second step is to choose an appropriate failure criterion. The given configuration consists of a thick plate where plane strain conditions exist and the appropriate fracture toughness criterion based on the K_{Ic} value can be used. Substituting the value of K_{Ic} for K_A and K_B as a failure condition in Equations 4.3.4 and 4.3.5, the equations can be solved for σ for various values of a . The residual strength diagram for the open hole configuration can be constructed through the following equations.

$$\sigma_f^A = \frac{K_{Ic}}{\beta_A \sqrt{\pi a}} \quad (4.3.10)$$

and

$$\sigma_f^B = \frac{K_{Ic}}{\beta_B \sqrt{\frac{b}{a}} \sqrt{\pi a}} \quad (4.3.11)$$

The solutions to Equations 4.3.10 and 4.3.11 are presented in Figure 4.3.7 for the radial quarter circular crack geometry and in Figure 4.3.8 for the radial embedded semicircular crack geometry. Note that the conditions associated with Point B in both crack geometries is more severe and actually defines the residual strength of this radially cracked structure.

4.3.2 Built-Up Structure Residual Strength Diagrams

In single load path structures, the residual strength analysis involved only one failure criterion for a given structural geometry; whereas in built-up structures, due to the complex geometrical configuration, one or more failure criterion may have to be considered in the determination of residual strength for the whole structure. The following paragraphs examine these aspects of the residual strength analysis of built-up structures.

It was explained earlier that safety can be achieved by designing aircraft structure either as slow crack growth or as fail-safe. The latter case can further be classified into two cases: Multiple Load Path and Crack Arrest. Typically, both Multiple Load Path and Crack Arrest structures are built-up structures. In Chapter 2, the definitions and requirements for these two types of built-up structure are discussed. For completeness, the structure shown in Figure 4.3.9 is analyzed to further explain the features inherent in multiple load path, built-up structure. As long as the central member is not failed, all three elements

carry a share of the total load P . In the event of failure of the center member, the total load P (actually $1.15P$) must be transmitted by the other two members at the instant of failure, if the structure is to stay intact. The residual strength capability for the multiple load path structure shown in Figure 4.3.9 can be explained with Figure 4.3.10. When one element fails, Figure 4.3.10 shows that the remaining parallel members are able to carry the required load without failure. The residual capability is shown to degrade as the crack in the central member extends and as the cracks in the remaining elements fail. Figure 4.3.10 shows the discontinuous change in the strength capability as a result of element failures. Since the load levels in other members dramatically increase, if the load P must be maintained, the remaining members will have short lives. Thus, the second member may fail after the time (t_2). The residual strength capability is shown to drop below the safe level somewhere in time between t_1 and t_2 . The duration of the time interval between the failure of the first element and the failure of the structure may be short or long depending on the "type of failure" of the first member and the load requirements subsequent to this failure. This time interval is available for the detection of the failure of the first member and the repair of the structure.

The failure stress or the critical flaw size level of the central member (any one of the parallel members) can be estimated by treating the problem in a manner similar to the single load path structure. Using a

fatigue crack growth analysis, the crack propagation curve is obtained from the minimum detectable crack size to the critical crack length as illustrated in Figure 4.3.11. In multiple load path structure, partial failure of the structure can occur during its operating period. But this failure must be detected at an inspection before catastrophic failure of the entire structure occurs. A suitable inspection schedule must include analysis of structural characteristics along with the operational requirements for the intervals between inspections.

To illustrate the analysis involved in the estimation of residual strength of complex structures, consider an axially loaded skin-stringer combination with longitudinal stiffening as shown in Figure 4.3.12. Assuming that the fasteners are rigid, the displacements of adjacent points in skin and stringers will be equal. (If skin and stringers are made from the same material, the stresses in the two will also be equal for the case of no crack.) Let a transverse crack develop in the skin. This will cause larger displacement in the skin. The stringers must follow this larger displacement. As a result, they take load from the skin, thus decreasing the skin stress at the expense of higher stringer stress. Consequently, the displacements in the cracked skin will be smaller than in an unstiffened plate with the same size of crack. This implies that the skin stresses are lower and that the stress-intensity factor is lower. The closer the stringers are to the crack, the more effective is the load transfer.

If the stress-intensity factor for a small crack in an unstiffened panel is approximated by $K = \sigma\sqrt{\pi a}$, the stress-intensity factor for the stiffened plate will be $K = \beta\sigma\sqrt{\pi a}$. The reduction factor, $\beta = K/\sigma\sqrt{\pi a}$, will decrease when the crack tip approaches a stringer. Since the stringers take load from the skin, the stringer stress will increase from σ to $L\sigma$, where L increases as the crack tip approaches the stringer. Obviously, $0 < \beta \leq 1$, and $L \geq 1$. These values depend upon stiffening ratios, the stiffness of the attachment, and the ratio of crack size to stringer spacing. As will be shown subsequently, β and L can be readily calculated; at this point it is sufficient to note that β and L vary with crack length as shown in Figure 4.3.13.

Due to the complexity of stiffened skin structure, the construction of a residual strength diagram is considerably more difficult. Consider first the condition where an abrupt failure in the skin occurs. When the crack is small as compared to the stiffener spacing, the residual strength of the skin is not influenced by the stiffeners and the initial portion of the diagram follows the plot for an unstiffened panel (See point A in Figure 4.3.14). Once the crack size is long enough that the skin cannot sustain the applied load any further, the stringer will take some of the load from the skin, thus decreasing the skin stress. Consequently, the crack-tip stress-intensity factor will be lower due to the reduced stress and so the residual strength of the skin structure will increase with crack length as shown in Figure 4.3.13. As the crack size increases further toward the

stiffener location, the load transferred from the skin to the stiffener also increases significantly, thus reducing the stress-intensity factor. The residual strength of the stiffened panel continues to increase as shown in the figure for longer cracks. It can also be noted from the figure that the residual strength diagram for an unstiffened panel would have followed the dotted line, i.e., the continuous decay in the residual strength as the crack size increases. This is because there is no inherent feature present in the single load path structure to decrease the crack tip stress-intensity factor.

The residual strength diagram for the skin-stiffened structure is repeated in Figure 4.3.15 where several additional points of interest are defined for the analyst. For a structure with a crack of length a_A , the residual strength is identified as point A. Since point A is associated with a failure stress that is above the peak stress (σ_{peak}), the crack extends abruptly and completely fails the panel. If the structure contains a crack of length a_C , in the range between a_B and a_D , the crack extends abruptly but then arrests at crack length a_E , where the residual strength available is greater than the applied (failure) stress. This crack extension and arrest feature of skin-stringer construction greatly facilitates meeting inspection requirements for fail-safe structures.

Before the panel fails completely, the failure stress level at point C/E must be increased to the level associated with point F, i.e. to σ_{peak} . As the stress is increased above the level of point E, the crack extends

from a_E to maintain an equilibrium between the input stress and the residual strength. When the stress reaches σ_{peak} , the crack has extended to a_F , at which point the crack abruptly extends causing failure of the panel. A schematic illustrating the load crack length diagram observed during an abrupt crack extension/arrest situation in a skin-stringer structure is presented in Figure 4.3.16. Thus, it is seen that the residual strength curve ABCDEF shown in Figure 4.3.15 can be replaced for all practical purposes with a curve that connects points ABF.

In the design of fail-safe structure, a frequent objective is to design the structure for limiting or arresting unstable crack growth so that catastrophic failure can be prevented. A number of arrest techniques are described in References 11 through 13. The fundamental concept in crack arrest design is to provide within the structure a means to reduce the crack tip stress intensity factor. This concept requires the use of additional stiffening members such as stiffeners, reinforcing rings, etc., to produce a decrease in the stress. These are inherently present in built-up structures, such as aircraft wings, fuselages, etc. as shown in Figure 4.3.12.

In general, the residual strength analysis of a structure with crack arrest capabilities may involve more than one failure criterion. For instance, in a stiffened skin structure or an aircraft wing, the analysis should consider stringer failure, fastener failure, and skin crack failure criteria. Built-up panels loaded to fail-safe levels tend to

exhibit substantial local deformations of critical elements. Failure criteria are thus dependent also on elastic-plastic deflection allowables for both fastener and skin/stringer elements. Gunther and Wozumi⁽¹⁴⁾ provide additional details on the residual strength analysis of complex panels based on the ultimate stringer strain.

The residual strength diagram for the structure which exhibits slow crack growth behavior will contain two curves as shown in Figure 4.3.17. The lower curve corresponds to the critical level of stress at which slow crack extension starts. The onset of slow tearing is then described by this lower curve. The upper curve provides the critical stress level at which the unstable rapid crack extension occurs. When the crack approaches the stiffener, as explained earlier, the residual strength levels, corresponding to the onset of slow cracking and the rapid extension, start increasing.

For a crack length a_1 , as shown in Figure 4.3.17, the slow crack extension begins at point B. This stable extension continues up to point B' where the rapid failure is supposed to occur. However, due to the continuous rise in the residual strength of the stiffened panel, the stable crack extension continues to occur beyond point B' and up to point C. Since the residual strength of the panel starts reducing at this point, any further increase in the applied load will lead to the rapid unstable crack extension.

The construction of the residual strength diagram follows the three steps presented in Section 4.3.1. Due to the complexity of the structural geometry, however, estimating requires the calculation of the loads that are transferred to the stiffening or secondary members from the main load carrying member of the structure. Depending upon the complexity, the K vs a curves can be obtained either through an appropriate numerical method or through the method of superposition. The methods for constructing residual strength diagrams and for the residual strength capability analyses are further discussed in the following sections with various example problems.

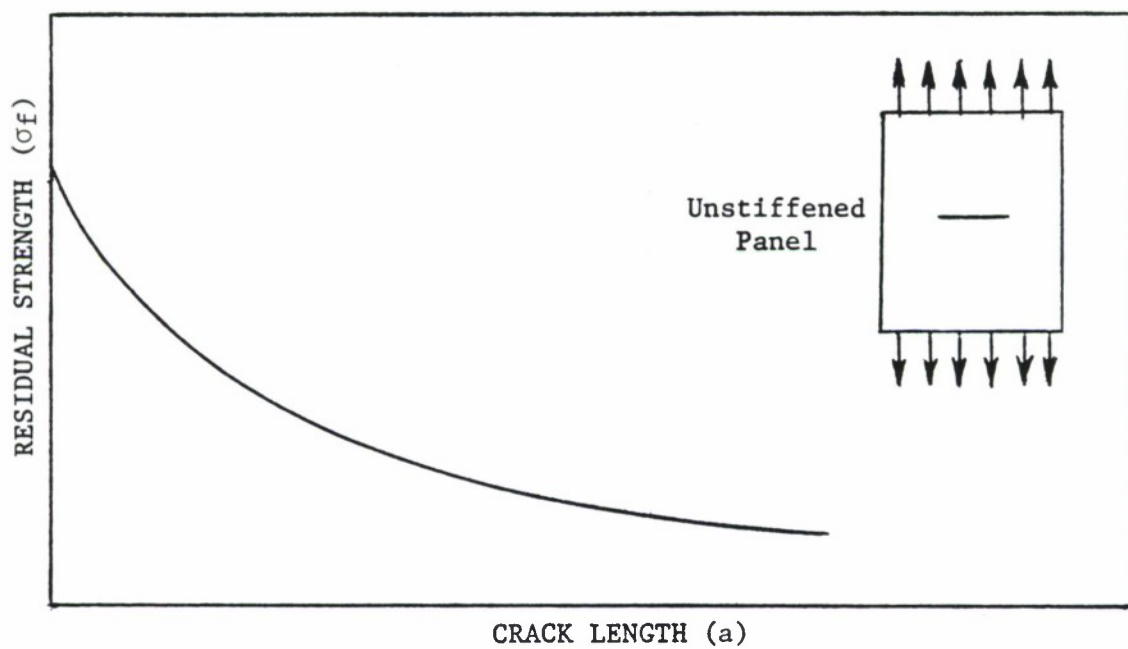


Figure 4.3.1. Residual Strength Diagram for Abrupt Failure of a Single Load Path Structure.

MATERIAL PROPERTIES

yield strength (σ_{ys}) = 74 ksi

Fracture Toughness
(K_C) = 40 ksi $\sqrt{\text{in}}$

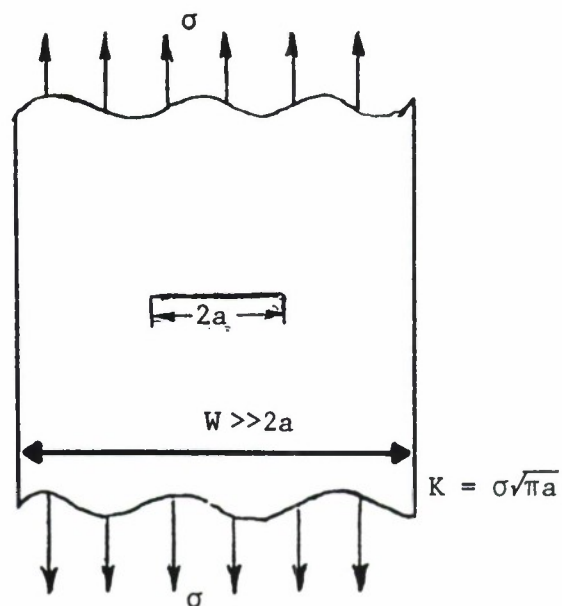
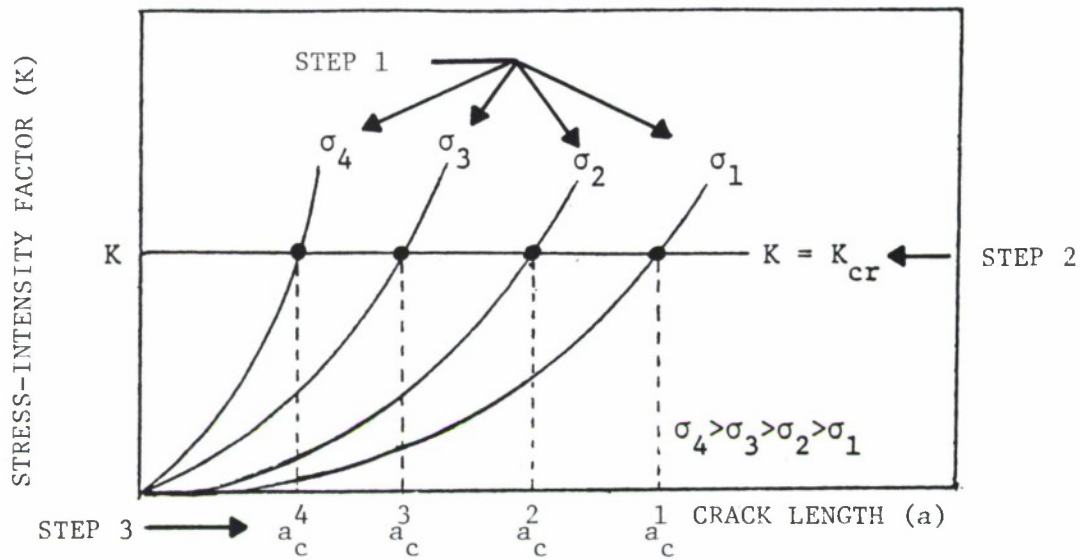
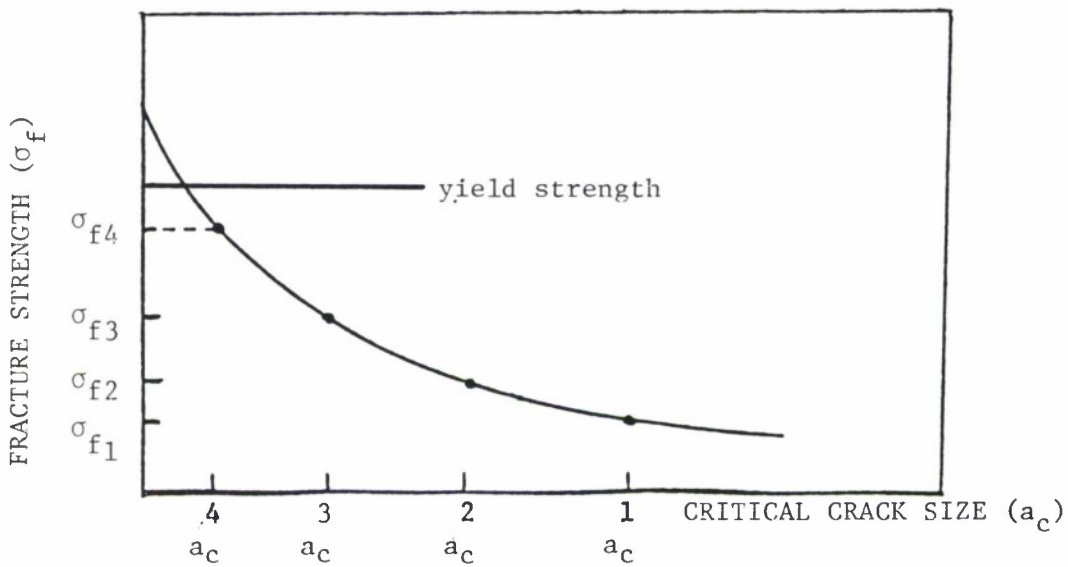


Figure 4.3.2. Structural Geometry and Material Properties for Example 4.3.1.



(a) Stress-Intensity Factor as a Function of Crack Length for Constant Values of Stress



(b) Residual Strength Diagram

Figure 4.3.3. Description of Procedures that One Might Follow to Obtain the Residual Strength Diagram Graphically.

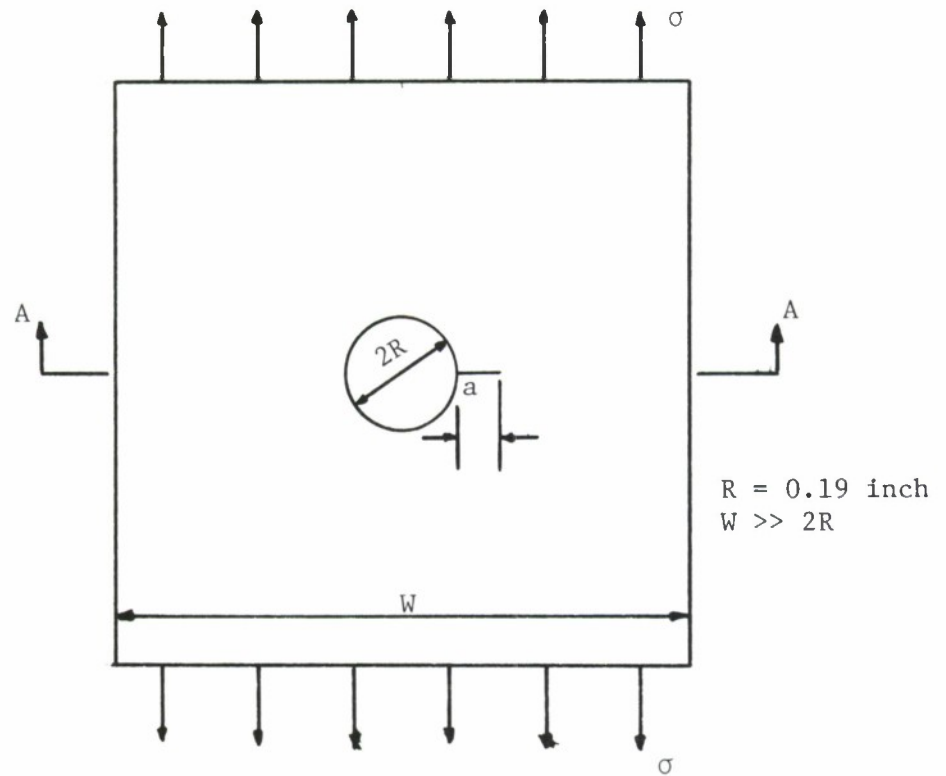
MATERIAL

AISI 4340 STEEL

MATERIAL
PROPERTIES

$$\sigma_{ys} = 200 \text{ Ksi}$$

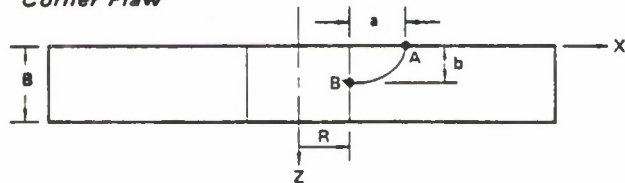
$$K_{Ic} = 75 \text{ Ksi}$$



$$R = 0.19 \text{ inch}$$
$$W \gg 2R$$

(a) In Plane View of Radial Hole Crack

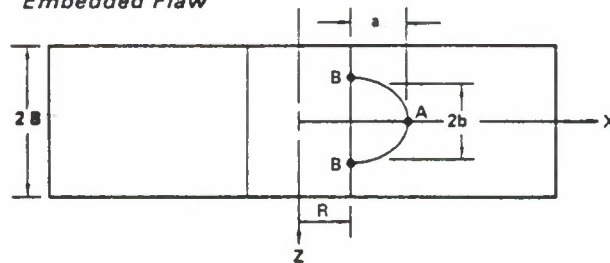
Corner Flaw



$$\frac{a}{b} = 1.0$$

$$B = 0.76 \text{ inch}$$

Embedded Flaw



(b) Section A-A. Definition of Crack Geometries

Figure 4.3.4. Crack Geometries Considered for a Radial Crack Growing from a Hole for Example 4.3.2.

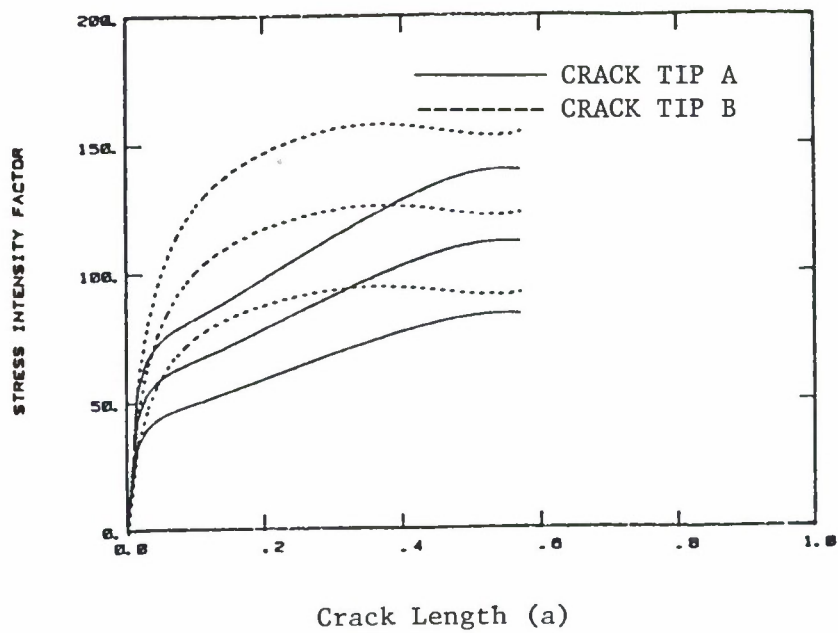


Figure 4.3.5. Stress-Intensity Factor Relationships at Points A and B for the Radial Quarter Circular Crack Geometry.

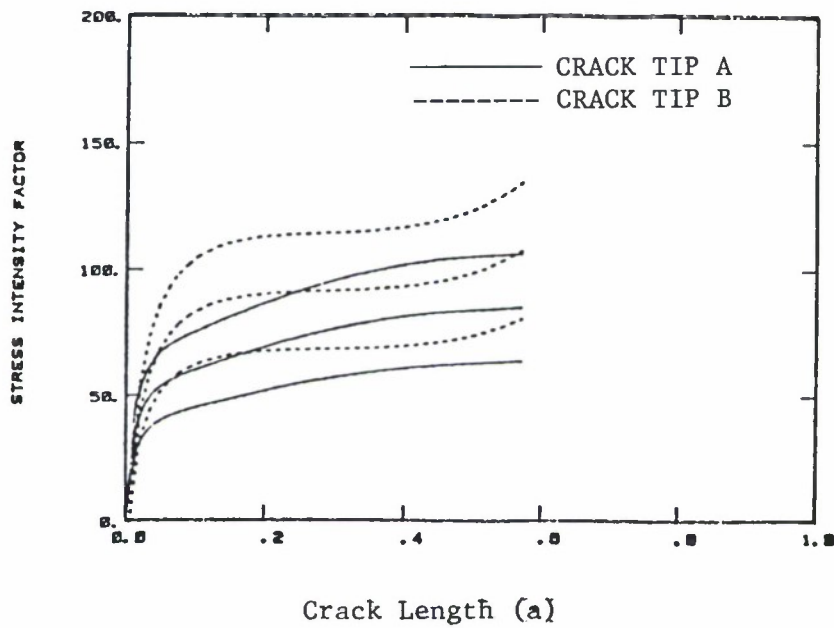


Figure 4.3.6. Stress-Intensity Factor Relationships at Points A and B for the Radial Embedded Semi-Circular Crack Geometry.

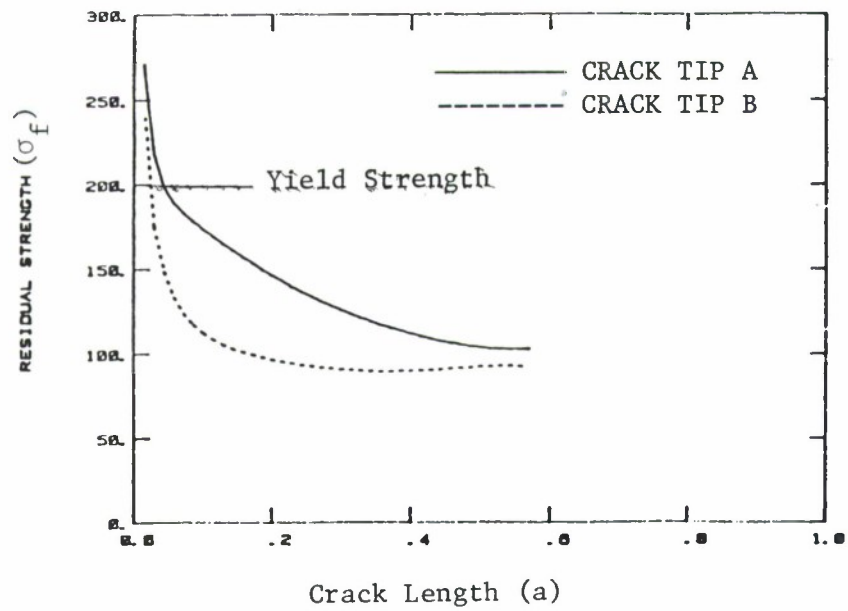


Figure 4.3.7. Residual Strength Diagram for Points A and B Located on the Radial Quarter Circular Crack Geometry Shown in Figure 4.3.4.

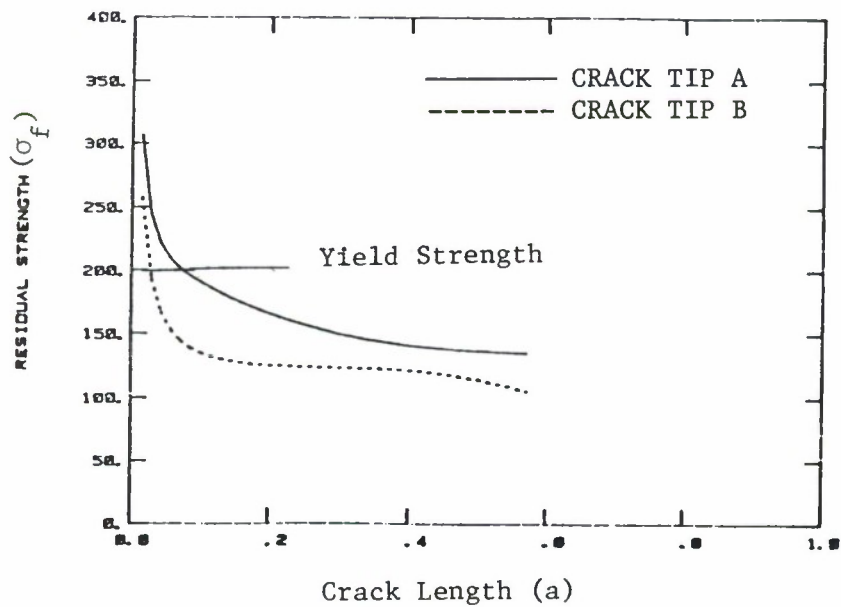


Figure 4.3.8. Residual Strength Diagram for Points A and B Located on the Embedded Semi-Circular Crack Geometry Shown in Figure 4.3.4.

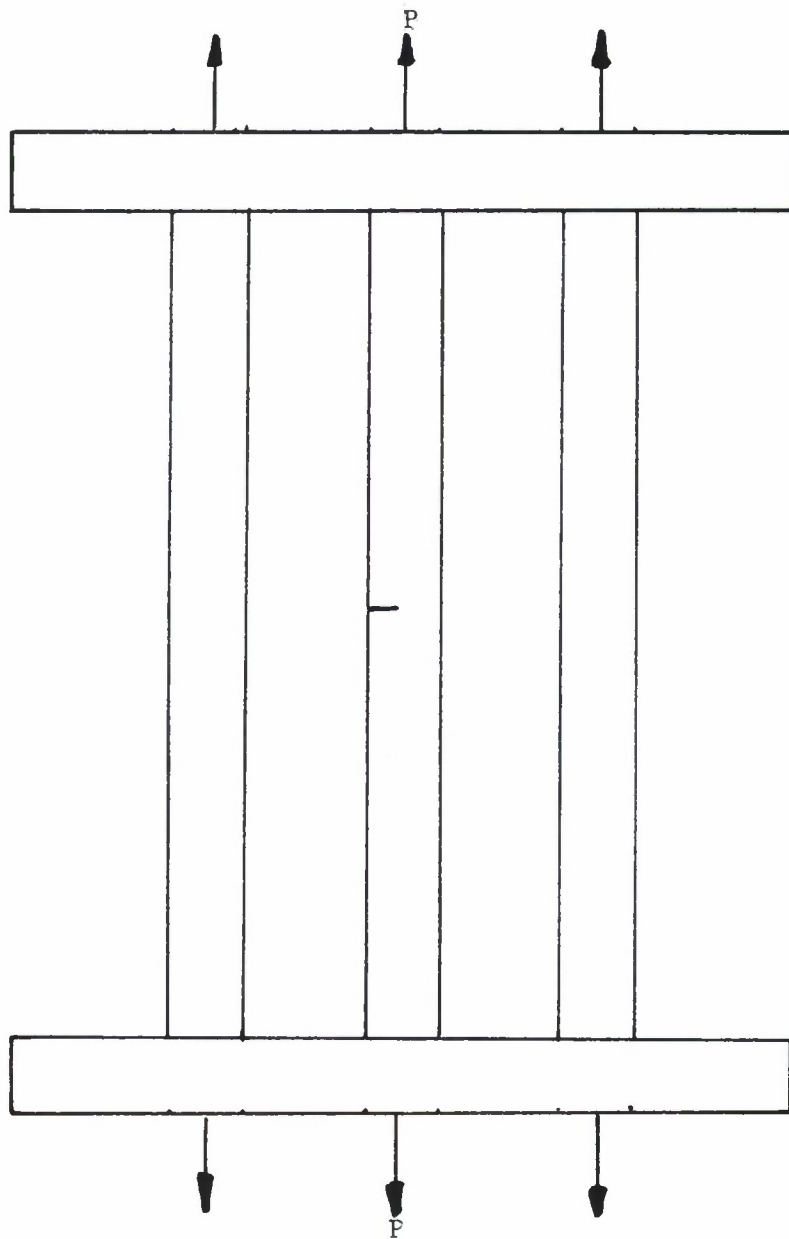


Figure 4.3.9. Multiple Load Path (Built-up) Structure with a Crack in the Central Member.

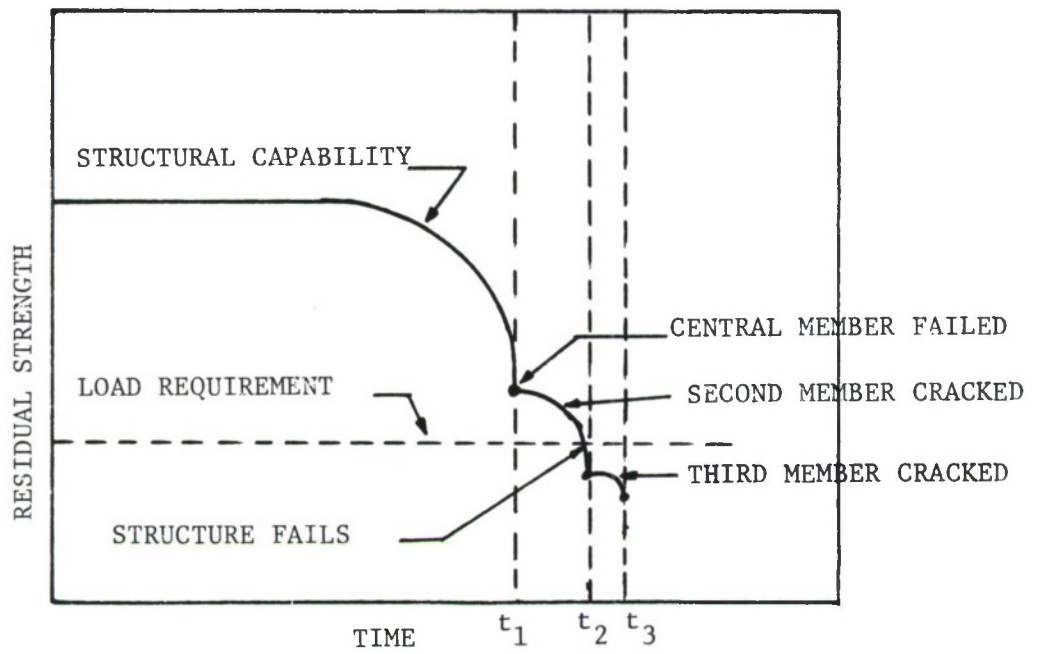


Figure 4.3.10. Reduction of Residual Strength During Successive Failure of Members in the Structure Shown in Figure 4.3.9.

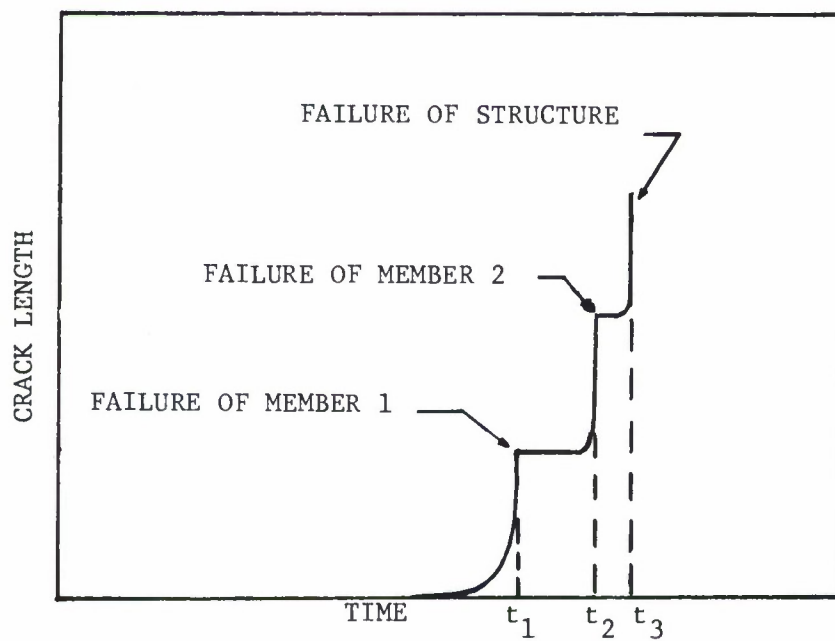


Figure 4.3.11. Crack Growth Curve for Multiple Load Path Structure Shown in Figure 4.3.9.

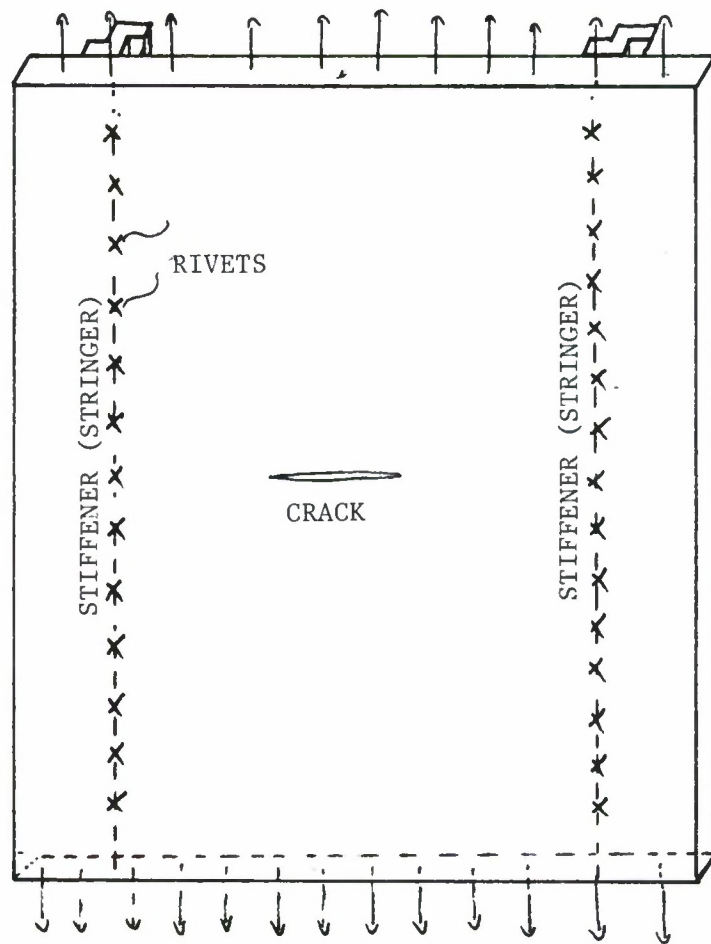


Figure 4.3.12. Skin-Stringer Built-Up Structure.

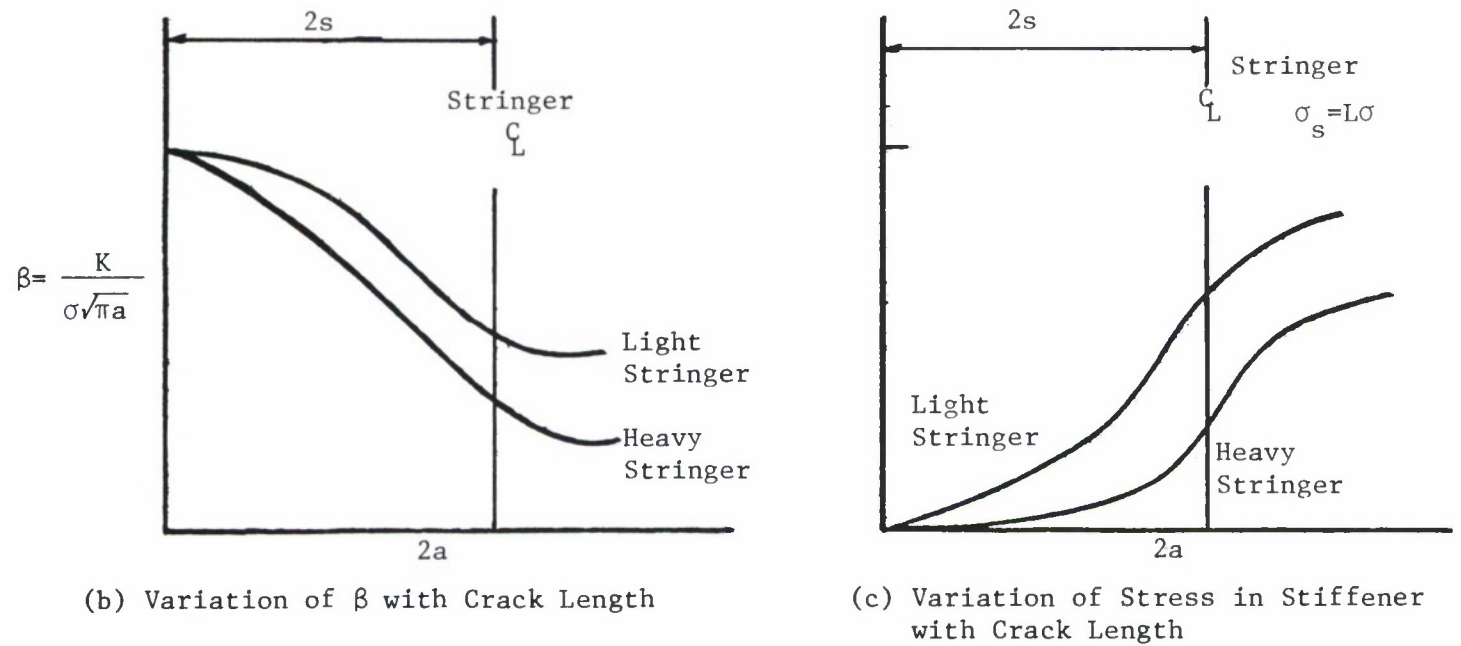
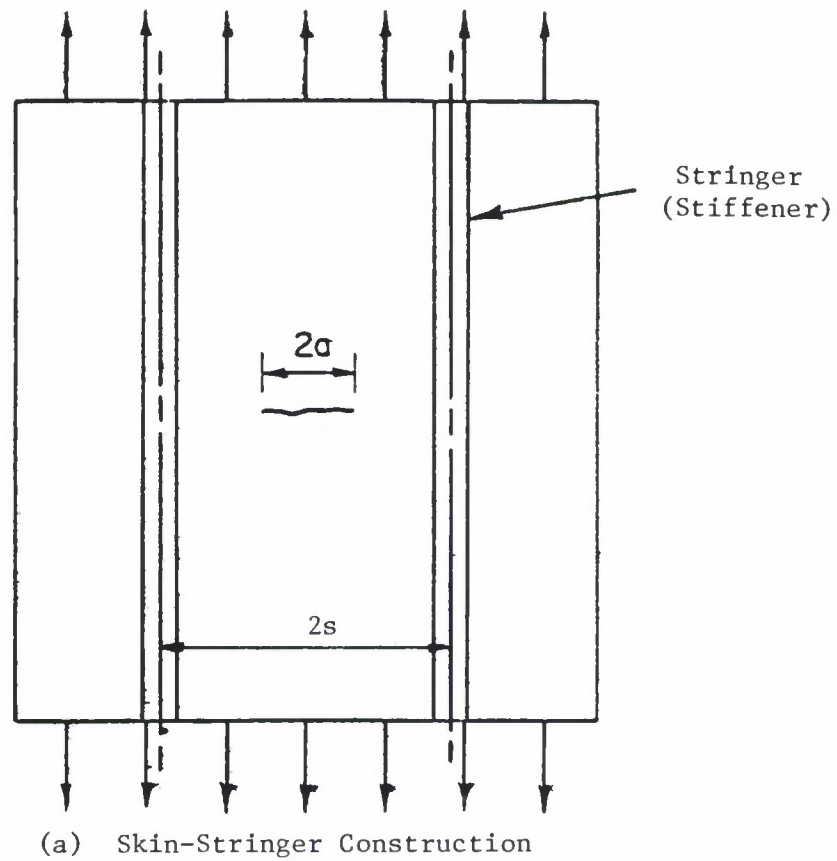


Figure 4.3.13. Variation of β and L with Crack Length in Stiffened Panel with a Crack Between the Stiffeners.

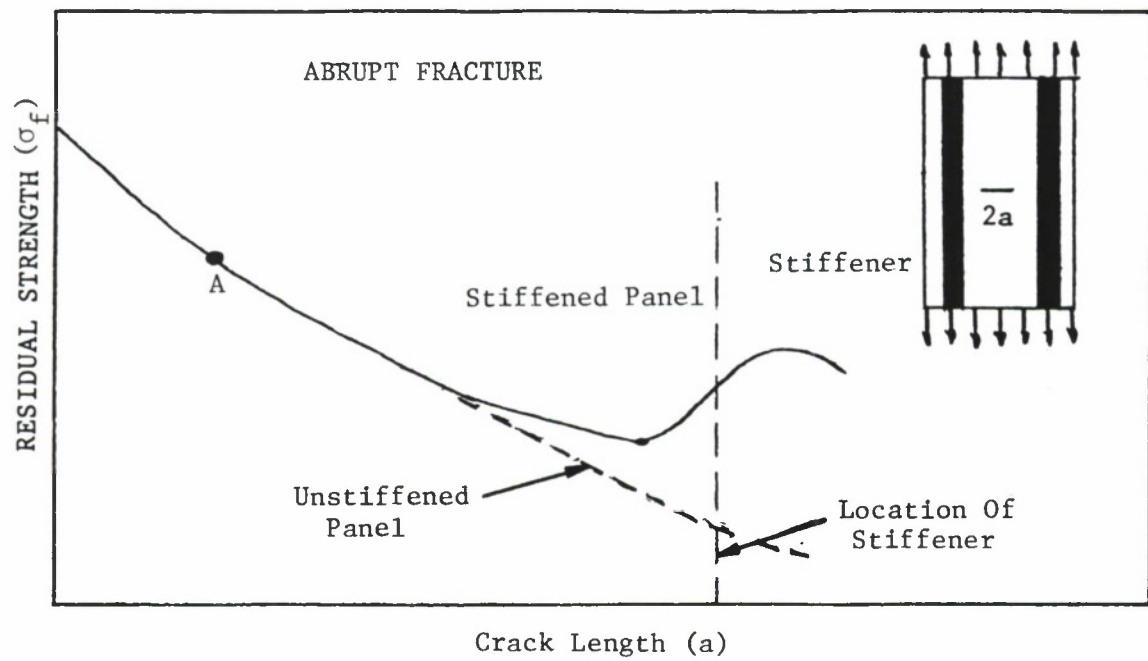


Figure 4.3.14. Residual Strength of the Cracked Panel as a Function of Crack Length for Built-Up Skin-Stiffened Structure Compared with Unstiffened Panel. Abrupt Failure Criterion Used to Determine Residual Strength.

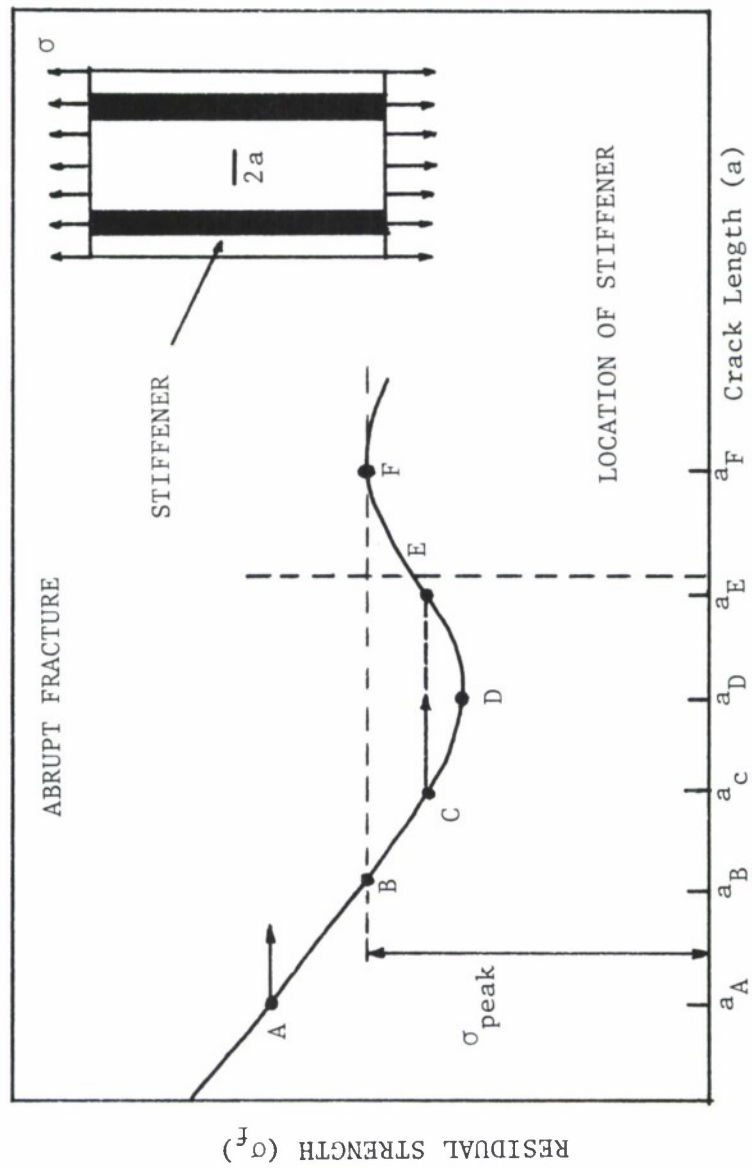


Figure 4.3.15. Residual Strength of the Cracked Panel as a Function of Crack Length for Built-Up Skin Stiffened Structure. Only Skin Failure Mode Considered. Abrupt Failure Criterion Used to Determine Residual Strength.

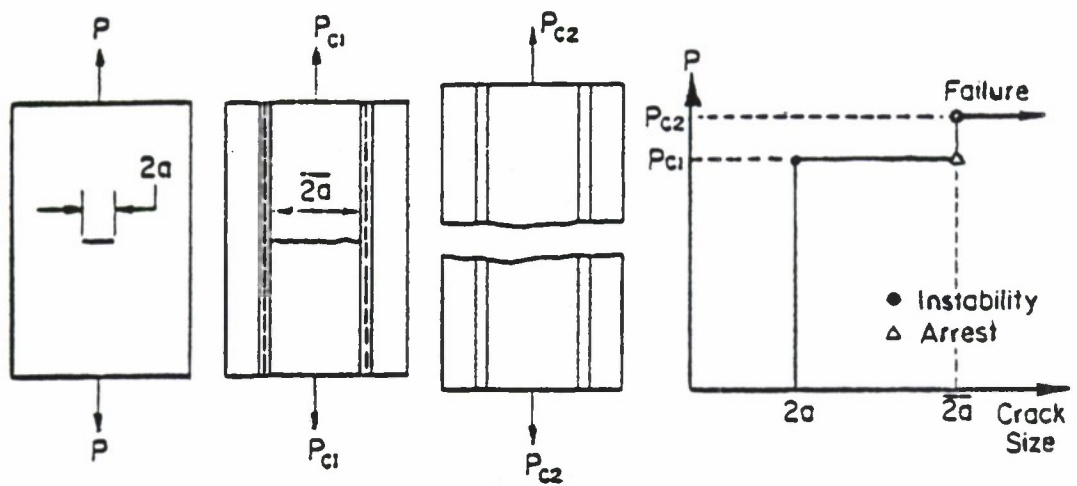


Figure 4.3.16. Load-Crack Length Behavior Observed in Skin-Stiffened Construction with Arrest Features.

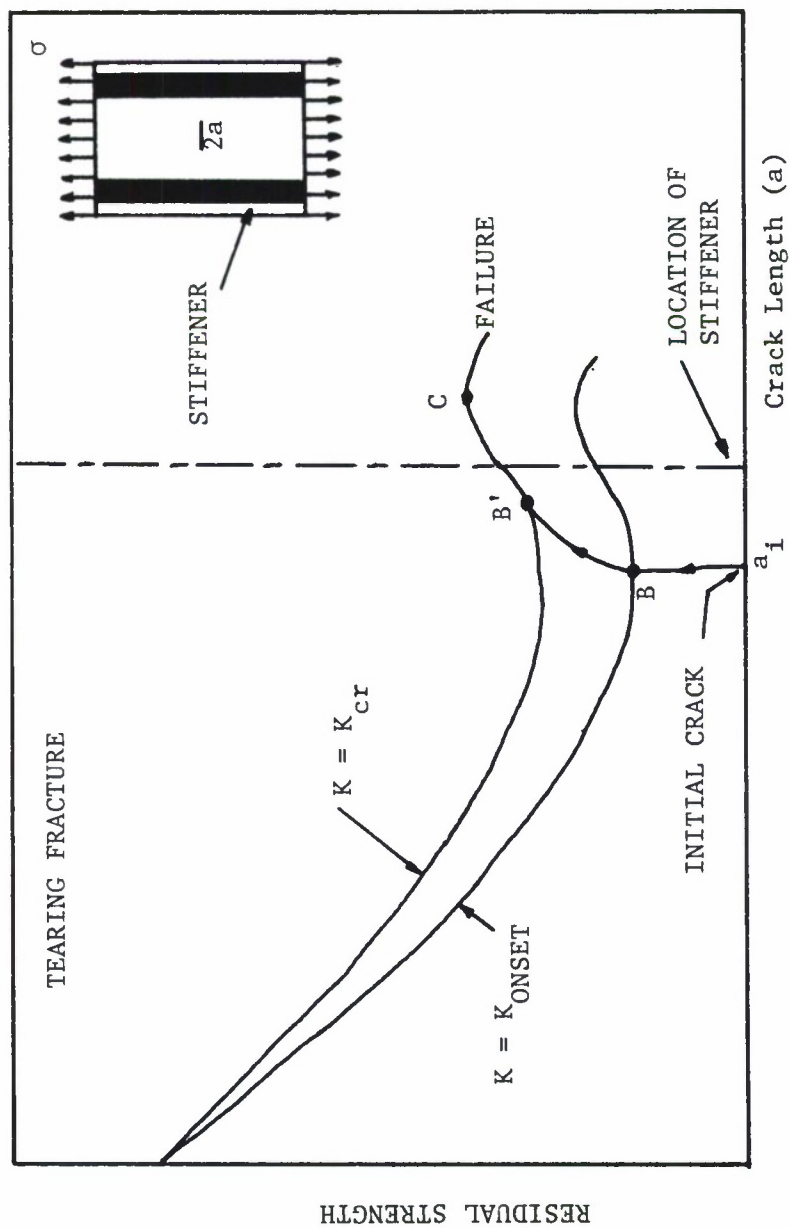


Figure 4.3.17. Residual Strength of Cracked Panel as a Function of Crack Length for Built-up Skin-Stringer Structure. Tearing Failure Criterion Used to Determine Residual Strength.

4.4 SINGLE LOAD PATH STRUCTURE

For a single load path structure, the only means to protect the safety is to prevent the damage growth from degrading the strength of the structure to less than the design limit load. This applies for all structures classified as slow crack growth, regardless of the type of construction (such as single load path or multiple load path). The residual strength capability of the structure depends mainly on the material's resistance to fracture.

4.4.1 Abrupt Fracture

For materials which exhibit abrupt failure, the start of slow crack extension will be followed immediately by the onset of rapid fracture. The residual strength capability then requires a strict evaluation of the initial flaw sizes in the structure. The allowable initial crack length necessary to maintain the required residual strength will be less than a_f ; the design limit load must also be such that the stress level in the structure is less than σ_1 as shown in Figure 4.4.1. The residual strength diagram can be evaluated as described earlier through the plot of σ_f vs a_c using the relationship $K = \sigma_f \sqrt{\pi a}$ for the structural geometry of interest and also employing the failure criterion based on a critical fracture toughness value, K_{cr} . The margin of safety as shown in Figure 4.4.1 allows for undetected cracks or for subcritical crack growth such that the initial crack size will not become greater than a_f .

In the following paragraphs, two different example problems are presented to demonstrate the application of the steps in constructing the residual strength diagram and also to analyze the structure for its residual strength capabilities. The first example illustrates the centrally cracked finite width panel. The second example considers an eccentrically cracked finite width panel problem. These examples demonstrate the basic concepts involved in the residual strength capabilities of a single load path structure.

EXAMPLE 4.4.1 Residual Strength of Center Cracked Panel

Develop the residual strength diagram for the cracked finite width panel shown in Figure 4.4.2.

SOLUTION:

For the center-cracked geometry configuration shown in Figure 4.4.2, the stress-intensity factor K is expressed by the relationship (See Section 1.7):

$$K = \sigma \sqrt{\pi a \sec\left(\frac{\pi a}{W}\right)} \quad (4.4.1)$$

Since we have an explicit expression for K , using the fracture toughness failure criterion (plane strain), the residual strength diagram can be obtained directly. The corresponding equation is

$$\sigma_f = K_{Ic} / \left(\sqrt{\pi a_c \sec\left(\frac{\pi a_c}{W}\right)} \right) \quad (4.4.2)$$

where $K_{Ic} = 40 \text{ ksi}\sqrt{\text{in}}$ and $W = 20 \text{ inch}$ are given as data and σ_f can be obtained for any selected crack length. The σ_f vs a_c curve, which is the

required residual strength diagram, can now be plotted.

The residual strength of the panel can be estimated from Equation 4.4.2 which is described in the diagram presented in Figure 4.4.3. From this figure, for the given operating stress level (20 Ksi), the critical crack size at which unstable crack extension would occur, can be estimated as 1.2 inch. Thus, to avoid a fracture type failure of the panel, the structure should not develop a crack of this size. Assume that based on an established visual inspection schedule, the simple rectangular aluminum panel, uniformly loaded in tension as shown, could develop a 2.0 inch long, central through-the-thickness crack (normal to loading) before detection. This crack length is slightly smaller than the critical crack size ($2.4 = 2 \times 1.2$ inch) under the operating conditions so that the margin of safety is small when this inspection process is employed.

To establish the required residual strength level to fit the inspection schedule, the designer must reduce the crack-tip stress-intensity factor for the same applied load. One method is to transfer portions of the load to a stiffening member. Another method is to reduce the operating load level below the failure level corresponding to the inspection crack size, although this is not always practiced.

EXAMPLE 4.4.2 Residual Strength of Eccentrically Cracked Panel

Establish the residual strength diagram for a finite-width panel with the eccentric crack shown in Figure 4.4.4.

SOLUTION:

For the given configuration, the stress intensity factor is expressed by the following relationship (See Section 1.7),

$$K = \sigma \beta \sqrt{\pi a} \quad (4.4.3)$$

where $\beta = \beta(\epsilon, \frac{a}{W})$ and $\epsilon = \frac{2e}{W}$; $W' = \frac{W}{2} - e$. Since it is an eccentric crack, the K values at the crack tips A and E will be different and the corresponding β 's will also be different. From the plots of Figure 4.4.5⁽¹⁵⁾, β values for the crack tips A and E can be obtained for a given aspect ratio (a/W') and the eccentricity factor, ϵ . It is obvious from Figure 4.4.5 that the stress-intensity factor conditions at crack tip A, which is close to the panel edge, are higher than that for crack tip E so the conditions at point A will be critical in deciding the residual strength of the panel.

Applying the fracture toughness failure criterion, we can now obtain the direct relationship between the fracture stress and the critical crack size as

$$\sigma_f^A = K_{Ic} / \beta^A \sqrt{\pi a} \quad (4.4.4a)$$

and

$$\sigma_f^E = K_{Ic} / \beta^E \sqrt{\pi a} \quad , \quad (4.4.4b)$$

where the superscripts A and E represent the conditions at the crack tips A and E. We can now plot curves σ_f^A vs a and σ_f^E vs a for the given structural configuration. The residual strength diagram for crack tips A and E for $\epsilon = 0.9$ and $W' = 1.0$ are shown in Figure 4.4.6. As

anticipated on the basis of the differences in stress-intensity factor conditions, the residual strength curve associated with crack tip A controls the crack extension behavior of the eccentric crack. For the 20 Ksi maximum stress operating condition, the critical crack size is approximately 0.73 inch, based on the crack tip A curve (see point G). If a crack with a half crack length (a) of 0.73 inch develops in the panel, crack tip A will extend rapidly and the crack will be arrested at the free edge. Now the crack growth behavior at crack tip E needs further analysis corresponding to the panel configuration as shown in Figure 4.4.7. The crack length a' is equal to $(W' + a)$ where W' and a are known, i.e., $a' = 1.73$ inch.

The critical stress level at crack tip E can now be calculated using the expression, $K_{Ic} = \sigma_f \beta \sqrt{\pi a'}$ corresponding to the single edge crack. The value of β can be obtained from Figure 4.4.7. For $a' = 1.73$ inch and $W = 20$ inch, β is estimated as 1.1. The value of σ_f for these values of β and a , is obtained from the relationship $K_{Ic} = \sigma_f \beta \sqrt{\pi a'}$ and is equal to 15.6 ksi, which is lower than the given maximum operating stress level of 20 ksi, and thus the crack extends from tip E causing complete fracture of the plate.

Even though extension of crack tip A is arrested at the free edge, the residual strength level of the panel is not sufficient to prevent extension at crack tip E for the given maximum operating stress level.

To further illustrate the analysis that would be required for the determination of the crack growth behavior of each crack tip, consider the residual strength diagram presented in Figure 4.4.8. Again two curves are illustrated, one for crack tip A, the other for crack tip E. The analysis for crack tip A is as shown in Figure 4.4.6. The analysis and data presentation for crack tip E is based on the assumption that crack tip A has extended to the edge of the panel and the residual strength is given by

$$\sigma_f = \frac{K_{Ic}}{1.1\sqrt{\pi(1+a)}} \quad (4.4.5)$$

It is noted that the crack tip E will remain stationary when the crack tip A extends if the crack length size (a) exceeds the size associated with the intersection of the two residual strength curves. The next example describes an analysis of such a situation.

EXAMPLE 4.4.3 Residual Strength of Eccentrically Cracked Panel - Crack Arrest Conditions

Repeat the residual strength analysis of Example 4.4.2 with a maximum operating stress level of 13 ksi. From Figure 4.4.6, it can be seen that the critical crack size for the given load level is 0.9 inch. If the panel develops a crack of this size, rapid extension will occur at crack tip A, Point F identifies the point of instability. The crack extension will be arrested at the free edge as in the earlier case. To continue the analysis for residual strength capabilities of the panel,

consider the crack extension behavior of the single edge crack at crack tip E. The new crack length is given by $W' + a$ where $W' = 1$ inch and $a = 0.9$ inch. Thus, for a crack length of 1.9 inch, β is obtained from Figure 4.4.7 as 1.1. Using the relationship, $K_{Ic} = \sigma_f \beta \sqrt{\pi a}$, the critical stress level for crack tip E to extend rapidly is calculated as 14.9 ksi. However, the maximum operating stress level is given as 13 ksi which is less than this critical strength level. Thus, the panel does have the capacity to be effective without failure even when it develops a maximum crack of half length size 0.9 inch, leading to the rapid extension of crack tip A.

4.4.2 Tearing Fracture

Materials with medium or high fracture toughness exhibit a type of subcritical crack extension behavior prior to reaching the maximum load carrying capacity of the structure. When a limited amount of yielding occurs in front of the crack tip, the initial extension of an existing crack in these materials will be slow and stable threshold values of the stress-intensity factor (K_{ONSET}). To understand this behavior, consider an unreinforced, center-cracked panel. The stress-intensity factor (K) at the crack tip increases linearly with the value of the normal tensile stress component acting on the structure for a stationary crack. As the K level increases, some point (point A) will be reached at which the crack length will begin to extend as shown in Figure 4.4.9. The crack will extend gradually as the load continues to increase, until reaching the critical size at which the crack extension becomes unstable (point B in Figure 4.4.9). The point of crack initiation and instability are determined by the appropriate failure criteria.

When the subcritical growth of the crack, as shown in Figure 4.4.9a between the points A and B, is not significant the fracture toughness criterion K_{CR} values can be used in the analysis. In this case, fracture is assumed to occur immediately after the start of crack extension as under abrupt failure conditions. However, for materials exhibiting substantial crack growth between points A and B as shown in Figure 4.4.9b, the crack resistance curve approach can be used in the residual strength analysis. The crack resistance (R) curve approach might be based on either K_R vs ΔA or $\sqrt{J_R}$ vs. a . The K_R vs Δa curve is normally used when the fracture strength is associated with

stress levels below net section yield conditions; in other words, when limited crack tip plasticity occurs prior to fracture. The $\sqrt{J_R}$ vs a curve is used for those conditions where the fracture strength is expected to result in gross yielding.

In the calculation of residual strength when the cracked structure exhibits a tearing instability, one normally follows the following steps:

1. Obtain K_{eff} ($=\beta\sqrt{\pi(a+r_p)}$) values for the structure for various crack lengths and applied stresses using a suitable plastic zone model (e.g. Dugdale Model). Evaluation of the K values involves methods described in Chapter 1. Plot K versus a curves for various applied stresses as shown in Figure 4.4.10a.

2. Obtain the experimentally determined R -curve (K_R versus Δa) for the sheet material (Figure 4.4.10b).

3. Determine the point of instability from the K curves of the structure and the K_R curves of the material as shown schematically in Figure 4.4.10c.

4. Obtain different values for the fracture strength and the corresponding crack lengths from step 3 and plot these points to establish the failure strength (σ_f) crack length (a_c) curve. This provides the necessary residual strength diagram of the structure.

The residual strength diagram for intermediate or high fracture toughness materials can be constructed by using either the K_R curve or the $\sqrt{J_R}$ method. To understand the use of the R -curve failure criteria in evaluating the residual strength, consider the following example in which failure criterion based on the K_R curve is applied.

EXAMPLE 4.4.4 Residual Strength of Tearing Radial Hole Crack

Construct the residual strength diagram for a large and relatively thin (0.063) plate of 7075-T73 aluminum alloy having a through crack emanating (radially) from a hole with a diameter (D) equal to one inch, such as illustrated in Figure 4.4.11. Assume the material inhibits a limited amount of crack tip yielding. Also calculate the crack length associated with a fracture strength associated with a crack length of 2.0 inch.

SOLUTION:

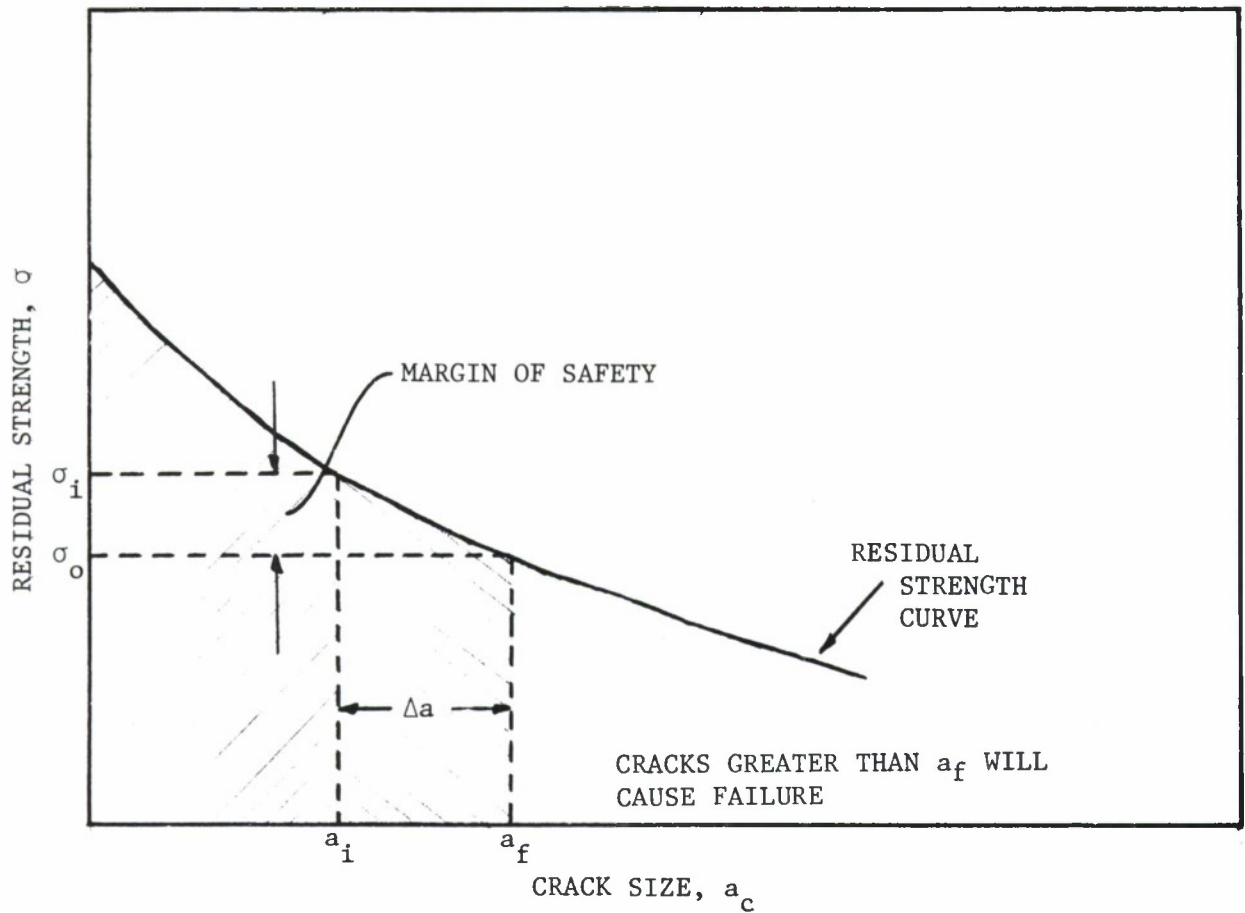
As the first step, the appropriate expression for the stress-intensity factor is obtained from Section 1.7, Table 1.7.3, Case 1.7.3.1, where the Grandt ⁽¹⁶⁾ approximation of the Bowie ⁽¹⁷⁾ radial hole crack solution is given (Also see Figure 4.4.11). Figure 4.4.12 describes the variation in stress-intensity factor with crack length and stress level.

The second step is to consider the appropriate failure criterion. The given geometry is a thin sheet and the material exhibits limited crack tip yielding behavior. So the R-curve method based on K_R values can be applied to evaluate the fracture strength.

For the given 7075-T73 aluminum alloy material (0.063 inch thick), an experimentally obtained R-curve is shown in Figure 4.4.13. By superposing the R-curve onto the plot obtained in step one, as explained in Section 4.2, the points where the R-curve is tangent to the K-curves, as shown in Figure 4.4.14 are obtained. At these points the failure criterion, i.e., $K = K_R$ and $\frac{\partial K}{\partial a} = \frac{\partial K_R}{\partial a}$, is satisfied. The corresponding stress σ_c is the

is the critical (fracture) stress at which the initiation of rapid fracture will occur. From a diagram like Figure 4.4.14, we can obtain the critical initial sizes of the crack and the respective fracture stresses.

The final step is to plot the σ_f vs a_c curve. The required residual strength diagram is shown in Figure 4.4.15 for the 7075-T73 Aluminum plate with a crack emanating radially from a hole. It can be seen from this figure that the critical crack size a for a 20 Ksi operating stress level is equal to 4.0 inches. As can also be seen from the figure, for an observed crack of 2.0 inches, the residual strength available is 27 ksi.



a_f = critical flaw size for the maximum operating load.

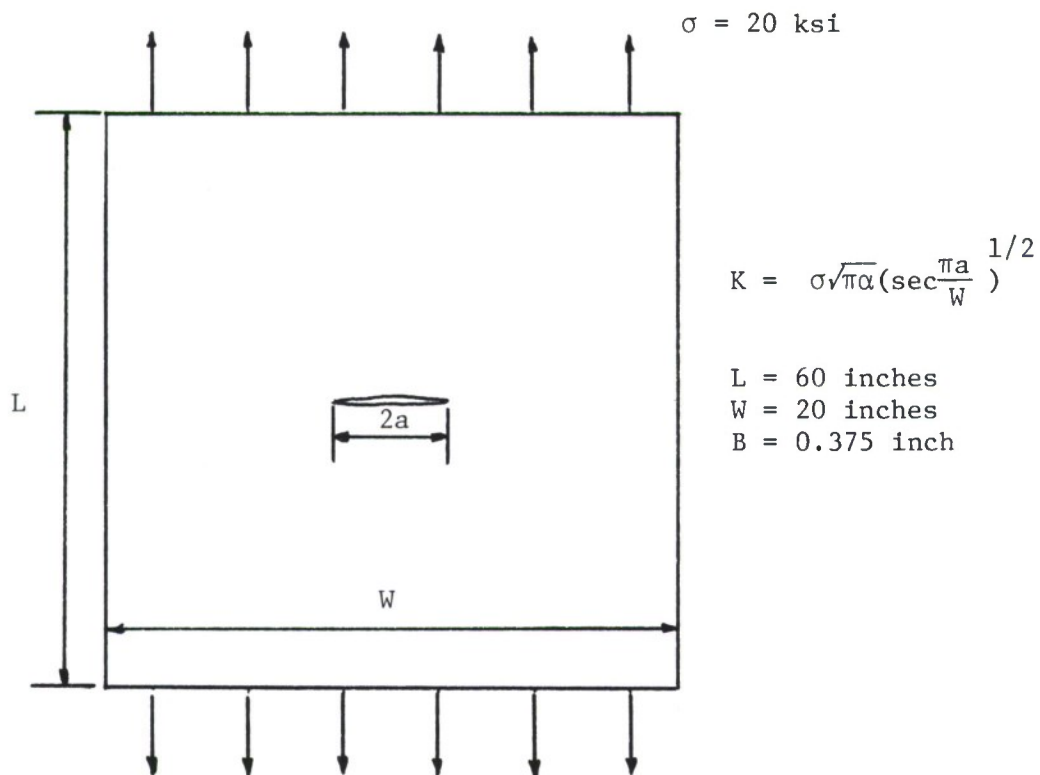
a_i = observed initial crack length.

Δa = available additional length. (allowance for undetected initial crack size and for subcritical crack growth).

σ_i = residual strength level for an initial crack a_i .

σ_o = maximum operating stress level.

Figure 4.4.1. Residual Strength Diagram Showing Defining Cracks and Residual Strength Parameters.



MATERIAL PROPERTIES

$\sigma_{ys} = 78 \text{ ksi}$
 $\sigma_{ult} = 83 \text{ ksi}$
 $K_{IC} = 40 \text{ ksi } \sqrt{\text{in}}$

INSPECTION PROCEDURE

VISUAL INSPECTION

$2a_{NDE} = 2 \text{ inch}$

Figure 4.4.2. Center Crack Panel and Material Properties for Example 4.4.1.

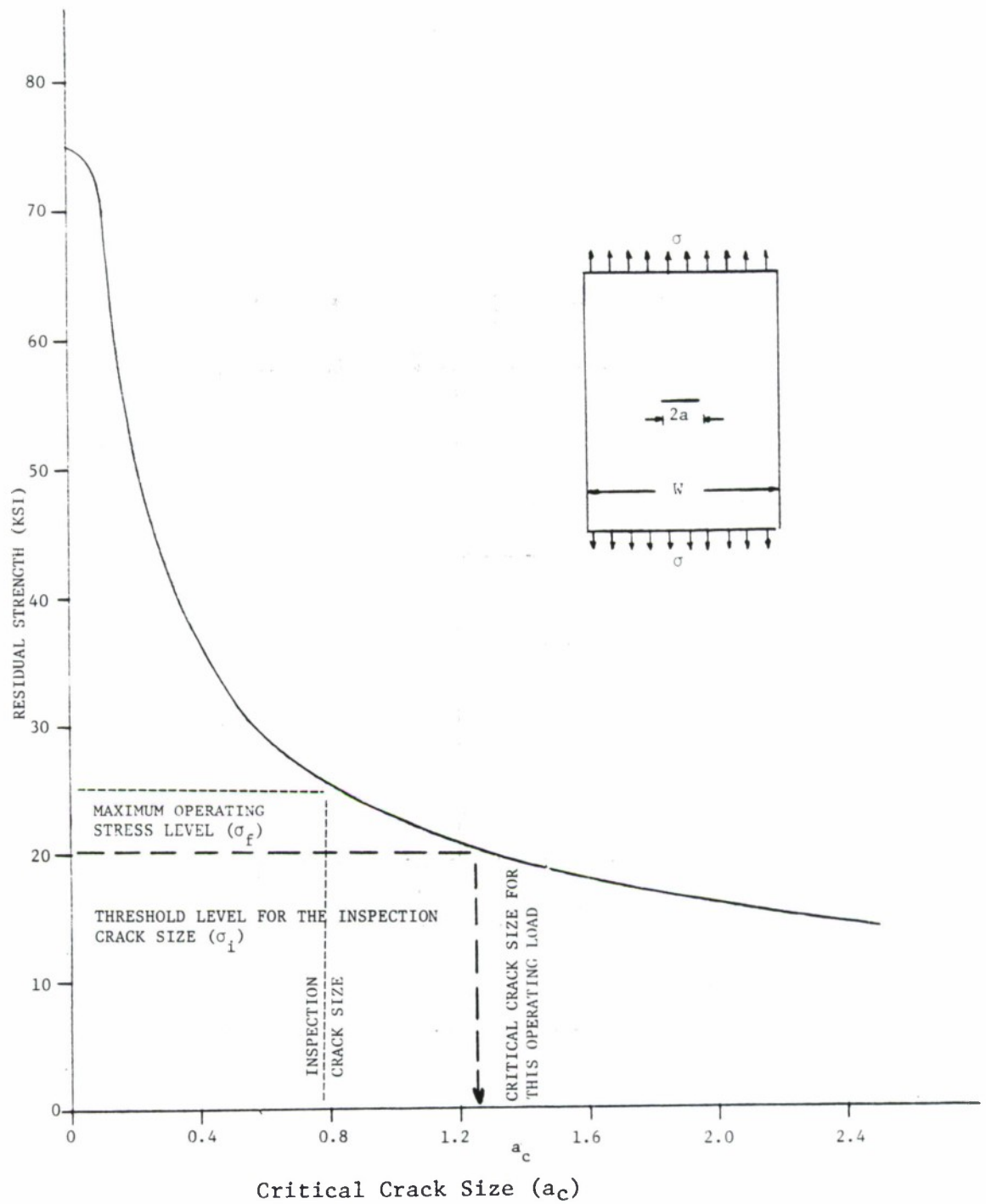
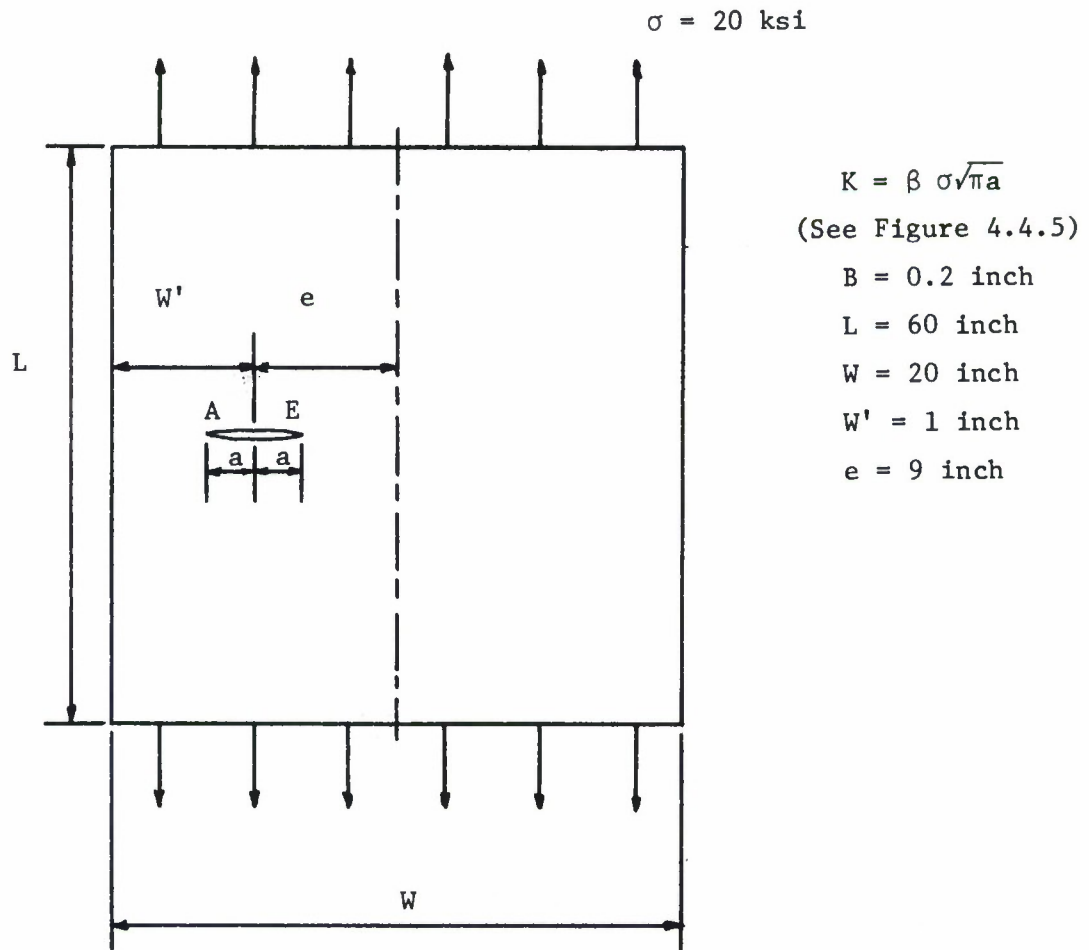


Figure 4.4.3. Residual Strength Diagram Determining Critical Crack Size at 20 Ksi Operating Level.



MATERIAL PROPERTIES

$$\sigma_{ys} = 78 \text{ ksi}$$

$$\sigma_{ult} = 83 \text{ ksi}$$

$$K_{IC} = 40 \text{ ksi } \sqrt{\text{in}}$$

Figure 4.4.4. Excentrically Cracked Panel Associated with Examples 4.4.2 and 4.4.3.

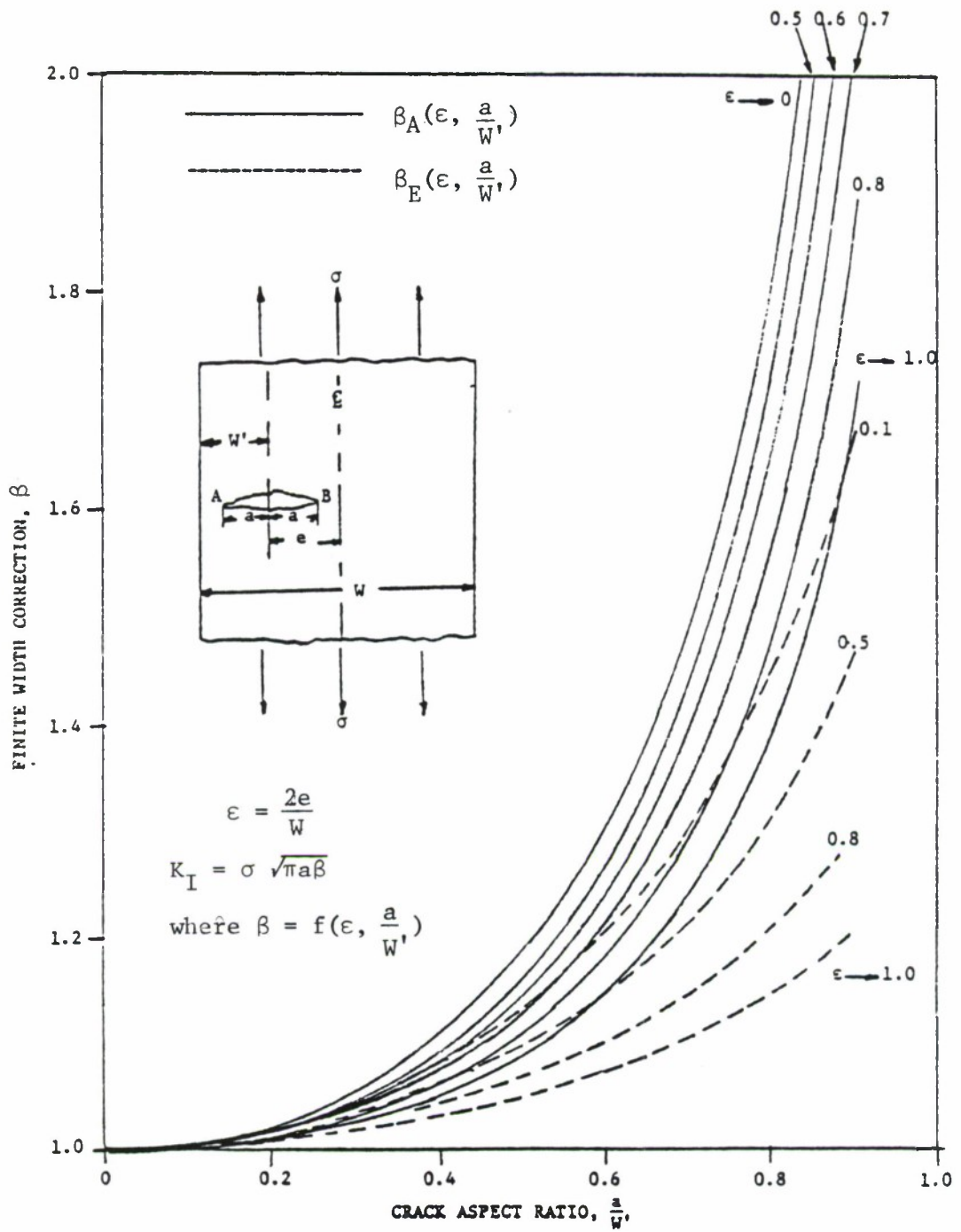


Figure 4.4.5. Finite-Width Correction-Eccentric Crack (Tension) (Reference 15).

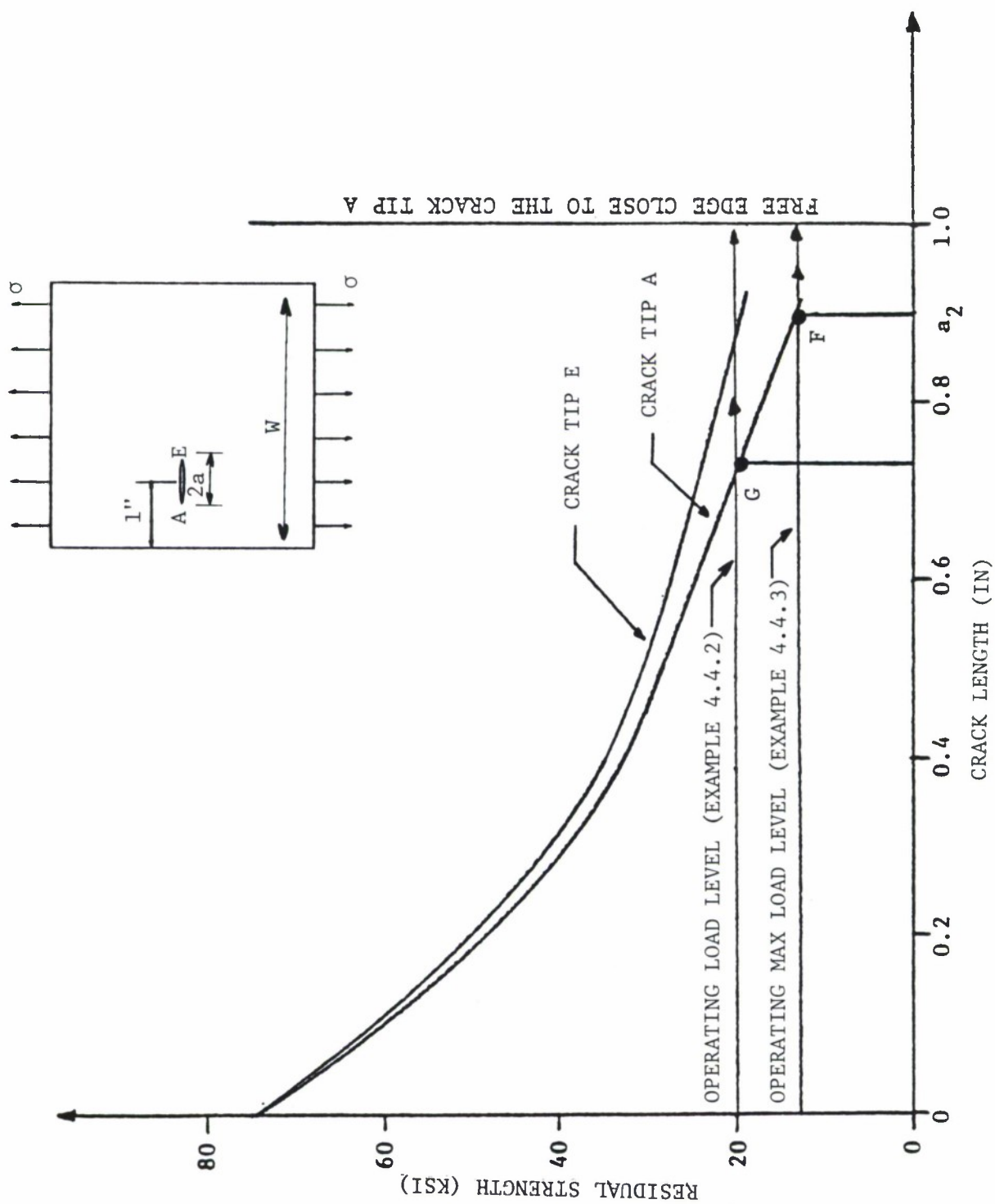


Figure 4.4.6. Residual Strength Diagram for Panel with Eccentric Crack Given in Figure 4.4.4. Crack with Lowest Fracture Resistance Curve Extends First.

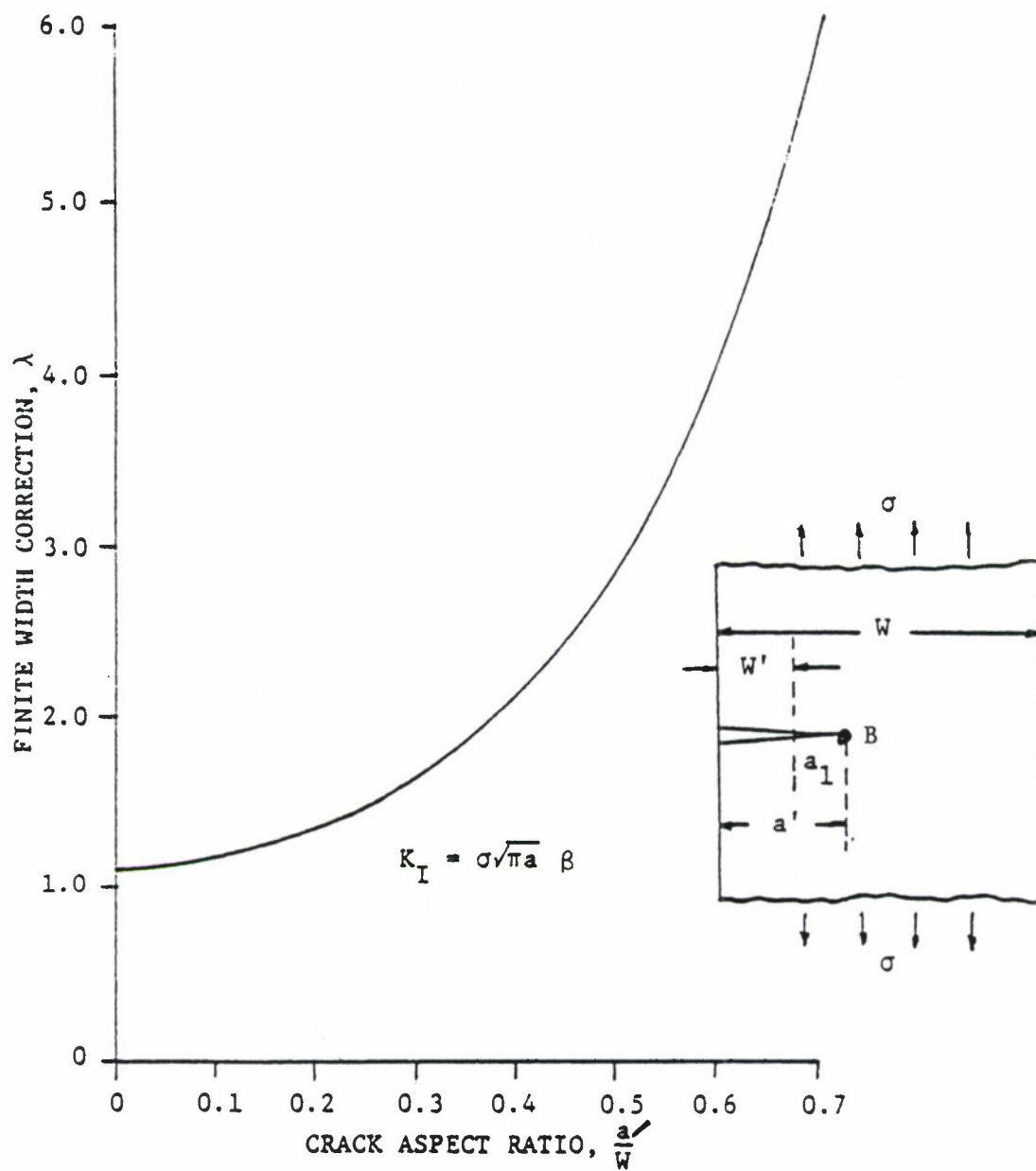


Figure 4.4.7. Finite Width Correction-Single Edge Crack, After the Eccentric Crack Extends from Tip A.

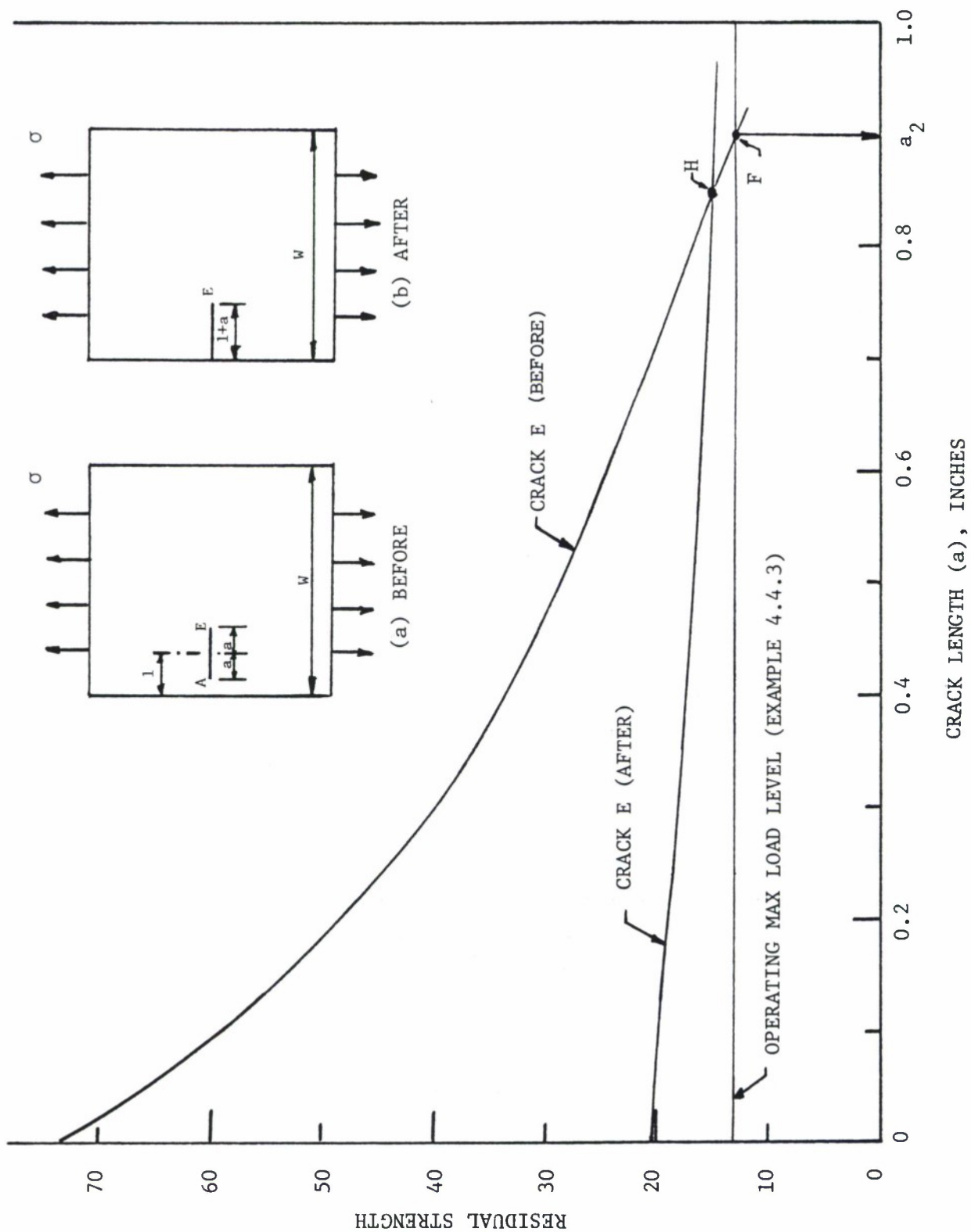
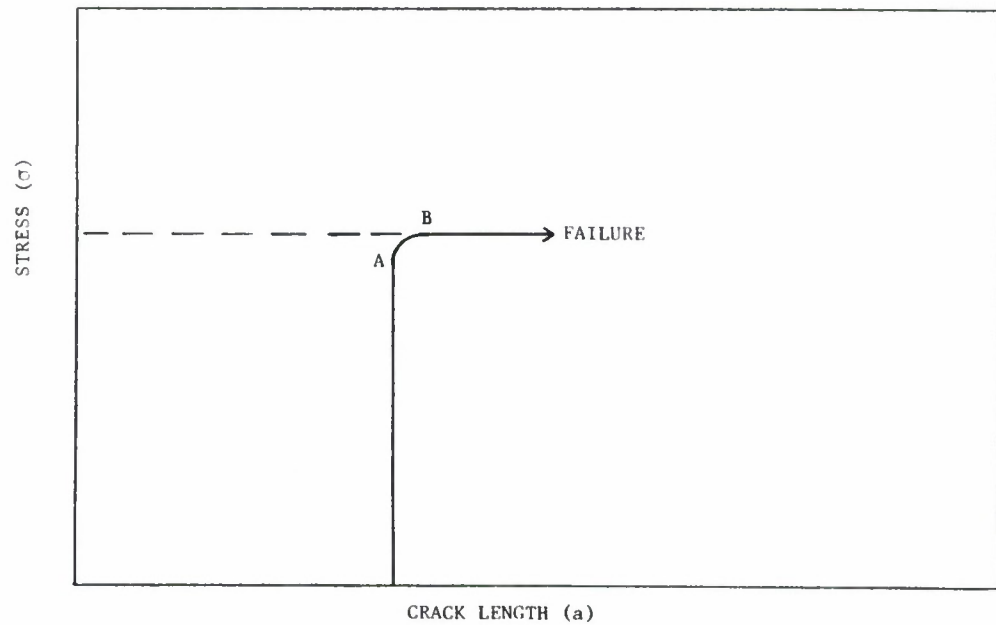
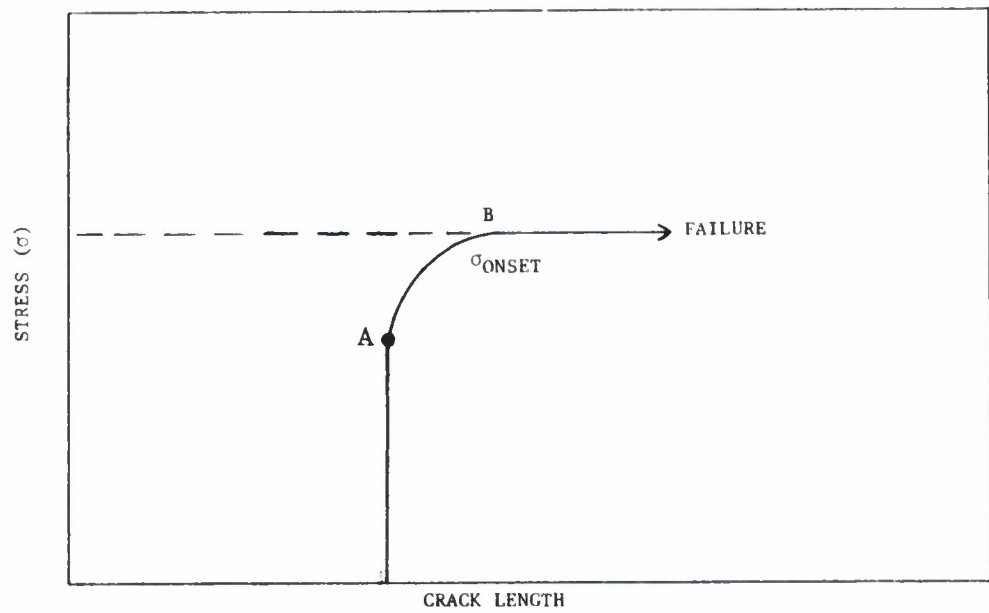


Figure 4.4.8. Residual Strength Diagram Used to Consider Arrest Features as Crack Tip A Reaches the Edge of the Plate.

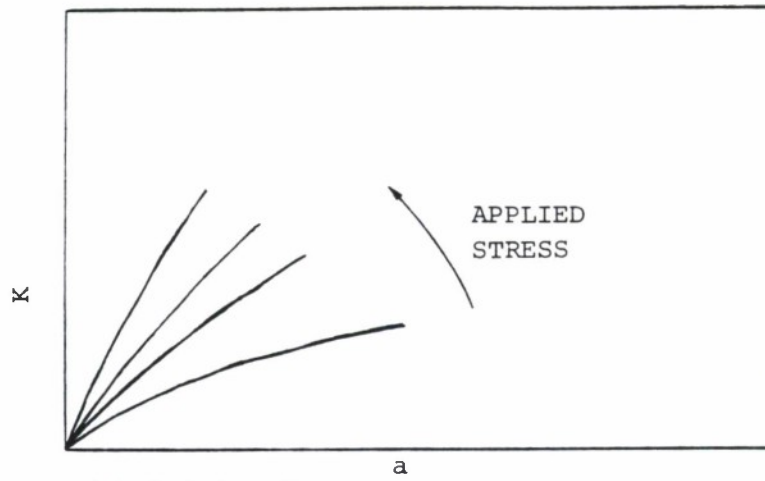


(a) Limited Crack Extension

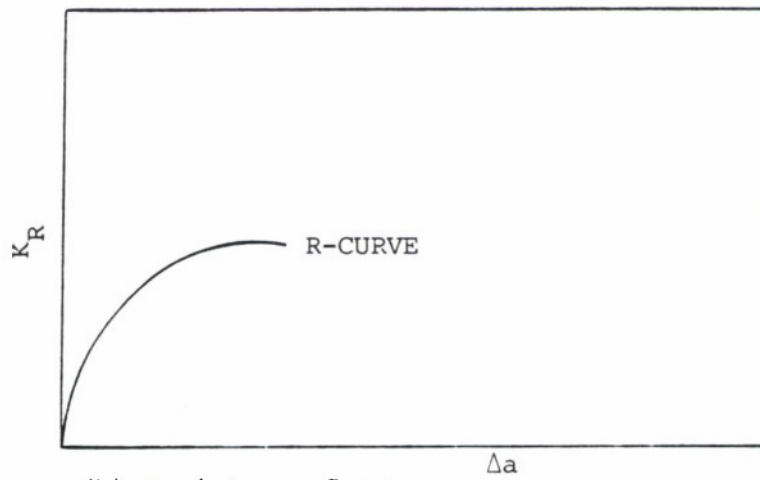


(b) Extensive Crack Extension

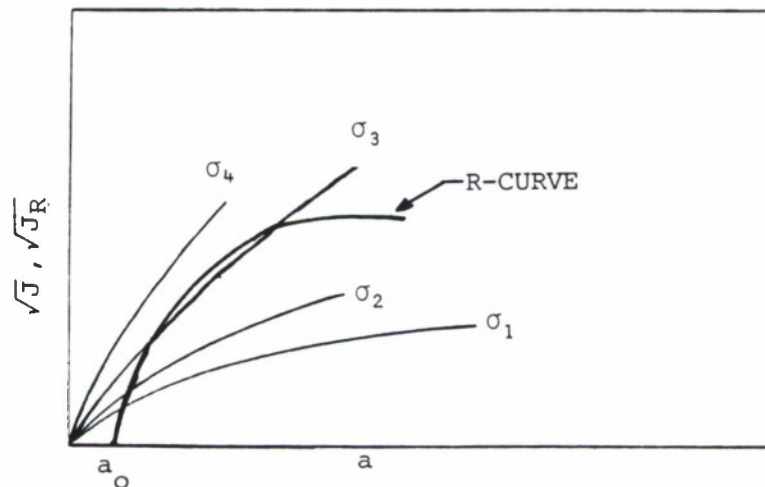
Figure 4.4.9. Diagrams Showing Onset of Unstable Crack Growth for Conditions of Limited or Extensive Crack Extension.



(a) Driving Factor

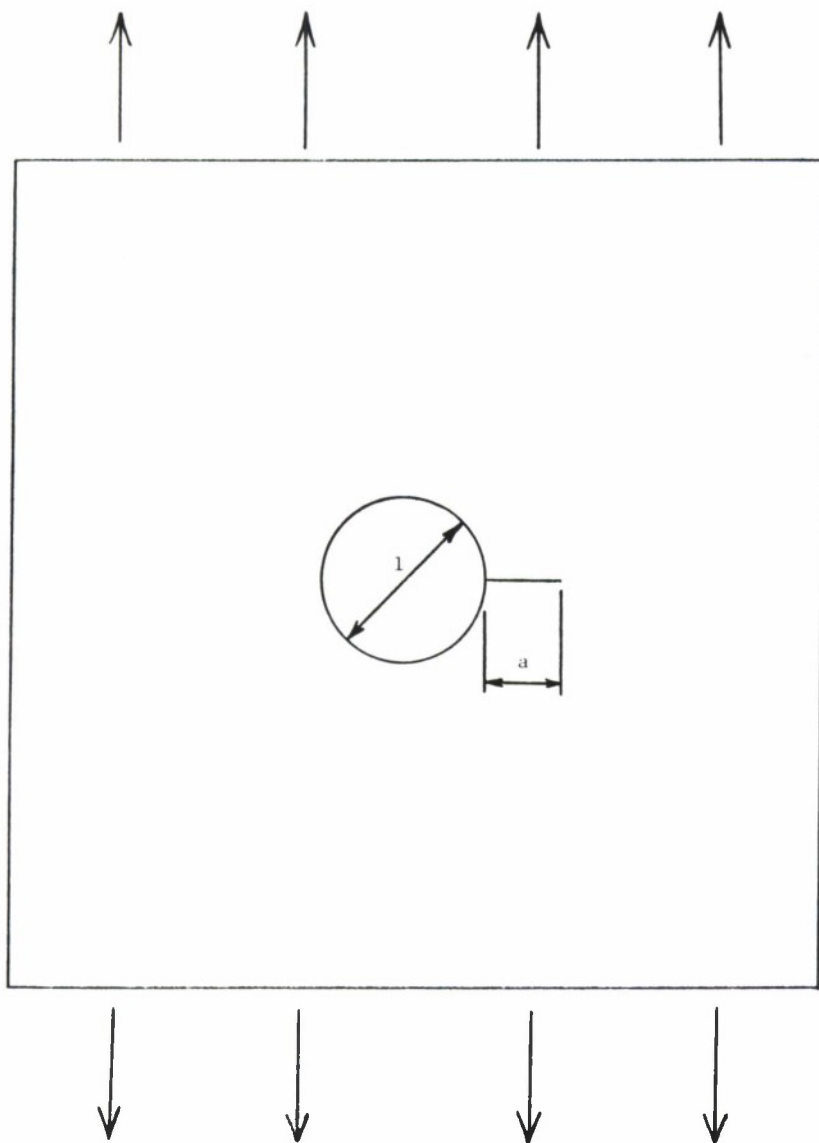


(b) Resistance Curve



(c) Matching Driving Factor with Resistance Curve

Figure 4.4.10. Steps Associated with Calculating Residual Strength of Cracked Structures with Tearing Fractures.



DIMENSIONS

$$D = 2R = 1 \text{ inch}$$

$$B = 0.063 \text{ inch}$$

MATERIAL

7075-T73

ALUMINUM

$$K = \sigma \beta \sqrt{\pi a} \text{ where}$$

$$\beta = \frac{0.8734}{(0.3246 + \frac{a}{r})} + 0.6762$$

Figure 4.4.11. Structural Geometry Associated with EXAMPLE 4.4.4.

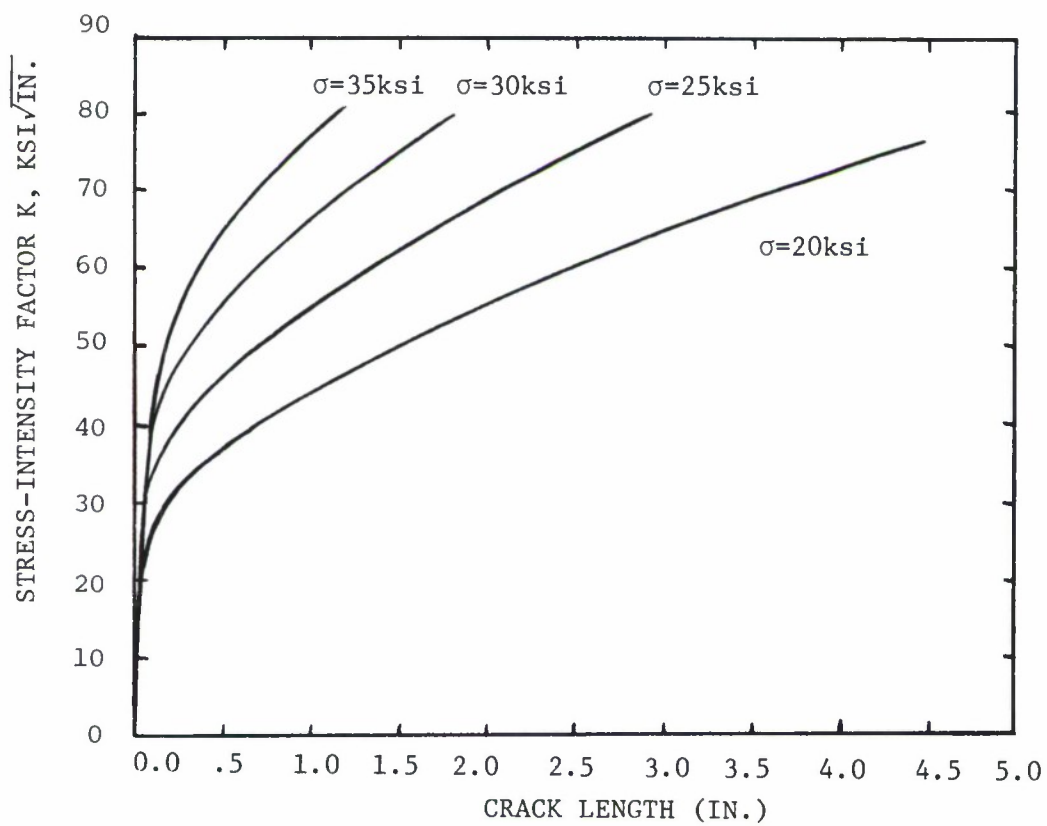


Figure 4.4.12. Stress-Intensity Factor Relationship for Various Values of Applied Stress.

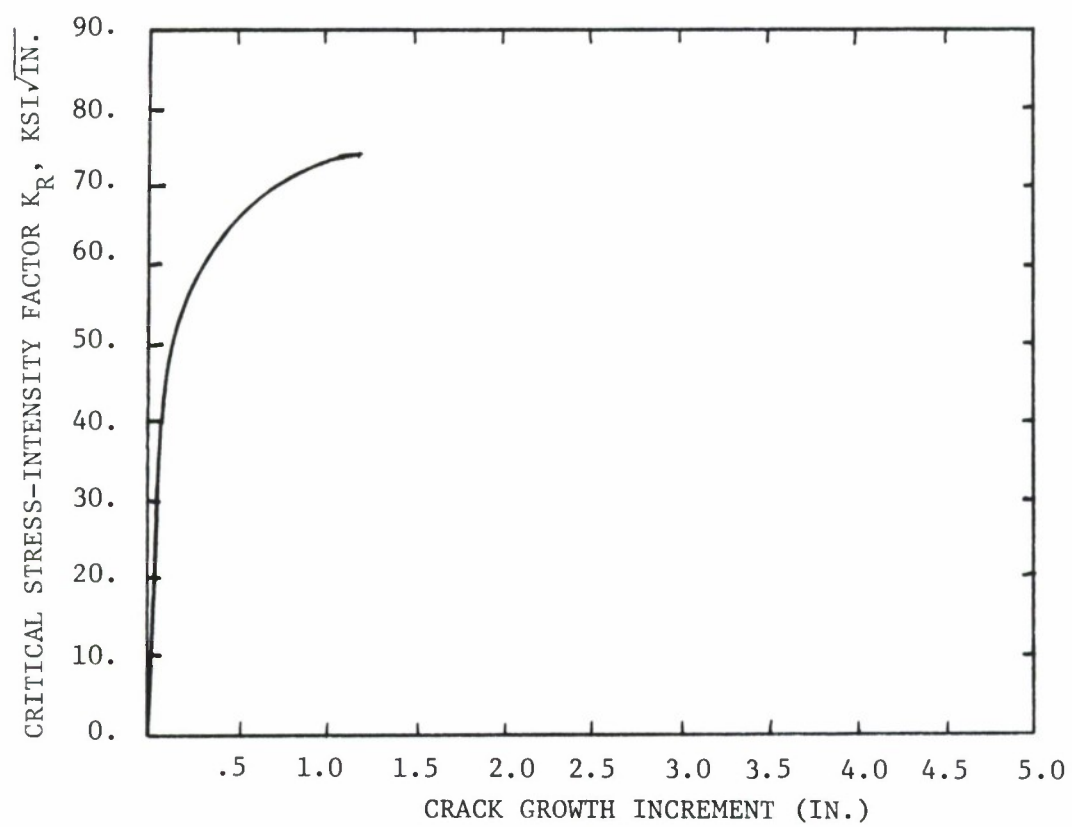


Figure 4.4.13. Resistance Curve for 7075-T73 Aluminum for a Thickness of 0.063 Inches.

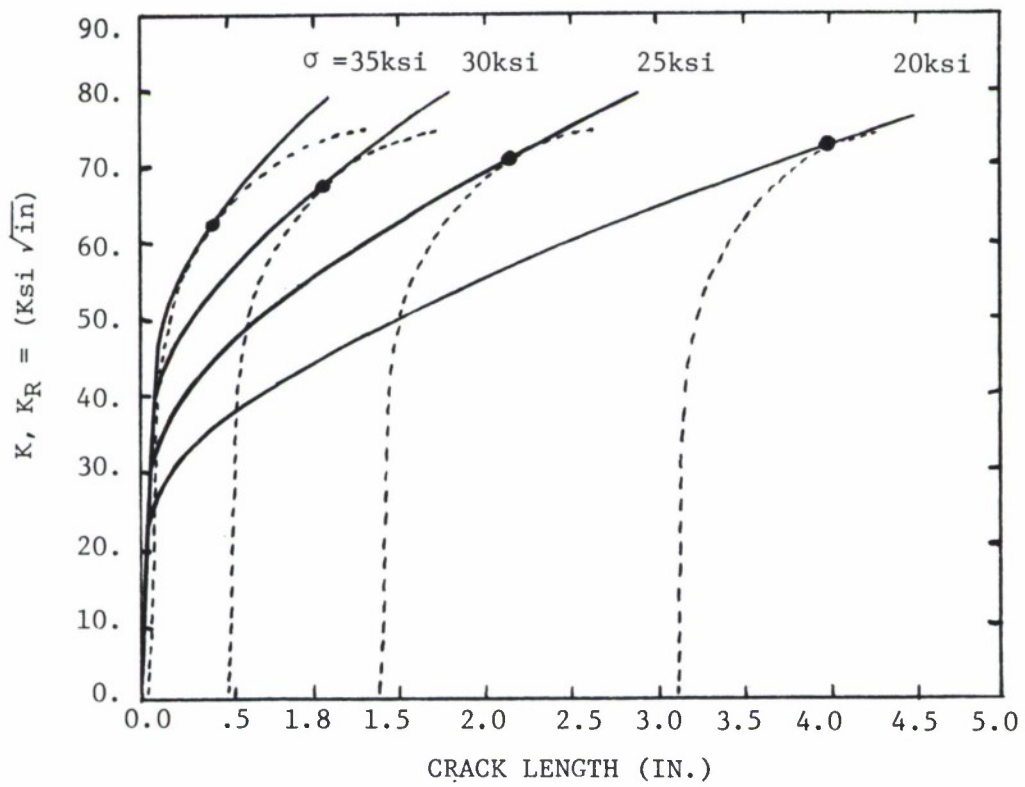


Figure 4.4.14. Matching the R-Curve and Stress-Intensity Factor Curves.

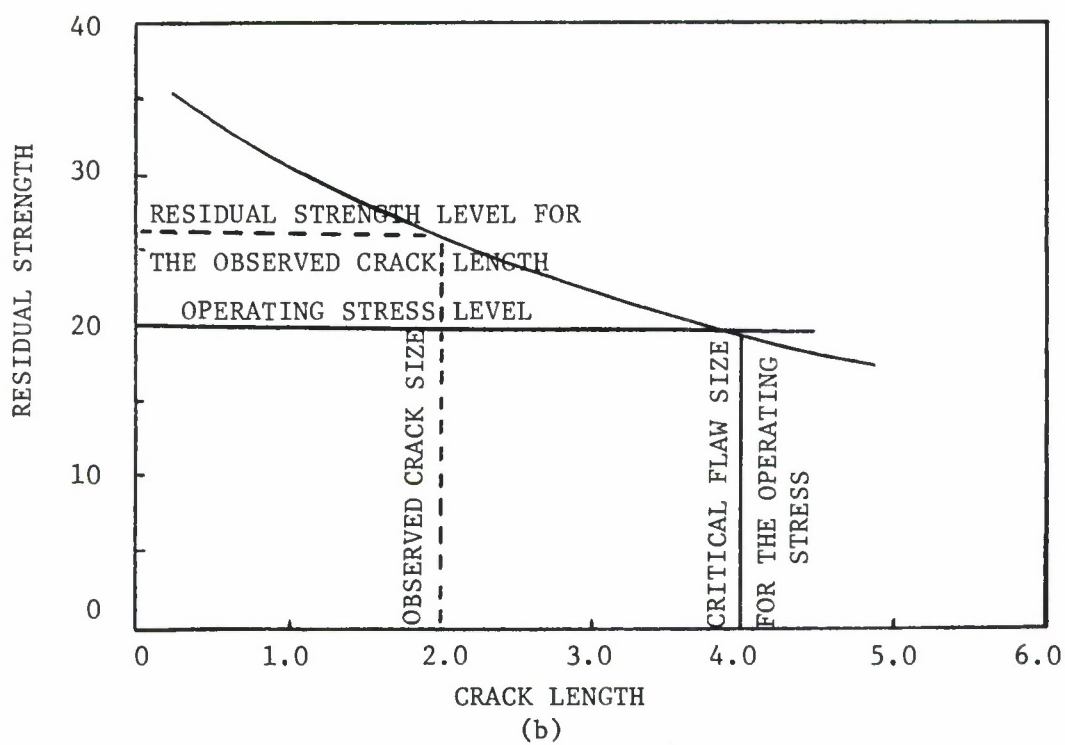


Figure 4.4.15. Residual Strength Diagram Obtained for Structure Shown in Figure 4.4.11 (EXAMPLE 4.4.4).

4.5 BUILT-UP STRUCTURES

Built-up structures normally require more than one failure criterion to determine the residual strength of the total structure. The development of the residual strength diagram of a given structure will involve the analysis of failures of each part of the load support system.

The structural configuration essentially determines the complexity of the residual strength analysis. Typical structural parameters which must be considered for skin-stiffened structure are:

- a. Type of Construction
 - 1. Monolithic (Unreinforced/Forgings)
 - 2. Skin (Longerons, stringer)
 - 3. Integrally Stiffened
 - 4. Planked
 - 5. Layered (Honeycomb/Laminated)
- b. Panel Geometry
 - 1. Planform
 - 2. Curvature
 - 3. Stiffener Spacing and Orientation
 - 4. Attachments (Spar Caps, Webs, Frames, etc.)
- c. Details of Construction
 - 1. Stiffener Geometry (hat, Z, Channel, etc.)
 - 2. Attachment Details (Bolted, Riveted, Welded, etc.)
 - 3. Fastener Flexibility
 - 4. Eccentricity

Ideally, the residual strength analysis will take all these parameters into consideration. In practice, many are treated empirically and others are not considered except in extremely detailed analyses.

This section provides details of the analysis methods used for built-up skin-stringer structure and the effects of many of the structural parameters listed above. In the order of their presentation, the subsections provide: overviews of the analysis for edge stiffened and for centrally stiffened skin structure, the analysis methods used to determine the stress-intensity factor in the skin structure and the loading transferred to the stringers, the analysis of stiffener failure, the analysis of fastener failure, the analysis methodology and an Example.

4.5.1 Edge Stiffened Panel With a Central Crack

The residual strength diagram of a simple panel with two stringers and a central crack can be constructed as follows. Consider first a crack in plane stress which starts propagating slowly at $\sigma_o = K_{onset}/\sqrt{\pi a_o}$ and becomes unstable at $\sigma_c = K_c/\sqrt{\pi a_c}$ in a sheet without stringers as shown in Figure 4.5.1a.

When the panel is stiffened with stringers, the stress-intensity factor is reduced to $K = \beta\sigma\sqrt{\pi a}$, where $\beta < 1$. As a result, both the stress for slow stable crack growth, σ_o , and the stress for unstable crack growth, σ_f , are altered to give $\sigma_o = K_{onset}/\beta\sqrt{\pi a_o}$ and $\sigma_{cf} = K_c/\beta\sqrt{\pi a_c}$, respectively.

4.5.2

Hence, these events take place at higher stresses in the stiffened panel than in the unstiffened panel. This means that the lines in Figure 4.5.1a are raised by a factor $1/\beta$ for the case of the stiffened panel, as depicted in Figure 4.5.1b. Since β decreases as the crack approaches the stringer, the curves in Figure 4.5.1b turn upward for crack sizes on the order of the stringer spacing.

The possibility of stringer failure should be considered also. The stringer will fail when its stress reaches the ultimate tensile stress (σ_{UTS}). As the stringer stress is $L\sigma$, where σ is the nominal stress in the panel away from the crack, failure will occur at σ_{sf} , given by $L\sigma_{sf} = \sigma_{UTS}$. Using L , a measure of the load transferred to the stringer, the panel stress at which stringer failure occurs is shown in Figure 4.5.1c. The stringer may yield before it fails. This means that its capability to take overload from the cracked skin decreases. As a result, β will be higher and L will be lower. The stress-intensity analysis should account for this effect.

Figure 4.5.2 shows the residual strength diagram of the stiffened panel. It is a composite of the critical conditions shown in Figure 4.5.1. In the case when the crack is still small at the onset of instability ($2a \ll 2s$, where $2s$ is stringer spacing), the stress condition at the crack tip will hardly be influenced by the stringers and the stress at unstable crack growth initiation will be the same as that of an

unstiffened sheet of the same size (Point B in Figure 4.5.2). When the unstably growing crack approaches the stiffener, the load concentration in the stiffener will be so high that the stiffener fails (Point C) without stopping the unstable crack growth (line BC).

When the panel contains a crack extending almost from one stiffener to the other ($2a \approx 2s$), the stringer will be extremely effective in reducing the peak stress at the crack tips (β small), resulting in a higher value of the stress at crack growth initiation. With increasing load, the crack will grow stably to the stiffener (line LMIF) and due to the inherent increase of stiffener effectiveness, the crack growth will remain stable. Fracture of the panel will occur at the same stress level corresponding to the point F due to the fact that the stiffener has reached its failure stress and the stress reduction in the skin is no longer effective after stringer failure.

For cracks of intermediate size ($2a = 2a_1$), there will be unstable crack growth at a stress slightly above the fracture strength of the unstiffened sheet (point H), but this will be stopped under the stiffeners at I. After crack arrest, the panel load can be further increased at the cost of some additional stable crack growth until F, where the ultimate stringer load is reached.

Since β and L depend upon stiffening ratio, the residual strength diagram of Figure 4.5.2 is not unique. Figure 4.5.2 shows the case where stringer failure is the critical event. For other stiffening ratios, skin failure may be the critical event as depicted in Figure 4.5.3. Due to a low stringer load concentration, the curves e and g do not intersect. A crack of size $2a_1$ will show stable growth at point B and become unstable at point C. Crack arrest occurs at D from where further slow growth can occur if the load is raised. Finally, at point E, the crack will again become unstable, resulting in panel fracture. It is therefore obvious then that a criterion for crack arrest has to involve the two alternatives of stringer failure and skin failure, and these depend upon the relative stiffness of sheet and stringer.

The foregoing clearly shows that for crack arrest it is not essential that the crack run into a fastener hole. Crack arrest basically results from the reduction of stress-intensity factor due to load transmittal to the stringer.

For the particular case depicted in Figure 4.5.4, the residual strength is not determined by stringer failure solely but also by fastener failure (point K). A crack of length $2a_1$ will show slow growth from E to F and instability from F to G. After crack arrest at G, further slow growth occurs until at point K the fasteners fail. The latter could cause panel failure, but this cannot be directly determined from the diagram.

In fact, a new residual strength diagram must now be calculated with omission of the first row of rivets at either side of the crack. Fastener failure will affect load transmittal from the skin to the stringer: line e will be lowered, line g will be raised. The intersection point H' of the new lines g' and e' may still be above K and hence, the residual strength will still be determined by stringer failure at H'.

In reality, the behavior will be more complicated due to plastic deformation. Shear deformation of the fasteners, hole deformation, and plastic deformation of the stringers will occur before fracture takes place. Plastic deformation always reduces the ability of the stringer to take load from the skin which implies that line g in actuality will be raised and line e will be lowered. The intersection of the two lines (failure point) will not be affected a great deal, however, (compare points H and H' in Figure 4.5.4). For this reason the residual strength of a stiffened panel can still be predicted reasonably well, even if plasticity effects are ignored. Nevertheless, a proper treatment of the problem requires that plasticity effects be taken into account.

4.5.2 Centrally and Edge Stiffened Panel With a Central Crack

In the previous subsection, the cases considered pertain to cracks between two stiffeners. In practice, however, cracks frequently start at a fastener hole and then there will be a stringer across the

crack which will have a high load concentration factor. The problem can be dealt with in a manner similar to a crack between stringers, using either analytical or finite-element procedures. A schematic residual strength diagram for this case is presented in Figure 4.5.5. Apart from the residual strength curve g for the edge stiffeners, there will now be an additional residual strength curve k for the central stiffener.

For the case where the crack in the skin is small ($2a \ll 2s$), the first failure in the structure is noted to occur at point B in Figure 4.5.5 where the skin fails and the crack starts to run. When the crack reaches a size such that point C is reached, the central stiffener residual strength has dropped to the operating stress level and then the central stringer fails, immediately causing additional loading to be transferred to the edge stiffeners and the skin structure. The effect of losing the capability of the central stringer is noted in Figure 4.5.5 with a repositioning of the residual strength curves for the edge stiffeners (from curve g to curve g') and skin structure (from curve e to curve e'). As the crack in the skin structure continues to grow after causing the ultimate tensile strength failure in the central stringer at point C, it reaches a size that causes the ultimate tensile strength failure of the two edge stringers at point D, at which point all potential arrest capability is lost and the structure is lost.

For the case of longer cracks, Figure 4.5.5 shows that skin cracks may start running (line EF), arrest (point F), and tear along curve FL as the stress is increased. At point L, the crack has reached a length that has resulted in sufficient stress being transferred to the central stringer so that this stiffener now fails. Again, this failure causes a redistribution of stress in the entire structure so that a new set of residual strength diagrams are required to determine the consequences associated with failing the central stringer. The new edge stringer and skin structure residual strength curves are presented by curves g' and e' , respectively.

Due to the high load concentration, the middle stringer will usually fail fairly soon by fatigue and therefore lines e' and g' , with the middle stringer failed, will have to be used and the residual strength is determined by point H' . (Note that e' , g' , and H' will have different positions in the absence of the middle stringer; a failed central stringer will induce higher stresses in both the skin and the edge stiffeners.) The foregoing discussion provides the concepts required to establish a complete residual strength diagram.

4.5.3 Analytical Methods

In this subsection analytical procedures are presented for the residual strength capability analyses. Methods for evaluating the unknown fastener force and the stress-intensity factors for the stiffened

panel are presented. Since the equations for the solution procedures have been based on linear elastic fracture mechanics, the failure criterion used in these analyses are also based on fracture toughness values for abrupt fracture conditions and K_R resistance curve data for tearing fracture conditions.

Analysis methods for stiffened panels have been developed independently by Romualdi, et al.⁽¹⁸⁾, Poe^(19,20), Vlieger⁽²¹⁾, Swift and Wang⁽²²⁾, Swift⁽²³⁾, Creager and Liu⁽²⁵⁾, and Wilhem and Ratwani⁽²⁶⁾.

Application of the stress intensity factor parameter, β , and the stringer load concentration factor, L , were proposed by Vlieger⁽²¹⁾ and Swift and Wang⁽²²⁾.

From the residual strength capability analysis as discussed in the preceding subsections, it is evident that the construction of residual strength diagrams for built-up structures also requires the estimation of the stress-intensity factor K . A number of approaches for determining K have been developed. Solutions for complicated structural geometries can sometimes be obtained from the basic stress field solutions combined with displacement compatibility requirements for all the structural members involved. This approach has been shown by several investigators to be useful in the analysis of built-up sheet structure. While the analysis is based on closed form solutions, the actual analyses are computerized for efficient solutions. The essentials of this technique are described below.

In calculating β and L , two methods can be used. There are the finite-element method and an analytical method based on closed-form solutions. The analytical method has advantages over the finite-element method in that the effect of different panel parameters on the residual strength of a certain panel configuration can be easily assessed, so that the stiffened panel can be optimized with respect to fail-safe strength. It allows direct determination of the residual-strength diagram. In the case of the finite-element method, a new analysis has to be carried out when the dimensions of certain elements are changed because a new idealization has to be made. An advantage of the finite-element analysis, on the other hand, is that such effects as stringer eccentricity, hole deformation, and stringer yielding can be incorporated with relative ease. Details of the calculations can be found in the referenced papers.

The procedure for analytical calculation is outlined in Figure 4.5.6. The stiffened panel is split up into its composite parts, the skin and the stringer. Load transmission from the skin to the stringer takes place through the fasteners. As a result, the skin will exert forces F_1 , F_2 , etc., on the stringer, and the stringer will exert reaction forces F_1 , F_2 , etc. on the skin. This is depicted in the upper line of Figure 4.5.6.

The problem is now reduced to that of an unstiffened plate loaded by a uniaxial stress, σ , and fastener forces $F_1 \dots F_n$. This case can be considered as superposition of three others, shown in the second line of Figure 4.5.6. Namely:

- a. A uniformly loaded cracked sheet.
- b. A sheet without a crack, loaded with forces $F_1 \dots F_n$.
- c. A cracked sheet with forces on the crack edges given by the function $p(x)$. The forces $p(x)$ represent the load distribution given by Love⁽²⁷⁾. When the slit CD is cut, these forces have to be exerted on the edges of the slit to provide the necessary crack-free edges.

The three cases have to be analyzed individually. For case a, the stress-intensity factor is $K = \sigma\sqrt{\pi a}$. For case b, $K = 0$. The stress intensity for case c is a complicated expression that has to be solved numerically. However, once the K value for case c is determined, the stress-intensity factor for the whole stiffened panel can be obtained by adding the K values for cases a and b. The determination of K requires calculations of fastener forces $F_1, F_2 \dots F_n$. To calculate these forces, the displacement compatibility conditions which require equal displacements in sheet and stringer at the corresponding fastener locations, can be used. These compatibility requirements deliver a set of n (n = number of fasteners) independent algebraic equations from which the fastener forces can be obtained. These equations can be solved numerically using Gauss-Seidal or Gauss-Jordan iterative methods.

The number of fasteners to be included in the calculation depends somewhat upon geometry and crack size. According to Swift⁽²⁴⁾ and shown in Figure 4.5.7, 15 fasteners at either side of the crack seems to be sufficient

to get a consistent result. Similar results were obtained by Sanga⁽²⁸⁾. Swift's analysis provides a detailed description of how to incorporate nonelastic behavior in this kind of analysis. The method can account for (1) stiffener flexibility and stiffener bending, (2) fastener flexibility, and (3) biaxiality. Stringer yielding, fastener flexibility, and hole flexibility are lumped together in an empirical equation for fastener deflection.

The effect of fastener flexibility and stiffener bending on β and L is shown in Figure 4.5.8. Although the effects are quite large, the vertical position of the crossover of critical stress-intensity factor curve and stringer stress curve is not affected too much (compare points A and B in Figure 4.5.8). The level of the crossover determines the residual strength, as pointed out in the previous subsections. This explains why the residual strength can be reasonably well predicted if the flexibility of the fasteners is neglected.

In the case of adhesively bonded stiffeners, the displacement compatibility approach was used to calculate the fastener loads $F_1, F_2 \dots F_n$. The adhesive was considered by dividing it into a series of discrete segments. The forces $F_1, F_2 \dots F_n$ which correspond to the segments shown in Figure 4.5.9. Using an appropriate computational method as explained for riveted fastener, the unknown fastener forces can be evaluated. The method of superposition results in an expression in terms of a complex integral for the stress-intensity factor. A typical

residual strength diagram for a bonded structure as compared to the riveted structure is shown in Figure 4.5.10. The required expressions and the solution techniques are discussed in the example problem for a riveted skin-stringer combination with a central crack in the skin (see subsection 4.5.7).

4.5.4 Stiffener Failure

Stiffener failures are based on the following three stiffener conditions:

1. Intact Stiffener (no cracks).
2. Partially failed stiffener (with cracks).
3. Totally failed stiffener.

The failure criterion for the intact stiffener is based on the ultimate strength criterion. As mentioned earlier, the ratio between the stiffener load in the cracked region (P_{\max}) and the remote region from the crack (P) is defined as the load concentration factor L_s or

$$L_s = \frac{P_{\max}}{P} = \frac{P_{\max}}{\sigma A_s} \quad (4.5.1)$$

where σ is the uniform stress in the skin at the loaded end of the panel and A_s is the stiffener cross sectional area. Failure of the stiffener will occur when the value of P_{\max} is equal to the ultimate strength of the stiffener (P_{ult}), or when

$$P_{\max} = P_{\text{ult}} = \Psi \sigma_{\text{ult}} A_s \quad (4.5.2)$$

where σ_{ult} is the ultimate tensile strength of the stiffener material and $\Psi \leq 1$ is a factor accounting for load eccentricity and notch effects in the stiffener. For a uniform stress distribution in the panel remote from the crack the stress in the stringer will equal the nominal stress σ in the skin, i.e.,

$$P = \sigma A_s. \quad (4.5.3)$$

Combining equations 4.5.1 to 4.5.3, yields the following stiffener failure criterion:

$$\sigma = \Psi \frac{\sigma_{ult}}{L_s} \quad (4.5.4)$$

When the stress in the stringer reaches the value of $\Psi \sigma_{ult}$, the stringer will fail. The parameter Ψ is determined by tests.

When load eccentricity and notch effects are not considered for a stringer, Ψ equals one. The stiffener failure curve obtained using Equation 4.5.4 is shown in Figure 4.5.11. The initial portion of the residual strength curve is flat because the load concentration factor L_s is equal to one for small skin crack lengths. As the skin crack increases in size, L_s becomes significantly greater than one and the stringer carries a large portion of the total structural load which eventually leads to stringer yielding and failure. The portion of the curve in Figure 4.5.11 corresponding to $L_s > 1$ shows the gradual reduction of the residual strength.

When the load eccentricity and notch effects in the stiffener are considered, the parameter Ψ in Equation 4.5.4 is less than one. The residual strength corresponding to a case where $\Psi < 1$ is shown in Figure 4.5.11. The curve CD does not have the initial flaw portion exhibited by the case $\Psi = 1$. Instead, the residual strength starts decreasing even for small skin crack lengths. The residual strength diagram for the stringer can be constructed knowing the values of L_s and Ψ . Determining L_s requires numerical solution techniques which are discussed in the example presented in subsection 4.5.7.

According to MIL-A-83444 requirements, cracks are assumed in all load carrying members. This means that all structural elements, stringer included, are assumed to be damaged. The residual strength diagram for the stringer will involve using the fracture mechanics approach of predicting unstable crack growth. The critical stress for a partially cracked stringer is given by $\sigma_f = \frac{K_{cr}}{L_s \beta_s \sqrt{\pi a_s}}$ where K_{cr} is the appropriate fracture toughness, β_s is the stringer geometric parameter, and a_s is the stringer crack size. When the crack in the panel approaches the stringer, the load transmitted to the stringer will become large ($L_s \gg 1$) and thus the critical stress level required to fail the stringer rapidly decreases as shown by curve CE in Figure 4.5.11. Curve CE corresponds to the total failure of the stringer. This may happen when a large crack emanates from a stringer rivet hole. Total failure of the stiffener occurs before the skin crack approaches the stiffeners.

The residual strength diagram for the stiffened panel in this case, would, in fact, be approximately that of the unstiffened panel.

The foregoing discussion presented analysis of a riveted built-up structure. However, built-up structures exist in which the stringer is adhesively bonded to the skin. The load transfer from the skin to the stringer is more effective in the bonded structure due to the increased rigidity in the stiffener. The corresponding load transfer parameter L_s will have higher values as shown schematically in Figure 4.5.12a. Due to the effective load transfer from the skin to the stiffener, the applied stress-intensity factor will be reduced when the panel crack approaches the stiffener. Figure 4.5.12b illustrates the levels of stress-intensity factor that occur for riveted and bonded stiffeners. The figure also shows that the bonded stiffener is subjected to higher loads due to the effective load transfer; the higher load causes the stiffener failure of the bonded structure to be more critical than that of the riveted structure. Figure 4.5.13 compares the decay of residual strength for these two types of structures. The residual strength of the bonded stiffener decreases faster than the riveted stiffener. In the determination of the residual strength diagram, the parameter L_s is usually calculated by numerical methods. The steps to obtain L_s are discussed later in this section.

4.5.5 Fastener Failure

In subsections 4.5.3 and 4.5.4, the discussion focused on skin and stiffener failures. A third mode of failure involves the fasteners. This paragraph will discuss the failure of the fastener system. Load is transmitted from the skin to the stringers through fasteners. If the fastener loads become too high, fastener failure may occur by shear. Fastener failure will reduce the effectivity of the stringer; and therefore, the residual strength of the panel will drop. The highest loads (F) in the stringer/skin connections will occur in the fasteners adjacent to the crack path. Fastener failure will occur when the fastener forces F transmitted by the fasteners adjacent to the crack exceed the critical shear load of the fastener. The fastener failure criterion is given by

$$F = \pi/4 d^2 \tau_{ult} \quad (4.5.5)$$

where d is the fastener diameter and τ_{ult} is the ultimate shear stress of the fastener material. It is emphasized that fastener failure need not necessarily cause total failure of the panel. Once the fastener failure criterion is met, however, the values of L_s and β will change since the loads transferred to the stiffener and skin changes. Once the fastener fails, the values of β and L_s will be recalculated in order to proceed further with the residual strength analysis. The load that causes the fasteners to fail by shear can be calculated from Equation 4.5.5; the corresponding nominal stress in the panel then gives the residual

strength curve for the fasteners as shown in Figure 4.5.14. At zero crack length, and for the case where the skin and stringers are made from common materials, the fasteners do not carry any load; the curve therefore tends to increase rapidly for $a \rightarrow 0$. The fastener forces F_i can be computed through the displacement compatibility between the stiffener and the panel. The necessary steps involved in the computation of F_i are discussed in the example presented in subsection 4.5.7.

In the case of adhesively bonded structures, the adhesive (fastener) failure criterion is based on a maximum adhesive strain value. The residual strength analysis is fairly complicated (see for example, reference 24). Based on the displacement compatibility between the panel and the stiffener, the adhesive segment strain deflection can be numerically computed for different amounts of disbond. Figure 4.5.15a shows the adhesive strain versus gross stress for various levels of adhesive delamination. The vertical line AB represents average failure strain of the adhesive. The intersection points between the line AB and the curves give the critical gross stress versus amount of adhesive failed as shown in Figure 4.5.15b. The corresponding curve ABC can be used for panel failure analysis. The area above the curve defines the failure of adhesive.

4.5.6 Methodology Basis for Stiffened Panel Example Problem

The residual strength analysis of an edge stiffened, centrally cracked skin structure of the type shown in Figure 4.5.16 can be performed by following the general steps described in the preceding subsections.

In this subsection, the specific details are covered which are associated with conducting the stress-intensity factor analysis as well as the analysis to determine the stresses in the stringers and fastener loads. To simplify the detailed calculations, it is assumed that only one fastener (rivet) on either side of the crack is active as shown in Figure 4.5.17 and that this rivet is assumed to be rigid. Thus, there is only one unknown fastener force F transferred between the stringers and the skin by this rivet.

Typically, the analysis proceeds by splitting up the structure shown in Figure 4.5.16 into its component parts as shown in Figure 4.5.17. The unknown force F can be calculated from the displacement compatibility condition between the skin and the stringer. The complicated expressions which correspond to the displacements V_σ , V_F , and V_P due to the applied stress, σ , the fastener force F and the distributed pressure $P(x)$, respectively, can be obtained using a procedure suggested by Westergaard⁽²⁹⁾ and by Love⁽²⁷⁾. The detailed discussions on the methods of obtaining the required relationships are presented by Broek⁽¹³⁾. The necessary

relationships for V_σ , V_F , V_p and V_{st} (displacement in the stringer) are given as:

$$V_\sigma = \frac{\sigma}{E} f_\sigma \quad (4.5.6)$$

$$V_F = \frac{-F}{EB} f_F \quad (4.5.7)$$

$$V_p = \frac{-F}{EB} f_p \quad (4.5.8)$$

and
$$V_{st} = \frac{F}{E_{st} B_{st}} f_{st} + \frac{\sigma}{E_s} p \quad (4.5.9)$$

where

$$f_\sigma = \sqrt{\rho_1 \rho_2} \left\{ 2 \sin\left[\frac{\theta_1 + \theta_2}{2}\right] \frac{(1+\nu)pr}{\rho_1 \rho_2} \cos\left[\theta - \frac{\theta_1 + \theta_2}{2}\right] \right\} + \nu p \quad (4.5.10)$$

$$f_F = \frac{(1+\nu)}{4\pi} \left\{ (3-\nu) \left[\ln \frac{d}{4p} - 1 \right] + (1+\nu) \left[2 - \frac{s^2}{2^2 + p^2} \right] + (3-\nu) \ln \left(\frac{s^2}{2^2 + p^2} \right) \right\} \quad (4.5.11)$$

$$f_p = \frac{\bar{P}}{\pi a} \left\{ 2 \left[\sqrt{\rho_1 \rho_2} \sin\left(\frac{\theta_1 + \theta_2}{2}\right) - p \right] - (1+\nu) p \left[\frac{r}{\sqrt{\rho_1 \rho_2}} \cos\left(\theta - \frac{\theta_1 + \theta_2}{2}\right) - 1 \right] \right\} \quad (4.5.12)$$

where $\bar{P} = \left\{ \tan^{-1}\left(\frac{a+s}{p}\right) + \tan^{-1}\left(\frac{a-s}{p}\right) + \frac{p(1+\nu)}{2} \left[\frac{a+s}{p^2 + (a+s)^2} + \frac{a-s}{p^2 + (a-s)^2} \right] \right\} \quad (4.5.13)$

and

$$f_{st} = - \frac{(1+\nu)}{4\pi} \left\{ \left[(3-\nu) \left(\ln \frac{d}{4y_o} - 1 \right) + (1+\nu) \right] + 2 \sum_{n=1}^{\infty} \left[(3-\nu) \ln \frac{nw}{\sqrt{n^2 w^2 + 4p^2}} + (1+\nu) \left(\frac{4p^2}{n^2 w^2 + 4p^2} \right) \right] \right\} \quad (4.5.14)$$

The geometric variables r , ρ_1 , ρ_2 , θ_1 , θ_2 and θ are shown in Figure 4.5.18.

The displacement compatibility condition requires equal displacements in corresponding points of sheet and stringer; it yields the following equation to calculate the unknown fastener force F .

$$V_{\sigma} + V_F + V_p = V_{st} \quad (4.5.15)$$

substituting the expressions 4.5.6-4.5.9 for V_{σ} , V_F , V_p , and V_{st} in the above relationship, and reassembling, we get

$$F = \sigma \lambda \text{ where } \lambda = \left\{ \frac{\frac{f_{\sigma}}{E} - \frac{p}{E_{st}}}{\frac{f_F + f_p}{EB} + \frac{f_{st}}{E_{st} B_{st}}} \right\}. \quad (4.5.16)$$

The next step is to obtain an expression for the stress-intensity factor for the entire stiffened panel configuration. Using superposition, the stress-intensity factor is obtained as the sum of the stress-intensity factors for the three cases shown in Figure 4.5.17. It can easily be seen that for Case I: $K = \sigma \sqrt{\pi a}$ and for Case II: $K = 0$. The stress-intensity factor (K) for Case III is a fairly complicated expression and it is given by,

$$K_{III} = -2 \sqrt{\frac{a}{\pi}} \frac{1}{\pi} \frac{F}{B_p} \left[\frac{(3 + \nu)}{2} I_1 + (1 + \nu) I_2 \right] \quad (4.5.17)$$

$$\text{where } I_1 = \int_0^a \frac{d\bar{x}}{\sqrt{a^2 - \bar{x}^2}} \left\{ \frac{1}{(1 + (\bar{x} - \bar{s})^2)} + \frac{1}{(1 + (\bar{x} + \bar{s})^2)} \right\} \quad (4.5.18a)$$

$$\text{and } I_2 = \int_0^a \frac{d\bar{x}}{\sqrt{a^2 - \bar{x}^2}} \left\{ \frac{(\bar{x} - \bar{s})^2}{(1 + (\bar{x} - \bar{s})^2)^2} + \frac{(\bar{x} + \bar{s})^2}{(1 + (\bar{x} + \bar{s})^2)^2} \right\}. \quad (4.5.18b)$$

where \bar{a} , \bar{x} and \bar{s} are normalized with respect to the rivet pitch. The estimation of K_{III} requires solution of the above integrals by numerical methods. Replacing the fastener force F by the expression and rearranging the expression for K_{III} , the stress-intensity factor K for the stiffened panel then becomes

$$K = \sigma\sqrt{\pi a} - \sigma\sqrt{\pi a} \lambda_1 \lambda_2 \quad (4.5.19)$$

where
$$\lambda_1 = \frac{(3+\nu)}{2} I_1 + (1+\nu) I_2 \quad (4.5.20a)$$

and
$$\lambda_2 = \frac{2\lambda}{\pi^2 B_p} . \quad (4.5.20b)$$

The stress-intensity factor K can be finally expressed in the following form,

$$K = \sigma\beta\sqrt{\pi a} \quad (4.5.21)$$

where
$$\beta = (1 - \lambda_1 \lambda_2) . \quad (4.5.22)$$

To calculate K for a given stiffened panel the values of f_σ , f_F , f_p , f_{st} , and λ_1 have to be obtained. These variables are numerically calculated and plotted as shown in Figures 4.5.19 to 4.5.23 for various values of \bar{s} , \bar{a} , and \bar{d} . For the given example data, we can now construct the residual strength diagram using the values obtained from these plots.

4.5.7 Example Residual Strength Analysis of Stiffened Panel

Determine the residual strength capabilities of a stiffened panel of 7075 Aluminum with a central crack between the two stringers as shown in Figure 4.5.24.

For a critical crack size ($2a$) of 4.0 inch, what is the fracture strength and for an operating stress of 20 Ksi, what is the critical crack size?

SOLUTION:

The first step is to obtain the stress-intensity factor by means of Equation 4.5.21 which involves the parameters λ_1 and λ_2 . For various crack lengths, these two variables can be calculated using Equation 4.5.20. The calculations involve the values of f_σ , f_F , f_p , f_{st} and λ which are obtained from the plots for various values of \bar{a} for the given $\bar{s} = 20$ and $d/p = 3/16$. Knowing the values of λ_1 and λ_2 , the geometric parameter β can be estimated from Equation 4.5.22. It is then straightforward to obtain the K vs. a plot by substituting the sets of values of a and β in the stress-intensity factor Equation 4.5.21 for a particular value of the applied stress σ . The corresponding K vs. a plot is shown in Figure 4.5.25 for $\sigma = 5, 10, \text{ and } 15$ Ksi. This figure shows that the stress-intensity factor decreases rapidly when the crack approaches the stringer. The figure also shows the effect of stringer to panel thickness ratio on the stress-intensity factor.

The next step is to apply a failure criterion to evaluate the fracture stresses, σ_{cr} , for various crack sizes. Assuming that the material exhibits negligible subcritical crack growth, the fracture toughness failure criterion ($K = K_{cr}$) based on the plane stress condition can then be applied. For $K = K_c$ in Equation 4.5.21, σ_f can be evaluated for a

particular crack size and the corresponding β which was obtained through equation 4.5.22. The residual strength diagram, i.e., the plot of σ_f vs. a_c for the given data ($K_c = 65 \text{ Ksi}\sqrt{\text{inch}}$) is shown in Figure 4.5.26.

The residual strength curves of the fastener and stiffeners are obtained by combining equations 4.5.5 and 4.5.16 for fastener failure and equations 4.5.1, 4.5.4, and 4.5.16 for stringer failure. The corresponding equations are given by,

$$\sigma_f = \frac{\pi d^2 \tau_{ult}}{4 \lambda} \text{ (Fastener)} \quad (4.5.23)$$

and

$$\sigma_f = \psi \frac{\sigma_{ult}}{(1 + \frac{\lambda}{A_s})} \text{ (Stringer)} \quad (4.5.24)$$

where λ is a function of 'a' and the values of λ for various crack lengths can be obtained using the Equation 4.5.16. To obtain Equation 4.5.24, note that the maximum stringer load (P_{max}) is the source of the fastener force ($F = \sigma \lambda$) and the remote stringer force (σA_s). The composite residual strength diagram as shown in Figure 4.5.26 contains the three failure curves corresponding to panel, stringer, and fastener. The stringer failure curve corresponds to $\alpha = 1$ (light stringer).

For the crack length given ($2a = 4$ inches), the corresponding residual strength is found from Figure 4.5.26 for a half crack length (a) of 2 inches. Point A in this figure identifies the skin failure condition which occurs at a stress level of 25.9 Ksi. For the operating stress level of

20 Ksi, the panel can be effective without catastrophic failure for cracks with length less than the critical crack (a_{cr}) of 3.4 inch (note $2a_{cr} = 6.8$ inch). If the panel develops a crack less than a_{cr} , it will not fail by unstable crack growth. However, for any other crack size which is equal or greater than the a_{cr} (3.4 inch), the residual strength level will fall below the operating stress level, leading to the rapid extension of the crack. Nevertheless, the structure has to be fully analyzed for its crack arrest capabilities when it develops cracks of length greater than a_{cr} .

Assume that the panel develops a crack of size a_{cr} . At point B in the figure, the crack extends rapidly. When the rapidly extending crack becomes 15 inches, the stress level in the stiffener (point C) reaches its critical value and the stiffener fails. Due to the stiffener failure, the stiffener becomes ineffective, leading to the total failure of the panel without any crack arrest possibilities.

In Figure 4.5.27, the stiffener failure curve is plotted for a strong stiffener with $\alpha = 4$ (the stiffener thickness is "assumed" four times the panel thickness). If the panel develops a crack size a_{cr} , the crack will extend rapidly from point D to point E as shown in Figure 4.5.27. At point E, the fastener fails, leading to an ineffective stringer (loads are no longer transferred to the stringer). Thus, the failure of the panel is unavoidable and the unstable crack growth without effective crack arrest leads to the total failure of the structure.

4.5.8 Tearing Failure Analysis

When the cracked thin sheet structure of high fracture toughness material is considered, the solutions based on linear elastic behavior for the calculation of residual strength are no longer valid due to the large scale yielding at the crack tip. For fail-safe structures with crack arrest capabilities, the residual strength analysis becomes complicated. However, using the R-curve based on $\sqrt{J_R}$ concept as the failure criterion Ratwani and Wilhem⁽²⁶⁾ developed a step-by-step procedure for predicting the residual strength of built-up skin stringer structure composed of tough material exhibiting tearing type fractures.

The residual strength prediction procedure is briefly outlined here to show, step-by-step, the required data and analysis. It should not be assumed that by reading this step-by-step procedure that the uninitiated can perform a residual strength prediction. It is strongly recommended that the details of the preceding subsections and reference 26 be examined prior to attempting a structural residual strength analysis based on the following ten procedural steps.

STEP 1. Model the structure for finite-element analysis or use an existing finite-element model remembering --

- a. That structural idealizations are typically two-dimensional,
- b. That no out-of-plane bending is permitted,
- c. To use a proper fastener model (a flexible fastener model for riveted or bolted structure, or a shear spring model for bonded structure).

- d. To use material property data from skin and substructure of interest (i.e., E , E_{ty} and F_{tu}),
- e. To select the most critical crack location (normally highest stressed area),
- f. To take advantage of structural symmetry.

STEP 2. Select one crack length ($2a$ or a) of interest (based on inspection capability or detailed damage tolerance requirement). Based on this "standard" crack length, five other crack lengths are selected for a Dugdale type elastic plastic analysis. These crack lengths should be selected such that crack length to stiffener spacing ($2a$) ratios vary between 0.15 to 1.1 remembering --

- a. That the greatest variation in J values will take place near reinforcements, and
- b. To select at least one crack size shorter than "standard".

STEP 3. With the finite-element model (from Step 1) and assumed crack lengths (from Step 2), perform an analysis assuming Dugdale type plastic zones for each crack size remembering --

- a. To select the first increment of plastic zone length at 0.2 inches and sufficient successive increments (normally 6) to reach Bueckner-Hayes calculated stresses up to 85 percent to F_{ty} .
- b. To make judicious selection of plastic zone increments so as to take advantage of overlapping a_e (effective crack length) (e.g., 3.2, 3.5, 4.2, 5.0 inches for a 3 inch physical crack

and 4.2, 4.5, 5.0 inches, etc., for a 4 inch physical crack). If overlapping is done, those cases where the crack surfaces are loaded throughout the crack length will be common for two or more physical crack sizes hence the computer programs need be run only once (e.g., 4.2 and 5.0 inches) thus reducing computer run times.

STEP 4. From Step 3, obtain stresses in stiffeners for Dugdale analysis and elastic analysis. Plot stiffener stresses as function of applied stress.

STEP 5. From the crack surface displacement data of Step 3, plot \sqrt{J} (obtained by Bueckner-Hayes approach) versus applied stress to F_{ty} ratio for each crack size.

STEP 6. From Step 5, cross plot the data in the form of \sqrt{J} versus crack size (a) at specific values of applied stress to F_{ty} ratio.

STEP 7. Employing the data of Step 4 and the "standard" crack size determine, gross panel stress to yield strength ratio, σ/F_{ty} at ultimate strength (F_{tu}) for the stiffener material - assuming zero slow crack growth. This information will be used subsequently to determine if a skin or stiffener critical case is operative.

STEP 8. Obtain crack growth resistance data for skin material (see Volume II of reference 26) remembering --

- a. To use thickness of interest (i.e., if the skin material is chemically milled, use the experimentally obtained R-curve for the same chemically milled material)
- b. Use proper crack orientation (LT, TL, or off angle) corresponding to anticipated direction structural cracking.

STEP 9. Plot \sqrt{J} versus Δa_{PHY} curve as shown in Figure 4.5.28 from the data obtained in Step 8.

STEP 10. Determine structural residual strength. On the \sqrt{J} versus crack size (a) plots obtained in Step 6 for the structure, overlay the $\sqrt{J_R}$ versus Δa_{PHY} material plot of Step 9 at the initial crack length of interest as shown in Figure 4.5.29. Determine if --

At the gross panel stress obtained from Step 7, significant slow tear (≥ 0.25 inch) will occur as indicated from the intersection of the $\sqrt{J_R}$ versus Δa_{PHY} curve with the constant σ/F_{ty} curve at a stringer ultimate strength (see Step 7). Interpolation will probably be necessary between values of constant σ/F_{ty} . Then proceed as follows:

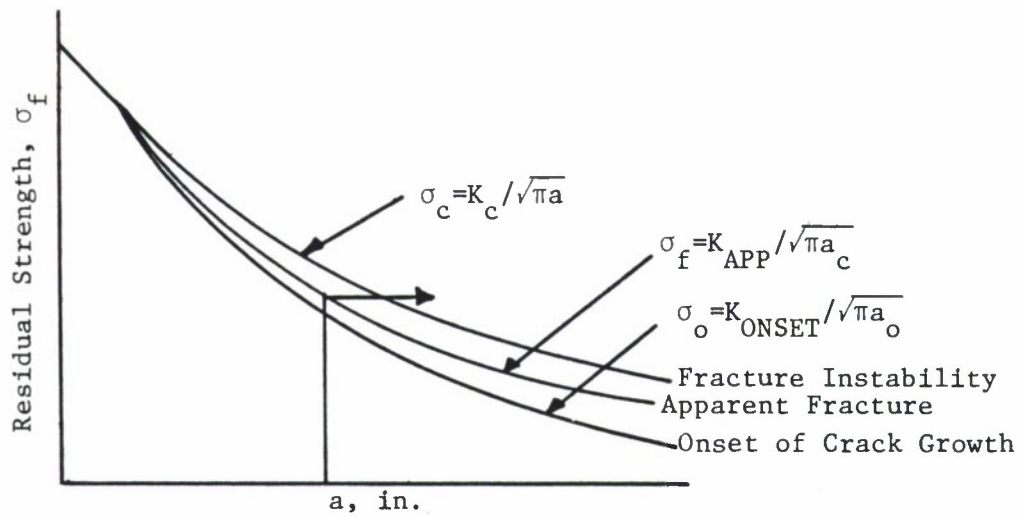
- If significant slow tear occurs (≥ 0.25 inch) the structure can be considered to be skin critical (at that particular crack length). Tangency of $\sqrt{J_R}$ versus Δa_{PHY} and \sqrt{J}

versus a_{PHY} at constant applied stress can be used to determine extent of slow tear and residual strength at failure as a percentage of F_{ty} .

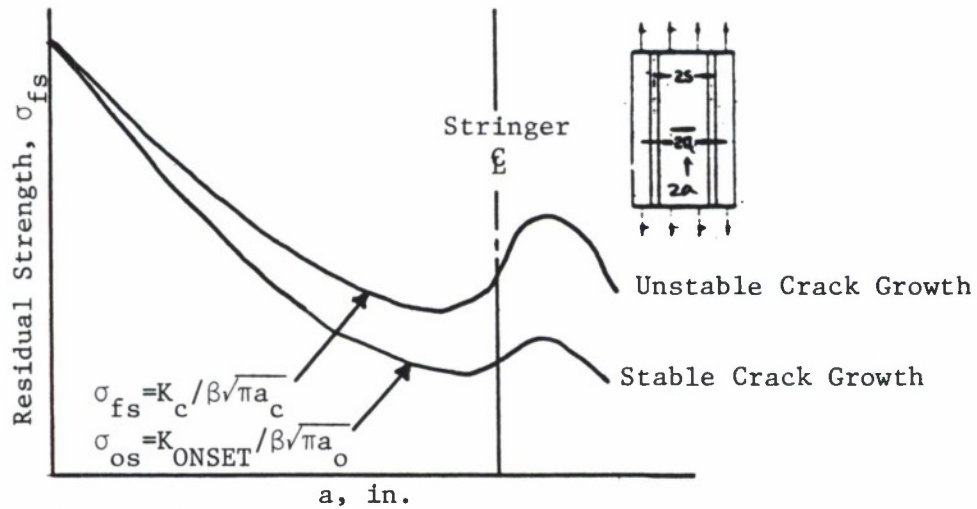
- If significant slow tear does not occur ($\Delta a_{PHY} < 0.25$ inch) the structure will normally be stiffener critical. To determine a conservative value of residual strength (for that crack length) use the Dugdale curve of Step 4 and stiffener ultimate strength.

4.5.9 Summary

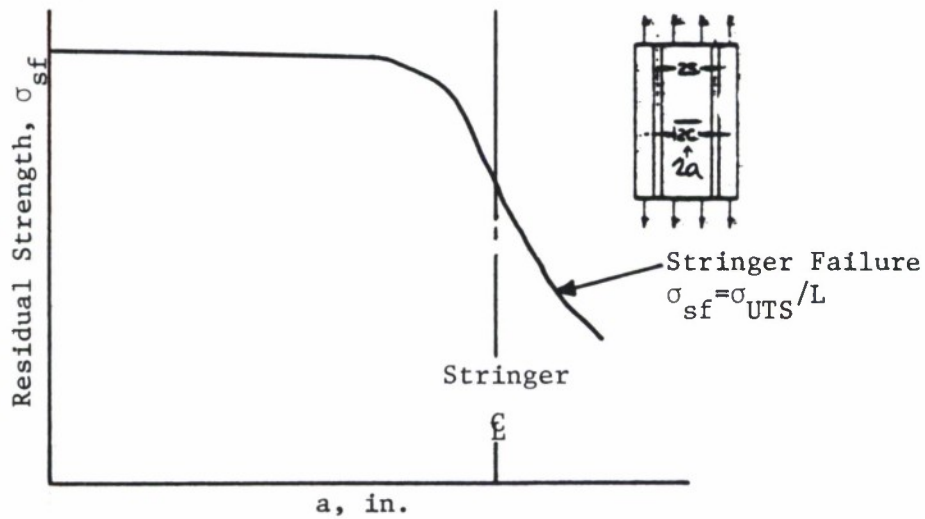
The most important factor to consider in residual strength prediction of a cracked built-up structure is to decide whether the structure is skin or stiffener critical. Normally, a short crack length is likely to be a skin critical case and a long crack length a stiffener critical case. However, there is no clear cut demarcation between the two cases. Factors such as percentage stiffening, spacing of stringers, lands in the structure and other structural details will influence the type of failure. Hence, a good technique is to determine the residual strength of a given structure based on both skin critical and stiffener critical cases. The minimum fracture stress of the two will then represent the residual strength of the structure and should be considered to be the governing case.



(a) Unstiffened Panel



(b) Stiffened Panel



(c) Stringer

Figure 4.5.1. Elements of Residual Strength Diagram.
4.5.31

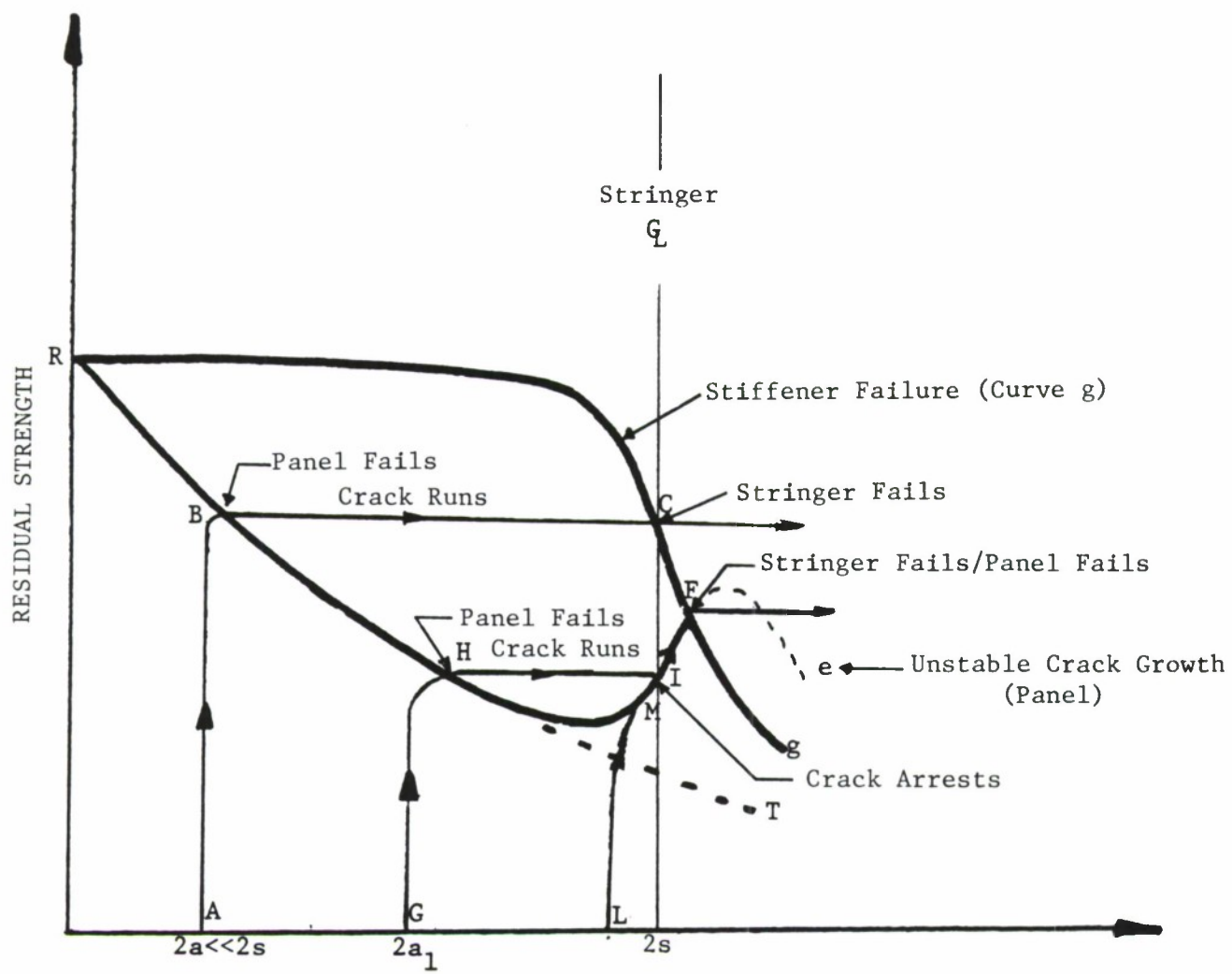


Figure 4.5.2. Residual Strength Diagram for a Stiffened Panel.

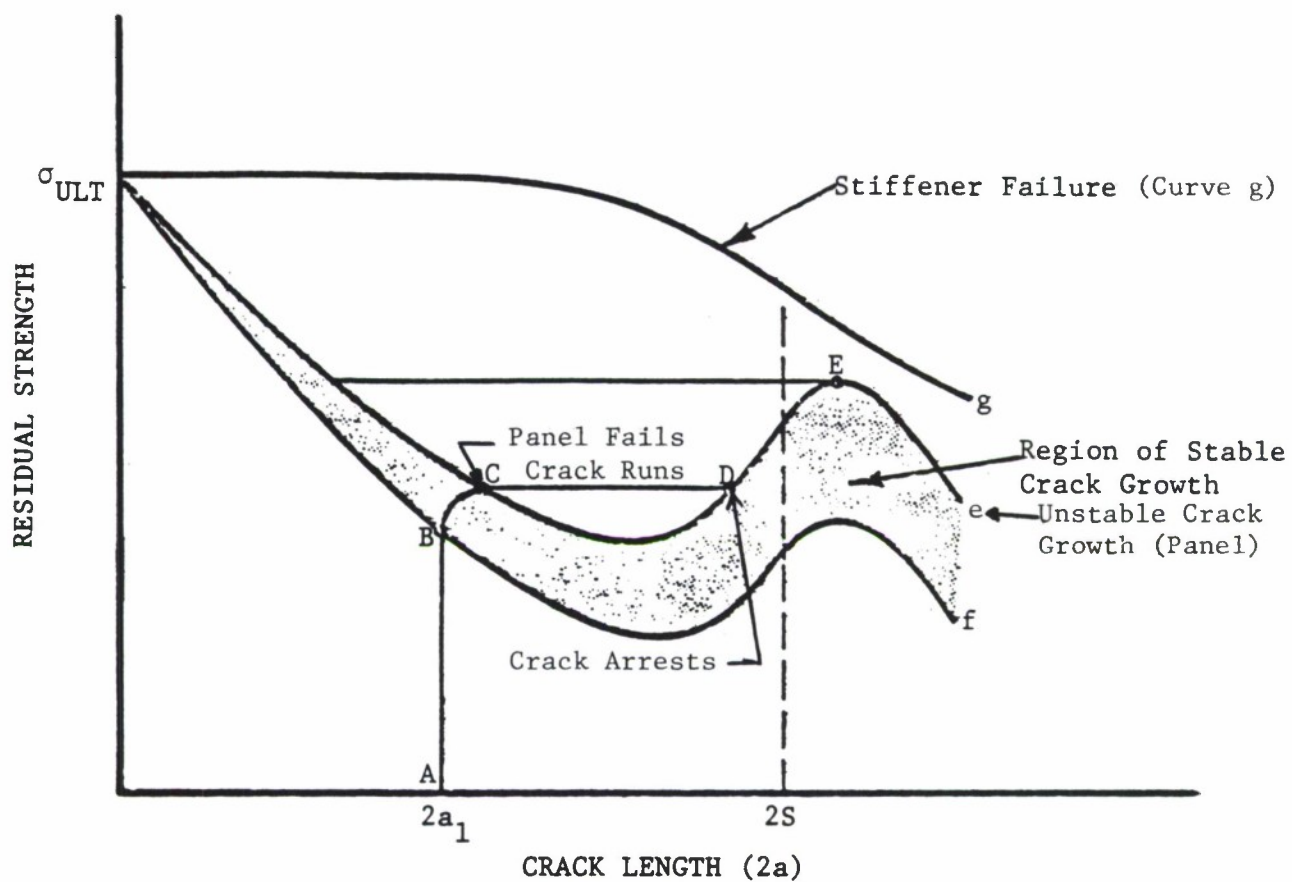


Figure 4.5.3. Panel Configuration with Heavy Stringers; Skin-Critical Case.

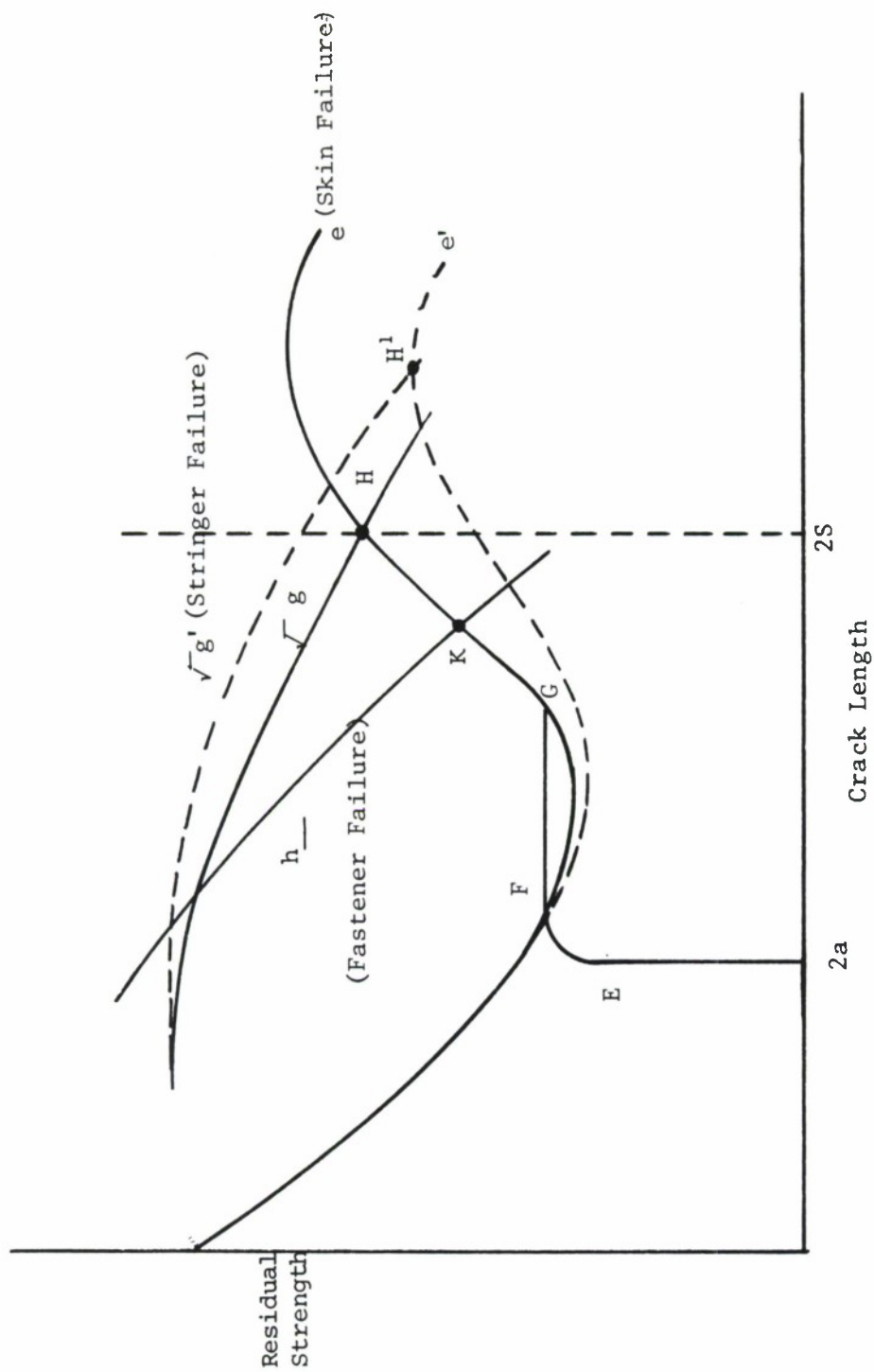
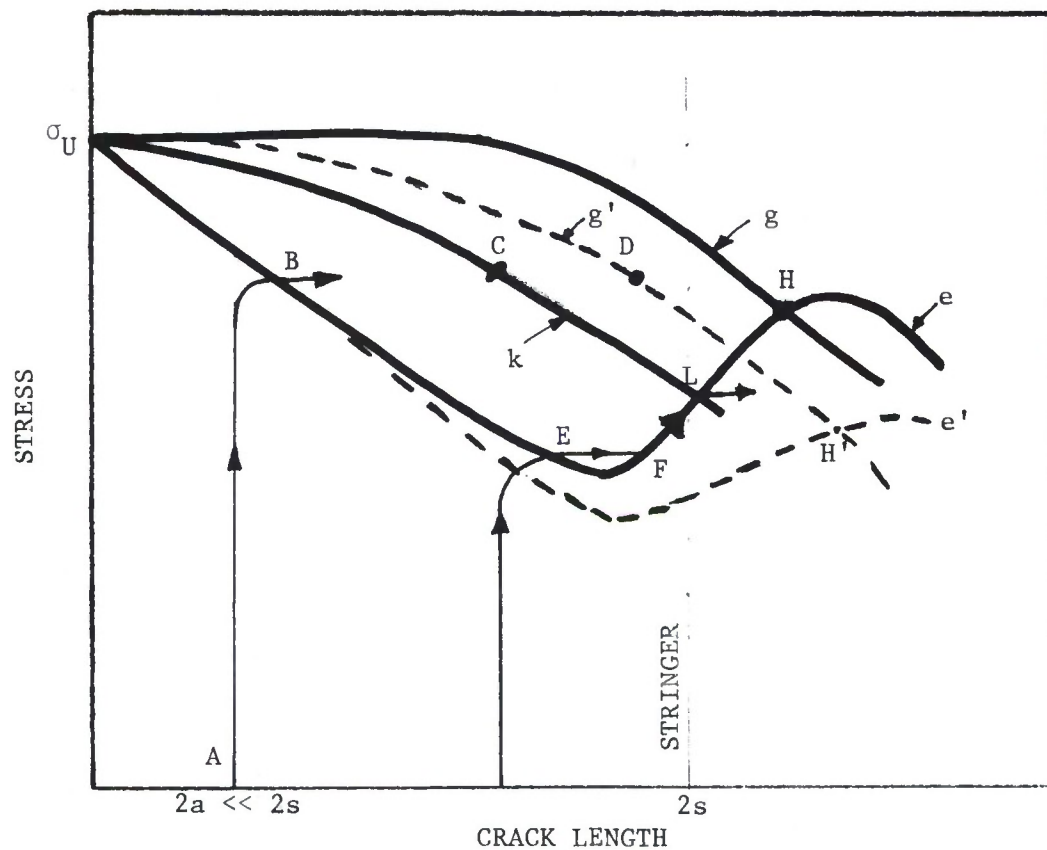
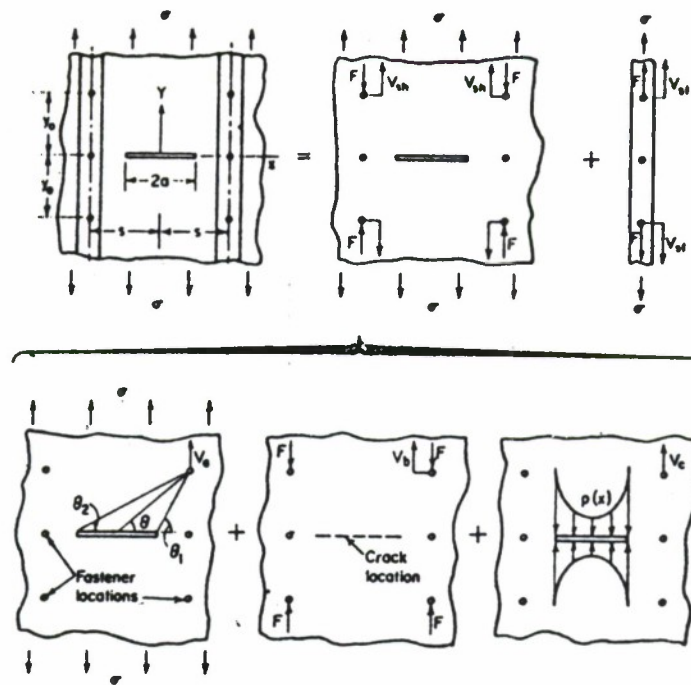


Figure 4.5.4. Criterion for Fastener Failure.

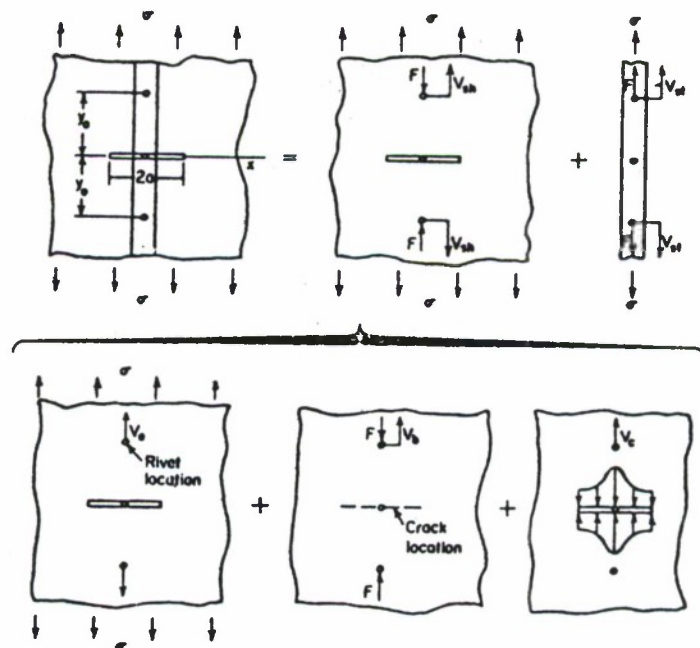


- f: Residual Strength Curve of Skin Alone
- g: Residual Strength Curve of Two Edge Stiffeners
- k: Residual Strength Curve of Central Stiffener (Failing).
- g': Residual Strength Curve of Two Edge Stiffeners After the Failure of Central Stiffener

Figure 4.5.5. Residual Strength Diagram for a Panel With Three Stiffeners and a Central Crack Emanating from a Rivet Hole.



a. Crack Between Stiffeners



b. Crack Across Stiffener

Figure 4.5.6. Analysis of Stiffened Panel.

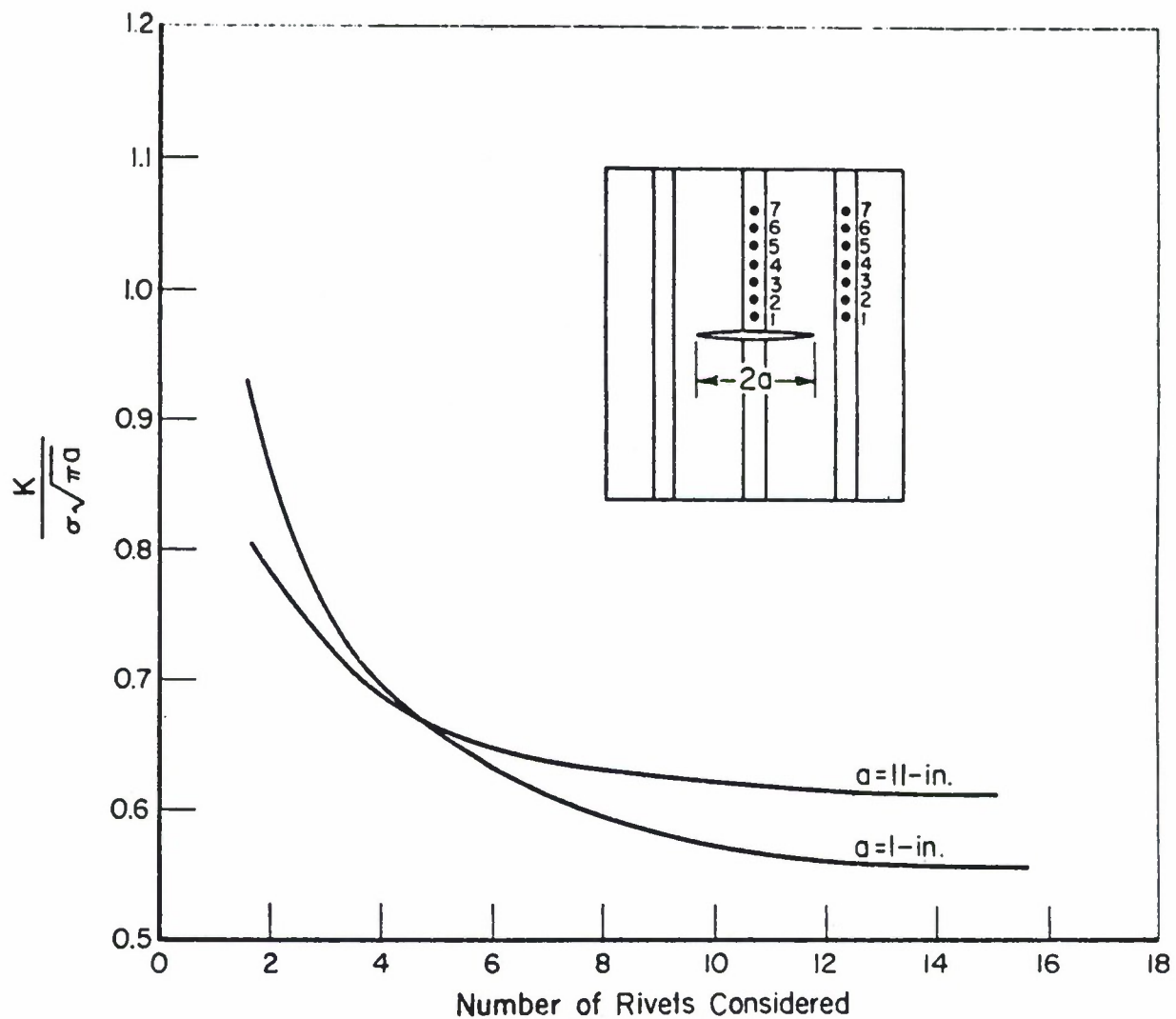


Figure 4.5.7. Effect of Number of Fasteners Included in Analysis on Calculated Stress-Intensity Factor.

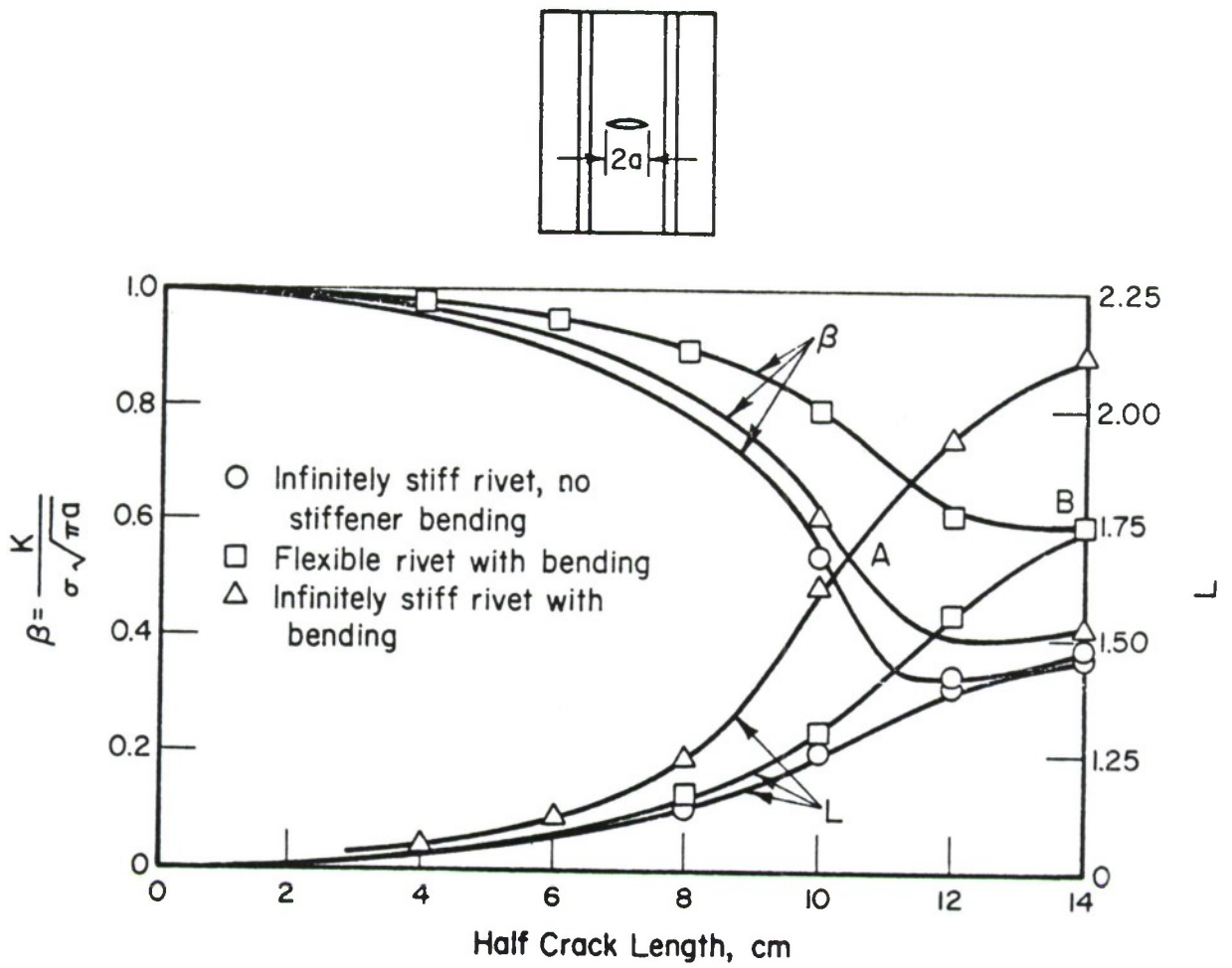


Figure 4.5.8. Skin-Stress-Reduction β and Stringer-Load-Concentration L as Affected by Fastener Flexibility and Stiffener Bending.

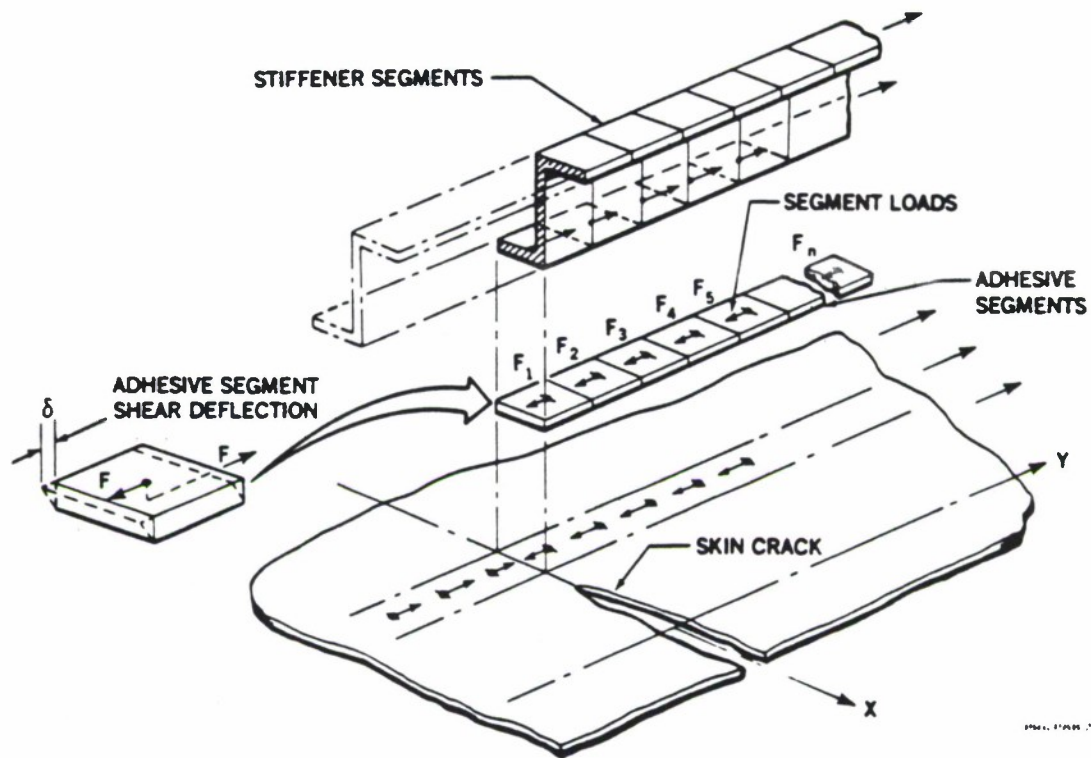


Figure 4.5.9. Bonded Fastener Divided into Discrete Segments.

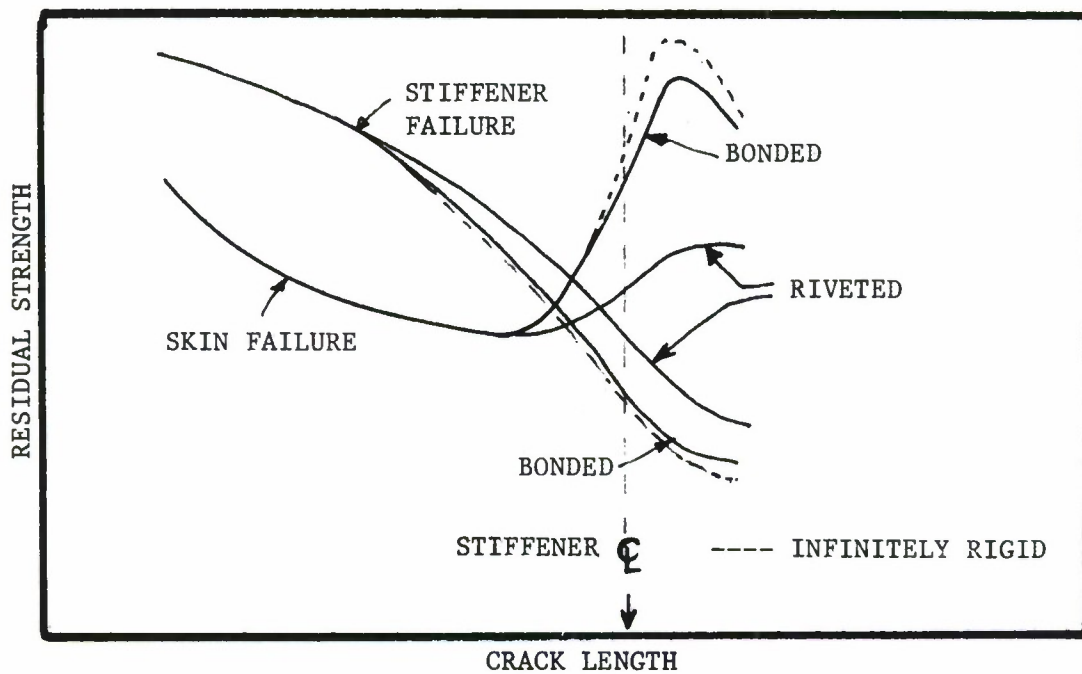


Figure 4.5.10. Residual Strength Diagram Comparing Riveted and Bonded Structures.

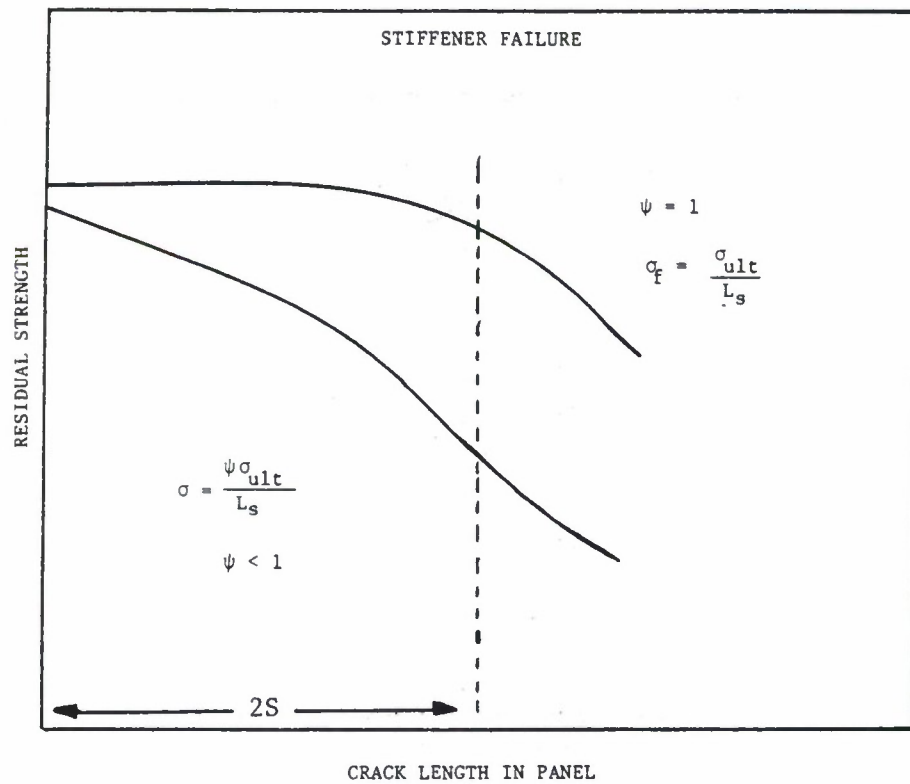
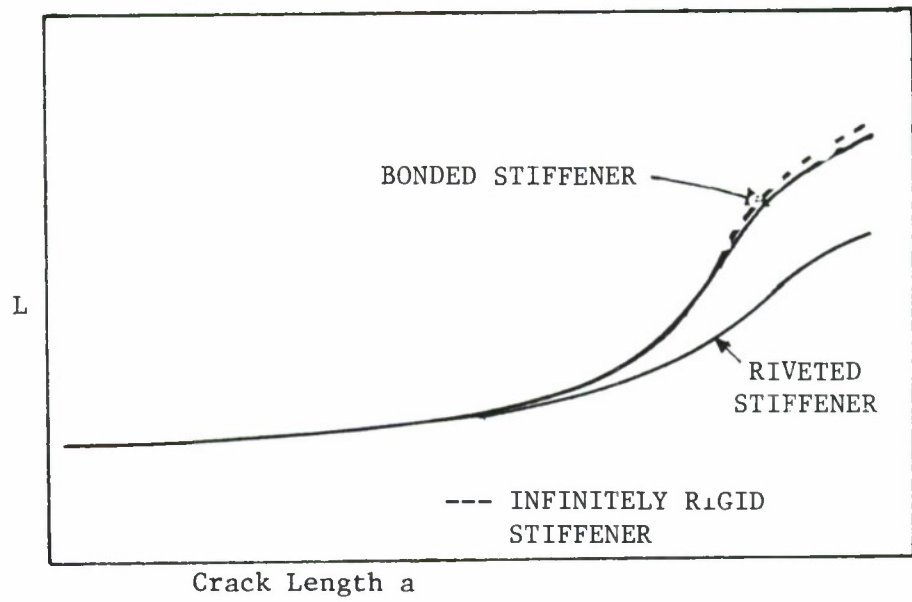
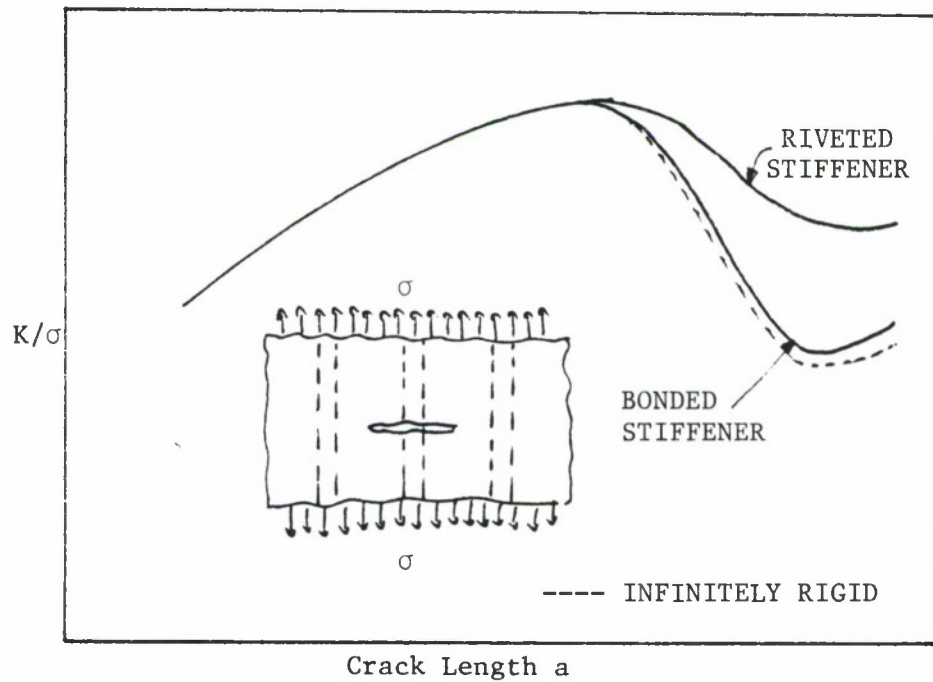


Figure 4.5.11. Residual Strength Diagram for Stiffener.



(a) Load Transfer Parameter (L)



(b) Stress-Intensity Factor Coefficient (K/σ)

Figure 4.5.12. Comparison of L_s and K/σ_s for Riveted and Bonded Structures.

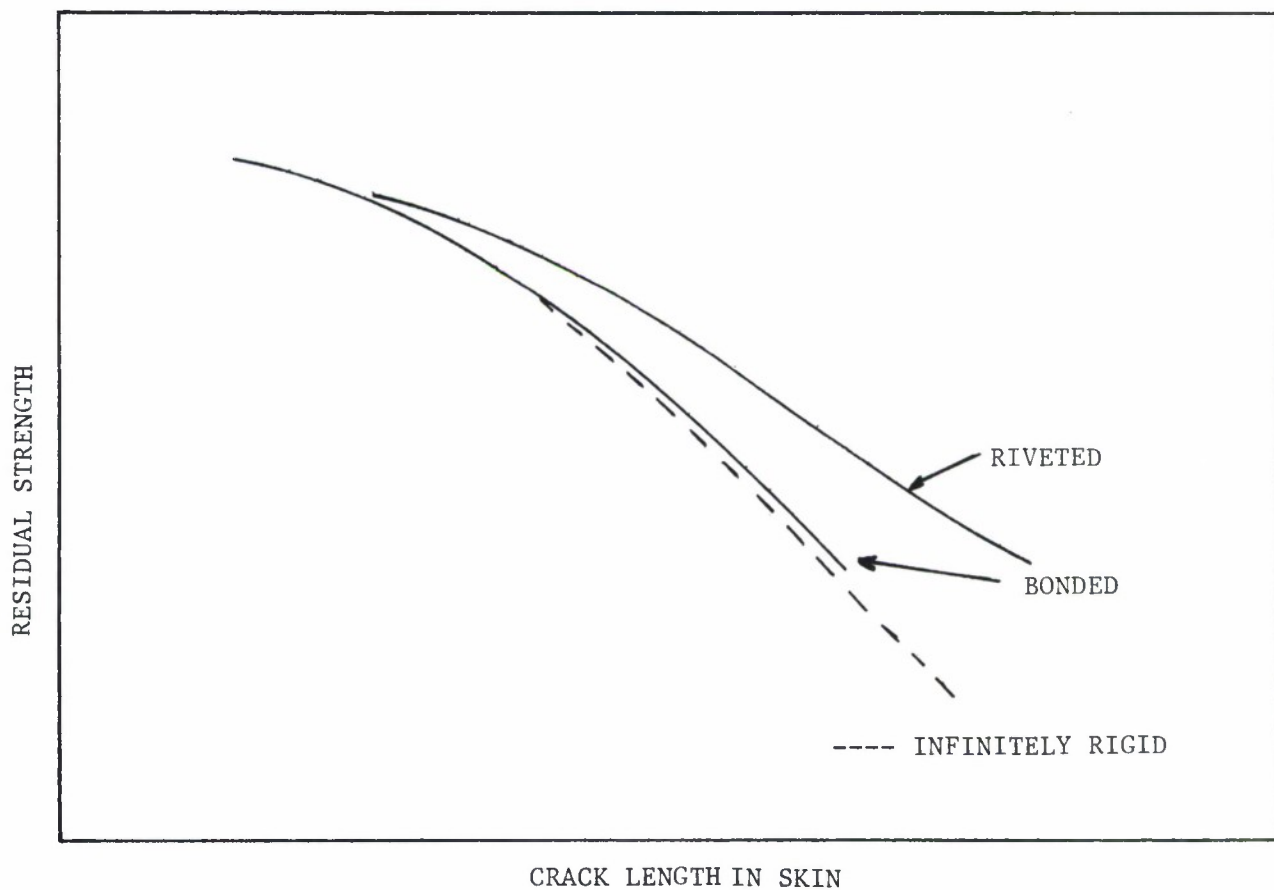


Figure 4.5.13. Comparison of Residual Strength for Riveted and Bonded Stiffeners.

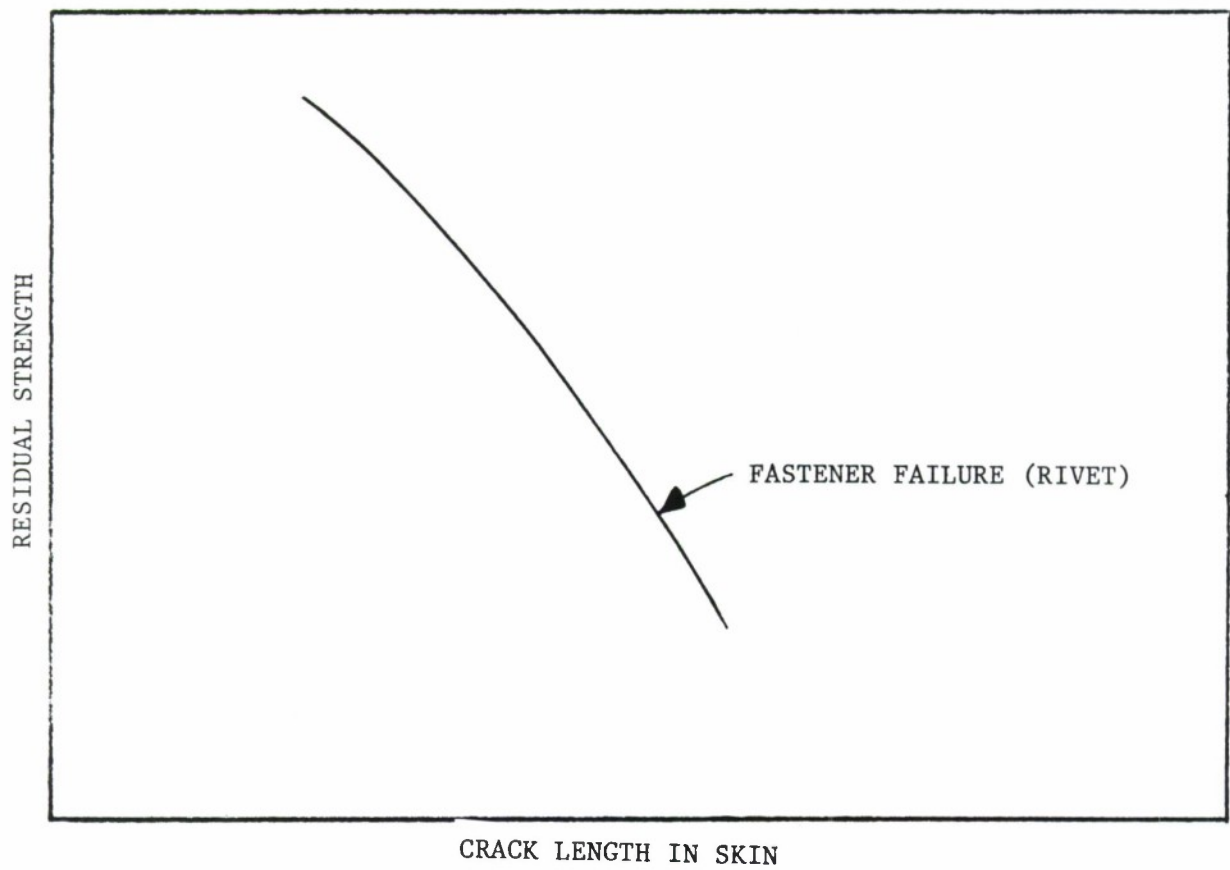
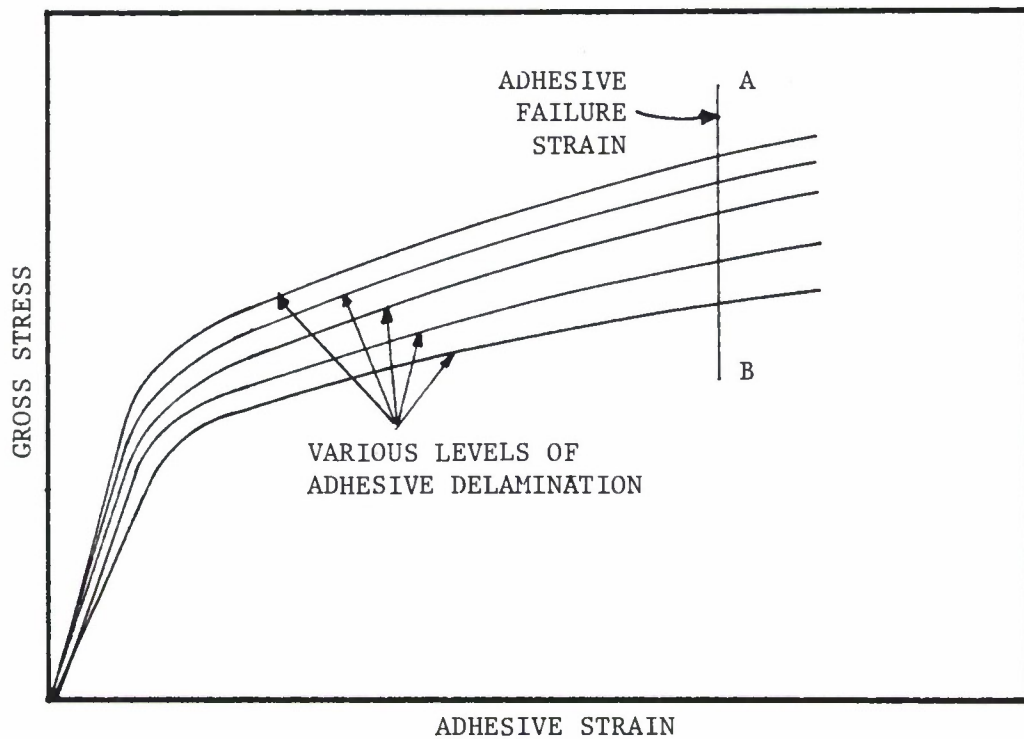
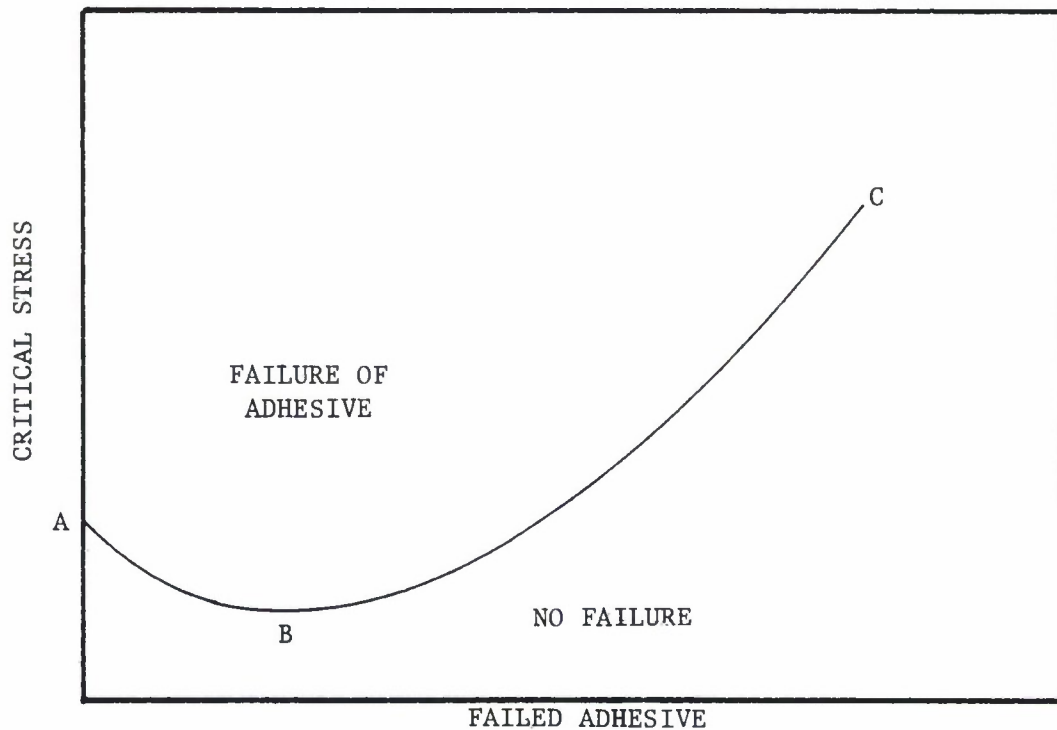


Figure 4.5.14. Residual Strength Diagram for the Fasteners in a Built-Up Structure.



(a) Stress-Strain Curves for Adhesively Bonded Stringer With Various Levels of Delamination.



(b) Critical Levels of Stress for Adhesively Bonded Stringer.

Figure 4.5.15. Gross Stress and Critical Stress Diagram for Adhesively Bonded Stringer.

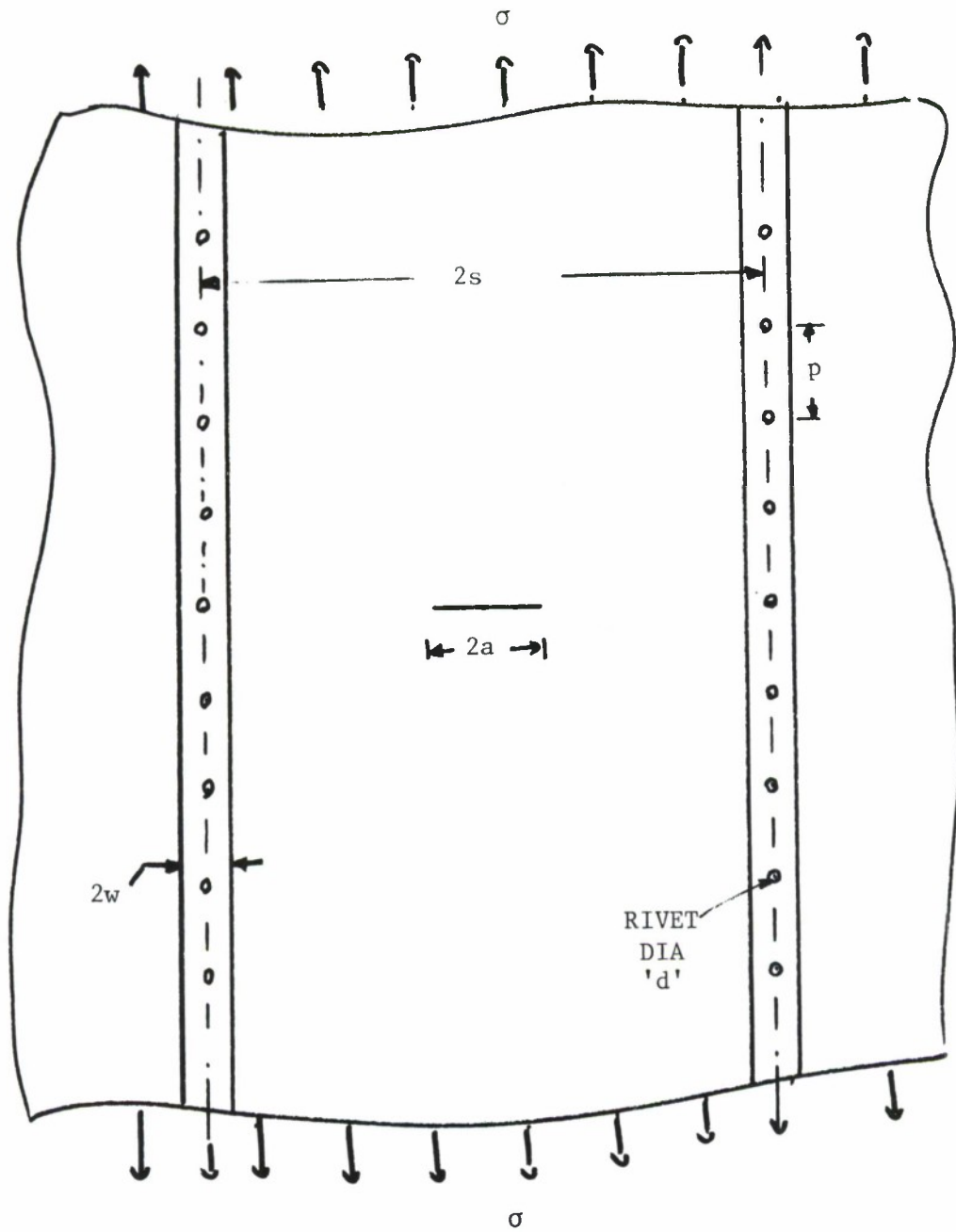


Figure 4.5.16. Riveted Panel with a Central Crack Between Two Stringers.

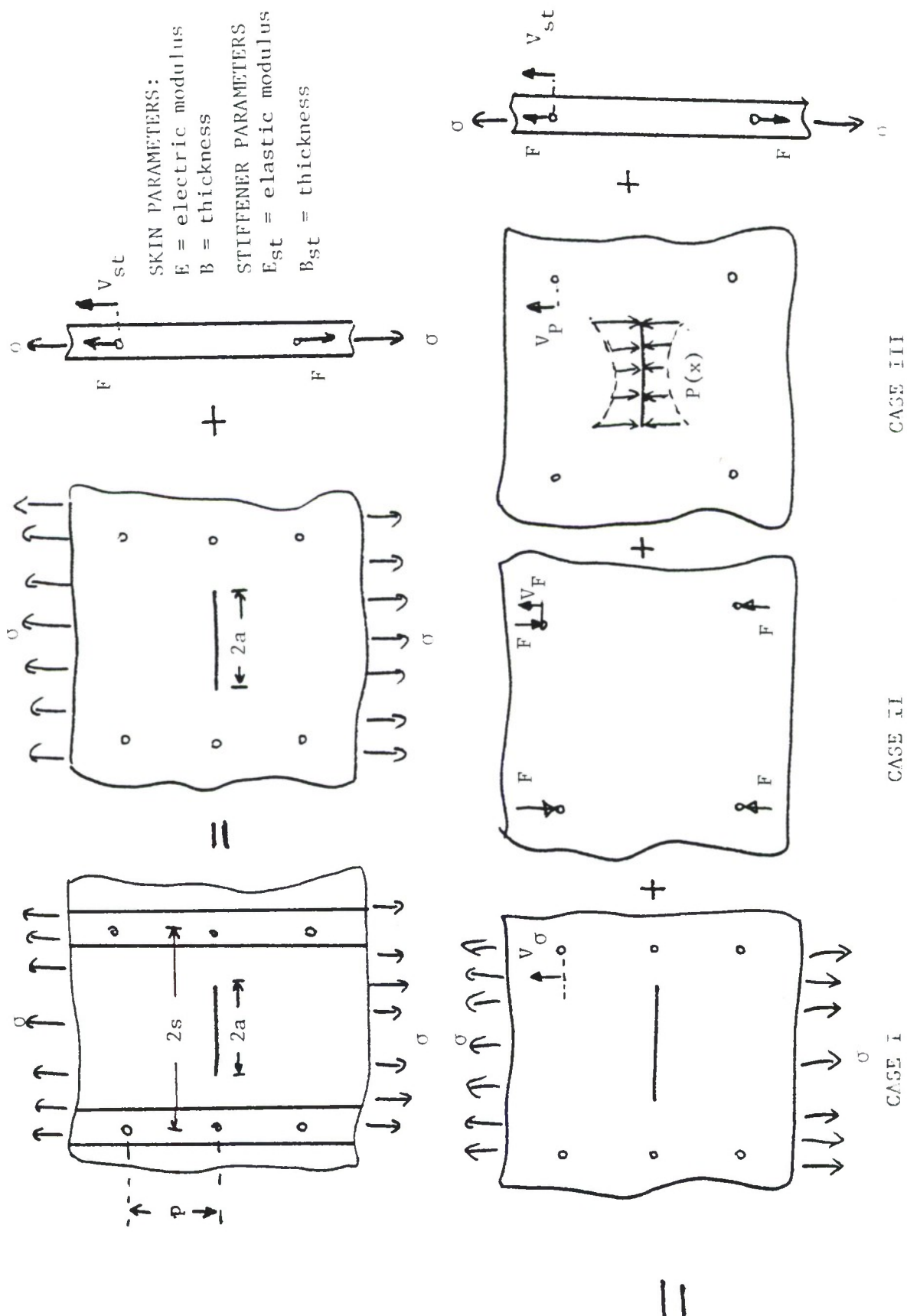


Figure 4.5.17. Stiffened Structure Broken Into Components.

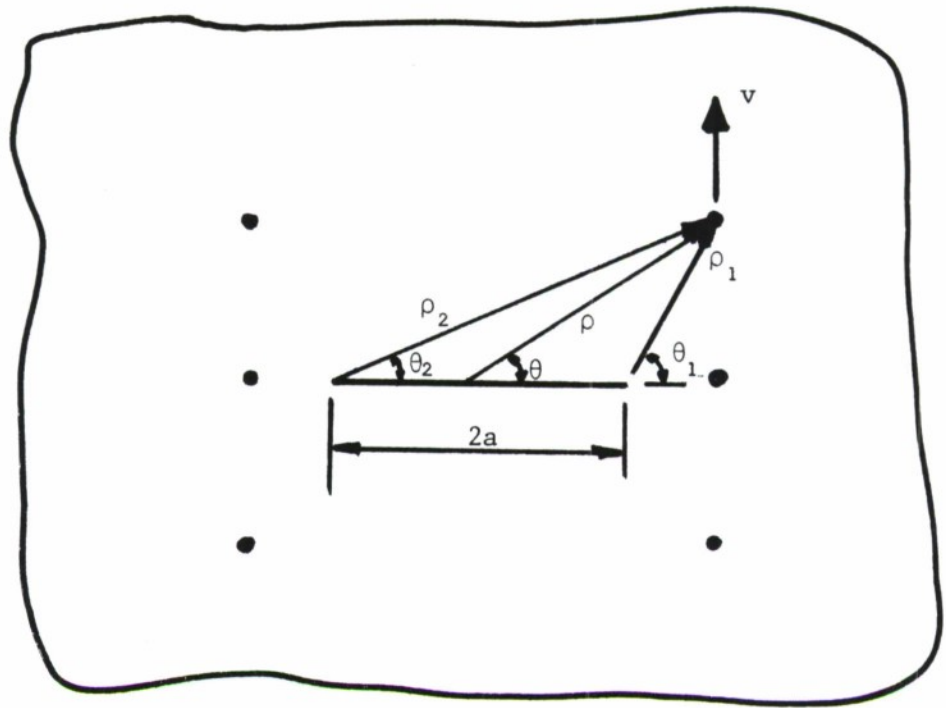


Figure 4.5.18. Geometrical and Displacement Parameters Relative to the Crack Tip.

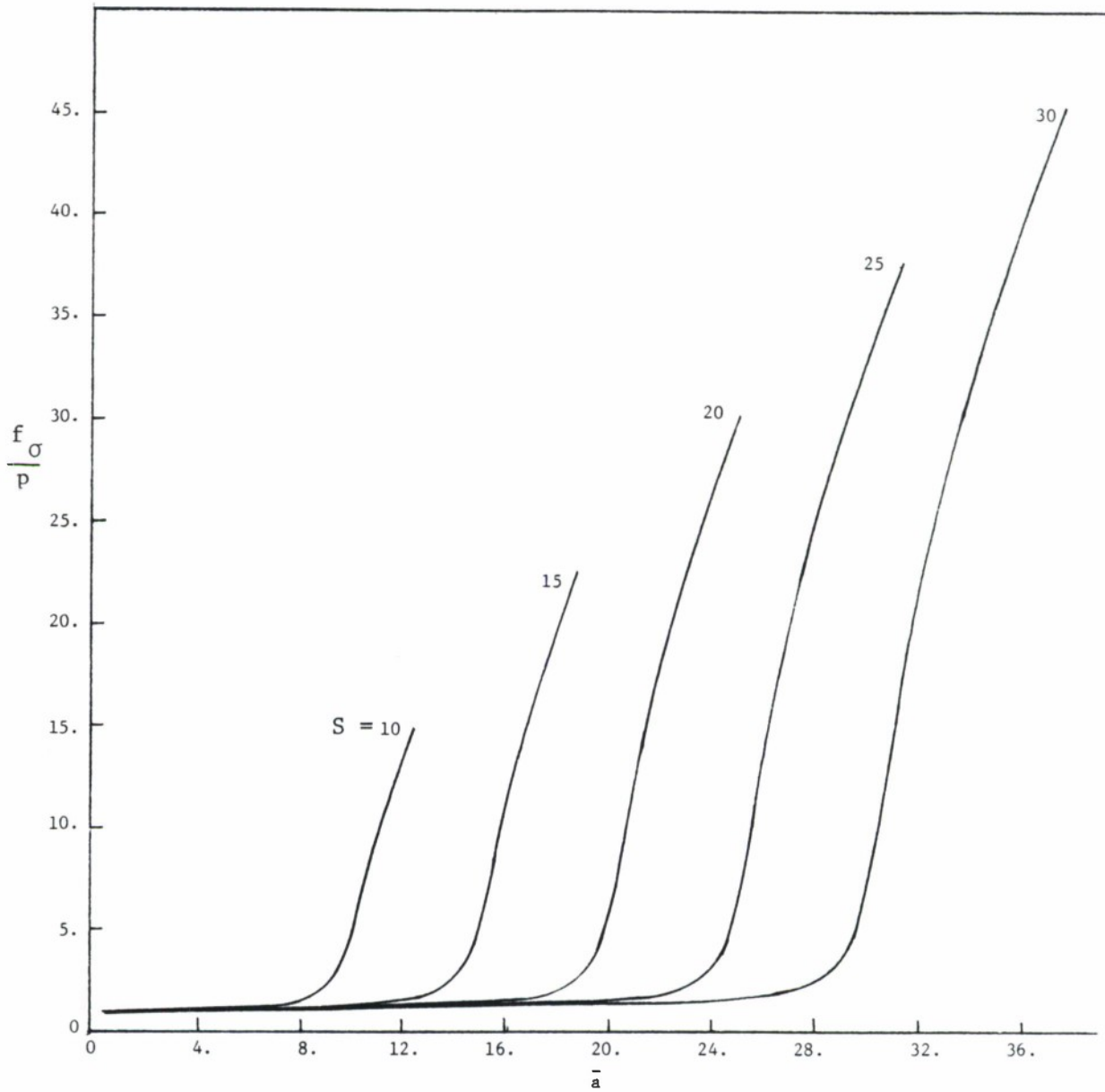


Figure 4.5.19. Normalized Panel Displacement Function (f_σ/p) Due to Applied Stress Vs. Normalized Crack Length (a/p) for Various Stringer Spacings ($\bar{S} = S/p$).

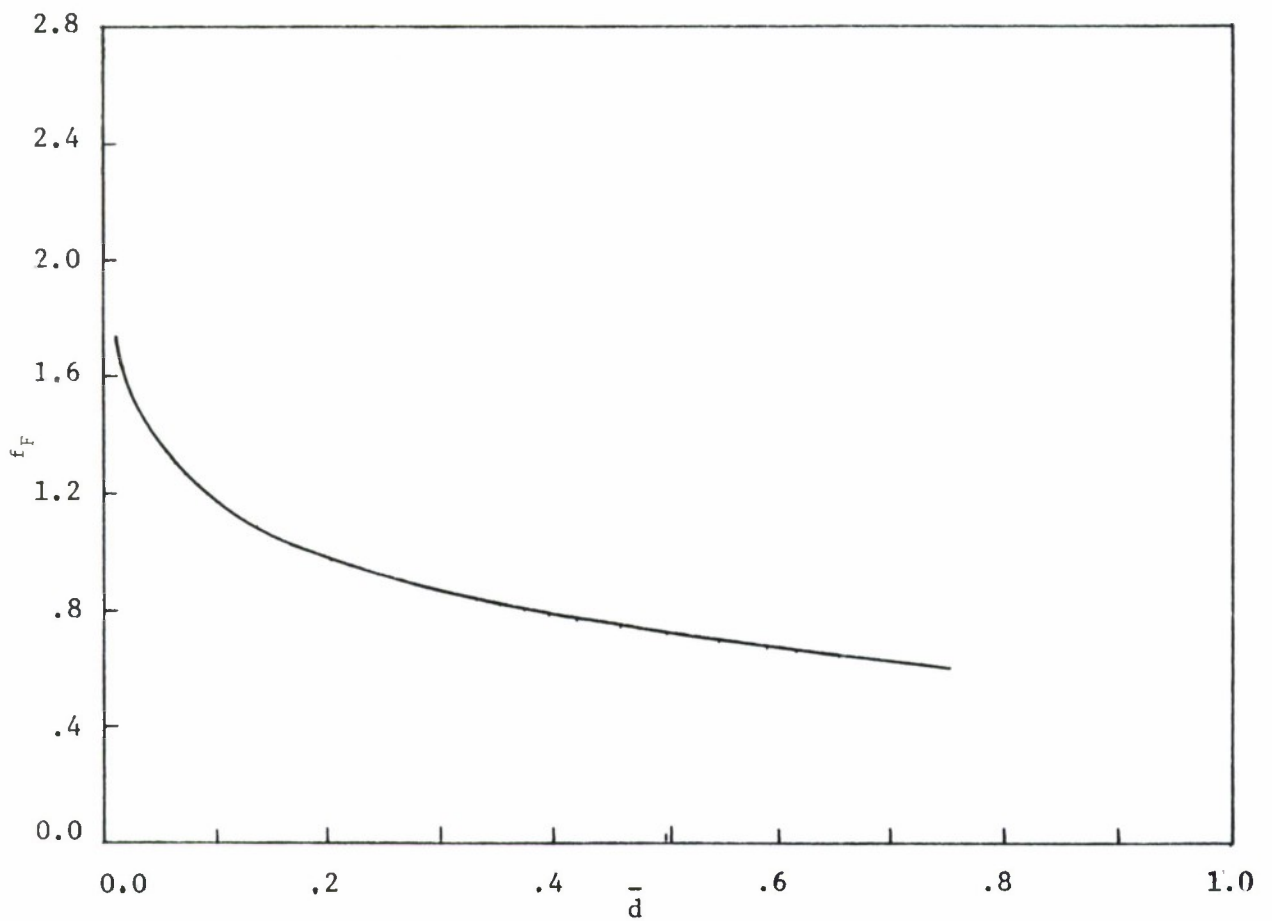


Figure 4.5.20. Panel Displacement Function Due to Fastener Force Vs. Normalized Rivet Diameter (d/p) for All Stiffener Spacings.

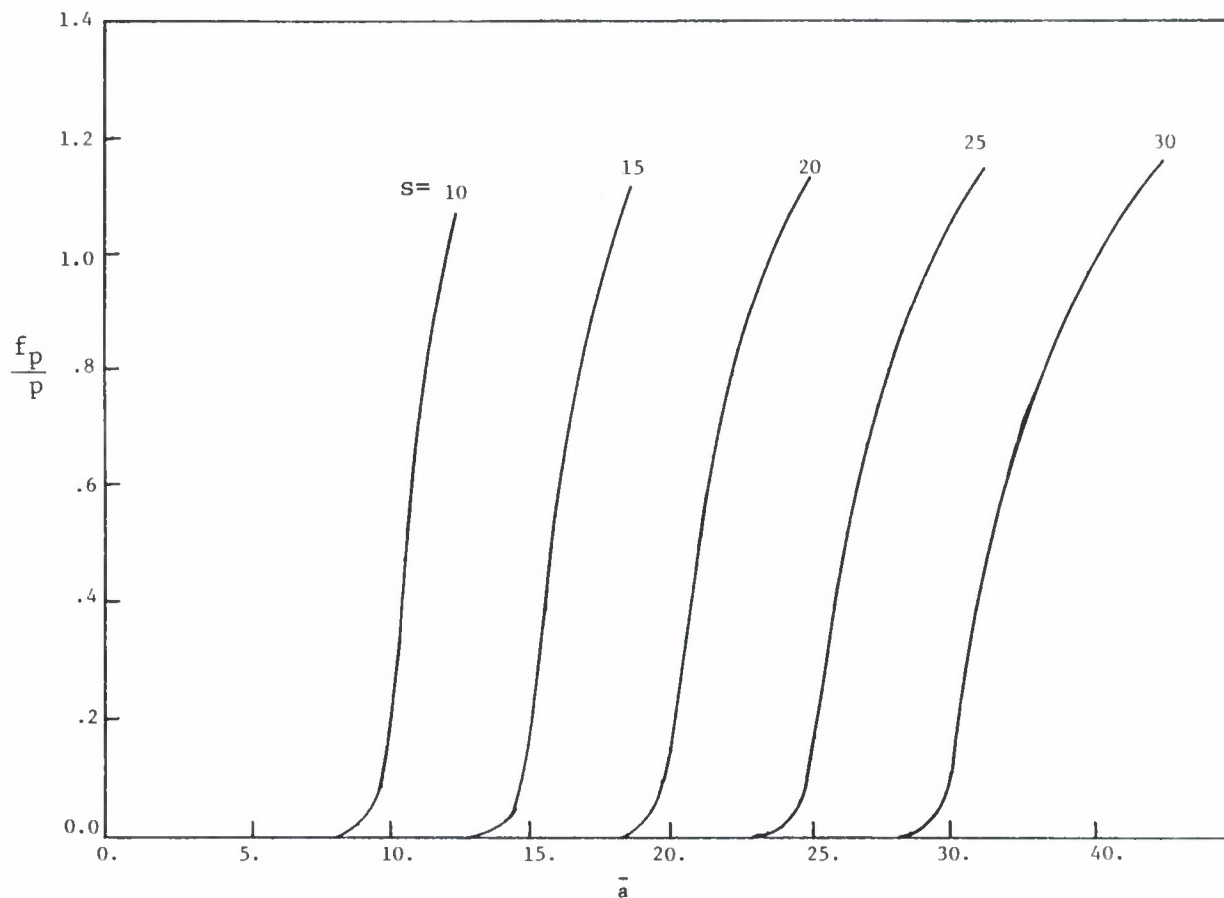


Figure 4.5.21. Normalized Panel Displacement Function (f_p/p) Due to Distributed Pressure Along Crack Vs. Normalized Crack Length (a/p) for Various Stringer Spacings ($\bar{s} = s/p$),

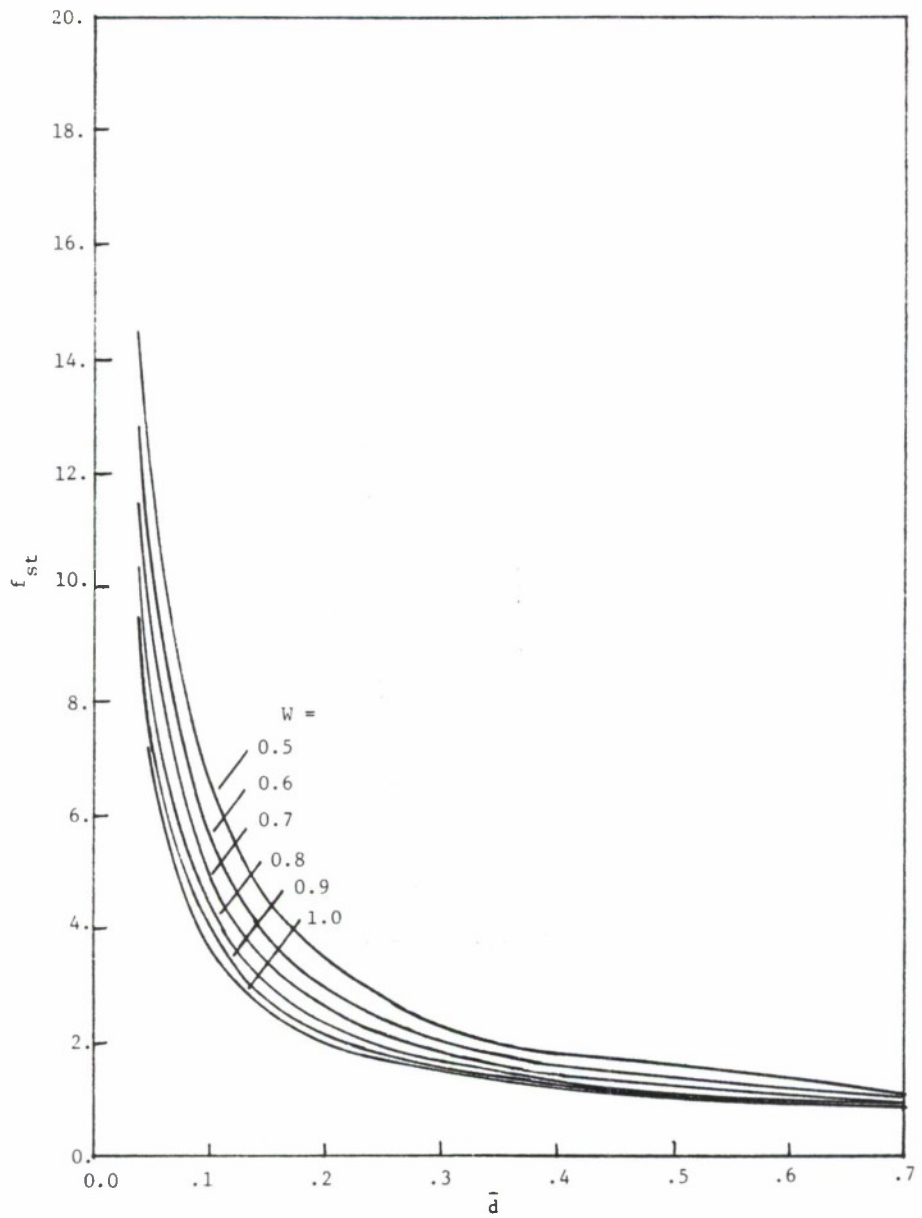


Figure 4.5.22. Stringer Displacement Function Vs. Normalized Rivet Diameter (d/p) for Various Half Stringer Widths.

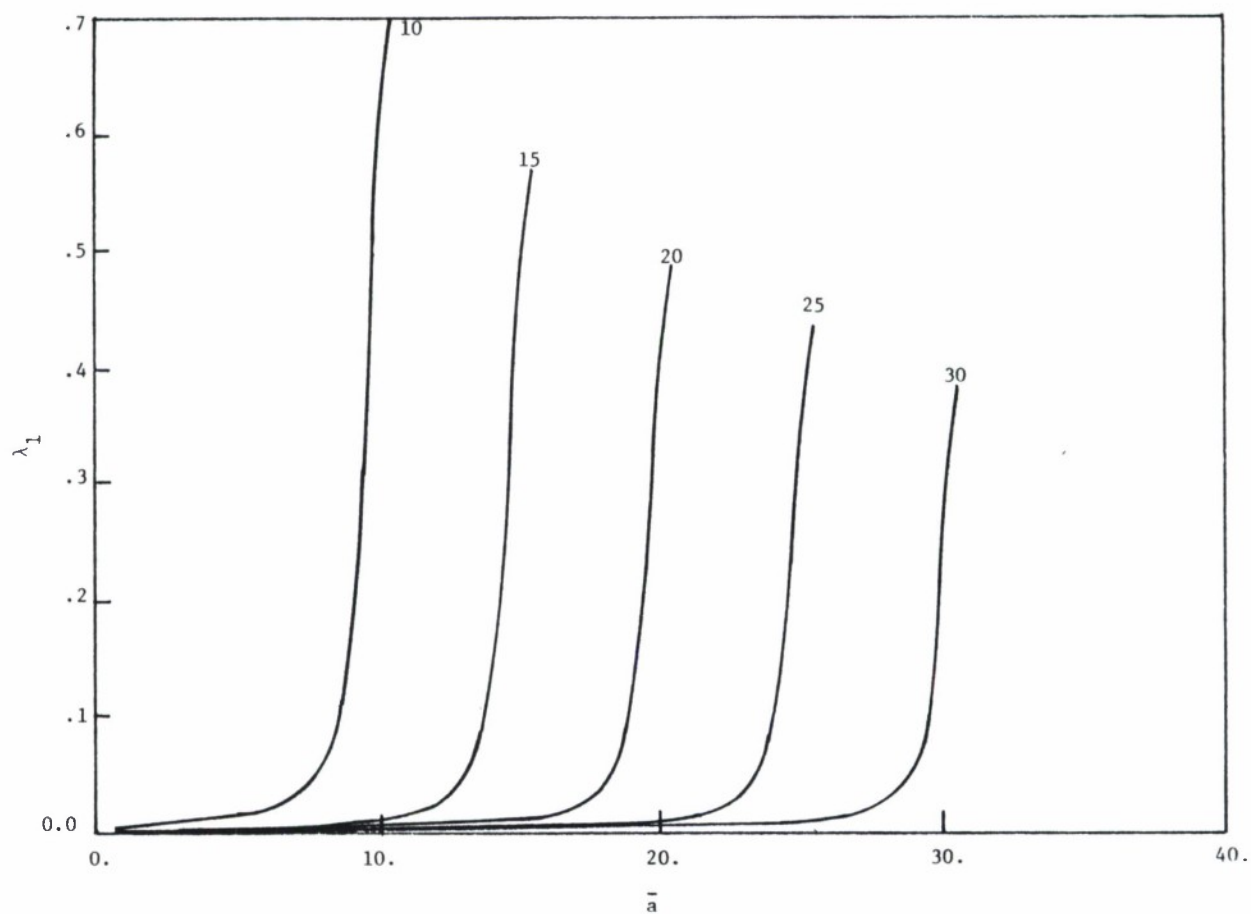
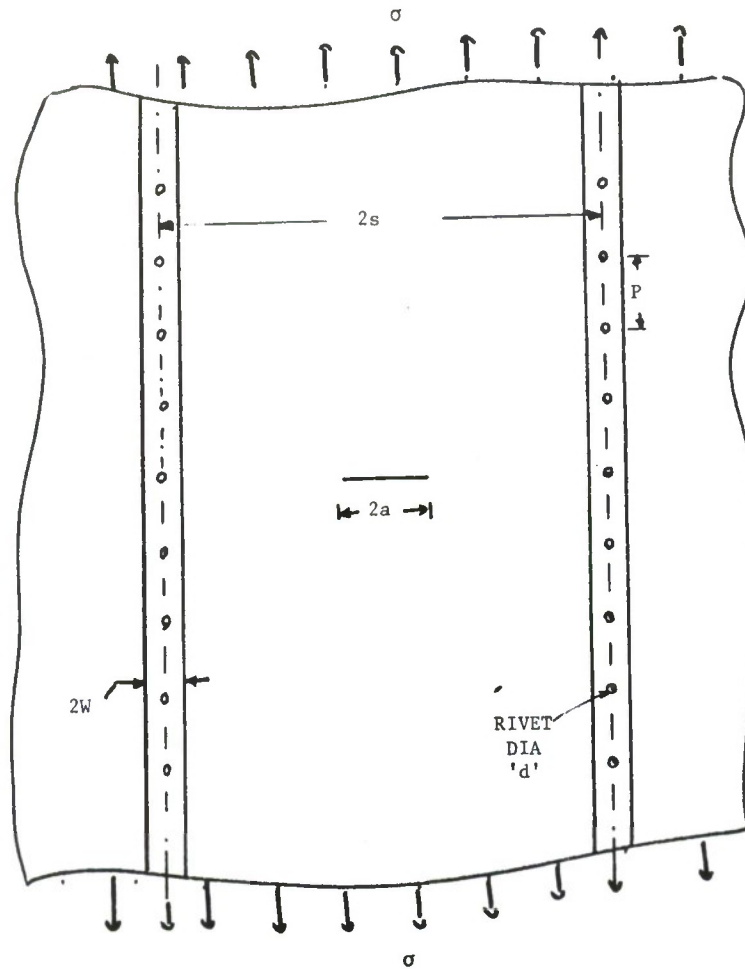


Figure 4.5.23. Parameter λ_1 Vs. Normalized Crack Length (a/p) for Various Normalized Stringer Spacings (s/p).

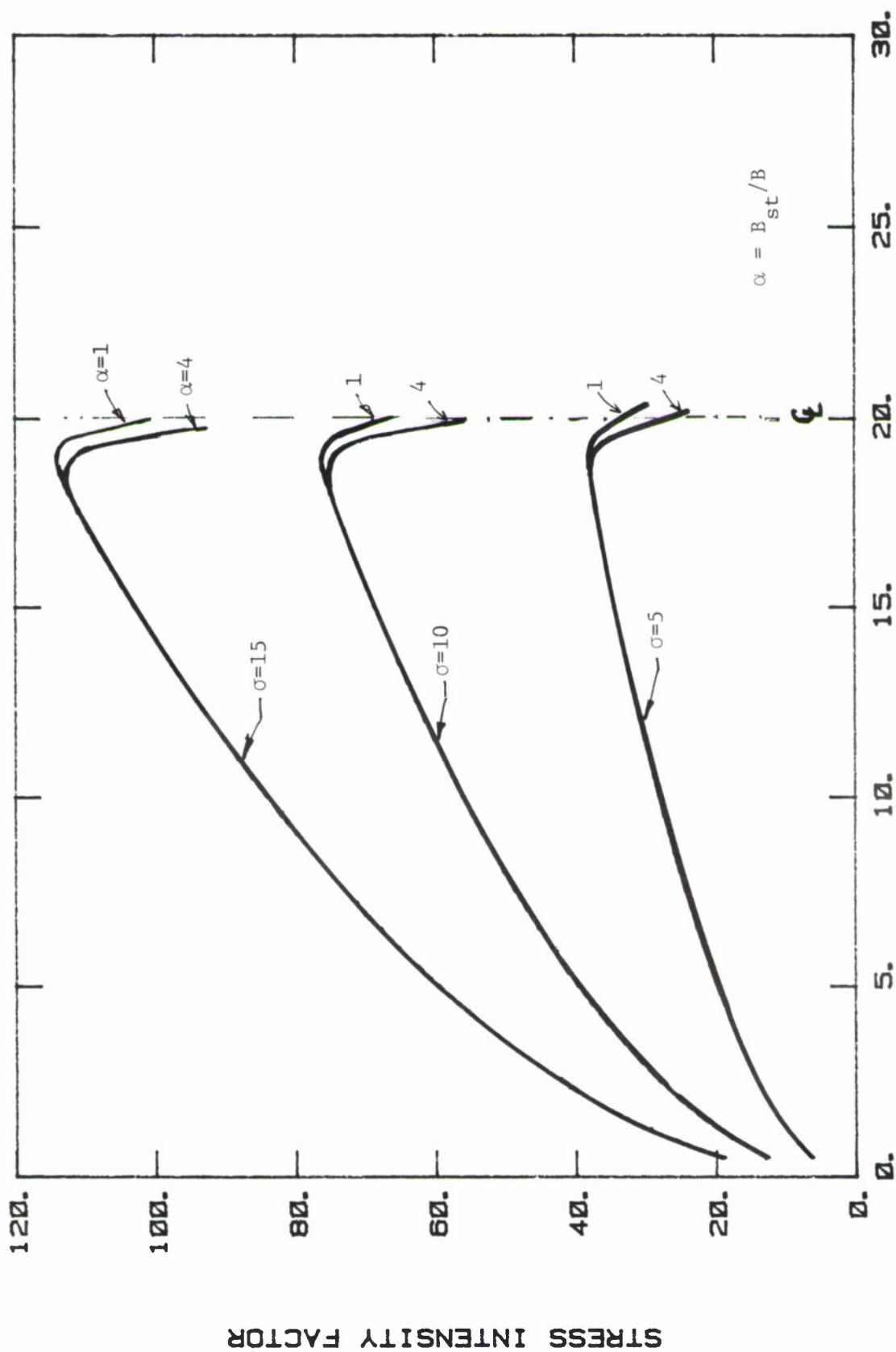


given the following data:

Maximum operating stress: 20 Ksi
 Stiffener spacing ($2s$): 40 inch
 Stiffener width (w): 0.5 inch
 Stiffener thickness (B_{st}): 0.063 inch
 Panel thickness (B): 0.063 inch
 Rivet pitch (p): 1 inch
 Rivet diameter (d): 3/16 inch
 Material: 7075-T6 Aluminum
 Fracture toughness: 65 Ksi $\sqrt{\text{inch}}$
 Ultimate Strength: 78 Ksi

Figure 4.5.24. Structural Geometry and Material Properties for Example of Subsection 4.5.7.

STRESS INTENSITY FACTOR DIAG.



CRACK LENGTH

Figure 4.5.25. Stress Intensity Factor Diagram for Panel and Riveted Stringers.

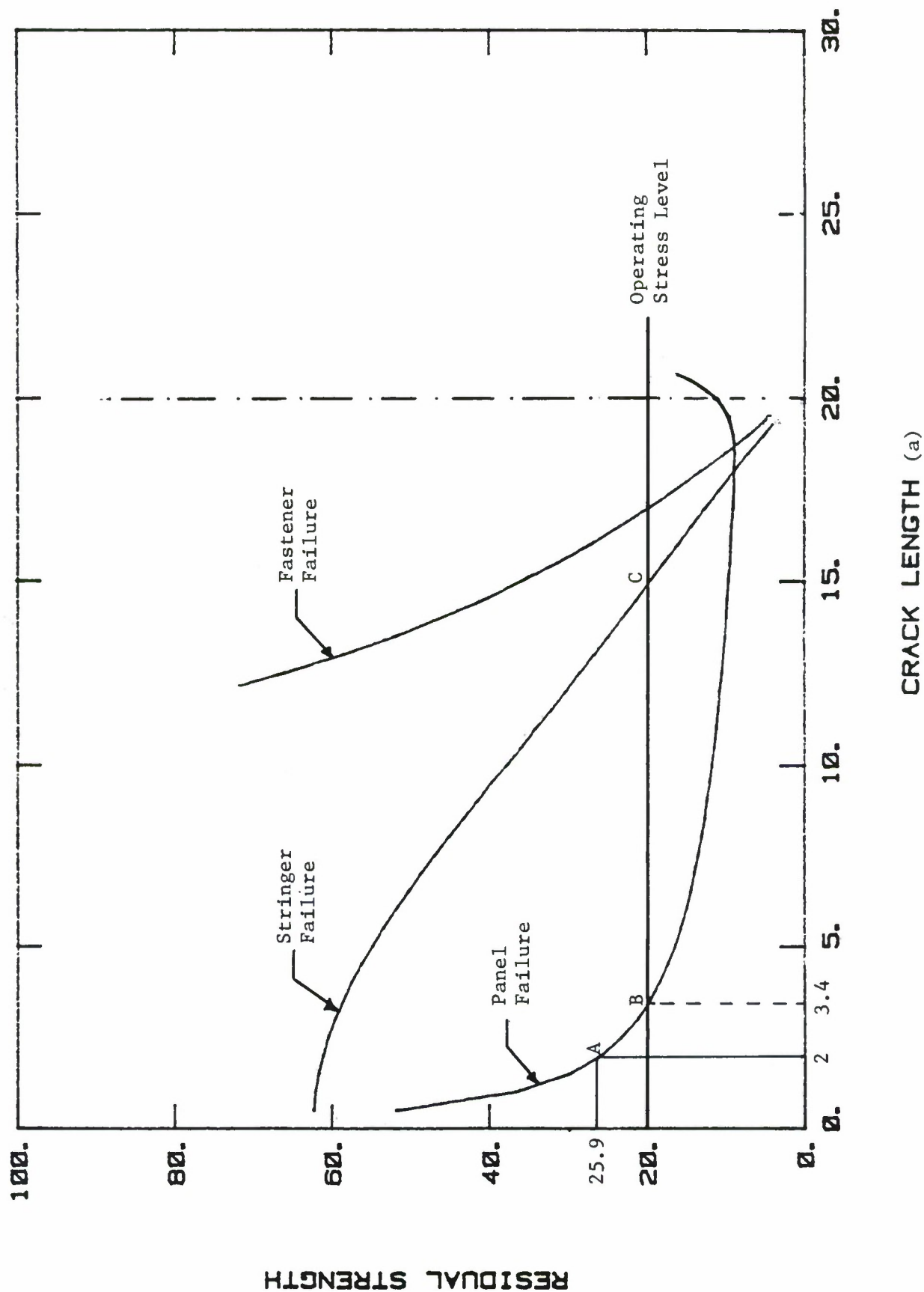


Figure 4.5.26. Residual Strength Diagram for Panel and Riveted Stringers (Light Stringers).

RESIDUAL STRENGTH DIAGRAM

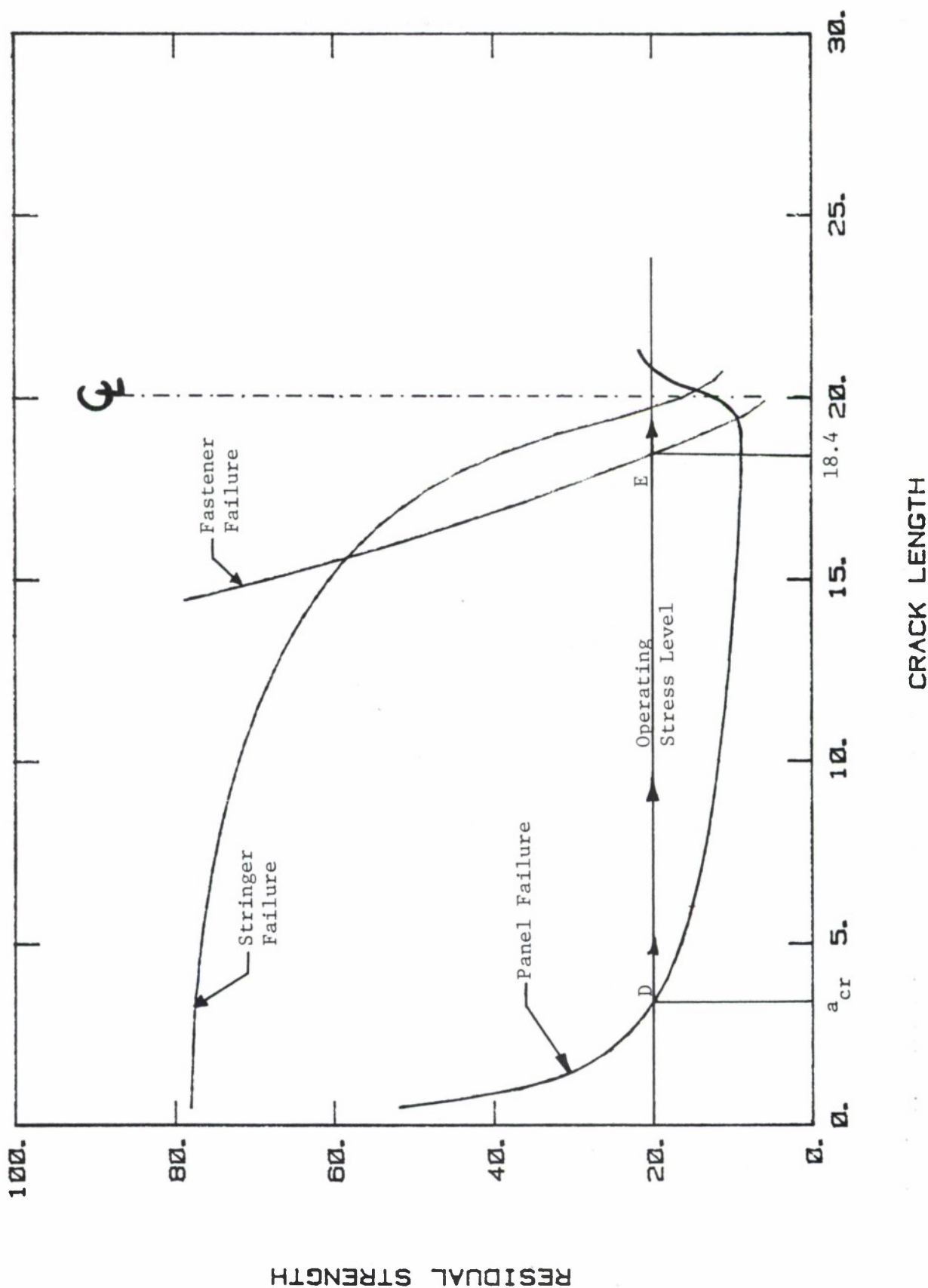


Figure 4.5.27. Residual Strength Diagram for Panel and Riveted Stringers (Heavy Stringers).

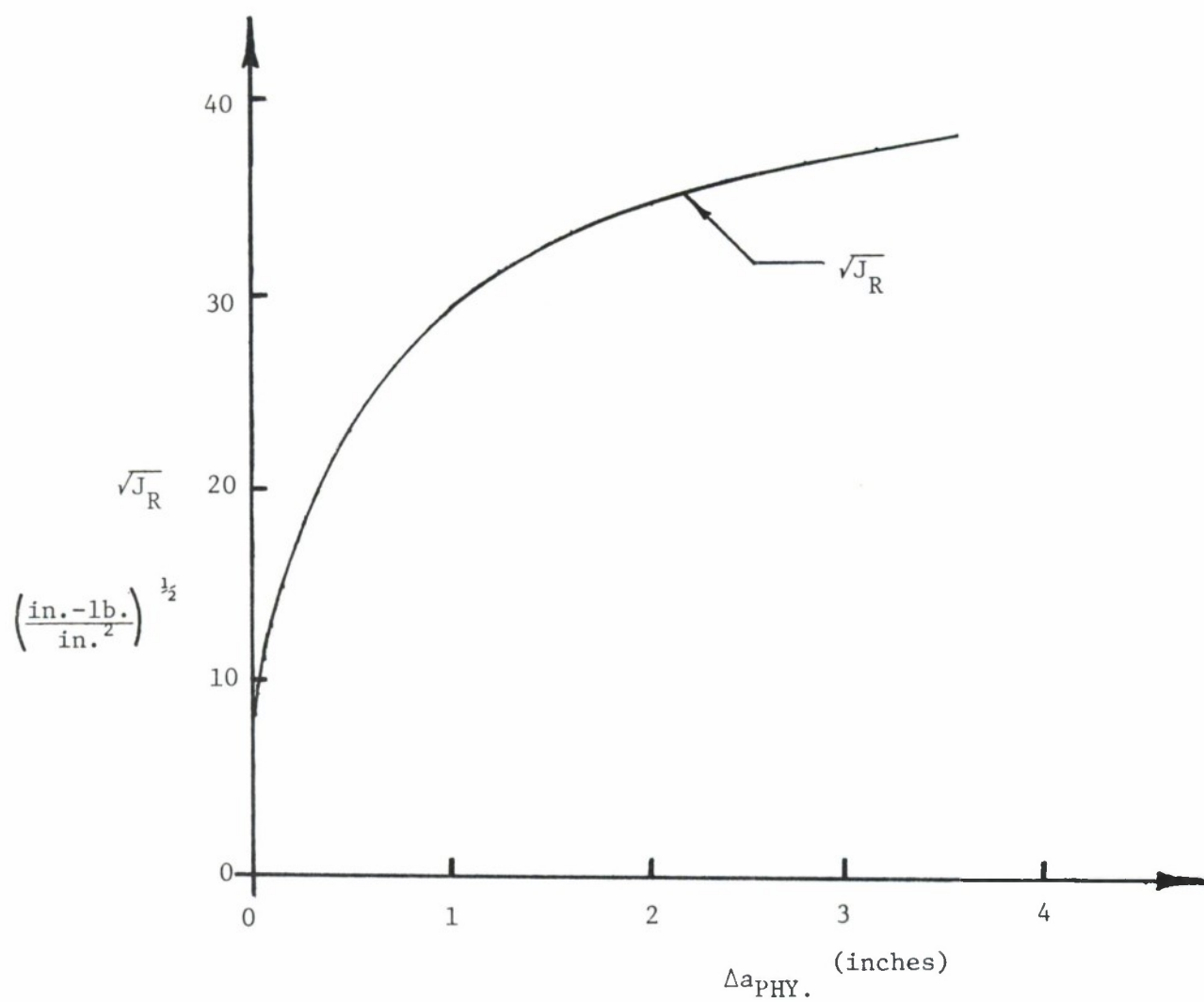


Figure 4.5.28. Square Root of J_R Resistance Curve.

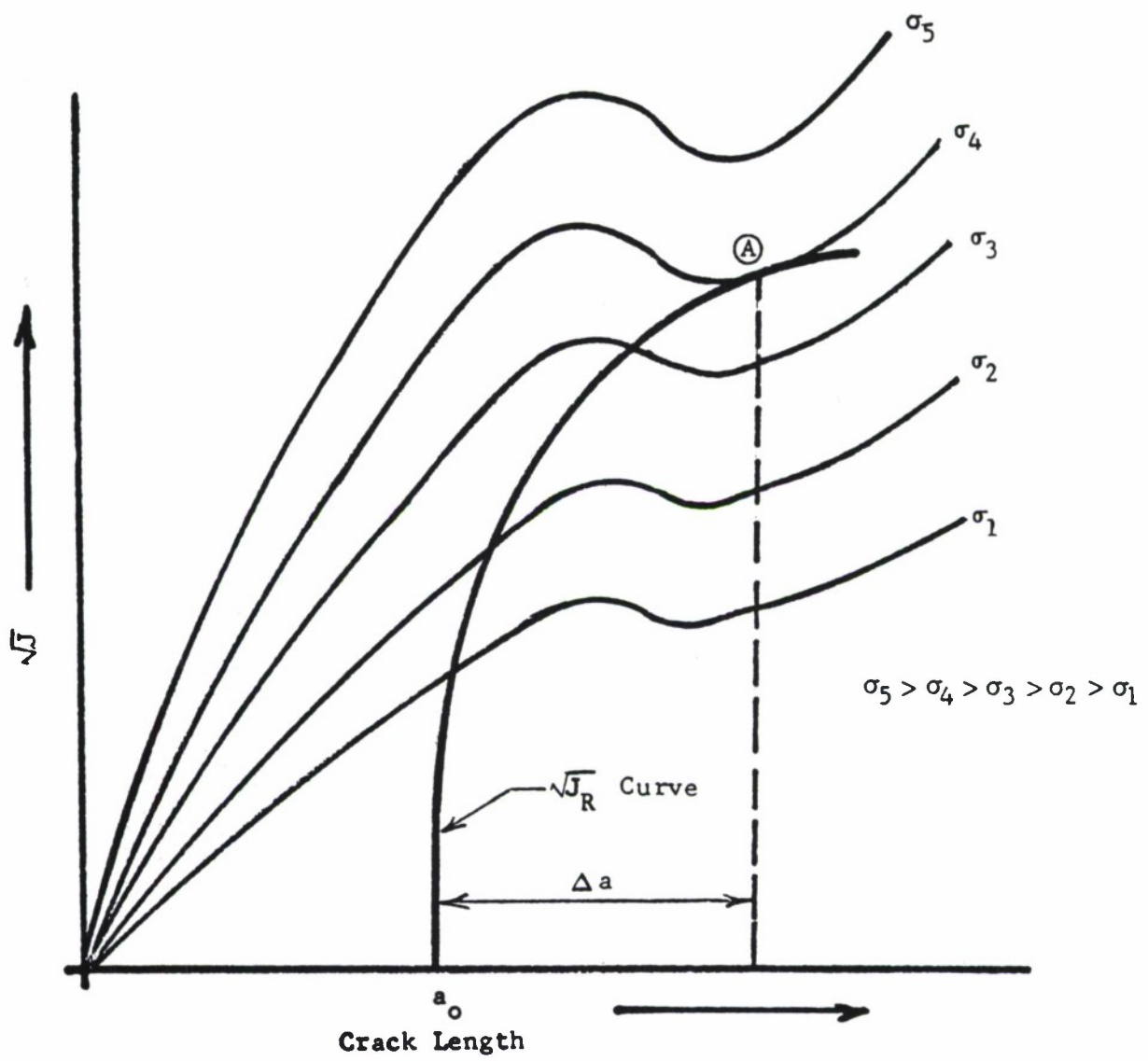


Figure 4.5.29. Failure Analysis Based on J_{Critical} Curve.

4.6 REFERENCES

1. Damage Tolerant Design (Data) Handbook, Revision to MCIC-HB-01, (1975), covered under USAF Contract No. F33615-80-C-3229.
2. W. S. Margolis and F. C. Nordquist, "Plane Stress Fracture Toughness (K_{IC}) of Aluminum Alloy 7475 - $\frac{1}{2}$ Inch Plate, Tempers - T7651 and T7351 and of Aluminum Alloy 2024 - $\frac{1}{8}$ Inch Sheet - T81 and T62 Temper," General Dynamics, Fort Worth Div., F-16 Air Combat Fighter Technical Report TIS GA2300, CDRL A031, USAF Contract F33657-75-C-0310.
3. J. M. Krafft, A. M. Sullivan and R. W. Boyle, "Effect of Dimensions on Fast Fracture Instability of Notched Sheets," Cranfield Crack Propagation Symposium, Vol. 1, (1961), pp. 8-28.
4. J. E. Srawley and W. F. Brown, "Fracture Toughness Testing Methods," ASTM STP 381, (1965), pp. 133-195.
5. Fracture Toughness Evaluation by R-Curve Method, ASTM STP 527, D. E. McCabe, Ed, Am Soc for Testing and Mat'l, (1973).
6. D. P. Wilhem, "An Improved Technique for Residual Strength Prediction - A Modified Crack Growth Resistance Approach," Paper presented at Conference on Prospects of Fracture Mechanics, Delft University, The Netherlands, (June 1974).
7. J. R. Rice, "A Path Independent Integral and the Approximate Analyses of Strain Concentration by Notches and Cracks," J. Appl. Mech., ASME, Vol. 35, (June 1968), pp. 379-386.
8. C. A. Griffis and G. R. Yoder, "Application of the J-Integral to Crack Initiation in a 2024-T-351 Aluminum Alloy," Naval Research Lab Report 7676, (April 1974).
9. R. Verette and D. P. Wilhem, "Development & Evaluation of Methods of Plane Stress Fracture Analysis, Review and Evaluation of Structural Residual Strength Prediction Techniques," AFFDL-TR-73-42, (May 1973).
10. W. T. Fujimoto, "Determination of Crack Growth and Fracture Toughness Parameters for Surface Flaws Emanating from Fastener Holes," MCAIR Report A4093, (17 March 1976); Presented at the AIAA/ASME/SAE Structures, Structural Dynamics and Materials Conference, Valley Forge, PA, (4-7 May 1976).

11. J. I. Bluhm, "Fracture Arrest," Fracture, Vol. V, Liebowitz ed., Academic Press, (1969), pp. 1-63.
12. J. P. Romauldi and P. H. Sanders, "Fracture Arrest By Rivited Stiffeners," Proceedings of Fourth Midwest Conference on Solid Mechanics, University of Texas Press, (1959-1960).
13. D. Broek, Elementary Engineering Fracture Mechanics, Noordhoff (1974).
14. C. K. Gunther and J. T. Wozumi, "Critical Failure Mod-s in Cracked Mechanically Fastened Stiffened Panels," Design of Fatigue and Fracture Resistant Structures, ASTM STP761, P. R. Abelkis and C. M. Hudson, Eds., Am. Soc. for Testing and Mat'ls, (1982), pp. 310-327.
15. D. P. Wilhem, "Fracture Mechanics Guidelines for Aircraft Structural Applications," AFFDL-TR-69-111, Air Force Flight Dynamics Laboratory, (Feb. 1970).
16. A. F. Grandt, "A General Stress-Intensity Factor Solution for Through-Cracked Fastener Holes," Int. J. Fracture, 11, (1975), pp. 283-294.
17. O. L. Bowie, "Analysis of an Infinite Plate Containing Radial Cracks Originating at the Boundary of an Internal Circular Hole," J Math. and Phys., 35, (1956), pp. 60-71.
18. J. P. Romualdi, J. T. Frasier, and G. R. Irwin, "Crack-Extension Force Near a Riveted Stringer, NRL Memo Report No. 4956, (1957).
19. C. C. Poe, "The Effect of Riveted and Uniformly Space Stringers on the Stress-Intensity Factor of a Cracked Sheet," Air Force Conference on Fatigue and Fracture, (1969), AFFDL-TR-70-144, (1970), pp. 207-216.
20. C. C. Poe, "Fatigue-Crack Propagation in Stiffened Panels," ASTM STP 486, (1971), pp. 79-97.
21. H. Vlieger, "The Residual Strength Characteristics of Stiffened Panels Containing Fatigue Cracks," Engineering Fracture Mechanics, 5, (1973), pp. 447-478.
22. T. Swift and D. Y. Wang, "Damage Tolerant Design Methods and Test Verification of Fuselage Structure," Air Force Conference on Fatigue and Fracture, (1969), AFFDL-TR-70-144, pp. 653-683.

23. T. Swift, "Development of the Fail-Safe Design Features of the DC-10," ASTM STP 486, (1971), pp. 164-214.
24. T. Swift, "The Effects of Fastener Flexibility and Stiffener Geometry on the Stress Intensity in Stiffened Cracked Sheet," Prospects of Fracture Mechanics, Sih, Van Esh, Broek, eds., Nordhoff, (1974), pp. 419-436.
25. M. Creager and A. F. Liu, "The Effect of Reinforcements on the Slow Stable Tear and Catastrophic Failure of Thin Metal Sheet," AIAA Paper 71-113, (1971).
26. M. M. Ratwani and D. P. Wilhem, "Development and Evaluation of Methods of Plane Stress Fracture Analysis, A Technique for Predicting Residual Strength of Structure," AFFDL-TR-73-42, (December 1974).
27. A. E. H. Love, "A Treatise on the Mathematical Theory of Elasticity," New York, Dover, 4th Ed., (1944), p. 209.
28. R. V. Sanga, "The 747 Fail-Safe Structural Program," Fail-Safe Aircraft Structures, Vol. II, I CAF Symp. 1973, RAE TR 73 183, (1974), pp. 3.1/1-3.1/66.
29. H. M. Westergaard, "Bearing Pressures and Cracks," Transactions, Am. Soc. Mech. Engrs., J. of Applied Mechanics, Vol. 6, (1939), pp. 49-53.

5.0 ANALYSIS OF DAMAGE GROWTH

<u>SECTION</u>		<u>PAGE</u>
5.1	BASIC INFORMATION	5.1.1
5.1.1	<u>Introduction</u>	5.1.1
5.1.2	<u>Fatigue-Crack Growth and Stress-Intensity</u>	5.1.2
5.1.3	<u>Fatigue Crack-Growth Rate (FCGR) Descriptions</u>	5.1.6
5.1.4	<u>Factors Affecting Crack Growth</u>	5.1.17
5.1.5	<u>Use of Data; Data Scatter</u>	5.1.19
5.1.6	<u>Stress-Corrosion Cracking and Stress-Intensity</u>	5.1.22
5.2	VARIABLE-AMPLITUDE LOADING	5.2.1
5.2.1	<u>Introduction</u>	5.2.1
5.2.2	<u>Retardation</u>	5.2.1
5.2.3	<u>Retardation Under Spectrum Loading</u>	5.2.3
5.2.4	<u>Retardation Models</u>	5.2.5
5.2.5	<u>Integration Routines</u>	5.2.11
5.2.6	<u>Cycle-by-Cycle Analysis</u>	5.2.16
5.3	STRESS SEQUENCE DEVELOPMENT	5.3.1
5.3.1	<u>Service Life Description and Mission Profiles</u>	5.3.1
5.3.2	<u>Sequence Development Techniques</u>	5.3.4
5.3.3	<u>Application of Simplified Stress Sequences for Design Studies</u>	5.3.14
5.4	CRACK GROWTH PREDICTION	5.4.1
5.4.1	<u>Introduction</u>	5.4.1
5.4.2	<u>Cycle Definition and Sequencing</u>	5.4.1
5.4.3	<u>Clipping</u>	5.4.4
5.4.4	<u>Truncation</u>	5.4.8
5.4.5	<u>Crack Shape</u>	5.4.9
5.4.6	<u>Interaction of Cracks</u>	5.4.11
5.5	LIST OF REFERENCES	5.5.1

LIST OF FIGURES

<u>FIGURE</u>		<u>PAGE</u>
5.1.1	Typical Crack Growth-Life Curve.	5.1.26
5.1.2	Definition of Terms.	5.1.27
5.1.3	Fatigue Crack Growth Rate Data Presentation Format Used in Revised Damage Tolerant Design (Data) Handbook. Data for Two Stress Ratios Presented for 7075-T7351 Aluminum Alloy (Reference 1).	5.1.28
5.1.4	Sample Fatigue Crack Growth Rate Data Set for 7075-T6 Aluminum Alloy Sheet After Mil Handbook-5 (Reference 2).	5.1.29
5.1.5	Sample Fatigue Crack Growth Rate Data Set for 7075-T7351 Aluminum Alloy Plate After Mil-Handbook-5 (Reference 2).	5.1.30
5.1.6	Schematic of Fatigue Crack Growth Rate Behavior.	5.1.31
5.1.7	Description of FCGR Data Fitting and the Comparison of Predicted to Actual Behaviors.	5.1.32
5.1.8	Possible Variation of Crack Growth in Materials from Different Sources (Reference 12).	5.1.33
5.1.9	Example of Effect of Thickness on Crack Growth (Reference 13).	5.1.34
5.1.10	Effect of Humidity on Fatigue Crack Propagation (Reference 18).	5.1.35
5.1.11	Example of Temperature Effect on Crack Growth (Reference 29).	5.1.36
5.1.12	Crack Growth Data Scatter for Identical Conditions.	5.1.37
5.1.13	Stress Corrosion Cracking Data (Reference 33).	5.1.38
5.1.14	Stress Corrosion Cracking.	5.1.39
5.1.15	K_{Isc} Data as Presented by the Damage Tolerant Design (Data) Handbook (Reference 1).	5.1.40
5.1.16	Stress Corrosion Cracking Rate Data for 2024-T351 Aluminum in the Format of Reference 1.	5.1.41

LIST OF FIGURES
Cont'd

<u>FIGURE</u>		<u>PAGE</u>
5.1.17	Stress Required for Stress Corrosion Cracking.	5.1.42
5.2.1	Retardation Due to Positive Overloads and Due to Positive-Negative Overload Cycles (Reference 40).	5.2.20
5.2.2	Effect of Magnitude of Overload on Retardation (Reference 27).	5.2.21
5.2.3	Retardation in Ti-6V-4Al; Effect of Hold Periods and Multiple Overloads (Reference 42).	5.2.22
5.2.4	Effect of Clipping of Higher Loads in Random Flight-by-Flight Loading on Crack Propagation in 2024-T3 Al Alloy (Reference 43 and 44).	5.2.23
5.2.5	Effect of Block Programming and Block Size on Crack Growth Life (All Histories Have Same Cycle Content) Alloy: 2024-T3 Aluminum (Reference 27).	5.2.24
5.2.6	Yield Zone Due to Overload (r_{poL}), Current Crack Size (a_i), and Current Yield Zone (r_{pi}).	5.2.25
5.2.7	Crack Growth Predictions by Wheeler Model Using Different Retardation Exponents (Reference 45).	5.2.26
5.2.8	Predictions of Crack Growth Lives with the Generalized Willenborg Model, and Comparison with Test Data (Reference 59). Compressive Stress Levels Were Ignored in this Analysis.	5.2.27
5.2.9	Predictions by Crack Closure Model as Compared with Data Resulting from Constant-Amplitude Tests with Overload Cycles (Reference 52).	5.2.28
5.2.10	Steps Required for Crack-Growth Integration.	5.2.29
5.2.11	Statistical Crack-Incrementation Scheme Used to Determine Spectrum Induced Variations in Crack Growth-Rate Behavior (Reference 16).	5.2.29
5.2.12	Steps Required for Crack-Growth Integration.	5.2.30

LIST OF FIGURES
Cont'd

<u>FIGURE</u>		<u>PAGE</u>
5.3.1	Mission Profile and Mission Segments.	5.3.19
5.3.2	Maneuver Spectra According to MIL-A-08866B (USAF).	5.3.20
5.3.3	Exceedance Spectra for 1000 Hrs.	5.3.21
5.3.4	Stepped Approximation of Spectrum.	5.3.22
5.3.5	Fatigue-Crack Growth Behavior Under Various Spectra Approximations.	5.3.23
5.3.6	Approximate Stress Spectrum for 1000 Flights Based on MIL-A-08866B (USAF).	5.3.24
5.4.1	Definition of Cycles.	5.4.14
5.4.2	Rain Flow Count.	5.4.15
5.4.3	Calculated Crack Growth Curves for Random Flight-by-Flight Fighter Spectrum (Reference 67).	5.4.16
5.4.4	Spectrum Fatigue Crack Growth Behavior Willenborg Retardation Model.	5.4.17
5.4.5	Spectrum Fatigue Crack Growth Behavior Wheeler Retardation Model.	5.4.18
5.4.6	Effect of Clipping Level on Calculated Crack Growth for Spectrum B-Trainer.	5.4.19
5.4.7	Effect of Clipping for Various Spectra.	5.4.20
5.4.8	Calculated and Experimental Data for Gust Spectrum Clipping (Reference 43 and 44).	5.4.21
5.4.9	Effect of Lowest Stress Amplitude in Flight-by-Flight Tests Based on Gust Spectrum (Reference 43 and 44).	5.4.22
5.4.10	Improper and Correct Truncation.	5.4.23
5.4.11	Development of Flaws.	5.4.24
5.4.12	Interaction of Cracks.	5.4.25

LIST OF TABLES

<u>TABLE</u>		<u>PAGE</u>
5.1.1	ACTIVE PARTICIPANTS AND THEIR ORGANIZATIONS (REFERENCE 10)	5.1.11
5.1.2	FCGR DESCRIPTIONS	5.1.12
5.1.3	MEANS AND STANDARD DEVIATION OF SETS OF LIFE-PREDICTION RATIOS FOR THE FULL CRACK GROWTH INTERVAL	5.1.12
5.1.4	A FURTHER COMPARISON OF FCGR DESCRIPTIONS	5.1.14
5.1.5	EXAMPLE FATIGUE CRACK GROWTH RATE TABLE (2219-T851 ALUMINUM)	5.1.15
5.3.1	SIMPLE FLIGHT-BY-FLIGHT SPECTRUM FOR EARLY DESIGN ANALYSIS AND TRADE-OFF STUDIES	5.3.16

5.0 ANALYSIS OF DAMAGE GROWTH

5.1 BASIC INFORMATION

5.1.1 Introduction

MIL-A-83444, "Airplane Damage Tolerance Design Requirements," specifies that cracks shall be assumed to exist in all primary aircraft structure. These cracks shall not grow to a size to cause loss of the aircraft at a specified load within a specified period. Showing compliance with these requirements implies that the rate of growth of the assumed flaws must be predicted.

Crack growth is a result of cyclic loading due to gusts and maneuvers (fatigue cracking), or of the combined action of sustained loading and environment (stress-corrosion cracking), or both. The most common crack-growth mechanisms are fatigue-crack growth and environment-assisted (corrosion) fatigue-crack growth. Certain aircraft parts (especially high-strength forgings) may be liable to stress-corrosion cracking. Since there is a design threshold for stress corrosion, proper detail design and proper material selection can minimize or prevent stress corrosion. Fatigue cracking is difficult to prevent, but it can be controlled.

The information concerning the determination of stress-intensity factors, that was presented in Chapter 1 can be directly applied to crack-growth analysis.

To predict crack growth behavior such as illustrated in Figure 5.1.1, the following information must be available:

1. The stress-intensity factor, described as a function of crack size, for the relevant structural and crack geometry;
2. The stress (load)-time history, described for the structural location component or structure under consideration;
3. The baseline crack-growth properties (constant amplitude crack-growth rate data), described as a function of the stress-intensity factor, for the material and for the relevant environment;
4. A damage integration routine that integrates the crack-growth rate (from (3)) to produce a crack-growth curve, using the proper stress-time history (from (2)), the proper stress-intensity formulation (from (1)), and an appropriate integration rule.

This chapter provides guidelines to arrive at crack growth estimates, and points out where deficiencies in knowledge and analysis methods lead to inaccuracies.

5.1.2 Fatigue-Crack Growth and Stress-Intensity

Consider constant-amplitude fatigue loading as in Figure

5.1.2a. The following parameters are defined:

σ_m	mean stress
σ_a	stress amplitude
$\Delta\sigma$	stress range
σ_{\max}	maximum stress
σ_{\min}	minimum stress
R	stress ratio: $R = \frac{\sigma_{\min}}{\sigma_{\max}} = \frac{\sigma_m - \sigma_a}{\sigma_m + \sigma_a} = 1 - \frac{\Delta\sigma}{\sigma_{\max}}$

The cyclic stress can be fully characterized (apart from the frequency) by any combination of two of these parameters. The stress range, $\Delta\sigma$, and the stress ratio, R, are the two most commonly used. Note that in a constant-amplitude test each of these parameters has a constant value with respect to time.

The stress history can be converted into a stress-intensity factor history (Figure 5.1.2b) at a given crack length by multiplying the stress history by the stress-intensity factor coefficient. The following parameters are defined:

K_m	mean stress-intensity factor = $\beta\sigma_m\sqrt{\pi a}$
K_a	amplitude of the stress-intensity factor = $\beta\sigma_a\sqrt{\pi a}$
ΔK	range of the stress-intensity factor = $\beta\Delta\sigma\sqrt{\pi a}$
K_{\max}	maximum stress-intensity factor = $\beta\sigma_{\max}\sqrt{\pi a}$
K_{\min}	minimum stress-intensity factor = $\beta\sigma_{\min}\sqrt{\pi a}$
R_K	cycle ratio: $R_K = \frac{K_{\min}}{K_{\max}}$

The above calculation schemes for stress-intensity factor parameters, while being the most straightforward algebraically, have an operational quality about them. For example, it is theoretically difficult to define a negative stress-intensity factor which happens if the stress becomes compressive. In this case, the crack closes and the crack tip stress field loses its singularity character; thus, the stress-intensity factor ceases to have meaning. The operational quality of the negative stress-intensity factors calculated for compressive stress situations has been given a lot of consideration by the aerospace industry and by the American Society of Testing Materials (ASTM), specifically its subcommittee on subcritical crack growth (ASTM E24.04). ASTM has chosen to provide the following definitions when $\sigma_{\min} < 0$:

$$K_{\min} = 0 \text{ if } \sigma_{\min} < 0$$

$$\Delta K = K_{\max} \text{ if } \sigma_{\min} < 0$$

The reader should be aware of the ASTM ΔK definition since that convention is used in the Damage Tolerant Design (Data) Handbook⁽¹⁾ for the presentation of crack growth rate data when part of the fatigue cycle is compressive, i.e., when $\sigma_{\min} < 0$ ($R < 0$). The algebraic definition of ΔK is used in the current version of MIL-HDBK-5⁽²⁾. Before negative stress ratio ($R < 0$) data are used, it is important to establish what the operational definition of ΔK is. The reader should note that the behavior of the material under negative stress ratio conditions is itself independent of the operational definition of ΔK .

In the elastic case, the stress-intensity factor alone is sufficient to describe the stress field at the tip of a crack. When the plastic zone at the crack tip is small compared with the crack size, the stress-intensity factor still gives a good indication of the stress environment of the crack tip. Two different cracks which have the same stress environment (equal stress-intensity factors) will behave in the same manner and show the same rate of growth.

Since two parameters are required to characterize the fatigue cycle, two parameters are required to characterize crack growth rate behavior. The crack-growth rate per cycle, da/dN , where N is the number of cycles, can be generally described with functional relations of the type:

$$\frac{da}{dN} = f(\Delta K, R) \text{ or } = g(K_{\max}, R) \quad (5.1.1)$$

where R is the stress ratio associated with the stress cycle.

EXAMPLE 5.1.1: Meaning of Equation 5.1.1

For a wide center crack panel subjected to constant amplitude loading conditions, Equation 5.1.1 implies that the crack growth rate of a 2-inch long crack subjected to a remote loading of $\Delta\sigma = 10$ ksi for $R=0$ will be identical to the rate of growth of a 0.5-inch long crack subjected to a remote loading of $\Delta\sigma = 20$ ksi for $R=0$. The rates for the two different crack length - loading conditions will be the same because the stress-intensity factor range (ΔK) and the stress ratio (R) are the same in both cases.

Typically, fatigue crack growth rate data is described using plots of da/dN versus ΔK on double-logarithmic scale graph paper. Figure 5.1.3 presents fatigue crack growth rate data for 7075 Aluminum in the graphical format that is being used in the revised version of the Damage Tolerant Design (Data) Handbook⁽¹⁾. Figures 5.1.4 and 5.1.5 describe example composite da/dN data plots for 7075 Aluminum as a function of ΔK (algebraic definition) for different stress ratio (R) values⁽²⁾. Both Figures 5.1.4 and 5.1.5 provide mean trend curves that represent the function $f(\Delta K, R)$ in Equation 5.1.1. On the basis of these figures, it can be seen that $f(\Delta K, R)$ is not a simple function. Figure 5.1.6 is a schematic illustration of fatigue crack growth rate behavior from the threshold region (below 10^{-8} inch/cycle) to the onset of rapid cracking in the fracture toughness region (above 10^{-3} inch/cycle). As can be seen from Figures 5.1.3 - 5.1.6, the behavior exhibits a sigmoidial shape suggesting that there might be asymptotes at the two extreme regions.

5.1.3 Fatigue Crack-Growth Rate (FCGR) Descriptions

Many descriptions of the function $f(\Delta K, R)$ in Equation 5.1.1 have been proposed. In the early literature⁽³⁻⁶⁾, most of the descriptions were either based on physical models of the crack growth process (referred to as "laws") or on equations that appeared to describe the trends in the data. Currently, the fatigue crack growth rate (FCGR) descriptions are carefully selected to provide accurate mean trend descriptions of the specific data collected to support a materials evaluation or structural

design. Before introducing these more accurate FCGR descriptions, the Paris power law⁽⁷⁾, the Walker equation⁽⁸⁾, and Forman equations will be reviewed⁽⁹⁾.

The Paris power law equation was initially proposed to describe the crack growth rate behavior in the central region for specific values of stress ratio. It is given by the general form:

$$\frac{da}{dN} = C \Delta K^p \quad (5.1.2)$$

where C and p are experimentally determined constants. Equation 5.1.2 is still extensively used to develop first order approximations of life behavior when only limited amounts of data are available. The reader is cautioned that Equation 5.1.2, as well as any other FCGR description, should not be extrapolated beyond its limits of applicability without a great deal of care and experience. Greater life prediction errors can result from data extrapolation errors than almost all other design methodology errors combined.

The Walker equation⁽⁸⁾ provided one of the first simple equations that accounted for the stress ratio shift. It is a subtle modification of Equation 5.1.2 and is given by

$$\frac{da}{dN} = C [(1-R)^m K_{\max}]^p \quad (5.1.3)$$

where C, m, and p are empirical constants. The exponent m typically ranges from 0.4 to 0.6 for many materials. Because Equation 5.1.3 is a

power law, it has been noted to be most useful in describing the central region of the growth rate behavior.

The Forman equation⁽⁹⁾ was initially proposed to describe both the central and high crack growth regions of the behavior. To account for the acceleration of the cracking rates as the stress-intensity factors levels approached critical, the Paris power law equation was divided by a factor that would reach zero when the stress-intensity factor reached a critical level. The general form of the Forman equation is:

$$\frac{da}{dN} = \frac{C \Delta K^p}{(1-R) K_c - \Delta K} \quad (5.1.4)$$

where C, p, and K_c are experimentally evaluated for the given material and thickness. Equation 5.1.4 can be rearranged to yield:

$$\frac{da}{dN} = \frac{C (1-R)^{p-1} \cdot K_{max}^p}{K_c - K_{max}} \quad (5.1.5)$$

which shows that the equation has the capability to describe multiple stress ratio data sets.

The empirical constants in Equations 5.1.2-5.1.4 are typically derived using least square fitting procedures. Note that the simplicity of Equations 5.1.2 and 5.1.3 allow for a graphical fit to the data on log-log coordinate paper and the direct evaluation of the constants from the graph. The usefulness of Equations 5.1.2-5.1.4 comes from the ease in

which their constants can be evaluated from available data, as well as the direct application of the equations to simplified life integration calculations. When considering the general expression for crack growth life (N_f)

$$N_f = \int_{a_o}^{a_f} \frac{da}{f(\Delta K, R)} , \quad (5.1.6)$$

it is seen that the function f is simple for Equations 5.1.2-5.1.4.

ASTM task group E24.04.04 (on FCGR descriptions) recently conducted two analytical round robin investigations of the utility of various FCGR descriptions that describe FCGR behavior (See References 10 and 11). These round robin investigations have clearly demonstrated that FCGR descriptions which are classified as "good" from a life analysis standpoint must adequately represent the mean trend of the FCGR data. Figure 5.1.7 outlines a general procedure whereby the FCGR behavior is first described by least square regression analysis (Figure 5.1.7a) and then the regression equation (in conjunction with the stress-intensity factor analysis for the test geometry) is used in integral form to obtain an estimate of the fatigue crack growth life N_f (Figure 5.1.7b). In Figure 5.1.7a, the mean trend behavior is described along with bounds on the regression equation. Those descriptions which fail to model the mean trend of the FCGR data, either because they are preconceived to have a specific form (sinh, power law, Forman, etc.) or due to a lack of care in performing the regression analysis, lead to life prediction errors that are biased or exhibit significant scatter.

To support the first round robin, FCGR data from compact and center crack test geometries fabricated from 0.25 inch thick 2219-T851 aluminum alloy were supplied to the participants. The tests were conducted between threshold and fracture toughness levels for five separate stress ratios (-1, 0.1, 0.3, 0.5, and 0.8). A number of individuals from government, industry, and academia participated in the round robin (See Table 5.1.1) and chose to evaluate the ten (10) descriptions defined in Table 5.1.2. Each participant was given FCGR data and asked to describe the mean trend of the behavior using equations or other procedures. The participants then integrated their mean trend analysis to establish predicted life values. They were each given the initial and final crack sizes as well as the loading conditions for these life predictions of center cracked specimens and compact specimens.

One of the procedures utilized to evaluate the ten descriptions was to summarize the sixteen (16) life prediction ratios (life predicted divided by life measured, N_f^P/N_f , see Figure 5.1.7b) associated with each description. The means and standard deviations for the life prediction ratios associated with each participant/FCGR description is presented in Table 5.1.3.

TABLE 5.1.1 - Active Participants and their Organizations⁽¹⁰⁾

Name	Affiliation
C. G. Annis	Pratt & Whitney Aircraft
F. K. Haake	
J. Fitzgerald	Northrop Corporation
J. P. Gallagher*	University of Dayton Research Institute
M. S. Miller	
S. J. Hudak, Jr.	Westinghouse R&D Center
A. Saxena	
J. M. Krafft	Naval Research Laboratory
D. E. Macha	Air Force Materials Laboratory
L. Mueller ⁺	Alcoa Laboratories
B. Mukherjee	Ontario Hydro
M. L. Vanderglas	
J. C. Newman	NASA Langley Research Center

* Chairman, ASTM Task Group E24.04.04 on FCGR Descriptions (1975-80)

⁺ Chairman, ASTM Task Group E24.04.04 on FCGR Descriptions (1980-83)

TABLE 5.1.2 - FCGR Descriptions

Participant/ FCGR Description No.	Form
(1)	$\frac{da}{dN} = C_1 \overline{\Delta K}^{C_2}$
(2)	$\frac{da}{dN} = P_1 \frac{(\Delta K - \Delta K_t)^{P_2}}{(\Delta K_c - \Delta K)^{P_3}}$
(3)	$\frac{1}{da/dN} = \frac{A_1}{(\Delta K)^{n_1}} + A_2 \left[\frac{1}{(\Delta K)^{n_2}} - C' \right]$
(4)	$\frac{da}{dN} = C(K_{max})^m \left[(K_{max} + K_e)(1 - R_{eff}) + *K \right]^2$
(5)	$\log_{10} \left(\frac{da}{dN} \right) = P_1 \exp(P_2 x) + P_3 \exp(P_4 x) + P_5$
(6) ⁺	$\frac{da}{dN} = {}_{10}\{C_1 \sinh[C_2(\log \Delta K + C_3)] + C_4\}$
(7) ⁺	$\frac{da}{dN} = {}_{10}\{C_1 \sinh[C_2(\log \Delta K + C_3)] + C_4\}$
(8)	$\frac{da}{dN} = e + (v - e) \left[-\ln \left(1 - \frac{\Delta K}{K_b} \right) \right]^{1/k}$
(9)	tensile ligament instability model
(10)	table lookup procedure

⁺The hyperbolic sine model is listed twice because two separate organizations chose to evaluate this description.

TABLE 5.1.3 - Means and Standard Deviation of Sets of Life-Prediction Ratios for the Full Crack Growth Interval

	Participant/FCGR Description No.									
	1	2	3	4	5	6	7	8	9	10
	Mean	Standard Deviation								
Mean	0.95	0.72	1.00	0.76	0.96	0.97	2.32	0.99	1.05	0.96
Standard Deviation	0.27	0.16	0.27	0.15	0.12	0.24	5.81	0.10	0.32	0.12

The life prediction ratio (LPR) numbers in Table 5.1.3 can be interpreted by comparing the mean LPR to 1.0 and the standard deviation to 0.0. A mean LPR less than 1.0 implies a conservative prediction. A further interpretation of the results of the round-robin are presented in Table 5.1.4 which contains percentage of life prediction ratios that fall within the ranges of 0.80 and 1.20 and of 0.90 and 1.10. Note that four descriptions were able to achieve LPR numbers between 0.80 and 1.20 for at least 80 percent of the number of predictions made.

One modeling procedure that has consistently shown itself to rank among the most accurate FCGR descriptions for predicting lives is the table look-up scheme (FCGR Description no. 10 in Table 5.1.2). For life prediction purposes, most aircraft companies have gone to a table look-up scheme in which they describe crack growth rate as a function of ΔK for specific values of fatigue crack growth rate or vice versa, i.e., da/dN is described for specific values of ΔK . Table 5.1.5 summarizes the mean trend FCGR behavior of the 2219-T851 aluminum alloy employed by the ASTM Task Group E24.04.04. This table format will be close to the format utilized to present mean trend data in the revised Damage Tolerant Design (Data) Handbook⁽¹⁾. Within the main body of Table 5.1.5, da/dN will be presented as a function of prechosen ΔK levels for specific levels of stress ratio (or environment, etc.). In the rows directly above and directly below the main body of the table, the data extreme values are defined. In the bottom rows of the table, statistical summaries that define the accuracy

TABLE 5.1.4 - A Further Comparison of FCGR Descriptions

Participant/ FCGR Description No.	Percent of All Predictions Within:	
	<u>+20%</u> of 1.0	<u>+10%</u> of 1.0
1	53.3	20.0
2	33.3	20.0
3	86.7	26.7
4	38.5	15.4
5	100.0	73.3
6	73.3	53.3
7	80.0	66.7
8	89.5	57.9
9	31.3	18.8
10	100.0	80.0

TABLE 5.1.5 - Example Fatigue Crack Growth Rate Table
(2219-T851 Aluminum)

ΔK (Ksi $\sqrt{\text{in}}$)			$da/dN \times 10^6$ inches/cycle				
			R1=-1.0	R2=0.1	R3=0.3	R4=0.6	R5=0.8
ΔK_{min} at:	R1	1.09	0.00730	0.00336	0.00369	0.00351	0.00112
	R2	2.55					
	R3	2.11					
	R4	1.38					
	R5	1.17					
	1.3	0.0167					0.00429
	1.6	0.0351				0.0176	0.0251
	2.0	0.0676				0.0569	0.0689
	2.5	0.127			0.0451	0.0911	0.128
	3.0	0.216		0.0166	0.152	0.139	0.228
	3.5	0.336		0.0639	0.246	0.218	0.431
	4.0	0.488		0.171	0.355	0.339	0.809
	5.0	0.884		0.566	0.691	0.753	2.60
	6.0	1.37		1.14	1.30	1.46	7.83
	7.0	1.91		1.93	2.28	2.50	46.3
	8.0	2.47		3.09	3.60	3.95	
	9.0	3.08		4.78	5.14	6.07	
	10.0	3.80		7.04	6.86	9.38	
	13.0	7.16		17.0	14.4	38.4	
	16.0	13.2		36.2	30.9		
	20.0	28.3		126.0			
ΔK_{max} at:	R1	20.7	32.0	887.0	81.3	146.0	47.4
	R2	24.7					
	R3	19.3					
	R4	15.8					
	R5	7.01					
root mean square percent error			2.2	80.4	8.6	6.4	6.1
life prediction ratio summary							
0.0 - 0.5							
0.5 - 0.8				1			
0.8 - 1.25			1	3	1	2	2
1.25 - 2.0							
> 2.0							

of the mean trend (tabular) description (1) to relative to the FCGR data (The parameter RMSPE is the root mean square percentage error) and (2) with respect to life prediction (life prediction ratios based on original a vs N data). The RMSPE is a statistic that measures the deviation of fatigue crack growth rate data from the table; and, it is somewhat akin to the coefficient of (life) variation.

The mean trend data presented in the revised Damage Tolerant Design (Data) Handbook⁽¹⁾ can be directly utilized with table look-up algorithms in crack growth life prediction computer codes. These data might also be utilized with least square fitting procedures to generate wider ranging predictive schemes that account for the effects of stress ratio, frequency, environment, temperature, and other controlling conditions.

The Damage Tolerant Design (Data) Handbook⁽¹⁾ provides crack-growth data for a variety of materials. The data are presented in the form of graphs (See Figure 5.1.3) and tables (See Table 5.1.5). Multiple parameter equation fitting should not be attempted if only limited sets of data are available. In case limited data sets have to be used, a comparison should be made with similar alloys for which complete data are available, and curves may be fitted through the limited data sets on the basis of this comparison.

5.1.4 Factors Affecting Crack Growth

Unlike tensile strength and yield strength, fatigue crack growth rate (FCGR) behavior is not a consistent material characteristic. The FCGR is influenced by many uncontrollable factors. As a result, a certain amount of scatter occurs. Therefore, crack growth predictions should be based on factors relevant to the conditions in service.

Among the many factors that affect crack propagation, the following should be taken into consideration for crack growth properties.

- A.
 - Type of product (plate, extrusion, forging)
 - Heat treatment
 - Orientation with respect to grain direction
 - Manufacturer and batch
 - Thickness
- B.
 - Environment
 - Temperature
 - Frequency.

No attempt will be made to illustrate the effects of all these factors with data, particularly because some factors have largely different (and sometimes opposite) effects on different materials. Rather, some general trends will be briefly mentioned.

The factors under A pertain to the material. The crack propagation characteristics for a particular alloy differ for plates, extrusions, and forgings. The latter may exhibit large anisotropy, which may have to be considered in the growth of surface flaws and corner cracks, which grow simultaneously in two perpendicular directions. Closely related to this are other processing variables, particularly the heat treatment.

An alloy of nominally the same composition but produced by different manufacturers may have quite different crack propagation properties⁽¹²⁾. This is illustrated in Figure 5.1.8. The differences are associated with slight variations in composition, inclusion content, heat treatment (precipitates), and cold work. Similar variations in crack growth occur for different batches of the same alloy produced by the same manufacturer. Data presented in Figure 5.1.9 show that growth rates can vary with sheet thickness⁽¹³⁻¹⁷⁾.

In view of the factors which influence crack growth properties, predictions of crack growth should be based on material data which pertain to the product form. Spot checks may be necessary to account for variabilities in heats and/or manufacturer.

The factors under B are associated with the environmental circumstances. A lightly corrosive environment (humid air) gives rise to higher crack growth rates than a dry environment⁽¹⁸⁻²⁷⁾. The effect is illustrated in Figure 5.1.10. Although opinions differ in explaining the environmental

effect, there is concurrence that the principal factor is corrosive action, which is time and temperature dependent. The effect of cyclic frequency^(19,22,26,28) is related to the environmental effect, with slower cyclic frequencies usually associated with accelerated fatigue crack growth rates.

At low temperatures, the reaction kinetics are slower and the air contains less water vapor. This may reduce crack propagation rates in certain alloys^(29,30). Figure 5.1.11 shows the influence of low temperature on crack growth for 7075-T6 alloy compared with growth at normal temperatures⁽²⁹⁾. Temperatures higher than ambient may increase crack growth rates^(31,32). In view of the effect of environment on crack growth, the data used for life predictions should represent the effect of the expected environment and temperature.

5.1.5 Use of Data; Data Scatter

Fatigue-crack-propagation data for a variety of materials can be found in data handbooks. In many cases, however, the data for a particular application (with regard to material condition, thickness, and environment) will have to be generated in the manner prescribed by Chapter 7.

As indicated by the results presented in subsection 5.1.3, accurate mean trend FCGR descriptions result in accurate fatigue crack life descriptions. People have worried in the past about trying to account for the substantial

amount of scatter which exists in the crack growth rate data. The amount of crack growth between crack measurements and the accuracy of this incremental crack growth measurement determines a large part of the scatter. Another inherent reason for data scatter is due to the differentiation techniques that one uses to reduce the data.

Shown in Figure 5.1.12a is a hypothetical example of the crack growth-life behavior observed in a single laboratory test; Figure 5.1.12b represents the FCGR data derived from this test. Outlying data points are indicated by an asterisk in Figure 5.1.12a and b. The mean trend curves faired through the data can be shown to be directly related to each other; the integral of the curve in Figure 5.1.12b gives the curve in Figure 5.1.12a for the test conditions. If more tests are run and all the data compiled, the plot will be as in Figure 5.1.12c: each test might have a few outlying data points, but the compilation has many outlying points. When all data points, including the outliers, are plotted, the data exhibit a wide scatterband, noted as the apparent scatterband, shown in Figure 5.1.12c. However, as previously seen from Figures 5.1.12a and b, the outlier points did not significantly affect the crack growth curve or the mean trend FCGR curve. When considered collectively, the outlying data points in Figure 5.1.12c can be misleading since they do not represent the mean trend behavior of any specimen. If the wide scatterband were considered for a crack growth prediction, the upper bound would predict a consistent

high growth rate at each crack size (whereas it happened only incidentally as shown in Figure 5.1.12a). As a result, the diagram would reflect a large apparent scatter in crack growth lives (Figure 5.1.12d) whereas the real scatter in crack growth lives is much smaller.

As indicated by the above remarks, worrying about the random (within specimen) scatter in fatigue crack growth rates is really not that important from a life estimation standpoint. What has been found from analyses of multiple specimen data sets is that the width of the scatterbands associated with specimen to specimen mean trend variations in FCGR is closely related to the variability in crack growth-life behavior. The scatterband associated with specimen to specimen variations is identified in Figures 5.1.12c and d as the real scatterband since it focuses on the variability in crack growth life-behavior.

The coefficient in variation of crack growth lives is sometimes similar in magnitude to the root mean square (percentage) error associated with fatigue crack growth rate modeling. When conservative estimates in crack growth lives are desired, the upper bound of the real scatterband (identified in Figure 5.1.12c) determined on the basis of four or more specimens should be used.

5.1.6 Stress-Corrosion Cracking and Stress Intensity

Many engineering materials exhibit some cracking behavior under sustained loading in the presence of an environment (thermal and/or chemical). The type of cracking behavior for many chemical environments is referred to as stress-corrosion cracking behavior. The mechanism for this attack process has been attributed to the chemical reactions that take place at the crack tip and to diffusion of reactive species (particularly Hydrogen) into the high stressed region ahead of the crack. The cracking process has been noted to be a function of time and it is highly dependent on the environment, the material, and the applied stress (or stress-intensity factor) level.

For a given material-environment interaction, the stress-corrosion-cracking rate has been noted to be governed by the stress-intensity factor. Similar specimens with the same size of initial crack but loaded at different levels (different initial K values) show different times to failure⁽³³⁻³⁵⁾ as shown in Figure 5.1.13. A specimen initially loaded to K_{Ic} fails immediately. The level below which cracks are not observed to grow is the threshold level which is denoted as K_{Isc} .

If the load is kept constant during the stress-corrosion-cracking process, the stress-intensity factor will gradually increase due to the growing crack. As a result the crack-growth rate per unit of time, da/dt , increases according to

$$\frac{da}{dt} = f(K). \quad (5.1.7)$$

When the crack has grown to a size that K becomes equal to K_{Ic} , the specimen fails. This is shown schematically in Figure 5.1.14. In typical tests, specimens may be loaded to various initial K 's such as K_1 , K_2 , and K_3 . The time to failure is recorded giving rise to the typical data point (t_1, K_1) . During the test, K will increase (as a result of crack extension) from its initial value to K_{Ic} , where final failure occurs. The times t_2 and t_3 represent the times to failure for higher K 's such as K_2 and K_3 .

The stress-corrosion threshold and the rate of growth depend on the material and the environmental conditions. Data on K_{Isc} and da/dt can be found in the Damage Tolerant Design (Data) Handbook ⁽¹⁾. Typical examples of K_{Isc} and da/dt data presentation formats are shown in Figures 5.1.15 and 5.1.16.

As illustrated in Figure 5.1.17, a component with a given crack fails at a stress given by $\sigma_c = K_{Ic} / \beta \sqrt{\pi a}$. It will exhibit stress-corrosion-crack growth when loaded to stresses in excess of $\sigma_{scc} = K_{Isc} / \beta \sqrt{\pi a}$.

In service, stress-corrosion cracks have been found to be predominantly a result of residual stresses and secondary stresses. Stress-corrosion failure due to primary loading seldom occur because most stress-corrosion cracks favor the short transverse direction (S-L), which is usually not the primary load direction. In many materials, the long transverse (T-L) and longitudinal (L-T) directions are not very susceptible to stress corrosion.

Prevention of stress corrosion cracking is preferred as a design policy over controlling it as is done for fatigue cracking. This means that stress-corrosion critical components must be designed to operate at a stress level lower than $\sigma_{scc} = K_{Iscc} / \beta \sqrt{\pi a_i}$ in which a_i is the initial flaw sizes as specified in the Damage Tolerance Requirements per MIL-A-83444. However, if stress corrosion can occur, it must be accounted for in damage tolerance analyses by using an integral form of Equation 5.1.7.

Stress-corrosion cracking may occur in fatigue-critical components. This means that in addition to growth by fatigue, cracks might show some growth due to stress corrosion. In dealing with this problem, the following should be considered:

- Stress-corrosion cracking is a phenomenon that basically occurs under a steady stress. Hence, the in-flight stationary stress level (lg) is the governing factor. Most fatigue cycles are of relatively short duration and do not contribute to stress-corrosion cracking. Moreover, the cyclic crack growth would be properly treated already on the basis of data for environment-assisted fatigue-crack growth. When stress corrosion cracking is expected, the stress corrosion cracking rate should be superimposed on the fatigue crack growth rate⁽³⁶⁻³⁹⁾.

- Stress-corrosion cracking is generally confined to forgings, heavy extrusions, and other heavy sections, made of susceptible materials. Thus, the problem is generally limited to cases where plane strain prevails.
- The maximum crack size to be expected in service is $a_c = K_{Ic}^2 / \pi \beta^2 \sigma^2$, where σ equals σ_{LT} or σ_{DM} depending upon the inspectability level.

If stress-corrosion cracking is not expected at any crack size, the l-g stress, σ_{lg} , should be lower than $\sigma_{scc} = K_{Isc} / \beta \sqrt{\pi a_c}$. With a_c given as above, it follows that complete prevention of stress corrosion extension of a fatigue crack requires selection of a material for which:

$$K_{Isc} > \frac{\sigma_{lg}}{\sigma_{LT} \text{ (or } \sigma_{DM})} K_{Ic} . \quad (5.1.8)$$

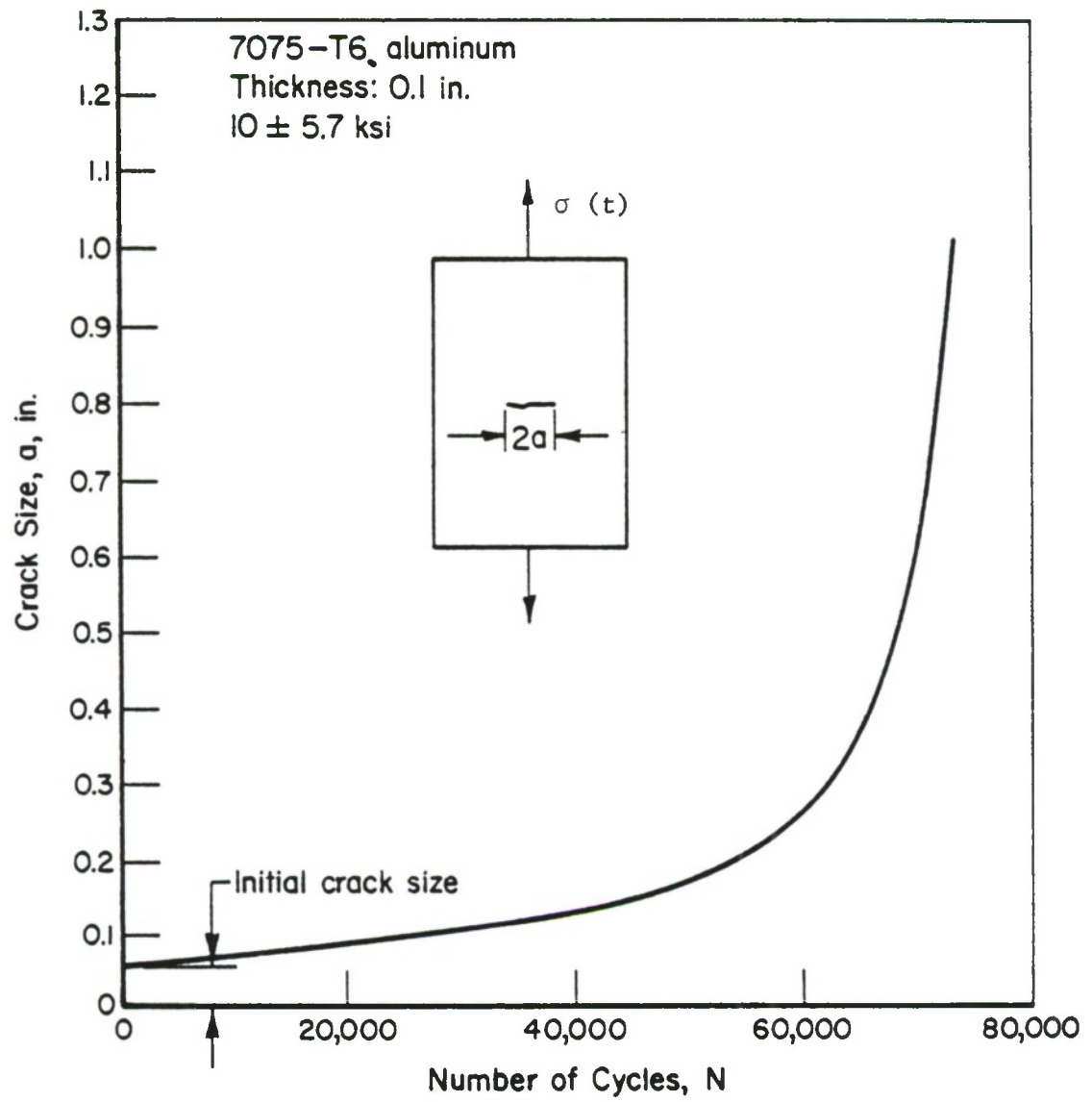


Figure 5.1.1. Typical Crack Growth-Life Curve.

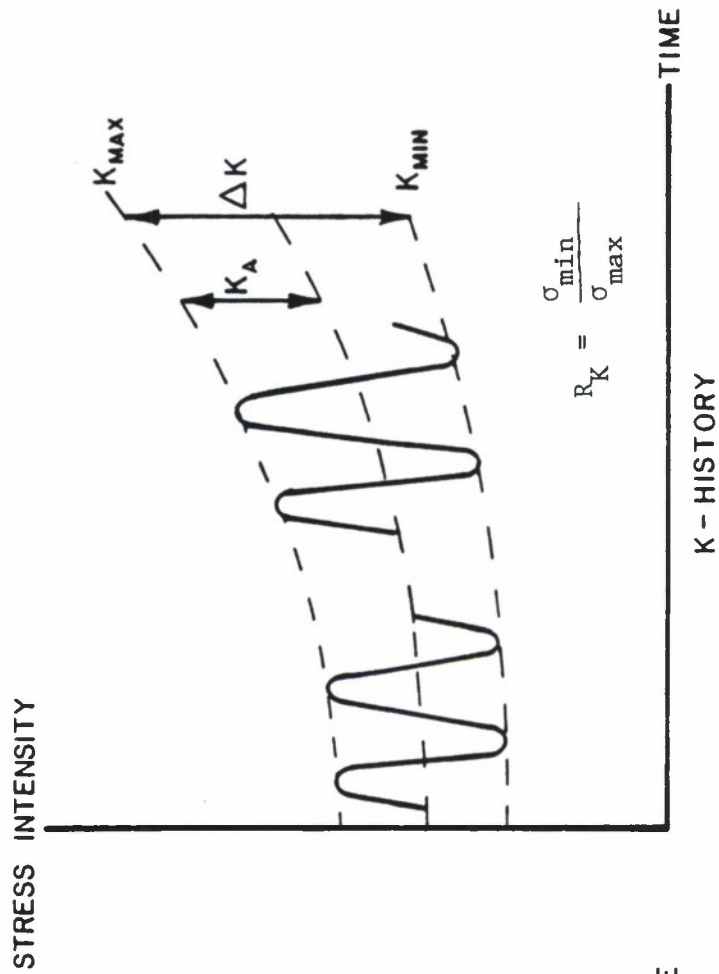
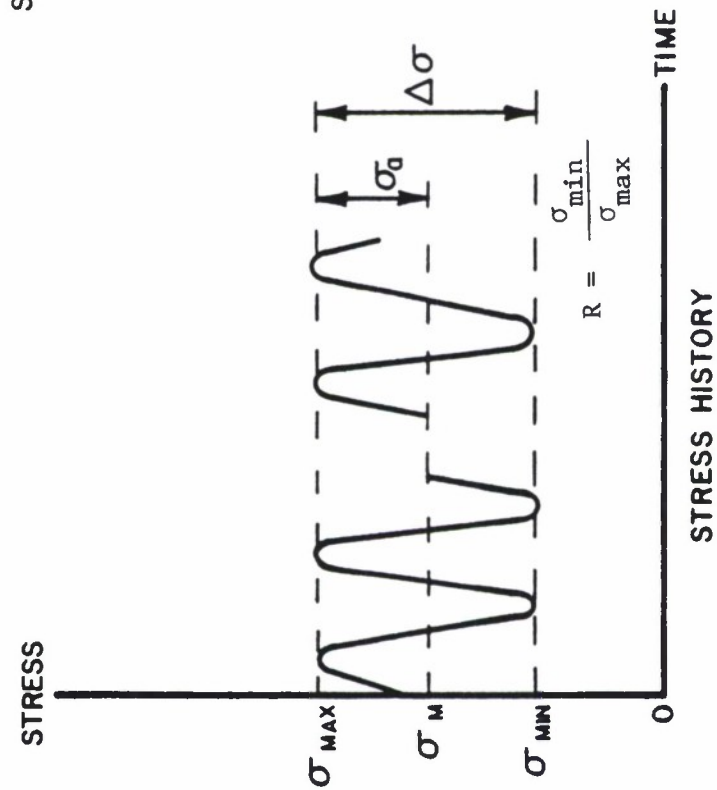


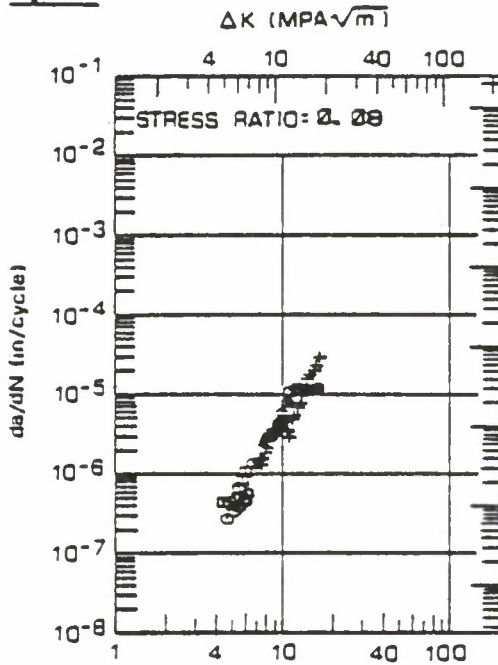
Figure 5.1.2. Definition of Terms.

FORM: 2.00" TH PLATE
 DIRECTION: L-T
 ENVIRONMENT: R.T. L.H.A.
 FREQUENCY: 6.0 HZ

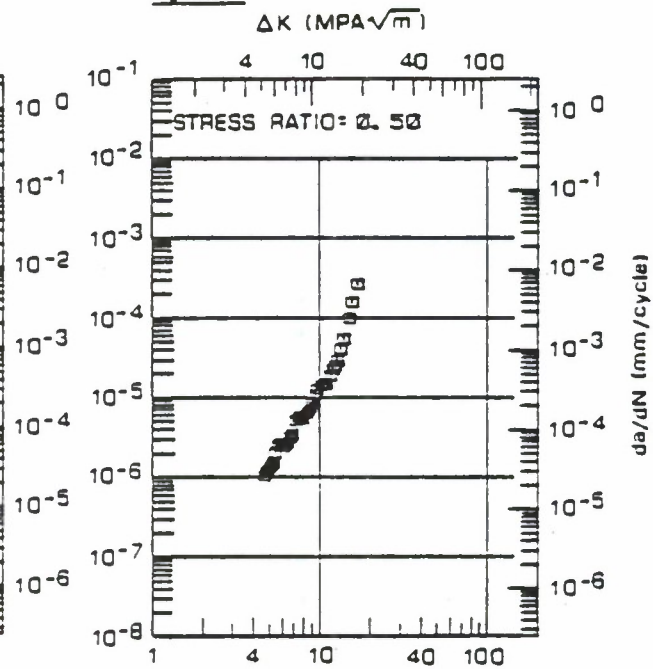
YIELD STRENGTH: 85.0 KSI
 SPECIMEN TYPE: CT
 SPECIMEN SIZE: 0.10" T, 6.00" W
 REFERENCE: 85837, 88579

ALUM
 7075
 T7351

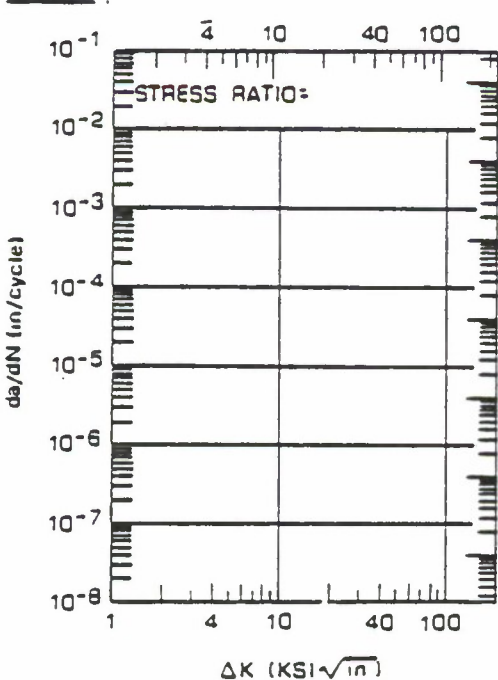
Figure



Figure



Figure



Figure

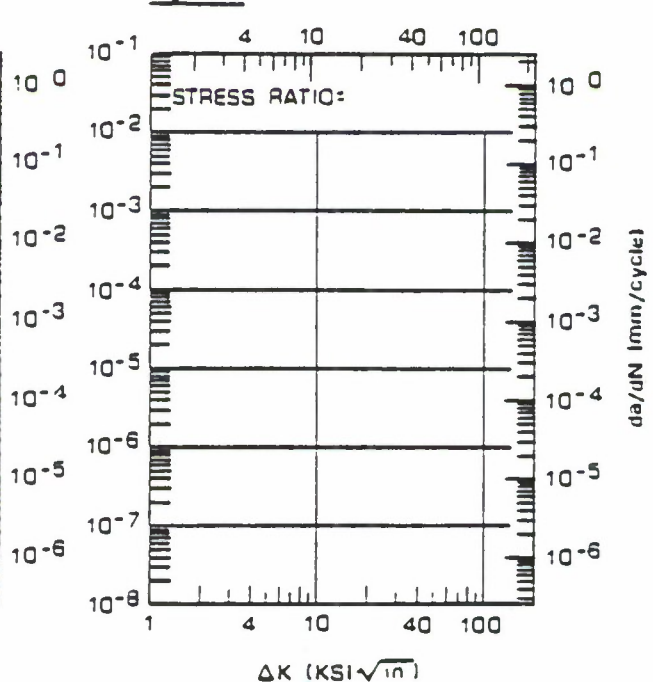


Figure 5.1.3. Fatigue Crack Growth Rate Data Presentation Format Used in Revised Damage Tolerant Design (Data) Handbook. Data for Two Stress Ratios Presented for 7075-T7351 Aluminum Alloy (Reference 1).

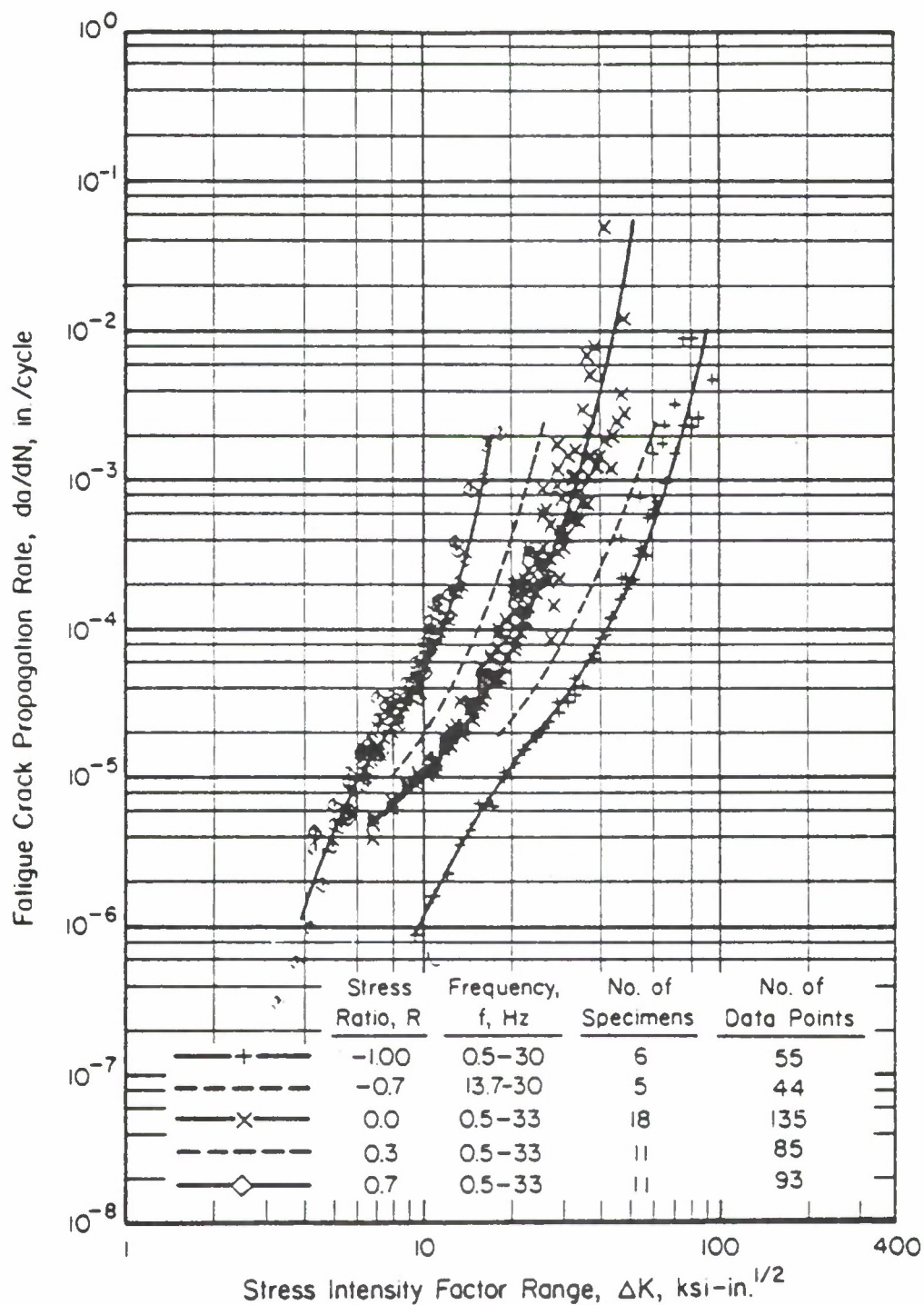


Figure 5.1.4. Sample Fatigue Crack Growth Rate Data Set for 7075-T6 Aluminum Alloy Sheet After Mil Handbook-5 (Reference 2).

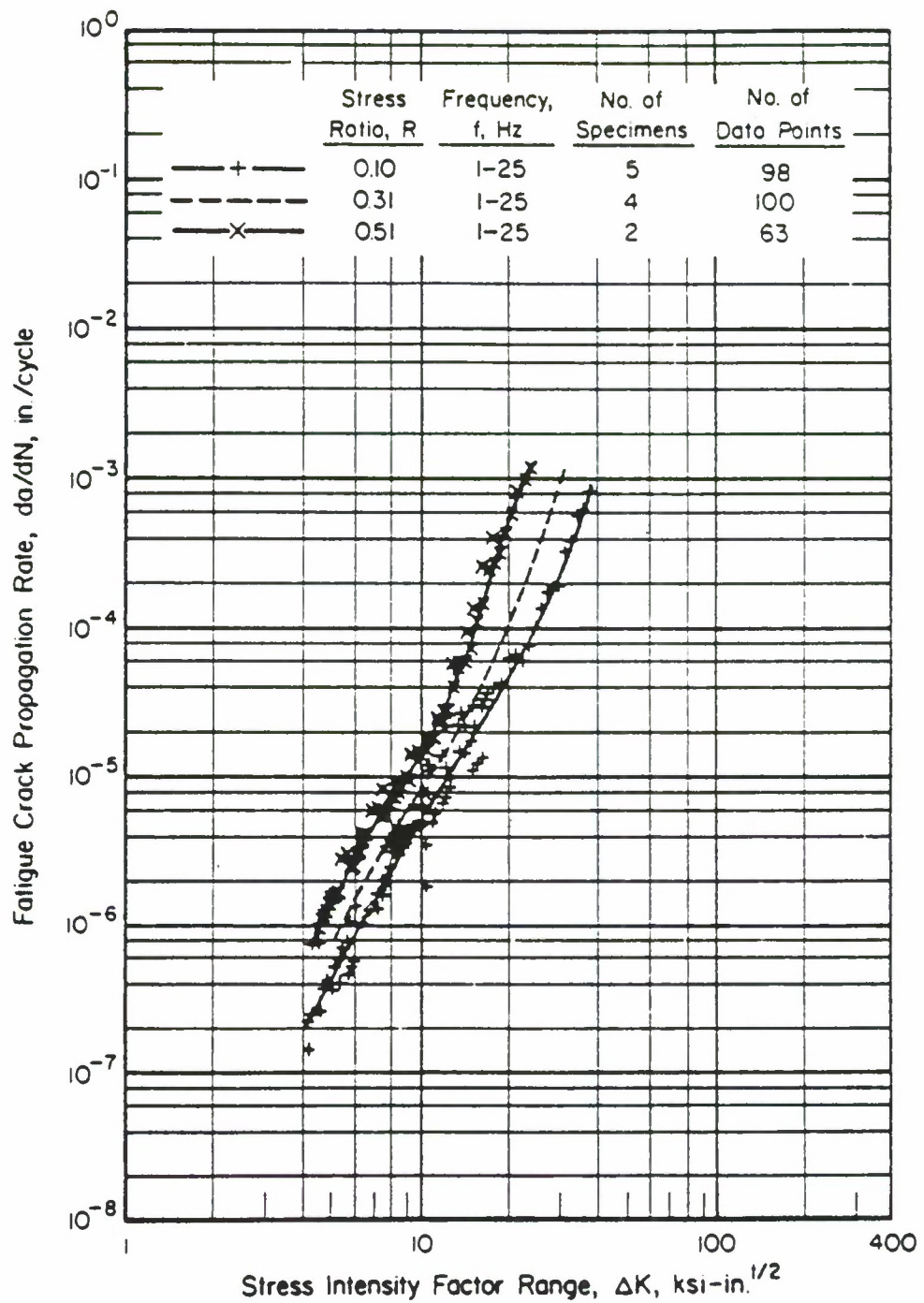


Figure 5.1.5. Sample Fatigue Crack Growth Rate Data Set for 7075-T7351 Aluminum Alloy Plate After Mil-Handbook-5 (Reference 2).

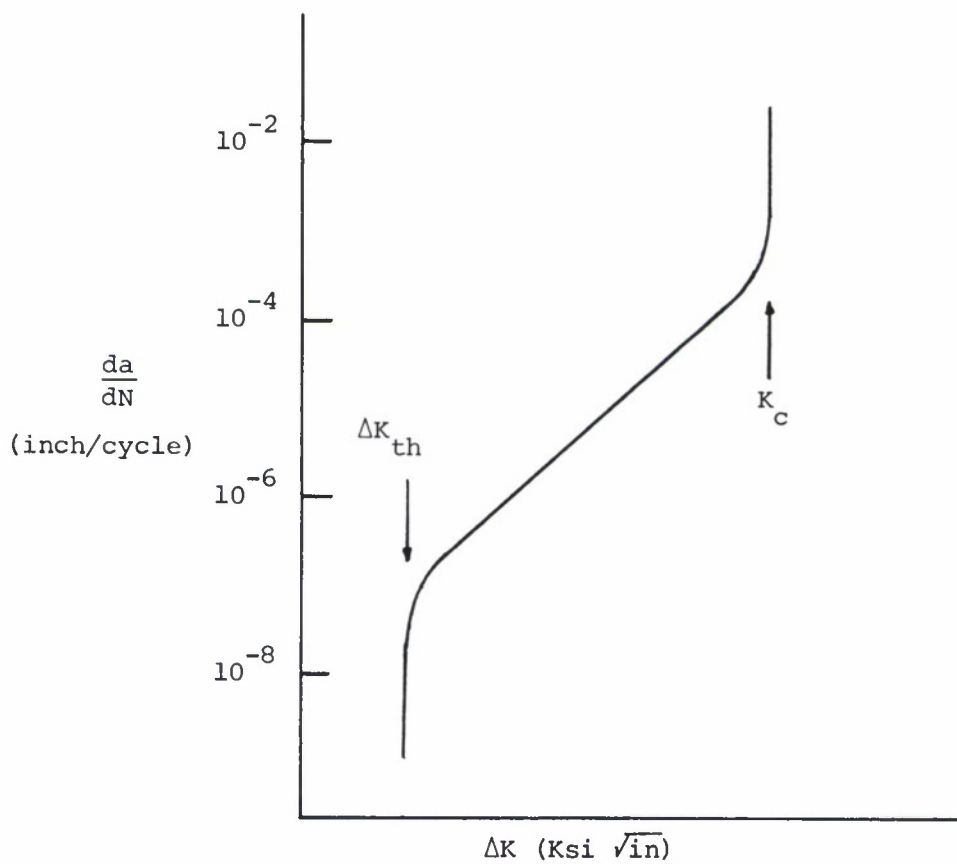


Figure 5.1.6. Schematic of Fatigue Crack Growth Rate Behavior.

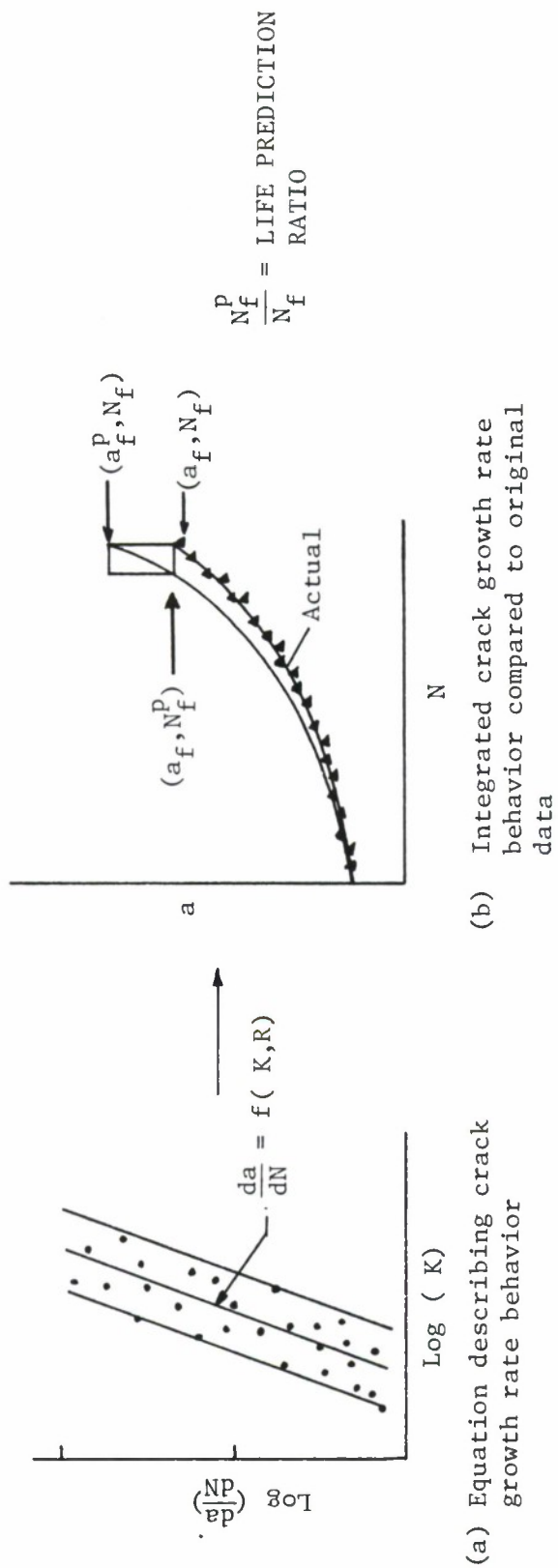


Figure 5.1.7. Description of FCGR Data Fitting and the Comparison of Predicted to Actual Behaviors.

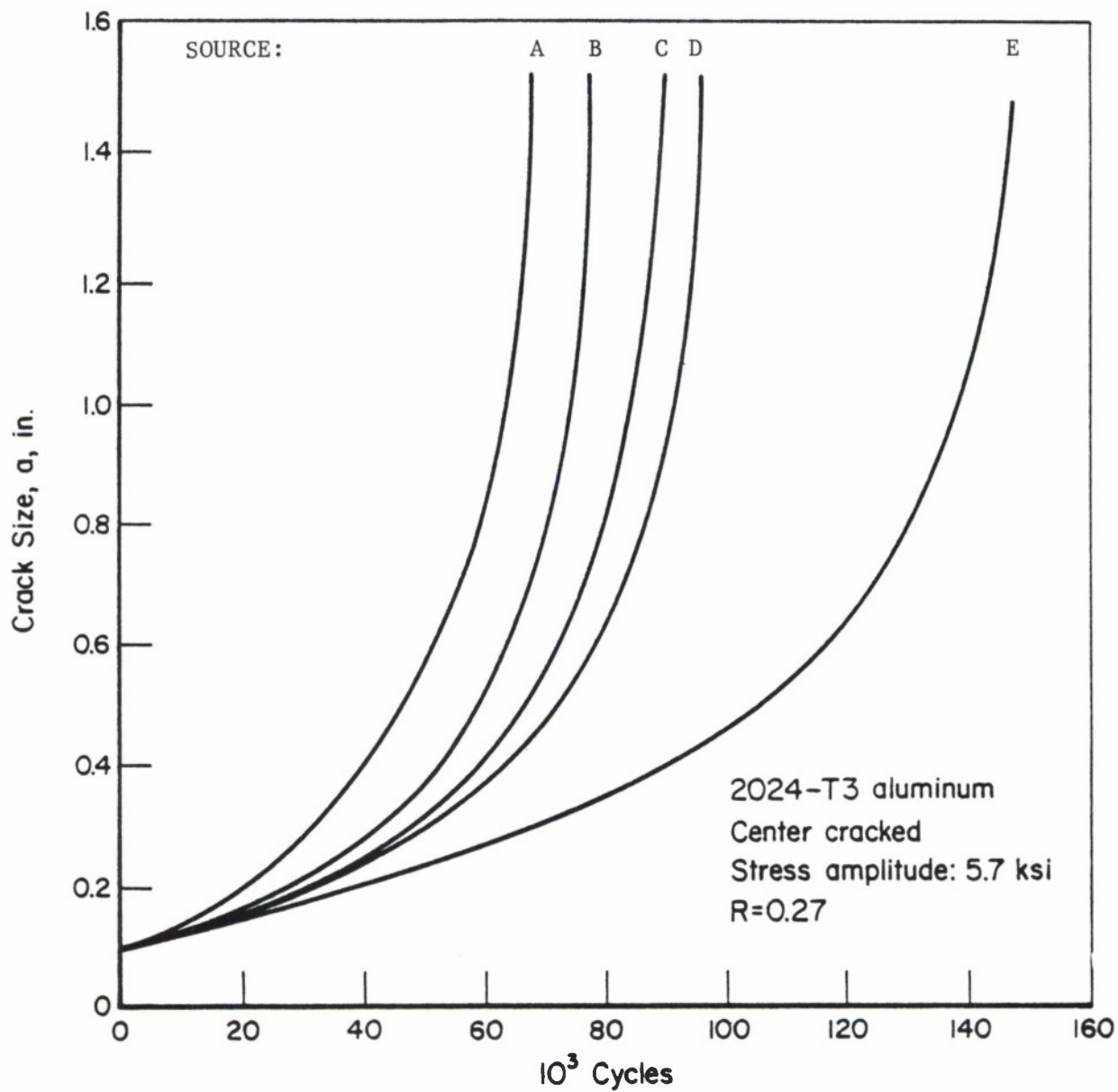


Figure 5.1.8. Possible Variation of Crack Growth in Materials from Different Sources (Reference 12).

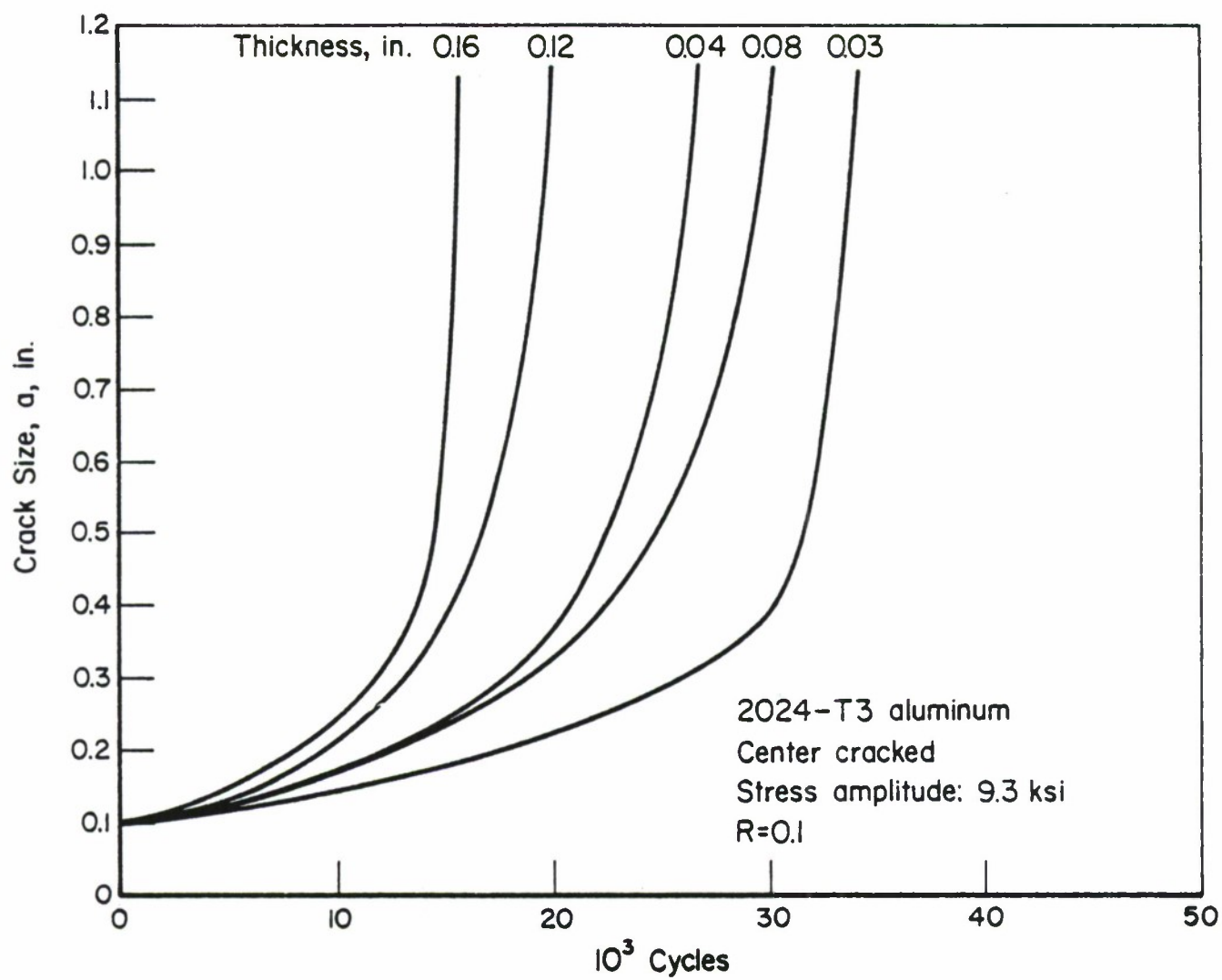


Figure 5.1.9. Example of Effect of Thickness on Crack Growth (Reference 13).

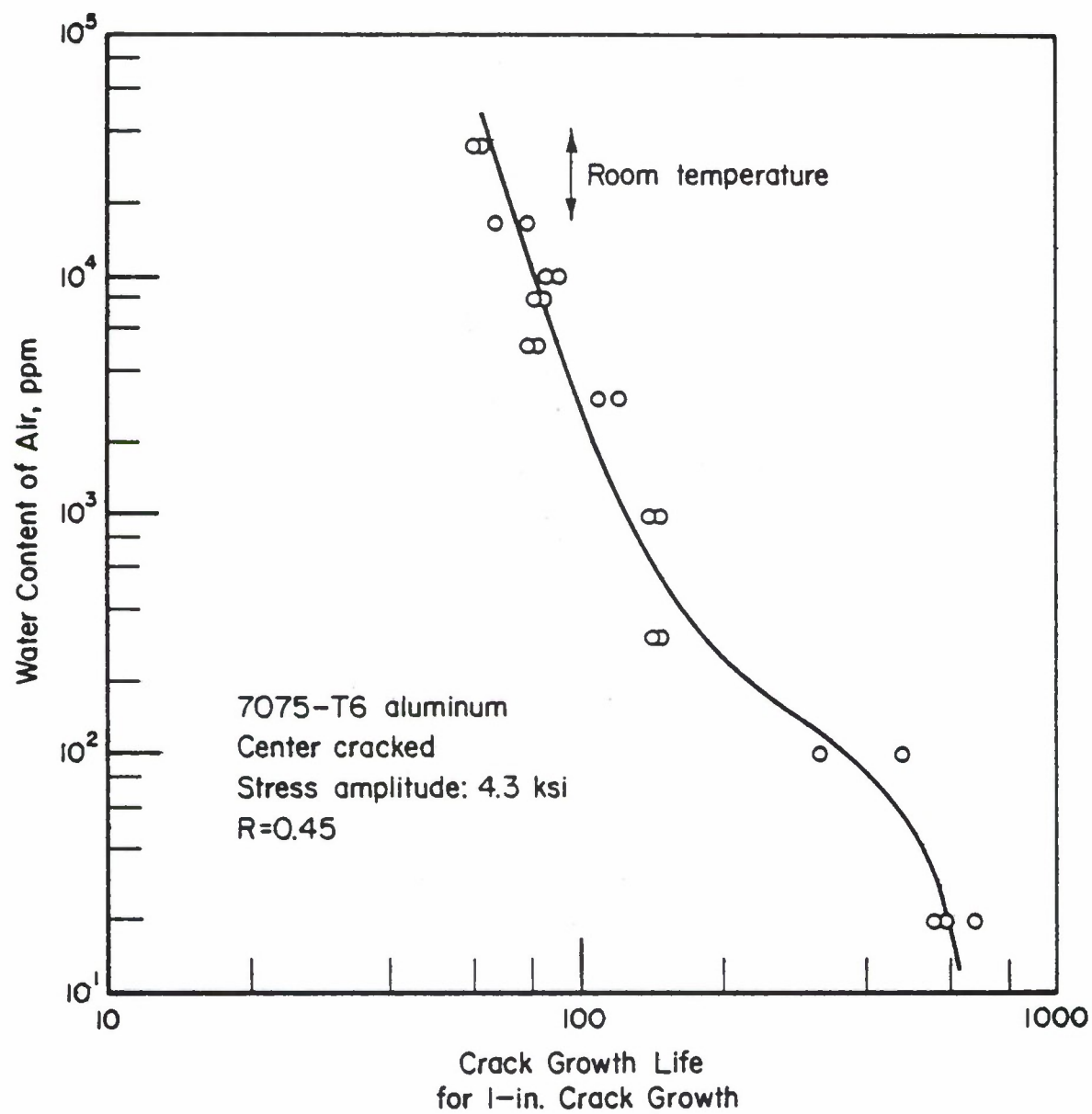


Figure 5.1.10. Effect of Humidity on Fatigue Crack Propagation (Reference 18).

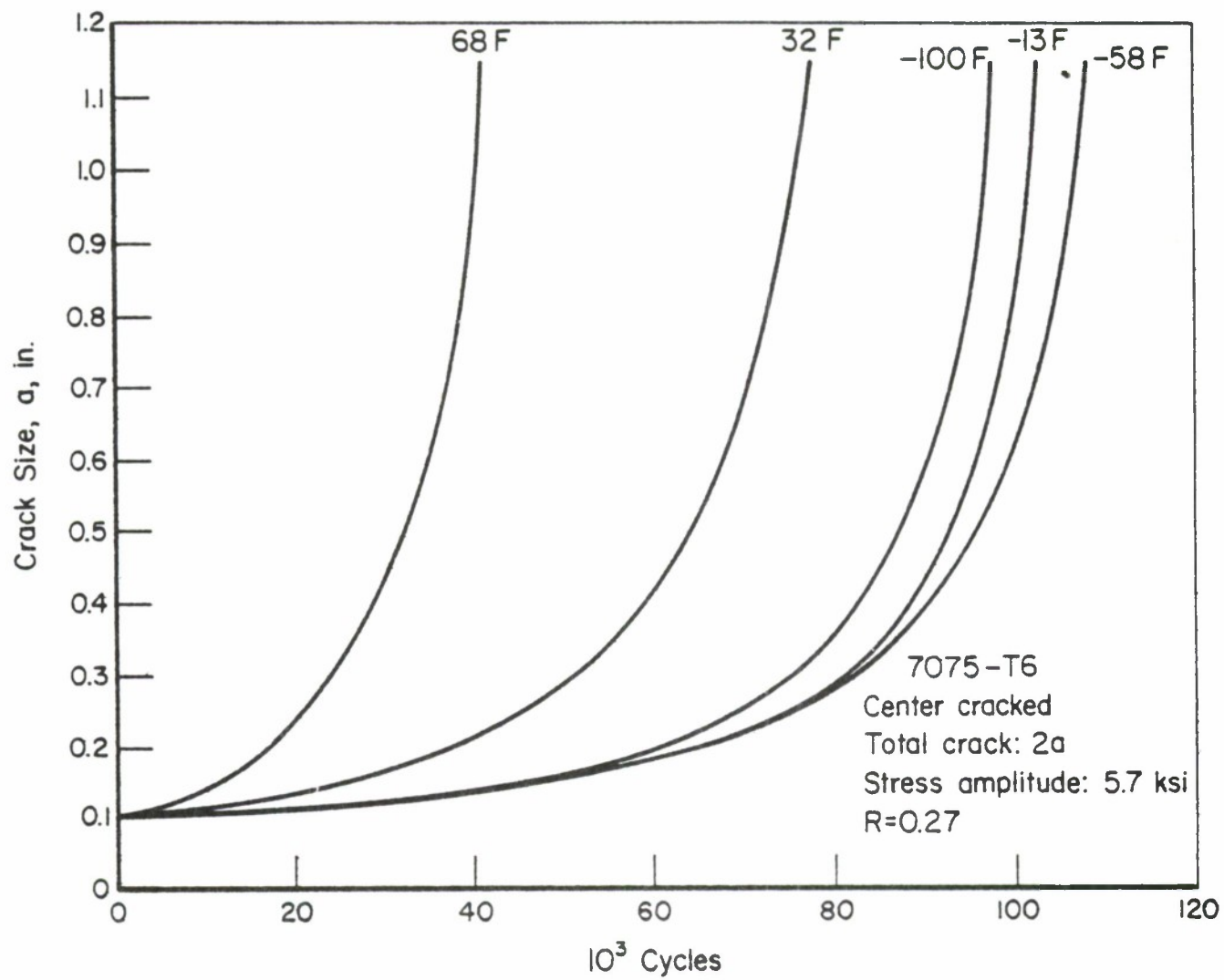


Figure 5.1.11. Example of Temperature Effect on Crack Growth (Reference 29).

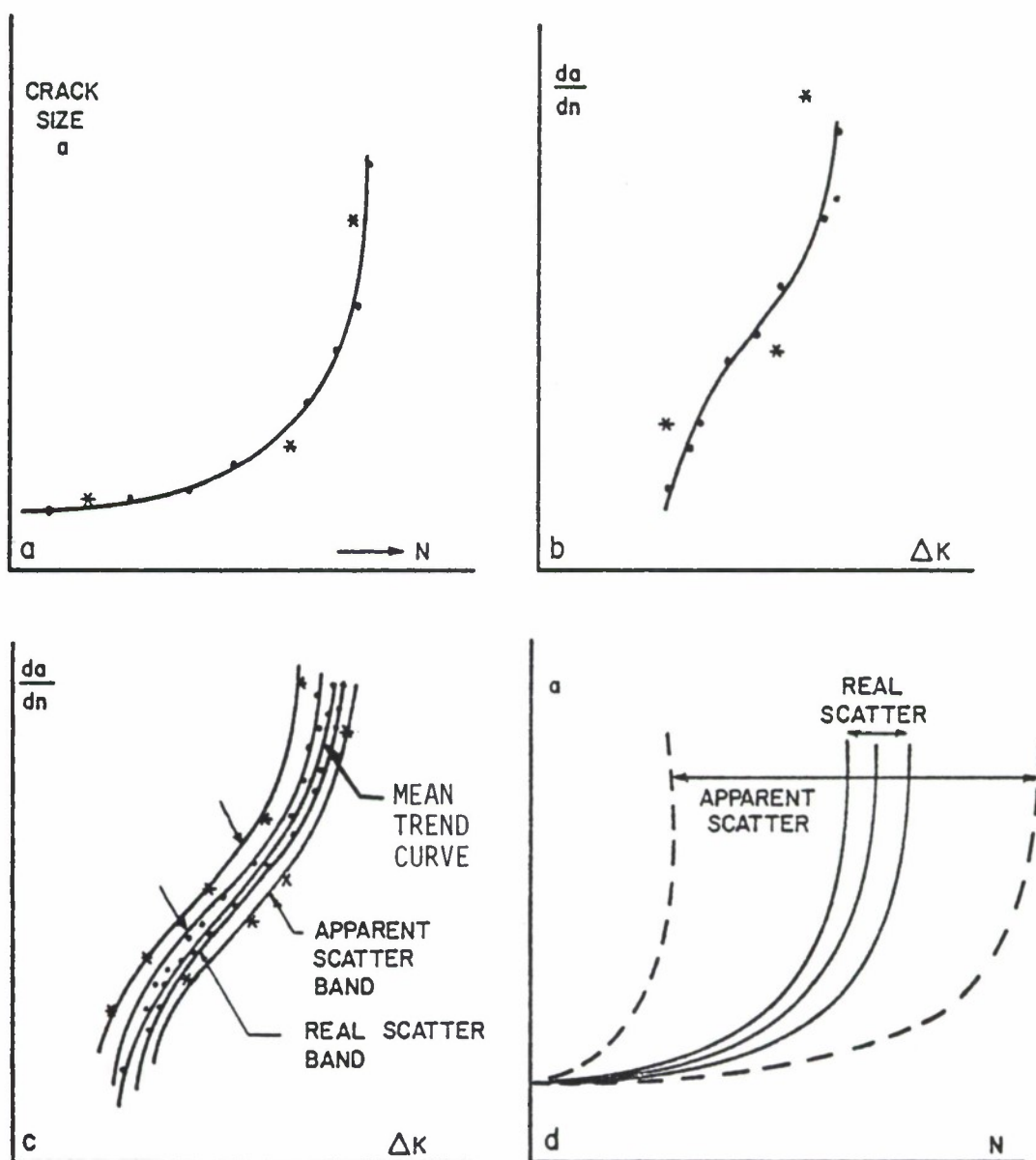


Figure 5.1.12. Crack Growth Data Scatter for Identical Conditions.

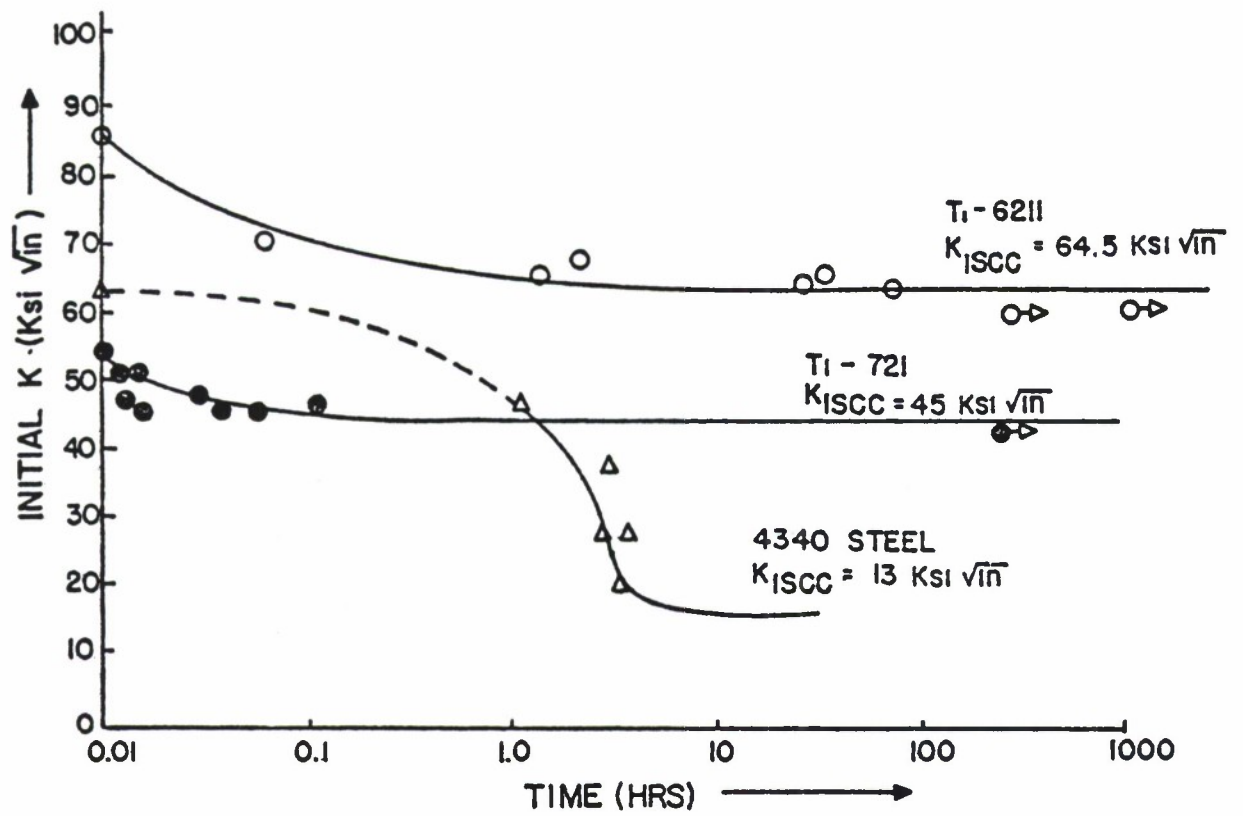


Figure 5.1.13. Stress Corrosion Cracking Data (Reference 33).

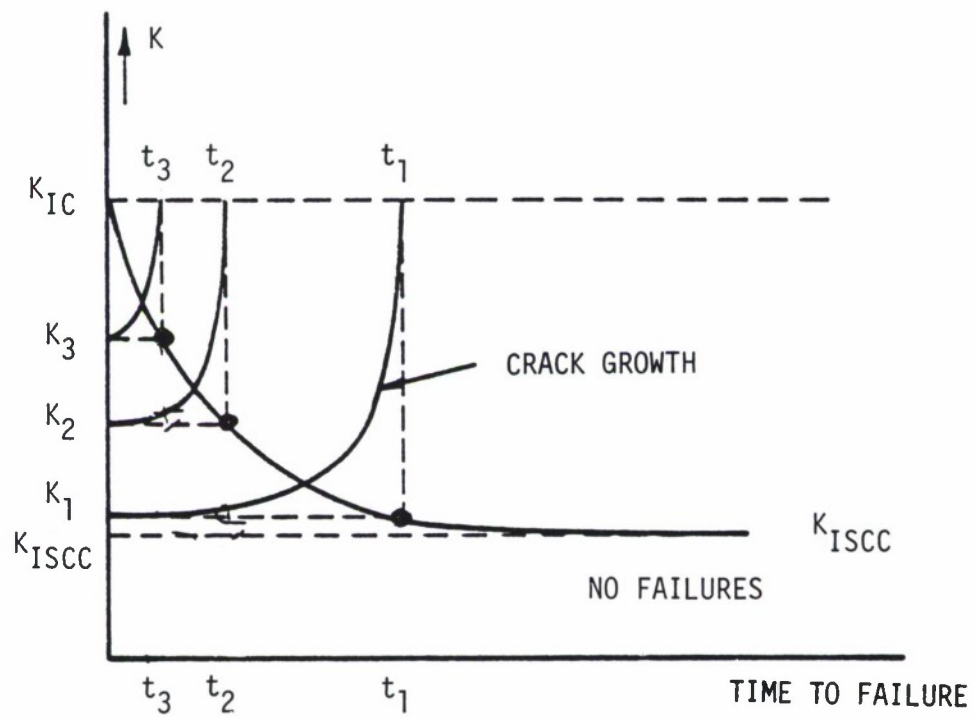


Figure 5.1.14. Stress Corrosion Cracking.

CONDITION	ALUMINUM				7075		K (ISCC)		STAN DEV	FAIL TIME (MIN)	DATE REFER						
	--PRODUCT-- FORM THICK (IN)	TEST SPEC OR STR (KSI)	YIELD ENVIRONMENT	-----SPECIMEN-----		CRACK											
				WIDTH (IN) W	THICK (IN) B	DESIGN (IN) A	LENGTH (IN) A	K (Q) (KSI*SQRT IN)				MEAN					
T352	F	6.00	R. T.	S-L	56.3	3.5	PCT NACL	1.400	0.700	CANT	----	20.10	18.00	----	1972	82675	
T6	P	1.00	R. T.	S-L	73.0	3.5	PCT NACL	4.000	1.000	DCB	----	23.00	19.00	----	1968	84331	
T651	P	3.00	R. T.	L-T	70.2	AIR	74PCT RH	5.000	1.250	TDCB	----	30.00	25.30	----	1971	84361	
T651	P	3.00	R. T.	L-T	70.2	DIST	WATER	5.000	1.250	TDCB	----	30.00	24.00	----	1971	84361	
T651	P	3.00	R. T.	L-T	70.2	3.5	PCT NACL	5.000	1.250	TDCB	----	30.00	28.30	----	1971	84361	
T651	P	2.50	R. T.	S-L	66.7	INDUSTRIAL	ATM	2.000	1.000	CT	----	19.60	10.00	----	1973	86681	
T651	P	2.50	R. T.	S-L	66.7	SALT-DICHRO- MATE-ACETATE		2.000	1.000	CT	----	19.60	5.00	----	1973	86681	
T651	P	2.50	R. T.	S-L	66.7	SEACOAST	ATM	2.000	1.000	CT	----	19.60	10.00	----	1973	86681	
T651	P	1.00	R. T.	S-L	78.0	3.5	PCT NACL	4.000	1.000	DCB	----	21.00	17.00	----	1968	84331	
T651	E	-----	R. T.	T-L	-----	CARBON TET, CCL4		3.000	0.750	DCB	----	-----	10.00	-----	1969	75781	
T651	E	-----	R. T.	T-L	-----	ETHANOL		3.000	0.750	DCB	----	-----	12.00	11.0/ 1.4	-----	1969	75781
T7351	P	4.00	R. T.	T-L	53.2	DIST	WATER	5.000	1.250	TDCB	----	29.00	24.80	----	1972	84361	
T7351	P	4.00	R. T.	T-L	53.2	3.5	PCT NACL	5.000	1.250	TDCB	----	29.00	23.90	----	1972	84361	
T7351	P	2.50	R. T.	S-L	55.1	SEACOAST	ATM	2.000	1.000	CT	----	21.00	20.00	----	1973	86681	
T7351	P	2.50	R. T.	S-L	55.1	SALT-DICHRO- MATE-ACETATE		2.000	1.000	CT	----	21.00	19.00	----	1972	86681	
T7351	P	2.50	R. T.	S-L	55.1	INDUSTRIAL	ATM	2.000	1.000	CT	----	21.00	20.00	----	1973	86681	
T7351	P	1.00	R. T.	S-L	52.0	3.5	PCT NACL	4.000	1.000	DCB	----	24.00	21.00	----	1968	84331	
T76511	E	-----	R. T.	T-L	64.5	3.5	PCT NACL	-----	-----	DCB	----	31.80	29.10	----	1973	86211	

Figure 5.1.15. K_{Isc} Data as Presented by the Damage Tolerant Design (Data) Handbook (Reference 1).

CONDITION/HT: T351
 ENVIRONMENT: WET 3 TIMES/DAY
 SPECIMEN TYPE:
 ORIENTATION: S-L
 YIELD STRENGTH:
 ULT. STRENGTH:

SPECIMEN THK: 1.00"
 SPECIMEN WIDTH: 5.00"
 CRACK LENGTH (A_0):
 K_{ISCC} :
 REFERENCES: 78313, 84284

ALUM

2024

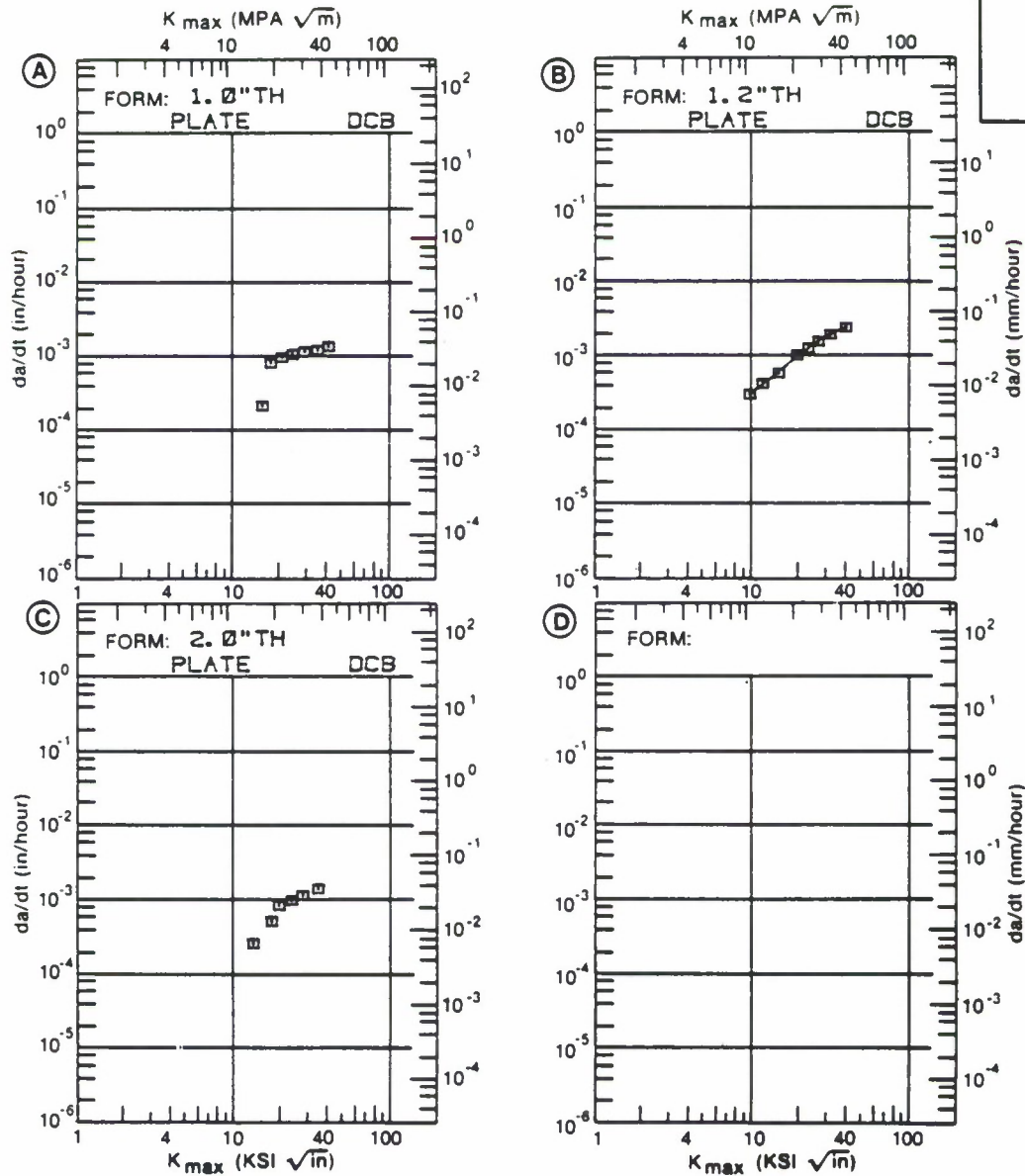


Figure 5.1.16. Stress Corrosion Cracking Rate Data for 2024-T351 Aluminum in the Format of Reference 1.

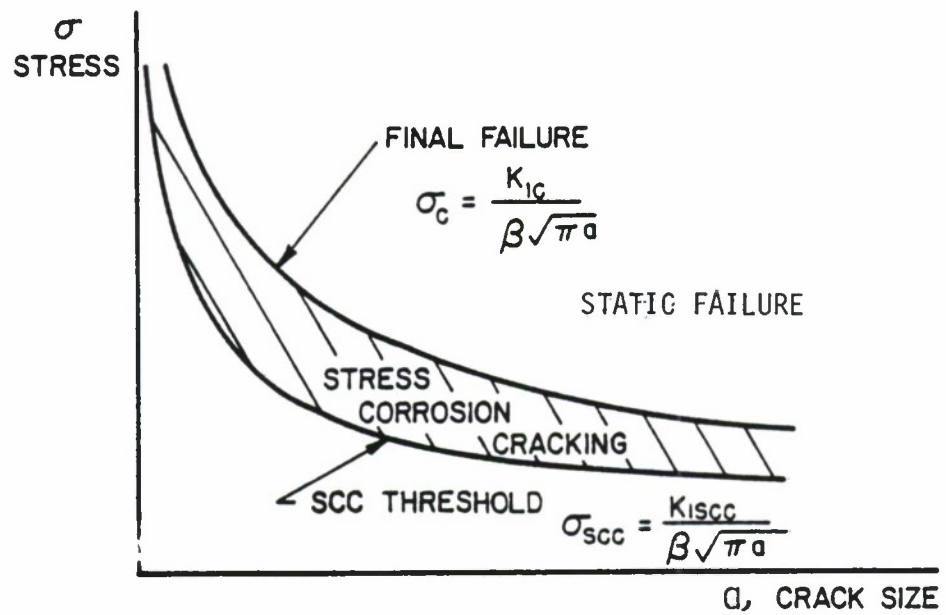


Figure 5.1.17. Stress Required for Stress Corrosion Cracking.

5.2 VARIABLE-AMPLITUDE LOADING

5.2.1 Introduction

Baseline fatigue data are derived under constant-amplitude loading conditions, but aircraft components are subjected to variable amplitude loading. If there were not interaction effects of high and low loads in the sequence, it would be relatively easy to establish a crack-growth curve by means of a cycle-by-cycle integration (see Section 5.2.5). However, crack-growth under variable-amplitude cycling is largely complicated by interaction effects of high and low loads.

In the following sections these interaction effects will be briefly discussed. Crack-growth-prediction procedures which take interaction effects into account will be presented in Section 5.2.5.

5.2.2 Retardation

A high load occurring in a sequence of low-amplitude cycles significantly reduces the rate of crack-growth during the cycles applied subsequent to the overload. This phenomenon is called retardation. Figure 5.2.1 shows a baseline crack-growth curve obtained in a constant-amplitude test⁽⁴⁰⁾. In a second experiment, the same constant-amplitude loading was interspersed with overload cycles. After each application of the overload, the crack virtually stopped growing during many cycles, after which the original crack-growth behavior was gradually restored.

Retardation results from the plastic deformations that occur as the crack propagates. During loading, the material at the crack tip is plastically deformed and a tensile plastic zone is formed. Upon load release, the surrounding material is elastically unloaded and a part of the plastic zone experiences compressive stresses. The larger the load, the larger the zone of compressive stresses. If the load is repeated in a constant amplitude sense, there is no observable direct effect of the residual stresses on the crack-growth behavior; in essence, the process of growth is steady state. Measurements have indicated, however, that the plastic deformations occurring at the crack tip remain as the crack propagates so that the crack surfaces open and close at non zero (positive) load levels. These observations have given rise to constant amplitude crack-growth models referred to as closure models⁽⁴¹⁾ after the concept that the crack may be closed during part of the load cycle.

When the load history contains a mix of constant amplitude loads and discretely applied higher level loads, the patterns of residual stress and plastic deformation are perturbed. As the crack propagates through this perturbed zone under the constant amplitude loading cycles, it grows slower (the crack is retarded) than it would have if the perturbation had not occurred. After the crack has propagated through the perturbed zone, the crack growth rate returns to its typical steady state level. Two basic models have been proposed to describe the phenomenon

of crack retardation. The first model is based on the concept of the compressive residual stress perturbation and the second on the concept of plastic deformation (enhanced crack wedging - more closure).

If the tensile overload is followed by a compressive overload, the material at the crack tip may undergo reverse plastic deformation and this reduces the residual stresses. Thus, a negative overload in whole or in part annihilates the beneficial effect of tensile overloads, as is also shown in Figure 5.2.1.

Retardation depends upon the ratio between the magnitude of the overload and subsequent cycles. This is illustrated in Figure 5.2.2. Sufficiently large overloads may cause total crack arrest. Hold periods at zero stress can partly alleviate residual stresses and thus reduce the retardation effect^(27,42), while hold periods at load increase retardation. Multiple overloads significantly enhance the retardation. This is shown in Figure 5.2.3.

5.2.3 Retardation Under Spectrum Loading

An actual service load history contains high- and low-stress amplitudes and positive and negative "overloads" in random order. Retardation and annihilation of retardation becomes complex, but qualitatively the loading produces behavior that is similar to a constant-amplitude history with incidental overloads. The higher the maximum

stresses in the service load history, the larger the retardation effect during the low-amplitude cycles. Negative stress excursions reduce the retardation effect and tend to enhance crack-growth. These effects have been documented in various sources (e.g., References 43-49); a few examples are now presented.

When the magnitude of the higher loads are reduced (or clipped) without eliminating the cycle, i.e., higher loads are reset to a defined lower level, the cracking rates are observed to speed up as shown in Figure 5.2.4^(43,44). Figure 5.2.4 describes the crack growth life results for a study in which a (random) flight-by-flight stress history was systematically modified by "clipping" the highest load excursions to the three levels shown.

In References 43 and 44, it was also observed that negative stress excursions reduce the retardation effect and omission of the ground-air-ground (G-A-G) cycles (negative loads) in the tests with the highest clipping level resulted in a longer crack growth life for the same amount of crack growth.

Figure 5.2.5 shows the importance of load sequence. The crack-propagation life for random load cycling is shown at the top. Ordering the sequences of the loads, lo-hi, lo-hi-lo, or hi-lo increases the crack-growth life, the more so for larger block sizes. Hence, ordering should only be permitted if the block size is small. Lo-hi ordering gives more conservative results than hi-lo ordering. In the latter case, the retardation effect caused by the highest load is effective during all subsequent cycles.

5.2.4 Retardation Models

Some mathematical models have been developed to account for retardation in crack-growth-integration procedures. All models are based on simple assumptions, but within certain limitations and when used with experience, each model will produce results that can be used with reasonable confidence. The two yield zone models by Wheeler⁽⁵⁰⁾ and by Willenborg, et al⁽⁵¹⁾, and a crack-closure model by Bell and Creager⁽⁵²⁾ will be briefly discussed. Detailed information and applications of closure models can be found in References⁽⁵²⁻⁵⁵⁾.

Wheeler defines a crack-growth reduction factor, C_p :

$$\left(\frac{da}{dN}\right)_r = C_p f(\Delta K), \quad (5.2.1)$$

where $f(\Delta K)$ is the usual crack-growth function, and (da/dN) is the retarded crack-growth rate. The retardation factor, C_p is given as

$$C_p = \left(\frac{r_{pi}}{a_{oL} + r_{poL} - a_i}\right)^m, \quad (5.2.2)$$

in which (see Figure 5.2.6):

r_{pi} is the current plastic zone size in the i th cycle under consideration

a_i is the current crack size

r_{poL} is the plastic size generated by a previous higher load excursion

a_{oL} is the crack size at which the higher load excursion occurred

m is an empirical constant.

There is retardation as long as the current plastic zone is contained within a previously generated plastic zone; this is the fundamental assumption of yield zone models.

Some examples of crack-growth predictions made by means of the Wheeler model are shown in Figure 5.2.7. Selection of the proper value for the exponent m will yield adequate crack-growth predictions. In fact, one of the earlier advantages of the Wheeler model was that exponent m could be tailored to allow for reasonably accurate life predictions of spectrum test results. Through the course of time, it has become recognized, however, that the exponent m was dependent on material, crack size, and stress-intensity factor level as well as spectrum. The reader is cautioned against using the Wheeler model for service life predictions based on limited amounts of supporting test data and more specifically against estimating the service life of structures with spectra radically different from those for which the exponent m was derived. Estimates made without the supporting data required to tailor the exponent m can lead to inaccurate and unconservative results.

The Willenborg model also relates the magnitude and extent of the retardation factor to the overload plastic zone. The extent of the retardation is handled exactly the same as that of the Wheeler model. The magnitude of the retardation factor is established through the use of an effective stress-intensity factor that senses the differences in

compressive residual stress state caused by differences in load levels. The effective stress-intensity factor (K_i^{eff}) is equal to the typical remote stress-intensity factor (K_i) for the i th cycle minus the residual stress-intensity factor (K_R):

$$K_i^{\text{eff}} = K_i - K_R \quad (5.2.3)$$

where in the original formulation (References 51,56-58)

$$K_R = K_R^W = K_{\text{max}}^{\text{oL}} \sqrt{1 - \frac{a_i - a_{\text{oL}}}{r_{\text{poL}}}} - K_{\text{max},i} \quad (5.2.4)$$

in which (see Figure 5.2.6):

a_i is the current crack size

a_{oL} is the crack size at the occurrence of the overload

r_{poL} is the yield zone produced by the overload

$K_{\text{max}}^{\text{oL}}$ is the maximum stress intensity of the overload

$K_{\text{max},i}$ is the maximum stress intensity for the current cycle.

The equations show that retardation will occur until the crack has generated a plastic zone size that reaches the boundary of the overload yield zone. At that time, $a_i - a_{\text{oL}} = r_{\text{poL}}$ and the reduction becomes zero.

Equation 5.2.3 indicates that the complete stress-intensity factor cycle, and therefore, its maximum and minimum levels ($K_{\text{max},i}$ and $K_{\text{min},i}$), are reduced by the same amount (K_R). Thus, the retardation effect is sensed by the change in the effective stress ratio calculated by

$$R_{eff} = \frac{K_{min,i}^{eff}}{K_{max,i}^{eff}} = \frac{K_{min,i}^{-K_R}}{K_{max,i}^{-K_R}} \quad (5.2.5)$$

since the range in stress-intensity factor is unchanged by the uniform reduction. Thus, for the i th load cycle, the crack growth increment (Δa_i) is:

$$\Delta a_i = \frac{da}{dN} = f(\Delta K, R_{eff}) \quad (5.2.6)$$

For many of the early calculations with the Willenborg model, it was assumed that R_{eff} was never less than zero and that $\Delta K = K_{max,i}^{eff}$ when R_{eff} was calculated to be less than zero. Recent evidence, however, supports the calculations of R_{eff} as given by Equation 5.2.5 and the use of a negative stress ratio cut-off in the crack growth rate calculation (Equation 5.2.6) for more accurate modeling of crack growth behavior.

Another problem that was identified with the original Willenborg model was that it was always assigned the same level of residual stress effect independent of the type of loading. In particular, it can be noted (through the use of Equation 5.2.3 and 5.2.4) that the model predicts that $K_{max,i}^{eff} = 0$, and therefore crack arrest, immediately after overload if $K_{max}^{OL} = 2 K_{max,i}$. That is, if the overload is twice as large as (or larger than) the following loads, the crack arrests. To account for the observations of continuing crack propagation after overloads larger than a factor of two or more, Gallagher and Hughes⁽⁵⁷⁾ introduced an empirical (spectra/material) constant into the calculations. Specifically, they

suggested that

$$K_R = \phi K_R^W \quad (5.2.7)$$

where ϕ is given by

$$\phi = \frac{1 - \frac{K_{\max,th}}{K_{\max,i}}}{S^{OL} - 1} \quad (5.2.7a)$$

There are two empirical constants in Equation 5.2.7a: $K_{\max,th}$ which is the threshold stress-intensity factor level associated with zero fatigue crack growth rates (see Section 5.1.3), and S^{OL} which is the overload (shut-off) ratio required to cause crack arrest for the given material. This ratio is affected by the type of underload/overload cycle as well as the frequency of overload cycle occurrence. Results of some life predictions made using what has become to be called the "Generalized" Willenborg model are presented in Figure 5.2.8 (Reference 59).

One of the earliest crack-closure models developed for aircraft structural applications is attributed to Bell and Creager⁽⁵²⁾. The closure model makes use of a crack-growth-rate equation based on an effective stress-intensity range ΔK_{eff} . The effective stress intensity is the difference between the applied stress intensity and the stress intensity for crack closure. Some examples of predictions made with the model are presented in Figure 5.2.9. The final equations contain many experimental constants, which reduces the versatility of the model and make it difficult to apply. Recent work by Dill and Saff⁽⁶⁰⁾ shows that

the closure model can be simplified to the point of practicality while retaining a high level of accuracy in life prediction.

Crack-growth calculations are the most useful for comparative studies, where variations of only a few parameters are considered (i.e., trade-off studies to determine design details, design stress levels, material selection, etc.). The predictions must be verified by experiments. (See Analysis Substantiation Tests in Section 7.3). Example calculations of crack-growth curves will be given in Section 5.4.

Other factors contributing to uncertainties in crack-growth predictions are:

- Scatter in baseline da/dN data
- Unknowns in the effects of service environment
- Necessary assumptions on flaw shape development (Section 5.4.4)
- Deficiencies in K calculation (Section 5.4.4)
- Assumptions on interaction of cracks (see 5.4.5)
- Assumptions on service stress history (see 5.3).

In view of these additional shortcomings of crack-growth predictions, the shortcomings of a retardation model become less pronounced; therefore, no particular retardation model has preference over the others. From a practical point of view, the Generalized Willenborg model is easier to use since it contains a minimum number of empirical constants.

5.2.5 Integration Routines

The determination of a crack growth increment due to any particular stress history depends upon an integration of the growth rate relation such as given by equations 5.1.2-5.1.4. Four general methods are available for this purpose.

The first approach is based on extensive spectrum crack growth data. Tests which incorporate the important stress levels, part geometry, crack shape details and loading sequences are run to determine the effect of the particular variables of interest on the component life.

A second approach, and one used extensively, is the cycle-by-cycle crack growth analysis where crack rates are integrated over the crack length of interest as a function of stress and crack length (61-62).

A third approach is based on the statistical stress-parameter-characterization. The actual service stress histories are replaced with equivalent constant amplitude stress histories for the analytical prediction of component life (17).

A fourth approach, recently developed, utilizes a crack-incrementation scheme to analytically generate "miniblock" crack growth rate behavior prior to predicting life. It combines some features of the first three methods (61-63).

The application of the second through fourth approaches requires methods for integrating the crack growth rate relations requires the knowledge of the following items:

- (1) An initial flaw distribution,
- (2) The aircraft loading spectrum,
- (3) Constant amplitude crack growth rate material properties,
- (4) Crack tip stress-intensity factor analysis,
- (5) A damage integrator model relating crack growth to applied stress and which accounts for load-history interactions,
- (6) The criteria which establishes the life-limiting end point of the calculation.

These items are described in detail in Section 1.4 of this handbook. The basic damage integrating equation is also presented as equation 1.4.1 but is repeated here:

$$a_{cr} = a_o + \sum_{j=1}^{t_f} \Delta a_j \quad (1.4.1R)$$

where Δa_j is the growth increment associated with the j^{th} time increment, a_o is the initial crack length, a_{cr} is the critical crack length and t_f is the life of the structure. The determination of t_f is the objective of this equation.

Of the integration methods described above, the second and third are most frequently used. The generation of the data required for the first method is very expensive and is only recommended for extremely critical parts.

The second method, the cycle-by-cycle integration method, uses a type of integrating relation whereby the effect of each cycle is considered separately. This is generally the least efficient method, but if the spectrum under consideration cannot be considered as statistically repetitive, it may be the most accurate of the analytical methods. This method is covered in detail in subsection 5.2.6.

The third method, using a statistical characterization of a crack growth parameter is based on the similarity of certain variable amplitude crack growth behavior to the constant amplitude functional relationship;

$$\frac{da}{dF} = C (\bar{K})^P \quad (5.2.8)$$

where (da/dF) is the flight-by-flight crack growth behavior and \bar{K} is a stress-intensity factor parameter that is derived using the product of a statistically characterizing stress parameter $(\bar{\sigma})$ and the stress-intensity factor coefficient (K/σ) , i.e.,

$$\bar{K} = \bar{\sigma} \cdot (K/\sigma) \quad (5.2.9)$$

The statistically characterizing parameters that have been employed in the past to some success are derived using a root mean square (RMS) or similar type analysis of the stress range or stress maximum. The crack growth behavior of both fighter and transport aircraft stress histories have been described using various forms of equation 5.2.8.

One might imply from equations 5.2.8 and 5.2.9 that the use of a single stress characterizing parameter for stress histories would allow one to utilize equivalent constant amplitude histories to derive the same crack growth rate behavior. Unfortunately, relating constant amplitude behavior to variable amplitude behavior has not been that successful.

The damage integration Equation (1.4,1R) is now expressed for the flight as

$$a_k = a_o + \sum_{j=1}^{N_f} \Delta a_j \quad (5.2.10)$$

where N_f is the number of flights corresponding to crack length a_k , and Δa_j is computed from Equation 5.2.8 evaluated for the given conditions. The parameters C and p of Equation 5.2.8 are determined by a least squares curve fit to previously determined data. The value that comes from employing the third method comes from the fact that a somewhat limited variable amplitude data base might be extended to cover other crack lengths, structural geometry, or stress level differences.

The fourth approach provides an analytical extension of the cycle-by-cycle analysis to predict flight-by-flight crack growth rates. In essence, this approach combines some of the best features of the other three methods. The basic element in this analysis is what is referred to as a miniblock which is taken to be a flight (includes takeoff, landing and all intermediate stress events) or a group of flights. The approach hinges on the identification of the statistically repeating stress group that approximates the loading and sequence effects for the complete spectrum.

The basic damage integration equation can be written in the miniblock form to compute the crack increment (Δa) due to application of N_G Flights:

$$\Delta a = a_k - a_o = \sum_{j=1}^{N_G} \sum_{i=1}^{N_j} (\Delta a_i) \quad (5.2.11)$$

where there are N_j stress cycles in the j^{th} flight. The most direct method for applying the equation is called the simple crack-incrementation-miniblock approach. Successive crack increments are obtained at successively larger initial-crack-lengths. Figure 5.2.10 illustrates this method. The resulting values of $\Delta a/\Delta F$ and the corresponding K_{max} values are fit with a curve of the desired type, usually similar to Equation 5.2.8, which can now be used to compute life.

An alternate method, called the statistical crack-incrementation-miniblock approach, is illustrated in Figure 5.2.11. This method allows evaluation of the effect of miniblock group-to-group variation in the crack growth rate behavior. A number of different miniblock groups are used at each initial crack length. A curve can be fit through the mean $\Delta a/\Delta F$ vs. \bar{K}_{max} values and the variation of $\Delta a/\Delta F$ at each K_{max} can be observed. Confidence limits can be determined for each set of data.

The fourth approach provides a more efficient integration scheme than the cycle-by-cycle analysis. However, its use is determined by the type of stress history that has to be integrated.

In summary, there are a number of integration schemes available. These schemes all employ modeling approaches based on either limited or extensive variable amplitude data bases so that the analyst might properly account for loading and sequence effects in the most direct and most accurate manner.

5.2.6 Cycle-by-Cycle Analysis

Several computer programs are available for general use that include one or more of the retardation models in a crack-growth-integration scheme. The most well known of these is CRACKS^{*(64)}, the latest version of which should be used. The user has the option of using any of the three retardation models discussed in the previous section. Most airframe companies, however, have their own inhouse computer program for performing variable-amplitude fatigue life calculations.

In general, the crack-growth-damage-integration procedure consists of the following steps schematically outlined in Figure 5.2.12.

- Step 1. The initial crack size follows from the damage tolerance assumptions as a_1 . The stress range in the first cycle is $\Delta\sigma_1$ (See Section 5.4). Then determine $\Delta K_1 = \beta\Delta\sigma_1\sqrt{\pi a_1}$ by using the appropriate β for the given structural geometry and crack geometry. (Computer programs frequently have a library of stress-intensity factors or schemes for tabular data input).
- Step 2. Determine $(da/dN)_1$, at ΔK_1 from the $da/dN - \Delta K$ baseline information, taking into account the appropriate R value. (The $da/dN - \Delta K$ baseline information may use one of the crack-growth equations discussed in Section 5.1.3. The computer program may contain options for any of these equations, or it may use data in tabular form and

* Available through AFWAL/FIBEC, Fatigue and Fracture Group.

interpolate between data points). The crack extension

Δa_1 in cycle 1 is

$$\Delta a_1 = \left(\frac{da}{dN} \right)_1 \times 1 .$$

The new crack size will be $a_2 = a_1 + \Delta a_1$.

Step 3. The extent of the yield zone in Cycle 1 is determined as

$$Y_2 = a_{oL} + r_{pL}, \text{ where } a_{oL} = a_1$$

$$\text{with } r_{pL} = \frac{1}{2\pi} \left(\frac{K_{\max,1}}{\sigma_{ys}} \right)^2 \text{ for plane stress}$$

$$\text{or } r_{pL} = \frac{1}{4\sqrt{2}\pi} \left(\frac{K_{\max,1}}{\sigma_{ys}} \right)^2 \text{ for plane strain.}$$

Step 4. The crack size is now a_2 . The stress range in the next cycle is $\Delta \sigma_2$. Calculate ΔK with $\Delta K_2 = \beta \Delta \sigma_2 \sqrt{\pi a_2}$.

Step 5. Calculate the extent of the yield zone

$$Y_{22} = a_2 + r_{p2} .$$

Step 6. If $Y_{22} < Y_2$ calculate C_p according to Equation 5.2.2 when using the Wheeler model, or calculate K_{\max}^{eff} or K_{\min}^{eff} and R_{eff} according to Equations 5.2.3, 5.2.4, 5.2.5, and 5.2.7 when using the Generalized Willenborg model. Skip Steps 7 and 8, go to Step 9.

Step 7. If $Y_{22} \geq Y_2$, determine $(da/dN)_2$ from ΔK_2 . Determine the new crack size

$$a_3 = a_2 + \Delta a_2 = a_2 + \left(\frac{da}{dN} \right)_2 \times 1 .$$

Step 8. Replace Y_2 by Y_{22} which is now called Y_2 . Replace $a_{oL} = a_1$ by $a_{oL} = a_2$. Skip Step 9, go to Step 10.

Step 9. When using the Wheeler model, determine the amount of crack growth on the basis of ΔK_2 from the $da/dN - \Delta K$ data. Find the new crack size from

$$a_3 = a_2 + \Delta a_2 + C_p \left(\frac{da}{dN} \right)_2 \times 1.$$

When using the Generalized Willenborg model, determine the amount of crack growth using the ΔK and R_{eff} value determined in Step 6 from the $da/dN - \Delta K$ data. Determine the new crack size as

$$a_3 = a_2 + \Delta a_2 = a_2 + \left(\frac{da}{dN} \right)_2 \times 1.$$

Step 10. Repeat Steps 4 through 9 for every following cycle, while for the i th cycle replacing a_2 by a_i and a_3 by a_{i+1} .

This routine of cycle-by-cycle integration is not always necessary.

The integration is faster if the crack size is increased stepwise in the following way.

- At a certain crack size, the available information is a_i , a_{oL} , Y_2 .
- Calculate Δa_i for the i_{th} cycle in the same way as in Steps 4 through 9.
- Calculate $\Delta a_{j+1}, \dots, \Delta a_j, \dots, \Delta a_n$ for the following cycles but let the current crack size remain a_i constant. This eliminates recalculation of β every cycle.

- Calculate Y_{2k} for every cycle. If $Y_{2k} > Y_2$, then replace Y_2 by Y_{2k} and call it Y_2 . Then replace a_{oL} by a_i and call it a_{oL} .
- Sum the crack-growth increments to give

$$\Delta a = \sum_{k=i}^j \Delta a_k.$$

- Continue increasing j until Δa exceeds a previously determined size or until $j = n$ and the cycles are exhausted. Then increment the crack size by

$$a = a_i + \Delta a,$$

and repeat the procedure.

A reasonable size for the crack-growth increment is $\Delta a = \frac{1}{20} a_i$; this choice of increment typically keeps the change in K small. It can also be based on the extent of the yield zone, e.g., $\Delta a = \frac{1}{10} (Y_2 - a_i)$. The advantage of the incremental crack-growth procedure is especially obvious if series of constant-amplitude cycles occur. Since the crack size (a_i) is fixed, the stress intensity does not change. Hence, each cycle produces the same amount of growth. This means that all n constant-amplitude cycles can be treated as one cycle to give

$$\Delta a = n \frac{da}{dN}.$$

The integration scheme is a matter of individual judgement, but may be dictated by available computer facilities.

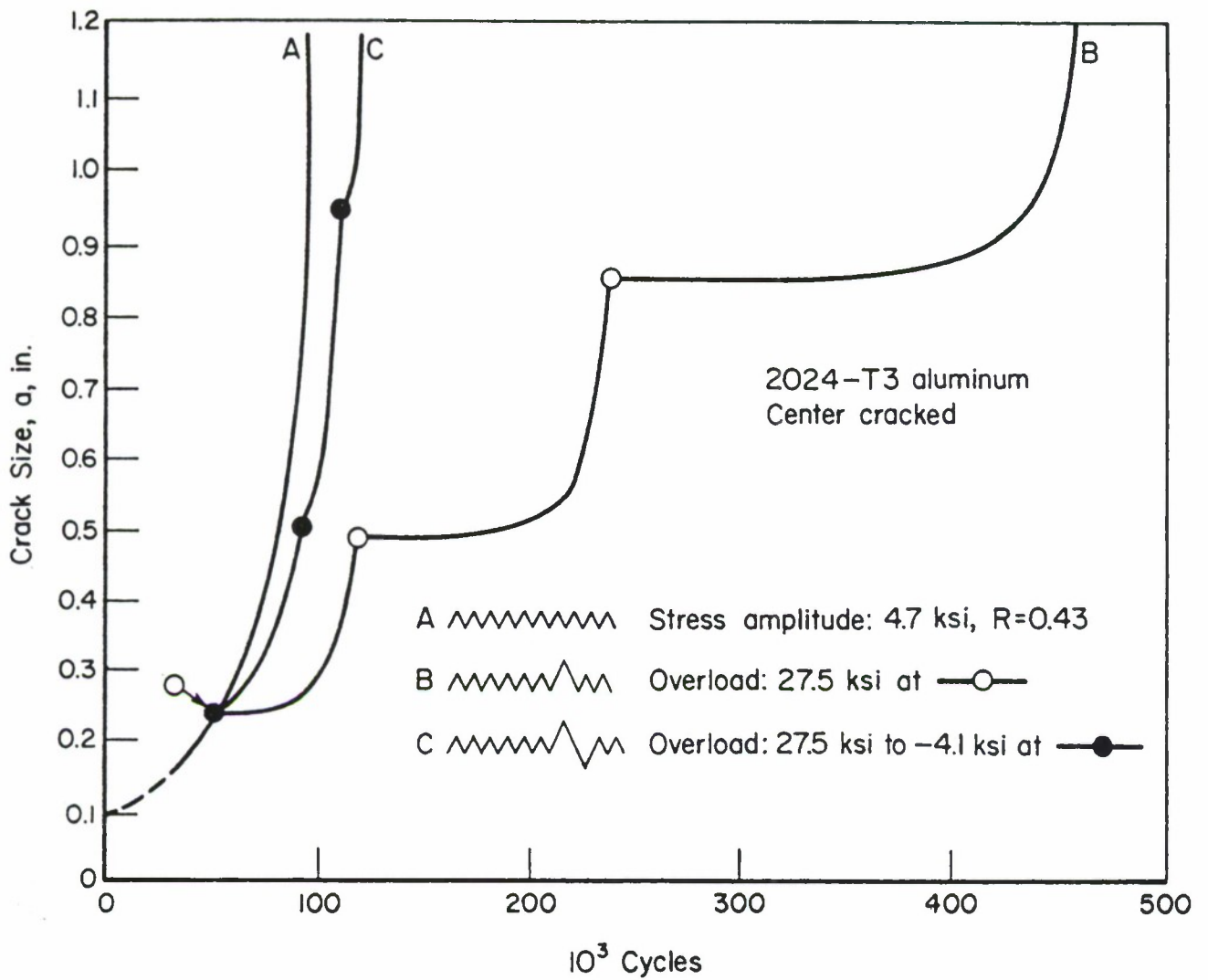


Figure 5.2.1. Retardation Due to Positive Overloads, and Due to Positive-Negative Overload Cycles (Ref. 40).

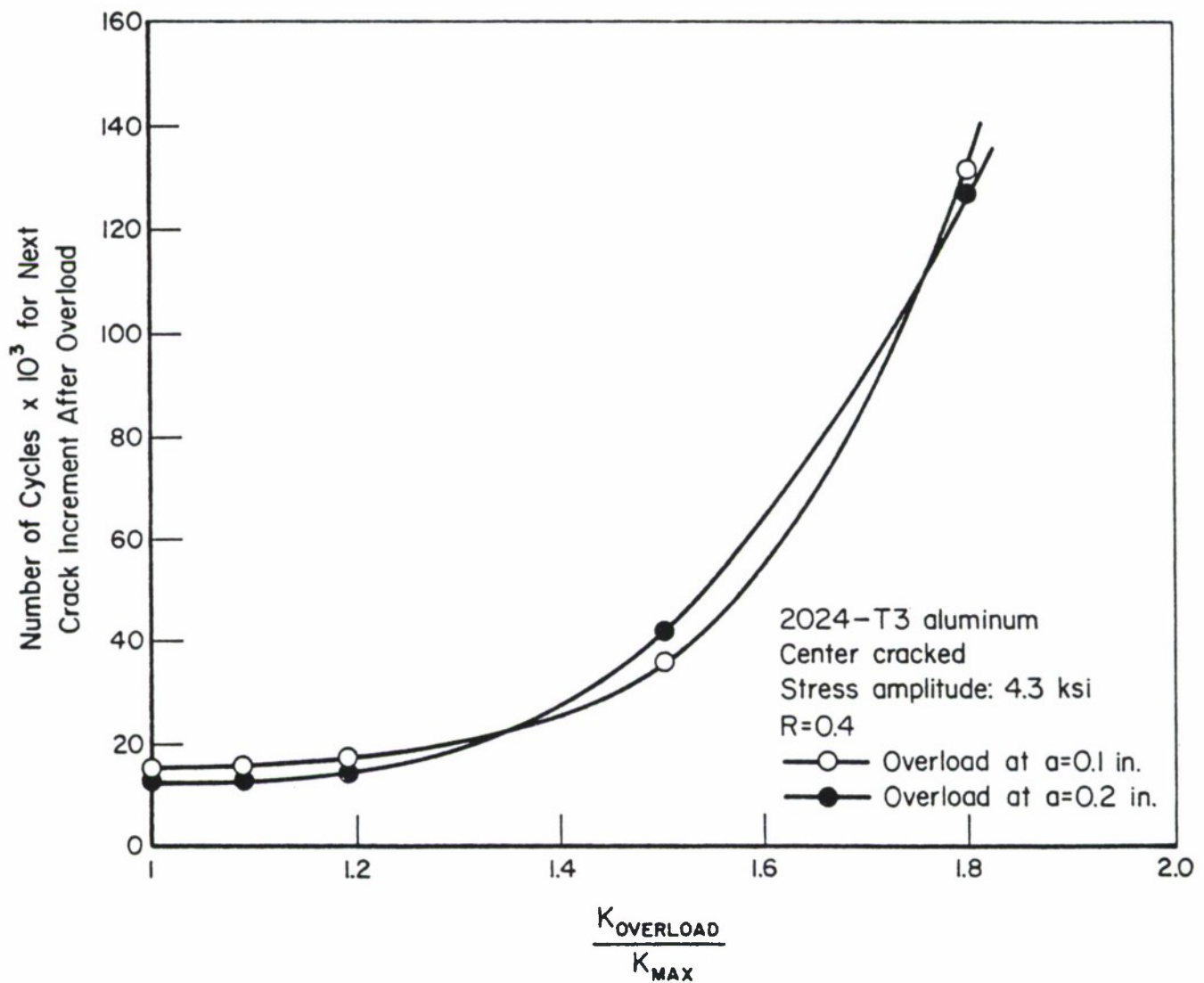


Figure 5.2.2. Effect of Magnitude of Overload on Retardation (Ref. 27).

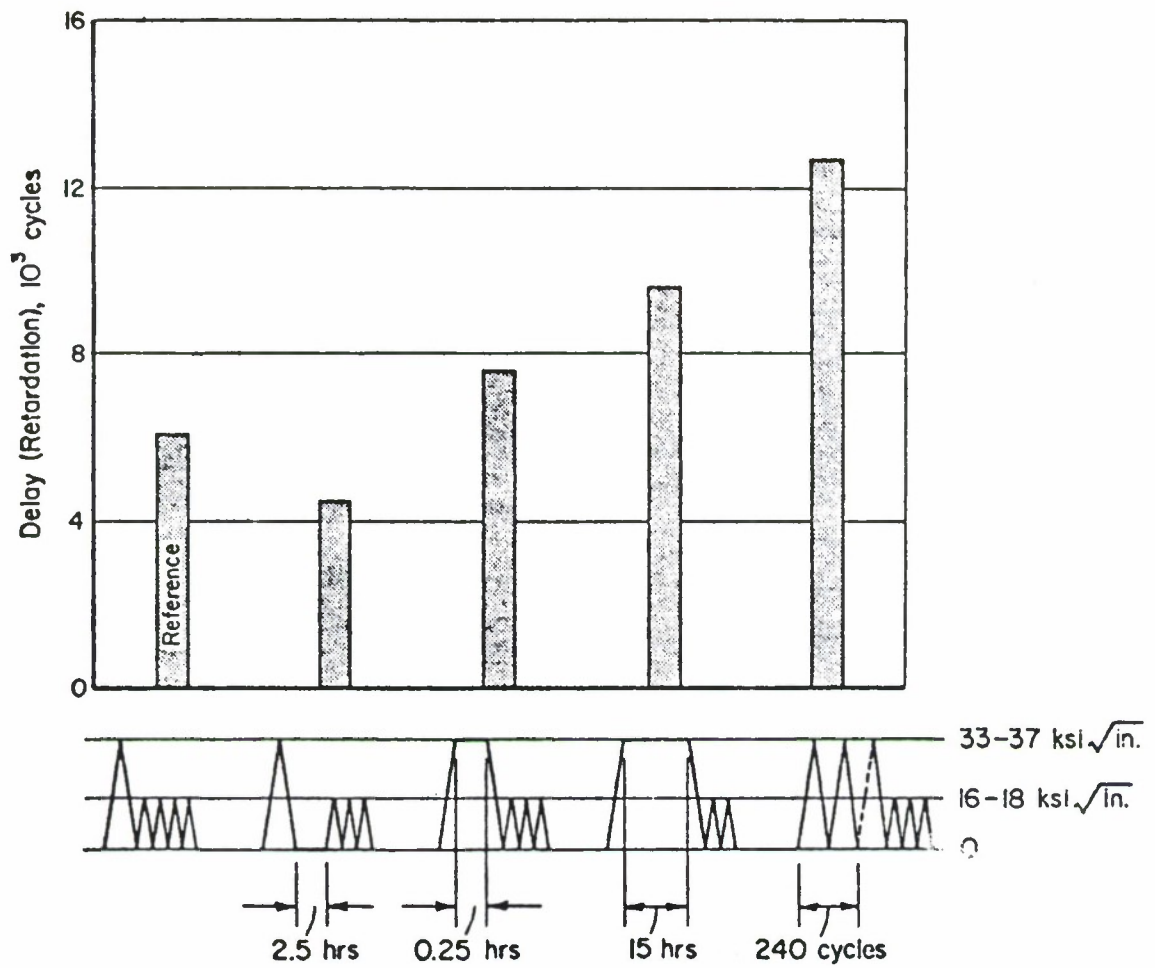


Figure 5.2.3. Retardation in Ti-6V-4Al; Effect of Hold Periods and Multiple Overloads (Ref. 42).

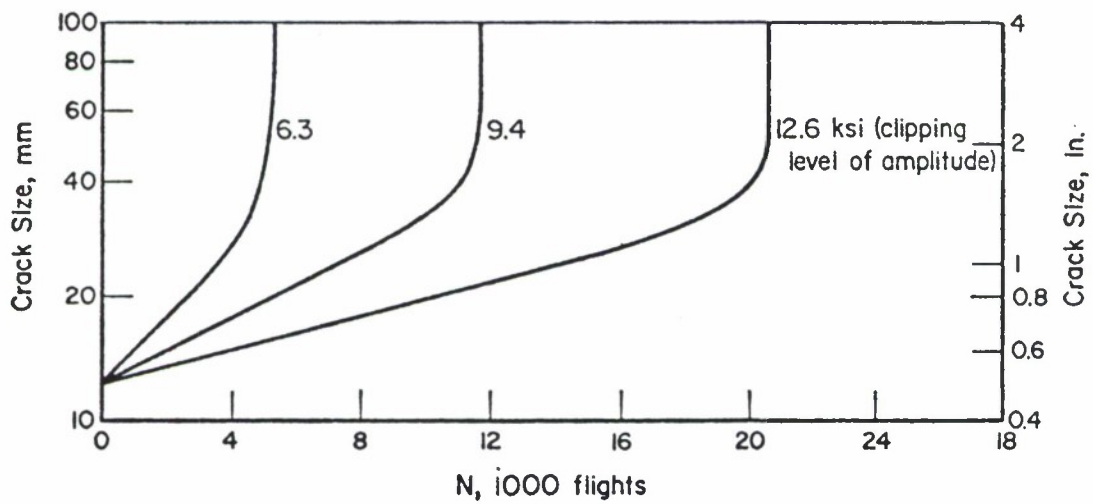


Figure 5.2.4. Effect of Clipping of Higher Loads in Random Flight-by-Flight Loading on Crack Propagation In 2024-T3 Al Alloy (Ref. 43, 44).

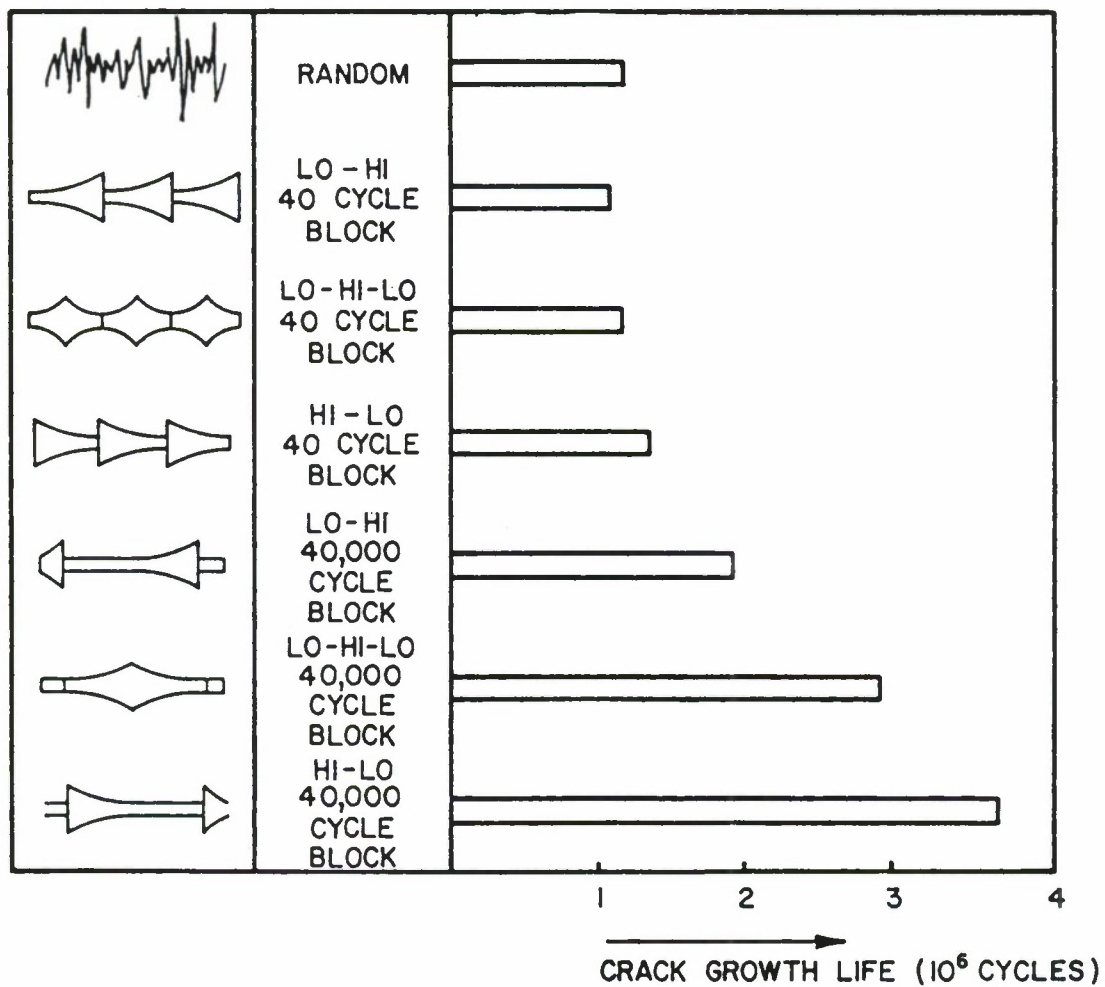


Figure 5.2.5. Effect of Block Programming and Block Size On Crack Growth Life (All Histories Have Same Cycle Content) Alloy: 2024-T3 Aluminum (Ref. 27).

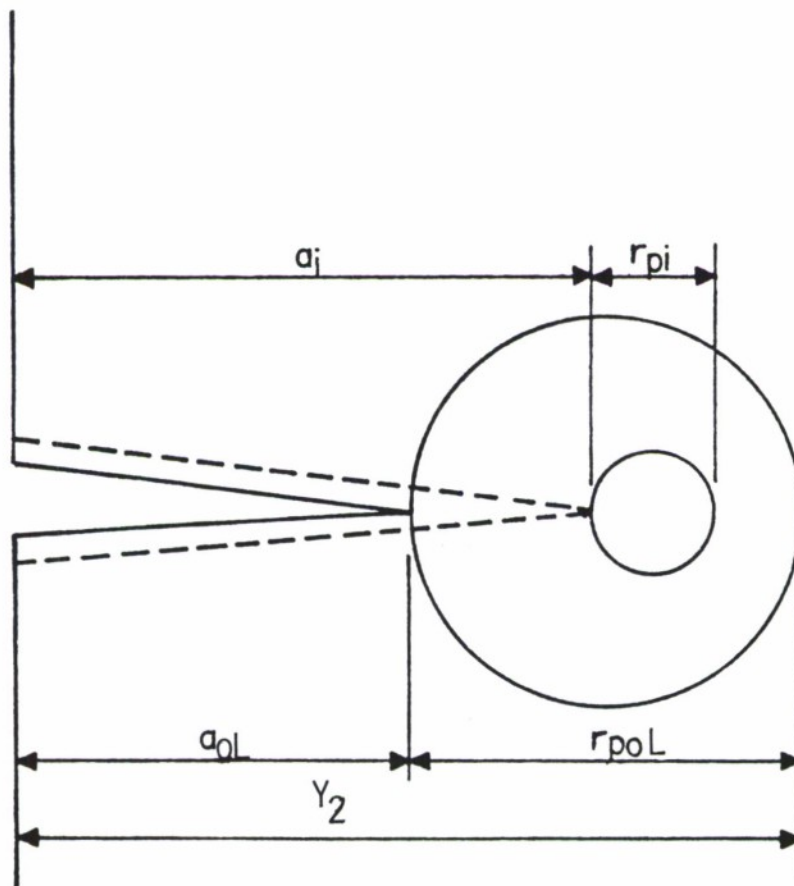


Figure 5.2.6. Yield Zone Due to Overload (r_{poL}), Current Crack Size (a_i), and Current Yield Zone (r_{pi}).

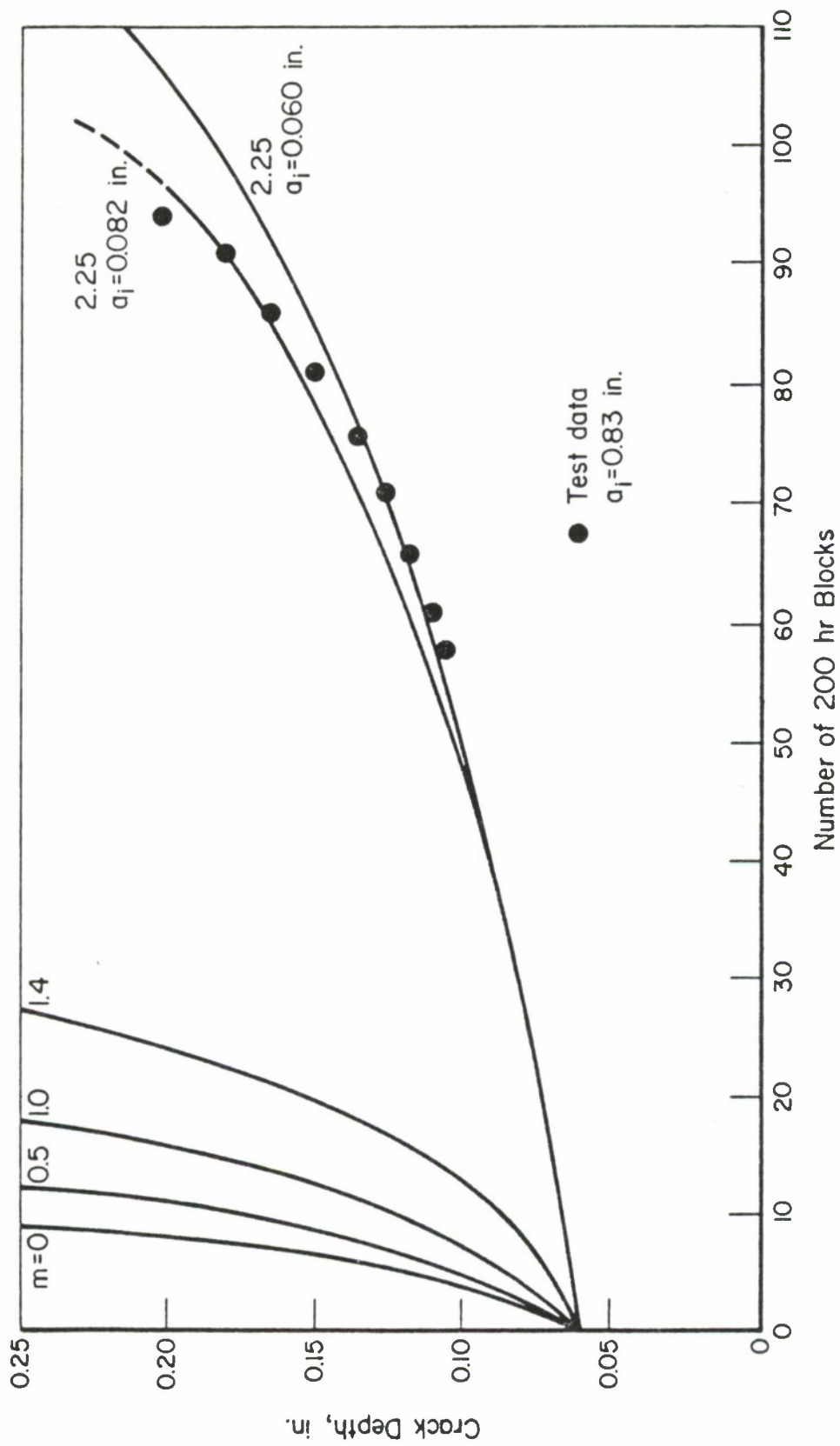


Figure 5.2.7. Crack Growth Predictions by Wheeler Model Using Different Retardation Exponents (Ref. 45).

SECTION 3.5
LIST OF REFERENCES

1. Walker, E. K., Ekvall, J. C. and Rhodes, J. E., "Design for Continuing Structural Integrity," Structural Integrity Technology, A.S.M.E., N.Y., (1979).
2. Packman, P. F., Klima, S. J., Davies, R., Malpani, J., Moyzis, J., Walker, W., Yee, B. G. W. and Johnson, D. P., "Reliability of Flaw Detection by Nondestructive Inspection," ASM Metal Handbook, Vol. 11, 8th Edition, Metals Park, Ohio, (1976), pp. 214-224.
3. McGonnagle, W. J., Nondestructive Testing, McGraw-Hill, N.Y., (1961).
4. McMaster, R. C., Nondestructive Testing Handbook, Ronal Press Co., N.Y., (1959).
5. Corlin, B., Ultrasonics, McGraw-Hill, N.Y., (1960).
6. Betz, C. E., Principles of Penetrants, Magnaflux Corp., (1963).
7. Schaffer, G., "Nondestructive Testing," Special Report 692, American Mechanist, (1976).
8. Berens, A. P. and Hovey, P. W., "Evaluation of NDE Reliability Characterization," AFWAL-TR-81-4160, Air Force Wright Aeronautical Laboratories, Wright-Patterson Air Force Base, Ohio, Nov., 1981.
9. Southworth, H. L., Steel, N. W., and Torelli, P. P., "Practical Sensitivity Limits of Production Nondestructive Testing Methods in Aluminum and Steel," AFML-TR-74-241, (1974).
10. Rummel, W. O., Rathke, R. A., Jr., Todd, P. H., Tedrow, T. L. and Mullen, S. J., "Detection of Tightly Closed Flaws by Nondestructive Testing (NDT) Methods in Steel and Titanium," NAS9-14653, (1976).
11. Lewis, W. H., Dodd, B. D., Sproat, W. H., and Hamilton, J. M., "Reliability of Nondestructive Inspections - Final Report," Report No. SA-ALC/MEE 76-6-38-1, United States Air Force, San Antonio Air Logistics Center, Kelly Air Force Base, Texas, (1978).
12. Smith, D. K., "Improved Penetrant Process Evaluation Criteria," Pratt and Whitney Aircraft Report Number FR-15223, October 1981.

13. Yee, B. G. W., Chang, F. H., Couchman, J. C., Lemon, G. H., and Packman, P. F., "Assessment of NDE Reliability Data," NASA CR-134991, National Aeronautics and Space Administration, Lewis Research Center, Cleveland, Ohio, (1976).
14. Chang, F. H., Bell, J. R., Walker, T. C., Norton, J. M., Packman, P. F., and Gilstrap, L. O., "Methods for the Determination of the Sensitivity of NDE Techniques," AFML-TR-76-246, Air Force Materials Laboratory, Wright-Patterson Air Force Base, Ohio, December 1976.
15. Cargill, J. S., "Retirement for Cause Inspection System Design," Presented at AF/DARPA Review of Progress in Quantitative NDE, Boulder, Colorado, August, 1981.
16. Natrella, M. G., Experimental Statistics, Handbook 91, National Bureau of Standards, (1963).
17. Mood, A. M., Introduction to the Theory of Statistics, McGraw-Hill Book Company, Inc., New York, (1950).
18. Tiffany, C. F., and Masters, J. N., "Applied Fracture Mechanics," Fracture Toughness Testing and Its Applications," ASTM STP 381, American Society for Testing and Materials, Baltimore, MD, (1965), pp. 249-277.
19. Buntin, W. D., "Concept and Conduct of Proof Test of F-111 Production Aircraft," paper presented to the Royal Aeronautical Society, 27 Oct. 1971, London, England.
20. Cowie, W. D., "Turbine Engine Structural Integrity Program (ENSIP)," AIAA, J. of Aircraft, Vol. 12, No. 4, Special Issue (April 1975), pp. 366-369.
21. Horsley, J. J., Bryan, D. F., and Fuller, J. E., "B-52D Proof Load Program, Laboratory Crack Growth Tests," The Boeing Company, Wichita Division, Document No. D3-9700, Feb. 1976, (Restricted Publication).
22. Gunderson, A. W., "Fracture Mechanics Tests and Analyses of the AEDC APTU Storage Vessel Material," AFML-TR-74-133, Air Force Materials Laboratory, October 1974.
23. Albrechtsen, U. and Aitken-Cade, P., Briefing Charts on C-141 Loading Gear Proof Test Conditions, Ogden Air Logistics Center/MMIRCL, Hill Air Force Base, March 1976.
24. White, et al., "Fatigue Life Evaluation of the A-7E Arresting Gear Hool Shank," Vought Report No. 2-30400/9R-52133, Vought Corporation, Dallas, Texas, May 1979.

25. MIL-HDBK-5C, Military Standardization Handbook, Metallic Materials and Elements for Aerospace Vehicle Structures, Vol. 1, 15 September 1976, pp. 3-8.
26. Rudd, J. L. and Gray, T. D., "Equivalent Initial Quality Method," Air Force Flight Dynamics Laboratory, AFFDL-TM-76-83-FBE, Sept. 1976.
27. Rudd, J. L. and Gray, T. D., "Quantification of Fastener-Hole Quality," Journal of Aircraft, Vol. 15, No. 3, (1978), pp. 143-147.
28. Pinckert, R. E., "Damage Tolerance Assessment of F-4 Aircraft," AIAA-76-904, presented at AIAA Aircraft Systems & Technology Meeting, Dallas, Texas, 26-27 September 1976.
29. Dumesnil, C. E., Aratki, S. D., Wilson, R. P., Martin, C. P., White, D. J., and Hooks, O. L., "A-7D ASIP Part I, Damage Tolerance and Fatigue Assessment Program," Vought Corp., Report No. 2-53440/7R-5928, Vol. I, Jan. 1977.
30. Potter, J. M., "Advances in Fastener Hole Quality Through the Application of Solid Mechanics," Proceedings of the Army Symposium on Solid Mechanics, (1978) - Case Studies on Structural Integrity and Reliability, AMMRC-MS 78-3, Watertown, MA, (1978).

4.0 RESIDUAL STRENGTH

<u>SECTION</u>	<u>PAGE</u>
4.1 INTRODUCTION	4.1.1
4.1.1 <u>Slow Crack Growth Structure</u>	4.1.3
4.1.2 <u>Fail-Safe Structure</u>	4.1.4
4.2 FAILURE CRITERIA	4.2.1
4.2.1 <u>Ultimate Strength</u>	4.2.2
4.2.2 <u>Fracture Toughness - Abrupt Fracture</u>	4.2.3
4.2.3 <u>Crack Growth Resistance - Tearing Fracture</u>	4.2.5
4.2.3.1 The Apparent Fracture Toughness Approach	4.2.6
4.2.3.2 The Resistance (R) Curve Approach	4.2.7
4.2.3.3 The J-Integral Resistance Curve Approach	4.2.9
4.3 RESIDUAL STRENGTH CAPABILITY	4.3.1
4.3.1 <u>Single Load Path Residual Strength Diagrams</u>	4.3.2
4.3.2 <u>Built-Up Structure Residual Strength Diagrams</u>	4.3.9
4.4 SINGLE LOAD PATH STRUCTURE	4.4.1
4.4.1 <u>Abrupt Fracture</u>	4.4.1
4.4.2 <u>Tearing Fracture</u>	4.4.8
4.5 BUILT-UP STRUCTURES	4.5.1
4.5.1 <u>Edge Stiffened Panel with a Central Crack</u>	4.5.2
4.5.2 <u>Centrally and Edge Stiffened Panel with a Central Crack</u>	4.5.6
4.5.3 <u>Analytical Methods</u>	4.5.8
4.5.4 <u>Stiffener Failure</u>	4.5.13
4.5.5 <u>Fastener Failure</u>	4.5.17
4.5.6 <u>Methodology Basis for Stiffened Panel Example Problem</u>	4.5.19
4.5.7 <u>Example Residual Strength Analysis of Stiffened Panel</u>	4.5.22
4.5.8 <u>Tearing Failure Analysis</u>	4.5.26
4.5.9 <u>Summary</u>	4.5.30
4.6 LIST OF REFERENCES	4.6.1

LIST OF FIGURES

<u>FIGURE</u>		<u>PAGE</u>
4.1.1	The Structural Configuration or Degree of Inspectability Controls the Subsequent Choices of Design Concept and Inspection Level.	4.1.5
4.1.2	Relationship Between the Life Expended and Residual Strength Capability Showing Monotonic Decrease in Load Carrying Capacity Due to Increased Structural Damage. Failure Occurs when the Residual Strength Capability Curve Intersects the Required Residual Strength Level.	4.1.6
4.1.3	Relationship Between Crack Length and Life Expended Showing a Monotonic Increase in Crack Length Up Until Failure. Shown are the Various Technology and Specification Requirements Needed to Define the Crack Growth Curve Which, in Turn, Establishes the Life Limit.	4.1.7
4.1.4	Strength Criteria for Periodically Inspected Damage Tolerant Structure.	4.1.8
4.2.1	Description of Crack Geometry and Residual Strength Results.	4.2.12
4.2.2	Fracture Data Described as a Function of Crack Length.	4.2.13
4.2.3	The Fracture Mechanics Basis for Establishing Residual Strength.	4.2.14
4.2.4	Plane-Strain Fracture Toughness (K_{IC}) Data for 7075 Aluminum in the format of Reference 1.	4.2.15
4.2.5	Plane-Stress Fracture Toughness (K_C) Data for 7075 Aluminum in the Format of Reference 1.	4.2.16
4.2.6	Fracture Toughness Behavior as a Function of Thickness.	4.2.17
4.2.7	Schematic Illustration of Tearing Fracture Behavior and the Development of a Crack Growth Resistance Curve (R-Curve).	4.2.18

LIST OF FIGURES
(Con't)

<u>FIGURE</u>	<u>PAGE</u>
4.2.8 K_R Curves from 7475 Alloy, 16 Inch Wide Panels, 0.5 Inch Thickness (Reference 2).	4.2.19
4.2.9 Schematic Illustration of Tearing Fracture Behavior Which Further Defines the Change in Critical Level of Fracture Toughness as a Function of Crack Length (Also see Figure 4.2.7).	4.2.20
4.2.10 Description of the Three Fracture Toughness Criteria that are Utilized to Estimate Residual Strength Under Tearing Fracture Conditions.	4.2.21
4.2.11 Schematic Illustration of the Individual and Collective Parts of A K_R Fracture Analysis.	4.2.22
4.2.12 Schematic Illustration of the Individual and Collective Parts of a $\sqrt{J_R}$ Fracture Analysis.	4.2.23
4.3.1 Residual Strength Diagram for Abrupt Failure of a Single Load Path Structure.	4.3.17
4.3.2 Structural Geometry and Material Properties for Example 4.3.1.	4.3.18
4.3.3 Description of Procedures that One Might Follow to Obtain the Residual Strength Diagram Graphically.	4.3.19
4.3.4 Crack Geometries Considered for a Radial Crack Growing from a Hole for Example 4.3.2.	4.3.20
4.3.5 Stress-Intensity Factor Relationships at Points A and B for the Radial Quarter Circular Crack Geometry.	4.3.21
4.3.6 Stress-Intensity Factor Relationships at Points A and B for the Radial Embedded Semi-Circular Crack Geometry.	4.3.21
4.3.7 Residual Strength Diagram for Points A and B Located on the Radial Quarter Circular Crack Geometry Shown in Figure 4.3.4.	4.3.22
4.3.8 Residual Strength Diagram for Points A and B Located on the Embedded Semi-Circular Crack Geometry Shown in Figure 4.3.4.	4.3.22

LIST OF FIGURES
(Con't)

<u>FIGURE</u>		<u>PAGE</u>
4.3.9	Multiple Load Path (Built-Up) Structure with a Crack in the Central Member.	4.3.23
4.3.10	Reduction of Residual Strength During Successive Failure of Members in the Structure Shown in Figure 4.3.9.	4.3.24
4.3.11	Crack Growth Curve for Multiple Load Path Structure Shown in Figure 4.3.9.	4.3.25
4.3.12	Skin-Stringer Built-Up Structure.	4.3.26
4.3.13	Variation of β and L with Crack Length in Stiffened Panel with a Crack Between the Stiffeners.	4.3.27
4.3.14	Residual Strength of the Cracked Panel as a Function of Crack Length for Built-Up Skin-Stiffened Structure Compared with Unstiffened Panels. Abrupt Failure Criterion Used to Determine Residual Strength.	4.3.28
4.3.15	Residual Strength of a Cracked Panel as a Function of Crack Length for Built-Up Skin-Stiffened Structure. Only Skin Failure Mode Considered. Abrupt Failure Criterion Used to Determine Residual Strength.	4.3.29
4.3.16	Load-Crack Length Behavior Observed in Skin-Stiffened Construction with Arrest Features.	4.3.30
4.3.17	Residual Strength of Cracked Panel as a Function of Crack Length for Built-Up Skin-Stringer Structure. Tearing Failure Criterion Used to Determine Residual Strength.	4.3.31
4.4.1	Residual Strength Diagram Showing Defining Crack and Residual Strength Parameters.	4.4.12
4.4.2	Center Crack Panel and Materials Properties for Example 4.4.1.	4.4.13
4.4.3	Residual Strength Diagram Determining Critical Crack Size at 20 Ksi Operating Level.	4.4.14

LIST OF FIGURES
(Con't)

<u>FIGURE</u>		<u>PAGE</u>
4.4.4	Excentrically Cracked Panel Associated with Examples 4.4.2 and 4.4.3.	4.4.15
4.4.5	Finite-Width Correction-Eccentric Crack (Tension) (Reference 15).	4.4.16
4.4.6	Residual Strength Diagram for Panel with Eccentric Crack Given in Figure 4.4.4. Crack with Lowest Fracture Resistance Curve Extends First.	4.4.17
4.4.7	Finite Width Correction-Single Edge Crack, After the Eccentric Crack Extends from Tip A.	4.4.18
4.4.8	Residual Strength Diagram Used to Consider Arrest Features as Crack Tip A Reaches the Edge of the Plate.	4.4.19
4.4.9	Diagrams Showing Onset of Unstable Crack Growth for Conditions of Limited or Extensive Crack Extension.	4.4.20
4.4.10	Steps Associated with Calculating Residual Strength of Cracked Structures with Tearing Fractures.	4.4.21
4.4.11	Structural Geometry Associated with Example 4.4.4.	4.4.22
4.4.12	Stress-Intensity Factor Relationship for Various Values of Applied Stress.	4.4.23
4.4.13	Resistance Curve for 7075-T73 Aluminum for a Thickness of 0.063 Inches.	4.4.24
4.4.14	Matching the R-Curve and Stress-Intensity Factor Curves.	4.4.25
4.4.15	Residual Strength Diagram Obtained for Structure Shown in Figure 4.4.11 (Example 4.4.4).	4.4.26
4.5.1	Elements of Residual Strength Diagram.	4.5.31
4.5.2	Residual Strength Diagram for a Stiffened Panel.	4.5.32
4.5.3	Panel Configuration with Heavy Stringers; Skin-Critical Case.	4.5.33

LIST OF FIGURES
(Con't)

<u>FIGURE</u>		<u>PAGE</u>
4.5.4	Criterion for Fastener Failure	4.5.34
4.5.5	Residual Strength Diagram for a Panel with Three Stiffeners and a Central Crack Emanating from a Rivet Hole.	4.5.35
4.5.6	Analysis of Stiffened Panel.	4.5.36
4.5.7	Effect of Number of Fasteners Included in Analysis on Calculated Stress-Intensity Factor.	4.5.37
4.5.8	Skin-Stress-Reduction β and Stringer-Load-Concentration L as Affected by Fastener Flexibility and Stiffener Bending.	4.5.38
4.5.9	Bonded Fastener Divided into Discrete Segments.	4.5.39
4.5.10	Residual Strength Diagram Comparing Riveted and Bonded Structures.	4.5.40
4.5.11	Residual Strength Diagram for Stiffener.	4.5.41
4.5.12	Comparison of L_S and K/σ_S for Riveted and Bonded Structures.	4.5.42
4.5.13	Comparison of Residual Strength for Riveted and Bonded Stiffeners.	4.5.43
4.5.14	Residual Strength Diagram for the Fasteners in a Built-Up Structure.	4.5.44
4.5.15	Gross Stress and Critical Stress Diagram for Adhesively Bonded Stringer.	4.5.45
4.5.16	Riveted Panel with a Central Crack Between Two Stringers.	4.5.46
4.5.17	Stiffened Structure Broken into Components.	4.5.47
4.5.18	Geometrical and Displacement Parameters Relative to the Crack Tip.	4.5.48
4.5.19	Normalized Panel Displacement Function (f_{σ}/p) Due to Applied Stress Vs. Normalized Crack Length (a/p) for Various Stringer Spacings ($\bar{S} = S/p$).	4.5.49

LIST OF FIGURES
(Con't)

<u>FIGURE</u>		<u>PAGE</u>
4.5.20	Panel Displacement Function Due to Fastener Force Vs. Normalized Rivet Diameter (d/p) for All Stiffener Spacings.	4.5.50
4.5.21	Normalized Panel Displacement Function (f_p/p) Due to Distributed Pressure Along Crack Vs. Normalized Crack Length ($a/;$) for Various Stringer Spacings ($\bar{s} = s/p$).	4.5.51
4.5.22	Stringer Displacement Function Vs. Normalized Rivet Diameter (d/p) for Various Half Stringer Widths.	4.5.52
4.5.23	Parameter λ_1 Vs. Normalized Crack Length (a/p) for Various Normalized Stringer Spacings (s/p).	4.5.53
4.5.24	Structural Geometry and Material Properties for Example of Subsection 4.5.7.	4.5.54
4.5.25	Stress-Intensity Factor Diagram for Panel and Riveted Stringers.	4.5.55
4.5.26	Residual Strength Diagram for Panel and Riveted Stringers (Light Stringers).	4.5.56
4.5.27	Residual Strength Diagram for Panel and Riveted Stringers (Heavy Stringers).	4.5.57
4.5.28	Square Root of J_R Resistance Curve.	4.5.58
4.5.29	Failure Analysis Based on $J_{Critical}$ Curve.	4.5.59

CHAPTER 4

RESIDUAL STRENGTH

4.1 INTRODUCTION

The strength of a structure can be significantly affected by the presence of a crack and is usually substantially lower than the strength of the undamaged structure. To prevent catastrophic failure, one must evaluate the load carrying capacity that will exist in the potentially cracked structure throughout its expected service life. The load carrying capacity of a cracked structure is the residual strength of that structure and it is a function of material toughness, crack size, crack geometry and structural configuration.

The basic concept in damage tolerance design is to ensure the safety of the structure throughout the expected service life. To provide the required safety, a structure must be designed to withstand service loads even when cracks are present or when part of the structure has already failed; i.e., the structure has to be damage tolerant. The overriding philosophy is to maintain a minimum required residual strength so that catastrophic failure of the structure is prevented.

Figure 4.1.1 identifies the major sequence of events that ultimately define the residual strength requirements. As can be noted from the figure, once a safety-of-flight-critical element is identified, either its structural configuration or its degree of inspectability will

establish the allowable structural design concept and the inspection level categories. Every safety-of-flight-critical element must be qualified in at least one design concept category and in one inspection category. Each allowable combination of design concept and inspection category is coupled in MIL-A-83444 to a residual strength requirement, a service life requirement, and a requirement to assume a level of initial damage.

Figure 4.1.2 illustrates the residual strength and the service life interval requirements as well as a residual strength capability curve. The residual strength capability curve defines the level of load that the structure can withstand without failing in the presence of a growing crack. To account for the change in residual strength capacity as a function of time, it is necessary to determine the crack size as a function of time. The crack-growth-life curve and its various properties are shown schematically in Figure 4.1.3.

As can be seen from Figure 4.1.2, when the residual strength of the structure falls below the maximum stress in the service load history, failure can be expected. To avoid such a failure, a thorough understanding of the problem is essential. Significant advances have been made in recent years in procedures for analyzing damaged structures. Assessments now consider residual strength, damage growth, interactive multiple damage sites and quantitative structural maintenance and in-service evaluations.

The application of existing fracture mechanics solution techniques has yielded effective methods for analyzing the residual strength of the cracked structure. The necessary theories and methods for determining the residual strength capability of cracked structures are presented in this chapter. Prior to presenting this information in the following sections, a few remarks are made about the residual strength requirements for the two damage tolerant design categories: slow crack growth structure and fail-safe structure.

4.1.1 Slow Crack Growth Structure

In a slow crack growth structure, the damage tolerance must be assured by the maintenance of a slow rate of crack growth, a residual strength capacity, and the assurance that subcritical damage will either be detected at the depot⁺ or will not reach unstable dimensions within the design lifetime of the structure. The residual strength curve for a structure which is inspected periodically is schematically shown in Figure 4.1.4. As a result of the inspections, the initially assumed cracks do not grow to a critical size and the structure is restored to its original load carrying capability when an inspection capability equal to that of the manufacturer's is employed.

Single-load-path "monolithic" structure must be qualified in this category; the residual strength estimation procedure for this type of

⁺depot level inspections have been eliminated as a design option by ASD for new slow crack growth structure in airframes.

structure is fairly straightforward. Built-up (multiple-load-path) structure can be qualified either in this category or in the fail-safe category.

4.1.2 Fail-Safe Structure

The residual strength requirement of a fail-safe structure is to assure damage tolerance following a partial failure of the structure. Damage tolerance is maintained through detection of this failure prior to total loss of the structure and sufficient residual strength capability for operating safely with the partial failure prior to inspection. The fail-safe structure is typically a built-up structure with multiple load paths or crack arrest features in its design. In the event of failure of a structural member, its load must be transferred to and withstood by the remainder of the structure, which also contains crack damage, without causing the loss of whole structure. The residual strength of the built-up structure must be determined under such critical circumstances so that the fail-safe design requirements are met.

The analysis of residual strength capability for built-up structure requires the estimation of the critical stress level at which the partial failure occurs, as well as an understanding of the capability of the total structure to withstand this partial failure at and subsequent to the time of failure. The required load associated with the time subsequent to failure is based on the inspection category; and, the partially failed structure must be able to maintain this load until the time of inspection.

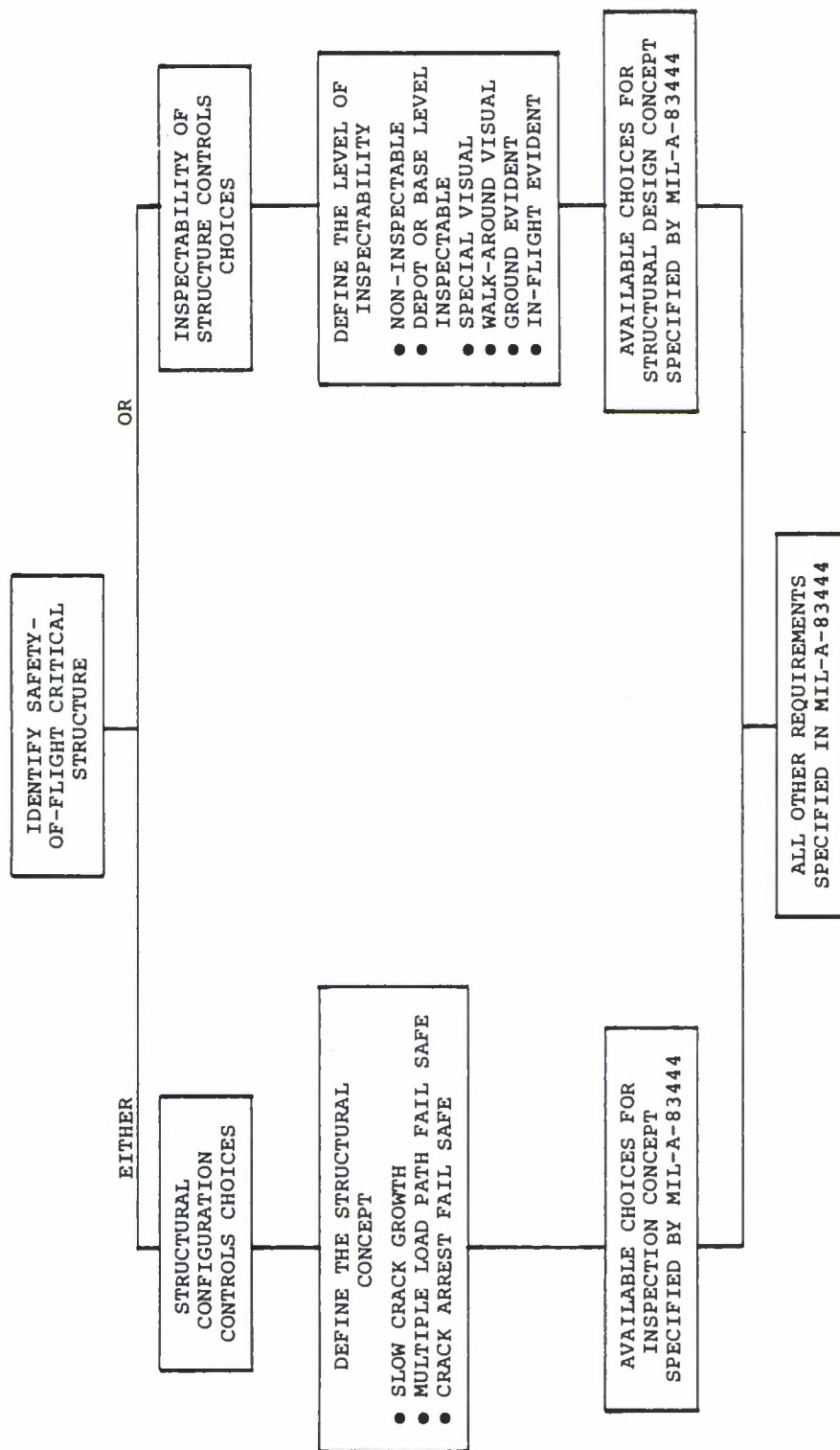


Figure 4.1.1. The Structural Configuration or Degree of Inspectability Controls the Subsequent Choices of Design Concept and Inspection Level.

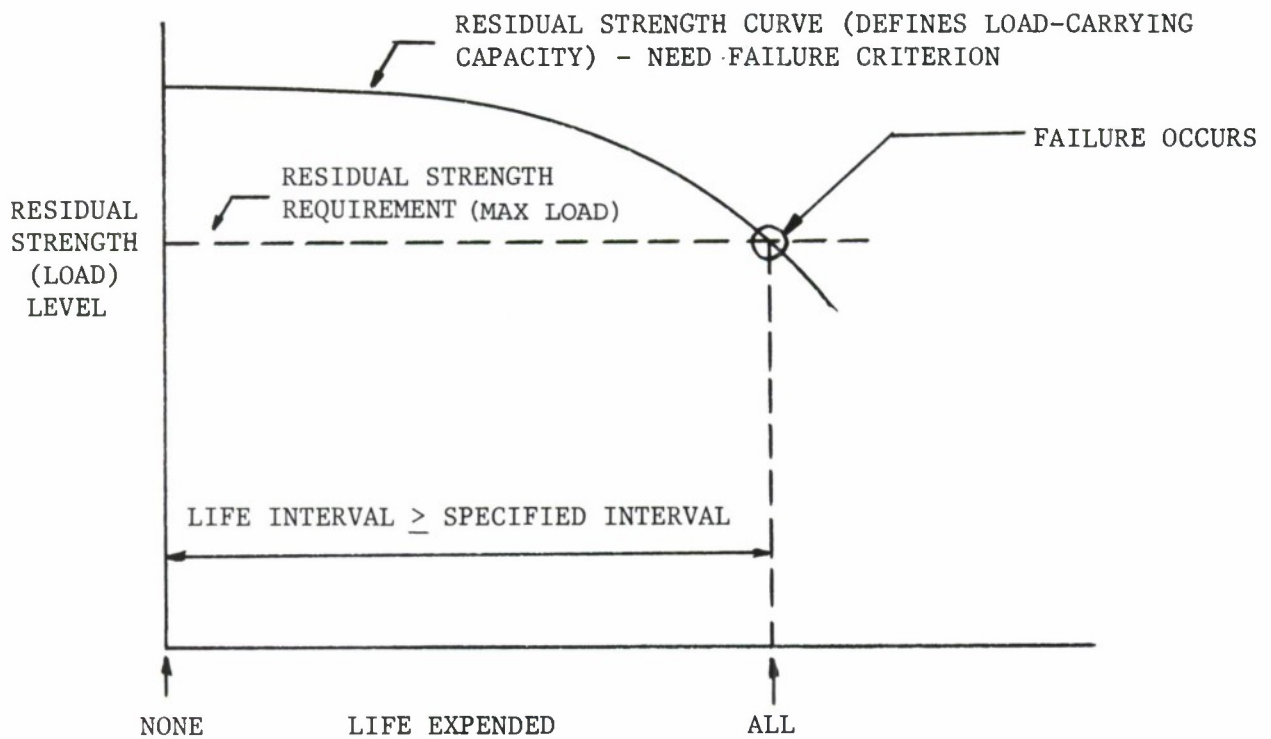


Figure 4.1.2. Relationship Between the Life Expended and Residual Strength Capability Showing a Monotonic Decrease in Load Carrying Capacity Due to Increased Structural Damage. Failure Occurs When the Residual Strength Capability Curve Intersects the Required Residual Strength Level.

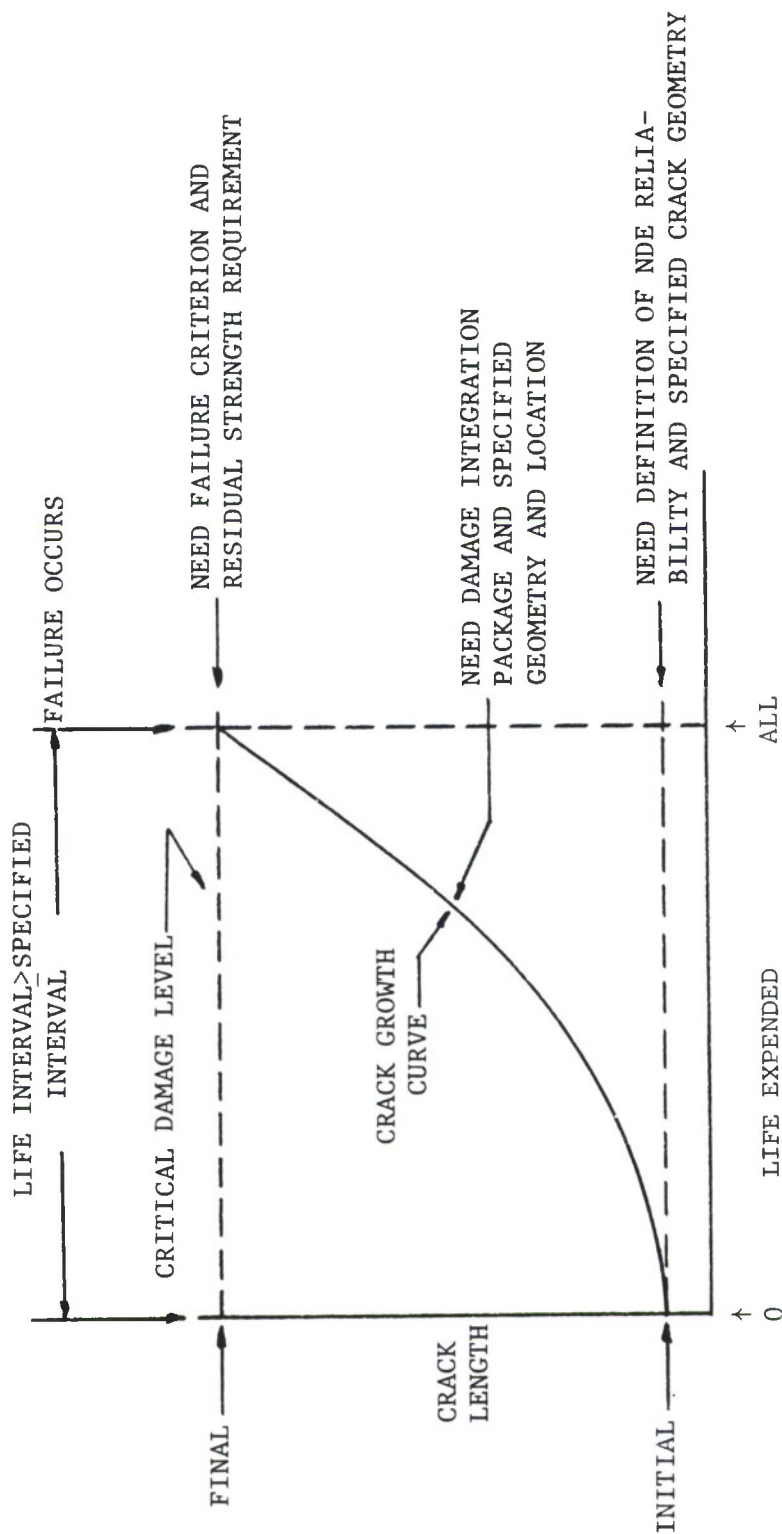


Figure 4.1.3. Relationship Between Crack Length and Life Expended Showing a Monotonic Increase in Crack Length Up Until Failure. Shown are the Various Technology and Specification Requirements Needed to Define the Crack Growth Curve Which, in Turn, Establishes the Life Limit.

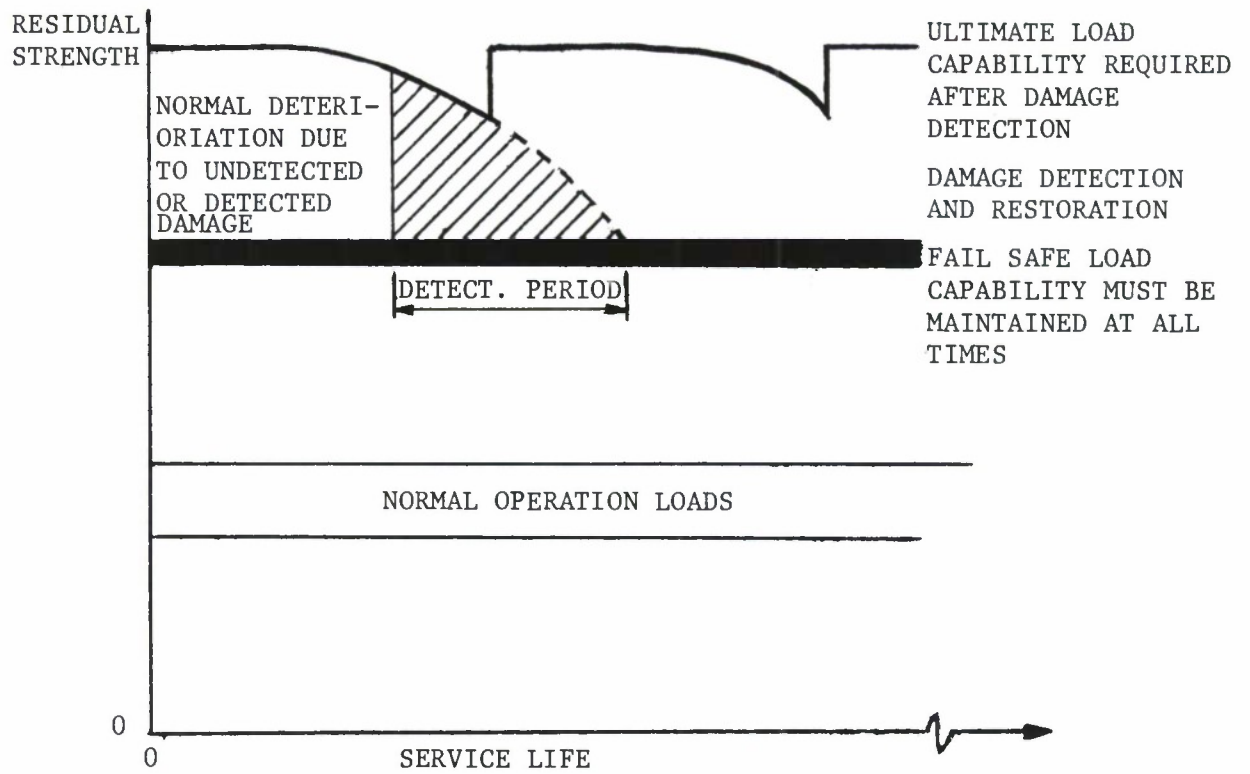


Figure 4.1.4. Strength Criteria for Periodically Inspected Damage Tolerant Structure.

4.2 FAILURE CRITERIA

The determination of residual strength for uncracked structures is straightforward because the ultimate strength of the material is the residual strength; whereas, a crack in a structure causes a high stress concentration resulting in a reduced residual strength. When the load on the structure exceeds a certain limit, the crack will extend. The crack extension may become immediately unstable and the crack may propagate in a fast uncontrollable manner causing complete fracture of the component.

Figure 4.2.1 illustrates the results obtained from a series of tests conducted on a lug geometry containing a crack. The lug geometry shown in Figure 4.2.1a is a single-load-path structure. Figure 4.2.1b indicates that the cracks in each of the three tests extended abruptly at a critical level of load which is noted to be a function of crack length. The crack length-critical load level data shown in Figure 4.2.1b provide the basis for establishing the residual strength capability curve (See Figure 4.1.2). The locus of critical load levels as a function of crack length is shown in Figure 4.2.1c where the residual strength capability of the lug structure is shown to decrease with increasing crack length.

Considering the preceding in terms of applied stress (σ) rather than load gives the σ versus a and σ_c versus a_c plots as shown in Figure 4.2.2

parts a and b. Schematically, the plots exhibit the same abrupt fracture behavior as the curves presented in Figure 4.2.1. As also shown in Figure 4.2.2 parts c and d, crack extension can first occur at a load level that is well below the fracture critical level. The point A' corresponds to the start of slow and stable extension of the crack. The unstable rapid extension leading to total failure occurs at Point A. This kind of behavior is observed typically in thin metal sheets or in tough materials. When different crack lengths are considered, the σ_c versus a_c plot will contain two distinct curves as shown in Figure 4.2.2d. The curve A'B'C' corresponds to the start of slow and stable crack extension and the curve ABC corresponds to failure.

In general, unstable crack propagation results in fracture of the component. Hence, unstable crack growth is what determines the residual strength. In order to estimate the residual strength of a structure, a thorough understanding of the crack growth behavior is needed. Also, the point at which the crack growth becomes unstable must be defined and this necessitates the need for a failure criterion. There are several criteria available; these criteria are tailored to represent the ability of a material to resist failure.

4.2.1 Ultimate Strength

The simplest failure criterion assumes that failure occurs at the ultimate (or yield) strength of the material. Thus, the failure

criterion becomes simply

$$\sigma_f = F_{tu}, \quad (4.2.1)$$

where σ_f is the fracture stress and F_{tu} is the ultimate strength. This criterion is applicable primarily to uncracked structures and is included here for completeness. In past analyses of failure of built-up structure, the residual strength of stiffeners was based upon this criterion. When the main panel between the stiffeners fails due to catastrophic crack growth, the panel loads are transferred to the stringers (or stiffeners). The transferred loads may increase the stress level in the stringer high enough to reach the value of σ_f , causing stiffener failure.

4.2.2 Fracture Toughness - Abrupt Fracture

In a cracked structure, as discussed in Chapter 1, the stress intensity factor (K) interrelates the local stresses in the region of the crack tip with: crack geometry, structural geometry, and the level of load on the structure. When the applied load level increases, the K value also increases and reaches a critical value at which time the crack growth becomes unstable as shown in Figure 4.2.3. This critical level of K, which is independent of the crack length, is a material property called fracture toughness. The fracture toughness is a measure of the material's resistance to unstable cracking. Several test procedures are available to evaluate the fracture toughness. Also, various theoretical and numerical solution techniques are available as discussed in Chapter 1, which can be used to estimate the (applied) stress intensity factor, K, for a given structure.

4.2.3

The failure criterion (Irwin's Criterion) states that abrupt fracture occurs when the crack-tip stress-intensity factor reaches or exceeds the fracture toughness of the material. The corresponding applied stress at failure is called the fracture strength. The failure criterion becomes simply

$$K \geq K_{cr} \quad (4.2.2)$$

where K_{cr} is the material's fracture toughness.

The critical K_{cr} for abrupt fracture mode is denoted as K_{Ic} for plane strain conditions and K_c for plane stress conditions; and the conditions for plane stress or plane strain are determined by experiment. The test requirements necessary for generating K_{Ic} and K_c are discussed in Chapter 7.

The Damage Tolerant Design (Data) Handbook⁽¹⁾ contains a large quantity of fracture toughness data. Examples of the formats associated with individual test data for 7075 aluminum alloy are shown in Figures 4.2.4 and 4.2.5 for plane strain and plane stress fracture toughness values, respectively. In general, a material's toughness depends on thickness as shown in Figure 4.2.6. When the thickness is such that the crack tip plastic zone size is on the order of the plate thickness, the toughness reaches a maximum value, $K_{c(max)}$. With increasing thickness of the plate, the plastic zone size reduces and thus the toughness gradually decreases, from $K_{c(max)}$ to K_{Ic} . When the thickness is large enough that the crack tip deformation is not affected by the thickness, plane strain conditions prevail at the crack tip. The toughness in the plane strain regime is

virtually independent of thickness. For increasing thickness, the toughness asymptotically approaches the plane strain fracture toughness, K_{Ic} .

4.2.3 Crack Growth Resistance - Tearing Fracture

As illustrated in Figures 4.2.2c and d, when the crack extends by a tearing mode of fracture, which typically occurs in thin metal sheets or in tough materials, the crack extension is essentially slow and stable. The failure condition for tearing fractures depends on the crack growth resistance (K_R) behavior of the material and the applied stress-intensity factor K , which in turn depends on the crack and structural configurations. Figure 4.2.7 describes the observations that lead to the development of the crack growth resistance curve (K_R vs. Δa). Figure 4.2.7 parts a and b present the tearing behavior as a function of applied stress and the corresponding stress-intensity factor, respectively. Figure 4.2.7c presents the crack growth resistance curve which is a composite of the three stress-intensity factor curves shown in Figure 4.2.7b. Note that the composite was created by using the amount of physical crack movement observed in each case as the independent variable. As implied by the data points on the crack growth resistance curve in Figure 4.2.7c, the stress-intensity factor level associated with material failure is not necessarily constant.

Shown in Figure 4.2.8 is a resistance curve for a 7475 aluminum alloy described as a function effective crack length (Ref. 2). The effective

crack length is the sum of the physical crack length and the plastic zone size corresponding to the current crack length and loading conditions.

Indeed, while the shape of the resistance curve is basically independent of crack length or other geometrical effects, the fracture level is a function of crack length (See Figure 4.7.9). To account for this variation in fracture critical level, a two parameter failure criterion was required. However, before introducing the two parameter criteria that are used for more accurate estimates, approximate single parameter criteria for tearing failures are presented.

4.2.3.1 The Apparent Fracture Toughness Approach

Due to the complexity of the two parameter fracture criteria for tearing fracture behavior, engineers sometimes obtain preliminary estimates of the residual strength using a single parameter fracture toughness criterion. Figure 4.2.10 describes the stress-crack length levels associated with the onset of cracking ($K = K_{\text{ONSET}}$) and fast fracture ($K = K_{\text{cr}}$) conditions for a tearing material. Intermediate between the two curves established from material observations is a third curve referred to as the apparent fracture curve. The apparent fracture toughness (K_{APP}) is established from the same data employed to derive K_{ONSET} and K_{cr} . The calculation procedure uses the onset (or initial) crack length (a_i) and the final recorded stress level (σ_{cr}) for the tests conducted. Thus, K_{APP} represents a fracture toughness level bounded by the onset and fast fracture levels.

For lower bound estimates of the residual strength for fast fracture of a tearing material, one could equate the level of applied stress-intensity factor (K) to the apparent fracture toughness (K_{APP}), i.e., assume that fracture occurs when

$$K = K_{APP} \quad (4.2.3)$$

in order to determine the critical level of stress. Equation 4.2.3 is an abrupt failure criterion for a tearing fracture.

4.2.3.2 The Resistance (R) Curve Approach

If the crack tip plastic zone size is estimated to be on the order of the structural thickness but substantially smaller than other geometrical variables (crack length, ligament size, height, etc.), a linear elastic fracture mechanics analysis can still be sensibly used to predict the catastrophic cracking event. The failure criterion for tearing type fractures under these conditions states that fracture will occur when (1) the stress-intensity factor K reaches or exceeds the material's fracture resistance K_R and (2) the rate of change of K (with respect to crack length) reaches or exceeds the rate of change of K_R (with respect to crack length). Physically, the criterion means that at failure, the energy available to extend the crack equals or exceeds the material resistance to crack growth. The failure criterion becomes simply,

$$K \geq K_R; \quad \frac{\partial K}{\partial a} \geq \frac{\partial K_R}{\partial a} \quad (4.2.4)$$

The corresponding applied stress, σ_f , at this point is defined as the fracture stress which determines the residual strength of the cracked structure. The criterion presented in Equation 4.2.4 is noted to be a two parameter criterion rather than the single parameter criteria that was presented in paragraph 4.2.3.1. To interpret the meaning of this criterion, first consider the structural parameters that are a function of the geometry and stress, i.e. K and $\frac{\partial K}{\partial a}$.

In general, the estimation of K involves the relationship $K = \sigma\beta\sqrt{\pi a}$ as given in Chapter 1; using this equation, the variation of K with respect to crack length (a) can be obtained for various values of stress (σ) as shown in Figure 4.2.11a. Shown in Figure 4.2.11b is the variation of K_R with respect to the crack extension (Δa) that was developed for the given material using the procedures outlined in Figure 4.2.7. Since this R-curve is assumed to be independent of the initial crack length, it can be superimposed on the plot of K versus a as shown in Figure 4.2.11c. The tangency point between the applied stress intensity factor curve (K vs. a) and the R-curve (K_R vs. Δa) determines the commencement of unstable crack propagation. In general, the accurate method of determining the tangency point involves the numerical solution based on the experimentally obtained R-curve. Using a least squares determined polynomial expression for R-curve and knowing an expression for K in terms of crack length, the common tangent point can be obtained by equating the functional values ($K = K_R$) and also the first derivatives with respect to the crack length ($\frac{dK}{da} = \frac{dK_R}{da}$) of these two expressions.

The slow stable tear is dependent on a structural configuration in which the plastic zone at the crack tip is no longer negligible but not enormous. References 3, 4 and 5 explain the dependence of the R-curve on structural configuration as well as with test procedures used to evaluate the R-curve. See Chapter 7 for additional information on test procedures and the Damage Tolerant Design (Data) Handbook⁽¹⁾ for a summary of available data.

4.2.3.3 The J-Integral Resistance Curve Approach

The crack growth resistance curve (K_R) has shown good promise for materials where limited (small-scale) yielding occurs in front of the crack tip. Difficulties in estimating crack tip plasticity under large-scale yielding conditions, led Wilhem⁽⁶⁾ to an alternate failure criterion based on the J-integral⁽⁷⁾. For a basic introduction to the J-integral see Section 1.9.

Wilhem's J-integral criterion is similar to the K_R - curve criterion; it states that failure will occur when the following conditions are met:

$$\sqrt{J} \geq \sqrt{J_R} ; \frac{d\sqrt{J}}{da} \geq \frac{\partial \sqrt{J_R}}{\partial a} \quad (4.2.5)$$

where J is the value of the applied J-integral and J_R is the value of the J-integral representing the material resistance to fracture. The applied stress (σ_f) corresponding to Equation 4.2.5 is defined as the fracture stress. Since the effect of large-scale yielding can be appropriately incorporated through a suitable elastic-plastic model in the estimation of J-integral, it becomes an effective parameter for predicting failure

under plane stress conditions where the plastic zone size is significantly large.

The crack resistance curve for the tearing failure is now represented by $\sqrt{J_R}$ vs. Δa curve instead of K_R vs. Δa curve. The use of $\sqrt{J_R}$ rather than J_R is justified by the fact that \sqrt{J} is directly related to the stress-intensity factor for elastic behavior through the equation

$$J = K^2/E' \quad (4.2.6)$$

where E' is the elastic modulus (E) for plane stress conditions and $E/(1-\nu^2)$ for plane strain conditions.

For different levels of applied load, the J-integral can be computed using finite element techniques for the structure of interest for a series of different crack sizes; the \sqrt{J} versus crack length curve is illustrated in Figure 4.2.12a for a constant level of applied stress. It is noted that this curve will incorporate the influence of material properties (yield strength and strain hardening exponent) through the finite element analysis. In a manner similar to the stress-intensity factor type resistance curve, i.e. the K_R curve, the resistance curve based on $\sqrt{J_R}$ can be experimentally obtained^(8,9). A $\sqrt{J_R}$ versus crack movement (Δa) curve, i.e. the J-integral resistance curve, is schematically illustrated in Figure 4.2.12b. The failure criterion is also based on the tangency conditions between the \sqrt{J} versus crack length curve and the $\sqrt{J_R}$ versus crack movement curve. To obtain this condition, the $\sqrt{J_R}$ vs. Δa curve can be superimposed on the plot of \sqrt{J} vs. a curve such

that at some crack length these two curves are tangent to each other as shown in Figure 4.2.12c. The corresponding crack length then defines the critical crack size of the structure for the fracture stress, σ_f .

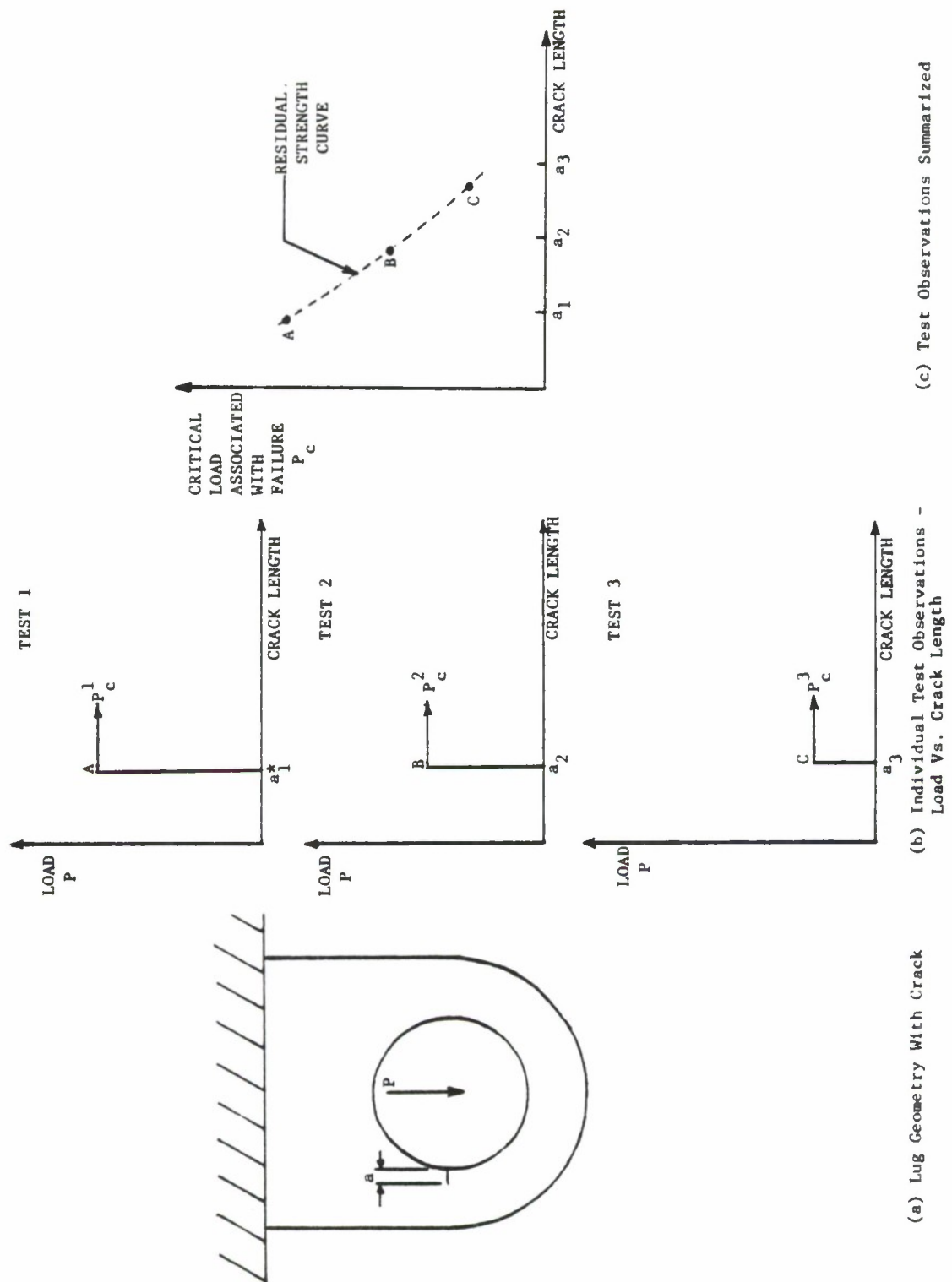
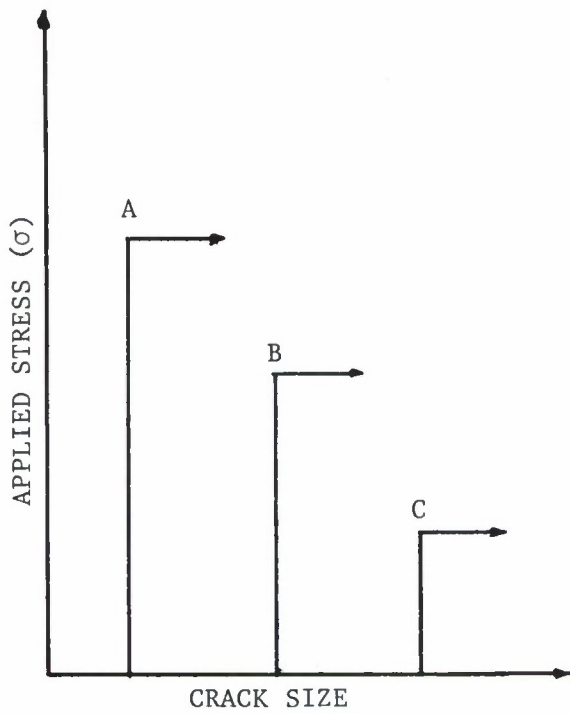
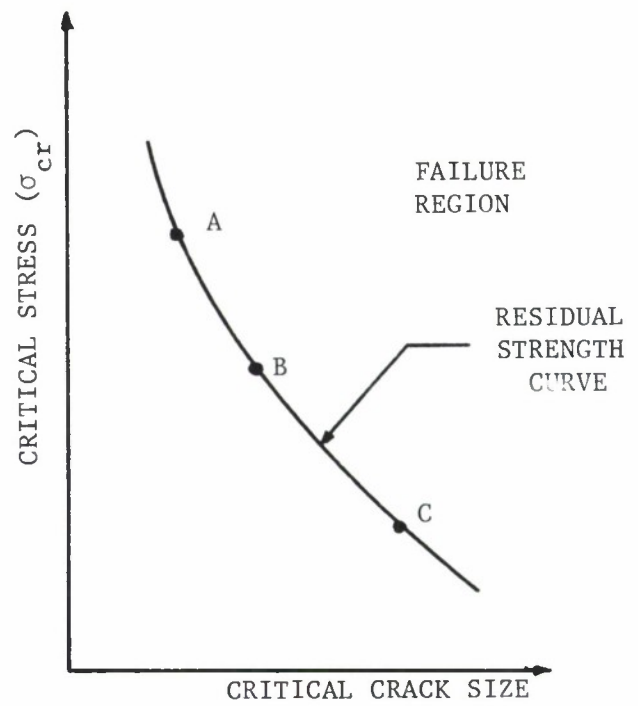


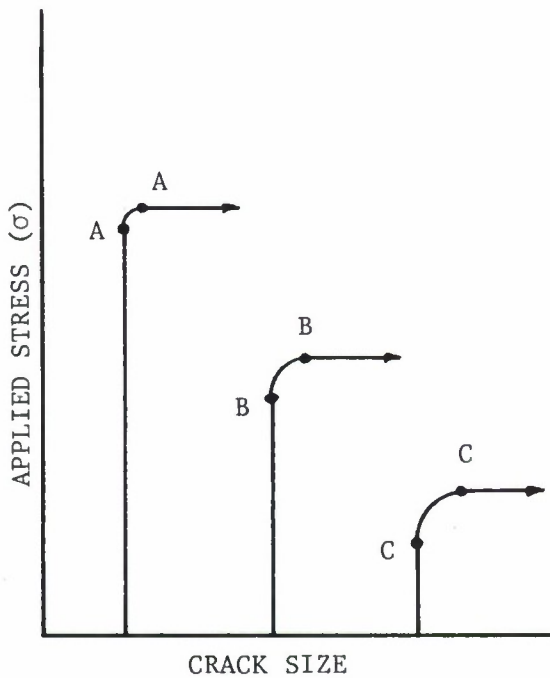
Figure 4.2.1.1. Description of Crack Geometry and Residual Strength Results.



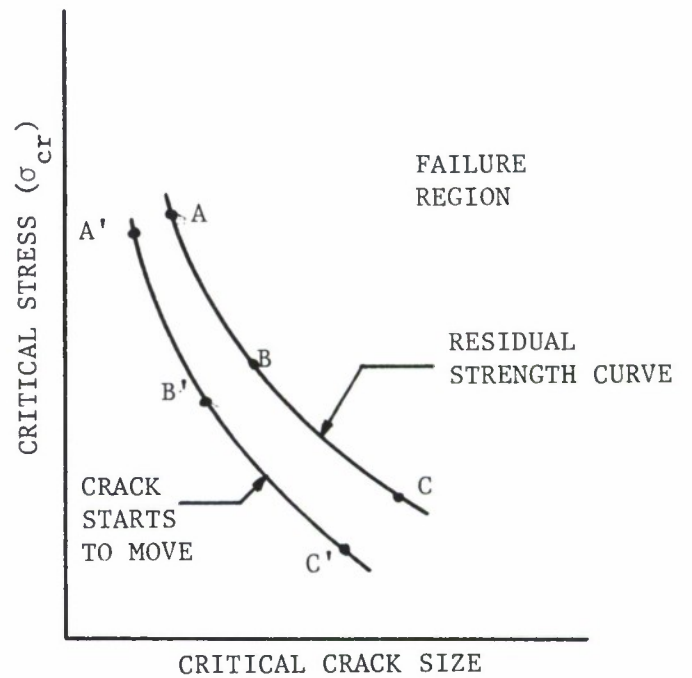
(a) Individual Test Data-
Abrupt Failure



(b) Critical Stress Data Summarized-
Abrupt Failure

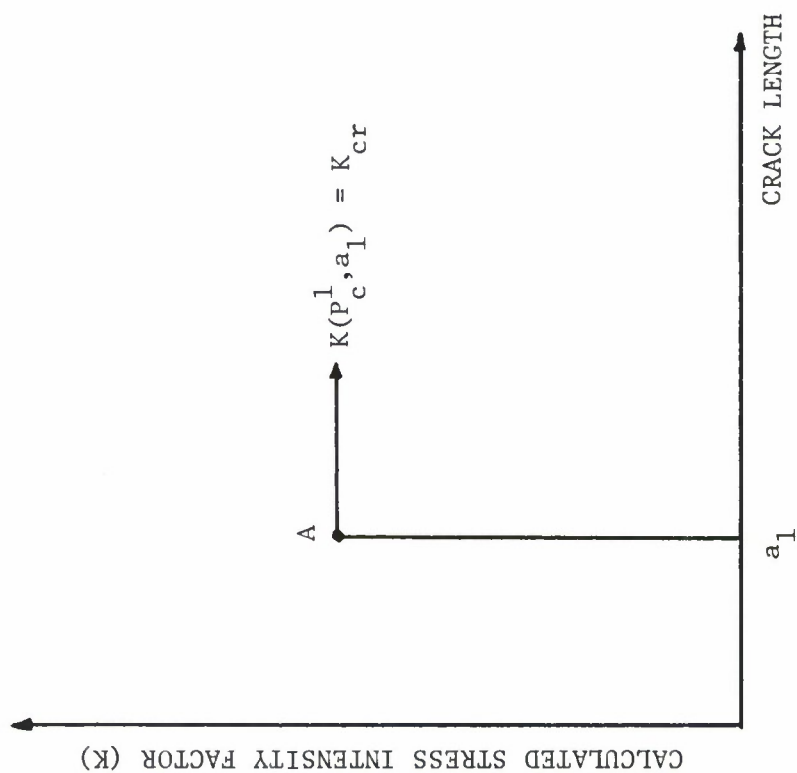


(c) Individual Test Data-
Tearing Failure

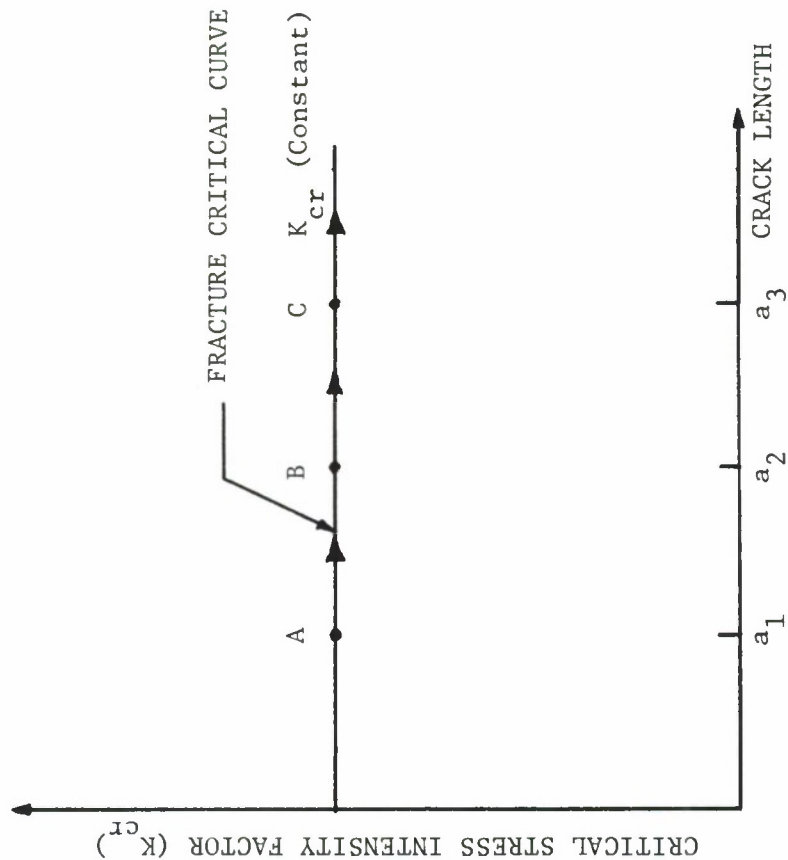


(d) Critical Stress Data Summarized-
Tearing Failure

Figure 4.2.2. Fracture Data Described as a Function of Crack Length.



(a) Stress Intensity Factor Calculated as a Function of Load and Crack Length.



(b) Critical Stress Intensity Factor Levels Described as a Function of Crack Length.

Figure 4.2.3. The Fracture Mechanics Basis for Establishing Residual Strength.

ALUMINUM													
7075													
K (IC)													
CONDITION	--PRODUCT--		TEST	SPECIMEN	YIELD	-----SPECIMEN-----		CRACK	2.5* (k/c) ²	K (IC) MEAN	STAN	DATE	REFER
	FORM	THICK				THICK	THICK						
	(IN)	(F)		ORIENT	(KSI)	(IN)	(IN)	(IN)	(IN)				
											</		

Figure 4.2.4. Plane-Strain Fracture Toughness (K_{Ic}) Data for 7075 Aluminum in the Format of Reference 1.

CONDITION	ALUMINUM 7075										K(C)		STAN				DATE	REFER
	--PRODUCT-- FORM	THICK (IN)	TEST TEMP (F)	SPEC OR	YIELD STR (KSI)	---SPECIMEN---			CRACK LENGTH		---STRESS---			STAN DEV	MEAN (KSI*SGRT IN)	K(C)		
						WIDTH (IN)	THICK (IN)	B	INIT (IN)	FINAL (IN)	ONSET (KSI)	MAX (KSI)	K(APP) (KSI*SGRT IN)					
BUCKLING OF CRACK EDGES NOT RESTRAINED																		
T6	S	0.06	R. T.	T-L	75.5	4.500	0.063		1.130	1.130	---	40.00	55.46	55.5/ 0.0	58.3/ 4.0	55.46	1966	86731
		0.06			75.5	4.500	0.063		1.130	1.330	---	40.00	55.46					
T6	S	0.06	R. T.	T-L	75.5	6.000	0.063		1.500	1.770	---	35.20	56.21			62.06	1966	86731
T6	S	0.06	R. T.	T-L	75.5	10.000	0.064		2.250	2.500	---	30.10	58.42			62.06	1966	86731
T6	S	0.06	R. T.	T-L	75.5	12.000	0.063		3.000	3.500	---	24.10	54.43			59.67	1966	86731
T6	S	0.06	R. T.	T-L	75.5	15.000	0.063		3.750	4.250	---	21.80	55.05	54.8/ 1.7	61.7/ 3.3	58.81	1966	86213
		0.06			72.9	15.810	0.063		5.580	6.960	---	15.80	53.20					
		0.06			72.9	15.810	0.063		3.010	3.500	---	25.40	56.50					
		0.06			72.9	15.810	0.063		3.010	4.000	---	25.70	57.17					
		0.06			72.9	15.820	0.063		1.000	1.400	---	42.90	53.90					
T6	S	0.06	R. T.	T-L	72.9	15.820	0.063		4.000	4.720	---	20.40	53.25			57.70	1966	86731
T6	S	0.06	R. T.	T-L	75.5	18.000	0.064		4.500	5.000	---	19.60	54.21	58.56		57.70	1966	86731
		0.06	R. T.	T-L	75.5	21.000	0.064		5.250	5.250	---	19.60	58.56					
T6	S	0.06	R. T.	T-L	69.0	24.000	0.063		8.000	-----	---	11.40	43.43	46.0/ 5.4	54.8/ 0.7	55.23	1966	86731
		0.06			69.0	24.000	0.063		8.000	-----	---	11.30	43.04					
		0.06			69.0	24.000	0.063		8.000	-----	---	10.90	41.52					
		0.06			69.0	24.000	0.063		8.000	-----	---	11.25	42.85					
		0.06			69.0	24.000	0.063		8.000	-----	---	11.40	43.43					
T6	S	0.06	R. T.	T-L	75.5	24.000	0.064		6.000	6.360	---	16.71	53.37	56.00		56.17	1966	86731
		0.06			75.5	24.000	0.064		6.000	6.000	---	17.00	54.30					
T6	S	0.08	R. T.	T-L	73.3	29.990	0.081		15.000	15.050	---	9.70	56.00					

BUCKLING OF CRACK EDGES NOT RESTRAINED

Figure 4.2.5. Plane-Stress Fracture Toughness (K_{IC}) Data for 7075 Aluminum in the Format of Reference 1.

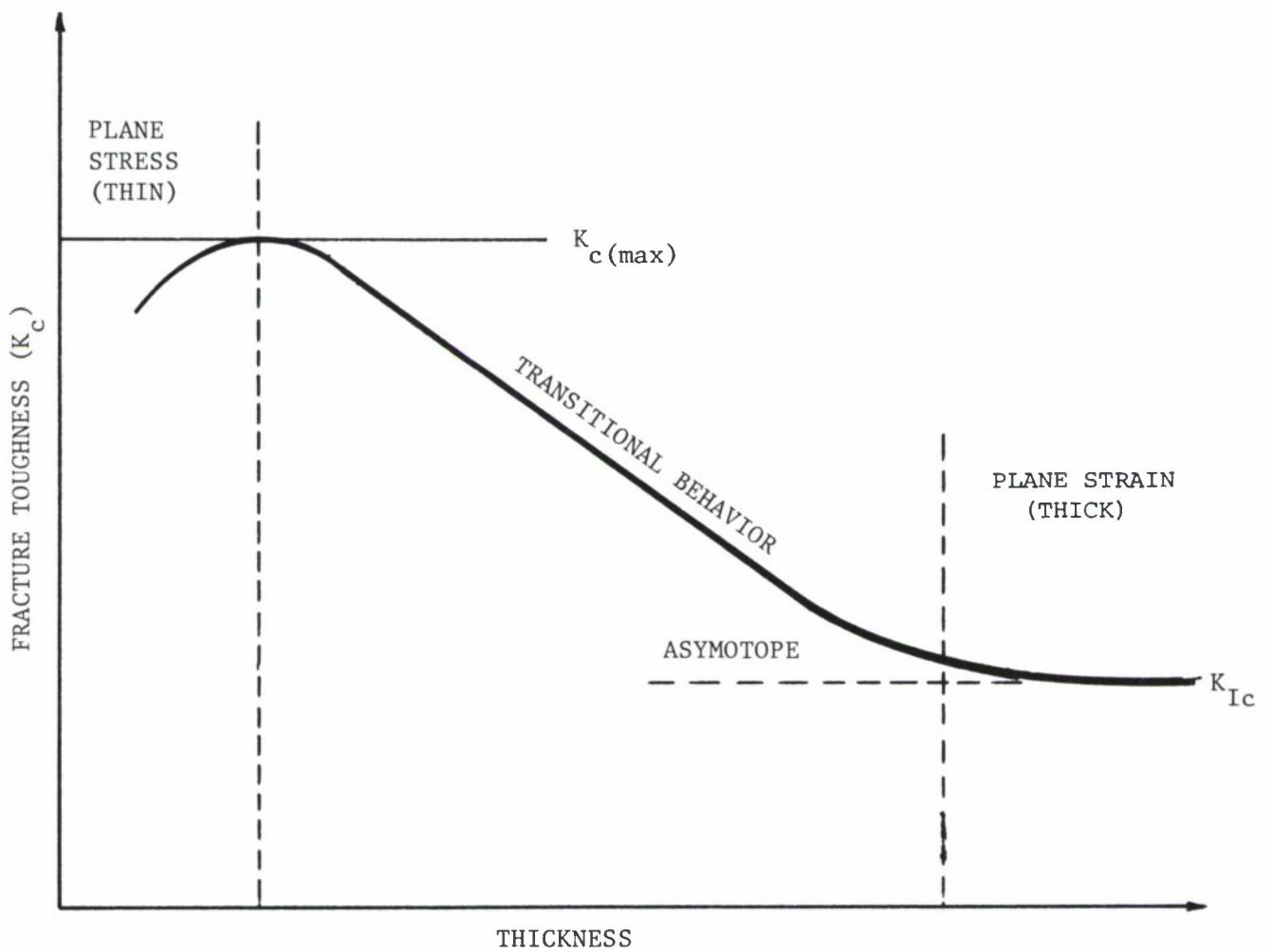


Figure 4.2.6. Fracture Toughness Behavior as a Function of Thickness.

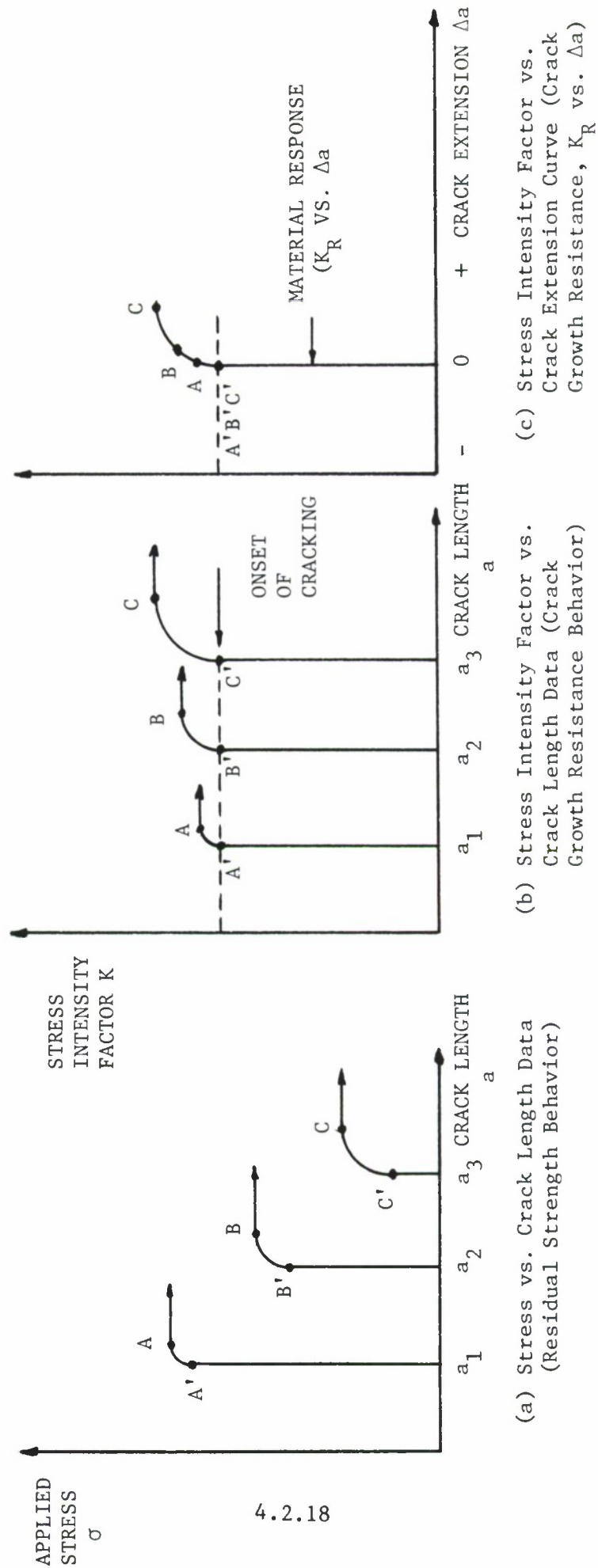


Figure 4.2.7. Schematic Illustration of Tearing Fracture Behavior and the Development of a Crack Growth Resistance Curve (R-Curve).

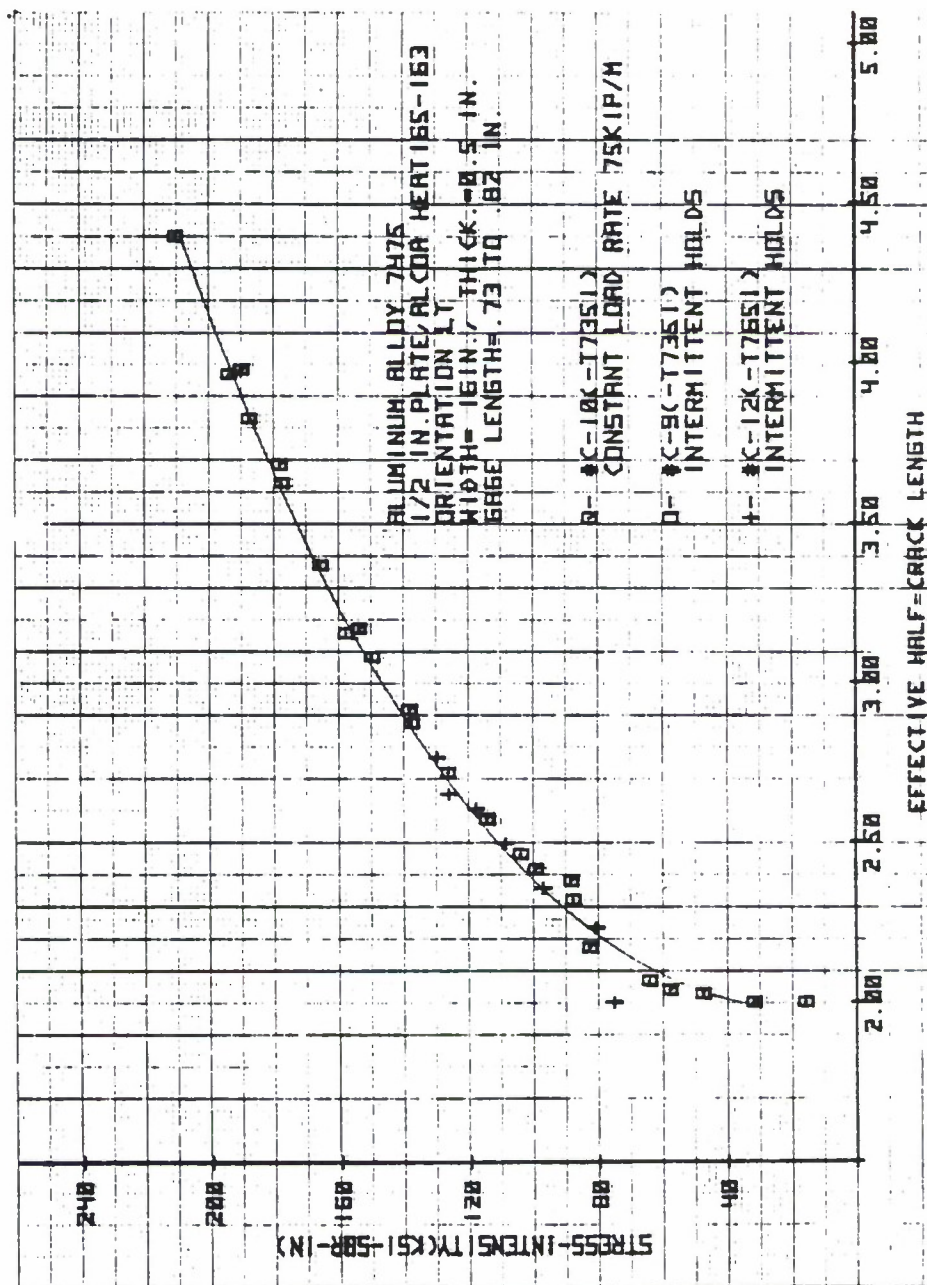


Figure 4.2.8. K_R Curves from 7475 Alloy, 16 Inch Wide Panels, 0.5 Inch Thickness (Reference 2).

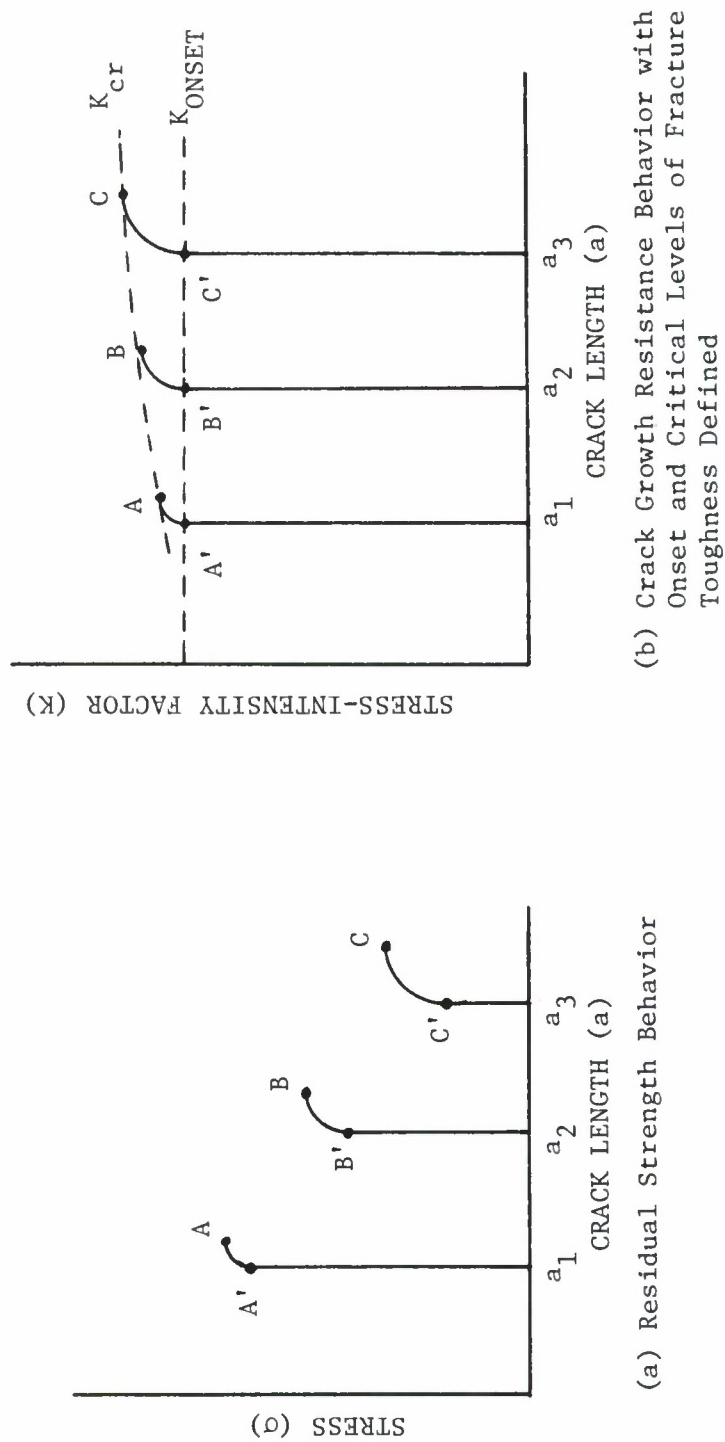


Figure 4.2.9. Schematic Illustration of Tearing Fracture Behavior Which Further Defines the Change in Critical Level of Fracture Toughness as a Function of Crack Length (Also See Figure 4.2.7).

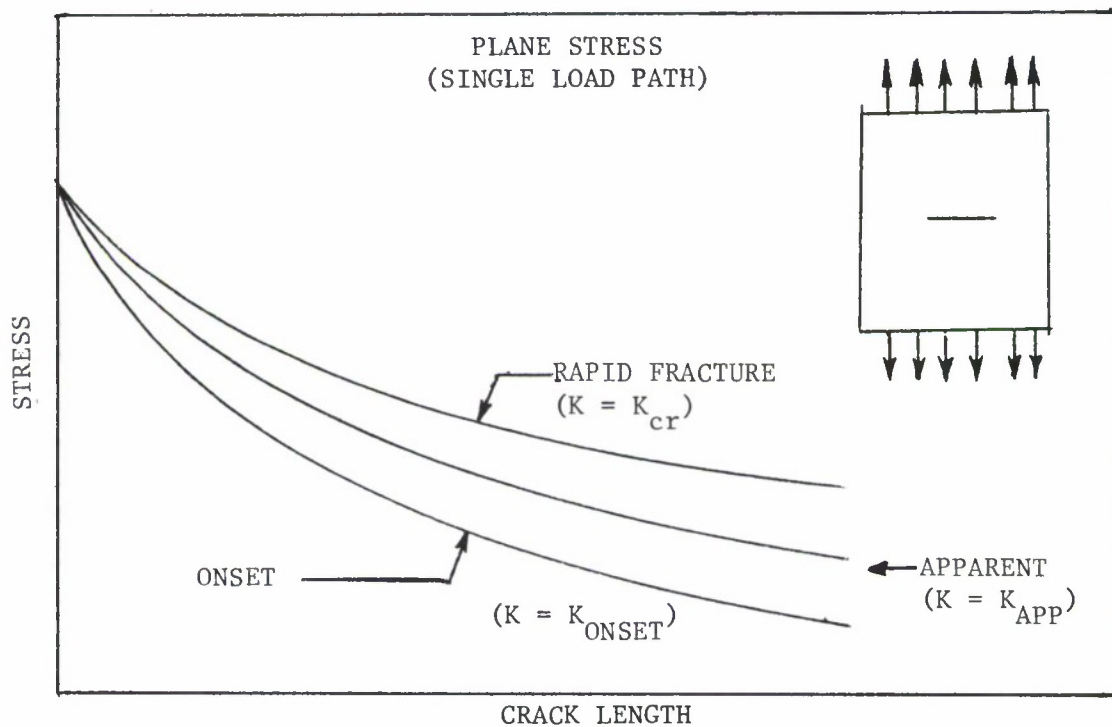
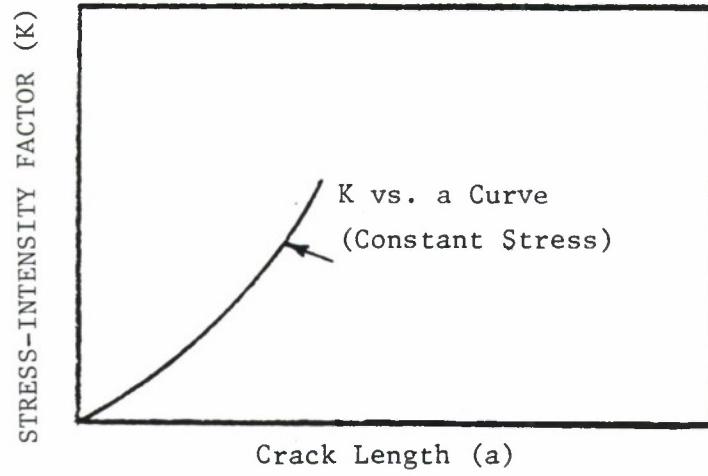
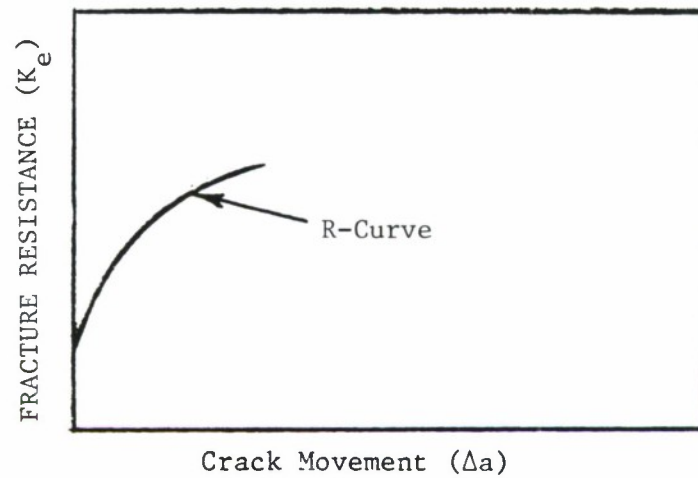


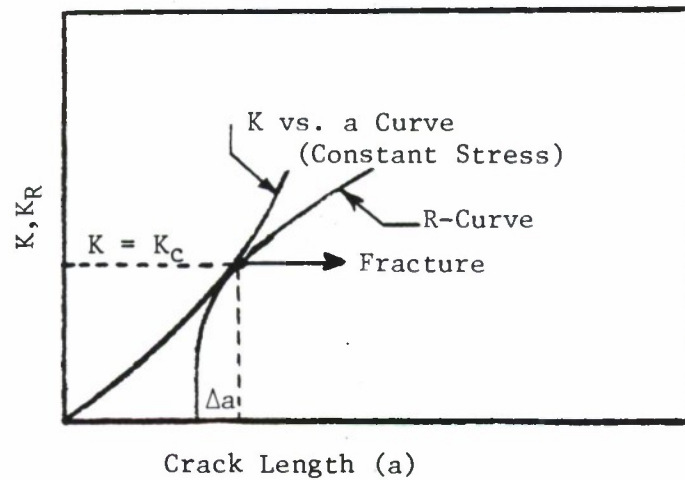
Figure 4.2.10. Description of the Three Fracture Toughness Criteria that are Utilized to Estimate Residual Strength Under Tearing Fracture Conditions.



(a) Driving Force

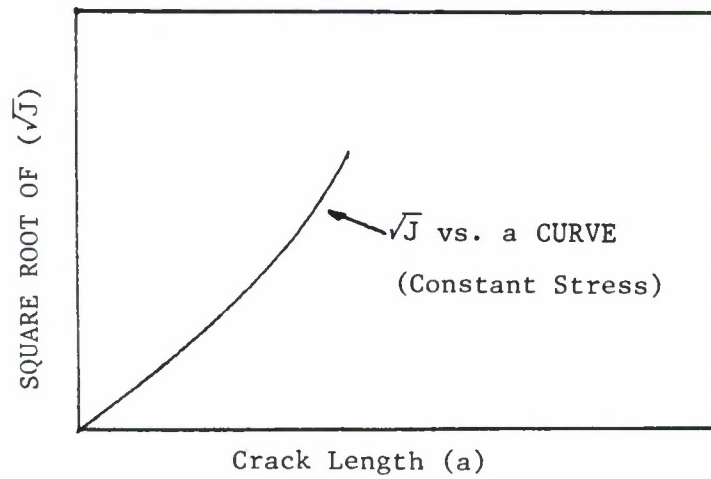


(b) Resistance to Crack Growth

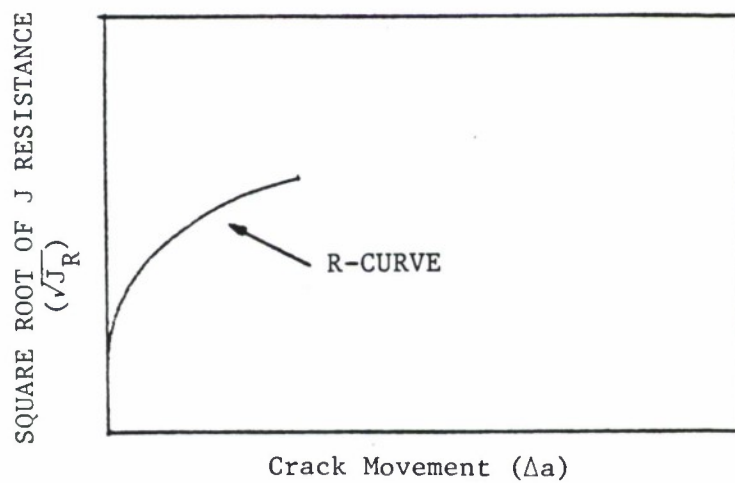


(c) Establishment of Critical Conditions

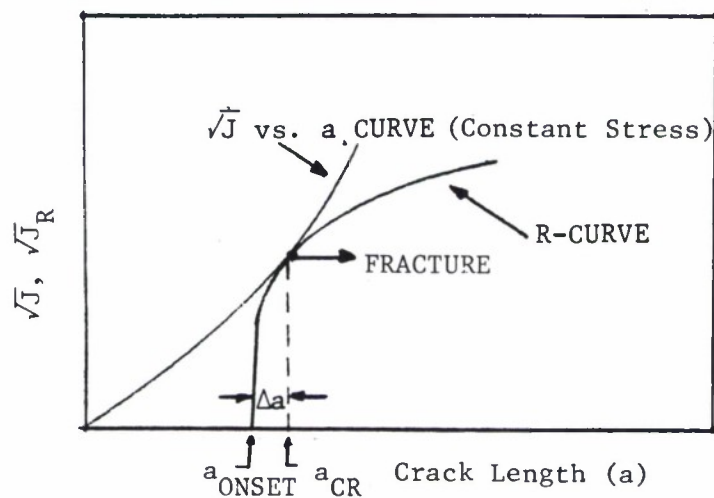
Figure 4.2.11. Schematic Illustration of the Individual and Collective Parts of A K_R Fracture Analysis.



a. Driving Force



b. Resistance to Crack Growth



c. Establishment of Critical Conditions

Figure 4.2.12. Schematic Illustration of the Individual and Collective Parts of a $\sqrt{J_R}$ Fracture Analysis.

4.3 RESIDUAL STRENGTH CAPABILITY

To establish the residual strength capability of a given structure under certain loading conditions, prediction techniques must be developed with a thorough understanding of the complexities involved in evaluating the residual strength. For monolithic or single load path structures which must be classified as slow crack growth structures, the estimation of residual strength capability is straightforward. In multiple load path (built-up) structures, whether classified as slow crack growth or fail-safe structures, the strength analysis can become complicated, due to the complex geometric construction of the built-up components. In general, the prediction techniques are based on the critical value of the stress-intensity factor for a given geometry and loading. Using fracture toughness failure criteria as explained earlier, the decay in critical stress can be obtained in terms of crack size.

As described by Figure 4.1.2, the residual strength capability is a function of service time for a given structure. This is because the residual strength capability depends on the size of the crack in the structure and the crack grows as a function of time. Thus to obtain a residual strength capability curve (Figure 4.1.2), one needs two types of data: (a) the relationship between crack length and time and (b) the relationship between fracture strength (σ_f) and crack length. Chapter 5 is devoted to obtaining the crack length-time relationship and the remainder of this chapter is devoted to presenting methods and procedures

for obtaining the fracture strength-crack length (σ_f vs. a) relationship. It is to be noted that the σ_f vs. a relationship is independent of time and has been referred to in the general literature as the residual strength diagram. This section presents useful information about residual strength diagrams for single load path and for multiple load path structures.

4.3.1 Single Load Path Residual Strength Diagrams

For a single load path structure, such as an unstiffened panel, the residual strength diagram under plane strain conditions, consists of a single curve as shown in Figure 4.3.1. The procedure for developing the residual strength diagram involves the calculation of the critical stress σ_f , for the critical crack length a_c , using the relationship $K_{cr} = \sigma_f \beta \sqrt{\pi a_c}$ where K_{cr} is the known value of fracture toughness of the material. (K_{cr} may be equal to K_{Ic} or K_{Ic} depending on the problem.) The plot of σ_f vs a_c then provides the necessary residual strength diagram required in design analysis for the simple configuration.

The available fracture mechanics solution techniques, as given in Chapter 1, can be employed in the calculation of the crack-tip stress-intensity factor K to construct the residual strength diagram. Depending on the complexity of the structure, K can be calculated either numerically or through closed form solutions. These techniques, in conjunction with an appropriate failure criterion, can then be used to determine the residual strength capabilities of a given structure.

4.3.2

In general, the construction of a residual strength diagram involves three steps:

- (a) The development of the relationship between the applied stress σ , the crack length parameter a , and the applied stress-intensity factor K for the given structural configuration (See Section 1.6).
- (b) The selection of an appropriate failure criterion based for the expected material behavior at the crack tip (See Section 4.2).
- (c) The fracture strength (σ_f) values for critical crack sizes (a_c) are obtained utilizing the results of the first two steps and residual strength diagram (σ_f vs a_c) for the given structural configuration is plotted.

To understand these three steps for constructing a residual strength diagram, the following two examples are considered. The first example considers a wide thin panel with a central crack which has a simple relationship for the stress intensity factor. The second example considers corner and embedded cracks emanating from a hole; the second configuration does not have a simple relationship for the stress-intensity factor. These two examples will illustrate the importance of the stress-intensity factor for constructing the residual strength diagram.

EXAMPLE 4.3.1 Unstiffened Center Crack Panel

Construct the residual strength diagram for the wide unstiffened panel shown in Figure 4.3.2, assuming that the structure is made from 7075-T6 aluminum sheet material, with a fracture toughness of $40 \text{ ksi}\sqrt{\text{in}}$.

SOLUTION:

Following the three step process, the first step that must be taken is to define the stress-intensity factor relationship. From Table 1.7.1, the stress intensity factor for a wide unstiffened, center crack panel is given by

$$K = \sigma\sqrt{\pi a} \quad (4.3.1)$$

The second step is to define the failure criterion. For this problem, it is assumed that an abrupt fracture occurs and the condition that defines the fracture is

$$K = K_{cr} = K_c = 40 \text{ ksi}\sqrt{\text{in}} \quad (4.3.2)$$

The third and final step is to utilize the results of the first two steps to derive a relationship between fracture strength (σ_f) and critical crack size (a_c) from Equations 4.3.1 and 4.3.2, the σ_f vs a_c relationship is given by

$$\sigma_f\sqrt{a_c} = 40/\sqrt{\pi} \quad (4.3.3)$$

For a half crack size (a_c) of 2.0 inch, the fracture strength (σ_f) is about 16. ksi. Other (σ_f vs a_c) values can be similarly obtained. Once a sufficient number of values are available, the residual strength diagram can be developed.

One could also attack the problem in the graphic manner which will now be explained using Figure 4.3.3. The three steps are identified in Figure 4.3.3a.

The first step is to construct a plot of K vs a using Equation 4.3.1 for

various values of stress. The second step requires that one superimpose the horizontal line $K = K_{cr} = 40 \text{ Ksi}\sqrt{\text{in}}$ on the diagram. This line represents the critical stress intensity, i.e., fracture toughness, for this material and is independent of crack length. Step 3 utilizes the intersection points of the horizontal line with curves where the failure criterion is satisfied, i.e. where $K_{cr} = \sigma_f \sqrt{\pi a_c}$. The values of the respective stresses and the crack sizes at these points are termed to be the failure stresses and the critical crack sizes for the given structure, i.e., the unstiffened panel. In Figure 4.3.2b, the residual strength diagram is finally constructed by plotting the σ_f vs a_c curve.

EXAMPLE 4.3.2 Cracked Fastener Hole

Construct the residual strength diagrams for the radially cracked structure shown in Figure 4.3.4. Consider the two radial crack geometries separately, i.e., construct one residual strength diagram for the corner cracked hole and one residual strength diagram for the embedded (bore type) cracked hole illustrated in Figure 4.3.4b. For purposes of this example, the crack geometry is assumed to maintain the same crack shape (a/b ratio) as the crack grows. Also assume the fastener hole is unloaded and the plate is subjected to remote uniform stress along the edge as shown in Figure 4.3.4.

SOLUTION:

The first step in the construction of the residual strength diagram

is to obtain the stress-intensity factor relationships ($K = \sigma\beta\sqrt{\pi a}$) for the structural configuration. The estimation of β may involve closed form solutions or numerical solutions, depending on the complexities of the structural geometry. Fujimoto⁽¹⁰⁾ has presented one method for obtaining the stress intensity factors at points A and B shown in Figure 4.3.4b for the given geometry (See Section 1.7 for other solutions). The required stress intensity factor relationship has the following form⁽¹⁰⁾,

$$K_A = \beta_A \sigma\sqrt{\pi a} \quad (4.3.4)$$

and

$$K_B = \beta_B \sigma\sqrt{\pi b} \quad (4.3.5)$$

where

$$\beta_A = \sum_{i=0}^4 A_i \left(\frac{R}{R+a}\right)^i \quad (4.3.6)$$

and

$$\beta_B = \sum_{i=0}^4 B_i \left(\frac{R}{R+a}\right)^i \quad (4.3.7)$$

The coefficients A_i and B_i are evaluated by:

$$A_i = \sum_{j=0}^2 \sum_{k=0}^3 A_{ijk} \left(\frac{a}{b}\right)^j \left(\frac{b}{B}\right)^k \quad (4.3.8)$$

and

$$B_i = \sum_{j=0}^2 \sum_{k=0}^3 B_{ijk} \left(\frac{a}{b}\right)^j \left(\frac{b}{B}\right)^k \quad (4.3.9)$$

The constants A_{ijk} and B_{ijk} for the various configurations are summarized in Table 4.3.1⁽¹⁰⁾. The solutions presented by Equations 4.3.4 through 4.3.9 are suggested to be accurate to within $\pm 7\%$ for $0.5 \leq a/b \leq 2$, $a/R \leq 3$ and $b/B \leq 0.8$ (corner crack) and $b/B \leq 0.95$ (embedded flaw). For

TABLE 4.3.1

COEFFICIENTS FOR CORNER (A_{ijk}) AND EMBEDDED (B_{ijk}) FLAWS

Table I

A _{ijk} Coefficients				
A _{ijk}	Open Hole Corner Flaw	Loaded Hole Corner Flaw	Open Hole Embedded Flaw	Loaded Hole Embedded Flaw
A ₀₀₀	-1.73913	-0.44699	-1.26736	-0.27428
A ₀₀₁	2.18447	-0.41009	0.22793	-0.37981
A ₀₀₂	-12.31660	-0.17500	-0.31572	1.06466
A ₀₀₃	12.28036	-0.28705	0.27700	-0.70431
A ₀₁₀	2.03400	0.49602	1.46408	0.22855
A ₀₁₁	-5.54602	-1.17354	-0.51878	0.80844
A ₀₁₂	26.30347	0.05565	0.60348	-2.20899
A ₀₁₃	-28.83108	0.52655	-0.64122	1.42081
A ₀₂₀	-0.62550	-0.15949	-0.42884	-0.04803
A ₀₂₁	2.04171	0.52542	0.59595	-0.31512
A ₀₂₂	-10.08710	-0.15182	-1.10433	0.82786
A ₀₂₃	11.28916	-0.12493	0.82250	-0.51180
A ₁₀₀	20.44604	3.62963	16.35029	2.04350
A ₁₀₁	-12.98692	-3.42947	-1.36796	3.18371
A ₁₀₂	79.06818	1.25362	0.90021	-8.85802
A ₁₀₃	-81.39789	2.58161	-1.10382	5.83154
A ₁₁₀	-19.15893	-4.24345	-14.44464	-1.80365
A ₁₁₁	32.54240	9.71349	3.18175	-6.91026
A ₁₁₂	-153.17228	0.99495	-0.90493	18.66301
A ₁₁₃	183.89616	-5.61054	2.48066	-11.94847
A ₁₂₀	5.63804	1.38285	3.97690	0.38262
A ₁₂₁	-11.48757	-4.33299	-4.73213	2.70521
A ₁₂₂	57.78026	0.50822	8.12799	-7.01695
A ₁₂₃	-71.50791	1.70251	-6.10715	4.30908
A ₂₀₀	-54.07142	-8.73901	-40.03081	-3.66265
A ₂₀₁	26.28259	10.12695	1.69908	-9.40318
A ₂₀₂	-173.61978	-2.81193	5.31024	26.26181
A ₂₀₃	186.67485	-8.39172	-2.33583	-17.22762
A ₂₁₀	55.38509	12.06427	37.64427	4.07100
A ₂₁₁	-65.48530	-28.54288	-4.94141	20.73286
A ₂₁₂	310.31737	-4.71604	-11.78825	-55.81962
A ₂₁₃	-414.90592	18.60957	3.89408	35.80193
A ₂₂₀	-16.99852	-4.10506	-10.77498	-0.88681
A ₂₂₁	21.87818	12.64776	12.74285	-8.14196
A ₂₂₂	-113.03797	-0.10892	-19.73785	21.00805
A ₂₂₃	159.51377	-6.34499	14.67313	-12.89406
A ₃₀₀	63.91046	9.86487	44.09282	3.18017
A ₃₀₁	-21.34684	-12.58513	1.30029	11.71907
A ₃₀₂	155.66256	2.41823	-17.28515	-32.85878
A ₃₀₃	-177.54153	11.37710	10.22270	21.47714
A ₃₁₀	-69.55437	-14.91176	-42.79166	-4.23316
A ₃₁₁	53.27534	35.32007	-0.41580	-26.09328
A ₃₁₂	-239.17594	9.64735	34.36822	70.23733
A ₃₁₃	382.87850	-26.68173	-19.03715	-45.03193
A ₃₂₀	21.97211	5.18043	12.56399	0.94129
A ₃₂₁	-16.45864	-15.54508	-13.63744	10.23302
A ₃₂₂	81.63436	-2.04295	18.05169	-26.34017
A ₃₂₃	-144.56350	9.86170	-13.65703	16.12578
A ₄₀₀	-25.48746	-3.45644	-15.57989	-0.32568
A ₄₀₁	6.07411	5.63847	-2.29626	-5.26245
A ₄₀₂	-47.33858	-0.47231	12.79822	14.81260
A ₄₀₃	58.83734	-5.58817	-7.87547	-9.62040
A ₄₁₀	30.61973	6.33835	16.18676	1.20944
A ₄₁₁	-15.30575	-15.72380	3.64549	11.77369
A ₄₁₂	56.77733	-5.25457	-24.86827	-31.67043
A ₄₁₃	-123.39537	13.06793	15.10964	20.30113
A ₄₂₀	-10.04444	-2.28421	-4.93434	-0.27841
A ₄₂₁	4.18466	6.85458	4.68604	-4.60124
A ₄₂₂	-16.39237	1.58956	-4.47318	11.81074
A ₄₂₃	45.39223	-5.06460	3.88566	-7.22032

Table II

B _{ijk} Coefficients				
B _{ijk}	Open Hole Corner Flaw	Loaded Hole Corner Flaw	Open Hole Embedded Flaw	Loaded Hole Embedded Flaw
B ₀₀₀	0.54048	0.15717	-0.14090	-0.04578
B ₀₀₁	-8.13585	-0.18905	-0.19118	0.23456
B ₀₀₂	38.74291	0.36964	-1.42513	-1.03245
B ₀₀₃	-36.61072	-0.55842	2.70092	1.04606
B ₀₁₀	-0.51374	-0.34371	0.24126	0.02019
B ₀₁₁	20.70229	0.67188	-0.06062	-0.68745
B ₀₁₂	-96.53400	-1.02481	3.50309	2.60507
B ₀₁₃	94.56232	2.24038	-5.56386	-2.53181
B ₀₂₀	0.23259	0.13161	-0.03900	-0.01654
B ₀₂₁	-8.10325	-0.24870	0.14748	0.39027
B ₀₂₂	37.49696	0.15076	-1.79208	-1.40898
B ₀₂₃	-36.02049	-0.43639	2.62247	1.30659
B ₁₀₀	-3.93066	-1.40838	1.51775	0.39092
B ₁₀₁	54.54817	3.05268	2.95869	-1.89716
B ₁₀₂	-267.23920	-5.58993	6.91519	8.31125
B ₁₀₃	257.44638	5.83453	-18.34105	-8.38878
B ₁₁₀	10.54763	4.21388	2.99000	0.49356
B ₁₁₁	-137.75080	-8.95923	1.42239	5.83529
B ₁₁₂	658.29611	13.40329	-33.45103	-22.27612
B ₁₁₃	-664.66240	-20.77969	51.72551	21.67629
B ₁₂₀	-3.12356	-1.39814	-0.63004	0.03033
B ₁₂₁	53.58138	3.40310	-0.68160	-3.10127
B ₁₂₂	-250.42133	-2.82250	12.97239	11.27094
B ₁₂₃	246.15655	3.95030	-20.04903	-10.45358
B ₂₀₀	12.31339	4.73501	-4.21283	-1.00774
B ₂₀₁	-130.01489	-13.23293	-14.43670	4.85151
B ₂₀₂	652.54759	23.67186	1.64581	-21.38737
B ₂₀₃	-639.45674	-20.29833	33.74666	21.56301
B ₂₁₀	-25.20873	-11.55251	-4.32532	-0.24067
B ₂₁₁	329.32411	36.63884	8.63271	-14.25572
B ₂₁₂	-1601.55759	-56.47692	47.76155	54.50932
B ₂₁₃	1664.84801	69.79620	-103.79259	-53.08007
B ₂₂₀	8.01373	4.12442	1.06179	-0.25385
B ₂₂₁	-126.43281	-13.84244	-2.78214	7.75229
B ₂₂₂	602.66553	14.96288	-18.70448	-28.10606
B ₂₂₃	-608.02169	-15.00235	40.49219	26.14542
B ₃₀₀	-14.68582	-6.15314	5.54863	1.21024
B ₃₀₁	130.65565	21.26107	23.96607	-5.08309
B ₃₀₂	-678.54260	-39.04345	-27.28160	22.36259
B ₃₀₃	680.29731	30.88059	-18.01680	-22.53679
B ₃₁₀	32.19384	15.42347	6.56869	0.72364
B ₃₁₁	-329.36748	-56.34595	-20.61094	15.16998
B ₃₁₂	1648.82514	89.92427	-16.75978	-57.78589
B ₃₁₃	-1780.81402	-99.14050	88.27022	56.49131
B ₃₂₀	-10.69055	-5.64651	-2.00699	0.07354
B ₃₂₁	124.22248	21.24180	8.57289	-7.89956
B ₃₂₂	-605.34757	-24.65551	1.19613	28.37763
B ₃₂₃	632.49290	21.54101	-28.78621	-26.44062
B ₄₀₀	6.62558	2.93506	-2.17015	-0.40455
B ₄₀₁	-47.11327	-11.40477	-12.23145	1.91775
B ₄₀₂	252.80634	20.97539	19.85932	-8.33485
B ₄₀₃	-260.05599	-15.75597	-0.06542	8.32499
B ₄₁₀	-15.12721	-7.31732	-3.18803	-0.37767
B ₄₁₁	118.27654	29.53266	12.75632	-5.49372
B ₄₁₂	-604.94418	-46.78340	-9.48745	20.67719
B ₄₁₃	681.55676	47.49374	-21.42362	-20.07632
B ₄₂₀	5.12997	2.70455	0.99823	-0.00082
B ₄₂₁	-43.91149	-11.21255	-5.70704	2.73978
B ₄₂₂	217.00926	13.56194	8.16120	-9.63864
B ₄₂₃	-234.55121	-10.63665	3.75003	8.91080

the detailed solution procedures involved in obtaining these expressions, refer to the paper by Fujimoto⁽¹⁰⁾ who also presents solutions for the condition where the fastener is loaded.

Subjected to the conditions when the crack size ratio (a/b) is equal to 1.0, the stress-intensity factor solutions for points A and B are given in Figure 4.3.5 for the quarter-circular corner crack and in Figure 4.3.6 for the embedded semicircular crack. The K_A and K_B curves in these two figures were obtained from Equations 4.3.4 through 4.3.9 with the appropriate coefficients taken from Table 4.3.1.

Having established a relationship for the applied stress intensity factors K_A and K_B , the second step is to choose an appropriate failure criterion. The given configuration consists of a thick plate where plane strain conditions exist and the appropriate fracture toughness criterion based on the K_{Ic} value can be used. Substituting the value of K_{Ic} for K_A and K_B as a failure condition in Equations 4.3.4 and 4.3.5, the equations can be solved for σ for various values of a . The residual strength diagram for the open hole configuration can be constructed through the following equations.

$$\sigma_f^A = \frac{K_{Ic}}{\beta_A \sqrt{\pi a}} \quad (4.3.10)$$

and

$$\sigma_f^B = \frac{K_{Ic}}{\beta_B \sqrt{\frac{b}{a}} \sqrt{\pi a}} \quad (4.3.11)$$

The solutions to Equations 4.3.10 and 4.3.11 are presented in Figure 4.3.7 for the radial quarter circular crack geometry and in Figure 4.3.8 for the radial embedded semicircular crack geometry. Note that the conditions associated with Point B in both crack geometries is more severe and actually defines the residual strength of this radially cracked structure.

4.3.2 Built-Up Structure Residual Strength Diagrams

In single load path structures, the residual strength analysis involved only one failure criterion for a given structural geometry; whereas in built-up structures, due to the complex geometrical configuration, one or more failure criterion may have to be considered in the determination of residual strength for the whole structure. The following paragraphs examine these aspects of the residual strength analysis of built-up structures.

It was explained earlier that safety can be achieved by designing aircraft structure either as slow crack growth or as fail-safe. The latter case can further be classified into two cases: Multiple Load Path and Crack Arrest. Typically, both Multiple Load Path and Crack Arrest structures are built-up structures. In Chapter 2, the definitions and requirements for these two types of built-up structure are discussed. For completeness, the structure shown in Figure 4.3.9 is analyzed to further explain the features inherent in multiple load path, built-up structure. As long as the central member is not failed, all three elements

carry a share of the total load P . In the event of failure of the center member, the total load P (actually $1.15P$) must be transmitted by the other two members at the instant of failure, if the structure is to stay intact. The residual strength capability for the multiple load path structure shown in Figure 4.3.9 can be explained with Figure 4.3.10. When one element fails, Figure 4.3.10 shows that the remaining parallel members are able to carry the required load without failure. The residual capability is shown to degrade as the crack in the central member extends and as the cracks in the remaining elements fail. Figure 4.3.10 shows the discontinuous change in the strength capability as a result of element failures. Since the load levels in other members dramatically increase, if the load P must be maintained, the remaining members will have short lives. Thus, the second member may fail after the time (t_2). The residual strength capability is shown to drop below the safe level somewhere in time between t_1 and t_2 . The duration of the time interval between the failure of the first element and the failure of the structure may be short or long depending on the "type of failure" of the first member and the load requirements subsequent to this failure. This time interval is available for the detection of the failure of the first member and the repair of the structure.

The failure stress or the critical flaw size level of the central member (any one of the parallel members) can be estimated by treating the problem in a manner similar to the single load path structure. Using a

fatigue crack growth analysis, the crack propagation curve is obtained from the minimum detectable crack size to the critical crack length as illustrated in Figure 4.3.11. In multiple load path structure, partial failure of the structure can occur during its operating period. But this failure must be detected at an inspection before catastrophic failure of the entire structure occurs. A suitable inspection schedule must include analysis of structural characteristics along with the operational requirements for the intervals between inspections.

To illustrate the analysis involved in the estimation of residual strength of complex structures, consider an axially loaded skin-stringer combination with longitudinal stiffening as shown in Figure 4.3.12.

Assuming that the fasteners are rigid, the displacements of adjacent points in skin and stringers will be equal. (If skin and stringers are made from the same material, the stresses in the two will also be equal for the case of no crack.) Let a transverse crack develop in the skin. This will cause larger displacement in the skin. The stringers must follow this larger displacement. As a result, they take load from the skin, thus decreasing the skin stress at the expense of higher stringer stress. Consequently, the displacements in the cracked skin will be smaller than in an unstiffened plate with the same size of crack. This implies that the skin stresses are lower and that the stress-intensity factor is lower. The closer the stringers are to the crack, the more effective is the load transfer.

If the stress-intensity factor for a small crack in an unstiffened panel is approximated by $K = \sigma\sqrt{\pi a}$, the stress-intensity factor for the stiffened plate will be $K = \beta\sigma\sqrt{\pi a}$. The reduction factor, $\beta = K/\sigma\sqrt{\pi a}$, will decrease when the crack tip approaches a stringer. Since the stringers take load from the skin, the stringer stress will increase from σ to $L\sigma$, where L increases as the crack tip approaches the stringer. Obviously, $0 < \beta \leq 1$, and $L \geq 1$. These values depend upon stiffening ratios, the stiffness of the attachment, and the ratio of crack size to stringer spacing. As will be shown subsequently, β and L can be readily calculated; at this point it is sufficient to note that β and L vary with crack length as shown in Figure 4.3.13.

Due to the complexity of stiffened skin structure, the construction of a residual strength diagram is considerably more difficult. Consider first the condition where an abrupt failure in the skin occurs. When the crack is small as compared to the stiffener spacing, the residual strength of the skin is not influenced by the stiffeners and the initial portion of the diagram follows the plot for an unstiffened panel (See point A in Figure 4.3.14). Once the crack size is long enough that the skin cannot sustain the applied load any further, the stringer will take some of the load from the skin, thus decreasing the skin stress. Consequently, the crack-tip stress-intensity factor will be lower due to the reduced stress and so the residual strength of the skin structure will increase with crack length as shown in Figure 4.3.13. As the crack size increases further toward the

stiffener location, the load transferred from the skin to the stiffener also increases significantly, thus reducing the stress-intensity factor. The residual strength of the stiffened panel continues to increase as shown in the figure for longer cracks. It can also be noted from the figure that the residual strength diagram for an unstiffened panel would have followed the dotted line, i.e., the continuous decay in the residual strength as the crack size increases. This is because there is no inherent feature present in the single load path structure to decrease the crack tip stress-intensity factor.

The residual strength diagram for the skin-stiffened structure is repeated in Figure 4.3.15 where several additional points of interest are defined for the analyst. For a structure with a crack of length a_A , the residual strength is identified as point A. Since point A is associated with a failure stress that is above the peak stress (σ_{peak}), the crack extends abruptly and completely fails the panel. If the structure contains a crack of length a_C , in the range between a_B and a_D , the crack extends abruptly but then arrests at crack length a_E , where the residual strength available is greater than the applied (failure) stress. This crack extension and arrest feature of skin-stringer construction greatly facilitates meeting inspection requirements for fail-safe structures.

Before the panel fails completely, the failure stress level at point C/E must be increased to the level associated with point F, i.e. to σ_{peak} . As the stress is increased above the level of point E, the crack extends

from a_E to maintain an equilibrium between the input stress and the residual strength. When the stress reaches σ_{peak} , the crack has extended to a_F , at which point the crack abruptly extends causing failure of the panel. A schematic illustrating the load crack length diagram observed during an abrupt crack extension/arrest situation in a skin-stringer structure is presented in Figure 4.3.16. Thus, it is seen that the residual strength curve ABCDEF shown in Figure 4.3.15 can be replaced for all practical purposes with a curve that connects points ABF.

In the design of fail-safe structure, a frequent objective is to design the structure for limiting or arresting unstable crack growth so that catastrophic failure can be prevented. A number of arrest techniques are described in References 11 through 13. The fundamental concept in crack arrest design is to provide within the structure a means to reduce the crack tip stress intensity factor. This concept requires the use of additional stiffening members such as stiffeners, reinforcing rings, etc., to produce a decrease in the stress. These are inherently present in built-up structures, such as aircraft wings, fuselages, etc. as shown in Figure 4.3.12.

In general, the residual strength analysis of a structure with crack arrest capabilities may involve more than one failure criterion. For instance, in a stiffened skin structure or an aircraft wing, the analysis should consider stringer failure, fastener failure, and skin crack failure criteria. Built-up panels loaded to fail-safe levels tend to

exhibit substantial local deformations of critical elements. Failure criteria are thus dependent also on elastic-plastic deflection allowables for both fastener and skin/stringer elements. Gunther and Wozumi⁽¹⁴⁾ provide additional details on the residual strength analysis of complex panels based on the ultimate stringer strain.

The residual strength diagram for the structure which exhibits slow crack growth behavior will contain two curves as shown in Figure 4.3.17. The lower curve corresponds to the critical level of stress at which slow crack extension starts. The onset of slow tearing is then described by this lower curve. The upper curve provides the critical stress level at which the unstable rapid crack extension occurs. When the crack approaches the stiffener, as explained earlier, the residual strength levels, corresponding to the onset of slow cracking and the rapid extension, start increasing.

For a crack length a_1 , as shown in Figure 4.3.17, the slow crack extension begins at point B. This stable extension continues up to point B' where the rapid failure is supposed to occur. However, due to the continuous rise in the residual strength of the stiffened panel, the stable crack extension continues to occur beyond point B' and up to point C. Since the residual strength of the panel starts reducing at this point, any further increase in the applied load will lead to the rapid unstable crack extension.

The construction of the residual strength diagram follows the three steps presented in Section 4.3.1. Due to the complexity of the structural geometry, however, estimating requires the calculation of the loads that are transferred to the stiffening or secondary members from the main load carrying member of the structure. Depending upon the complexity, the K vs a curves can be obtained either through an appropriate numerical method or through the method of superposition. The methods for constructing residual strength diagrams and for the residual strength capability analyses are further discussed in the following sections with various example problems.

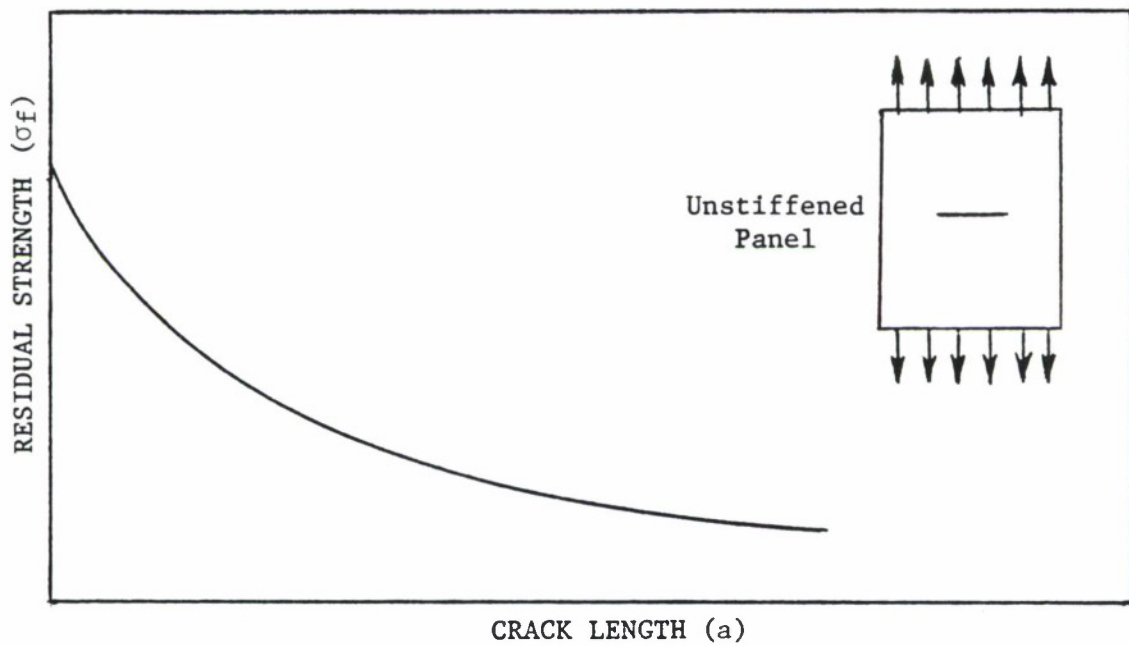


Figure 4.3.1. Residual Strength Diagram for Abrupt Failure of a Single Load Path Structure.

MATERIAL PROPERTIES

yield strength (σ_{ys}) = 74 ksi

Fracture Toughness
(K_C) = 40 ksi $\sqrt{\text{in}}$

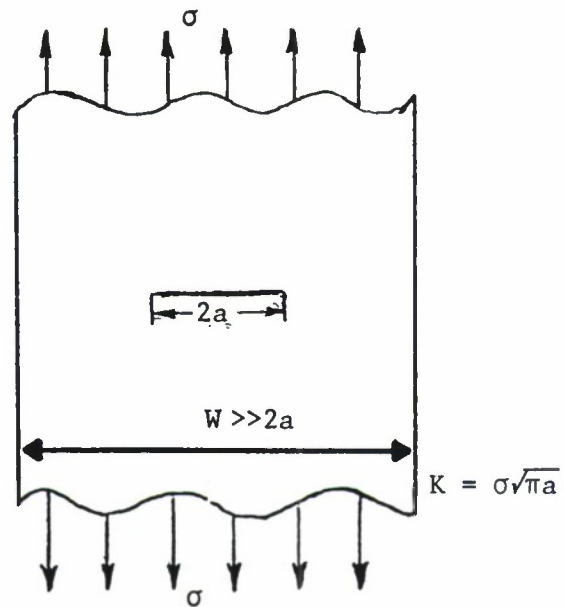
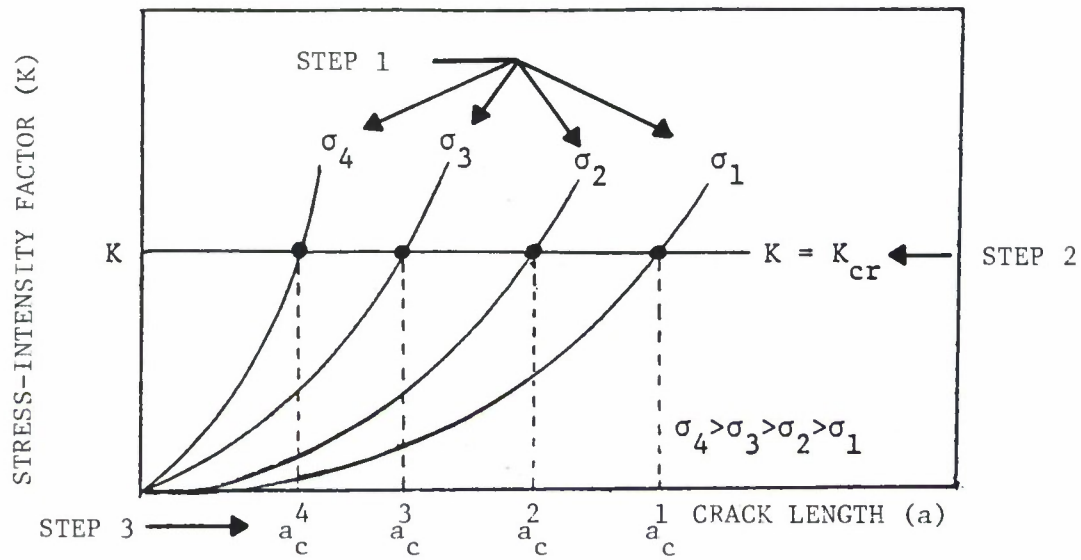
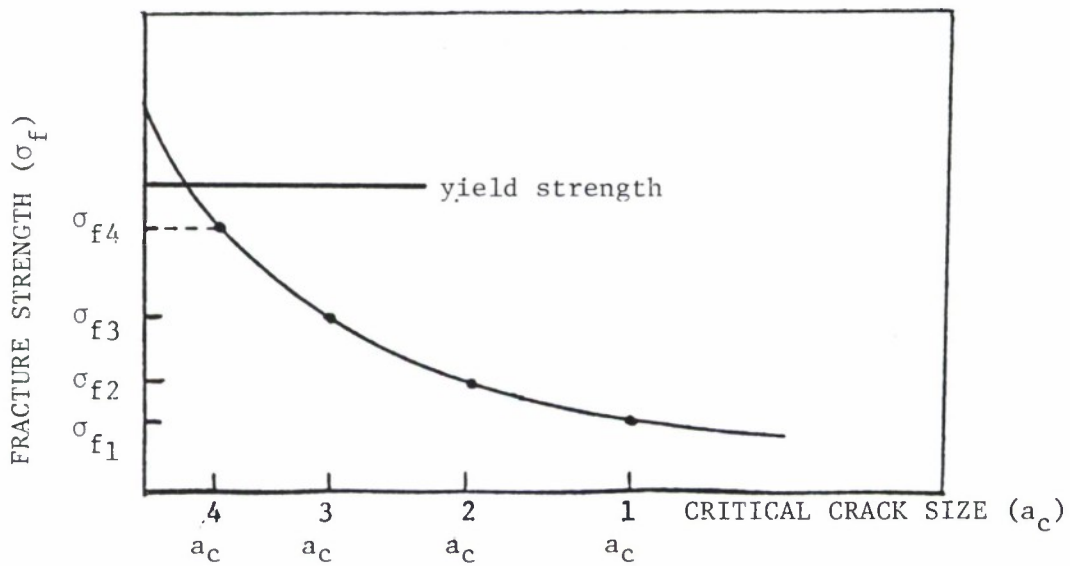


Figure 4.3.2. Structural Geometry and Material Properties for Example 4.3.1.



(a) Stress-Intensity Factor as a Function of Crack Length for Constant Values of Stress



(b) Residual Strength Diagram

Figure 4.3.3. Description of Procedures that One Might Follow to Obtain the Residual Strength Diagram Graphically.

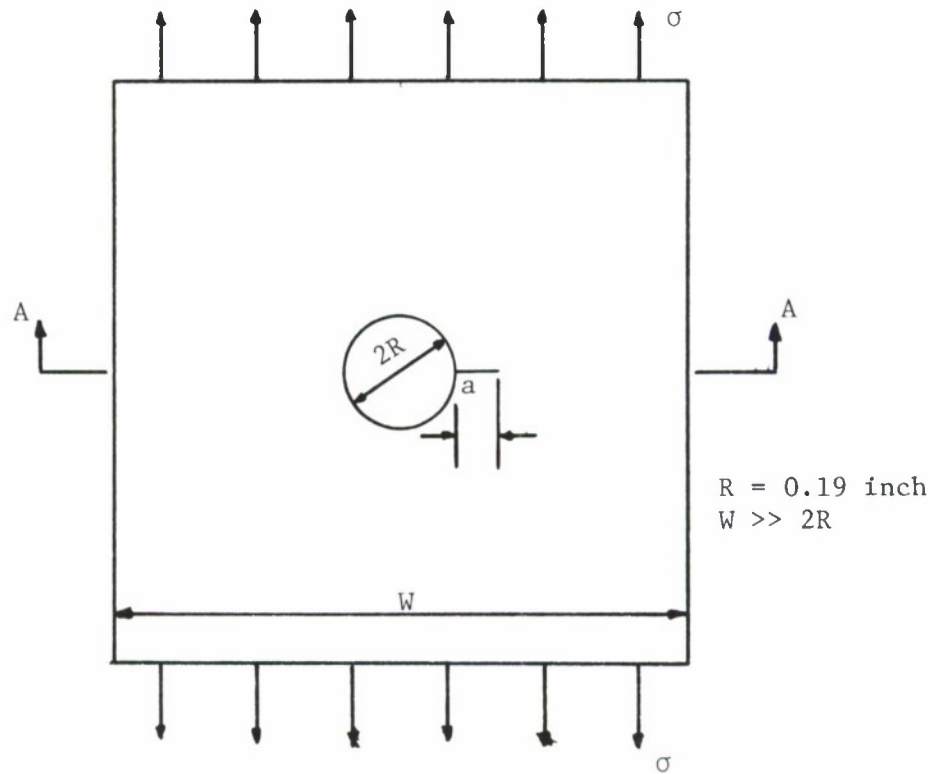
MATERIAL

AISI 4340 STEEL

MATERIAL
PROPERTIES

$$\sigma_{ys} = 200 \text{ Ksi}$$

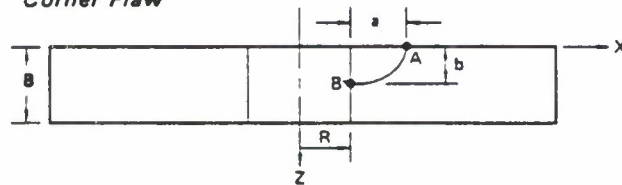
$$K_{Ic} = 75 \text{ Ksi}$$



$$R = 0.19 \text{ inch}$$
$$W \gg 2R$$

(a) In Plane View of Radial Hole Crack

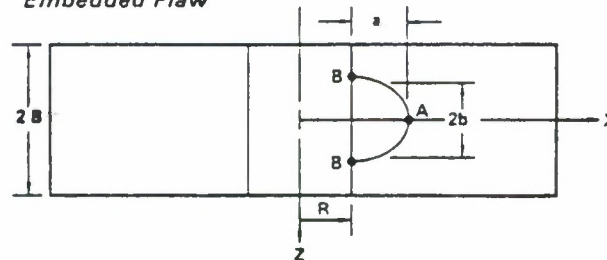
Corner Flaw



$$\frac{a}{b} = 1.0$$

$$B = 0.76 \text{ inch}$$

Embedded Flaw



(b) Section A-A. Definition of Crack Geometries

Figure 4.3.4. Crack Geometries Considered for a Radial Crack Growing from a Hole for Example 4.3.2.

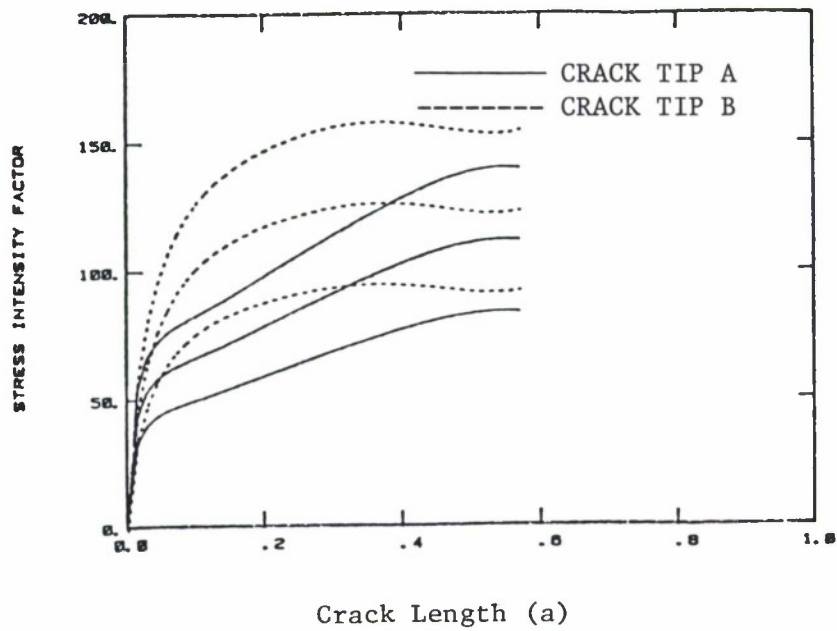


Figure 4.3.5. Stress-Intensity Factor Relationships at Points A and B for the Radial Quarter Circular Crack Geometry.

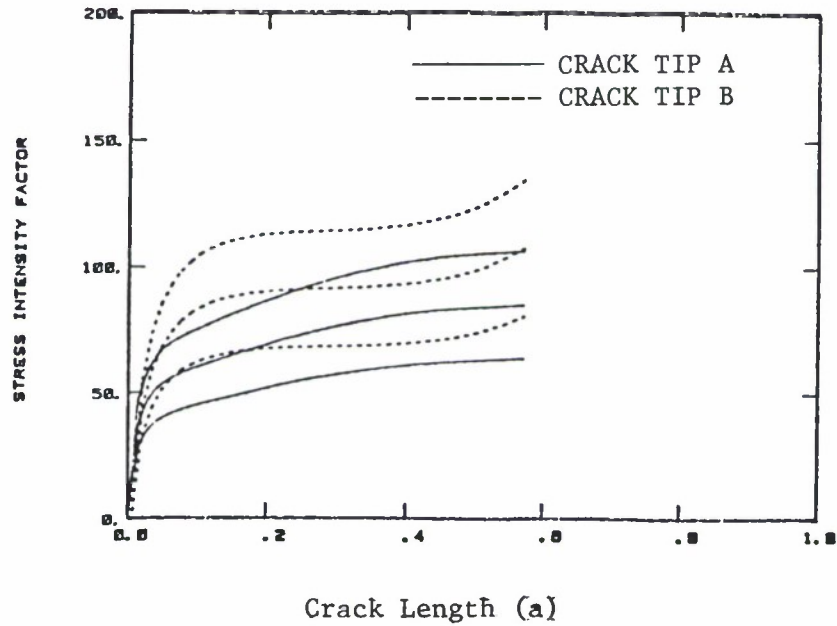


Figure 4.3.6. Stress-Intensity Factor Relationships at Points A and B for the Radial Embedded Semi-Circular Crack Geometry.

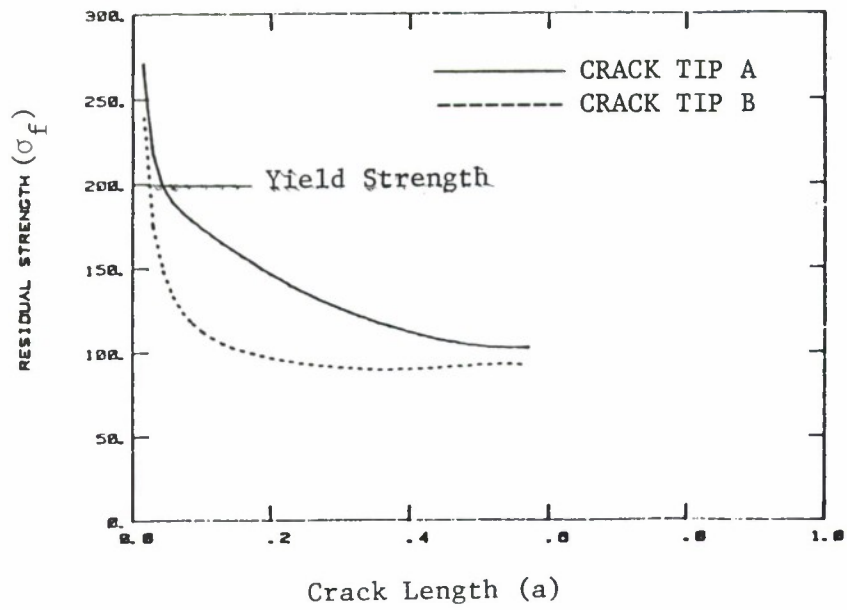


Figure 4.3.7. Residual Strength Diagram for Points A and B Located on the Radial Quarter Circular Crack Geometry Shown in Figure 4.3.4.

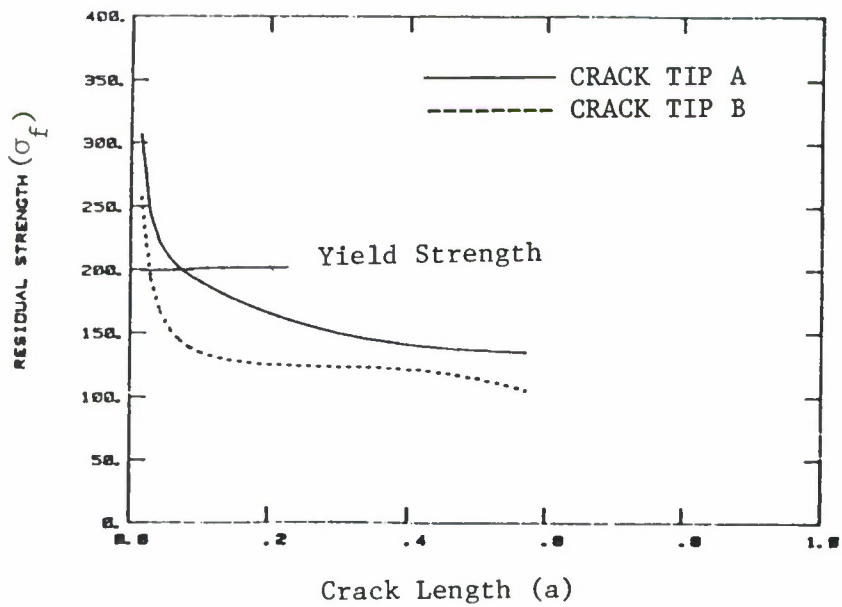


Figure 4.3.8. Residual Strength Diagram for Points A and B Located on the Embedded Semi-Circular Crack Geometry Shown in Figure 4.3.4.

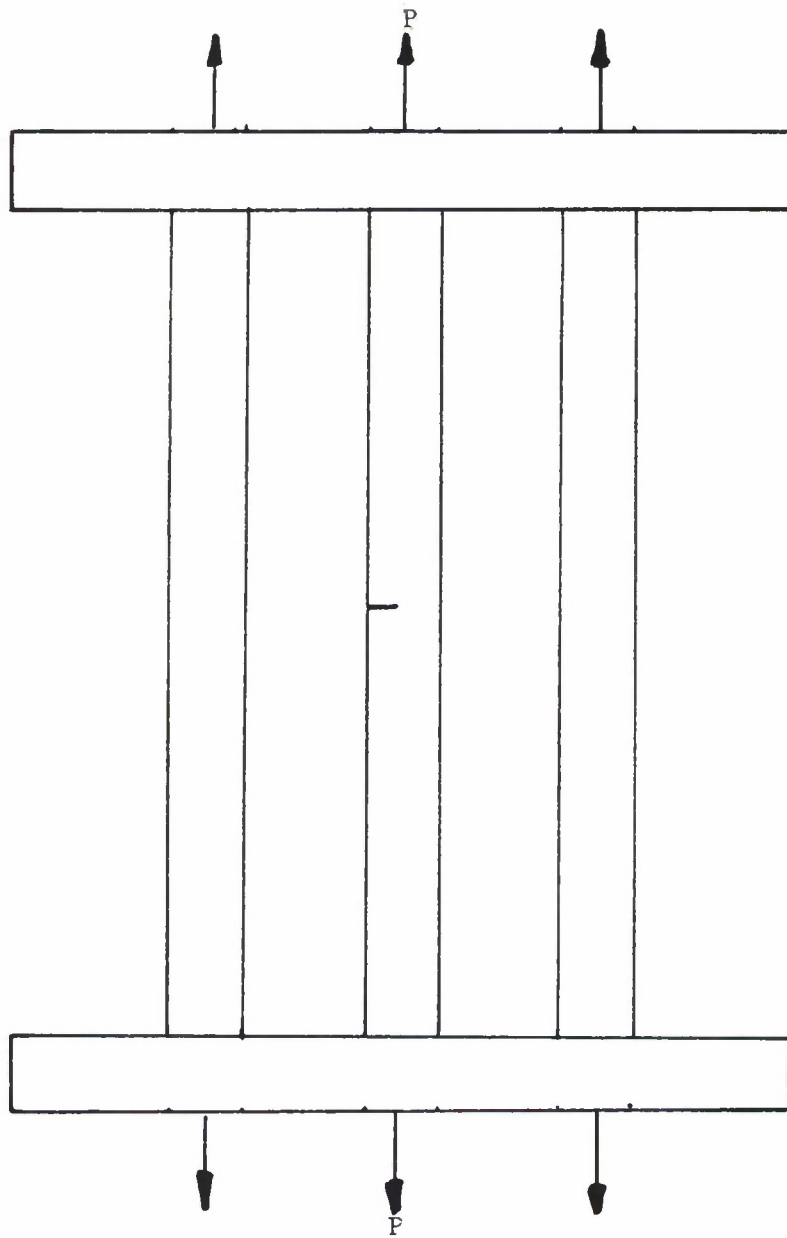


Figure 4.3.9. Multiple Load Path (Built-up) Structure with a Crack in the Central Member.

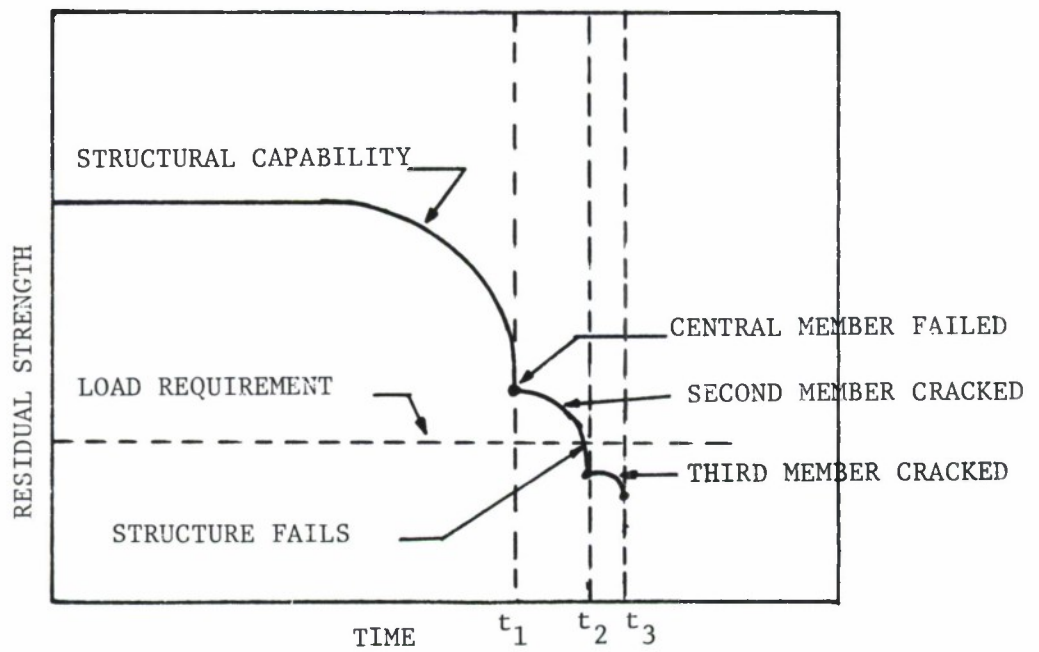


Figure 4.3.10. Reduction of Residual Strength During Successive Failure of Members in the Structure Shown in Figure 4.3.9.

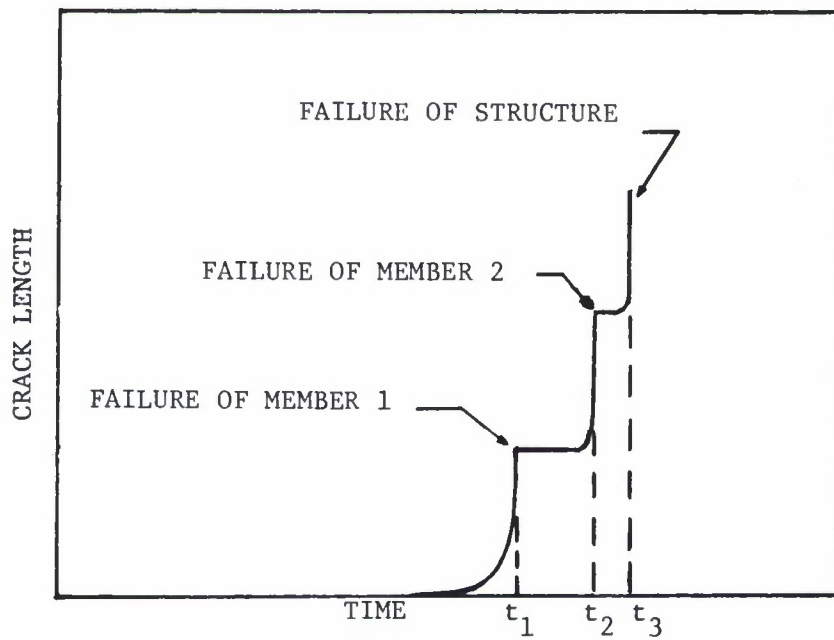


Figure 4.3.11. Crack Growth Curve for Multiple Load Path Structure Shown in Figure 4.3.9.

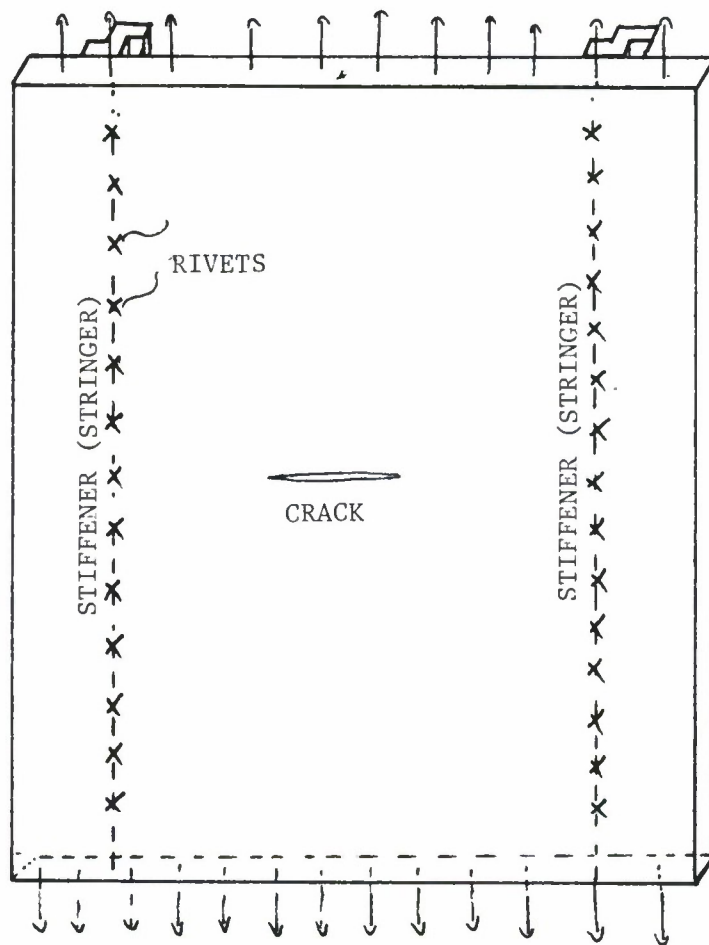


Figure 4.3.12. Skin-Stringer Built-Up Structure.

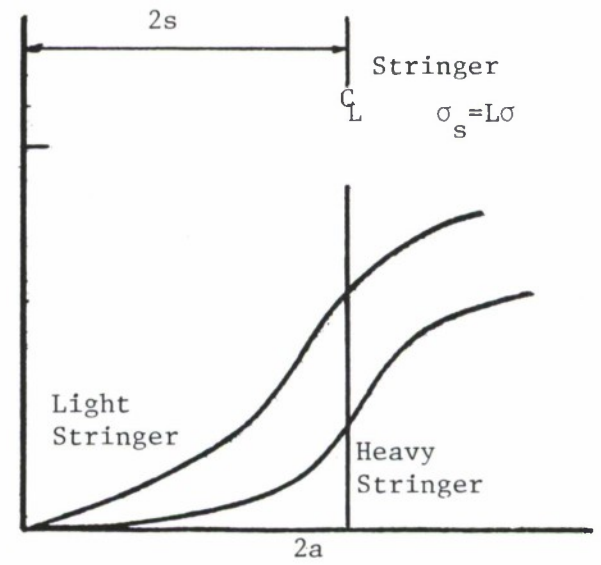
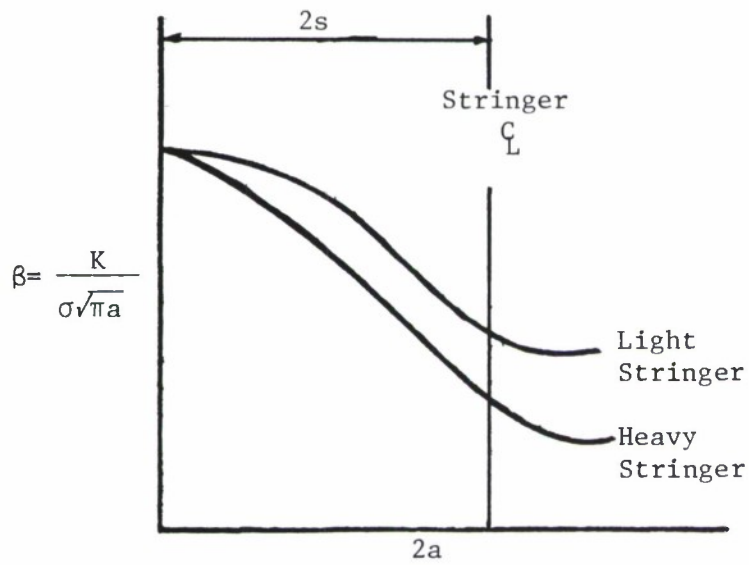
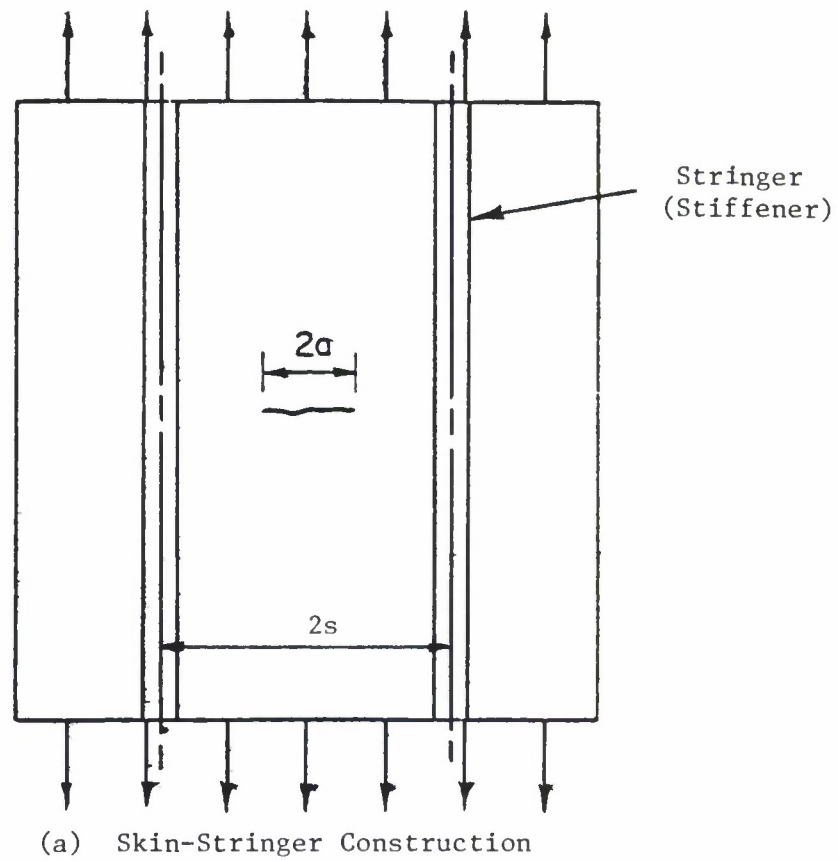


Figure 4.3.13. Variation of β and L with Crack Length in Stiffened Panel with a Crack Between the Stiffeners.

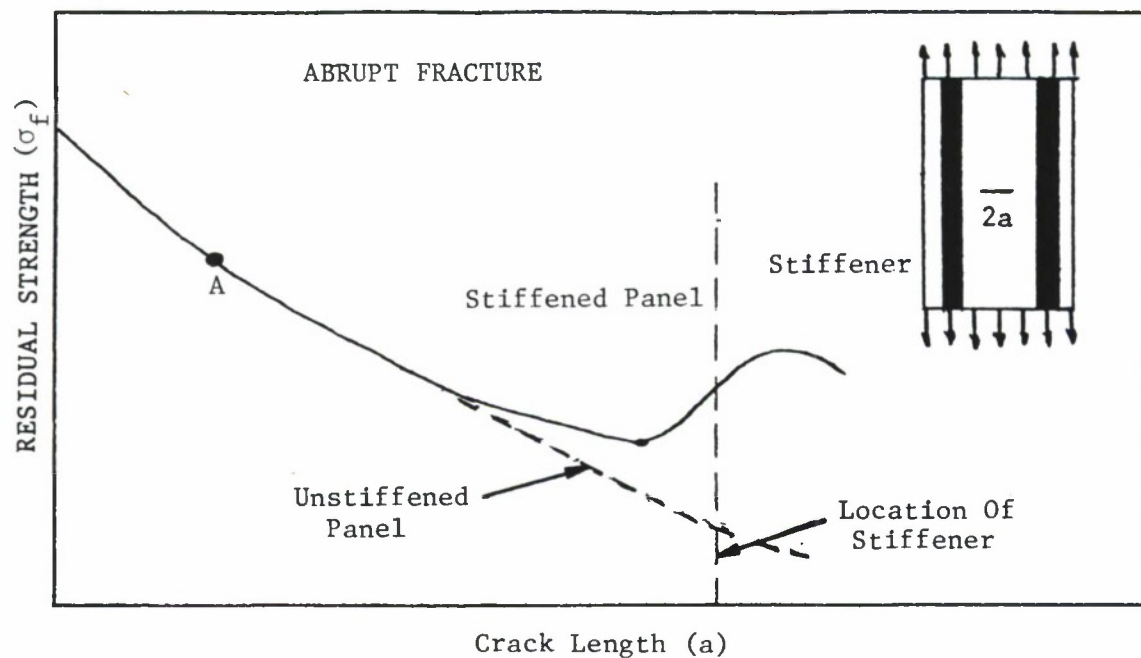


Figure 4.3.14. Residual Strength of the Cracked Panel as a Function of Crack Length for Built-Up Skin-Stiffened Structure Compared with Unstiffened Panel. Abrupt Failure Criterion Used to Determine Residual Strength.

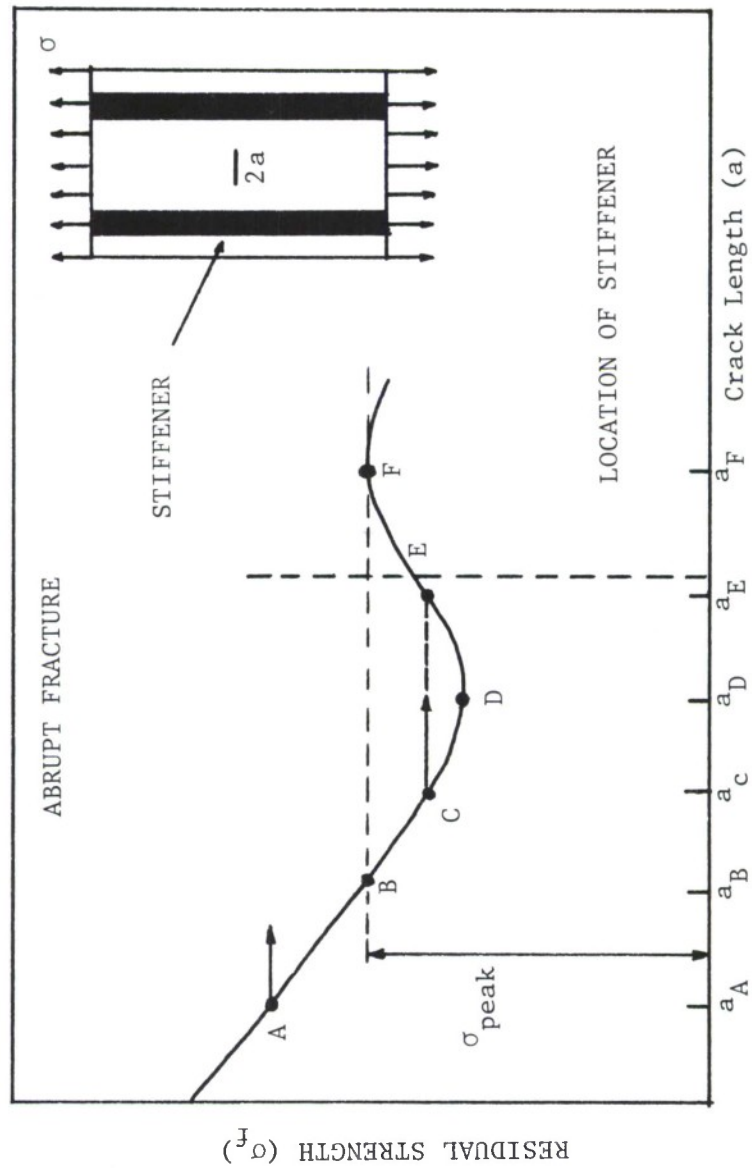


Figure 4.3.15. Residual Strength of the Cracked Panel as a Function of Crack Length for Built-Up Skin Stiffened Structure. Only Skin Failure Mode Considered. Abrupt Failure Criterion Used to Determine Residual Strength.

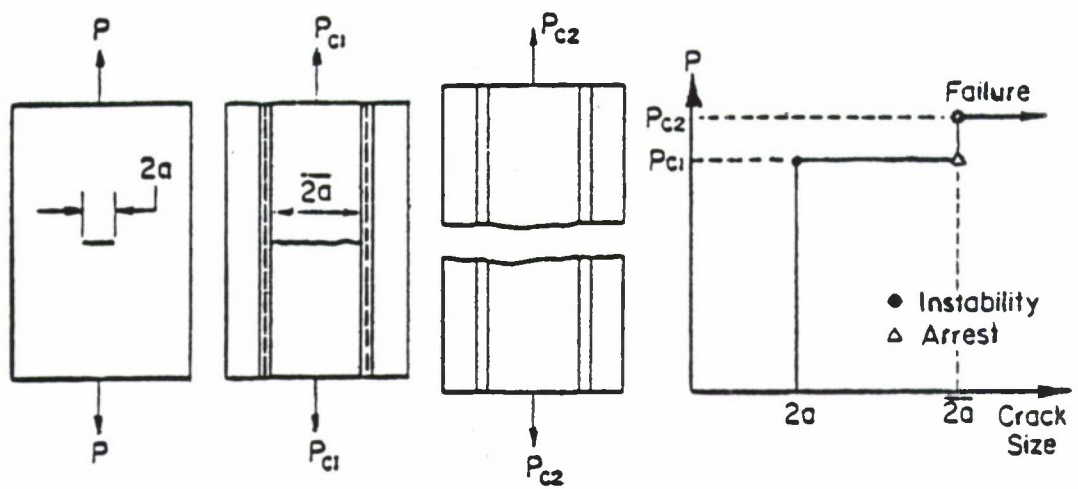


Figure 4.3.16. Load-Crack Length Behavior Observed in Skin-Stiffened Construction with Arrest Features.

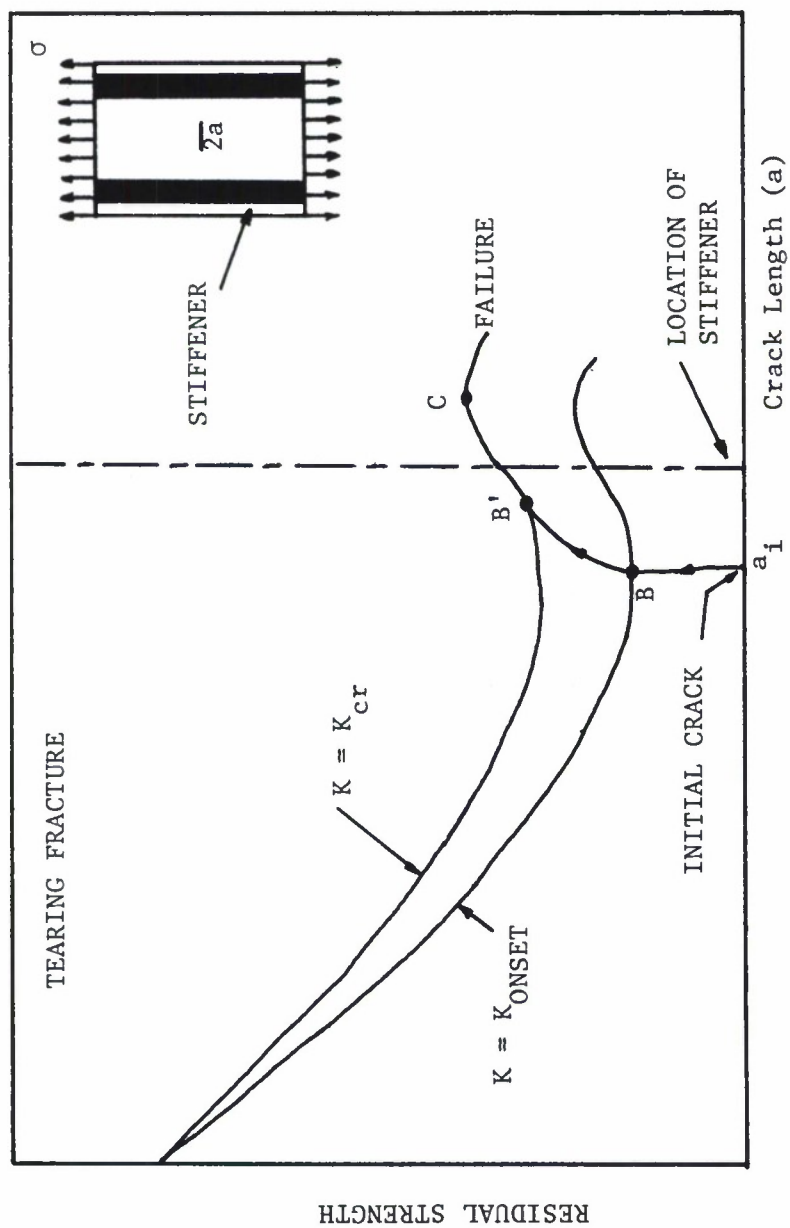


Figure 4.3.17. Residual Strength of Cracked Panel as a Function of Crack Length for Built-up Skin-Stringer Structure. Tearing Failure Criterion Used to Determine Residual Strength.

4.4 SINGLE LOAD PATH STRUCTURE

For a single load path structure, the only means to protect the safety is to prevent the damage growth from degrading the strength of the structure to less than the design limit load. This applies for all structures classified as slow crack growth, regardless of the type of construction (such as single load path or multiple load path). The residual strength capability of the structure depends mainly on the material's resistance to fracture.

4.4.1 Abrupt Fracture

For materials which exhibit abrupt failure, the start of slow crack extension will be followed immediately by the onset of rapid fracture. The residual strength capability then requires a strict evaluation of the initial flaw sizes in the structure. The allowable initial crack length necessary to maintain the required residual strength will be less than a_f ; the design limit load must also be such that the stress level in the structure is less than σ_i as shown in Figure 4.4.1. The residual strength diagram can be evaluated as described earlier through the plot of σ_f vs a_c using the relationship $K = \sigma_f \sqrt{\pi a}$ for the structural geometry of interest and also employing the failure criterion based on a critical fracture toughness value, K_{cr} . The margin of safety as shown in Figure 4.4.1 allows for undetected cracks or for subcritical crack growth such that the initial crack size will not become greater than a_f .

In the following paragraphs, two different example problems are presented to demonstrate the application of the steps in constructing the residual strength diagram and also to analyze the structure for its residual strength capabilities. The first example illustrates the centrally cracked finite width panel. The second example considers an eccentrically cracked finite width panel problem. These examples demonstrate the basic concepts involved in the residual strength capabilities of a single load path structure.

EXAMPLE 4.4.1 Residual Strength of Center Cracked Panel

Develop the residual strength diagram for the cracked finite width panel shown in Figure 4.4.2.

SOLUTION:

For the center-cracked geometry configuration shown in Figure 4.4.2, the stress-intensity factor K is expressed by the relationship (See Section 1.7):

$$K = \sigma \sqrt{\pi a \sec\left(\frac{\pi a}{W}\right)} \quad (4.4.1)$$

Since we have an explicit expression for K , using the fracture toughness failure criterion (plane strain), the residual strength diagram can be obtained directly. The corresponding equation is

$$\sigma_f = K_{Ic} / \left(\sqrt{\pi a_c \sec\left(\frac{\pi a_c}{W}\right)} \right) \quad (4.4.2)$$

where $K_{Ic} = 40 \text{ ksi}\sqrt{\text{in}}$ and $W = 20 \text{ inch}$ are given as data and σ_f can be obtained for any selected crack length. The σ_f vs a_c curve, which is the

required residual strength diagram, can now be plotted.

The residual strength of the panel can be estimated from Equation 4.4.2 which is described in the diagram presented in Figure 4.4.3. From this figure, for the given operating stress level (20 Ksi), the critical crack size at which unstable crack extension would occur, can be estimated as 1.2 inch. Thus, to avoid a fracture type failure of the panel, the structure should not develop a crack of this size. Assume that based on an established visual inspection schedule, the simple rectangular aluminum panel, uniformly loaded in tension as shown, could develop a 2.0 inch long, central through-the-thickness crack (normal to loading) before detection. This crack length is slightly smaller than the critical crack size ($2.4 = 2 \times 1.2$ inch) under the operating conditions so that the margin of safety is small when this inspection process is employed.

To establish the required residual strength level to fit the inspection schedule, the designer must reduce the crack-tip stress-intensity factor for the same applied load. One method is to transfer portions of the load to a stiffening member. Another method is to reduce the operating load level below the failure level corresponding to the inspection crack size, although this is not always practiced.

EXAMPLE 4.4.2 Residual Strength of Eccentrically Cracked Panel

Establish the residual strength diagram for a finite-width panel with the eccentric crack shown in Figure 4.4.4.

SOLUTION:

For the given configuration, the stress intensity factor is expressed by the following relationship (See Section 1.7),

$$K = \sigma \beta \sqrt{\pi a} \quad (4.4.3)$$

where $\beta = \beta(\epsilon, \frac{a}{W})$ and $\epsilon = \frac{2e}{W}$; $W' = \frac{W}{2} - e$. Since it is an eccentric crack, the K values at the crack tips A and E will be different and the corresponding β 's will also be different. From the plots of Figure 4.4.5⁽¹⁵⁾, β values for the crack tips A and E can be obtained for a given aspect ratio (a/W') and the eccentricity factor, ϵ . It is obvious from Figure 4.4.5 that the stress-intensity factor conditions at crack tip A, which is close to the panel edge, are higher than that for crack tip E so the conditions at point A will be critical in deciding the residual strength of the panel.

Applying the fracture toughness failure criterion, we can now obtain the direct relationship between the fracture stress and the critical crack size as

$$\sigma_f^A = K_{Ic} / \beta^A \sqrt{\pi a} \quad (4.4.4a)$$

and

$$\sigma_f^E = K_{Ic} / \beta^E \sqrt{\pi a} \quad , \quad (4.4.4b)$$

where the superscripts A and E represent the conditions at the crack tips A and E. We can now plot curves σ_f^A vs a and σ_f^E vs a for the given structural configuration. The residual strength diagram for crack tips A and E for $\epsilon = 0.9$ and $W' = 1.0$ are shown in Figure 4.4.6. As

anticipated on the basis of the differences in stress-intensity factor conditions, the residual strength curve associated with crack tip A controls the crack extension behavior of the eccentric crack. For the 20 Ksi maximum stress operating condition, the critical crack size is approximately 0.73 inch, based on the crack tip A curve (see point G). If a crack with a half crack length (a) of 0.73 inch develops in the panel, crack tip A will extend rapidly and the crack will be arrested at the free edge. Now the crack growth behavior at crack tip E needs further analysis corresponding to the panel configuration as shown in Figure 4.4.7. The crack length a' is equal to $(W' + a)$ where W' and a are known, i.e., $a' = 1.73$ inch.

The critical stress level at crack tip E can now be calculated using the expression, $K_{Ic} = \sigma_f \beta \sqrt{\pi a'}$ corresponding to the single edge crack. The value of β can be obtained from Figure 4.4.7. For $a' = 1.73$ inch and $W = 20$ inch, β is estimated as 1.1. The value of σ_f for these values of β and a , is obtained from the relationship $K_{Ic} = \sigma_f \beta \sqrt{\pi a'}$ and is equal to 15.6 ksi, which is lower than the given maximum operating stress level of 20 ksi, and thus the crack extends from tip E causing complete fracture of the plate.

Even though extension of crack tip A is arrested at the free edge, the residual strength level of the panel is not sufficient to prevent extension at crack tip E for the given maximum operating stress level.

To further illustrate the analysis that would be required for the determination of the crack growth behavior of each crack tip, consider the residual strength diagram presented in Figure 4.4.8. Again two curves are illustrated, one for crack tip A, the other for crack tip E. The analysis for crack tip A is as shown in Figure 4.4.6. The analysis and data presentation for crack tip E is based on the assumption that crack tip A has extended to the edge of the panel and the residual strength is given by

$$\sigma_f = \frac{K_{Ic}}{1.1\sqrt{\pi(1+a)}} \quad (4.4.5)$$

It is noted that the crack tip E will remain stationary when the crack tip A extends if the crack length size (a) exceeds the size associated with the intersection of the two residual strength curves. The next example describes an analysis of such a situation.

EXAMPLE 4.4.3 Residual Strength of Eccentrically Cracked Panel - Crack Arrest Conditions

Repeat the residual strength analysis of Example 4.4.2 with a maximum operating stress level of 13 ksi. From Figure 4.4.6, it can be seen that the critical crack size for the given load level is 0.9 inch. If the panel develops a crack of this size, rapid extension will occur at crack tip A, Point F identifies the point of instability. The crack extension will be arrested at the free edge as in the earlier case. To continue the analysis for residual strength capabilities of the panel,

consider the crack extension behavior of the single edge crack at crack tip E. The new crack length is given by $W' + a$ where $W' = 1$ inch and $a = 0.9$ inch. Thus, for a crack length of 1.9 inch, β is obtained from Figure 4.4.7 as 1.1. Using the relationship, $K_{IC} = \sigma_f \beta \sqrt{\pi a}$, the critical stress level for crack tip E to extend rapidly is calculated as 14.9 ksi. However, the maximum operating stress level is given as 13 ksi which is less than this critical strength level. Thus, the panel does have the capacity to be effective without failure even when it develops a maximum crack of half length size 0.9 inch, leading to the rapid extension of crack tip A.

4.4.2 Tearing Fracture

Materials with medium or high fracture toughness exhibit a type of subcritical crack extension behavior prior to reaching the maximum load carrying capacity of the structure. When a limited amount of yielding occurs in front of the crack tip, the initial extension of an existing crack in these materials will be slow and stable threshold values of the stress-intensity factor (K_{ONSET}). To understand this behavior, consider an unreinforced, center-cracked panel. The stress-intensity factor (K) at the crack tip increases linearly with the value of the normal tensile stress component acting on the structure for a stationary crack. As the K level increases, some point (point A) will be reached at which the crack length will begin to extend as shown in Figure 4.4.9. The crack will extend gradually as the load continues to increase, until reaching the critical size at which the crack extension becomes unstable (point B in Figure 4.4.9). The point of crack initiation and instability are determined by the appropriate failure criteria.

When the subcritical growth of the crack, as shown in Figure 4.4.9a between the points A and B, is not significant the fracture toughness criterion K_{CR} values can be used in the analysis. In this case, fracture is assumed to occur immediately after the start of crack extension as under abrupt failure conditions. However, for materials exhibiting substantial crack growth between points A and B as shown in Figure 4.4.9b, the crack resistance curve approach can be used in the residual strength analysis. The crack resistance (R) curve approach might be based on either K_R vs Δa or $\sqrt{J_R}$ vs. a . The K_R vs Δa curve is normally used when the fracture strength is associated with

stress levels below net section yield conditions; in other words, when limited crack tip plasticity occurs prior to fracture. The $\sqrt{J_R}$ vs a curve is used for those conditions where the fracture strength is expected to result in gross yielding.

In the calculation of residual strength when the cracked structure exhibits a tearing instability, one normally follows the following steps:

1. Obtain K_{eff} ($=\beta\sqrt{\pi(a+r_p)}$) values for the structure for various crack lengths and applied stresses using a suitable plastic zone model (e.g. Dugdale Model). Evaluation of the K values involves methods described in Chapter 1. Plot K versus a curves for various applied stresses as shown in Figure 4.4.10a.

2. Obtain the experimentally determined R-curve (K_R versus Δa) for the sheet material (Figure 4.4.10b).

3. Determine the point of instability from the K curves of the structure and the K_R curves of the material as shown schematically in Figure 4.4.10c.

4. Obtain different values for the fracture strength and the corresponding crack lengths from step 3 and plot these points to establish the failure strength (σ_f) crack length (a_c) curve. This provides the necessary residual strength diagram of the structure.

The residual strength diagram for intermediate or high fracture toughness materials can be constructed by using either the K_R curve or the $\sqrt{J_R}$ method.

To understand the use of the R-curve failure criteria in evaluating the residual strength, consider the following example in which failure criterion based on the K_R curve is applied.

EXAMPLE 4.4.4 Residual Strength of Tearing Radial Hole Crack

Construct the residual strength diagram for a large and relatively thin (0.063) plate of 7075-T73 aluminum alloy having a through crack emanating (radially) from a hole with a diameter (D) equal to one inch, such as illustrated in Figure 4.4.11. Assume the material inhibits a limited amount of crack tip yielding. Also calculate the crack length associated with a fracture strength associated with a crack length of 2.0 inch.

SOLUTION:

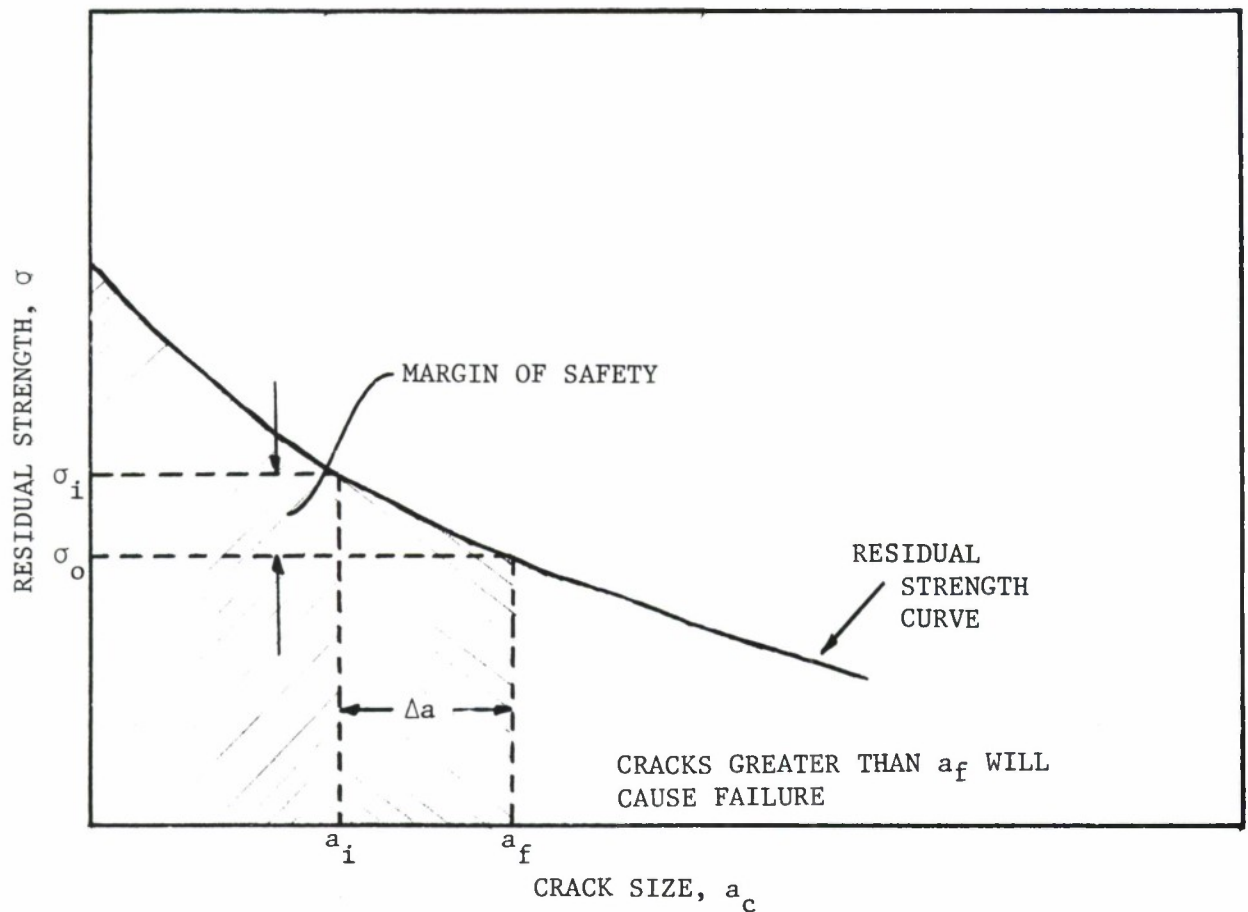
As the first step, the appropriate expression for the stress-intensity factor is obtained from Section 1.7, Table 1.7.3, Case 1.7.3.1, where the Grandt ⁽¹⁶⁾ approximation of the Bowie ⁽¹⁷⁾ radial hole crack solution is given (Also see Figure 4.4.11). Figure 4.4.12 describes the variation in stress-intensity factor with crack length and stress level.

The second step is to consider the appropriate failure criterion. The given geometry is a thin sheet and the material exhibits limited crack tip yielding behavior. So the R-curve method based on K_R values can be applied to evaluate the fracture strength.

For the given 7075-T73 aluminum alloy material (0.063 inch thick), an experimentally obtained R-curve is shown in Figure 4.4.13. By superposing the R-curve onto the plot obtained in step one, as explained in Section 4.2, the points where the R-curve is tangent to the K-curves, as shown in Figure 4.4.14 are obtained. At these points the failure criterion, i.e., $K = K_R$ and $\frac{\partial K}{\partial a} = \frac{\partial K_R}{\partial a}$, is satisfied. The corresponding stress σ_c is the

is the critical (fracture) stress at which the initiation of rapid fracture will occur. From a diagram like Figure 4.4.14, we can obtain the critical initial sizes of the crack and the respective fracture stresses.

The final step is to plot the σ_f vs a_c curve. The required residual strength diagram is shown in Figure 4.4.15 for the 7075-T73 Aluminum plate with a crack emanating radially from a hole. It can be seen from this figure that the critical crack size a for a 20 Ksi operating stress level is equal to 4.0 inches. As can also be seen from the figure, for an observed crack of 2.0 inches, the residual strength available is 27 ksi.



a_f = critical flaw size for the maximum operating load.

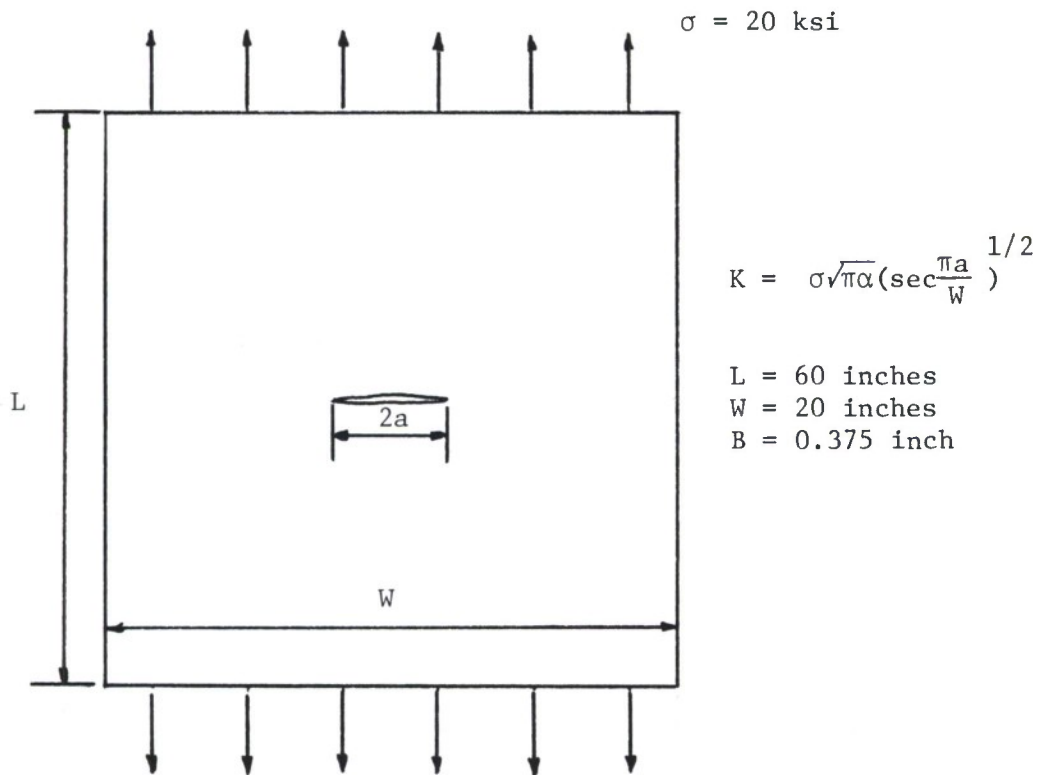
a_i = observed initial crack length.

Δa = available additional length. (allowance for undetected initial crack size and for subcritical crack growth).

σ_i = residual strength level for an initial crack a_i .

σ_o = maximum operating stress level.

Figure 4.4.1. Residual Strength Diagram Showing Defining Cracks and Residual Strength Parameters.



MATERIAL PROPERTIES

$\sigma_{ys} = 78 \text{ ksi}$
 $\sigma_{ult} = 83 \text{ ksi}$
 $K_{IC} = 40 \text{ ksi } \sqrt{\text{in}}$

INSPECTION PROCEDURE

VISUAL INSPECTION

$2a_{NDE} = 2 \text{ inch}$

Figure 4.4.2. Center Crack Panel and Material Properties for Example 4.4.1.

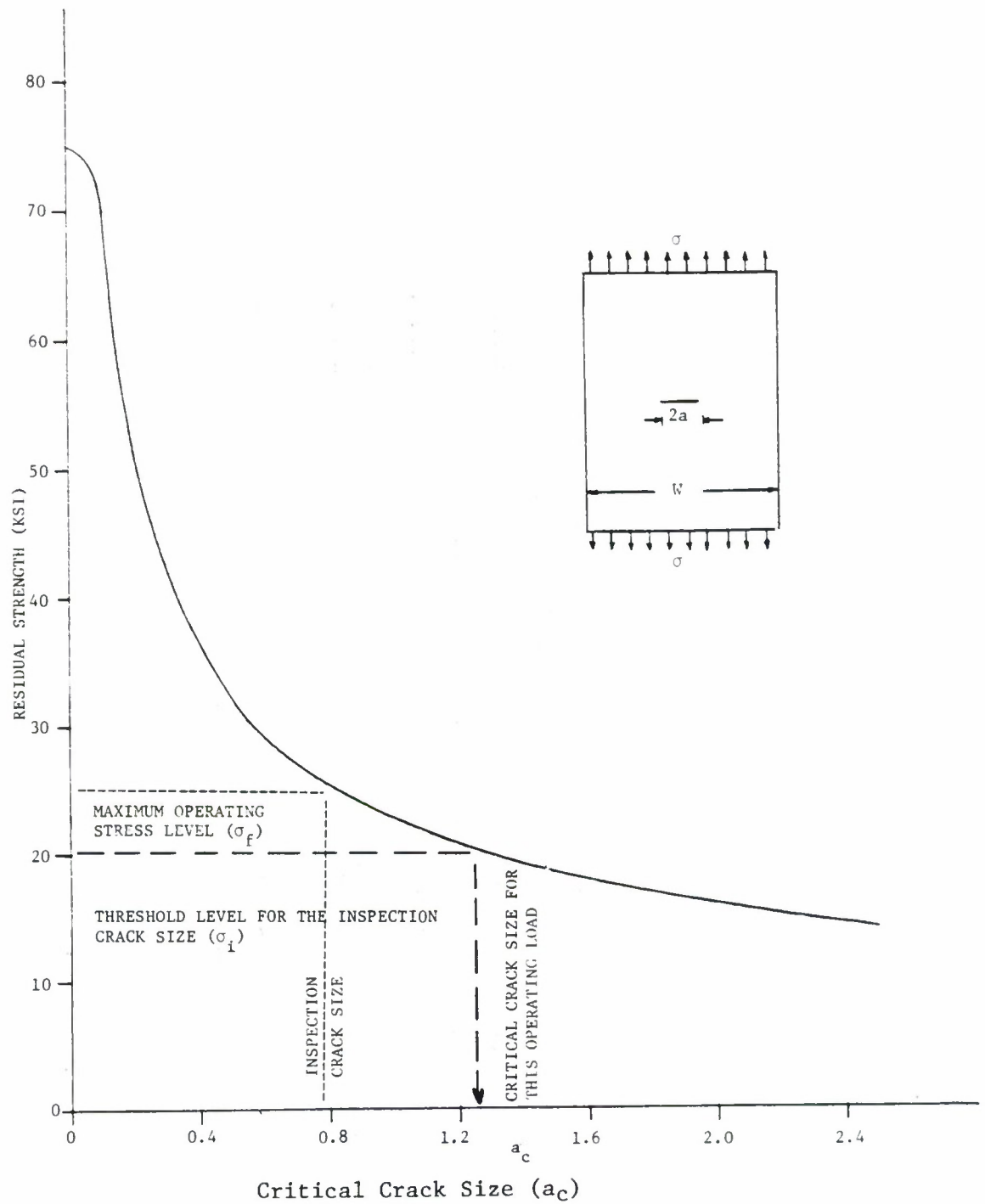
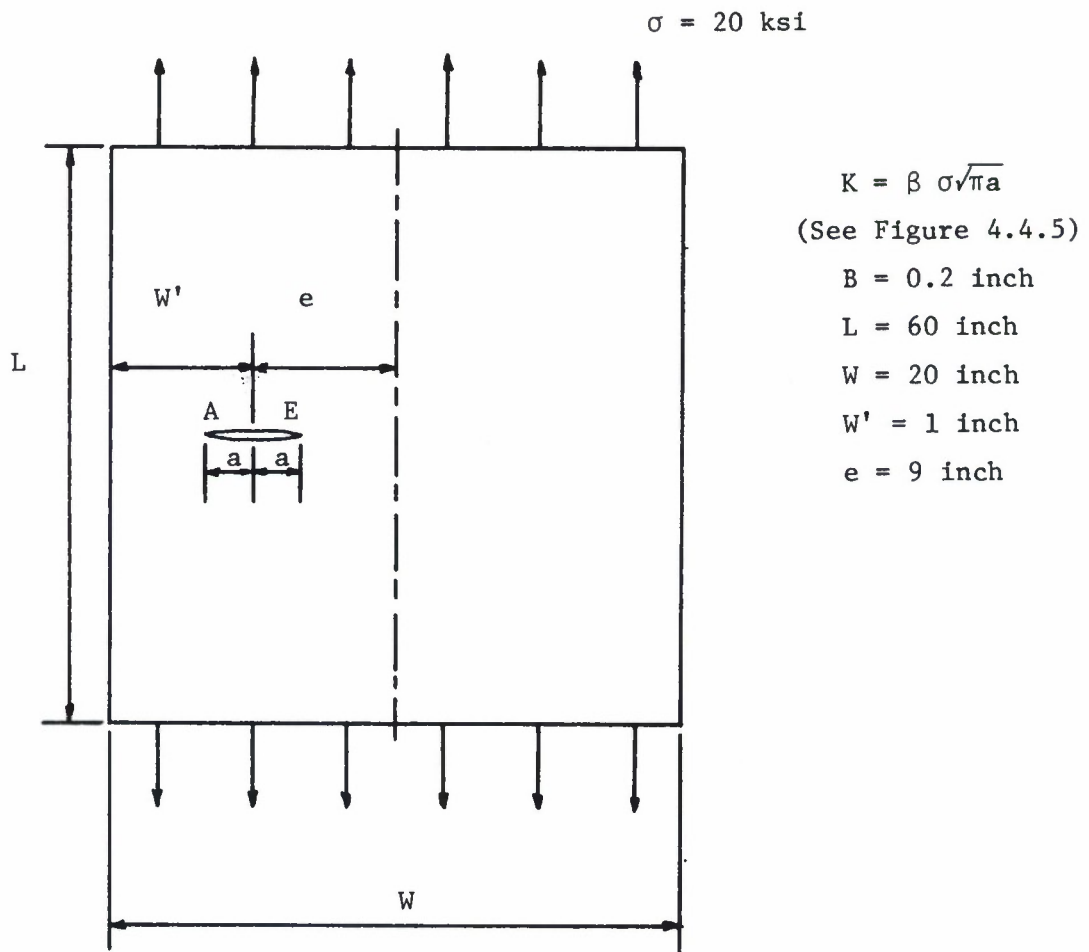


Figure 4.4.3. Residual Strength Diagram Determining Critical Crack Size at 20 Ksi Operating Level.



MATERIAL PROPERTIES

$$\sigma_{ys} = 78 \text{ ksi}$$

$$\sigma_{ult} = 83 \text{ ksi}$$

$$K_{IC} = 40 \text{ ksi } \sqrt{\text{in}}$$

Figure 4.4.4. Excentrically Cracked Panel Associated with Examples 4.4.2 and 4.4.3.

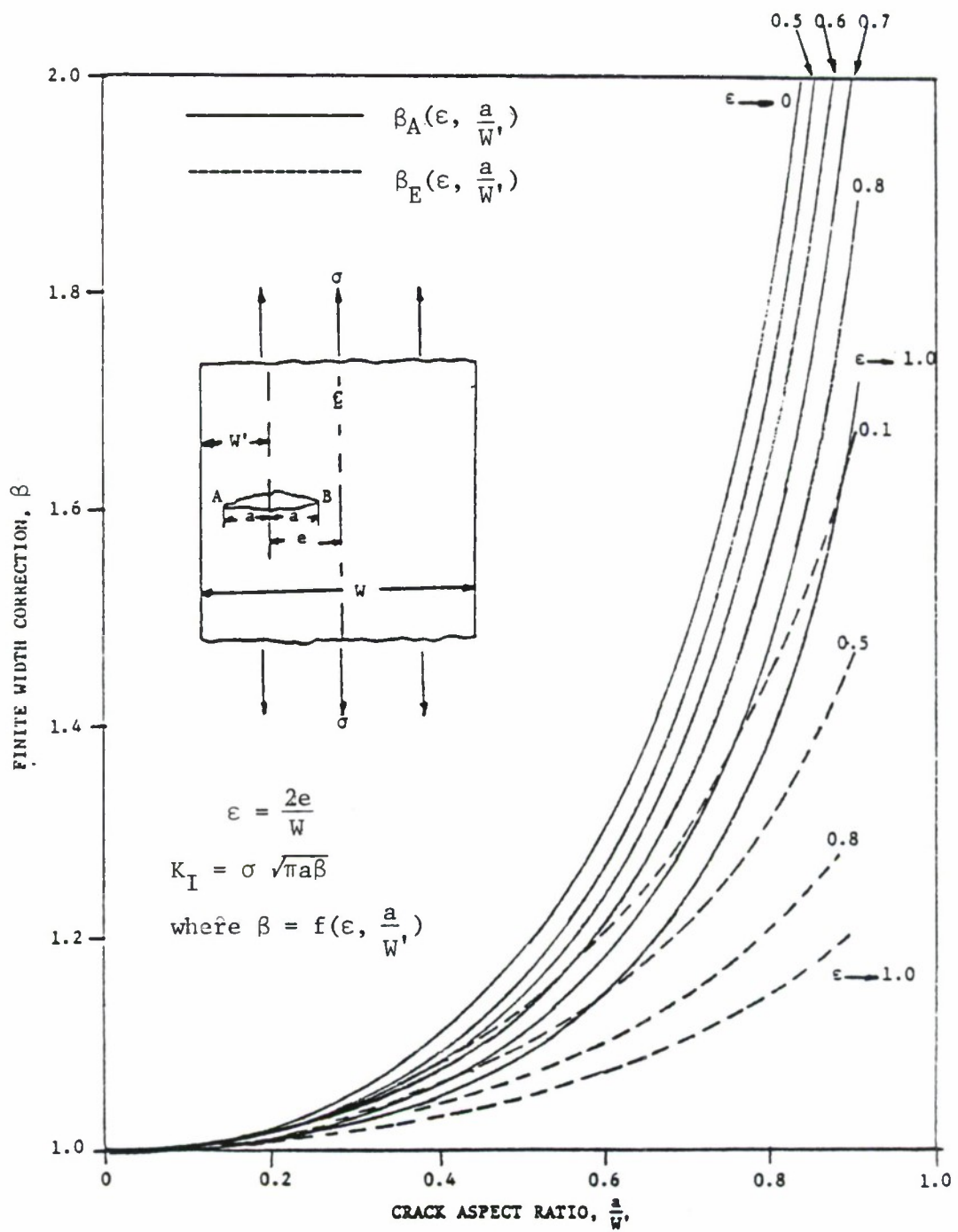


Figure 4.4.5. Finite-Width Correction-Eccentric Crack (Tension) (Reference 15).

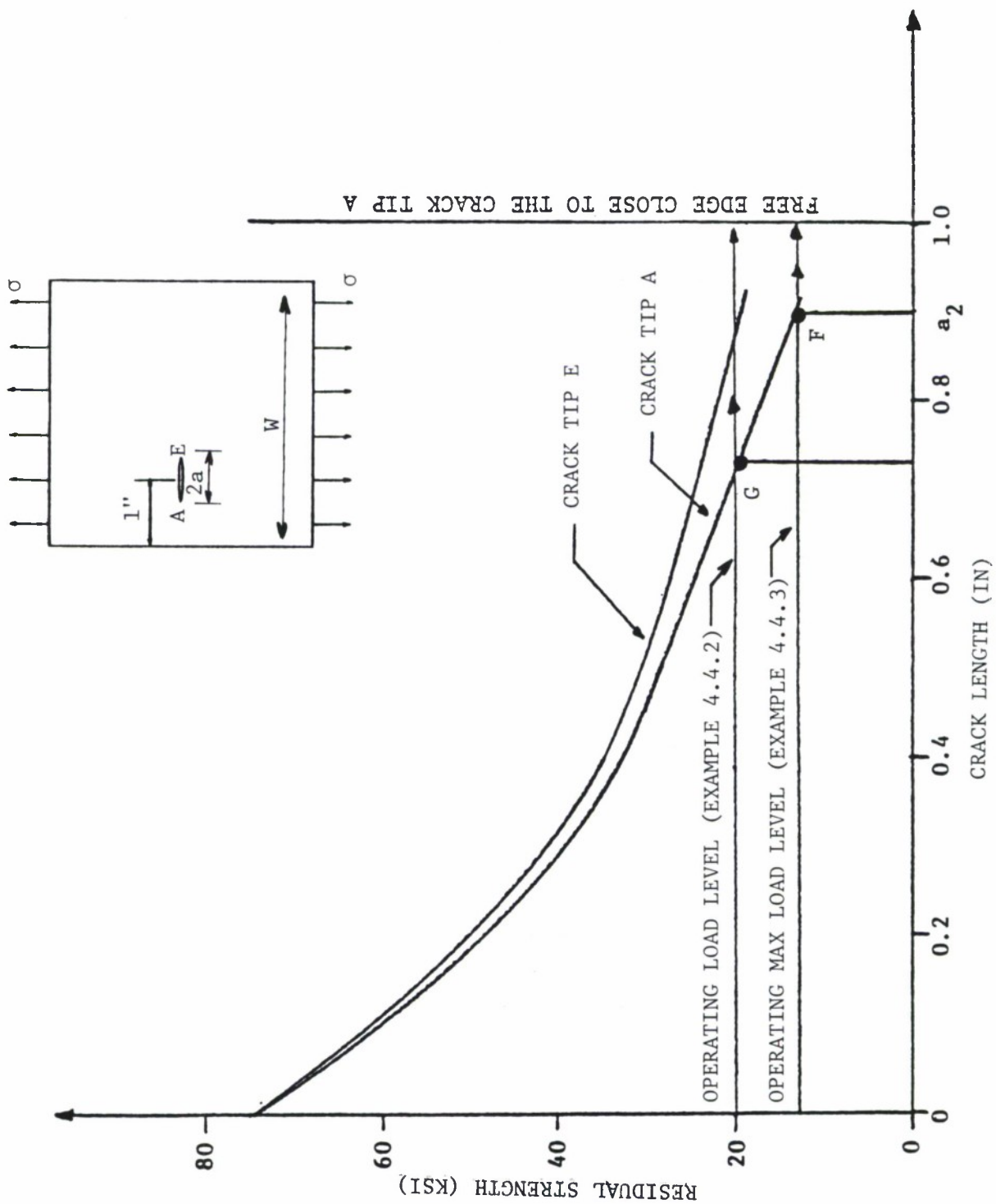


Figure 4.4.6. Residual Strength Diagram for Panel with Eccentric Crack Given in Figure 4.4.4. Crack with Lowest Fracture Resistance Curve Extends First.

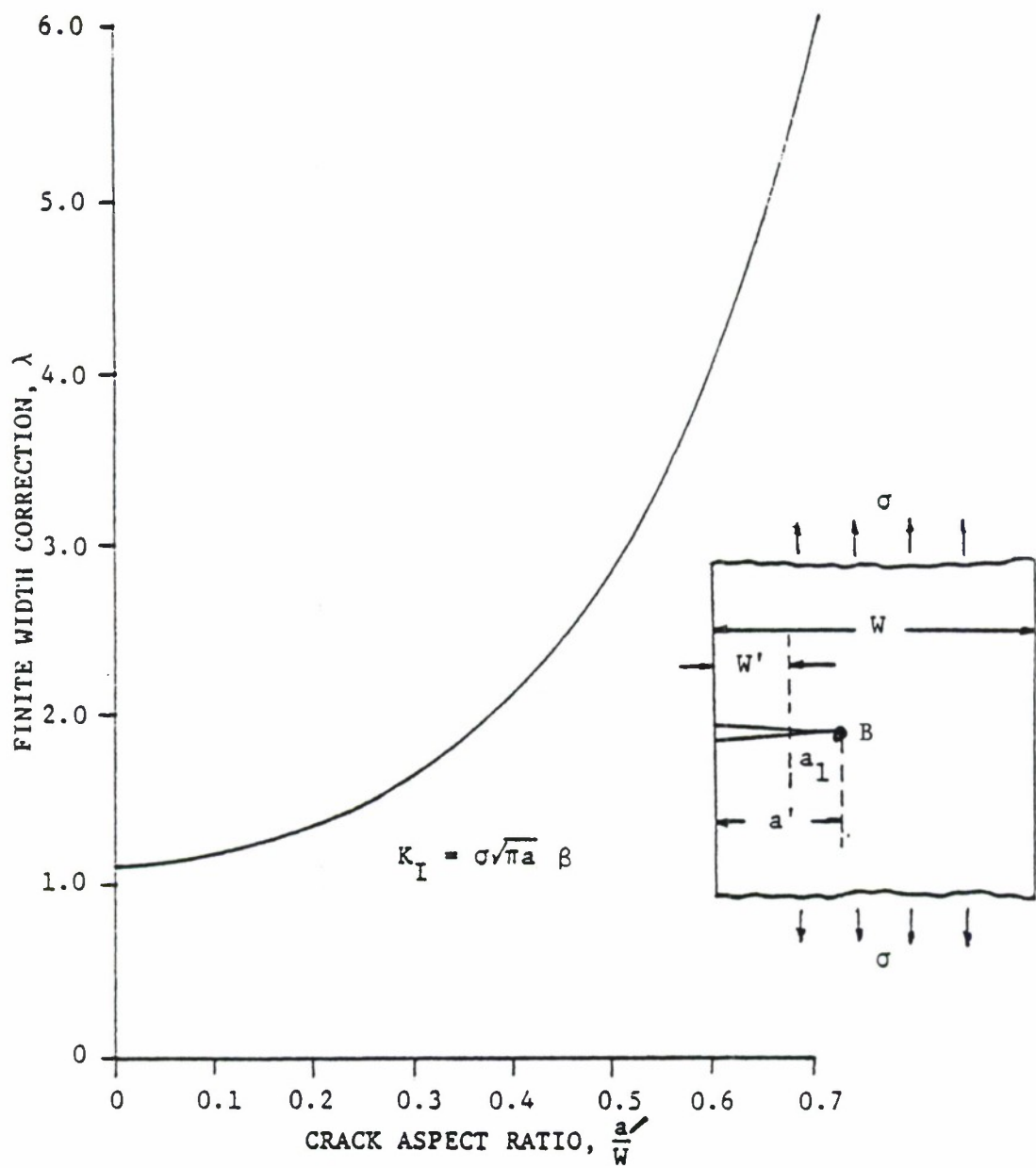


Figure 4.4.7. Finite Width Correction-Single Edge Crack, After the Eccentric Crack Extends from Tip A.

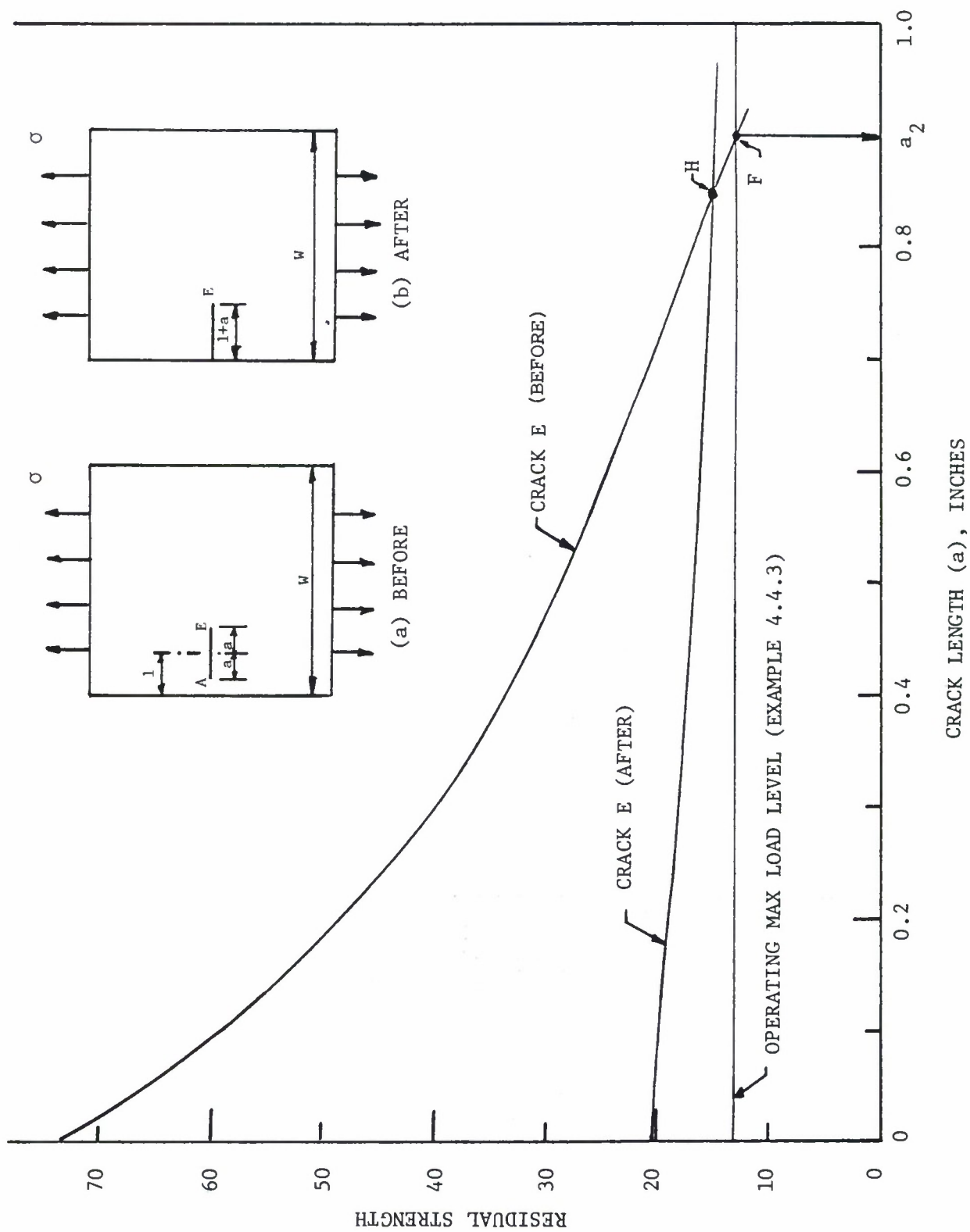


Figure 4.4.8. Residual Strength Diagram Used to Consider Arrest Features as Crack Tip A Reaches the Edge of the Plate.

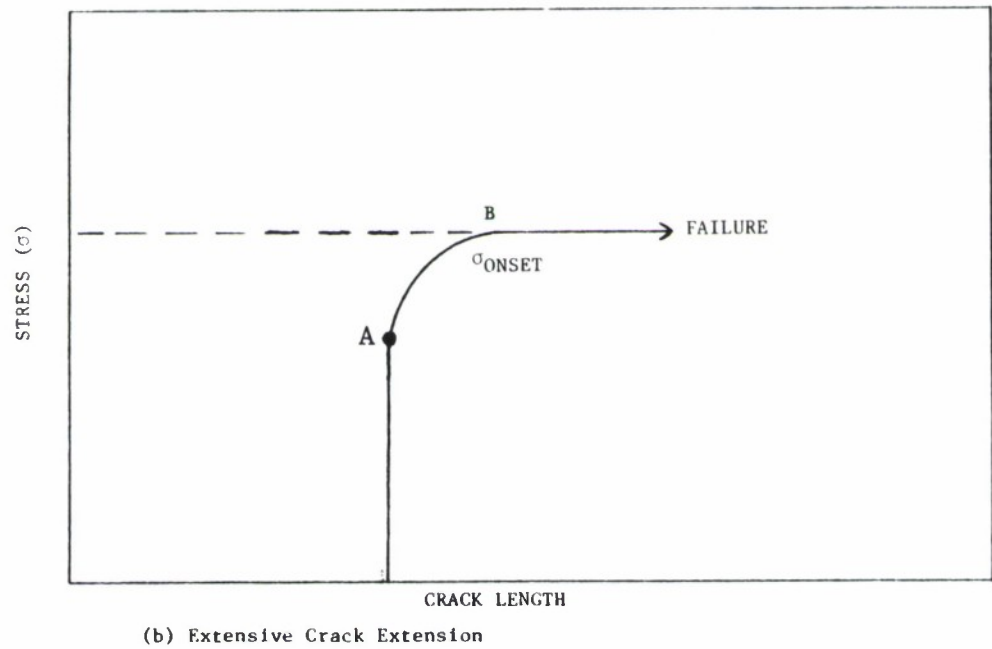
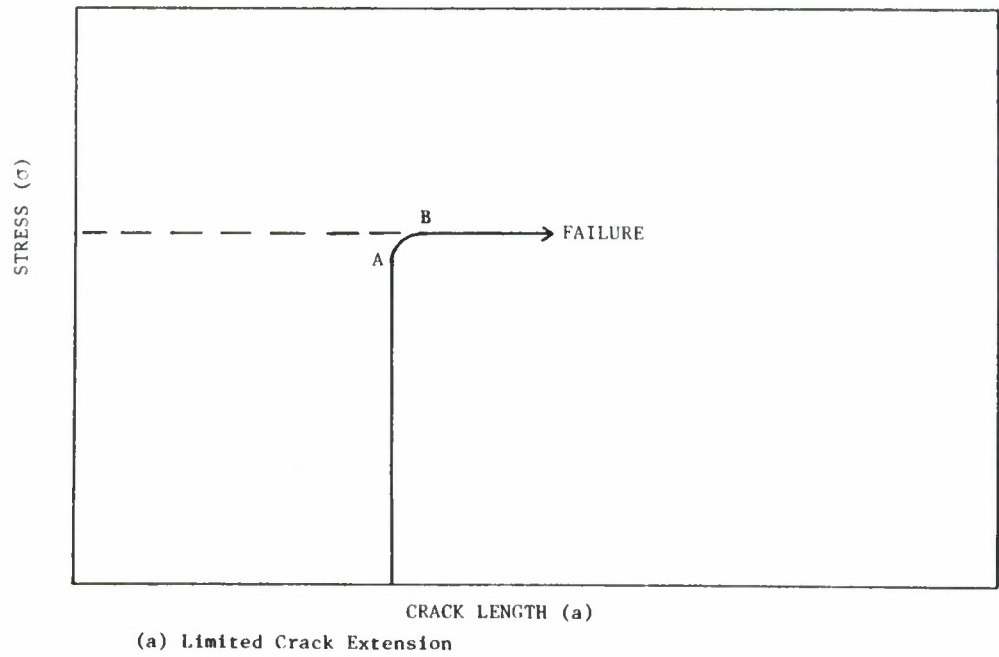
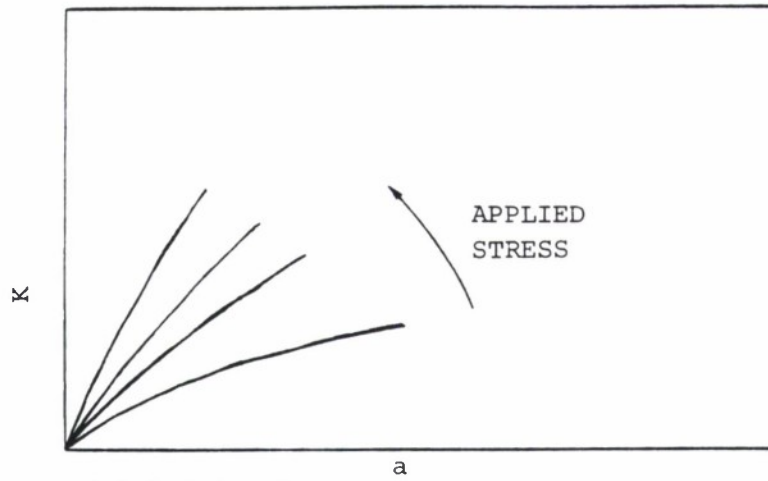
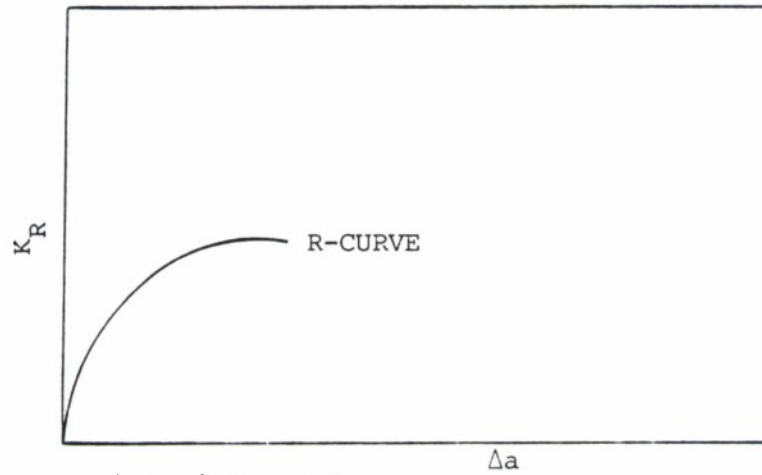


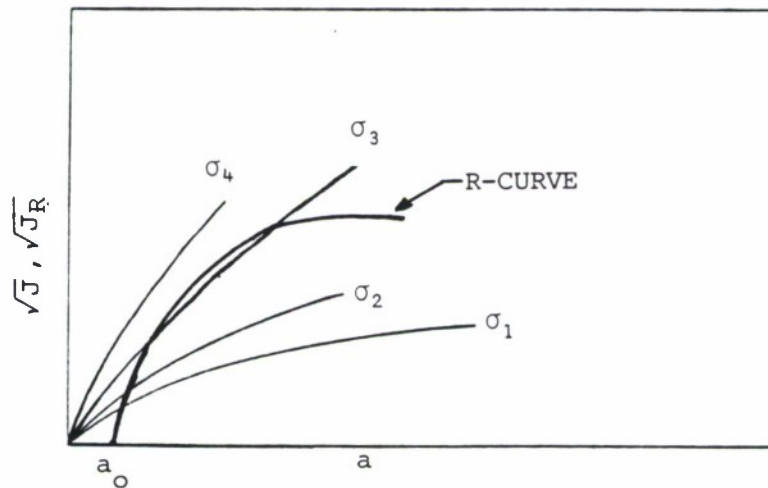
Figure 4.4.9. Diagrams Showing Onset of Unstable Crack Growth for Conditions of Limited or Extensive Crack Extension.



(a) Driving Factor

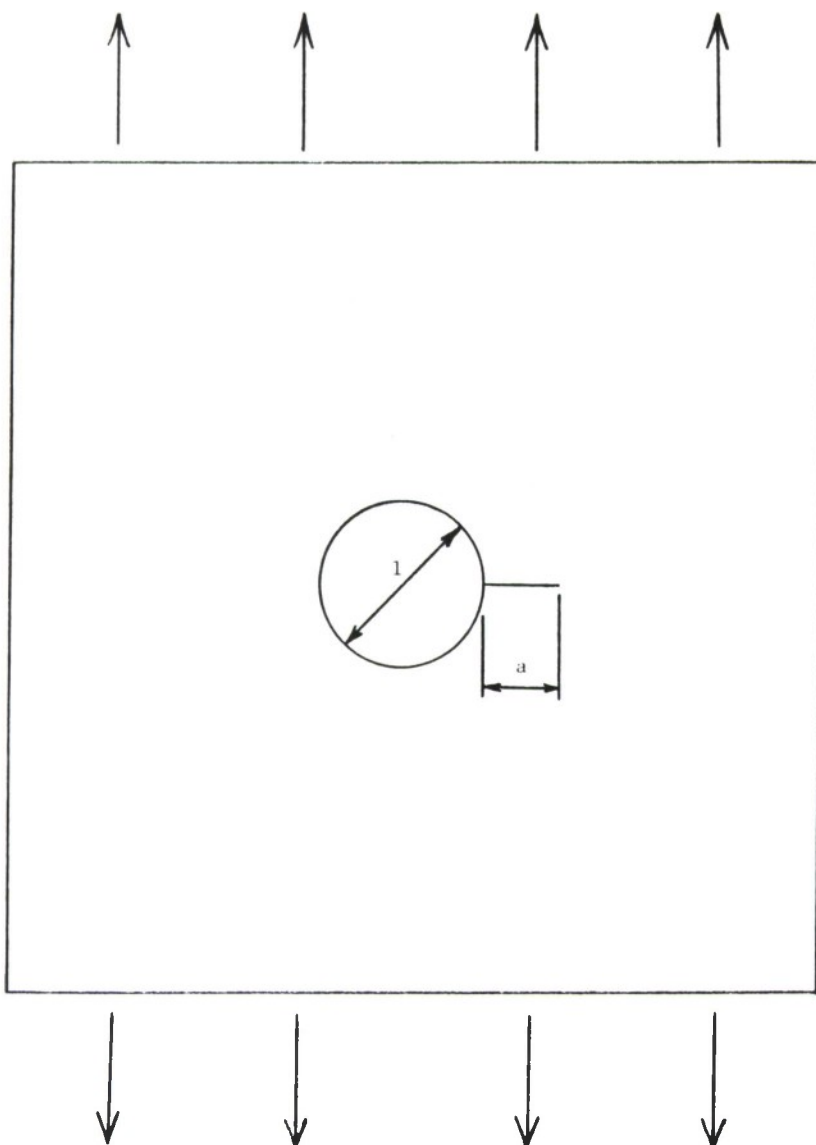


(b) Resistance Curve



(c) Matching Driving Factor with Resistance Curve

Figure 4.4.10. Steps Associated with Calculating Residual Strength of Cracked Structures with Tearing Fractures.



DIMENSIONS

$$D = 2R = 1 \text{ inch}$$

$$B = 0.063 \text{ inch}$$

MATERIAL

7075-T73

ALUMINUM

$$K = \sigma \beta \sqrt{\pi a} \text{ where}$$

$$\beta = \frac{0.8734}{(0.3246 + \frac{a}{r})} + 0.6762$$

Figure 4.4.11. Structural Geometry Associated with EXAMPLE 4.4.4.

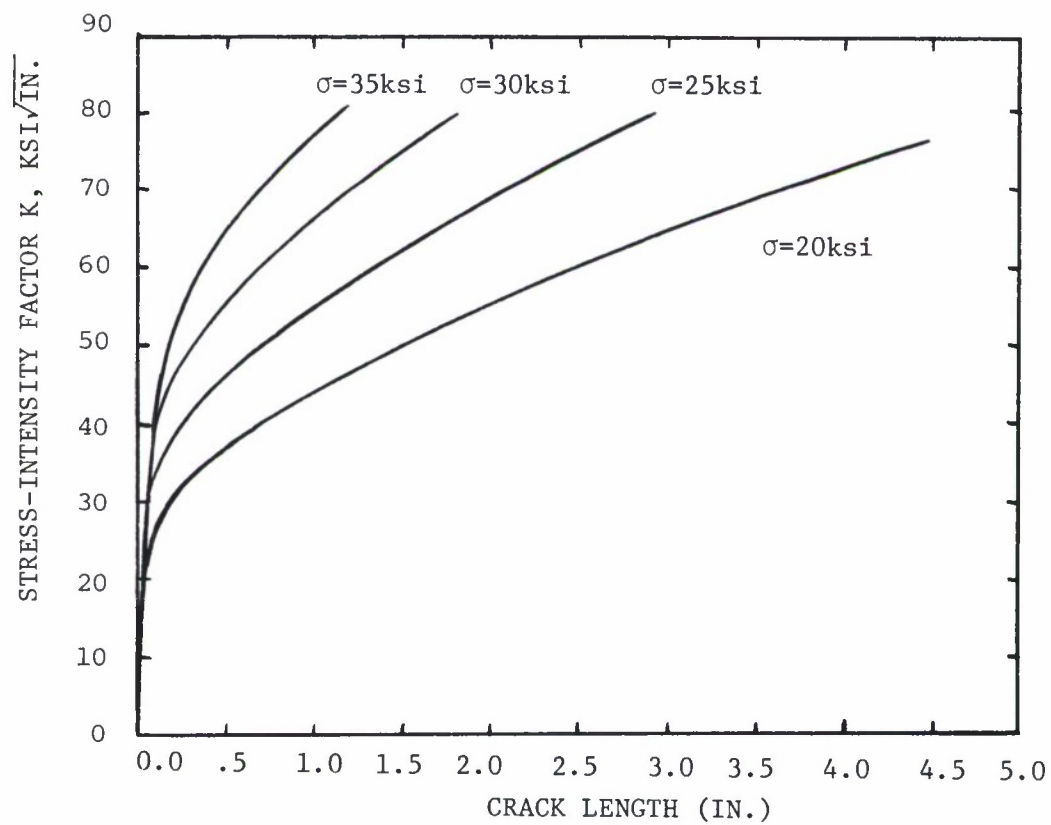


Figure 4.4.12. Stress-Intensity Factor Relationship for Various Values of Applied Stress.

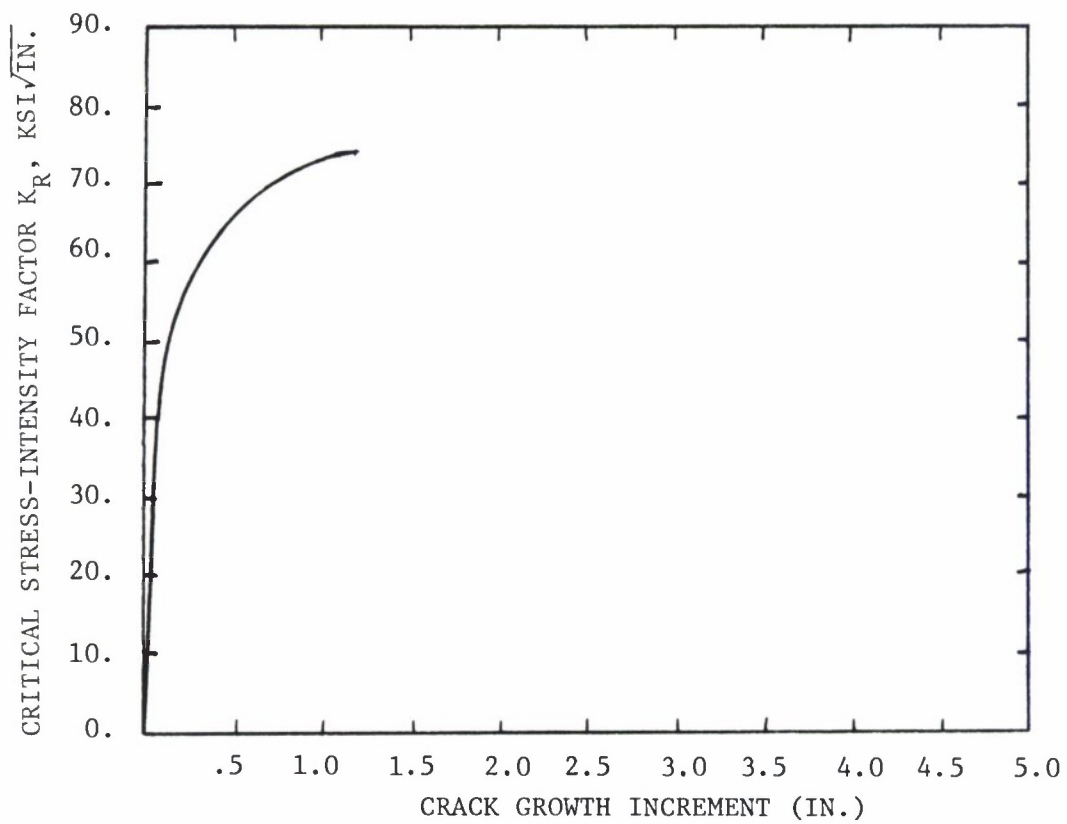


Figure 4.4.13. Resistance Curve for 7075-T73 Aluminum for a Thickness of 0.063 Inches.

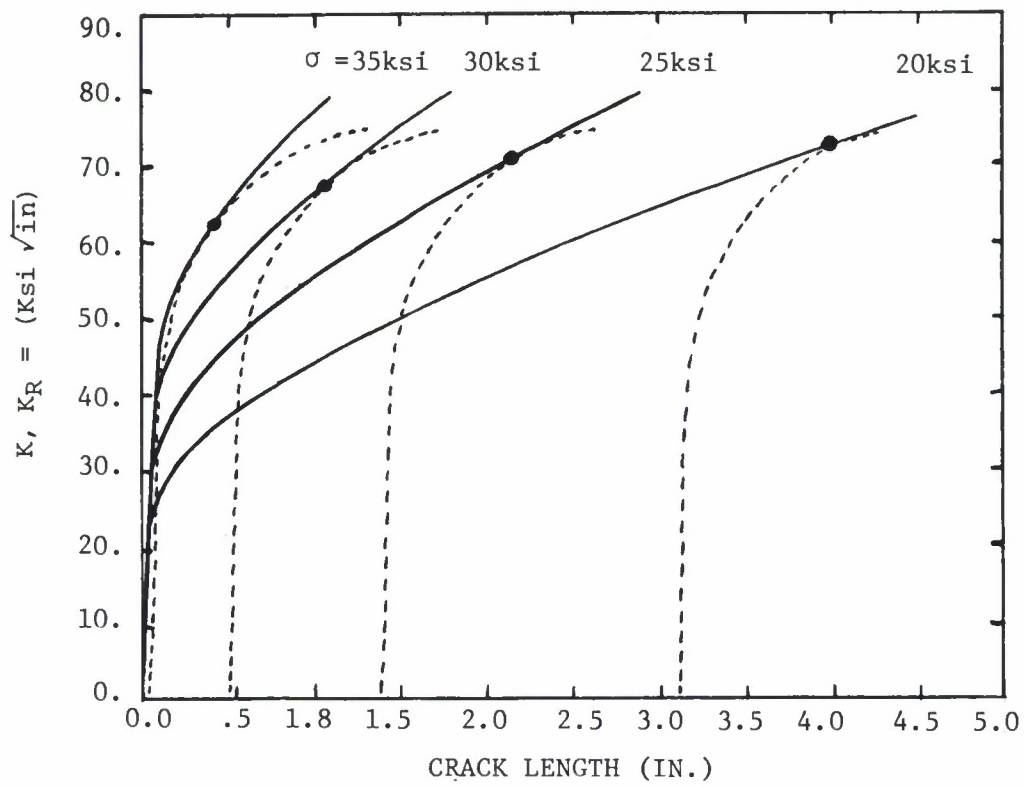


Figure 4.4.14. Matching the R-Curve and Stress-Intensity Factor Curves.

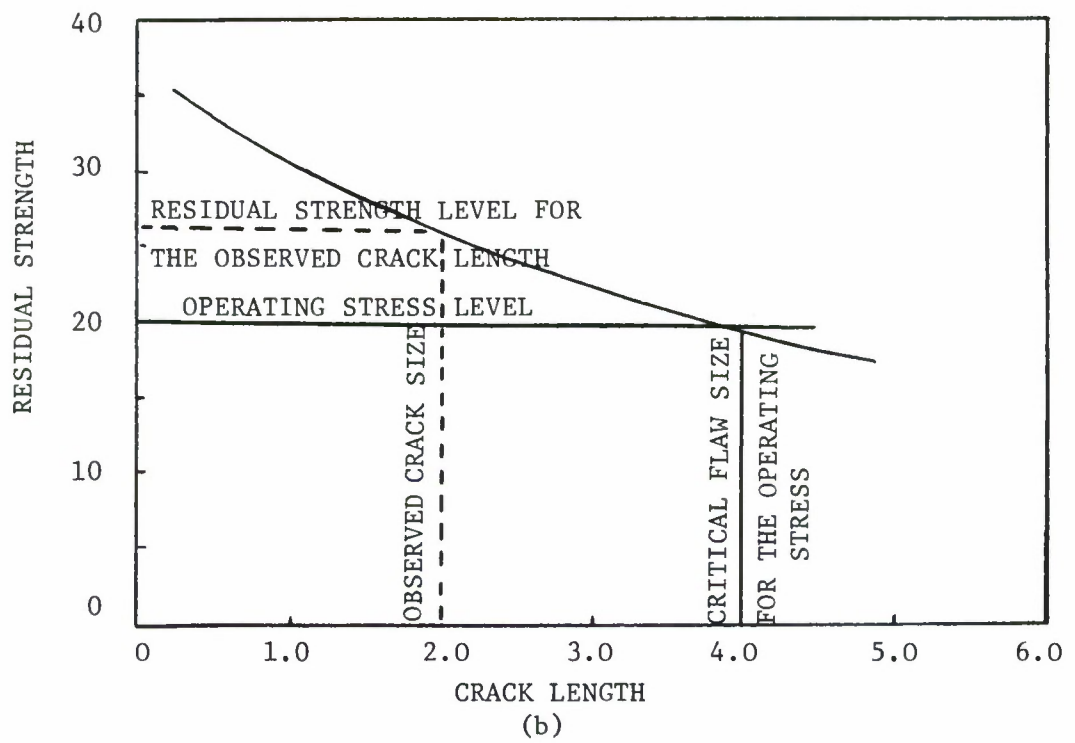


Figure 4.4.15. Residual Strength Diagram Obtained for Structure Shown in Figure 4.4.11 (EXAMPLE 4.4.4).

4.5 BUILT-UP STRUCTURES

Built-up structures normally require more than one failure criterion to determine the residual strength of the total structure. The development of the residual strength diagram of a given structure will involve the analysis of failures of each part of the load support system.

The structural configuration essentially determines the complexity of the residual strength analysis. Typical structural parameters which must be considered for skin-stiffened structure are:

- a. Type of Construction
 - 1. Monolithic (Unreinforced/Forgings)
 - 2. Skin (Longerons, stringer)
 - 3. Integrally Stiffened
 - 4. Planked
 - 5. Layered (Honeycomb/Laminated)
- b. Panel Geometry
 - 1. Planform
 - 2. Curvature
 - 3. Stiffener Spacing and Orientation
 - 4. Attachments (Spar Caps, Webs, Frames, etc.)
- c. Details of Construction
 - 1. Stiffener Geometry (hat, Z, Channel, etc.)
 - 2. Attachment Details (Bolted, Riveted, Welded, etc.)
 - 3. Fastener Flexibility
 - 4. Eccentricity

Ideally, the residual strength analysis will take all these parameters into consideration. In practice, many are treated empirically and others are not considered except in extremely detailed analyses.

This section provides details of the analysis methods used for built-up skin-stringer structure and the effects of many of the structural parameters listed above. In the order of their presentation, the subsections provide: overviews of the analysis for edge stiffened and for centrally stiffened skin structure, the analysis methods used to determine the stress-intensity factor in the skin structure and the loading transferred to the stringers, the analysis of stiffener failure, the analysis of fastener failure, the analysis methodology and an Example.

4.5.1 Edge Stiffened Panel With a Central Crack

The residual strength diagram of a simple panel with two stringers and a central crack can be constructed as follows. Consider first a crack in plane stress which starts propagating slowly at $\sigma_o = K_{onset}/\sqrt{\pi a_o}$ and becomes unstable at $\sigma_c = K_c/\sqrt{\pi a_c}$ in a sheet without stringers as shown in Figure 4.5.1a.

When the panel is stiffened with stringers, the stress-intensity factor is reduced to $K = \beta\sigma\sqrt{\pi a}$, where $\beta < 1$. As a result, both the stress for slow stable crack growth, σ_o , and the stress for unstable crack growth, σ_f , are altered to give $\sigma_o = K_{onset}/\beta\sqrt{\pi a_o}$ and $\sigma_{cf} = K_c/\beta\sqrt{\pi a_c}$, respectively.

Hence, these events take place at higher stresses in the stiffened panel than in the unstiffened panel. This means that the lines in Figure 4.5.1a are raised by a factor $1/\beta$ for the case of the stiffened panel, as depicted in Figure 4.5.1b. Since β decreases as the crack approaches the stringer, the curves in Figure 4.5.1b turn upward for crack sizes on the order of the stringer spacing.

The possibility of stringer failure should be considered also. The stringer will fail when its stress reaches the ultimate tensile stress (σ_{UTS}). As the stringer stress is $L\sigma$, where σ is the nominal stress in the panel away from the crack, failure will occur at σ_{sf} , given by $L\sigma_{sf} = \sigma_{UTS}$. Using L , a measure of the load transferred to the stringer, the panel stress at which stringer failure occurs is shown in Figure 4.5.1c. The stringer may yield before it fails. This means that its capability to take overload from the cracked skin decreases. As a result, β will be higher and L will be lower. The stress-intensity analysis should account for this effect.

Figure 4.5.2 shows the residual strength diagram of the stiffened panel. It is a composite of the critical conditions shown in Figure 4.5.1. In the case when the crack is still small at the onset of instability ($2a \ll 2s$, where $2s$ is stringer spacing), the stress condition at the crack tip will hardly be influenced by the stringers and the stress at unstable crack growth initiation will be the same as that of an

unstiffened sheet of the same size (Point B in Figure 4.5.2). When the unstably growing crack approaches the stiffener, the load concentration in the stiffener will be so high that the stiffener fails (Point C) without stopping the unstable crack growth (line BC).

When the panel contains a crack extending almost from one stiffener to the other ($2a \approx 2s$), the stringer will be extremely effective in reducing the peak stress at the crack tips (β small), resulting in a higher value of the stress at crack growth initiation. With increasing load, the crack will grow stably to the stiffener (line LMIF) and due to the inherent increase of stiffener effectiveness, the crack growth will remain stable. Fracture of the panel will occur at the same stress level corresponding to the point F due to the fact that the stiffener has reached its failure stress and the stress reduction in the skin is no longer effective after stringer failure.

For cracks of intermediate size ($2a = 2a_1$), there will be unstable crack growth at a stress slightly above the fracture strength of the unstiffened sheet (point H), but this will be stopped under the stiffeners at I. After crack arrest, the panel load can be further increased at the cost of some additional stable crack growth until F, where the ultimate stringer load is reached.

Since β and L depend upon stiffening ratio, the residual strength diagram of Figure 4.5.2 is not unique. Figure 4.5.2 shows the case where stringer failure is the critical event. For other stiffening ratios, skin failure may be the critical event as depicted in Figure 4.5.3. Due to a low stringer load concentration, the curves e and g do not intersect. A crack of size $2a_1$ will show stable growth at point B and become unstable at point C. Crack arrest occurs at D from where further slow growth can occur if the load is raised. Finally, at point E, the crack will again become unstable, resulting in panel fracture. It is therefore obvious then that a criterion for crack arrest has to involve the two alternatives of stringer failure and skin failure, and these depend upon the relative stiffness of sheet and stringer.

The foregoing clearly shows that for crack arrest it is not essential that the crack run into a fastener hole. Crack arrest basically results from the reduction of stress-intensity factor due to load transmittal to the stringer.

For the particular case depicted in Figure 4.5.4, the residual strength is not determined by stringer failure solely but also by fastener failure (point K). A crack of length $2a_1$ will show slow growth from E to F and instability from F to G. After crack arrest at G, further slow growth occurs until at point K the fasteners fail. The latter could cause panel failure, but this cannot be directly determined from the diagram.

In fact, a new residual strength diagram must now be calculated with omission of the first row of rivets at either side of the crack. Fastener failure will affect load transmittal from the skin to the stringer: line e will be lowered, line g will be raised. The intersection point H' of the new lines g' and e' may still be above K and hence, the residual strength will still be determined by stringer failure at H'.

In reality, the behavior will be more complicated due to plastic deformation. Shear deformation of the fasteners, hole deformation, and plastic deformation of the stringers will occur before fracture takes place. Plastic deformation always reduces the ability of the stringer to take load from the skin which implies that line g in actuality will be raised and line e will be lowered. The intersection of the two lines (failure point) will not be affected a great deal, however, (compare points H and H' in Figure 4.5.4). For this reason the residual strength of a stiffened panel can still be predicted reasonably well, even if plasticity effects are ignored. Nevertheless, a proper treatment of the problem requires that plasticity effects be taken into account.

4.5.2 Centrally and Edge Stiffened Panel With a Central Crack

In the previous subsection, the cases considered pertain to cracks between two stiffeners. In practice, however, cracks frequently start at a fastener hole and then there will be a stringer across the

crack which will have a high load concentration factor. The problem can be dealt with in a manner similar to a crack between stringers, using either analytical or finite-element procedures. A schematic residual strength diagram for this case is presented in Figure 4.5.5. Apart from the residual strength curve g for the edge stiffeners, there will now be an additional residual strength curve k for the central stiffener.

For the case where the crack in the skin is small ($2a \ll 2s$), the first failure in the structure is noted to occur at point B in Figure 4.5.5 where the skin fails and the crack starts to run. When the crack reaches a size such that point C is reached, the central stiffener residual strength has dropped to the operating stress level and then the central stringer fails, immediately causing additional loading to be transferred to the edge stiffeners and the skin structure. The effect of losing the capability of the central stringer is noted in Figure 4.5.5 with a repositioning of the residual strength curves for the edge stiffeners (from curve g to curve g') and skin structure (from curve e to curve e'). As the crack in the skin structure continues to grow after causing the ultimate tensile strength failure in the central stringer at point C, it reaches a size that causes the ultimate tensile strength failure of the two edge stringers at point D, at which point all potential arrest capability is lost and the structure is lost.

For the case of longer cracks, Figure 4.5.5 shows that skin cracks may start running (line EF), arrest (point F), and tear along curve FL as the stress is increased. At point L, the crack has reached a length that has resulted in sufficient stress being transferred to the central stringer so that this stiffener now fails. Again, this failure causes a redistribution of stress in the entire structure so that a new set of residual strength diagrams are required to determine the consequences associated with failing the central stringer. The new edge stringer and skin structure residual strength curves are presented by curves g' and e' , respectively.

Due to the high load concentration, the middle stringer will usually fail fairly soon by fatigue and therefore lines e' and g' , with the middle stringer failed, will have to be used and the residual strength is determined by point H' . (Note that e' , g' , and H' will have different positions in the absence of the middle stringer; a failed central stringer will induce higher stresses in both the skin and the edge stiffeners.) The foregoing discussion provides the concepts required to establish a complete residual strength diagram.

4.5.3 Analytical Methods

In this subsection analytical procedures are presented for the residual strength capability analyses. Methods for evaluating the unknown fastener force and the stress-intensity factors for the stiffened

panel are presented. Since the equations for the solution procedures have been based on linear elastic fracture mechanics, the failure criterion used in these analyses are also based on fracture toughness values for abrupt fracture conditions and K_R resistance curve data for tearing fracture conditions.

Analysis methods for stiffened panels have been developed independently by Romualdi, et al.⁽¹⁸⁾, Poe^(19,20), Vlieger⁽²¹⁾, Swift and Wang⁽²²⁾, Swift⁽²³⁾, Creager and Liu⁽²⁵⁾, and Wilhem and Ratwani⁽²⁶⁾.

Application of the stress intensity factor parameter, β , and the stringer load concentration factor, L , were proposed by Vlieger⁽²¹⁾ and Swift and Wang⁽²²⁾.

From the residual strength capability analysis as discussed in the preceding subsections, it is evident that the construction of residual strength diagrams for built-up structures also requires the estimation of the stress-intensity factor K . A number of approaches for determining K have been developed. Solutions for complicated structural geometries can sometimes be obtained from the basic stress field solutions combined with displacement compatibility requirements for all the structural members involved. This approach has been shown by several investigators to be useful in the analysis of built-up sheet structure. While the analysis is based on closed form solutions, the actual analyses are computerized for efficient solutions. The essentials of this technique are described below.

In calculating β and L , two methods can be used. There are the finite-element method and an analytical method based on closed-form solutions. The analytical method has advantages over the finite-element method in that the effect of different panel parameters on the residual strength of a certain panel configuration can be easily assessed, so that the stiffened panel can be optimized with respect to fail-safe strength. It allows direct determination of the residual-strength diagram. In the case of the finite-element method, a new analysis has to be carried out when the dimensions of certain elements are changed because a new idealization has to be made. An advantage of the finite-element analysis, on the other hand, is that such effects as stringer eccentricity, hole deformation, and stringer yielding can be incorporated with relative ease. Details of the calculations can be found in the referenced papers.

The procedure for analytical calculation is outlined in Figure 4.5.6. The stiffened panel is split up into its composite parts, the skin and the stringer. Load transmission from the skin to the stringer takes place through the fasteners. As a result, the skin will exert forces F_1, F_2 , etc., on the stringer, and the stringer will exert reaction forces F_1, F_2 , etc. on the skin. This is depicted in the upper line of Figure 4.5.6.

The problem is now reduced to that of an unstiffened plate loaded by a uniaxial stress, σ , and fastener forces $F_1 \dots F_n$. This case can be considered as superposition of three others, shown in the second line of Figure 4.5.6. Namely:

- a. A uniformly loaded cracked sheet.
- b. A sheet without a crack, loaded with forces $F_1 \dots F_n$.
- c. A cracked sheet with forces on the crack edges given by the function $p(x)$. The forces $p(x)$ represent the load distribution given by Love⁽²⁷⁾. When the slit CD is cut, these forces have to be exerted on the edges of the slit to provide the necessary crack-free edges.

The three cases have to be analyzed individually. For case a, the stress-intensity factor is $K = \sigma\sqrt{\pi a}$. For case b, $K = 0$. The stress intensity for case c is a complicated expression that has to be solved numerically. However, once the K value for case c is determined, the stress-intensity factor for the whole stiffened panel can be obtained by adding the K values for cases a and b. The determination of K requires calculations of fastener forces $F_1, F_2 \dots F_n$. To calculate these forces, the displacement compatibility conditions which require equal displacements in sheet and stringer at the corresponding fastener locations, can be used. These compatibility requirements deliver a set of n (n = number of fasteners) independent algebraic equations from which the fastener forces can be obtained. These equations can be solved numerically using Gauss-Seidal or Gauss-Jordan iterative methods.

The number of fasteners to be included in the calculation depends somewhat upon geometry and crack size. According to Swift⁽²⁴⁾ and shown in Figure 4.5.7, 15 fasteners at either side of the crack seems to be sufficient

to get a consistent result. Similar results were obtained by Sanga⁽²⁸⁾. Swift's analysis provides a detailed description of how to incorporate nonelastic behavior in this kind of analysis. The method can account for (1) stiffener flexibility and stiffener bending, (2) fastener flexibility, and (3) biaxiality. Stringer yielding, fastener flexibility, and hole flexibility are lumped together in an empirical equation for fastener deflection.

The effect of fastener flexibility and stiffener bending on β and L is shown in Figure 4.5.8. Although the effects are quite large, the vertical position of the crossover of critical stress-intensity factor curve and stringer stress curve is not affected too much (compare points A and B in Figure 4.5.8). The level of the crossover determines the residual strength, as pointed out in the previous subsections. This explains why the residual strength can be reasonably well predicted if the flexibility of the fasteners is neglected.

In the case of adhesively bonded stiffeners, the displacement compatibility approach was used to calculate the fastener loads $F_1, F_2 \dots F_n$. The adhesive was considered by dividing it into a series of discrete segments. The forces $F_1, F_2 \dots F_n$ which correspond to the segments shown in Figure 4.5.9. Using an appropriate computational method as explained for riveted fastener, the unknown fastener forces can be evaluated. The method of superposition results in an expression in terms of a complex integral for the stress-intensity factor. A typical

residual strength diagram for a bonded structure as compared to the riveted structure is shown in Figure 4.5.10. The required expressions and the solution techniques are discussed in the example problem for a riveted skin-stringer combination with a central crack in the skin (see subsection 4.5.7).

4.5.4 Stiffener Failure

Stiffener failures are based on the following three stiffener conditions:

1. Intact Stiffener (no cracks).
2. Partially failed stiffener (with cracks).
3. Totally failed stiffener.

The failure criterion for the intact stiffener is based on the ultimate strength criterion. As mentioned earlier, the ratio between the stiffener load in the cracked region (P_{\max}) and the remote region from the crack (P) is defined as the load concentration factor L_s or

$$L_s = \frac{P_{\max}}{P} = \frac{P_{\max}}{\sigma A_s} \quad (4.5.1)$$

where σ is the uniform stress in the skin at the loaded end of the panel and A_s is the stiffener cross sectional area. Failure of the stiffener will occur when the value of P_{\max} is equal to the ultimate strength of the stiffener (P_{ult}), or when

$$P_{\max} = P_{\text{ult}} = \Psi \sigma_{\text{ult}} A_s \quad (4.5.2)$$

where σ_{ult} is the ultimate tensile strength of the stiffener material and $\Psi \leq 1$ is a factor accounting for load eccentricity and notch effects in the stiffener. For a uniform stress distribution in the panel remote from the crack the stress in the stringer will equal the nominal stress σ in the skin, i.e.,

$$P = \sigma A_s. \quad (4.5.3)$$

Combining equations 4.5.1 to 4.5.3, yields the following stiffener failure criterion:

$$\sigma = \Psi \frac{\sigma_{ult}}{L_s} \quad (4.5.4)$$

When the stress in the stringer reaches the value of $\Psi \sigma_{ult}$, the stringer will fail. The parameter Ψ is determined by tests.

When load eccentricity and notch effects are not considered for a stringer, Ψ equals one. The stiffener failure curve obtained using Equation 4.5.4 is shown in Figure 4.5.11. The initial portion of the residual strength curve is flat because the load concentration factor L_s is equal to one for small skin crack lengths. As the skin crack increases in size, L_s becomes significantly greater than one and the stringer carries a large portion of the total structural load which eventually leads to stringer yielding and failure. The portion of the curve in Figure 4.5.11 corresponding to $L_s > 1$ shows the gradual reduction of the residual strength.

When the load eccentricity and notch effects in the stiffener are considered, the parameter Ψ in Equation 4.5.4 is less than one. The residual strength corresponding to a case where $\Psi < 1$ is shown in Figure 4.5.11. The curve CD does not have the initial flaw portion exhibited by the case $\Psi = 1$. Instead, the residual strength starts decreasing even for small skin crack lengths. The residual strength diagram for the stringer can be constructed knowing the values of L_s and Ψ . Determining L_s requires numerical solution techniques which are discussed in the example presented in subsection 4.5.7.

According to MIL-A-83444 requirements, cracks are assumed in all load carrying members. This means that all structural elements, stringer included, are assumed to be damaged. The residual strength diagram for the stringer will involve using the fracture mechanics approach of predicting unstable crack growth. The critical stress for a partially cracked stringer is given by $\sigma_f = \frac{K_{cr}}{L_s \beta_s \sqrt{\pi a_s}}$ where K_{cr} is the appropriate fracture toughness, β_s is the stringer geometric parameter, and a_s is the stringer crack size. When the crack in the panel approaches the stringer, the load transmitted to the stringer will become large ($L_s \gg 1$) and thus the critical stress level required to fail the stringer rapidly decreases as shown by curve CE in Figure 4.5.11. Curve CE corresponds to the total failure of the stringer. This may happen when a large crack emanates from a stringer rivet hole. Total failure of the stiffener occurs before the skin crack approaches the stiffeners.

The residual strength diagram for the stiffened panel in this case, would, in fact, be approximately that of the unstiffened panel.

The foregoing discussion presented analysis of a riveted built-up structure. However, built-up structures exist in which the stringer is adhesively bonded to the skin. The load transfer from the skin to the stringer is more effective in the bonded structure due to the increased rigidity in the stiffener. The corresponding load transfer parameter L_s will have higher values as shown schematically in Figure 4.5.12a. Due to the effective load transfer from the skin to the stiffener, the applied stress-intensity factor will be reduced when the panel crack approaches the stiffener. Figure 4.5.12b illustrates the levels of stress-intensity factor that occur for riveted and bonded stiffeners. The figure also shows that the bonded stiffener is subjected to higher loads due to the effective load transfer; the higher load causes the stiffener failure of the bonded structure to be more critical than that of the riveted structure. Figure 4.5.13 compares the decay of residual strength for these two types of structures. The residual strength of the bonded stiffener decreases faster than the riveted stiffener. In the determination of the residual strength diagram, the parameter L_s is usually calculated by numerical methods. The steps to obtain L_s are discussed later in this section.

4.5.5 Fastener Failure

In subsections 4.5.3 and 4.5.4, the discussion focused on skin and stiffener failures. A third mode of failure involves the fasteners. This paragraph will discuss the failure of the fastener system. Load is transmitted from the skin to the stringers through fasteners. If the fastener loads become too high, fastener failure may occur by shear. Fastener failure will reduce the effectivity of the stringer; and therefore, the residual strength of the panel will drop. The highest loads (F) in the stringer/skin connections will occur in the fasteners adjacent to the crack path. Fastener failure will occur when the fastener forces F transmitted by the fasteners adjacent to the crack exceed the critical shear load of the fastener. The fastener failure criterion is given by

$$F = \pi/4 d^2 \tau_{ult} \quad (4.5.5)$$

where d is the fastener diameter and τ_{ult} is the ultimate shear stress of the fastener material. It is emphasized that fastener failure need not necessarily cause total failure of the panel. Once the fastener failure criterion is met, however, the values of L_s and β will change since the loads transferred to the stiffener and skin changes. Once the fastener fails, the values of β and L_s will be recalculated in order to proceed further with the residual strength analysis. The load that causes the fasteners to fail by shear can be calculated from Equation 4.5.5; the corresponding nominal stress in the panel then gives the residual

strength curve for the fasteners as shown in Figure 4.5.14. At zero crack length, and for the case where the skin and stringers are made from common materials, the fasteners do not carry any load; the curve therefore tends to increase rapidly for $a \rightarrow 0$. The fastener forces F_i can be computed through the displacement compatibility between the stiffener and the panel. The necessary steps involved in the computation of F_i are discussed in the example presented in subsection 4.5.7.

In the case of adhesively bonded structures, the adhesive (fastener) failure criterion is based on a maximum adhesive strain value. The residual strength analysis is fairly complicated (see for example, reference 24). Based on the displacement compatibility between the panel and the stiffener, the adhesive segment strain deflection can be numerically computed for different amounts of disbond. Figure 4.5.15a shows the adhesive strain versus gross stress for various levels of adhesive delamination. The vertical line AB represents average failure strain of the adhesive. The intersection points between the line AB and the curves give the critical gross stress versus amount of adhesive failed as shown in Figure 4.5.15b. The corresponding curve ABC can be used for panel failure analysis. The area above the curve defines the failure of adhesive.

4.5.6 Methodology Basis for Stiffened Panel Example Problem

The residual strength analysis of an edge stiffened, centrally cracked skin structure of the type shown in Figure 4.5.16 can be performed by following the general steps described in the preceding subsections.

In this subsection, the specific details are covered which are associated with conducting the stress-intensity factor analysis as well as the analysis to determine the stresses in the stringers and fastener loads. To simplify the detailed calculations, it is assumed that only one fastener (rivet) on either side of the crack is active as shown in Figure 4.5.17 and that this rivet is assumed to be rigid. Thus, there is only one unknown fastener force F transferred between the stringers and the skin by this rivet.

Typically, the analysis proceeds by splitting up the structure shown in Figure 4.5.16 into its component parts as shown in Figure 4.5.17. The unknown force F can be calculated from the displacement compatibility condition between the skin and the stringer. The complicated expressions which correspond to the displacements V_σ , V_F , and V_P due to the applied stress, σ , the fastener force F and the distributed pressure $P(x)$, respectively, can be obtained using a procedure suggested by Westergaard⁽²⁹⁾ and by Love⁽²⁷⁾. The detailed discussions on the methods of obtaining the required relationships are presented by Broek⁽¹³⁾. The necessary

relationships for V_σ , V_F , V_p and V_{st} (displacement in the stringer) are given as:

$$V_\sigma = \frac{\sigma}{E} f_\sigma \quad (4.5.6)$$

$$V_F = \frac{-F}{EB} f_F \quad (4.5.7)$$

$$V_p = \frac{-F}{EB} f_p \quad (4.5.8)$$

and
$$V_{st} = \frac{F}{E_{st} B_{st}} f_{st} + \frac{\sigma}{E_s} p \quad (4.5.9)$$

where

$$f_\sigma = \sqrt{\rho_1 \rho_2} \left\{ 2 \sin\left[\frac{\theta_1 + \theta_2}{2}\right] \frac{(1+\nu)pr}{\rho_1 \rho_2} \cos\left[\theta - \frac{\theta_1 + \theta_2}{2}\right] \right\} + \nu p \quad (4.5.10)$$

$$f_F = \frac{(1+\nu)}{4\pi} \left\{ (3-\nu) \left[\ln \frac{d}{4p} - 1 \right] + (1+\nu) \left[2 - \frac{s^2}{2p^2} \right] + (3-\nu) \ln \left(\frac{s^2}{s^2 + p^2} \right) \right\} \quad (4.5.11)$$

$$f_p = \frac{\bar{P}}{\pi a} \left\{ 2 \left[\sqrt{\rho_1 \rho_2} \sin\left(\frac{\theta_1 + \theta_2}{2}\right) - p \right] - (1+\nu) p \left[\frac{r}{\sqrt{\rho_1 \rho_2}} \cos\left(\theta - \frac{\theta_1 + \theta_2}{2}\right) - 1 \right] \right\} \quad (4.5.12)$$

where $\bar{P} = \left\{ \tan^{-1}\left(\frac{a+s}{p}\right) + \tan^{-1}\left(\frac{a-s}{p}\right) + \frac{p(1+\nu)}{2} \left[\frac{a+s}{p^2 + (a+s)^2} + \frac{a-s}{p^2 + (a-s)^2} \right] \right\} \quad (4.5.13)$

and

$$f_{st} = - \frac{(1+\nu)}{4\pi} \left\{ \left[(3-\nu) \left(\ln \frac{d}{4y_o} - 1 \right) + (1+\nu) \right] + 2 \sum_{n=1}^{\infty} \left[(3-\nu) \ln \frac{nw}{\sqrt{n^2 w^2 + 4p^2}} + (1+\nu) \left(\frac{4p^2}{n^2 w^2 + 4p^2} \right) \right] \right\} \quad (4.5.14)$$

The geometric variables r , ρ_1 , ρ_2 , θ_1 , θ_2 and θ are shown in Figure 4.5.18.

The displacement compatibility condition requires equal displacements in corresponding points of sheet and stringer; it yields the following equation to calculate the unknown fastener force F .

$$V_{\sigma} + V_F + V_p = V_{st} \quad (4.5.15)$$

substituting the expressions 4.5.6-4.5.9 for V_{σ} , V_F , V_p , and V_{st} in the above relationship, and reassembling, we get

$$F = \sigma \lambda \text{ where } \lambda = \left\{ \frac{\frac{f_{\sigma}}{E} - \frac{p}{E_{st}}}{\frac{f_F + f_p}{EB} + \frac{f_{st}}{E_{st} B_{st}}} \right\}. \quad (4.5.16)$$

The next step is to obtain an expression for the stress-intensity factor for the entire stiffened panel configuration. Using superposition, the stress-intensity factor is obtained as the sum of the stress-intensity factors for the three cases shown in Figure 4.5.17. It can easily be seen that for Case I: $K = \sigma \sqrt{\pi a}$ and for Case II: $K = 0$. The stress-intensity factor (K) for Case III is a fairly complicated expression and it is given by,

$$K_{III} = - 2 \sqrt{\frac{a}{\pi}} \frac{1}{\pi} \frac{F}{Bp} \left[\frac{(3 + \nu)}{2} I_1 + (1 + \nu) I_2 \right] \quad (4.5.17)$$

$$\text{where } I_1 = \int_0^a \frac{d\bar{x}}{\sqrt{a^2 - \bar{x}^2}} \left\{ \frac{1}{(1 + (\bar{x} - \bar{s})^2)} + \frac{1}{(1 + (\bar{x} + \bar{s})^2)} \right\} \quad (4.5.18a)$$

$$\text{and } I_2 = \int_0^a \frac{d\bar{x}}{\sqrt{a^2 - \bar{x}^2}} \left\{ \frac{(\bar{x} - \bar{s})^2}{(1 + (\bar{x} - \bar{s})^2)^2} + \frac{(\bar{x} + \bar{s})^2}{(1 + (\bar{x} + \bar{s})^2)^2} \right\}. \quad (4.5.18b)$$

where \bar{a} , \bar{x} and \bar{s} are normalized with respect to the rivet pitch. The estimation of K_{III} requires solution of the above integrals by numerical methods. Replacing the fastener force F by the expression and rearranging the expression for K_{III} , the stress-intensity factor K for the stiffened panel then becomes

$$K = \sigma\sqrt{\pi a} - \sigma\sqrt{\pi a} \lambda_1 \lambda_2 \quad (4.5.19)$$

where
$$\lambda_1 = \frac{(3+\nu)}{2} I_1 + (1+\nu) I_2 \quad (4.5.20a)$$

and
$$\lambda_2 = \frac{2\lambda}{\pi^2 B_p} . \quad (4.5.20b)$$

The stress-intensity factor K can be finally expressed in the following form,

$$K = \sigma\beta\sqrt{\pi a} \quad (4.5.21)$$

where
$$\beta = (1 - \lambda_1 \lambda_2) . \quad (4.5.22)$$

To calculate K for a given stiffened panel the values of f_σ , f_F , f_p , f_{st} , and λ_1 have to be obtained. These variables are numerically calculated and plotted as shown in Figures 4.5.19 to 4.5.23 for various values of \bar{s} , \bar{a} , and \bar{d} . For the given example data, we can now construct the residual strength diagram using the values obtained from these plots.

4.5.7 Example Residual Strength Analysis of Stiffened Panel

Determine the residual strength capabilities of a stiffened panel of 7075 Aluminum with a central crack between the two stringers as shown in Figure 4.5.24.

For a critical crack size ($2a$) of 4.0 inch, what is the fracture strength and for an operating stress of 20 Ksi, what is the critical crack size?

SOLUTION:

The first step is to obtain the stress-intensity factor by means of Equation 4.5.21 which involves the parameters λ_1 and λ_2 . For various crack lengths, these two variables can be calculated using Equation 4.5.20. The calculations involve the values of f_σ , f_F , f_p , f_{st} and λ which are obtained from the plots for various values of \bar{a} for the given $\bar{s} = 20$ and $d/p = 3/16$. Knowing the values of λ_1 and λ_2 , the geometric parameter β can be estimated from Equation 4.5.22. It is then straightforward to obtain the K vs. a plot by substituting the sets of values of a and β in the stress-intensity factor Equation 4.5.21 for a particular value of the applied stress σ . The corresponding K vs. a plot is shown in Figure 4.5.25 for $\sigma = 5, 10, \text{ and } 15$ Ksi. This figure shows that the stress-intensity factor decreases rapidly when the crack approaches the stringer. The figure also shows the effect of stringer to panel thickness ratio on the stress-intensity factor.

The next step is to apply a failure criterion to evaluate the fracture stresses, σ_{cr} , for various crack sizes. Assuming that the material exhibits negligible subcritical crack growth, the fracture toughness failure criterion ($K = K_{cr}$) based on the plane stress condition can then be applied. For $K = K_c$ in Equation 4.5.21, σ_f can be evaluated for a

particular crack size and the corresponding β which was obtained through equation 4.5.22. The residual strength diagram, i.e., the plot of σ_f vs. a_c for the given data ($K_c = 65 \text{ Ksi}\sqrt{\text{inch}}$) is shown in Figure 4.5.26.

The residual strength curves of the fastener and stiffeners are obtained by combining equations 4.5.5 and 4.5.16 for fastener failure and equations 4.5.1, 4.5.4, and 4.5.16 for stringer failure. The corresponding equations are given by,

$$\sigma_f = \frac{\pi d^2 \tau_{ult}}{4 \lambda} \text{ (Fastener)} \quad (4.5.23)$$

and

$$\sigma_f = \Psi \frac{\sigma_{ult}}{(1 + \frac{\lambda}{A_s})} \text{ (Stringer)} \quad (4.5.24)$$

where λ is a function of 'a' and the values of λ for various crack lengths can be obtained using the Equation 4.5.16. To obtain Equation 4.5.24, note that the maximum stringer load (P_{max}) is the source of the fastener force ($F = \sigma \lambda$) and the remote stringer force (σA_s). The composite residual strength diagram as shown in Figure 4.5.26 contains the three failure curves corresponding to panel, stringer, and fastener. The stringer failure curve corresponds to $\alpha = 1$ (light stringer).

For the crack length given ($2a = 4$ inches), the corresponding residual strength is found from Figure 4.5.26 for a half crack length (a) of 2 inches. Point A in this figure identifies the skin failure condition which occurs at a stress level of 25.9 Ksi. For the operating stress level of

20 Ksi, the panel can be effective without catastrophic failure for cracks with length less than the critical crack (a_{cr}) of 3.4 inch (note $2a_{cr} = 6.8$ inch). If the panel develops a crack less than a_{cr} , it will not fail by unstable crack growth. However, for any other crack size which is equal or greater than the a_{cr} (3.4 inch), the residual strength level will fall below the operating stress level, leading to the rapid extension of the crack. Nevertheless, the structure has to be fully analyzed for its crack arrest capabilities when it develops cracks of length greater than a_{cr} .

Assume that the panel develops a crack of size a_{cr} . At point B in the figure, the crack extends rapidly. When the rapidly extending crack becomes 15 inches, the stress level in the stiffener (point C) reaches its critical value and the stiffener fails. Due to the stiffener failure, the stiffener becomes ineffective, leading to the total failure of the panel without any crack arrest possibilities.

In Figure 4.5.27, the stiffener failure curve is plotted for a strong stiffener with $\alpha = 4$ (the stiffener thickness is "assumed" four times the panel thickness). If the panel develops a crack size a_{cr} , the crack will extend rapidly from point D to point E as shown in Figure 4.5.27. At point E, the fastener fails, leading to an ineffective stringer (loads are no longer transferred to the stringer). Thus, the failure of the panel is unavoidable and the unstable crack growth without effective crack arrest leads to the total failure of the structure.

4.5.8 Tearing Failure Analysis

When the cracked thin sheet structure of high fracture toughness material is considered, the solutions based on linear elastic behavior for the calculation of residual strength are no longer valid due to the large scale yielding at the crack tip. For fail-safe structures with crack arrest capabilities, the residual strength analysis becomes complicated. However, using the R-curve based on $\sqrt{J_R}$ concept as the failure criterion Ratwani and Wilhem⁽²⁶⁾ developed a step-by-step procedure for predicting the residual strength of built-up skin stringer structure composed of tough material exhibiting tearing type fractures.

The residual strength prediction procedure is briefly outlined here to show, step-by-step, the required data and analysis. It should not be assumed that by reading this step-by-step procedure that the uninitiated can perform a residual strength prediction. It is strongly recommended that the details of the preceding subsections and reference 26 be examined prior to attempting a structural residual strength analysis based on the following ten procedural steps.

STEP 1. Model the structure for finite-element analysis or use an existing finite-element model remembering --

- a. That structural idealizations are typically two-dimensional,
- b. That no out-of-plane bending is permitted,
- c. To use a proper fastener model (a flexible fastener model for riveted or bolted structure, or a shear spring model for bonded structure).

- d. To use material property data from skin and substructure of interest (i.e., E , E_{ty} and F_{tu}),
- e. To select the most critical crack location (normally highest stressed area),
- f. To take advantage of structural symmetry.

STEP 2. Select one crack length ($2a$ or a) of interest (based on inspection capability or detailed damage tolerance requirement). Based on this "standard" crack length, five other crack lengths are selected for a Dugdale type elastic plastic analysis. These crack lengths should be selected such that crack length to stiffener spacing ($2a$) ratios vary between 0.15 to 1.1 remembering --

- a. That the greatest variation in J values will take place near reinforcements, and
- b. To select at least one crack size shorter than "standard".

STEP 3. With the finite-element model (from Step 1) and assumed crack lengths (from Step 2), perform an analysis assuming Dugdale type plastic zones for each crack size remembering --

- a. To select the first increment of plastic zone length at 0.2 inches and sufficient successive increments (normally 6) to reach Bueckner-Hayes calculated stresses up to 85 percent to F_{ty} .
- b. To make judicious selection of plastic zone increments so as to take advantage of overlapping a_e (effective crack length) (e.g., 3.2, 3.5, 4.2, 5.0 inches for a 3 inch physical crack

and 4.2, 4.5, 5.0 inches, etc., for a 4 inch physical crack). If overlapping is done, those cases where the crack surfaces are loaded throughout the crack length will be common for two or more physical crack sizes hence the computer programs need be run only once (e.g., 4.2 and 5.0 inches) thus reducing computer run times.

STEP 4. From Step 3, obtain stresses in stiffeners for Dugdale analysis and elastic analysis. Plot stiffener stresses as function of applied stress.

STEP 5. From the crack surface displacement data of Step 3, plot \sqrt{J} (obtained by Bueckner-Hayes approach) versus applied stress to F_{ty} ratio for each crack size.

STEP 6. From Step 5, cross plot the data in the form of \sqrt{J} versus crack size (a) at specific values of applied stress to F_{ty} ratio.

STEP 7. Employing the data of Step 4 and the "standard" crack size determine, gross panel stress to yield strength ratio, σ/F_{ty} at ultimate strength (F_{tu}) for the stiffener material - assuming zero slow crack growth. This information will be used subsequently to determine if a skin or stiffener critical case is operative.

STEP 8. Obtain crack growth resistance data for skin material (see Volume II of reference 26) remembering --

- a. To use thickness of interest (i.e., if the skin material is chemically milled, use the experimentally obtained R-curve for the same chemically milled material)
- b. Use proper crack orientation (LT, TL, or off angle) corresponding to anticipated direction structural cracking.

STEP 9. Plot \sqrt{J} versus Δa_{PHY} curve as shown in Figure 4.5.28 from the data obtained in Step 8.

STEP 10. Determine structural residual strength. On the \sqrt{J} versus crack size (a) plots obtained in Step 6 for the structure, overlay the $\sqrt{J_R}$ versus Δa_{PHY} material plot of Step 9 at the initial crack length of interest as shown in Figure 4.5.29. Determine if --

At the gross panel stress obtained from Step 7, significant slow tear (≥ 0.25 inch) will occur as indicated from the intersection of the $\sqrt{J_R}$ versus Δa_{PHY} curve with the constant σ/F_{ty} curve at a stringer ultimate strength (see Step 7). Interpolation will probably be necessary between values of constant σ/F_{ty} . Then proceed as follows:

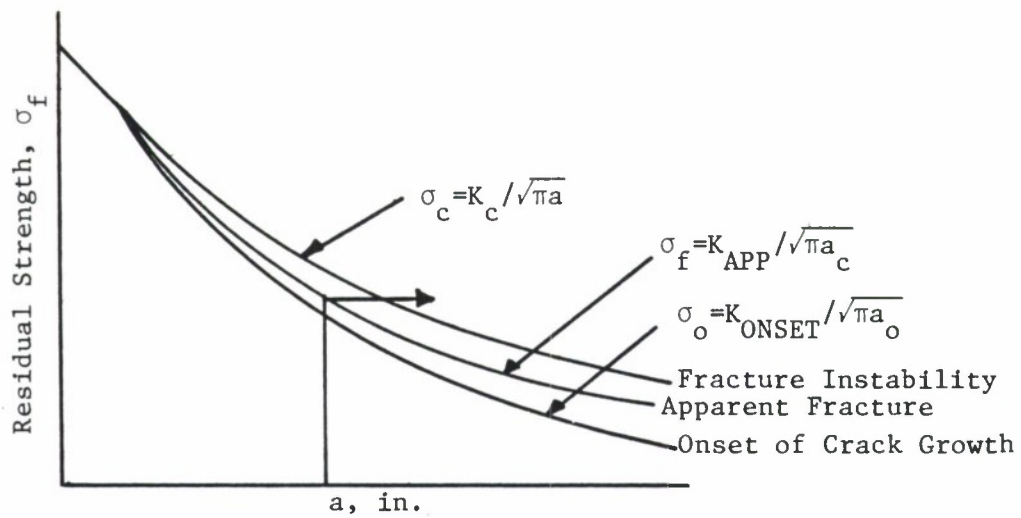
- If significant slow tear occurs (≥ 0.25 inch) the structure can be considered to be skin critical (at that particular crack length). Tangency of $\sqrt{J_R}$ versus Δa_{PHY} and \sqrt{J}

versus a_{PHY} at constant applied stress can be used to determine extent of slow tear and residual strength at failure as a percentage of F_{ty} .

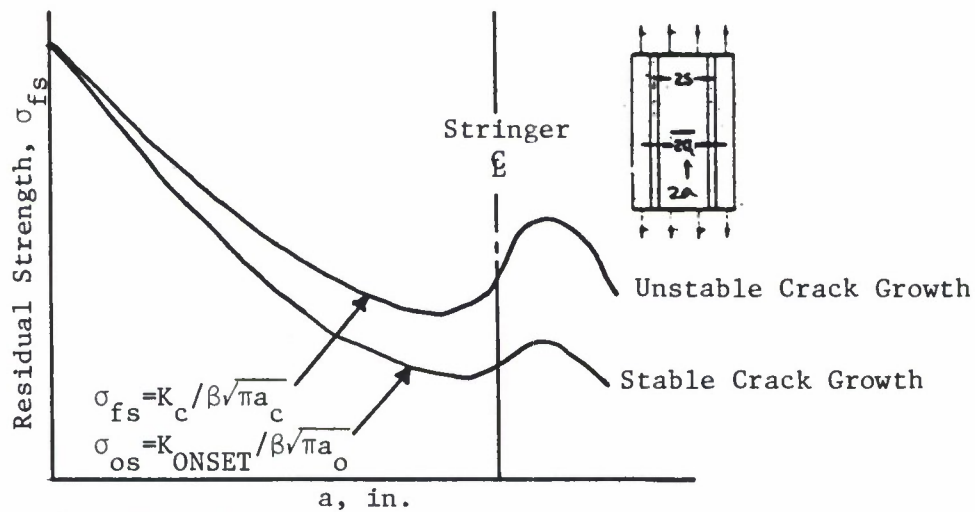
- If significant slow tear does not occur ($\Delta a_{PHY} < 0.25$ inch) the structure will normally be stiffener critical. To determine a conservative value of residual strength (for that crack length) use the Dugdale curve of Step 4 and stiffener ultimate strength.

4.5.9 Summary

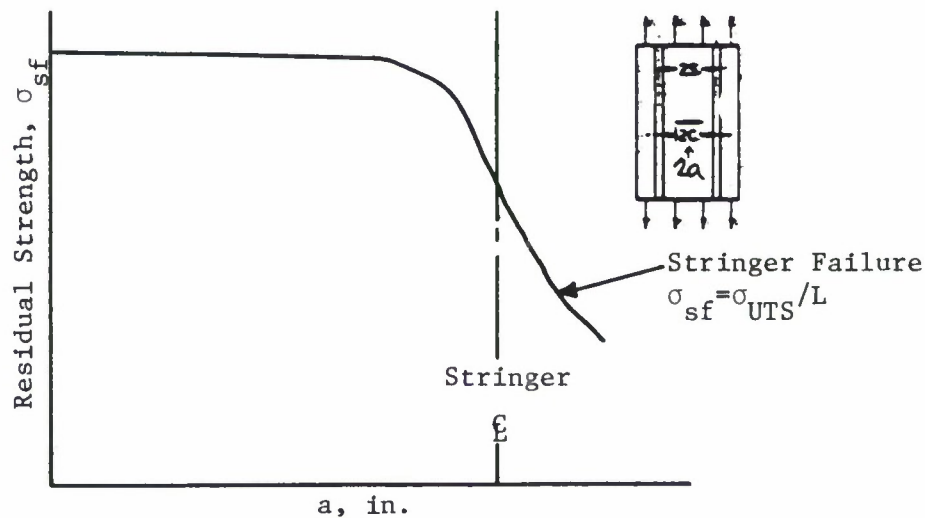
The most important factor to consider in residual strength prediction of a cracked built-up structure is to decide whether the structure is skin or stiffener critical. Normally, a short crack length is likely to be a skin critical case and a long crack length a stiffener critical case. However, there is no clear cut demarcation between the two cases. Factors such as percentage stiffening, spacing of stringers, lands in the structure and other structural details will influence the type of failure. Hence, a good technique is to determine the residual strength of a given structure based on both skin critical and stiffener critical cases. The minimum fracture stress of the two will then represent the residual strength of the structure and should be considered to be the governing case.



(a) Unstiffened Panel



(b) Stiffened Panel



(c) Stringer

Figure 4.5.1. Elements of Residual Strength Diagram.
4.5.31

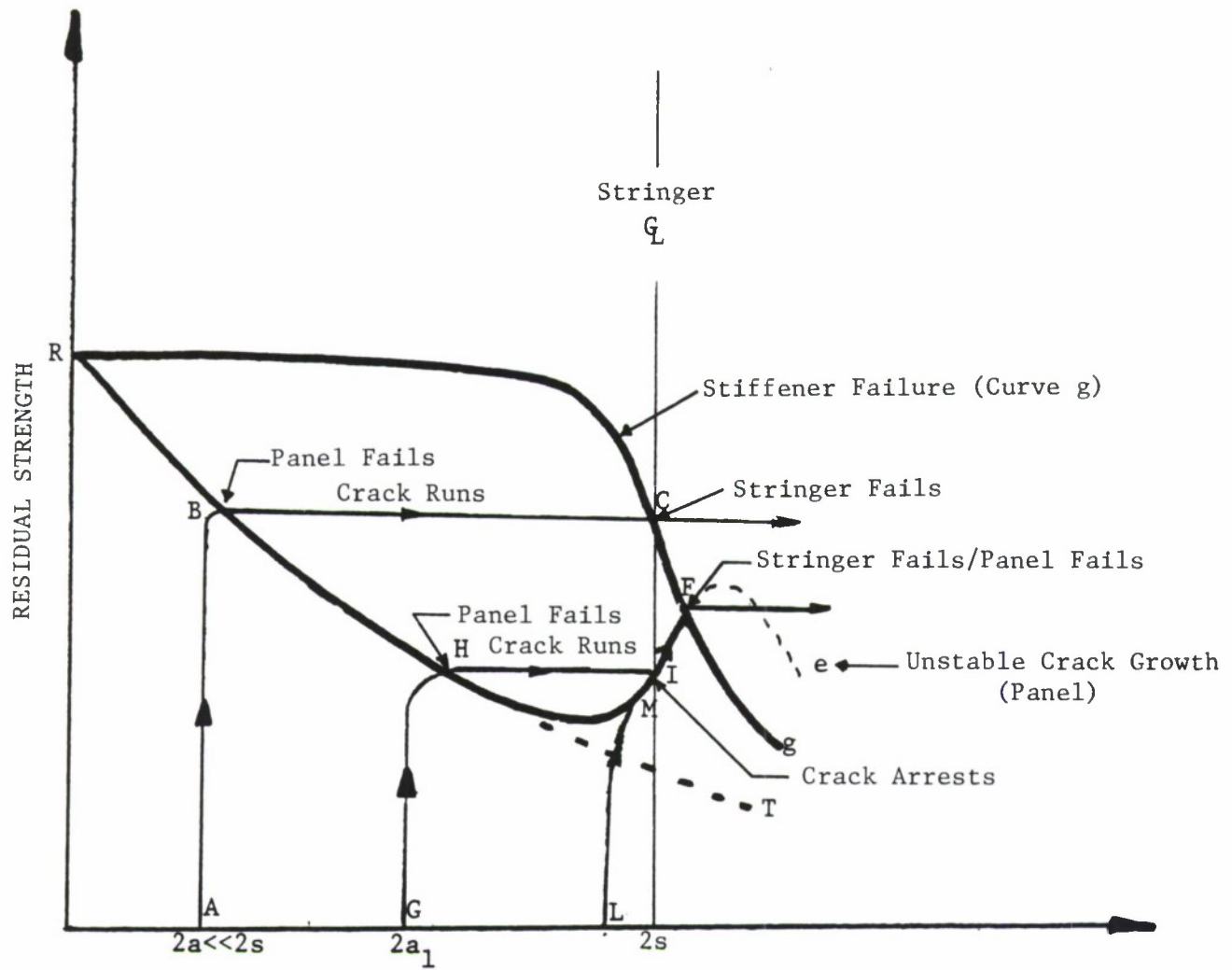


Figure 4.5.2. Residual Strength Diagram for a Stiffened Panel.

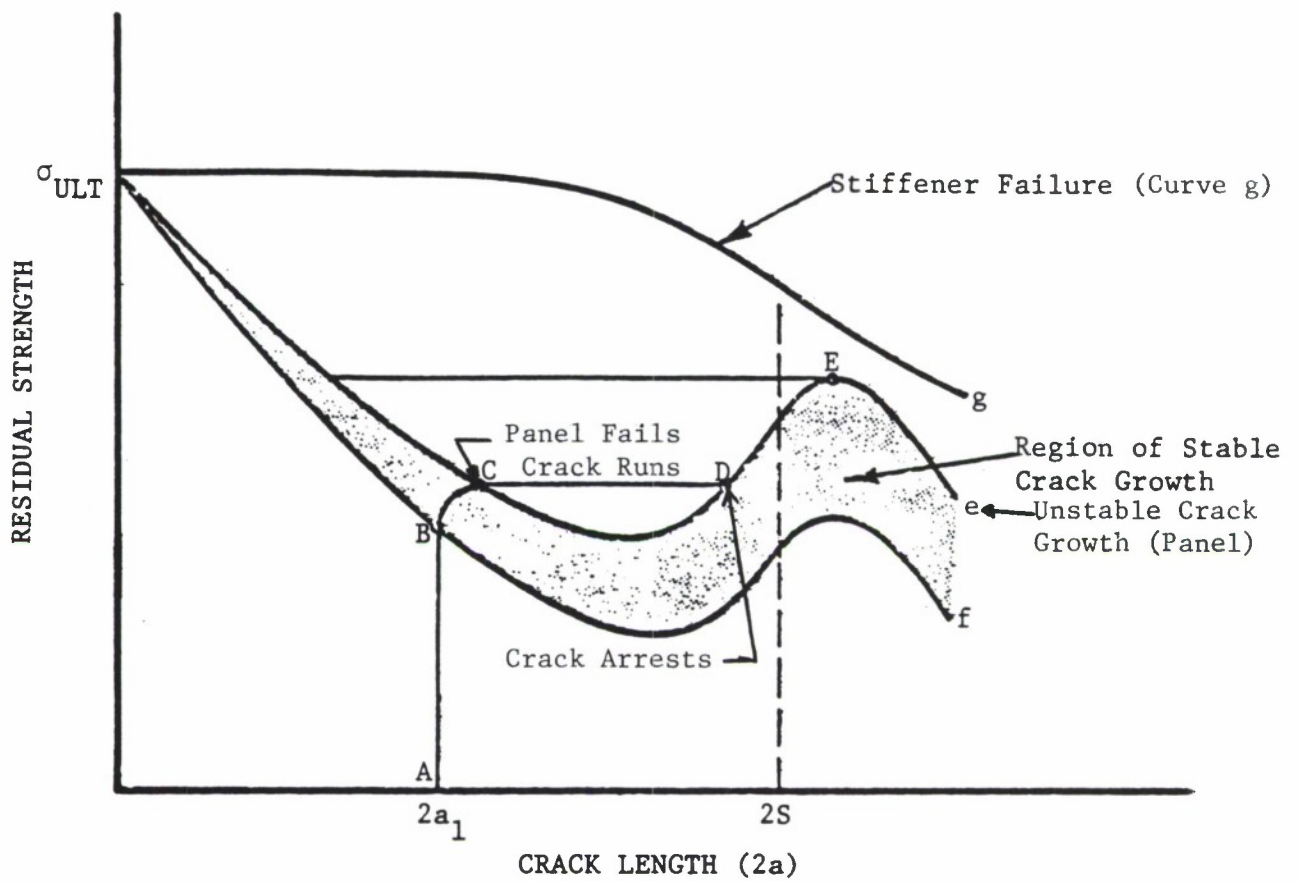


Figure 4.5.3. Panel Configuration with Heavy Stringers; Skin-Critical Case.

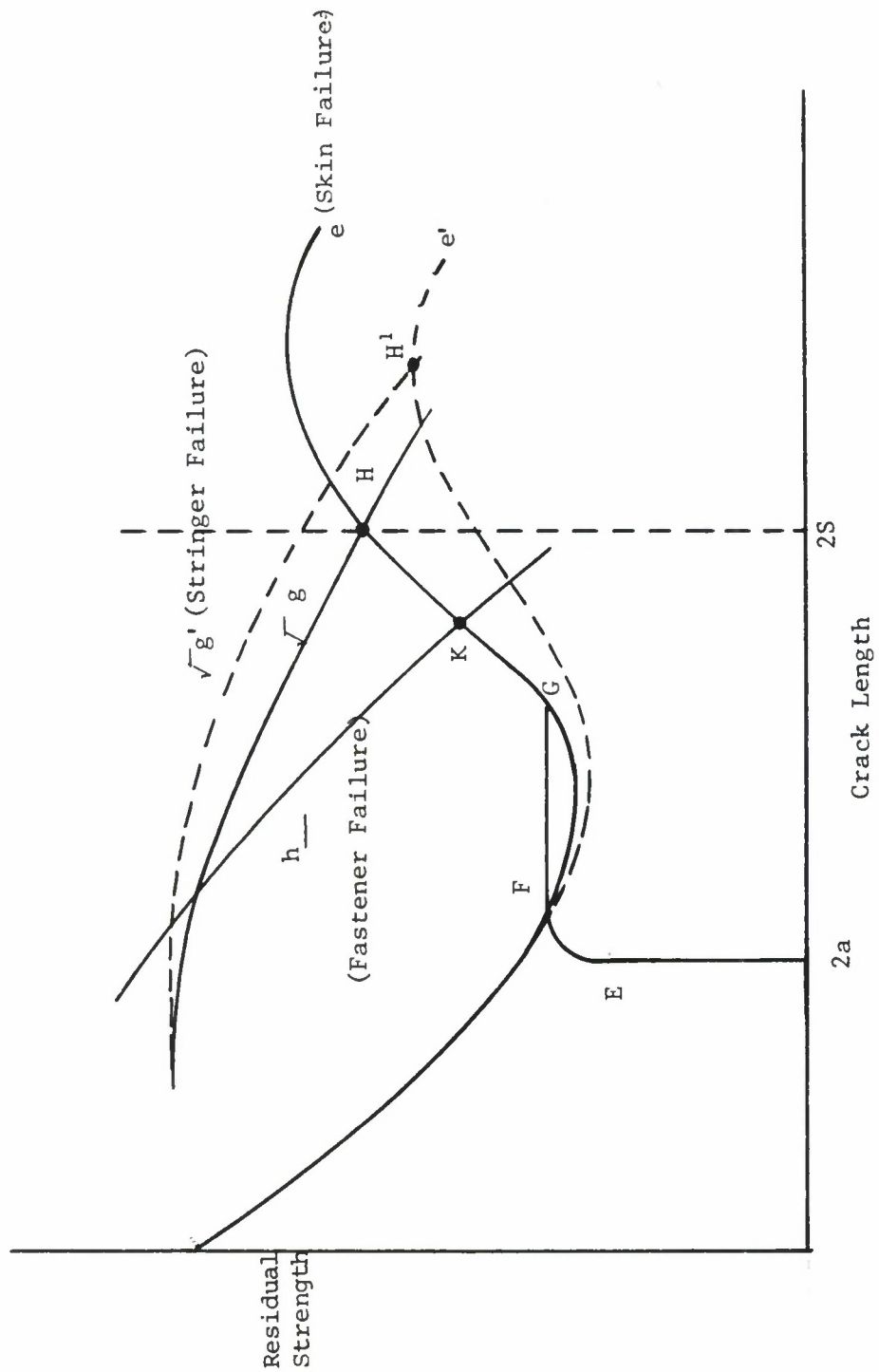
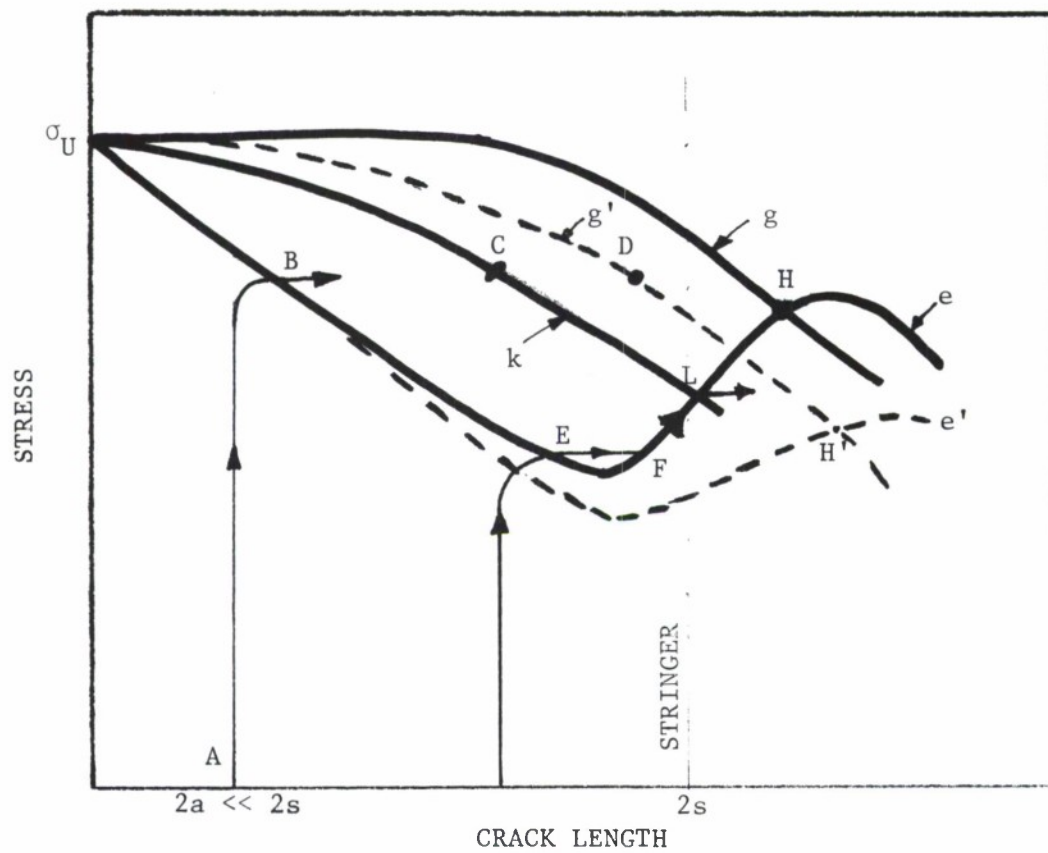
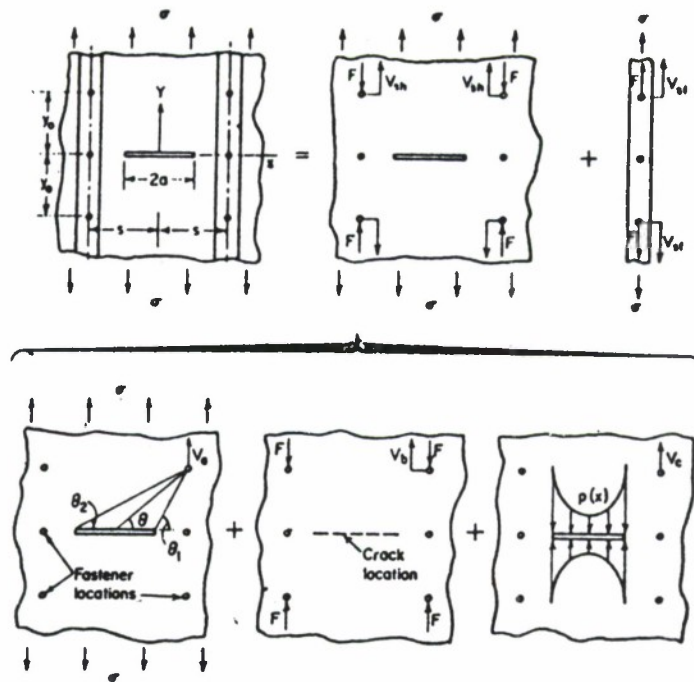


Figure 4.5.4. Criterion for Fastener Failure.

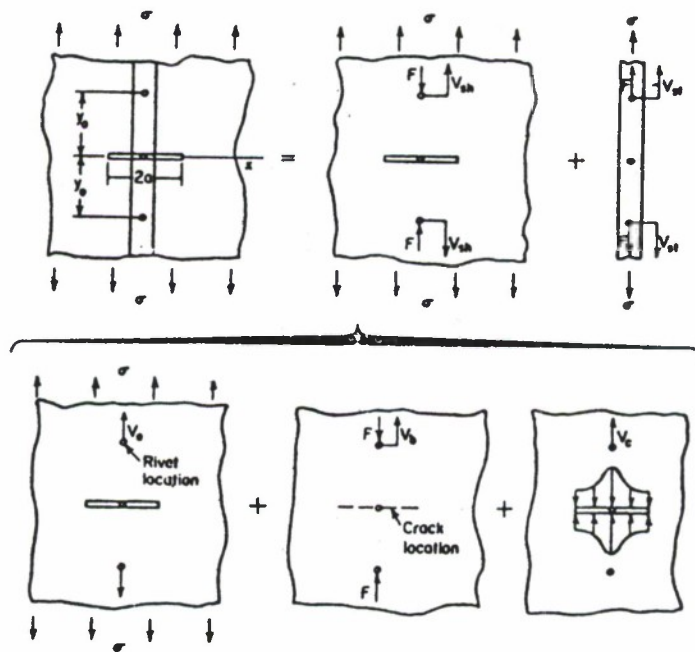


- f: Residual Strength Curve of Skin Alone
- g: Residual Strength Curve of Two Edge Stiffeners
- k: Residual Strength Curve of Central Stiffener (Failing).
- g': Residual Strength Curve of Two Edge Stiffeners After the Failure of Central Stiffener

Figure 4.5.5. Residual Strength Diagram for a Panel With Three Stiffeners and a Central Crack Emanating from a Rivet Hole.



a. Crack Between Stiffeners



b. Crack Across Stiffener

Figure 4.5.6. Analysis of Stiffened Panel.

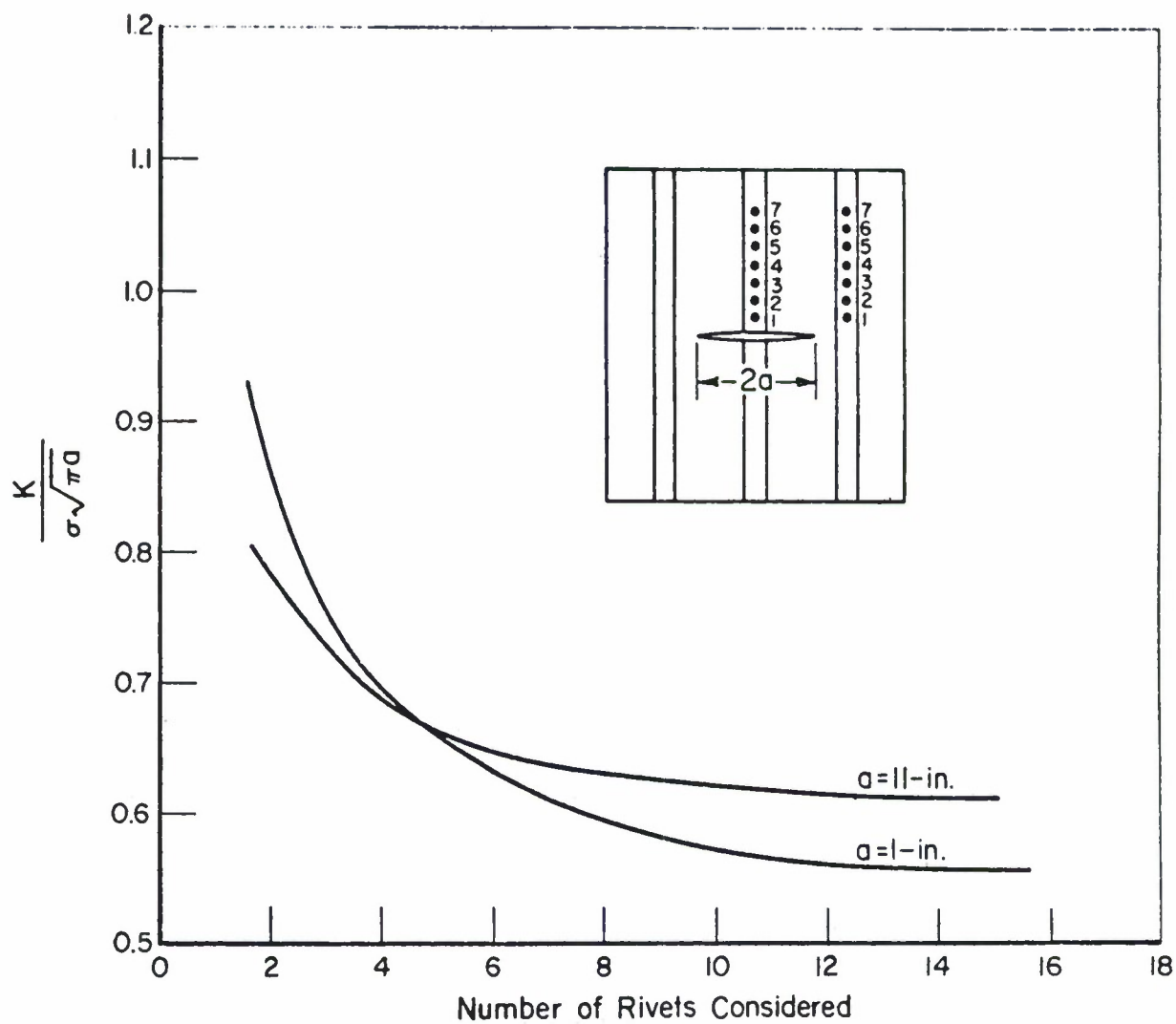


Figure 4.5.7. Effect of Number of Fasteners Included in Analysis on Calculated Stress-Intensity Factor.

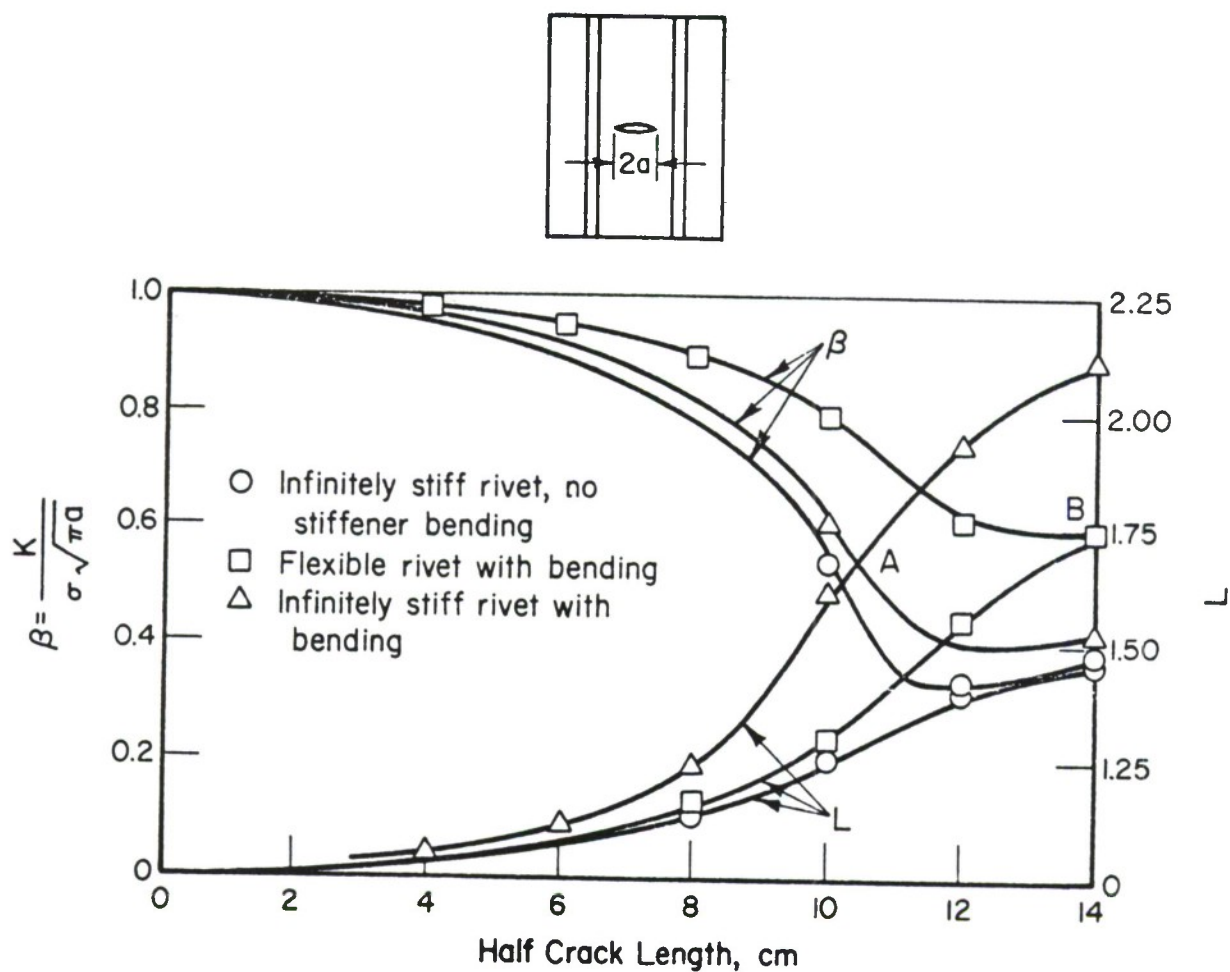


Figure 4.5.8. Skin-Stress-Reduction β and Stringer-Load-Concentration L as Affected by Fastener Flexibility and Stiffener Bending.

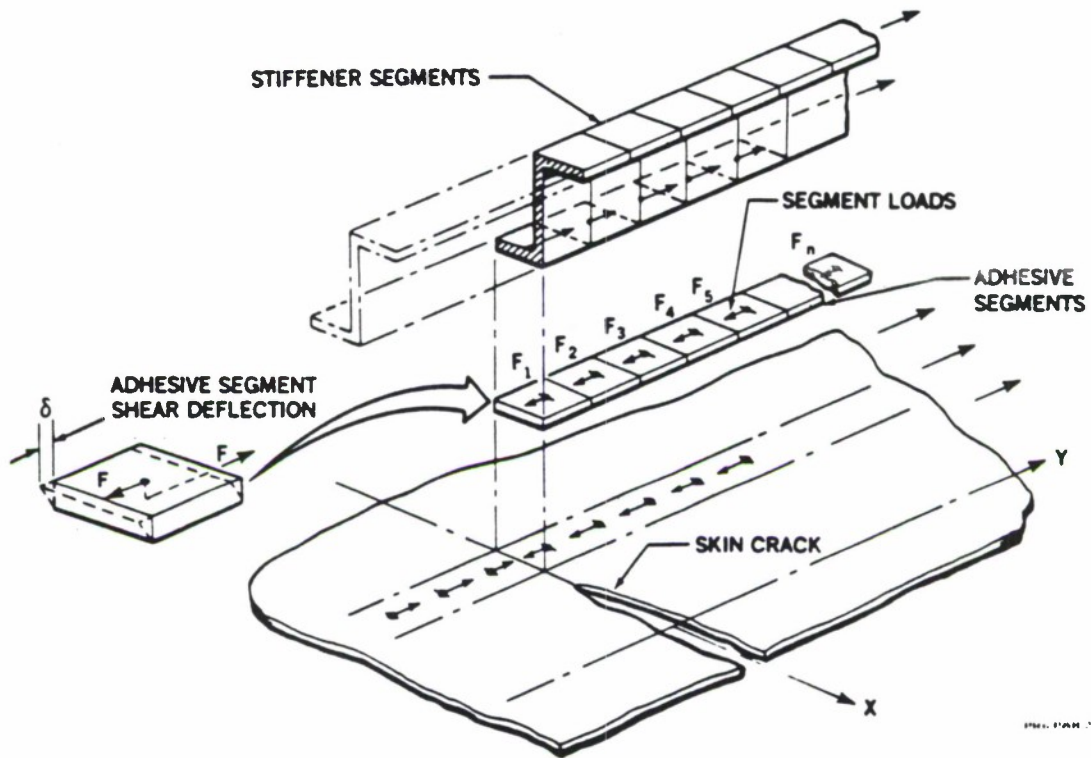


Figure 4.5.9. Bonded Fastener Divided into Discrete Segments.

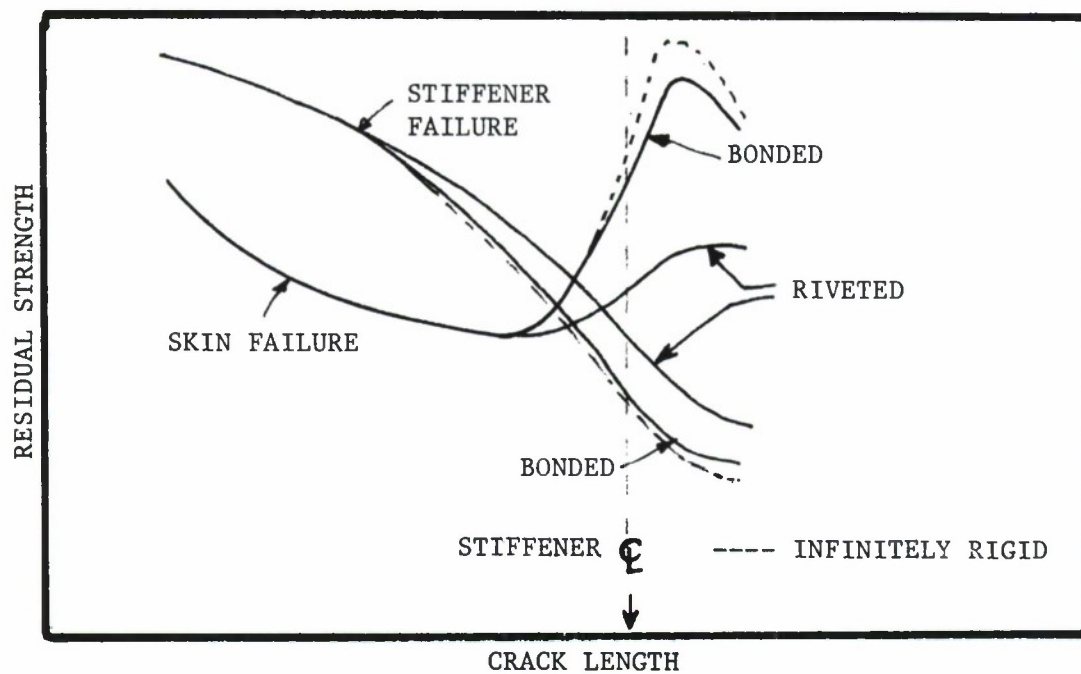


Figure 4.5.10. Residual Strength Diagram Comparing Riveted and Bonded Structures.

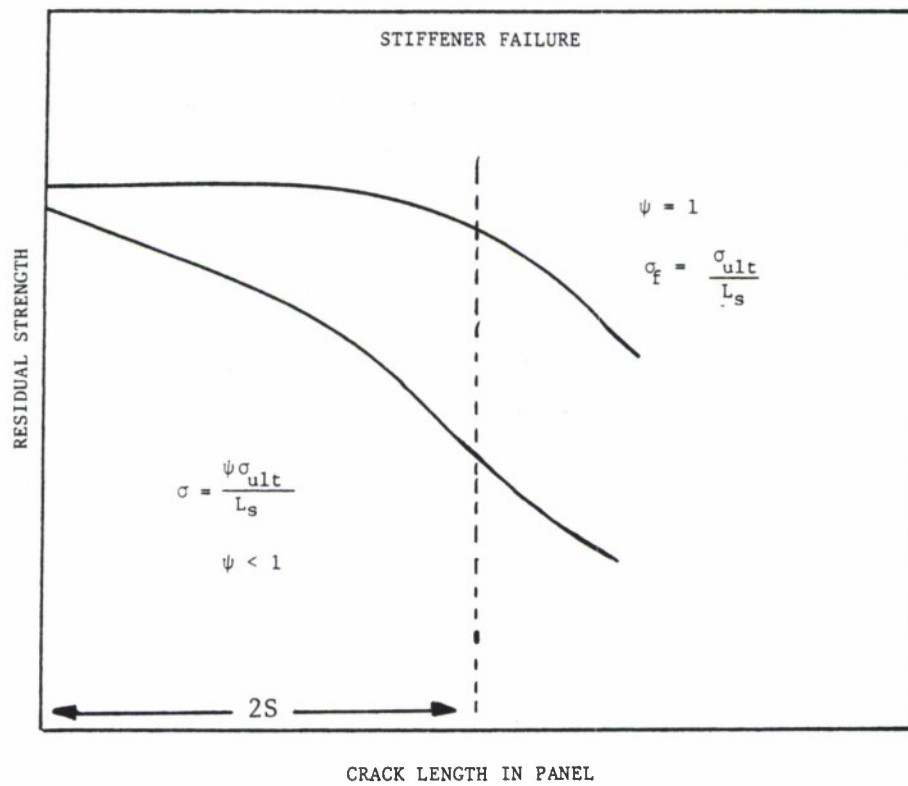
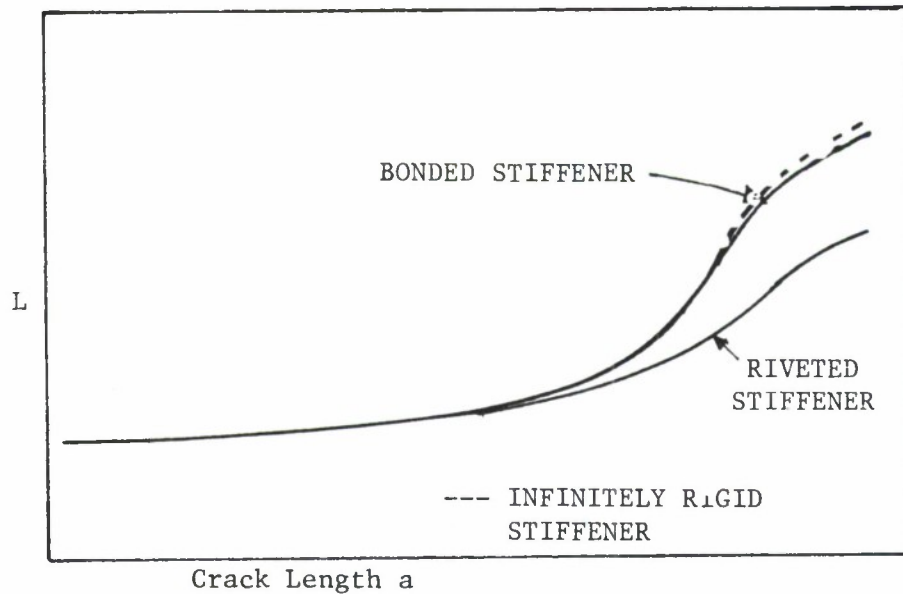
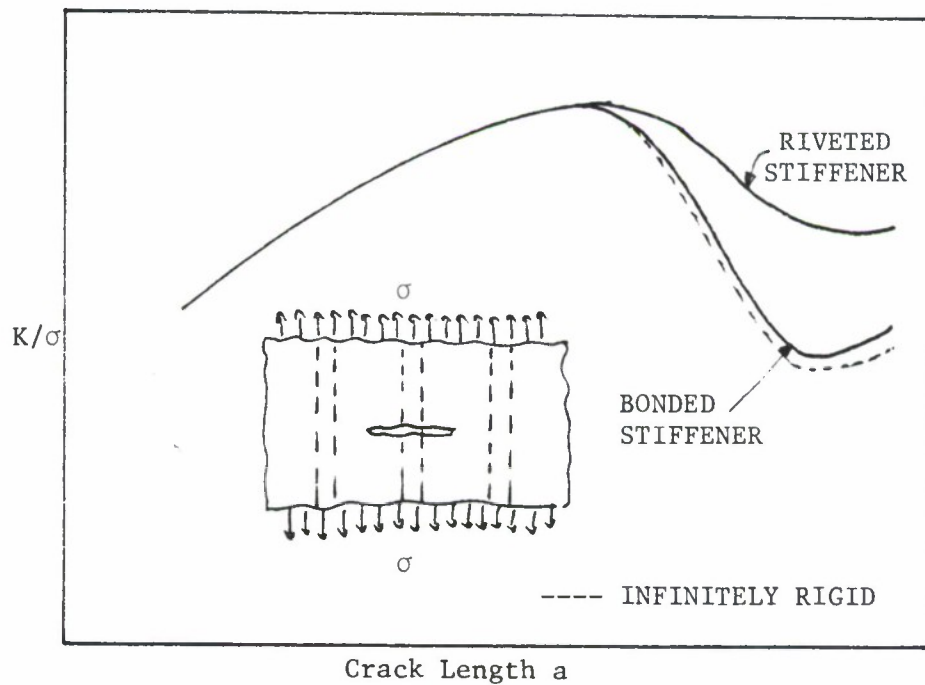


Figure 4.5.11. Residual Strength Diagram for Stiffener.



(a) Load Transfer Parameter (L)



(b) Stress-Intensity Factor Coefficient (K/σ)

Figure 4.5.12. Comparison of L_s and K/σ_s for Riveted and Bonded Structures.

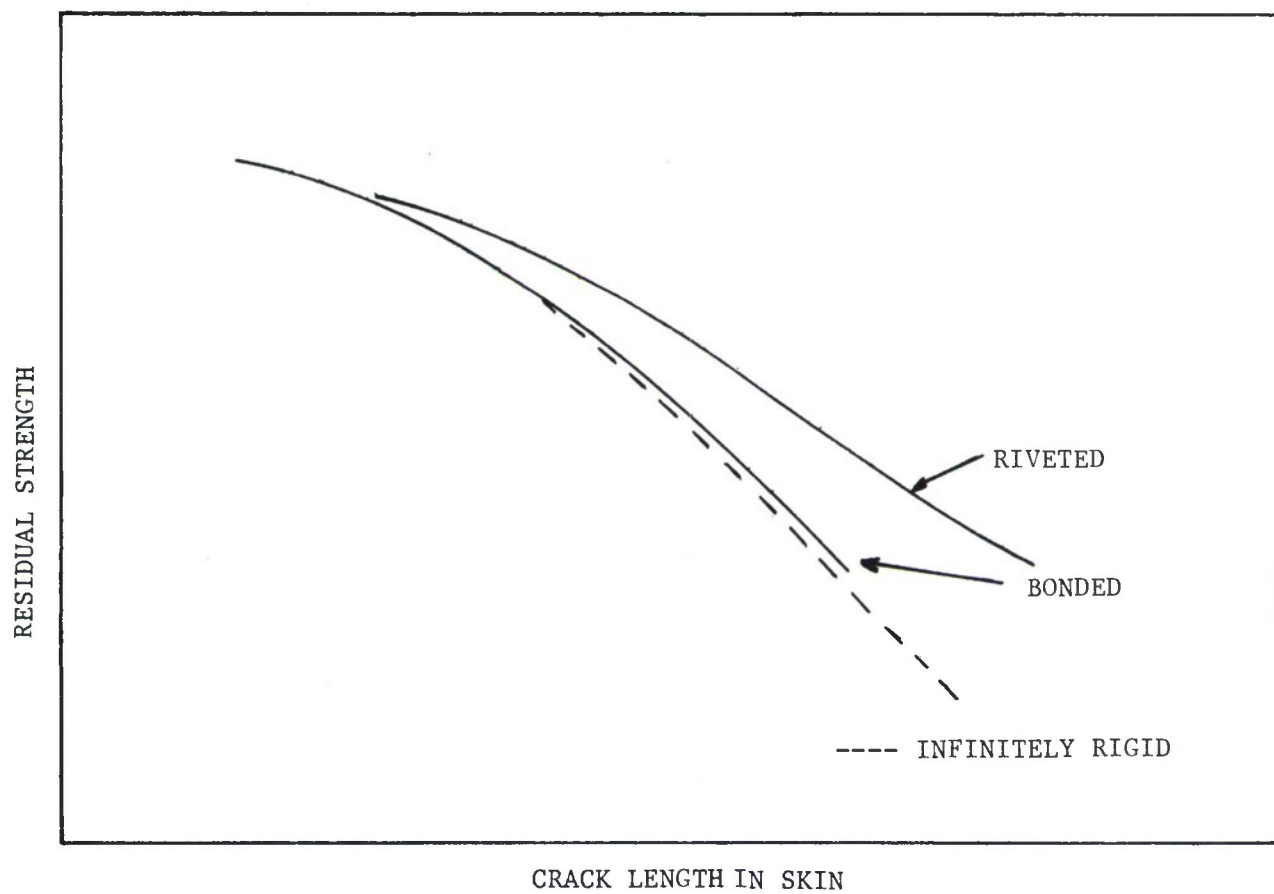


Figure 4.5.13. Comparison of Residual Strength for Riveted and Bonded Stiffeners.

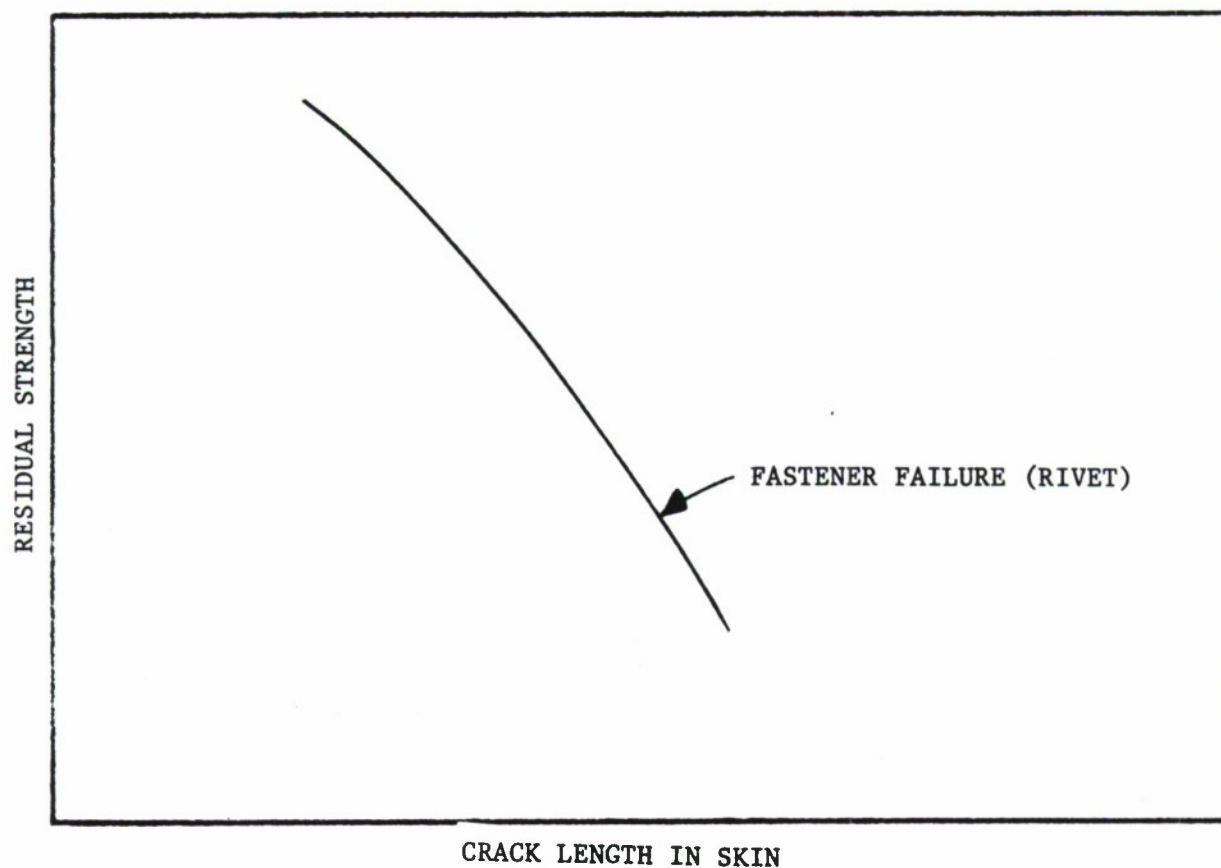
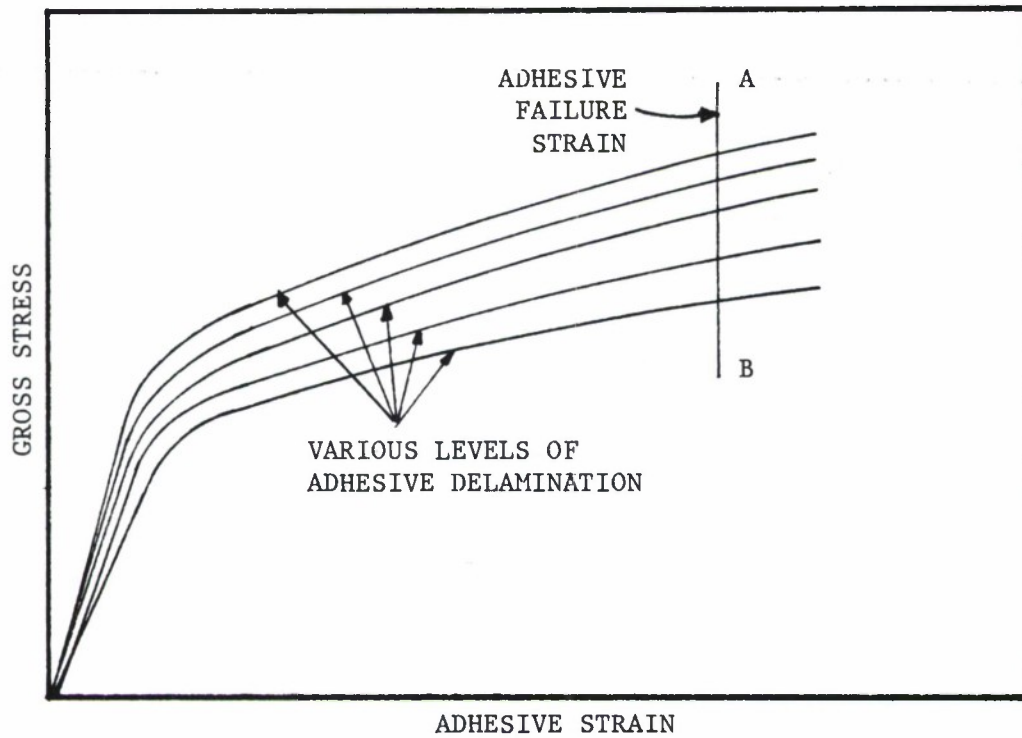
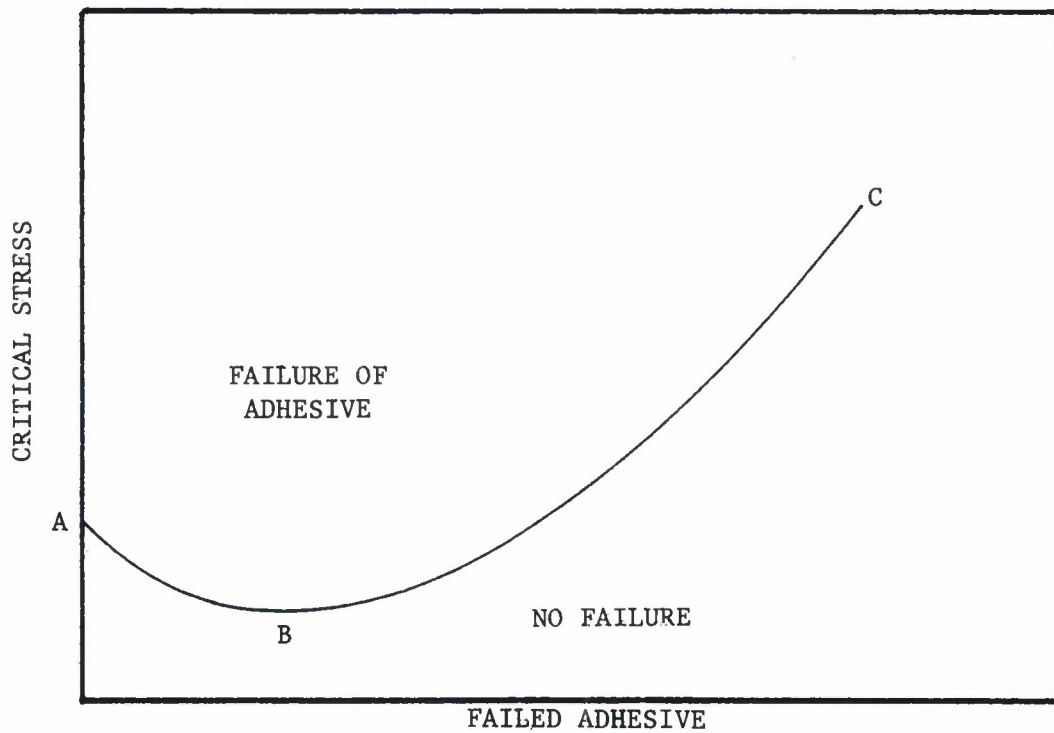


Figure 4.5.14. Residual Strength Diagram for the Fasteners in a Built-Up Structure.



(a) Stress-Strain Curves for Adhesively Bonded Stringer With Various Levels of Delamination.



(b) Critical Levels of Stress for Adhesively Bonded Stringer.

Figure 4.5.15. Gross Stress and Critical Stress Diagram for Adhesively Bonded Stringer.

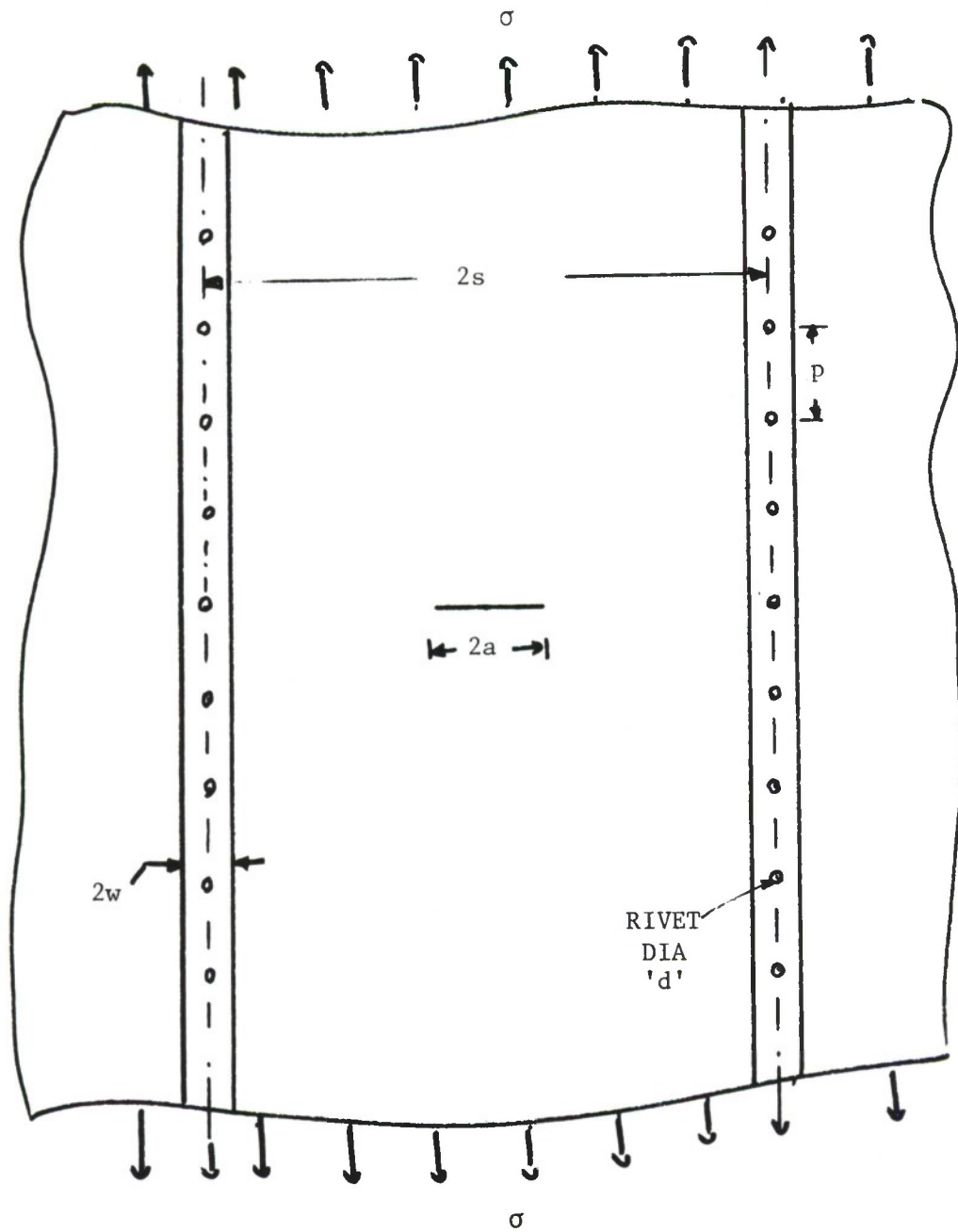


Figure 4.5.16. Riveted Panel with a Central Crack Between Two Stringers.

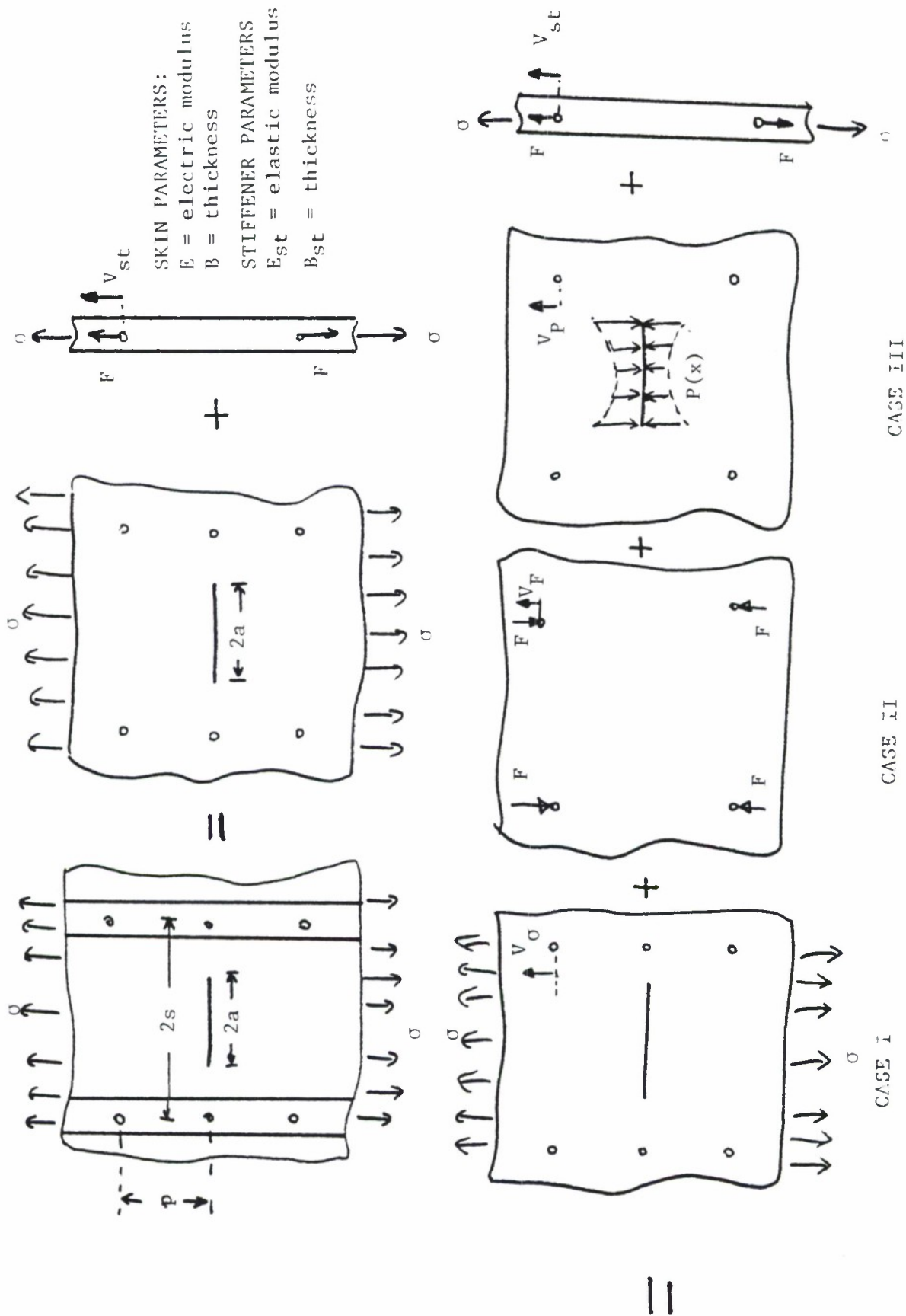


Figure 4.5.17. Stiffened Structure Broken Into Components.

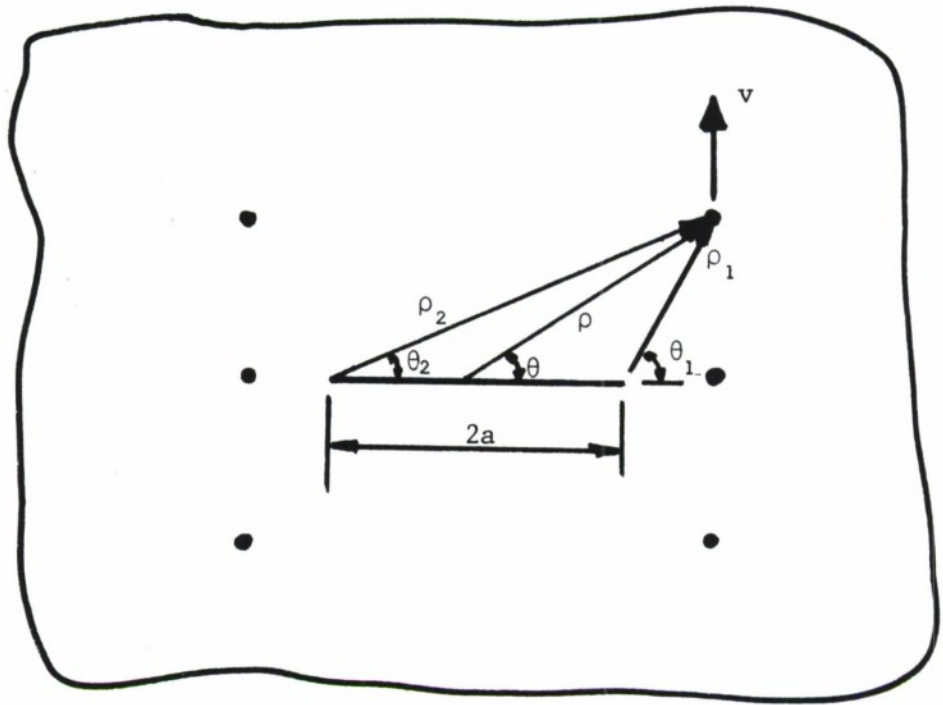


Figure 4.5.18. Geometrical and Displacement Parameters Relative to the Crack Tip.

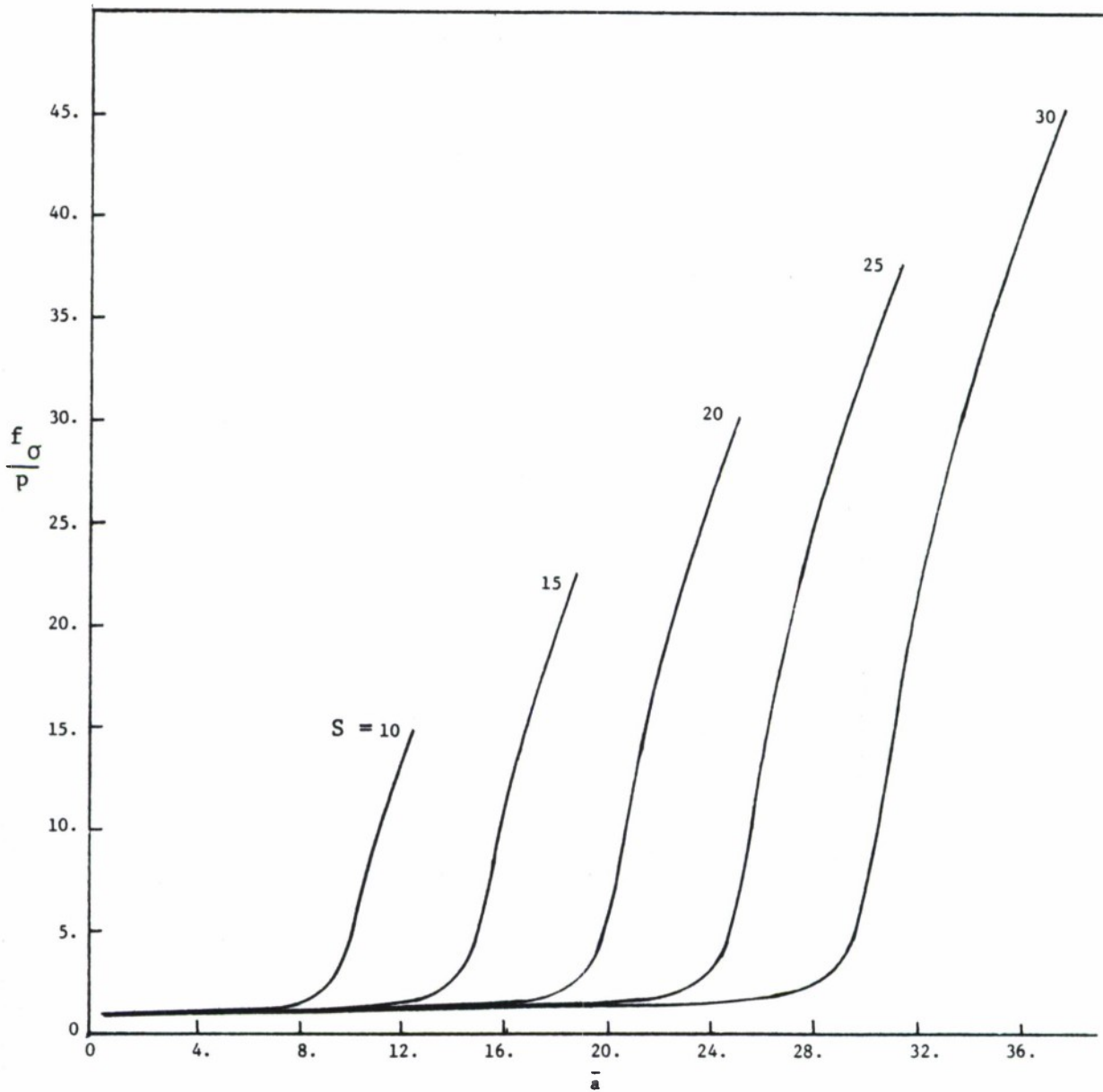


Figure 4.5.19. Normalized Panel Displacement Function (f_σ/p) Due to Applied Stress Vs. Normalized Crack Length (a/p) for Various Stringer Spacings ($\bar{S} = S/p$).

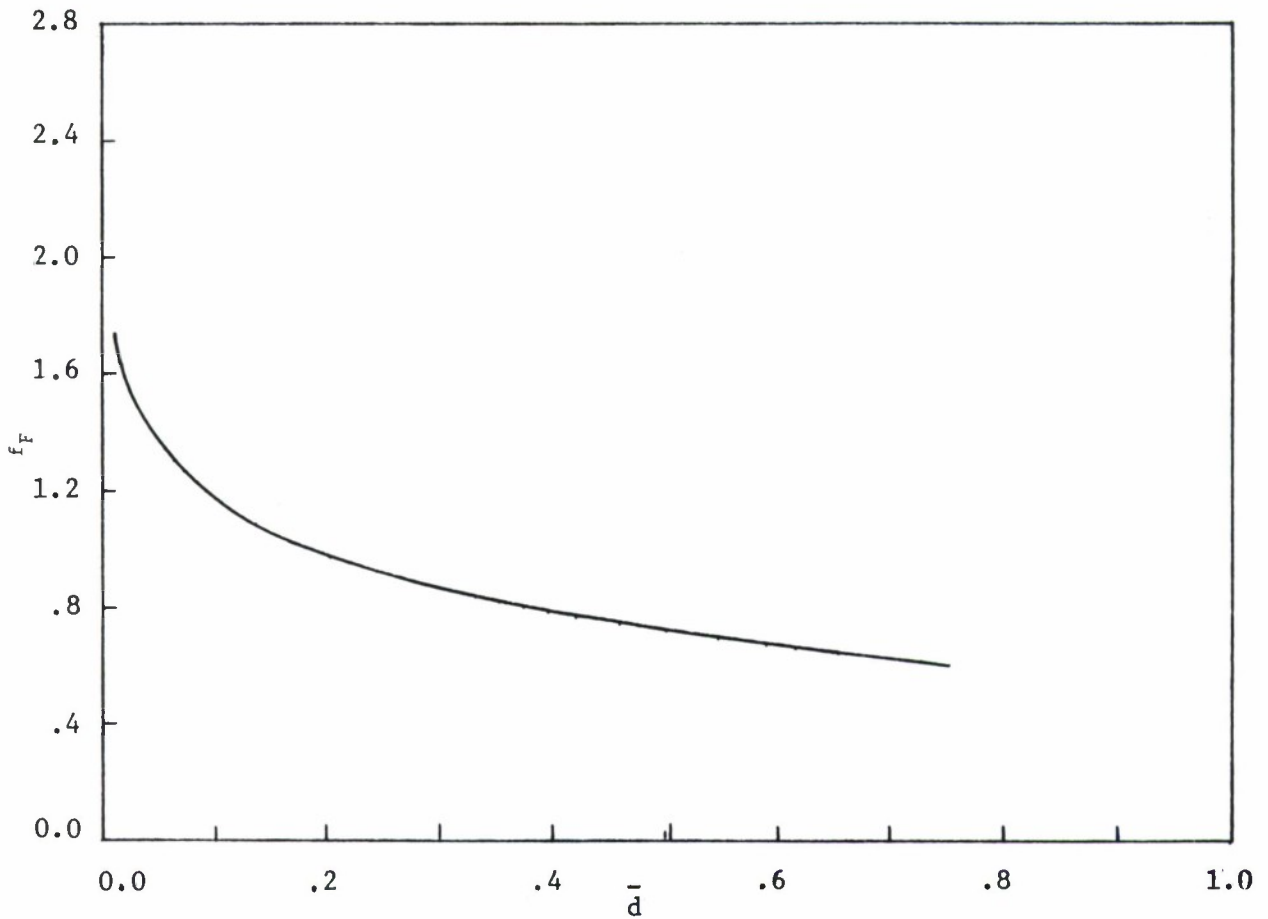


Figure 4.5.20. Panel Displacement Function Due to Fastener Force Vs. Normalized Rivet Diameter (d/p) for All Stiffener Spacings.

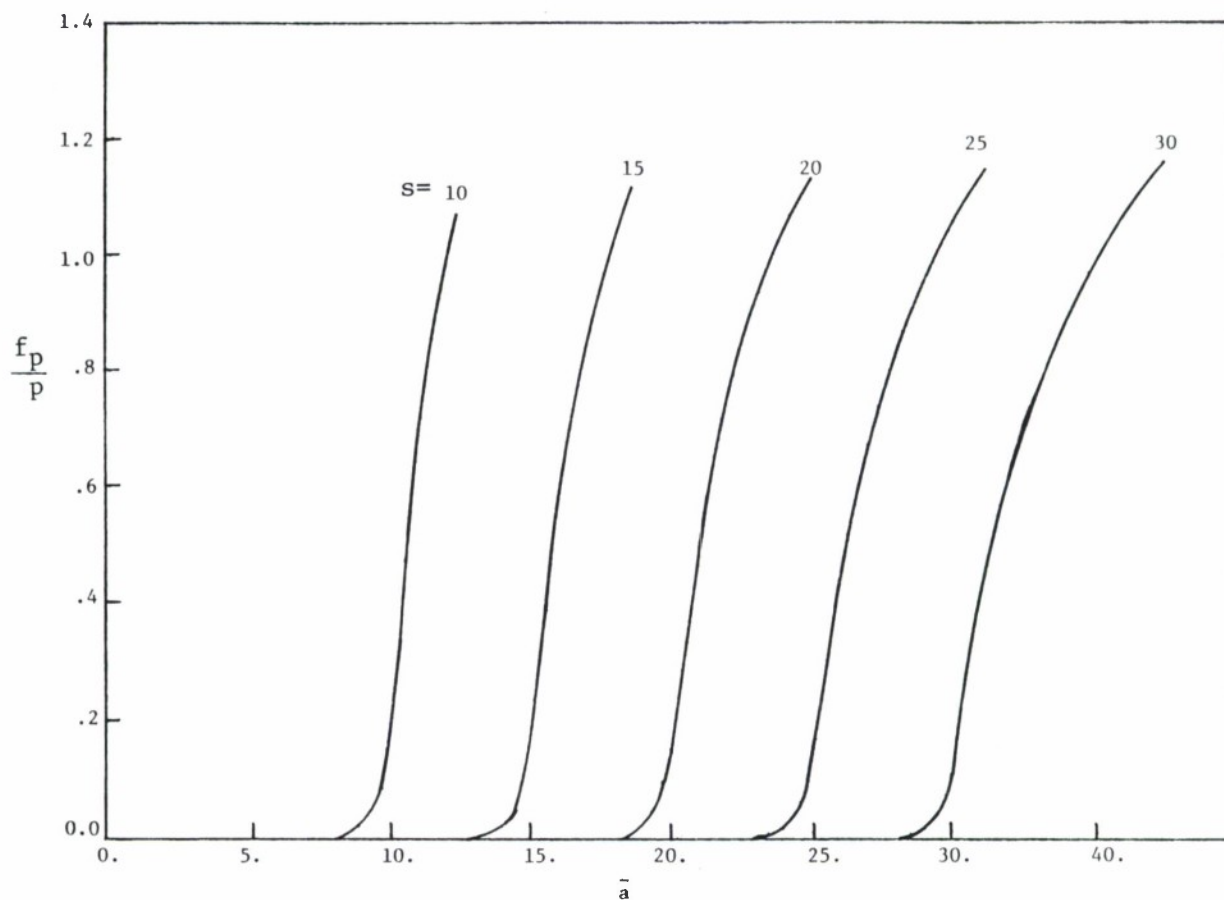


Figure 4.5.21. Normalized Panel Displacement Function (f_p/p) Due to Distributed Pressure Along Crack Vs. Normalized Crack Length (a/p) for Various Stringer Spacings ($\bar{s} = s/p$).

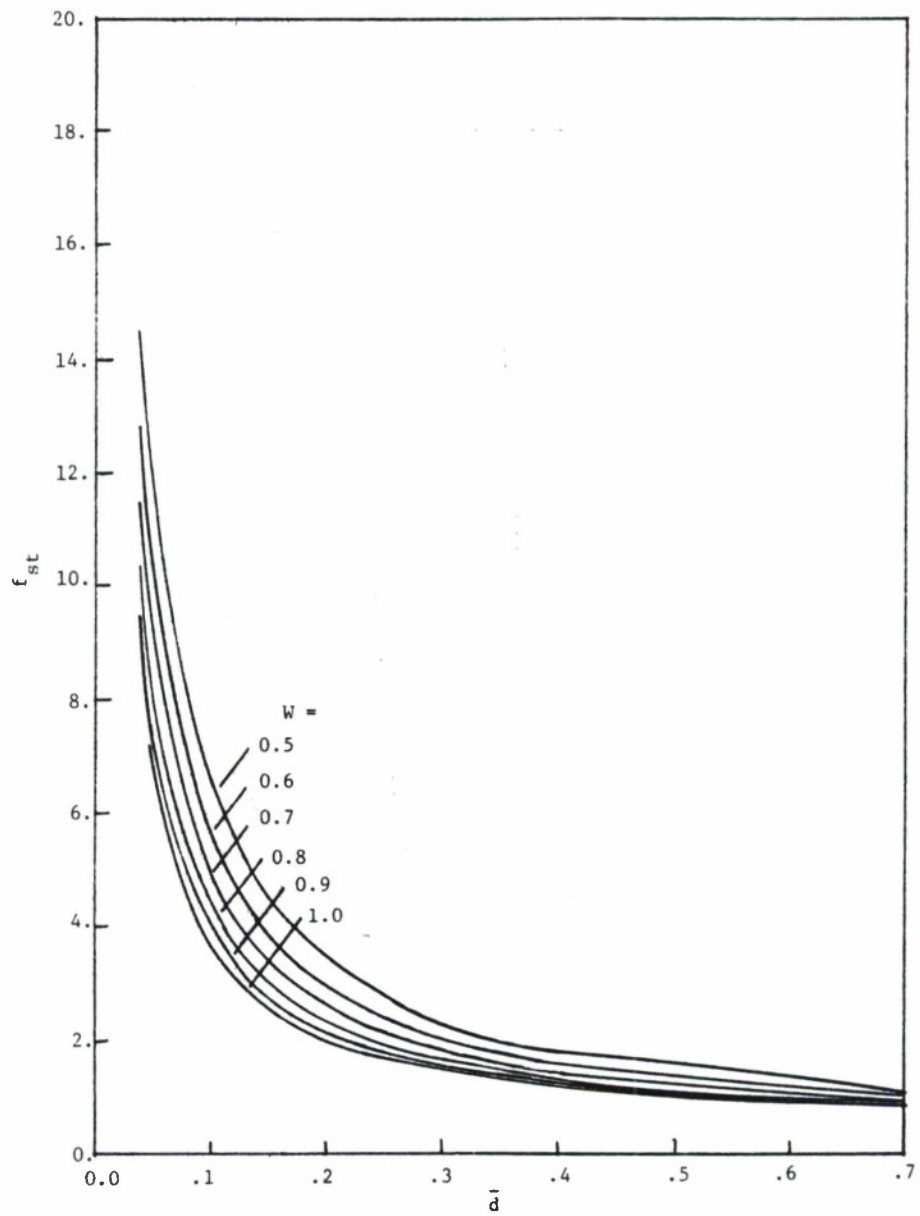


Figure 4.5.22. Stringer Displacement Function Vs. Normalized Rivet Diameter (d/p) for Various Half Stringer Widths.

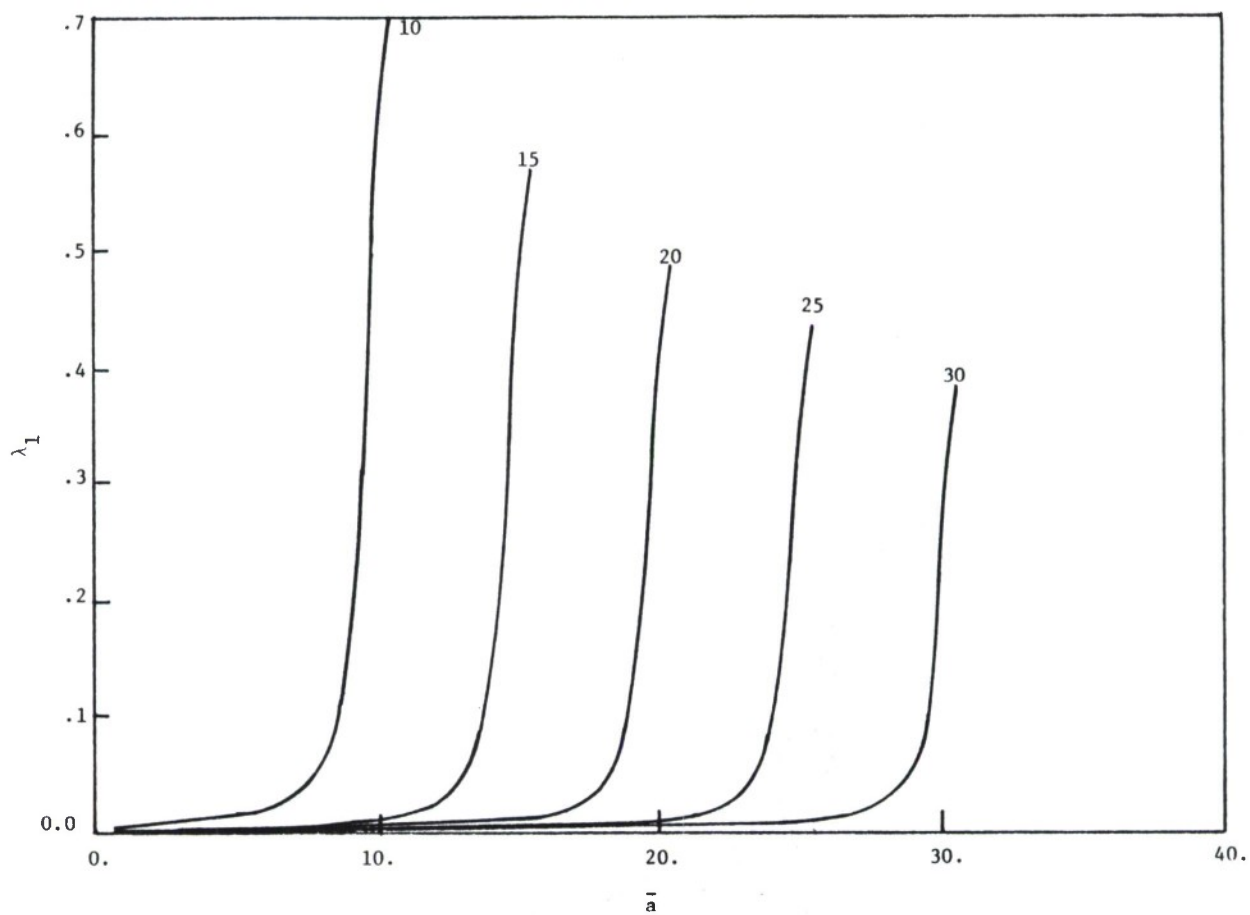
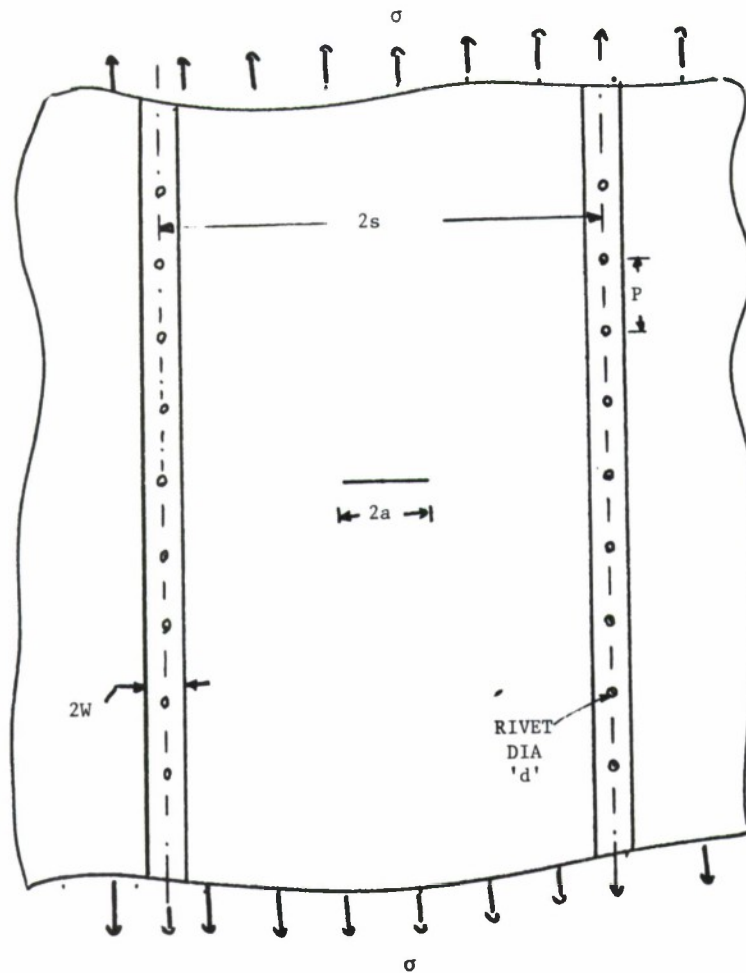


Figure 4.5.23. Parameter λ_1 Vs. Normalized Crack Length (a/p) for Various Normalized Stringer Spacings (s/p).

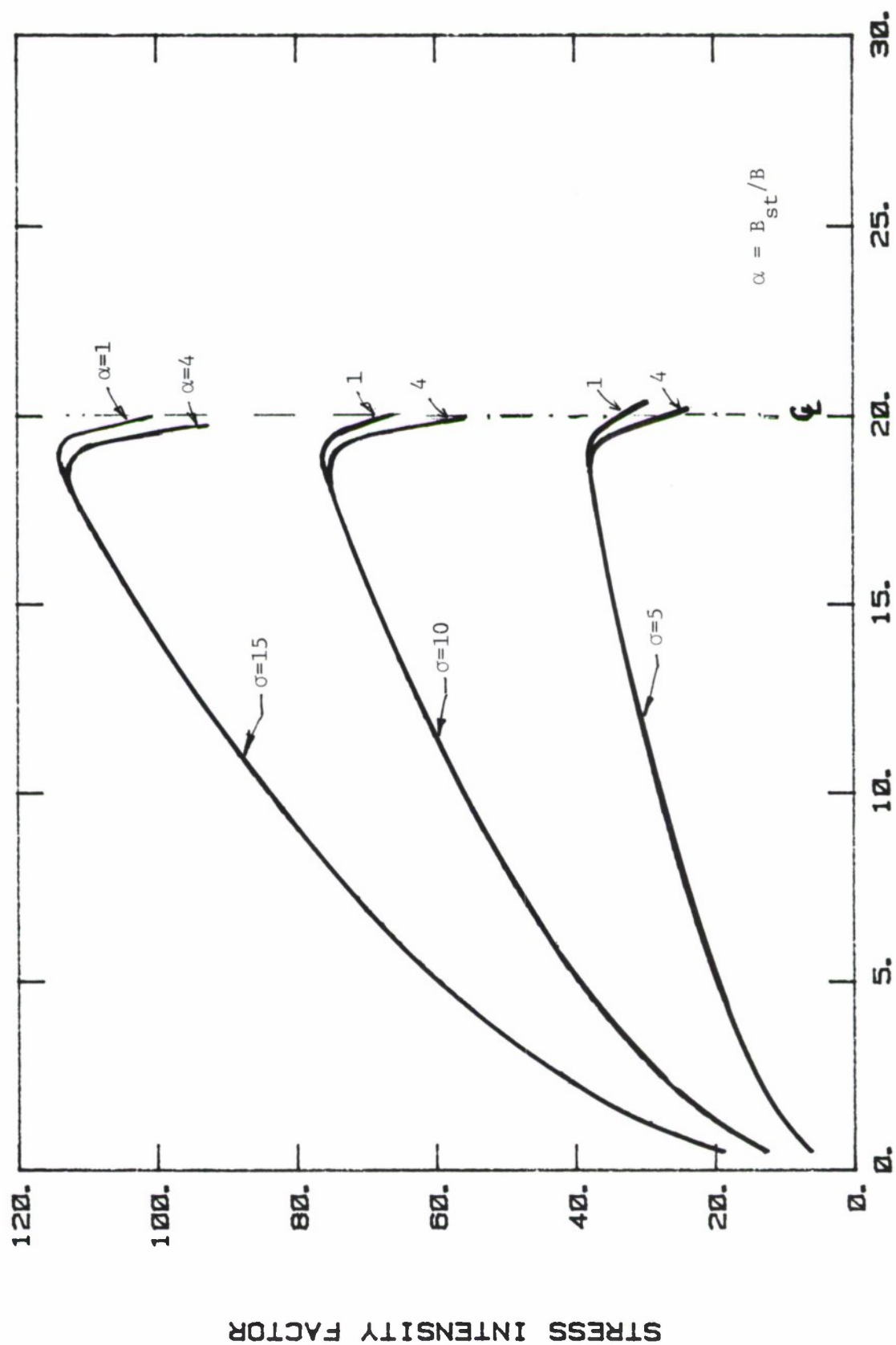


given the following data:

Maximum operating stress: 20 Ksi
 Stiffener spacing ($2s$): 40 inch
 Stiffener width (w): 0.5 inch
 Stiffener thickness (B_{st}): 0.063 inch
 Panel thickness (B): 0.063 inch
 Rivet pitch (p): 1 inch
 Rivet diameter (d): 3/16 inch
 Material: 7075-T6 Aluminum
 Fracture toughness: 65 Ksi $\sqrt{\text{inch}}$
 Ultimate Strength: 78 Ksi

Figure 4.5.24. Structural Geometry and Material Properties for Example of Subsection 4.5.7.

STRESS INTENSITY FACTOR DIAG.



CRACK LENGTH

Figure 4.5.25. Stress Intensity Factor Diagram for Panel and Riveted Stringers.

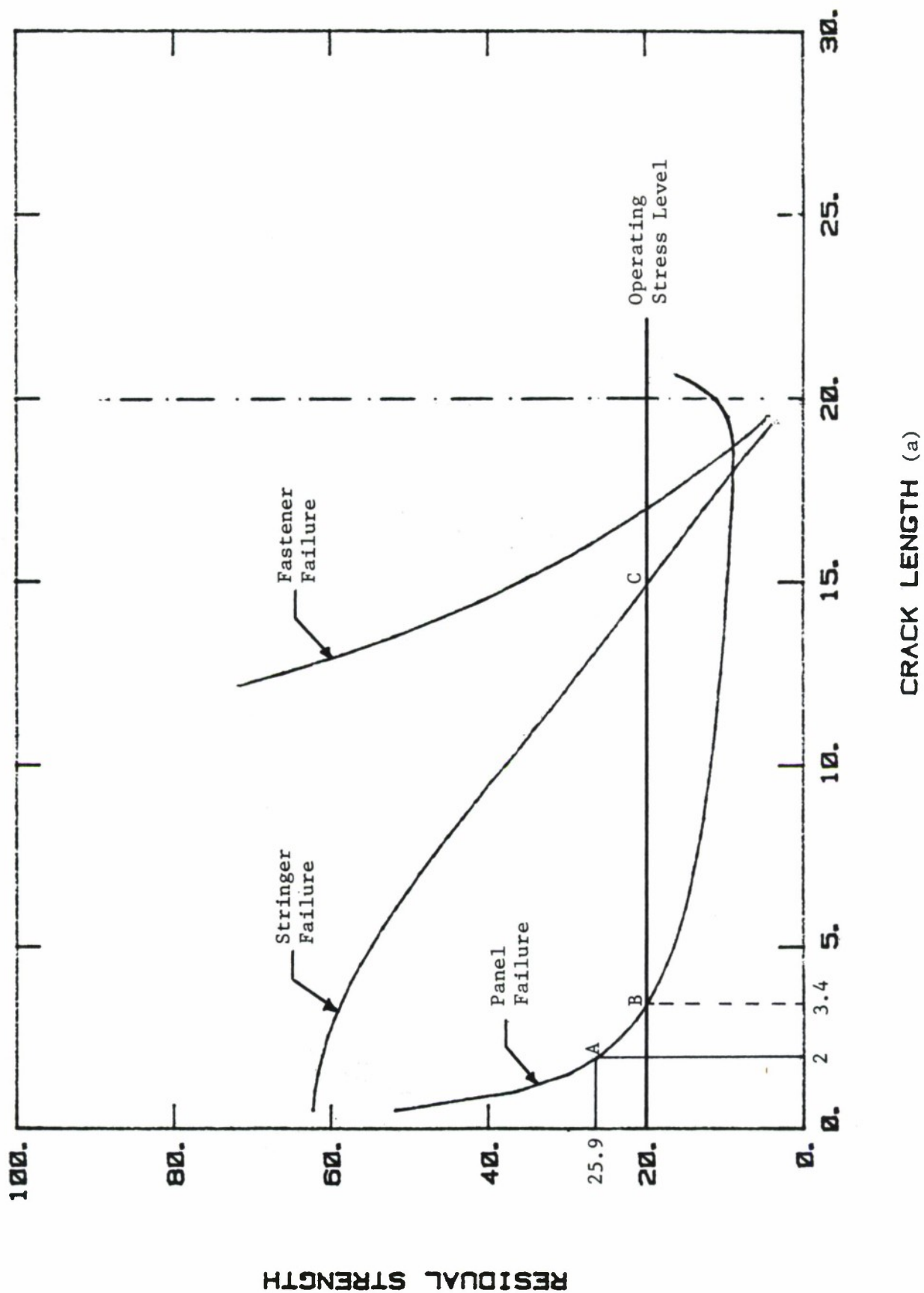
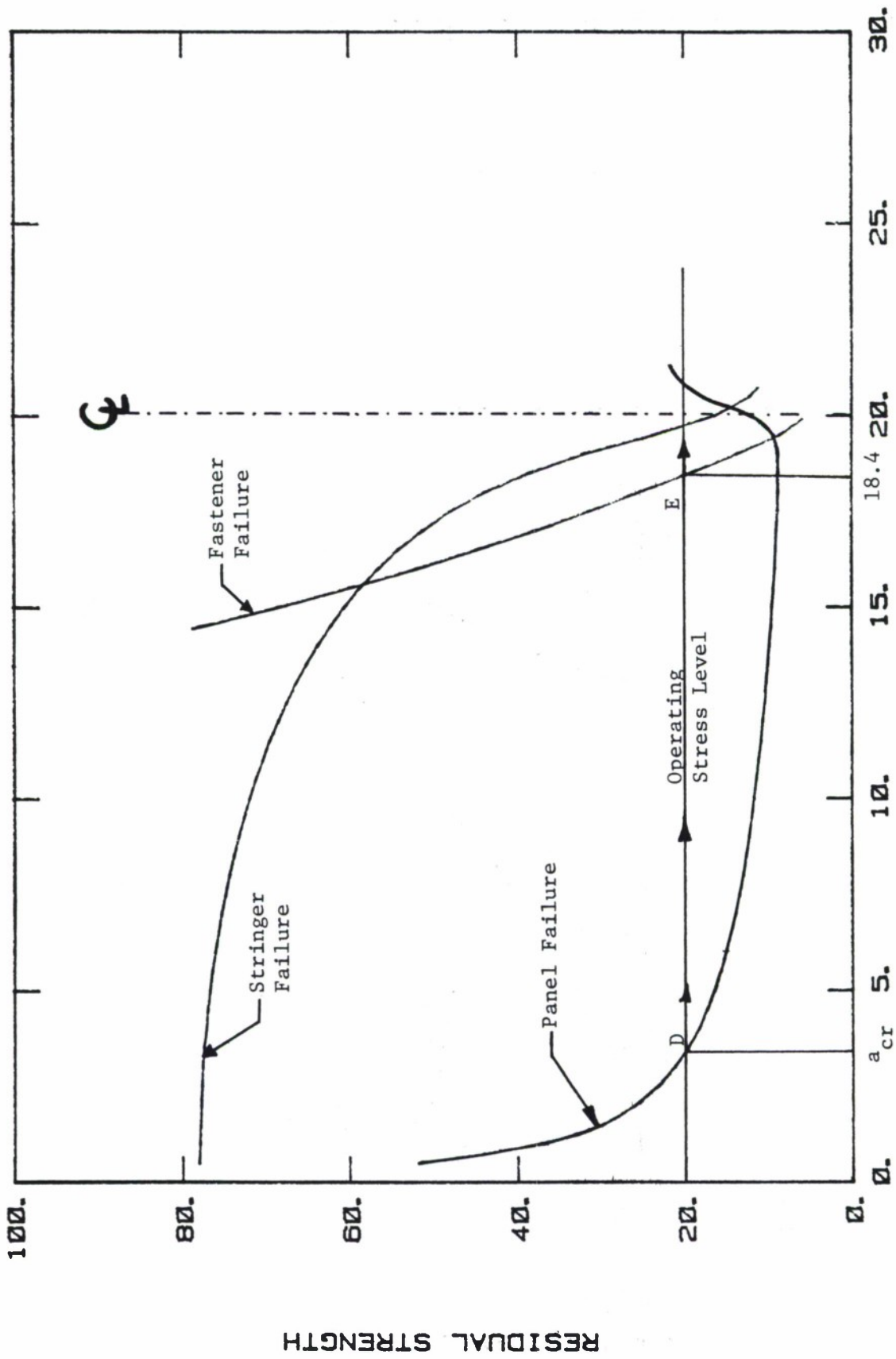


Figure 4.5.26. Residual Strength Diagram for Panel and Riveted Stringers (Light Stringers).

RESIDUAL STRENGTH DIAGRAM



CRACK LENGTH

Figure 4.5.27. Residual Strength Diagram for Panel and Riveted Stringers (Heavy Stringers).

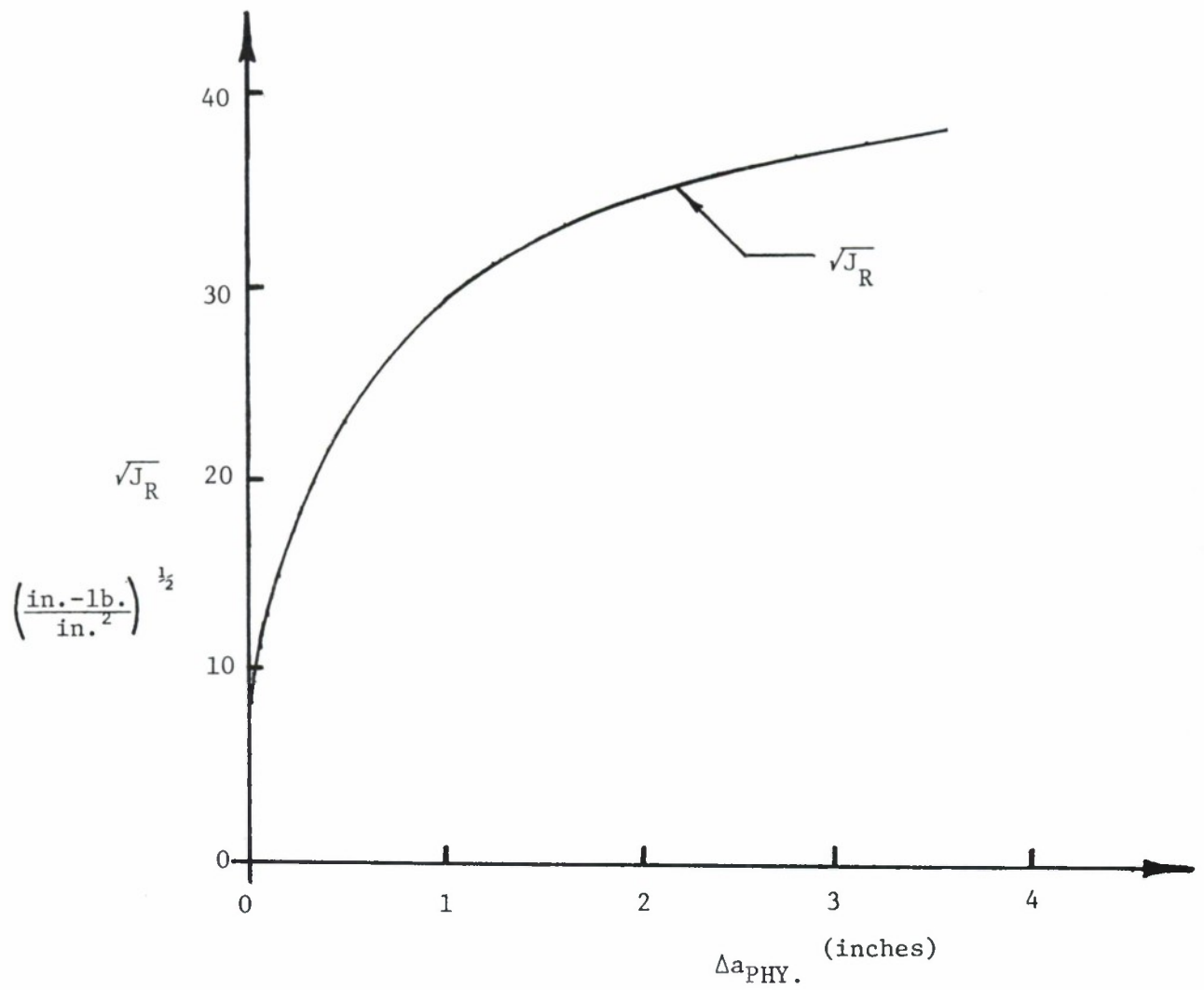


Figure 4.5.28. Square Root of J_R Resistance Curve.

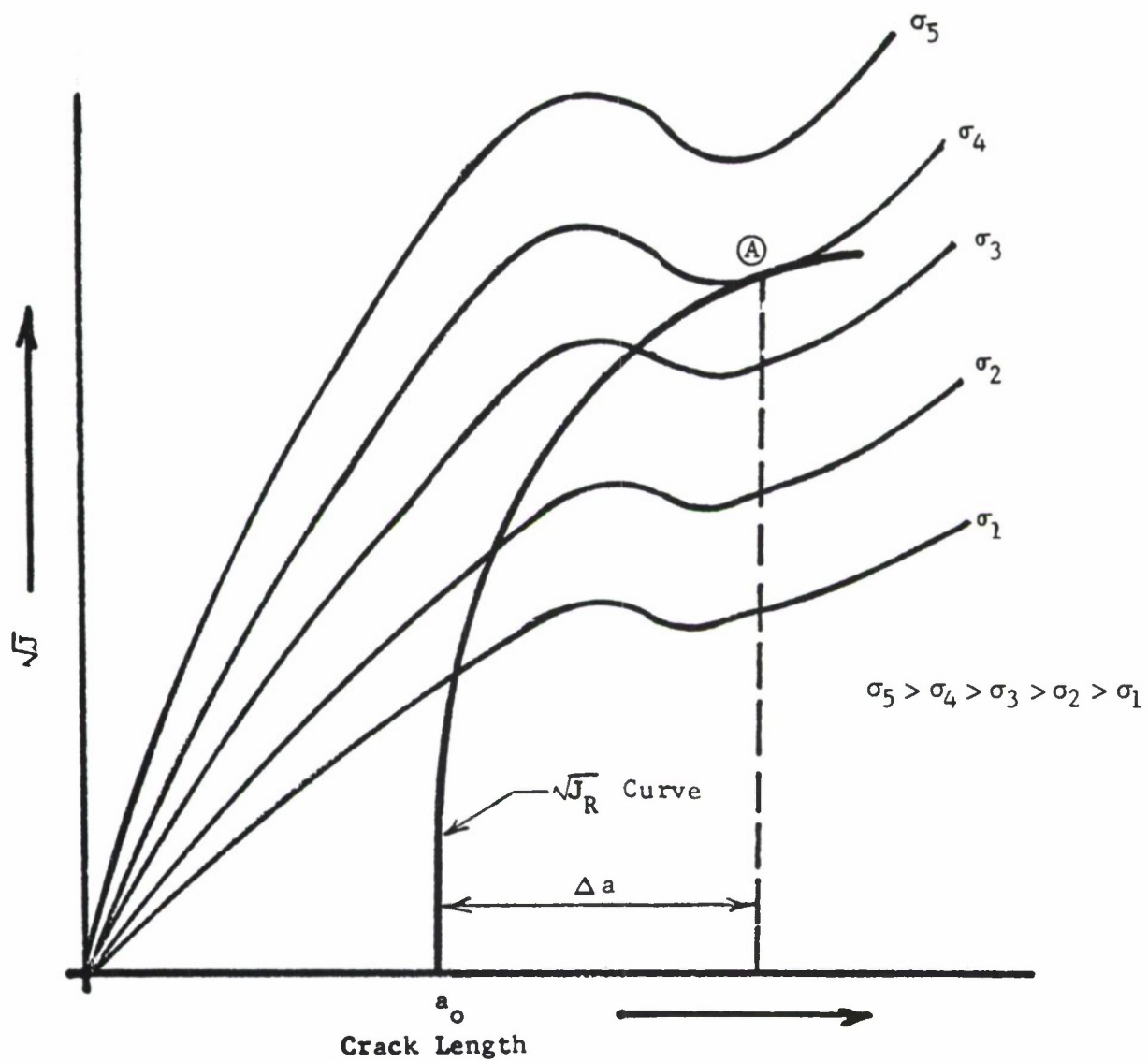


Figure 4.5.29. Failure Analysis Based on J_{Critical} Curve.

4.6 REFERENCES

1. Damage Tolerant Design (Data) Handbook, Revision to MCIC-HB-01, (1975), covered under USAF Contract No. F33615-80-C-3229.
2. W. S. Margolis and F. C. Nordquist, "Plane Stress Fracture Toughness (K_{IC}) of Aluminum Alloy 7475 - $\frac{1}{2}$ Inch Plate, Tempers - T7651 and T7351 and of Aluminum Alloy 2024 - $\frac{1}{8}$ Inch Sheet - T81 and T62 Temper," General Dynamics, Fort Worth Div., F-16 Air Combat Fighter Technical Report TIS GA2300, CDRL AO31, USAF Contract F33657-75-C-0310.
3. J. M. Krafft, A. M. Sullivan and R. W. Boyle, "Effect of Dimensions on Fast Fracture Instability of Notched Sheets," Cranfield Crack Propagation Symposium, Vol. 1, (1961), pp. 8-28.
4. J. E. Srawley and W. F. Brown, "Fracture Toughness Testing Methods," ASTM STP 381, (1965), pp. 133-195.
5. Fracture Toughness Evaluation by R-Curve Method, ASTM STP 527, D. E. McCabe, Ed, Am Soc for Testing and Mat'l, (1973).
6. D. P. Wilhem, "An Improved Technique for Residual Strength Prediction - A Modified Crack Growth Resistance Approach," Paper presented at Conference on Prospects of Fracture Mechanics, Delft University, The Netherlands, (June 1974).
7. J. R. Rice, "A Path Independent Integral and the Approximate Analyses of Strain Concentration by Notches and Cracks," J. Appl. Mech., ASME, Vol. 35, (June 1968), pp. 379-386.
8. C. A. Griffis and G. R. Yoder, "Application of the J-Integral to Crack Initiation in a 2024-T-351 Aluminum Alloy," Naval Research Lab Report 7676, (April 1974).
9. R. Verette and D. P. Wilhem, "Development & Evaluation of Methods of Plane Stress Fracture Analysis, Review and Evaluation of Structural Residual Strength Prediction Techniques," AFFDL-TR-73-42, (May 1973).
10. W. T. Fujimoto, "Determination of Crack Growth and Fracture Toughness Parameters for Surface Flaws Emanating from Fastener Holes," MCAIR Report A4093, (17 March 1976); Presented at the AIAA/ASME/SAE Structures, Structural Dynamics and Materials Conference, Valley Forge, PA, (4-7 May 1976).

11. J. I. Bluhm, "Fracture Arrest," Fracture, Vol. V, Liebowitz ed., Academic Press, (1969), pp. 1-63.
12. J. P. Romauldi and P. H. Sanders, "Fracture Arrest By Rivited Stiffeners," Proceedings of Fourth Midwest Conference on Solid Mechanics, University of Texas Press, (1959-1960).
13. D. Broek, Elementary Engineering Fracture Mechanics, Noordhoff (1974).
14. C. K. Gunther and J. T. Wozumi, "Critical Failure Mod-s in Cracked Mechanically Fastened Stiffened Panels," Design of Fatigue and Fracture Resistant Structures, ASTM STP761, P. R. Abelkis and C. M. Hudson, Eds., Am. Soc. for Testing and Mat'ls, (1982), pp. 310-327.
15. D. P. Wilhem, "Fracture Mechanics Guidelines for Aircraft Structural Applications," AFFDL-TR-69-111, Air Force Flight Dynamics Laboratory, (Feb. 1970).
16. A. F. Grandt, "A General Stress-Intensity Factor Solution for Through-Cracked Fastener Holes," Int. J. Fracture, 11, (1975), pp. 283-294.
17. O. L. Bowie, "Analysis of an Infinite Plate Containing Radial Cracks Originating at the Boundary of an Internal Circular Hole," J Math. and Phys., 35, (1956), pp. 60-71.
18. J. P. Romualdi, J. T. Frasier, and G. R. Irwin, "Crack-Extension Force Near a Riveted Stringer, NRL Memo Report No. 4956, (1957).
19. C. C. Poe, "The Effect of Riveted and Uniformly Space Stringers on the Stress-Intensity Factor of a Cracked Sheet," Air Force Conference on Fatigue and Fracture, (1969), AFFDL-TR-70-144, (1970), pp. 207-216.
20. C. C. Poe, "Fatigue-Crack Propagation in Stiffened Panels," ASTM STP 486, (1971), pp. 79-97.
21. H. Vlieger, "The Residual Strength Characteristics of Stiffened Panels Containing Fatigue Cracks," Engineering Fracture Mechanics, 5, (1973), pp. 447-478.
22. T. Swift and D. Y. Wang, "Damage Tolerant Design Methods and Test Verification of Fuselage Structure," Air Force Conference on Fatigue and Fracture, (1969), AFFDL-TR-70-144, pp. 653-683.

23. T. Swift, "Development of the Fail-Safe Design Features of the DC-10," ASTM STP 486, (1971), pp. 164-214.
24. T. Swift, "The Effects of Fastener Flexibility and Stiffener Geometry on the Stress Intensity in Stiffened Cracked Sheet," Prospects of Fracture Mechanics, Sih, Van Ebst, Broek, eds., Nordhoff, (1974), pp. 419-436.
25. M. Creager and A. F. Liu, "The Effect of Reinforcements on the Slow Stable Tear and Catastrophic Failure of Thin Metal Sheet," AIAA Paper 71-113, (1971).
26. M. M. Ratwani and D. P. Wilhem, "Development and Evaluation of Methods of Plane Stress Fracture Analysis, A Technique for Predicting Residual Strength of Structure," AFFDL-TR-73-42, (December 1974).
27. A. E. H. Love, "A Treatise on the Mathematical Theory of Elasticity," New York, Dover, 4th Ed., (1944), p. 209.
28. R. V. Sanga, "The 747 Fail-Safe Structural Program," Fail-Safe Aircraft Structures, Vol. II, I CAF Symp. 1973, RAE TR 73 183, (1974), pp. 3.1/1-3.1/66.
29. H. M. Westergaard, "Bearing Pressures and Cracks," Transactions, Am. Soc. Mech. Engrs., J. of Applied Mechanics, Vol. 6, (1939), pp. 49-53.

5.0 ANALYSIS OF DAMAGE GROWTH

<u>SECTION</u>		<u>PAGE</u>
5.1	BASIC INFORMATION	5.1.1
5.1.1	<u>Introduction</u>	5.1.1
5.1.2	<u>Fatigue-Crack Growth and Stress-Intensity</u>	5.1.2
5.1.3	<u>Fatigue Crack-Growth Rate (FCGR) Descriptions</u>	5.1.6
5.1.4	<u>Factors Affecting Crack Growth</u>	5.1.17
5.1.5	<u>Use of Data; Data Scatter</u>	5.1.19
5.1.6	<u>Stress-Corrosion Cracking and Stress-Intensity</u>	5.1.22
5.2	VARIABLE-AMPLITUDE LOADING	5.2.1
5.2.1	<u>Introduction</u>	5.2.1
5.2.2	<u>Retardation</u>	5.2.1
5.2.3	<u>Retardation Under Spectrum Loading</u>	5.2.3
5.2.4	<u>Retardation Models</u>	5.2.5
5.2.5	<u>Integration Routines</u>	5.2.11
5.2.6	<u>Cycle-by-Cycle Analysis</u>	5.2.16
5.3	STRESS SEQUENCE DEVELOPMENT	5.3.1
5.3.1	<u>Service Life Description and Mission Profiles</u>	5.3.1
5.3.2	<u>Sequence Development Techniques</u>	5.3.4
5.3.3	<u>Application of Simplified Stress Sequences for Design Studies</u>	5.3.14
5.4	CRACK GROWTH PREDICTION	5.4.1
5.4.1	<u>Introduction</u>	5.4.1
5.4.2	<u>Cycle Definition and Sequencing</u>	5.4.1
5.4.3	<u>Clipping</u>	5.4.4
5.4.4	<u>Truncation</u>	5.4.8
5.4.5	<u>Crack Shape</u>	5.4.9
5.4.6	<u>Interaction of Cracks</u>	5.4.11
5.5	LIST OF REFERENCES	5.5.1

LIST OF FIGURES

<u>FIGURE</u>		<u>PAGE</u>
5.1.1	Typical Crack Growth-Life Curve.	5.1.26
5.1.2	Definition of Terms.	5.1.27
5.1.3	Fatigue Crack Growth Rate Data Presentation Format Used in Revised Damage Tolerant Design (Data) Handbook. Data for Two Stress Ratios Presented for 7075-T7351 Aluminum Alloy (Reference 1).	5.1.28
5.1.4	Sample Fatigue Crack Growth Rate Data Set for 7075-T6 Aluminum Alloy Sheet After Mil Handbook-5 (Reference 2).	5.1.29
5.1.5	Sample Fatigue Crack Growth Rate Data Set for 7075-T7351 Aluminum Alloy Plate After Mil-Handbook-5 (Reference 2).	5.1.30
5.1.6	Schematic of Fatigue Crack Growth Rate Behavior.	5.1.31
5.1.7	Description of FCGR Data Fitting and the Comparison of Predicted to Actual Behaviors.	5.1.32
5.1.8	Possible Variation of Crack Growth in Materials from Different Sources (Reference 12).	5.1.33
5.1.9	Example of Effect of Thickness on Crack Growth (Reference 13).	5.1.34
5.1.10	Effect of Humidity on Fatigue Crack Propagation (Reference 18).	5.1.35
5.1.11	Example of Temperature Effect on Crack Growth (Reference 29).	5.1.36
5.1.12	Crack Growth Data Scatter for Identical Conditions.	5.1.37
5.1.13	Stress Corrosion Cracking Data (Reference 33).	5.1.38
5.1.14	Stress Corrosion Cracking.	5.1.39
5.1.15	K_{Isc} Data as Presented by the Damage Tolerant Design (Data) Handbook (Reference 1).	5.1.40
5.1.16	Stress Corrosion Cracking Rate Data for 2024-T351 Aluminum in the Format of Reference 1.	5.1.41

LIST OF FIGURES
Cont'd

<u>FIGURE</u>		<u>PAGE</u>
5.1.17	Stress Required for Stress Corrosion Cracking.	5.1.42
5.2.1	Retardation Due to Positive Overloads and Due to Positive-Negative Overload Cycles (Reference 40).	5.2.20
5.2.2	Effect of Magnitude of Overload on Retardation (Reference 27).	5.2.21
5.2.3	Retardation in Ti-6V-4Al; Effect of Hold Periods and Multiple Overloads (Reference 42).	5.2.22
5.2.4	Effect of Clipping of Higher Loads in Random Flight-by-Flight Loading on Crack Propagation in 2024-T3 Al Alloy (Reference 43 and 44).	5.2.23
5.2.5	Effect of Block Programming and Block Size on Crack Growth Life (All Histories Have Same Cycle Content) Alloy: 2024-T3 Aluminum (Reference 27).	5.2.24
5.2.6	Yield Zone Due to Overload (r_{pol}), Current Crack Size (a_1), and Current Yield Zone (r_{pi}).	5.2.25
5.2.7	Crack Growth Predictions by Wheeler Model Using Different Retardation Exponents (Reference 45).	5.2.26
5.2.8	Predictions of Crack Growth Lives with the Generalized Willenborg Model, and Comparison with Test Data (Reference 59). Compressive Stress Levels Were Ignored in this Analysis.	5.2.27
5.2.9	Predictions by Crack Closure Model as Compared with Data Resulting from Constant-Amplitude Tests with Overload Cycles (Reference 52).	5.2.28
5.2.10	Steps Required for Crack-Growth Integration.	5.2.29
5.2.11	Statistical Crack-Incrementation Scheme Used to Determine Spectrum Induced Variations in Crack Growth-Rate Behavior (Reference 16).	5.2.29
5.2.12	Steps Required for Crack-Growth Integration.	5.2.30

LIST OF FIGURES

Cont'd

<u>FIGURE</u>		<u>PAGE</u>
5.3.1	Mission Profile and Mission Segments.	5.3.19
5.3.2	Maneuver Spectra According to MIL-A-08866B (USAF).	5.3.20
5.3.3	Exceedance Spectra for 1000 Hrs.	5.3.21
5.3.4	Stepped Approximation of Spectrum.	5.3.22
5.3.5	Fatigue-Crack Growth Behavior Under Various Spectra Approximations.	5.3.23
5.3.6	Approximate Stress Spectrum for 1000 Flights Based on MIL-A-08866B (USAF).	5.3.24
5.4.1	Definition of Cycles.	5.4.14
5.4.2	Rain Flow Count.	5.4.15
5.4.3	Calculated Crack Growth Curves for Random Flight-by-Flight Fighter Spectrum (Reference 67).	5.4.16
5.4.4	Spectrum Fatigue Crack Growth Behavior Willenborg Retardation Model.	5.4.17
5.4.5	Spectrum Fatigue Crack Growth Behavior Wheeler Retardation Model.	5.4.18
5.4.6	Effect of Clipping Level on Calculated Crack Growth for Spectrum B-Trainer.	5.4.19
5.4.7	Effect of Clipping for Various Spectra.	5.4.20
5.4.8	Calculated and Experimental Data for Gust Spectrum Clipping (Reference 43 and 44).	5.4.21
5.4.9	Effect of Lowest Stress Amplitude in Flight-by-Flight Tests Based on Gust Spectrum (Reference 43 and 44).	5.4.22
5.4.10	Improper and Correct Truncation.	5.4.23
5.4.11	Development of Flaws.	5.4.24
5.4.12	Interaction of Cracks.	5.4.25

LIST OF TABLES

<u>TABLE</u>		<u>PAGE</u>
5.1.1	ACTIVE PARTICIPANTS AND THEIR ORGANIZATIONS (REFERENCE 10)	5.1.11
5.1.2	FCGR DESCRIPTIONS	5.1.12
5.1.3	MEANS AND STANDARD DEVIATION OF SETS OF LIFE-PREDICTION RATIOS FOR THE FULL CRACK GROWTH INTERVAL	5.1.12
5.1.4	A FURTHER COMPARISON OF FCGR DESCRIPTIONS	5.1.14
5.1.5	EXAMPLE FATIGUE CRACK GROWTH RATE TABLE (2219-T851 ALUMINUM)	5.1.15
5.3.1	SIMPLE FLIGHT-BY-FLIGHT SPECTRUM FOR EARLY DESIGN ANALYSIS AND TRADE-OFF STUDIES	5.3.16

5.0 ANALYSIS OF DAMAGE GROWTH

5.1 BASIC INFORMATION

5.1.1 Introduction

MIL-A-83444, "Airplane Damage Tolerance Design Requirements," specifies that cracks shall be assumed to exist in all primary aircraft structure. These cracks shall not grow to a size to cause loss of the aircraft at a specified load within a specified period. Showing compliance with these requirements implies that the rate of growth of the assumed flaws must be predicted.

Crack growth is a result of cyclic loading due to gusts and maneuvers (fatigue cracking), or of the combined action of sustained loading and environment (stress-corrosion cracking), or both. The most common crack-growth mechanisms are fatigue-crack growth and environment-assisted (corrosion) fatigue-crack growth. Certain aircraft parts (especially high-strength forgings) may be liable to stress-corrosion cracking. Since there is a design threshold for stress corrosion, proper detail design and proper material selection can minimize or prevent stress corrosion. Fatigue cracking is difficult to prevent, but it can be controlled.

The information concerning the determination of stress-intensity factors, that was presented in Chapter 1 can be directly applied to crack-growth analysis.

To predict crack growth behavior such as illustrated in Figure 5.1.1, the following information must be available:

1. The stress-intensity factor, described as a function of crack size, for the relevant structural and crack geometry;
2. The stress (load)-time history, described for the structural location component or structure under consideration;
3. The baseline crack-growth properties (constant amplitude crack-growth rate data), described as a function of the stress-intensity factor, for the material and for the relevant environment;
4. A damage integration routine that integrates the crack-growth rate (from (3)) to produce a crack-growth curve, using the proper stress-time history (from (2)), the proper stress-intensity formulation (from (1)), and an appropriate integration rule.

This chapter provides guidelines to arrive at crack growth estimates, and points out where deficiencies in knowledge and analysis methods lead to inaccuracies.

5.1.2 Fatigue-Crack Growth and Stress-Intensity

Consider constant-amplitude fatigue loading as in Figure

5.1.2a. The following parameters are defined:

σ_m	mean stress
σ_a	stress amplitude
$\Delta\sigma$	stress range
σ_{\max}	maximum stress
σ_{\min}	minimum stress
R	stress ratio: $R = \frac{\sigma_{\min}}{\sigma_{\max}} = \frac{\sigma_m - \sigma_a}{\sigma_m + \sigma_a} = 1 - \frac{\Delta\sigma}{\sigma_{\max}}$

The cyclic stress can be fully characterized (apart from the frequency) by any combination of two of these parameters. The stress range, $\Delta\sigma$, and the stress ratio, R, are the two most commonly used. Note that in a constant-amplitude test each of these parameters has a constant value with respect to time.

The stress history can be converted into a stress-intensity factor history (Figure 5.1.2b) at a given crack length by multiplying the stress history by the stress-intensity factor coefficient. The following parameters are defined:

K_m	mean stress-intensity factor = $\beta\sigma_m\sqrt{\pi a}$
K_a	amplitude of the stress-intensity factor = $\beta\sigma_a\sqrt{\pi a}$
ΔK	range of the stress-intensity factor = $\beta\Delta\sigma\sqrt{\pi a}$
K_{\max}	maximum stress-intensity factor = $\beta\sigma_{\max}\sqrt{\pi a}$
K_{\min}	minimum stress-intensity factor = $\beta\sigma_{\min}\sqrt{\pi a}$
R_K	cycle ratio: $R_K = \frac{K_{\min}}{K_{\max}}$

The above calculation schemes for stress-intensity factor parameters, while being the most straightforward algebraically, have an operational quality about them. For example, it is theoretically difficult to define a negative stress-intensity factor which happens if the stress becomes compressive. In this case, the crack closes and the crack tip stress field loses its singularity character; thus, the stress-intensity factor ceases to have meaning. The operational quality of the negative stress-intensity factors calculated for compressive stress situations has been given a lot of consideration by the aerospace industry and by the American Society of Testing Materials (ASTM), specifically its subcommittee on subcritical crack growth (ASTM E24.04). ASTM has chosen to provide the following definitions when $\sigma_{\min} < 0$:

$$K_{\min} = 0 \text{ if } \sigma_{\min} < 0$$

$$\Delta K = K_{\max} \text{ if } \sigma_{\min} < 0$$

The reader should be aware of the ASTM ΔK definition since that convention is used in the Damage Tolerant Design (Data) Handbook⁽¹⁾ for the presentation of crack growth rate data when part of the fatigue cycle is compressive, i.e., when $\sigma_{\min} < 0$ ($R < 0$). The algebraic definition of ΔK is used in the current version of MIL-HDBK-5⁽²⁾. Before negative stress ratio ($R < 0$) data are used, it is important to establish what the operational definition of ΔK is. The reader should note that the behavior of the material under negative stress ratio conditions is itself independent of the operational definition of ΔK .

In the elastic case, the stress-intensity factor alone is sufficient to describe the stress field at the tip of a crack. When the plastic zone at the crack tip is small compared with the crack size, the stress-intensity factor still gives a good indication of the stress environment of the crack tip. Two different cracks which have the same stress environment (equal stress-intensity factors) will behave in the same manner and show the same rate of growth.

Since two parameters are required to characterize the fatigue cycle, two parameters are required to characterize crack growth rate behavior. The crack-growth rate per cycle, da/dN , where N is the number of cycles, can be generally described with functional relations of the type:

$$\frac{da}{dN} = f(\Delta K, R) \text{ or } = g(K_{\max}, R) \quad (5.1.1)$$

where R is the stress ratio associated with the stress cycle.

EXAMPLE 5.1.1: Meaning of Equation 5.1.1

For a wide center crack panel subjected to constant amplitude loading conditions, Equation 5.1.1 implies that the crack growth rate of a 2-inch long crack subjected to a remote loading of $\Delta\sigma = 10$ ksi for $R=0$ will be identical to the rate of growth of a 0.5-inch long crack subjected to a remote loading of $\Delta\sigma = 20$ ksi for $R=0$. The rates for the two different crack length - loading conditions will be the same because the stress-intensity factor range (ΔK) and the stress ratio (R) are the same in both cases.

Typically, fatigue crack growth rate data is described using plots of da/dN versus ΔK on double-logarithmic scale graph paper. Figure 5.1.3 presents fatigue crack growth rate data for 7075 Aluminum in the graphical format that is being used in the revised version of the Damage Tolerant Design (Data) Handbook⁽¹⁾. Figures 5.1.4 and 5.1.5 describe example composite da/dN data plots for 7075 Aluminum as a function of ΔK (algebraic definition) for different stress ratio (R) values⁽²⁾. Both Figures 5.1.4 and 5.1.5 provide mean trend curves that represent the function $f(\Delta K, R)$ in Equation 5.1.1. On the basis of these figures, it can be seen that $f(\Delta K, R)$ is not a simple function. Figure 5.1.6 is a schematic illustration of fatigue crack growth rate behavior from the threshold region (below 10^{-8} inch/cycle) to the onset of rapid cracking in the fracture toughness region (above 10^{-3} inch/cycle). As can be seen from Figures 5.1.3 - 5.1.6, the behavior exhibits a sigmoidial shape suggesting that there might be asymptotes at the two extreme regions.

5.1.3 Fatigue Crack-Growth Rate (FCGR) Descriptions

Many descriptions of the function $f(\Delta K, R)$ in Equation 5.1.1 have been proposed. In the early literature⁽³⁻⁶⁾, most of the descriptions were either based on physical models of the crack growth process (referred to as "laws") or on equations that appeared to describe the trends in the data. Currently, the fatigue crack growth rate (FCGR) descriptions are carefully selected to provide accurate mean trend descriptions of the specific data collected to support a materials evaluation or structural

design. Before introducing these more accurate FCGR descriptions, the Paris power law⁽⁷⁾, the Walker equation⁽⁸⁾, and Forman equations will be reviewed⁽⁹⁾.

The Paris power law equation was initially proposed to describe the crack growth rate behavior in the central region for specific values of stress ratio. It is given by the general form:

$$\frac{da}{dN} = C \Delta K^p \quad (5.1.2)$$

where C and p are experimentally determined constants. Equation 5.1.2 is still extensively used to develop first order approximations of life behavior when only limited amounts of data are available. The reader is cautioned that Equation 5.1.2, as well as any other FCGR description, should not be extrapolated beyond its limits of applicability without a great deal of care and experience. Greater life prediction errors can result from data extrapolation errors than almost all other design methodology errors combined.

The Walker equation⁽⁸⁾ provided one of the first simple equations that accounted for the stress ratio shift. It is a subtle modification of Equation 5.1.2 and is given by

$$\frac{da}{dN} = C [(1-R)^m K_{max}]^p \quad (5.1.3)$$

where C, m, and p are empirical constants. The exponent m typically ranges from 0.4 to 0.6 for many materials. Because Equation 5.1.3 is a

power law, it has been noted to be most useful in describing the central region of the growth rate behavior.

The Forman equation⁽⁹⁾ was initially proposed to describe both the central and high crack growth regions of the behavior. To account for the acceleration of the cracking rates as the stress-intensity factors levels approached critical, the Paris power law equation was divided by a factor that would reach zero when the stress-intensity factor reached a critical level. The general form of the Forman equation is:

$$\frac{da}{dN} = \frac{C \Delta K^p}{(1-R) K_c - \Delta K} \quad (5.1.4)$$

where C, p, and K_c are experimentally evaluated for the given material and thickness. Equation 5.1.4 can be rearranged to yield:

$$\frac{da}{dN} = \frac{C (1-R)^{p-1} \cdot K_{max}^p}{K_c - K_{max}} \quad (5.1.5)$$

which shows that the equation has the capability to describe multiple stress ratio data sets.

The empirical constants in Equations 5.1.2-5.1.4 are typically derived using least square fitting procedures. Note that the simplicity of Equations 5.1.2 and 5.1.3 allow for a graphical fit to the data on log-log coordinate paper and the direct evaluation of the constants from the graph. The usefulness of Equations 5.1.2-5.1.4 comes from the ease in

which their constants can be evaluated from available data, as well as the direct application of the equations to simplified life integration calculations. When considering the general expression for crack growth life (N_f)

$$N_f = \int_{a_0}^{a_f} \frac{da}{f(\Delta K, R)} , \quad (5.1.6)$$

it is seen that the function f is simple for Equations 5.1.2-5.1.4.

ASTM task group E24.04.04 (on FCGR descriptions) recently conducted two analytical round robin investigations of the utility of various FCGR descriptions that describe FCGR behavior (See References 10 and 11). These round robin investigations have clearly demonstrated that FCGR descriptions which are classified as "good" from a life analysis standpoint must adequately represent the mean trend of the FCGR data. Figure 5.1.7 outlines a general procedure whereby the FCGR behavior is first described by least square regression analysis (Figure 5.1.7a) and then the regression equation (in conjunction with the stress-intensity factor analysis for the test geometry) is used in integral form to obtain an estimate of the fatigue crack growth life N_f (Figure 5.1.7b). In Figure 5.1.7a, the mean trend behavior is described along with bounds on the regression equation. Those descriptions which fail to model the mean trend of the FCGR data, either because they are preconceived to have a specific form (sinh, power law, Forman, etc.) or due to a lack of care in performing the regression analysis, lead to life prediction errors that are biased or exhibit significant scatter.

To support the first round robin, FCGR data from compact and center crack test geometries fabricated from 0.25 inch thick 2219-T851 aluminum alloy were supplied to the participants. The tests were conducted between threshold and fracture toughness levels for five separate stress ratios (-1, 0.1, 0.3, 0.5, and 0.8). A number of individuals from government, industry, and academia participated in the round robin (See Table 5.1.1) and chose to evaluate the ten (10) descriptions defined in Table 5.1.2. Each participant was given FCGR data and asked to describe the mean trend of the behavior using equations or other procedures. The participants then integrated their mean trend analysis to establish predicted life values. They were each given the initial and final crack sizes as well as the loading conditions for these life predictions of center cracked specimens and compact specimens.

One of the procedures utilized to evaluate the ten descriptions was to summarize the sixteen (16) life prediction ratios (life predicted divided by life measured, N_f^P/N_f , see Figure 5.1.7b) associated with each description. The means and standard deviations for the life prediction ratios associated with each participant/FCGR description is presented in Table 5.1.3.

TABLE 5.1.1 - Active Participants and their Organizations⁽¹⁰⁾

Name	Affiliation
C. G. Annis	Pratt & Whitney Aircraft
F. K. Haake	
J. Fitzgerald	Northrop Corporation
J. P. Gallagher*	University of Dayton Research Institute
M. S. Miller	
S. J. Hudak, Jr.	Westinghouse R&D Center
A. Saxena	
J. M. Krafft	Naval Research Laboratory
D. E. Macha	Air Force Materials Laboratory
L. Mueller ⁺	Alcoa Laboratories
B. Mukherjee	Ontario Hydro
M. L. Vanderglas	
J. C. Newman	NASA Langley Research Center

* Chairman, ASTM Task Group E24.04.04 on FCGR Descriptions (1975-80)

⁺ Chairman, ASTM Task Group E24.04.04 on FCGR Descriptions (1980-83)

TABLE 5.1.2 - FCGR Descriptions

Participant/ FCGR Description No.	Form
(1)	$\frac{da}{dN} = C_1 \Delta K^{C_2}$
(2)	$\frac{da}{dN} = P_1 \frac{(\Delta K - \Delta K_1)^{P_2}}{(\Delta K_c - \Delta K)^{P_3}}$
(3)	$\frac{1}{da/dN} = \frac{A_1}{(\Delta K)^{n_1}} + A_2 \left[\frac{1}{(\Delta K)^{n_2}} - C' \right]$
(4)	$\frac{da}{dN} = C(K_{\max})^m \left[(K_{\max} + K_c)(1 - R_{eff}) + *K \right]^2$
(5)	$\log_{10} \left(\frac{da}{dN} \right) = P_1 \exp(P_2 x) + P_3 \exp(P_4 x) + P_5$
(6) ⁺	$\frac{da}{dN} = {}_{10}\{C_1 \sinh[C_2(\log \Delta K + C_3)] + C_4\}$
(7) ⁺	$\frac{da}{dN} = {}_{10}\{C_1 \sinh[C_2(\log \Delta K + C_3)] + C_4\}$
(8)	$\frac{da}{dN} = e + (v - e) \left[-\ln \left(1 - \frac{\Delta K}{K_b} \right) \right]^{1/k}$
(9)	tensile ligament instability model
(10)	table lookup procedure

⁺The hyperbolic sine model is listed twice because two separate organizations chose to evaluate this description.

TABLE 5.1.3 - Means and Standard Deviation of Sets of Life-Prediction Ratios for the Full Crack Growth Interval

	Participant/FCGR Description No.									
	1	2	3	4	5	6	7	8	9	10
	Mean	Standard	Deviation							
Mean	0.95	0.72	1.00	0.76	0.96	0.97	2.32	0.99	1.05	0.96
Standard Deviation	0.27	0.16	0.27	0.15	0.12	0.24	5.81	0.10	0.32	0.12

The life prediction ratio (LPR) numbers in Table 5.1.3 can be interpreted by comparing the mean LPR to 1.0 and the standard deviation to 0.0. A mean LPR less than 1.0 implies a conservative prediction. A further interpretation of the results of the round-robin are presented in Table 5.1.4 which contains percentage of life prediction ratios that fall within the ranges of 0.80 and 1.20 and of 0.90 and 1.10. Note that four descriptions were able to achieve LPR numbers between 0.80 and 1.20 for at least 80 percent of the number of predictions made.

One modeling procedure that has consistently shown itself to rank among the most accurate FCGR descriptions for predicting lives is the table look-up scheme (FCGR Description no. 10 in Table 5.1.2). For life prediction purposes, most aircraft companies have gone to a table look-up scheme in which they describe crack growth rate as a function of ΔK for specific values of fatigue crack growth rate or vice versa, i.e., da/dN is described for specific values of ΔK . Table 5.1.5 summarizes the mean trend FCGR behavior of the 2219-T851 aluminum alloy employed by the ASTM Task Group E24.04.04. This table format will be close to the format utilized to present mean trend data in the revised Damage Tolerant Design (Data) Handbook⁽¹⁾. Within the main body of Table 5.1.5, da/dN will be presented as a function of prechosen ΔK levels for specific levels of stress ratio (or environment, etc.). In the rows directly above and directly below the main body of the table, the data extreme values are defined. In the bottom rows of the table, statistical summaries that define the accuracy

TABLE 5.1.4 - A Further Comparison of FCGR Descriptions

Participant/ FCGR Description No.	Percent of All Predictions Within:	
	+20% of 1.0	+10% of 1.0
1	53.3	20.0
2	33.3	20.0
3	86.7	26.7
4	38.5	15.4
5	100.0	73.3
6	73.3	53.3
7	80.0	66.7
8	89.5	57.9
9	31.3	18.8
10	100.0	80.0

TABLE 5.1.5 - Example Fatigue Crack Growth Rate Table
(2219-T851 Aluminum)

ΔK (Ksi $\sqrt{\text{in}}$)			$da/dN \times 10^6$ inches/cycle				
			R1=-1.0	R2=0.1	R3=0.3	R4=0.6	R5=0.8
ΔK_{\min} at:	R1 R2 R3 R4 R5	1.09 2.55 2.11 1.38 1.17	0.00730	0.00336	0.00369	0.00351	0.00112
	1.3 1.6 2.0 2.5 3.0 3.5 4.0 5.0 6.0 7.0 8.0 9.0 10.0 13.0 16.0 20.0		0.0167 0.0351 0.0676 0.127 0.216 0.336 0.488 0.884 1.37 1.91 2.47 3.08 3.80 7.16 13.2 28.3		0.0451 0.152 0.246 0.355 0.691 1.30 2.28 3.60 5.14 6.86 14.4 30.9 126.0	0.0176 0.0569 0.0911 0.139 0.218 0.339 0.753 1.46 2.50 3.95 6.07 9.38 38.4	0.00429 0.0251 0.0689 0.128 0.228 0.431 0.809 2.60 7.83 46.3
ΔK_{\max} at:	R1 R2 R3 R4 R5	20.7 24.7 19.3 15.8 7.01	32.0	887.0	81.3	146.0	47.4
root mean square percent error			2.2	80.4	8.6	6.4	6.1
life prediction ratio summary							
0.0 - 0.5 0.5 - 0.8 0.8 - 1.25 1.25 - 2.0 > 2.0			1	1 3	1	2	2

of the mean trend (tabular) description (1) to relative to the FCGR data (The parameter RMSPE is the root mean square percentage error) and (2) with respect to life prediction (life prediction ratios based on original a vs N data). The RMSPE is a statistic that measures the deviation of fatigue crack growth rate data from the table; and, it is somewhat akin to the coefficient of (life) variation.

The mean trend data presented in the revised Damage Tolerant Design (Data) Handbook⁽¹⁾ can be directly utilized with table look-up algorithms in crack growth life prediction computer codes. These data might also be utilized with least square fitting procedures to generate wider ranging predictive schemes that account for the effects of stress ratio, frequency, environment, temperature, and other controlling conditions.

The Damage Tolerant Design (Data) Handbook⁽¹⁾ provides crack-growth data for a variety of materials. The data are presented in the form of graphs (See Figure 5.1.3) and tables (See Table 5.1.5). Multiple parameter equation fitting should not be attempted if only limited sets of data are available. In case limited data sets have to be used, a comparison should be made with similar alloys for which complete data are available, and curves may be fitted through the limited data sets on the basis of this comparison.

5.1.4 Factors Affecting Crack Growth

Unlike tensile strength and yield strength, fatigue crack growth rate (FCGR) behavior is not a consistent material characteristic. The FCGR is influenced by many uncontrollable factors. As a result, a certain amount of scatter occurs. Therefore, crack growth predictions should be based on factors relevant to the conditions in service.

Among the many factors that affect crack propagation, the following should be taken into consideration for crack growth properties.

- A.
 - Type of product (plate, extrusion, forging)
 - Heat treatment
 - Orientation with respect to grain direction
 - Manufacturer and batch
 - Thickness
- B.
 - Environment
 - Temperature
 - Frequency.

No attempt will be made to illustrate the effects of all these factors with data, particularly because some factors have largely different (and sometimes opposite) effects on different materials. Rather, some general trends will be briefly mentioned.

The factors under A pertain to the material. The crack propagation characteristics for a particular alloy differ for plates, extrusions, and forgings. The latter may exhibit large anisotropy, which may have to be considered in the growth of surface flaws and corner cracks, which grow simultaneously in two perpendicular directions. Closely related to this are other processing variables, particularly the heat treatment.

An alloy of nominally the same composition but produced by different manufacturers may have quite different crack propagation properties⁽¹²⁾. This is illustrated in Figure 5.1.8. The differences are associated with slight variations in composition, inclusion content, heat treatment (precipitates), and cold work. Similar variations in crack growth occur for different batches of the same alloy produced by the same manufacturer. Data presented in Figure 5.1.9 show that growth rates can vary with sheet thickness⁽¹³⁻¹⁷⁾.

In view of the factors which influence crack growth properties, predictions of crack growth should be based on material data which pertain to the product form. Spot checks may be necessary to account for variabilities in heats and/or manufacturer.

The factors under B are associated with the environmental circumstances. A lightly corrosive environment (humid air) gives rise to higher crack growth rates than a dry environment⁽¹⁸⁻²⁷⁾. The effect is illustrated in Figure 5.1.10. Although opinions differ in explaining the environmental

effect, there is concurrence that the principal factor is corrosive action, which is time and temperature dependent. The effect of cyclic frequency^(19,22,26,28) is related to the environmental effect, with slower cyclic frequencies usually associated with accelerated fatigue crack growth rates.

At low temperatures, the reaction kinetics are slower and the air contains less water vapor. This may reduce crack propagation rates in certain alloys^(29,30). Figure 5.1.11 shows the influence of low temperature on crack growth for 7075-T6 alloy compared with growth at normal temperatures⁽²⁹⁾. Temperatures higher than ambient may increase crack growth rates^(31,32). In view of the effect of environment on crack growth, the data used for life predictions should represent the effect of the expected environment and temperature.

5.1.5 Use of Data; Data Scatter

Fatigue-crack-propagation data for a variety of materials can be found in data handbooks. In many cases, however, the data for a particular application (with regard to material condition, thickness, and environment) will have to be generated in the manner prescribed by Chapter 7.

As indicated by the results presented in subsection 5.1.3, accurate mean trend FCGR descriptions result in accurate fatigue crack life descriptions. People have worried in the past about trying to account for the substantial

amount of scatter which exists in the crack growth rate data. The amount of crack growth between crack measurements and the accuracy of this incremental crack growth measurement determines a large part of the scatter. Another inherent reason for data scatter is due to the differentiation techniques that one uses to reduce the data.

Shown in Figure 5.1.12a is a hypothetical example of the crack growth-life behavior observed in a single laboratory test; Figure 5.1.12b represents the FCGR data derived from this test. Outlying data points are indicated by an asterisk in Figure 5.1.12a and b. The mean trend curves faired through the data can be shown to be directly related to each other; the integral of the curve in Figure 5.1.12b gives the curve in Figure 5.1.12a for the test conditions. If more tests are run and all the data compiled, the plot will be as in Figure 5.1.12c: each test might have a few outlying data points, but the compilation has many outlying points. When all data points, including the outliers, are plotted, the data exhibit a wide scatterband, noted as the apparent scatterband, shown in Figure 5.1.12c. However, as previously seen from Figures 5.1.12a and b, the outlier points did not significantly affect the crack growth curve or the mean trend FCGR curve. When considered collectively, the outlying data points in Figure 5.1.12c can be misleading since they do not represent the mean trend behavior of any specimen. If the wide scatterband were considered for a crack growth prediction, the upper bound would predict a consistent

high growth rate at each crack size (whereas it happened only incidentally as shown in Figure 5.1.12a). As a result, the diagram would reflect a large apparent scatter in crack growth lives (Figure 5.1.12d) whereas the real scatter in crack growth lives is much smaller.

As indicated by the above remarks, worrying about the random (within specimen) scatter in fatigue crack growth rates is really not that important from a life estimation standpoint. What has been found from analyses of multiple specimen data sets is that the width of the scatterbands associated with specimen to specimen mean trend variations in FCGR is closely related to the variability in crack growth-life behavior. The scatterband associated with specimen to specimen variations is identified in Figures 5.1.12c and d as the real scatterband since it focuses on the variability in crack growth life-behavior.

The coefficient in variation of crack growth lives is sometimes similar in magnitude to the root mean square (percentage) error associated with fatigue crack growth rate modeling. When conservative estimates in crack growth lives are desired, the upper bound of the real scatterband (identified in Figure 5.1.12c) determined on the basis of four or more specimens should be used.

5.1.6 Stress-Corrosion Cracking and Stress Intensity

Many engineering materials exhibit some cracking behavior under sustained loading in the presence of an environment (thermal and/or chemical). The type of cracking behavior for many chemical environments is referred to as stress-corrosion cracking behavior. The mechanism for this attack process has been attributed to the chemical reactions that take place at the crack tip and to diffusion of reactive species (particularly Hydrogen) into the high stressed region ahead of the crack. The cracking process has been noted to be a function of time and it is highly dependent on the environment, the material, and the applied stress (or stress-intensity factor) level.

For a given material-environment interaction, the stress-corrosion-cracking rate has been noted to be governed by the stress-intensity factor. Similar specimens with the same size of initial crack but loaded at different levels (different initial K values) show different times to failure⁽³³⁻³⁵⁾ as shown in Figure 5.1.13. A specimen initially loaded to K_{Ic} fails immediately. The level below which cracks are not observed to grow is the threshold level which is denoted as K_{Isc} .

If the load is kept constant during the stress-corrosion-cracking process, the stress-intensity factor will gradually increase due to the growing crack. As a result the crack-growth rate per unit of time, da/dt , increases according to

$$\frac{da}{dt} = f(K). \quad (5.1.7)$$

When the crack has grown to a size that K becomes equal to K_{IC} , the specimen fails. This is shown schematically in Figure 5.1.14. In typical tests, specimens may be loaded to various initial K 's such as K_1 , K_2 , and K_3 . The time to failure is recorded giving rise to the typical data point (t_1, K_1) . During the test, K will increase (as a result of crack extension) from its initial value to K_{IC} , where final failure occurs. The times t_2 and t_3 represent the times to failure for higher K 's such as K_2 and K_3 .

The stress-corrosion threshold and the rate of growth depend on the material and the environmental conditions. Data on K_{Isc} and da/dt can be found in the Damage Tolerant Design (Data) Handbook (1). Typical examples of K_{Isc} and da/dt data presentation formats are shown in Figures 5.1.15 and 5.1.16.

As illustrated in Figure 5.1.17, a component with a given crack fails at a stress given by $\sigma_c = K_{IC} / \beta\sqrt{\pi a}$. It will exhibit stress-corrosion-crack growth when loaded to stresses in excess of $\sigma_{scc} = K_{Isc} / \beta\sqrt{\pi a}$.

In service, stress-corrosion cracks have been found to be predominantly a result of residual stresses and secondary stresses. Stress-corrosion failure due to primary loading seldom occur because most stress-corrosion cracks favor the short transverse direction (S-L), which is usually not the primary load direction. In many materials, the long transverse (T-L) and longitudinal (L-T) directions are not very susceptible to stress corrosion.

Prevention of stress corrosion cracking is preferred as a design policy over controlling it as is done for fatigue cracking. This means that stress-corrosion critical components must be designed to operate at a stress level lower than $\sigma_{scc} = K_{Iscc} / \beta \sqrt{\pi a_i}$ in which a_i is the initial flaw sizes as specified in the Damage Tolerance Requirements per MIL-A-83444. However, if stress corrosion can occur, it must be accounted for in damage tolerance analyses by using an integral form of Equation 5.1.7.

Stress-corrosion cracking may occur in fatigue-critical components. This means that in addition to growth by fatigue, cracks might show some growth due to stress corrosion. In dealing with this problem, the following should be considered:

- Stress-corrosion cracking is a phenomenon that basically occurs under a steady stress. Hence, the in-flight stationary stress level (lg) is the governing factor. Most fatigue cycles are of relatively short duration and do not contribute to stress-corrosion cracking. Moreover, the cyclic crack growth would be properly treated already on the basis of data for environment-assisted fatigue-crack growth. When stress corrosion cracking is expected, the stress corrosion cracking rate should be superimposed on the fatigue crack growth rate⁽³⁶⁻³⁹⁾.

- Stress-corrosion cracking is generally confined to forgings, heavy extrusions, and other heavy sections, made of susceptible materials. Thus, the problem is generally limited to cases where plane strain prevails.
- The maximum crack size to be expected in service is $a_c = K_{Ic}^2 / \pi \beta^2 \sigma^2$, where σ equals σ_{LT} or σ_{DM} depending upon the inspectability level.

If stress-corrosion cracking is not expected at any crack size, the l-g stress, σ_{lg} , should be lower than $\sigma_{scc} = K_{Isc} / \beta \sqrt{\pi a_c}$. With a_c given as above, it follows that complete prevention of stress corrosion extension of a fatigue crack requires selection of a material for which:

$$K_{Isc} > \frac{\sigma_{lg}}{\sigma_{LT} \text{ (or } \sigma_{DM})} K_{Ic} . \quad (5.1.8)$$

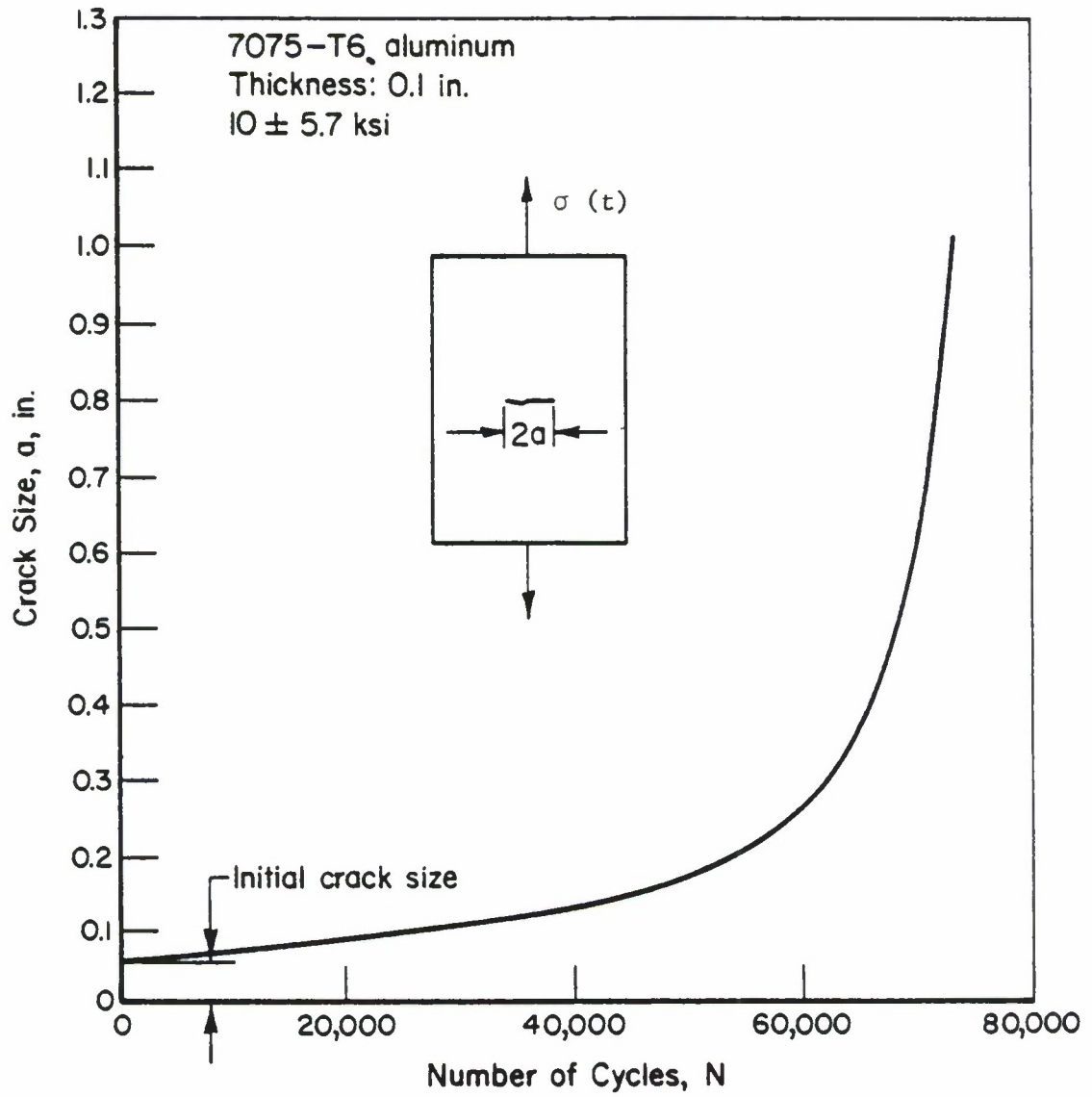


Figure 5.1.1. Typical Crack Growth-Life Curve.

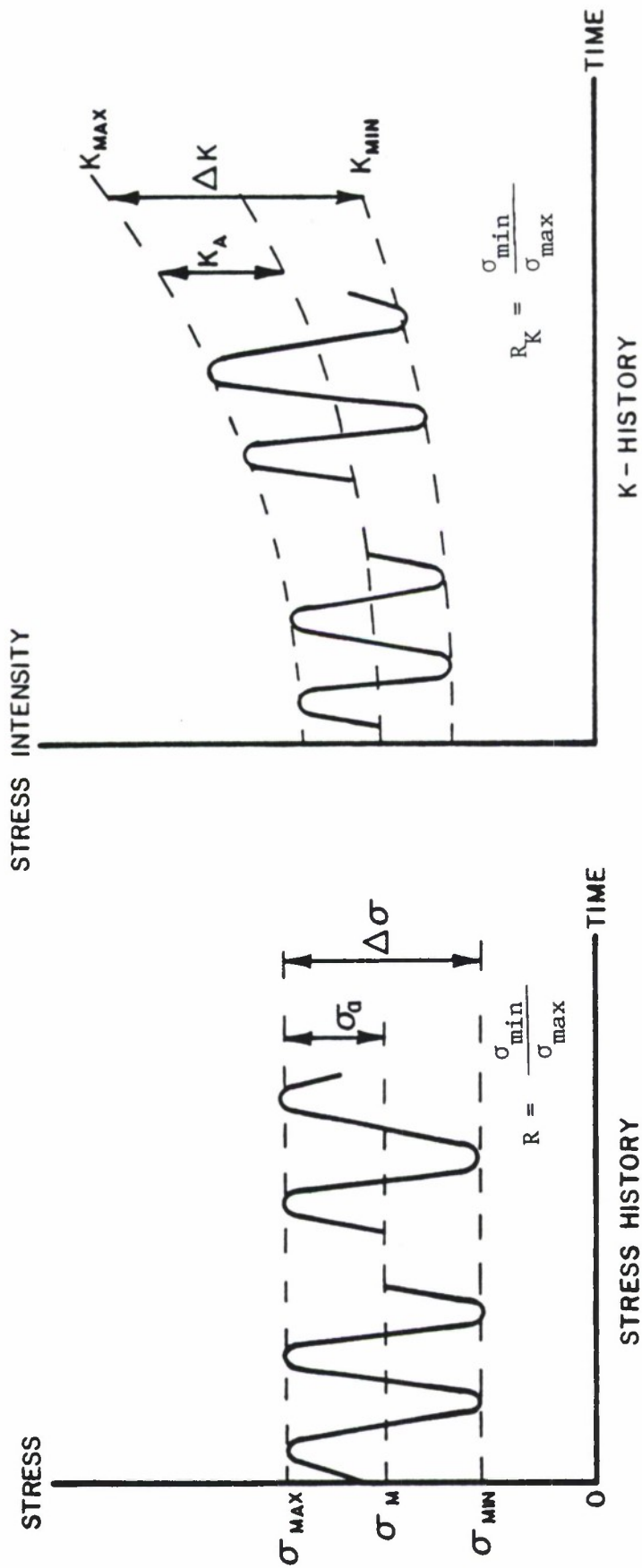


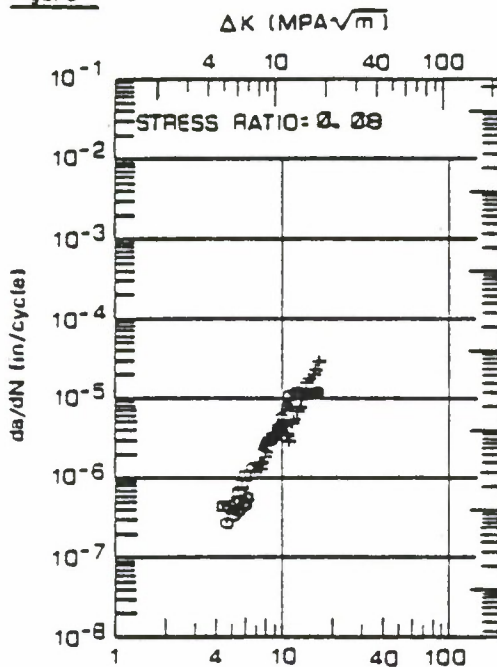
Figure 5.1.2. Definition of Terms.

FORM: 2.00" TH PLATE
 DIRECTION: L-T
 ENVIRONMENT: R. T. L. H. A.
 FREQUENCY: 6.0 HZ

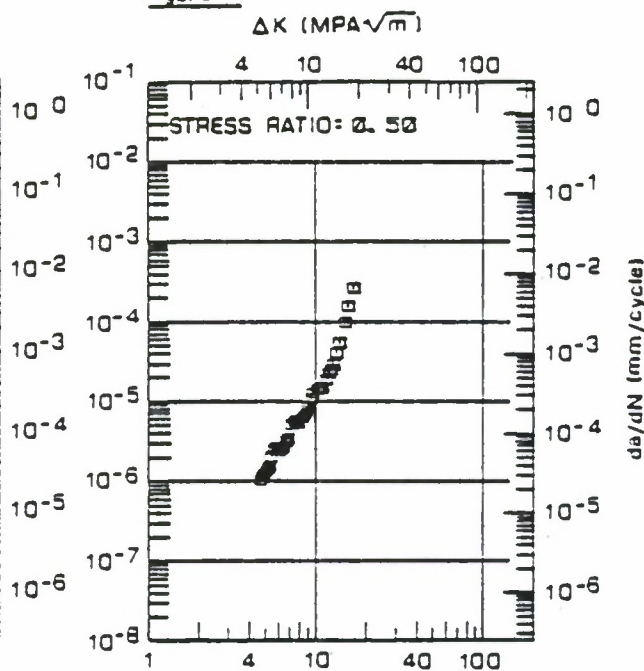
YIELD STRENGTH: 85.0 KSI
 SPECIMEN TYPE: CT
 SPECIMEN SIZE: .812" T, 6.00" W
 REFERENCE: 85837, 88579

ALUM
 7075
 T7351

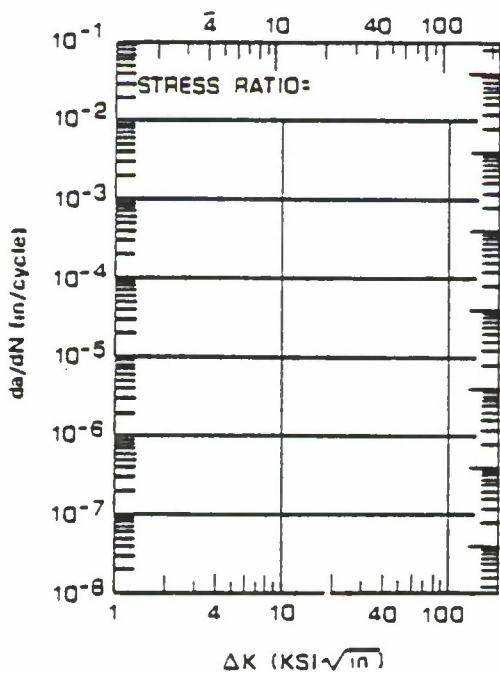
Figure



Figure



Figure



Figure

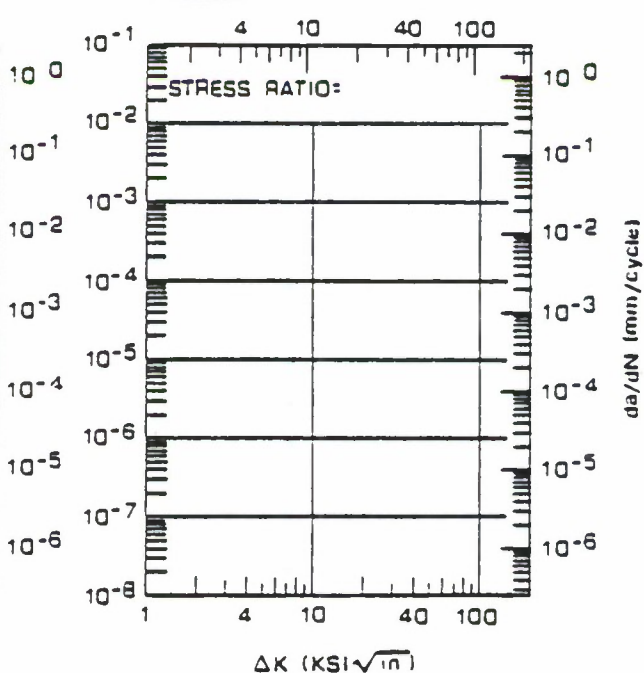


Figure 5.1.3. Fatigue Crack Growth Rate Data Presentation Format Used in Revised Damage Tolerant Design (Data) Handbook. Data for Two Stress Ratios Presented for 7075-T7351 Aluminum Alloy (Reference 1).

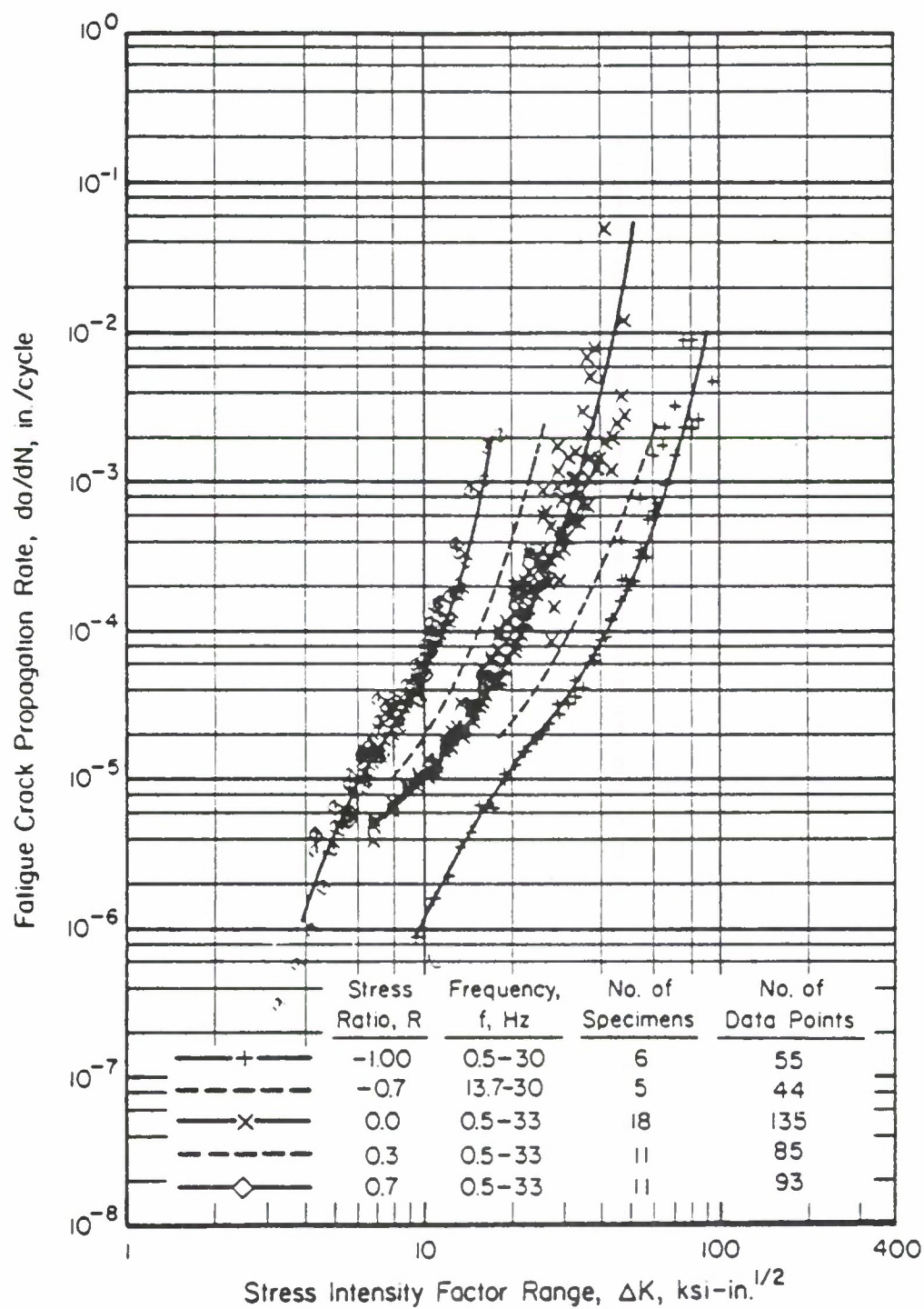


Figure 5.1.4. Sample Fatigue Crack Growth Rate Data Set for 7075-T6 Aluminum Alloy Sheet After Mil Handbook-5 (Reference 2).

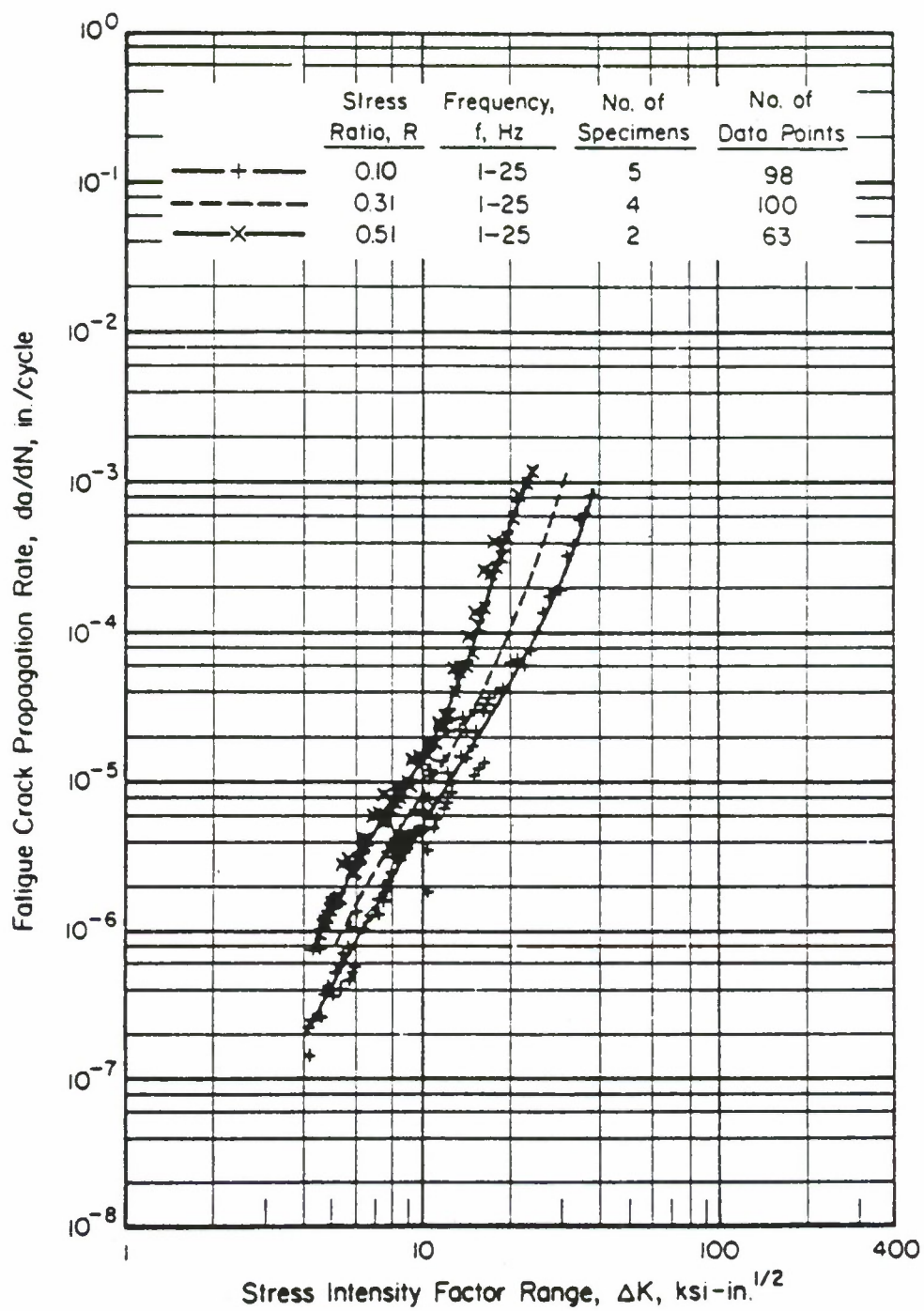


Figure 5.1.5. Sample Fatigue Crack Growth Rate Data Set for 7075-T7351 Aluminum Alloy Plate After Mil-Handbook-5 (Reference 2).

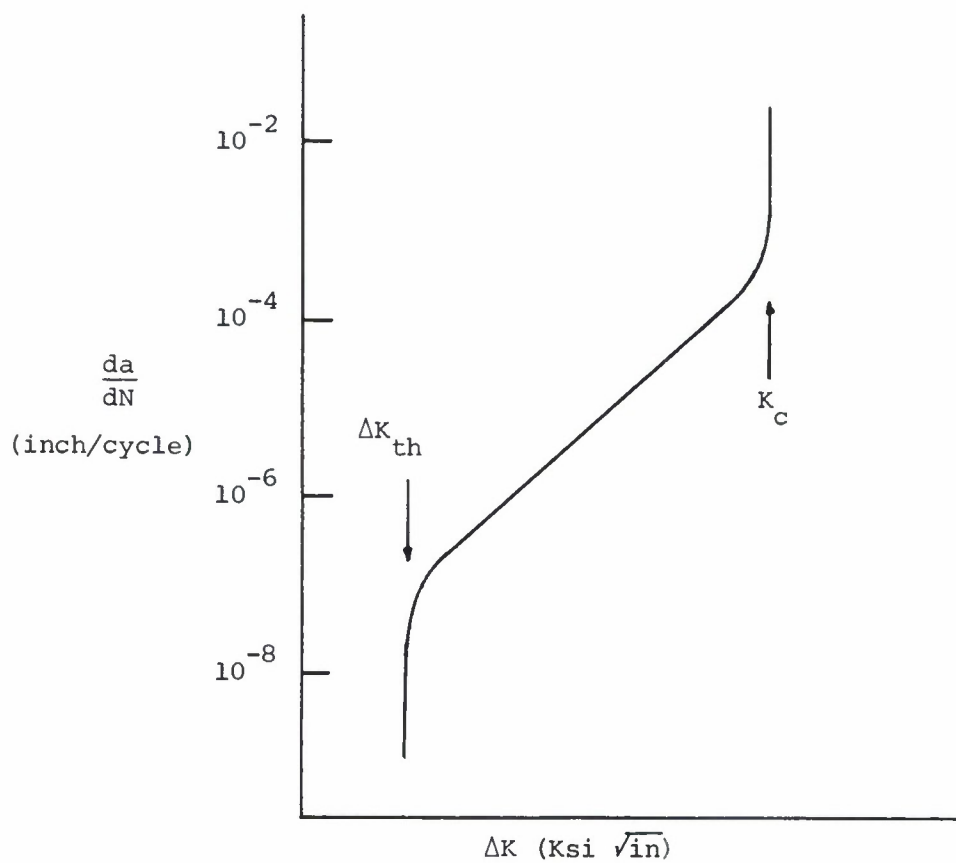


Figure 5.1.6. Schematic of Fatigue Crack Growth Rate Behavior.

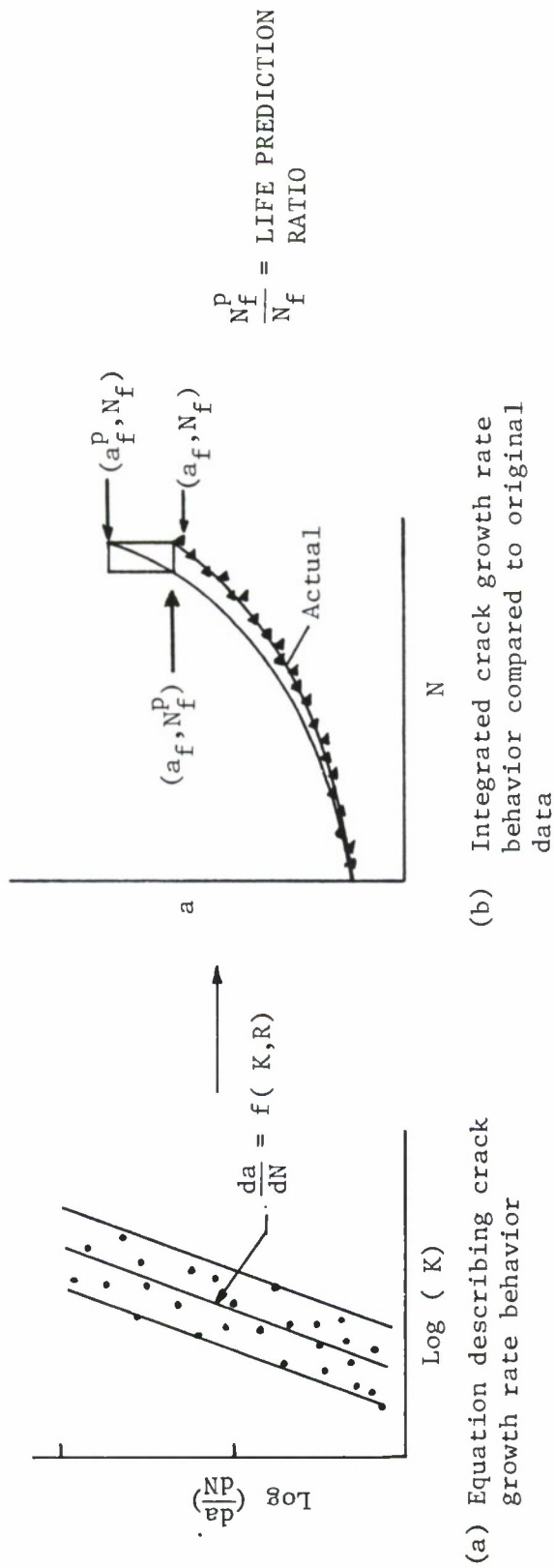


Figure 5.1.7. Description of FCGR Data Fitting and the Comparison of Predicted to Actual Behaviors.

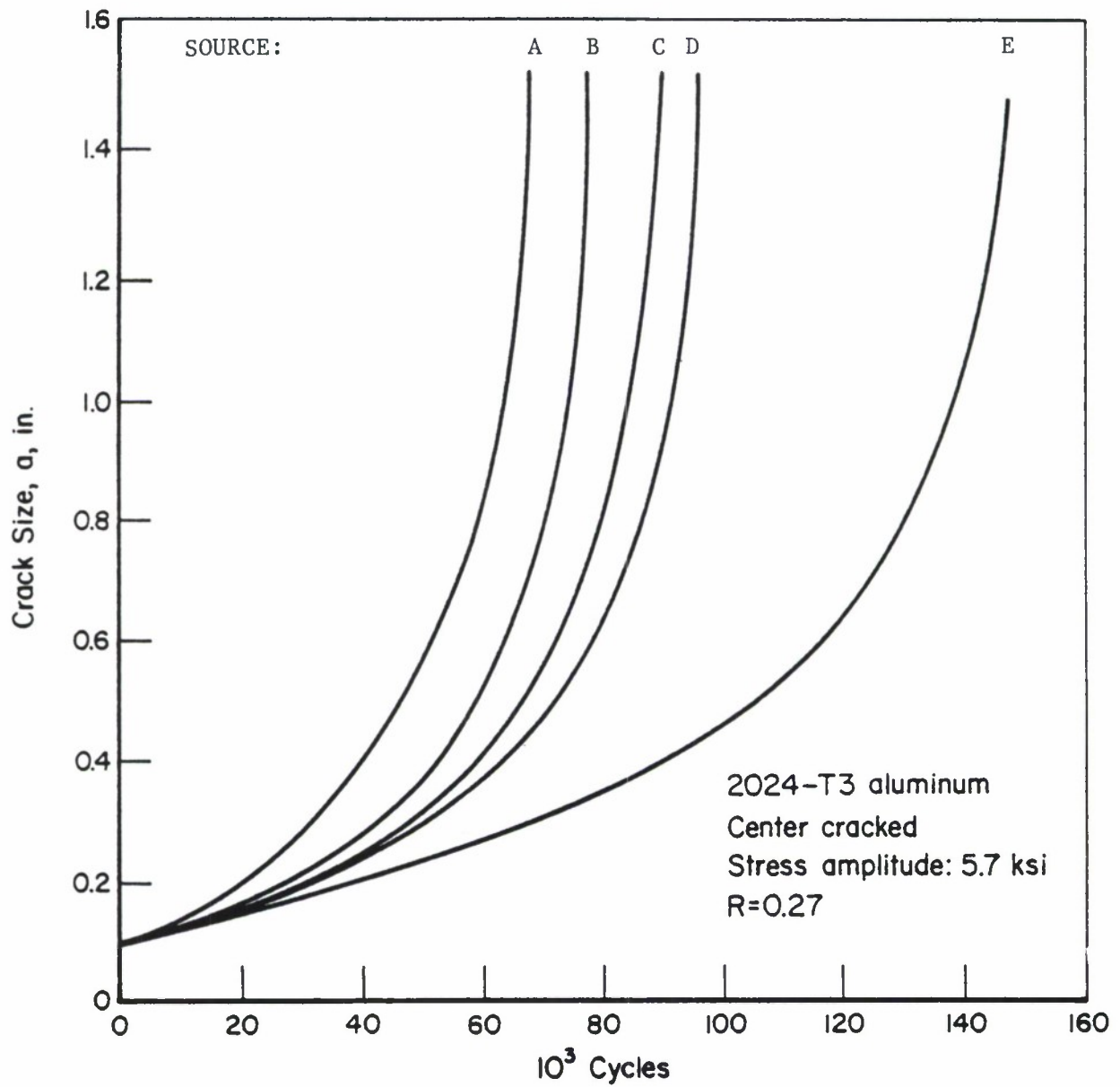


Figure 5.1.8. Possible Variation of Crack Growth in Materials from Different Sources (Reference 12).

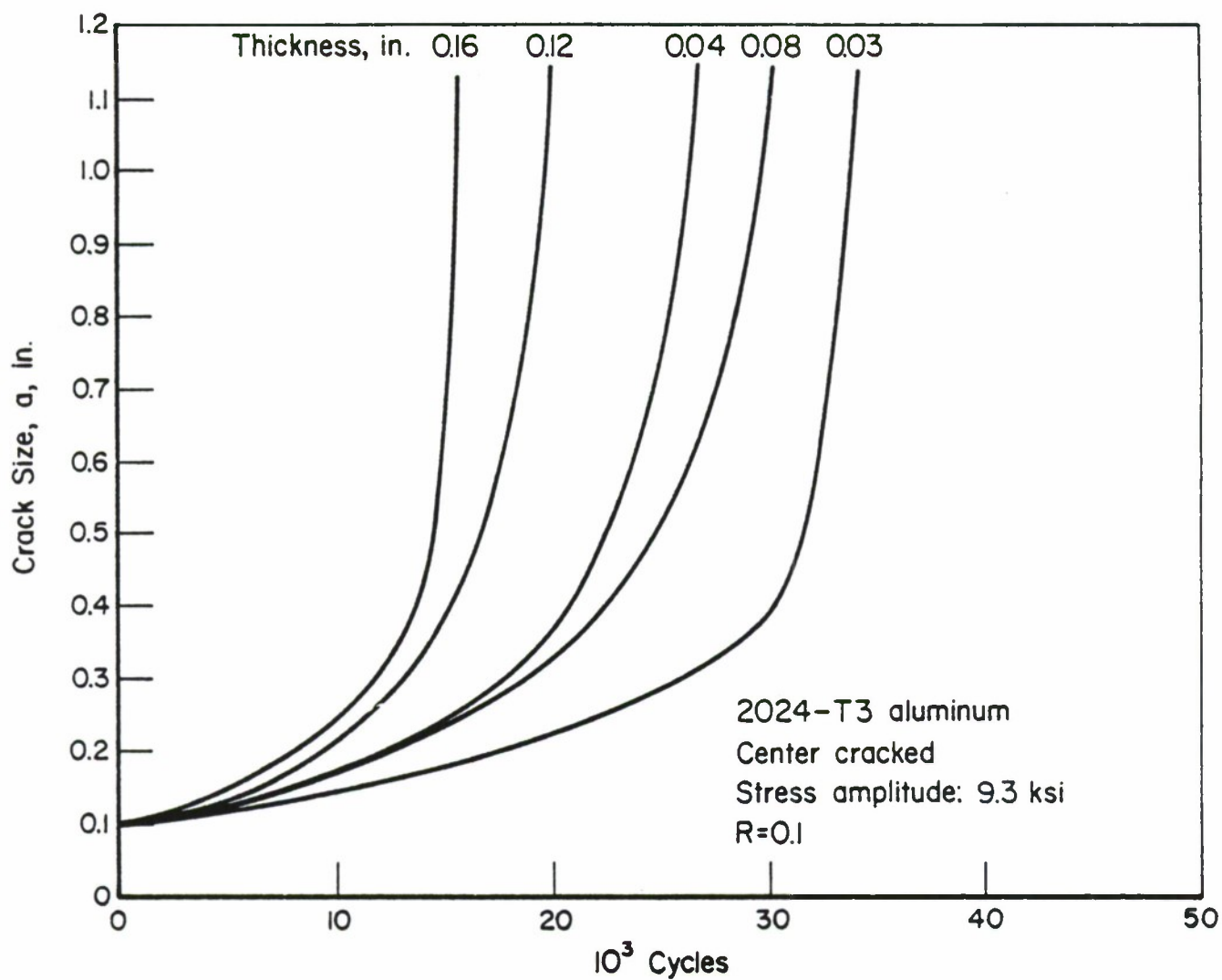


Figure 5.1.9. Example of Effect of Thickness on Crack Growth (Reference 13).

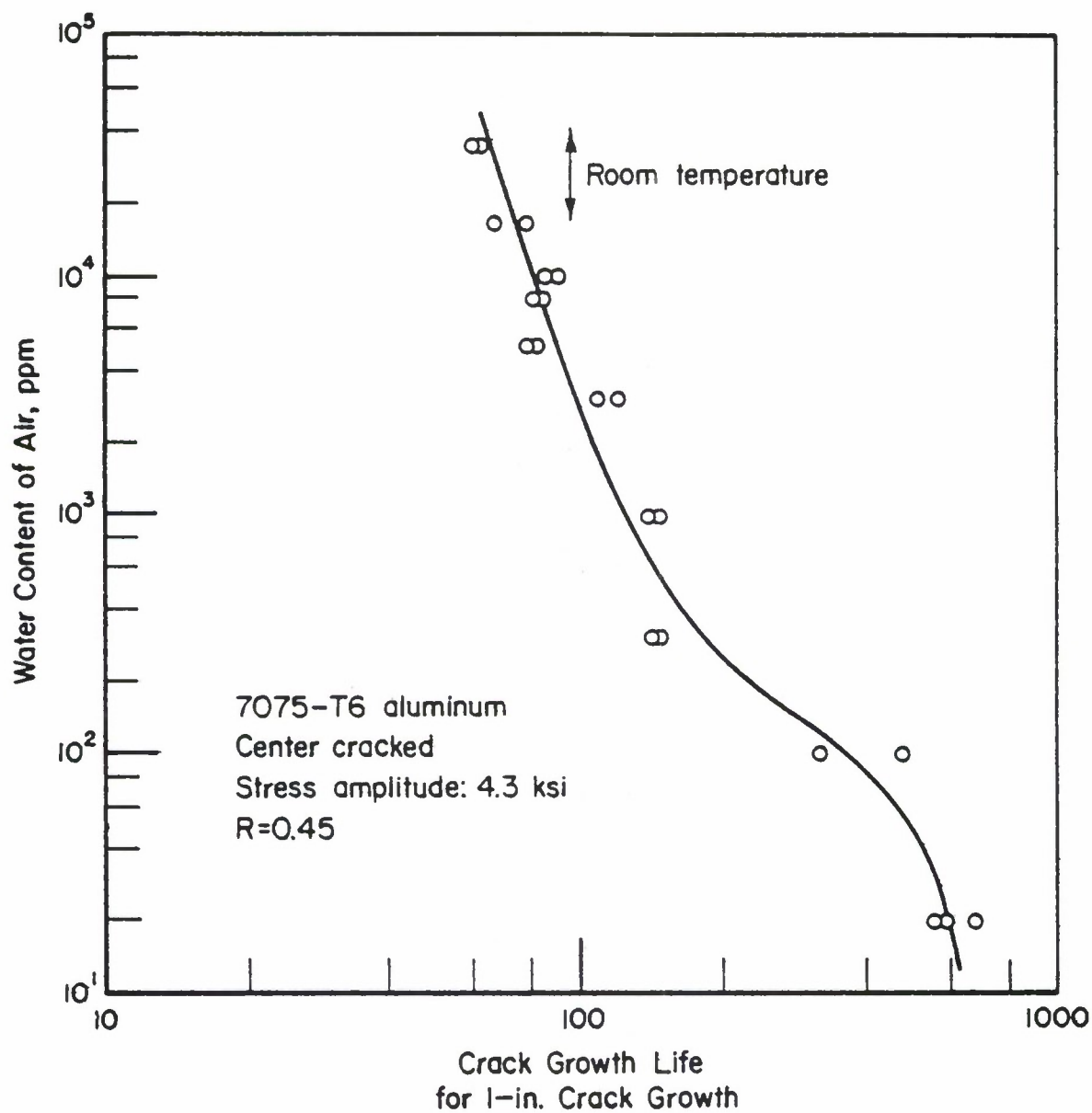


Figure 5.1.10. Effect of Humidity on Fatigue Crack Propagation (Reference 18).

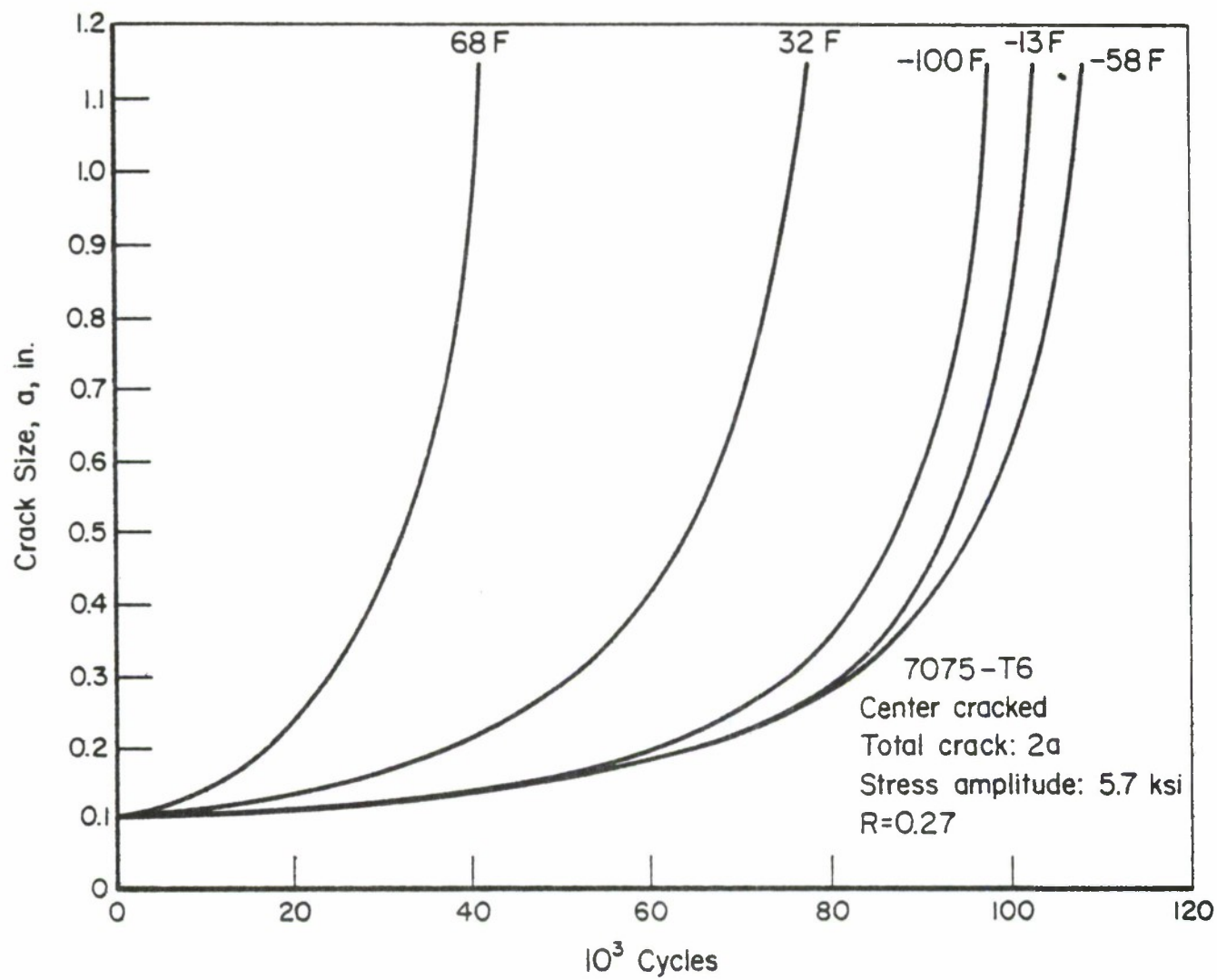


Figure 5.1.11. Example of Temperature Effect on Crack Growth (Reference 29).

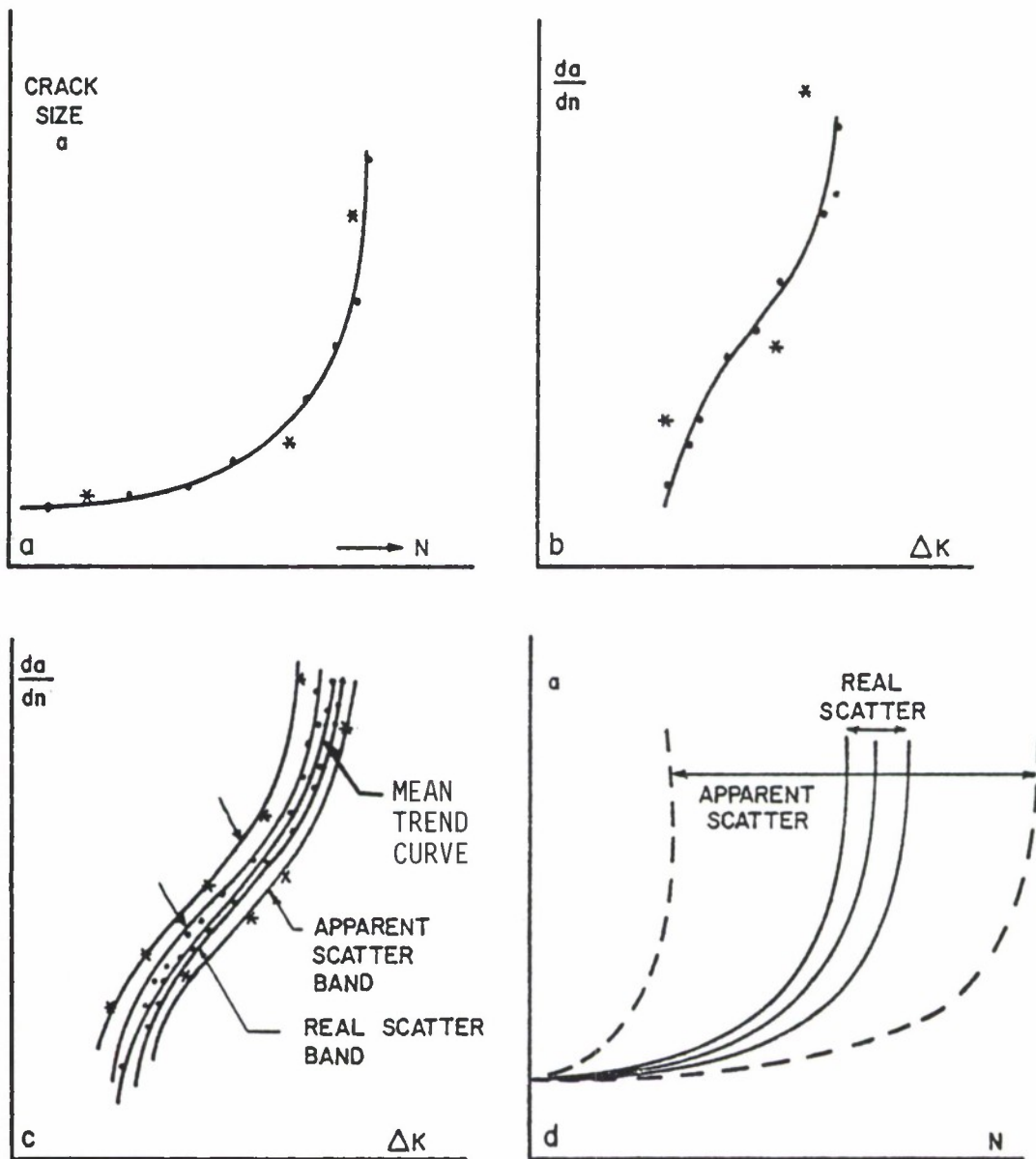


Figure 5.1.12. Crack Growth Data Scatter for Identical Conditions.

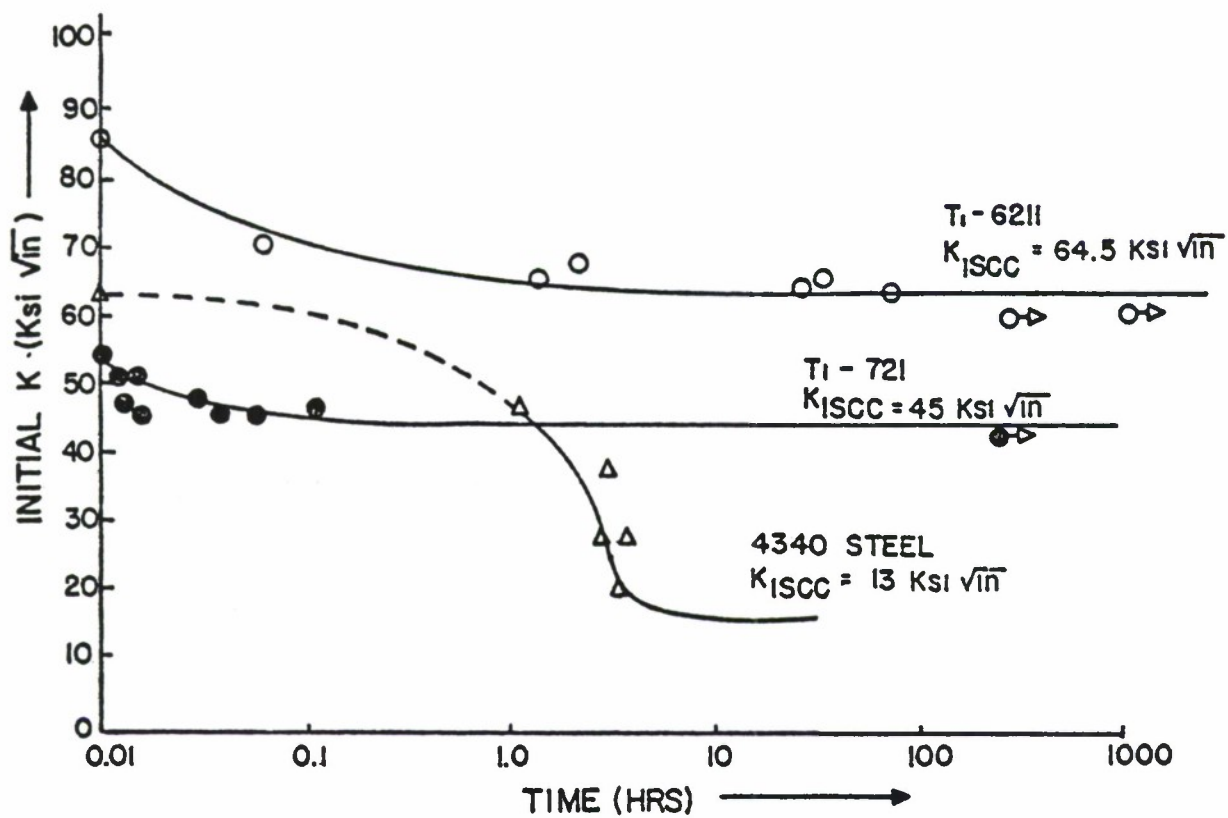


Figure 5.1.13. Stress Corrosion Cracking Data (Reference 33).

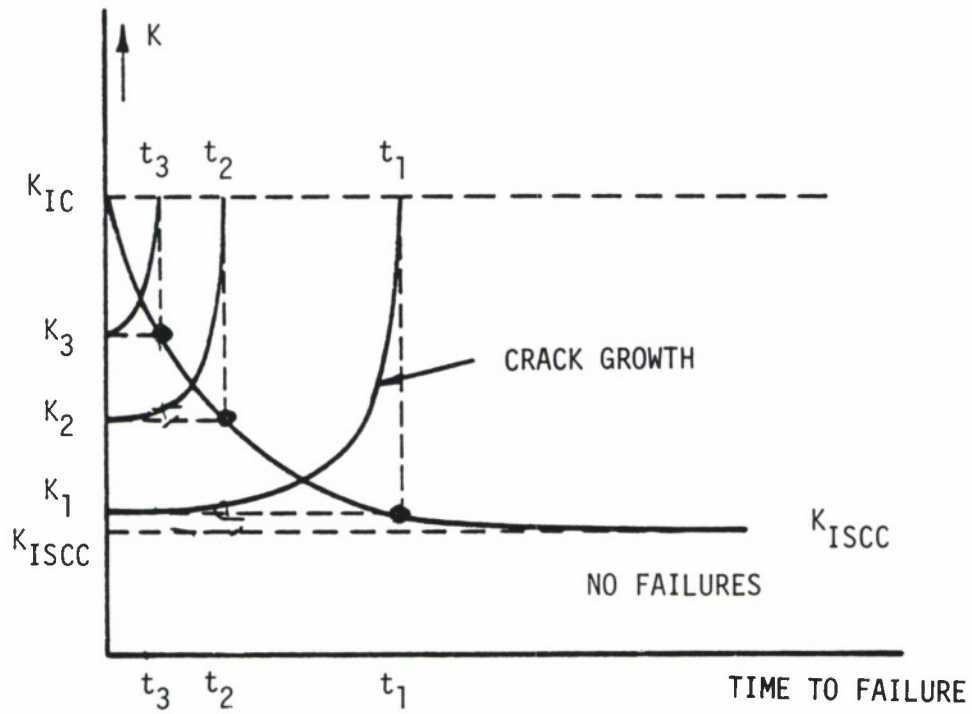


Figure 5.1.14. Stress Corrosion Cracking.

CONDITION	ALUMINUM				7075				K (ISCC)		STAN DEV	FAIL TIME (MIN)	DATE REFER		
	--PRODUCT-- FORM THICK (IN)	TEST SPEC OR STR (F)	YIELD (KSI)	ENVIRONMENT	-----SPECIMEN-----		CRACK								
					WIDTH (IN) W	THICK DESIGN (IN) B	THICK DESIGN (IN) A	K (G) (KSI*SGRT IN)							
T352	F	6.00	R. T.	S-L	56.3	3.5	PCT NACL	1.400	0.700	CANT	----	20.10	18.00	----	1972 82675
T6	P	1.00	R. T.	S-L	73.0	3.5	PCT NACL	4.000	1.000	DCB	----	23.00	19.00	----	1968 84331
T651	P	3.00	R. T.	L-T	70.2	AIR	74PCT RH	5.000	1.250	TDCB	----	30.00	25.30	----	1971 84360
T651	P	3.00	R. T.	L-T	70.2	DIST	WATER	5.000	1.250	TDCB	----	30.00	24.00	----	1971 84360
T651	P	3.00	R. T.	L-T	70.2	3.5	PCT NACL	5.000	1.250	TDCB	----	30.00	28.30	----	1971 84360
T651	P	2.50	R. T.	S-L	66.7	INDUSTRIAL	ATM	2.000	1.000	CT	----	19.60	10.00	----	1973 86689
T651	P	2.50	R. T.	S-L	66.7	SALT-DICHROR- MATE-ACETATE		2.000	1.000	CT	----	19.60	5.00	----	1973 86689
T651	P	2.50	R. T.	S-L	66.7	SEACOAST	ATM	2.000	1.000	CT	----	19.60	10.00	----	1973 86689
T651	P	1.00	R. T.	S-L	78.0	3.5	PCT NACL	4.000	1.000	DCB	----	21.00	17.00	----	1968 84331
T651	E	-----	R. T.	T-L	-----	CARBON TET, CCL4		3.000	0.750	DCB	----	-----	10.00	-----	1969 75787
T651	E	-----	R. T.	T-L	-----	ETHANOL		3.000	0.750	DCB	----	-----	9.00	-----	1969 75787
T7351	P	4.00	R. T.	T-L	53.2	DIST	WATER	5.000	1.250	TDCB	----	29.00	24.80	----	1972 84360
T7351	P	4.00	R. T.	T-L	53.2	3.5	PCT NACL	5.000	1.250	TDCB	----	29.00	23.90	----	1972 84360
T7351	P	2.50	R. T.	S-L	55.1	SEACOAST	ATM	2.000	1.000	CT	----	21.00	20.00	----	1973 86689
T7351	P	2.50	R. T.	S-L	55.1	SALT-DICHROR- MATE-ACETATE		2.000	1.000	CT	----	21.00	19.00	----	1973 86689
T7351	P	2.50	R. T.	S-L	55.1	INDUSTRIAL	ATM	2.000	1.000	CT	----	21.00	20.00	----	1973 86689
T7351	P	1.00	R. T.	S-L	52.0	3.5	PCT NACL	4.000	1.000	DCB	----	24.00	21.00	----	1968 84331
T76511	E	-----	R. T.	T-L	64.5	3.5	PCT NACL	-----	-----	DCB	----	31.80	29.10	----	1973 86211

CONDITION/HT: T351
 ENVIRONMENT: WET 3 TIMES/DAY
 SPECIMEN TYPE:
 ORIENTATION: S-L
 YIELD STRENGTH:
 ULT. STRENGTH:

SPECIMEN THK: 1.00"
 SPECIMEN WIDTH: 5.00"
 CRACK LENGTH (A_0):
 K_{ISCC} :
 REFERENCES: 78313, 84284

ALUM

2024

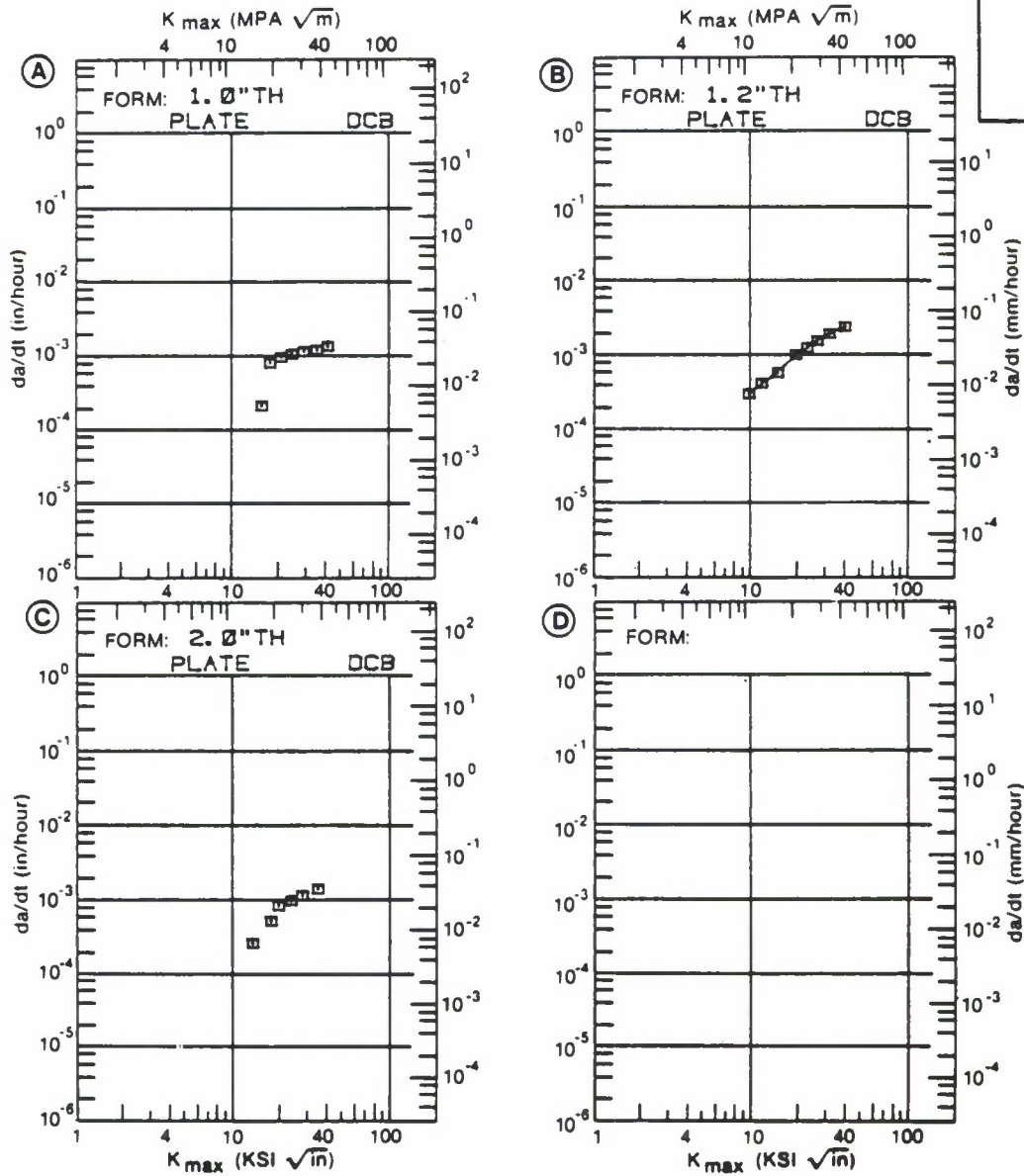


Figure 5.1.16. Stress Corrosion Cracking Rate Data for 2024-T351 Aluminum in the Format of Reference 1.

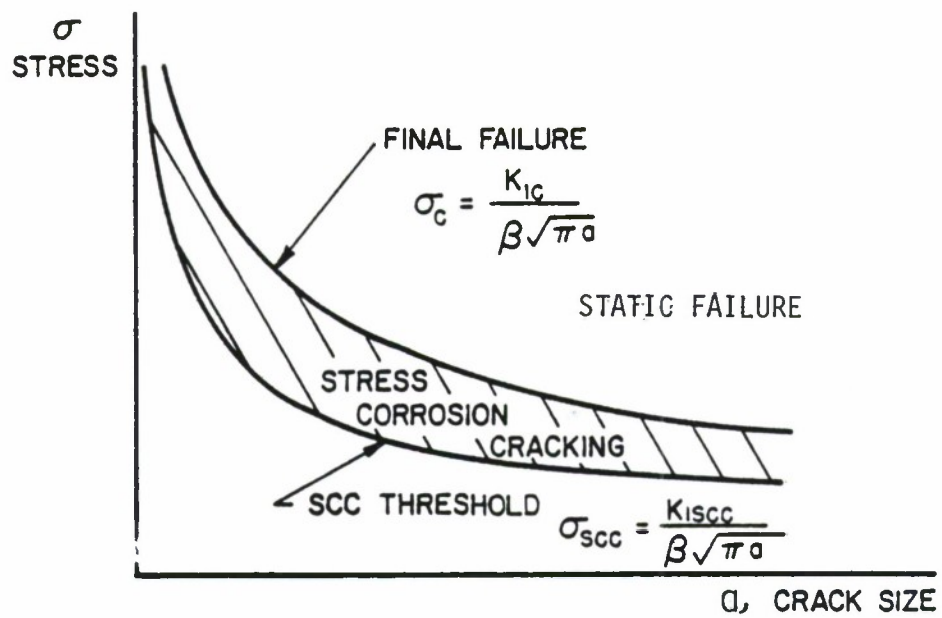


Figure 5.1.17. Stress Required for Stress Corrosion Cracking.

5.2 VARIABLE-AMPLITUDE LOADING

5.2.1 Introduction

Baseline fatigue data are derived under constant-amplitude loading conditions, but aircraft components are subjected to variable amplitude loading. If there were not interaction effects of high and low loads in the sequence, it would be relatively easy to establish a crack-growth curve by means of a cycle-by-cycle integration (see Section 5.2.5). However, crack-growth under variable-amplitude cycling is largely complicated by interaction effects of high and low loads.

In the following sections these interaction effects will be briefly discussed. Crack-growth-prediction procedures which take interaction effects into account will be presented in Section 5.2.5.

5.2.2 Retardation

A high load occurring in a sequence of low-amplitude cycles significantly reduces the rate of crack-growth during the cycles applied subsequent to the overload. This phenomenon is called retardation. Figure 5.2.1 shows a baseline crack-growth curve obtained in a constant-amplitude test⁽⁴⁰⁾. In a second experiment, the same constant-amplitude loading was interspersed with overload cycles. After each application of the overload, the crack virtually stopped growing during many cycles, after which the original crack-growth behavior was gradually restored.

Retardation results from the plastic deformations that occur as the crack propagates. During loading, the material at the crack tip is plastically deformed and a tensile plastic zone is formed. Upon load release, the surrounding material is elastically unloaded and a part of the plastic zone experiences compressive stresses. The larger the load, the larger the zone of compressive stresses. If the load is repeated in a constant amplitude sense, there is no observable direct effect of the residual stresses on the crack-growth behavior; in essence, the process of growth is steady state. Measurements have indicated, however, that the plastic deformations occurring at the crack tip remain as the crack propagates so that the crack surfaces open and close at non zero (positive) load levels. These observations have given rise to constant amplitude crack-growth models referred to as closure models⁽⁴¹⁾ after the concept that the crack may be closed during part of the load cycle.

When the load history contains a mix of constant amplitude loads and discretely applied higher level loads, the patterns of residual stress and plastic deformation are perturbed. As the crack propagates through this perturbed zone under the constant amplitude loading cycles, it grows slower (the crack is retarded) than it would have if the perturbation had not occurred. After the crack has propagated through the perturbed zone, the crack growth rate returns to its typical steady state level. Two basic models have been proposed to describe the phenomenon

of crack retardation. The first model is based on the concept of the compressive residual stress perturbation and the second on the concept of plastic deformation (enhanced crack wedging - more closure).

If the tensile overload is followed by a compressive overload, the material at the crack tip may undergo reverse plastic deformation and this reduces the residual stresses. Thus, a negative overload in whole or in part annihilates the beneficial effect of tensile overloads, as is also shown in Figure 5.2.1.

Retardation depends upon the ratio between the magnitude of the overload and subsequent cycles. This is illustrated in Figure 5.2.2. Sufficiently large overloads may cause total crack arrest. Hold periods at zero stress can partly alleviate residual stresses and thus reduce the retardation effect^(27,42), while hold periods at load increase retardation. Multiple overloads significantly enhance the retardation. This is shown in Figure 5.2.3.

5.2.3 Retardation Under Spectrum Loading

An actual service load history contains high- and low-stress amplitudes and positive and negative "overloads" in random order. Retardation and annihilation of retardation becomes complex, but qualitatively the loading produces behavior that is similar to a constant-amplitude history with incidental overloads. The higher the maximum

stresses in the service load history, the larger the retardation effect during the low-amplitude cycles. Negative stress excursions reduce the retardation effect and tend to enhance crack-growth. These effects have been documented in various sources (e.g., References 43-49); a few examples are now presented.

When the magnitude of the higher loads are reduced (or clipped) without eliminating the cycle, i.e., higher loads are reset to a defined lower level, the cracking rates are observed to speed up as shown in Figure 5.2.4^(43,44). Figure 5.2.4 describes the crack growth life results for a study in which a (random) flight-by-flight stress history was systematically modified by "clipping" the highest load excursions to the three levels shown.

In References 43 and 44, it was also observed that negative stress excursions reduce the retardation effect and omission of the ground-air-ground (G-A-G) cycles (negative loads) in the tests with the highest clipping level resulted in a longer crack growth life for the same amount of crack growth.

Figure 5.2.5 shows the importance of load sequence. The crack-propagation life for random load cycling is shown at the top. Ordering the sequences of the loads, lo-hi, lo-hi-lo, or hi-lo increases the crack-growth life, the more so for larger block sizes. Hence, ordering should only be permitted if the block size is small. Lo-hi ordering gives more conservative results than hi-lo ordering. In the latter case, the retardation effect caused by the highest load is effective during all subsequent cycles.

5.2.4 Retardation Models

Some mathematical models have been developed to account for retardation in crack-growth-integration procedures. All models are based on simple assumptions, but within certain limitations and when used with experience, each model will produce results that can be used with reasonable confidence. The two yield zone models by Wheeler⁽⁵⁰⁾ and by Willenborg, et al⁽⁵¹⁾, and a crack-closure model by Bell and Creager⁽⁵²⁾ will be briefly discussed. Detailed information and applications of closure models can be found in References⁽⁵²⁻⁵⁵⁾.

Wheeler defines a crack-growth reduction factor, C_p :

$$\left(\frac{da}{dN}\right)_r = C_p f(\Delta K), \quad (5.2.1)$$

where $f(\Delta K)$ is the usual crack-growth function, and (da/dN) is the retarded crack-growth rate. The retardation factor, C_p is given as

$$C_p = \left(\frac{r_{pi}}{a_{oL} + r_{poL} - a_i}\right)^m, \quad (5.2.2)$$

in which (see Figure 5.2.6):

r_{pi} is the current plastic zone size in the i th cycle under consideration

a_i is the current crack size

r_{poL} is the plastic size generated by a previous higher load excursion

a_{oL} is the crack size at which the higher load excursion occurred

m is an empirical constant.

There is retardation as long as the current plastic zone is contained within a previously generated plastic zone; this is the fundamental assumption of yield zone models.

Some examples of crack-growth predictions made by means of the Wheeler model are shown in Figure 5.2.7. Selection of the proper value for the exponent m will yield adequate crack-growth predictions. In fact, one of the earlier advantages of the Wheeler model was that exponent m could be tailored to allow for reasonably accurate life predictions of spectrum test results. Through the course of time, it has become recognized, however, that the exponent m was dependent on material, crack size, and stress-intensity factor level as well as spectrum. The reader is cautioned against using the Wheeler model for service life predictions based on limited amounts of supporting test data and more specifically against estimating the service life of structures with spectra radically different from those for which the exponent m was derived. Estimates made without the supporting data required to tailor the exponent m can lead to inaccurate and unconservative results.

The Willenborg model also relates the magnitude and extent of the retardation factor to the overload plastic zone. The extent of the retardation is handled exactly the same as that of the Wheeler model. The magnitude of the retardation factor is established through the use of an effective stress-intensity factor that senses the differences in

compressive residual stress state caused by differences in load levels. The effective stress-intensity factor (K_i^{eff}) is equal to the typical remote stress-intensity factor (K_i) for the i th cycle minus the residual stress-intensity factor (K_R):

$$K_i^{eff} = K_i - K_R \quad (5.2.3)$$

where in the original formulation (References 51,56-58)

$$K_R = K_R^W = K_{max}^{oL} \sqrt{1 - \frac{a_i - a_{oL}}{r_{poL}}} - K_{max,i} \quad (5.2.4)$$

in which (see Figure 5.2.6):

a_i is the current crack size

a_{oL} is the crack size at the occurrence of the overload

r_{poL} is the yield zone produced by the overload

K_{max}^{oL} is the maximum stress intensity of the overload

$K_{max,i}$ is the maximum stress intensity for the current cycle.

The equations show that retardation will occur until the crack has generated a plastic zone size that reaches the boundary of the overload yield zone. At that time, $a_i - a_{oL} = r_{poL}$ and the reduction becomes zero.

Equation 5.2.3 indicates that the complete stress-intensity factor cycle, and therefore, its maximum and minimum levels ($K_{max,i}$ and $K_{min,i}$), are reduced by the same amount (K_R). Thus, the retardation effect is sensed by the change in the effective stress ratio calculated by

$$R_{eff} = \frac{K_{min,i}^{eff}}{K_{max,i}^{eff}} = \frac{K_{min,i} - K_R}{K_{max,i} - K_R} \quad (5.2.5)$$

since the range in stress-intensity factor is unchanged by the uniform reduction. Thus, for the i th load cycle, the crack growth increment (Δa_i) is:

$$\Delta a_i = \frac{da}{dN} = f(\Delta K, R_{eff}) \quad (5.2.6)$$

For many of the early calculations with the Willenborg model, it was assumed that R_{eff} was never less than zero and that $\Delta K = K_{max,i}^{eff}$ when R_{eff} was calculated to be less than zero. Recent evidence, however, supports the calculations of R_{eff} as given by Equation 5.2.5 and the use of a negative stress ratio cut-off in the crack growth rate calculation (Equation 5.2.6) for more accurate modeling of crack growth behavior.

Another problem that was identified with the original Willenborg model was that it was always assigned the same level of residual stress effect independent of the type of loading. In particular, it can be noted (through the use of Equation 5.2.3 and 5.2.4) that the model predicts that $K_{max,i}^{eff} = 0$, and therefore crack arrest, immediately after overload if $K_{max}^{OL} = 2 K_{max,i}$. That is, if the overload is twice as large as (or larger than) the following loads, the crack arrests. To account for the observations of continuing crack propagation after overloads larger than a factor of two or more, Gallagher and Hughes⁽⁵⁷⁾ introduced an empirical (spectra/material) constant into the calculations. Specifically, they

suggested that

$$K_R = \phi K_R^W \quad (5.2.7)$$

where ϕ is given by

$$\phi = \frac{1 - \frac{K_{\max,th}}{K_{\max,i}}}{S^{OL} - 1} \quad (5.2.7a)$$

There are two empirical constants in Equation 5.2.7a: $K_{\max,th}$ which is the threshold stress-intensity factor level associated with zero fatigue crack growth rates (see Section 5.1.3), and S^{OL} which is the overload (shut-off) ratio required to cause crack arrest for the given material. This ratio is affected by the type of underload/overload cycle as well as the frequency of overload cycle occurrence. Results of some life predictions made using what has become to be called the "Generalized" Willenborg model are presented in Figure 5.2.8 (Reference 59).

One of the earliest crack-closure models developed for aircraft structural applications is attributed to Bell and Creager⁽⁵²⁾. The closure model makes use of a crack-growth-rate equation based on an effective stress-intensity range ΔK_{eff} . The effective stress intensity is the difference between the applied stress intensity and the stress intensity for crack closure. Some examples of predictions made with the model are presented in Figure 5.2.9. The final equations contain many experimental constants, which reduces the versatility of the model and make it difficult to apply. Recent work by Dill and Saff⁽⁶⁰⁾ shows that

the closure model can be simplified to the point of practicality while retaining a high level of accuracy in life prediction.

Crack-growth calculations are the most useful for comparative studies, where variations of only a few parameters are considered (i.e., trade-off studies to determine design details, design stress levels, material selection, etc.). The predictions must be verified by experiments. (See Analysis Substantiation Tests in Section 7.3). Example calculations of crack-growth curves will be given in Section 5.4.

Other factors contributing to uncertainties in crack-growth predictions are:

- Scatter in baseline da/dN data
- Unknowns in the effects of service environment
- Necessary assumptions on flaw shape development (Section 5.4.4)
- Deficiencies in K calculation (Section 5.4.4)
- Assumptions on interaction of cracks (see 5.4.5)
- Assumptions on service stress history (see 5.3).

In view of these additional shortcomings of crack-growth predictions, the shortcomings of a retardation model become less pronounced; therefore, no particular retardation model has preference over the others. From a practical point of view, the Generalized Willenborg model is easier to use since it contains a minimum number of empirical constants.

5.2.5 Integration Routines

The determination of a crack growth increment due to any particular stress history depends upon an integration of the growth rate relation such as given by equations 5.1.2-5.1.4. Four general methods are available for this purpose.

The first approach is based on extensive spectrum crack growth data. Tests which incorporate the important stress levels, part geometry, crack shape details and loading sequences are run to determine the effect of the particular variables of interest on the component life.

A second approach, and one used extensively, is the cycle-by-cycle crack growth analysis where crack rates are integrated over the crack length of interest as a function of stress and crack length (61-62).

A third approach is based on the statistical stress-parameter-characterization. The actual service stress histories are replaced with equivalent constant amplitude stress histories for the analytical prediction of component life (17).

A fourth approach, recently developed, utilizes a crack-incrementation scheme to analytically generate "miniblock" crack growth rate behavior prior to predicting life. It combines some features of the first three methods (61-63).

The application of the second through fourth approaches requires methods for integrating the crack growth rate relations requires the knowledge of the following items:

- (1) An initial flaw distribution,
- (2) The aircraft loading spectrum,
- (3) Constant amplitude crack growth rate material properties,
- (4) Crack tip stress-intensity factor analysis,
- (5) A damage integrator model relating crack growth to applied stress and which accounts for load-history interactions,
- (6) The criteria which establishes the life-limiting end point of the calculation.

These items are described in detail in Section 1.4 of this handbook. The basic damage integrating equation is also presented as equation 1.4.1 but is repeated here:

$$a_{cr} = a_o + \sum_{j=1}^{t_f} \Delta a_j \quad (1.4.1R)$$

where Δa_j is the growth increment associated with the j^{th} time increment, a_o is the initial crack length, a_{cr} is the critical crack length and t_f is the life of the structure. The determination of t_f is the objective of this equation.

Of the integration methods described above, the second and third are most frequently used. The generation of the data required for the first method is very expensive and is only recommended for extremely critical parts.

The second method, the cycle-by-cycle integration method, uses a type of integrating relation whereby the effect of each cycle is considered separately. This is generally the least efficient method, but if the spectrum under consideration cannot be considered as statistically repetitive, it may be the most accurate of the analytical methods. This method is covered in detail in subsection 5.2.6.

The third method, using a statistical characterization of a crack growth parameter is based on the similarity of certain variable amplitude crack growth behavior to the constant amplitude functional relationship;

$$\frac{da}{dF} = C (\bar{K})^P \quad (5.2.8)$$

where (da/dF) is the flight-by-flight crack growth behavior and \bar{K} is a stress-intensity factor parameter that is derived using the product of a statistically characterizing stress parameter $(\bar{\sigma})$ and the stress-intensity factor coefficient (K/σ) , i.e.,

$$\bar{K} = \bar{\sigma} \cdot (K/\sigma) \quad (5.2.9)$$

The statistically characterizing parameters that have been employed in the past to some success are derived using a root mean square (RMS) or similar type analysis of the stress range or stress maximum. The crack growth behavior of both fighter and transport aircraft stress histories have been described using various forms of equation 5.2.8.

One might imply from equations 5.2.8 and 5.2.9 that the use of a single stress characterizing parameter for stress histories would allow one to utilize equivalent constant amplitude histories to derive the same crack growth rate behavior. Unfortunately, relating constant amplitude behavior to variable amplitude behavior has not been that successful.

The damage integration Equation (1.4,1R) is now expressed for the flight as

$$a_k = a_o + \sum_{j=1}^{N_f} \Delta a_j \quad (5.2.10)$$

where N_f is the number of flights corresponding to crack length a_k , and Δa_j is computed from Equation 5.2.8 evaluated for the given conditions. The parameters C and p of Equation 5.2.8 are determined by a least squares curve fit to previously determined data. The value that comes from employing the third method comes from the fact that a somewhat limited variable amplitude data base might be extended to cover other crack lengths, structural geometry, or stress level differences.

The fourth approach provides an analytical extension of the cycle-by-cycle analysis to predict flight-by-flight crack growth rates. In essence, this approach combines some of the best features of the other three methods. The basic element in this analysis is what is referred to as a miniblock which is taken to be a flight (includes takeoff, landing and all intermediate stress events) or a group of flights. The approach hinges on the identification of the statistically repeating stress group that approximates the loading and sequence effects for the complete spectrum.

The basic damage integration equation can be written in the miniblock form to compute the crack increment (Δa) due to application of N_G Flights:

$$\Delta a = a_k - a_o = \sum_{j=1}^{N_G} \sum_{i=1}^{N_j} (\Delta a_i) \quad (5.2.11)$$

where there are N_j stress cycles in the j^{th} flight. The most direct method for applying the equation is called the simple crack-incrementation-miniblock approach. Successive crack increments are obtained at successively larger initial-crack-lengths. Figure 5.2.10 illustrates this method. The resulting values of $\Delta a/\Delta F$ and the corresponding K_{max} values are fit with a curve of the of the desired type, usually similar to Equation 5.2.8, which can now be used to compute life.

An alternate method, called the statistical crack-incrementation-miniblock approach, is illustrated in Figure 5.2.11. This method allows evaluation of the effect of miniblock group-to-group variation in the crack growth rate behavior. A number of different miniblock groups are used at each initial crack length. A curve can be fit through the mean $\Delta a/\Delta F$ vs. \bar{K}_{max} values and the variation of $\Delta a/\Delta F$ at each K_{max} can be observed. Confidence limits can be determined for each set of data.

The fourth approach provides a more efficient integration scheme than the cycle-by-cycle analysis. However, its use is determined by the type of stress history that has to be integrated.

In summary, there are a number of integration schemes available. These schemes all employ modeling approaches based on either limited or extensive variable amplitude data bases so that the analyst might properly account for loading and sequence effects in the most direct and most accurate manner.

5.2.6 Cycle-by-Cycle Analysis

Several computer programs are available for general use that include one or more of the retardation models in a crack-growth-integration scheme. The most well known of these is CRACKS^{*(64)}, the latest version of which should be used. The user has the option of using any of the three retardation models discussed in the previous section. Most airframe companies, however, have their own inhouse computer program for performing variable-amplitude fatigue life calculations.

In general, the crack-growth-damage-integration procedure consists of the following steps schematically outlined in Figure 5.2.12.

- Step 1. The initial crack size follows from the damage tolerance assumptions as a_1 . The stress range in the first cycle is $\Delta\sigma_1$ (See Section 5.4). Then determine $\Delta K_1 = \beta\Delta\sigma_1\sqrt{\pi a_1}$ by using the appropriate β for the given structural geometry and crack geometry. (Computer programs frequently have a library of stress-intensity factors or schemes for tabular data input).
- Step 2. Determine $(da/dN)_1$, at ΔK_1 from the $da/dN - \Delta K$ baseline information, taking into account the appropriate R value. (The $da/dN - \Delta K$ baseline information may use one of the crack-growth equations discussed in Section 5.1.3. The computer program may contain options for any of these equations, or it may use data in tabular form and

* Available through AFWAL/FIBEC, Fatigue and Fracture Group.

interpolate between data points). The crack extension Δa_1 in cycle 1 is

$$\Delta a_1 = \left(\frac{da}{dN} \right)_1 \times 1 .$$

The new crack size will be $a_2 = a_1 + \Delta a_1$.

Step 3. The extent of the yield zone in Cycle 1 is determined as

$$Y_2 = a_{oL} + r_{pL}, \text{ where } a_{oL} = a_1$$

with $r_{pL} = \frac{1}{2\pi} \left(\frac{K_{\max,1}}{\sigma_{ys}} \right)^2$ for plane stress

or $r_{pL} = \frac{1}{4\sqrt{2}\pi} \left(\frac{K_{\max,1}}{\sigma_{ys}} \right)^2$ for plane strain.

Step 4. The crack size is now a_2 . The stress range in the next cycle is $\Delta \sigma_2$. Calculate ΔK with $\Delta K_2 = \beta \Delta \sigma_2 \sqrt{\pi a_2}$.

Step 5. Calculate the extent of the yield zone

$$Y_{22} = a_2 + r_{p2} .$$

Step 6. If $Y_{22} < Y_2$ calculate C_p according to Equation 5.2.2 when using the Wheeler model, or calculate K_{\max}^{eff} or K_{\min}^{eff} and R_{eff} according to Equations 5.2.3, 5.2.4, 5.2.5, and 5.2.7 when using the Generalized Willenborg model. Skip Steps 7 and 8, go to Step 9.

Step 7. If $Y_{22} \geq Y_2$, determine $(da/dN)_2$ from ΔK_2 . Determine the new crack size

$$a_3 = a_2 + \Delta a_2 = a_2 + \left(\frac{da}{dN} \right)_2 \times 1 .$$

Step 8. Replace Y_2 by Y_{22} which is now called Y_2 . Replace $a_{oL} = a_1$ by $a_{oL} = a_2$. Skip Step 9, go to Step 10.

Step 9. When using the Wheeler model, determine the amount of crack growth on the basis of ΔK_2 from the $da/dN - \Delta K$ data. Find the new crack size from

$$a_3 = a_2 + \Delta a_2 + C_p \left(\frac{da}{dN} \right)_2 \times 1.$$

When using the Generalized Willenborg model, determine the amount of crack growth using the ΔK and R_{eff} value determined in Step 6 from the $da/dN - \Delta K$ data. Determine the new crack size as

$$a_3 = a_2 + \Delta a_2 = a_2 + \left(\frac{da}{dN} \right)_2 \times 1.$$

Step 10. Repeat Steps 4 through 9 for every following cycle, while for the i th cycle replacing a_2 by a_1 and a_3 by a_{i+1} .

This routine of cycle-by-cycle integration is not always necessary.

The integration is faster if the crack size is increased stepwise in the following way.

- At a certain crack size, the available information is a_i , a_{oL} , Y_2 .
- Calculate Δa_i for the i_{th} cycle in the same way as in Steps 4 through 9.
- Calculate $\Delta a_{j+1}, \dots, \Delta a_j, \dots, \Delta a_n$ for the following cycles but let the current crack size remain a_i constant. This eliminates recalculation of β every cycle.

- Calculate Y_{2k} for every cycle. If $Y_{2k} > Y_2$, then replace Y_2 by Y_{2k} and call it Y_2 . Then replace a_{oL} by a_i and call it a_{oL} .
- Sum the crack-growth increments to give

$$\Delta a = \sum_{k=1}^j \Delta a_k.$$

- Continue increasing j until Δa exceeds a previously determined size or until $j = n$ and the cycles are exhausted. Then increment the crack size by

$$a = a_i + \Delta a,$$

and repeat the procedure.

A reasonable size for the crack-growth increment is $\Delta a = \frac{1}{20} a_i$; this choice of increment typically keeps the change in K small. It can also be based on the extent of the yield zone, e.g., $\Delta a = \frac{1}{10} (Y_2 - a_i)$. The advantage of the incremental crack-growth procedure is especially obvious if series of constant-amplitude cycles occur. Since the crack size (a_i) is fixed, the stress intensity does not change. Hence, each cycle produces the same amount of growth. This means that all n constant-amplitude cycles can be treated as one cycle to give

$$\Delta a = n \frac{da}{dN}.$$

The integration scheme is a matter of individual judgement, but may be dictated by available computer facilities.

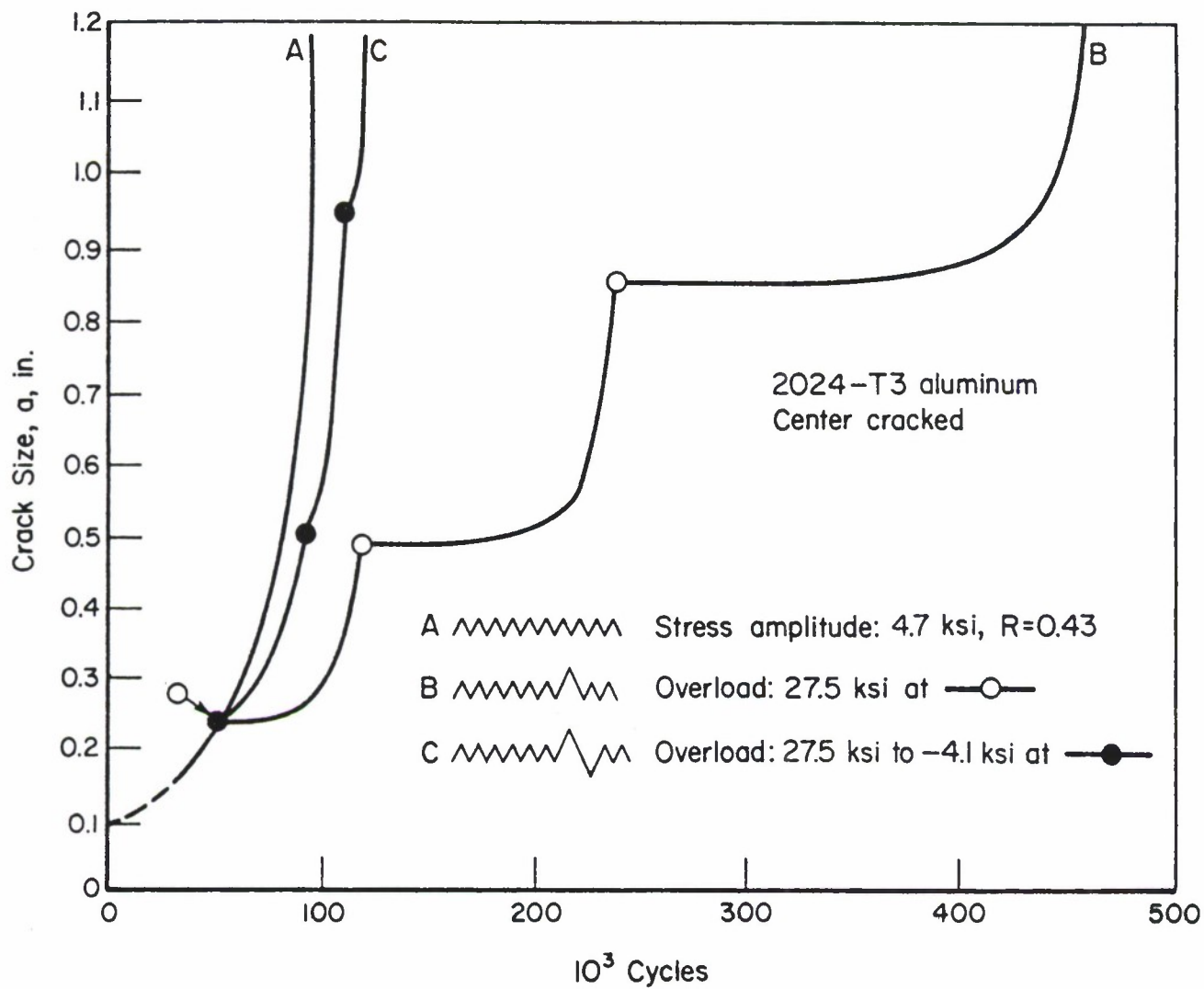


Figure 5.2.1. Retardation Due to Positive Overloads, and Due to Positive-Negative Overload Cycles (Ref. 40).

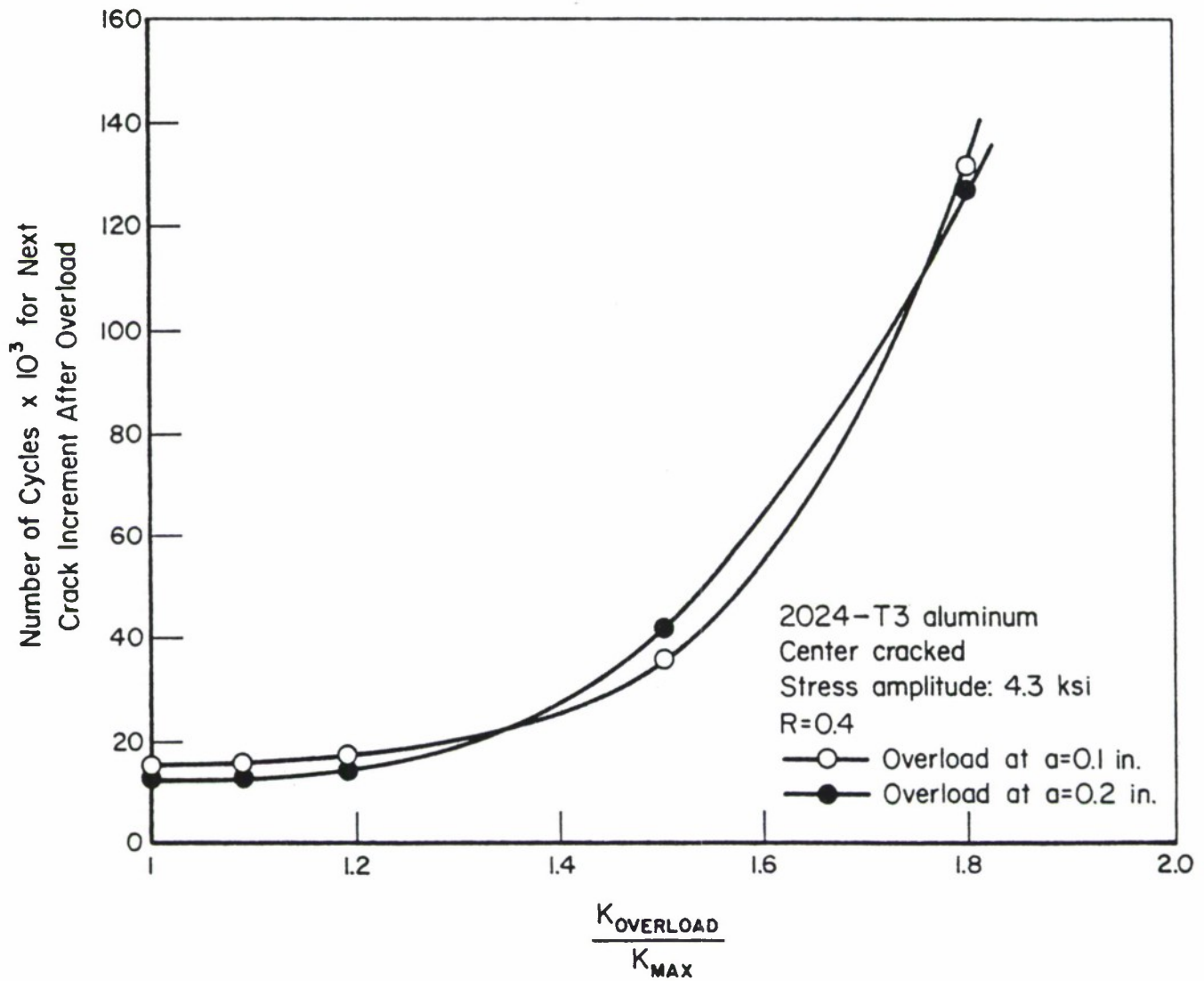


Figure 5.2.2. Effect of Magnitude of Overload on Retardation (Ref. 27).

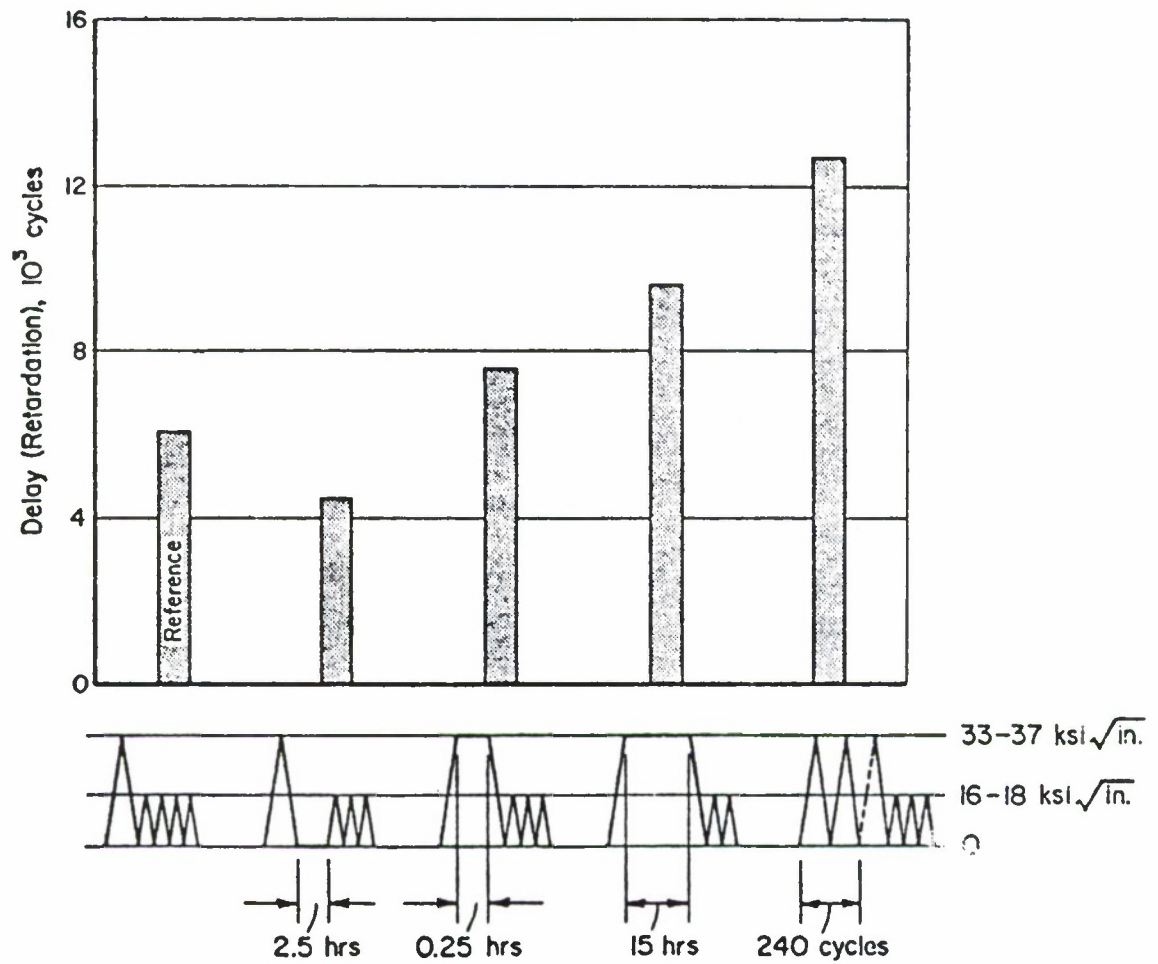


Figure 5.2.3. Retardation in Ti-6V-4Al; Effect of Hold Periods and Multiple Overloads (Ref. 42).

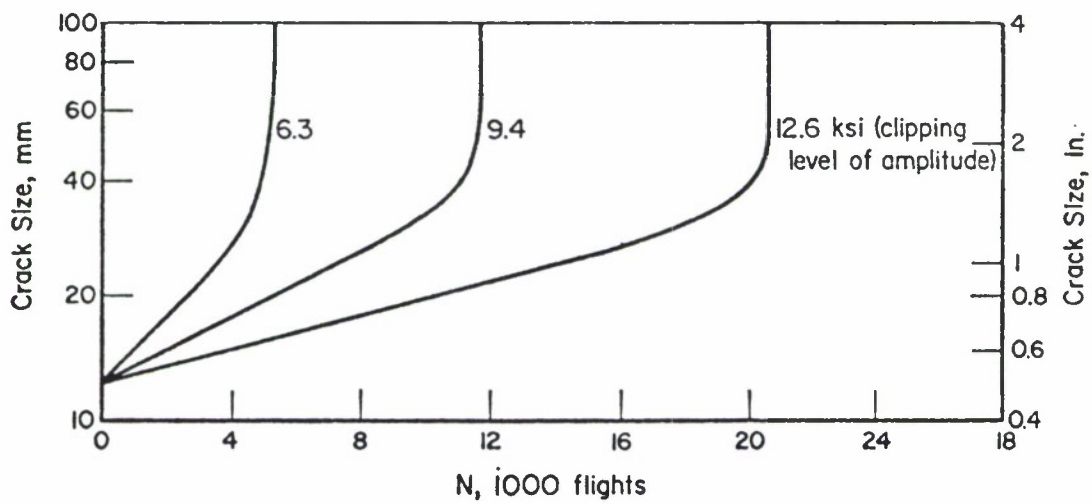


Figure 5.2.4. Effect of Clipping of Higher Loads in Random Flight-by-Flight Loading on Crack Propagation In 2024-T3 Al Alloy (Ref. 43, 44).

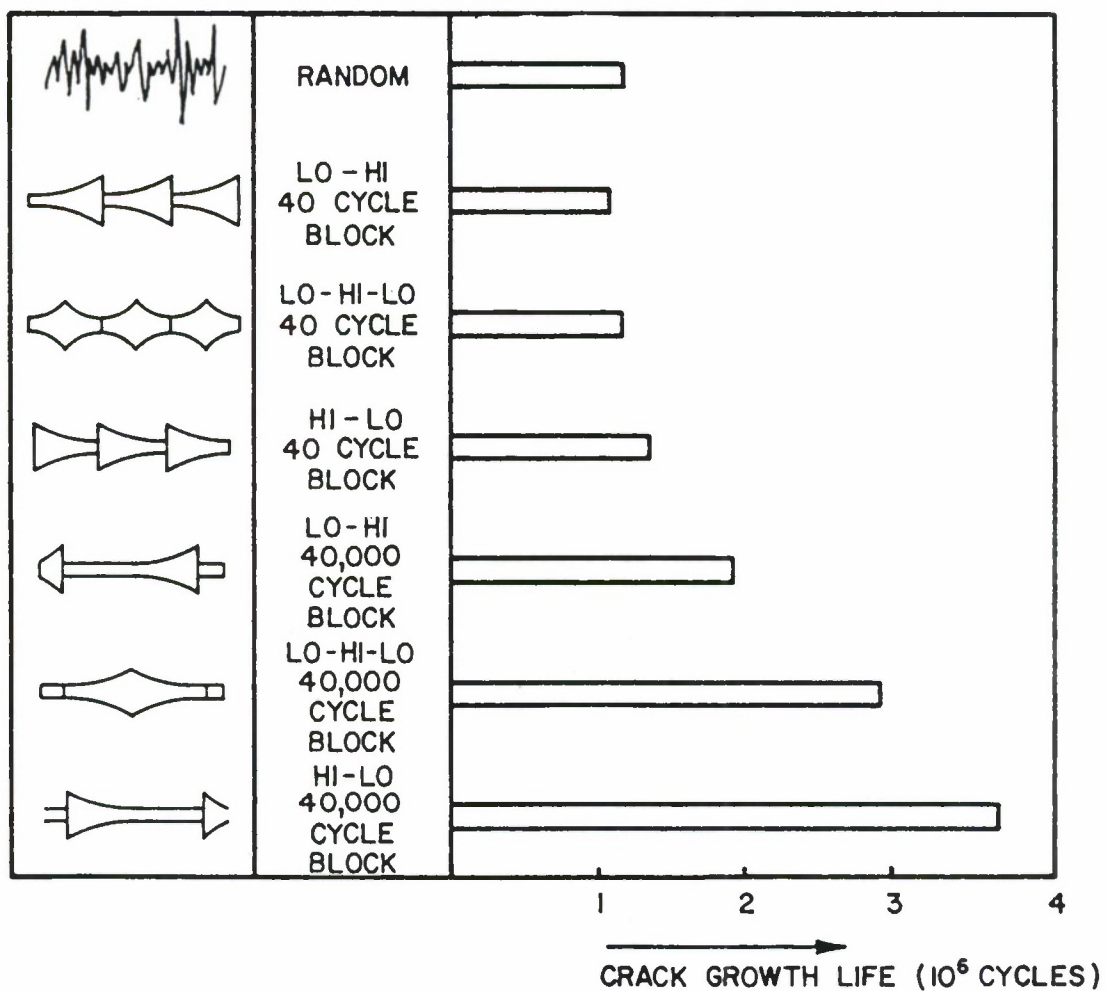
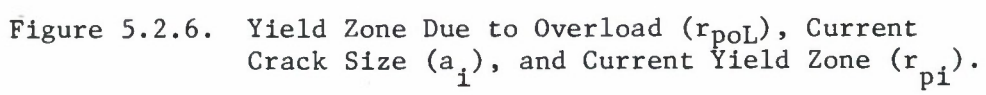


Figure 5.2.5. Effect of Block Programming and Block Size On Crack Growth Life (All Histories Have Same Cycle Content) Alloy: 2024-T3 Aluminum (Ref. 27).



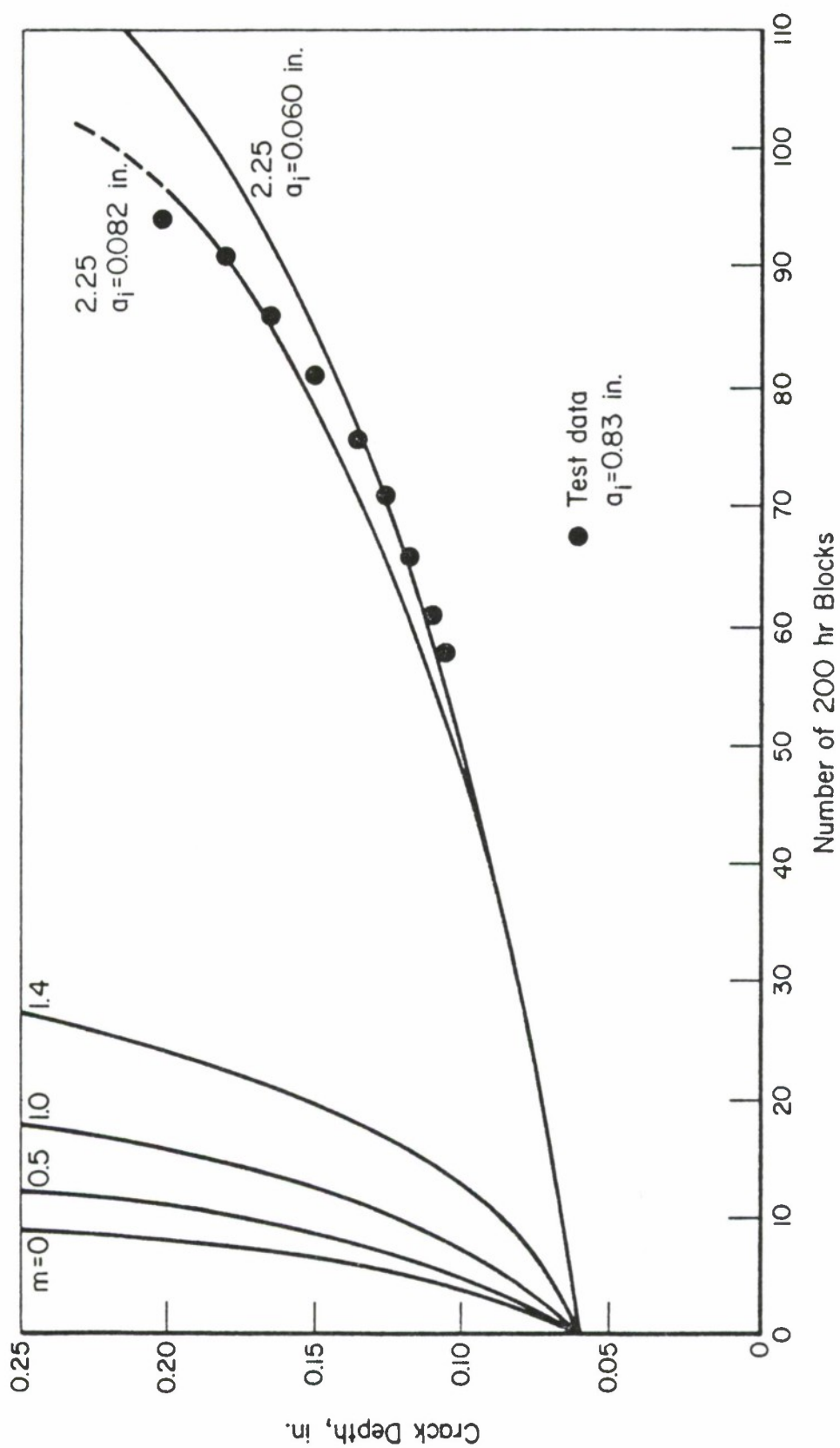


Figure 5.2.7. Crack Growth Predictions by Wheeler Model Using Different Retardation Exponents (Ref. 45).

8.3 OPERATIONAL IMPLICATIONS OF TRACKING SCHEMES

Figure 8.3.1 shows an overview of the various elements which compose the IAT system. The selection of specific methods to implement each of the elements should consider the effects on the system. Of concern should be the required system accuracy and the extent of the processing which is required.

8.3.1 Accuracy Requirements as a Parameter

One of the items which is not usually discussed in detail is the accuracy requirement of the tracking system. It has been postulated (Reference 4) that "The perfectly accurate tracking system is that which can reproduce exactly the output of the 'Best' computational model of the DADTA." This reference then proceeds to define an error analysis model and to determine which elements of the tracking system are major contributions to error.

The analysis is defined around three major causes of error in the estimate of the projected months to a maintenance action. They are the variability in average flying rates per month, the variability of average usage severity, and the variability in the estimate of the baseline age due to the inability to exactly calculate the crack length at the critical point ⁽⁹⁾. The first two quantities relate to the variation from the average of any particular aircraft. Over a long enough period these deviations should begin to show a stable distribution among the airplanes. Figures 8.3.2 and 8.3.3, from Reference 9, show examples of the variability of these quantities. The estimation of the variability of crack length estimate is the most difficult to make. Figure 8.3.4 ⁽⁹⁾ shows an example of how this error may affect the baseline hours and thus the remaining time to a maintenance action. This is a very important

consideration since it can be expected to increase as the current crack increment is a function of prior crack length.

This brief description of the causes of variability in projecting life is meant to alert the designer of an IAT system to some of the concerns that must be considered. However, the IAT system should not be more accurate than necessary. The required accuracy should be based on the risk involved in not scheduling an aircraft for a maintenance action within a specified time of projected crack size. Here, the unacceptable risk is usually not the loss of an airplane, but an unrepairable crack which requires replacement of a part. To be compared with this risk is the increased cost of requiring inspections much sooner than is necessary. The economic system will balance these two considerations to find a minimum cost.

8.3.2 Effect of Processing Method on Results

The method of processing the IAT data should also be selected so as to be consistent with the data collection and the desired results. Reference 3 recommends the combinations of data collection and analysis methods listed in Table 8.3.1.

Another consideration should be the relative ease of accounting for missed data. This, of course, varies with the system used. Since aircraft flight hours are a known quantity and since mission identification is also usually known, some method of equivalent mission analysis is a reasonable gap filler. It is acknowledged that in general the gap filled data is not as accurate as the basic data, but the gap filling should be done in a fashion to at least be conservative.

TABLE 8.3.1

RECOMMENDED IAT METHODS
(REFERENCE 3)

<u>Method</u>	<u>Data Collection</u>	<u>Tracked Parameter</u>	<u>Analysis</u>
1	Aircraft Records	Flt hrs & Landings	Percent Hrs/Ldgs
4	Pilots Log	Time by Data Block	Parametric Crack Growth Tables
5	Pilots Log	Equivalent Missions	Mission Crack Growth Tables
10	Counting Accel.	Equivalent n_z Spectra	Normalized Crack Growth Curves
11	Mechanical Strain Recorder	Equivalent Stress Spectra	Normalized Crack Growth Curves

8.3.3 Criteria for Selection of an IAT System

A number of criteria for selection of an IAT system can be formulated. Table 8.3.2 presents some which have been developed. These items have applicability to all types of IAT systems. Some of them appear to be more applicable to those systems requiring onboard hardware, but all should be considered.

It is recognized that these criteria cannot be absolutes, that is, there must be an associated degree of compliance. The degree of compliance to be sought must be considered for each system. It is in this area that various systems can be compared and the opportunity for trade-off studies exists. This table is not considered to be an exhaustive list. The system designer should add an item which may be desirable or required for a specific IAT system.

TABLE 8.3.2

CRITERIA FOR THE SELECTION OF AN
INDIVIDUAL AIRCRAFT TRACKING SYSTEM

- The system shall provide for rank ordering of aircraft according to usage severity
- The system output shall be related to the aircraft maintenance scheduling
- The system shall indicate relative damage accumulation rates
- The system shall continue to operate under all variations of aircraft usage
- The system shall give a repeatable result under the same usage experience
- The system shall not degrade the aircraft serviceability
- Failure of the system shall not affect the aircraft's performance
- The system shall be applicable to a variety of initial conditions
- The system shall not be sensitive to installation variability
- The system shall provide easily usable results

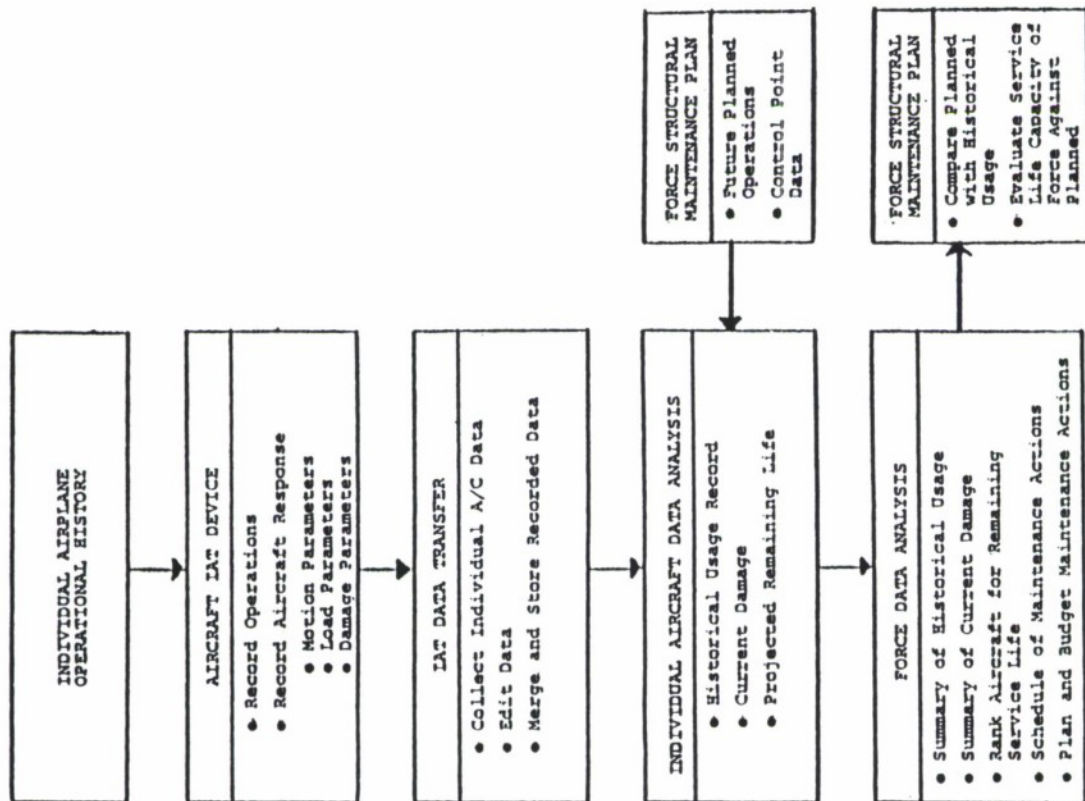


Figure 8.3.1.1. The Various Elements that are Inherent in IAT Systems.

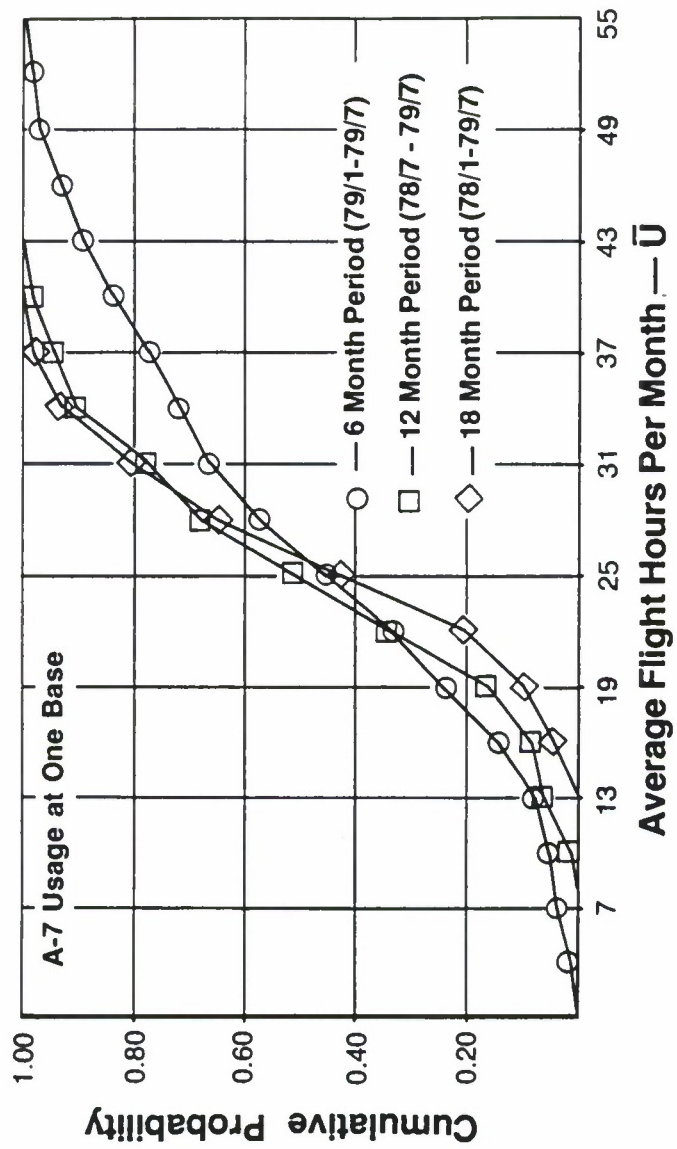


Figure 8.3.2. Example of Cumulative Distribution of Average Flying Rates.

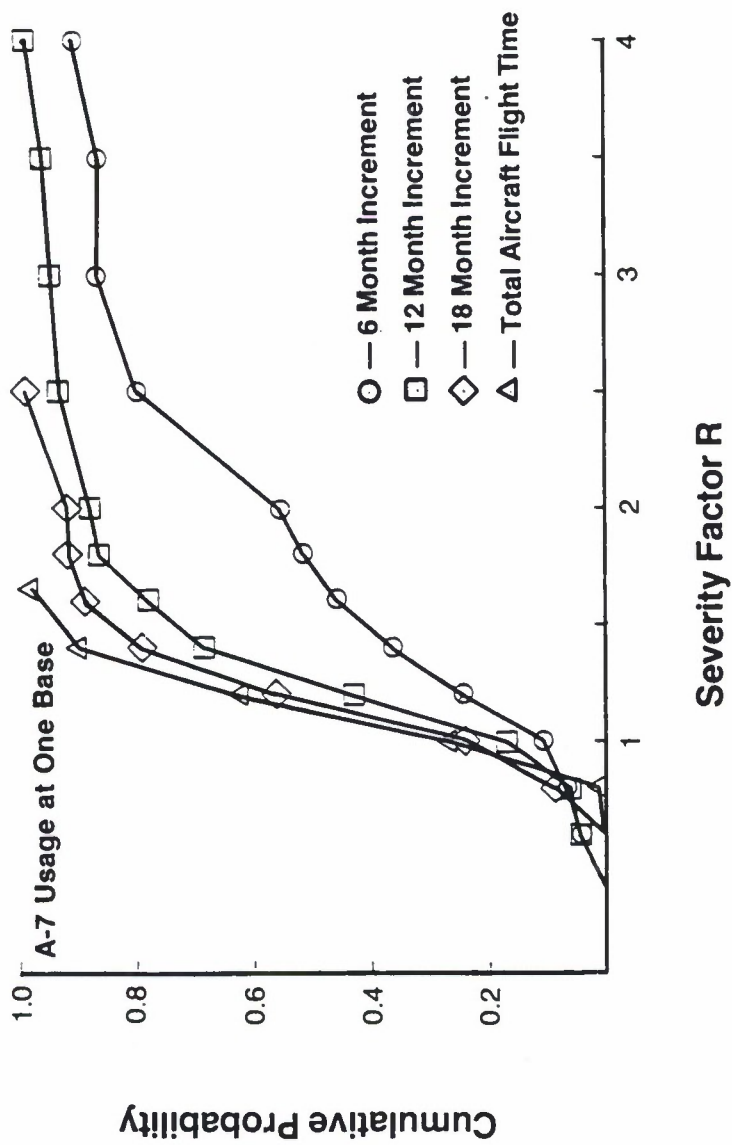


Figure 8.3.3. Example of Cumulative Distribution of Severity Factor.

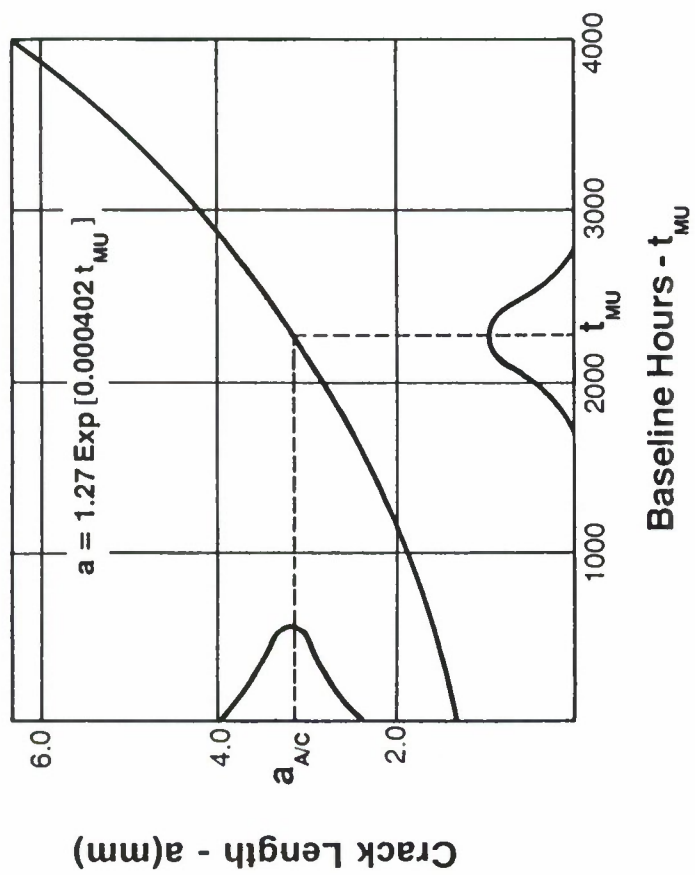


Figure 8.3.4. Example of the Effect of Error in Crack Length on the Error in Baseline Hours.

8.4 THE RELATIONSHIP BETWEEN USAGE AND DAMAGE

The parameter of concern in a fracture mechanics based tracking system is the length of a crack at the analysis location. This is defined as the damage to the structure caused by the accumulated usage. At the present time, there is no one proven method which gives a direct reading of crack length. All current methods require some sort of indirect determination of crack length. This is usually through measurement of parameters which are representative of the load cycles or the stress cycles acting on the structure. These in turn can be converted to crack length through a growth incrementation method. Some of these methods in current use are described in this section.

8.4.1 Types of Usage Descriptions

The usage of a particular aircraft can be described in a variety of ways. The simplest is to use a group of preanalyzed mission types and then merely to make a record of the mission types as they are flown. This requires the assumption that mission load sequences are insignificant to the crack growth problem. A variation of this method is to assume that missions are repeated but that other information, in addition to a mission name, is required before an identification can be made. This requires such data as concurrent values of airspeed, altitude, and weight with associated times. These parameters are recorded each time one of them makes a significant change. Evaluation of these patterns leads to an assignment of a particular mission. A very similar description can be obtained by assigning flight segment identifications as the flight data varies rather than on a complete mission basis. All of these methods use a

predetermined crack growth computation for each mission or segment. After either the mission or the segment is identified the load sequence is assumed to be known.

Moving in the direction of increasing complexity the recording of load indicators may be necessary. Parameters such as load factor, strain and angular rates can be recorded and translated into load sequences. Usually additional data such as configuration and/or take-off weight is also necessary for an adequate description. Such data is usually processed by summing the number of occurrences at given parameter range levels and converting into loads or stresses. An alternate technique is to compare the summed and blocked results to various predetermined spectra and select the one most closely approximated for the analysis.

More complicated methods involve the time history recording of several load indicating parameters and computing a load and stress sequence for each flight. This should only be done if the other methods do not yield adequate results or if the computation can be done in a cost-effective manner. Some variation of this technique of determining usage is usually discussed in relation to using a microprocessor-based tracking method. The mechanical strain recorder (MSR) is a variant of this technique. However, only one parameter, strain, is recorded and typically at only a single location.

The method for determining usage is influenced by the desired frequency of data retrieval. Methods which require relatively long times to retrieve the data, such as recorder unloading or reading of counters are usually used if individual flight data is not required. Pilot logs and forms can be

efficiently retrieved after each flight. Examples of two types of data retrieval forms are shown in Figures 8.4.1 and 8.4.2. Figure 8.4.1 shows a flight data and counter form to be filled out after each flight. Figure 8.4.2 shows a flight data form used for mission analysis, which is also filled out after each flight.

Figure 8.4.3 shows various data transcription methods in use at the processing facility to handle various types of IAT data coming from the field.

8.4.2 Usage to Damage Schemes Summarized

The conversion of the aircraft usage data to damage accumulation as described by the crack length at the control point requires the integration of the crack growth rate information. Chapter 5 of this handbook presents a complete description of the basic elements in the calculation of crack growth increments. The different applications of this calculation to the tracking function can be categorized by how much of the effort is precomputed and used in the form of parametric tables. In general, the less detailed the tracking data, the more extensive the use of precomputed crack growth tables.

Five damage integration schemes will be described in this handbook. They are listed in Table 8.4.1.

TABLE 8.4.1
DAMAGE INTEGRATION SCHEMES

- Mission-by-Mission Integration (Figure 8.4.4)
- Mission-Segment-by-Mission-Segment Integration (Figure 8.4.5)
- Time In-Usage Category Integration (Figure 8.4.6)
- Strain History Integration (Figure 8.4.7)
- Damage Parameter Integration (Figure 8.4.8)

8.4.2.1 Mission-By-Mission Integration

Figure 8.4.4 describes the method of determining control point crack growth by a mission identification scheme. The pilot log data is analyzed to determine the mission assignment for a particular flight. This may vary from a simple mission identification on the log to a rather complicated pseudo time history of flight activities. Figure 8.4.2 showed a form capable of handling the more complicated mission descriptions. Such data is analyzed in the processing program to identify the mission. As many missions as considered necessary may be used. It is not uncommon to use several hundred missions if the variation of weight, altitude, weight and flight activity is wide.

Each mission used in the analysis has been previously characterized as to all details of the flight as indicated in the second box of Figure 8.4.4. A detailed cycle-by-cycle stress history is derived for the mission and a crack growth rate chart or table is developed based on the crack length. If retardation is to be considered in the analysis, the initial plastic zone size is also an input. As the flight-by-flight analysis continues,

the final crack length and the final plastic zone size for a flight becomes the input for the next flight and the incremental growth is determined as indicated in the figure. This operation is done for each control point and the crack is incremented flight-by-flight.

This method provides a very rapid method for converting from usage data to crack length. The disadvantage may be the large number of missions required to adequately describe the aircraft usage. Its use is most efficient in the case of cargo/transport aircraft and large bombers which experience relatively few maneuvering loads and where the majority of load cycles are due to atmospheric turbulence which can be characterized by time in altitude bands.

8.4.2.2 Mission-Segment-By-Mission-Segment Integration

In cases where it is not convenient or practical to obtain parametric crack growth tables for the entire mission, it may be possible to consider the mission as a series of identifiable segments. Figure 8.4.5 shows the series of steps which comprise this method. The pilot log data is used to define which of a series of mission segments may be assigned to describe the flight. Each segment is characterized by a stress exceedance curve or table which is usually also presented as a function of the flight data parameters such as airspeed, altitude and weight. Both maneuver and turbulence induced stresses may be used. From the time spent in each segment a number of stress occurrences at each level is obtained. This is formed into a stress sequence and is input to a crack growth calculation program. Crack growth is computed sequentially according

to segment occurrence and a crack length for the flight is determined for each control point.

This method is complicated and usually requires substantial amounts of calculation effort. However, it provides a more flexible analysis of the flight data and may provide more accurate results than some other methods.

8.4.2.3 Time-In-Usage-Category Integration

This method, illustrated in Figure 8.4.6, requires the logged data to be obtained in the form of coincident values of flight data in ranges of airspeed, altitude, weight, linear acceleration and angular acceleration. Each such combination is called a usage category or data block. The exact combination of parameters required depends on the aircraft and on the control point location. Precomputed crack growth rates for each usage category are then converted into crack growth per flight. Retardation can be considered if desired by including it in the growth rate tables as a function of an additional input, such as the previous plastic zone size, or other parameters that measure the effect of prior history.

This method requires a large amount of computational time if many usage category blocks are used. However, it may be a good method for aircraft which have had to categorize missions and flight profiles which show large variations, and the mission or mission segment method is not adequate.

8.4.2.4 Strain-History Integration

Figure 8.4.7 outlines a method which uses strain history data as the usage indicator. The figure assumes that the data is being recorded on a mechanical strain recorder (MSR). However, the procedure can be used with any method of strain history recording.

The method depends on the use of the normalized crack growth curves discussed in Section 8.2. Initial normalized crack growth curves are computed for each of a series of selected stress spectra, for each critical point. Also computed are normalized usage spectra. This observed data is also normalized and used to determine interpolation factors to be used with normalized crack growth curves. This leads to an increment crack growth for the control point of interest. This procedure is repeated for each control point.

This technique has the potential of being one of the "most accurate" tracking systems at a single location. This technique eliminates the need for recording other parameters and is less time consuming than if the strain cycles were analyzed on a cycle-by-cycle basis.

8.4.2.5 Damage Parameter Integration

The method of integration outlined in Figure 8.4.8 is used when a damage indicator parameter is used as the measure of the usage. The figure is drawn showing the use of the normal load factor, n_z , as the damage parameter. This is the most common quantity, but any other parameter can be used for which a relation between it and crack growth can be developed. The method relates the spectra of known sequences to the observed spectra and based on the use of two normalized curves. The first

normalized curve is used to correlate crack growth at different locations when exposed to the same stress spectrum and the second is used to correlate crack growth due to two stress spectra at the same location. This was illustrated in Figure 8.2.1. These assumptions allow tracking only one location and accounting for variations from a baseline spectrum.

The figure also uses a Damage Index instead of Flight Hours to specify when maintenance actions are required. This is a device to assign an arbitrary number to the operational limit of a particular spectrum. It provides a scaling factor for the abscissa of the normalized crack growth curve. Now the time to maintenance action is obtained from the damage index curve. A linear relation for the damage index in terms of the measured load indicator values is obtained from test data. Known load spectra are used to test a model of the critical location. The observations of the times to achieve a critical crack length for multiple tests are related to the damage index and the coefficients of the following equation are determined

$$D.I. = C_1X_1 + C_2X_2 + C_3X_3 + C_4X_4.$$

This is a four-level equation in terms of the X_1 level of the n_z occurrences during a time period.

The accuracy of this method depends upon the correlation between the measured parameter and the stress at the original point. The load factor, n_z , for example, is quite well correlated with wing root stresses but very slightly correlated with vertical stabilizer stresses.

8.4.3 Individual Systems Compared

The methods of usage descriptions and damage calculation discussed individually in the preceeding sections require some comparison reviews before a selection can be made for a particular application. The following paragraphs discuss some of the comparisons that should be made and some of the criteria to be used in judging the comparisons. It is observed that almost all of the systems previously described either are in current use or have been proposed, or have been in use in the past.

8.4.3.1 Stand-Alone Versus Continuously Interacting Systems

A stand-alone system is defined as using one type of data collection and usage description which can be directly transformed into the damage. Such a system would be a counting accelerometer from which the exceedance data is used as input to an algorithm which directly computes damage increment from a previously determined equation as a function of the occurrences at each measured acceleration level.

To make this an interacting system a pilot log might be included which tabulates such things as take-off weight and external store configuration. Now a more complicated analysis can be made where the damage relation can also be based on actual weight and configuration. Such a system is in fact quite common for tracking fighter/attack/trainer type aircraft.

A more complicated system might require time history recording of parameters such as airspeed, altitude and normal acceleration and be combined with a log

sheet giving weights and configurations. The use of this system requires processing the flight data, integrating it with the log sheet data and using the combined data to compute damage.

As the degree of interaction increases so does the processing complexity and the cost. However, it is expected that accuracy of damage computation also increases. The stand alone system usually requires more assumptions for the total usage characteristic while the interacting system does not.

The relation of the tracking system to the loads/environmental spectral survey (L/ESS) needs to be considered. The L/ESS provides the complete data used to characterize the various mission usage upon which the IAT is based. The more information obtained in the IAT, the more accurately the L/ESS data can be used. For example, if the L/ESS has developed mission data based on time spent in various mission segments, then, if the IAT collects enough data to allow identification of mission segments, the L/ESS data can be fully utilized. If this is not the case then an approximation must be made of the time spent in various segments for a particular mission.

8.4.3.2 Simple Vs. Complex Algorithms

The selection of an algorithm to compute the crack growth per unit time determines the amount of data and processing required. Simple systems which use only a few parameters require more initial development effort for a parametric damage accumulation table or equation. More complex systems which utilize a cycle-by-cycle analysis on each flight require more data and more processing time per flight. If this complexity is decided upon for

the IAT then it should be justified by either a very sensitive structure or by a usage pattern which cannot be easily characterized by the L/ESS, such as a constantly changing usage pattern. Fortunately, most aircraft are not in this category.

8.4.3.3 Level of Accuracy Achieved Within Operating System

Although accuracy has been previously discussed, it is of sufficient importance to emphasize that the type of IAT system selected affects the accuracy of the results. The analysis in Reference 4 compares the accuracy of forms data, strain measurements, and counting accelerometers. Two error sources exist in a forms data program. One is inaccuracies of the average crack growth per flight due to sampling errors in the L/ESS or from a change in usage. The other is the variability in individual usage from the average usage. However, this method, particularly pilot logs, is the currently accepted method for tracking large transport/bomber aircraft.

Strain measure tracking can be in error due to three sources: stress transfer, missing data, and inaccurate recording or reduction. Stress transfer errors result when many tracking locations are monitored from one data station. Increasing the data stations helps this problem. Missing data errors depend upon the amount and the method of gap filling. Only subjective judgements of this error can be made at this time. Inaccurate processing and recording errors must be determined for each system.

The counting accelerometer system is a long used IAT method for aircraft which have highly active maneuvering flight. The first source of error is due to the assumption that the normal acceleration can be used to determine crack growth without any other parameters. If this is not the case and the usage changes significantly, the method may be in error. A second source of error is the regression equation used to compute damage. If the actual usage differs from that used to develop this equation, the results could be in error.

These considerations of the possible error in each system are discussed in much more detail in Reference 4.

Figure 8.4.2. C-5 Aircraft Fatigue Tracking Record (MAC Form 89).

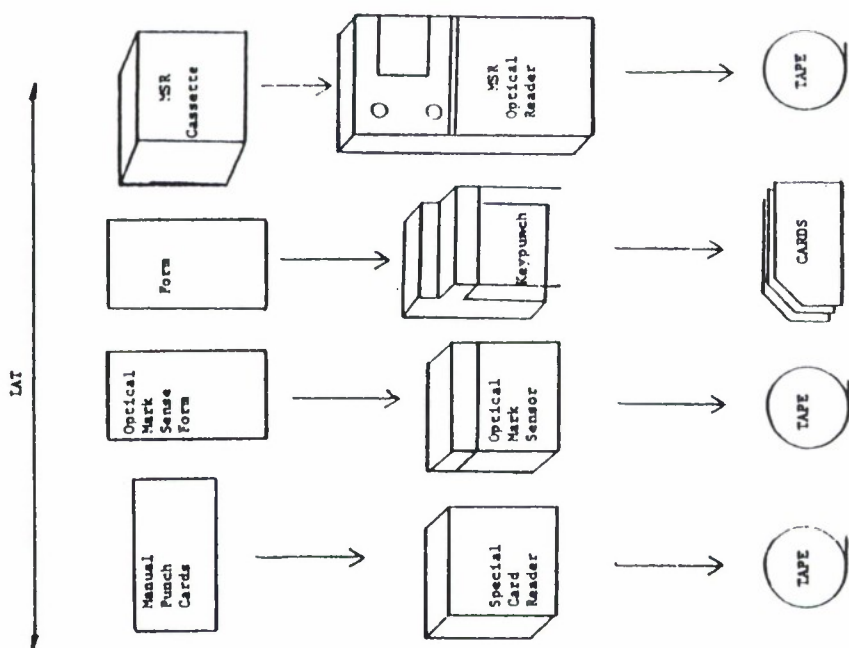


Figure 8.4.3. Data Transcription Methods.

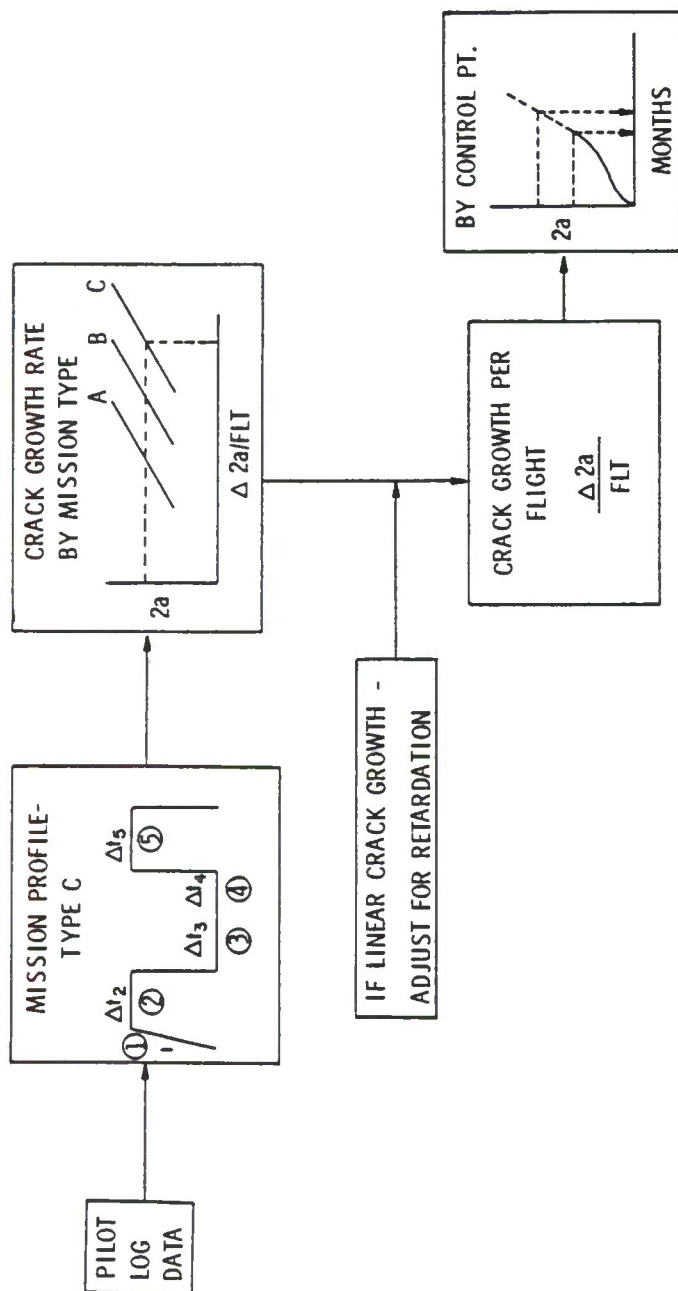


Figure 8.4.4. Mission-By-Mission Integration (Reference 3).

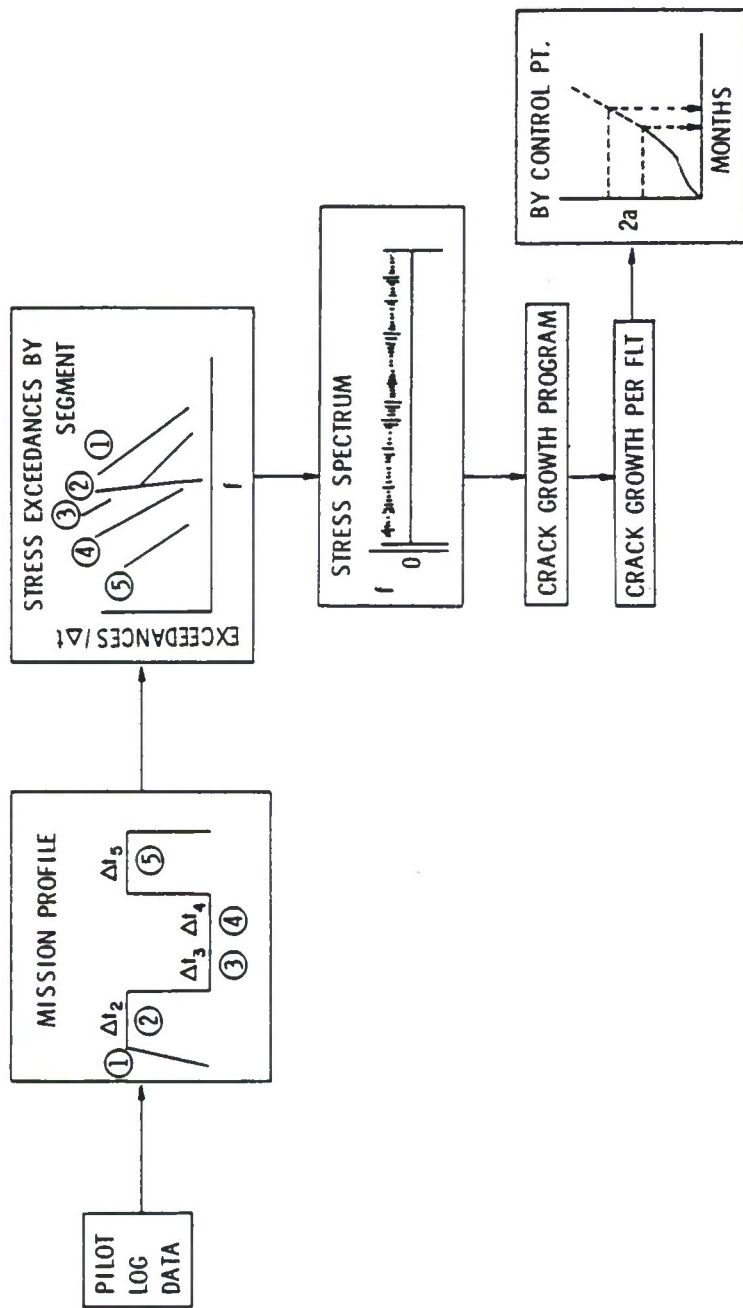


Figure 8.4.5. Mission-Segment-By-Mission Segment Integration (Reference 3).

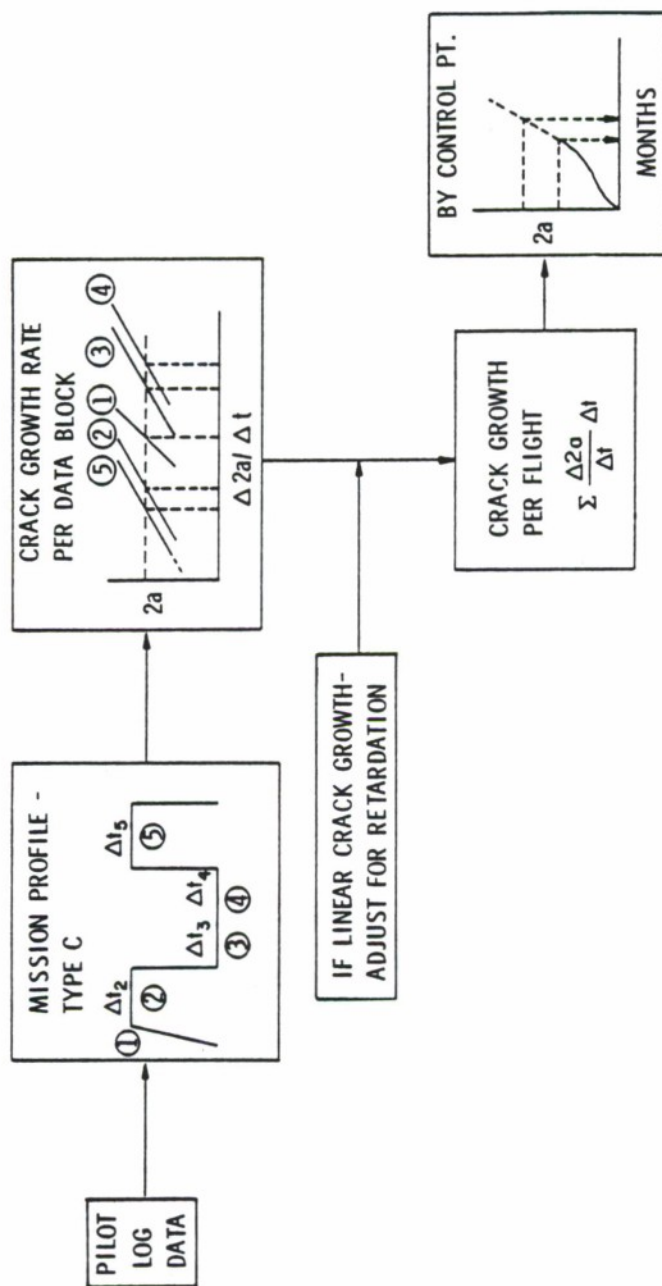


Figure 8.4.6. Time In-Usage Category Integration (Reference 3).

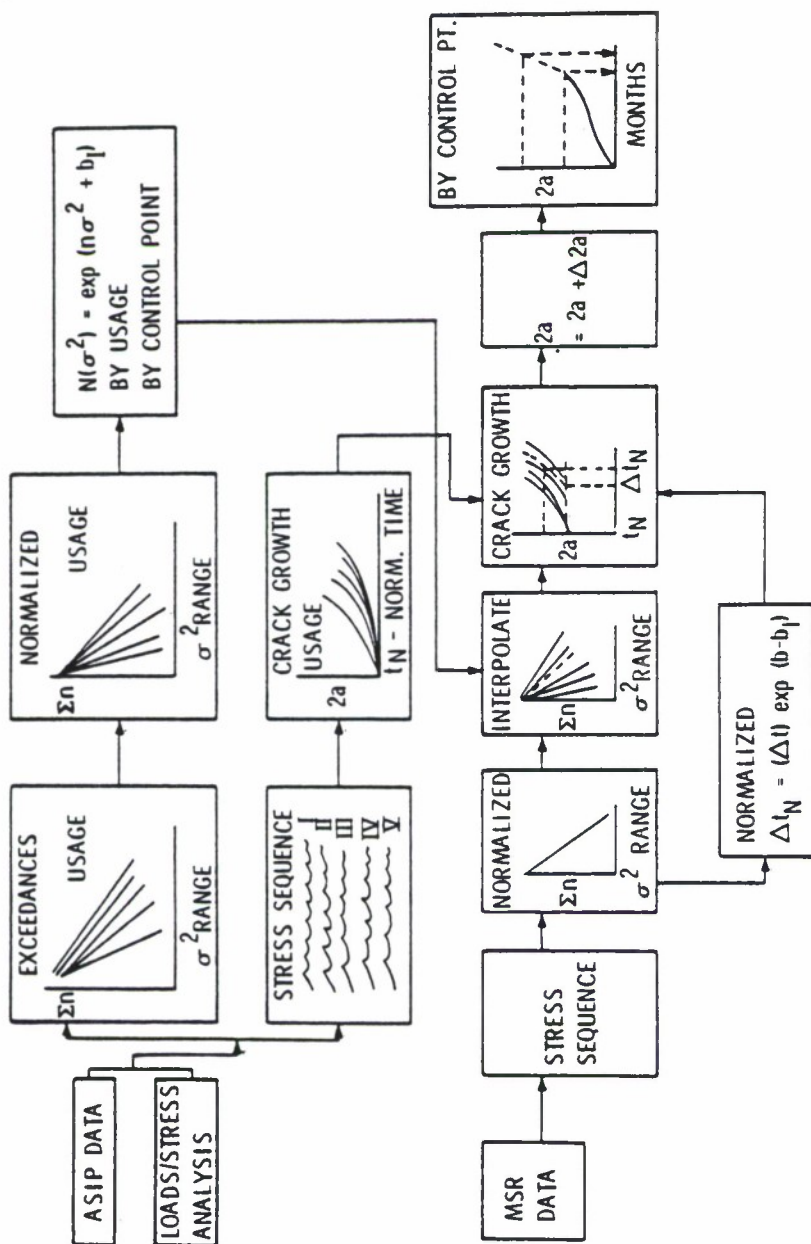


Figure 8.4.7. Strain History Integration (Reference 3).

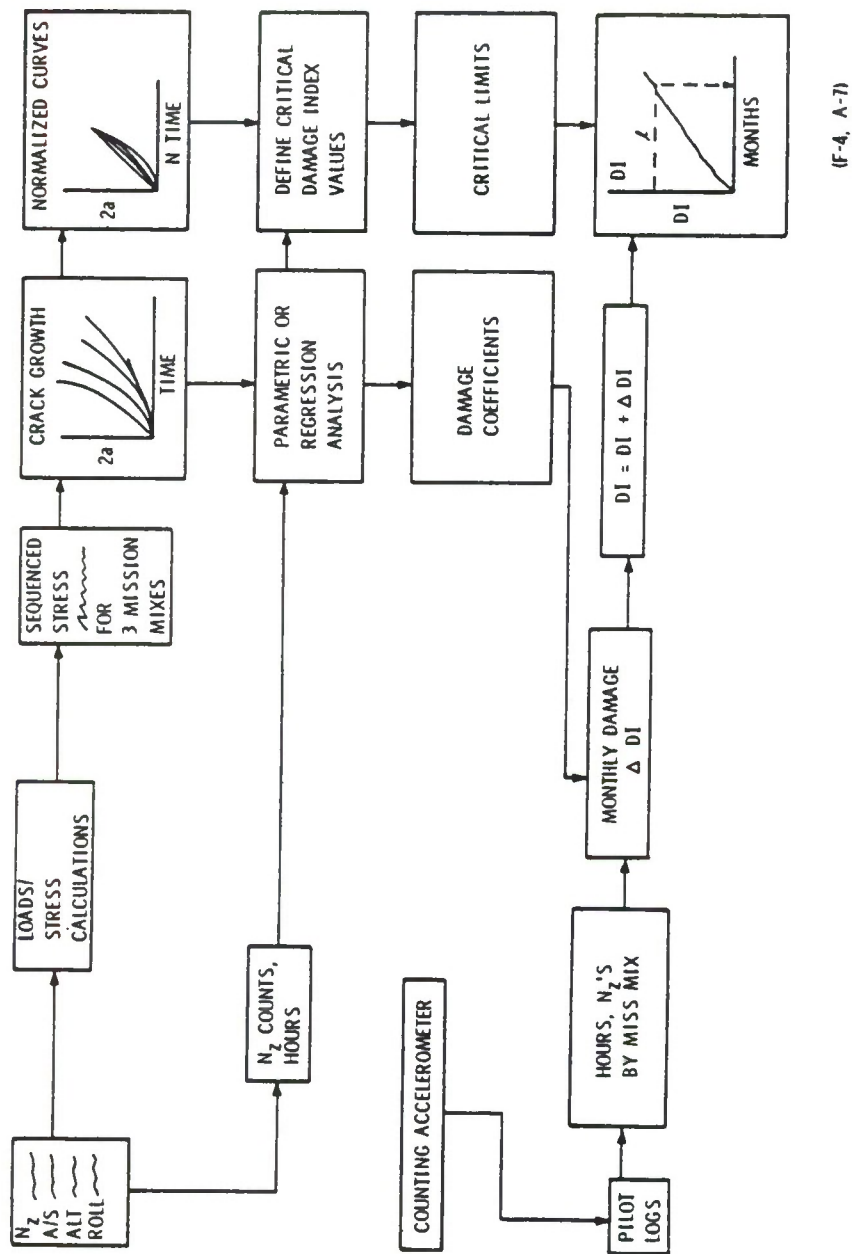


Figure 8.4.8. Damage Parameter Integration Scheme (Reference 3).

8.5 RECOMMENDED METHODS

Although there are a variety of methods which can be used for IAT systems, the experience obtained has indicated that there are preferred systems for each type of aircraft. The division can be made simply into two types, large flexible aircraft with wings of high aspect ratio such as cargo, transport and some bombers. The second type includes aircraft with wings of low aspect ratio such as fighters, trainers and most attack aircraft. The large aircraft are usually not highly maneuverable and experience most of the load history from encounters with atmospheric turbulence. The smaller aircraft are usually highly maneuverable and less sensitive to turbulence. The IAT systems generally recommended for the two classes of aircraft are discussed below. Detailed discussions of these methods are presented in Reference 1.

8.5.1 Large Flexible Aircraft

The recommended method for tracking large flexible aircraft is with a flight log form and parametric crack growth tables for damage calculations. The log form can be as complex as required. If the missions are well defined and have little variation then recording only the mission designation is sufficient. For usage where the missions are more variable then the values of airspeed, altitude, weight and configuration during the flight are recorded. The amount of variation allowed before recording a new set of data is determined by how sensitive the crack growth is to data block changes. The data needed from the L/ESS and the load survey programs to develop the crack growth tables must be coordinated with the data to be obtained during tracking. This is a very important item in using this method.

8.5.2 Stiff Aircraft

The aircraft which are generally considered to be small and stiff and which receive most of their loading through maneuvering must be tracked by a method sensitive to flight activity. Two methods can be easily applied to these type aircraft. Either the normalized n_z exceedance method or the normalized stress exceedance method.

The n_z method uses the counting accelerometer form on which data is transcribed on a monthly basis. This along with airframe hours and total landings is usually sufficient to determine what level of activity should be used to calculate the crack growth increment.

The stress method uses a device such as the MSR or may use some type of microprocessor based device as they are developed. The application to determine crack growth is similar to the n_z method.

Both of these methods require extensive use of the L/ESS data and loads survey data to develop the normalized crack growth curves for a variety of spectra of the measured parameter.

SECTION 8.6
LIST OF REFERENCES

1. Coffin, M. D., and Tiffany, C. F., "New Air Force Requirements for Structural Safety, Durability, and Life Management," *Journal of Aircraft*, Vol. 13, February 1976, pp. 93-98.
2. Tiffany, C. F., ed., "Analysis of USAF Aircraft Structural Durability and Damage Tolerance," AIAA Professional Study Workshop, April 6-7, 1978.
3. Clay, L. E., et al., "Force Management Methods Task I Report - Current Methods," AFFDL-TR-78-183, December 1978.
4. Berens, A. P., et al., "Force Management Methods Task II Volume I - Summary and Analysis Considerations," AFWAL-TR-80-3120, Volume I, November 1980.
5. Berens, A. P., et al., "Handbook of Force Management Methods," AFWAL-TR-81-3079, April 1981.
6. Gallagher, J. P., and Stalnaker, H. D., "Developing Normalized Crack Growth Curves for Tracking Damage in Aircraft," *Journal of Aircraft*, Vol. 15, No. 2, February 1978, pp. 114-120.
7. Denyer, A. G., "Fracture Mechanics Technology Applied to Individual Aircraft Tracking," Fracture Mechanics: Thirteenth Conference, ASTM STP 743, Richard Roberts, Ed., American Society for Testing and Materials, (1981), pp. 288-302.
8. Parker, G. S. and Pinckert, R. E., "Generalized Procedures for Tracking Crack Growth in Fighter Aircraft," McDonnell Aircraft Co., MCAIR 77-015, Presented at American Society for Testing and Materials Symposium, Atlanta, GA, 14-18 November 1972.
9. Berens, A. P. and Gallagher, J. P., "Maintenance Scheduling Based on Accumulated Crack Growth," Design of Fatigue and Fracture Resistant Structures, ASTM STP 761, P. R. Abelkis and C. M. Hudson, Eds., American Society for Testing and Materials, (1982), pp. 172-187.

9.0 GUIDELINES FOR DAMAGE TOLERANCE DESIGN
AND FRACTURE CONTROL PLANNING

<u>SECTION</u>		<u>PAGE</u>
9.1	INTRODUCTION	9.1.1
9.2	DESIGN LOADS SPECTRUM	9.2.1
9.3	MATERIAL SELECTION	9.3.1
	9.3.1 <u>Crack Growth Resistance and Fracture Toughness</u>	9.3.1
	9.3.2 <u>Material Property Control</u>	9.3.3
9.4	STRUCTURAL CONFIGURATION ANALYSIS	9.4.1
	9.4.1 <u>Critical Parts List</u>	9.4.1
	9.4.2 <u>Inspection Method Development</u>	9.4.3
	9.4.3 <u>Demonstration Test Development</u>	9.4.5
9.5	MANUFACTURING PROCESS	9.5.1
	9.5.1 <u>Control of Quality of Processes</u>	9.5.1
	9.5.2 <u>Development of Critical Parts Accountability</u>	9.5.2
9.6	FORCE STRUCTURAL MANAGEMENT	9.6.1
	9.6.1 <u>Force Management Plan</u>	9.6.1
	9.6.2 <u>Implementation of FSM Plan</u>	9.6.3
9.7	LIST OF REFERENCES	9.7.1

LIST OF FIGURES

<u>FIGURE</u>		<u>PAGE</u>
9.1.1	Elements of Damage Tolerant Design.	9.1.4
9.1.2	Damage Tolerance Design Requirements.	9.1.5
9.2.1	A Procedure for Development of Design Loads Spectra (Reference 4).	9.2.3
9.3.1	A Method of Presenting Comparative Material Data (Reference 4).	9.3.6
9.3.2	Illustration of Effects of Environment on Crack Growth Rates (Reference 5).	9.3.7
9.3.3	Fracture Control System for Subcontractors (Reference 8).	9.3.8
9.4.1	Illustration of Selection Logic for Fracture Critical Parts (Reference 8).	9.4.6
9.4.2	Fracture Control Analyses for Design Trade Studies.	9.4.7
9.4.3	Classes of Structural Arrangements.	9.4.8
9.4.4	Selecting Design Stress Level to Meet Residual Strength Crack Growth and Inspectability Requirements (Reference 9).	9.4.9
9.5.1	Representation of Elements in a Fracture Control Plan (Reference 4).	9.5.4

LIST OF TABLES

<u>TABLE</u>		
9.4.1	EXAMPLES OF NDE CAPABILITIES (REFERENCE 8)	9.4.4

9.0 GUIDELINES FOR DAMAGE TOLERANCE DESIGN AND FRACTURE CONTROL PLANNING

9.1 INTRODUCTION

The attainment of trouble-free and damage tolerant design for safety-of-flight structure on aircraft is a continuing multiple element process which begins in the preliminary design phase and extends through manufacturing into the operational planning and use of the aircraft. The purpose of this process is to develop a planned approach to the control of fracture damage in the aircraft. Figure 9.1.1 illustrates the main elements of the process.

The design criteria includes the service loads history, the functional requirements, and the desired life of the structure. The initial damage assumptions to be used with each type of design concept and degree of inspectability are also specified in the criteria. Figure 9.1.2 illustrates the interaction of these criteria elements based on MIL-A-83444 requirements.

Material selection is a critical element of the process. Trade-off studies are conducted between competing materials and use of comparative property data is necessary in the selection process. Ultimate strength, yield strength, fracture toughness and stress corrosion resistance must be considered together with the expected aircraft environment. The crack growth rate as a function of stress-intensity factor is required.

The structural configuration development must consider the effects of design details on fracture control. The inspection level is defined and a list of critical parts is begun. Consideration of the inspection procedures to be used at each critical location is important. The analysis methods used and

the stress-intensity factor computations are a function of the structural configuration and design details, and are set at this time. Testing methods for each critical part and assembly are also developed and incorporated into the damage tolerant design process.

Manufacturing processes must be selected for the critical parts such that they do not reduce the damage tolerance level required by the design. Control of processes and selection of inspection procedures to maintain process quality are the prime considerations of this element.

Procedures for inspecting the aircraft during operational maintenance and the development of the force structural management plan constitute the last element of the total damage tolerant design process.

This introduction of the elements illustrates the strong connections between design, testing, manufacturing, inspection and use in order to obtain and maintain the desired damage tolerant structure and to reduce the incidence of fracture related failures and loss.

The documents which outline the requirements for this activity and describe the various functions are military standards and specifications. MIL-STD-1530A establishes the requirements for aircraft structural integrity program (ASIP) and MIL-A-83444 (USAF) describes the airplane damage tolerance design requirements. These documents have been reproduced in the appendix of this handbook to serve as a reference.

Reference 1 provides discussion of the ASIP technology. Reference 2 presents extensive discussions of the durability and damage tolerance problem of USAF aircraft structures. In particular, the review by Mr. C. F. Tiffany,

"Durability and Damage Tolerance Assessments of United States Air Force Aircraft," provides a thorough review of the background of this topic. This chapter of the handbook describes these tolerant design elements in some detail, and when the described functions are followed, the resultant aircraft structure should have the required level of damage tolerance.

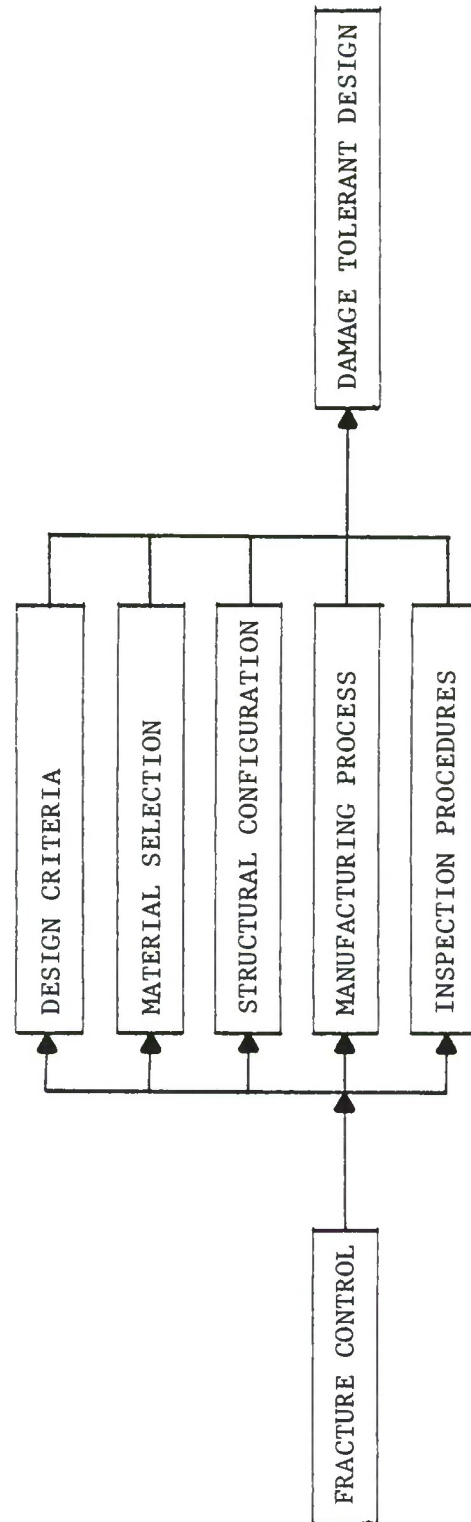


Figure 9.1.1.1 Elements of Damage Tolerant Design.

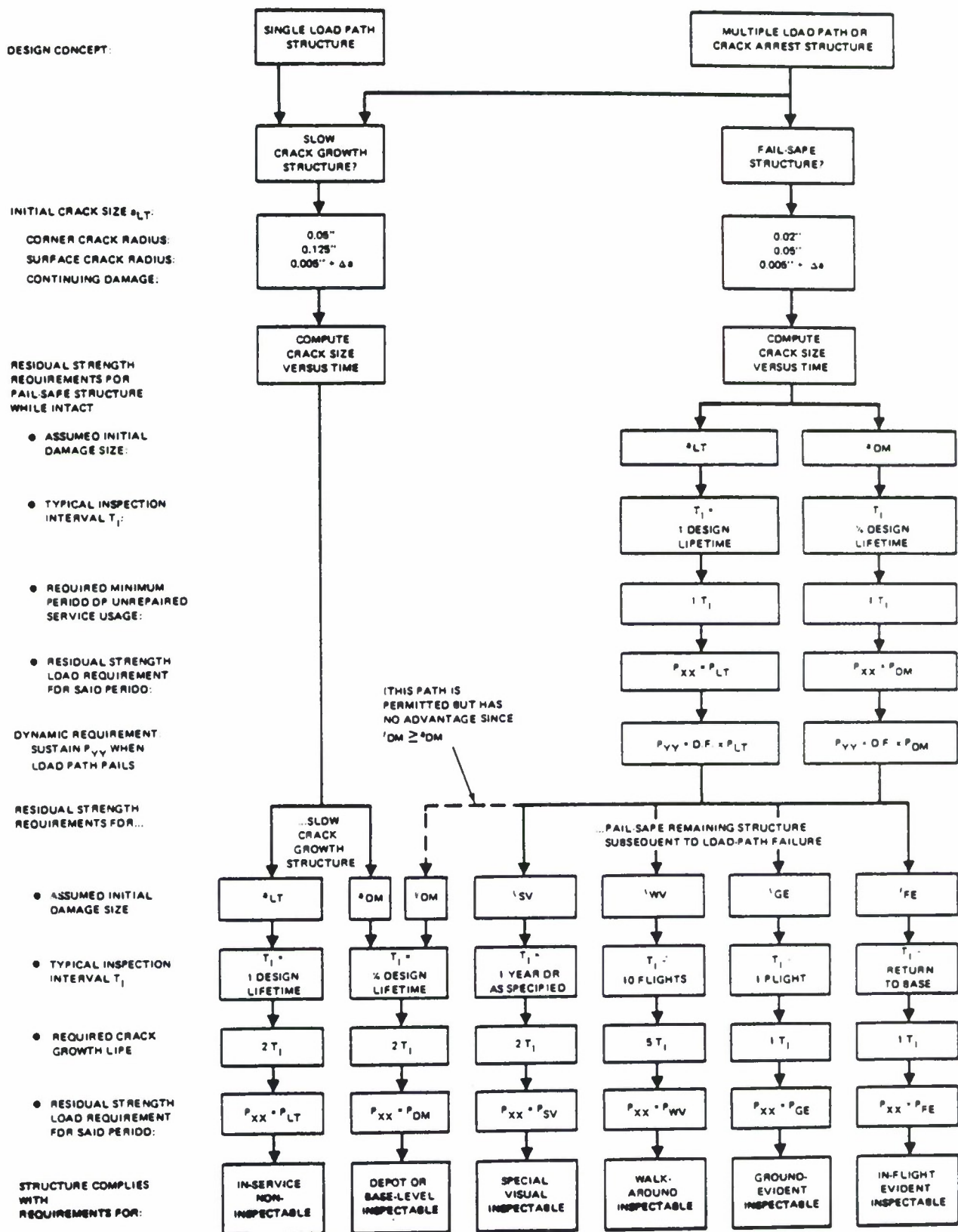


Figure 9.1.2 Damage Tolerance Design Requirements.

9.2 DESIGN LOADS SPECTRUM

The design load spectrum is used to determine the damage growth in each critical part during analysis and testing. It is based on the specified mission profile information and the required aircraft life. A description of the load sequence development is given in Section 5.3 of this handbook. A brief review is presented here. Reference 3 presents a detailed description of load sequence development methodology.

The load sequence is composed of the load cycles which can be expected to occur during the lifetime operation of the aircraft. They are the result of ground operations, such as towing, taxiing, turning, braking, take-off and landing, and of airborne operations of maneuvering, turbulence encounters, store ejection and refueling. The specification documents include the numbers of these loads to be anticipated at various levels during the aircraft life.

The design spectrum must be based on a reasonable estimate of the anticipated mission usage history. All load sources should be included and the anticipated severity should reflect on both previously observed data and on any performance advances being designed into the new aircraft. It has become somewhat of an axiom that the full maneuvering capability of the aircraft will be used during its operation. Thus, it is essential that the design load sequence be representative of the aircraft capability. Figure 9.2.1 from Reference 4 illustrates a basic procedure for the development of a design loads spectrum. This is an interactive program involving several different data sources and other design activities.

The design loads spectra usually progresses from a preliminary effort based on the initial aerodynamics to a final form based on the final aerodynamics and aircraft configuration.

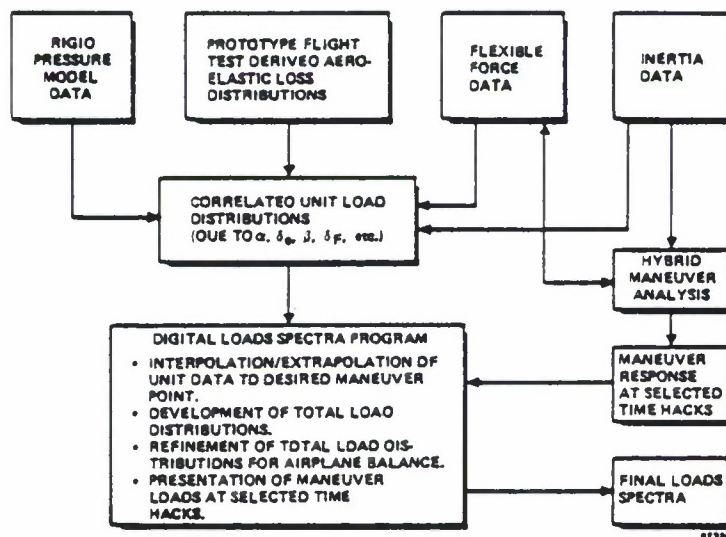


Figure 9.2.1 A Procedure for Development of Design Loads Spectra (Reference 4).

9.3 MATERIAL SELECTION

The selection of materials for damage tolerant design is one of the most important functions. Materials must be evaluated and selected on both their static strength and their toughness and flaw growth characteristics. The properties used for these comparisons are:

Yield Strength, F_{ty}

Ultimate Strength, F_{tu}

Fracture Toughness, K_c or K_{IC}

Stress Corrosion Factor, K_{ISCC} .

Crack Growth Rate, da/dN vs. ΔK .

Figure 9.3.1 from reference 4 shows how some of these properties can be compared. In addition, analysis of typical crack growth characteristics is also done for each material.

9.3.1 Crack Growth Resistance and Fracture Toughness

The material properties used for the selection criteria must be obtained for conditions which correspond to those expected in the structural usage environment.

Crack growth resistance as expressed in the da/dN data should be obtained from tests conducted using thicknesses similar to the anticipated structure applications and in similar environments. Some alloys are quite susceptible to corrosive media such as may be experienced in aircraft fuel bays or during operation near salt water. Effects of these variables are shown in Figure 9.3.2 (Reference 5).

For ease of application in the design process, the crack propagation data is usually described by an empirical relationship, such as the Forman equation, given as:

$$\frac{da}{dN} = \frac{C(\Delta K)^n}{(1-R) K_c - \Delta K}$$

where

- K_c , Fracture Toughness
- ΔK , Stress-Intensity Factor Range
- C, n , Constants, Dependent on Material, Obtained From
Curve Fitting Techniques.

It may be necessary to model the data in several parts over the ΔK range of interest in order to achieve adequate representation.

Reference 6 presents a method for evaluation of weight savings due to the use of advanced materials. The utilization of materials having improved damage tolerance characteristics as evidenced by a higher allowable stress value was shown to effect a weight savings from 1-3 percent for an improvement in allowable stress of 10-25 percent.

Reference 7 discusses material properties and characteristics of some new materials based on obtaining high strength with good durability and damage tolerance properties. This is mentioned to make the reader aware of current efforts to improve structural materials. Goals stated in this report are to increase the static strength, decrease the crack growth, and increase the temperature capability of aluminum alloy.

9.3.2 Material Property Control

Along with the selection of various materials for use on the structure, it is essential that a control system be established. Reference 8 describes such a system as including the areas of source selection, usage, evaluation, documentation, and tracking of all materials. The establishment of material control specifications is necessary to achieve the desired end result. It is suggested that a rating system be established for each material based on the expected usage. Reference 8 suggests a five-level system (A, B, C, U, X) which may be defined as:

- A - Acceptable for Usage,
- B - Acceptable with Specific Controls,
- C - Acceptable with Demonstration Evaluation,
- U - Not Evaluated for a Given Usage,
- X - Not Acceptable.

The development of a material selection list includes all properties which are required for each material usage. A pre-release material approval is suggested as a screening device. This would be by a material review board which would pass on all selected materials.

After the approval of all selected materials, the next step is to assure that only approved materials are actually used and that they meet the requirements. An accountability procedure must be implemented. As a minimum, this system must do the following:

1. Identify the part,
2. List all material data required,
3. List all supplemental data related to part;
 - a. Test Data,
 - b. Change Notices,
 - c. Deviations,
 - d. Process Specifications,
 - e. Inspection Reports,
 - f. Rework Required.

This system should be easily accessible and usable throughout the design, manufacturing, and usage phases of the aircraft life cycle. It would provide the information necessary to solve any future problems and will be the basis for the next design. This system is directed toward fracture critical parts, but it is evident that such material control is necessary for all parts. If such is the case, then fracture critical parts can be easily identified and tracked as part of the total aircraft design and development.

As a part of this system, it is necessary to establish a material quality control program. Sample testing of all material which is identified for fracture critical parts should include verification of crack growth rate and toughness properties. Special handling instructions for this material to preserve initial quality should be implemented. Non-destructive testing techniques must be developed and incorporated into the manufacturing process to insure that manufacturing quality is maintained.

While such systems of material control are easily established by a prime contractor, it is also necessary to extend them to subcontractors and parts vendors who furnish fracture critical parts. All procurement specifications for such parts must include the same requirements for incorporation and maintenance of quality as practiced by the prime. Figure 9.3.3 from Reference 8 illustrates how such vendor interfaces can be achieved.

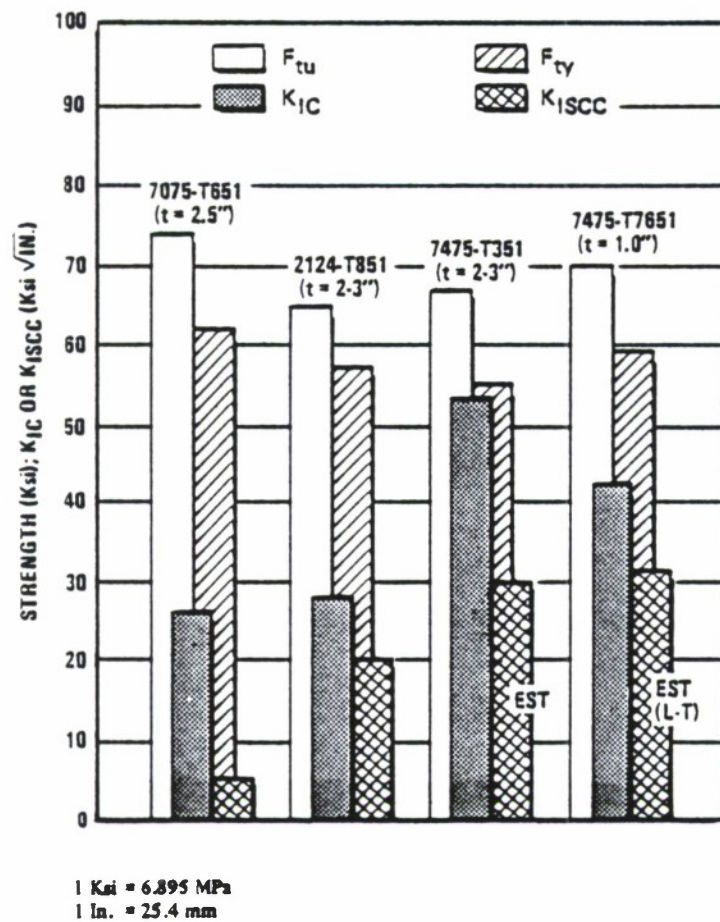


Figure 9.3.1 A Method of Presenting Comparative Material Data (Reference 4).

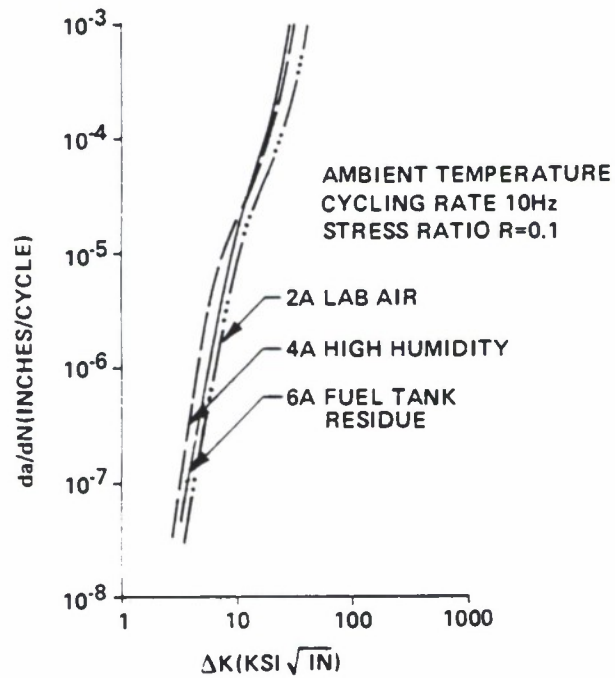
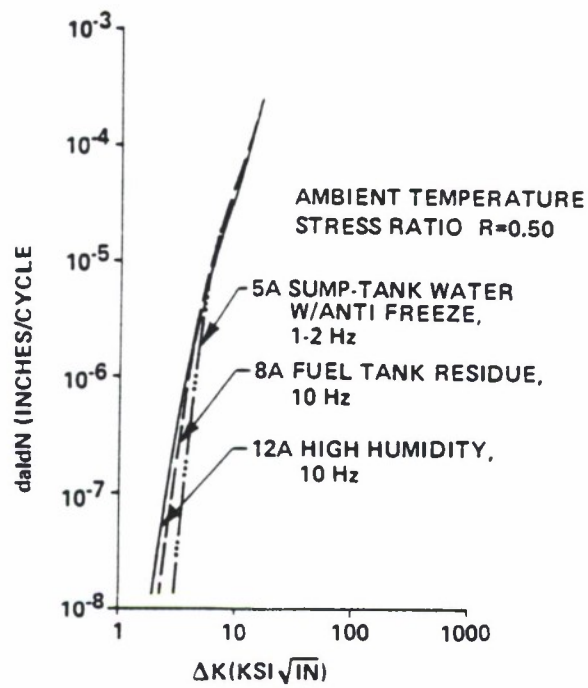


Figure 9.3.2 Illustration of Effects of Environment on Crack Growth Rates (Reference 5).

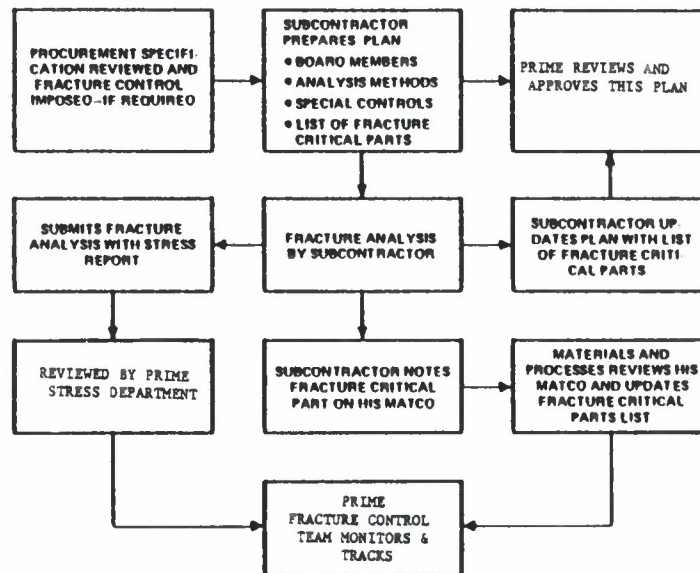


Figure 9.3.3. Fracture Control System for Subcontractors (Reference 8).

9.4 STRUCTURAL CONFIGURATION ANALYSIS

The fracture control program must consider all of the design details incorporated into the structural configurations as possible critical items. It is as a part of this function that the critical parts list is developed and each part analyzed for its fracture propagation characteristics. The method to be used to inspect the critical parts must also be established. This will set the initial flaw size which is used in the analysis. Any testing which must be done to establish the damage tolerance of a part is also done during this phase of the development.

9.4.1 Critical Parts List

The development of the fracture critical parts list begins with the first design studies. The list is then maintained throughout the life of the aircraft. It identifies those parts which would cause loss of the aircraft or endanger personnel and cargo if they failed as a result of flaw propagation. The logic pattern and analysis necessary to identify critical parts is outlined in Figure 9.4.1 (Reference 8). Initially, the static analysis is used to identify the highly stressed areas of safety of flight items. A crack growth analysis using the best estimate of an initial flaw at the time of the analysis and the design load spectrum is run until either the required life has been exceeded without a predicted failure or until a failure is predicted in the part. Failure is usually related to a critical crack size and the required residual strength load. This analysis is usually conducted as a part of the design trade studies used to select materials, select stress loads and to size the part.

An outline of these design trade studies is shown in Figure 9.4.2. Figure 9.4.3 illustrates three classes of structural arrangements which are analysed. The factors affecting the selection of design stress levels are illustrated in Figure 9.4.4 (Reference 9).

Redesign is done as necessary until the required life is attained. Figure 9.4.1 shows a decision point at four lifetimes. Actual life requirements will vary depending on the part; however, the logic is similar for all parts. The accurate determination of the component stress field for identification of critical areas is important. The best results can be achieved with fine grid finite element models. Unfortunately, cost is high for these so judgement must be used to decide when such sophistication is necessary.

Each part finally identified as a fracture critical part is then added to the list and identified for controlled handling during the manufacturing process. Establishment of this procedure early results in little disruption of standard procedures and makes the handling of fracture critical parts an integral part of the design and manufacturing process.

When the design load spectrum is developed to its final form, which should also be relatively early in the design process, the initial analysis of the most critical items should be repeated to determine if there are any changes in results. Any differences must be evaluated and redesign accomplished as indicated.

The selection of the manufacturing processes for the critical parts should be made with care. Such things as surface finish, edge finish, location of parting planes, location of identification marks, and amount of metal removal

per part must be considered during the design. Considerations of these and other items is presented in publications such as Reference 10, 11 and 12. It is not considered appropriate to present a large number of details in this handbook, but a catalogue of acceptable and unacceptable design and machining details should be developed by the manufacturer as a guide to design and fabrication.

9.4.2 Inspection Method Development

The initial assumed flaw used in all crack growth computations is determined either by a specified minimum flaw based on standard inspection techniques or by a special minimum flaw which can be substantiated by special inspection techniques. Table 9.4.1 from Reference 8 lists an example of what may be expected from several inspection methods. These will vary with specific equipment.

During the development of the critical parts list, it is necessary to consider how each part will be inspected for flaws. This must be considered not only during the manufacturing process but also during the periodic inspections to be performed during the aircraft life. The results of the fracture analysis can be significantly affected by the inspection method and the selection of initial flaw sizes.

As improved inspection methods are incorporated into production use, it is to be expected that improved design will result. The trade-off between inspection cost and performance may also be considered.

TABLE 9.4.1
EXAMPLES OF NDE CAPABILITIES
(Reference 8)

Inspection method	Flaw type	Standard NOE	Special NOE
Penetrant or magnetic particle	Surface flaw (Depth x length)	0.19 x 0.38 cm (0.075 x 0.150 in.) or equivalent area	0.083 x 0.127 cm (0.025 x 0.050 in.) or equivalent area
Ultrasonics	Embedded flaw (diameter)	0.254 cm (0.100 in.)	0.12 cm (0.047 in.)
Radiographic	Surface or embedded (depth x length)	0.7t x 1.4t Min length = 0.38 cm (0.150 in.)	0.6t x 1.2t Min length = 0.127 cm (0.050 in.)
t = thickness			

9.4.3 Demonstration Test Development

The use of tests to demonstrate the existence of damage tolerant design is necessary when design details depart from past acceptable usage and when various environments are present for which data is not available. It is suggested that such testing begin early and start with element and small component tests. This testing should also use the flight-by-flight design load spectrum being used for analysis.

As the design progresses, large component tests of critical areas should be conducted. As much as possible, the anticipated environments should be a part of the test. As mentioned earlier, the influence of environment can be quite extensive on crack growth behavior.

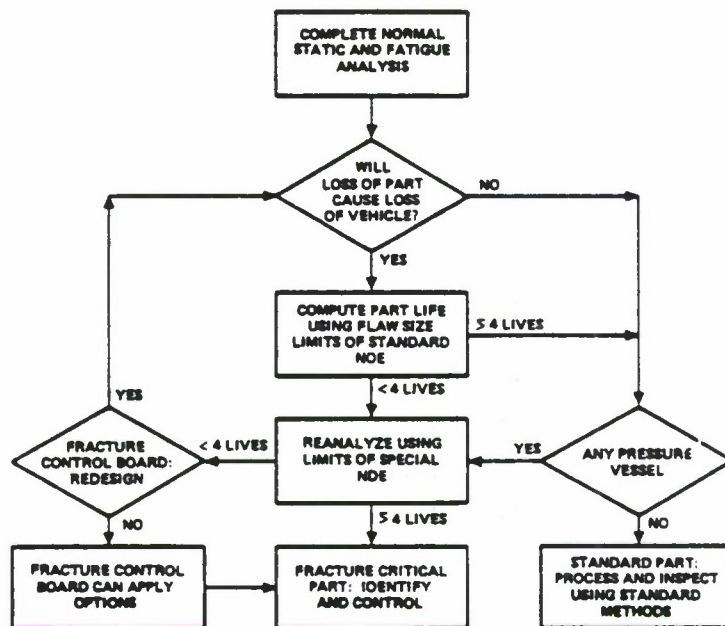


Figure 9.4.1 Illustration of Selection Logic for Fracture Critical Parts (Reference 8).

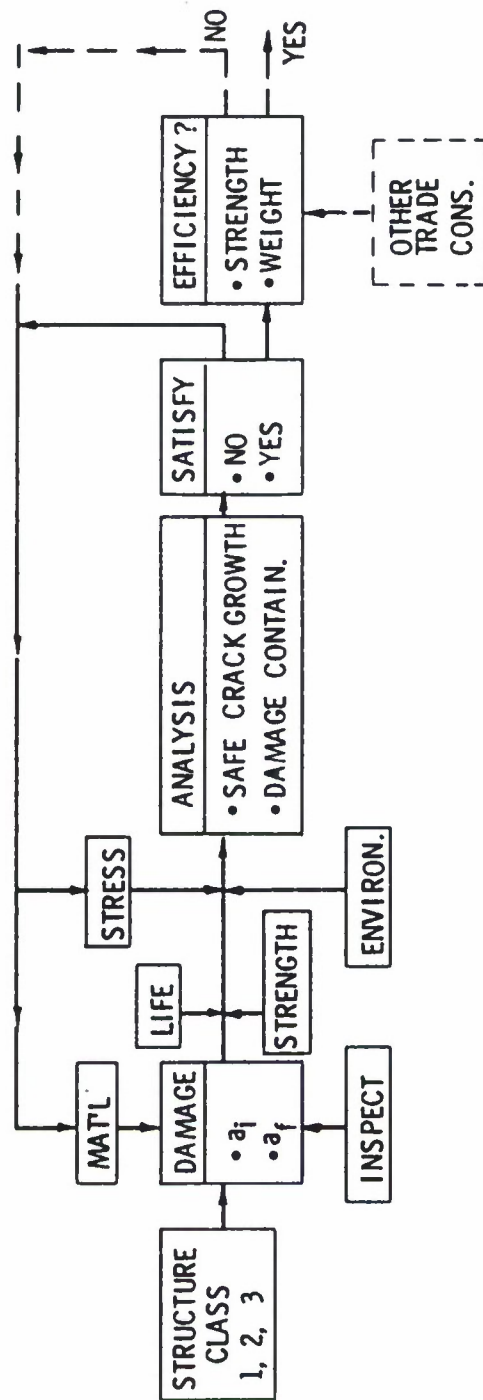


Figure 9.4.2 Fracture Control Analyses for Design Trade Studies.

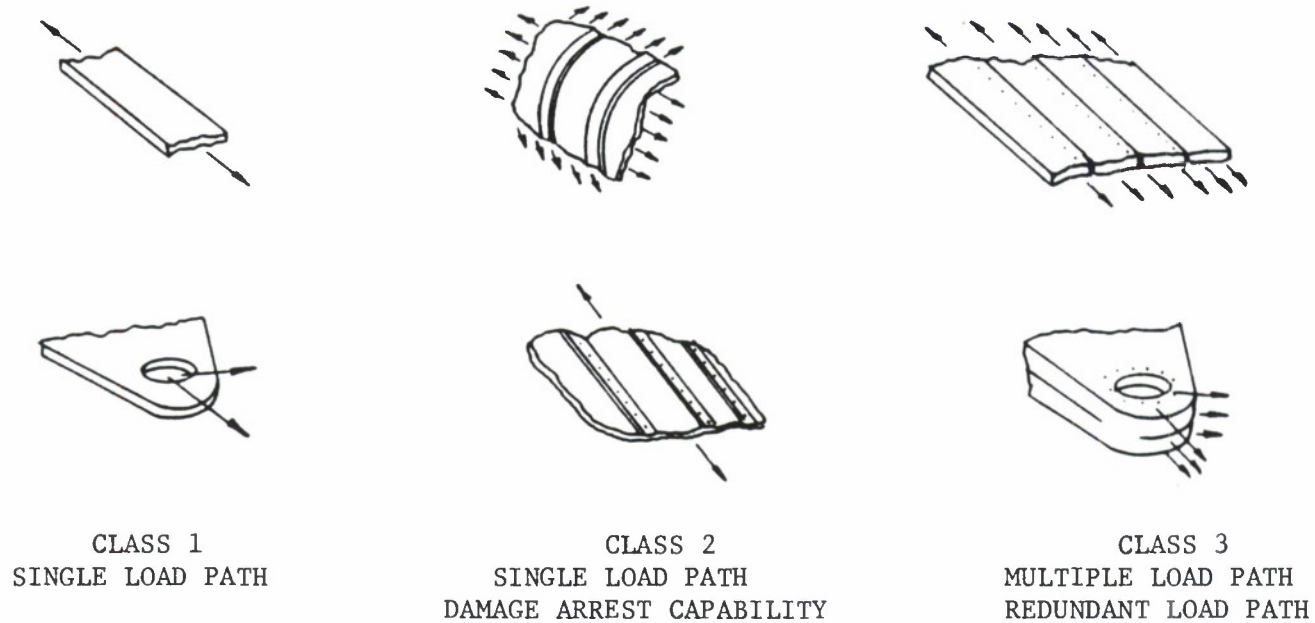


Figure 9.4.3. Classes of Structural Arrangements.

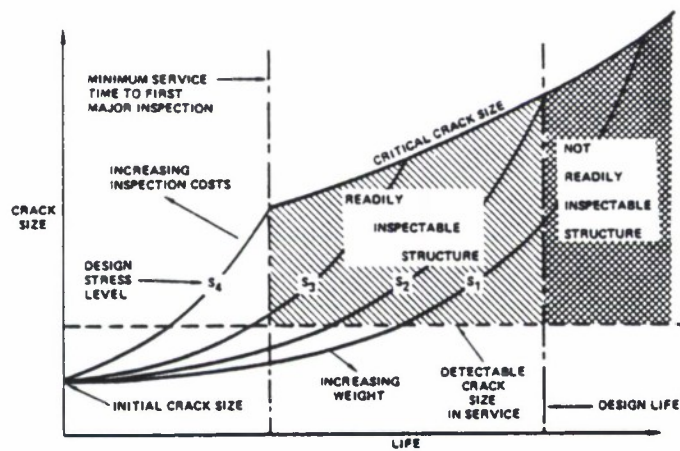
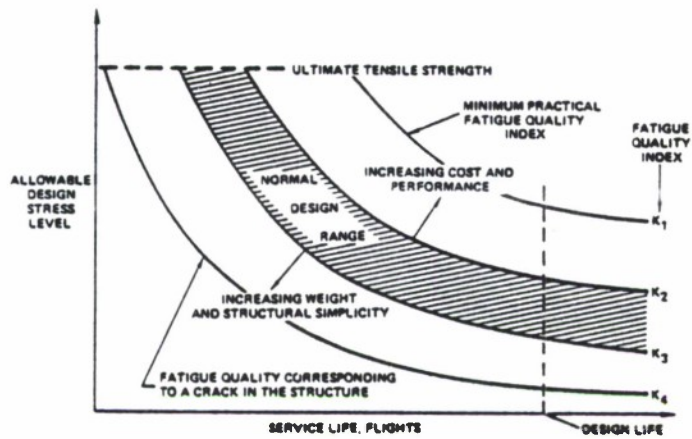


Figure 9.4.4 Selecting Design Stress Level to Meet Residual Strength Crack Growth and Inspectability Requirements (Reference 9).

9.5 MANUFACTURING PROCESS

The realization of the design during the manufacturing process is where the fracture control plan reaches its ultimate test. It is now that a diverse group of participants must be brought into control to insure the production of the required quality.

Each manufacturing step of the fracture critical parts must be monitored and controlled. Procedures must be developed which provide strict accountability and sign-off from step to step but which also do not unduly hinder the normal flow of manufacturing processes. Two major items are involved at this point: (1) Establishing the control of manufacturing quality, and (2) Developing the methods for critical parts accountability. Figure 9.5.1 shows an example of a fracture control plan which illustrates these items.

9.5.1 Control of Quality of Processes

Three major items comprise the function of the manufacturing process quality control. They are:

- (1) Definition of inspection requirements,
- (2) Demonstration of inspection methods,
- (3) Review of manufacturing process and inspections.

The basic document for the manufacture of each fracture critical part is the process specification. It lists all of the processes which must be performed on the part. This forms the basis for selection of the inspection methods. Limits for acceptance are also a part of the process specification. The scheduling of inspections during the process must be considered. A trade-off

between inspection cost, rework cost, and loss due to scrap must be made. This process may be more critical in a fracture critical part than in another part since there may not be as many rework options open. Thus, it may be more efficient to have more inspections than to risk losing a large amount of process time. Parts which do not pass an early inspection may be reclaimed through rework options still available at this time.

The demonstration of the efficiency of nondestructive process inspections can be made through destructive testing or through a more rigorous nondestructive inspection. This demonstration is made early in the program and may be subject to periodic checking over the life of the project. As experience is gained with the process, the inspection frequency may be decreased.

It should be noted that whenever either new process equipment is installed or inspection equipment is changed, the inspection procedure should be tightened until confidence is again attained. This also should include periodic review of the inspection process to insure that the quality of the inspection is being maintained.

9.5.2 Development of Critical Parts Accountability

The critical parts list is only the first step in the control process. It also includes the damage review procedure, material procurement and acceptance, handling of the part during manufacture, installation procedures, incorporation of design changes, and disposition of manufactured parts. This entire process is one of accountability. In order to do this, a method of serial numbering is used and a work routing sheet is suggested which identifies the source of the stock material used in the part during its

manufacture and provides sign-off and transfer records for each process. In order for this process of control to be effective, the personnel involved during manufacture must have an awareness of the objective. They must realize the development of an individual commitment to achieve a damage tolerant aircraft. References 11 and 12 present discussions of how damage tolerant design has been incorporated into transport aircraft design and construction.

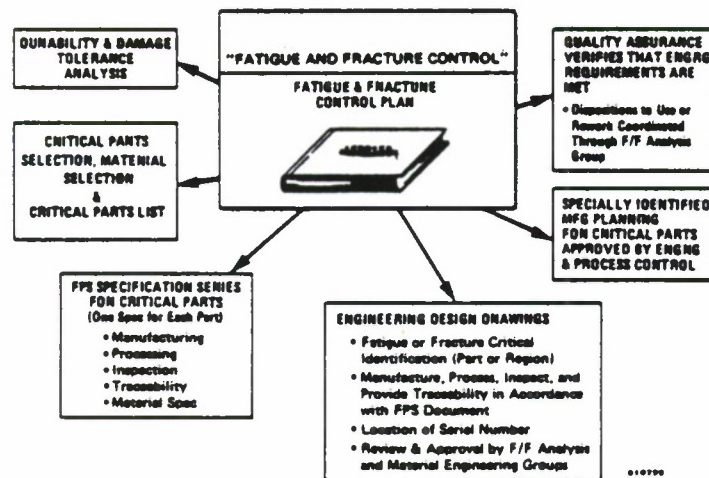


Figure 9.5.1 Representation of Elements in a Fracture Control Plan (Reference 4).

9.6 FORCE STRUCTURAL MANAGEMENT

The maintenance of the damage tolerant capability of an aircraft after it enters the force is the function of an activity called Force Structural Management. This has been mentioned in reference to the Individual Aircraft Tracking (IAT) Plan described in Chapter 8 and is covered in detail in Reference 13. As this activity can be considered to be the final phase of fracture control, a summary of the elements contained in Force Management are presented here. The concept is to monitor the usage of each aircraft and compare the computed damage accumulation, as described by a crack growth analysis, with the predicted damage accumulation of a baseline usage aircraft. The maintenance schedule of the monitored aircraft is modified as necessary to account for differences of usage from the baseline. This section discusses the elements of the FSM plan and how they are implemented.

9.6.1 Force Management Plan

The airframe contractor is required, under current Air Force requirements, to devise a Force Management Plan. It contains three essential parts: The Force Structural Maintenance (FSM) Plan, the Loads/Environment Spectra Survey (L/ESS), and the Individual Aircraft Tracking (IAT) Program. The initial FSM plan presents the schedule for inspections and maintenance actions for an aircraft which is accumulating damage according to the design loads spectra usage predictions. It is to be updated when the baseline operational loads spectra are developed.

The L/ESS is a data collection and analysis program designed to provide the data to develop the baseline operational load spectra. A number of the force aircraft, usually about twenty percent, are fitted with data measuring and recording equipment. Parameters such as accelerations, angular rates, airspeed, altitude, weight and other load indicative quantities are obtained in a time history form as the aircraft are flown. It is categorized by mission type and segment, and load histories are calculated for the critical areas of the aircraft. These are the same areas which were identified in the critical parts list and which will be subjected to subsequent inspection and possible repair or modification during maintenance actions. The new baseline operational damage accumulation rates based on the L/ESS data are used to update the FSM plan.

The IAT program is also a data collection and analysis effort which is applied to each aircraft of the force. The minimum amount of data is collected which will allow the estimation of the damage being accumulated. Comparison with the baseline damage accumulation predictions allows modification of the FSM plan to account for the differences in usage of each aircraft. Chapter 8 provides more detail of the IAT programs.

The planning for these three parts of the FSM plan should begin with the initial design studies and the fracture control plan. Crack growth techniques used during the design are also those used in the IAT and FSM portions of the program and should be formulated to permit easy incorporation. Studies made for evaluation of the effect of different load parameters on the loads computation and subsequently on crack growth calculations should be used in

the development of the parameter list for the L/ESS program. Accuracy requirements and parameter ranges should be selected to be commensurate with the methods of analysis.

9.6.2 Implementation of FSM Plan

The final FSM plan and all of the test results and analysis conducted during the design, manufacture, and testing of the aircraft form the final data package which is delivered to the Air Force. It substantiates the damage tolerance characteristics of the structure and describes how it may be maintained during the life of the aircraft.

A transition period normally occurs during which the contractor trains the user in all stages of the L/ESS, IAT, and FSM plan. It is essential that the user assume the same regard for the treatment of damage critical parts that was practiced during manufacture. As emphasized during this chapter, the damage tolerance analysis is highly dependent on the size of the initial quality flaw. Manufacturing processes and handling were watched so that quality was preserved. It is now the responsibility of the user to handle the aircraft in the same manner. Disregard for the structure could result in complete loss of all of the previous efforts and could invalidate all of the tracking efforts.

It is the responsibility of the Air Force user to obtain the data from the L/ESS to be used in the baseline analysis update. Early collection of that data will lead to the most accurate use of the IAT data. Recognition of this operation as part of the fracture control plan should aid in the proper

conduct of the task. Keeping the equipment in service and striving for the maximum amount of data return will lead to the most accurate final results. (This is, in part, also dependent on a selection of parameters which are easy to record.) Recording equipment and transducers selected should have a high reliability and be easy to use.

The IAT implementation must also be such that a high return of data is assured. Again, the feeling of being a part of the fracture control plan should pervade the IAT personnel. The timely and complete recording and processing of this data will result in accurate scheduling of maintenance actions.

These ideas are meant to emphasize the connection between the follow-on FSM activities and the damage control plan. Additional ideas and discussions on this topic are presented in Reference 13. It is most highly recommended that the reader also obtain a copy of this reference for further reading.

SECTION 9.7

LIST OF REFERENCES

1. H. A. Wood, "Structural Integrity Technology for Aerospace Applications," Structural Integrity Technology, J. P. Gallagher and T. W. Crooker, Eds., The American Society of Mechanical Engineers, May 1979.
2. C. F. Tiffany, Ed., "Analysis of United States Air Force Aircraft Structural Durability and Damage Tolerance," Notebook for AIAA Short Course, April 1978.
3. F. Joseph Giessler, Seth J. Duell and Robert F. Cook, "Handbook of Guidelines for the Development of Design Usage and Environmental Sequences for United States Air Force Aircraft," AFWAL-TR-80-3156, February 1981.
4. W. D. Buntin, "Durability and Safety in the F-16 Airframe," Structural Integrity Technology, J. P. Gallagher and T. W. Crooker, Eds., The American Society of Mechanical Engineers, May 1979.
5. R. L. Circle and F. M. Conley, "A Quantitative Assessment of the Variables Involved in Crack Propagation Analysis for In-Service Aircraft," 21st Structures, Structural Dynamics and Materials Conference, AIAA, ASME, ASCE, AHS, Part I, pp. 512-521, May 1980.
6. J. C. Ekvall, J. E. Rhodes, and C. G. Wald, "Methodology for Evaluating Weight Savings from Basic Material Properties," Design of Fatigue and Fracture Resistant Structures, ASTM STP 761, P. R. Abelkis and C. M. Hudson, Eds., American Society for Testing and Materials, 1982, pp. 328-341.
7. R. F. Simenz and M. K. Guess, "Structural Aluminum Materials for the 1980's," Journal of Aircraft, Vol. 17, No. 7, July 1980, pp. 514-520.
8. R. M. Ehert, "Material Control and Fracture Control Planning for the Space Shuttle Orbiter Program," Structural Integrity Technology, J. P. Gallagher and T. W. Crooker, Eds., The American Society of Mechanical Engineers, May 1979.
9. E. K. Walker, J. C. Ekvall, and J. E. Rhodes, "Design for Continuing Structural Integrity," Structural Integrity Technology, J. P. Gallagher and T. W. Crooker, Eds., The American Society of Mechanical Engineers, May 1979.
10. T. Lunde, "Fatigue and Stress Corrosion Guidelines," Lockheed-California Company, 1976.

11. U. G. Goranson, J. Hall, J. R. Maclin, and R. T. Watanabe, "Long Life Damage Tolerant Jet Transport Structures," Design of Fatigue and Fracture Resistant Structures, ASTM STP 761, P. R. Abelkis and C. M. Hudson, Eds., American Society for Testing and Materials, 1982. pp. 47-87.
12. R. E. Watson, "Structural Integrity Development of Commercial Aircraft," Structural Integrity Technology, J. P. Gallagher and T. W. Crooker, Eds., The American Society of Mechanical Engineers, May 1979.
13. A. P. Berens, et al., "Handbook of Force Management Methods," AFWAL-TR-81-3079, April 1981.

10.0 ANALYSIS OF STRUCTURAL REPAIRS

<u>SECTION</u>	<u>PAGE</u>
10.1 INTRODUCTION	10.1.1
10.1.1 <u>Repairs/Changes Requiring Analysis</u>	10.1.1
10.1.2 <u>Levels of Damage Tolerance Analysis</u>	10.1.3
10.2 USAGE CHARACTERIZATION FOR SIMPLE REPAIRS	10.2.1
10.2.1 <u>Variable Amplitude Crack Growth Behavior</u>	10.2.2
10.2.2 <u>Other Methods for Generating Rate Descriptions</u>	10.2.5
10.2.3 <u>Power Law Descriptions</u>	10.2.8
10.2.4 <u>Analytical Concerns</u>	10.2.9
10.3 SPECTRUM ANALYSIS FOR REPAIR	10.3.1
10.3.1 <u>Definition of Stress Histories</u>	10.3.1
10.3.2 <u>Spectra Descriptions</u>	10.3.4
10.3.2.1 Exceedance Curve Descriptions	10.3.4
10.3.2.2 RMS Descriptions	10.3.6
10.3.3 <u>Crack Growth Analysis</u>	10.3.9
10.3.3.1 Generation of Crack Growth Curves	10.3.11
10.3.3.2 Analysis of Observed Behavior	10.3.13
10.3.3.3 Interpretation and Use of Crack Growth Rate Curves	10.3.14
10.3.3.4 Analysis for Multiple Stress Histories	10.3.19
10.4 LIFE SENSITIVITY FOR STRESS EFFECTS	10.4.1
10.5 LIFE SENSITIVITY ANALYSIS FOR HOLE REPAIR	10.5.1
10.6 BLEND-OUT REPAIRS	10.6.1
10.7 RESIDUAL STRENGTH PARAMETRIC ANALYSIS	10.7.1
10.8 RESIDUAL STRENGTH ANALYSIS OF COCKPIT LONGERON REPAIR	10.8.1
10.9 RESIDUAL STRENGTH ANALYSIS OF A SKIN PANEL REPAIR	10.9.1
10.10 LIST OF REFERENCES	10.10.1

LIST OF FIGURES

<u>FIGURE</u>		<u>PAGE</u>
10.1.1	Relationships Between Residual Strength, Crack and Time-in-Service.	10.1.6
10.2.1a	Experimental Propagation Behavior of Corner Crack with Full F-4E/S Wing Spectrum (68000 cycles/1000 flight hours) Scaled to Two Stress Levels (36 and 30.5 ksi).	10.2.13
10.2.1b	Experimental Flight-By-Flight Fatigue Crack Growth Behavior of a B-1A Wing Spectrum Scaled to Three Stress Levels (24.17, 31.12, and 36.31 ksi).	10.2.14
10.2.2	Method for Reducing Fatigue Crack Growth Life Data to Fatigue Crack Growth Rate Data.	10.2.15
10.2.3	Fatigue Crack Growth Rate Data for Two Transport Spectra (A = Upper Wing, B = Lower Wing).	10.2.16
10.2.4	Crack Incrementation Scheme Based on Cycle-by-Cycle Crack Growth Analysis.	10.2.17
10.2.5	Crack Growth Rate Description of Crack Incrementation Data for Two Transport Wing Stress Histories ($\Delta F=50$ Flights).	10.2.17
10.3.1a	Center Wing Stress History for Mission 1.	10.3.22
10.3.1b	Inner Wing Stress History for Mission 1.	10.3.23
10.3.1c	Outer Wing Stress History for Mission 1.	10.3.24
10.3.2	Exceedance Curves for the Three Transport Wing Stress Histories.	10.3.25
10.3.3	Common Geometry Used to Evaluate Stress History Effect on Crack Growth Behavior.	10.3.27
10.3.4	Crack Growth Behavior for the Center Wing Location; Part a Generated Using CRKGRO Part b Generated by Secant Slope Method.	10.3.28

LIST OF FIGURES (Cont'd)

<u>FIGURE</u>	<u>PAGE</u>
10.3.5 Flight-by-Flight Crack Growth Life Behavior for Inner Wing (WS-733) and Outboard Wing Stress Histories.	10.3.29
10.3.6 Flight-by-Flight Fatigue Crack Growth Rate Behavior for Three Transport Wing Histories.	10.3.30
10.3.7 Comparison Between Outer Wing Data and the Least Squares Determined Curve.	10.3.31
10.3.8 Flight-by-Flight Crack Growth Behavior Exhibited for the Inner Wing (WS733) Stress History Scaled to Two Different Stress Levels.	10.3.32
10.3.9 Cyclic Crack Growth Rate Behavior for Three Transport Wing Stress Histories. $\bar{K} = \sigma_{\max_{\text{RMS}}} \cdot (K/\sigma)$	10.3.33
10.3.10 Cyclic Crack Growth Rate Behavior for Three Transport Wing Stress Histories. $\bar{K} = \Delta\sigma_{\text{RMS}} \cdot (K/\sigma)$	10.3.34
10.3.11 Schematic of Elements Required to Analyse for Crack Growth Life at Specific Locations.	10.3.35
10.4.1 Schematic Describing the Use of Equation 10.4.3 to Scale the Crack Growth Life Curve Based on a Stress Level Change from σ to $x \cdot \sigma$ where $x < 1$.	10.4.9
10.4.2 Life Scaling Factor (New Life \div Current Life) as a Function of the Stress Scaling Factor (x = New Stress/Current Stress).	10.4.10
10.4.3 Doubler Analysed in EXAMPLE 10.4.1.	10.4.11
10.4.4 Description of Structural Geometry and Defini- tion of Analysis Location and of Crack Site.	10.4.12
10.4.5 Details of Cracking Process at Location B and Life Curve.	10.4.13

LIST OF FIGURES (Cont'd)

<u>FIGURE</u>		<u>PAGE</u>
10.5.1	Crack Growth Ratio as a Function of Initial Crack Size Based on Results Presented in EXAMPLE 10.5.1.	10.5.8
10.5.2	Three Stages in the Life of A Cracked Hole.	10.5.9
10.5.3	Geometrical Parameters Associated with Blueprint and Post Rework Crack Configurations for EXAMPLE 10.5.2.	10.5.10
10.6.1	Geometry of Structure with Small Crack.	10.6.15
10.6.2	Geometry of Blend-Out Repair Assumed for Analysis.	10.6.15
10.6.3	Tabular Data Page From the Damage Tolerant Design (Data) Handbook Used in EXAMPLE 10.6.1.	10.6.16
10.6.4	Graphical Data Page From the Damage Tolerant Design (Data) Handbook Used in EXAMPLE 10.6.1.	10.6.17
10.6.5	Tabular Data From Damage Tolerant Design (Data) Handbook (Figure 10.6.3) Plotted and Compared to Graphically Established Power Law Equation.	10.6.18
10.6.6	Short and Long Crack Limiting Cases and Numerical Solution, for Cracks Growing From a Circular Hole in an Infinite Plate (Newman).	10.6.19
10.6.7	Geometry of Blend-Out with Edge Crack Present.	10.6.20
10.7.1	Types of Residual Strength Relationships	10.7.17
10.7.2	Tension-Loaded, Open Hole with Radial-Through-The-Thickness Crack.	10.7.18
10.7.3	Effect of Fracture Toughness on the Residual Strength-Crack Length Relationship for a Radially Cracked Hole.	10.7.19
10.7.4	Crack Growth-Life Relationship for the Baseline Geometry.	10.7.19
10.7.5	Effect of Fracture Toughness on the Residual Strength-Life Relationship.	10.7.20

LIST OF FIGURES (Cont'd)

<u>FIGURE</u>		<u>PAGE</u>
10.7.6	Effect of Stress Level on Crack Growth-Life Relationship.	10.7.21
10.7.7	Effect of Stress Level on Residual Strength-Life Relationship.	10.7.21
10.7.8	Variation of Crack Growth Behavior Resulting from a Shift in the Power Law Curve.	10.7.22
10.7.9	Effect of Pre-exponential Constant (C) on Residual Strength-Life Relationship.	10.7.23
10.7.10	Crack Growth Curves Shown Passing Through Common Point, Used in EXAMPLE 10.7.4.	10.7.24
10.7.11	Effect of Exponent n on the Crack Growth Life Relationship.	10.7.25
10.7.12	Effect of Exponent n on the Residual Strength-Life Relationship.	10.7.25
10.7.13	Effect of Geometry on the Residual Strength-Crack Length Relationship.	10.7.26
10.7.14	Effect of Geometry on the Crack Growth-Life Relationship.	10.7.26
10.7.15	Effect of Geometry on the Residual Strength-Life Relationship.	10.7.27
10.7.16	Pin Loading Configuration for a Radial Through-The-Thickness Crack.	10.7.28
10.7.17	Effect of Pin Loading on the Residual Strength-Crack Length Relationship.	10.7.29
10.7.18	Effect of Pin Loading on the Crack Growth-Life Relationship.	10.7.29
10.7.19	Effect of Pin Loading on the Residual Strength-Life Relationship.	10.7.30
10.8.1	Cracked Longeron, Top (Material 7178-T6).	10.8.12
10.8.2	Specified Longeron Repair.	10.8.12

LIST OF FIGURES (Cont'd)

<u>FIGURE</u>		<u>PAGE</u>
10.8.3	Section Geometry.	10.8.13
10.8.4	Steps in Computation of Maximum Allowable Stress for Damage Tolerance Analysis.	10.8.14
10.9.1	Example of Airframe Lower Wing Skin Crack Repair.	10.9.11
10.9.2	View of Repair Installaion on Outer Wing Lower Surface.	10.9.12
10.9.3	Rotation of Generalized Stress Element to Produce Principal Stress Orientation.	10.9.13
10.9.4	Rotation of Stress Element in Lower Wing Skin to Principal Stress Direction (stresses in psi).	10.9.13
10.9.5	Reproduction of Figure 1.7.3 for Use in EXAMPLE 10.9.2.	10.9.14

LIST OF TABLES

<u>TABLE</u>		<u>PAGE</u>
10.2.1	BOMBER/TRANSPORT BEHAVIOR	10.2.10
10.2.2	FIGHTER/ATTACK/TRAINER BEHAVIOR (BASED ON 1000 FLIGHT HOUR BLOCK SPECTRA)	10.2.11
10.3.1	MISSION ORDERING FOR TRANSPORT FLIGHT-BY-FLIGHT SPECTRUM	10.3.3
10.3.2	REPLACEMENT STRESSES FOR MISSION 1 FOR THE THREE WING LOCATIONS	10.3.4
10.3.3	PER CYCLE ROOT MEAN SQUARE REPRESENTATIVE STRESS VALUES FOR THE THREE WING STRESS HISTORIES	10.3.7
10.3.4	PER FLIGHT ROOT MEAN SQUARE REPRESENTATIVE STRESS VALUES FOR THREE WING STRESS HISTORIES	10.3.9
10.3.5	CONSTANTS C AND p FOR EQUATION 10.3.1	10.3.14
10.3.6	EFFECT OF STRESS MAGNIFICATION FACTOR ON CRACK GROWTH LIVES (L) CALCULATED BY CRKGRO FOR A CENTER CRACK (2a) GROWING BETWEEN 2a = 0.22 AND 1.60 INCH	10.3.15
10.3.7	RATIO OF POWER LAW LIFE PREDICTIONS (L_{PL}) TO CRKGRO LIFE PREDICTIONS (L_{CG}) (RATIO > 1, UNCONSERVATIVE)	10.3.18
10.4.1	RELATIONSHIP BETWEEN STRESS SCALING FACTOR x AND LIFE SCALING FACTOR $L_{x\sigma}$ FOR DEFINED VALUES OF THE CRACK GROWTH EXPONENT p	10.4.3
10.5.1	CRACK GROWTH LIFE AS A FUNCTION OF INITIAL SIZE FOR $\bar{\sigma} = 30$ ksi AND $a_f = 0.550$	10.5.4
10.5.2	COMPARATIVE ANALYSIS TO DETERMINE THE EFFECT OF ENLARGING THE HOLE (INITIAL CRACK LENGTH = 0.050 INCH)	10.5.7

LIST OF TABLES (Cont'd)

<u>TABLE</u>		<u>PAGE</u>
10.6.1	EFFECTS OF BLEND-OUT SHAPE ON CRACK GROWTH LIFE RATIO	10.6.13
10.6.2	EFFECT OF REPAIR INITIAL CRACK SIZE ON CRACK GROWTH LIFE RATIO	10.6.14
10.9.1	SUMMARY OF K_{APP} DATA FOR 7075-T6 SHEET AT ROOM TEMPERATURE (Abstracted from DTD HB TABLE 8.9.2.2)	10.9.9

CHAPTER 10

ANALYSIS OF STRUCTURAL REPAIRS

10.1 INTRODUCTION

The structural integrity of a force of operational aircraft is primarily ensured by implementing the periodic inspection and maintenance program defined in the Force Structural Maintenance (FSM) plan and the associated technical order (T.O.)-3 repair and -36 inspection manuals. In addition to this formal method of addressing known or potential cracking problems, the structural integrity of individual aircraft is also ensured through the timely identification of new cracking problems and by implementing repairs that will return cracked structure to a safe operational condition. This chapter is presented as a supplement to the other chapters and only specifically addresses those guidelines applicable to ensuring that adequate damage tolerance exists in structural repairs. Adequate damage tolerance implies that cracks do not reduce the structure's load carrying capability below a predefined level throughout a required period of in-service usage.

10.1.1 Repairs/Changes Requiring Analysis

All repairs made to cracked structure and all structural changes made to in-service aircraft require some form of damage tolerance analysis. The degree of intensity of each analysis, however, depends on the consequences of failure in the repaired or modified structure if cracks are present. For example, the extent of the analysis of a repair to replace a compressively loaded fuselage member that is removed for corrosion damage would be minimal, while a force-wide modification to the tension-loaded,

primary-load-path, lower wing skin structure of a fighter aircraft would require an indepth evaluation of expected fracture and fatigue crack growth behavior.

The best categorization of what requires an indepth damage tolerance analysis can be directly taken from the MIL-A-83444 specification applicable to new structure. This specification requires that all safety-of-flight critical structure be designed using a damage tolerance analysis. The analysis ensures that cracks potentially present in this type of structure will not cause loss of the aircraft during flight for some predefined period of in-service operation. The above suggests the first guideline for structural repairs and modifications, i.e., all structural repairs and modifications to safety-of-flight critical structure, must be subjected to indepth damage tolerance analyses to ensure that the structure is not degraded as a result of the repair (or modification) below a level considered satisfactory for the subsequent in-service operational period contemplated.

A question arises relative to the definition of what constitutes safety-of-flight critical structure and their locations within the airframe. Based on the information required by MIL-STD-1530A for the support of force management operations, a critical parts list is prepared by the airframe contractor and appended to the Force Structural Maintenance (FSM) plan supplied to the Air Force. It is suggested then that clear definitions for safety-of-flight critical structure be provided with each aircraft's FSM plan along with the appendix that lists and illustrates safety-of-flight critical structure. If the manufacturer can conceive of potential problems associated with the

repair or modification of specially designed (or manufactured) safety-of-flight critical structure, then the manufacturer should identify such problems in the FSM plan with reference to additional details in the T.O.-3 repair manual.

The intensity of the analysis also varies as a function of the extensiveness of the change to the force. If the repair or modification can be incorporated into any given aircraft or will be applied to all aircraft in the force, then a more careful analysis of the impact of cracks potentially existing in the structure should be conducted. For one-of-a-kind repairs applied to an airframe in order to return the aircraft to a depot for more extensive repair, the type of damage tolerance analysis would be primarily of a residual strength type, without much consideration being given to variable amplitude fatigue loading.

10.1.2 Levels of Damage Tolerance Analysis

There are two basic elements in a damage tolerance analysis: a residual strength analysis and a subcritical crack growth analysis. In the residual strength analysis, one develops a relationship between load carrying capability and crack length. In the subcritical crack growth analysis, one determines a relationship between time-in-service and crack length for a given type of operation.

In a damage tolerance analysis, one obtains an estimate of the structural life to grow the initial crack damage in the structure to critical size. The residual strength analysis determines the critical crack size required to fail the structure; the subcritical crack growth analysis is used to obtain the life

10.1.3

estimate. One could also determine the decay in residual strength as the crack extends under service loading by coupling the residual strength analysis with the subcritical crack growth analysis. Figure 10.1.1a illustrates the relationship between residual strength and crack length. Figure 10.1.1c describes the relationship between crack length and time-in-service. Figure 10.1.1b couples the information in parts a and b to obtain the relationship between the decay in residual strength and time-in-service.

As described in Chapters 1, 4, and 5, the analyst needs the following structural/material information to conduct a damage tolerance analysis:

- Definition of quality - to obtain the initial crack length (a_0) for the subcritical crack growth analysis.
- Definition of operational loading and environmental conditions - (a) to establish the residual strength requirement and (b) to grow the crack in the subcritical crack growth analysis.
- Definition of the structural parameter that relates loading, global geometry, as well as crack size and geometry to crack tip conditions - this parameter makes it possible to relate laboratory behavior to in-service hardware.
- Definition of material properties that characterize resistance to fracture and to subcritical crack growth - to provide the basis for estimating fracture level and the rate of crack growth in the structure.
- A damage summation model - to integrate the effects of variable amplitude loading and time dependent behavior in the subcritical crack growth analysis.

- A fracture model - to provide the criteria for estimating the critical crack length.

For a safety-of-flight critical structural component, detailed analysis and understanding is required for the above structural/material information.

For such detailed analysis, the other chapters have been prepared. This chapter has been prepared to highlight what might be accomplished with both limited information and structural analysis capability. The method of approach in this chapter will be to illustrate how approximate methods can reduce the complexity of a residual strength analysis or full-scale cycle-by-cycle subcritical crack growth rate analysis. The approximate methods facilitate parameter studies that isolate those features of the structure, its material, the usage, the environment, or method of inspection, which control the level of damage tolerance associated with the structure, in an unrepaired or repaired condition.

The remainder of this chapter is organized to present (a) some general observations about usage characterization for crack growth life estimates, (b) a detailed analysis of three transport wing stress histories and the effects of stress scaling, (c) fatigue life sensitivity analysis for stress effects, (d) fatigue life sensitivity analysis for hole repair, (e) fatigue life sensitivity analysis for blend-out repairs, (f) a residual strength parametric analysis to establish limits for return to depot, (g) a detailed residual strength analysis of a cockpit longeron repair, and (h) a detailed residual strength analysis of a wing skin repair.

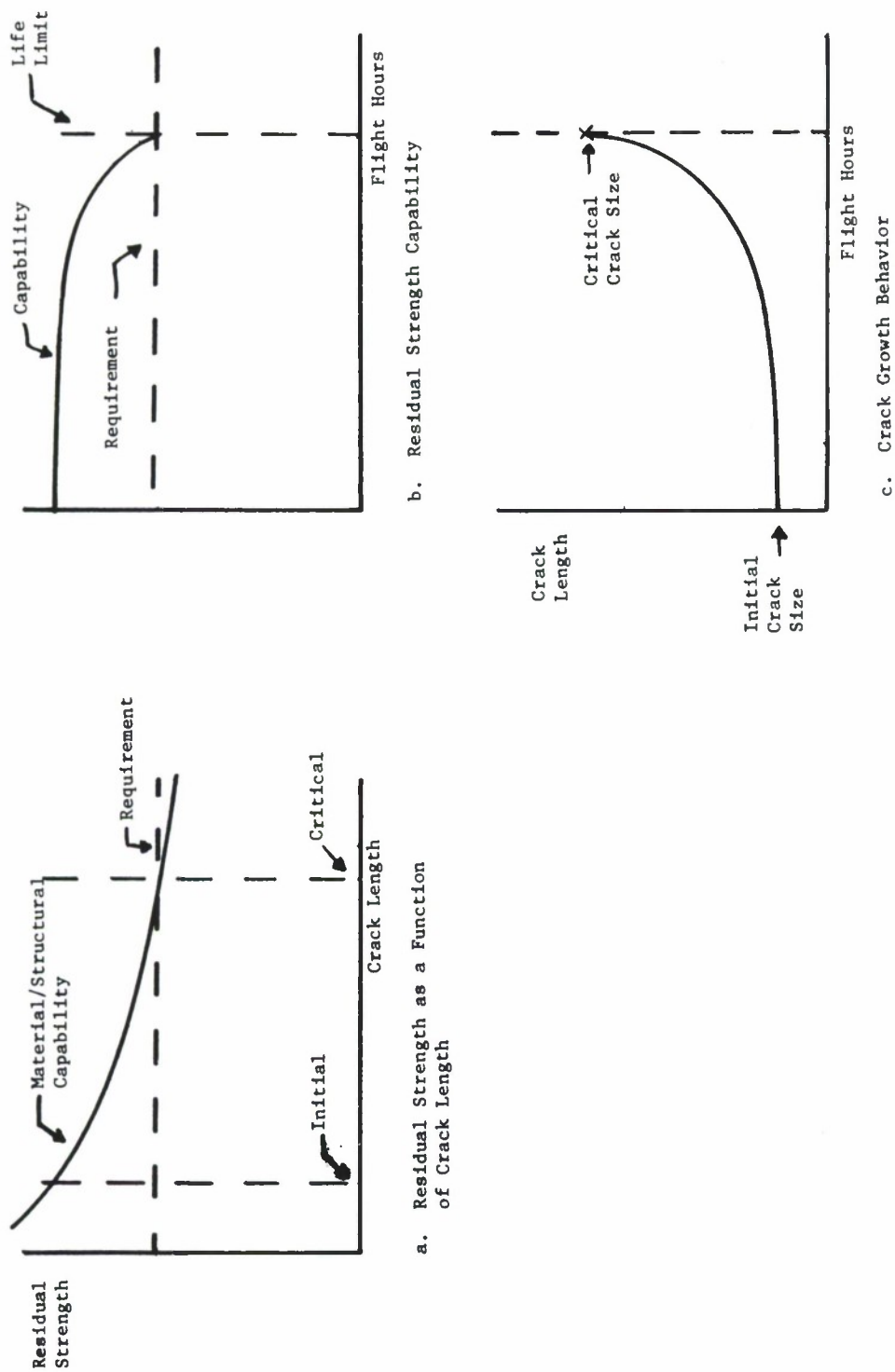


Figure 10.1.1.1 Relationships Between Residual Strength, Crack and Time-in-Service.

10.2 USAGE CHARACTERIZATION FOR SIMPLE REPAIRS

As explained in Section 10.1, there are two reasons for characterizing the usage for a damage tolerance analysis: (a) to establish the residual strength requirement and (b) to grow the crack in the subcritical crack growth analysis. The maximum loading conditions and their frequency (likelihood of occurrence) determine the loading (residual strength) requirement that the structural element must withstand without failure. Typically the more frequently occurring loading conditions are those responsible for growing a crack from its initial size to failure.

For a residual strength analysis of a structural repair, one would want to characterize the maximum loading condition that the structure might experience in its anticipated service life. A simple choice might be based on returning the load carrying capability of the cracked structure to the original ultimate load carrying capability of the structural member without a crack. Sections 10.7, 10.8, and 10.9 describe in more detail the methods for conducting a residual strength analysis.

For a subcritical crack growth analysis, one is more typically interested in characterizing the average per flight loading conditions that will be experienced by the cracked or repaired structure. It is the relatively large, frequently occurring load excursions that drive the crack growth process. From a repair analysis standpoint, it is important that the analyst know what are the sources of large (and frequently occurring) stress excursions and have some indication of the maximum to minimum stress ratios as well as frequency of these excursions on a per flight (or per flight hour) basis.

The more critical the repair, the more important is the definition of the specifics of per flight average loading conditions for a life analysis. If one can identify those loading conditions (even in a general way) that affect the rate at which cracks grow in a given structural member, then simple calculations can be made to obtain first order estimates of this member's structural life. While first order estimates can be questioned from an absolute sense, such estimates, when used in a relative (comparative) sense, can provide the necessary guidance for designing a repair, or releasing an individual aircraft for flight.

In the following subsections, a subcritical crack growth analysis approach which was introduced in Chapter 5, Subsection 5.2.5, is further described and justified for its application for repair analysis. In Section 10.3, an example analysis of three transport wing stress histories will be utilized to illustrate how a generic stress history for a given structural member could be employed to estimate the life at any given location in that member.

10.2.1 Variable Amplitude Crack Growth Behavior

Many airframe loading conditions are sufficiently repetitive over a number of flights (~ 100 to 500 flights) that crack growth damage accumulates in a relatively continuous manner. Figure 10.2.1 describes two examples of experimental crack growth data generated under typical flight-by-flight loadings involving multiple missions. Figure 10.2.1a represents the behavior experienced at a hole subjected to a fighter wing stress history and Figure 10.2.1b represents the behavior observed at a hole subjected to a bomber aircraft wing stress history. Both behaviors illustrate the regular

10.2.2

and relatively continuous crack growth pattern exhibited by many flight-by-flight histories.

As a result of the regularity of such flight-by-flight induced crack growth behavior, there was a recognition as early as 1963 that aircraft stress histories can induce crack growth behavior similar to constant amplitude behavior. This early recognition has led to a number of schemes for utilizing limited information to characterize the behavior of cracks in aircraft structure. These schemes all focus on the translation of variable amplitude crack growth life data to variable amplitude crack growth "rate" data so that the simple analysis schemes for constant amplitude loadings can be used to establish life estimates. These replace the more complicated numerical, computer-based algorithms used for a load interaction, cycle-by-cycle analysis of the complete stress history.

The translation of the variable amplitude crack growth life data to that of variable amplitude crack growth rate data follows most of the procedures used to convert constant amplitude crack growth life data to constant amplitude crack growth rate data (see Subsection 7.2.2, and more specifically Figure 7.2.9, which is repeated as Figure 10.2.2). The major differences between describing variable amplitude rate behavior and constant amplitude rate behavior is in the choice of the rate variable and the characterizing stress history parameter. In variable amplitude descriptions, the crack growth rate may be described as rate per flight, rate per flight hour, or rate per cycle. Also, since the magnitude of the individual stress events in the stress history is a random variable, the characteristic stress parameter that describes the history is a

statistical measure of the individual events in the history.

Figure 10.2.3 describes a variable amplitude crack growth rate behavior ($da/d(\text{Flight})$) as a function of a spectra dependent characteristic stress-intensity factor (\bar{K}) for two transport wing histories. The \bar{K} is calculated based on the formula

$$\bar{K} = \bar{\sigma} \cdot \frac{(K)}{\sigma} \quad (10.2.1)$$

where K/σ is the stress-intensity factor coefficient for the geometry and $\bar{\sigma}$ is the characteristic stress parameter, here chosen as the root mean square (RMS) of the maximum stresses in the history, i.e.

$$\bar{\sigma} = \bar{\sigma}_{\max} = \left[\sum_{i=1}^N (\sigma_{\max_i})^2 / N \right]^{1/2} \quad (10.2.2)$$

In Equation 10.2.2, N is the number of stress events, and σ_{\max_i} denotes the maximum stress for the i th stress event.

It is seen from Figure 10.2.3 that the crack growth rate (on a per flight basis) behavior for the two spectra might be described by a power law equation of the form

$$\frac{da}{dF} = C \bar{K}^p \quad (10.2.3)$$

The corresponding damage integration equation can be expressed as

$$F = \int_{a_o}^a \frac{da}{C \bar{K}^p} \quad (10.2.4)$$

or as

$$a = a_o + \sum_{j=1}^F \Delta a_j \quad (10.2.5)$$

where F is the number of flights required to grow the crack from a_0 to a , and

where Δa_j is evaluated for the current crack length using Equation 10.2.3.

The coefficients C and p are evaluated using least squares procedures applied to data of the type shown in Figure 10.2.3.

The value of the data shown in Figure 10.2.3 and its description with a simple equation, e.g. Equation 10.2.3, is that parametric studies can be conducted in a relatively simple manner. Such parametric studies could cover (a) other ranges of crack length for the same geometry, (b) other structural geometries, and (c) other stress magnification factors applied to the same spectra.

10.2.2 Other Methods for Generating Rate Descriptions

Translating experimental crack growth life data to flight-by-flight crack growth rate only provides one method for generating the flight-by-flight power law growth rate relationship given by Equation 10.2.3. The power law rate equation can also be generated using two different analytic methods. One popular analytical method is to calculate the RMS range and maximum parameters and to substitute these parameters into a constant amplitude - stress ratio equation. This method results in a single curve that describes the effects of this stress combination. The following example illustrates the procedure.

EXAMPLE 10.2.1 - RMS Power Law Analysis

The constant amplitude crack growth equation for a particular alloy is given by (units: in/cycles, ksi $\sqrt{\text{in}}$)

$$\frac{da}{dN} = 8.63 \times 10^{-8} K_{\text{eff}}^{2.347} \quad (10.2.6)$$

where the effective stress-intensity factor has been determined to be of the form:

$$K_{\text{eff}} = [K_{\text{max}} - \frac{3}{(1-R)^{0.35}}] \cdot (1-R)^{0.696} \quad (10.2.6a)$$

When the values of maximum stress (σ_{max}) and stress range ($\Delta\sigma$) for a given constant amplitude loading are known, these values are used with the stress-intensity factor coefficient (K/σ) for the geometry of interest to generate K_{max} , i.e.

$$K_{\text{max}} = \sigma_{\text{max}} \cdot \left(\frac{K}{\sigma} \right), \quad (10.2.7)$$

and with the stress ratio formula

$$R = 1 - \frac{\Delta\sigma}{\sigma_{\text{max}}} \quad (10.2.8)$$

to generate the parameters defined in Equation 10.2.6. To obtain the power law relation that would result for a flight-by-flight spectrum, the RMS values are substituted into Equations 10.2.6 through 10.2.8.

If the RMS range ($\overline{\Delta\sigma}$) and maximum ($\overline{\sigma_{\text{max}}}$) stresses for a given stress history are 4.45 and 12.30 ksi, respectively, the the RMS stress ratio (\overline{R}) is given by (from Equation 10.2.8)

$$\overline{R} = 1 - \frac{\overline{\Delta\sigma}}{\overline{\sigma_{\text{max}}}} = 1 - \frac{4.45}{12.30} = 0.640 \quad (10.2.9)$$

From Equation 10.2.7, the RMS maximum stress-intensity factor is

$$\overline{K}_{\text{max}} = \overline{\sigma_{\text{max}}} \left(\frac{K}{\sigma} \right) = 12.3 \left(\frac{K}{\sigma} \right) \quad (10.2.10)$$

and Equation 10.2.6 becomes

$$\frac{da}{dN} = 8.63 \times 10^{-8} \overline{K}_{\text{eff}}^{2.347} \quad (10.2.11)$$

where

$$\bar{K}_{\text{eff}} = [\bar{K}_{\text{max}} - \frac{3}{0.35}] \cdot (1-0.640)^{0.696} \quad (10.2.11a)$$

or

$$\bar{K}_{\text{eff}} = [\bar{K}_{\text{max}} - 4.29] \cdot (0.491) \quad (10.2.11b)$$

Notice that the rate in Equation 10.2.11 is given on a per cycle basis so one must multiply this rate by the average number of cycles per flight (flight hour) to obtain the corresponding average growth rate per flight (or flight hour).

A method that substitutes RMS (or other statistically derived) parameters into constant amplitude equations has one major limitation. This limitation is that load interaction effects (retardation or acceleration) are ignored. Thus, the analyst must be wary of comparisons between spectra when using this method, since it will only provide first order approximations of spectra effects.

It is possible to account for load interaction effects with a cycle-by-cycle analysis, but as indicated above, the processing of the complete stress history requires extensive numerical analysis. An approach was suggested in the early 1970's for processing a limited portion of a stress history with a cycle-by-cycle analysis for the purpose of generating crack increments at several crack lengths. Most of the details for generating crack increments for such an analysis were discussed in subsection 5.2.5 relative to Figures 5.2.10 and 5.2.11. Figure 5.2.10 is repeated here as Figure 10.2.4, and the corresponding

crack growth rate data is presented in Figure 10.2.5. The choice of methods that one might employ for the cycle-by-cycle analysis is dictated by the success that a given analysis has had in predicting crack growth behavior of the type under consideration. In Section 10.3, a detailed example of an analytical analysis of the crack growth behavior (life and rate) of three transport wing stress histories is conducted. This example should provide additional insight into how the simplified rate method can be used to assess spectra and their differences.

10.2.3 Power Law Descriptions

This subsection was written to illustrate the generality of the flight-by-flight rate approach. The next subsection describes the concerns that an analyst should have before using the approach.

A number of experimental and analytical investigations have revealed that the flight-by-flight crack growth rate behavior of military aircraft can be described with a power law relationship (Equation 10.2.3). Specifically, the stress histories considered were developed to facilitate the design of a new structure or an analysis of an in-service aircraft for force management purposes. As such, these stress histories represented an expected average usage based on a force wide composition mission mix; most of the stresses in these histories repeated after an application of a large block of flights or flight hours. None of the histories involved any major mission change during the expected life of the aircraft. For these histories, one might say that the operations today will be like the operation next year or five years from now.

Nevertheless, the generalized observations of power law flight-by-flight crack growth rate behavior here are immediately applicable to the study of parameters affecting structural repair. Thus, the results of these studies are summarized in Tables 10.2.1 and 10.2.2 for bomber/transport behavior and for fighter/attack/trainer behavior, respectively. Table 10.2.1 presents the coefficients for a crack growth rate per flight type equation, while Table 10.2.2 presents the coefficients for a crack growth rate per flight hour type equation.

The reader can note from Table 10.2.1 that the exponent p for bomber/transport aircraft wing stress histories only varies from about 3.0 to 3.5; Table 10.2.2 indicates a wider variation in the exponent for the aircraft and conditions indicated ($2.2 \leq p \leq 3.7$). Based on a close analysis of the results, it can be said that the largest variations in the exponent p are generated due to the wide variations in spectrum content (load magnitude and frequency).

10.2.4 Analytical Concerns

Before employing a flight-by-flight crack growth rate type analysis to estimate the life of a repair, the analyst should be concerned with the adequacy of such an analysis. The most important part of the analysis is the definition of the stress history that the repaired member will experience in the future. If the history is anticipated to be statistically repetitive as a function of time-in-service then the results from a flight-by-flight rate analysis will be comparable to a cycle-by-cycle analysis.

TABLE 10.2.1

BOMBER/TRANSPORT BEHAVIOR

Aircraft	History	Flights/ Block	$\bar{\sigma}_{\max}$ (ksi)	C^+	p	Aluminum Alloy
B-1A	Wing Pivot	100	27.3	4.91×10^{-8}	3.025	2219
C-5A	Upper Wing	100	11.7	1.70×10^{-8}	3.111	7075
C-5A	Lower Wing	300	12.3	1.05×10^{-7}	3.183	7075
B-52D	Lower Wing	200	16.4	2.61×10^{-8}	3.529	7075
KC 135	Proof Test, Lower Wing	200	17.8	5.97×10^{-9}	3.454	7178
KC 135	Lower Wing	200	18.4	1.01×10^{-8}	3.338	7178

+ inch/flight, $\text{Ksi}/\sqrt{\text{in}}$ units

TABLE 10.2.2

FIGHTER/ATTACK/TRAINER BEHAVIOR
(BASED ON 1000 FLIGHT HOUR BLOCK SPECTRA)

Aircraft	History	C^+	p	Aluminum Alloy
T-38	Lower Wing (Baseline)	2.66×10^{-8}	2.678	7075
T-38	Lower Wing (Severe)	1.07×10^{-8}	3.152	7075
T-38	Lower Wing (Mild)	5.32×10^{-9}	2.460	7075
F-4	Lower Wing (Baseline)	1.68×10^{-8}	2.242	7075
F-4	Lower Wing (High Stress Baseline)	1.77×10^{-8}	2.242	7075
F-4	Lower Wing (Severe)	1.76×10^{-8}	2.395	7075
F-4	Lower Wing (Mild)	5.77×10^{-9}	2.395	7075
F-16	Lower Wing (Mix)	6.92×10^{-10}	3.62	7175
F-16	Tail (Mix)	1.33×10^{-10}	3.67	7175
F-16	Lower Wing (Air to Air)	1.07×10^{-9}	2.905	7175
F-16	Lower Wing (Air to Ground)	8.94×10^{-11}	3.464	7175

+ inch/flight hour, ksi $\sqrt{\text{in}}$ units

If the mission type or mix is expected to change significantly as a function of time, then projecting a predefined rate of crack growth without detailed consideration of how the damage will be changing could lead to nonconservative errors. One method for addressing mission type or mix changes is to utilize one rate curve before the time of change and another rate curve subsequently. A more exact method for addressing mission changes is by using a cycle-by-cycle crack growth analysis applied to the stress history that accounts for the changes.

Rate methods have one inherent problem; they tend to minimize the effects of the infrequently applied large loads. These large loads will cause retardation effects and tend to slow the growth process (if, in application, failure is not induced). Thus rate methods will normally predict somewhat shorter (more conservative) lives than cycle-by-cycle analyses.

Based on Tables 10.2.1 and 10.2.2 the analyst should note that the crack growth rate equation is a function of material, location, and usage. An equation generated for the horizontal tail should not be used for the vertical tail (nor wing); an equation generated for air-to-ground operations should not be utilized for air-to-air operations.

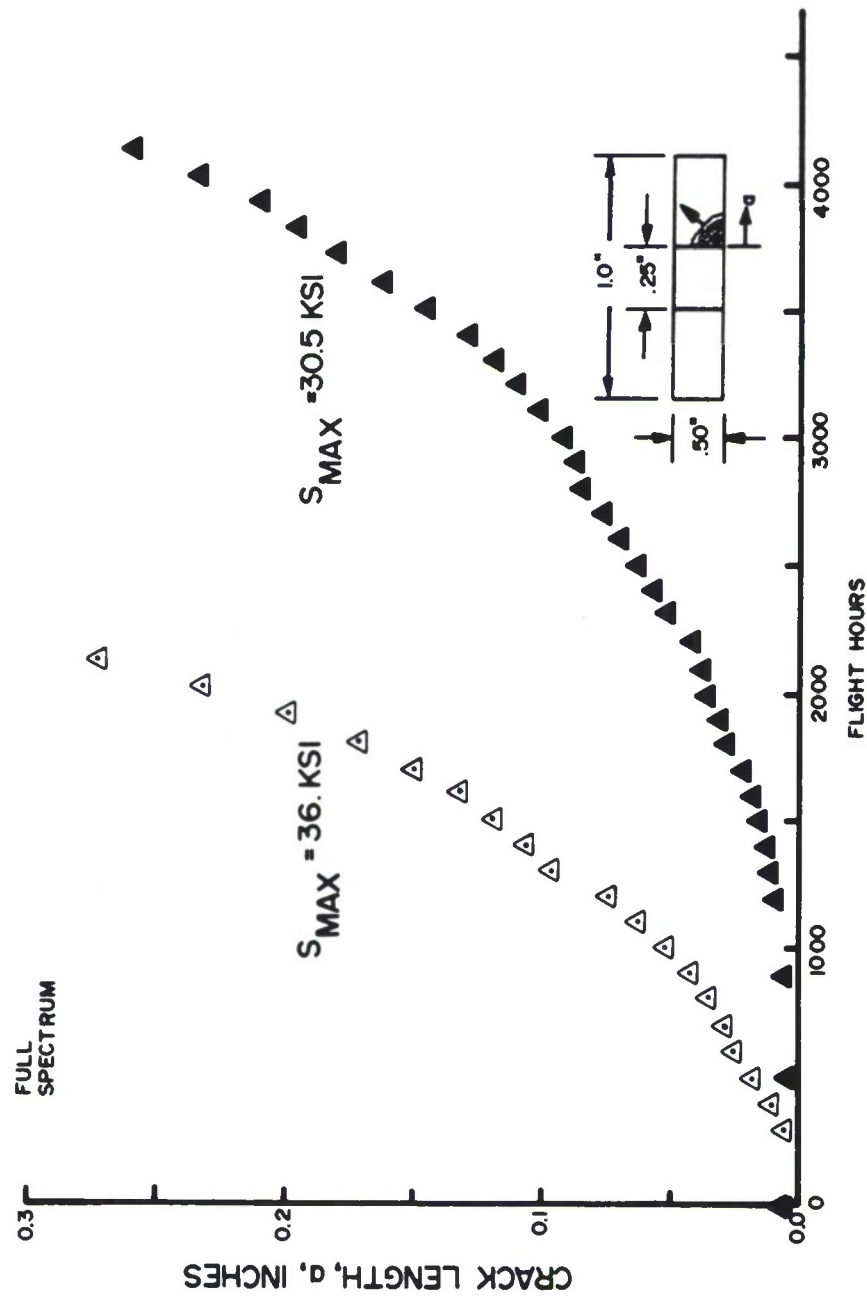


Figure 10.2.1a. Experimental Propagation Behavior of Corner Crack with Full F-4E/S Wing Spectrum (68000 cycles/1000 flight hours) Scaled to Two Stress Levels (36 and 30.5 ksi).

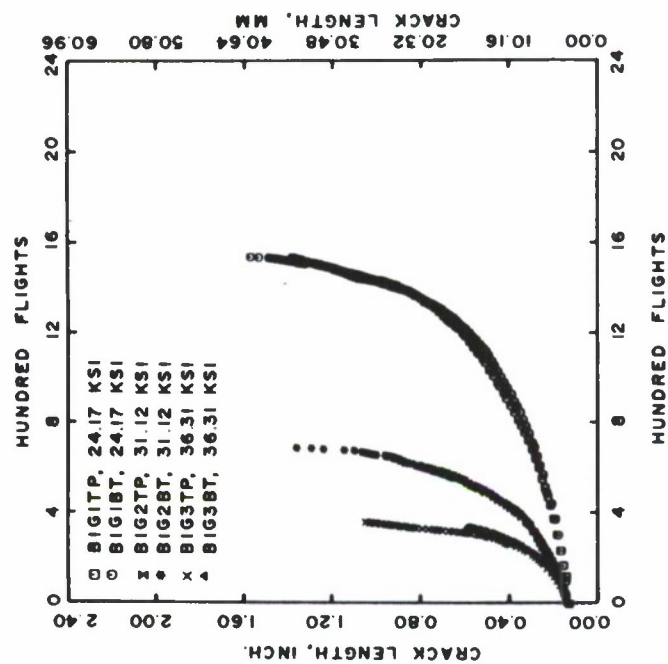


Figure 10.2.1b. Experimental Flight-By-Flight Fatigue Crack Growth Behavior for a B-1A Wing Spectrum Scaled to Three Stress Levels (24.17, 31.12, and 36.31 ksi).

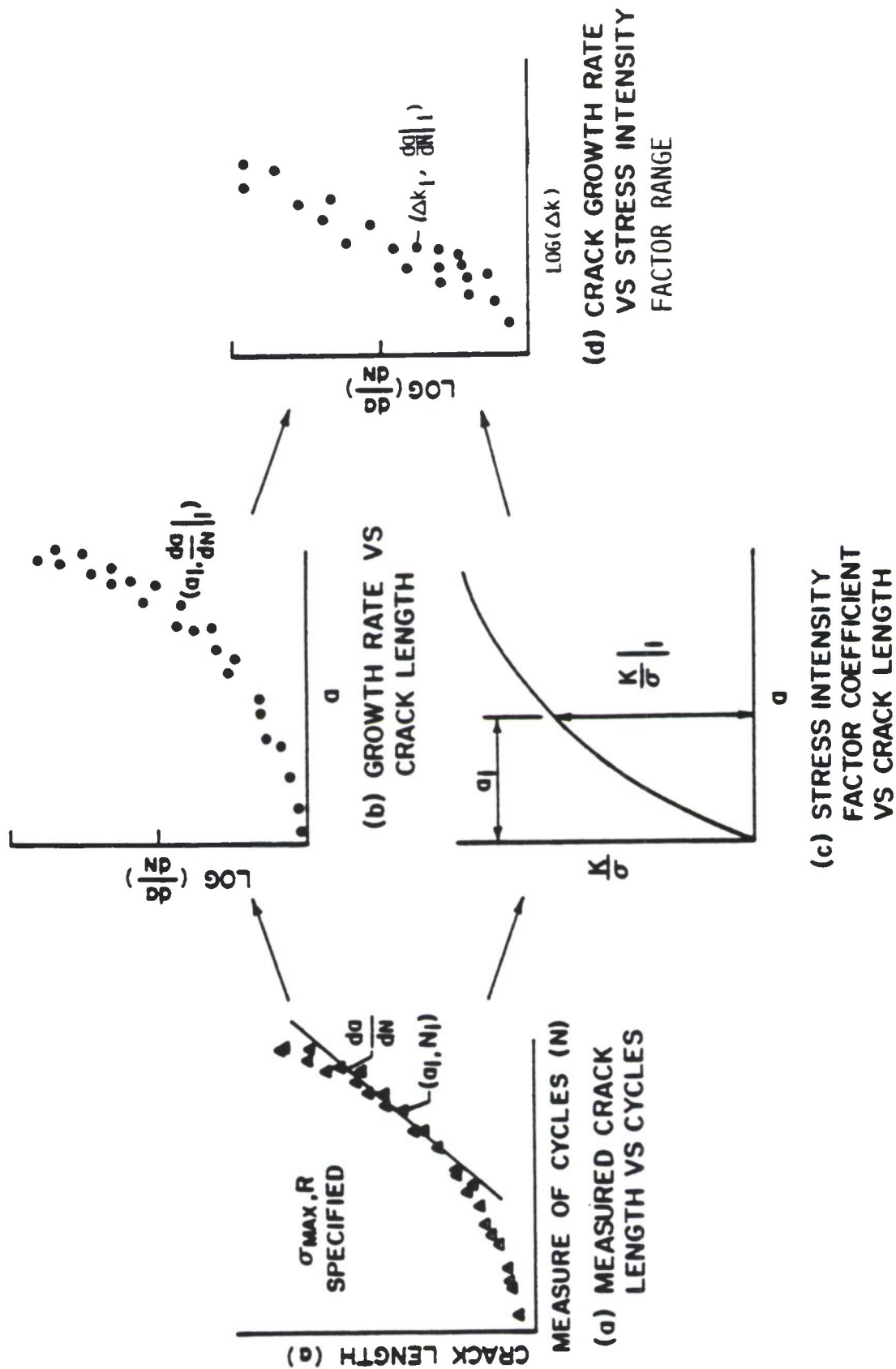


Figure 10.2.2.2. Method for Reducing Fatigue Crack Growth Life Data to Fatigue Crack Growth Rate Data.

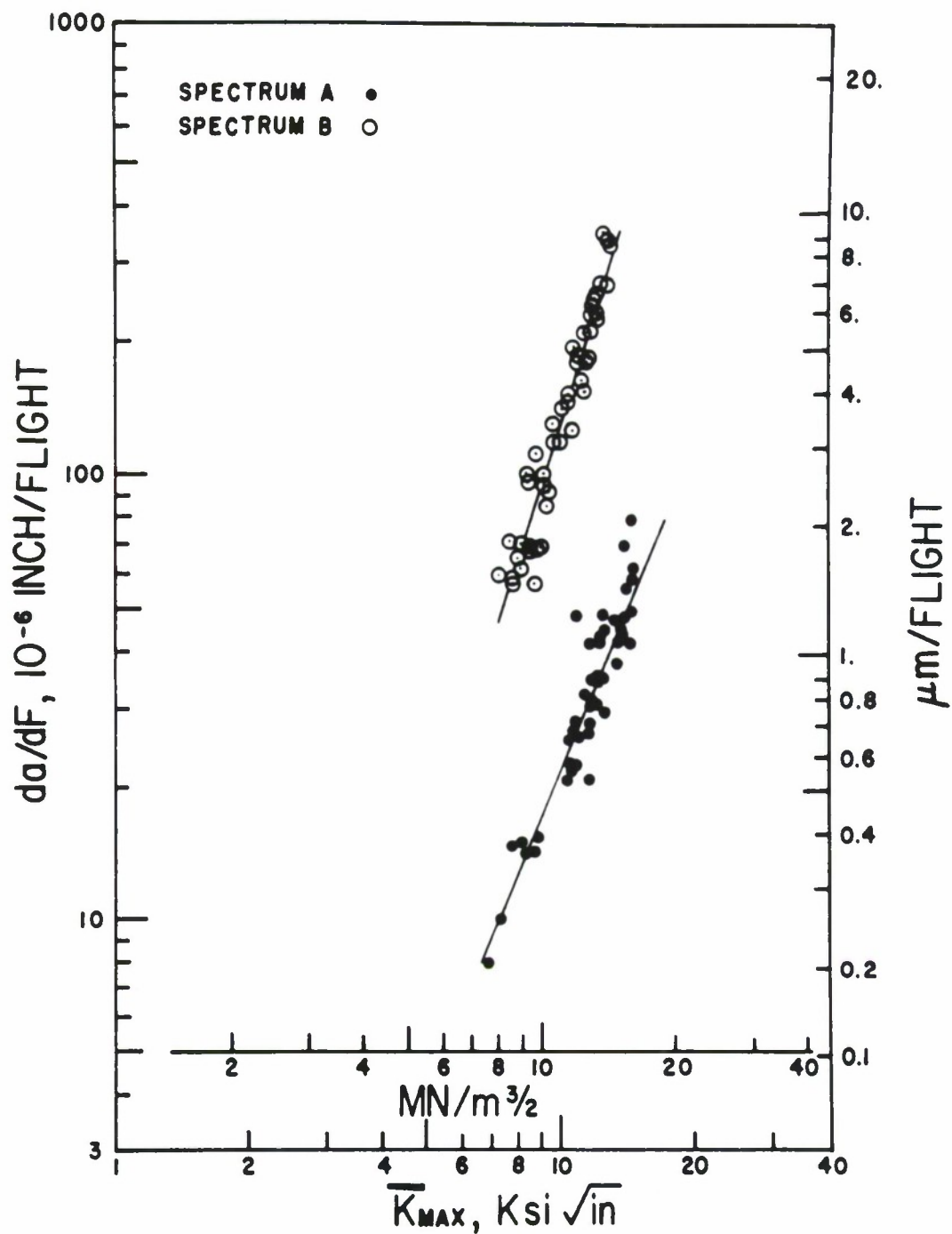


Figure 10.2.3. Fatigue Crack Growth Rate Data for Two Transport Spectra (A = Upper Wing, B = Lower Wing).

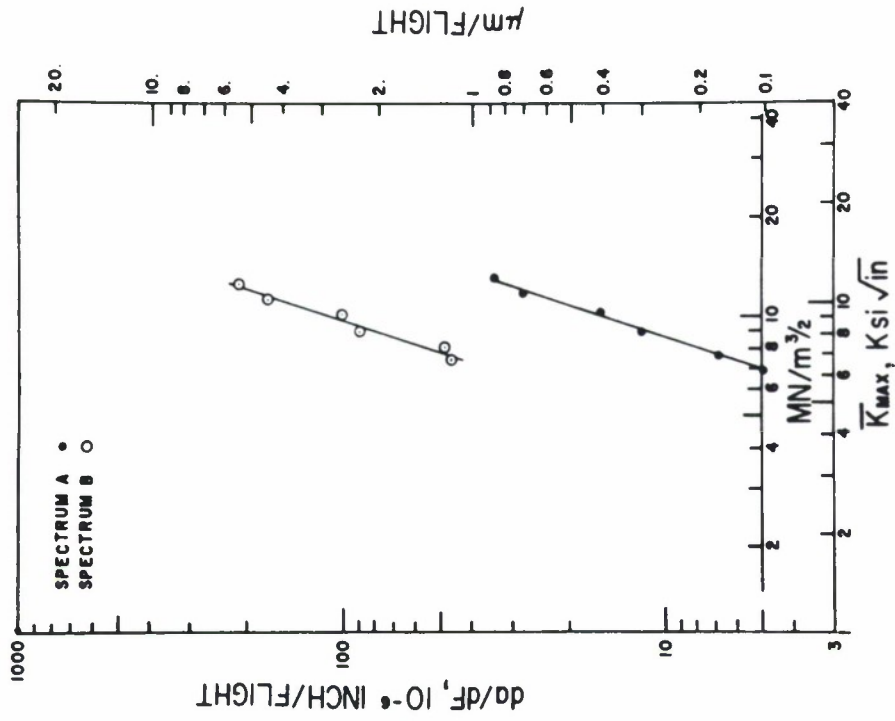


Figure 10.2.5 Crack Growth Rate Description of Crack Incrementation Data for Two Transport Wing Stress Histories ($\Delta F=50$ Flights).

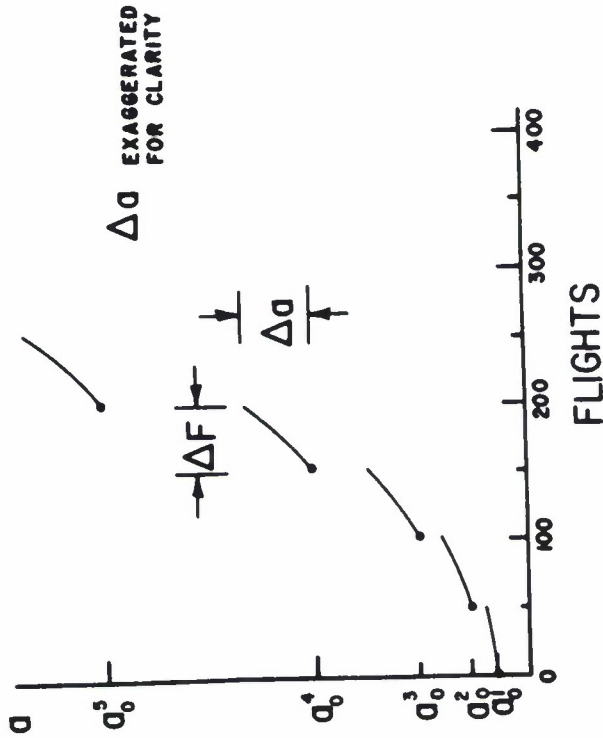


Figure 10.2.4 Crack Incrementation Scheme Based on Cycle-by-Cycle Crack Growth Analysis.

10.3 SPECTRUM ANALYSIS FOR REPAIR

As discussed in Section 10.2, the flight-by-flight crack growth rate behavior for many structural loading conditions can be defined using a power law that relates crack growth rate to a characteristic stress-intensity factor, i.e.

$$\frac{da}{dF} = C\bar{K}^P \quad (10.3.1)$$

An example analysis is conducted using three transport wing stress histories to illustrate how such equations can be generated. Subsequent to the generation of the flight-by-flight crack growth rate equations, additional analysis is conducted to evaluate the effects of stress level and structural location on the use of these equations for the analysis of structural repairs.

10.3.1 Definition of Stress Histories

The transport stress histories utilized for this example were developed during a force management update and represent the expected behavior at three separate locations on the lower wing surface. The force management update involved a complete durability and damage tolerant analysis of the airframe as well as a reassessment of past and future usage of the aircraft force. Stress histories were generated for durability and damage tolerant studies at those structural locations identified as potentially critical to the continuing safe operation of the force.

The lower wing stress histories chosen for this example analysis represent locations in the center wing (BL 70), in the inner wing (WS 733) and the outer wing. All three stress histories were developed assuming the same operational (mission mix) history. The operational history was considered

to be represented by a block of 100 flights with a defined mission order. Eight (8) separate missions were identified as representative of service operations. Each mission in the 100-flight block averaged 4.8 hours per flight.

The 100-flight block of ordered missions repeated until the service life of 40,000 flight hours was exceeded; thus, more than 83 applications of the repeating 100-flight blocks were required to define one lifetime of operation. The mission order for the eight representative missions is defined by Table 10.3.1. For comparison purposes, Figure 10.3.1 presents the stress histories for mission 1 at the three locations. The stress histories for the other seven missions could be defined in a similar manner.

The stress history for each location is now defined except for the infrequently occurring maximum stresses. The infrequently occurring stresses in each mission were inserted into the history on a periodic basis as a replacement for the first maximum stress in the mission. The period of occurrence of these replacement load events was during the tenth, the one-hundredth, and the two-hundredth repeat occurrence of any of the individual eight missions. The replacement maximum stresses for mission 1 for the three locations are listed in Table 10.3.2. Each mission had a similar set of replacement stresses.

Table 10.3.1

MISSION ORDERING FOR TRANSPORT
FLIGHT-BY-FLIGHT SPECTRUM

Order Per 20 Flight Group	Flights 1-20	Flights 21-40	Flights 41-60	Flights 61-80	Flights 80-100
1	4	6	7	6	5
2	1	7	7	1	4
3	1	7	6	1	6
4	7	2	3	7	1
5	6	1	6	6	1
6	4	4	2	5	8
7	5	3	6	3	2
8	2	8	7	7	3
9	5	5	3	4	8
10	8	4	8	2	6
11	2	3	8	3	7
12	8	1	7	6	5
13	2	6	3	5	6
14	7	6	1	6	6
15	1	3	8	7	6
16	6	8	5	7	5
17	7	6	7	6	1
18	7	1	6	2	5
19	2	2	2	5	4
20	7	4	4	4	7

Table 10.3.2

REPLACEMENT STRESSES FOR MISSION 1 FOR THE
THREE WING LOCATIONS

Occurance Frequency (per no. of mission repeats)	Center Wing (BL-70) Location (ksi)	Inner Wing (WS-733) Location (ksi)	Outer Wing Location (ksi)
1/1	14.64	14.43	16.34
1/10	16.16	16.14	18.36
1/100	17.96	18.20	20.79
1/200	18.60	18.89	21.56

10.3.2 Spectra Descriptions

The stress history uniquely defines the sequence and magnitude of the individual stress events applied at a specific location. While this information is essential for conducting a cycle-by-cycle crack growth analysis that accounts for load interaction, it is both difficult to use and interpret without computer programs that perform such analyses. One of the side benefits associated with describing flight-by-flight crack growth rates as a function of a characteristic stress-intensity factor is that one is forced into presenting stress history information simply. This subsection addresses two such schemes - the exceedance curve and an RMS characterization.

10.3.2.1 Exceedance Curve Descriptions

One normally generates a stress history for a given mission based upon exceedance information; however, the starting exceedance information is typically based on operational parameters, e.g. n_z , airspeed, weight, altitude, etc., for given mission functions. After a stress history has been generated for a collection of missions, it is

recommended that stress exceedance curves be generated for the maximum stress, the minimum stress, and the positive (load-increasing) stress range associated with all stress events. The exceedance curves for the maximum, minimum, and range of the individual stress events in the three wing stress histories are presented in Figure 10.3.2.

The exceedance curves for each stress event characteristic are noted (from Figure 10.3.2) to be similar in shape but somewhat displaced relative to number of exceedances. The behavior observed might have been expected since all three locations are experiencing the same operational history. Both the minimum stress and stress range exceedance curves indicate a plateau around 8300 exceedances, which is the dividing line between once per flight occurrences and those that occur more frequently. Thus, because we are dealing with a transport aircraft, it can be noted that the once per flight ground-air-ground (GAG) cycle has a stress range typically larger than 16 ksi, while the gust/maneuver cycles have stress ranges less than 8 ksi.

In anticipating the level of damage that a stress history might generate, the exceedance curve becomes a useful tool. The highest stresses (all events) are noted to be present in the outboard wing (followed by the inner wing and then center wing). Also, for a given magnitude of any stress characteristic, the number of exceedances are the highest for the outboard wing location (followed by the inner wing and then center wing). The implication is that, on a per flight basis, more damage is generated at the outer wing location than at the other two locations, all other things being equal (structural geometry, material, crack geometry, etc.).

The shape of the exceedance curve can also be used to determine if the stress history might be expected to introduce major perturbations in the crack growth behavior. If the exceedance curve associated with the maximum stress characteristic is relatively continuous from the infrequent to the once per flight event, then the flight-by-flight crack growth rate curve would also be expected to be relatively continuous. Except for the outboard wing location curve between 40-60 exceedances, Figure 10.3.2a shows that the maximum stress exceedance curves are relatively continuous. It is therefore expected that the flight-by-flight crack growth rate curves for the three wing histories will be relatively continuous (not show major effects of retardation).

10.3.2.2 RMS Descriptions

The presentation of complicated variable amplitude stress histories can be simplified by defining average or RMS values of the stress event characteristics, i.e. the maximum stresses and positive stress ranges of the history. The difference between the average value and the RMS value of a given characteristic is normally not more than 3 percent when one is considering stress histories with more than 1000 stress events. For average stress analysis, one uses

$$\sigma_{\text{mean}} = \frac{1}{N} \sum_{i=1}^N (\sigma_i / N) \quad (10.3.2)$$

while for RMS analysis, one uses

$$\sigma_{\text{RMS}} = \left[\frac{1}{N} \sum_{i=1}^N \sigma_i^2 / N \right]^{1/2} \quad (10.3.3)$$

where σ_i is the characteristic (maximum stress or stress range) for the i th stress event and N is the total number of stress events.

Similar analysis schemes have also been employed where the slope (p) of the crack growth rate power law expression (Equation 10.3.1) is used to calculate a representative stress, i.e.

$$\sigma_{REP} = \left[\sum_{i=1}^N \sigma_i^{p/N} \right]^{1/p} \quad (10.3.4)$$

Experience has shown that such schemes (Equation 10.3.4) are not appreciably of more value than the average or RMS determined characteristics.

The RMS equation (Equation 10.3.3) was applied to the three transport wing stress histories to obtain RMS values for the maximum stress and stress range. The results are summarized in Table 10.3.3.

Table 10.3.3

PER CYCLE ROOT MEAN SQUARE REPRESENTATIVE STRESS
VALUES FOR THE THREE WING STRESS HISTORIES

Stress History	Maximum Stress (ksi)	Stress Range (ksi)	Cycles Per 100 Flights
Center Wing (BL-70)	8.00	3.52	18268
Inner Wing (WS-733)	7.24	3.33	41174
Outer Wing	8.01	3.38	62562

Based on the RMS analyses presented in Table 10.3.3, it appears as if the three stress histories are quite similar on a per cycle basis (the stress ranges are within five (5) percent, and the maximum stresses are within ten (10) percent). Based on a constant amplitude analysis of these stress conditions, the damage per cycle would be expected also to be similar. From Table 10.3.3, one can note that the number of cycles applied per 100 flight block differs substantially from stress history to stress history. If the RMS stresses are similar and the number of stresses per flight differ, then one would expect that the damage per flight would favor the stress history with the most stress events per flight.

One of the reasons that the RMS representative stresses can not be blindly used in a constant amplitude equation to accurately estimate crack growth behavior is because the damage is a non-linear function of the different events in the history. The analyst must understand where the damage is coming from and isolate on those events. For example, a transport wing stress history generates damage as a result of both GAG cycle loading and gust/maneuver cycle loading. A second analysis was therefore conducted on the three wing histories to obtain per flight characteristics for the GAG and gust/maneuver cycles. This analysis is presented in Table 10.3.4.

Table 10.3.4
PER FLIGHT ROOT MEAN SQUARE REPRESENTATIVE STRESS
VALUES FOR THREE WING STRESS HISTORIES

Stress History	GAG Maximum Stress (ksi)	GAG Stress Range (ksi)	Gust/Manu. Maximum Stress (Ksi)	Gust/Manu. Stress Range (ksi)	Number of Gust/Manu. Cycles
Center Wing (BL-70)	12.23	18.64	7.97	3.35	182
Inner Wing (WS-733)	13.14	18.13	7.21	3.31	411
Outer Wing	14.73	20.01	7.99	3.29	625

Relative to the per flight RMS representative stress values for GAG and gust/maneuver cycles, the three stress histories are shown to be relatively similar. The magnitude of the GAG cycle appears to be increasing as the location moves outboard; this would indicate that the GAG cycle causes more damage per flight in the outboard wing than at the inner and center wing locations. We note that the largest number of gust/maneuver cycles occur at the outer wing location and this would also favor more damage per flight (due to gust/maneuver cycles) than the other two locations.

10.3.3 Crack Growth Analysis

To obtain a flight-by-flight crack growth rate equation (Equation 10.3.1), it is necessary to have either a crack growth life curve or the capability for generating such a curve. As described in Section 10.2, once a flight-by-flight crack growth life curve exists, it can be differentiated to obtain crack growth rates.

The simplest manner for differentiating a curve is by using the secant method, i.e.

$$\frac{da}{dF} = \frac{a_2 - a_1}{F_2 - F_1} \quad (10.3.5)$$

where (a_1, F_1) and $a_2, F_2)$ represent two different points on the crack growth life, crack length (a) versus flights (F) curve. The derivative (Equation 10.3.5) is considered to be the slope of the curve at the mean crack length of the two points, i.e.

$$a_{\text{mean}} = \frac{1}{2} (a_1 + a_2) \quad (10.3.6)$$

The mean crack length provides the ability to calculate the stress-intensity factor coefficient (K/σ) for the geometry associated with the crack growth life curve. To describe the crack growth rate as a function of stress-intensity factor, it is necessary to have either a formula or graph that relates stress-intensity factor to crack length for a known external loading condition. For example, if the stress-intensity factor is related to gross stress condition (σ_{gross}) by the formula

$$K = \sigma_{\text{gross}} \cdot \beta \sqrt{\pi a} \quad (10.3.7)$$

Then the stress-intensity factor coefficient is

$$\frac{K}{\sigma_{\text{gross}}} = \beta \sqrt{\pi a} \quad (10.3.8)$$

and Equation 10.3.8 is evaluated for $a = a_{\text{mean}}$ (Equation 10.3.6). Note that β is typically a function of crack length.

10.3.3.1 Generation of Crack Growth Curves

Crack growth life curves were generated for the three transport wing stress histories using the modular version of CRKGRO, a variable amplitude crack growth analysis computer code. The material chosen for the study was a 7075-T651 aluminum alloy; the associated constant amplitude crack growth rate curve was

$$\frac{da}{dN} = \frac{5 \times 10^{-7} (K_{\max} (1-R))^{2/3}}{K_C - K_{\max}} \quad (10.3.9)$$

with $K_C = 68 \text{ ksi } \sqrt{\text{in}}$ and a $R = -0.12$ negative cutoff. The Willenborg-Chang retardation model embedded within CRKGRO was used to account for load-interaction effects. These modeling choices affect the absolute accuracy of the crack growth predictions but not the implications of the analysis which are presented in a relative sense.

Rather than dealing directly with the actual structural geometries for the three wing locations, it was decided that the crack growth analysis would be applied for a common geometry for all three stress histories. This choice does not affect the crack growth rate analysis as will be further discussed below. The choice of common geometry for all three stress histories makes it possible to evaluate the relative effects of per flight and per cycle damage in a straightforward manner. Since a common geometry is being chosen for the analyses, we decided also to choose a simple geometry: a four (4) inch wide center cracked panel was the choice, giving a stress-intensity factor coefficient of

$$\frac{K}{\sigma} = \left(\pi a \cdot \sec \frac{\pi a}{W} \right)^{1/2} \quad (10.3.10)$$

The initial and final crack length chosen for the configuration were 0.11 and 1.25 inch, respectively. Figure 10.3.3 summarizes the common configuration employed in this analytical study.

Figure 10.3.4 presents both the crack growth life curve generated by CRKGRO and its crack growth rate counterpart for the center wing stress history. The crack growth rate curve was generated by forming the secant defined slope for consecutive points on the life curve and relating this slope to the stress-intensity factor calculated using the mean crack length and the RMS maximum stress value (given in Table 10.3.3). The stress-intensity factor in Figure 10.3.4 is given by

$$K = \left(\sigma_{\max} \right)_{\text{RMS}} \cdot \left(\frac{K}{\sigma} \right) \quad (10.3.11)$$

where $\left(\sigma_{\max} \right)_{\text{RMS}} = 8.0$ ksi and (K/σ) is given by Equation 10.3.10. The curve through the center of the points in Figure 10.3.4 is the mean trend curve that connects all the points.

Figure 10.3.5 presents the crack growth life curves generated for the other two wing locations, again using the computer code CRKGRO. Figure 10.3.6 summarizes the crack growth rate behavior associated with all three stress histories. The inner and outboard wing crack growth rate data points were also generated by the secant method of analysis. The RMS maximum stresses used for the stress multiplier in Equation 10.3.11 were 7.24 and 8.01 ksi for the inner wing and outer wing location, respectively.

10.3.3.2 Analysis of Observed Behavior

A number of observations can be made from the data presented in Figures 10.3.4 through 10.3.6. First, the life is shortest and the rates are fastest for the outer wing stress history; this stress history is the most damaging from a crack growth point of view. The next most damaging history is the inner wing stress history; the least damaging history is associated with the center wing location. Second, the three crack growth rate curves appear to be almost parallel and relatively continuous throughout the range shown. There are discontinuities in the outer and inner wing curves which tend to locally depress the rate curves. These discontinuities are not severe and are associated with the exceptionally high but frequently occurring maximum stress events in the stress history.

As a result of the relatively continuous nature of the crack growth rate curves, least square procedures were applied to the data in Figure 10.3.6 in order to generate the constants in Equation 10.3.1. These constants are presented in Table 10.3.5 along with another set of constants derived using graphical procedures and the assumption that the crack growth rate curves were parallel. Figure 10.3.7 illustrates the degree of fit achieved by the curve established using least squares procedures for the outer wing data. The least squares determined power law curve is seen to adequately describe the outer wing data. The other two least squares power law curves provided similarly adequate descriptions of their respective crack growth rate data.

Table 10.3.5

CONSTANTS C AND p FOR EQUATION 10.3.1

Stress History	Least Squares Method		Graphical Method	
	C	p	C	p
Center Wing (BL-70)	2.54×10^{-7}	2.93	3.35×10^{-7}	2.89
Inner Wing (WS-733)	7.29×10^{-7}	2.73	5.10×10^{-7}	2.89
Outer Wing	7.74×10^{-7}	2.86	9.05×10^{-7}	2.89

A second crack growth life analysis was conducted using the three transport wing stress histories scaled to a lower stress level; all stress events in the three histories were scaled to 0.903 of their original level (both tensile and compressive levels were scaled equally). The modular version of CRKGRO was employed for this second analysis and all geometry and material properties were kept the same. The stress history mission mix and order (stress sequence) were the same as described in subsection 10.3.1. As expected, longer crack growth lives were associated with the lower stress magnitude stress histories. Table 10.3.6 summarizes the life predictions required to grow the crack between the previously defined limits, i.e. (between $2a_o = 0.22$ inch and $2a_f = 1.60$ inch).

10.3.3.3 Interpretation and Use of Crack Growth Rate Curves

It can be noted from Table 10.3.6 that the ratios of crack growth lives for the two stress magnification factors are nearly the same (within 2 percent) for the three stress histories. The reason for this happening

TABLE 10.3.6

EFFECT OF STRESS MAGNIFICATION FACTOR ON CRACK GROWTH
LIVES (L) CALCULATED BY CRKGRO FOR A CENTER CRACK (2a)
GROWING BETWEEN 2a = 0.22 AND 1.60 INCH

Stress History	Lives for Two Stress Magnification Factor Values		Life Ratio
	L_1 (Flights)	$L_{0.903}$ (Flights)	
Center Wing (BL-70)	6220	8300	1.33
Inner Wing (WS-733)	4115	5345	1.30
Outer Wing	2385	3117	1.31

can be justified on the basis of the crack growth rate behavior. Consider Figure 10.3.8 where both the crack growth life and crack growth rate behavior associated with the scaled inner wing stress histories are described. Figure 10.3.8 shows that while the life behavior is different, the crack growth rate behavior can be described by a common curve. If the common crack growth rate curve is a power law equation (Equation 10.3.1) then its integral form, i.e.

$$F = \int_{a_o}^{a_f} \frac{da}{C\bar{K}^P} \quad (10.3.12)$$

can be rewritten, using Equations 10.3.10 and 10.3.11, as

$$F = \frac{1}{C(\sigma_{\max_{RMS}} \sqrt{\pi})^P} \int_{a_o}^{a_f} \frac{da}{\left(a \cdot \sec \frac{\pi a}{W}\right)^{P/2}} \quad (10.3.13)$$

If all the stresses in a stress history are scaled, then the σ_{\max} characterizing stress will be scaled by the same factor. So, if the crack growth interval remains the same, the life ratio ($L_{0.903} / L_1$; where $L_1 = F$ and $L_{0.903} = F$ with lower stress) is given by

$$\frac{L_{0.903}}{L_1} = \frac{(\sigma_{\max_{RMS}})^P}{(0.903 \sigma_{\max_{RMS}})^P} = (0.903)^{-P} \quad (10.3.14)$$

Since all other factors in Equation 10.3.13 are constant, note that the integral is only a function of geometry and once the geometry is defined the stress level does not influence its value.

Using Equation 10.3.14 and the power law exponents given in Table 10.3.5, the life ratio for the scaled stress histories is noted to vary between 1.32 and 1.35 (lowest value of exponent yield lowest life ratio). The life ratio estimate based on the crack growth rate power law exponent is noted to closely approximate the life ratios given in Table 10.3.6. Thus, if one can obtain an estimate of the crack growth rate power law exponent, then one can closely approximate the effect of stress scaling on the crack growth life behavior. Section 10.4 provides additional information on the use of this analysis approach for estimating the lives of structural repairs.

Independent of the above remarks, Equation 10.3.12 has an important application for directly estimating the structural life of cracked components. As an example of its use for conducting such analysis, we compared the results of the CRKGRO analysis with life estimates made using the data presented in Table 10.3.5 and Equation 10.3.13. These results are presented in Table 10.3.7, where it is seen that the power law life prediction ratios, which are conservative relative to the least squares procedure, result in estimates which more closely approximate the CRKGRO estimates for all three stress histories.

Because the least squares determined coefficients are insensitive to the accuracy with which the crack growth rate data are described, it is suggested that the analyst comparatively review the least squares results in a graphical format

TABLE 10.3.7
RATIO OF POWER LAW LIFE PREDICTIONS (L_{PL}) TO CRKGRO LIFE PREDICTIONS (L_{CG})
(RATIO > 1, UNCONSERVATIVE)

Stress History	Stress Magnitude Factor = 1			Stress Magnitude Factor = 0.903		
	CRKGRO (Flights)	L_{PL}/L_{CG}		CRKGRO (Flights)	L_{PL}/L_{CG}	
		Least Squares	Graphical		Least Squares	Graphical
Center Wing (BL-70)	6220	0.961	0.789	8300	0.773	0.632
Inner Wing (WS-733)	4115	0.752	0.769	5345	0.772	0.803
Outer Wing	2385	0.945	0.761	3117	0.977	0.790

such as Figure 10.3.7. One reason for choosing the graphical method is to emphasize the (log-log) lower portion of the crack growth rate behavior. (The least squares procedure results in a "best" fit to all the data).

When flight-by-flight crack growth rate behavior is shown to be independent of stress scaling effects, the behavior will also be independent of the geometry used to collect the crack growth life data. This has been shown for a number of aircraft stress histories similar to those analyzed in this section.

One cautionary remark must be made relative to geometrical effects - if one reduces crack growth life data using a stress-intensity factor which is substantially in error of the actual stress-intensity factor for the geometry, then the transference of the crack growth rate data from one geometry to another will not be possible. In other words, take care in reducing crack growth life data from structural geometries where the stress-intensity factor is not well defined.

10.3.3.4 Analysis for Multiple Stress Histories

Air Logistic Center (ALC) engineers typically need to analyze structural locations within a component for which no stress history is available. Frequently, a stress analysis of these structural locations must be performed based on a strength of materials approach. One question asked repeatedly is: What is available that facilitates conducting a simple crack growth life analysis of these structural locations?

One method that has potential for a relatively large component is a wide area crack growth rate equation that describes the rate of damage growth within the

area identified. This numbered paragraph provides an example of how a wide area crack growth rate equation might be generated and then utilized. The three transport wing stress histories provide the basis for this example.

To develop a wide area crack growth rate equation it is necessary to have crack growth life behavior described at a number of locations within the area of application. The mission mix and stress sequencing must be the same at all locations considered. It is anticipated that crack growth lives might be generated for ten or more locations experiencing loading conditions which produce similar contributions of damage. For the example, only three locations were analyzed for the entire wing; however, the approach and interpretation of results would be similar independent of the component and numbers of location.

As was shown in Figure 10.3.6, the flight-by-flight crack growth rate behavior associated with the three stress histories was different; the rate behavior of each was seen to be relatively continuous and parallel to the others. To obtain a wide area crack growth rate equation, the analyst must find a method for collapsing the rate curves into one master curve. This collapsing can only be accomplished (with confidence) if the analyst understands the relationship between the damage generation process and the stress events in the history. The damage may be generated primarily either by the gust/maneuver cycles or by the GAG cycles.

Figure 10.3.6 shows that the crack growth rates are ordered for the three histories according to the number of gust/maneuver cycles that occur per flight. The data in Figure 10.3.6 were therefore converted to a crack growth rate per

cycle basis and replotted. Figure 10.3.9 describes the result of this scaling of crack growth rates. As is shown by Figure 10.3.9, the crack growth rates are found to collapse to tight scatter band with the inner wing location behavior forming the upper curve on the band.

The collapsing of crack growth rate data observed in Figure 10.3.9 does not always occur when the $\sigma_{\max_{\text{RMS}}}$ parameter is used as the stress history characterizing parameters. If the analyst uses a characterizing parameter that does not describe those events that create damage, one would not expect the crack growth rate data to collapse. Another good characterizing stress parameter for the three transport wing stress histories is the root mean square (RMS) stress range ($\Delta\sigma_{\text{RMS}}$). Figure 10.3.10 describes the cycle-by-cycle crack growth rate behavior for the three stress histories where the characterizing stress-intensity factor (\bar{K}) was calculated using

$$\bar{K} = \Delta\sigma_{\text{RMS}} \left(\frac{K}{\sigma} \right) \quad (10.3.14)$$

As Figure 10.3.10 illustrates, the characterizing stress-intensity factor given by Equation 10.3.14 also collapses the rate data. Additional choices of the characterizing stress maybe necessary when the damage contributions are not dominated by a single loading source.

Once a master crack growth rate curve exists, the curve can be used to integrate the crack growth rate curve at a specific location to produce a crack growth life curve. Figure 10.3.11 highlights the elements of the analysis.

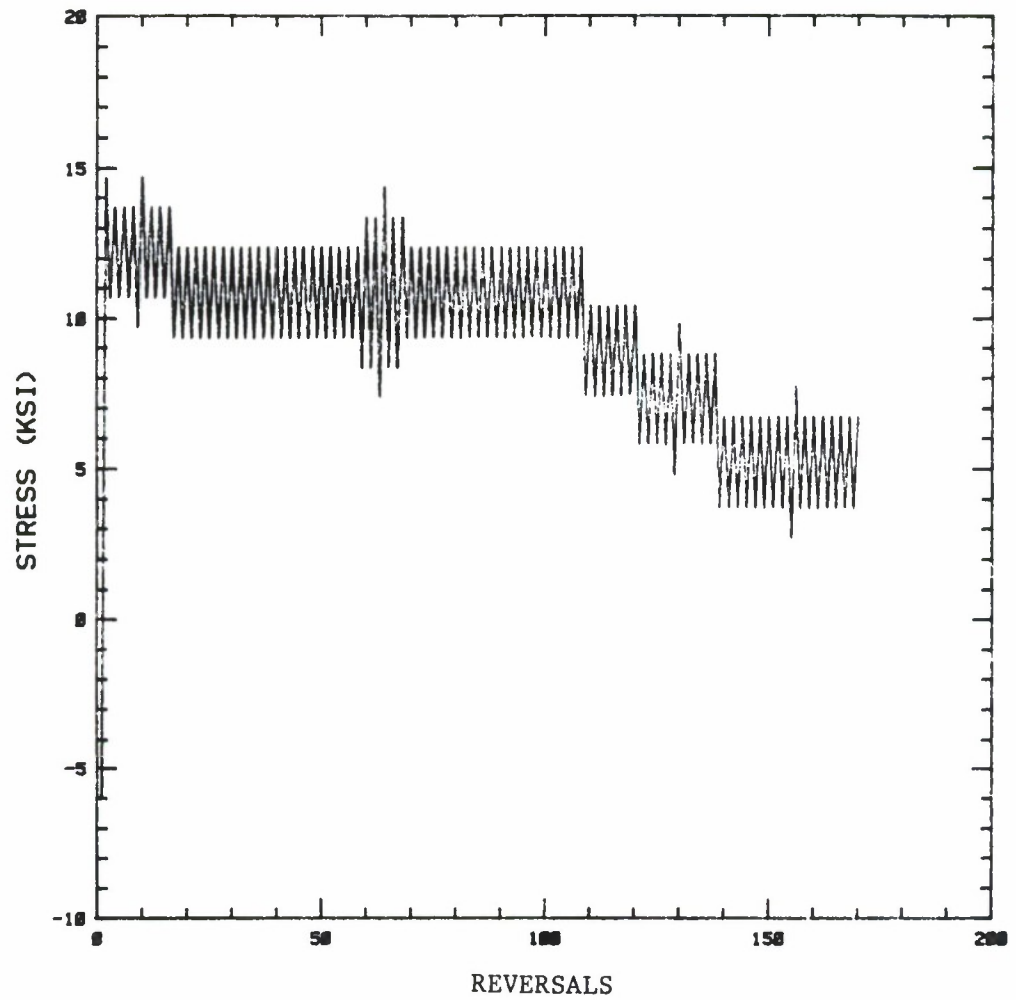


Figure 10.3.1a. Center Wing Stress History for Mission 1.

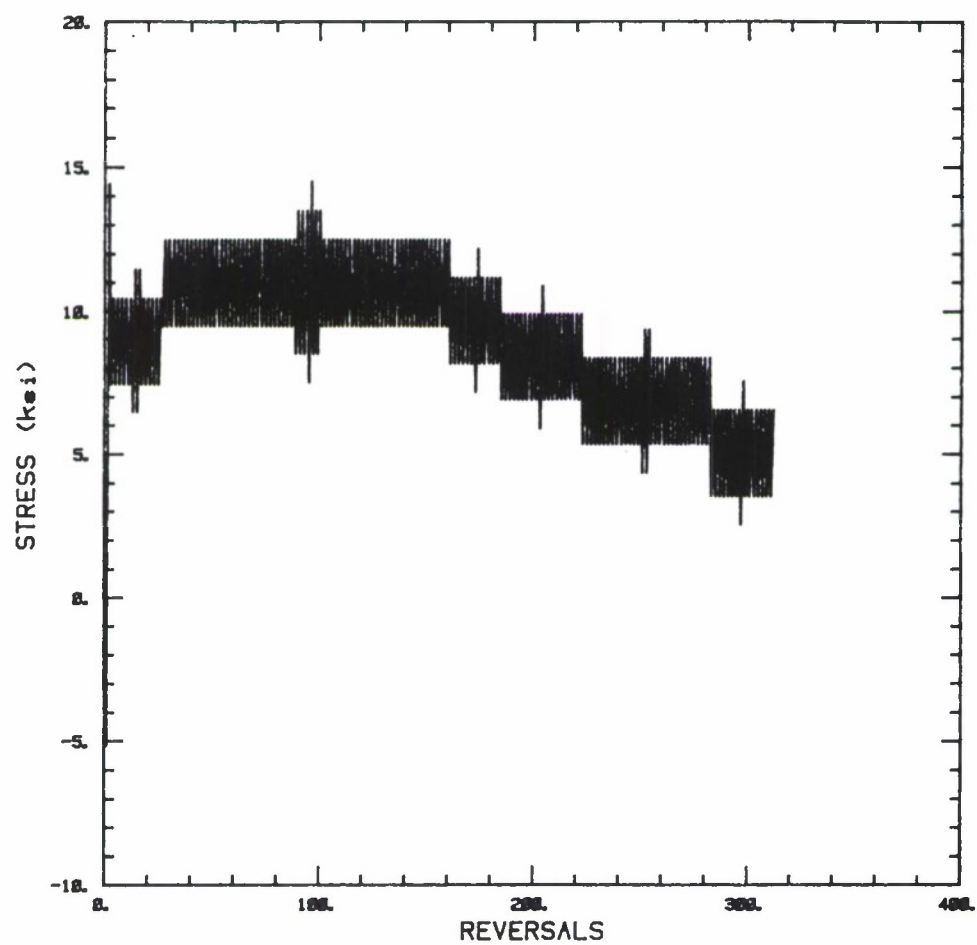


Figure 10.3.lb. Inner Wing Stress History for Mission 1.

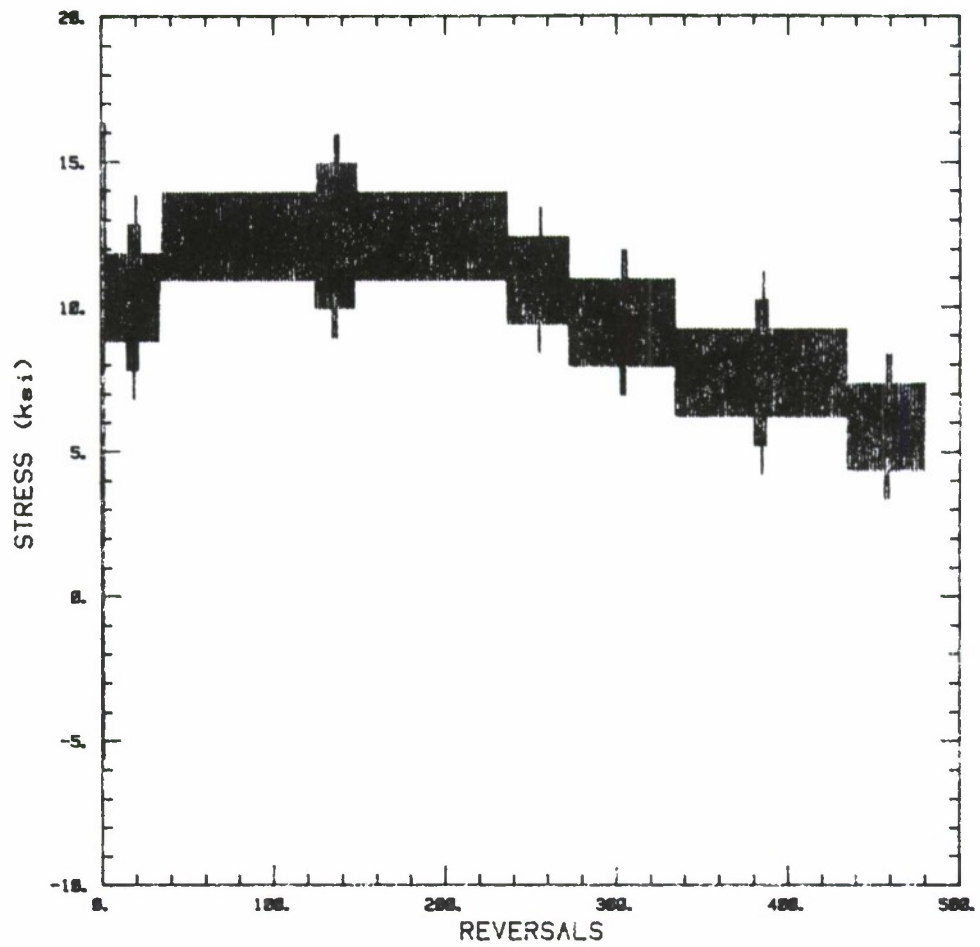
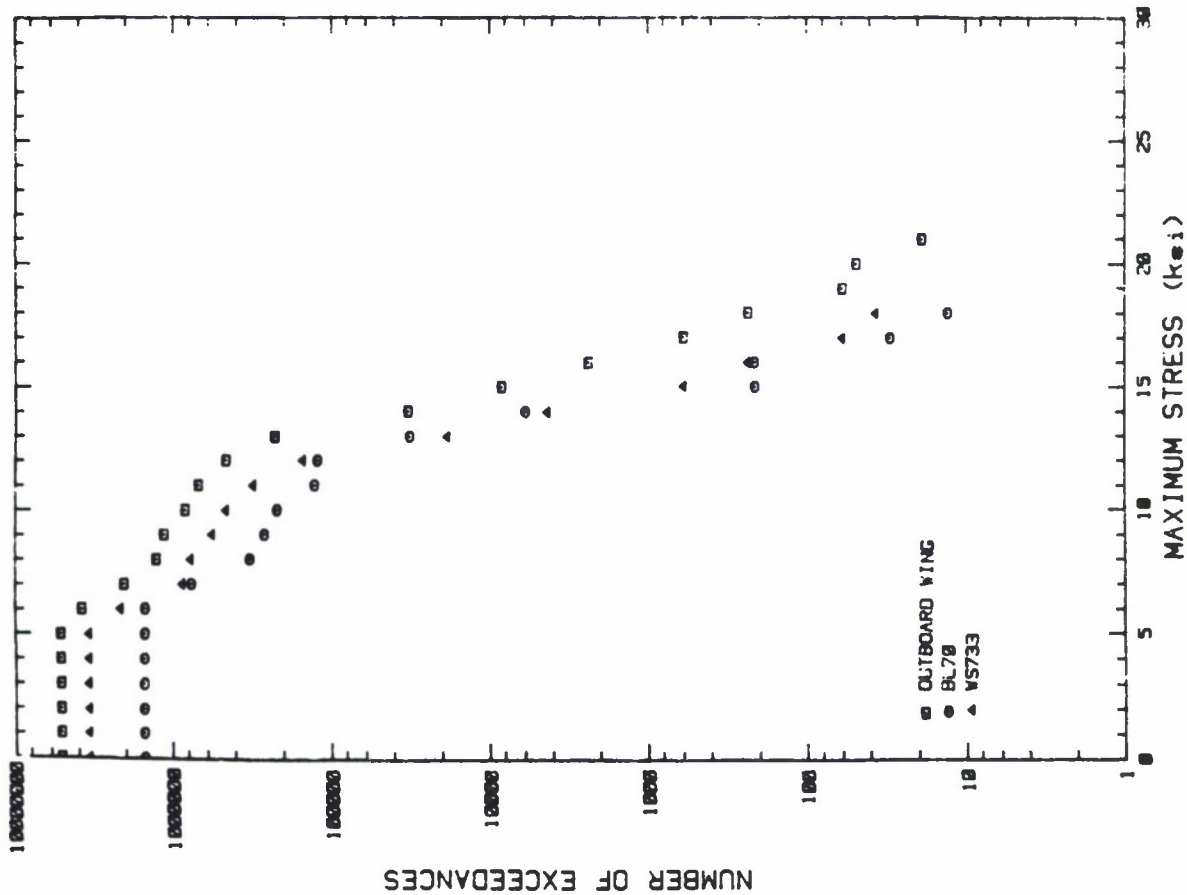


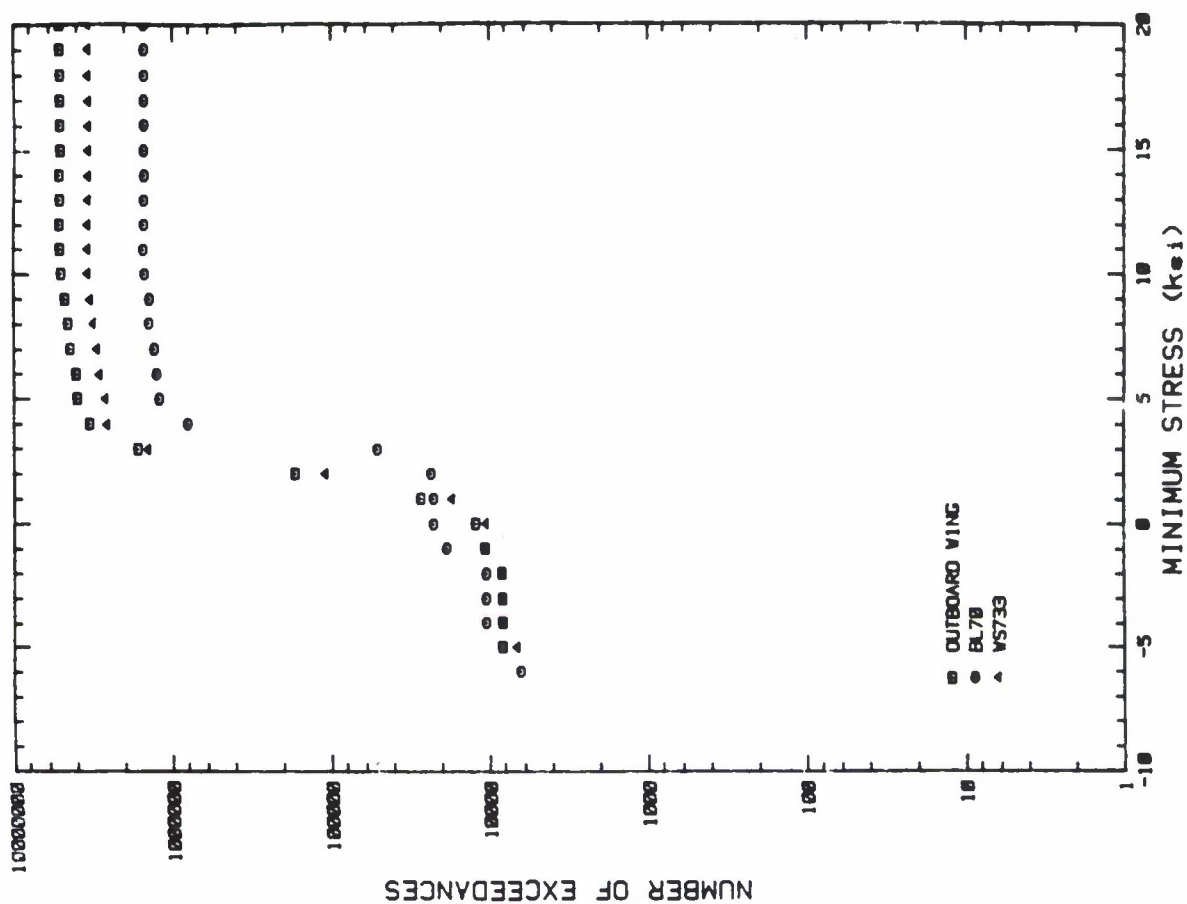
Figure 10.3.1c. Outer Wing Stress History for Mission 1.

MAXIMUM STRESS



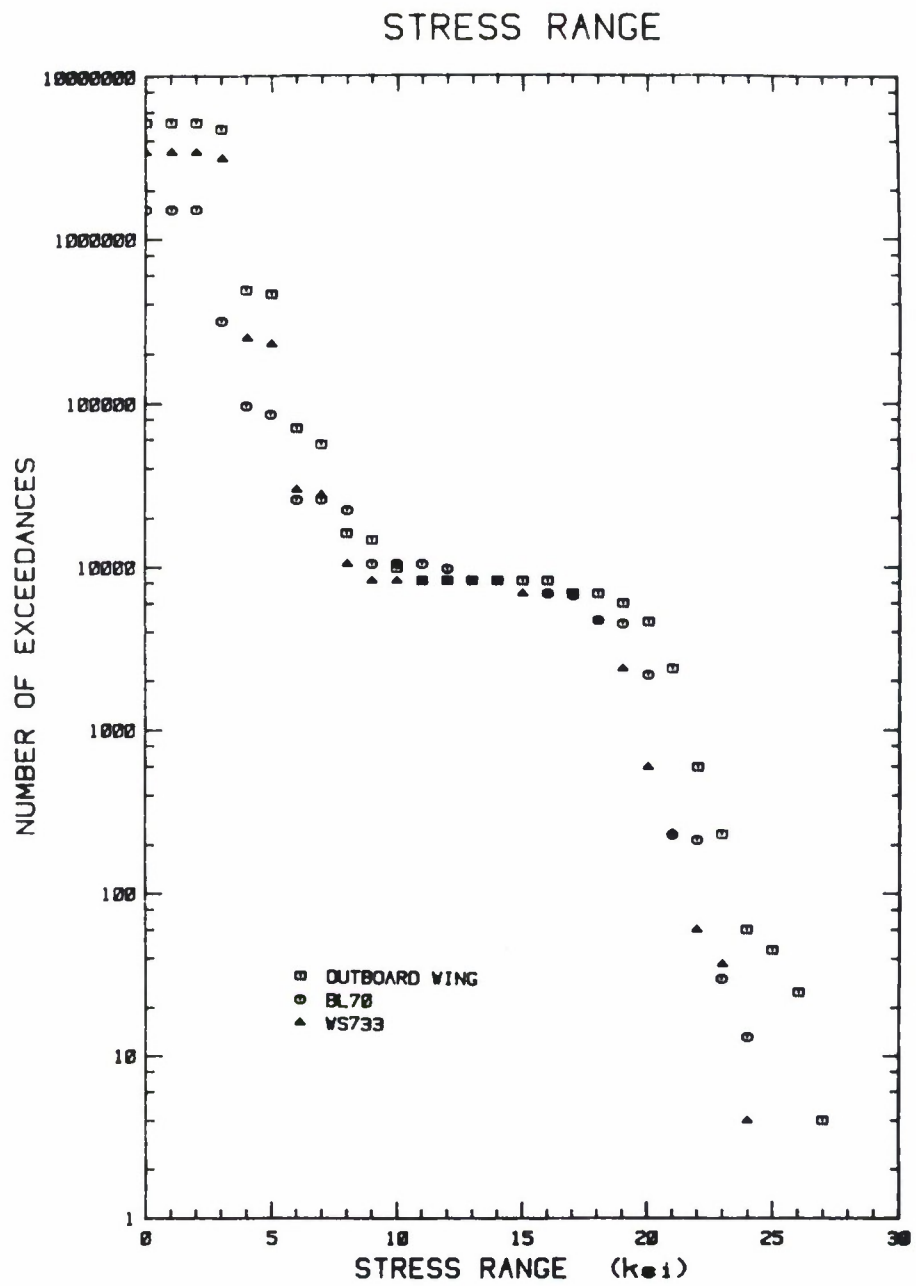
a. Maximum Stress Exceedance

MINIMUM STRESS



b. Minimum Stress Exceedance

Figure 10.3.2. Exceedance Curves for the Three Transport Wing Stress Histories.



c. Stress Range Exceedance

Figure 10.3.2 (Concluded).

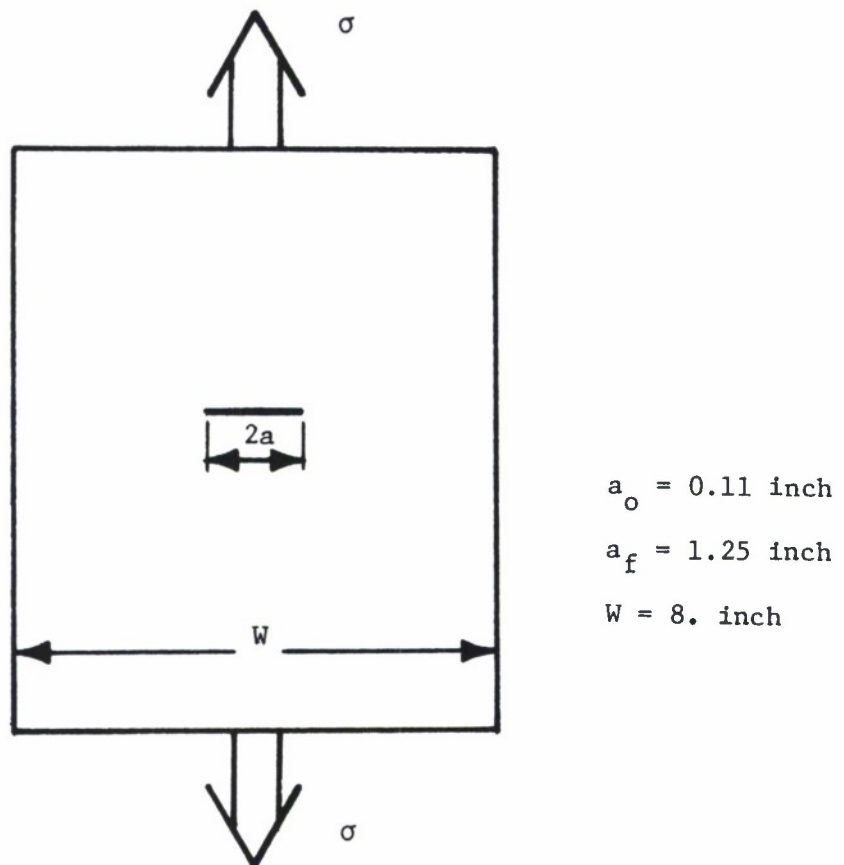


Figure 10.3.3 Common Geometry Used to Evaluate Stress History Effect on Crack Growth Behavior.

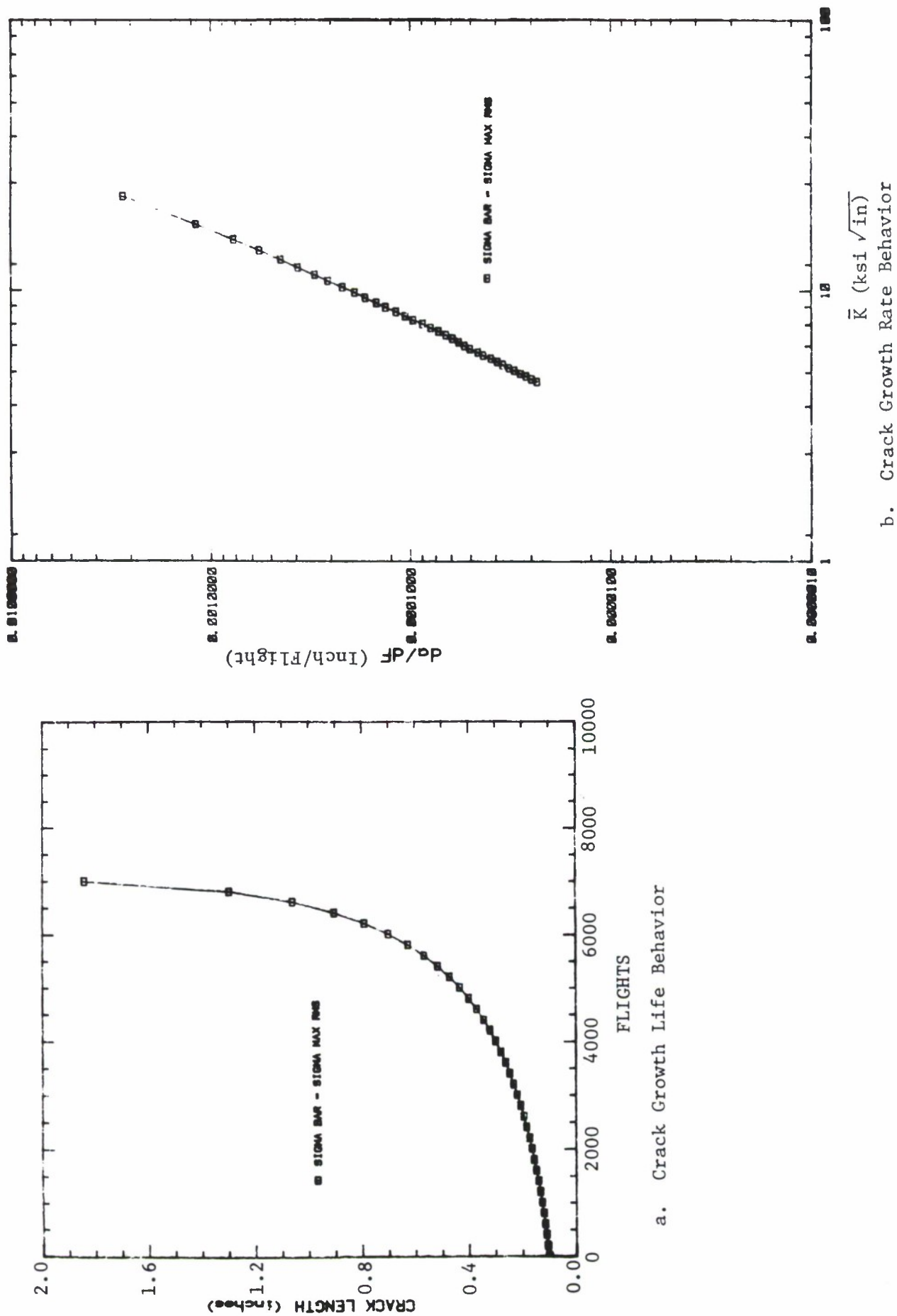
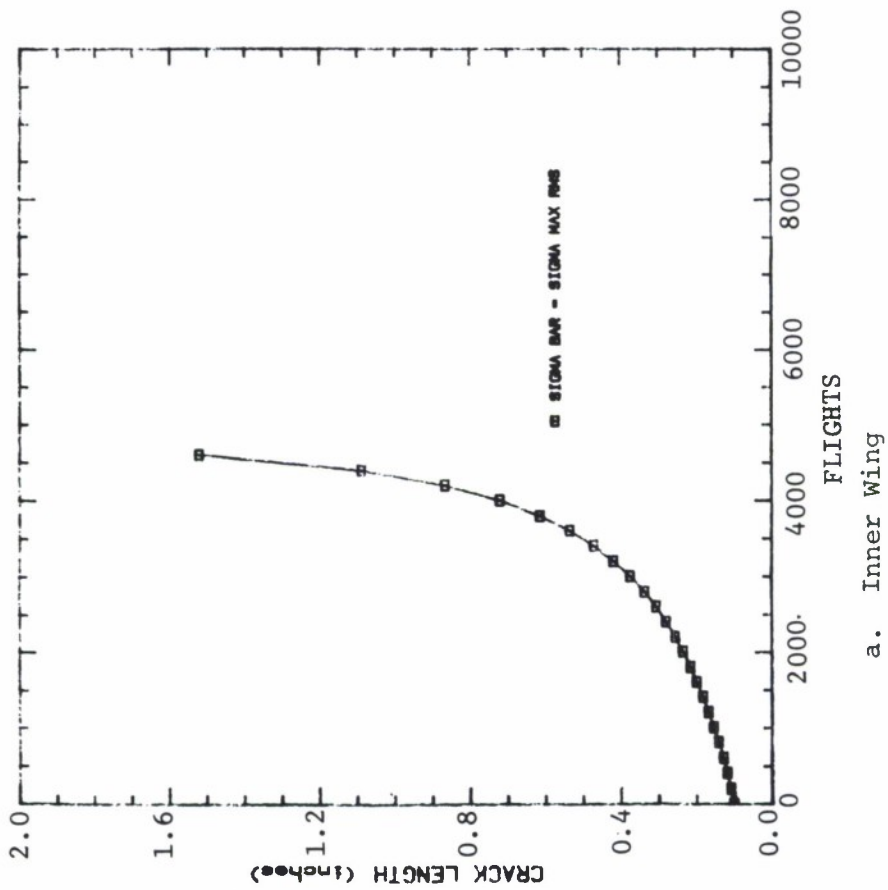
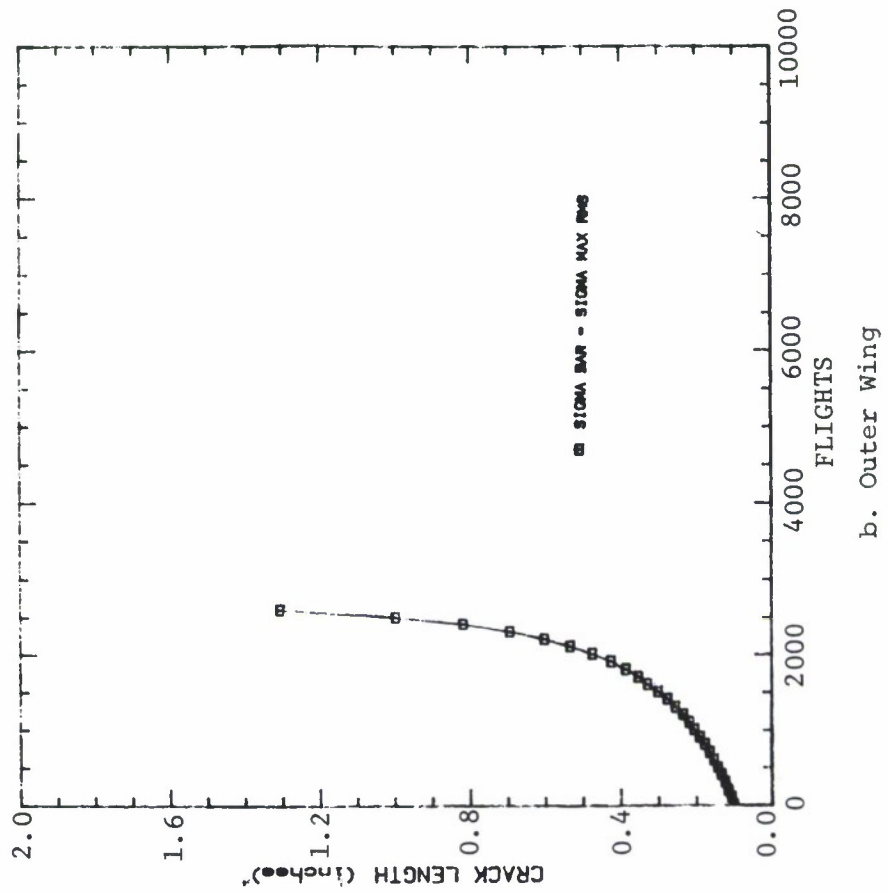


Figure 10.3.4 Crack Growth Behavior for the Center Wing Location; Part a Generated Using CRKGRO
Part b Generated by Secant Slope Method.



a. Inner Wing



b. Outer Wing

Figure 10.3.5 Flight-by-Flight Crack Growth Life Behavior for Inner Wing (WS-733) and Outboard Wing Stress Histories.

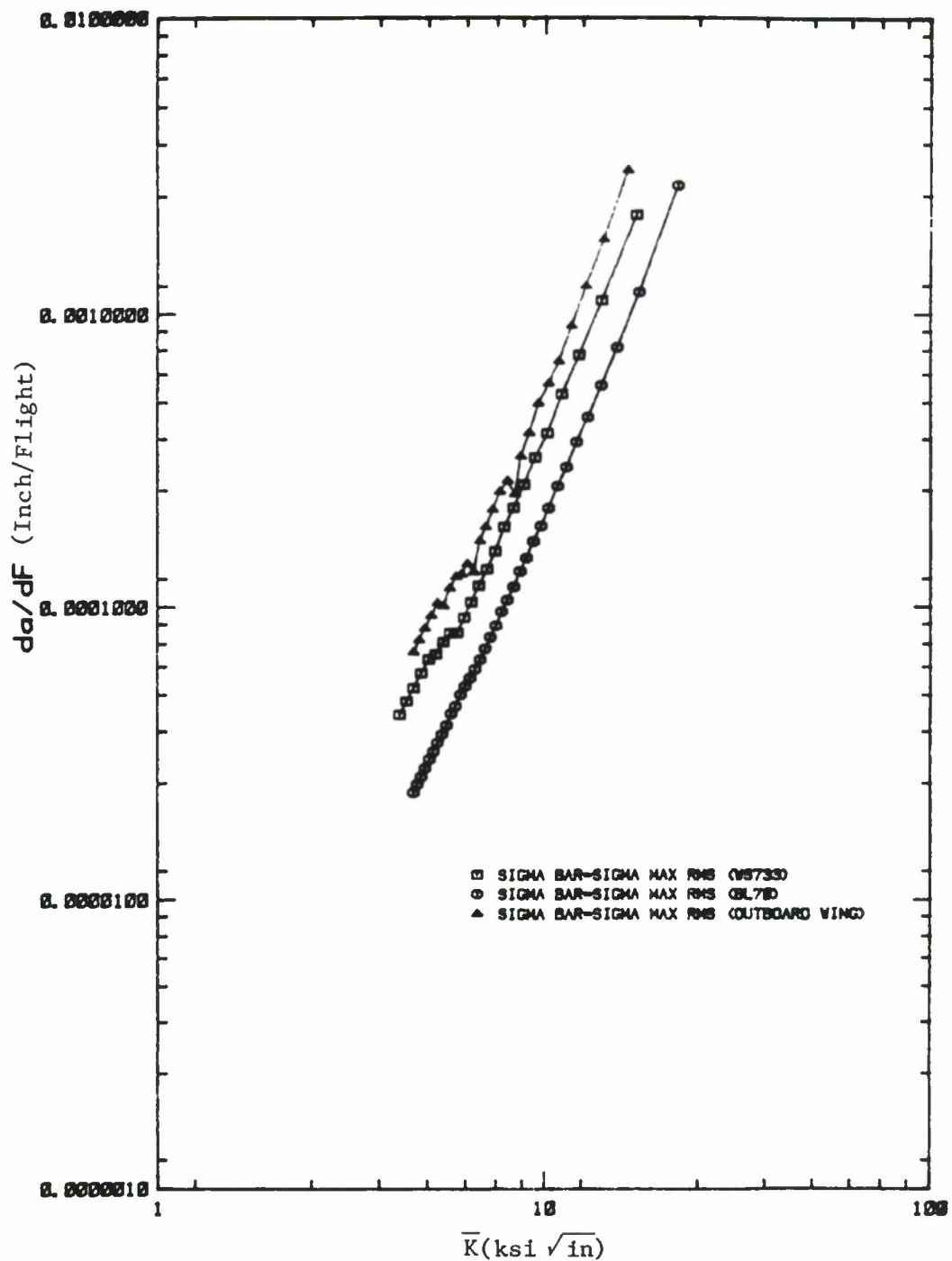


Figure 10.3.6 Flight-by-Flight Fatigue Crack Growth Rate Behavior for Three Transport Wing Histories.

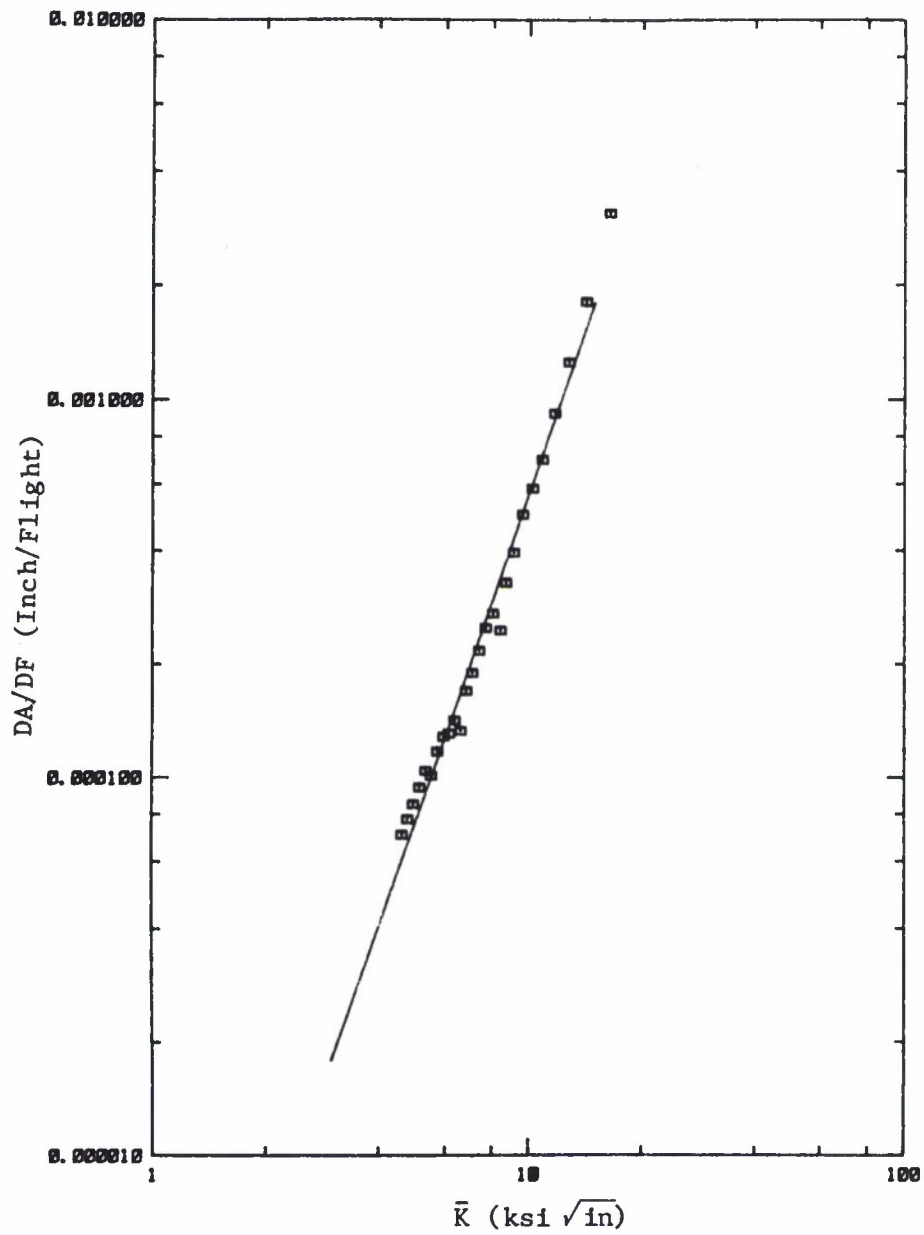
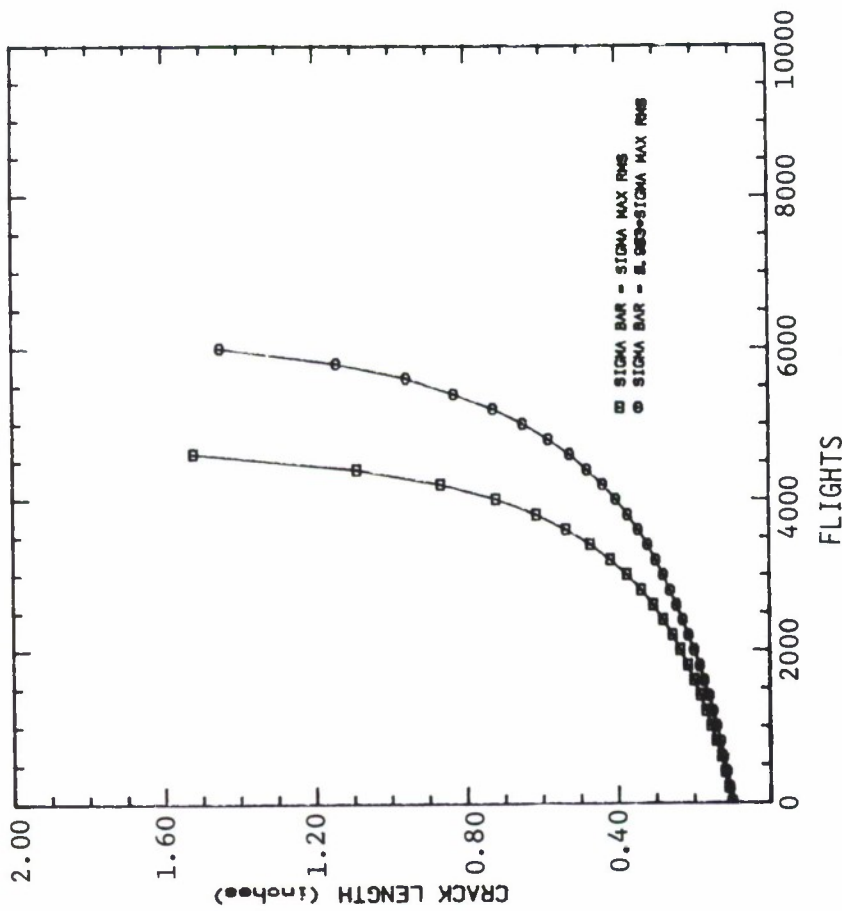
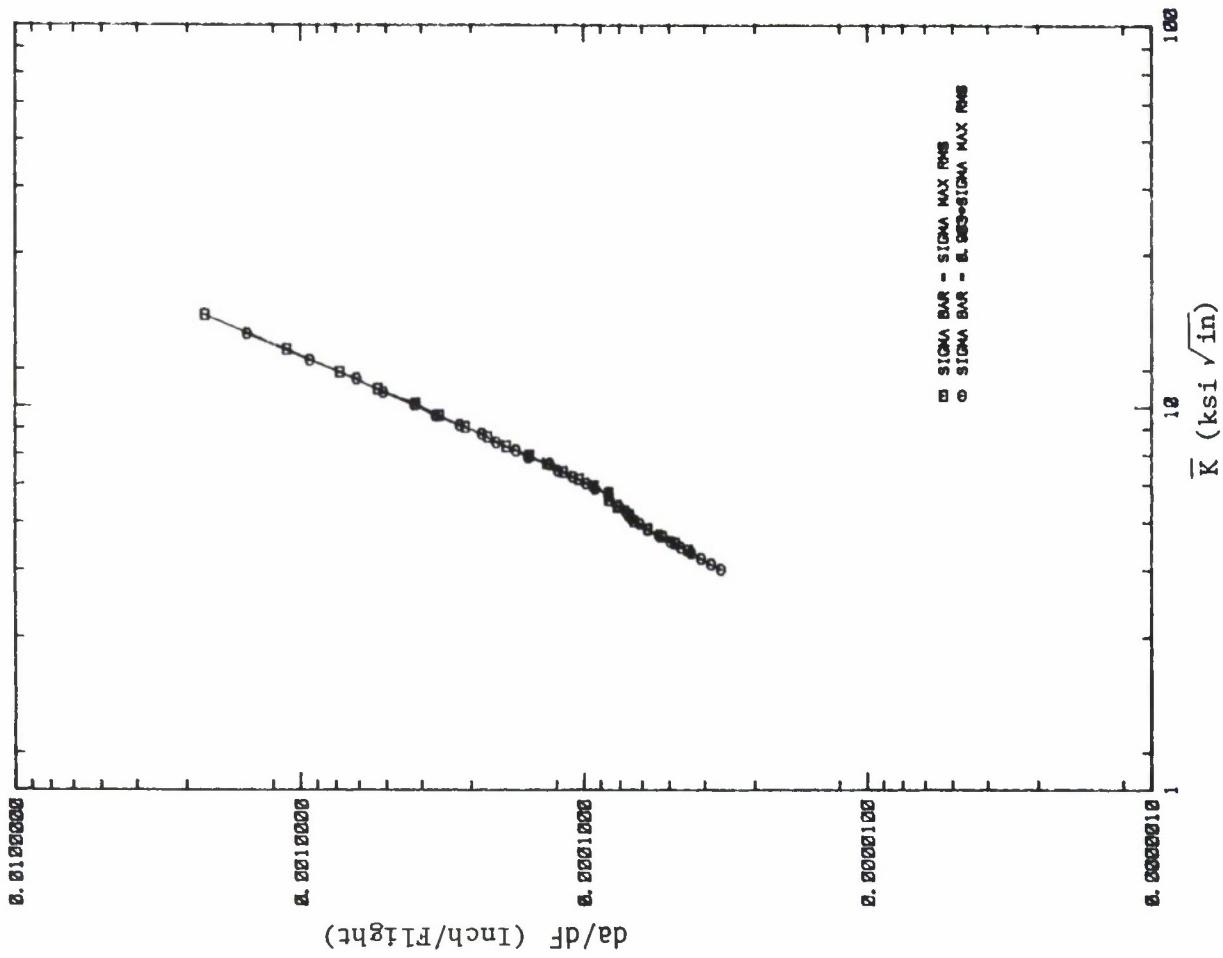


Figure 10.3.7 Comparison Between Outer Wing Data and the Least Squares Determined Curve.



a. Crack Growth Life Behavior



b. Crack Growth Rate Behavior

Figure 10.3.8 Flight-by-Flight Crack Growth Behavior Exhibited for the Inner Wing (WS733) Stress History Scaled to Two Different Stress Levels.

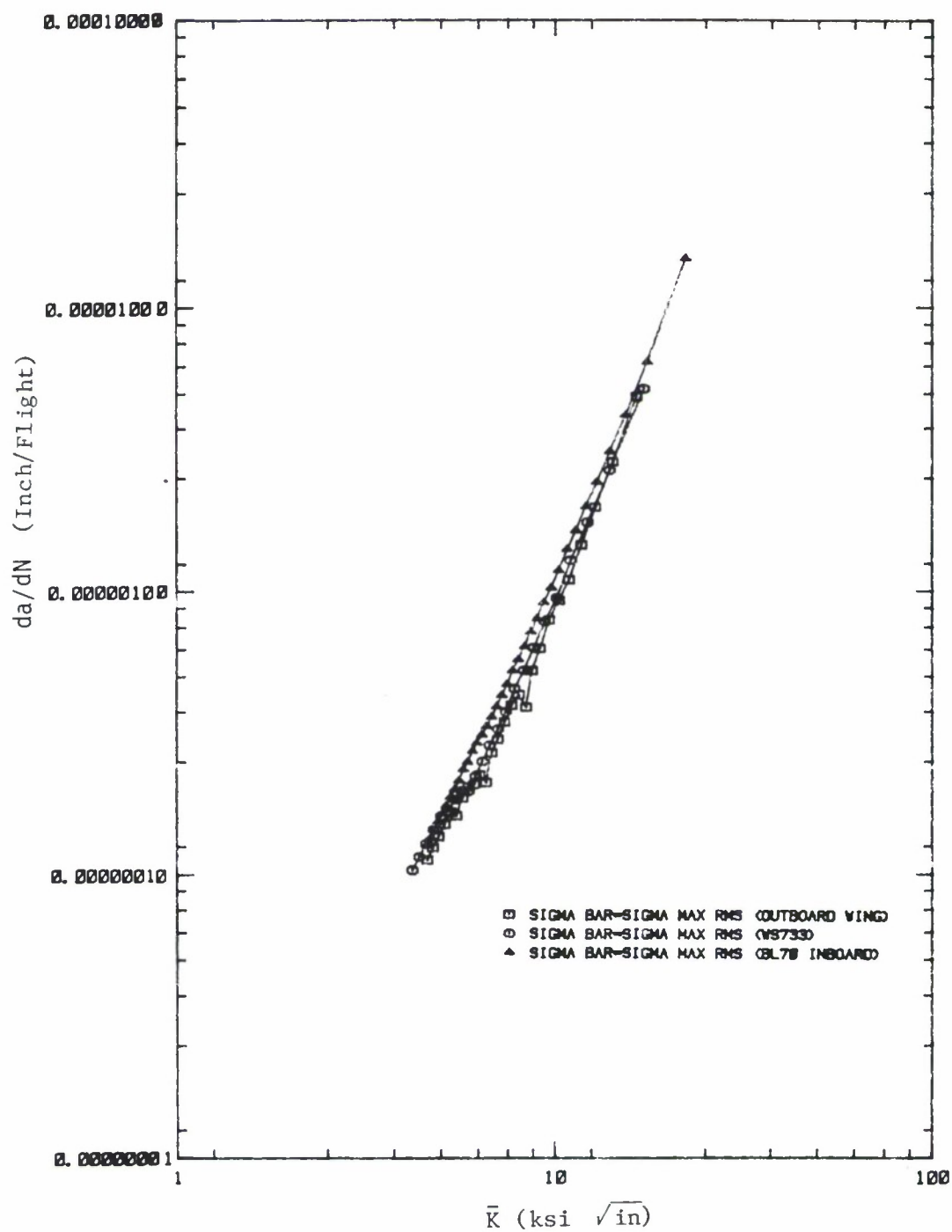
$$\sigma_{\text{BAR}} = \sigma_{\text{MAX RMS}}$$


Figure 10.3.9 Cyclic Crack Growth Rate Behavior for Three Transport Wing Stress Histories.

$$\bar{K} = \sigma_{\max_{\text{RMS}}} \cdot (K/\sigma)$$

SIGMA BAR = DELTA SIGMA RMS

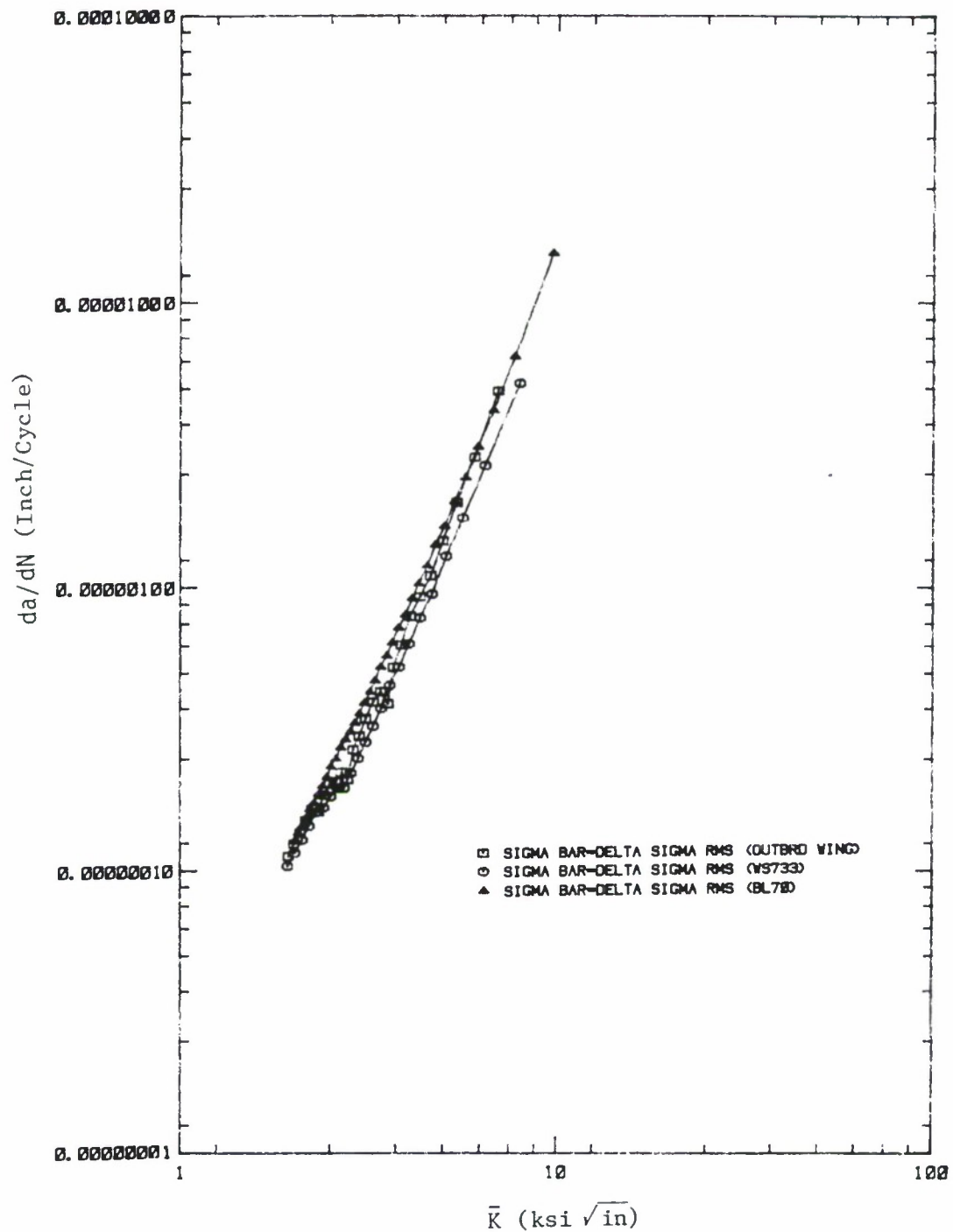
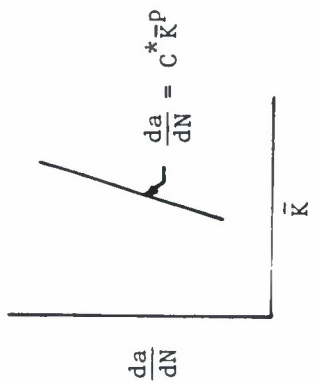
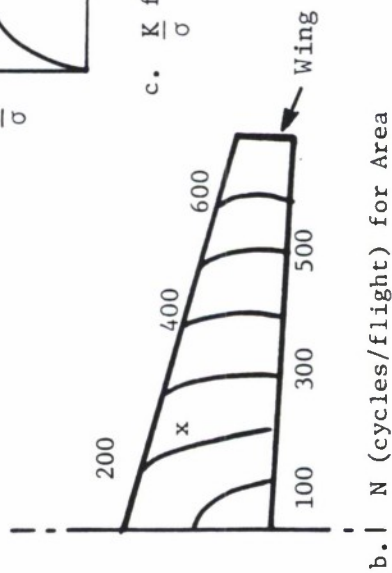
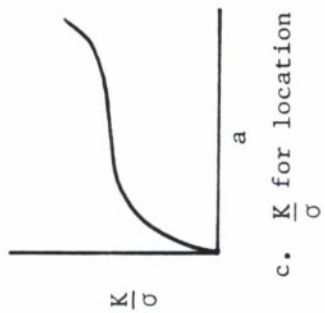
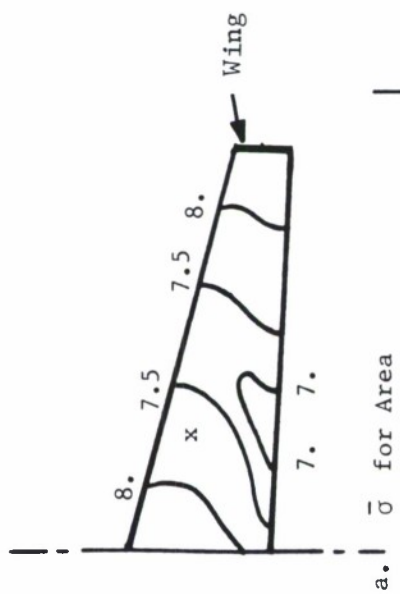


Figure 10.3.10 Cyclic Crack Growth Rate Behavior for Three Transport Wing Stress Histories.

$$\bar{K} = \Delta\sigma_{\text{RMS}} \cdot (K/\sigma)$$



$$\bar{\sigma} = 7.75 \text{ ksi}$$

$$\bar{K} = \bar{\sigma} \cdot \left(\frac{K}{\sigma} \right)$$

$$N = 250 \text{ cycles/flight}$$

$$\frac{da}{dF} = \frac{da}{dN} \cdot \frac{dN}{dF}$$

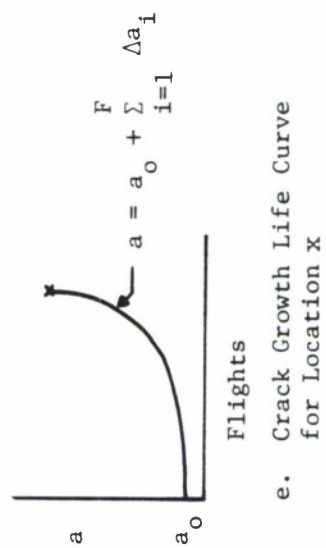


Figure 10.3.11 Schematic of Elements Required to Analyse for Crack Growth Life at Specific Locations.

10.4 LIFE SENSITIVITY FOR STRESS EFFECTS

The fatigue crack growth life of structural components is significantly affected by the level of applied (repeating) stress and the initial crack size. This section addresses the effect of applied stress level on any structural component and provides examples whereby relative life estimates can be utilized to facilitate the damage tolerant analysis of structural repairs. Section 10.5 discusses the effect that initial crack size has on the crack growth life of a repaired hole.

The simplest method for evaluating the effect of stress level on the fatigue crack growth life is based on the general form of Equation 10.3.14 and an available crack growth life curve for the structural geometry of interest. The general form of Equation 10.3.14 related the life (L_σ) at the current stress level (σ) to the life ($L_{x\sigma}$) at the new stress level ($x\cdot\sigma$) through the equation

$$\frac{L_{x\sigma}}{L_\sigma} = \left(\frac{1}{x} \right)^p = x^{-p} \quad (10.4.1)$$

As explained in Subsection 10.3.3, Equation 10.4.1 will estimate life in a relative sense for any structural detail if (1) the crack growth life is known for a defined stress history and (2) the flight-by-flight crack growth rate behavior is described by the power law equation

$$\frac{da}{dF} = C \bar{K}^p \quad (10.4.2)$$

Equation 10.4.1 does not allow one to calculate relative life for changes in crack interval, in crack geometry, or in mission mix (unless a master crack growth curve is available for different mission mixes). The above restrictions do not minimize the extensive usefulness of Equation 10.4.1.

Rewriting equation 10.4.1 so that it relates the unknown crack growth life ($L_{x\sigma}$) to the known life results in

$$L_{x\sigma} = x^{-p} \cdot L_{\sigma} \quad (10.4.3)$$

Equation 10.4.3, in essence, provides a scaling factor that would be applied to the complete crack growth life curve for any structural detail; Figure 10.4.1 illustrates this concept schematically. Note that the life scaling factor (x^{-p}) is independent of the shape of the crack growth life curve.

Due to the generality of the life scaling factor for constructing life estimates it is instructive to evaluate this factor as a function of the stress scaling factor. The relationship is described in Table 10.4.1 for four different values of the crack growth rate exponent p . Table 10.4.1 shows that the smallest life scaling factors for $x < 1$ are associated with the lowest exponential value ($p = 2.2$). For $x < 1$, the new stress level is lower than the current level and as one would guess (see Table 10.4.1 and Figure 10.4.2), the greater the reduction in stress the longer the life (the higher the life scaling factors).

The life benefit achieved by reducing the general level of stress in a structural detail that has experienced crack problems can be estimated from Equation 10.4.3

TABLE 10.4.1

RELATIONSHIP BETWEEN STRESS SCALING FACTOR x
 AND LIFE SCALING FACTOR $L_{x\sigma}$ FOR DEFINED
 VALUES OF THE CRACK GROWTH EXPONENT p

Stress Scaling Factor $x = \frac{\sigma_{\text{new}}}{\sigma_{\text{current}}}$	Life Scaling Factor (for x^{-p})			
	$p = 2.2$	$p = 2.5$	$p = 3.0$	$p = 3.0$
0.50	4.60	5.66	8	11.31
0.60	3.08	3.59	4.63	5.98
0.70	2.19	2.44	2.92	3.48
0.80	1.63	1.75	1.95	2.18
0.85	1.43	1.50	1.63	1.77
0.90	1.26	1.30	1.37	1.46
0.92	1.20	1.23	1.28	1.34
0.94	1.15	1.17	1.20	1.24
0.96	1.09	1.11	1.13	1.15
0.98	1.04	1.05	1.06	1.07
1.00	1.00	1.00	1.00	1.00
1.02	0.96	0.95	0.94	0.93
1.04	0.92	0.91	0.89	0.87
1.06	0.88	0.86	0.84	0.81
1.08	0.84	0.83	0.79	0.76
1.10	0.81	0.79	0.75	0.72
1.15	0.73	0.71	0.66	0.61
1.20	0.67	0.63	0.58	0.53
1.30	0.56	0.52	0.46	0.40
1.40	0.48	0.43	0.36	0.31
1.50	0.41	0.36	0.30	0.24

If the power law exponent p is not available for this particular structural detail, it is recommended that a conservative estimate of p be made, i.e. for a stress reduction chose $p = 2.2$, and evaluate the increase in life on this basis.

EXAMPLE 10.4.1 Modify to Achieve Lower Stress Levels

The doubler shown in Figure 10.4.3 has been modified to reduce the general level of stress at the cracking site identified by ten (10) percent. The original doubler on a 6000 hour aircraft had a mean service life of 3400 flight hours to a crack size which would functionally impare the use of this aircraft. How much life will the replacement doubler have? No crack growth life curve exists for the doubler nor for the general area of the wing where it is located. A wide area master curve for the wing is described by a power law equation with exponent $p = 2.89$.

SOLUTION:

The aircraft is presumed to fly the same type of missions with the same frequency after the repair modification as before. Since a master crack growth rate curve is available for the wing, the analyst would evaluate the life of the repair using Equation 10.4.3 with a power law exponent of 2.89. The modification is expected to result in a new life (L_{new}) for a ten (10) percent reduction in stress level (the new stress level is 0.9 times the current stress level).

The new life is given by

$$L_{\text{new}} = x^{-p} \cdot L_{\text{current}} \quad (10.4.4)$$

when L_{current} is equal to 3400 flight hours, Equation 10.4.4 reduces to

$$\begin{aligned} L_{\text{new}} &= (0.9)^{-2.89} \cdot (3400) \\ &= 1.356 \cdot 3400 \\ &= 4610 \text{ flight hours.} \end{aligned}$$

Thus, a first order estimate indicates the life of the replacement doubler will be 35 percent greater than the original doubler. If the original doublers are removed at 2500 hours and replaced with the doubler with the lower stress, it is anticipated that the replacement doubler will not fail during the remaining life of the aircraft ($2500 + 4610 = 7110 \text{ hours} > 6000 \text{ hour life requirement}$). If no information on the crack growth rate behavior existed for region where the doubler was located, then it is suggested that Equation 10.4.4 be evaluated with $p = 2.2$. The result of this evaluation is 4285 hours which still indicates that the replacement doubler will out last the aircraft ($2500 + 4285 = 6785 \text{ hours} > 6000 \text{ hour life requirement}$).

As a cautionary note, it is important to recognize that the best estimate of the exponent p will result in the best life estimate. The exponent p is expected to vary as a function of location (due to material and stress event effects on damage) so if values of the exponent p are available for a given location in a component, it is more accurate to utilize the exponent p for that location.

Another direct application of Equation 10.4.4 comes from moving from a stress analysis control point where a complete crack growth life analysis is available to a new location where the cracking behavior is expected to be similar due to

geometrical and material conditions, but where only a strength of materials analysis is available. An example illustrates the approach here.

EXAMPLE 10.4.2 Local Stress Scaling

Figure 10.4.4 describes a local area (Location A) of an aircraft structure that has been experiencing distress. Only the most critical hole (Location B) in the region was analyzed during a damage tolerance analysis; this analysis is summarized in Figure 10.4.5. The exponent p associated with the aircraft's standard operational missions is 3.2 for Location B.

A strength of materials analysis was conducted to evaluate the difference in stress levels at the two location (A & B) for a given external loading; these stress levels are defined in Figure 10.4.4. Please provide an estimate of the life for the hole identified in Figure 10.4.4.

SOLUTION:

The crack at Location A is presumed to grow in the same manner illustrated in Figure 10.4.5. The stress history at Location A is identical to that at Location B except that the stresses are scaled to a lower level x given by

$$x = \frac{\sigma_A}{\sigma_B} = \frac{13.6}{14.3} = 0.951$$

So that the life (L_A) at Location A is found using Equation 10.4.4 and the crack growth life curve in Figure 10.4.5 which describes the life (L_B) to any given crack size for Location B:

$$L_A = (0.951)^{-3.2} (L_B) \quad (10.4.5)$$

From the Location B crack growth life curve, the flights required to break the ligament and to fracture the component are 7300 and 12100 flights, respectively. From Equation 10.4.5, the corresponding lives at Location A are 8570 and 14210 flight, respectively, a 17 percent increase over that of Location B.

If cracks are observed with a greater frequency at Location A than at Location B, and if the crack sizes at Location A are longer than that anticipated at Location B for the same operational conditions, then the analyst might reverse the analysis, i.e. use the life ratios for specific crack sizes to obtain a better indication of the stresses at the distressed location. EXAMPLE 10.4.3 describes this calculation.

EXAMPLE 10.4.3 Stress Estimated from Crack Behavior

Cracks have been noted during PDM in a number of aircraft at Location A (Figure 10.4.4). From the available inspection data, it appears that the cracks reach a length of 0.150 inches after about 3600 flights. The DTA established crack growth life curve indicated that 0.150 inch long cracks should not appear until 5800 flights. Estimate the stress level difference between Locations A and B. Also estimate the number of flights required to fail the ligament and the component.

SOLUTION:

The method suggested for determining the stress level difference is with Equation 10.4.4, i.e.

$$L_A = x^{-p} \cdot L_B \quad (10.4.6)$$

where L_A , L_B , and p are known ($L_A = 3600$, $L_B = 5800$, $p = 3.2$). Solving for x , the stress ratio between Location A and B yields

$$x = \frac{(\sigma_A)}{(\sigma_B)} = \frac{(L_B)^{\frac{1}{p}}}{L_A} \quad (10.4.7)$$

and the stress ratio is

$$x = \frac{(5800)^{\frac{1}{3.2}}}{3600} = 1.16 \quad (10.4.7a)$$

So the stresses at the cracking site (Location A) are expected to be 16 percent greater than that at the DTA location (Location B).

Equation 10.4.6 can be now used to estimate the lives to grow the crack (at Location A) to fail the ligament and the component with x known, the lives are given by

$$L_A = (1.16)^{-3.2} L_B \quad (10.4.6a)$$

and with $L_B = 7300$ and 12100 flights for the Location B critical conditions, $L_A = 4540$ and 7525 flights, respectively, to fail the ligament and the component at Location A.

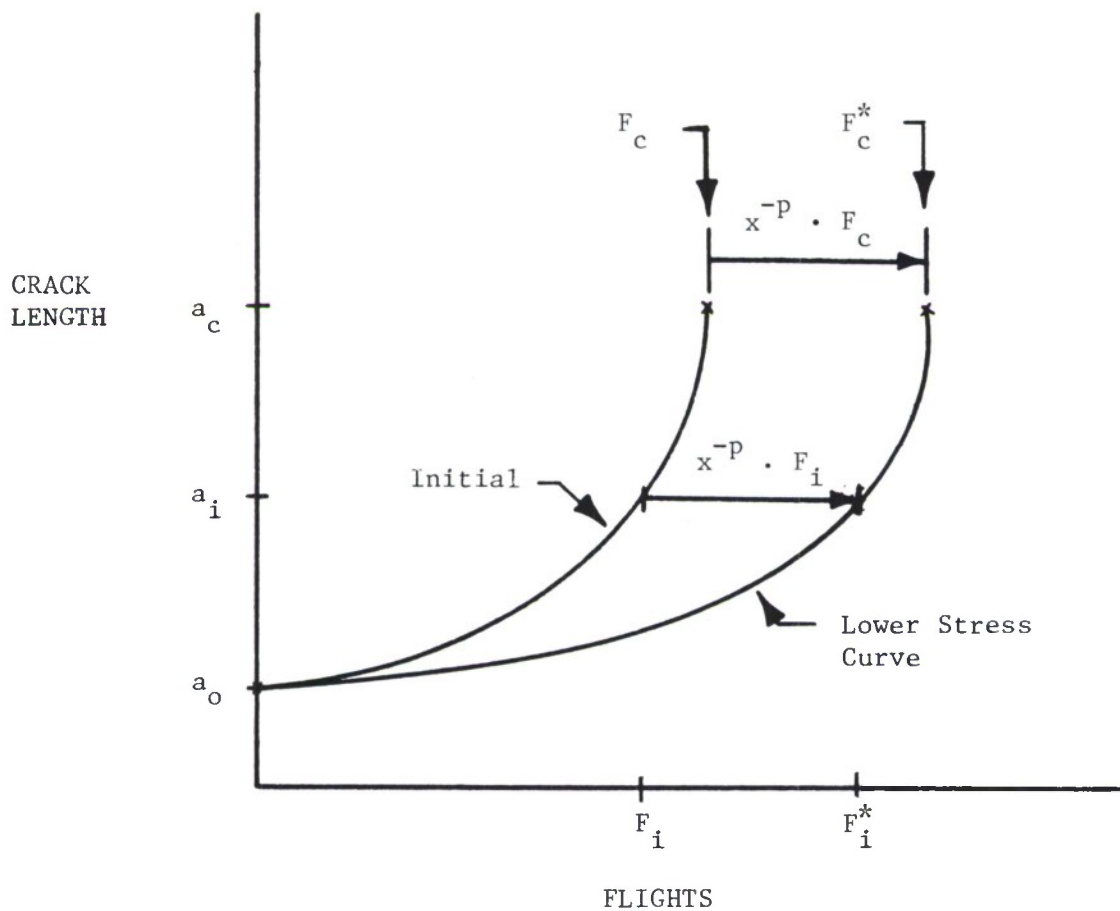


Figure 10.4.1 Schematic Describing the Use of Equation 10.4.3 to Scale the Crack Growth Life Curve Based on a Stress Level Change from σ to $x \cdot \sigma$ where $x < 1$.

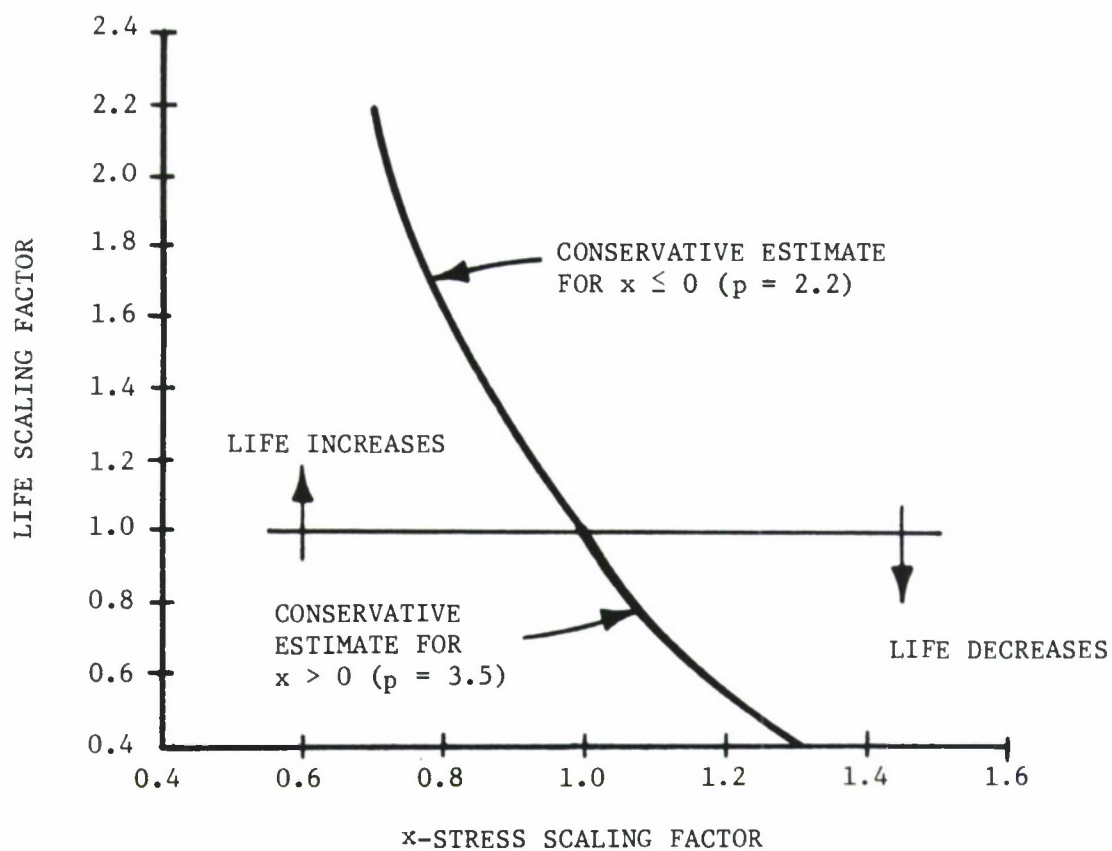


Figure 10.4.2 Life Scaling Factor (New Life \div Current Life) as a Function of the Stress Scaling Factor (x = New Stress/Current Stress).

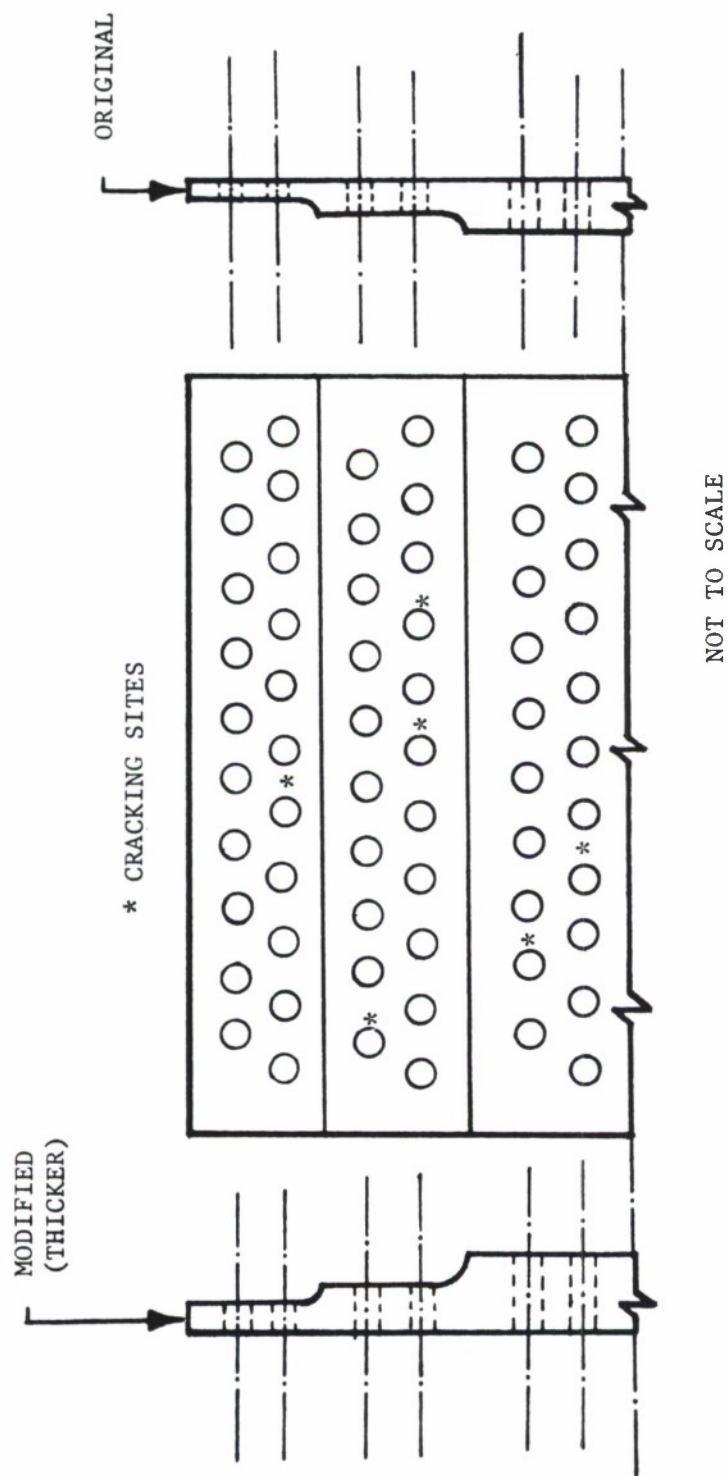


Figure 10.4.3 Doubler Analysed in Example 10.4.1.

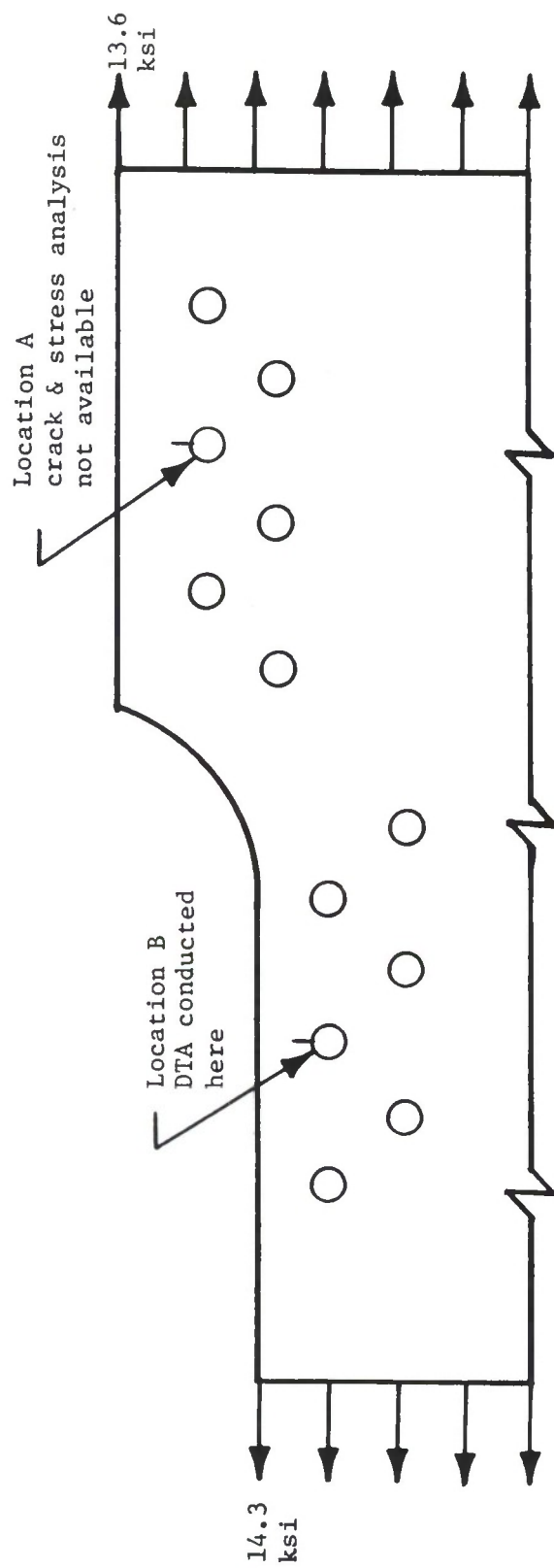
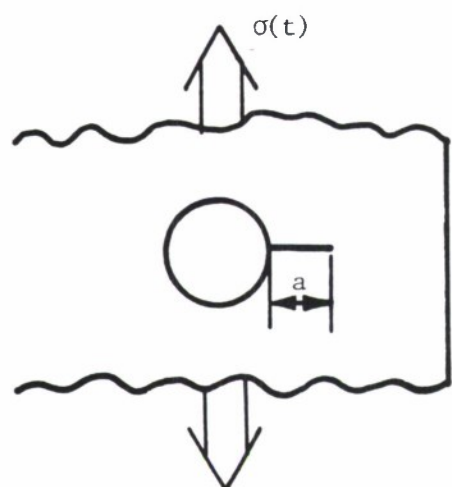
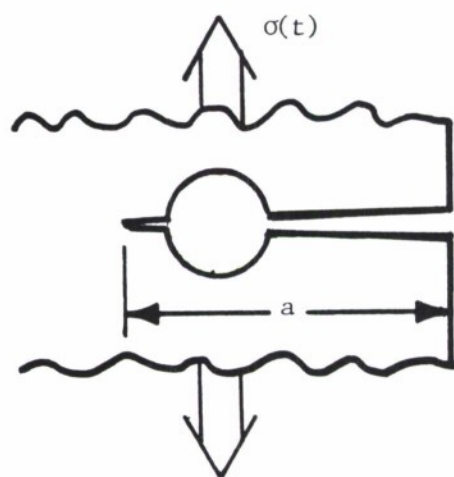


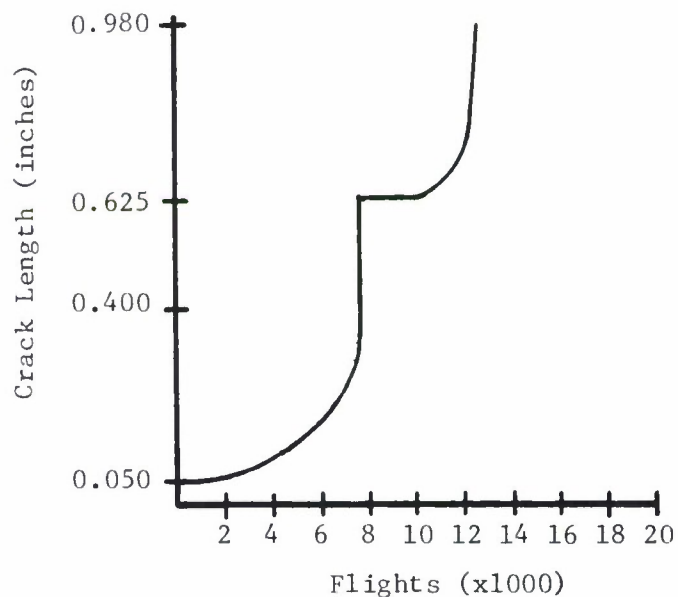
Figure 10.4.4 Description of Structural Geometry and Definition of Analysis Location and of Crack Site.



a. Initial Crack



b. Broken Ligament



c. Crack Growth Behavior

Figure 10.4.5 Details of Cracking Process at Location B and Life Curve.

10.5 LIFE SENSITIVITY ANALYSIS FOR HOLE REPAIR

Because holes are stress concentration sites, it is not surprising that a large number of holes are drilled oversize and repaired to remove crack indications identified during inspection. It is not possible to conduct a detailed damage tolerance analysis on every repair of this type; however, engineers can assess the life of many components before and after the hole is enlarged using Equation 10.3.1 and its integral counterpart (Equation 10.3.12). Detailed evaluations should always be conducted for critical locations; in some cases, the detailed evaluations will become the building blocks for other simplified repair analyses.

Hole repairs are made to remove crack indications from the edge of the hole. Several example damage tolerance analyses are presented in this section to summarize the effect of oversizing the hole to remove some (but not all) of the crack damage. Practically speaking, the objective is to remove all the crack damage. But, because nondestructive evaluation (NDE) capability is what it is, the analyst can not presume that all traces of the crack are removed when the hole is oversized. From an economics and safety viewpoint, all traces of the crack should be removed and the aircraft restored to its original condition. When conducting a damage tolerance analysis to protect safety, it is wise to err on the conservative side in defining the initial crack size after a hole oversizing operation.

10.5.1

Before introducing the example analyses, it is instructive to review the integral counterpart of Equation 10.3.1, i.e. Equation 10.3.12, which is presented as Equation 10.5.1

$$F = \int_{a_o}^{a_f} \frac{da}{C \bar{K}^P} \quad (10.5.1)$$

or

$$F = \frac{1}{C(\bar{\sigma} \sqrt{\pi})^P} \int_{a_o}^{a_f} \frac{da}{(\beta \sqrt{a})^P} \quad (10.5.2)$$

The parameter β is the geometry correction factor which is normally a function of crack length. We again note that the integral

$$I = \int_{a_o}^{a_f} \frac{da}{(\beta \sqrt{a})^P} \quad (10.5.3)$$

is independent of stress effects and is only dependent on the geometry of the structure and of the crack. So if the stress parameter, i.e., the stress history, is constant, then the impact of geometry changes on life can be assessed by studying the variation of I as the geometry changes. The following example will be used to illustrate this point.

EXAMPLE 10.5.1 Variation of Initial Crack Size on Life

structural member made from D6AC steel has been experiencing cracking problems at a 1/4 diameter weep hole. If the crack growth rate per flight hour is given by

$$\frac{da}{d(FH)} = 16 \times 10^{-8} \bar{K}^{2.6} \quad (10.5.4)$$

Calculate the life required to grow a thru-thickness crack from several initial crack sizes to a 0.550 inch long radial crack. Assume the stress is 30 ksi.

SOLUTION:

The integral counterpart of Equation 10.5.4 for this problem is

$$FH = \frac{1}{16 \times 10^{-7} (30 \sqrt{\pi})^{2.6}} \int_{a_o}^{0.550} \frac{da}{(\beta \sqrt{a})^{2.6}} \quad (10.5.5)$$

where β is associated with the radially cracked hole geometry, see Subsection 1.7.3, Table 1.7.3, Case 1.7.3.1, Equation 1.7.4:

$$\beta = F_1 \frac{(a)}{r} = \frac{0.8734}{(0.3246 + \frac{a}{r})} + 0.6762 \quad (10.5.6)$$

The life results (solutions to Equation 10.5.5) for several initial crack lengths are presented in Table 10.5.1

TABLE 10.5.1

CRACK GROWTH LIFE AS A FUNCTION OF INITIAL SIZE
 FOR $\bar{\sigma} = 30$ ksi AND $a_f = 0.550$

a_o (inch)	Life (L_{a_o}) (flight hours)	Life Ratio ($L_{a_o}/L_{0.050}$)
0.001	8894	4.03
0.002	7360	3.34
0.005	5625	2.55
0.010	4465	2.02
0.020	3416	1.55
0.025	3102	1.41
0.040	2480	1.12
0.050	2205	1.00
0.075	1736	0.78
0.100	1428	0.65
0.125	1204	0.55

It is important to note that the life ratios generated by dividing all the life values by the life value associated with $a_o = 0.050$ inch is independent of stress level. The reader might try the same calculation for life ratio using a stress of 50 ksi. The life ratio results in Table 10.5.1 are described in Figure 10.5.1 which illustrates the importance of initial crack size on life. While the values of the life ratios would change for changes in the material, structural geometry, and probably aircraft operation (as sensed by p), the conclusion that life is significantly affected by initial flaw size would not change.

Equation 10.5.3 can also provide a simplified method for determining the effect of increasing the diameter of a cracked hole. Consider Figure 10.5.2 which defines the three stages associated with increasing the hole diameter to remove a pre-existing crack. One of the first steps in the analysis is to obtain an estimate of the initial structural life (this life is referred to as the DTA result or the Blueprint life). For purposes of this analysis, the DTA result is presumed available for the region of interest.

As indicated in EXAMPLE 10.5.1, the larger the initial crack size, the shorter the life. Thus, the decision of choosing the initial flaw size after oversizing is an important one - both for economy and for safety. Based on conversations with NDE engineers at several ALC depots, the minimum crack size that can be assumed after an oversizing operation is 0.015 inch based on current capability. For consistency of analysis with MIL Spec. 83444 requirements, however, it is recommended that crack sizes be no smaller than that associated with initial

manufacturing. An example problem is presented later in the section to consider the influence that the initial post rework crack size has on the remaining structural life. First, let us consider the influence that the reworked oversized hole has on life relative to that of the initial hole.

EXAMPLE 10.5.2 Effect of Rework Hole Size on Life

In this example, the blueprint diameter is 0.250 inches and the final crack length is 0.550. For comparative purposes, the initial crack length (both manufacturer's and post rework) is 0.050 inches and is assumed to be a through-thickness crack. See Figure 10.5.3 for a description of the geometrical conditions both initially and post-rework.

Present a comparative life analysis that defines the effect of enlarging the 0.250 inch diameter hole to larger sizes during repair of hole crack damage. Allow the crack growth rate exponent p to vary from 2.5 to 3.5. Assess the effect of the exponent p on the results.

SOLUTION:

Since a comparative analysis is being conducted, it is not necessary to know the stress level nor the crack growth rate constant C , i.e., only those parameters that affect the integral I (Equation 10.5.3) need be considered. Table 10.5.2 presents the results of the calculations where the lives have been normalized to the Blueprint life $I_{r=0.125}$, using $(I_r - I_{r=0.125}) * 100 / I_{r=0.125}$ where I_r is the value of Equation 10.5.3 for radius r .

TABLE 10.5.2

COMPARATIVE ANALYSIS TO DETERMINE THE
EFFECT OF ENLARGING THE HOLE
(INITIAL CRACK LENGTH = 0.050 INCH)

Initial Hole Radius (inch)	Rework Change in Radius (inch)	Final Hole Radius (inch)	% Life Reduction		
			p=2.5	p=3.0	p=3.5
0.125	0	0.125	0	0	0
0.125	1/64	0.140625	10.6	12.2	13.7
0.125	1/32	0.15625	19.7	22.3	24.9
0.125	3/64	0.171875	27.5	30.9	34.1
0.125	1/16	0.1815	34.3	38.2	41.9
0.125	5/64	0.203125	40.2	44.5	48.4
0.125	3/32	0.21875	45.5	49.9	54.0
0.125	7/64	0.234375	50.2	54.7	58.9
0.125	1/8	0.250	54.4	58.9	63.0
0.125	9/64	0.265625	58.2	62.7	66.7
0.125	5/32	0.28125	61.6	66.0	69.9

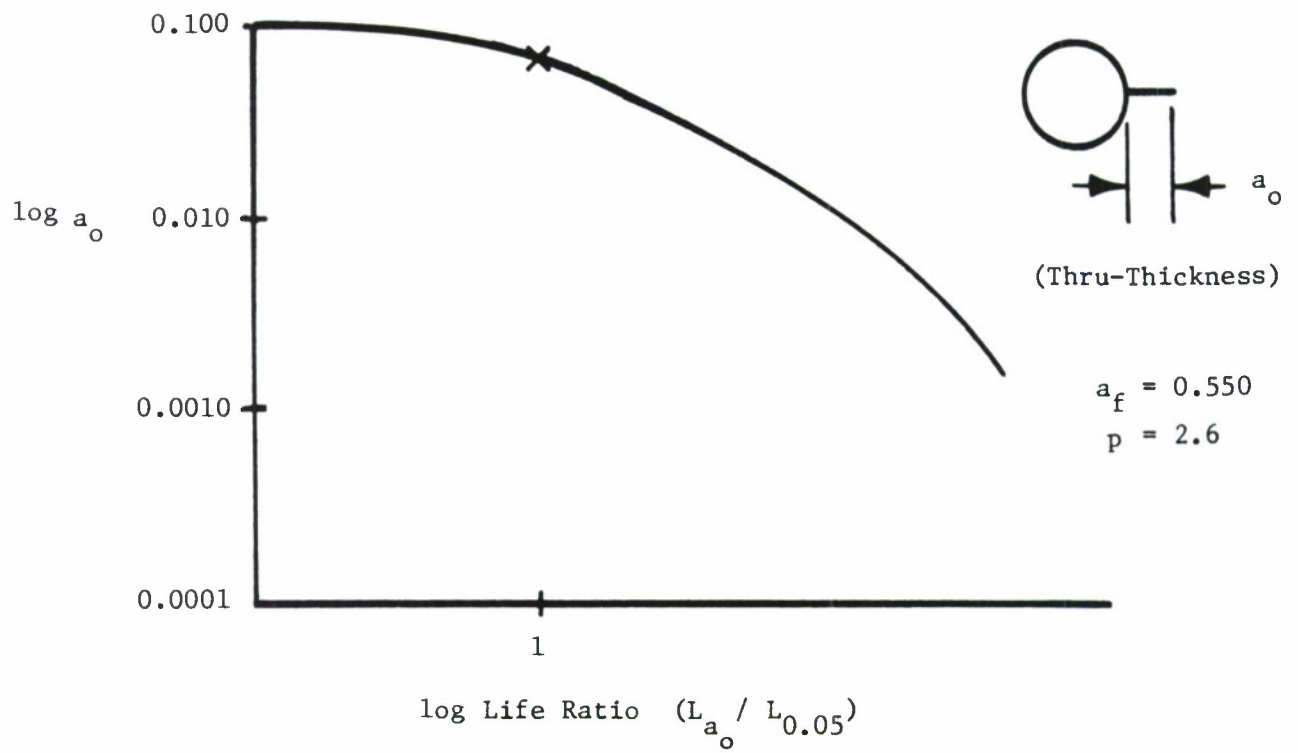
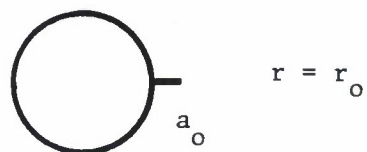
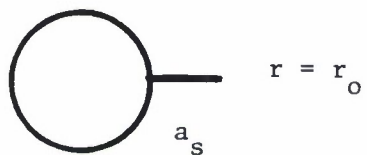


Figure 10.5.1 Crack Growth Life Ratio as a Function of Initial Crack Size Based on Results Presented in EXAMPLE 10.5.1.

a. Initial Configuration



b. In Service Configuration



c. Initial Reworked Configuration



Figure 10.5.2 Three Stages in the Life of A Cracked Hole.

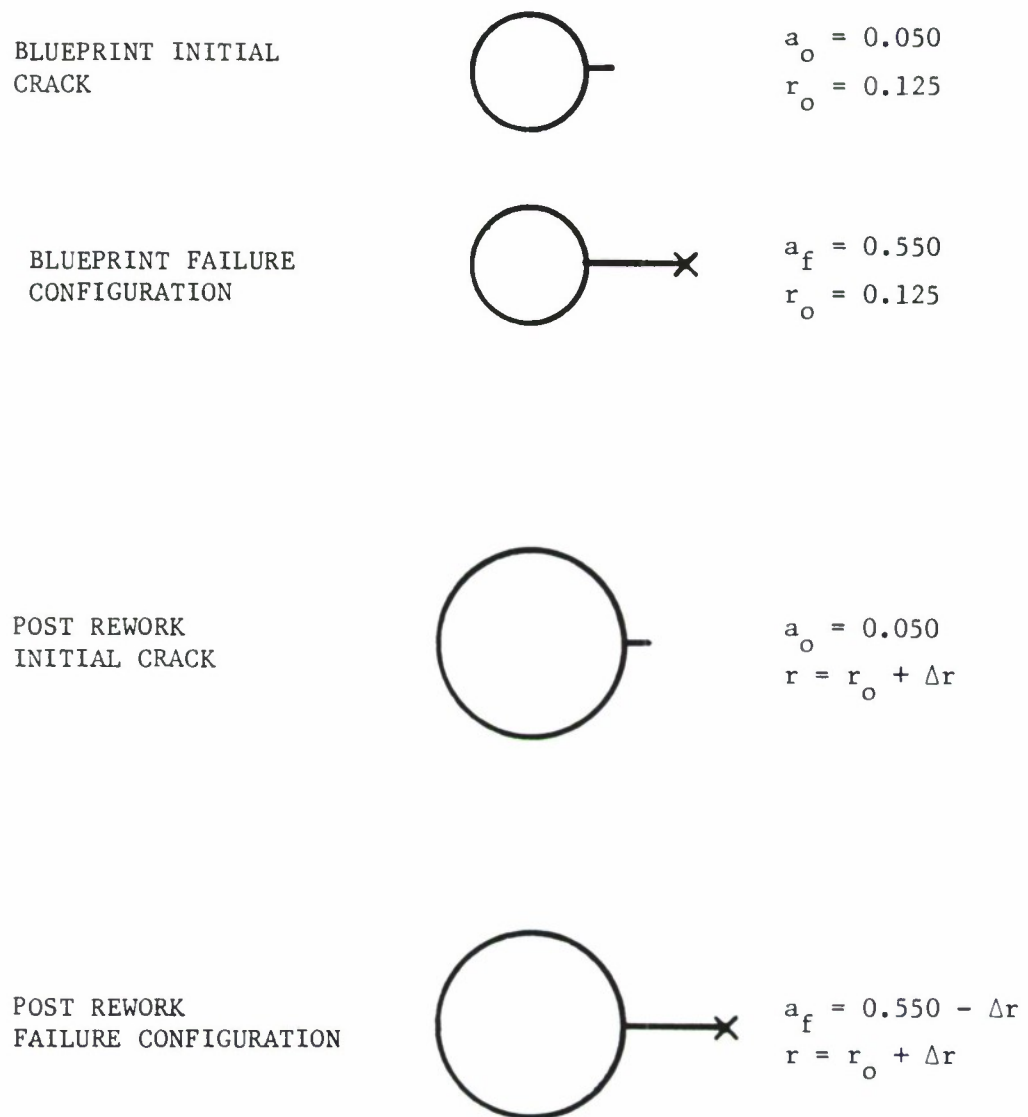


Figure 10.5.3 Geometrical Parameters Associated with Blueprint and Post Rework Crack Configurations for EXAMPLE 10.5.2.

One of the accepted procedures for removing a small amount of crack damage in the field is through the use of blend-out repairs. These repairs are efficiently accomplished and for the most part, return the structure close to its original static strength and design crack growth life interval. This subsection was prepared to specifically address the type of fatigue crack growth life analysis one might conduct to ensure that a blend-out repair has not significantly degraded the anticipated service life of the structure.

There are two basic conditions that might degrade the life of the structure as a result of blend-out: (1) the accidental gouging, scraping, or otherwise damaging of the material during the repair and (2) the development of a stress concentration site. Both conditions must be actively avoided since both tend to accelerate the development of new cracks which could cause safety-of-flight problems.

As discussed in Section 10.5, one of the more difficult aspects of repair analysis is the definition of initial crack size utilized for life calculations. If the initial crack size assumed after repair is greater than or equal to the initial crack size assumed during design, then the structure life after repair is less than or equal to the initial design life. To determine the fractional loss in structural life, an engineer could utilize the ratio

$$\text{Fractional Loss (FL)} = 1 - \frac{\text{Life(Repair)}}{\text{Life(Blueprint)}} \quad (10.6.1)$$

Alternately, the engineer could evaluate the loss in blueprint life by forming the life ratio:

$$LR = \frac{\text{Life(Repair)}}{\text{Life(Blueprint)}} \quad (10.6.2)$$

For comparison purposes, it would probably be advisable to calculate both the repair life and blueprint life based on the same initial crack length and thereby assess the effects of stress concentration introduced by the blend-out operation. To establish the crack growth life of the repair in an absolute sense would require that the choice of initial crack length be given careful engineering consideration.

Two examples have been prepared to illustrate the types of analyses which could be conducted to evaluate the damage tolerance of blend-out type repairs.

EXAMPLE 10.6.1 presents the calculations where the initial crack size for the repair is assumed to be equal to the crack size in as-manufactured structure. A sensitivity study is presented to demonstrate the impact that blend-out shape has on repair life. In EXAMPLE 10.6.2, the crack size after repair is assumed to be smaller than that in the as-manufactured structure, and a sensitivity study is presented to illustrate the effect of crack size.

EXAMPLE 10.6.1 Blend-out Repair - Effect of Shape

The angle transition component shown in Figure 10.6.1 periodically exhibits evidence of cracking in the location identified and the engineer has recommended a blend-out repair to remove all evidence of cracking. Based on the manufacturer's stress report, the tensile stress in the angle transition component is 27 Ksi for the critical load condition. Evaluate the damage tolerance of the component

assuming that the initial crack size in the repair (see Figure 10.6.2) and the as-manufactured structure are the same ($a_o = 0.050$ inch).

SOLUTION:

The damage tolerance evaluation will be based on an assessment of both the change in crack growth lives and the change in critical crack sizes. Based on a lack of both a stress history and a wide area crack growth rate equation (discussed in paragraph 10.3.3), an engineer might choose a worst case loading environment to conduct the evaluation. Since the stress condition is known ($\sigma_{\max} = 27$ Ksi), the engineer could approximate the loading with a once per flight maximum stress of 27 Ksi applied in a constant amplitude manner. For simplicity, the minimum stress per flight is presumed to be zero so that the assumed loading is zero-tension ($R=0$) constant amplitude with a stress maximum of 27 Ksi.

To conduct the life analysis, the life equation based on continuous crack growth (consistent with the constant amplitude loading assumption) will be utilized, i.e., life will be calculated using

$$\text{LIFE} = \int_{a_o}^{a_f} \frac{da}{f(K)} \quad (10.6.3)$$

The function $f(K)$ describes the crack growth rate for the material and loading condition; a_o and a_f are the initial and critical crack sizes, respectively. Three elements are necessary for the life calculation: (1) the function $f(K)$, (2) the stress-intensity factor relationship for the geometry, and (3) the critical crack size (a_f). Each element will be separately determined in the paragraphs below; subsequently, LIFE will be determined.

Function f(K) Established

The function f(K) describes crack growth rate as a function of a stress-intensity factor parameter (such as ΔK). As a result of the constant amplitude loading condition, the engineer would consult the Damage Tolerant Design (Data) Handbook⁽¹⁾ to find data consistent with the material and stress ratio conditions. The data in Table 8.11.3.3 (page 8.11-16) and Figure 8.11.3.3 (page 8.11-17) are considered representative of the 7079-T6 Aluminum Alloy; the table and figure are reproduced here as Figures 10.6.3 and 10.6.4, respectively. While it is possible to utilize the mean trend data given in tabular form (as presented in Figure 10.6.3) in conjunction with computer codes that employ table look-up schemes, it is instructive to plot the mean trend data and determine if a simple (power law) crack growth rate equation, i.e.

$$\frac{da}{dN} = C\Delta K^n \quad (10.6.4)$$

describes the behavior. Figure 10.6.5 presents both the mean trend data for the R = 0.05 data set and a power law equation that describes these data. The power law equation was determined (graphically evaluated) to be

$$\frac{da}{dN} = 5.84 \times 10^{-10} \Delta K^{4.09} \quad (10.6.5)$$

Because the stress ratio (R) for the assumed loading (R=0) and the data set (R=0.05) are relatively close, no stress ratio correction factor is applied to Equation 10.6.5. If a stress ratio correction must be applied to a handbook data set, it is suggested that a Walker type correction be considered. The suggested Walker correction factor for aluminum alloys is given by

$$\frac{da}{dN} \bigg|_{R = R_{\text{desired}}} = C_{\text{data set}} \left[\frac{1 - R_{\text{data set}}}{1 - R_{\text{desired}}} \right]^{\frac{1}{2}} \Delta K^n \quad (10.6.6)$$

where $R_{\text{data set}}$ and R_{desired} are the stress ratios associated with the Handbook data set and the assumed loading, respectively, and where n is the power law exponent for the data set ($n = 4.09$ for the 7079-T6 Aluminum data set). A quick evaluation of Equation 10.6.6 with the appropriate constants shows that the crack growth rate expression given by Equation 10.6.5 is approximately 10 percent higher than a corresponding stress ratio corrected expression, and thus not overly conservative for a first order approximation.

Stress-Intensity Factor Established

The stress-intensity factor for the blend-out cracking problem can be solved without access to exact finite element stress analyses through the use of some recent work of Dowling⁽²⁾. For the purpose of providing a methodology for estimating total fatigue life (crack initiation plus crack propagation lives) of notched structures, Dowling needed a transition crack length that separated the initiation life analysis from the crack propagation life analysis. His studies of the conditions controlling small crack growth behavior led him to the stress-intensity factor evaluation shown in Figure 10.6.6. The point M in Figure 10.6.6 identifies the condition where the short crack stress-intensity factor (K_s) is equal to the long crack solution (K_l). Dowling noted that these two crack solutions provided reasonably accurate estimates of the finite element solution in their respective crack length regions. For crack initiation life analysis, Dowling restricted crack length size measured in smooth fatigue samples to sizes

less than the crack length associated with the point M in Figure 10.6.6. This is because the stress concentration effect dominates in this region.

For the purpose of analysis, the engineer could estimate the stress-intensity factor for the blend-out repair using a Dowling type approach where for small cracks, a short crack stress-intensity factor would apply and for longer cracks, a long crack stress-intensity factor would apply. Thus, for the blend-out repair, the engineer could describe the stress-intensity factor as:

$$K = \begin{cases} K_s, & a \leq a_M \\ K_\ell, & a > a_M \end{cases} \quad (10.6.7)$$

with the short and long crack stress-intensity factors given by:

$$K_s = 1.12 k_t \sigma \sqrt{\pi a} \quad (10.6.8)$$

and

$$K_\ell = 1.12 \sigma \sqrt{\pi(a+d)} \quad (10.6.9)$$

where k_t in Equation 10.6.8 is the stress concentration factor associated with the blend-out shape.

The equations are written in a form slightly different than those presented in Figure 10.6.6 because (1) the geometry of the blend-out is more in line with an edge crack rather than a central crack (Dowling's solution) and (2) the crack length a is measured from the surface of the blend-out, see Figure 10.6.7 for a definition of " a " and " d ". Based on an analysis of Equations 10.6.8 and 10.6.9, one can see that the blend-out geometry affects the stress-intensity factor solutions through the stress concentration factor (k_t) and blend-out depth (d).

An estimate of the stress concentration k_t for a blend-out repair is made using the solution of an elliptical cut out in a plate. For an ellipse oriented with the major axis in line with the direction of the stress axis, the stress concentration is given by^(3,4)

$$k_t = \frac{3 + 2M - M^2}{1 + 2M + M^2} \quad (10.6.10)$$

where

$$M = \frac{L - d}{L + d} . \quad (10.6.11)$$

with L and d defined as the major and minor radii of the ellipse. As can be noted from Figure 10.6.7, L and d define a segment of a circle which we are approximating with a semi-ellipse. Thus, if one has a measure of L and d for a blend-out repair, one can estimate k_t and the corresponding short crack stress-intensity factor using Equations 10.6.10 and 10.6.8, respectively.

Critical Crack Size, a_f

The critical crack size for both as-manufactured (blueprint) and repaired structure will be based on the Irwin hypothesis for abrupt failure, i.e. when

$$K = K_{cr} \quad (10.6.12)$$

failure occurs. The critical stress-intensity factor is obtained by estimating the stress-intensity factor range required to achieve a growth rate of 1000 micro-inches/cycle. Solving Equation 10.6.5 in an inverse manner, i.e., solving

$$\Delta K = \left[\frac{1 \times 10^{-3}}{5.84 \times 10^{-10}} \right]^{\frac{1}{4.09}} \quad (10.6.13)$$

yields $\Delta K = 33.34 \text{ Ksi} \sqrt{\text{in}}$. As a lower bound to this estimate, one might chose $K_{cr} = 30 \text{ Ksi} \sqrt{\text{in}}$ for convenience. $K_{cr} = 30 \text{ Ksi} \sqrt{\text{in}}$ corresponds to a crack growth rate of 642 microinches/cycle.

The stress-intensity factor for the blueprint structure is given by

$$K = 1.12 \sqrt{\pi a} \quad (10.6.14)$$

where as that for the repaired structure is given by

$$K = 1.12 \sigma \sqrt{\pi(a+d)} \quad (10.6.15)$$

(Note that the long crack solution is being used for the repair). In both equations, "a" is measured from the surface; d is 0.0 in Equation 10.6.14 since the surface is flat. Solving Equation 10.6.12 for $K_{cr} = 30 \text{ Ksi} \sqrt{\text{in}}$ and the above stress-intensity factor solutions yields

$$a_f = 0.325 \text{ inch} \quad (10.6.16)$$

for the blueprint critical size and

$$a_f = (0.325-d) \text{ inch} \quad (10.6.17)$$

for the repair critical size.

Life Estimating

While Equation 10.6.3 could be used directly for life estimates of the as-manufactured (blueprint) structure, the stress-intensity factor analysis of Equation 10.6.7 requires that the integral equation (Equation 10.6.3) be broken into two intervals. For this repair analysis, LIFE is calculated using

$$\text{LIFE} = \int_{a_o}^{a_M} \frac{da}{f(K_s)} + \int_{a_M}^{a_f} \frac{da}{f(K_\ell)} \quad (10.6.18)$$

where the crack size a_M is associated with the transition between the short and long crack stress-intensity factor solutions. This crack size is obtained by equating the two solutions and solving for a_M , thus

$$K_s = K_l \quad (10.6.19)$$

in conjunction with Equations 10.6.8 and 10.6.9 results in

$$a_m = \frac{d}{k_t^2 - 1} \quad (10.6.20)$$

Since for a blend-out repair k_t would be greater than 1.0 and hopefully less than 1.4, a_M will be greater than d .

Numerical Details of Blueprint Life

For an edge crack problem with the material crack growth rate response given by a power law expression, i.e. Equation 10.6.4, Equation 10.6.3 can be written as

$$\text{LIFE} = \frac{1}{C(1.12 \sigma \sqrt{\pi})^n} \left[\int_{a_o}^{a_f} \frac{da}{a^{n/2}} \right] \quad (10.6.21)$$

When integrated, Equation 10.6.21 becomes

$$\text{LIFE} = \frac{1}{C(1.12 \sigma \sqrt{\pi})^n} \left[\frac{1}{\left(1 - \frac{n}{2}\right)} \cdot \left(a_f^{\frac{1-n}{2}} - a_o^{\frac{1-n}{2}} \right) \right] \quad (10.6.22)$$

Given the growth rate constants C , n (from Equation 10.6.5), the critical crack size (from Equation 10.6.16), the given stress ($\sigma = 27$ Ksi) and the given initial crack size ($a_o = 0.050$ inch), the crack growth life for the blueprint conditions is determined to be

$$\text{LIFE} = 2910 \text{ cycles} \quad (10.6.23)$$

of zero-tension loading.

Numerical Details of Repair Life

For the blend-out repair with the material crack growth rate response given by a power law expression, Equation 10.6.18 can be expressed as

$$\text{LIFE} = \frac{1}{C(1.12 \sigma \sqrt{\pi})^n} \left[\frac{1}{k_t^2} \int_{a_o}^{a_M} \frac{da}{a^{n/2}} + \int_{a_M}^{a_f} \frac{da}{(a+d)^{n/2}} \right] \quad (10.6.24)$$

When integrated Equation 10.6.24 becomes

$$\begin{aligned} \text{LIFE} = \frac{1}{C(1.12 \sigma \sqrt{\pi})^n} & \left(\frac{1}{k_t^2} \right) \left[\frac{1}{k_t^2} \cdot \left(a_M^{\frac{1-n}{2}} - a_o^{\frac{1-n}{2}} \right) \right. \\ & \left. + \left((a_f + d)^{\frac{1-n}{2}} - (a_M + d)^{\frac{1-n}{2}} \right) \right] \end{aligned} \quad (10.6.25)$$

Given the growth rate constants C , n (from Equation 10.6.4, the critical crack size from 10.6.17), the given stress ($\sigma = 27$ Ksi), and the given initial crack size ($a_o = 0.050$ inch), one can estimate the LIFE for defined values of k_t and d . For example, when d and L are 0.08 inch and 1.0 inch, k_t is 1.16, $a_f = 0.245$ inch, $a_M = 0.231$ inch, and

$$\text{LIFE} = 2033 \text{ cycles} \quad (10.6.26)$$

of zero-tension loading, approximately 30 percent lower than that given by Equation 10.6.23.

Comparative Analysis of Shape Effect

To summarize the analysis for different blend-out shapes, Equation 10.6.25 was repetitively solved for several different length ($2L$) and depth (d) conditions for $a_o = 0.050$ inch. These results are presented in Table 10.6.1 in the form of life

ratios (Equation 10.6.2) and utilize the blueprint life obtained from Equation 10.6.22(23). Focusing on three crack depths (0.050, 0.100 and 0.150 inches) as representative, one can immediately note from Table 10.6.1 even for the more gradual blend-out case, the life is substantially reduced (to approximately 80, 65, and 50 percent, respectively) of the original life estimate.

The life ratios presented in Table 10.6.1 show the close correlation between life and the stress concentration factor. These results only reinforce common sense since they show that the more gradual the blend-out, the closer to initial life one achieves.

EXAMPLE 10.6.2 Effect of Repair Initial Crack Size

To justify removing shallow cracks with blend-out repair procedures, EXAMPLE 10.6.1 is extended by considering the effect of repair initial crack size. As a basis for comparison, the life ratio equation, Equation 10.6.2, will again be employed and the blueprint (as-manufacturing) LIFE is calculated using Equation 10.6.22) with $a_o = 0.050$ inch. Thus, the blueprint LIFE will be as calculated in EXAMPLE 10.6.1, and is given by Equation 10.6.23. The purpose of this example is to show that if only part of the crack remains after blend-out there can be substantial life improvement over that calculated for the blueprint LIFE.

The effect of repair initial crack size on crack growth life was calculated using Equation 10.6.25 whereas the initial crack size a_o was varied along with length ($2L$) and depth (d) of the blend-out. The results are summarized in Table 10.6.2 as a function of the various geometric parameters considered. As expected, Table 10.6.2 shows that initial repair crack size substantially affects the damage tolerant life of the blend-out. In fact, compared to the

other parameters considered, it dominates. Based on Table 10.6.2, the importance of the variables on life is a_o - most significant, k_t - significant, and d - least significant. Thus, during a blend-out repair, the objective is to remove as much of the damage as possible (and hopefully all) with a minimum amount of shape change.

TABLE 10.6.1

EFFECTS OF BLEND-OUT SHAPE ON CRACK
GROWTH LIFE RATIO

Depth (d) inch	Length (2L) inch	k_t	Life Ratio $\left(\frac{\text{Equation 10.6.25}}{\text{Equation 10.6.23}}\right)$	Condition
0.005	2	1.01	0.977	<div><div></div><div></div><div></div><div></div><div></div><div></div><div></div><div></div><div></div><div></div><div></div><div></div><div></div><div></div><div></div><div></div><div></div><div></div><div></div><div></div><div></div><div></div><div></div><div></div><div></div><div></div><div></div><div></div><div></div><div></div><div></div><div></div><div></div><div></div><div></div><div></div><div></div><div></div><div></div><div></div><div></div><div></div><div></div><div></div><div></div><div></div><div></div><div></div><div></div><div></div><div></div><div></div><div></div><div></div><div></div><div></div><div></div><div></div><div></div><div></div><div></div><div></div><div></div><div></div><div></div><div></div><div></div><div></div><div></div><div></div><div></div><div></div><div></div><div></div><div></div><div></div><div></div><div></div><div></div><div></div><div></div><div></div><div></div><div></div><div></div><div></div><div></div><div></div><div></div><div></div><div></div><div></div><div></div><div></div><div></div><div></div><div></div><div></div><div></div><div></div><div></div><div></div><div></div><div></div><div></div><div></div><div></div><div></div><div></div><div></div><div></div><div></div><div></div><div></div><div></div><div></div><div></div><div></div><div></div><div></div><div></div><div></div><div></div><div></div><div></div><div></div><div></div><div></div><div></div><div></div><div></div><div></div><div></div><div></div><div></div><div></div><div></div><div></div><div></div><div></div><div></div><div></div><div></div><div></div><div></div><div></div><div></div><div></div><div></div><div></div><div></div><div></div><div></div><div></div><div></div><div></div><div></div><div></div><div></div><div></div><div></div><div></div><div></div><div></div><div></div><div></div><div></div><div></div><div></div><div></div><div></div><div></div><div></div><div></div><div></div><div></div><div></div><div></div><div></div><div></div><div></div><div></div><div></div><div></div><div></div><div></div><div></div><div></div><div></div><div></div><div></div><div></div><div></div><div></div><div></div><div></div><div></div><div></div><div></div><div></div><div></div><div></div><div></div><div></div><div></div><div></div><div></div><div></div><div></div><div></div><div></div><div></div><div></div><div></div><div></div><div></div><div></div><div></div><div></div><div></div><div></div><div></div><div></div><div></div><div></div><div></div><div></div><div></div><div></div><div></div><div></div><div></div><div></div><div></div><div></div><div></div><div></div><div></div><div></div><div></div><div></div><div></div><div></div><div></div><div></div><div></div><div></div><div></div><div></div><div></div><div></div><div></div><div></div><div></div><div></div><div></div><div></div><div></div><div></div><div></div><div></div><div></div><div></div><div></div><div></div><div></div><div></div><div></div><div></div><div></div><div></div><div></div><div></div><div></div><div></div><div></div><div></div><div></div><div></div><div></div><div></div><div></div><div></div><div></div><div></div><div></div><div></div><div></div><div></div><div></div><div></div><div></div><div></div><div></div><div></div><div></div><div></div><div></div><div></div><div></div><div></div><div></div><div></div><div></div><div></div><div></div><div></div><div></div><div></div><div></div><div></div><div></div><div></div><div></div><div></div><div></div><div></div><div></div><div></div><div></div><div></div><div></div><div></div><div></div><div></div><div></div><div></div><div></div><div></div><div></div><div></div><div></div><div></div><div></div><div></div><div></div><div></div><div></div><div></div><div></div><div></div><div></div><div></div><div></div><div></div><div></div><div></div><div></div><div></div><div></div><div></div><div></div><div></div><div></div><div></div><div></div><div></div><div></div><div></div><div></div><div></div><div></div><div></div><div></div><div></div><div></div><div></div><div></div><div></div><div></div><div></div><div></div><div></div><div></div><div></div><div></div><div></div><div></div><div></div><div></div><div></div><div></div><div></div><div></div><div></div><div></div><div></div><div></div><div></div><div></div><div></div><div></div><div></div><div></div><div></div><div></div><div></div><div></div><div></div><div></div><div></div><div></div><div></div><div></div><div></div><div></div><div></div><div></div><div></div><div></div><div></div><div></div><div></div><div></div><div></div><div></div><div></div><div></div><div></div><div></div><div></div><div></div><div></div><div></div><div></div><div></div><div></div><div></div><div></div><div></div><div></div><div></div><div></div><div></div><div></div><div></div><div></div><div></div><div></div><div></div><div></div><div></div><div></div><div></div><div></div><div></div><div></div><div></div><div></div><div></div><div></div><div></div><div></div><div></div><div></div><div></div><div></div><div></div><div></div><div></div><div></div><div></div><div></div><div></div><div></div><div></div><div></div><div></div><div></div><div></div><div></div><div></div><div></div><div></div><div></div><div></div><div></div><div></div><div></div><div></div><div></div><div></div><div></div><div></div><div></div><div></div><div></div><div></div><div></div><div></div><div></div><div></div><div></div><div></div><div></div><div></div><div></div><div></div><div></div><div></div><div></div><div></div><div></div><div></div><div></div><div></div><div></div><div></div><div></div><div></div><div></div><div></div><div></div><div></div><div></div><div></div><div></div><div></div><div></div><div></div><div></div><div></div><div></div><div></div><div></div><div></div><div></div><div></div><div></div><div></div><div></div><div></div><div></div><div></div><div></div><div></div><div></div><div></div><div></div><div></div><div></div><div></div><div></div><div></div><div></div><div></div><div></div><div></div><div></div><div></div><div></div><div></div><div></div><div></div><div></div><div></div><div></div><div></div><div></div><div></div><div></div><div></div><div></div><div></div><div></div><div></div><div></div><div></div><div></div><div></div><div></div><div></div><div></div><div></div><div></div><div></div><div></div><div></div><div></div><div></div><div></div><div></div><div></div><div></div><div></div><div></div><div></div><div></div><div></div><div></div><div></div><div></div><div></div><div></div><div></div><div></div><div></div><div></div><div></div><div></div><div></div><div></div><div></div><div></div><div></div><div></div><div></div><div></div><div></div><div></div><div></div><div></div><div></div><div></div><div></div><div></div><div></div><div></div><div></div><div></div><div></div><div></div><div></div><div></div><div></div><div></div><div></div><div></div><div></div><div></div><div></div><div></div><div></div><div></div><div></div><div></div><div></div><div></div><div></div><div></div><div></div><div></div><div></div><div></div><div></div><div></div><div></div><div></div><div></div><div></div><div></div><div></div><div></div><div></div><div></div><div></div><div></div><div></div><div></div><div></div><div></div><div></div><div></div><div></div><div></div><div></div><div></div><div></div><div></div><div></div><div></div><div></div><div></div><div></div><div></div><div></div><div></div><div></div><div></div><div></div><div></div><div></div><div></div><div></div><div></div><div></div><div></div><div></div><div></div><div></div><div></div><div></div><div></div><div></div><div></div><div></div><div></div><div></div><div></div><div></div><div></div><div></div><div></div><div></div><div></div><div></div><div></div><div></div><div></div><div></div><div></div><div></div><div></div><div></div><div></div><div></div><div></div><div></div><div></div><div></div><div></div><div></div><div></div><div></div><div></div><div></div><div></div><div></div><div></div><div></div><div></div><div></div><div></div><div></div><div></div><div></div><div></div><div></div><div></div><div></div><div></div><div></div><div></div><div></div><div></div><div></div><div></div><div></div><div></div><div></div><div></div><div></div><div></div><div></div><div></div><div></div><div></div><div></div><div></div><div></div><div></div><div></div><div></div><div></div><div></div><div></div><div></div><div></div><div></div><div></div><div></div><div></div><div></div><div></div><div></div><div></div><div></div><div></div><div></div><div></div><div></div><div></div><div></div><div></div><div></div><div></div><div></div><div></div><div></div><div></div><div></div><div></div><div></div><div></div><div></div><div></div><div></div><div></div><div></div><div></div><div></div><div></div><div></div><div></div><div></div><div></div><div></div><div></div><div></div><div></div><div></div><div></div><div></div><div></div><div></div><div></div><div></div><div></div><div></div><div></div><div></div><div></div><div></div><div></div><div></div><div></div><div></div><div></div><div></div><div></div><div></div><div></div><div></div><div></div><div></div><div></div><div></div><div></div><div></div><div></div><div></div><div></div><div></div><div></div><div></div><div></div><div></div><div></div><div></div><div></div><div></div><div></div><div></div><div></div><div></div><div></div><div></div><div></div><div></div><div></div><div></div><div></div><div></div><div></div><div></div><div></div><div></div><div></div><div></div><div></div><div></div><div></div><div></div><div></div><div></div><div></div><div></div><div></div><div></div><div></div><div></div><div></div><div></div><div></div><div></div><div></div><div></div><div></div><div></div><div></div><div></div><div></div><div></div><div></div><div></div><div></div><div></div><div></div><div></div><div></div><div></div><div></div><div></div><div></div><div></div><div></div><div></div><div></div><div></div><div></div><div></div><div></div><div></div><div></div><div></div><div></div><div></div><div></div><div></div><div></div><div></div><div></div><div></div><div></div><div></div><div></div><div></div><div></div><div></div><div></div><div></div><div></div><div></div><div></div><div></div><div></div><div></div><div></div><div></div><div></div><div></div><div></div><div></div><div></div><div></div><div></div><div></div><div></div><div></div><div></div><div></div><div></div><div></div><div></div><div></div><div></div><div></div><div></div><div></div><div></div><div></div><div></div><div></div><div></div><div></div><div></div><div></div><div></div><div></div><div></div><div></div><div></div><div></div><div></div><div></div><div></div><div></div><div></div><div></div><div></div><div></div><div></div><div></div><div></div><div></div><div></div><div></div><div></div><div></div><div></div><div></div><div></div><div></div><div></div><div></div><div></div><div></div><div></div><div></div><div></div><div></div><div></div><div></div><div></div><div></div><div></div><div></div><div></div><div></div><div></div><div></div><div></div><div></div><div></div><div></div><div></div><div></div><div></div><div></div><div></div><div></div><div></div><div></div><div></div><div></div><div></div><div></div><div></div><div></div><div></div><div></div><div></div><div></div><div></div><div></div><div></div><div></div><div></div><div></div><div></div><div></div><div></div><div></div><div></div><div></div><div></div><div></div><div></div><div></div><div></div><div></div><div></div><div></div><div></div><div></div><div></div><div></div><div></div><div></div><div></div><div></div><div></div><div></div><div></div><div></div><div></div><div></div><div></div><div></div><div></div><div></div><div></div><div></div><div></div><div></div><div></div><div></div><div></div><div></div><div></div><div></div><div></div><div></div><div></div><div></div><div></div><div></div><div></div><div></div><div></div><div></</div></div>

TABLE 10.6.2

EFFECT OF REPAIR INITIAL CRACK SIZE
ON CRACK GROWTH LIFE RATIO

Repair Initial Crack Size (a_o) inch	Depth (d) inch	Length (2L) inch	k_t	Life Ratio $\left(\frac{\text{Equation 10.6.25}}{\text{Equation 10.6.23}} \right)$
0.005	0.02	2.0	1.04	11.81
0.005	0.05	2.0	1.10	10.55
0.005	0.10	2.0	1.20	8.83
0.005	0.15	2.0	1.30	7.49
<hr/>				
0.010	0.02	2.0	1.04	5.63
0.010	0.05	2.0	1.10	5.02
0.010	0.10	2.0	1.20	4.19
0.010	0.15	2.0	1.30	3.52
<hr/>				
0.010	0.02	1.0	1.08	5.21
0.010	0.05	1.0	1.20	4.20
0.010	0.10	1.0	1.40	3.02
0.010	0.15	1.0	1.60	2.28
<hr/>				
0.020	0.02	2.0	1.04	2.64
0.020	0.05	2.0	1.10	2.34
0.020	0.10	2.0	1.20	1.94
0.020	0.15	2.0	1.30	1.61
<hr/>				
0.050	0.02	2.0	1.04	0.91
0.050	0.05	2.0	1.10	0.80
0.050	0.10	2.0	1.20	0.64
0.050	0.15	2.0	1.30	0.50

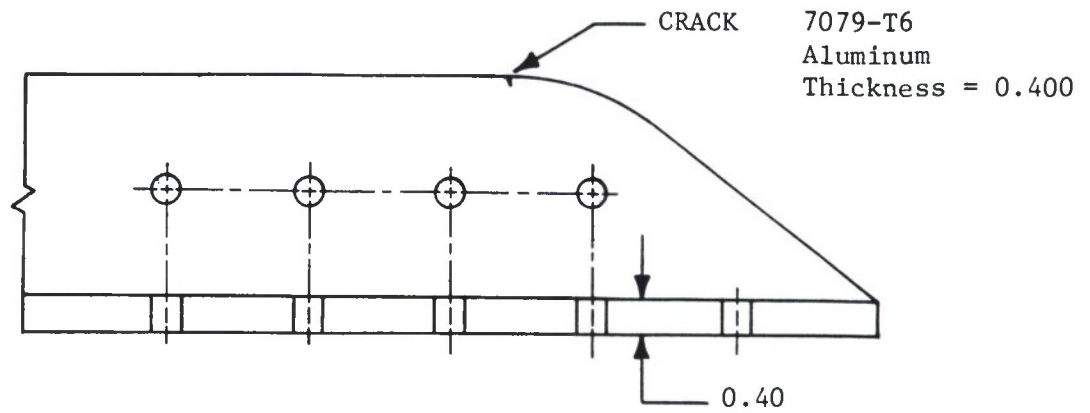


Figure 10.6.1 Geometry of Structure with Small Crack.

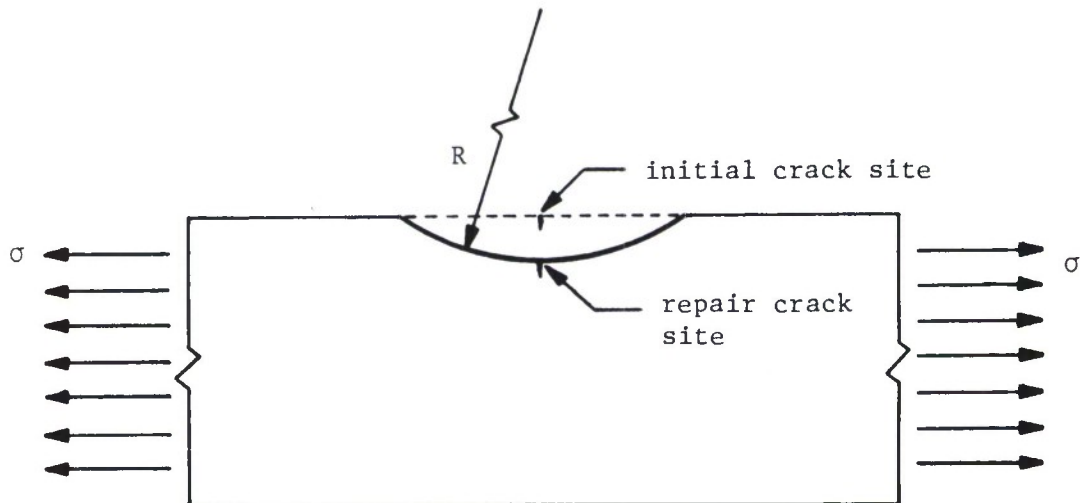


Figure 10.6.2 Geometry of Blend-Out Repair Assumed for Analysis.

TABLE 8.11.3.3

**FATIGUE CRACK GROWTH RATES AT DEFINED LEVELS
OF STRESS INTENSITY FACTOR**

DATA ASSOCIATED WITH FIGURE 8.11.3.3 INDICATING EFFECT

OF STRESS RATIO

MATERIAL: ALUMINUM		7079			
CONDITION: T6					
ENVIRONMENT: R. T., LAB AIR					
DELTA K		DA/DN (10** ⁻⁶ IN./CYCLE)			
(KSI*IN**1/2)					
		A	B	C	D
		R=+0.05	R=+0.50		
A:	4.14	.284			
DELTA K B:	2.16		.137		
MIN C:					
D:					
	2.50		.193		
	3.00		.317		
	3.50		.517		
	4.00		.833		
	5.00	.387	2.08		
	6.00	.922	4.65		
	7.00	1.91	8.94		
	8.00	3.29	15.3		
	9.00	5.17	21.3		
	10.00	7.81	22.0		
	13.00	21.8			
	16.00	35.7			
	20.00	42.8			
	25.00	55.4			
A:	27.05	67.8			
DELTA K B:	10.09		21.7		
MAX C:					
D:					
ROOT MEAN SQUARE		41.55	30.01		
PERCENT ERROR					
LIFE	0.0-0.5				
PREDICTION	0.5-0.8				
RATIO	0.8-1.25				
SUMMARY	1.25-2.0				
(NP/NA)	>2.0				

8.11-16

Figure 10.6.3 Tabular Data Page From the Damage Tolerant Design (Data)
Handbook Used in EXAMPLE 10.6.1.

CONDITION/HT: T8
 FORM: FORGING
 SPECIMEN TYPE: CT
 ORIENTATION: T-L
 FREQUENCY: 9.00 HZ
 ENVIRONMENT: R.T., LAB AIR

YIELD STRENGTH: 72.8 KSI
 ULT. STRENGTH: 83.4 KSI
 SPECIMEN THK: 0.400"
 SPECIMEN WIDTH:
 REFERENCES: BW001

ALUM.
 ALLOY

7079

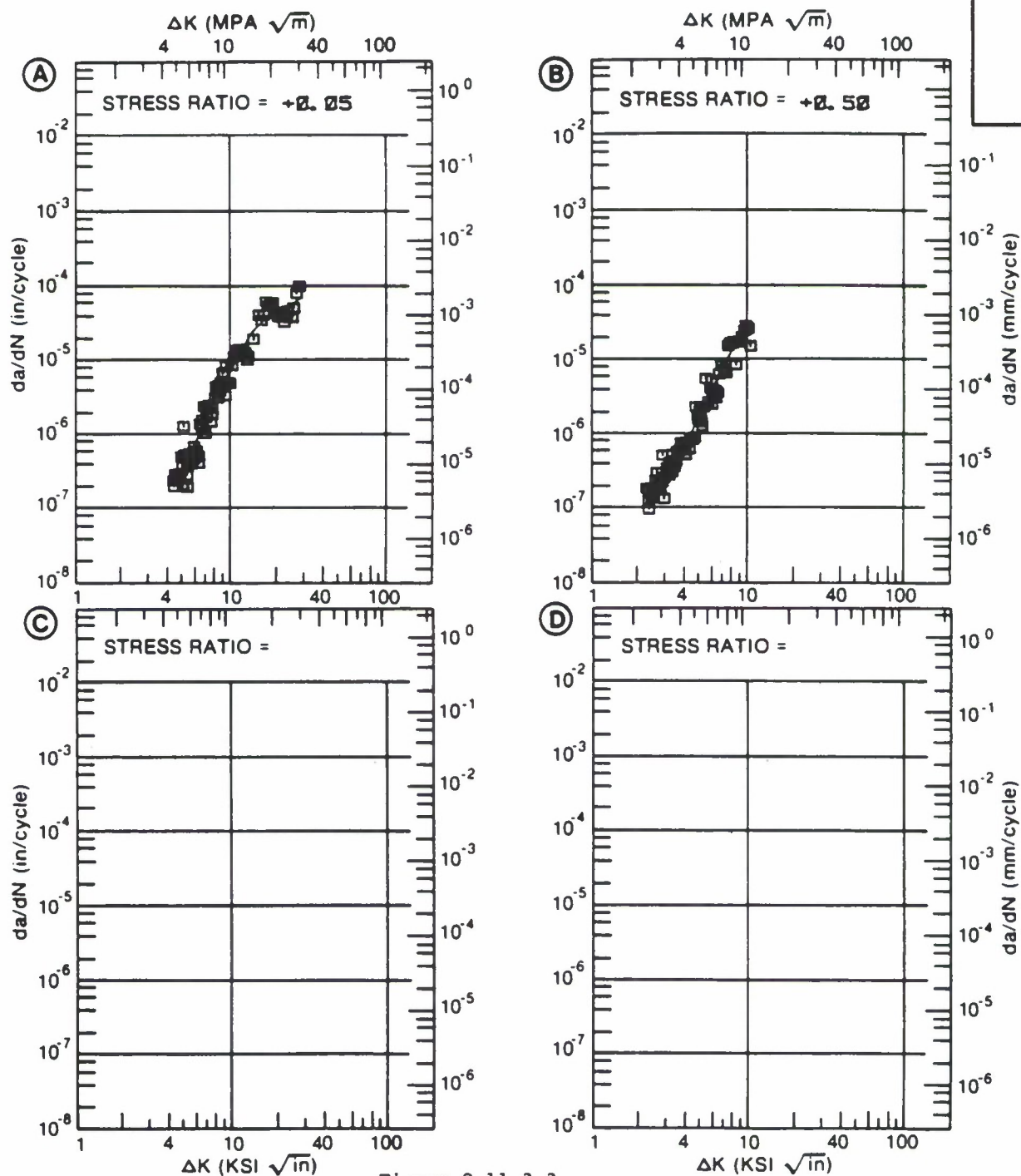


Figure 8.11.3.3

8.11-17

Figure 10.6.4 Graphical Data Page From the Damage Tolerant Design (Data) Handbook Used in EXAMPLE 10.6.1.

10.6.17

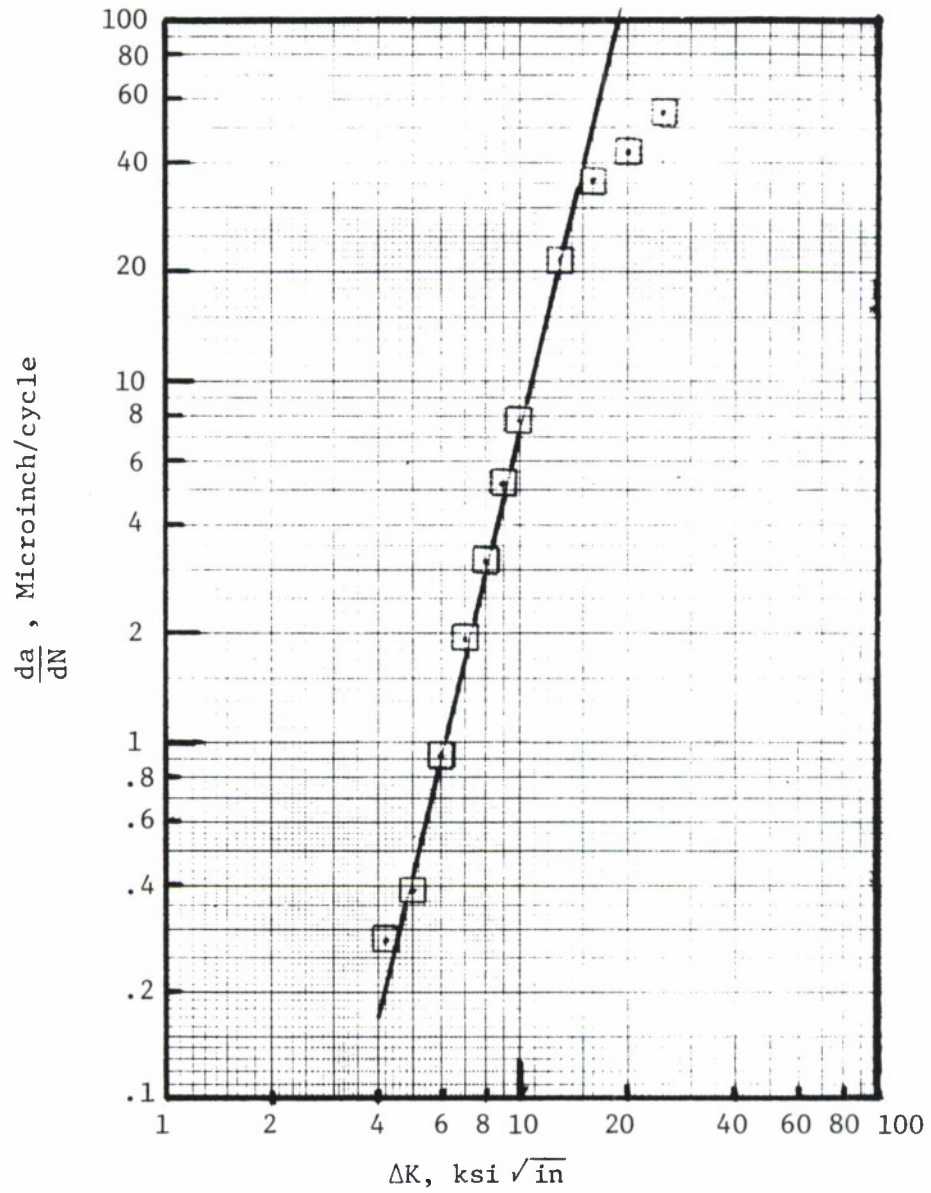


Figure 10.6.5 Tabular Data From Damage Tolerant Design (Data) Handbook (Figure 10.6.3) Plotted and Compared to Graphically Established Power Law Equation.

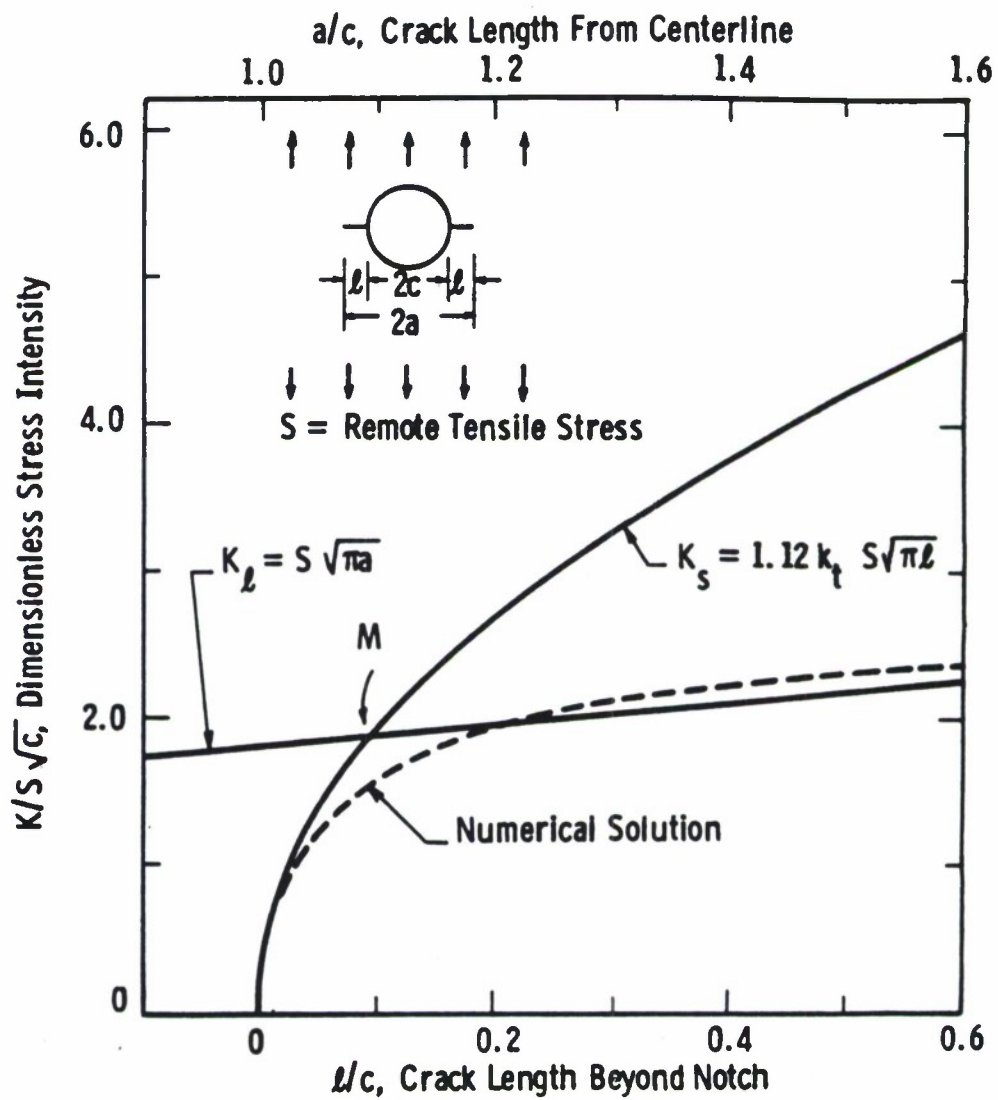


Figure 10.6.6 Short and Long Crack Limiting Cases and Numerical Solution, for Cracks Growing From a Circular Hole in an Infinite Plate (Newman).

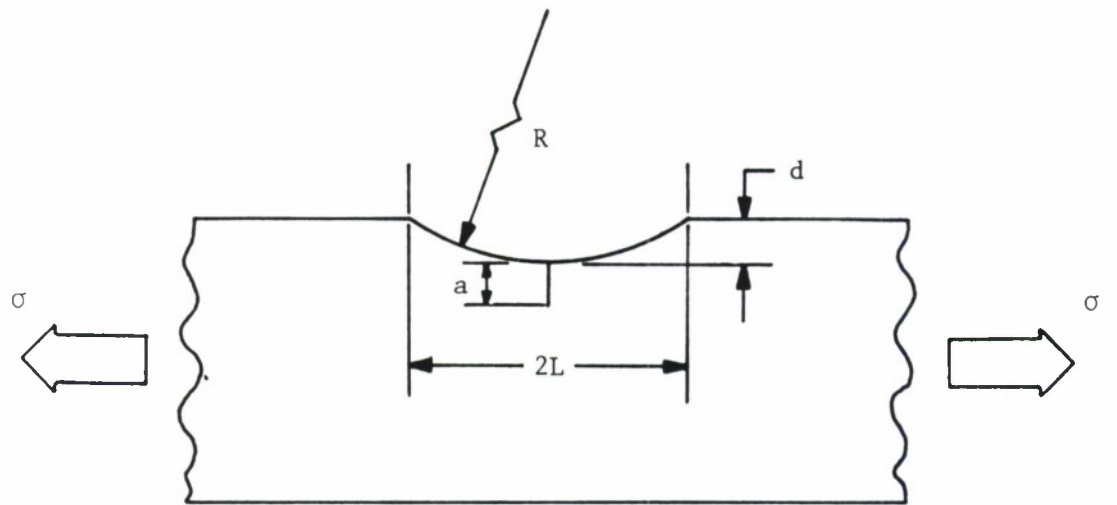


Figure 10.6.7 Geometry of Blend-Out with Edge Crack Present.

This section illustrates parametric analyses available to an engineer for evaluating the sensitivity of residual strength to geometric and material parameters. As discussed in Chapter 4, the residual strength relates load carrying capability to material toughness and crack size in a unique way for each structure. Two methods are generally available for describing the residual strength of a structure: the first is with a relationship between residual strength and crack length and the second is with a relationship between residual strength and time. These relationships are summarized in Figure 10.7.1. The first relationship (Figure 10.7.1a) is best used to describe the effects of toughness or of global geometry. The second relationship (Figure 10.7.1b) is best used to describe the effects of crack growth resistance and of global geometry.

Constructing residual strength-crack length relationships are relatively straight forward. To do so requires both fracture toughness data for the material and a stress-intensity factor analysis for the cracked structure. Fracture toughness data can be found in the Damage Tolerant Design (Data) Handbook. The stress-intensity factor for a given cracked structure can be obtained through either the exact or approximate methods discussed in Sections 1.6, 1.7, and 1.8.

Constructing residual strength-life relationships requires the same information as above plus a description of the crack growth life behavior under the service loading. This additional information can be generated by integrating wide area crack growth rate equations (Paragraph 10.3.3) or by summing incremental damage on a cycle-by-cycle basis. Cycle-by-cycle damage summation presumes (a) that a stress history is available for the cracked structure and (b) that constant

amplitude fatigue crack growth rate data are available for the material. The additional complexity associated with generating residual strength-life relationships is one reason why residual strength data are normally only presented as a function of crack length.

A series of examples have been prepared to describe the effects of material properties, spectrum stress level, and structural geometry on the residual strength of relatively simple structures. The approach taken could be duplicated for other more complicated situations related to specific structural repairs.

For each example, the Irwin abrupt fracture criterion is employed to obtain the relationship between residual strength and crack size. Simply stated, failure is presumed to occur when the applied stress-intensity factor (K) is greater than or equal to the fracture toughness (K_{cr}) of the material, i.e.

$$K \geq K_{cr} \quad (10.7.1)$$

then failure occurs. Because the stress-intensity factor is a function of stress and crack size, Equation 10.7.1 provides the relationship between residual strength and critical crack length.

To facilitate a general overview of the residual strength-life relationship, the wide area crack growth rate equation methods developed in Section 10.3 are utilized. In this section, the wide area equation is expressed as

$$\frac{da}{dN} = C \bar{K}^n \quad (10.7.2)$$

where the crack growth rate (da/dN) is given appropriately as a function of cycles, flights, or flight hours depending on the given structural situation. Also, the

characteristic stress-intensity factor (\bar{K}) in Equation 10.7.2 is related to the characteristic stress ($\bar{\sigma}$) through

$$\bar{K} = \bar{\sigma} \left(\frac{K}{\sigma} \right) \quad (10.7.3)$$

where (K/σ) is the stress-intensity factor coefficient (dependent only on geometric parameters, such as crack length and edge distances). The residual strength-life relationship is obtained by cross correlating the residual strength calculated from Equation 10.7.1 with the life calculated from

$$\text{LIFE} = \int_{a_o}^{a_{cr}} \frac{da}{C \bar{K}^n} \quad (10.7.4)$$

The cross correlation is accomplished using the same value of critical crack length (a_{cr}) for both the residual strength and life calculations.

The first example (10.7.1) considers the effect of fracture toughness on both the residual strength-crack length and residual strength-life relationships. These relationships are established for an open hole with a through-the-thickness radial crack, and for a wide area crack growth rate equation defined as

$$\frac{da}{dN} = 1 \times 10^{-8} \bar{K}^{3.0} \quad (10.7.5)$$

(When $\bar{K} = 10 \text{ ksi } \sqrt{\text{in}}$, the crack growth rate is $10 \times 10^{-6} \text{ inch/cyclic unit}$).

Examples 10.7.2, 10.7.3, and 10.7.4 consider how (1) the characteristic stress level ($\bar{\sigma}$), (2) the pre-exponential constant (C in Equation 10.7.2) and (3) the exponential constant (n in Equation 10.7.2), respectively, affect the residual strength-life relationship. Subsequently, Examples 10.7.5 and 10.7.6 present the effect of geometrical and loading changes on the residual strength-crack length and residual strength-life relationships.

EXAMPLE 10.7.1 Effect of Fracture Toughness

The structural geometry and loading are as described in Figure 10.7.2 and it is desired that the residual strength relationships be evaluated as a function of fracture toughness. To determine the residual strength-crack length relationship, Equation 10.7.1 is utilized in conjunction with the stress-intensity factor coefficient obtained from Subsection 1.7, and specifically employing Equation 1.7.4 to describe the Beta factor. The stress-intensity factor coefficient for the tension-loaded, open-hole with a radial-through-the-thickness crack is given by

$$\frac{K}{\sigma} = \sqrt{\pi a} \cdot \left(0.6762 + \frac{0.8734}{0.3246 + \frac{a}{r}} \right) \quad (10.7.6)$$

Solving Equation 10.7.1 in conjunction with Equation 10.7.6 leads to the relationship between residual stress and critical crack size, thus

$$\sigma_{\text{res}} \cdot \sqrt{\pi a_{\text{cr}}} \left(0.6762 + \frac{0.8734}{0.3246 + \frac{a_{\text{cr}}}{r}} \right) = K_{\text{cr}} \quad (10.7.7)$$

Defining a series of critical crack sizes for a given value of K_{cr} is the easiest method for evaluating the relationship. Figure 10.7.3 describes the relationship between residual strength and crack length (evaluated in this manner) for several given values of K_{cr} . As Figure 10.7.3 illustrates, a substantial difference exists between the residual strength curves at any crack length; this difference is linearly related to the fracture toughness level (For a defined crack length, Equation 10.7.6 gives a constant value of (K/σ) so an increase in K_{cr} leads to a similar increase in σ_{res}).

Evaluating the difference between the residual strength curves in Figure 10.7.3 based on a constant residual strength level illustrates that a greater improvement factor on critical crack size accompanies an increase in fracture toughness. For a $\sigma_{res} = 40$ ksi requirement, the critical crack size for the $K_{cr} = 30$ ksi $\sqrt{\text{in}}$ material is about 0.050 inch whereas that for a 50 ksi $\sqrt{\text{in}}$ material is about 0.750 inch. As a first order approximation of the improvement factor, one might neglect the influence of the Beta factor and arrive at a simplified ratio

$$\frac{a_{cr}^{new}}{a_{cr}^{old}} = \left(\frac{K_{cr}^{new}}{K_{cr}^{old}} \right)^2 \quad (10.7.8)$$

that illustrates the reason for the dramatic increase in critical crack length for fracture toughness improvements.

One function of an engineer is to provide the structure with sufficient fracture toughness in order to maintain the required residual strength throughout the anticipated service lifetime. A choice of high fracture toughness is appropriate when the engineer is attempting to ensure that potentially damaging cracks are large and easily inspectable prior to the loss of a residual strength requirement. To determine how rapidly the residual strength decays, it is necessary to perform a crack growth life calculation.

When the crack growth life calculation is based on the integral formulation of Equation 10.7.2 (a power law), i.e. on Equation 10.7.4, the shape of the crack growth-life curve is as shown in Figure 10.7.4. The specific curve generated in Figure 10.7.4 was obtained for a characteristic stress level ($\bar{\sigma}$) of 20 ksi and employed $C = 1 \times 10^{-8}$ and $n = 3.0$ as the constants in Equation 10.7.4. The initial crack length (a_0) in Equation 10.7.4 was chosen as 0.050 inches.

The curve in Figure 10.7.4 has been marked to indicate the stress-intensity factor at various crack length levels. These levels correspond to the lower fracture toughness levels shown in Figure 10.7.3. One consequence of using a power law equation to describe crack growth rate behavior is that the crack growth life curve does not indicate a rapid increase as the stress-intensity factor approaches the fracture toughness level. From a practical standpoint, only a slight error in the life calculation occurs due to inaccurately modeling the crack growth rate in the fracture toughness regime.

When the crack length-life data in Figure 10.7.4 are cross correlated with the residual strength-crack length data in Figure 10.7.3, one obtains the relationships between residual strength and life shown in Figure 10.7.5. Each residual strength-life data point identified in Figure 10.7.5 is associated with a common crack length that relates the data in Figures 10.7.3 and 10.7.4. Figure 10.7.5 shows that the highest values of fracture toughness are again associated with the highest values of residual strength. Figure 10.7.5 also shows that a material with high fracture toughness will maintain a high residual strength capability longer than one with low fracture toughness, all other conditions being equal. Interestingly, for the conditions given for this example, the residual strength capability decays in a linear fashion for most of the life. The only nonlinearity occurs in the earliest part of life where the crack is in a severe stress-intensity factor gradient. Other factors which affect the extent of the nonlinear region will be discussed later.

EXAMPLE 10.7.2 Effect of Characteristic Stress Level

Because the operational stress level significantly affects the crack length life of a structure, an engineer might wish to consider its effect on residual strength. For this evaluation, assume that the material is known to have a fracture toughness (K_{cr}) of 30 ksi $\sqrt{\text{in}}$ and a crack growth rate behavior given by Equation 10.7.5.

The residual strength-crack length relationship will not be affected by the operational stress level; thus, the $K_{cr} = 30 \text{ ksi } \sqrt{\text{in}}$ curve in Figure 10.7.3 describes the relationship for this example. The corresponding crack growth-life curves for characteristic stress levels ($\bar{\sigma}$) of 15, 20, and 25 ksi are presented in Figure 10.7.6. As anticipated, the highest stress produces the fastest crack growth-life behavior. Based on Equation 10.7.4, the curves shown in Figure 10.7.6 are related to each other by a life factor given by

$$\frac{L_2}{L_1} = \left(\frac{\bar{\sigma}_1}{\bar{\sigma}_2} \right)^n \quad (10.7.9)$$

where the lives L_1 and L_2 are calculated at the same crack length (any choice of a_{cr} applies) for characteristic stress levels $\bar{\sigma}_1$ and $\bar{\sigma}_2$.

If one cross correlates the crack length-life behavior given in Figure 10.7.6 with the $K_{cr} = 30 \text{ ksi } \sqrt{\text{in}}$ residual strength-crack length behavior given in Figure 10.7.3, then the residual strength-life behavior is as presented in Figure 10.7.7. Note that the residual strength capability decays more slowly for the lower characteristic stress levels. As a method for predicting the residual strength-life behavior as a function of stress level, one could utilize the base-line curve identified in Figure 10.7.7 and Equation 10.7.9 to provide the

appropriate life factor (at any given residual strength level). For example, as shown in Figure 10.7.7, the $\bar{\sigma} = 15$ ksi residual strength-life curve is displaced by a factor of

$$\frac{L_{15}}{L_{20}} = \left(\frac{20}{15}\right)^{3.0} = 2.37 \quad (10.7.10)$$

from the $\bar{\sigma} = 20$ ksi residual strength-life curve (check this at say $\sigma_{\text{res}} = 30$ ksi where $L_{20} \approx 5300$ and where $L_{15} \approx 12600$.)

Thus, one could construct residual strength-life curves as a function of characteristic stress levels by generating a baseline curve and applying the life factor given by Equation 10.7.9.

EXAMPLE 10.7.3 Effect of Pre-exponential Constants

This example and EXAMPLE 10.7.4 collectively consider the effect of modifying the material's crack growth rate response on the residual strength capability. In both examples, the baseline conditions stated in Figure 10.7.2 are used unless otherwise specified. It is noted that the crack growth rate resistance can be changed independent of the fracture toughness (fracture resistance), so that the residual strength-crack length relationship is again given by the $K_{\text{cr}} = 30 \text{ ksi} \sqrt{\text{in}}$ curve in Figure 10.7.3.

In a somewhat decoupling fashion, the effect of varying the coefficients in Equation 10.7.2 are considered separately. In this example, only the pre-exponential constant (C) is varied to reflect decreasing the crack growth rate response in a systematic manner from the baseline condition ($C = 1 \times 10^{-8}$). In EXAMPLE 10.7.4, the effect of varying the exponent n is considered.

A change in the pre-exponential constant in Equation 10.7.2 is equivalent to shifting the crack growth rate curve to a new position but with the same slope (see Figure 10.7.8).

Based on an analysis of Equation 10.7.4, it is seen that the life difference that results from a change in C can be expressed as a life ratio

$$\frac{L_2}{L_1} = \frac{C_1}{C_2} \quad (10.7.11)$$

Thus, if a baseline crack growth-life curve and a baseline residual strength-life curve exist, new curves can be generated by factoring the lives from the baseline condition to the new material conditions using Equation 10.7.11.

Figure 10.7.9 describes the residual strength-life curves for the baseline and two lower values of the pre-exponential constants. From the figure, it is seen that the increased crack growth resistance, i.e. lower C values, results in slower rates of residual strength decay. The new curves are exactly a factor of two and of four removed from the baseline curve as suggested by Equation 10.7.11.

Increasing the material's crack growth resistance has an immediate effect of increasing the number of flights (amount of flight hours) until the residual strength capability decays to the residual strength requirement.

EXAMPLE 10.7.4 Effect of Exponential Constant

In this example, the exponential constant (n) in Equation 10.7.2 is varied along with the pre-exponential constant C to reflect a defined rate of crack growth ($\frac{da}{dN} = 10 \times 10^{-6}$ in/cyclic unit) for a given characteristic stress-intensity

factor level ($\bar{K} = 10 \text{ ksi } \sqrt{\text{in}}$). The baseline constants of $n = 3.0$ and $C = 1 \times 10^{-8}$ yield an equation (Equation 10.7.5) which passes through the point $(10, 10 \times 10^{-6})$. Figure 10.7.10 illustrates the three choices of n considered in this example.

For this baseline geometry, fracture toughness level, and stress level, the characteristic stress-intensity factor varies between about 15 and 30 $\text{ksi } \sqrt{\text{in}}$ (as a result of the crack growth change). When the common point for the power law equations is located at a stress-intensity factor level that corresponds to a crack length within the crack length interval associated with the life calculation, one can not immediately interpret the effect of the crack growth rate behavior. However, based on the crack growth rate behavior defined in Figure 10.7.10, the curve with $n = 3.5$ will yield crack growth rates faster than the baseline throughout the crack length interval of interest. Thus for the conditions stated, an engineer would expect a more accelerated crack growth behavior and a more rapidly decaying residual strength behavior for the $n = 3.5$ material than for the baseline. The curves in Figures 10.7.11 and 10.7.12 bear out this expectation.

One observation made in studying the residual strength-life behavior presented in Figure 10.7.12 is that the decay in residual strength is slightly nonlinear in the long life region for the two nonbaseline crack growth rate behaviors. For the $n = 2.5$ material, the residual strength-life curve is slightly concave up while the $n = 3.5$ material produces a slightly concave-down shape. Thus, a second factor that produces nonlinear decay effects is the exponent n . Generally speaking, nonlinear decay effects would be expected when the crack growth rate behavior can not be described by a power law equation with $n = 3$. While the nonlinear

behavior is evident, it is important to note that it is slight. As a result, local regions of the residual strength life curve can be easily described by linear line segments, and the procedures presented in EXAMPLES 10.7.1, 10.7.2, and 10.7.3 can be utilized to extrapolate from a segmented baseline curve.

The rate of decay in residual strength as a function of service loading has been shown by the above examples to be an important function of material behavior and of load level. The residual strength decay rate can also be significantly affected by geometric parameters and loading conditions. In EXAMPLE 10.7.5, the effect of global and crack geometry is considered; and then in EXAMPLE 10.7.6, the effect of localized fastener loading is evaluated.

EXAMPLE 10.7.5 Effect of Geometrical Parameters

Using the through-the-thickness, radially-cracked, open hole geometry (Figure 10.7.2) as the baseline geometry, two other geometrical configurations are considered: (1) the through-the-thickness, center-crack and (2) an open hole with a radial crack which transitions from a one-quarter-circular, corner-crack shape to a through-the-thickness-crack shape. In all cases, the width of the structure is considered sufficient so that it does not influence the results. Baseline material properties (K_{cr} , C , and n), initial crack length (a_o), and characteristic stress level ($\bar{\sigma}$) are as defined in Figure 10.7.2 and apply to all three geometries. The center crack geometry does not have a central (starter) hole; its total initial length is $2a_o$. The radius (r) of the hole with the transitioning crack is 0.125 inch, the same as the baseline geometry.

The information presented at the introduction of this section described how the residual stress relationships could be developed using Equations 10.7.1 and 10.7.4 and the stress-intensity factor coefficient for the geometry. The only factor that changes as a function of geometrical parameters is the stress-intensity factor coefficient; Equation 10.7.6 provided this coefficient for the baseline case. For the through-the-thickness, center crack configuration, the stress-intensity factor coefficient is given by

$$\frac{K}{\sigma} = \sqrt{\pi a} \quad (10.7.12)$$

The case of the transitioning corner crack requires that the crack growth shape be known throughout the interval of crack growth. As an approximation of the stress-intensity factor coefficient for this complicated problem EXAMPLE 1.8.5 was prepared and its results are used herein. The coefficient is presented for three crack length intervals:

for $a \leq 0.050$ inch

$$\frac{K}{\sigma} = 1.12 \cdot \frac{2}{\pi} \cdot \sqrt{\pi a} \left(0.6762 + \frac{0.8734}{0.3246 + \frac{a}{\sqrt{2} r}} \right) \quad (10.7.13)$$

for $0.050 \leq a \leq 0.250$

$$\frac{K}{\sigma} = 1.376 a^{0.2783} \quad (10.7.14)$$

and for $a > 0.250$, Equation 10.7.6 is used.

When the stress-intensity factor coefficients for the given geometries are utilized in conjunction with Equation 10.7.1, the residual strength-crack length relationships shown in Figure 10.7.13 are determined ($K_{cr} = 30 \text{ ksi } \sqrt{\text{in}}$). As expected, the transitioning corner crack geometry exhibits residual strength which

is greater than that of the through-the-thickness crack geometry (baseline) for shorter cracks. For crack lengths greater than 0.250 inch, the transitioning radial crack and baseline configurations exhibit the same residual strength (since the stress-intensity factor coefficients are the same here). One interesting feature of Figure 10.7.13 is that the residual strength of the center crack configuration is higher than the radially cracked holes for short crack lengths but rapidly decreases with crack length and eventually falls below the residual strength exhibited by the cracked hole. One might puzzle through this observation by noting that the center crack has a total length of $2a$, whereas the radially cracked hole has an equivalent length of $(a + 2r)$.

Equation 10.7.4 was utilized to calculate the crack growth life relationships for the three geometries and these are shown in Figure 10.7.14. Because the stress-intensity factor for the through-the-thickness radial crack is initially higher than those of the other two configurations, the baseline configuration exhibits the fastest crack growth behavior. The transitioning radial-corner-crack configuration initially exhibits slower crack growth behavior than the baseline but eventually these two crack growth curves become parallel (when the stress-intensity factor is the same, i.e. when $a > 0.250$ inch). The center crack configuration exhibits the slowest initial growth behavior, and this is primarily because the stress-intensity factor for small crack lengths is substantially below that of the other two configurations.

By cross-correlating the information presented in Figures 10.7.13 and 10.7.14, one is able to construct the residual strength-life relationships shown in Figure 10.7.15. As anticipated, the baseline configuration has the lowest residual

strength capability and the center crack configuration exhibits the highest residual strength capacity. Both the baseline and center crack configurations are also shown to exhibit an extensive region of linear residual strength decay as a function of time-in-service. The nonlinear residual strength decay exhibited by the transitioning radial corner crack is attributed to the gradient in the stress-intensity factor coefficient for relatively short cracks. Based on observations in this and other examples in Section 10.7, it would appear that one of the most important factors contributing to nonlinear behavior is the severity of stress-intensity factor gradient (as a function of crack length).

EXAMPLE 10.7.6 Effect of Hole Loading

As a means of evaluating the effect of fastener loading on the residual strength, this example combines the baseline remote loading configuration described in Figure 10.7.2 with the localized pin loading described in Figure 10.7.16. To calculate residual strength, the baseline material properties are utilized in Equations 10.7.1 and 10.7.4 along with the stress-intensity factor associated with the combined loading. Because the structural response is linear elastic, stress-intensity factor solutions for the remote (Figure 10.7.2) and localized (Figure 10.7.16) loadings can be added to obtain the stress-intensity factor for the combined loading; thus,

$$K_{\text{TOTAL}} = K_{\text{REMOTE}} + K_{\text{LOCAL}} \quad (10.7.15)$$

where K_{REMOTE} is obtained from the product of the remote stress ($\bar{\sigma}$) and the stress-intensity factor coefficient given by Equation 10.7.6. K_{LOCAL} is the stress-intensity factor associated with the pin loading. Reviewing Subsection 1.7.3,

one finds that the pin loaded hole solution was presented by Newman (Equation 1.7.9), i.e.,

$$K_{LOCAL} = \frac{P}{2rB} \sqrt{\pi a} \beta_{PR}\left(\frac{a}{r}\right) \quad (10.7.16)$$

where

$$\beta_{PR} = f_w \cdot F_1 \cdot f_h \cdot G_1 \quad (10.7.17)$$

For a wide plate, f_w and f_h are approximately 1.0 (see Equation 1.7.11 a and b with $W \rightarrow \infty$) and via Equation 1.7.13

$$G_1 = \frac{1}{\pi} \left(\frac{r}{r + \frac{a}{2}} \right) \sqrt{\frac{1}{1 + \frac{a}{r}}} \quad (10.7.18)$$

The function F_1 is the Bowie Beta factor that can be obtained from Equation 10.7.6

$$F_1 = \frac{K_{BOWIE}}{\sigma \sqrt{\pi a}} = \left(0.6762 + \frac{0.8734}{0.3246 + \frac{a}{r}} \right) \quad (10.7.19)$$

(Newman used an alternate estimate of the Bowie Beta factor but Newman's estimate and that of 10.7.19 were shown to be equivalent). The pin loading identified in Equation 10.7.16 could also be written using the bearing stress (σ_{BR}) given by

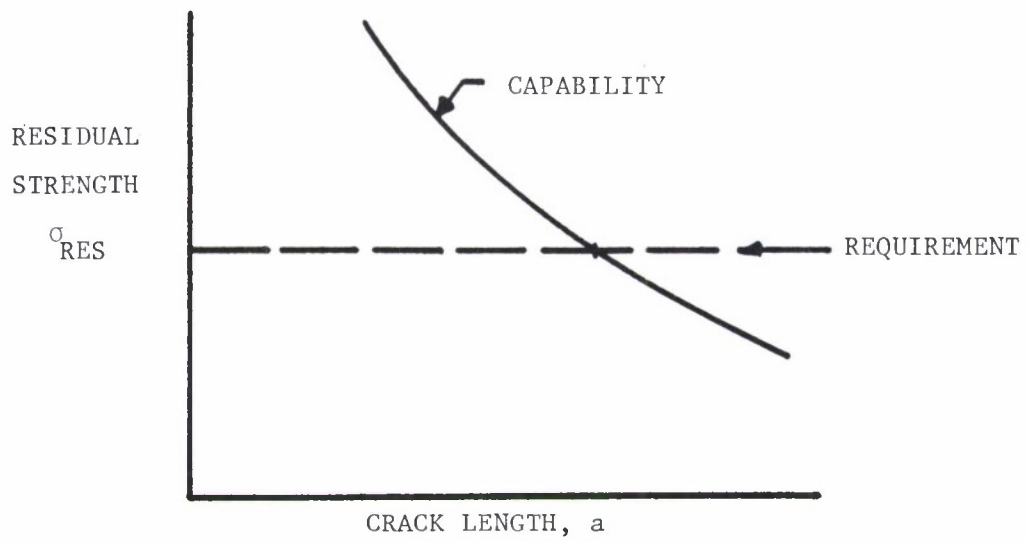
$$\sigma_{BR} = \frac{P}{2rB} \quad (10.7.20)$$

As a method of comparing the effect of pin loading in conjunction with remote stress loading, the bearing to bypass ratio was used. The bearing to bypass ratio is the ratio between the bearing stress (calculated by Equation 10.7.20) and the remote stress $\bar{\sigma}$, i.e.

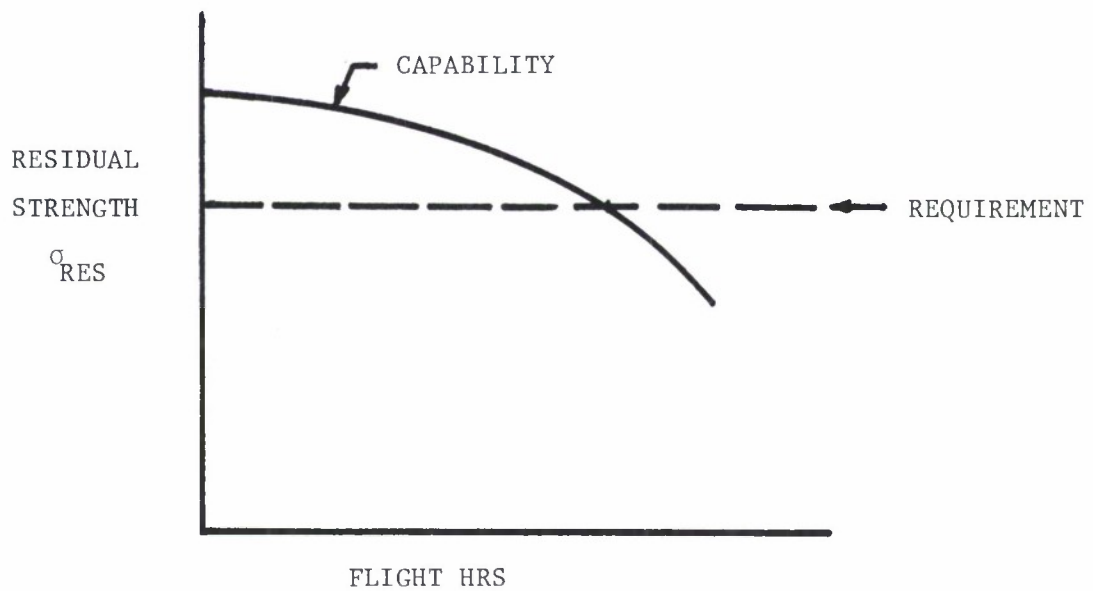
$$\frac{\sigma_{BR}}{\sigma_{BP}} = \frac{\frac{P}{2rB}}{\bar{\sigma}} \quad (10.7.21)$$

Various combinations of 10.7.31 were chosen and the residual strength relationships were then generated using Equations 10.7.1 and 10.7.4. The residual strength-crack length relationships are shown in Figure 10.7.17 for $K_{cr} = 30 \text{ ksi} \sqrt{\text{in}}$; and, the crack length-life are shown in Figure 10.7.18 for $C = 1 \times 10^{-8}$ and $n = 3.0$. By cross-correlating the information in Figures 10.7.17 and 10.7.18, one can generate the residual strength-life relationships presented in Figure 10.7.19.

Based on the results presented in Figures 10.7.17 through 10.7.19, it would appear that bearing to bypass ratios less than 0.4 cause a relatively small change in the residual strength/crack length/life relationships. As the bearing to bypass ratio increases from 0 to 0.2, (a) the residual strength decays very rapidly in the short crack region (Figure 10.7.17), (b) a significant reduction occurs in the crack growth-life curves (Figure 10.7.18), and (c) the residual strength-life curves are progressively lower (Figure 10.7.19). The collective sum of these observations indicate that when substantial hole loading is present, it is necessary to account for the hole loading when assessing the residual strength and crack growth life behavior.



a. Residual Strength as a Function of Crack Length.



b. Residual Strength as a Function of Service Life.

Figure 10.7.1 Types of Residual Strength Relationships.

Baseline Conditions

$$a_o = 0.050 \text{ inch}$$

$$r = 0.125 \text{ inch}$$

$$K_{Ic} = 30 \text{ ksi } \sqrt{\text{in}}$$

$$C = 1 \times 10^{-8}$$

$$n = 3.0$$

$$\bar{\sigma} = 20 \text{ ksi}$$

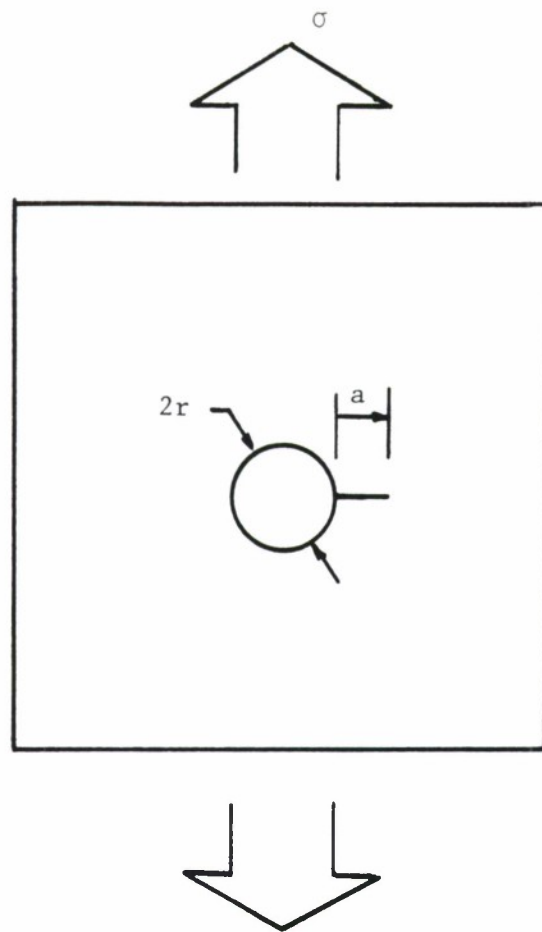


Figure 10.7.2 Tension-Loaded, Open Hole with Radial-Through-The-Thickness Crack.

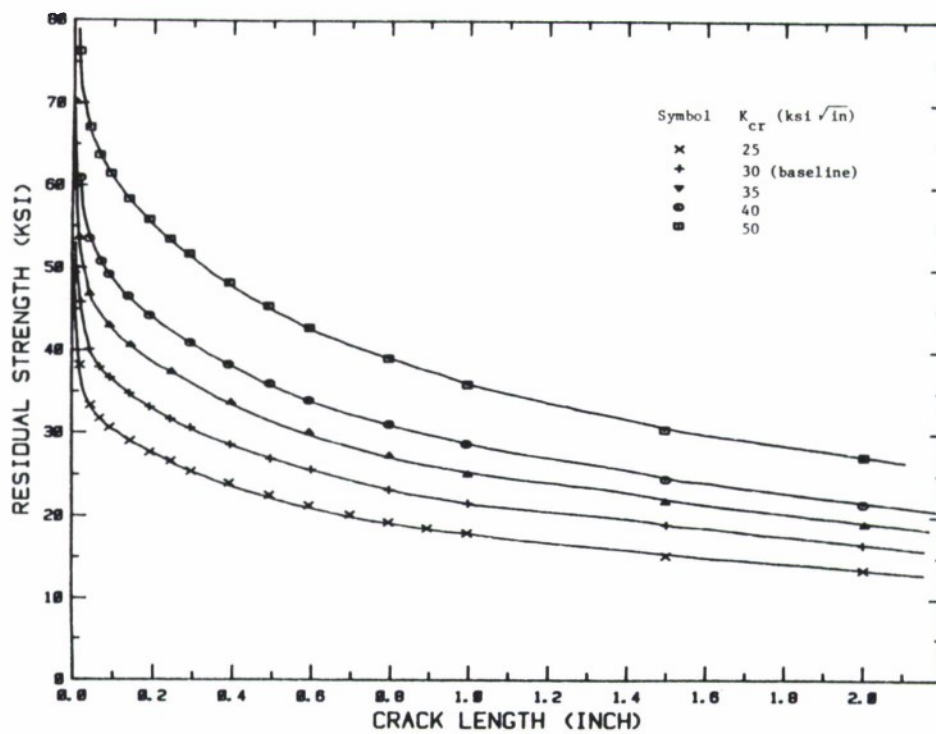


Figure 10.7.3 Effect of Fracture Toughness on the Residual Strength-Crack Length Relationship for a Radially Cracked Hole.

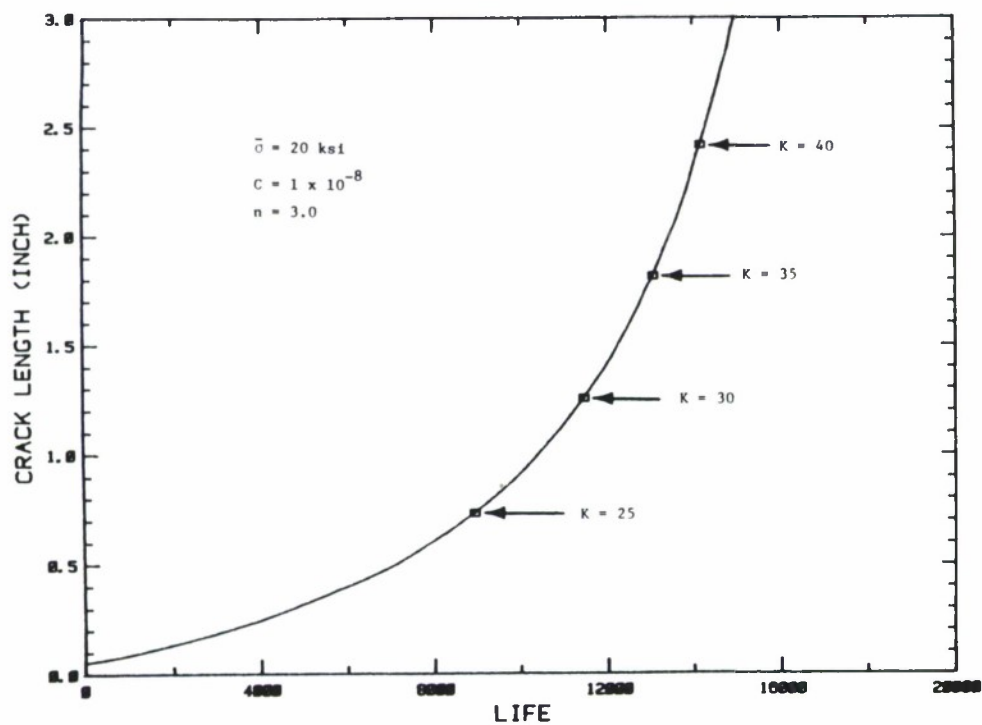


Figure 10.7.4 Crack Growth-Life Relationship for the Baseline Geometry.

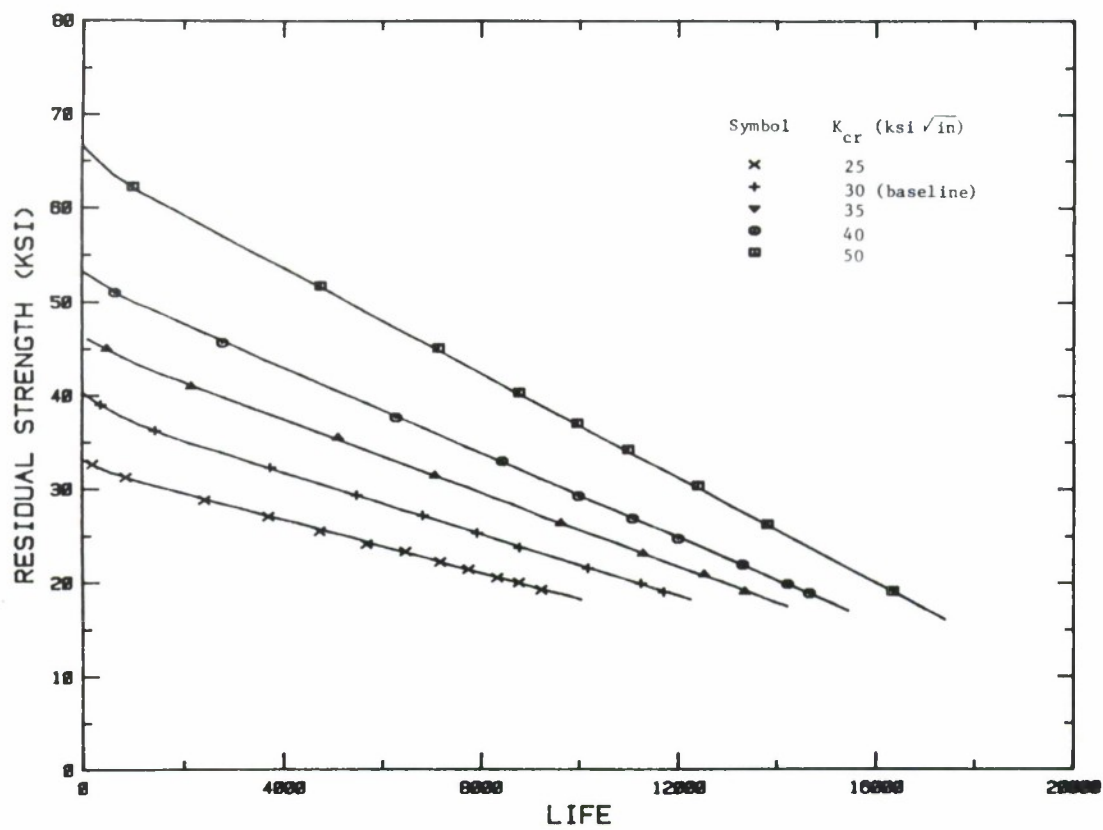


Figure 10.7.5 Effect of Fracture Toughness on the Residual Strength-Life Relationship.

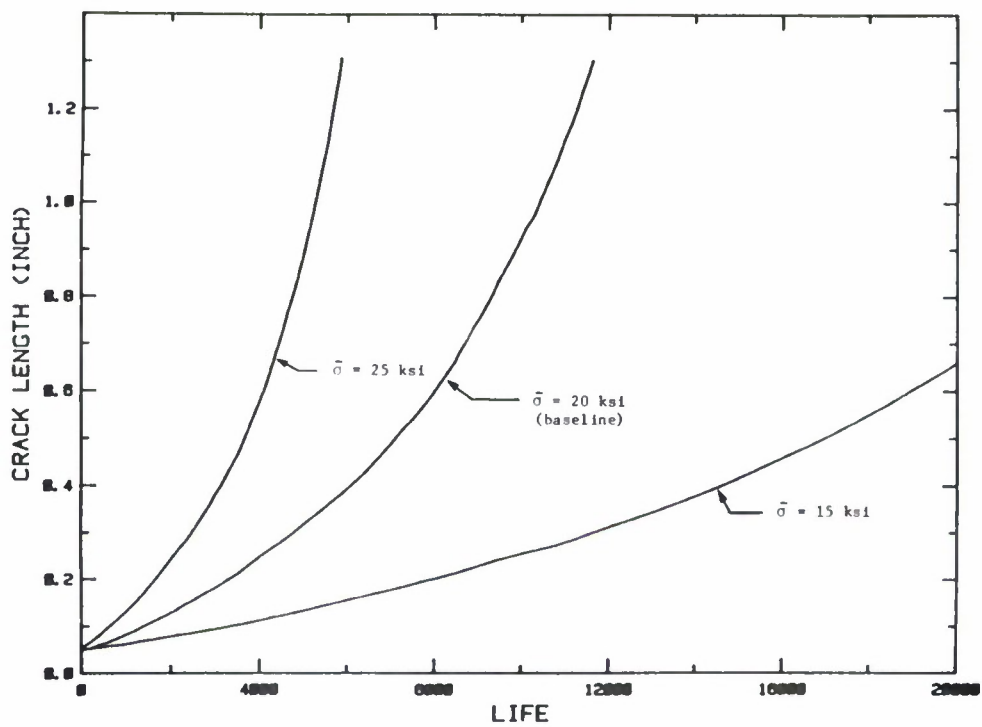


Figure 10.7.6 Effect of Stress Level on Crack Growth-Life Relationship.

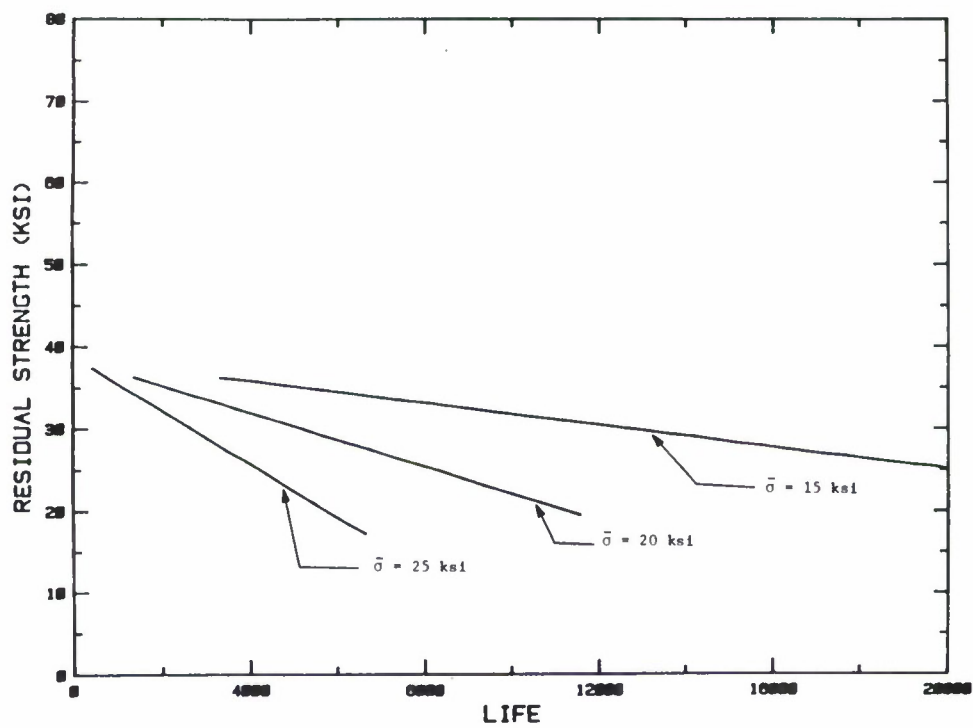


Figure 10.7.7 Effect of Stress Level on Residual Strength-Life Relationship.

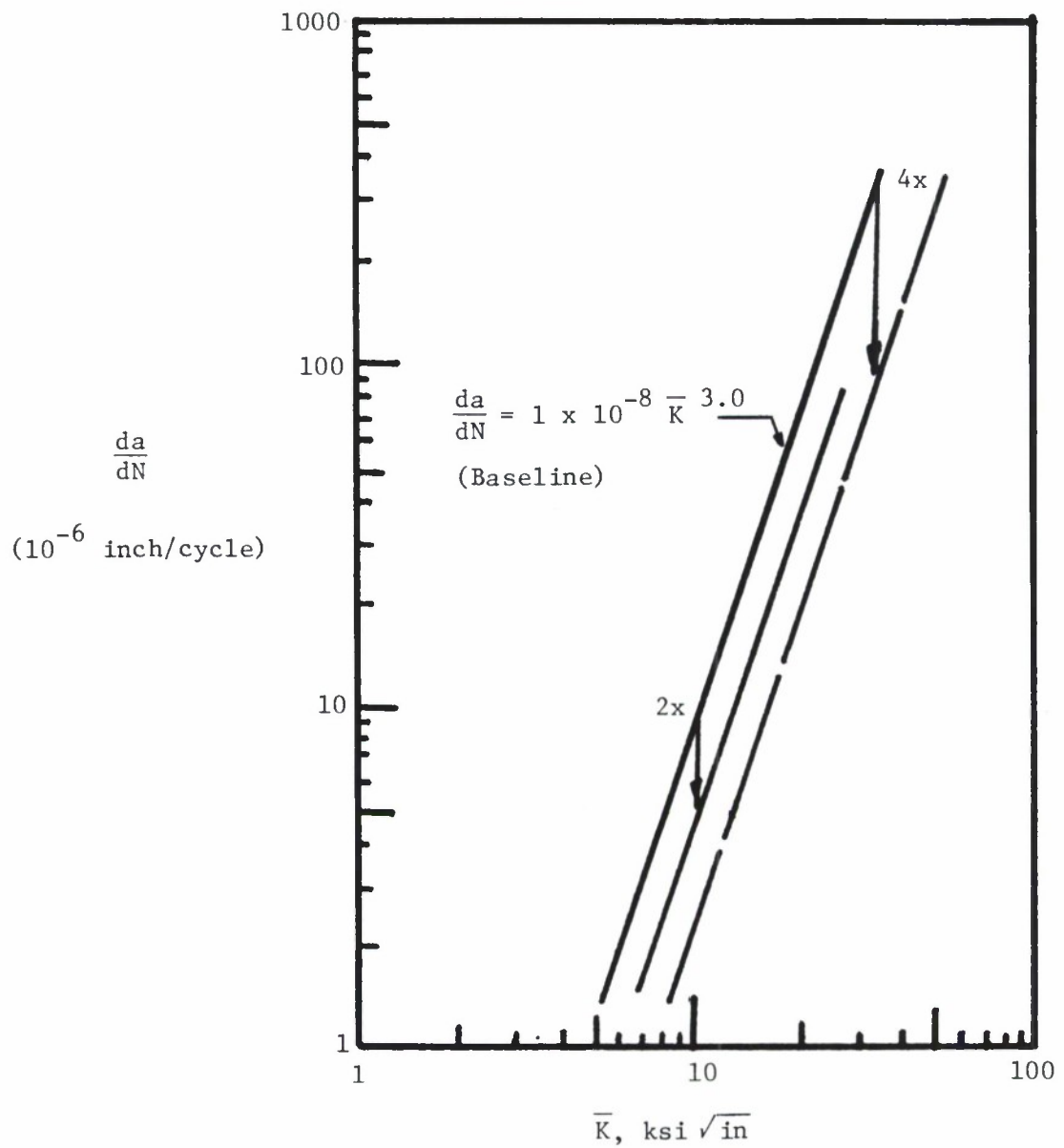


Figure 10.7.8 Variation of Crack Growth Behavior Resulting from a Shift in the Power Law Curve.

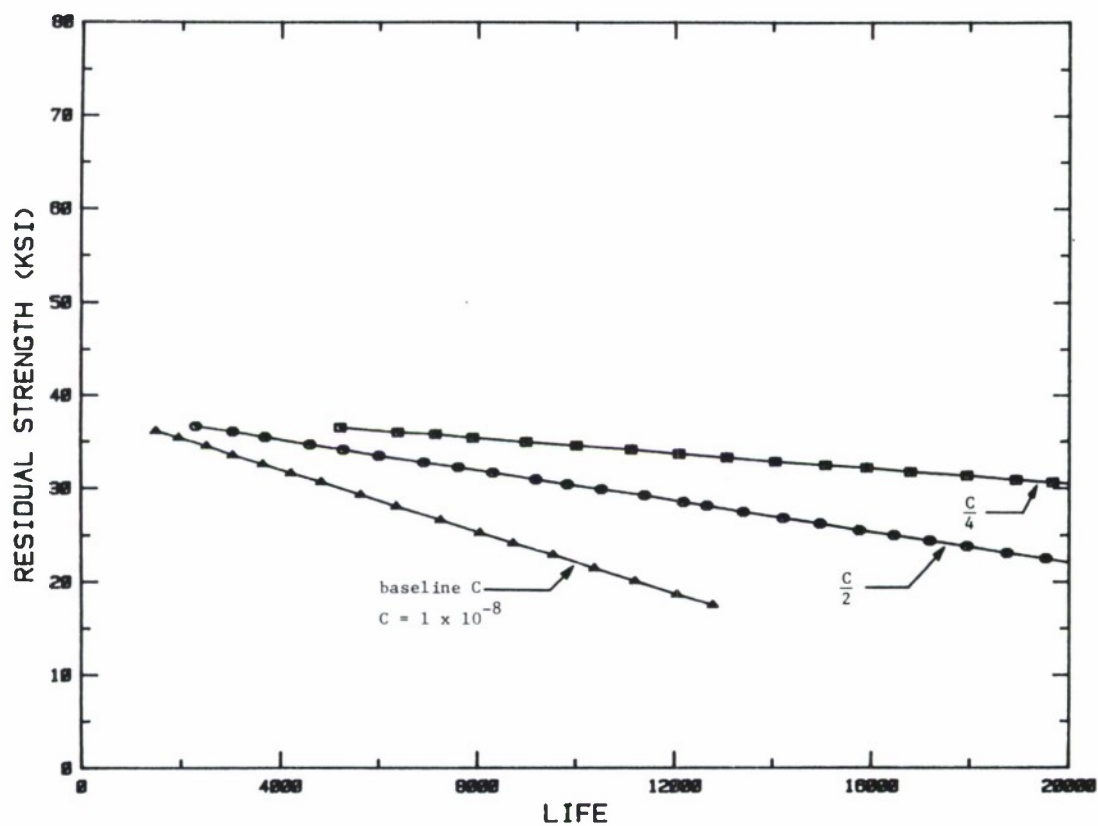


Figure 10.7.9 Effect of Pre-exponential Constant (C) on Residual Strength-Life Relationship.

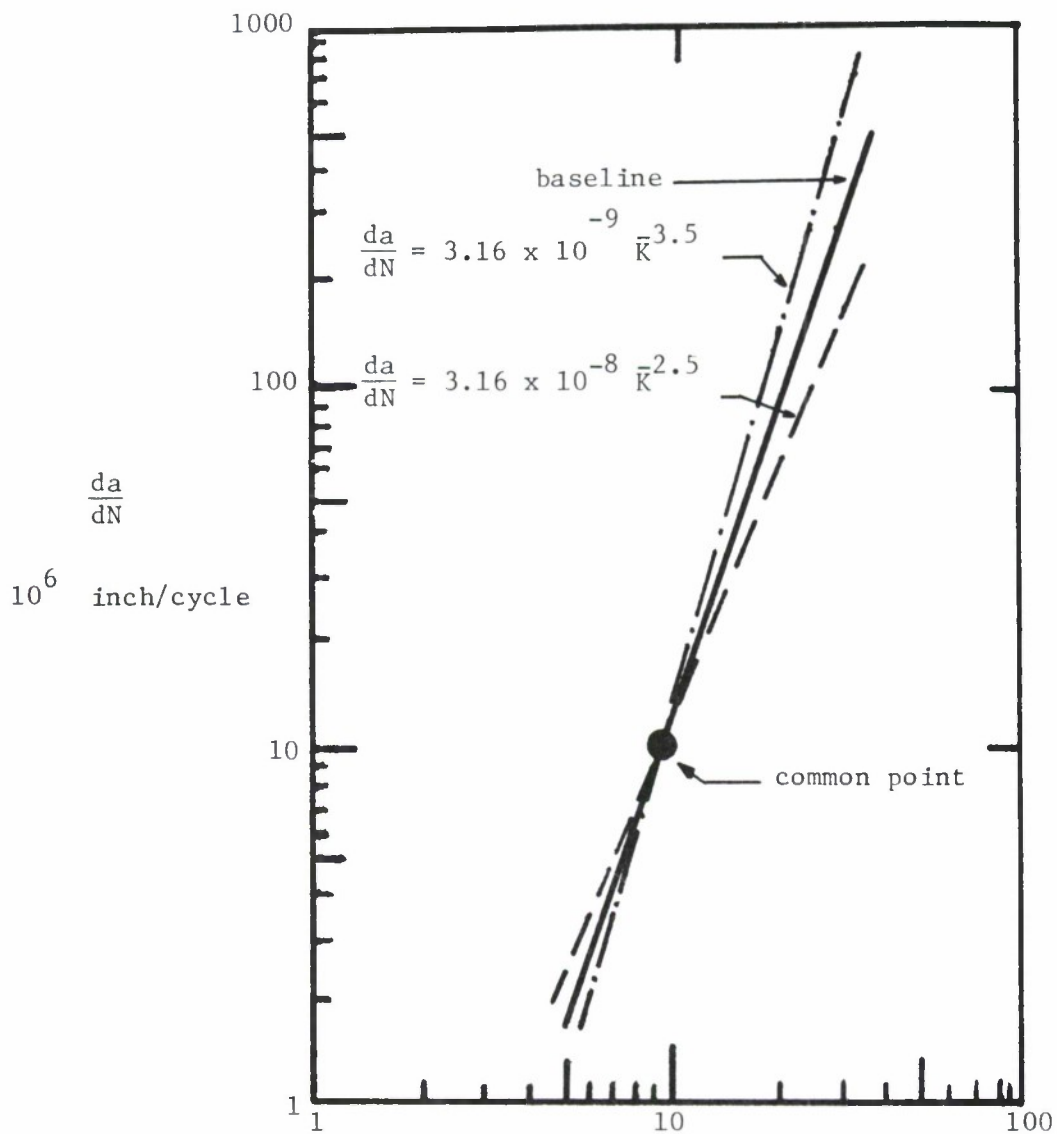


Figure 10.7.10 Crack Growth Curves Shown Passing Through Common Point, Used in EXAMPLE 10.7.4.

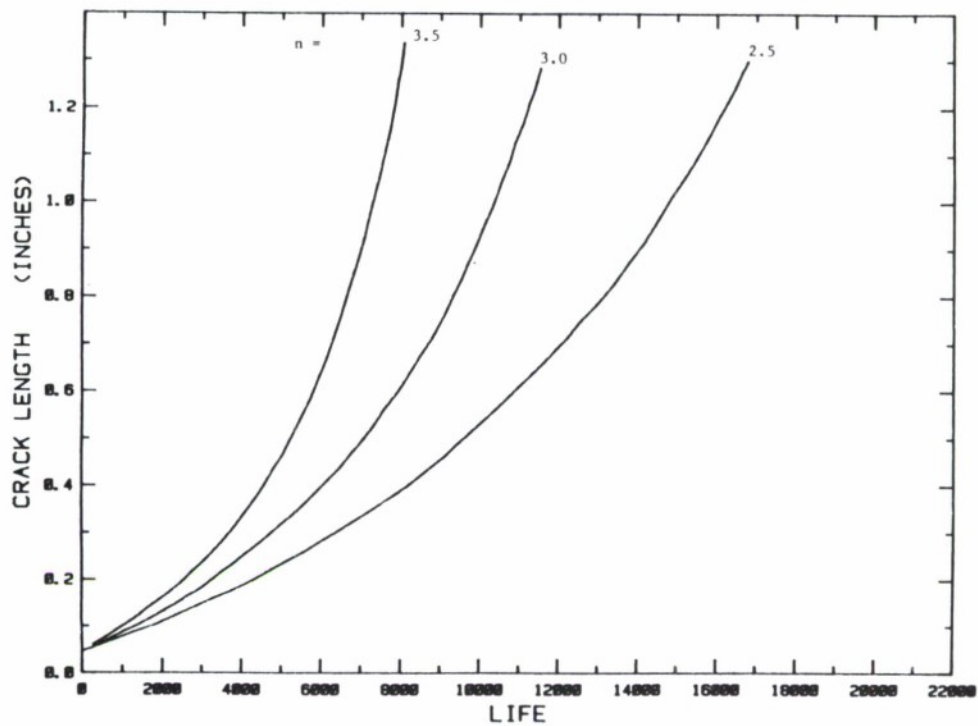


Figure 10.7.11 Effect of Exponent n on the Crack Growth Life Relationship.

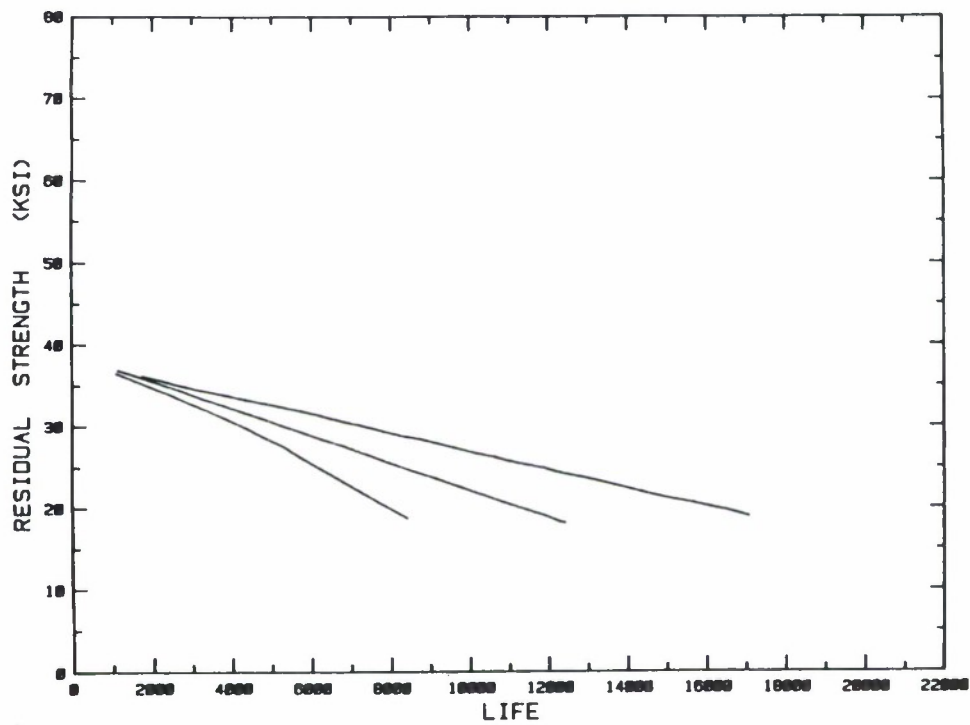


Figure 10.7.12 Effect of Exponent n on the Residual Strength-Life Relationship.

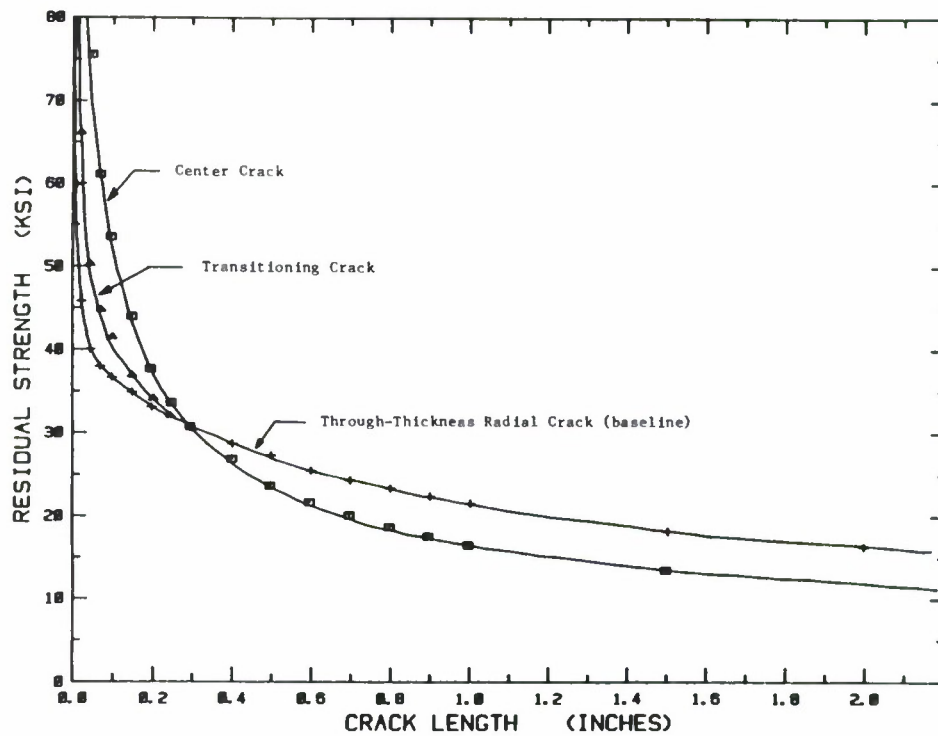


Figure 10.7.13 Effect of Geometry on the Residual Strength-Crack Length Relationship.

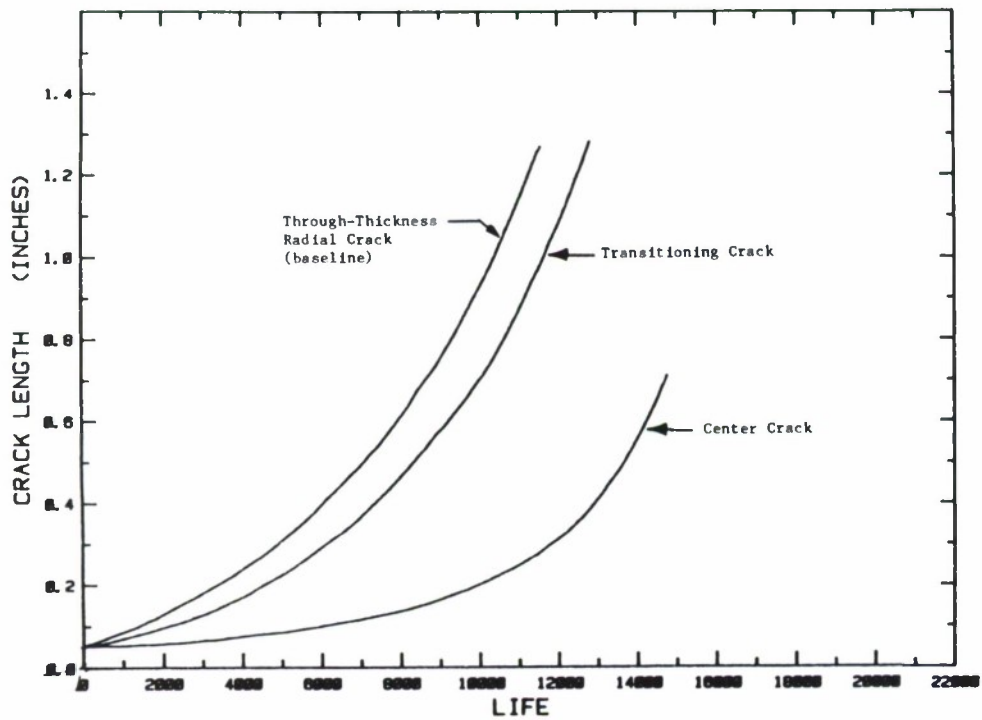


Figure 10.7.14 Effect of Geometry on the Crack Growth-Life Relationship.

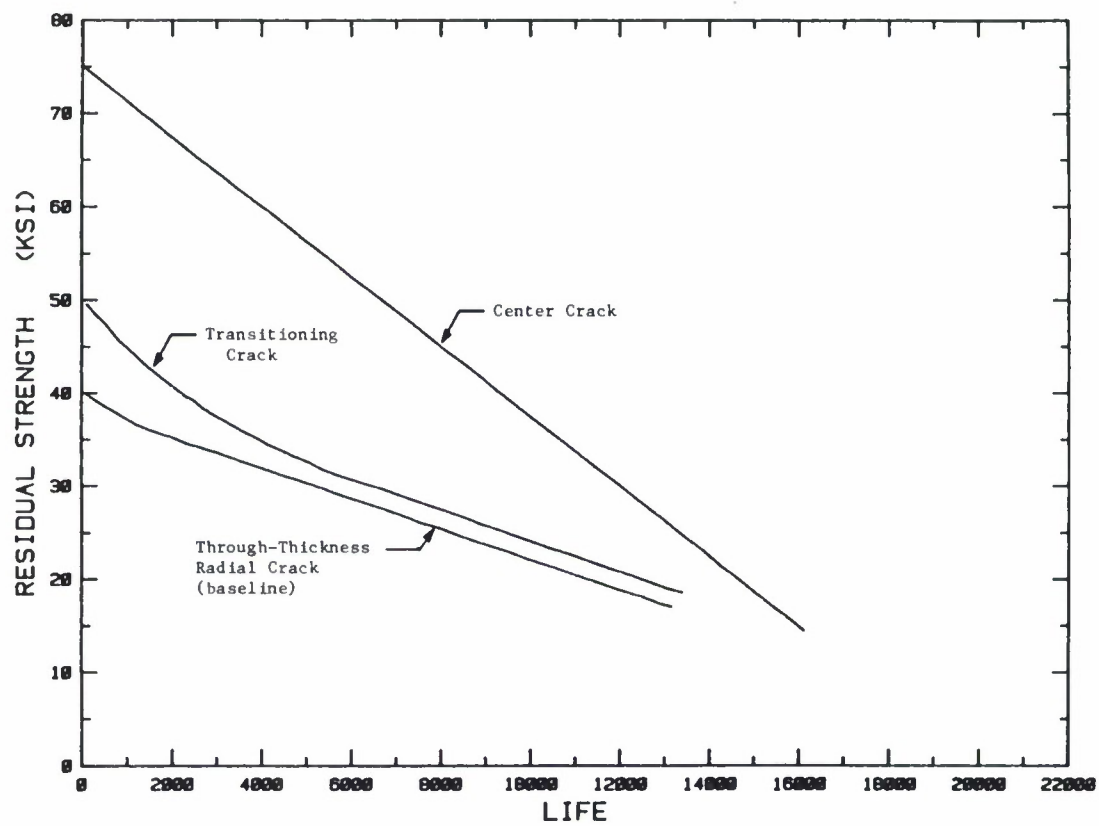


Figure 10.7.15 Effect of Geometry on the Residual Strength-Life Relationship.

$$\sigma_{BR} = \frac{P}{2rB}$$

Baseline Properties

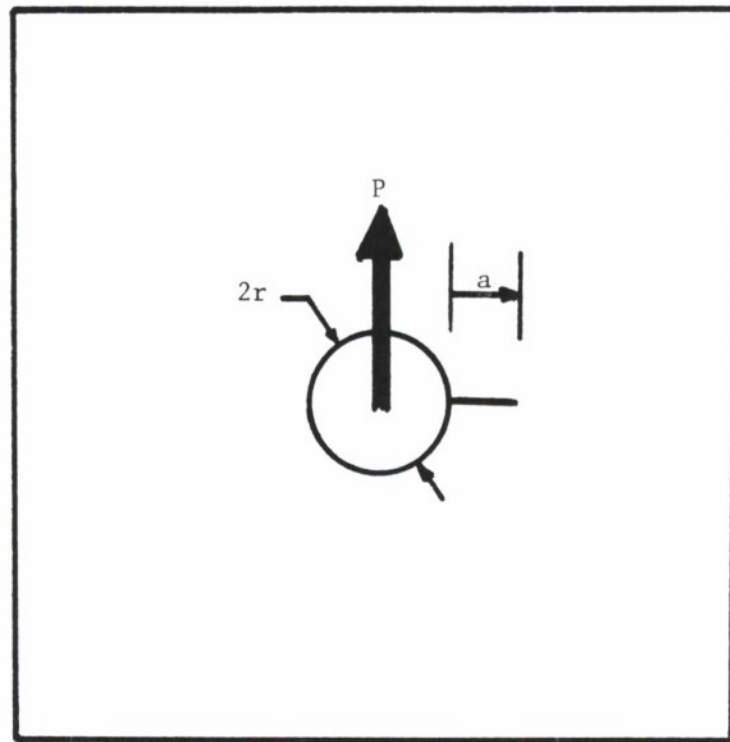
$$a_o = 0.050 \text{ inch}$$

$$r = 0.125 \text{ inch}$$

$$K_{cr} = 30 \text{ ksi} \sqrt{\text{in}}$$

$$C = 1 \times 10^{-8}$$

$$n = 3.0$$



B = thickness
(unspecified)

Figure 10.7.16 Pin Loading Configuration for a Radial Through-The-Thickness Crack.

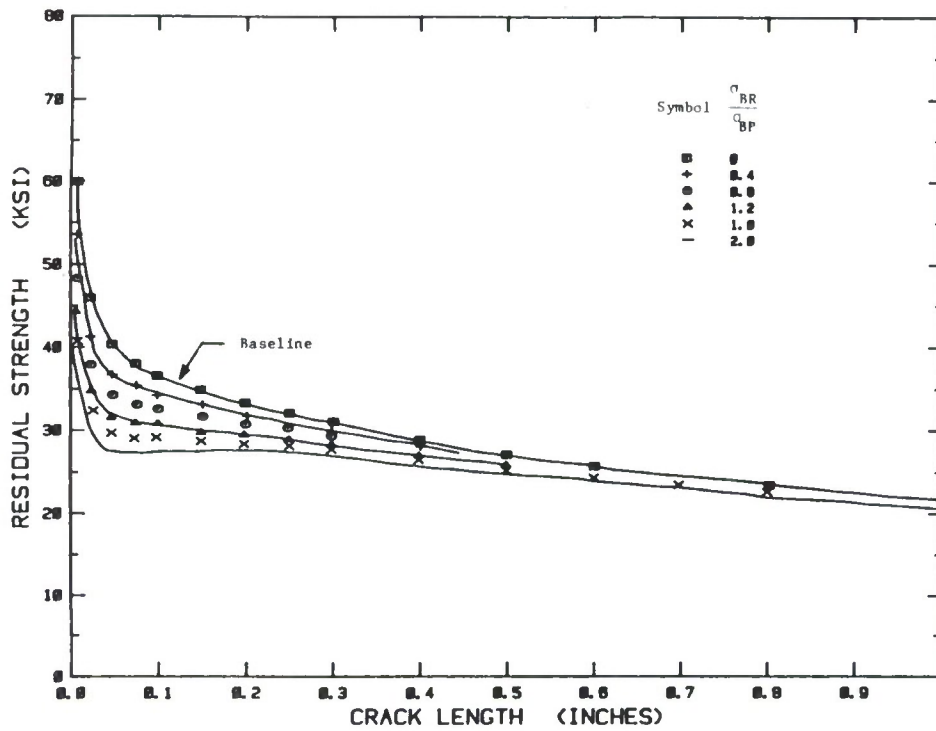


Figure 10.7.17 Effect of Pin Loading on the Residual Strength-Crack Length Relationship.

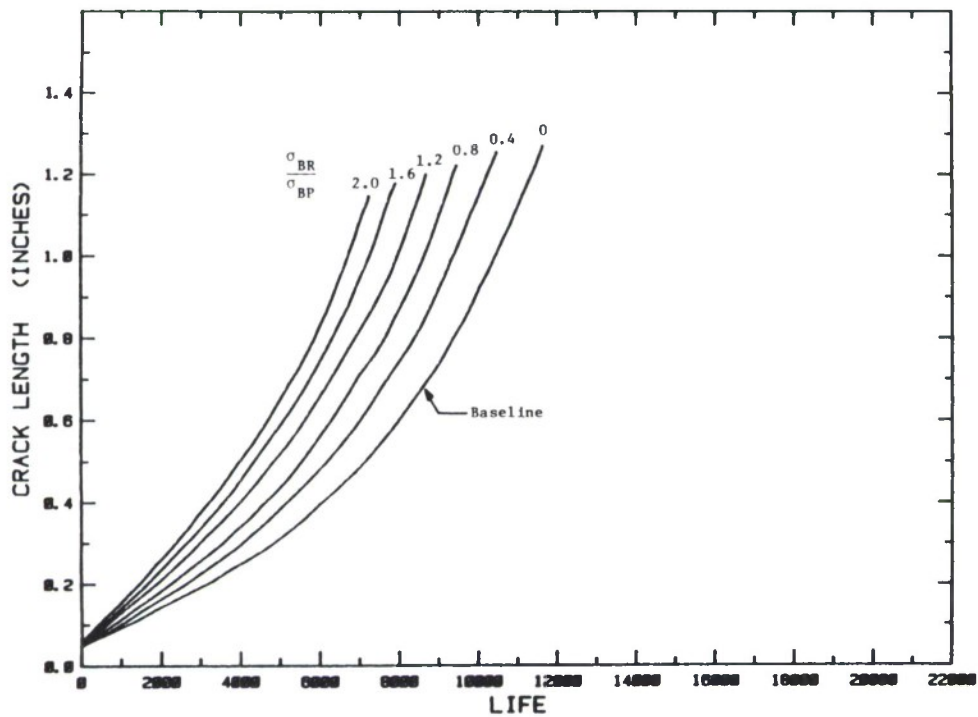


Figure 10.7.18 Effect of Pin Loading on the Crack Growth-Life Relationship.

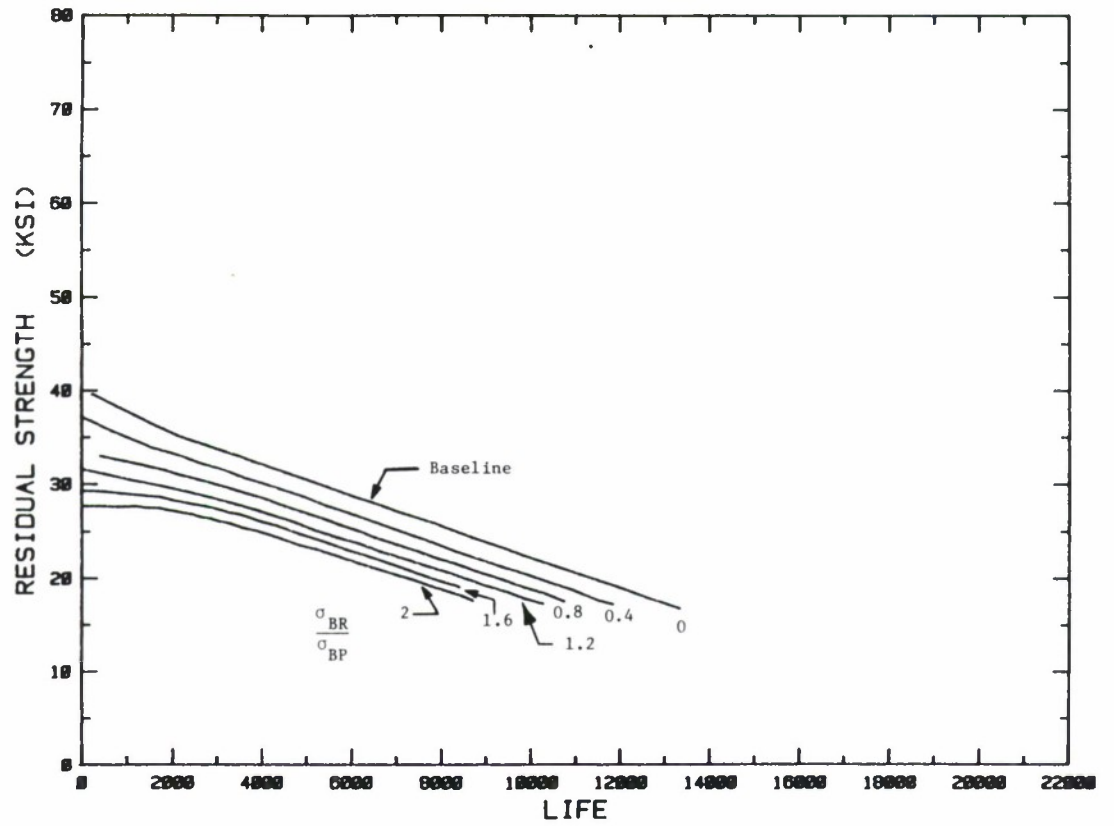


Figure 10.7.19 Effect of Pin Loading on the Residual Strength-Life Relationship.

This section provides example residual strength calculations for a cockpit longeron cracking problem. The calculations consider both the as-manufactured (unrepaired) and repaired structure. To provide a point of reference, two example calculations are also performed to evaluate the (uncracked) static strength of the as-manufactured and repaired structure.

Figure 10.8.1 shows a cracked longeron on a multipurpose fighter aircraft. The repair of such a crack is illustrated in Figure 10.8.2 and consists of placing a steel doubler over the cracked portion as shown. An examination of the stress analysis report for this aircraft shows that this part is critical in crippling (localized static compressive failure), so the first step in the analysis is to determine the effect that the doubler has on the ability of the longeron to withstand the primary static compressive loading which may result in crippling failure of this component. The analysis of the as-manufactured and repaired structure to withstand crippling failure is provided in EXAMPLE 10.8.1; subsequently in EXAMPLE 10.8.2, the residual strength behavior for the cracked structure is determined.

EXAMPLE 10.8.1 Uncracked Structure Crippling Failure

This example static analysis follows the standard methods typically used prior to the introduction of finite element methods. This type of static analysis provides the maximum amount of help to field engineering personnel who may not have access to finite element modeling capabilities or to fatigue crack growth analysis. It is expected that engineers designing repairs will have a basic understanding of strength of materials type analyses and the associated

terminology. Additional support for basic strength and deflection analyses as well as standard information used for structural repairs can be found in the general manual on repairs (T.O. 1-01-1A).

Figure 10.8.3 shows a typical section geometry for this part and the definition of the three elements used for the analysis. The slight overlap between element 1 and 2 is considered to be negligible. As the geometry may vary between models the analytical results are given only for illustration and should not be applied to any specific repair situation.

The crippling allowable stress (F_{cc}) is first determined for the uncracked part from the relation:

$$F_{cc} = \frac{\sum bt (F_{cc})_i}{\sum bt} \quad (10.8.1)$$

where $(F_{cc})_i$ = element crippling allowable, psi

b = element width, in.

t = element thickness, in.

The element crippling allowable is obtained from design manuals. This analysis uses the relation for a hinged element (conservative) from the AFFDL Stress Analysis Manual⁽⁵⁾, pp. 2-89, 2-90. This relation is

$$(F_{cc})_i = \frac{0.416 E}{(1 - \mu^2) \left(\frac{b}{t}\right)^2} \quad (10.8.2)$$

where E = modulus of elasticity (10.7×10^6 psi assumed), and

μ = Poisson's ratio (0.3 assumed).

Now setting up a work table for the present problem gives:

<u>Elem</u>	<u>b</u>	<u>t</u>	<u>bt</u>	<u>b/t</u>	<u>(F_{cc})_i</u>	<u>bt(F_{cc})_i</u>
1	1.68	0.156	0.262	10.76	42248	11068
2	1.90	0.156	0.296	12.17	33016	9772
3	1.59	0.250	<u>0.397</u>	6.36	120926	<u>48007</u>
			Σ = 0.955			
						Σ = 68847

Based on Equation 10.8.1, the crippling allowable stress is:

$$F_{cc} = \frac{68,847}{0.955} = 72,091 \text{ psi} \quad (10.8.3)$$

Also from the aircraft stress analysis report, the maximum compressive load on the longeron is 51,000 lb. Thus, the applied compressive stress (f_c) is:

$$f_c = \frac{51,000}{0.955} = 53,403 \text{ psi} \quad (10.8.4)$$

and the margin of safety is

$$M. S. = \frac{F_{cc}}{f_c} - 1 = \frac{72,091}{53,403} - 1 = +0.349 \quad (10.8.5)$$

Now the analysis must be modified to account for the replacement of the cracked leg (element 2) with the added doubler. The aircraft repair manual specifies a repair using a 4130 steel sheet 0.090 inches thick.

For the repair analysis, consider only the portion of the added part which replaces the cracked leg (element 2) and do not include the portion which doubles the uncracked leg. This is a conservative analysis.

The working analysis table thus becomes

<u>Elem</u>	<u>b</u>	<u>t</u>	<u>bt</u>	<u>b/t</u>	<u>(F_{cc})_i</u>	<u>bt(F_{cc})_i</u>
1	1.68	0.156	0.262	10.86	42248	11068
2*	1.90	0.090	0.171	21.11	30772	5262
3	1.59	0.250	<u>0.397</u>	6.36	120926	<u>48007</u>
			Σ = 0.830			
						Σ = 64337

* New element (E = 30 x 10⁶ psi assumed)

And the corresponding calculations for the repair are:

$$F_{cc} = \frac{64,337}{0.830} = 77,514 \text{ psi}, \quad (10.8.6)$$

$$f_c = \frac{51,000}{0.830} = 61,445 \text{ psi, and} \quad (10.8.7)$$

$$M. S. = \frac{F_{cc}}{f_c} = \frac{77,514}{61,445} = +0.261 \quad (10.8.8)$$

Thus, the repair leg can withstand the static applied compressive load without failure by crippling, but with a slightly lower margin than the initial design.

Now consider the damage tolerance analysis of this part. The crack in the side longeron is caused by a side loading, represented by P in Figure 10.8.1. Only the crippling stress is given in the aircraft stress report for the critical static condition, and it is necessary to estimate the load P in order to determine if the repair reduces the potential for failure.

To conduct a residual strength analysis with a crack present in the structure, one should follow the five-step process suggested in Figure 10.8.4. This five-step process includes;

- 1) Defining a structural model of the crack/load/geometry.
- 2) Obtaining the stress-intensity factor relation for the model (the model selection may be influenced by the availability of stress-intensity factor vs crack length relationships).
- 3) Defining the longest allowable crack.
- 4) Obtaining the fracture toughness, K_{cr} , for the material. A major source is the Damage Tolerant Design (Data) Handbook⁽¹⁾. (This property is a function of thickness. If no applicable K_{cr} value is available, the plane-strain fracture toughness, K_{Ic} , can be used as a lower bound.)
- 5) Calculating the maximum allowable load or stress.

For some problems, steps 3 and 5 are interchanged: Under step 3 one defines the maximum allowable load or stress on the component and then under step 5 one calculates the longest crack that the structure could resist without failure. Example 10.8.2 illustrates the application of these steps to both unrepaired and repaired structure. Additional details that support the development of residual strength estimate can be found in Chapter 4.

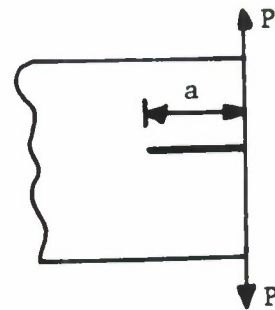
EXAMPLE 10.8.2 Comparative Residual Strength Analysis

The structural analysis for estimating the residual strength of unrepaired and repaired structure should follow the steps schematically illustrated in Figure 10.8.4. In the absence of information in the aircraft stress analysis report, it is necessary to estimate the load (and sometimes the loading conditions) associated with fracture. After the maximum allowable load or stress is obtained, a similar procedure is followed to estimate the maximum allowable crack length in the repair for the same load. For this problem, one additional piece of information is available and that is; the T0-3 repair manual states the the longeron should not be repaired (but replaced) if the crack is longer than seven inches. As a first approximation, the maximum applied load should not cause failure at this maximum crack size.

For the cracked side longeron, the details associated with the five steps (Figure 10.8.4) in the damage tolerant analysis are given below.

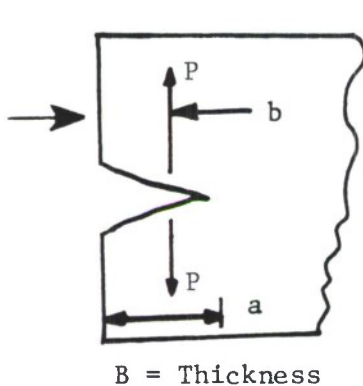
STEP 1. Model the Situation:

Assume that the structure is a semi-infinite plate with an edge crack with the loads applied to the edge of the plate.



STEP 2. Determine the Stress Intensity Factor Coefficient:

Table 1.7.2 of Section 1.7 of this handbook gives a situation which is similar to the desired model;



$$K = \frac{2}{\pi} \frac{1 + F \left(\frac{b}{a}\right)}{\sqrt{a^2 - b^2}} \frac{P}{B} \sqrt{\pi a} \quad (10.8.9)$$

$$\begin{aligned} F \left(\frac{b}{a}\right) = & 0.2045 \left(1 - \frac{b}{a}\right) + 0.3912 \left(\frac{b}{a}\right)^2 \\ & + 0.7685 \left(\frac{b}{a}\right)^4 - 0.9942 \left(\frac{b}{a}\right)^6 \\ & + 0.5094 \left(\frac{b}{a}\right)^8 \end{aligned} \quad (10.8.10)$$

Step 3. Define the Longest Crack Length:

The longest crack length (a_{cr}) was given in the T.O.-3 repair manual as 7 inches; so determine the corresponding value of the stress-intensity factor coefficient $(K/P)_{cr}$, given that the thickness (B) is 0.156 inch and that the loading is applied at a position which makes the offset parameter b (in Equation 10.8.10) zero. Thus, substituting these values into Equations 10.8.9 and 10.8.10 yields:

$$\left(\frac{K}{P}\right)_{CR} = 3.293 \frac{\text{ksi} \sqrt{\text{in.}}}{\text{kip}} \quad (10.8.11)$$

Step 4. Obtain the Fracture Toughness Value;

Table 8.18.2.2 on pp 8.18-10 through 8.18-12 in the Damage Tolerant Design (Data) Handbook (MIC-HB-Q1R) provides the following fracture toughness. (K_{APP}) data for 7178-T6 and T651 Aluminum:

Mean K_{APP} (ksi $\sqrt{\text{in}}$)	Thickness (inch)	Direction	Number of Tests
39.9	0.064	L-T	13
46.3	0.064	L-T	5
40.9	0.123	L-T	15
35.6	0.25	L-T	2

Step 5. Calculate the Maximum Allowable Load:

Using a fracture toughness value linearly interpolated from the Step 4 given values,

$$K_{cr}(=K_{APP}) = 39.5 \text{ ksi } \sqrt{\text{in.}}, \text{ for } B = 0.156$$

and the stress-intensity factor coefficient (K/P) given by Equation 10.8.11, one obtains

$$P_{\max} = \frac{K_{cr}}{\left(\frac{K}{P}\right)_{CR}} = \frac{39.5}{3.293} = 12.0 \text{ kip} \quad (10.8.12)$$

Applying this five step process to the cracked member has resulted in an estimate of the maximum load that could be applied to the member without failing the member with a 7 inch long crack. The proposed repair is a patch that is fastened to the longeron in such a manner that the patch can be assumed to carry all the load if the longeron is cracked (a conservative approximation).

For the comparison with cracked (unrepaired) structure, the analyst can estimate (a) the load required to cause the patch to fracture given the same crack length conditions ($a_{cr} = 7$ inch), or (b) the critical crack length associated with fracture of the patch at the same loading condition ($P_{max} = 12.0$ kip) that implied failure of the unrepaired structure. Either estimate can be used in a comparative sense, relative to the results of the unrepaired structural analysis.

Using the same five step process, we estimate the applied load that would cause failure of the 4130 steel patch illustrated in Figure 10.8.2 with a coinciding 7 inch long crack. Step 1 required that we have a structural model; again, the edge crack geometry is chosen. In step 2, the stress-intensity factor is chosen as before (Equations 10.8.9 and 10.8.10 with $b = 0$). In this analysis, the crack length was established as 7 inches long (Step 3). In step 4, the Damage Tolerant Design (Data) Handbook is reviewed to establish a fracture toughness for the 4130 steel. No values for this steel are reported in the Handbook. The properties for comparable steels 4140 and 4340 are summarized below for the lowest yield strengths available in the Handbook.

Product Form	Table No.	Page No.	Material	K_{Ic} (ksi $\sqrt{\text{in}}$)	Thickness (inch)	σ_{ys} (ksi)	Direction
Plate	6.27.2.1	6.27-2	4140	85.3	0.994	159	T-L
Plate	6.27.2.1	6.27-2	4140	58.7	0.994	175	T-L
Forged Bar	6.29.2.1	6.29-6	4340	59.5	0.600	195	L-T
Billet	6.29.2.1	6.29-7	4340	76.8	0.600	195	L-T

The plane strain fracture toughness (K_{Ic}) varies between 58.7 and 85.3 ksi for the conditions given in the table, and should be used only for guidance, considering (a) that the plane stress or transition fracture toughness value should be higher than the plane strain values, and (b) that fracture toughness goes down with increasing yield strength. A first order guess for the plane stress fracture toughness of the 4130 steel at 160 - 180 ksi yield strength would be 75 ksi $\sqrt{\text{in}}$ or higher for the 0.090 inch thick doubler. Using this value ($K_{cr} = 75 \text{ ksi } \sqrt{\text{in}}$), in step 5, the load is determined from

$$P_{\max} = \frac{K_{Ic}}{\left(\frac{K}{P}\right)_{CR}} \quad (10.8.13)$$

where $(K/P)_{CR} = 5.708$ was established from Equations 10.8.9 and 10.8.10 with $a_{cr} = 7$ inch, thickness (B) = 0.090 inch, and force location parameter b equal to zero. Solving Equation 10.8.13 with K_{Ic} and $(K/P)_{CR}$ known, results in

$$P_{\max} = \frac{75.0}{5.708} = 13.14 \text{ kip} \quad (10.8.14)$$

for the repair (Patch capability only, independent of supporting/underlying structure). It can be noted that the loading condition associated with failure of the unrepaired structure (per Equation 10.8.12) is about 10 percent less than that required to fail the patch, i.e.,

$$\begin{aligned} MS &= \frac{(P_{\max})_{\text{repair}}}{(P_{\max})_{\text{unrepaired}}} - 1 \\ &= \frac{13.14}{12.00} - 1 = + 0.095 \end{aligned} \quad (10.8.15)$$

indicating that a positive margin of safety exists for the same type of loading condition. Conducting an alternate type of analysis whereby the load on the repaired structure is held equal to that on the unrepaired structure shows that the critical crack in the repaired structure (patch) is longer than 7 inch.

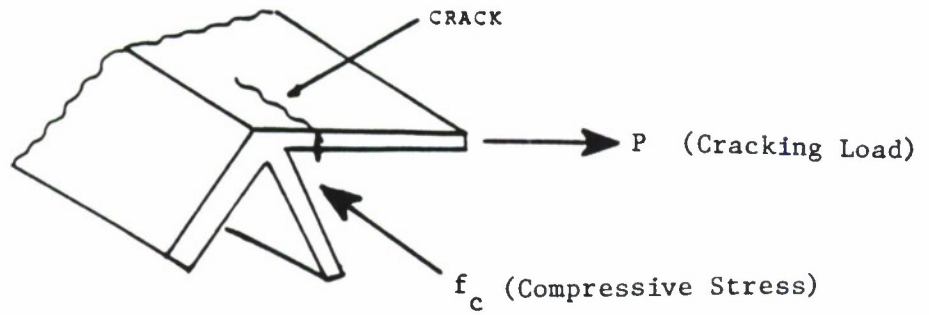


Figure 10.8.1 Cracked Longeron, Top (Material 7178-T6).

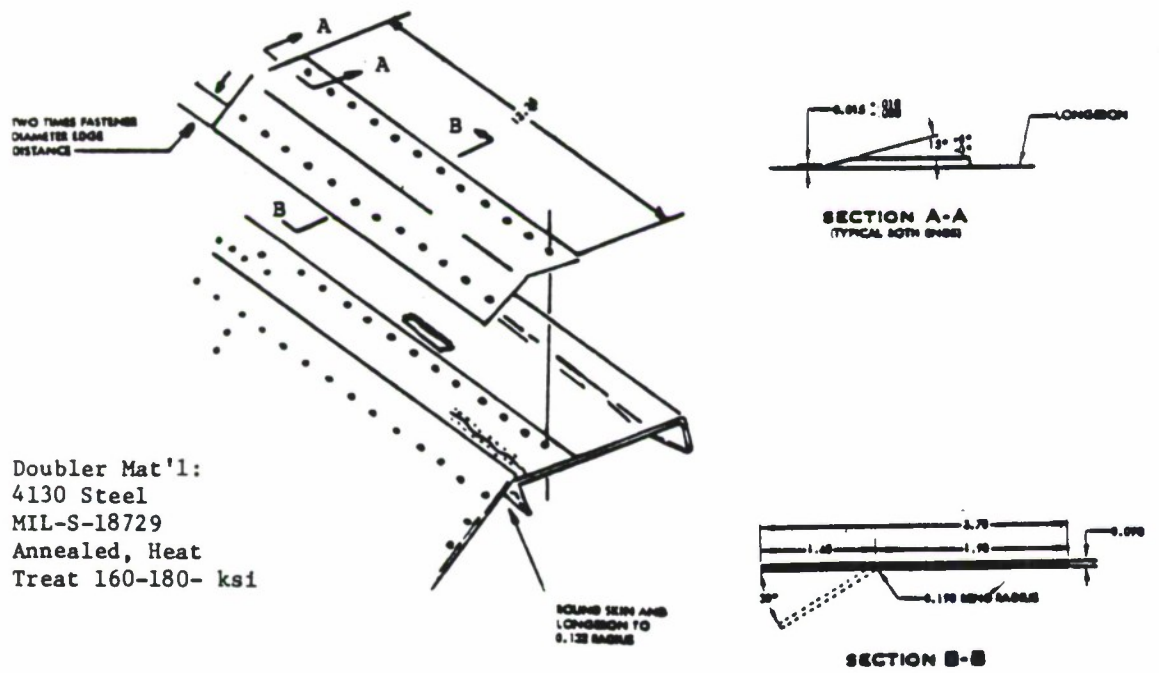
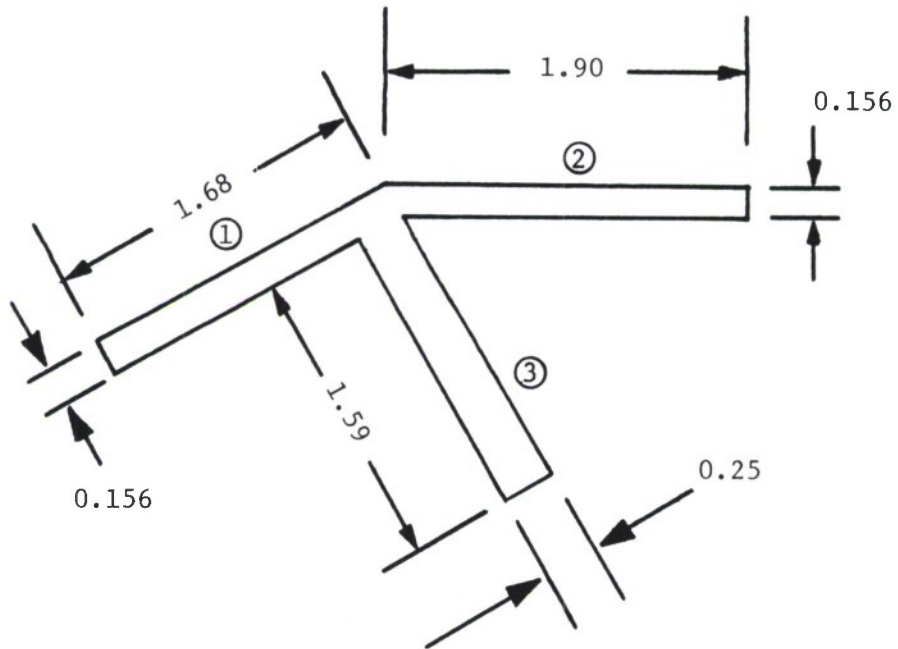


Figure 10.8.2 Specified Longeron Repair.



All Dimensions in Inches

Figure 10.8.3 Section Geometry.

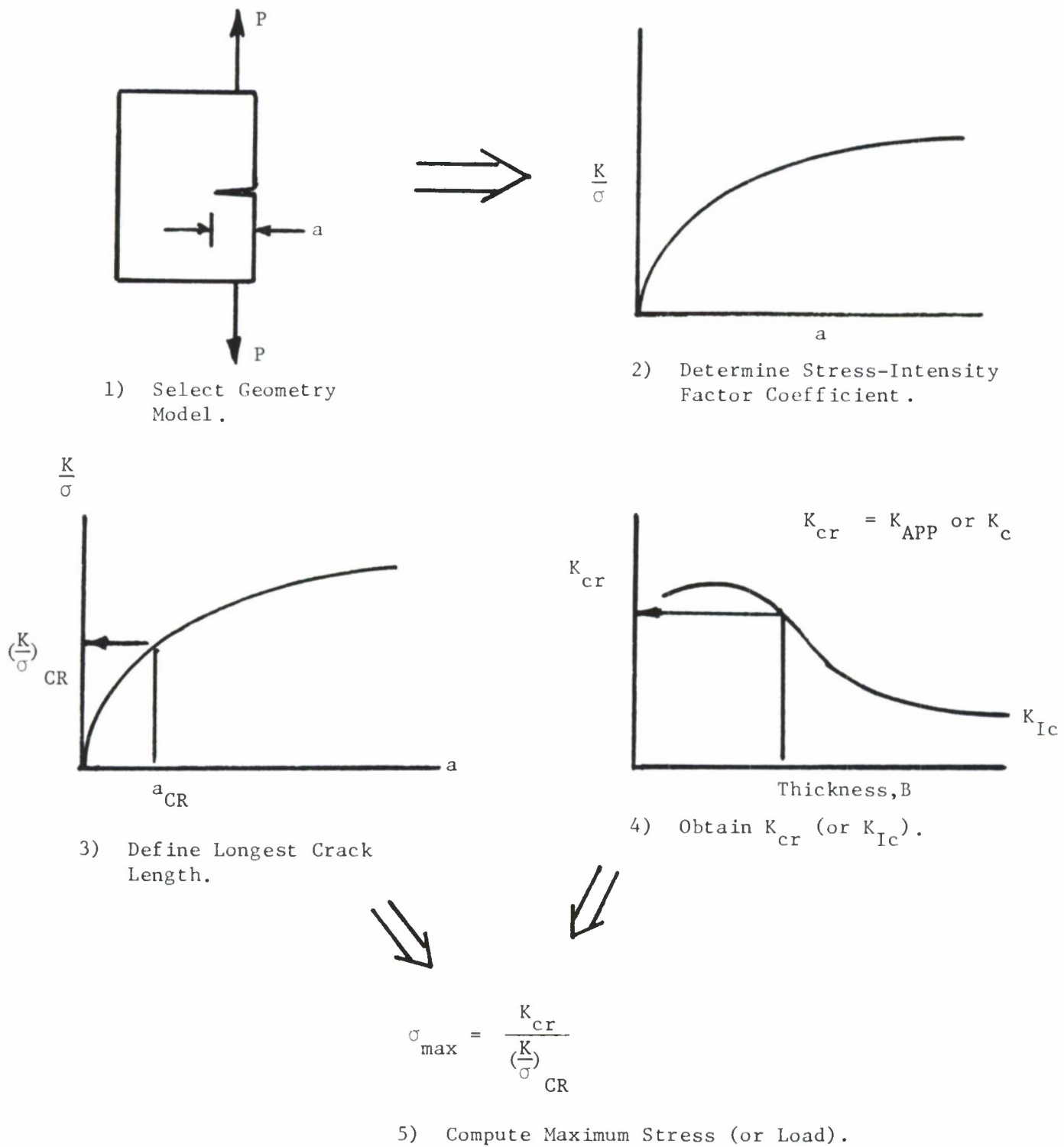


Figure 10.8.4 Steps in Computation of Maximum Allowable Stress for Damage Tolerance Analysis.

This example describes the analysis that might be applied to a typical one-of-a-kind type repair involving patching cracked skin panels. Figure 10.9.1 describes a cracked lower wing skin panel as well as a suggested repair. The repair is expected to provide an interim fix until a more comprehensive repair can be implemented. The repair is for a crack condition whereby a crack is growing from a hole centered between two ribs. Figure 10.9.2 shows the view looking up at the lower skin.

Based on the aircraft stress analysis report, the critical loading condition in this region of the lower wing skin results from a symmetrical high load factor. The aircraft stress analysis report also provided the axial and shear stresses in the subject area of the wing; these are:

$$\begin{aligned}\text{axial stress } (f_A) &= +22,192 \text{ psi} \\ \text{shear stress } (f_S) &= +20,500 \text{ psi}\end{aligned}\tag{10.9.1}$$

The repair must be analysed to determine if it provides an adequate margin of static load capability from both an uncracked and cracked point of view. The uncracked (static strength) analysis is presented in EXAMPLE 10.9.1; the cracked structural (damage tolerance) analysis then follows in EXAMPLE 10.9.2.

EXAMPLE 10.9.1 Uncracked Structural Analysis

The lower wing skin has a thickness of 0.040 inch and the panel is 6.0 inches wide. These dimensions give axial loads and shear flows of;

$$\text{Axial Load, } P_A = f_A A = (22,192) (0.240)$$

$$P_A = +5326 \text{ lb.} \quad (10.9.2)$$

$$\text{Shear Flow, } q = f_s t = (20,500) (0.040)$$

$$q = +820 \text{ lb/in}$$

Since the patch replaces one-fourth of the panel, assume that it also must support one-fourth of the axial load as well as all of the shear flow. Based on a patch thickness of 0.090 inches, and a width of 1.50 inches ($A_p = 0.135 \text{ inches}^2$) the stresses in the patch are:

$$\text{Axial Stress } f_{Ap} = \frac{1}{4} \frac{P}{A_p} = \frac{5326}{(4)(0.135)} = 9862 \text{ psi} \quad (10.9.3)$$

$$\text{Shear Stress } f_{sp} = \frac{q}{t} = \frac{820}{0.090} = 9100 \text{ psi}$$

Making allowance for the fastener holes, the net area of the patch is

$A_{pN} = 0.101 \text{ in}^2$. This gives net stresses as:

$$f_{A_{\text{net}}} = 9862 (0.135/0.101) = + 13,181 \text{ psi} \quad (10.9.4)$$

$$f_{s_{\text{net}}} = 9100 (0.135/0.101) = +12,162 \text{ psi}$$

This combined axial and shear stress state must be analysed to determine the values of the largest axial and shear stresses that could occur under a rotation of the stress element. Figure 10.9.3 shows a rotation of the stress element that produces the condition of principal (axial) stress -- no shear

stresses exist on the rotated element. A rotation of 45° from the principal stress directions, defines the direction where the shear stresses reach a maximum condition. The maximum principal (axial) stresses ($f_{A_{\max}}$, $f_{A_{\min}}$) can be determined using the following stress transformation equation:

$$f_{A_{\max}} = \frac{f_{A_1} + f_{A_2}}{2} + f_{s_{\max}} \quad (10.9.5a)$$

$$f_{A_{\min}} = \frac{f_{A_1} + f_{A_2}}{2} - f_{s_{\max}} \quad (10.9.5b)$$

$$f_{s_{\max}} = \sqrt{\left(\frac{f_{A_1} - f_{A_2}}{2}\right)^2 + f_s^2} \quad (10.9.5c)$$

For the given problem, $f_{A_1} = f_{A_{\text{net}}}$, $f_{A_2} = 0$, and $f_s = f_{s_{\text{net}}}$. Substituting numerical values for f_{A_1} and f_s in Equation 10.9.5 results in:

$$f_{s_{\max}} = \sqrt{\left(\frac{13,181}{2}\right)^2 + (12,162)^2} = 13,833 \text{ psi} \quad (10.9.6)$$

$$f_{A_{\max}} = \left(\frac{13,181}{2}\right) + 13,833 = 20,423 \text{ psi}$$

$$f_{A_{\min}} = \left(\frac{13,181}{2}\right) - 13,833 = -7,242 \text{ psi}$$

for the maximum shear stress, and the maximum and minimum principal axial stress, respectively. Based on a conventional strength of materials analysis, the element must be rotated about 31° counter clockwise from its current orientation to achieve the maximum principal stress orientation.

For 7075-T6, the following ultimate shear and tensile stress values, respectively, are obtained from MIL-HDBK-5, Table 3.7.3.0(b) (A values)

$$\begin{aligned} F_{Su} &= 47,000 \text{ psi} \\ F_{tu} &= 78,000 \text{ psi} \end{aligned} \quad (10.9.7)$$

Check margins:

$$\begin{aligned} \text{Tension M. S.} &= \frac{F_{tu}}{f_{A_{\max}}} - 1 = \frac{78,000}{20,423} - 1 = +2.82 \\ \text{Shear M. S.} &= \frac{F_{Su}}{f_{s_{\max}}} - 1 = \frac{47,000}{13,833} - 1 = +2.40 \end{aligned} \quad (10.9.8)$$

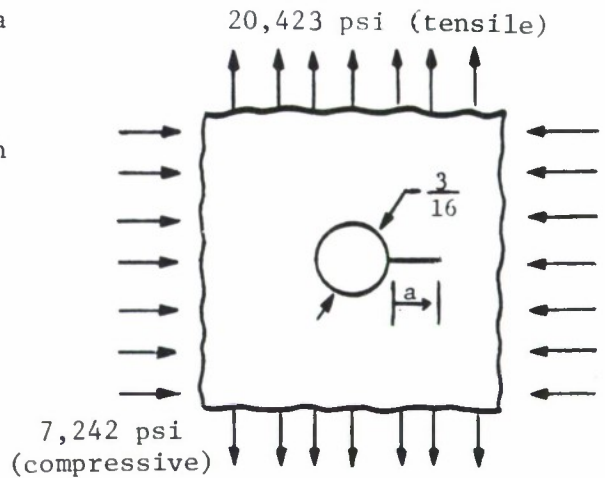
Thus, the repair is satisfactory for the static loading condition.

EXAMPLE 10.9.2 Cracked Structural Analysis

As a different application of a damage tolerant analysis, the repaired skin panel shown in Figure 10.9.1 is analysed for residual strength in the presence of a crack at the edge of one hole. Following the steps outlined in Figure 10.8.4, we obtain:

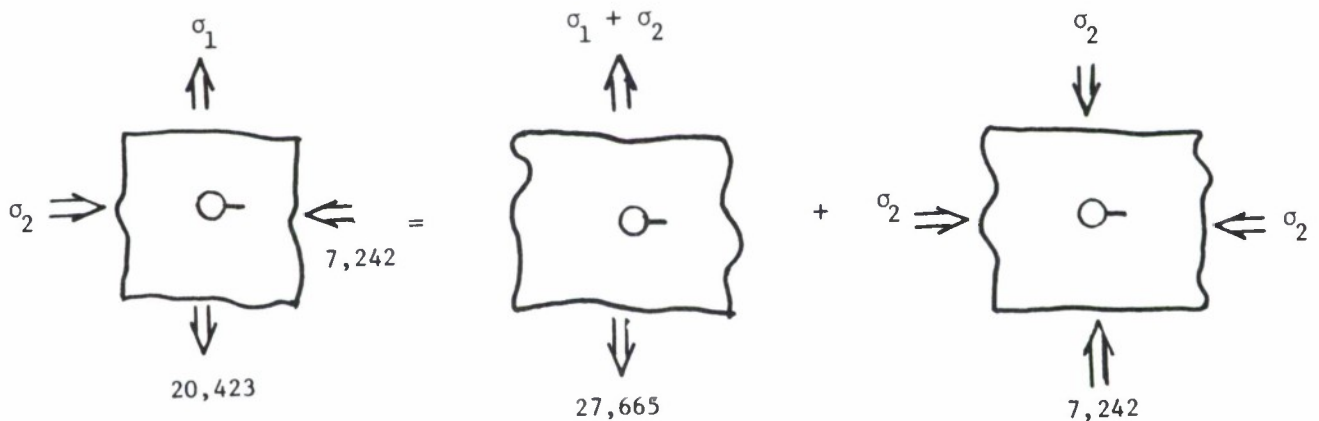
Step 1. Definition of Crack/Load Model

The repair panel is subjected to a biaxial stress consisting of a maximum principal stress of 20,423 psi and a minimum principal stress of -7,242 psi. It is expected that the crack will propagate in a direction perpendicular to the maximum principal normal stress. Thus, a first order model of the crack and loading would be as shown, which neglects both width effects and fastener hole loading effects.



Step 2. Determine Stress-Intensity Factor Coefficient

Based on the information presented in subsection 1.7.3 concerning cracked holes, and more specifically biaxially loaded, radially cracked holes, an engineer would be able to construct a stress-intensity factor for the crack/load model. One interim step would include developing an equal biaxial loading and an uniaxial loading from the crack/load model shown above, i.e., decompose the unequal biaxial load model into the models shown below.



The purpose of the decomposition is to allow the use of the solutions given in Figure 1.7.3 repeated here as Figure 10.9.5. Thus, the stress-intensity factor is obtained by adding the individual solutions to the decomposed crack/load models presented above; thus,

$$K_{\text{TOTAL}} = K_{\text{UNIAXIAL}} + K_{\text{EQUAL BIAXIAL}} \quad (10.9.9)$$

where

$$K_{\text{UNIAXIAL}} = (20,423 + 7,242) \sqrt{\pi a} * F_1\left(\frac{a}{r}\right)_{\text{UNIAXIAL}} \quad (10.9.9a)$$

and

$$K_{\text{EQUAL BIAXIAL}} = -7,242 \sqrt{\pi a} * F_1\left(\frac{a}{r}\right)_{\text{BIAXIAL}} \quad (10.9.9b)$$

and the $F_1\left(\frac{a}{r}\right)$ Beta factors are defined in Figure 10.9.5

Step 3. Determination of K_I from Maximum Crack Length

The repair procedure for this item specifies that if the crack in the skin exceeds 0.75 in. the depot should be contacted. For the present example, assume that this is a maximum crack length that could appear in the repair.

Thus, for the 3/16 inch diameter hole:

$$r = 0.09375 \text{ inches}$$

and

$$\frac{a}{r} = \frac{0.75}{0.09375} = 8$$

From Figure 10.9.5, it is seen that the Beta factors decrease as a function of (a/r) and are equal at the two a/r values closest to $a/r = 8$. We estimate that $F_1(a/r)_{\text{UNIAXIAL}}$ and $F_1(a/r)_{\text{BIAXIAL}} = 0.774$ based on linear extrapolation. Note that the influence of the parallel stress diminishes as the crack length increases.

Calculating the stress-intensity factor based on Equation 10.9.9 gives

$$\begin{aligned} K &= 0.774 (20,423) \sqrt{\pi(0.75)} & (10.9.10) \\ &= 24,265 \text{ psi } \sqrt{\text{in}} = 24.3 \text{ Ksi } \sqrt{\text{in}} \end{aligned}$$

Step 4. Obtain the Fracture Toughness

The fracture toughness of 7075-T6 aluminum is obtained from Table 8.9.2.2 in the Damage Tolerant Design Data Handbook, and also is given by the third value in Table 10.9.1. For the 0.090 inch skin thickness and crack direction (across the rolling direction), the fracture toughness (K_{APP}) is 64.6 Ksi $\sqrt{\text{in}}$, with a standard deviation of 3.2 Ksi $\sqrt{\text{in}}$. This was a lucky find! More frequently one would not find a fracture toughness value for the exact set of circumstances required for positive reassurance.

Table 10.9.1 illustrates how an engineer might organize and summarize data for a given alloy system for comparison purposes. The information presented makes it possible to compare the effect of crack growth direction, thickness, test specimen width, and buckling restraint on the fracture toughness.

The L-T direction data suggest that the fracture toughness increases as thickness increases from 0.039 to 0.090 inch, whereas the T-L direction data appears to be independent of thickness. It is also interesting to note from Table 10.9.1, that the fracture toughness levels associated with L-T and T-L directions are within ten percent of each other for a given thickness. On the basis of metallurgical considerations, one would expect that the toughness in the L-T direction should be higher than the T-L direction, and indeed for the 0.039 and 0.090 thickness condition, higher values are associated with the L-T direction. At the 0.063

thickness, however, the higher values are associated with the T-L direction. The above remarks should indicate that if one wishes to make fracture toughness estimates in the absence of data in the direction of interest then one might use data from another direction, but only with caution and with an understanding of data trends.

One interesting point relative to the T-L direction/0.063 inch thickness data in Table 10.9.1 is that the buckling restrained fracture toughness tests generated increasing fracture toughness values as the width increased. The unrestrained tests developed data that were relatively independent of test specimen width. We also note that the unrestrained and restrained tests gave about the same fracture toughness values for test specimen widths which were at and below 6.0 inches. Thus, for small patches, while one might prefer to use buckling restrained data, one could use buckling unrestrained data from small width test specimens with reasonable confidence in the data.

In the absence of data for a specific set of circumstances, an engineer could construct tables such as illustrated in Table 10.9.1 and puzzle through to an estimate. For safety considerations, the engineer will also chose to err on the conservative side when making such estimates.

Step 5. Determine the Maximum Stress

Comparing the fracture toughness ($K_{APP} = 64.6 \text{ Ksi} \sqrt{\text{in}}$) with the applied stress-intensity factor ($K = 24.3 \text{ Ksi}$) shows that a substantial margin of safety is available before failure; thus,

$$\text{Fracture M.S.} = \frac{K_{APP}}{K} - 1 = \frac{64.6}{24.3} - 1 = 1.66 \quad (10.9.11)$$

TABLE 10.9.1

SUMMARY OF K_{APP} DATA FOR 7075-T6 SHEET AT ROOM TEMPERATURE

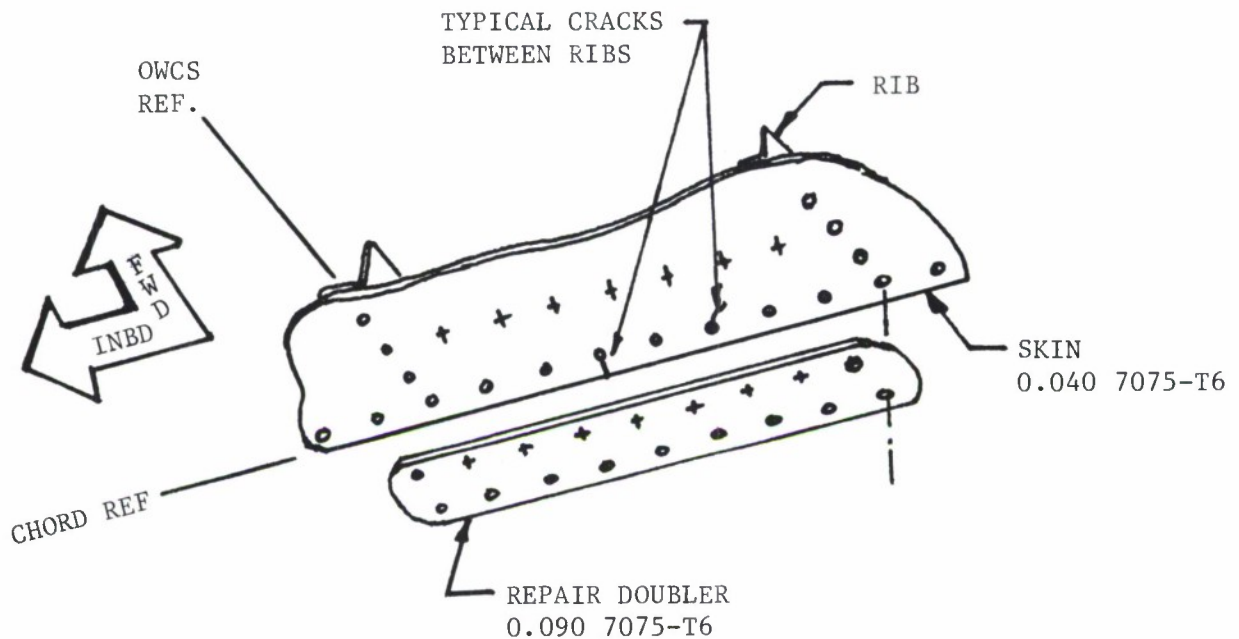
(Abstracted from DTD HB TABLE 8.9.2.2)

Thickness	K_{APP} mean (Ksi $\sqrt{\text{in}}$)	K_{APP} std. dev. (Ksi $\sqrt{\text{in}}$)	Direction	Width (inch)	Buckling Restraint	Page No.
0.039	49.4	6.3	L-T	6	NO	8.9-54
0.063	51.1	2.7	L-T	15.8	NO	8.9-54
0.090	64.6	3.2	L-T	12	YES	8.9-51
0.039	45.2	4.9	T-L	6	NO	8.9-56
0.063	53.3	-	T-L	3.03	YES	8.9-52
0.063	54.3	1.9	T-L	4.5	YES	8.9-52
0.064	56.7	-	T-L	6	YES	8.9-52
0.061	59.2	-	T-L	7	YES	8.9-52
0.061	62.9	-	T-L	8	YES	8.9-52
0.062	65.0	4.4	T-L	10	YES	8.9-52
0.062	61.2	1.5	T-L	12	YES	8.9-52
0.064	65.7	-	T-L	18	YES	8.9-53
0.063	69.5	7.4	T-L	24	YES	8.9-53
0.061	50.1	0.8	T-L	3	NO	8.9-57
0.063	56.2	-	T-L	6	NO	8.9-57
0.064	58.4	-	T-L	10	NO	8.9-57
0.063	54.4	-	T-L	12	NO	8.9-57
0.063	55.0	-	T-L	15	NO	8.9-57
0.063	54.8	1.9	T-L	15.8	NO	8.9-57
0.063	46.0	5.4	T-L	24	NO	8.9-58
0.081	56.0	-	T-L	30	NO	8.9-58

The stress associated with producing a fracture in the patch is obtained from

$$\sigma_{\max} = \frac{K_{\text{APP}}}{\left(\frac{K}{\sigma}\right)_{a=0.75}} = \frac{64.6}{0.774} = 83.5 \text{ Ksi} \quad (10.9.12)$$

a level higher than the ultimate tensile strength (see Equation 10.9.7). It is therefore unlikely that the repair will fracture under the applied loading when the maximum crack is present, since the applied loading never approaches the ultimate tensile strength.

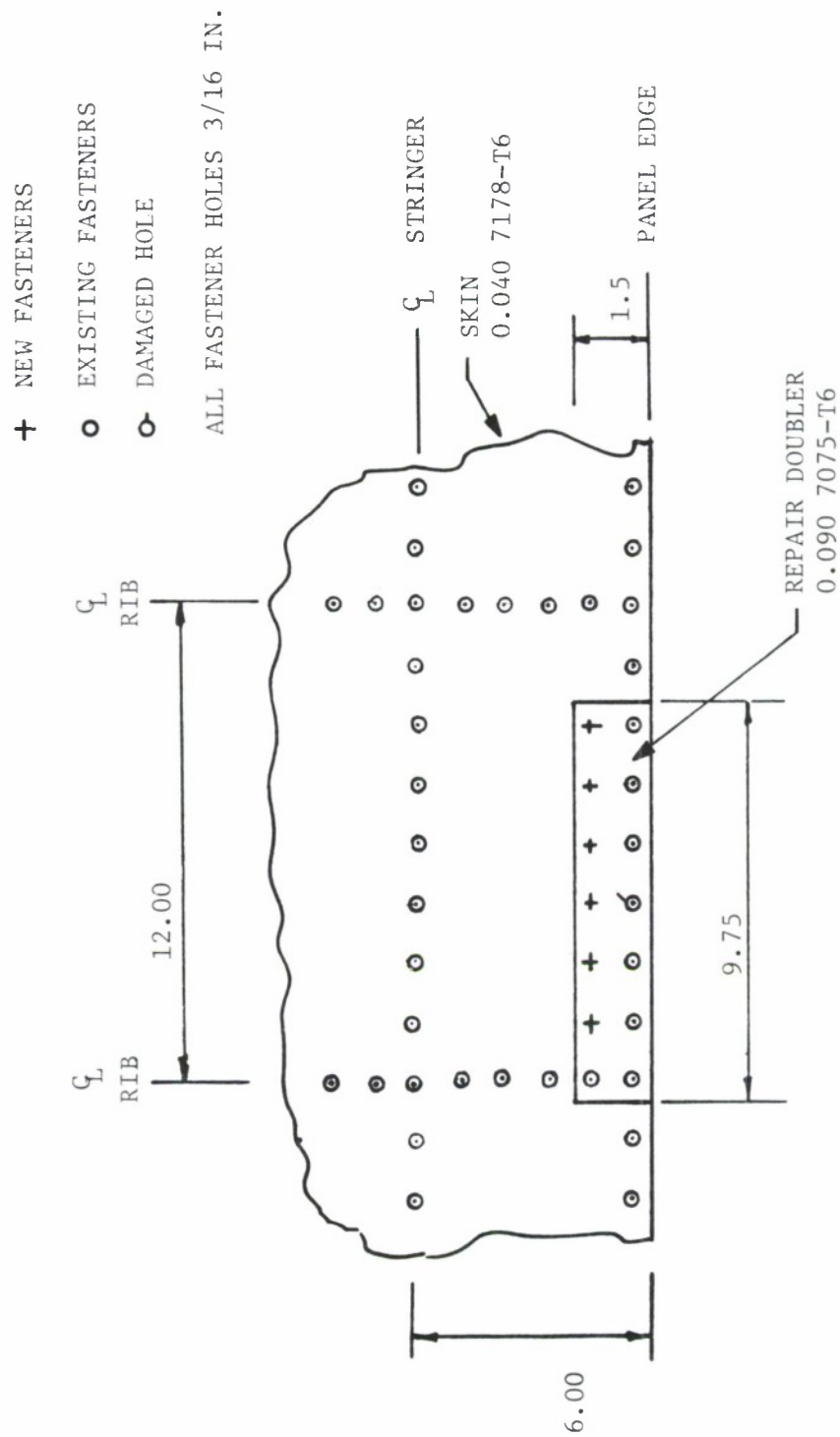


LOOKING UP AT LOWER SKIN

NOTES

1. Use repair doubler for cracks three fastener holes or more from ribs.
2. In cases where cracks exist both between ribs and at ribs in one bay, or there are cracks in adjacent bays, doubler will be extended to cover all cracks. Extend the doubler sufficient length to pick up three undamaged fastener holes beyond the last cracked hole.

Figure 10.9.1 Example of Airframe Lower Wing Skin Crack Repair.



10.9.12

Figure 10.9.2 View of Repair Installation on Outer Wing Lower Surface.

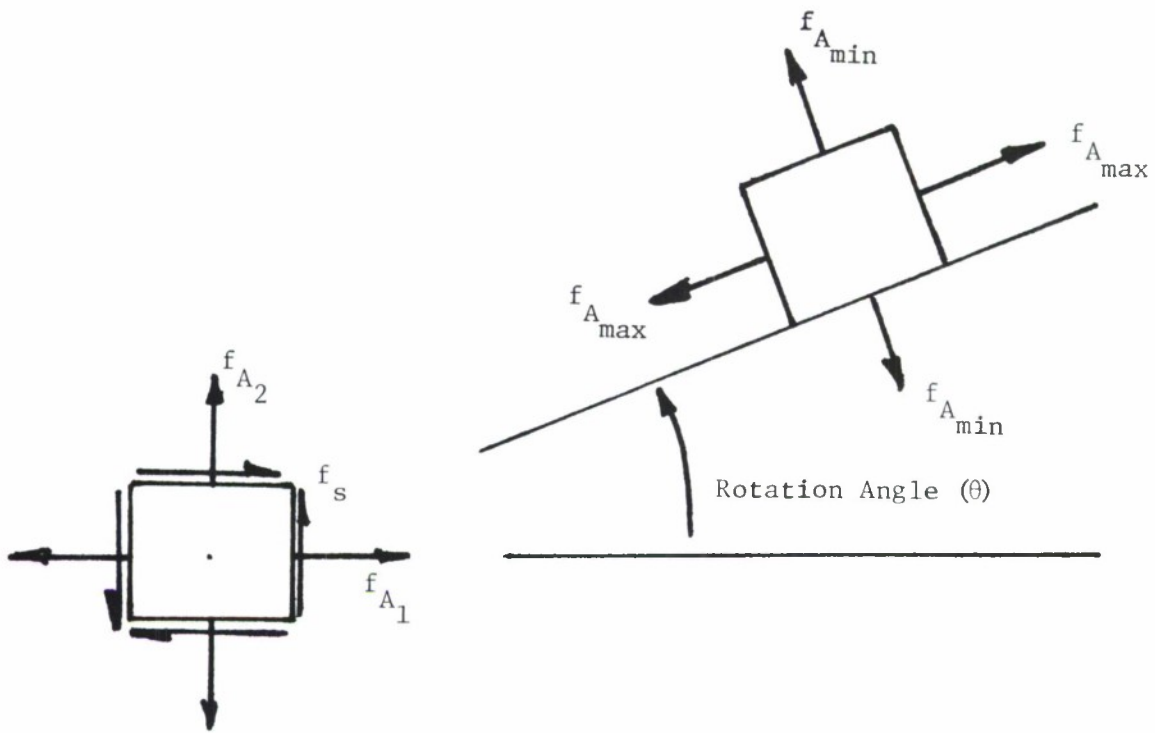


Figure 10.9.3 Rotation of Generalized Stress Element to Produce Principal Stress Orientation.

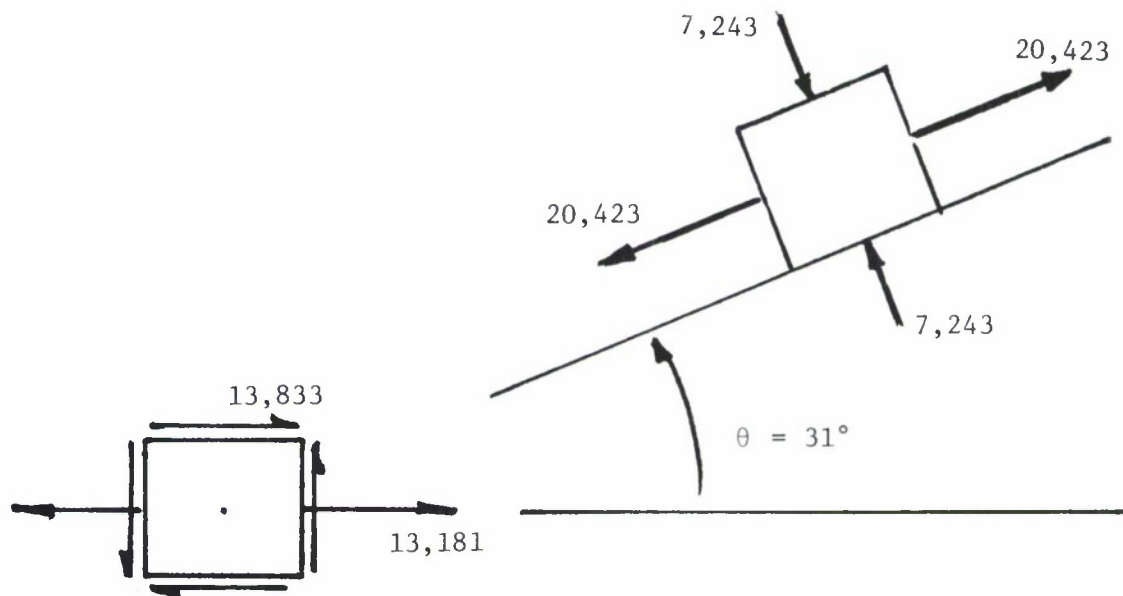
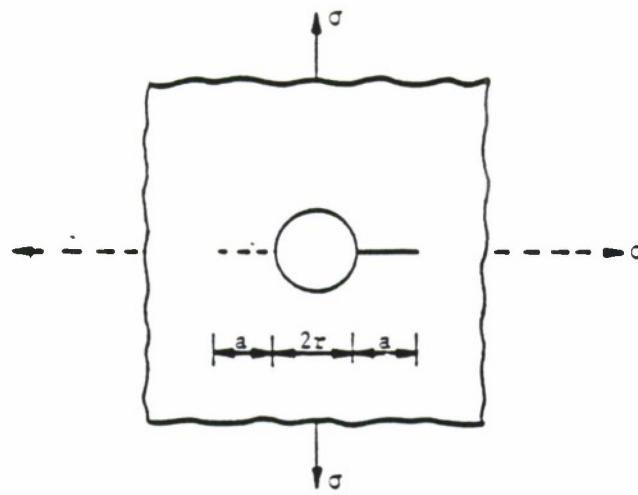


Figure 10.9.4 Rotation of Stress Element in Lower Wing Skin to Principal Stress Direction (stresses in psi).



$$K = \sigma \sqrt{\pi a} \beta$$

$$\beta = F_1 \left(\frac{a}{r} \right)$$

$\frac{a}{r}$	$F_1 \left(\frac{a}{r} \right)$, β Factor For Radially Cracked Hole		$F_2 \left(\frac{a}{r} \right)$, β Factor For Diametrically Cracked Hole	
	Uniaxial Loading Case 1.7.3.1	Equal Biaxial Loading	Uniaxial Loading Case 1.7.3.2	Equal Biaxial Loading
0.0	3.39	2.26	3.39	2.26
0.1	2.73	1.98	2.73	1.98
0.2	2.30	1.82	2.41	1.83
0.3	2.04	1.67	2.15	1.70
0.4	1.86	1.58	1.96	1.61
0.5	1.73	1.49	1.83	1.57
0.6	1.64	1.42	1.71	1.52
0.8	1.47	1.32	1.58	1.43
1.0	1.37	1.22	1.45	1.38
1.5	1.18	1.06	1.29	1.26
2.0	1.06	1.01	1.21	1.20
3.0	0.94	0.93	1.14	1.13
5.0	0.81	0.81	1.07	1.06
10.0	0.75	0.75	1.03	1.03
∞	0.707	0.707	1.00	1.00

Figure 1.7.3. Bowie β Factors for Through-Thickness Cracks at Remotely Loaded Circular Holes.

Figure 10.9.5 Reproduction of Figure 1.7.3 for Use in EXAMPLE 10.9.2.

SECTION 10.10

LIST OF REFERENCES

1. Stumpff, P. L., Gallagher, J. P., Johnson, E. L., and Hovey, P. W., "Damage Tolerant Design Handbook," MCIC-HB-01R, Metals and Ceramics Information Center, Battelle Columbus, May 1984.
2. Dowling, N. E., "Notched Member Fatigue Life Predictions Combining Crack Initiation and Propagation", Fatigue of Engineering Materials and Structures, Vol. 2, pp. 129-138, 1979.
3. Muskhelishvili, N. I., Some Basic Problems of the Mathematical Theory of Elasticity, Fourth, corrected and augmented edition, Moscow 1954, Translated from the Russian by J.R.M. Radok, P. Noordhoff Ltd., Groningen - the Netherlands, 1963.
4. Peterson, R. E., Stress Concentration Factors, Wiley-Interscience, New York, N.Y., 1974.
5. Maddux, G. E., Vorst, L. A., Giessler, F. J., Moritz, T., Stress Analysis Manual, AFFDL-TR-69-42, Air Force Flight Dynamics Laboratory, Wright Patterson Air Force Base, OH, February 1970.

APPENDIX A
AIR FORCE SPECIFICATIONS AND STANDARDS

MIL-STD-1530A(11)
11 December 1975
SUPERSEDING
MIL-STD-1530(USAF)
1 September 1972

MILITARY STANDARD

AIRCRAFT STRUCTURAL INTEGRITY PROGRAM,
AIRPLANE REQUIREMENTS



FSC 15GF

MIL-STD-1530A(11)

Airplane Structural Integrity Program, Airplane Requirements

MIL-STD-1530A(11)

1. This Military Standard is approved for use by all Departments and Agencies of the Department of Defense.
2. Recommended corrections, additions, or deletions should be addressed to Aeronautical Systems Division, ASD/ENFS, Wright-Patterson Air Force Base, Ohio 45433.

CONTENTS

PARAGRAPH		PAGE
1	SCOPE	1
1.1	Purpose	1
1.2	Applicability	1
1.2.1	Type of aircraft	1
1.2.2	Type of program	1
1.2.3	Type of structure	1
1.3	Modifications	1
2	REFERENCED DOCUMENTS	2
3	DEFINITIONS	3
3.1	Durability	3
3.2	Economic life	3
3.3	Initial quality	4
3.4	Structural operating mechanisms	4
3.5	Damage tolerance	4
4	GENERAL REQUIREMENTS	4
4.1	Discussion	4
4.2	Requirements	5
5	DETAIL REQUIREMENTS	5
5.1	Design information (Task I)	5
5.1.1	ASIP master plan	6
5.1.2	Structural design criteria	6
5.1.2.1	Damage tolerance and durability design criteria	6
5.1.2.1.1	Damage tolerance	6
5.1.2.1.2	Durability	7
5.1.2.2	Structural design criteria requirements	7
5.1.3	Damage tolerance and durability control plans	7
5.1.3.1	Damage tolerance control plan	8
5.1.3.2	Durability control plan	9
5.1.4	Selection of materials, processes and joining methods	10
5.1.4.1	Structural materials, processes, and joining methods selection requirements	10
5.1.5	Design service life and design usage	10
5.2	Design analyses and development tests (Task II)	10
5.2.1	Material and joint allowables	10
5.2.2	Loads analysis	11
5.2.3	Design service loads spectra	11
5.2.4	Design chemical/thermal environment spectra	11
5.2.5	Stress analysis	11
5.2.6	Damage tolerance analysis	12
5.2.6.1	Analysis procedures	12

CONTENTS (CONT'D)

PARAGRAPH		PAGE
5.2.7	Durability analysis	12
5.2.7.1	Analysis procedures	12
5.2.8	Sonic durability analysis	12
5.2.9	Vibration analysis	13
5.2.10	Flutter and divergence analysis	13
5.2.11	Nuclear weapons effects analyses	13
5.2.12	Nonnuclear weapons effects analysis	14
5.2.13	Design development tests	14
5.3	Full scale testing (Task III)	14
5.3.1	Static tests	14
5.3.1.1	Schedule requirement	15
5.3.2	Durability tests	15
5.3.2.1	Selection of test articles	15
5.3.2.2	Schedule requirements	15
5.3.2.3	Inspections	16
5.3.2.4	Test duration	17
5.3.3	Damage tolerance tests	17
5.3.4	Flight and ground operations tests	17
5.3.4.1	Flight and ground loads survey	17
5.3.4.2	Dynamic response tests	18
5.3.5	Sonic durability tests	18
5.3.6	Flight vibration tests	18
5.3.7	Flutter tests	18
5.3.7.1	Ground vibration tests	19
5.3.7.2	Structural rigidity tests	19
5.3.7.3	Flight flutter tests	19
5.3.8	Interpretation and evaluation of test results	19
5.4	Force management data package (Task IV)	19
5.4.1	Final analyses	20
5.4.1.1	Initial update of analyses	20
5.4.1.2	Final update of analyses	20
5.4.1.3	Development of inspection and repair criteria	20
5.4.2	Strength summary	20
5.4.3	Force structural maintenance plan	21
5.4.3.1	Initial force structural maintenance plan	21
5.4.3.2	Updated force structural maintenance plan	21
5.4.4	Loads/environment spectra survey	21
5.4.4.1	Data acquisition provisions	22
5.4.4.2	Data processing provisions	22
5.4.4.3	Analysis of data and development of baseline operational spectra	22
5.4.5	Individual airplane tracking program	23
5.4.5.1	Tracking analysis method	23
5.4.5.2	Data acquisition provisions	23

CONTENTS (CONT'D)

PARAGRAPH		PAGE
5.5	Force management (Task V)	23
5.5.1	Loads/environment spectra survey	24
5.5.2	Individual airplane tracking data	24
5.5.3	Individual airplane maintenance times	24
5.5.4	Structural maintenance records	25
6	NOTES	25
6.1	Data requirements	25
6.2	Relationship to system engineering management . .	25
TABLE I	USAF Aircraft Structural Integrity Program Tasks	26
FIGURES		
FIGURE 1	Aircraft Structural Integrity Program Task I - Design Information	27
	Task II - Design Analysis and Development Tests	27
FIGURE 2	Aircraft Structural Integrity Program Task III - Full Scale Testing	28
FIGURE 3	Aircraft Structural Integrity Program Task IV - Force Management Data Package	29
	Task V - Force Management	29
FIGURE 4	Interpretation and Evaluation of Test Results (Based on Design Service Life and Design Usage)	30

1. SCOPE

1.1 Purpose. The purpose of this standard is to describe the Air Force Aircraft Structural Integrity Program, define the overall requirements necessary to achieve structural integrity of USAF airplanes, and specify acceptance methods of contractor compliance. This standard shall be used by:

a. Contractors in conducting the development of an airframe for a particular weapon or support system

b. Government personnel in managing the development, production, and operational support of a particular airplane system throughout its life cycle.

1.2 Applicability. The degree of applicability of the various portions of this standard may vary between airplane systems as specified in 1.3.

1.2.1 Type of aircraft. This standard is directly applicable to manned power driven aircraft having fixed or adjustable fixed wings and to those portions of manned helicopter and V/STOL aircraft which have similar structural characteristics. Helicopter-type power transmission systems, including lifting and control rotors, and other dynamic machinery, and power generators, engines, and propulsion systems are not covered by this standard. For unmanned vehicles, certain requirements of this standard may be waived or factors of safety reduced commensurate with sufficient structural safety and durability to meet the intended use of the airframe. Waivers and deviations shall be specified in the contract specifications and shall have specific Air Force approval prior to commitment in the design.

1.2.2 Type of program. This standard applies to:

a. Future airplane systems

b. Airplane systems procured by the Air Force but developed under the auspices of another regulatory activity (such as the FAA or USN)

c. Airplanes modified or directed to new missions.

1.2.3 Type of structure. This standard applies to metallic and nonmetallic structures unless stated otherwise in the specifications referenced herein.

1.3 Modifications. The Air Force will make the decision regarding application of this standard and may modify requirements of this standard to suit system needs. The description of the modifications shall be documented in accordance with 5.1.1.

2. REFERENCED DOCUMENTS

2.1 Issues of documents. The following documents, of the issue in effect on date of invitation for bids or request for proposal, form a part of this standard to the extent specified herein:

SPECIFICATIONS

Military

MIL-I-6870	Inspection Program Requirements, Nondestructive, for Aircraft and Missile Materials and Parts
MIL-A-8860	Airplane Strength and Rigidity, General Specification for
MIL-A-8861	Airplane Strength and Rigidity, Flight Loads
MIL-A-8862	Airplane Strength and Rigidity, Landplane, Landing and Ground Handling Loads
MIL-A-8865	Airplane Strength and Rigidity, Miscellaneous Loads
MIL-A-8866	Airplane Strength and Rigidity, Reliability Requirements, Repeated Loads, and Fatigue
MIL-A-8867	Airplane Strength and Rigidity, Ground Tests
MIL-A-8869	Airplane Strength and Rigidity, Nuclear Weapons Effects
MIL-A-8870	Airplane Strength and Rigidity, Vibration Flutter and Divergence
MIL-A-8871	Airplane Strength and Rigidity, Flight and Ground Operations Tests
MIL-A-8892	Airplane Strength and Rigidity, Vibration
MIL-A-8893	Airplane Strength and Rigidity, Sonic Fatigue
MIL-R-83165	Recorder, Signal Data, MXU-553/A
MIL-C-83166	Converter-multiplexer, Signal Data, General Specification for
MIL-A-83444	Airplane Damage Tolerance Requirements

STANDARDS

Military

MIL-STD-499	Engineering Management
MIL-STD-882	System Safety Program for Systems and Associated Subsystems and Equipment, Requirements for
MIL-STD-1515	Fasteners to be Used in the Design and Construction of Aerospace Mechanical Systems
MIL-STD-1568	Materials and Processes for Corrosion and Prevention and Control in Aerospace Weapons Systems

HANDBOOKSMilitary

MIL-HDBK-5	Metallic Materials and Elements for Aerospace Vehicle Structures
MIL-HDBK-17	Plastics for Flight Vehicles
MIL-HDBK-23	Structural Sandwich Composites

Air Force Systems Command Design Handbooks

DH 1-0	General
DH 1-2	General Design Factors
DH 2-0	Aeronautical Systems
DH 2-7	System Survivability

(Copies of specifications, standards, drawings and publications required by contractors in connection with specific procurement functions should be obtained from the procuring activity or as directed by the contracting officer.)

2.2 Other publications. The following document forms a part of this standard to the extent specified herein. Unless otherwise indicated, the issue in effect on date of invitation for bids or request for proposal shall apply.

Other Publications

MCIC-HB-01	Damage Tolerance Design Handbook
------------	----------------------------------

(Application for copies should be addressed to the Metals and Ceramics Information Center, Battelle Memorial Institute, Columbus, Ohio 43201.)

3. DEFINITIONS. Definitions will be in accordance with the documents listed in Section 2 and as specified herein.

3.1 Durability. The ability of the airframe to resist cracking (including stress corrosion and hydrogen induced cracking), corrosion, thermal degradation, delamination, wear, and the effects of foreign object damage for a specified period of time.

3.2 Economic life. That operational life indicated by the results of the durability test program, i.e., test performance interpretation and evaluation in accordance with MIL-A-8867 to be available with the incorporation of Air Force approved and committed production or retrofit changes and supporting application of the force structural maintenance plan in accordance with this standard. In general, production or retrofit changes will be incorporated to correct local design and manufacturing deficiencies disclosed by test. It

will be assumed that the economic life of the test article has been attained with the occurrence of widespread damage which is uneconomical to repair and, if not repaired, could cause functional problems affecting operational readiness. This can generally be characterized by a rapid increase in the number of damage locations or repair costs as a function of cyclic test time.

3.3 Initial quality. A measure of the condition of the airframe relative to flaws, defects, or other discrepancies in the basic materials or introduced during manufacture of the airframe.

3.4 Structural operating mechanisms. Those operating, articulating, and control mechanisms which transmit structural forces during actuation and movement of structural surfaces and elements.

3.5 Damage tolerance. The ability of the airframe to resist failure due to the presence of flaws, cracks, or other damage for a specified period of unrepaired usage.

4. GENERAL REQUIREMENTS

4.1 Discussion. The effectiveness of any military force depends in part on the operational readiness of weapon systems. One major item of an airplane system affecting its operational readiness is the condition of the structure. The complete structure, herein referred to as the airframe, includes the fuselage, wing, empennage, landing gear, control systems and surfaces, engine mounts, structural operating mechanisms, and other components as specified in the contract specification. To maintain operational readiness, the capabilities, condition, and operational limitations of the airframe of each airplane weapon and support system must be established. Potential structural or material problems must be identified early in the life cycle to minimize their impact on the operational force, and a preventive maintenance program must be determined to provide for the orderly scheduling of inspections and replacement or repair of life-limited elements of the airframe.

4.1.1 The overall program to provide USAF airplanes with the required structural characteristics is referred to as the Aircraft Structural Integrity Program (ASIP). General requirements of the ASIP are to:

- a. Establish, evaluate, and substantiate the structural integrity (airframe strength, rigidity, damage tolerance, and durability) of the airplane.
- b. Acquire, evaluate, and utilize operational usage data to provide a continual assessment of the in-service integrity of individual airplanes.
- c. Provide a basis for determining logistics and force planning requirements (maintenance, inspections, supplies, rotation of airplanes, system phaseout, and future force structure).

d. Provide a basis to improve structural criteria and methods of design, evaluation, and substantiation for future airplanes.

4.1.2 The majority of detail requirements are published in the referenced military specifications. This standard repeats some of these requirements for emphasis and contains additional requirements which are not currently included in the military specifications. Any differences in detail requirements that may exist between this standard and the referenced documents listed in Section 2 shall be brought to the immediate attention of the Air Force for resolution. The applicable specifications, including the latest revisions thereto, for a particular airplane shall be as stated in the contract specifications.

4.2 Requirements. ASIP consists of the following five interrelated functional tasks as specified in table 1 and figures 1, 2, and 3:

- a. Task I (design information): Development of those criteria which must be applied during design so that the specific requirements will be met.
- b. Task II (design analysis and development tests): Development of the design environment in which the airframe must operate and the response of the airframe to the design environment.
- c. Task III (full scale testing): Flight and laboratory tests of the airframe to assist in determination of the structural adequacy of the design.
- d. Task IV (force management data package): Generation of data required to manage force operations in terms of inspections, modifications, and damage assessments.
- e. Task V (force management): Those operations that must be conducted by the Air Force during force operations to ensure damage tolerance and durability throughout the useful life of individual airplanes.

5. DETAIL REQUIREMENTS

5.1 Design information (Task I). The design information task encompasses those efforts required to apply the existing theoretical, experimental, applied research, and operational experience to specific criteria for materials selection and structural design for the airplane. The objective is to ensure that the appropriate criteria and planned usage are applied to an airplane design so that the specific operational requirements will be met. This task begins as early as possible in the conceptual phase and is finalized in subsequent phases of the airplane life cycle.

5.1.1 ASIP master plan. The contractor shall prepare an ASIP Master Plan in accordance with the detail requirements specified in the contract specifications. The purpose of the ASIP Master Plan is to define and document the specific approach for accomplishment of the various ASIP tasks throughout the life cycle of the airplane. The plan shall depict the time phased scheduling and integration of all required ASIP tasks for design, development, qualification, and tracking of the airframe. The plan shall include discussion of unique features, exceptions to the requirements of this standard and the associated rationale, and any problems anticipated in the execution of the plan. The development of the schedule shall consider all interfaces, impact of schedule delays (e.g., delays due to test failure), mechanisms for recovery programming, and other problem areas. The plan and schedules shall be updated annually and when significant changes occur. The ASIP Master Plan shall be subject to approval by the Air Force.

5.1.2 Structural design criteria. Detail structural design criteria for the specific airplane shall be established by the contractor in accordance with the requirements of the specifications as specified in 5.1.2.2. These specifications contain design criteria for strength, damage tolerance, durability, flutter, vibration, sonic fatigue, and weapons effects. The structural design criteria for damage tolerance and durability are further specified in 5.1.2.1 for special emphasis.

5.1.2.1 Damage tolerance and durability design criteria. The airframe shall incorporate materials, stress levels, and structural configurations which:

- a. Allow routine in-service inspection
- b. Minimize the probability of loss of the airplane due to propagation of undetected cracks, flaws, or other damage
- c. Minimize cracking (including stress corrosion and hydrogen induced cracking), corrosion, delamination, wear, and the effects of foreign object damage.

Damage tolerance design approaches shall be used to insure structural safety since undetected flaws or damage can exist in critical structural components despite the design, fabrication, and inspection efforts expended to eliminate their occurrence. Durability structural design approaches shall be used to achieve Air Force weapon and support systems with low in-service maintenance costs and improved operational readiness throughout the design service life of the airplane.

5.1.2.1.1 Damage tolerance. The damage tolerance design requirements are specified in MIL-A-83444, and shall apply to safety-of-flight structure. Damage tolerance designs are categorized into two general concepts:

- a. Fail-safe concepts where unstable crack propagation is locally contained through the use of multiple load paths or tear stoppers

- b. Slow crack growth concepts where flaws or defects are not allowed to attain the size required for unstable rapid propagation.

Either design concept shall assume the presence of undetected flaws or damage, and shall have a specified residual strength level both during and at the end of a specified period of unrepaired service usage. The initial damage size assumptions, damage growth limits, residual strength requirements and the minimum periods of unrepaired service usage depend on the type of structure and the appropriate inspectability level.

5.1.2.1.2 Durability. The durability design requirements are specified in MIL-A-8866. The airframe shall be designed such that the economic life is greater than the design service life when subjected to the design service loads/environment spectrum. The design service life and typical design usage requirements will be specified by the Air Force in the contract specifications for each new airplane. The design objective is to minimize cracking or other structural or material degradation which could result in excessive maintenance problems or functional problems such as fuel leakage, loss of control effectiveness, or loss of cabin pressure.

5.1.2.2 Structural design criteria requirements. Using the requirements in the System specification and the referenced military specifications the contractor shall prepare the detailed structural design criteria for the particular airplane. These criteria and all elements thereof shall require approval by the Air Force. Detail structural design criteria are specified in AFSC DH 1-0 and DH 2-0 and in MIL-A-8860, MIL-A-8861, MIL-A-8862, MIL-A-8865, MIL-A-8866, MIL-A-8869, MIL-A-8870, MIL-A-8892, MIL-A-8893, and MIL-A-83444. Where applicable, specific battle damage criteria will be provided by the Air Force. These criteria will include the threat, flight conditions, and load carrying capability and duration after damage is imposed, etc. The structure shall be designed to these criteria and to other criteria as specified in AFSC DH 2-7.

5.1.3 Damage tolerance and durability control plans. The contractor shall prepare damage tolerance and durability control plans and conduct the resulting programs in accordance with this standard, MIL-A-8866, and MIL-A-83444. The plans shall identify and define all of the tasks necessary to ensure compliance with the damage tolerance requirements as specified in 5.1.2.1.1 and MIL-A-83444, and the durability requirements as specified in 5.1.2.1.2 and MIL-A-8866. The plans and their individual elements shall require approval by the Air Force. The disciplines of fracture mechanics, fatigue, materials selection and processes, environmental protection, corrosion prevention and control, design, manufacturing, quality control, and nondestructive inspection are involved in damage tolerance and durability control. The corrosion prevention and control plan shall be in accordance with MIL-STD-1568. The plans shall include the requirement to perform damage tolerance and durability design concepts/material/weight/performance/cost trade studies during the early design phases to obtain low weight, cost effective designs which comply with the requirements of MIL-A-8866 and MIL-A-83444.

5.1.3.1 Damage tolerance control plan. The damage tolerance control plan shall include as a minimum the following tasks:

- a. Basic fracture data (i.e., K_{IC} , K_C , K_{ISCC} , da/dn , etc.) utilized in the initial trade studies and the final design and analyses shall be obtained from existing sources or developed as part of the contract in accordance with 5.2.1.
- b. A fracture critical parts list shall be established by the contractor in accordance with MIL-A-83444. The fracture critical parts list shall require approval by the Air Force and the list shall be kept current as the design of the airframe progresses.
- c. Design drawings for the fracture critical parts shall identify critical locations and special processing (e.g., shot peening) and inspection requirements.
- d. Complete nondestructive inspection requirements, process control requirements, and quality control requirements for fracture critical parts shall be established by the contractor and shall require approval by the Air Force. Nondestructive inspections shall comply with MIL-I-6870. This task shall include the proposed plan for certifying and monitoring subcontractor, vendor, and supplier controls.
- e. The damage tolerance control plan shall include any special nondestructive inspection demonstration programs conducted in accordance with the requirements of MIL-A-83444.
- f. Material procurement and manufacturing process specifications shall be developed and updated as necessary to minimize the possibility that basic materials and the resulting fracture critical parts have fracture toughness properties in the important loading directions which are less than those used in design.
- g. Traceability requirements shall be defined and imposed by the contractor on those fracture critical parts that receive prime contractor or subcontractor in-house processing and fabrication operations which could degrade the design material properties.
- h. Damage tolerance analyses, development testing, and full scale testing shall be performed in accordance with this standard, MIL-A-8867 and MIL-A-83444.
- i. For all fracture critical parts that are designed for a degree of inspectability other than in-service noninspectable, the contractor shall define the necessary inspection procedures for field use for each appropriate degree of inspectability as specified in MIL-A-83444.

5.1.3.2 Durability control plan. The durability control plan shall include as a minimum the following tasks:

a. A disciplined procedure for durability design shall be implemented to minimize the possibility of incorporating adverse residual stresses, local design details, materials, processing, and fabrication practices into the airplane design and manufacture which could lead to cracking or failure problems (i.e., those problems which have historically been found early during durability testing or early in service usage). The durability control plan shall encompass the requirements specified in the durability detail design procedures of MIL-A-8866.

b. Basic data (i.e., initial quality distribution, fatigue allowables, etc.) utilized in the initial trade studies and the final design and analyses shall be obtained from existing sources or developed as part of the contract in accordance with 5.2.1.

c. A criteria for identifying durability critical parts shall be established by the contractor and shall require approval by the Air Force. It is envisioned that durability critical parts will be expensive, noneconomical-to-replace parts that are either designed and sized by the durability requirements of MIL-A-8866 or could be designed and sized by the requirements of MIL-A-8866 if special control procedures are not employed. A durability critical parts list shall be established by the contractor and shall be kept current as the design of the airframe progresses.

d. Design drawings for the durability critical parts shall identify critical locations and special processing and inspection requirements.

e. Material procurement and manufacturing process specifications shall be developed and updated as necessary to minimize the possibility that initial quality is degraded below that assumed in the design.

f. Experimental determination sufficient to estimate initial quality by microscopic or fractographic examination shall be required for those structural areas where cracks occur during full scale durability testing. The findings shall be used in the full scale test data interpretation and evaluation task as specified in 5.3.8 and, as appropriate, in the development of the force structural maintenance plan as specified in 5.4.3.

g. Durability analyses, development testing, and full scale testing shall be performed in accordance with this standard, MIL-A-8866, and MIL-A-8867.

5.1.4 Selection of materials, processes, and joining methods. Materials, processes, and joining methods shall be selected to result in a light-weight, cost-effective airframe that meets the strength, damage tolerance, and durability requirements of this standard and supporting specifications. A primary factor in the final selection shall be the results of the design concept/material/weight/cost trade studies performed as a part of the damage tolerance and durability control programs.

5.1.4.1 Structural materials, processes, and joining methods selection requirements. In response to the request for proposal, prospective contractors shall identify the proposed materials, processes, and joining methods to be used in each of the structural components and the rationale for the individual selections. After contract award and during the design activity, the contractor shall document the complete rationale used in the final selection for each structural component. This rationale shall include all pertinent data upon which the selections were based including the data base, previous experience, and trade study results. The requirements of AFSC DH 1-2, Sections 7A, paragraph entitled, Materials, and 7B, paragraph entitled, Processes, shall be met as applicable. The selection of fasteners shall be in accordance with MIL-STD-1515. The materials, processes, and joining method selections for fracture and durability critical parts shall require approval by the Air Force.

5.1.5 Design service life and design usage. The Air Force will provide the required design service life and typical design usage as part of the contract specifications. These data shall be used in the initial design and analysis of the airframe. The design service life and design usage will be established through close coordination between the procuring activity and the advanced planning activities (i.e., Hq USAF, Hq AFSC, Hq AFLC, and using commands). Design mission profiles and mission mixes which are realistic estimates of expected service usage will be established. It is recognized that special force management actions will probably be required (i.e., early retirement, early modification, or rotation of selected airplanes) if the actual usage is more severe than the design usage. All revisions in these data subsequent to contract negotiations shall be at the discretion of the Air Force but will require separate negotiations between the Air Force and contractor.

5.2 Design analyses and development tests (Task II). The objectives of the design analyses and development tests task are to determine the environments in which the airframe must operate (load, temperature, chemical, abrasive, vibratory and acoustic environment) and to perform preliminary analyses and tests based on these environments to design and size the airframe to meet the required strength, damage tolerance, and durability requirements.

5.2.1 Material and joint allowables. The contractor shall utilize as appropriate the materials and joint allowables data in MIL-HDBK-5, MIL-HDBK-17, MIL-HDBK-23, and MCIC-HDBK-01 to support the various design analyses. Other data sources may also be used but will require approval by the Air Force.

For those cases where there are insufficient data available, the contractor shall formulate and perform experimental programs to obtain the data. Generation and analysis of test data shall meet the requirements of MIL-HDBK-5. The scope of these programs shall be defined by the prospective contractors in their responses to the request for proposal and shall require approval by the Air Force.

5.2.2 Loads analysis. The contractor shall comply with the detail requirements for loads analysis as specified in the contract specifications. The loads analysis shall consist of determining the magnitude and distribution of significant static and dynamic loads which the airframe may encounter when operating within the envelope established by the structural design criteria. This analysis consists of determining the flight loads, ground loads, power-plant loads, control system loads, and weapon effects. When applicable, this analysis shall include the effects of temperature, aeroelasticity, and dynamic response of the airframe.

5.2.3 Design service loads spectra. The contractor shall comply with the detail requirements for design service loads spectra in MIL-A-8866 as specified in the contract specifications. These spectra shall require approval by the Air Force. The purpose of the design service loads spectra is to develop the distribution and frequency of loading that the airframe will experience based on the design service life and typical design usage. The design service loads spectra and the design chemical/thermal environment spectra as specified in 5.2.4 will be used to develop design flight-by-flight stress/environment spectra as appropriate to support the various analyses and test tasks specified herein.

5.2.4 Design chemical/thermal environment spectra. The contractor shall comply with the detail requirements for design chemical/thermal environment spectra in MIL-A-8866 as specified in the contract specifications. These spectra shall require approval by the Air Force. These spectra shall characterize each environment (i.e., intensity, duration, frequency of occurrence, etc.).

5.2.5 Stress analysis. The contractor shall comply with the detail requirements for stress analysis as specified in the contract specifications. This analysis shall require approval by the Air Force. The stress analysis shall consist of the analytical determination of the stresses, deformation, and margins of safety resulting from the external loads and temperatures imposed on the airframe. The ability of the airframe to support the critical loads and to meet the specified strength requirements shall be established. In addition to verification of strength the stress analysis shall be used as a basis for durability and damage tolerance analyses, selection of critical structural components for design development tests, material review actions, and selection of loading conditions to be used in the structural testing.

The stress analysis shall also be used as a basis to determine the adequacy of structural changes throughout the life of the airplane and to determine the adequacy of the structure for new loading conditions that result from increased performance or new mission requirements. The stress analysis shall be revised to reflect any major changes to the airframe or to the loading conditions applied to the airframe.

5.2.6 Damage tolerance analysis. The contractor shall comply with the detail requirements for damage tolerance analysis in MIL-A-83444 as specified in the contract specifications. This analysis shall require approval by the Air Force. The purpose of this analysis is to substantiate the ability of the structural components to meet the requirements of MIL-A-83444.

5.2.6.1 Analysis procedures. The design flight-by-flight stress/environment spectra based on the requirements of 5.2.3 and 5.2.4 shall be used in the damage growth analysis and verification tests. The calculations of critical flaw sizes, residual strengths, safe crack growth periods, and inspection intervals shall be based on existing fracture test data and basic fracture allowables data generated as a part of the design development test program. The effect of variability in fracture properties on the analytical results shall be accounted for in the damage tolerance design.

5.2.7 Durability analysis. The contractor shall comply with the detail requirements for durability analysis in MIL-A-8866 as specified in the contract specifications. This analysis shall require approval by the Air Force. The purpose of this analysis is to substantiate the ability of the structure to meet the requirements of MIL-A-8866.

5.2.7.1 Analysis procedures. The design flight-by-flight stress/environment spectra based on the requirements of 5.2.3 and 5.2.4 shall be used in the durability analysis and verification tests. The analysis approach shall account for those factors affecting the time for cracks or equivalent damage to reach sizes large enough to cause uneconomical functional problems, repair, modification, or replacement. These factors shall include initial quality and initial quality variations, chemical/thermal environment, load sequence and environment interaction effects, material property variations, and analytical uncertainties. In addition to providing analytical assurance of a durable design, the durability analysis will provide a basis for development of test load spectra to be used in the design development and full scale durability tests.

5.2.8 Sonic durability analysis. The contractor shall comply with the detail requirements for sonic durability analysis in MIL-A-8893 as specified in the contract specifications. This analysis shall require approval by the Air Force. The objective of the sonic durability analysis is to ensure that the airframe is resistant to sonic durability cracking throughout the design service life.

The analysis shall define the intensity of the acoustic environment from potentially critical sources and shall determine the dynamic response, including significant thermal effects. Potentially critical sources include but are not limited to powerplant noise, aerodynamic noise in regions of turbulent and separated flow, exposed cavity resonance, and localized vibratory forces.

5.2.9 Vibration analysis. The contractor shall comply with the detail requirements for vibration analysis in MIL-A-8892 as specified in the contract specifications. This analysis shall require approval by the Air Force. The design shall control the structural vibration environment and the analysis shall predict the resultant environment in terms of vibration levels in various areas of the airplane such as the crew compartment, cargo areas, equipment bays, etc. The structure in each of these areas shall be resistant to unacceptable cracking as specified in 5.2.7.1 due to vibratory loads throughout the design service life. In addition, the design shall control the vibration levels to that necessary for the reliable performance of personnel and equipment throughout the design life of the airplane.

5.2.10 Flutter and divergence analysis. The contractor shall comply with the detail requirements for flutter and divergence analysis in MIL-A-8870 as specified in the contract specifications. This analysis shall require approval by the Air Force. The analysis shall consist of determination of the airplane flutter and divergence characteristics resulting from the interaction of the aerodynamic, inertia, and elastic characteristics of the components involved. The objective of the analysis is to substantiate the ability of the airplane structure to meet the specified flutter and divergence margins. Flutter analysis for failure modes as agreed to by the Air Force and the contractor shall also be conducted.

5.2.11 Nuclear weapons effects analyses. The contractor shall comply with the detail requirements for nuclear weapons effects analyses in MIL-A-8869 as specified in the contract specifications. These analyses shall require approval by the Air Force. The objectives of the nuclear weapons effects analyses are to:

- a. Verify that the design of the airframe will successfully resist the specified environmental conditions with no more than the specified residual damage
- b. Determine the structural capability envelope and crew radiation protection envelope for other degrees of survivability (damage) as may be required.

The contractor shall prepare detail design criteria and shall conduct the nuclear weapons effects analyses for transient thermal, overpressure, and gust loads and provide the substantiation of allowable structural limits on the structures critical for these conditions. The contractor shall also prepare and report the nuclear weapons effects capability envelope, including crew radiation protection, for a specified range of variations of weapon delivery trajectories, weapon size, aircraft escape maneuvers, and the resulting damage limits.

5.2.12 Non-nuclear weapons effects analysis. The contractor shall comply with the detail requirements for non-nuclear weapons effects analysis in AFSC DH 2-7 as specified in the contract specifications. This analysis shall require approval by the Air Force.

5.2.13 Design development tests. The contractor shall comply with the detail requirements for design development tests in MIL-A-8867, MIL-A-8870, MIL-A-8892, and MIL-A-8893 as specified in the contract specifications. The design development test program shall require approval by the Air Force. The objectives of the design development tests are to establish material and joint allowables; to verify analysis procedures; to obtain early evaluation of allowable stress levels, material selections, fastener systems, and the effect of the design chemical/thermal environment spectra; to establish flutter characteristics through wind tunnel tests; and to obtain early evaluation of the strength, durability (including sonic durability), and damage tolerance of critical structural components and assemblies. Examples of design development tests are tests of coupons; small elements; splices and joints; panels; fittings; control system components and structural operating mechanisms; and major components such as wing carry through, horizontal tail spindles, wing pivots, and assemblies thereof. Prospective contractors shall establish the scope of their proposed test program in their response to the request for proposal. After contract award and during the design analysis task, the contractor(s) shall finalize the plans and submit them to the Air Force for approval. The contractor shall revise and maintain approved updated versions of the test plans as the design develops. The plans shall consist of information such as rationale for selection of scope of tests; description of test articles, procedures, test loads and test duration; and analysis directed at establishing cost and schedule trade-offs used to develop the program.

5.3 Full scale testing (Task III). The objective of this task is to assist in determining the structural adequacy of the basic design through a series of ground and flight tests.

5.3.1 Static tests. The contractor shall comply with the detail requirements for static tests in MIL-A-8867 as specified in the contract specifications. Prior to initiation of testing, the test plans, procedures, and schedules shall be subject to approval by the Air Force. The static test program shall consist of a series of laboratory tests conducted on an instrumented airframe that simulates the loads resulting from critical flight and ground handling conditions. Thermal environment effects shall be simulated along with the load application on airframes where operational environments impose significant thermal effects. The primary purpose of the static test program is to verify the design ultimate strength capabilities of the airframe. Full scale static tests to design ultimate loads shall be required except:

- a. Where it is shown that the airframe and its loading are substantially the same as that used on previous aircraft where the airframe has been verified by full scale tests

- b. Where the strength margins (particularly for stability critical structure) have been demonstrated by major assembly tests.

When full scale ultimate load static tests are not performed, it shall be a program requirement to conduct a strength demonstration proof test. Deletion of the full scale ultimate load static tests shall require approval by the Air Force. Functional and inspection type proof test requirements shall be in accordance with MIL-A-8867.

5.3.1.1 Schedule requirement. The full scale static tests shall be scheduled such that the tests are completed in sufficient time to allow removal of the 80 percent limit restrictions on the flight test airplanes in accordance with MIL-A-8871 and allow unrestricted flight within the design envelope on schedule.

5.3.2 Durability tests. The contractor shall comply with the detail requirements for durability tests in MIL-A-8867 as specified by the contract specifications. Prior to initiation of testing, the test plans, procedures, and schedules shall require approval by the Air Force. Durability tests of the airframe shall consist of repeated application of the flight-by-flight design service loads/environment spectra. The objectives of the full scale durability tests are to:

- a. Demonstrate that the economic life of the test article is equal to or greater than the design service life when subjected to the design service loads/environment spectra
- b. Identify critical areas of the airframe not previously identified by analysis or component testing
- c. To provide a basis for establishing special inspection and modification requirements for force airplanes.

5.3.2.1 Selection of test articles. The test article shall be an early Full Scale Development (FSD) or Research Development Test & Evaluation (RDT&E) airframe and shall be as representative of the operational configuration as practical. If there are significant design, material, or manufacturing changes between the test article and production airplanes, durability tests of an additional article or selected components and assemblies thereof shall be required.

5.3.2.2 Schedule requirements. The full scale airframe durability test shall be scheduled such that one lifetime of durability testing plus an inspection of critical structural areas in accordance with 5.3.2.2.a and b shall be completed prior to full production go ahead decision. Two lifetimes of durability testing plus an inspection of critical structural areas in accordance with 5.3.2.3.a and b shall be scheduled to be completed prior to delivery of the first production airplane. If the economic life of the test article is reached

prior to two lifetimes of durability testing, sufficient inspection in accordance with 5.3.2.3.a and b and data evaluation shall be completed prior to delivery of the first production airplane to estimate the extent of required production changes and retrofit. In the event the original schedule for the production decision and production delivery milestones become incompatible with the above schedule requirements, a study shall be conducted to assess the technical risk and cost impacts of changing these milestones. An important consideration in the durability test program is that it be completed at the earliest practical time. This is needed to minimize force modifications due to deficiencies found during testing. To this end the following needs to be accomplished:

- a. Timely formulation of the test load spectra
- b. Early delivery of the test article
- c. Early establishment of managerial and contractual procedures for minimizing downtime in the event of a test failure.

Truncation, elimination, or substitution of load cycles in the test spectra to reduce test time and cost will be allowed. The contractor shall define by analysis and laboratory experiment the effect of any proposed truncation on the time to reach detrimental crack sizes to comply with the durability and damage tolerance requirements of MIL-A-8866 and MIL-A-83444 respectively. The results of these analyses and experiments shall be used to establish the final test spectra and, as necessary, to interpret the test results. The final test spectra shall require approval by the Air Force.

5.3.2.3 Inspections. Major inspection programs shall be conducted as an integral part of the full scale airframe durability test. The inspection programs shall require approval by the Air Force. These inspection programs shall include:

- a. In-service design inspections developed in accordance with the damage tolerance requirements of MIL-A-83444 and the durability requirements of MIL-A-8866
- b. Special inspections to monitor the status of critical areas and support the milestone schedule requirements of 5.3.2.2
- c. Teardown inspection at the completion of the full scale durability test including any scheduled damage tolerance tests to support the interpretation and evaluation task of 5.3.8.

A-21

5.3.2.4 Test duration. The minimum durability test duration shall be as specified in MIL-A-8867. It may be advantageous to the Air Force to continue testing beyond the minimum requirement to determine life extension capabilities and validate design life capability for usage that is more severe than design usage. The decision to continue testing beyond the minimum duration shall be made based upon a joint review by the contractor and appropriate Air Force activities. The prospective contractors shall provide, in their responses to the request for proposal, the estimated cost and schedule for two additional lifetimes of durability testing beyond the minimum requirement.

5.3.3 Damage tolerance tests. The contractor shall comply with the requirements for damage tolerance tests in MIL-A-8867 as specified in the contract specifications. Prior to initiation of testing, the test plans, procedures, and schedules shall require approval by the Air Force. The damage tolerance test program shall be of sufficient scope to verify Category I fracture critical parts in accordance with MIL-A-83444. The intent shall be to conduct damage tolerance tests on existing test hardware. This may include use of components and assemblies of the design development tests as well as the full scale static and durability test articles. When necessary, additional structural components and assemblies shall be fabricated and tested to verify compliance with the requirements of MIL-A-83444.

5.3.4 Flight and ground operations tests. The contractor shall comply with the detail requirements for flight and ground operations tests in MIL-A-8871 as specified in the contract specifications. Prior to initiation of testing, the test plans, procedures, and schedules shall require approval by the Air Force. An early Full Scale Development (FSD) or Research Development Test and Evaluation (RDT&E) airplane shall be used to perform the flight and ground operations tests. Load measurements shall be made by the strain gage or pressure survey methods agreed to between the contractor and the Air Force. An additional airplane, sufficiently late in the production program to ensure obtaining the final configuration, shall be the backup airplane for these flight tests and shall be instrumented similar to the primary test aircraft. Special types of instrumentation (e.g., recording equipment, mechanical strain recorders, strain gages, etc.) to be used during the loads/environment spectra survey and the individual airplane tracking programs shall be placed on the structural flight test airplane as appropriate for evaluation and correlation. The flight and ground operations tests shall include a flight and ground loads survey and dynamic response tests.

5.3.4.1 Flight and ground loads survey. The flight and ground loads survey program shall consist of operating an instrumented and calibrated airplane within and to the extremes of its limit structural design envelope to measure the resulting loads and, if appropriate, to also measure pertinent temperature profiles on the airplane structure. The objectives of the loads survey shall be as follows:

- a. Verification of the structural loads and temperature analysis used in the design of the airframe

- b. Evaluation of loading conditions which produce the critical structural load and temperature distribution
- c. Determination and definition of suspected new critical loading conditions which may be indicated by the investigations of structural flight conditions within the design limit envelope.

5.3.4.2 Dynamic response tests. The dynamic response tests shall consist of operating an instrumented and calibrated airplane to measure the structural loads and inputs while flying through atmospheric turbulence and during taxi, takeoff, towing, landing, refueling, store ejection, etc. The objectives shall be to obtain flight verification and evaluation of the elastic response characteristics of the structure to these dynamic load inputs for use in substantiating or correcting the loads analysis, fatigue analysis, and for interpreting the operational loads data.

5.3.5 Sonic durability tests. The contractor shall comply with the detail requirements for sonic durability tests in MIL-A-8893 as specified in the contract specifications. Prior to initiation of testing, the test plans, procedures, and schedules shall require approval by the Air Force. Measurements shall be made of the acoustic environments on a full scale airplane to verify or modify the initial design acoustic loads/environment. The sonic durability test shall be conducted on a representative airplane (or its major components) to demonstrate structural adequacy for the design service life. Sonic durability tests normally are accomplished by ground testing of the complete airplane with the power plants operating at full power for a time sufficient to assure design service life. However, testing of major portions of the airplane in special nonreverberant ground test stands using the airplane propulsion system as the noise source, or in high intensity noise facilities, may be acceptable.

5.3.6 Flight vibration tests. The contractor shall comply with the detail requirements for flight vibration tests in MIL-A-8892 as specified in the contract specifications. Prior to initiation of testing, the test plans, procedures, and schedules shall require approval by the Air Force. These tests shall be conducted to verify the accuracy of the vibration analysis. In addition, the test results shall be used to demonstrate that vibration control measures are adequate to prevent cracking and to provide reliable performance of personnel and equipment throughout the design service life.

5.3.7 Flutter tests. The contractor shall comply with the detail requirements for flutter related tests in MIL-A-8870 as specified in the contract specifications. Prior to initiation of testing, the test plans, procedures, and schedules shall require approval by the Air Force. Flutter related tests shall consist of ground vibration tests, thermoelastic tests, limit load rigidity tests, control surface free play and rigidity tests, and flight flutter tests.

5.3.7.1 Ground vibration tests. The ground vibration tests shall consist of the experimental determination of the natural frequencies, mode shapes, and structural damping of the airframe or its components. The objective is to verify mass, stiffness, and damping characteristics which are used in the aeroelastic analyses (flutter analysis, dynamic analysis, math models, etc.).

5.3.7.2 Structural rigidity tests. The thermoelastic tests, limit load rigidity test, and control surface free play and rigidity tests shall consist of the experimental determination of the structural elastic and free play properties of the airframe and its components. The objective of these tests is to verify supporting data used in aeroelastic analyses and dynamic model design.

5.3.7.3 Flight flutter tests. Flight flutter tests shall be conducted to verify that the airframe is free from aeroelastic instabilities and has satisfactory damping throughout the operational flight envelope.

5.3.8 Interpretation and evaluation of test results. Each structural problem (failure, cracking, yielding, etc.) that occurs during the tests required by this standard shall be analyzed by the contractor to determine the cause, corrective actions, force implications, and estimated costs. The scope and interrelations of the various tasks within the interpretation and evaluation effort are illustrated in figure 4. The results of this evaluation shall define corrective actions required to demonstrate that the strength, rigidity, damage tolerance and durability design requirements are met. The cost, schedule, operational, and other impacts resulting from correction of deficiencies will be used to make major program decisions such as major redesign, program cancellation, awards or penalties, and production airplane buys. Structural modifications or changes derived from the results of the full scale test to meet the specified strength, rigidity, damage tolerance, and durability design requirements shall be substantiated by subsequent tests of components, assemblies, or full scale article as appropriate. (See figure 3.) The test duration for durability modifications shall be as specified in MIL-A-8867 and the contract specifications. The contractor shall propose these additional test requirements together with the associated rationale to the Air Force for approval.

5.4 Force management data package (Task IV). Maintaining the strength, rigidity, damage tolerance, and durability is dependent on the capability of the appropriate Air Force commands to perform specific inspection, maintenance, and possibly modification or replacement tasks at specific intervals throughout the service life (i.e., at specified depot or base level maintenance times and special inspection periods). To properly perform these tasks, the Air Force must have detailed knowledge of the required actions. Additionally, experience has shown that the actual usage of military airplanes may differ significantly from the assumed design usage. It is necessary that the Air Force have the technical methods and actual usage data to assess the effect of these changes

in usage on airplane damage tolerance and durability. Task IV describes the minimum required elements of a data package which the contractor shall provide so that the Air Force can accomplish the force management tasks as specified in 5.5. It should be noted that Task IV contains basic ASIP requirements to be performed by the contractor but, unlike Tasks I through III, is not for the purpose of providing compliance to the basic structural design requirements.

5.4.1 Final analyses. The contractor shall revise the design analyses as appropriate to account for significant differences between analysis and test that are revealed during the full scale tests and later during the loads/environment spectra survey. These analyses updates shall be prepared as discussed below and shall require approval by the Air Force.

5.4.1.1 Initial update of analyses. The design analyses as specified in 5.2 shall be revised when the results of the design development and full scale tests as specified in 5.2.13 through 5.3.7 are available. These initial updates will be used to identify the causes of problems, corrective actions, and production and force modifications required by the interpretation and evaluation of test results task as specified in 5.3.8.

5.4.1.2 Final update of analyses. The initial update of the damage tolerance and durability analyses shall be revised to reflect the baseline operational spectra as specified in 5.4.3. These analysis updates shall form the basis for preparation of the updated force structural maintenance plan as specified in 5.4.3.2. The analyses shall identify the critical areas, damage growth rates, and damage limits required to establish the damage tolerance and durability inspection and modification requirements and economic life estimates required as part of the force structural maintenance plan.

5.4.1.3 Development of inspection and repair criteria. The appropriate analyses (stress, damage tolerance, durability, etc.) shall be used to develop a quantitative approach to inspection and repair criteria. Allowable damage limits and damage growth rates established by the analyses shall be used to develop inspection and repair times for structural components and assemblies. These analyses shall also be used to develop detail repair procedures for use at field or depot level. Special attention shall be placed on defining damage acceptance limits and damage growth rates for components utilizing bonded, honeycomb, or advanced composite types of construction. These inspection and repair criteria shall be incorporated into the force structural maintenance plan as specified in 5.4.3.

5.4.2 Strength summary. The contractor shall summarize the final analyses and other pertinent structures data into a format which will provide rapid visibility of the important structures characteristics, limitations and capabilities in terms of operational parameters. It is desirable that the summary be primarily in diagrammatic form showing the airplane structural limitations and capabilities as a function of the important operational parameters such as

speed, acceleration, center of gravity location, and gross weight. The summary shall include brief descriptions of each major structural assembly, also preferably in diagrammatic form, indicating structural arrangements, materials, critical design conditions, damage tolerance and durability critical areas, and minimum margins of safety. Appropriate references to design drawings, detail analyses, test reports, and other back-up documentation shall be indicated. The strength summary shall require approval by the Air Force.

5.4.3 Force structural maintenance plan. The contractor shall prepare a force structural maintenance plan to identify the inspection and modification requirements and the estimated economic life of the airframe. Complete detailed information (when, where, how, and cost data as appropriate) shall be included. It is intended that the Air Force will use this plan to establish budgetary planning, force structure planning, and maintenance planning. This plan shall require approval by the Air Force.

5.4.3.1 Initial force structural maintenance plan. The initial plan shall be based on the design service life, design usage spectra, the results of the full scale test interpretation and evaluation task as specified in 5.3.7 and the upgraded critical parts list required as specified in 5.1.3.

5.4.3.2 Updated force structural maintenance plan. The force structural maintenance plan shall be updated to include the baseline operational spectra through use of the final analyses update as specified in 5.4.1.2. The first update of the plan shall be based on the analyses that utilized data obtained from the initial phase of the loads/environment spectra survey. Additional updates that may be required to reflect significant changes determined during continuation of the loads/environment spectra survey will be provided through separate negotiation between the Air Force and contractor.

5.4.4 Loads/environment spectra survey. The objective of the loads/environment spectra survey shall be to obtain time history records of those parameters necessary to define the actual stress spectra for the critical areas of the airframe. It is envisioned that 10-20 percent of the operational airplanes will be instrumented to measure such parameters as velocity, accelerations, altitude, fuel usage, temperature, strains, etc. The data will be obtained by the Air Force as part of the force management task as specified in 5.5 and shall be used by the contractor to construct the baseline operational spectrum as specified in 5.4.4.3. Data acquisition shall start with delivery of the first operational airplane. The contractor shall propose, in response to the request for proposal, the number of airplanes to be instrumented and the parameters to be monitored. For the purposes of the program definition, cost estimating, and scheduling, it shall be assumed that the duration of the survey will be 3 years or when the total recorded flight hours of unrestricted operational usage equals one design lifetime, whichever occurs first. The contractor shall also propose the method to be used to detect when a significant change in

usage occurs to require an update in the baseline operational spectra. If the individual airplane tracking program as specified in 5.4.5 obtains sufficient data to develop the baseline operational spectra and detect significant usage changes, a separate survey program (or continuation thereof) as described herein may not be required. The scope of the program (e.g., the number of airplanes to be instrumented, and the number and type of parameters to be monitored) will be defined in the contract specifications.

5.4.4.1 Data acquisition provisions. The contractor shall select qualified functioning instrumentation and data recording systems in accordance with the requirements of this standard as specified in the contract specifications. The contractor shall select the specific instrumentation and data recording equipment to accomplish the survey task, obtain Air Force approval of the selections, and make the necessary instrumentation and data recording installations in the specified airplanes. If recording equipment and converter multiplexer equipment are selected, they shall meet the requirements of MIL-R-83165 and MIL-C-83166 respectively. Every effort should be made to use existing qualified instrumentation and recording equipment to reduce program costs and utilize proven operational capabilities. The contract shall specify whether the instrumentation and recording equipment (including spares) shall be Government Furnished Equipment (GFE) or Contractor Furnished Equipment (CFE).

5.4.4.2 Data processing provisions. The contractor shall coordinate with the Air Force the data processing provisions (including reformatting) to be used to ensure that the computer analysis methods will be compatible with the Air Force data analysis system. It is envisioned that contractor facilities and personnel, except for reformatting/transcribing and other data processing and analysis functions for which capabilities exist within the Air Force and are approved for use, will be used to process data collected during the 3-year period beginning with delivery of the first production airplane. Plans for transfer of data processing provisions from contractor to Air Force facilities including training of Air Force personnel shall be included.

5.4.4.3 Analysis of data and development of baseline operational spectra. The contractor shall use the flight data to assess the applicability of the design and durability test loads/environment spectra and to develop baseline operational spectra. The baseline operational spectra shall be used to update the durability and damage tolerance analyses as specified in 5.4.1.2 when a statistically adequate amount of data has been recorded. Subsequent revisions of the baseline operational spectra may be required but will require separate negotiations between the Air Force and contractor.

5.4.5 Individual airplane tracking program. The objective of the individual airplane tracking program shall be to predict the potential flaw growth in critical areas of each airframe that is keyed to damage growth limits of MIL-A-83444, inspection times, and economic repair times. Data acquisition shall start with delivery of the first operational airplane. The program shall include serialization of major components (e.g., wings, horizontal and vertical stabilizers, landing gears, etc.) so that component tracking can be implemented by the Air Force. The contractor shall propose for Air Force review and approval, an individual airplane tracking program for the specific airplane.

5.4.5.1 Tracking analysis method. The contractor shall develop an individual airplane tracking analysis method to establish and adjust inspection and repair intervals for each critical area of the airframe based on the individual airplane usage data. The damage tolerance and durability analyses and associated test data will be used to establish the analysis method. This analysis will provide the capability to predict crack growth rates, time to reach the crack size limits, and the crack length as a function of the total flight time and usage data. The contractor shall coordinate this effort with the Air Force to ensure that the computer analysis method will be compatible with the Air Force data analysis system. The individual airplane tracking analysis method shall require approval by the Air Force.

5.4.5.2 Data acquisition provisions. The contractor shall select qualified functioning instrumentation and data recording systems in accordance with the requirements of this standard as specified in the contract specifications. The recording system shall be as simple as possible and shall be the minimum required to monitor those parameters necessary to support the analysis methods as specified in 5.4.5.1. Counting accelerometers, electrical or mechanical strain recorders, electrical resistance gages, simplified manual data forms, etc. shall be considered. The contractor shall select the specific instrumentation and data recording equipment to accomplish the individual airplane usage tracking, obtain Air Force approval of the selections, and make the necessary instrumentation and data recording installations in the specified airplanes. The contract shall specify whether the instrumentation and recording equipment (including spares) shall be Government Furnished Equipment (GFE) or Contractor Furnished Equipment (CFE).

5.5 Force management (Task V). Task V describes those actions that must be conducted by the Air Force during force operations to ensure the damage tolerance and durability of each airplane. Task V will be primarily the responsibility of the Air Force and will be performed by the appropriate commands utilizing the data package supplied by the contractor in Task IV with the minimum amount of contractor assistance. Contractor responsibilities in Task V will be specified in the contract specifications.

5.5.1 Loads/environment spectra survey. The Air Force will be responsible for the overall planning and management of the loads/environment spectra survey and will:

- a. Establish data collection procedures and transmission channels within the Air Force
- b. Train squadron, base, and depot level personnel as necessary to ensure the acquisition of acceptable quality data
- c. Maintain and repair the instrumentation and recording equipment
- d. Ensure that the data are of acceptable quality and are obtained in a timely manner so that the contractor can analyze the results, develop the baseline spectrum (see 5.4.4.3), and update the analyses (see 5.4.1.2) and force structural maintenance plan (see 5.4.3.2).

The Air Force will also be responsible for ensuring that survey data are obtained for each type of usage that occurs within the force (training, reconnaissance, special tactics, etc.). Subsequent to completion of the initial data gathering effort, the Air Force will elect whether or not to continue to operate either all or a portion of the instrumentation and recording equipment aboard the survey airplanes to support additional updates of the baseline spectra and force structural maintenance plan.

5.5.2 Individual airplane tracking data. The Air Force will be responsible for the overall planning and management of the individual airplane tracking data gathering effort and will:

- a. Establish data collection procedures and data transmission channels within the Air Force
- b. Train squadron, base, and depot level personnel as necessary to ensure the acquisition of acceptable quality data
- c. Maintain and repair the instrumentation and recording equipment
- d. Ensure that the data are obtained and processed in a timely manner to provide adjusted maintenance times for each critical area of each airplane.

5.5.3 Individual airplane maintenance times. The Air Force will be responsible for deriving individual maintenance (inspection and repair) times for each critical area of each airplane by use of the tracking analysis methods as specified in 5.4.5.1 and the individual airplane tracking data as specified in 5.5.2. The objective is to determine adjusted times at which the force

structural maintenance actions as specified in 5.4.3 have to be performed on individual airplanes and each critical area thereof. With the force structural maintenance plan and the individual aircraft maintenance time requirements available, the Air Force can schedule force structural maintenance actions on a selective basis that accounts for the effect of usage variations on structural maintenance intervals.

5.5.4 Structural maintenance records. AFLC and the using command will be responsible for maintaining structural maintenance records (inspection, repair, modification, and replacement) for individual airplanes. These records shall contain complete listings of structural maintenance actions that are performed with all pertinent data included (Time Compliance Technical Order (TCTO) action, component flight time, component and airplane serial number, etc.).

6. NOTES

6.1 Data requirements. The data requirements in support of this standard will be selected from the DOD Authorized Data List (TD-3) and will be reflected in a contractor data requirements list (DD Form 1423) attached to the request for proposal, invitation for bids, or the contract as appropriate.

6.2 Relationship to system engineering management. When appropriate, the conduct of the work efforts by the contractor in achieving airplane structural integrity will be included in the System Engineering Management Plan in accordance with MIL-STD-499A(USAF) for the airplane and will be compatible with the system safety plan in accordance with MIL-STD-882.

Custodian:
Air Force - 11

Preparing activity:
Air Force - 11

Review activities:
Air Force - 01, 10, 16

Project No. 15GP-F019

TABLE I. USAF Aircraft structural integrity program tasks.

TASK I	TASK II	TASK III	TASK IV	TASK V
DESIGN INFORMATION	DESIGN ANALYSES AND DEVELOPMENT TESTS	FULL SCALE TESTING	FORCE MANAGEMENT DATA PACKAGE	FORCE MANAGEMENT
ASIP MASTER PLAN _____ STRUCTURAL DESIGN CRITERIA _____ DAMAGE TOLERANCE & DURABILITY CONTROL PLANS _____ SELECTION OF MAT'L'S, PROCESSES, & JOINING METHODS _____ DESIGN SERVICE LIFE AND DESIGN USAGE	MATERIALS AND JOINT ALLOWABLES _____ LOAD ANALYSIS _____ DESIGN SERVICE LOADS SPECTRA _____ DESIGN CHEMICAL/ THERMAL ENVIRONMENT SPECTRA _____ STRESS ANALYSIS _____ DAMAGE TOLERANCE ANALYSIS _____ DURABILITY ANALYSIS _____ SONIC ANALYSIS _____ VIBRATION ANALYSIS _____ FLUTTER ANALYSIS _____ NUCLEAR WEAPONS EFFECTS ANALYSIS _____ NON-NUCLEAR WEAPONS EFFECTS ANALYSIS _____ DESIGN DEVELOPMENT TESTS	STATIC TESTS _____ DURABILITY TESTS _____ DAMAGE TOLERANCE TESTS _____ FLIGHT & GROUND OPERATIONS TESTS _____ SONIC TESTS _____ FLIGHT VIBRATION TESTS _____ FLUTTER TESTS _____ INTERPRETATION & EVALUATION OF TEST RESULTS	FINAL ANALYSES _____ STRENGTH SUMMARY _____ FORCE STRUCTURAL MAINTENANCE PLAN _____ LOADS/ENVIRONMENT SPECTRA SURVEY _____ INDIVIDUAL AIRPLANE TRACKING PROGRAM	LOADS/ENVIRONMENT SPECTRA SURVEY _____ INDIVIDUAL AIRPLANE TRACKING DATA _____ INDIVIDUAL AIRPLANE MAINTENANCE TIMES _____ STRUCTURAL MAINTENANCE RECORDS

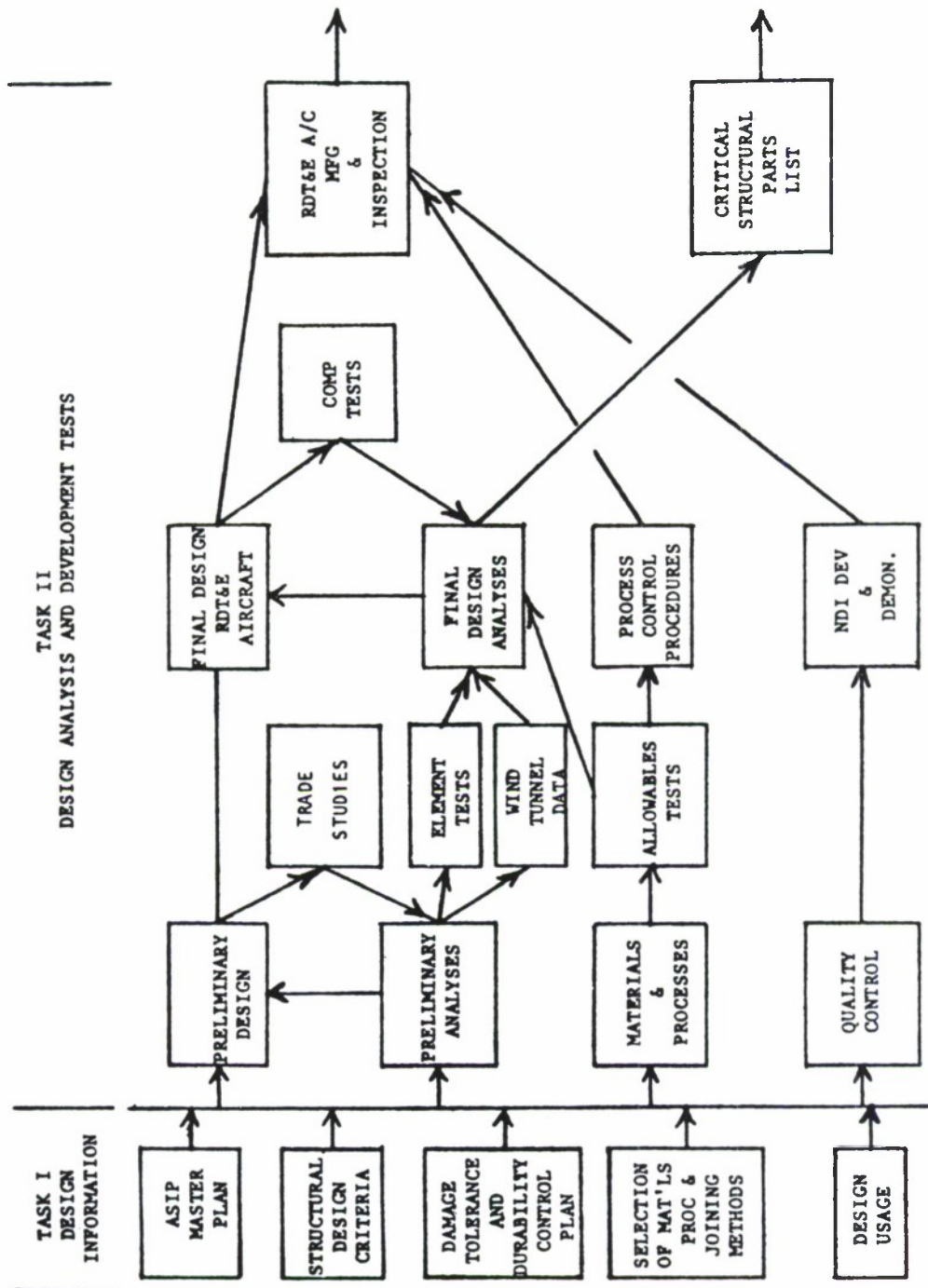


FIGURE 1. Aircraft structural integrity program.

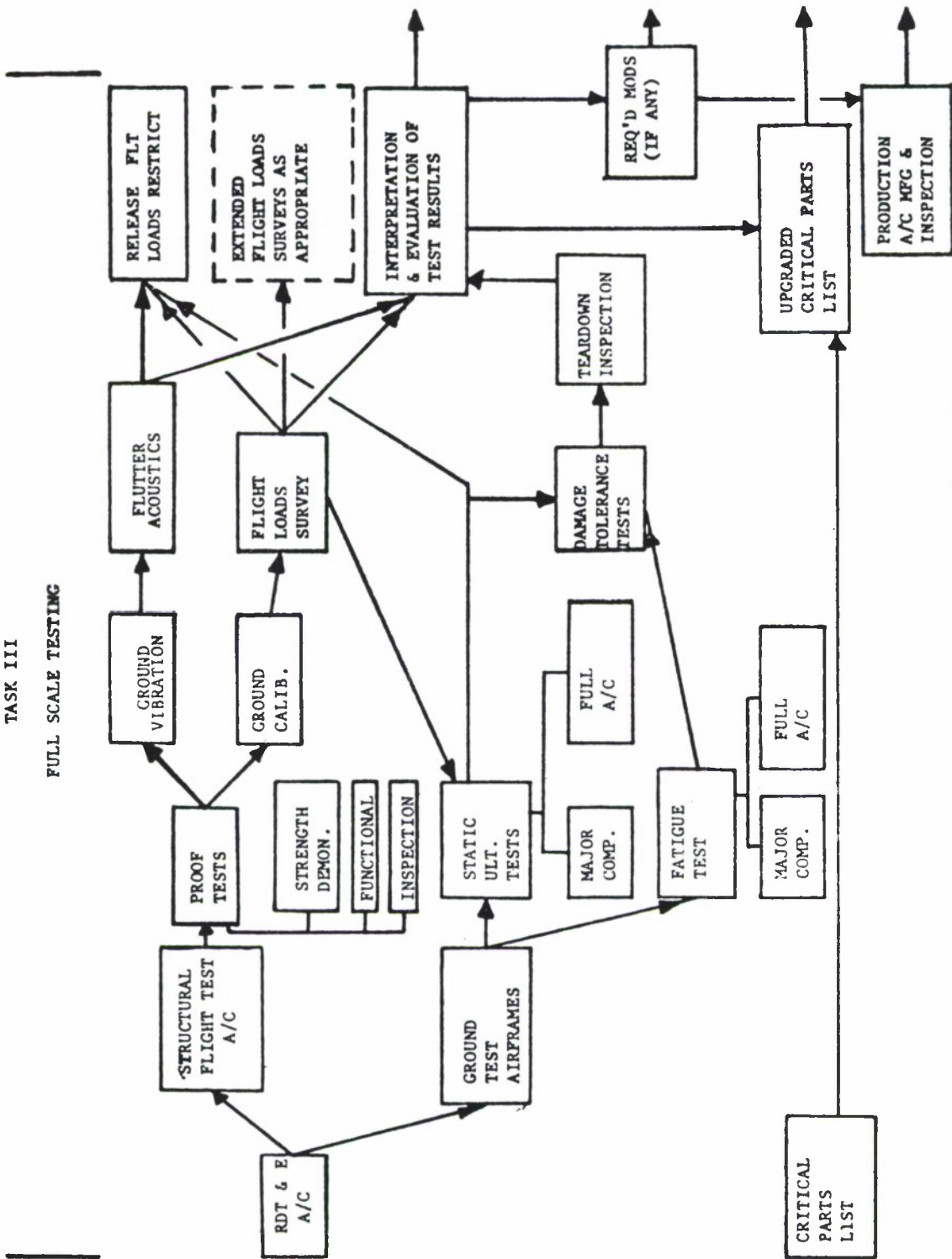


FIGURE 2. Aircraft structural integrity program.

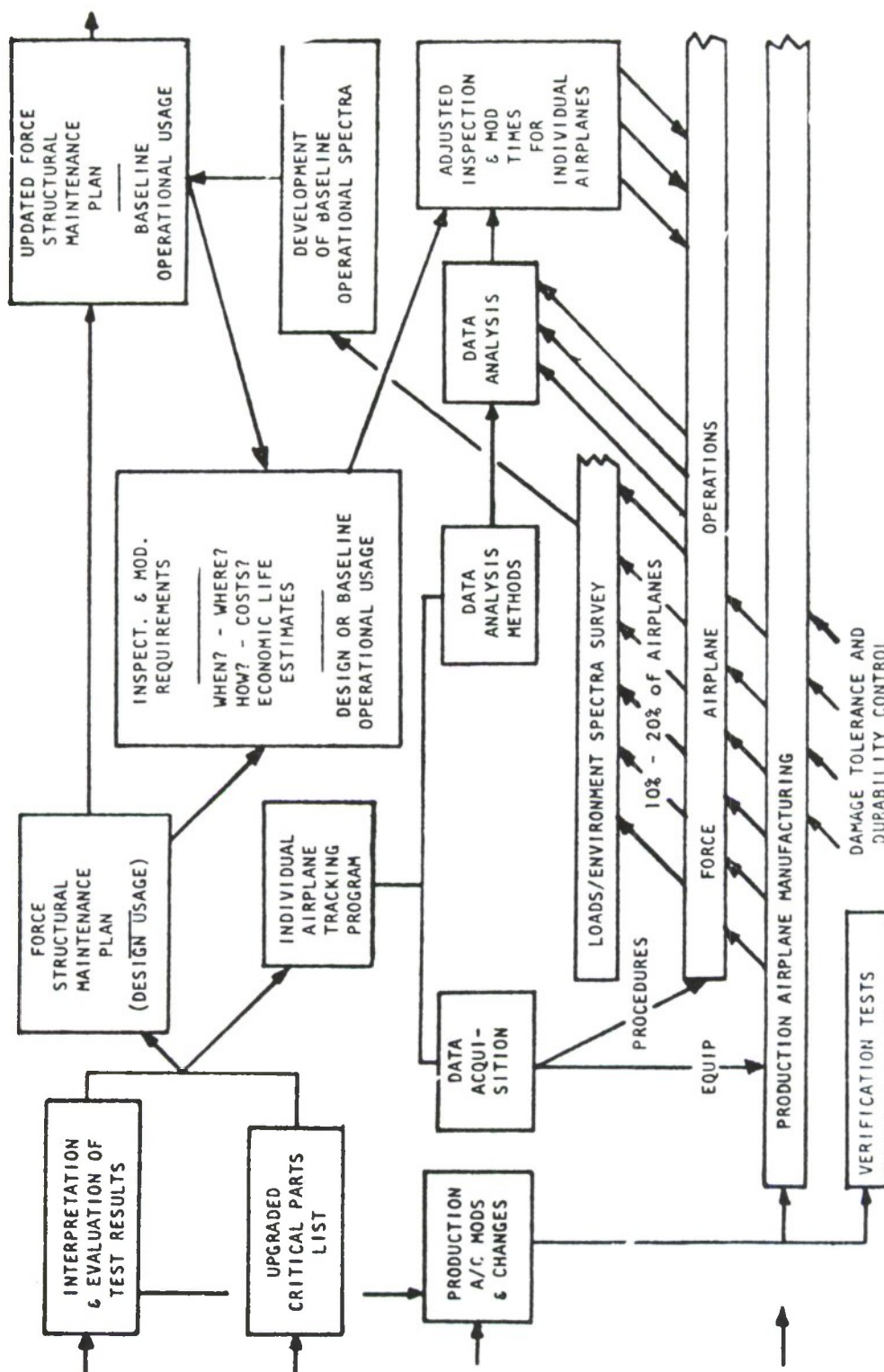


FIGURE 3. Aircraft structural integrity program.

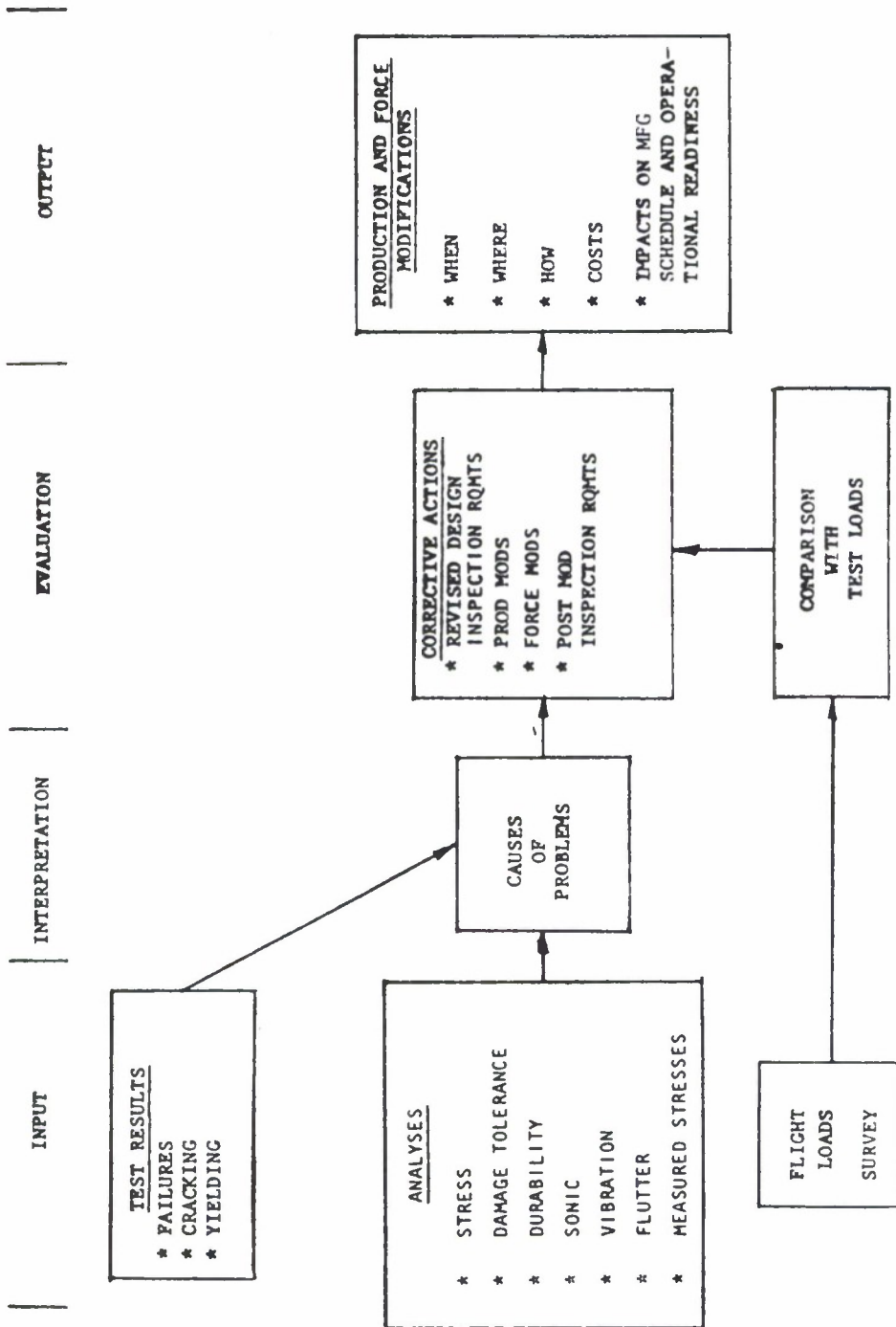


FIGURE 4. Interpretation and evaluation of test results
(based on design service life and design usage).

STANDARDIZATION DOCUMENT IMPROVEMENT PROPOSAL

OMB Approval
No. 22-R255

INSTRUCTIONS: The purpose of this form is to solicit beneficial comments which will help achieve procurement of suitable products at reasonable cost and minimum delay, or will otherwise enhance use of the document. DoD contractors, government activities, or manufacturers/vendors who are prospective suppliers of the product are invited to submit comments to the government. Fold on lines on reverse side, staple in corner, and send to preparing activity. Comments submitted on this form do not constitute or imply authorization to waive any portion of the referenced document(s) or to amend contractual requirements. Attach any pertinent data which may be of use in improving this document. If there are additional papers, attach to form and place both in an envelope addressed to preparing activity.

DOCUMENT IDENTIFIER AND TITLE

NAME OF ORGANIZATION AND ADDRESS

CONTRACT NUMBER

MATERIAL PROCURED UNDER A

☐ DIRECT GOVERNMENT CONTRACT ☐ SUBCONTRACT

1. HAS ANY PART OF THE DOCUMENT CREATED PROBLEMS OR REQUIRED INTERPRETATION IN PROCUREMENT USE?

A. GIVE PARAGRAPH NUMBER AND WORDING.

B. RECOMMENDATIONS FOR CORRECTING THE DEFICIENCIES

2. COMMENTS ON ANY DOCUMENT REQUIREMENT CONSIDERED TOO RIGID

3. IS THE DOCUMENT RESTRICTIVE?

☐ YES ☐ NO (If "Yes", in what way?)

4. REMARKS

SUBMITTED BY (Printed or typed name and address - Optional)

TELEPHONE NO.

DATE

DD FORM 1426
1 JAN 72

REPLACES EDITION OF 1 JAN 66 WHICH MAY BE USED

C 1 6 0 6 1

C. _____

ASD/ENYESS
Wright-Patterson AFB, O 45433
OFFICIAL BUSINESS
PENALTY FOR PRIVATE USE \$300

POSTAGE AND FEES PAID
DEPARTMENT OF THE AIR FORCE
DoD-318



ASD/ENYESS
Wright-Patterson AFB, Ohio 45433

FOLD

MILITARY SPECIFICATION

AIRPLANE DAMAGE TOLERANCE REQUIREMENTS

This specification is approved for use by all Departments
and Agencies of the Department of Defense

1. SCOPE

1.1 This specification contains the damage tolerance design requirements applicable to airplane safety of flight structure. The objective is to protect the safety of flight structure from potentially deleterious effects of material, manufacturing and processing defects through proper material selection and control, control of stress levels, use of fracture resistant design concepts, manufacturing and process controls and the use of careful inspection procedures.

2. APPLICABLE DOCUMENTS

2.1 The following documents, of the issue in effect on date of invitation for bids or request for proposal, form a part of this specification to the extent specified herein:

SPECIFICATIONS

Military

MIL-A-8866	Airplane Strength and Rigidity, Ground Tests
MIL-A-8867	Airplane Strength and Rigidity, Reliability Requirements, Repeated Loads and Fatigue

STANDARDS

Military

MIL-STD-1530	Aircraft Structural Integrity Program Airplane Requirements
--------------	---

(Copies of documents required by suppliers in connection with specific procurement functions should be obtained from the procuring activity or as directed by the contracting officer.)

3. REQUIREMENTS

3.1 General requirements. Detailed damage tolerance requirements are specified in 3.2 in various categories as a function of design concept and degree of inspectability. The design concepts and various degrees of inspectability are defined in 6.2. The contractor shall demonstrate that all safety of flight structures comply with the detailed requirements in a minimum of one of these categories (one design concept and one inspectability level). Design concepts utilizing multiple load paths and crack arrest features may be qualified under the appropriate inspectability level(s) as either slow crack growth or fail-safe structure. Single-load path structure without crack arrest features must be qualified at the appropriate inspectability level(s) as slow crack growth structure. The contractor shall perform all of the analytical and experimental work necessary to demonstrate compliance with the damage tolerance analyses and tests as specified herein, MIL-STD-1530, MIL-A-8867 and the procurement contract. This effort involves residual strength and crack growth analyses and tests. The analyses shall assume the presence of flaws placed in the most unfavorable location and orientation with respect to the applied stresses and material properties. The crack growth analyses shall predict the growth behavior of these flaws in the chemical, normal, and sustained and cyclic stress environments to which that portion of the component shall be subjected in service. The design flight by flight stress spectra and chemical and thermal environment spectra shall be developed by the contractor and approved by the procuring activity. Spectra interaction effects, such as variable loading and environment, shall be accounted for.

3.1.1 Initial flaw assumptions. Initial flaws shall be assumed to exist as a result of material and structure manufacturing and processing operations. Small imperfections equivalent to an .005 inch radius corner flaw resulting from these operations shall be assumed to exist in each hole of each element in the structure, and provide the basis for the requirements in 3.1.1.1c, 3.1.1.2, 3.1.1.3.1 and 3.1.1.3.2. If the contractor has developed initial quality data on fastener holes, (e.g., by fractographic studies, which provides a sound basis for determining equivalent initial flaw sizes), these data may be submitted to the procuring activity for review and serve as a basis for negotiating a size different than the specified .005 inch radius corner flaw. In addition, it shall be assumed that initial flaws of the sized specified in 3.1.1.1a, and b, can exist in any separate element of the structure. Each element of the structure shall be surveyed to determine the most critical location for the assumed initial flaws considering such features as edges, fillets, holes and other potentially high stressed areas. Only one initial flaw in the most critical hole and one initial flaw at a location other than a hole need be assumed to exist in any structural element. Interaction between these assumed initial flaws need not be considered. For multiple and adjacent elements, the initial flaws need not be situated at the same location, (e.g., chordwise plane in wing structure), except for structural elements where

fabrication and assembly operations are conducted such that flaws in two or more elements can exist at the same location. The most common example of such an operation is the assembly drilling of attachment holes. Except as noted in 3.1.1.2 and 3.1.1.3 more than one source of common initial cracks need not be assumed along the crack growth path. Initial flaw sizes are specified in terms of specific flaw shapes, such as through the thickness or corner flaws at holes and semi-elliptical surface flaws or through the thickness flaws at locations other than holes.

3.1.1.1 Initial flaw size. Specified initial flaw sizes presume the inspection of 100 percent of all fracture critical regions of all structural components as required by the fracture control provisions of MIL-STD-1530. This inspection shall include as a minimum a close visual inspection of all holes and cutouts and conventional ultrasonic, penetrant or magnetic particle inspection of the remainder of the fracture critical region. Where the use of automatic hole preparation and fastener installation equipment preclude close visual and dimensional inspection of 100 percent of the holes in the fracture critical regions of the structure, a plan to qualify and monitor hole preparation and fastener installation shall be prepared, approved by the procuring activity and implemented by the contractor. Where special nondestructive inspection procedures have demonstrated a detection capability better than indicated by the flaw sizes specified in (a) below, and the resulting smaller assumed flaw sizes are used in the design of the structure, these special inspection procedures shall be used in the aircraft manufacturing quality control.

a. Slow crack growth structure.

At holes and cutouts the assumed initial flaw shall be a .05 inch through the thickness flaw at one side of the hole when the material thickness is equal to or less than .05 inch. For material thicknesses greater than .05 inch, the assumed initial flaw shall be a .05 inch radius corner flaw at one side of the hole.

At locations other than holes, the assumed initial flaw shall be a through the thickness flaw .25 inch in length when the material thickness is equal to or less than .125 inch. For material thicknesses greater than .125 inch, the assumed initial flaw shall be a semicircular surface flaw with a length (2c) equal to .25 inch and a depth (a) equal to .125 inch. Other possible surface flaw shapes with the same initial stress intensity factor (K) shall be considered as appropriate. For example, corner flaws at edges of structural elements and longer and shallower surface flaws in plates which are subjected to high bending stresses.

Smaller initial flaw sizes than those specified above may be assumed subsequent to a demonstration, described in 4.2, that all flaws larger than these assumed sizes have at least a 90 percent probability of detection with a 95 percent confidence level. Smaller initial flaw sizes may also be assumed if proof test inspection is used. In this case, the minimum assumed initial flaw size shall be the calculated critical size at the proof test stress level and temperature using procuring activity approved upper bound of the material fracture toughness data.

b. Fail safe structure.

At holes and cutouts the assumed initial flaw shall be a .02 inch through the thickness flaw at one side of the hole when the material thickness is equal to or less than .02 inch. For material thicknesses greater than .02 inch the assumed initial flaw shall be a .02 inch radius corner flaw at one side of the hole.

At locations other than holes, the assumed initial flaw shall be a through the thickness flaw .10 inch in length when the material thickness is equal to or less than .05 inch. For material thicknesses greater than .05 inch, the assumed initial flaw shall be a semicircular surface flaw with a length (2c) equal to .10 inch and a depth (a) equal to .05 inch. Other possible surface flaw shapes with the same initial stress intensity factor (K) shall be considered as appropriate.

c. The fastener policy.

The beneficial effects of interference fasteners, cold expanded holes, joint clamp-up and other specific joint design and assembly procedures may be used in achieving compliance to the flaw growth requirements of this specification. These beneficial effects shall be demonstrated by laboratory tests of joints representative of the joints in the aircraft. The test specimens shall contain pre-cracked fastener holes. The limits of the beneficial effects to be used in design shall be approved by the procuring activity, but in no case shall the assumed initial flaw be smaller than an .005 inch radius corner flaw at one side of an as manufactured, non-expanded hole containing a net fit fastener in a non-clamped-up joint.

3.1.1.2 Continuing damage. Cyclic growth behavior of assumed initial flaws may be influenced by the particular geometry and arrangement of elements of the structure being qualified. The following assumptions of continuing crack growth shall be considered for those cases where the primary crack terminates due to structural discontinuities or element failure.

- a. When the primary damage and growth originates in a fastener hole and terminates prior to member or element failure, continuing damage shall be an .005 inch radius corner flaw emanating from the diametrically opposite side of the fastener hole at which the initial flaw was assumed to exist.
- b. When the primary damage terminates due to a member or element failure, the continuing damage shall be an .005 inch radius corner flaw in the most critical location of the remaining element or remaining structure or a surface flaw having $2c = .02$ inch and $a = .01$ inch, where, a , is measured in the direction of crack growth, plus the amount of growth (Δa) which occurs prior to element failure.
- c. When the crack growth from the assumed initial flaw enters into and terminates at a fastener hole, continuing damage shall be an .005 inch radius corner flaw $+ \Delta a$ emanating from the diametrically opposite side of the fastener hole at which the primary damage terminated.

3.1.1.3 Remaining structure damage

3.1.1.3.1 Fail safe multi-load path. The damage assumed to exist in the adjacent load path at the location of primary failure in fail safe multiple load path structure at the time of and subsequent to the failure of a primary load path shall be as follows:

- a. Multiple load path dependent structure. The same as specified in 3.1.1.1b plus the amount of growth (Δa) which occurs prior to load path failure.
- b. Multiple load path independent structure. The same as 3.1.1.2b plus the amount of growth (Δa) which occurs prior to load path failure.

3.1.1.3.2 Fail safe crack arrest structure. For structure classified as fail safe-crack arrest, the primary damage assumed to exist in the structure following arrest of a rapidly propagating crack shall depend upon the particular geometry. In conventional skin stringer (or frame) construction this shall be assumed as two panels (bays) of cracked skin plus the broken central stringer (or frames). Where tear straps are provided between stringers (or frames) this damage shall be assumed as cracked skin between tear straps plus the broken central stringer (or frame). Other configurations shall assume equivalent damage as mutually agreed upon by the contractor and the procuring activity. The damage assumed to exist in the structure adjacent to the primary damage shall be as specified in 3.1.1.2b or c.

3.1.2 In-Service inspection flaw assumptions. The smallest damage which can be presumed to exist in the structure after completion of a depot or base level inspection shall be as follows:

- a. If the component is to be removed from the aircraft and completely inspected with NDI procedures the same as those performed during fabrication, the minimum assumed damage size shall be as specified in 3.1.1.1.
- b. Where NDI techniques such as penetrant, magnetic particle or ultrasonics are applied without component or fastener removal, the minimum assumed flaw size at holes and cutouts shall be a through the thickness crack emanating from one side of the hole having a 0.25 inch uncovered length when the material thickness is equal to or less than 0.25 inch. For material thicknesses greater than 0.25 inch, the assumed initial flaw shall be a quarter-circular corner crack emanating from one side of the hole having a 0.25 inch uncovered length. The minimum assumed flaw size at locations other than holes shall be a through the thickness crack of length 0.50 inch when the material thickness is equal to or less than 0.25 inch. For material thicknesses greater than 0.25 inch, the assumed initial flaw shall be a semi-circular surface flaw with length (2c) equal to 0.50 inch and depth (a) equal to 0.25 inch. Other possible surface flaw shapes with the same initial stress intensity factor (K) shall be considered as appropriate such as corner flaws at edges of structural members and longer and shallower surface flaws in plates which are subjected to high bending stresses. While X-ray inspection may be used to supplement one or more of the other NDI techniques, it, by itself, shall not be considered capable of reliably detecting tight subcritical cracks.
- c. Where accessibility allows close visual inspection (using visual aid as necessary) an opening through the thickness crack having at least 2 inches of uncovered length shall be the minimum assumed damage size.
- d. Where accessibility, paint, sealant, or other factors preclude close visual inspection or the use of NDI techniques such as described in b above, slow crack growth structure shall be considered to be non-inspectable, and fail-safe structure shall be considered to be inspectable only for major damage such as a load path failure, or arrested unstable crack growth.

3.1.3 Residual strength requirements. The minimum required residual strength is specified in terms of the minimum internal member load, P_{XX} , which the aircraft must be able to sustain with damage present and without endangering safety of flight or degrading performance of the aircraft for the specified minimum period of unrepaired service usage. This includes loss of strength, loss of stiffness, excessive permanent deformation, loss of control, and reduction of the flutter speed below V_L . The magnitude of P_{XX} depends on the overall degree of inspectability of the structure and is intended to represent the maximum load the aircraft might encounter during a specified inspection interval or during a design lifetime for non-inspectable structure. The XX subscript is defined as a function of the specific degree of inspectability in table 1.

The aircraft loading spectrum shall be derived from a mission analysis where the mission mix and the loads in each mission segment represent average aircraft usage. The basic load factor exceedance data is specified in MIL-A-8866. To account for the fact that any individual aircraft may encounter loads considerably in excess of the average during their life, the required residual strength (i.e. the P_{XX} load) must be larger than the average load expected during a given interval between inspections. This is accomplished by magnifying the inspection interval. For example, the P_{XX} load for ground evident damage is the maximum average load that can be expected once in 100 flights. Table 1 defines the P_{XX} loads for the various degrees of inspectability.

TABLE 1

P_{XX}^*	Degree of Inspectability	Typical Inspection Interval	Magnification Factor, M
P_{FE}	In-Flight Evident	One Flight	100
P_{GE}	Ground Evident	One Flight	100
P_{WV}	Walk-Around Visual	Ten Flights	100
P_{SV}	Special Visual	One Year	50
P_{DM}	Depot or Base Level	1/4 Lifetime	20
P_{LT}	Non-Inspectable	One Lifetime	20

* P_{XX} = Maximum average internal member load that will occur once in M times the inspection interval. Where P_{DM} or P_{LT} is determined to be less than the design limit load, the design limit load shall be the required residual strength load level. P_{XX} need not be greater than 1.2 times the maximum load in one lifetime, if greater than design limit load.

For fail safe structure there is a requirement to sustain a minimum load, P_{YY} , at the instant of load path failure (or crack arrest) as well as being able to sustain the load, P_{XX} , subsequent to load path failure (or crack arrest) at any time during the specified inspection interval. The single load path failure (or crack arrest) load, P_{YY} , shall include a dynamic factor (D.F.). In lieu of test or analytical data to the contrary a dynamic factor of 1.15 shall be applied to the redistributed incremental load. P_{YY} should be equal to the internal member load at design limit load or D.F. times P_{XX} , whichever is greater.

3.2 Specific requirements. Specific damage tolerance requirements for Slow crack growth structure, Fail-Safe multiple load path structure, and Fail-Safe crack arrest structure as specified in 3.2.1, 3.2.2 and 3.2.3, respectively.

3.2.1 Slow crack growth structure. Of the degrees of inspectability in accordance with 6.2.1, only depot or base level inspectable and in-service non-inspectable are applicable to slow crack growth structures. The frequency of inspection for both shall be as stated below unless otherwise specified in the appropriate contractual documents.

Depot or Base Level inspectable - Once every one quarter of the design lifetime.

In-Service non-inspectable - Once at the end of one design lifetime.

3.2.1.1 Depot or base level inspectable. The damage which can be presumed to exist in the structure after completion of a depot or base level inspection shall be that specified for slow crack growth structure in 3.1.2. These damage sizes shall not grow to critical size and cause failure of the structure due to the application of P_{DM} in two (2) times the inspection interval as specified in 3.2.1.

3.2.1.2 In-Service non-inspectable. The initial damage size as specified in 3.1.1.1 shall not grow to critical size and cause failure of the structure due to the application of P_{LT} in two (2) design service lifetimes.

3.2.2 Fail-Safe multiple load path structure. The degrees of inspectability as specified in 6.2.1, which can be applicable to fail-safe multiple load path structure, are In-Flight evident inspectable, Ground evident inspectable, Walkaround inspectable, Special visual inspectable, and Depot or Base level inspectable.

3.2.2.1 Inspection intervals. The frequency of inspection for each of the inspectability levels shall be as stated below unless otherwise specified in the appropriate contractual documents.

In-Flight evident inspectable - Once per flight.

Ground evident inspectable - Once per flight.

Walkaround inspectable - Once every ten (10) flights.

Special visual inspectable - As proposed by the contractor and approved by the procuring activity, but not more frequently than once per year.

Depot or Base level inspectable - Once every one quarter of the design lifetime.

3.2.2.2 Residual strength requirements and damage growth limits. There are two sets of residual strength requirements and damage growth limits for fail-safe multiple load path structure. The first set applies to the required residual strength and damage growth limits for intact structure, (i.e., the structure prior to a load path failure), and the second set applies to the remaining structure subsequent to a load path failure. These are described in 3.2.2.2.1 and 3.2.2.2.2, respectively, and are summarized in table II.

3.2.2.2.1 Intact structure. The requirements for the intact structure are a function of the depot or base level inspectability of the intact structure for damage sizes which are less than a load path failure, (i.e., subcritical cracks and small element failures). If the structure is depot or base level inspectable the smallest damage sizes which can be presumed to exist in the structure after completion of a depot or base level inspection shall be those as specified in 3.1.2. These damage sizes shall not grow to a size such as to cause load path failure due to the application of P_{DM} in one depot or base level inspection interval. If the structure is not depot or base level inspectable for subcritical flaws or small element failures which are less than a load path failure (either by virtue of small critical flaw sizes or inspection problems) the initial material and manufacturing damage as specified in 3.1.1.1.b shall be assumed and it shall not grow to the size required to cause load path failure due to the application of P_{LT} in one design lifetime.

3.2.2.2.2 Remaining structure subsequent to a load path failure. For each of the five levels of inspectability specified in 3.2.2 the remaining structure at the time of a load path failure shall be able to sustain the P_{YY} load as described in 3.1.3 without loss of the aircraft. In addition, subsequent to load path failure, the failed load path plus the minimum assumed damage in the remaining adjacent structure as specified in 3.1.1.3.1 shall not grow to a size such as to cause loss of the aircraft due to the application of the P_{XX} load in the specified minimum period of unrepaired service usage. The P_{XX} loads and minimum periods of unrepaired service usage for each of the five inspectability levels shall be as follows:

<u>Inspectability</u>	<u>P_{XX} per 3.1.3</u>	<u>Minimum Period of Unrepaired Service Usage</u>
In-Flight Evident	P_{FE}	Return to base
Ground Evident	P_{GE}	One Flight
Walkaround	P_{WV}	5 X Inspection Interval*
Special Visual	P_{SV}	2 X Inspection Interval*
Depot or Base Level	P_{DM}	2 X Inspection Interval*

*See 3.2.2.1

TABLE II
FAIL-SAFE MULTIPLE LOAD PATH STRUCTURE

INSPECTABILITY	Residual strength req. and damage growth limits for intact structure	Residual strength req. and damage growth limits for remaining structure subsequent to load path failure
IN-FLIGHT EVIDENT	<p>○ If Structure is Depot or Base Level Inspectable for less than Failed Load Path (e.g. subcritical flaws):</p> <p>(a) P_{DM} shall not grow critical ϕ P_{DM} in one Depot or Base Level inspection interval</p>	<p>○ Must sustain P_{YY} at time of load path failure</p> <p>○ λ shall not cause aircraft failure @ P_{FE} during return to base</p>
GROUND EVIDENT	<p>(a) P_{DM} shall not grow critical ϕ P_{DM} in one Depot or Base Level inspection interval</p>	<p>○ Must sustain P_{YY} at time of failure.</p> <p>○ λ shall not cause aircraft failure @ P_{GE} in one flight</p>
WALK-ROUND VISUAL	<p>or</p> <p>○ If Structure is not Depot or Base Level inspectable for Less than Failed Load Path:</p>	<p>○ Must sustain P_{YY} at time of failure</p> <p>○ λ shall not cause aircraft failure @ P_{NW} in 5 times the inspection interval</p>
SPECIAL VISUAL	<p>a_i shall not grow to critical ϕ P_{LT} in one lifetime</p>	<p>○ Must sustain P_{YY} at time of failure</p> <p>○ λ shall not cause aircraft failure @ P_{SV} in 2 times the inspection interval</p>
DEPOT OR BASE LEVEL		<p>○ Must sustain P_{YY} at time of failure</p> <p>○ λ shall not cause aircraft failure @ P_{DM} in 2 times the inspection interval</p>

(a) P_{DM} = Assumed Depot or Base Level Damage Sizes specified in 3.1.2

λ = Failed Load Path plus assumed damage in remaining structure as specified in 3.1.1.3.1

a_i = Assumed initial flaw sizes specified in 3.1.1.1.b

P_{YY} = D.F. X P_{LIMIT} or D.F. X P_{XX} whichever is greater

3.2.3 Fail-Safe crack arrest structure. The degrees of inspectability as specified in 6.2.1 which can be applicable to fail-safe crack arrest structure are the same as those for the fail-safe multiple load path structure specified in 3.2.2.

3.2.3.1 Inspection intervals. The frequency of inspection for each of the inspectability levels shall be the same as those specified for fail-safe multiple load path structure in 3.2.2.1.

3.2.3.2 Residual strength requirements and damage growth limits. There are two sets of residual strength requirements and damage tolerance limits for fail-safe crack arrest structure. The first set applies to the intact structure (the structure prior to unstable crack growth and arrest equivalent to that as specified in 3.1.1.3.2) and the second set applies to the remaining structure subsequent to encountering unstable crack growth and arrest. These are described in 3.2.3.2.1 and 3.2.3.2.2, respectively and are summarized in table III.

3.2.3.2.1 Intact structure. The requirements for the intact structure are a function of the depot or base level inspectability of the intact structure for damage sizes which are less than the damage caused by unstable crack growth and arrest as specified in 3.1.1.3.2. If the structure is depot or base level inspectable the smallest damage sizes which can be presumed to exist in the structure after completion of a depot or base level inspection shall be those as specified in 3.1.2. These sizes shall not grow to a size such as to cause unstable crack growth due to the application of P_{DM} in one depot or base level inspection interval. If the structure is not depot or base level inspectable for subcritical flaws, the initial material and manufacturing damage as specified in 3.1.1.1.b shall be assumed and it shall not grow to critical size at P_{LT} in one design lifetime.

3.2.3.2.2 Remaining structure subsequent to crack arrest. For each of the five levels of inspectability applicable to this type of structure the remaining structure at the time of the unstable crack growth shall be able to sustain the P_{yy} load as specified in 3.1.3 without loss of the aircraft. In addition, subsequent to the unstable growth and arrest, damage as specified in 3.1.1.3.2 shall not grow to a size such as to cause loss of the aircraft due to the application of the P_{xx} load in the specified minimum periods of unrepaired usage. The P_{xx} loads and minimum periods of unrepaired service usage for each of the five inspectability levels shall be the same as those specified for fail-safe multiple load path structure in 3.2.2.2.2.

TABLE III
FAIL-SAFE CRACK ARREST STRUCTURE

INSPECTABILITY	Residual strength req. and damage growth limits for intact structure	Residual strength req. and damage growth limits for remaining structure subsequent to unstable growth and arrest
IN-FLIGHT EVIDENT	<p>Q If Structure is Depot or Base Level Inspectable for less than arrested Damage (e.g. subcritical flaws):</p> <p>(a) P_{DM} shall not grow to critical @ P_{DM} in one or Base level inspection interval</p> <p style="text-align: center;">or</p> <p>Q If Structure is not Depot or Base Level Inspectable for less than Arrested Damage:</p> <p>a_i shall not grow to critical @ P_{LT} in one lifetime</p>	<p>Q Must sustain P_{YY} at time of unstable cracking</p> <p>Q L' shall not cause A/C failure @ P_{FE} during return to base</p>
GROUND EVIDENT		<p>Q Must sustain P_{YY} at times of unstable cracking</p> <p>Q L' shall not cause A/C failure @ P_{GE} in one flight</p>
WALL AROUND VISUAL		<p>Q Must sustain P_{YY} at time of unstable cracking</p> <p>Q L' shall not cause A/C failure @ P_{WY} in 5 times the inspection interval</p>
SPECIAL VISUAL		<p>Q Must sustain P_{YY} at time of unstable cracking</p> <p>Q L' shall not cause A/C failure @ P_{SY} in 2 times inspection interval</p>
DEPOT OR BASE LEVEL		<p>Q Must sustain P_{YY} at time of unstable cracking</p> <p>Q L' shall not cause A/C Failure @ P_{DM} in 2 times inspection interval</p>

(a) P_{DM} = Assumed Depot or Base Level Damage Sizes specified in 3.1.2 L' = Damage as specified in 3.1.1.3.2

a_i = Assumed initial flaw sizes specified in 3.1.1.1.b $P_{YY} = D.F. \times P_{LIMIT}$ or D.F. P_{XX} whichever is greater

4. QUALITY ASSURANCE PROVISIONS

4.1 Design data. Design data shall be generated as required to support the analysis effort.

4.2 NDT demonstration program. Where designs are based on initial flaw size assumptions less than those as specified in 3.1.1.1a, a non-destructive testing demonstration program shall be performed by the contractor and approved by the procuring activity to verify that all flaws equal to or greater than the design flaw size will be detected to the specified reliability and confidence levels. The demonstration shall be conducted on each selected inspection procedure using production conditions, equipment and personnel. The defective hardware used in the demonstration shall contain cracks which simulate the case of tight fabrication flaws. Subsequent to successful completion of the demonstration program, specifications on these inspection techniques shall become the manufacturing inspection requirements and may not be changed without a requalifying program subject to procuring activity approval.

5. PREPARATION FOR DELIVERY

NOT APPLICABLE

6. NOTES

6.1 Intended use. This specification is intended for use in the design of all new military airplanes for the procuring activity. It is not intended to be directly applicable to advanced composite structures nor landing gear components. It is also not intended to dictate structural design concepts, however, other requirements that may be imposed on specific aircraft systems (battle or foreign object damage requirements) may limit the choices.

6.2 Definitions

6.2.1 Degree of inspectability. The degree of inspectability of safety of flight structure shall be established in accordance with the following definitions.

6.2.1.1 In-Flight evident inspectable. Structure is in-flight evident inspectable if the nature and extent of damage occurring in flight will result directly in characteristics which make the flight crew immediately and unmistakably aware that significant damage has occurred and that the mission should not be continued.

6.2.1.2 Ground evident inspectable. Structure is ground evident inspectable if the nature and extent of damage will be readily and unmistakably obvious to ground personnel without specifically inspecting the structure for damage.

6.2.1.3 Walkaround inspectable. Structure is walkaround inspectable if the nature and extent of damage is unlikely to be overlooked by personnel conducting a visual inspection of the structure. This inspection normally shall be a visual look at the exterior of the structure from ground level without removal of access panels or doors without special inspection aids.

6.2.1.4 Special visual inspectable. Structure is special visual inspectable if the nature and extent of damage is unlikely to be overlooked by personnel conducting a detailed visual inspection of the aircraft for the purpose of finding damaged structure. The procedures may include removal of access panels and doors, and may permit simple visual aids such as mirrors and magnifying glasses. Removal of paint, sealant, etc, and use of NDI techniques such as penetrant, X-ray, etc. are not part of a special visual inspection.

6.2.1.5 Depot or base level inspectable. Structure is depot or base level inspectable if the nature and extent of damage will be detected utilizing one or more selected nondestructive inspection procedures. The inspection procedures may include NDI techniques such as penetrant, X-ray, ultrasonic, etc. Accessibility considerations may include removal of those components designed for removal.

6.2.1.6 In-Service non-inspectable structure. Structure is in-service non-inspectable if either damage size or accessibility preclude detection during one or more of the above inspections.

6.2.2 Frequency of inspection. Frequency of inspection is the number of times that a particular type of inspection is to be conducted during the service life of the aircraft.

6.2.3 Minimum period of unrepaired service usage. Minimum period of unrepaired service usage is that period of time during which the appropriate level of damage (assumed initial or in-service) is presumed to remain unrepaired and allowed to grow within the structure.

6.2.4 Minimum assumed initial damage size. The minimum assumed initial damage size is the smallest crack-like defect which shall be used as a starting point for analyzing residual strength and crack growth characteristics of the structure.

6.2.5 Safety of flight structure. That structure whose failure could cause direct loss of the aircraft, or whose failure if it remained undetected could result in loss of the aircraft.

6.2.6 Fracture critical structure. Safety of flight structural components or regions of safety of flight structural components which are either sized by the requirements of this specification (Category I fracture critical parts), or could be sized by the requirements of this specification if fracture control procedures are not employed (Category II fracture critical parts).

6.2.7 Minimum assumed in-service damage size. The minimum assumed in-service damage size is the smallest damage which shall be assumed to exist in the structure after completion of an in-service inspection.

6.2.8 Slow crack growth structure. Slow crack growth structure consists of those design concepts where flaws or defects are not allowed to attain the critical size required for unstable rapid propagation. Safety is assured through slow crack growth for specified periods of usage depending upon the degree of inspectability. The strength of slow crack growth structure with subcritical damage present shall not be degraded below a specified limit for the period of unrepaired service usage.

6.2.9 Crack arrest fail safe structure. Crack arrest fail safe structure is structure designed and fabricated such that unstable rapid propagation will be stopped within a continuous area of the structure prior to complete failure. Safety is assured through slow crack growth of the remaining structure and detection of the damage at subsequent inspections. Strength of the remaining undamaged structure will not be degraded below a specified level for the specified period of unrepaired service usage.

6.2.10 Multiple load path-fail safe structure. Multiple load path fail safe structure is designed and fabricated in segments (with each segment consisting of one or more individual elements) whose function it is to contain localized damage and thus prevent complete loss of the structure. Safety is assured through slow crack growth in the remaining structure to the subsequent inspection. The strength and safety will not degrade below a specified level for a specified period of unrepaired service usage.

6.2.10.1 Multiple load path-dependent structure. Multiple load path structure is classified as dependent if, by design, a common source of cracking exists in adjacent load paths at one location due to the nature of the assembly or manufacturing procedures. An example of multiple load path-dependent structure is planked tension skin where individual members are spliced in the spanwise direction by common fasteners with common drilling and assembly operations.

6.2.10.2 Multiple load path-independent structure. Multiple load path structure is classified as independent if by design, it is unlikely that a common source of cracking exists in more than a single load path at one location due to the nature of assembly or manufacturing procedures.

MIL-A-83444 (USAF)

6.3 Ordering data. MIL-A-008866A(USAF) dated 31 March 1971 and MIL-A-008867A(USAF) dated 31 March 1971 or later issue will be used in conjunction with this specification.

Custodian:
Air Force - 11

Preparing activity:
Air Force - 11

Project No. 1510-F022

STANDARDIZATION DOCUMENT IMPROVEMENT PROPOSAL

OMB Approval
No. 32-R255

INSTRUCTIONS: The purpose of this form is to solicit beneficial comments which will help achieve procurement of suitable products at reasonable cost and minimum delay, or will otherwise enhance use of the document. DoD contractors, government activities, or manufacturers/vendors who are prospective suppliers of the product are invited to submit comments to the government. Fold on lines on reverse side, staple in corner, and send to preparing activity. Comments submitted on this form do not constitute or imply authorization to waive any portion of the referenced document(s) or to amend contractual requirements. Attach any pertinent data which may be of use in improving this document. If there are additional papers, attach to form and place both in an envelope addressed to preparing activity.

DOCUMENT IDENTIFIER AND TITLE

NAME OF ORGANIZATION AND ADDRESS

CONTRACT NUMBER

MATERIAL PROCURED UNDER A

☐ DIRECT GOVERNMENT CONTRACT ☐ SUBCONTRACT

1. HAS ANY PART OF THE DOCUMENT CREATED PROBLEMS OR REQUIRED INTERPRETATION IN PROCUREMENT USE?

A. GIVE PARAGRAPH NUMBER AND WORDING.

B. RECOMMENDATIONS FOR CORRECTING THE DEFICIENCIES

2. COMMENTS ON ANY DOCUMENT REQUIREMENT CONSIDERED TOO RIGID

3. IS THE DOCUMENT RESTRICTIVE?

☐ YES ☐ NO (If "Yes", in what way?)

4. REMARKS

SUBMITTED BY (Printed or typed name and address - Optional)

TELEPHONE NO.

DATE

DD FORM 1426
1 JAN 74

REPLACES EDITION OF 1 JAN 65 WHICH MAY BE USED

016001

FOLD

4950/TZS
Wright-Patterson AFB, O 45433
OFFICIAL BUSINESS
PENALTY FOR PRIVATE USE \$300

POSTAGE AND FEES PAID
DEPARTMENT OF THE AIR FORCE
DOD-318



4950/TZS
Wright-Patterson AFB, Ohio 45433

FOLD

MIL-A-008866B(USAF)
22 August 1975
SUPERSEDING
MIL-A-008866A(USAF)
31 March 1971
USED IN LIEU OF
MIL-A-8866(ASG)
18 May 1960

MILITARY SPECIFICATION

AIRPLANE STRENGTH AND RIGIDITY RELIABILITY REQUIREMENTS, REPEATED LOADS AND FATIGUE

This limited coordination Military Specification has been prepared by the Air Force based upon currently available technical information, but it has not been approved for promulgation as a coordinated revision of Military Specification MIL-A-8866(ASG). It is subject to modification. However, pending its promulgation as a coordinated Military Specification, it may be used in procurement.

1. SCOPE

1.1 This specification identifies the durability design requirements applicable to the structure of airplanes. The complete structure, herein referred to as the airframe, includes the fuselage, wing, empennage, landing gears, control systems and surfaces, engine mounts, structural operating mechanisms, and other components as specified in the contract. This specification applies to metallic and nonmetallic structures. The objective is to minimize the in-service maintenance costs and to obtain operational readiness through proper controls on materials selection and processing, inspections, design details, stress levels, and protection systems.

2. APPLICABLE DOCUMENTS

2.1 The following documents of the issue in effect on the date of invitation for bids or request for proposal, form a part of this specification to the extent specified herein.

SPECIFICATIONS

Military

MIL-A-8861	Airplane Strength and Rigidity, Flight Loads
MIL-A-8867	Airplane Strength and Rigidity Ground Tests
MIL-A-8870	Airplane Strength and Rigidity, Flutter, Divergence, and Other Aeroelastic Instabilities
MIL-A-8871	Airplane Strength and Rigidity, Flight and Ground Operations Tests

FSC 1510

MIL-A-008866B(USAF)

MIL-A-8892 Airplane Strength and Rigidity, Vibration
MIL-A-8893 Airplane Strength and Rigidity, Sonic Fatigue

(Copies of specifications, standards, drawings and publications required by suppliers in connection with specific procurement functions should be obtained from the procuring activity or as directed by the contracting officer.)

3. REQUIREMENTS

3.1 General requirements. The airframe shall be designed such that the economic life is greater than the design service life when subjected to the design service loads/environment spectra. The design objective is to minimize cracking or other structural or material degradation which could result in excessive maintenance problems or in functional problems such as fuel leakage, loss of control effectiveness or loss of cabin pressure. The contractor shall perform the analytical and experimental work necessary to demonstrate compliance with the analysis and tests as required herein, MIL-A-8867, and the contract. The design flight-by-flight load, stress, and environmental spectra shall be developed by the contractor. Spectra interaction effects such as that due to variable loading and environment shall be accounted for in the design.

3.2 Detail requirements

3.2.1 Design service life and design usage. The design service life and design usage will be specified by the procuring activity in the contract. The design service life and design usage will be based on the mission requirements and will be stipulated in terms of:

- a. Total flight hours.
- b. Total number of flights.
- c. Total number and type of landings.
- d. Total service years.
- e. Mission profiles for each type of mission to be flown. (These profiles will be divided into mission segments such as taxi, takeoff run, ascent, cruise, low altitude usage, inflight refueling, air-to-air combat, air-to-ground combat, etc. The mission profiles will also stipulate the approximate duration, altitude, speed, and payload configuration requirements for each mission segment.)
- f. Mission mix or number of flights of each mission.

g. Any other special requirements such as functional check flights, ground maintenance operational checks, etc.

3.2.2 Design service loads spectra. The design service loads spectra for the airframe shall be developed for the design service life and typical design usage of 3.2.1 and shall require approval by the procuring activity. The contractor shall include all significant sources of repeated loads. The sources of repeated loads shall include, but not be limited to, engine ground run-up, functional check-outs, jacking, towing, taxiing, landing, flight maneuvers, atmospheric turbulence, inflight refueling, control system operation, cabin pressurization, buffeting, and terrain following maneuvers. The individual spectra of repeated loads for a particular airplane shall be based on the data referenced in the following subparagraphs as modified and amplified due to the existence of more representative data or unique airplane requirements. The individual spectra of repeated loads shall be assembled on a flight-by-flight basis to form the design service loads sequence. Load occurrences less than once per mission segment or once per flight shall be rationally distributed (randomized or ordered, as appropriate) among appropriate segments and flights. The design service loads spectra shall not be arbitrarily limited to design static limit load if higher values are probable (e.g., once per lifetime airplane load level). An appropriate distribution of weight, center of gravity, configuration, speed, altitude, and other significant operational parameters shall be made within each mission segment.

3.2.2.1 Maneuver. Tables I through VI contain normal maneuver load factor spectra representative of USAF operations of several classes of airplanes prior to 1970 and are contained herein for reference. The contractor shall derive the final maneuver spectra by mission segment and account for variables such as maneuver capability, tactics, etc. These final spectra shall require approval by the procuring activity.

3.2.2.2 Gust. The gust loads spectra shall be developed in accordance with the procedures of MIL-A-8861, paragraph entitled, Continuous turbulence analysis.

3.2.2.3 Landing. The landing loads spectra shall be developed for the number of landings indicated in 3.2.1 including such variables as sinking speed, forward speed, attitude, wing stores, and fuel distribution. The distribution of sinking speeds specified in table VII is for reference.

3.2.2.4 Taxi. The taxi ground loads shall be based on vertical gear inputs resulting from taxi on prepared runways. Table VIII is presented for reference. For airplane classes BII, CASSAULT, and CTRANSPORT, the number of vertical load cycles shall be twice that as specified in table VIII; or the taxi ground loads spectra shall account for the increased frequency of

vertical gear inputs due to unprepared field operations. In lieu of a vertical load cycle spectra such as table VIII, the airplane may be designed for the effect of takeoff, taxiing, and rollout on deterministic runway profiles having power spectral density roughness characteristics as shown on figures 1, 2, and 3 or in the contract. For this option, the analysis shall include the significant rigid and flexible body modes, and gear dynamics. Aerodynamic and propulsion forces shall be included. The number of taxi operations for each of the runway roughness and airfield types shall be specified by the procuring activity, and taxi times and speeds shall require approval by the procuring activity.

3.2.2.5 Braking, pivoting, and turning. Taxi ground loads spectra shall include lateral and longitudinal loads resulting from braking, pivoting, and turning. Hard braking with maximum braking effects will be assumed to occur twice per full-stop landing and medium braking with half-maximum braking effects will be assumed to occur an additional five times per full-stop landing. During a given mission, each full-stop landing that occurs will be included. The effects of antiskid devices will also be included. Pivoting, with half-limit torque load, will be assumed to occur every 10 landings. Turning with a side load factor acting at the airplane center of gravity, reacted by the landing gears alternately inboard and outboard, will be assumed to occur. The magnitude and frequency of occurrences per landing of side load factor will be established by the contractor and will require approval by the procuring activity.

3.2.2.6 Pressurization. The number of pressurization cycles used for design shall be determined by, and be commensurate with, the design usage and design life requirements. Regulator valve nominal setting shall define the maximum pressure for cabins and cockpits.

3.2.2.7 Repeated operation of movable structures. Particular attention shall be given to the impact loads as well as the operational and residual loads that may occur when doors, cowling, landing gear, controls, and other devices are operated consistent with planned usage of the airplane.

3.2.2.8 Control surface balance weight attachments. Repeated load requirements for design of control surface balance weight attachments shall be in accordance with MIL-A-8870, paragraph entitled Mass-balance control surfaces and tabs [sub para (b).]

3.2.2.9 Control system inputs. The design service loads spectra shall include loads generated in performing the selected manual or automatic control functions. Rigid body and flexible modes of the airplane as well as the frequency response characteristics of the control system (including any filters used to modify response to structural modes) shall be considered in the derivation of the load spectra. The loads spectra due to pilot induced maneuvers shall be based on manual command inputs that are rationally derived.

3.2.2.10 Combined loadings. Loading conditions from individual sources of repeated loads shall be combined where appropriate. The contractor shall submit the rationale for combining individual sources of repeated loads to the procuring activity for approval.

3.2.3 Design chemical/thermal environment spectra. The contractor shall develop design chemical/thermal environment spectra. These spectra shall characterize each environment (i.e., intensity, duration, frequency of occurrence, etc.). The chemical/thermal environment spectra shall require approval by the procuring activity.

3.2.4 Analyses. An analysis shall be conducted to demonstrate that the economic life of the airframe is in excess of the design service life when subjected to the design service loads spectra and the design chemical/thermal environment spectra. The approach shall account for those factors affecting the time for cracks or other damage to reach sizes large enough to necessitate the repair, modification, or replacement of components. These factors shall include initial quality and initial quality variations, environment, load sequence and environment interaction effects, material property variations, and analytical uncertainties. The analysis shall demonstrate that cracks in the structure throughout one design lifetime shall not result in sustained crack growth under steady state flight (1G) and ground stress conditions. The design and analyses procedures shall be verified by test to selected design flight-by-flight stress and environment spectra and shall require approval by the procuring activity.

3.2.5 Durability detail design procedures. The contractor shall implement a disciplined procedure for durability design which will minimize the probability of incorporating adverse residual stresses, local design details, materials, processing and fabrication practices into the airplane design and manufacture which could lead to unexpected cracking or failure problems (i.e., those problems which have historically been found early in durability testing or early in service usage). The procedure shall be implemented concurrently with strength design. The procedure shall adequately reflect previous full scale test and fleet experiences as well as other laboratory and development test results. In addition, it shall encompass those managerial actions necessary to monitor and control the durability detail design activities.

3.2.6 Thermal protection. Where structural designs and thermal analyses defining temperature distributions, thermal strain histories, and material allowables are based on use of thermal protection systems (e.g., surface finishes, platings, primers, paints, fire retardant and insulating barriers, etc.), these systems shall be designed and demonstrated to endure the design environment spectra of 3.2.3 unless it can be shown that replacement, repair, or refurbishment at shorter intervals is cost effective. Designing to usage intervals less than the design service life shall require approval by the procuring activity, and the intervals shall not be less than the design inspection intervals specified in the contract.

3.2.7 Corrosion protection. Where structural designs and strength and durability analyses are based on the use of corrosion protection systems (e.g., corrosion resistant materials, ventilation, drainage, and chemically resistant finishes, coatings or barriers), these systems shall be designed and demonstrated to endure the design environment spectra of 3.2.3 unless it can be shown that replacement, repair, or refurbishment at shorter intervals is cost effective. Designing to usage intervals less than the design service life shall require approval by the procuring activity, and the intervals shall not be less than the design inspection intervals specified in the contract. The corrosion prevention and control plan shall be as specified in the contract.

3.2.8 Wear endurance. Excessive wear of structural components, elements, and major bearing surfaces which would interfere with function of the part shall not occur within the design service life and design usage unless it can be shown that replacement, repair, or refurbishment at shorter intervals is cost effective. Designing to usage intervals less than the design service life shall require approval by the procuring activity, and the intervals shall not be less than the design inspection intervals specified in the contract. Wear endurance during movement of structural surfaces and elements shall be considered as well as wear endurance of maintenance access panels, doors, and other removable parts during repeated removal, ground handling, and reinstallation.

3.2.9 Other durability considerations. The contractor shall develop and apply criteria for other durability considerations such as foreign object damage and special environments such as runway debris, sand, gravel, rain, hail, and lightning strikes. These considerations can arise due to airplane configurations, operation on substandard runways, or special atmospheric conditions. The criteria for these other durability considerations shall require approval by the procuring activity.

4. QUALITY ASSURANCE PROVISIONS

4.1 Design data. Structural design and analysis data shall be prepared and submitted as specified in the contract.

4.2 Laboratory tests. Laboratory tests shall be in accordance with MIL-A-8867.

4.3 Flight tests. Flight tests shall be in accordance with MIL-A-8871.

5. PREPARATION FOR DELIVERY

5.1 Section 5 is not applicable to this specification.

6. NOTES

6.1 Intended use. This specification is intended for use in the design of the airframe of all new USAF airplanes. Selected parts of this specification may also be used in the design of major modifications of existing USAF airplanes. Vibration and sonic durability design requirements are contained in MIL-A-8892 and MIL-A-8893, respectively.

6.2 Definitions. Definitions will be in accordance with the documents listed in Section 2 and as specified herein.

6.2.1 Durability. The ability of the airframe to resist cracking (including stress corrosion and hydrogen induced cracking), corrosion, thermal degradation, delamination, wear, and the effects of foreign object damage for a specified period of time.

6.2.2 Economic life. That operational life indicated by the results of the durability test program (i.e., test performance interpretation and evaluation in accordance with MIL-A-8867) to be available with the incorporation of USAF approved and committed production or retrofit changes and supporting application of the force structural maintenance plan in accordance with MIL-STD-1530. (In general, production or retrofit changes will be incorporated to correct local design and manufacturing deficiencies disclosed by the test. It will be assumed that the economic life of the test article has been attained with the occurrence of widespread damage which is uneconomical to repair and, if not repaired, could cause functional problems affecting operational readiness. This can generally be characterized by a rapid increase in the number of damage locations or repair costs as a function of cyclic test time.)

6.2.3 Initial quality. A measure of the condition of the airframe relative to flaws, defects, or other discrepancies in the basic materials or introduced during manufacture of the airframe.

6.2.4 Structural operating mechanisms. Those operating, articulating, and control mechanisms which transmit structural forces during actuation and movement of structural surfaces and elements.

6.3 Marginal indicia. Asterisks are not used in this revision to identify changes with respect to the previous issue due to the extensiveness of the changes.

Custodian:
Air Force - 11

Preparing activity
Air Force - 11

Project No. 1510-F023

MIL-A-008866B(USAF)

TABLE I. Maneuver-Load-Factor Spectra for A, F, TF Classes, Cumulative Occurrences per 1000 Flight Hours by Mission Segment

N_z	Ascent	Cruise	Descent	Loiter	Air-Grnd	Spec Wpn	Air-Air
Positive							
2.0	5000	10,000	20,000	15,000	175,000	70,000	300,000
3.0	90	2,500	5,500	2,200	100,000	25,000	150,000
4.0	1	400	500	250	40,000	7,500	50,000
5.0		1	1	25	10,000	2,000	13,000
6.0				1	1,500	250	3,300
7.0					200	15	900
8.0					15	1	220
9.0					1		60
10.0							15
Negative							
0.5					10,000		44,000
0					350		4,000
-0.5					30		1,200
-1.0					7		350
-1.5					3		60
-2.0					1		8
-2.5							1

TABLE II. Maneuver-Load-Factor Spectra for T, Trainer Class, Cumulative Occurrences per 1000 Flight Hours by Mission Type

N ₂	Transition		Formation	Instruments & Navigation	Administrative & Test
	Basic	Advanced			
Positive					
2.0	20,000	35,000	30,000	10,000	25,000
2.5	4,000	18,000	10,000	2,500	8,000
3.0	1,500	10,000	4,000	1,000	3,500
3.5	500	5,000	2,200	500	1,700
4.0	150	2,500	1,200	250	900
4.5	55	1,000	600	55	450
5.0	20	350	250	20	170
5.5	7	110	90	7	50
6.0	3	30	25	3	15
6.5		9	5	1	4
7.0		2.5	1		
7.5		1			
Negative					
0	280	3,700	4,800	1,200	2,800
-0.5	38	320	160	38	330
-1.0	20	100	20	3	110
-1.5	4	34	6	1	47
-2.0		10	1	0.6	18
-2.5		2			

TABLE III. Maneuver-Load-Factor Spectra for B_I, Bomber Class, Cumulative Occurrences per 1000 Flight Hours by Mission Type

N _z	Special Weapons	Transition	Air-Ground
Positive			
1.3	29,000	10,000	31,000
1.6	22,500	5,000	29,000
1.9	17,500	2,700	20,000
2.2	12,500	1,300	15,000
2.5	8,000	600	10,000
2.8	5,000	275	6,500
3.1	2,800	100	4,000
3.4	1,600	45	2,400
3.7	800	18	1,250
4.0	400	7	650
4.3	200	2	300
4.6	70	1	130
5.0	15		35
Negative			
0.7	525	250	1,300
0.5	450	150	1,000
0.3	350	85	700
0.1	235	35	450
0	170	17	350
-0.1	100	7	250
-0.3	1	1	90
-0.5			1

TABLE IV. Maneuver-Load-Factor Spectra for B₁₁, Bomber Class Cumulative Occurrences per 1000 Flight Hours by Mission Segment

N ₂	Ascent	Cruise	Descent	Refueling
Positive				
1.2	54,000	13,000	50,000	40,000
1.4	7,200	1,300	6,000	1,300
1.6	900	150	600	100
1.8	100	25	80	10
2.0	10	4	15	1
2.2	1	1	4	
2.4		0.15	1	
2.6		0.08	0.3	
2.8			0.1	
3.0			0.03	
Negative				
0.9	80,000	20,000	85,000	260,000
0.8	26,000	4,200	31,000	30,000
0.7	7,700	960	11,000	4,300
0.6	2,500	240	3,900	830
0.5	780	60	1,050	200
0.3	86	4	51	20
0.1	16	0.7	4	3.5
0	7		0.7	1
-0.2	1.5			
-0.4	0.4			
-0.6	0.1			

TABLE V. Maneuver-Load-Factor Spectra for CTRANSPORT, Cargo Class,
Cumulative Occurrences per 1000 Flight Hours by Mission Segment

N _z	Logistics			Training			Refuel
	Ascent	Cruise	Descent	Ascent	Cruise	Descent	
Positive							
1.2	11,000	825	13,000	60,000	45,000	35,000	8,000
1.4	380	30	435	5,600	4,000	3,500	850
1.6	25	3	28	500	350	800	110
1.8	4.5	0.7	5	70	35	250	20
2.0	1.8			15	5	90	2.5
2.2				4	1	35	
2.4				2		11	
2.6				1		4.5	
2.8						1.5	
Negative							
0.9	6,800	600	7,000	12,000	7,200	10,000	3,000
0.8	2,500	150	3,000	5,000	1,500	1,700	800
0.7	600	75	680	1,000	200	350	200
0.6	100	20	120	200	30	85	70
0.4	1	0.8	1	7	1	7	8
0.2						0.6	2

TABLE VI. Maneuver-Load-Factor Spectra for C_{ASSAULT}, Cargo Class,
Cumulative Occurrences per 1000 Flight Hours by Mission Segment

N ₂	Ascent	Cruise	Descent
Positive			
1.2	14,000	3,500	26,000
1.4	1,000	300	1,500
1.6	120	35	300
1.8	15	6	50
2.0	3	2	10
2.2	0.7	0.7	3
2.4		0.4	1
2.6		0.25	0.5
2.8			0.3
3.0			0.18
3.2			0.12
Negative			
0.8	4,700	1,000	5,000
0.6	105	30	100
0.4	8	3	3
0.2	2	0.3	
0	0.5		

TABLE VII. Cumulative Occurrences of Sinking Speed/1000 Landings

Sinking Speed FPS	Trainer	All Other Classes
0.5	1000	1000
1.5	870	820
2.5	680	530
3.5	460	270
4.5	270	115
5.5	145	37
6.5	68	11
7.5	31	3.0
8.5	14	1.5
9.5	6.0	0.5
10.5	3.0	0
11.5	1.5	
12.5	0.5	
13.5	0	

TABLE VIII. Cumulative Occurrences Per Thousand Runway Landings
That Load Factor N_z is Experienced at the Airplane CG

N_z	Cumulative Occurrences
1 \pm 0	494,000
1 \pm 0.1	194,000
1 \pm 0.2	29,000
1 \pm 0.3	2,100
1 \pm 0.4	94
1 \pm 0.5	4
1 \pm 0.6	0.155
1 \pm 0.7	0.005
1 \pm 0.8	0

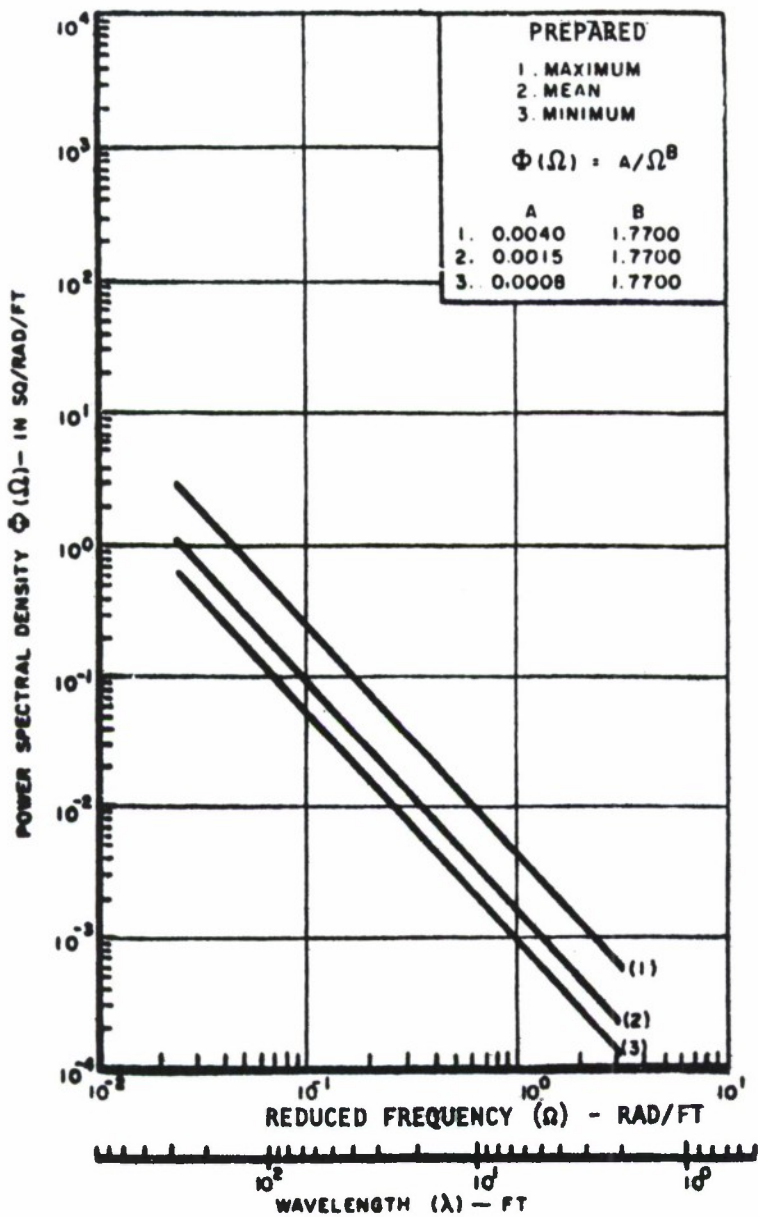


FIGURE 1. Roughness Levels For Prepared Airfields

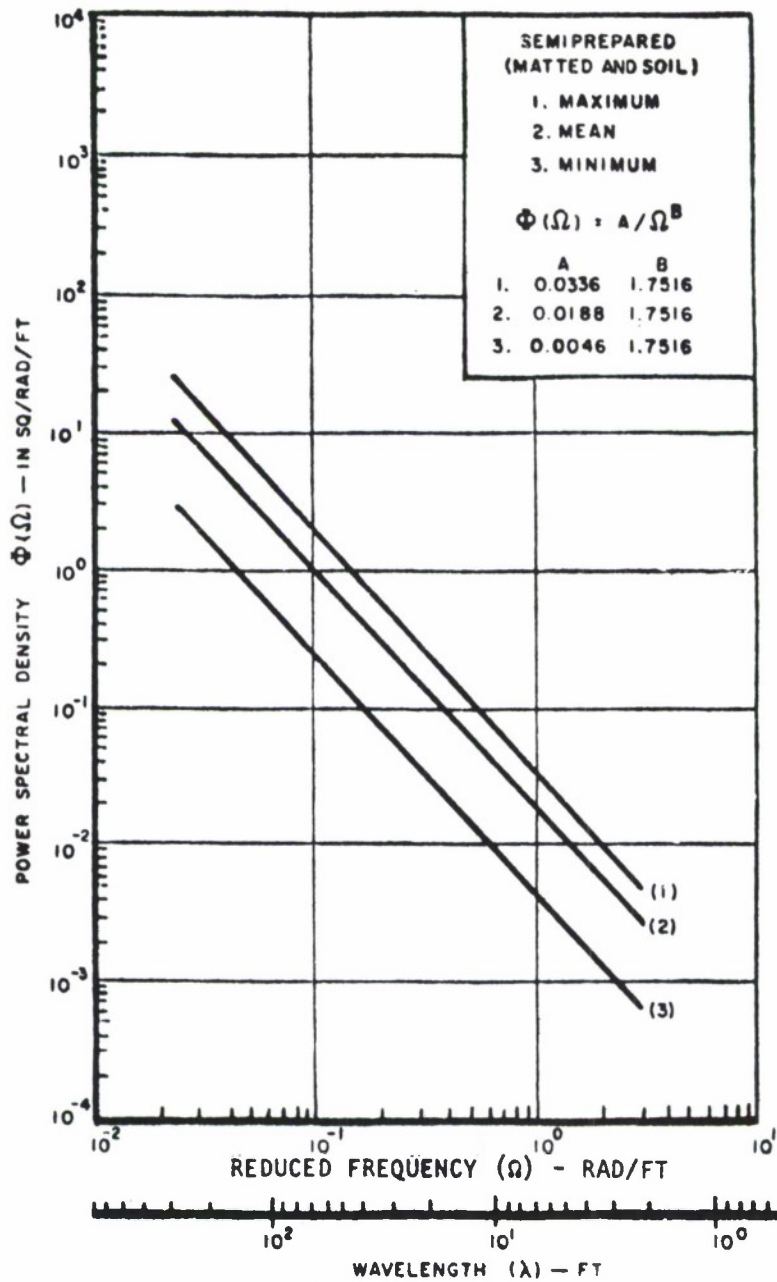


FIGURE 2. roughness Levels For Semiprepared Airfields

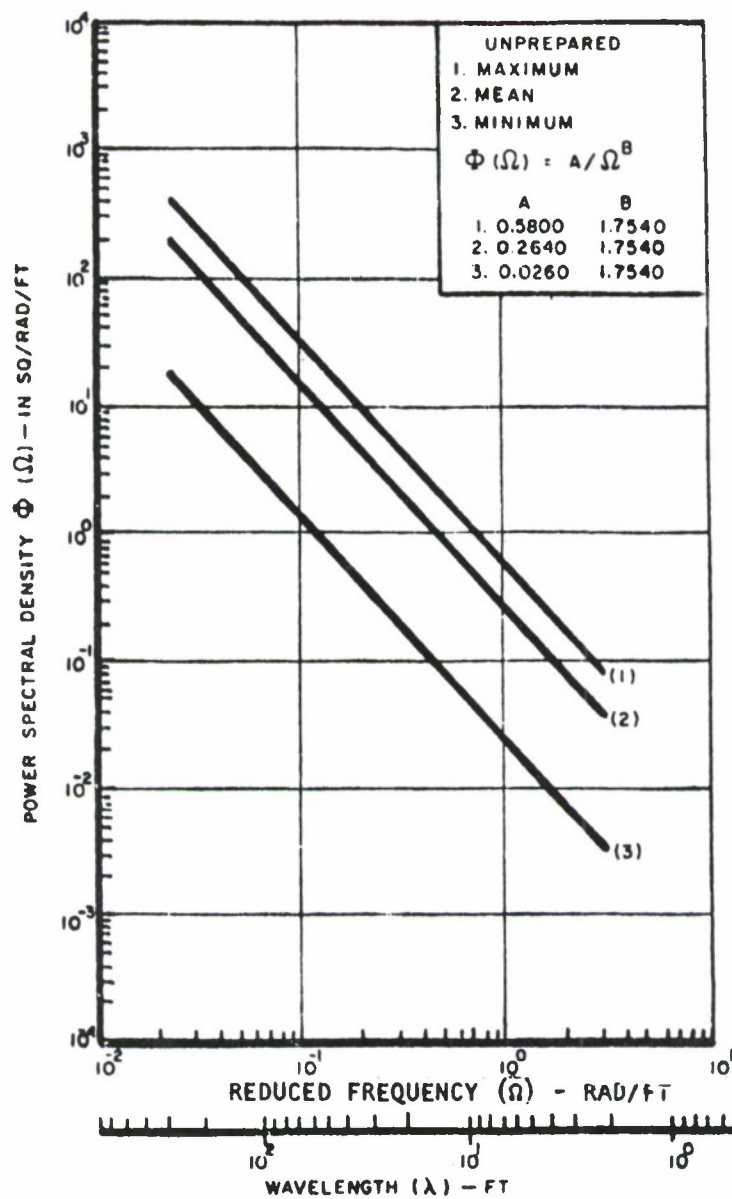


FIGURE 3. Roughness Levels For Unprepared Airfields ¹

NOTE 1: This figure shall not be used for design unless specified by the procuring activity.

ALPHABETICAL INDEX

	A	Paragraph
Analyses		3.2.4
APPLICABLE DOCUMENTS		2
	B	
Braking, pivoting, and turning		3.2.2.5
	C	
Combined loadings		3.2.2.10
Control surface balance weight attachments		3.2.2.8
Control system inputs		3.2.2.9
Corrosion protection		3.2.7
	D	
Definitions		6.2
Design chemical/thermal environment spectra		3.2.3
Design data		4.1
Design service life and design usage		3.2.1
Design service loads spectra		3.2.2
Detail requirements		3.2
Durability		6.2.1
Durability detail design procedures		3.2.5
	E	
Economic life		6.2.2
	F	
Flight tests		4.3
	G	
General requirements		3.1
Gust		3.2.2.2
	I	
Initial quality		6.2.3
Intended use		6.1

ALPHABETICAL INDEX (CONT'D)

	L	Paragraph
Laboratory tests		4.2
Landing		3.2.2.3
	M	
Maneuver		3.2.2.1
Marginal indicia		6.3
	N	
NOTES		6
	O	
Other durability considerations		3.2.9
	P	
PREPARATION FOR DELIVERY		5
Pressurization		3.2.2.6
	Q	
QUALITY ASSURANCE PROVISIONS		4
	R	
Repeated operation of movable structures		3.2.2.7
REQUIREMENTS		3
	S	
SCOPE		1
Structural operating mechanisms		6.2.4
	T	
Taxi		3.2.2.4
Thermal protection		3.2.6
	W	
Wear endurance		3.2.8

ALPHABETICAL INDEX (Cont'd)

TABLES

TABLE I	Maneuver Load Factor Spectra for A, F, TF Classes, Cumulative Occurrences per 1000 Flight Hours by Mission Segment
TABLE II	Maneuver Load Factor Spectra for T, Trainer Class, Cumulative Occurrences per 1000 Flight Hours by Mission Type
TABLE III	Maneuver Load Factor Spectra for B _I , Bomber Class, Cumulative Occurrences per 1000 Flight Hours by Mission Type
TABLE IV	Maneuver Load Factor Spectra for B _{II} , Bomber Class, Cumulative Occurrences per 1000 Flight Hours by Mission Segment
TABLE V	Maneuver Load Factor Spectra for C _{TRANSPORT} , Cargo Class, Cumulative Occurrences per 1000 Flight Hours by Mission Segment
TABLE VI	Maneuver Load Factor Spectra for C _{ASSAULT} , Cargo Class, Cumulative Occurrences per 1000 Flight Hours by Mission Segment
TABLE VII	Cumulative Occurrences of Sinking Speed per 1000 Landings
TABLE VIII	Cumulative Occurrences per 1000 Runway Landings That Load Factor N_z is Experienced at the Airplane CG

FIGURES

FIGURE 1	Roughness Levels for Prepared Airfields
FIGURE 2	Roughness Levels for Semiprepared Airfields
FIGURE 3	Roughness Levels for Unprepared Airfield

OMB Approval
No. 22-R255

DOCUMENT IDENTIFIER AND TITLE

CONTRACT NUMBER

☐ DIRECT GOVERNMENT CONTRACT ☐ SUBCONTRACT

A. GIVE PARAGRAPH NUMBER AND WORDING.

B. RECOMMENDATIONS FOR CORRECTING THE DEFICIENCIES

☐ YES ☐ NO (If "Yes", in what way?)

TELEPHONE NO.

DATE _____

REPLACES EDITION OF 1 JAN 66 WHICH MAY BE USED

C 1 6 0 6 1

FOLD

ASD/ENYESS
Wright-Patterson AFB, O 45433
OFFICIAL BUSINESS
PENALTY FOR PRIVATE USE \$300

POSTAGE AND FEES PAID
DEPARTMENT OF THE AIR FORCE
DoD-318



ASD/ENYESS
Wright-Patterson AFB, Ohio 45433

FOLD

MIL-A-008867B(USAF)
22 August 1975
SUPERSEDING
MIL-A-008867A(USAF)
31 March 1971
USED IN LIEU OF
MIL-A-8867(ASG)
18 May 1960

MILITARY SPECIFICATION

AIRPLANE STRENGTH AND RIGIDITY GROUND TESTS

This limited coordination Military Specification has been prepared by the Air Force based upon currently available technical information, but it has not been approved for promulgation as a coordinated revision of Military Specification MIL-A-8867(ASG). It is subject to modification. However, pending its promulgation as a coordinated Military Specification, it may be used in procurement.

1. SCOPE

1.1 Types of tests. This specification identifies the ground tests required for structural evaluation of airplanes. The complete structure, herein referred to as the airframe, includes the fuselage, wing, empennage, landing gears, control system and surfaces, engine mounts, structural operating mechanisms, and other components as specified in the contract. This specification applies to metallic and nonmetallic structures. The types of testing include, but are not limited to:

- a. Design development tests
- b. Proof, ultimate, and failing load static tests - full scale airframe
- c. Durability tests - full scale airframe
- d. Damage tolerance tests
- e. Fuel tank tests.

2. APPLICABLE DOCUMENTS

2.1 The following documents, of the issue in effect on the date of invitation for bids or request for proposal, form a part of this specification to the extent specified herein:

SPECIFICATIONS

Military

MIL-G-6021 Castings, Classification and Inspection of

FSC 1510

MIL-A-008867B(USAF)

MIL-A-8860	Airplane Strength and Rigidity, General Specification for
MIL-A-8866	Airplane Strength and Rigidity Reliability Requirements, Repeated Loads, and Fatigue
MIL-A-8871	Airplane Strength and Rigidity, Flight and Ground Operations Tests
MIL-C-45662	Calibration Systems Requirements
MIL-A-83444	Airplane Damage Tolerance Design Requirements

(Copies of specifications, standards, drawings and publications required by suppliers in connection with specific procurement functions should be obtained from the procuring activity or as directed by the contracting officer.)

3. REQUIREMENTS

3.1 General requirements. The contractor shall furnish component, assembly, and full scale airframe test specimens and shall perform tests in accordance with the test requirements specified herein and as modified and amplified by the contract.

3.1.1 Location of tests. The contract will specify whether the tests are to be performed by the Government or by the contractor. In the event that structural tests are performed by the Government, the contract will specify the type and amount of support to be provided by the contractor.

3.1.2 Schedule of tests. The test scheduling shall be as specified in the detail requirements of 3.2. In all cases, the test sequencing shall require approval by the procuring activity prior to starting the test program.

3.1.3 Test articles. Test article configuration shall require approval by the procuring activity. Changes, adjustments, reinforcements and repairs made to the test article to meet specified strength, rigidity, damage tolerance and durability requirements shall be representative of those that will be incorporated into operational flight articles. In addition, the test articles shall be identical with the structure of the flight articles except that:

a. Items such as fixed equipment and useful loads and their support structures may be omitted from the test structure provided the omission of these parts does not significantly affect the load, stress or thermal distributions and the structural characteristics of the parts of the structure to be tested, and provided the omitted parts are qualified by separate tests as agreed to by the procuring activity.

b. Substitute parts may be used when specific prior approval is obtained from the procuring activity, provided they produce the effects of the parts for which they are substituted, and provided the structural integrity of the parts for which substitutions are made are demonstrated in a manner that is satisfactory to the procuring activity.

c. Power plants and accessories shall be replaced by contractor designed-and-fabricated test fixtures that properly transmit the power plant loads to the engine mounts, vibration isolators, or both, as applicable. The means for applying the loads to these fixtures (such as loading rods through the fuselage or engine nacelle structure) shall be determined by the contractor. All structural modifications necessary to accommodate the loading devices shall be designed by the contractor in such a manner as to assure that the structural characteristics of the modified structure will be equivalent to those of the actual structure.

d. Paint or other finishes that do not affect the structural performance may be omitted from the test structures. When the structural test includes simulation of chemical or thermal environment (3.1.9), the test articles shall include the associated environmental protection systems developed in accordance with the durability design requirements of MIL-A-8866 paragraphs entitled Thermal protection and Corrosion protection.

e. Prior to shipping the test structures to Government facilities for testing, a number of buttock lines, water lines, fuselage stations, and wing stations shall be marked on the test structure. These shall be clearly identified and shall be of sufficient number to facilitate determining all desired reference points on the airframe.

f. To the extent required for adequate load simulation during test, mechanical portions of the flight control system and power actuators for the control systems shall be operable. When tests are conducted at Government facilities, special provisions shall be made for external power attachments to the actuating mechanisms to permit externally controlled operations. It is therefore permissible to omit any unnecessary portions of the normal internal power systems. Other actuators for landing gear doors, armament bay doors, etc., shall be externally operable as required for tests at Government facilities. Air actuated systems may be replaced by hydraulic systems to simplify testing procedures. The external actuation capability is also recommended for tests conducted by the contractor, if test operations can be simplified or costs reduced.

g. Structural parts and mechanisms which are subject to special qualification requirements outside the scope of this specification shall be qualified to the extent possible prior to incorporation in the test article (Class I castings in accordance with MIL-C-6021 paragraph entitled, Classes, weldments, actuators, etc.).

3.1.4 Instrumentation and test measurements. Structural test components, assemblies, and full scale airframe test articles shall be instrumented with strain gages, load cells, pressure transducers, deflection potentiometers, thermocouples, and other instrumentation as needed to (1) verify that external loads, pressure loads, environment and other external test parameters are correctly simulated and (2) monitor test article parameters such as strain, temperature distributions, and structural deflections for comparison with the appropriate structural analyses. Additional instrumentation shall be used as necessary to detect incipient structural failure, monitor crack growth, and monitor localized test areas. The instrumentation system sensor placement on the structural test articles shall be determined by the contractor and shall require approval by the procuring activity. Instrumentation used for obtaining test data shall be calibrated and certified in accordance with MIL-C-45662 as appropriate. Test facility measurement standards shall have certificates which are traceable to the National Bureau of Standards. The instrumentation shall be integrated into a read-out system for rapid and accurate presentation of the test parameters. Data measurements shall be taken at sufficient intervals and loadings to monitor and verify the test parameters consistent with the test program objectives. For tests conducted at discrete load increments, measurements shall be made at each load increment. The test article instrumentation requirements shall be coordinated with the instrumentation planned for the flight loads survey. Special types of instrumentation (e.g., mechanical strain recorders, strain gages, etc.) to be used during the individual airplane tracking program shall be placed on the static and durability articles as appropriate for evaluation and correlation. Analyses pertinent to the areas being instrumented shall be made available to the procuring activity prior to instrumentation. When tests are performed by the Government, required instrumentation (strain gages, thermocouples, pressure transducers, crack detection wires, etc.) shall be installed by the contractor to the maximum extent practicable, prior to delivery of the test article(s) to the testing agency. When tests are performed by the Government, the contractor shall consult with the testing agency to establish the instrumentation requirements relative to compatibility with Government data systems.

3.1.5 Use and disposition of test articles. Except for the case of proof testing of flight vehicle structures, parts of the test structure shall not be used on a flight article. In certain cases it may be a program requirement to store test articles for extended periods of time following completion of testing. The requirements for test article storage shall be as specified by the procuring activity in the contract.

3.1.6 Test loading system. The test loads shall be applied using a system capable of providing accurate load control to all load points simultaneously and shall contain emergency modes which will detect load errors and prevent excessive loads. When loads are applied in such a manner that they are not relieved when the rate of deformation of the specimen increases rapidly, as when failure occurs, safety devices such as shear links or pressure blowout valves shall be employed to minimize excessive deformation or overloading of other parts of the structure. Positive methods shall be employed to safely control the release of energy in the event of abrupt failure. Load application devices shall be designed to minimize local non-representative loading effects and to afford maximum accessibility for inspection of critical joints, cutouts, and areas of discontinuity. The test rig and associated equipment shall be capable of applying the maximum loads necessary to meet the required test objectives.

3.1.7 Test loads and distribution. In each test condition, parts of the structure critical for the pertinent design loading shall be tested and shall be loaded simultaneously, if practicable. Testing may be initiated using analytically derived loads and available wind tunnel data. Loads measured in the flight and ground loads survey program shall be used to correct the test loads and distribution at the earliest suitable time if the measured loads are significantly different than the analytical loads. The distribution of loads employed in the tests shall represent the actual distribution as closely as possible.

3.1.8 Deformations. It shall be demonstrated during structural tests that movable and removable structural components remain in their intended positions and do not deform within the load/deformation limits specified in MIL-A-8860 paragraph entitled, Deformations, to the extent that (1) deleterious aerodynamic effects are produced or (2) interference is such that functional impairment occurs when operation is required at the design condition. In addition, there shall be no permanent deformation as a result of application of the design loads specified in MIL-A-8860 paragraph entitled, Deformations which would impair the functioning of any aircraft component during subsequent flight and ground operations.

3.1.9 Environmental effects. The effect of chemical and thermal environments shall be evaluated during the material and joint allowables tests to the extent necessary. When deemed necessary, the design chemical and thermal environment shall be simulated during the full scale airframe tests. The method of simulating the environment shall require approval by the procuring activity.

3.1.10 Simplification and combination of loading. Loading conditions may be simplified during tests by modifying the distribution of loads applied to regions of a structure that will not be subjected to critical loads

during the loading condition being simulated or that are identical in construction to other regions of the structure that are subjected to critical loads during the same or another test condition. However, simplification of the method of loading shall not result in unrepresentative permanent deformations or failures. Simultaneously applying more than one loading condition to different portions of the structure shall be considered provided the interaction of the separate loadings does not affect the critical design loading on any portion of the structure. Loads resulting from pressurization shall be considered and, if critical, shall be simulated in combination with the applicable ground and flight loads during the appropriate component or full scale test.

3.1.11 Complete airframe versus separate assemblies. It will be a program option requiring approval by the procuring activity whether the full scale airframe static and durability tests are performed on a complete airframe or on separate major assemblies thereof (wing, fuselage, empennage, landing gear, etc.). When tests of components or separate assemblies are conducted, the test article shall be mounted in supporting and loading fixtures which accurately simulate the load and deflection interactions with the adjacent structure not being tested. If these actual interactions cannot be obtained, then the contractor shall provide sufficient transition test structure whose strength and stiffness is representative of the full scale airframe.

3.2 Detail requirements

3.2.1 Design development tests. The contractor shall conduct design development tests to establish material and joint allowables; to verify analysis procedures; to obtain early evaluation of allowable stress levels, material selections, fastener systems and the effect of the design chemical/thermal environment spectra; and to obtain early evaluation of the strength, durability, and damage tolerance of critical structural components and assemblies. Example of design development tests are tests of:

- a. Coupons
- b. Small elements
- c. Splices and joints
- d. Panels of basic section and panels with joints, cutouts, eccentricities and other discontinuities.
- e. Fittings
- f. Control system components and structural operating mechanisms.

In addition, design development tests shall include tests of critical major components and assemblies such as wing carry through, horizontal tail spindles, wing pivots, and assemblies thereof to obtain early validation of the static strength, durability, and damage tolerance. A design development test plan shall be developed by the contractor and shall require approval by the procuring activity.

3.2.2 Static tests - full scale airframe. The static test airframe shall meet the applicable general requirements of 3.1. Full scale static tests to design ultimate loads shall be required except (1) where it is shown that the airframe and its loading are substantially the same as that used on previous aircraft where the airframe has been verified by full scale tests or (2) where the strength margins (particularly for stability critical structure) have been demonstrated by major assembly tests. When full scale ultimate load static tests are not performed, it shall be a program requirement to conduct a strength demonstration proof test in accordance with 3.2.2.4. Deletion of the full scale ultimate load static tests shall require approval by the procuring activity. Prior to starting the static tests, structural modifications required as a result of failures that occur during design development tests shall be incorporated into the test article or qualified by separate tests as agreed to by the procuring activity.

3.2.2.1 Schedule. The full scale static tests shall be scheduled such that the tests are completed in sufficient time to allow removal of the 80 percent limit restrictions on the flight test airplanes in accordance with MIL-A-8871 paragraph entitled, Operating limitations, and allow unrestricted flight within the design envelope on schedule.

3.2.2.2 Functional proof tests prior to first flight. Proof testing requirements prior to first flight for major flight control systems and surfaces, and major operating mechanisms (e.g., wing sweep, droopnose, etc.) shall be established on an individual basis for each new airplane. The purpose of these tests is to demonstrate that systems and mechanisms function satisfactorily when subjected to the applicable maximum operating loads. These tests may be performed with the associated load induced deflection in the movable surface and the airframe to which the movable surface is attached, and may be performed on suitable components when approved by the procuring activity. Pressurized compartments shall be tested to 1.33 times maximum operating pressure (regulator valve nominal setting plus tolerance) on a flight article prior to pressurized flight. Each subsequent airplane shall be tested to at least 1.0 times the maximum operating pressure.

3.2.2.3 Inspection proof tests. Upon approval by the procuring activity and in conformance to MIL-A-83444, paragraph entitled, Initial flaw size; subparagraph Slow crack growth structure, the contractor may perform component, assembly, or complete airframe inspection proof tests on every

airplane for the purpose of defining maximum possible initial flaw sizes or other damage when design constraints make the use of conventional Non-Destructive Inspection impractical or not cost effective.

3.2.2.4 Strength demonstration proof tests. Strength demonstration proof tests shall be conducted when design ultimate load static tests are not required. The proof test load levels shall be equal to or greater than the maximum loads contained in the design service loads spectra and in no cases shall the load levels be less than design limit load. The structure shall be loaded during the strength demonstration proof tests in accordance with 3.1.7. Test conditions shall be selected which substantiate the design limit envelope for each component of the airframe. The internal loads and stress analysis shall be used as a guide in determining the most critical load conditions. The contractor shall submit a list of recommended test conditions including the basis for selection. Re-proof tests shall be required when flight test data confirms that actual load distributions are more severe than those used in design. Strength demonstration proof tests and re-proof test requirements shall require approval of the procuring activity.

3.2.2.4.1 Post proof test inspection and analysis requirements. A post proof test inspection program shall be conducted. Special emphasis shall be placed on determining if detrimental deformations (3.1.8) have occurred in the airframe that would prevent the use of any structural part on a flight vehicle. The analysis program shall include extensive examination of instrumentation data to determine whether extrapolated ultimate internal stresses are above predicted values to the extent that flight restrictions or modifications are required. The specific inspection and analysis program shall require approval by the procuring activity.

3.2.2.5 Ultimate load tests. In accordance with 3.2.2, the static test program shall include tests to design ultimate load on the full scale static test airframe to verify the static ultimate strength of the airframe. Design ultimate load test conditions shall be selected which substantiate the design envelope for each component of the airframe. The internal loads and stress analysis shall be used as a guide in determining the most critical load conditions. The contractor shall submit a list of recommended test conditions to the procuring activity for approval.

3.2.2.6 Failing load tests. When ultimate load static tests are conducted, consideration shall be given to conducting failing load tests at the end of the static test program to substantiate special capabilities such as growth potential or emergency operations. Failing load tests shall be specified in the contract unless other uses of the article are specified in the contract.

3.2.3 Durability tests - full scale airframe. The durability test article shall meet the applicable general requirements of 3.1. Prior to starting the durability tests, structural modifications required as a result of failures that occur during design development tests shall be incorporated into the test article or qualified by separate tests as agreed to by the procuring activity.

3.2.3.1 Selection of test articles. The test article shall be an early Full Scale Development (FSD) or Research Development Test and Evaluation (RDT&E) airframe to meet the scheduling requirements of 3.2.3.2. This article shall be as representative of the operational configuration as practical within the schedule constraints. If there are significant design, material, or manufacturing changes between the test article and production airplanes, durability test of an additional article or selected components and assemblies thereof shall be required. The contractor in conjunction with the procuring activity shall identify additional test requirements and these additional tests shall require separate contract negotiations.

3.2.3.2 Schedule requirements. The full scale airframe durability test shall be scheduled such that one lifetime of durability testing plus an inspection of critical structural areas in accordance with 3.2.3.4.1 and 3.2.3.4.2 shall be completed prior to full production go ahead decision. Two lifetimes of durability testing plus an inspection of critical structural areas in accordance with 3.2.3.4.1 and 3.2.3.4.2 shall be scheduled to be completed prior to delivery of the first production airplane. If the economic life of the test article is reached prior to two lifetimes of durability testing, sufficient inspection in accordance with 3.2.3.4.1 and 3.2.3.4.2 and data evaluation shall be completed prior to delivery of the first production airplane to estimate the extent of required production and retrofit changes. In the event the original schedule for the production decision and production delivery milestones becomes incompatible with the above schedule requirements, a study shall be conducted to assess the technical risks and cost impacts of changing these milestones.

3.2.3.3 Test spectra. The test spectra shall be based on the design service loads spectra and the design chemical/thermal environment spectra. The test spectra shall include rationally distributed missions, positive and negative loads (ordered or randomized, as appropriate), and shall be applied to the test article on a flight-by-flight basis. Test loads shall include significant sources of repeated loads and these loads shall be combined in the appropriate sequence. Chemical and thermal environment shall be included in accordance with 3.1.9. The test load and environment spectra shall require approval by the procuring activity.

3.2.3.3.1 Test spectra truncation. Truncation, elimination or substitution of load cycles in the test spectra to reduce test time and cost will be allowed. The contractor shall define by analysis and laboratory experiment the effect of the difference between the design spectra and the proposed test spectra on the time to reach detrimental crack sizes per the durability and damage tolerance requirements of MIL-A-8866 paragraph entitled General requirements and MIL-A-83444 paragraph entitled General requirements, respectively. The results of these analysis and experiments shall be used to establish the final test spectra and, as necessary, to interpret the test results. The final test spectra shall require approval by the procuring activity.

3.2.3.4 Inspections. Major inspection programs shall be conducted as an integral part of the full scale airframe durability test program. The inspection programs shall require approval by the procuring activity.

3.2.3.4.1 Design inspections. In-service inspections developed in accordance with the requirements of MIL-A-83444 paragraph entitled General requirements and the requirements of MIL-A-8866 paragraph entitled General requirements shall be programmed and conducted at the specified intervals and at the end of the test prior to the teardown inspection of 3.2.3.4.3. The inspection procedures shall be consistent with those proposed for use on force airplanes at the design inspection interval specified in the contract and shall account for the fact that accessibility to the test airframe may be different than for the flight configuration.

3.2.3.4.2 Special inspections. The contractor and procuring activity shall define special inspections (both type and interval) to monitor and status of critical areas identified during design, detecting additional critical areas not previously identified, and monitoring crack growth rates. These inspections shall be conducted at intervals as agreed to by the procuring activity and shall include the following intervals necessary to support the schedule requirements of 3.2.3.2: (1) at the end of one lifetime of test and (2) at the end of two lifetimes of test, or when the economic life of the test article is reached but prior to the teardown inspection of 3.2.3.4.3.

3.2.3.4.3 Teardown inspection. At the end of the full scale durability test including any scheduled damage tolerance tests, a destructive teardown inspection program shall be conducted. This inspection shall include disassembly and laboratory-type inspection of those critical structural areas identified in design as well as additional critical structure detected during the design and special inspections and during close visual examination while performing the disassembly. Fractographic examinations shall be conducted to obtain crack growth data and to assist in the assessment of the initial quality of the airframe and the degree of compliance with the durability requirements of MIL-A-8866 paragraph entitled General requirements and the damage tolerance requirements of MIL-A-83444 paragraph entitled General requirements.

3.2.3.5 Test duration. A minimum of two lifetimes of durability testing shall be conducted except when the economic life is reached prior to two lifetimes. If the economic life is reached prior to two lifetimes, the durability test shall be terminated and a decision made to perform either the teardown inspection or perform damage tolerance tests as required by 3.2.4 followed by the teardown inspection. If, at the end of two lifetimes, the economic life is not reached, a decision shall be made to (1) terminate durability testing and perform the teardown inspection, or (2) terminate the durability testing and perform damage tolerance testing, followed by the teardown inspection, or (3) continue durability testing for an approved extended duration followed by either (1) or (2). At each of the above decision points the contractor shall submit his recommended course of action together with the rationale supporting this recommendation to the procuring activity for approval. As a minimum, the rationale for continuing durability testing beyond two lifetimes shall be based on (1) effects of possible usage extremes on life, (2) possible force life extension needs, (3) development and production schedules, and (4) magnitude of cracking problems encountered in two lifetimes of testing.

3.2.4 Damage tolerance tests. Damage tolerance tests shall be conducted to demonstrate compliance with the design requirements of MIL-A-83444 paragraph entitled General requirements. The type and quantity of tests depend on the design concepts and the number of fracture critical areas. The types of tests shall include crack growth evaluation of slow crack growth and fail safe structure as well as residual strength and life tests of fail safe structure subsequent to load path failure or crack arrest. The amount of full scale damage tolerance testing that is conducted is also dependent upon the extent that damage tolerance is demonstrated during the design development or full scale durability tests (i.e., number of cracking incidents and subsequent crack growth). The damage tolerance test program shall be of sufficient scope to verify Category I fracture critical parts in accordance with MIL-A-83444 paragraph entitled Fracture critical structure. Deletion of verification of certain fracture critical areas can be proposed based on similarity of materials and structural configurations and demonstrated knowledge of the applied stresses. The intent shall be to conduct damage tolerance tests on existing test hardware. This may include use of components and assemblies of the design development tests as well as the full scale static and durability test articles. Fracture critical areas of existing test hardware shall be evaluated to determine the nature of physical changes caused by previous testing to insure validity of damage tolerance tests. When necessary, additional structural components and assemblies shall be fabricated and tested to verify compliance with the damage tolerance requirements of MIL-A-83444 paragraph entitled General requirements. Detail test requirements (type of tests, proposed deletions, quantity, choice of specimens, pre-crack locations, etc.) shall be proposed by the contractor and shall require approval by the procuring activity.

3.2.5 Fuel tank tests. The internal fuel tanks critical for repeated loads due to pressure, inertia, fluid acceleration heads, vibration, or other flight and ground loads shall be tested. When the critical stress conditions cannot be reasonably simulated in the durability test or other required test programs, durability tests shall be conducted on full scale representative tank sections as approved by the procuring activity. The contractor shall propose, for approval by the procuring activity, a plan to detect cracks, delaminations, or other material failures that would cause fuel leaks throughout the test duration. The test duration for fuel tank tests shall be as specified in 3.2.3.5. If the fuel tank is a Category I fracture critical part, it shall require damage tolerance tests as specified in 3.2.4. These test requirements do not supersede other test requirements for evaluation of fuel tanks (slosh and vibration).

3.2.6 Interpretation and evaluation of test results. Each structural problem (failure, cracking, yielding, etc.) that occurs during the tests required by this specification shall be analyzed by the contractor to determine the cause, corrective actions, force implications, and estimated costs. The scope and interrelations of the various tasks within the interpretation and evaluation effort are illustrated in figure 1. The results of this evaluation shall demonstrate that the strength, rigidity, damage tolerance and durability design requirements are met. Structural modifications or changes derived from the results of the full scale tests to meet the specified strength, rigidity, damage tolerance, and durability design requirements shall be substantiated by subsequent tests of components, assemblies, or full scale article as appropriate. The test duration for durability modifications shall be as specified in 3.2.3.5. The contractor shall propose these additional test requirements together with the associated rationale to the procuring activity for approval.

4. QUALITY ASSURANCE PROVISIONS

4.1 Additional tests. If the tests specified herein and performed by the contractor are inadequate to prove that the test structure meets the specified requirements, the contractor or the procuring activity will propose amendments to the contract to include additional tests.

4.2 Test witnesses. Before performing a required test, the procuring activity shall be notified in sufficient time so that a representative may witness the test and certify results and observations. The procuring activity shall be informed if the test is such that interpretation of the behavior of the structure under load is likely to require engineering knowledge and experience so that a qualified engineer may witness the test and certify the observations and results recorded during the test.

4.3 Test data. Structural test data shall be prepared and submitted as specified in the contract.

5. PREPARATION FOR DELIVERY

5.1 Section 5 is not applicable.

6. NOTES

6.1 Intended use. This specification is intended to be used in conjunction with MIL-T-6053, MIL-A-8870, MIL-A-8871, MIL-A-8892 and MIL-A-8893 for the structural substantiation of airframe structure of all new USAF airplanes. Selected portions of this specification may also be used in the substantiation of major modifications of existing USAF airplanes.

6.2 Definitions. Definitions will be in accordance with the documents listed in Section 2 and as specified herein.

3.2.1 Durability. The ability of the airframe to resist cracking (including stress corrosion and hydrogen induced cracking), corrosion, thermal degradation, delamination, wear, and the effects of foreign object damage for a specified period of time.

6.2.2 Economic life. That operational life indicated by the results of the durability test program (i.e., test performance interpretation and evaluation in accordance with MIL-A-8867) to be available with the incorporation of USAF approved and committed production or retrofit changes and supporting application of the force structural maintenance plan in accordance with MIL-STD-1530. (In general, production or retrofit changes will be incorporated to correct local design and manufacturing deficiencies disclosed by the test. It will be assumed that the economic life of the test article has been attained with the occurrence of widespread damage which is uneconomical to repair and, if not repaired, could cause functional problems affecting operational readiness. This can generally be characterized by a rapid increase in the number of damage locations or repair costs as a function of cyclic test time.)

6.2.3 Initial quality. A measure of the condition of the airframe relative to flaws, defects or other discrepancies in the basic materials or introduced during manufacture of the airframe.

6.2.4 Structural operating mechanisms. Those operating, articulating, and control mechanisms which transmit structural forces during actuation and movement of structural surfaces and elements.

MIL-A-008867B(USAF)

6.2.5 Damage tolerance. The ability of the airframe to resist failure due to the presence of flaws, cracks, or other damage for a specified period of unrepai red service usage.

6.2.6 Marginal indicia. Asterisks are not used in this revision to identify changes with respect to the previous issue due to the extensiveness of the changes.

Custodian:
Air Force - 11

Preparing activity:
Air Force - 11

Project No.: 1510-F024

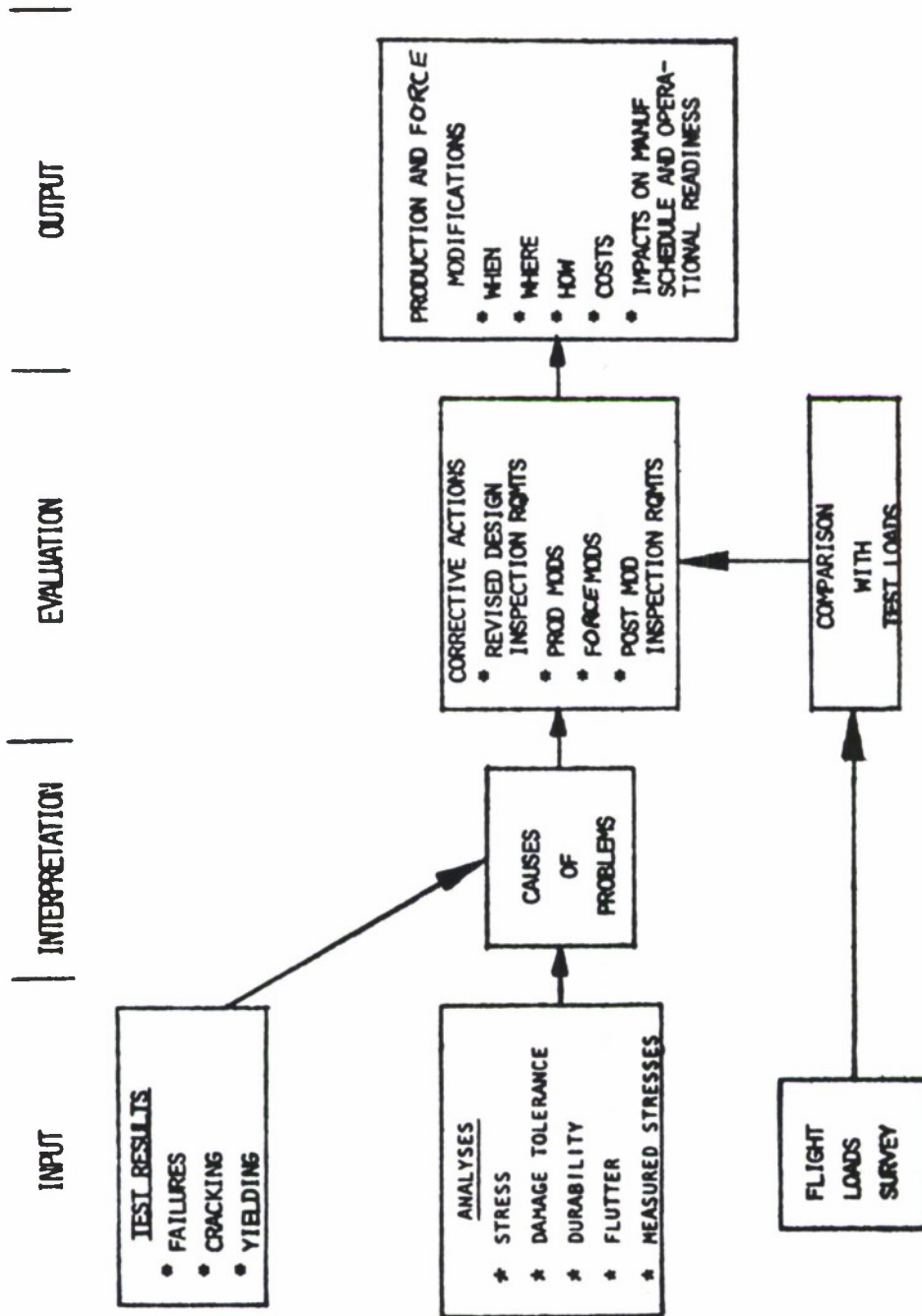


FIGURE 1. Interpretation and Evaluation of Test Results
(Based on Design Service Life and Design Usage)

ALPHABETICAL INDEX

	Paragraph
A	
Additional tests	4.1
APPLICABLE DOCUMENTS	2
C	
Complete airframe versus separate assemblies	3.1.11
D	
Damage tolerance	6.2.5
Damage tolerance tests	3.2.4
Definitions	6.2
Deformations	3.1.8
Design inspections	3.2.3.4.1
Design development tests	3.2.1
Detail requirements	3.2
Durability	6.2.1
Durability tests - full scale airframe	3.2.3
E	
Economic life	6.2.2
Environmental effects	3.1.9
F	
Failing load tests	3.2.2.6
Fuel tank tests	3.2.5
Functional proof tests prior to first flight	3.2.2.2
G	
General requirements	3.1
I	
Initial quality	6.2.3
Inspection proof tests	3.2.2.3
Inspections	3.2.3.4
Instrumentation and test measurements	3.1.4
Intended use	6.1
Interpretation and evaluation of test results	3.2.6

ALPHABETICAL INDEX (Cont'd)

	L	Paragraph
Location of tests		3.1.1
	M	
Marginal indicia		6.3
	N	
NOTES		6
	P	
Post proof test inspection and analysis requirements		3.2.2.4.1
PREPARATION FOR DELIVERY		5
	Q	
QUALITY ASSURANCE PROVISIONS		4
	R	
REQUIREMENTS		3
	S	
Schedule		3.2.2.1
Schedule of test		3.1.2
Schedule requirements		3.2.3.2
SCOPE		1
Selection of test articles		3.2.3.1
Simplification and combination of loading		3.1.10
Special inspections		3.2.3.4.2
Static tests - full scale airframe		3.2.2
Strength demonstration proof tests		3.2.2.4
Structural operating mechanisms		6.2.4
	T	
Teardown inspection		3.2.3.4.3
Test articles		3.1.3
Test data		4.3

ALPHABETICAL INDEX (Cont'd)

	Paragraph
Test duration	3.2.3.5
Test loading systems	3.1.6
Test loads and distribution	3.1.7
Test spectra	3.2.3.3
Test spectra truncation	3.2.3.3.1
Test witnesses	4.2
Types of tests	1.1

U

Ultimate load tests	3.2.2.5
Use and disposition of test articles	3.1.5

FIGURES

FIGURE 1	Interpretation and evaluation of test results (based on design service life and design usage)
----------	---

SPECIFICATION ANALYSIS SHEET		Form Approved Budget Bureau No. 22-R255
INSTRUCTIONS: This sheet is to be filled out by personnel, either Government or contractor, involved in the use of the specification in procurement of products for ultimate use by the Department of Defense. This sheet is provided for obtaining information on the use of this specification which will insure that suitable products can be procured with a minimum amount of delay and at the least cost. Comments and the return of this form will be appreciated. Fold on lines on reverse side, staple in corner, and send to preparing activity. Comments and suggestions submitted on this form do not constitute or imply authorization to waive any portion of the referenced document(s) or serve to amend contractual requirements.		
SPECIFICATION <div style="text-align: center; font-size: 1.2em; margin-top: 5px;">MIL-A-1435Q</div>		
ORGANIZATION		
CITY AND STATE	CONTRACT NUMBER	
MATERIAL PROCURED UNDER A <input type="checkbox"/> DIRECT GOVERNMENT CONTRACT <input type="checkbox"/> SUBCONTRACT		
1. HAS ANY PART OF THE SPECIFICATION CREATED PROBLEMS OR REQUIRED INTERPRETATION IN PROCUREMENT USE? A. GIVE PARAGRAPH NUMBER AND WORDING.		
B. RECOMMENDATIONS FOR CORRECTING THE DEFICIENCIES		
2. COMMENTS ON ANY SPECIFICATION REQUIREMENT CONSIDERED TOO RIGID		
3. IS THE SPECIFICATION RESTRICTIVE? <input type="checkbox"/> YES <input type="checkbox"/> NO (If "yes", in what way?)		
4. REMARKS (Attach any pertinent data which may be of use in improving this specification. If there are additional papers, attach to form and place both in an envelope addressed to preparing activity)		
SUBMITTED BY (Printed or typed name and activity - Optional)		DATE

DD FORM 1426
1 JAN 66

REPLACES EDITION OF 1 OCT 64 WHICH MAY BE USED.

FOLD

POSTAGE AND FEES PAID
DEFENSE SUPPLY AGENCY

DEFENSE SUPPLY AGENCY
OFFICIAL BUSINESS

Commander
US Army Tank-Automotive, Command
ATTN: AMSTA-GBS
Warren, MI 48090

FOLD

APPENDIX B
ASTM STANDARDS



Designation: E 616 - 81

AMERICAN SOCIETY FOR TESTING AND MATERIALS
1916 Race St., Philadelphia, Pa. 19103

Reprinted from the Annual Book of ASTM Standards, Copyright ASTM
If not listed in the current combined index, will appear in the next edition.

Standard Terminology Relating to FRACTURE TESTING¹

This standard is issued under the fixed designation E 616; the number immediately following the designation indicates the year of original adoption or, in the case of revision, the year of last revision. A number in parentheses indicates the year of last reapproval.

1. Scope

1.1 This terminology contains definitions, symbols, and abbreviations approved for use in standards on fracture testing. Terms defined under the heading General Definitions are presented in a sequence considered to be the most logical, for tutorial purposes, with definitions presented later calling upon those presented earlier. Terms under the heading Other Definitions are presented in the order in which they appear in each of the standards from which they are extracted. Preceding the definitions is an index that is intended to facilitate the use of this terminology. In the index are two lists. One is an alphabetical list of the terms, in which cross references are included. The other is an alphabetical list of the symbols, in which the Greek symbols are ordered according to their spelling in English.

2. Applicable Documents

2.1 Required ASTM Standards:

E 338 Sharp-Notch Tension Testing of High-Strength Sheet Materials²

E 399 Test for Plane-Strain Fracture Toughness of Metallic Materials²

E 561 Recommended Practice for R-Curve Determination²

E 602 Sharp-Notch Tension Testing with Cylindrical Specimens²

E 604 Test for Dynamic Tear Energy of Metallic Materials²

E 647 Test for Constant-Load-Amplitude Fatigue Crack Growth Rates Above 10^{-4} m/Cycle²

2.2 The following ASTM standard is listed below for information only:

E 436 Drop-Weight Tear Tests of Ferritic Steels²

3. Index of Terms

3.1 Alphabetical Listing by Term:

Term	Symbol	Section
crack (see ideal crack)		
crack displacement (see also displacement)		6
crack extension	Δa	18
crack-extension force	G	11
crack-extension resistance	K_{R}, G_R, J_R	21
crack, ideal (see ideal crack)		
crack length (see also crack size)	a	46
crack plane orientation		24
crack size	a	13
crack strength	σ_c	28
crack (tip) opening displacement, C(T)OD	δ	8
crack-tip plane strain		9
crack-tip plane stress (see crack-tip plane strain)		
crystallographic cleavage		29
cycle		47
displacement (see also crack displacement)	v	44
drop-weight tear test, DWTT		
dynamic tear (DT) energy		60
effective crack size	a_e	17
effective yield strength	σ_y	19
fatigue crack-growth rate	da/dN	52
fixed-load or fixed-displacement crack-extension force curve		59
fracture toughness		20
fracture toughness, plane-strain (see plane-strain fracture toughness)		
fracture toughness, plane stress (see plane-stress fracture toughness)		
ideal crack		4
ideal-crack-tip stress field		5
J-integral	J	12

¹ This terminology is under the jurisdiction of ASTM Committee E-24 on Fracture Testing, and is the direct responsibility of Subcommittee E24.05 on Terminology.

Current edition approved April 24, 1981. Published August 1981. Originally published as E 616 - 77. Last previous edition E 616 - 80.

² Annual Book of ASTM Standards, Part 10.

Term	Symbol	Section	C(T)OD	crack (tip) opening displacement
load range	ΔP	50	DT	dynamic tear
load ratio	R	51	DWTT	drop-weight tear test
maximum load	P_{max}	48		
maximum stress-intensity factor	K_{max}	55		
minimum load	P_{min}	49		
minimum stress-intensity factor	K_{min}	56		
mode		7		
nominal (net-section) stress	σ_R	25		
notch tensile strength, NTS		26		
original crack size	a_o	15		
physical crack size	a_p	14		
plane strain (see crack-tip plane strain)				
plane-strain fracture toughness	K_{Ic}	23		
plane-stress fracture toughness (see also plane-strain fracture toughness)	K_{Ic}	58		
plastic-zone adjustment	r_Y	16		
R-curve		22		
sharp-notch strength	σ_s	27		
strength (see effective yield strength, notch tensile strength, or sharp notch strength)				
stress field (see ideal-crack-tip stress field)				
stress-intensity calibration	K calibration	53		
stress-intensity factor	K, K_1, K_2, K_3	10		
stress-intensity factor range	ΔK	57		
yield strength, effective (see effective yield strength)				

3.2 Alphabetical Listing by Symbol:

a	crack length
a	crack size
a_e	effective crack size
a_o	original crack size
a_p	physical crack size
da/dN	fatigue crack-growth rate
Δa	crack extension
ΔK	stress-intensity factor range
ΔP	load range
δ	crack (tip) opening displacement
G	crack-extension force
G_R	crack-extension resistance
J	J-integral
J_R	crack-extension resistance
K	stress-intensity factor
K calibration	stress-intensity calibration
K_1, K_2, K_3	stress-intensity factor
K_{Ic}	plane-strain fracture toughness
K_{Ic}	plane stress fracture toughness
K_{max}	maximum stress-intensity factor
K_{min}	minimum stress intensity factor
K_R, G_R, J_R	crack-extension resistance
P_{max}	maximum load
P_{min}	minimum load
R	load ratio
r_Y	plastic-zone adjustment
σ_c	crack strength
σ_N	effective yield strength
σ_N	nominal (net-section) stress
σ_s	sharp-notch strength
v	displacement

3.3 Alphabetical Listing of Abbreviations:

GENERAL DEFINITIONS

4. ideal crack—a simplified model of a crack used in elastic stress analysis. In a stress-free body, the crack has two smooth surfaces that are coincident and join within the body along a smooth curve called the crack front; in two-dimensional representations the crack front is called the crack tip.

5. ideal-crack-tip stress field—the singular stress field, infinitesimally close to the crack front, that results from the dominant influence of an ideal crack in an elastic body that is deformed. In a linear-elastic homogeneous body, the significant stress components vary inversely as the square root of the distance from the crack tip.

NOTE—In a linear-elastic body, the crack-tip stress field can be regarded as the superposition of three component stress fields called modes.

6. crack displacement [L]—the separation vector between two points (on the surfaces of a deformed crack) that were coincident on the surfaces of an ideal crack in the undeformed condition.

7. mode—one of the three classes of crack (surface) displacements adjacent to the crack tip. These displacement modes are associated with stress-strain fields around the crack tip and are designated one, two, and three. Arabic numerals 1, 2, and 3 are used for the general case and roman numerals are used to specialize the mode to plane strain (I and II) or to anti-plane-strain (III).

NOTE 1—See definition of crack-tip plane strain for comments on plane strain and plane stress. See also crack displacement.

NOTE 2—It is recommended that the arabic subscript 1 be omitted except where needed for clarity.

Discussion—For isotropic materials, these three modes can be represented by the crack (surface) displacements presented in Table 1 and Fig. 1. For anisotropic materials, the displacements can be more complex.

Using the coordinates shown in Fig. 2 and assuming a homogeneous, isotropic elastic body, the singular stresses on an infinitesimal element just ahead of the crack front for modes I, II, and III are zero or non-zero as indicated in Table 1.

For linear-elastic bodies, the three stress-strain fields can be added to describe any crack-tip stress-strain field.

8. crack (tip) opening displacement (C(T)OD), δ [L]—the crack displacement due to elastic and plastic deformation at variously defined locations near the original (prior to an application load) crack tip.

NOTE—In common practice, δ is estimated for mode I by inference from observations of crack displacement nearby or away, or both, from the crack tip.

9. crack-tip plane strain—a stress-strain field, near a crack tip, that approaches plane strain to the degree required by an empirical criterion.

NOTE 1—For example in mode I, the criterion for crack-tip plane strain given in Method E 399 requires that plate thickness, B , must be equal to or greater than $2.5 (K/\sigma_Y)^2$.

NOTE 2—See text books on elasticity or solid mechanics for analytical definitions of plane strain.

NOTE 3—Crack-tip plane stress is a stress-strain field which is commonly used for a crack tip that is not in plane strain. In such situations the influences of the remaining degree of plane strain may be significant.

NOTE 4—For analytical discussions of plane stress and crack-tip plane stress, see text books on strength of materials, as well as J. N. Goodier, *Fracture*, Vol. II, H. Liebowitz, ed., Academic Press, New York (1968), p. 8 or N. E. Frost et al, *Metal Fatigue*, Clarendon Press, Oxford (1974), p. 210.

10. stress-intensity factor, K , K_1 , K_2 , K_3 [$\text{FL}^{-3/2}$]—the magnitude of the ideal-crack-tip stress field (a stress-field singularity) for a particular mode in a homogeneous, linear-elastic body.

NOTE—Values of K for the modes 1, 2, and 3 are given by:

$$K_1 = \lim_{r \rightarrow 0} [\sigma_y(2\pi r)^{1/2}],$$

$$K_2 = \lim_{r \rightarrow 0} [\tau_{xy}(2\pi r)^{1/2}], \text{ and}$$

$$K_3 = \lim_{r \rightarrow 0} [\tau_{yz}(2\pi r)^{1/2}],$$

where r = a distance directly forward from the crack tip to a location where the significant stress is calculated.

11. crack-extension force, G [FL^{-1}]—the elastic energy per unit of new separation area that is made available at the front of an ideal crack in an elastic solid during a virtual increment of forward crack extension.

NOTE—The above definition of G is useful for either static cracks or for running cracks. From past usage, G is commonly associated with linear-elastic methods of analysis, and J (see J-integral) may also be used for these analyses.

12. J-integral, J [FL^{-1}]—a mathematical expression, a line or surface integral that encloses the crack front from one crack surface to the other, used to characterize the local stress-strain field around the crack front.

NOTE 1—The J-integral expression for a two-dimensional crack, in the x - z plane with the crack front parallel to the y axis, is the line integral.

$$J = \int_{\Gamma} (W dy - \vec{T} \cdot \frac{\partial \vec{u}}{\partial x} ds),$$

where:

- W = loading work per unit volume or, for elastic bodies, strain energy density,
- Γ = the path of the integral, which encloses (that is, contains) the crack tip,
- ds = increment of the contour path,
- \vec{T} = outward traction vector on ds ,
- \vec{u} = displacement vector at ds ,
- x, y, z = rectangular coordinates (Fig. 2), and
- $\vec{T} \cdot \frac{\partial \vec{u}}{\partial x} ds$ = the rate of work input from the stress field into the area enclosed by Γ .

The value of J obtained from this equation is taken to be path independent in test specimens commonly used, but in service components (and perhaps in test specimens) caution is needed to adequately consider loading interior to Γ such as from rapid motion of the crack or the service component, and from residual or thermal stress.

NOTE 2—In elastic (linear or nonlinear) solids, the J-integral equals the crack-extension force, G . (See definition of G .)

NOTE 3—For those elastic (linear and nonlinear) solids for which the above equation is path independent, the J-integral is equal to the value obtained from two identical bodies with infinitesimally differing crack areas, each subject to stress, as the difference in loading work per unit difference in crack area at a fixed value of displacement or, where appropriate, at a fixed value of load. This approach is often used to define the value of J for inelastic solids.

NOTE 4—For further discussion, see J. R. Rice, *Journal of Applied Mechanics* Vol. 35, 1968, p. 379.

13. crack size, a [L]—a lineal measure of a principal planar dimension of a crack. This measure is commonly used in the calculation of quantities descriptive of the stress and displacement fields, and is often also termed crack length.

NOTE—In practice, the value of a is obtained from procedures for measurement of physical crack size, a_p , original crack size, a_o , and effective crack size, a_e , as appropriate to the situation being considered.

14. physical crack size, a_p [L]—the distance from a reference plane to the observed crack front. This distance may represent an average

of several measurements along the crack front. The reference plane depends on the specimen form, and it is normally taken to be either the boundary, or a plane containing either the load line or the centerline of a specimen or plate.

15. original crack size a_o [L]—the physical crack size at the start of testing.

16. plastic-zone adjustment, r_Y [L]—an addition to the physical crack size to account for plastic, crack-tip deformation enclosed by a linear-elastic stress field.

NOTE—Commonly the plastic-zone adjustment is given by:

$$r_Y = \frac{1}{2\pi} \frac{K^2}{\sigma_Y^2}, \text{ for plane-stress mode I, and}$$

$$r_Y = \frac{\alpha}{2\pi} \frac{K^2}{\sigma_Y^2}, \text{ for plane-strain mode I,}$$

where $\alpha \approx 1/3$ to $1/4$ and σ_Y is the effective yield strength.

17. effective crack size, a_e [L]—the physical crack size augmented for the effects of crack-tip plastic deformation.

NOTE—Sometimes the effective crack size, a_e , is calculated from a measured value of a physical crack size, a_p , plus a calculated value of a plastic-zone adjustment, r_Y . A preferred method for calculation of a_e compares compliance from the secant of a load-deflection trace with the elastic compliance from a calibration for the type of specimen.

18. crack extension, Δa [L]—an increase in crack size.

NOTE—For example, Δa_p or Δa_e is the difference between the crack size, either a_p (physical crack size) or a_e (effective crack size), and a_o (original crack size).

19. effective yield strength, σ_Y [FL⁻²]—an assumed value of uni-axial yield strength that represents the influences of plastic yielding upon fracture test parameters. It is variously defined for use in calculations.

NOTE 1—For example, the effective yield strength is sometimes the 0.2 % offset tensile-yield strength (σ_{YS}); other times it is the average of this value and the ultimate-tensile strength (σ_{TS}), that is $(\sigma_{YS} + \sigma_{TS})/2$.

NOTE 2—In estimating σ_Y , influences of testing conditions, such as loading rate and temperature, should be considered.

20. fracture toughness—a generic term for measures of resistance to extension of a crack.

NOTE—The term is sometimes restricted to results of fracture mechanics tests, which are directly applicable in fracture control. However, the term com-

monly includes results from simple tests of notched or precracked specimens not based upon fracture mechanics analysis. Results from tests of the latter type are often useful for fracture control, based upon either service experience or empirical correlations with fracture mechanics tests.

21. crack-extension resistance, K_R [FL^{-3/2}], and G_R or J_R (FL⁻¹)—a measure of the resistance of a material to crack extension expressed in terms of the stress-intensity factor, K , the crack-extension force, G , or values of J derived using the J-integral concept.

NOTE—See definition of *R-curve*.

22. R-curve—a plot of crack-extension resistance as a function of stable crack extension, Δa_p or Δa_e .

NOTE—For specimens discussed in Recommended Practice E 561, influence of in-plane geometry appears to be negligible, but *R*-curves normally depend upon specimen thickness and, for some materials, upon temperature and strain rate.

23. plane-strain fracture toughness—the crack-extension resistance under conditions of crack-tip plane strain.

NOTE 1—For example, in mode I for slow rates of loading and negligible plastic-zone adjustment, plane-strain fracture toughness is the value of stress-intensity factor designated K_{Ic} [FL^{-3/2}] as measured using the operational procedure (and satisfying all of the validity requirements) specified in Method E 399, which provides for the measurement of crack-extension resistance at the start of crack extension and provides operational definitions of crack-tip sharpness, start of crack extension, and crack-tip plane strain.

NOTE 2—See also definitions of crack-extension resistance, crack-tip plane strain, and mode.

Discussion—Plane-stress fracture toughness is the crack-extension resistance under conditions that do not approach crack-tip plane strain to a degree required by an empirical criterion. For example, by Recommended Practice E 561, plane-stress fracture toughness is represented by an *R-curve*.

When plane-stress fracture toughness is used to define conditions for crack instability it is designated K_{cs} , a quantity dependent on specimen geometry; by Recommended Practice E 561, K_c is the value of K at the point of tangency between the *R-curve* and the geometry-dependent stress-intensity-factor curve.

The effective crack size concept may be used to compute plasticity adjusted values of stress-intensity factor, K , if the crack-tip plastic zone is surrounded by an elastic stress field.

24. crack plane orientation—an identification of the plane and direction of a fracture in relation to product geometry. This identification is designated by a hyphenated code with

the first letter(s) representing the direction normal to the crack plane and the second letter(s) designating the expected direction of crack propagation.

Discussion—

24.1 The fracture toughness of a material usually depends on the orientation and direction of propagation of the crack in relation to the anisotropy of the material, which depends, in turn, on the principal directions of mechanical working or grain flow. The orientation of the crack plane should be identified wherever possible in accordance with the following systems.³ In addition, the product form should be identified (for example, straight rolled plate, cross rolled plate, pancake forging, etc.).

24.1.1 For rectangular sections, the reference directions are identified as in Figs. 3 and 4, which give examples for a rolled plate. The same system would be useful for sheet, extrusions, and forgings with nonsymmetrical grain flow.

L = direction of principal deformation (maximum grain flow),

T = direction of least deformation, and

S = third orthogonal direction.

24.1.1.1 Using a two letter code, the first letter designates the *direction normal* to the crack plane, and the second letter the *expected direction of crack propagation*. For example, in Fig. 3 the *T-L* specimen has a fracture plane whose normal is in the width direction of a plate and an expected direction of crack propagation coincident with the direction of maximum grain flow or longitudinal direction of the plate.

24.1.1.2 For specimens that are tilted in respect to two of the reference axes, Fig. 4, the orientation is identified by a three-letter code. The code *L-TS*, for example, means that the crack plane is perpendicular to the direction of principal deformation (*L* direction), and the expected fracture direction is intermediate between *T* and *S*. The code *TS-L* means the crack plane is perpendicular to a direction intermediate between *T* and *S*, and the expected fracture direction is in the *L* direction.

24.1.2 For certain cylindrical sections where the direction of principal deformation is parallel to the longitudinal axis of the cylinder, the reference directions are identified as in Fig. 5, which gives examples for a drawn bar. The same system would be useful for extrusions or forged parts having circular cross section.

L = direction of maximum grain flow,

R = radial direction, and

C = circumferential or tangential direction.

24.1.3 The C-shaped specimen is intended to measure the fracture toughness so that the normal-to-the-crack plane is in the circumferential or tangential direction and the direction of crack propagation is in the radial direction. This is the *C-R* orientation as defined in 24.1.2. For other orientations, a bend specimen or a compact specimen should be used.

25. **nominal (net-section) stress, σ_N [FL⁻²]**—in fracture testing, a measure of the stress on the net cross section calculated in a simplified man-

ner and without taking into account stress gradients produced by geometric discontinuities such as holes, grooves, fillets, etc.

NOTE 1—In tension specimens (tension only), the average stress is used: $\sigma_N = P/A$, where $A = B(W - a)$ for rectangulars, and $A = (\pi d^2)/4$ for circulars.

NOTE 2—In bend specimens (bending only), a fiber stress is used:

$$\sigma_N = \frac{6M}{B(W - a)^2}$$

NOTE 3—In compact specimens (tension and bending),

$$\sigma_N = \frac{2P(2W + a)}{B(W - a)^2}$$

NOTE 4—In C-shaped specimens (tension and bending),

$$\sigma_N = \frac{2P(3X + 2W + a)}{B(W - a)^2}$$

NOTE 5—In Notes 1 to 4,

d = diameter of notched section of a circumferentially-notched specimen, in. (or m),

P = load, lbf (or N),

B = specimen thickness, in. (or m),

W = specimen width, in. (or m),

a = crack size (length of notch or notch plus pre-crack), in. (or m),

X = loading hole offset, in. (or m), and

M = bending moment, in.·lbf (N·m), and the result, σ_N , is given in psi (or Pa). See Method E 399 for further explanations of symbols.

26. **notch tensile strength (NTS) [FL⁻²]**—the maximum nominal (net-section) stress that a notched tensile specimen is capable of sustaining.

NOTE 1—See definitions of **nominal (net-section) stress** and **sharp-notch strength**.

NOTE 2—Values of notch tensile strength may depend upon section size, notch sharpness, and eccentricity of the notch. See **sharp-notch strength**.

27. **sharp-notch strength, σ_s [FL⁻²]**—the maximum nominal (net-section) stress that a sharply notched specimen is capable of sustaining.

NOTE 1—See definition of **nominal (net-section) stress**.

NOTE 2—Values of sharp-notch strength may depend on notch and specimen configuration as these affect the net cross section and the elastic stress concentration.

NOTE 3—The tension specimens used in Methods E 388 and E 602 have notch root radii that approach the limit of machining capability. For these specimens, the radius is believed to be small enough that

³ Goode, R. J., "Identification of Fracture Plane Orientation," *Materials Research and Standards*, MIRSA, Am. Soc. Testing Mats., Vol. 12, No. 9, September 1972.

any smaller radius that is obtainable by standard machining methods would not produce changes in notch strength that are significant from an engineering viewpoint.

28. crack strength, σ_c [FL⁻²]—the maximum value of the nominal (net-section) stress that a cracked specimen is capable of sustaining.

NOTE 1—See definition of nominal (net-section) stress.

NOTE 2—Crack strength is calculated on the basis of the maximum load and the original minimum cross-sectional area (net cross section or ligament). Thus, it takes into account the original size of the crack, but ignores any crack extension that may occur during the test.

NOTE 3—Crack strength is analogous to the ultimate tensile strength, as it is based on the ratio of the maximum load to the minimum cross-sectional area of the specimen at the start of the test.

29. crystallographic cleavage—the separation of a crystal along a plane of fixed orientation relative to the three-dimensional crystal structure within which the separation process occurs, with the separation process causing the newly formed surfaces to move away from one another in directions containing major components of motion perpendicular to the fixed plane.

NOTE 1—Removed from the definition are all concepts of how the cleavage came about, including any inference of velocity, brittleness, energy, number of load applications, temperature, cohesive strength, atomic motions, etc. Only the crystallographic orientation relationship is used as the strict definition. However, when considering a specific fracture, it is helpful to know the conditions under which the cleavage was obtained, its appearance, velocity, etc., and the method by which the author concluded that the cracking event was cleavage.

NOTE 2—Cleavage usually occurs along planes having the largest interplanar spacings, or in other words, along planes with lowest indexes.

NOTE 3—Crystallographic cleavage has been identified in increasing numbers of materials and in increasing numbers of environments and stress conditions. Stress corrosion cracking, liquid metal-induced cracking, low-amplitude fatigue cracking, and hydrogen-assisted cracking, as well as the long-established low-temperature brittle fracture from a single load application, are known to frequently cause crystallographic cleavage.

NOTE 4—Proof that a fracture surface was formed by crystallographic cleavage is accomplished by a knowledge of the crystal structure, combined with a determination of the crystal orientation by techniques such as X-ray diffraction, electron diffraction, etch pit shapes, single- or multiple-surface trace analysis, etc. This form of cleavage is usually, but not always, recognizable by a number of fracture surface features, such as flat facets, steps between parallel facets, river

patterns formed by the joining of steps, and tongues and herringbone patterns caused by crystallographic twins at the crack tip. High magnifications (up to about 2000 ×) are often needed to see those characteristic features in fine-grained alloys.

NOTE 5—Separation along a matrix/twin interface is classified as parting, not cleavage.

NOTE 6—Although proof of cleavage is obtained from individual crystals, these crystals may be single crystals or incorporated into large-grained or fine-grained aggregates.

NOTE 7—A specific crystal may cleave along one family of planes under one combination of variables and along another family under another combination.

OTHER DEFINITIONS

Other definitions are extracted from Method E 338 - 78:

30. sharp-notch strength—(see Section 26 of this terminology).

Method E 399 - 78a:

31. stress-intensity factor—(See Section 10 of this terminology. See also *mode*.)

Discussion—In Method E 399, mode I is assumed.

32. plane-strain fracture toughness—(see Section 23 of this terminology).

33. crack plane orientation—(see Section 24 of this standard).

Recommended Practice E 561 - 80:

34. crack size—(see Section 13 of this terminology).

35. physical crack size—(see Section 14 of this terminology).

36. original crack size—(see Section 15 of this terminology).

37. effective crack size—(see Section 17 of this terminology).

38. plastic-zone adjustment, r_p [L]—(see Section 16 of this terminology).

Discussion—In this method, plane-stress mode I is assumed.

39. crack extension—(see Section 18 of this terminology).

40. stress-intensity factor—(See Section 10 of this terminology. See also *mode*.)

Discussion—In Recommended Practice E 561, mode I is assumed.

41. crack extension resistance—(see Section 21 of this terminology).

42. R-curve—(see Section 22 of this terminology).

43. crack displacement—(see Section 6 of this terminology).

Discussion—In Recommended Practice E 561, displacement (V) is the distance that a chosen measurement point on the specimen displaces normal to the crack plane. Total displacement as measured by clip gages or other devices spanning the crack is defined as $2v$. Measurement points on CLWL and CS specimens are identified as locations $V1$ and $V2$.

Method E 602 - 78 T:

44. sharp notch strength—(see Section 27 of this terminology).

Method E 647 - 78 T:

45. crack length, a [L]—*in fatigue*, the physical crack size used to determine the crack growth rate and the stress-intensity factor. For the CT specimen, a is measured from the line connecting the bearing points of load application, for the CCT specimen, a is measured from the perpendicular bisector of the central crack.

46. cycle—*in fatigue*, one complete sequence of values of applied load that is repeated periodically. The symbol N represents the number of cycles.

47. maximum load, P_{\max} [F]—*in fatigue*, the greatest algebraic value of applied load in a cycle. Tensile loads are considered positive and compressive loads negative.

48. minimum load, P_{\min} [F]—*in fatigue*, the least algebraic value of applied load in a cycle.

49. load range, ΔP [F]—*in fatigue*, the algebraic difference between the maximum and minimum loads in a cycle.

50. load ratio (also called stress ratio), R —*in fatigue*, the algebraic ratio of the minimum to maximum load in a cycle, that is, $R = P_{\min}/P_{\max}$.

51. fatigue crack growth rate, da/dN , [L]—the rate of crack extension caused by constant-amplitude fatigue loading, expressed in terms of crack extension per cycle of fatigue.

52. stress-intensity calibration, K calibration—a mathematical expression, based on empirical or analytical results, that relates the stress intensity factor to load and crack length for a specific specimen planar geometry.

53. stress-intensity factor—See Section 10 of this terminology. See also *mode*.)

Discussion—In Method E 647, mode I is assumed.

54. maximum stress-intensity factor, K_{\max} [$FL^{-3/2}$]—*in fatigue*, the maximum value of the

stress-intensity factor in a cycle. This value corresponds to P_{\max} .

55. minimum stress-intensity factor, K_{\min} [$FL^{-3/2}$]—*in fatigue*, the minimum value of the stress-intensity factor in a cycle. This value corresponds to P_{\min} when $R > 0$ and is taken to be zero when $R \leq 0$.

56. stress-intensity factor range, ΔK [$FL^{-3/2}$]—*in fatigue*, the variation in the stress-intensity factor in a cycle, that is, $K_{\max} - K_{\min}$.

NOTE 1—The loading variables R , ΔK , and K_{\max} are related such that specifying any two uniquely defines the third according to the following relationship: $\Delta K = (1 - R)K_{\max}$ for $R \geq 0$ and $\Delta K = K_{\max}$ for $R \leq 0$.

NOTE 2—These operational stress-intensity factor definitions do not include local crack-tip effects; for example, crack closure, residual stress, and blunting.

DESCRIPTIONS OF TERMS SPECIFIC TO A PARTICULAR STANDARD

Descriptions of terms are extracted from Recommended Practice E 561 - 80:

57. plane-stress fracture toughness, K_{IC} —in Recommended Practice E 561, the value of K_{IC} at the instability condition determined from the tangency between the R -curve and the critical crack-extension force curve of the specimen.

NOTE—See the discussion of plane-strain fracture toughness in Terminology E 616.

58. fixed-load or fixed-displacement crack-extension force curves—curves obtained from a fracture mechanics analysis for the test configuration; assuming a fixed applied load or displacement and generating a curve of K versus the effective crack size as the independent variable.

Method E 604 - 77:

59. dynamic tear (DT) energy is the total energy required to fracture standard $\frac{3}{8}$ -in. (16-mm) thick DT specimens tested in accordance with the provisions of Method E 604.

NOTE 1—With pendulum-type machines, the DT energy value recorded is the difference between the initial and the final potential energies of the pendulum or pendulums.

NOTE 2—With drop-weight machines, the DT energy value recorded is the difference between the initial potential energy of the hammer and the final energy of the hammer, as determined by a calibrated energy absorption system.

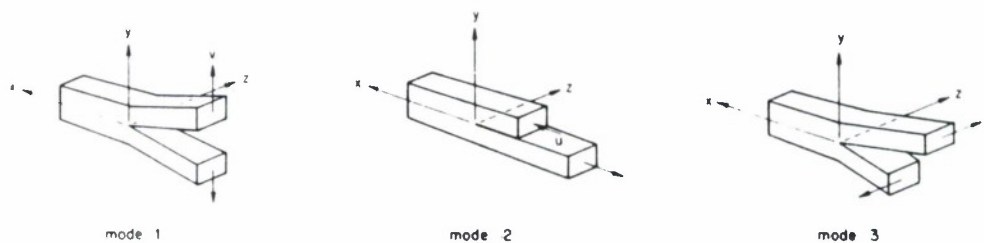
TABLE 1 Stress and Displacement Components^A for Plane-Strain and Anti-Plane-Strain Modes (see definition of mode)

	Mode I	Mode II	Mode III
Crack (surface) displacements ^B just behind the crack front (see Fig. 1):			
u	0	•	0
v	•	0	0
w	0	0	•
Stresses just ahead of the crack front (see Fig. 2):			
σ_x	•	0	0
σ_y	•	0	0
σ_z	•	0	0
τ_{xy}	0	•	0
τ_{yz}	0	0	•
τ_{xz}	0	0	0

^A • means non-zero.

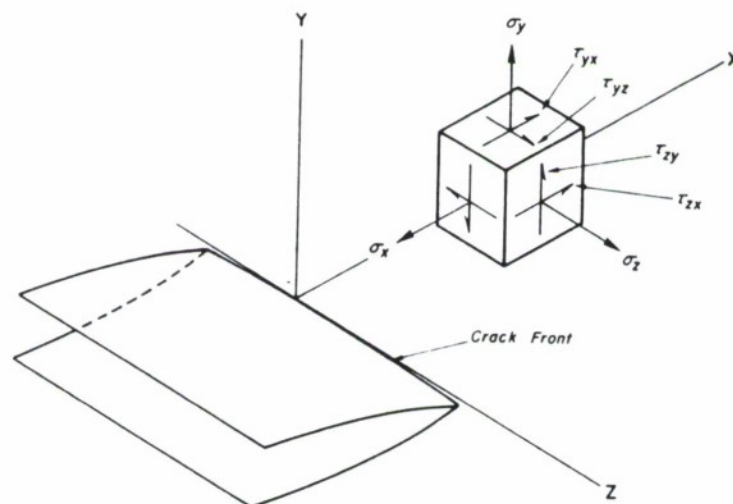
0 means zero.

^B Not applicable generally to anisotropic materials.



NOTE—See definition of mode.

FIG. 1 Basic Modes of Crack (Surface) Displacements for Isotropic Materials



NOTE—See definition of mode

FIG. 2 Customary Coordinate System and Stress on a Small Volume Element Located on the x Axis Just Ahead of the Crack Front

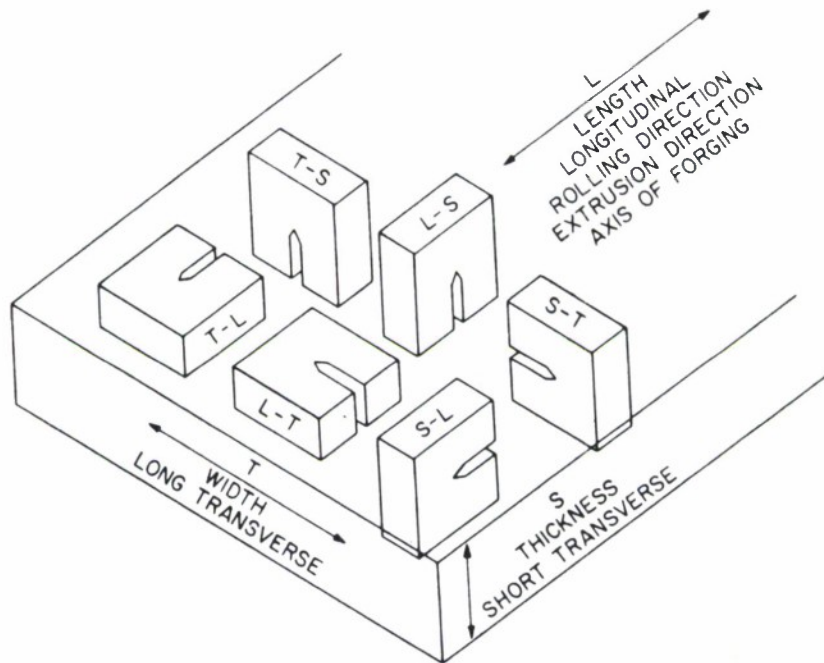


FIG. 3 Crack Plane Orientation Code for Rectangular Sections

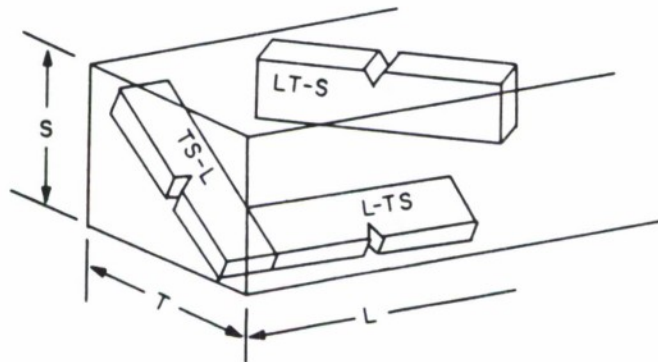


FIG. 4 Crack Plane Orientation Code for Rectangular Sections Where Specimens Are Tilted with Respect to the Reference Directions

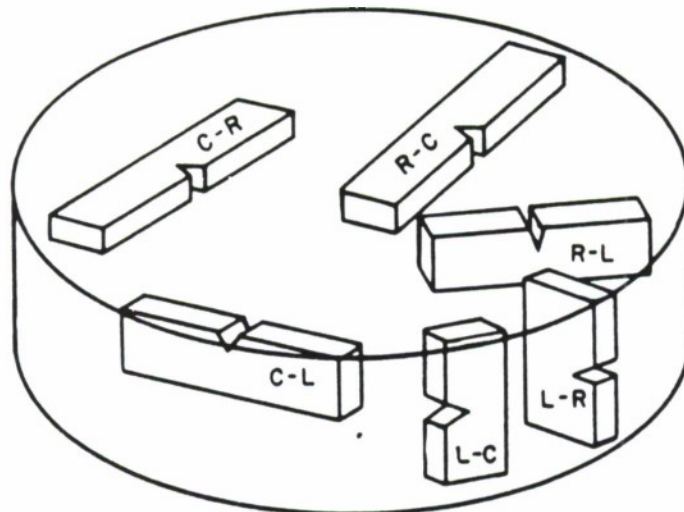


FIG. 5 Crack Plane Orientation Code for Bar and Hollow Cylinder

ANNEX

A1. UNITS

A1.1 For stress intensity factor, K , and any measure of fracture toughness expressed in terms of K , the recommended unit is $\text{MPa}(\text{m})^{1/2}$. The corresponding customary unit is $\text{ksi}(\text{in.})^{1/2}$.

A1.2 For the crack-extension force, G , and for the elastic energy release rate, which in plane measure-

ment problems is equal to J , and any measure of fracture toughness expressed in terms of G or J , the recommended unit is kJ/m^2 . The corresponding customary unit is $\text{in-lb}/\text{in.}^2$.

A1.3 For crack (tip) opening displacement, σ , and any measure of fracture toughness expressed in terms of σ , the recommended unit is metre. The corresponding inch-pound unit is mil.

This standard is subject to revision at any time by the responsible technical committee and must be reviewed every five years and if not revised, either reapproved or withdrawn. Your comments are invited either for revision of this standard or for additional standards and should be addressed to ASTM Headquarters. Your comments will receive careful consideration at a meeting of the responsible technical committee, which you may attend. If you feel that your comments have not received a fair hearing you should make your views known to the ASTM Committee on Standards, 1916 Race St., Philadelphia, Pa. 19103, which will schedule a further hearing regarding your comments. Failing satisfaction there, you may appeal to the ASTM Board of Directors.



Designation: E 399 – 81

AMERICAN SOCIETY FOR TESTING AND MATERIALS

1916 Race St., Philadelphia, Pa. 19103

Reprinted from the Annual Book of ASTM Standards, Copyright ASTM

If not listed in the current combined index, will appear in the next edition.

Standard Test Method for PLANE-STRAIN FRACTURE TOUGHNESS OF METALLIC MATERIALS¹

This standard is issued under the fixed designation E 399; the number immediately following the designation indicates the year of original adoption or, in the case of revision, the year of last revision. A number in parentheses indicates the year of last reapproval.

This method has been approved for use by agencies of the Department of Defense and for listing in the DoD Index of Specifications and Standards

1. Scope

1.1 This method covers the determination of the plane-strain fracture toughness (K_{Ic}) of metallic materials by tests using a variety of fatigue-cracked specimens having a thickness of 0.063 in. (1.6 mm) or greater.² The details of the various specimen configurations are shown in Annexes A1 through A6.

NOTE 1—Plane-strain fracture toughness tests of thinner materials that are sufficiently brittle (see 7.1) can be made with other types of specimens (1).³ There is no standard test method for testing such thin materials.

1.2 This method also covers the determination of the specimen strength ratio R_x , where x refers to the specific specimen configuration being tested. This strength ratio is a function of the maximum load the specimen can sustain, its initial dimensions and the yield strength of the material.

1.3 Measured values of plane-strain fracture toughness stated in inch-pound units are to be regarded as standard.

2. Applicable Documents

2.1 ASTM Standards:

B 645 Practice for Plain Strain Fracture Toughness Testing of Aluminium Alloys⁴

E 8 Tension Testing of Metallic Materials⁵

E 21 Practice for Elevated Temperature Tension Tests of Metallic Materials⁶

E 337 Test for Relative Humidity by Wet- and Dry-Bulb Psychrometer⁷

E 338 Sharp-Notch-Tension Testing of High-Strength Sheet Materials⁶

E 616 Terminology Relating to Fracture Testing⁶

3. Summary of Method

3.1 This method involves testing of notched specimens that have been precracked in fatigue by loading either in tension or three-point bending. Load versus displacement across the notch at the specimen edge is recorded autographically. The load corresponding to a 2 % apparent increment of crack extension is established by a specified deviation from the linear portion of the record. The K_{Ic} value is calculated from this load by equations that have been established on the basis of elastic stress analysis of specimens of the types described in this method. The validity of the determination of the K_{Ic} value by this method depends upon the establishment of a *sharp-crack* condition at the tip of the fatigue crack, in a specimen of adequate size. To establish a suitable crack-tip condition, the stress intensity level at which the fatigue precracking of the specimen is conducted is limited to a relatively low value.

3.2 The specimen size required for testing purposes increases as the square of the ratio of toughness to yield strength of the material;

¹ This method is under the jurisdiction of ASTM Committee E-24 on Fracture Testing and is the direct responsibility of Subcommittee E24.01 on Fracture Mechanics Test Methods.

Current edition approved April 24, 1981. Published July 1981. Originally published as E 399 – 70 T. Last previous edition E 399 – 78a.

² For additional information relating to the fracture toughness testing of aluminum alloys, see Method B 645.

³ The boldface numbers in parentheses refer to the list of references at the end of this method.

⁴ Annual Book of ASTM Standards, Part 7.

⁵ Annual Book of ASTM Standards, Parts 6, 7, 10.

⁶ Annual Book of ASTM Standards, Part 10.

⁷ Annual Book of ASTM Standards, Parts 20, 26, 32, 41.



therefore a range of proportional specimens is provided.

4. Significance and Use

4.1 The property K_{Ic} determined by this method characterizes the resistance of a material to fracture in a neutral environment in the presence of a sharp crack under severe tensile constraint, such that the state of stress near the crack front approaches triaxial plane strain, and the crack-tip plastic region is small compared with the crack size and specimen dimensions in the constraint direction. A K_{Ic} value is believed to represent a lower limiting value of fracture toughness. This value may be used to estimate the relation between failure stress and defect size for a material in service wherein the conditions of high constraint described above would be expected. Background information concerning the basis for development of this method in terms of linear elastic fracture mechanics may be found in Refs (1) and (2).

4.1.1 The K_{Ic} value of a given material is a function of testing speed and temperature. Furthermore, cyclic loads can cause crack extension at K_I values less than the K_{Ic} value. Crack extension under cyclic or sustained load will be increased by the presence of an aggressive environment. Therefore, application of K_{Ic} in the design of service components should be made with awareness to the difference that may exist between the laboratory tests and field conditions.

4.1.2 Plane-strain crack toughness testing is unusual in that there can be no advance assurance that a valid K_{Ic} will be determined in a particular test. Therefore it is essential that all of the criteria concerning validity of results be carefully considered as described herein.

4.1.3 Clearly it will not be possible to determine K_{Ic} if any dimension of the available stock of a material is insufficient to provide a specimen of the required size. In such a case the specimen strength ratio determined by this method will often have useful significance. However, this ratio, unlike K_{Ic} , is not a concept of linear elastic fracture mechanics, but can be a useful comparative measure of the toughness of materials when the specimens are of the same form and size, and that size is insufficient to provide a valid K_{Ic} determination, but sufficient that the maximum load results from pro-

nounced crack propagation rather than plastic instability.

4.1.3.1 The strength ratio for center-cracked plate specimens tested in uniaxial tension may be determined by Method E 338.

4.2 This method can serve the following purposes:

4.2.1 In research and development to establish, in quantitative terms, significant to service performance, the effects of metallurgical variables such as composition or heat treatment, or of fabricating operations such as welding or forming, on the fracture toughness of new or existing materials.

4.2.2 In service evaluation, to establish the suitability of a material for a specific application for which the stress conditions are prescribed and for which maximum flaw sizes can be established with confidence.

4.2.3 For specifications of acceptance and manufacturing quality control, but only when there is a sound basis for specification of minimum K_{Ic} values, and then only if the dimensions of the product are sufficient to provide specimens of the size required for valid K_{Ic} determination. The specification of K_{Ic} values in relation to a particular application should signify that a fracture control study has been conducted on the component in relation to the expected history of loading and environment, and in relation to the sensitivity and reliability of the crack detection procedures that are to be applied prior to service and subsequently during the anticipated life.

5. Definitions

5.1 *stress-intensity factor*, K_I ($\text{FL}^{-3/2}$)—the magnitude of the ideal-crack-tip stress field for mode I in a linear-elastic body.

NOTE 2—Values of K for mode I are given by:

$$K_I = \lim_{r \rightarrow 0} \sigma_y(2\pi r)^{1/2}$$

where r equals a distance directly forward from the crack tip to a location where the significant stress σ_y is calculated. σ_y is the principal stress normal to the crack plane. For modes 2 and 3, see General Definitions of Terminology E 616.

5.2 *plane-strain fracture toughness*, K_{Ic} ($\text{FL}^{-3/2}$)—the crack extension resistance under conditions of crack-tip plane-strain.

NOTE 3—In mode I Note 5 for slow rates of loading and negligible plastic zone adjustment, plane-strain fracture toughness is the value of stress-inten-

sity factor as measured using the operational procedure (and satisfying all of the validity requirements) specified in this method, which centers attention on the start of crack extension and provides operational definitions of crack tip sharpness, start of crack extension, and crack-tip plane strain.

NOTE 4—The roman numeral I signifies specialization to plane strain at the crack tip. As described in this method, mode I refers to a situation in which the crack faces are displaced apart in the direction normal to the crack plane.

NOTE 5—For definitions relating to measures of fracture toughness other than K_{Ic} , refer to General Definitions in Terminology E 616.

6. Apparatus

6.1 *Loading*—Specimens should be loaded in a testing machine that has provision for autographic recording of the load applied to the specimen.

6.2 *Fixtures*—Fixtures suitable for loading the specimen configurations covered by this method are shown in the appropriate annex. These fixtures are so designed as to minimize the frictional contributions to the measured load.

6.3 *Displacement Gage*—The displacement gage output shall indicate the relative displacement of two precisely located gage positions spanning the crack starter notch mouth. Exact and positive positioning of the gage on the specimen is essential, yet the gage must be released without damage when the specimen breaks. A recommended design for a self-supporting, releasable gage is shown in Fig. 1 and described in Annex A1. The strain gage bridge arrangement is also shown in Fig. 1.

6.3.1 The specimen must be provided with a pair of accurately machined knife edges that support the gage arms and serve as the displacement reference points. These knife edges can be machined integral with the specimen as shown in Fig. 1 and Fig. 2 or they may be separate pieces fixed to the specimen. A suggested design for such attachable knife edges is shown in Fig. 3. This design is based on a knife edge spacing of 0.2 in. (5.1 mm). The effective gage length is established by the points of contact between the screw and the hole threads. For the design shown the major diameter of the screw has been used in setting this gage length. A No. 2 screw will permit the use of attachable knife edges for specimens having $W > 1$ in. (25 mm).

6.3.2 Each gage shall be checked for linearity using an extensometer calibrator or other suitable device; the resettability of the calibrator at each displacement interval should be within $+0.000020$ in. (0.00050 mm). Readings shall be taken at ten equally spaced intervals over the working range of the gage (see Annex A1). This calibration procedure should be performed three times, removing and reinstalling the gage in the calibration fixture between each run. The required linearity shall correspond to a maximum deviation of $+0.0001$ in. (0.0025 mm) of the individual displacement readings from a least-squares-best-fit straight line through the data. The absolute accuracy, as such, is not important in this application, since the method is concerned with relative changes in displacement rather than absolute values (see 9.1).

6.3.3 It is not the intent of this method to exclude the use of other types of gages or gage-fixing devices provided the gage used meets the requirements listed below and provided the gage length does not exceed those limits given in the annex appropriate to the specimen being tested.

7. Specimen Size, Configurations, and Preparation

7.1 Specimen Size:

7.1.1 In order for a result to be considered valid according to this method it is required that both the specimen thickness, B , and the crack length, a , exceed $2.5 (K_{Ic}/\sigma_{YS})^2$, where σ_{YS} is the 0.2% offset yield strength of the material for the temperature and loading rate of the test (1, 5, 6).

7.1.2 The initial selection of a size of specimen from which valid values of K_{Ic} will be obtained may be based on an estimated value of K_{Ic} for the material. It is recommended that the value of K_{Ic} be overestimated, so that a conservatively large specimen will be employed for the initial tests. After a valid K_{Ic} result is obtained with the conservative-size initial specimen, the specimen size may be reduced to an appropriate size [a and $B \geq 2.5 (K_{Ic}/\sigma_{YS})^2$] for subsequent testing.

7.1.3 Alternatively, the ratio of yield strength to Young's modulus can be used for selecting a specimen size that will be adequate for all but the toughest materials:

σ_{YS}/E	Minimum Recommended Thickness and Crack Length	
	in.	mm
0.0050 to 0.0057	3	75
0.0057 to 0.0062	2½	63
0.0062 to 0.0065	2	50
0.0065 to 0.0068	1¾	44
0.0068 to 0.0071	1½	38
0.0071 to 0.0075	1¼	32
0.0075 to 0.0080	1	25
0.0080 to 0.0085	¾	20
0.0085 to 0.0100	½	12½
0.0100 or greater	¼	6½

When it has been established that $2.5 (K_{Ic}/\sigma_{YS})^2$ is substantially less than the minimum recommended thickness given in the preceding table, then a correspondingly smaller specimen can be used. On the other hand, if the form of the available material is such that it is not possible to obtain a specimen with both crack length and thickness greater than $2.5 (K_{Ic}/\sigma_{YS})^2$, then it is not possible to make a valid K_{Ic} measurement according to this method.

7.2 Specimen Configurations—The configurations of the various specimens are shown in the following annexes: Annex A3, Bend Specimen SE (B), Annex A4, Compact Specimen C (T), Annex A5, Arc-Shaped Specimen A (T), and Annex A6, Disk-Shaped Compact Specimen DC (T).

7.2.1 Standard Specimens—The crack length, a (crack starter notch plus fatigue crack) is nominally equal to the thickness, B , and is between 0.45 and 0.55 times the width, W . The ratio W/B is nominally equal to two.

7.2.2 Alternative Specimens—In certain cases it may be desirable to use specimens having W/B ratios other than two. Alternative proportions for bend specimens are $1 \leq W/B \leq 4$. For the other specimen configurations alternative specimens may have $2 \leq W/B \leq 4$. These alternative specimens shall have the same crack length-to-width ratio as the standard specimens. It should be appreciated that K_{Ic} values obtained using alternative specimen proportions may not agree with those obtained using the standard specimens (15).

7.3 Specimen Preparation—The dimensional tolerances and surface finishes shown on the specimen drawings given in Annexes A3 to A6 shall be followed in specimen preparation.

7.3.1 Fatigue Crack Starter Notch—Three forms of fatigue crack starter notches are shown in Fig. 4. To facilitate fatigue cracking at low

stress intensity levels, the root radius for a straight-through slot terminating in a V-notch should be 0.003 in. (0.08 mm) or less. If a chevron form of notch is used, the root radius may be 0.010 in. (0.25 mm) or less. In the case of a slot tipped with a hole it will be necessary to provide a sharp stress raiser at the end of the hole. Care should be taken to ensure that this stress raiser is so located that the crack plane orientation requirements (8.2.4) can be met.

7.3.2 Fatigue Cracking—Fatigue cracking shall be conducted in accordance with the procedures outlined in Annex A2. Fatigue cycling shall be continued until the fatigue crack will satisfy the requirements stated in the following two sections.

7.3.2.1 The crack length (total length of the crack starter configuration plus the fatigue crack) shall be between 0.45 and 0.55 W .

7.3.2.2 For a straight-through crack starter terminating in a V-notch (see Fig. 4), the length of the fatigue crack on each surface of the specimen shall not be less than 2.5 % of W or 0.050 in. (13 mm) min, and for a crack starter tipped with a drilled hole (see Fig. 4), the fatigue crack extension from the stress raiser tipping the hole shall be greater than 0.5 D on both surfaces of the specimen, where D is the diameter of the hole. For a chevron notch crack starter (see Fig. 4), the fatigue crack shall emerge from the chevron on both surfaces of the specimen.

8. General Procedure

8.1 Number of Tests—It is recommended that at least three replicate tests be made for each material condition.

8.2 Specimen Measurement—Specimen dimensions shall conform to the tolerances shown in the appropriate annex. Three fundamental measurements are necessary for the calculation of K_{Ic} , namely, the thickness, B , the crack length, a , and the width, W .

8.2.1 Measure the thickness, B , to the nearest 0.001 in. (0.025 mm) or to 0.1 %, whichever is larger, at not less than three equally spaced positions along the line of intended crack extension from the fatigue crack tip to the unnotched side of the specimen. The average of these three measurements should be recorded as B .

8.2.2 Measure the crack length, a , after fracture to the nearest 0.5 % at the following three



positions: at the center of the crack front, and midway between the center of the crack front, and the end of the crack front on each surface of the specimen. Use the average of these three measurements as the crack length to calculate K_Q . The following requirements shall apply to the fatigue crack front: (1) The difference between any two of the three crack length measurements shall not exceed 10 % of the average. (2) For a chevron notch starter (see Fig. 4), the fatigue crack shall emerge from the chevron on both surfaces of the specimen, neither surface crack length shall differ from the average length by more than 10 %, and the difference between these two surface measurements shall not exceed 10 % of the average crack length. (3) For a straight-through starter notch (see Fig. 4) no part of the crack front shall be closer to the machined starter notch than 2.5% W or 0.050 in. (13 mm) minimum, nor shall the surface crack length measurements differ from the average crack length by more than 15 %, and the differences between these two measurements shall not exceed 10 % of the average crack length.

8.2.3 Measure the width, W , as described in the annex appropriate to the specimen type being tested.

8.2.4 The plane of the crack shall be parallel to both the specimen width and thickness direction within $\pm 10^\circ$ (7).

8.3 *Loading Rate*—Load the specimen at a rate such that the rate of increase of stress intensity is within the range from 30 000 to 150 000 psi·in.^{1/2}/min (0.55 to 2.75 MPa·m^{1/2}/s). The loading rates corresponding to these stress intensity rates are given in the appropriate annex for the specimen being tested.

8.4 *Test Record*—Make a test record consisting of an autographic plot of the output of the load-sensing transducer versus the output of the displacement gage. The initial slope of the linear portion shall be between 0.7 and 1.5. It is conventional to plot the load along the vertical axis, as in an ordinary tension test record. Select a combination of load-sensing transducer and autographic recorder so that the load, P_Q , (see 9.1) can be determined from the test record with an accuracy of ± 1 %. With any given equipment, the accuracy of readout will be greater than the larger the scale of the test record.

8.4.1 Continue the test until the specimen

can sustain no further increase in load. In some cases the range of the chart will not be sufficient to include all of the test record up to maximum load, P_{max} . In any case, read the maximum load from the dial of the testing machine (or other accurate indicator) and record it on the chart.

9. Calculation and Interpretation of Results

9.1 *Interpretation of Test Record and Calculation of K_{Ic}* —In order to establish that a valid K_{Ic} has been determined, it is necessary first to calculate a conditional result, K_Q , which involves a construction on the test record, and then to determine whether this result is consistent with the size and yield strength of the specimen according to 7.1. The procedure is as follows:

9.1.1 Draw the secant line OP_S , shown in Fig. 5 through the origin of the test record with slope $(P/v)_S = 0.95 (P/v)_0$, where $(P/v)_0$ is the slope of the tangent OA to the initial linear part of the record (Note 6). The load P_Q is then defined as follows: if the load at every point on the record which precedes P_S is lower than P_Q then P_Q is P_S (Fig. 5 Type I); if, however, there is a maximum load preceding P_S which exceeds it, then this maximum load is P_Q (Fig. 5 Types II and III).

NOTE 6—Slight nonlinearity often occurs at the very beginning of a record and should be ignored. However, it is important to establish the initial slope of the record with high precision and therefore it is advisable to minimize this nonlinearity by a preliminary loading and unloading with the maximum load not producing a stress intensity level exceeding that used in the final stage of fatigue cracking.

9.1.2 Calculate the ratio P_{max}/P_Q , where P_{max} is the maximum load the specimen was able to sustain (see 8.4). If this ratio does not exceed 1.10, proceed to calculate K_Q as described in the annex appropriate to the specimen being tested. If P_{max}/P_Q does exceed 1.10, then the test is not a valid K_{Ic} test because it is then possible that K_Q bears no relation to K_{Ic} . In this case proceed to calculate the specimen strength ratio.

9.1.3 Calculate $2.5 (K_Q/\sigma_{YS})^2$ where σ_{YS} is the 0.2 % offset yield strength in tension (see Method E 8). If this quantity is less than both the specimen thickness and the crack length, then K_Q is equal to K_{Ic} . Otherwise, the test is not a valid K_{Ic} test.

9.1.4 If the test result fails to meet the requirements in 9.1.2 or in 9.1.3, or both, it will

be necessary to use a larger specimen to determine K_{Ic} . The dimensions of the larger specimen can be estimated on the basis of K_Q but generally will be at least 1.5 times those of the specimen that failed to yield a valid K_{Ic} value.

9.1.5 Calculate the specimen-strength ratio R_{xx} according to the annex appropriate to the specimen being tested.

9.2 *Crack Plane Orientation*—The fracture toughness of a material usually depends on the orientation and direction of propagation of the crack in relation to the anisotropy of the material, which depends, in turn, on the principal directions of mechanical working or grain flow. The orientation of the crack plane should be identified wherever possible in accordance with the following systems (11). In addition, the product form should be identified (for example, straight rolled plate, cross rolled plate, pancake forging, etc.).

9.2.1 For rectangular sections the reference directions are identified as in Figs. 6 and 7, which give examples for a rolled plate. The same system would be useful for sheet, extrusions, and forgings with nonsymmetrical grain flow.

L = direction of principal deformation (maximum grain flow),

T = direction of least deformation, and

S = third orthogonal direction.

9.2.1.1 Using a two letter code, the first letter designates the *direction normal* to the crack plane, and the second letter the *expected direction of crack propagation*. For example, in Fig 6 the T - L specimen has a fracture plane whose normal is in the width direction of a plate and an expected direction of crack propagation coincident with the direction of maximum grain flow or longitudinal direction of the plate.

9.2.1.2 For specimens that are tilted in respect to two of the reference axes, Fig. 17 the orientation is identified by a three-letter code. The code L - TS , for example, means that the crack plane is perpendicular to the direction of principal deformation (L direction), and the expected fracture direction is intermediate between T and S . The code TS - L means the crack plane is perpendicular to a direction intermediate between T and S , and the expected fracture direction is in the L direction.

9.2.2 For certain cylindrical sections where the direction of principal deformation is parallel to the longitudinal axis of the cylinder, the reference directions are identified as in Fig. 8

which gives examples for a drawn bar. The same system would be useful for extrusions or forged parts having circular cross section.

L = direction of maximum grain flow,

R = radial direction, and

C = circumferential or tangential direction.

9.3 *Fracture Appearance*—The appearance of the fracture is valuable supplementary information and shall be noted for each specimen. Common types of fracture appearance are shown in Fig. 9. For fractures of Types (a) or (b), measure the average width, f , of the central flat fracture area, and note and record the proportion of oblique fracture per unit thickness $(B-f)/B$. Make this measurement at a location midway between the crack tip and the unnotched edge of the specimen. Report fractures of Type (c) as full oblique fractures.

10. Report

10.1 The specimen configuration code as shown with the specimen drawing in the appropriate annex shall be reported. In addition, this code shall be followed with loading code (T for tension and B for bending) and the code for crack plane orientation (see 9.2). These latter two codes should appear in separate parentheses. For example, a test result obtained using the compact specimen (see Annex A4) might be designated as follows: $C(T)(S-T)$. The first letter indicates compact specimen. The second letter indicates the loading was tension and the first of the last two letters indicate that the normal to the crack plane is in the direction of principal deformation and the second of these letters indicates the intended direction of crack propagation is in the direction of least deformation.

10.2 In addition, the following information should be reported for each specimen tested.

10.2.1 The form of the product tested, that is, forging, plate, casting etc.

10.2.2 Thickness, B .

10.2.3 Width (depth), W .

10.2.3.1 Offset of the loading holes, X , for the arc-shaped specimen.

10.2.3.2 Outer and inner radii, r_2 and r_1 for the arc-shaped specimen.

10.2.4 Fatigue precracking conditions in terms of:

10.2.4.1 Maximum stress intensity, $K_I(\max)$ and number of cycles for terminal fatigue crack extension over a length at least 2.5 % of the overall length of notch plus crack, and

10.2.4.2 The stress intensity range for terminal crack extension.

10.2.5 Crack length measurements.

10.2.5.1 At center of crack front.

10.2.5.2 Midway between the center and the end of the crack front on each side, and

10.2.5.3 At each surface.

10.2.6 Test temperature.

10.2.7 Relative humidity as determined by Method E 337.

10.2.8 Loading rate in terms of K_I (change in stress intensity factor per unit time) (2).

10.2.9 Load-displacement record and associated calculations.

10.2.10 Fracture appearance.

10.2.11 Yield strength (offset = 0.2 %) as determined by Methods E 8.

10.2.12 K_{Ic} , or K_Q followed by the parenthetical statement: "invalid according to section(s)....of ASTM Method E 399," and

10.2.13 R_{ax} where x refers to the specimen configuration as given in the appropriate annex.

10.2.14 P_{max}/P_Q .

10.3 It is desirable to list the information required in 10.1 and 10.2 in the form of a table. A suggested form for such a table is given in Fig. 10.

11. Precision and Accuracy

11.1 *Accuracy*—There is no accepted "standard" value for the plane strain fracture toughness of any material. In the absence of such a true value, any statement concerning accuracy is not meaningful.

11.2 *Precision*—The precision of a K_{Ic} determination is a function of the precision and

accuracy of the various measurements of linear dimensions of the specimen and testing fixtures, the precision of the displacement measurement, and the accuracy of the load measurement as well as the accuracy of the recording devices used to produce the load displacement record and the precision of the constructions made on this record. It is not possible to make meaningful statements concerning precision and accuracy for all these measurements. However, it is possible to derive useful information concerning the precision of a K_{Ic} measurement in a global sense from three interlaboratory test programs (17) (18). The results of these programs are summarized in Table 1 which gives the standard deviation of K_{Ic} for the bend specimen, the compact specimen, and the arc-shaped specimen as derived from tests on several high-strength alloys which were all very uniform in composition and structure. It should be appreciated that the measures of precision shown in Table 1 apply to tests on high-strength alloys that do not exhibit strong transitional behavior in terms of temperature or strain rate. If temperature and rate effects have a large influence on the toughness, increased scatter in K_{Ic} measurements may be noted. For example, within or below the transition range of a structural steel the initial advance of the fatigue crack will be controlled by abrupt fracture of local elements at the crack tip accompanied by rapid transfer of load to adjacent regions which then exhibit cleavage fracture. Under these circumstances, a statistical size effect may be noticed as the specimen size is changed, and tests on small specimens will be characterized by larger scatter than will tests on larger specimens.

TABLE 1 Grand Means and Standard Deviations for K_{Ic} as Obtained from Three Interlaboratory Test Programs^a

	Bend Specimens			
	2219T851 $\sigma_{YS} = 51.0$ ksi (353 MPa)	4340 $\sigma_{YS} = 238$ ksi (1640 MPa)	18 Ni Marage $\sigma_{YS} =$ 276 ksi (1902 MPa)	4340 $\sigma_{YS} = 206$ ksi (1419 MPa)
Grand mean \bar{X} , ksi·in. ^{1/2}	32.7	44.2	51.8	79.8
Standard deviation, S	1.87	1.85	2.04	2.87
	Compact Specimens			
	32.4	45.5	53.9	79.4
Standard deviation, S	1.15	1.27	1.64	1.79
	Arc-Shaped Specimens (4335V, $\sigma_{YS} = 192$ ksi (1320 MPa))			
	$X/W = 0$	$X/W = 0.5$		
Grand mean \bar{X} , ksi·in. ^{1/2}	102.3	101.7		
Standard deviation, S	3.50	2.36		

^a The standard deviation has been pooled for all laboratories testing a given alloy. Data for the bend and compact specimen can be found in Ref (17) and for the arc-shaped specimen in Ref (18).

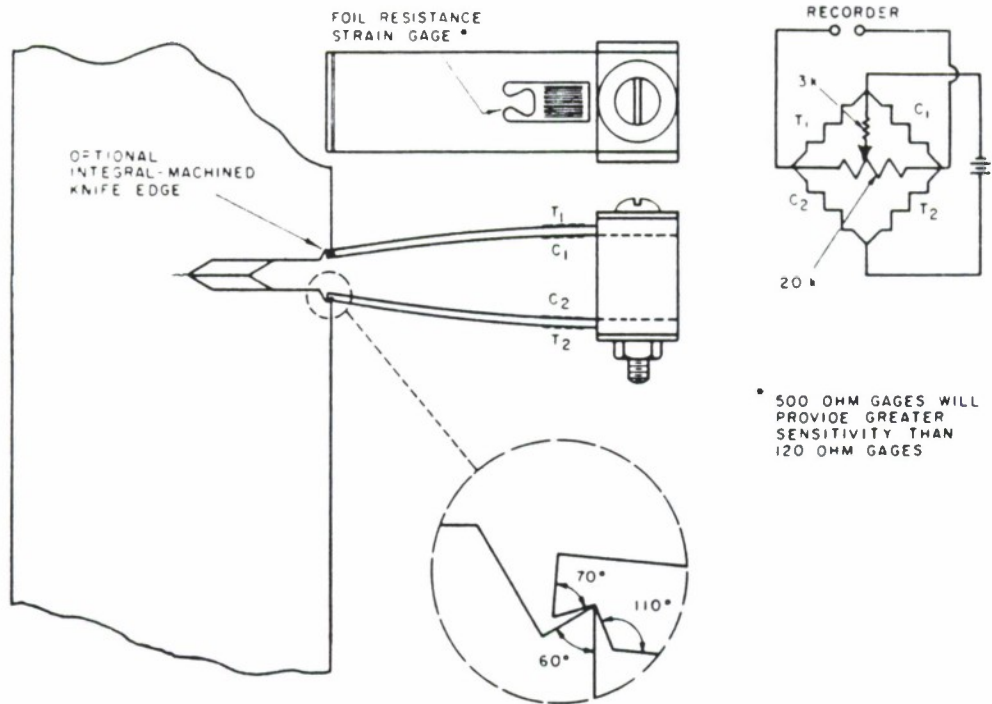
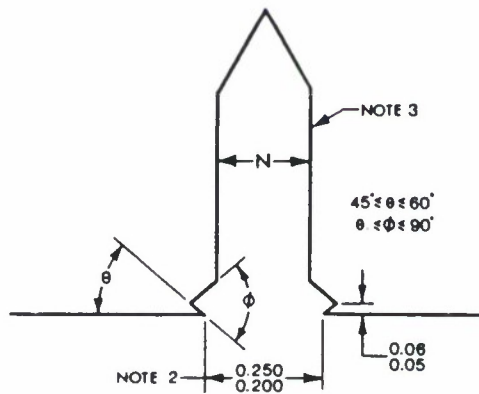


FIG. 1 Double-Cantilever Clip-In Displacement Gage Showing Mounting by Means of Integral Knife Edges (Gage Design Details are Given in Annex A1)



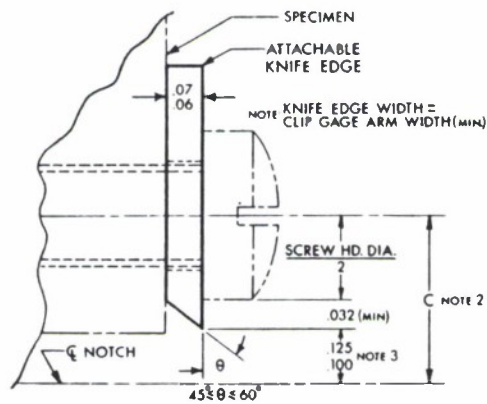
NOTE 1—Dimensions in inches.
 NOTE 2—Gage length shown corresponds to clip gage spacer block dimensions shown in Annex A1, but other gage lengths may be used provided they are appropriate to the specimen (see 6.3.3).
 NOTE 3—For starter notch configurations see Fig. 4.

Metric Equivalents

in.	0.050	0.060	0.200	0.250
mm	1.3	1.5	5.1	6.4

Fig. 2 Example of Integral Knife Edge Design

ASTM E 399



NOTE 1—Dimensions are in inches.

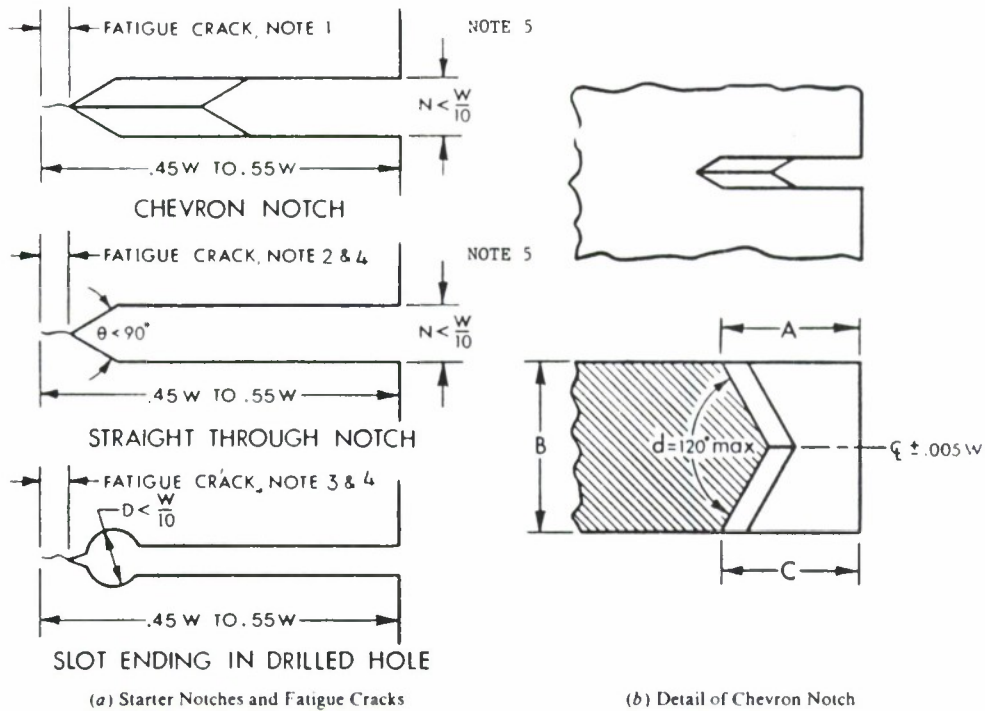
NOTE 2—Effective gage length = $2C + \text{Screw Thread Diameter} \leq W/2$. (This will always be greater than the gage length specified in A1.1.)

NOTE 3—Dimension shown corresponds to clip gage spacer block dimension in Annex A1.

Metric Equivalents

in.	0.032	0.06	0.07	0.100	0.125
mm	0.81	1.5	1.8	2.54	3.18

Fig. 3 Example of Attachable Knife Edge Design



- NOTE 1—For a chevron crack starter notch the fatigue crack shall emerge on both surfaces of the specimen.
- NOTE 2—Fatigue crack extension on each surface of the specimen containing a straight-through notch shall be at least $0.025 W$ or 0.050 in. (1.3 mm), whichever is larger.
- NOTE 3—Fatigue crack extension on each surface of the specimen from the stress raiser tipping the hole shall be at least $0.050 W$ or 0.050 in. (1.3 mm), whichever is larger.
- NOTE 4—Crack starter notch shall be perpendicular to the specimen surfaces and to the intended direction of crack propagation within $\pm 2^\circ$.
- NOTE 5—Notch width N need not be less than $1/16$ in. (1.6 mm).

FIG. 4 Crack Starter Notch and Fatigue Crack Configurations

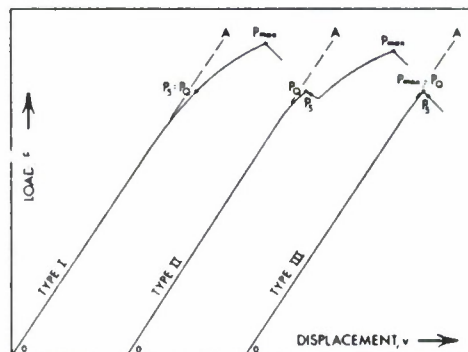


FIG. 5 Principal Types of Load-Displacement Records

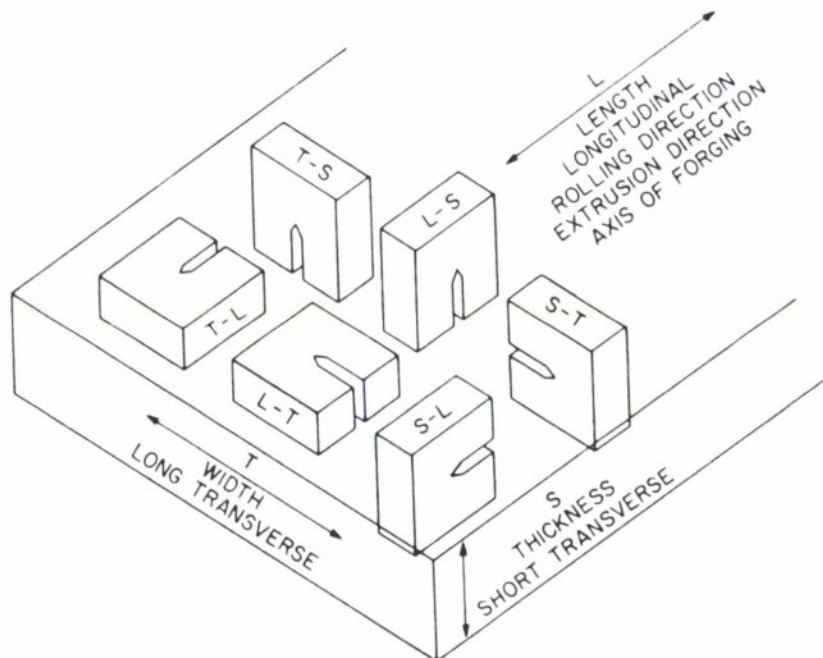


FIG. 6 Crack Plane Orientation Code for Rectangular Sections

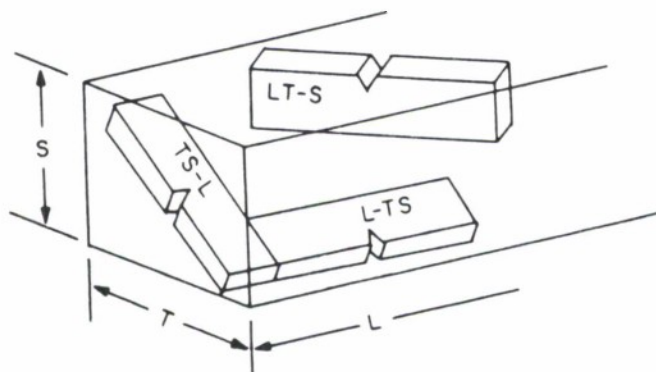


FIG. 7 Crack Plane Orientation Code for Rectangular Sections Where Specimens Are Tilted with Respect to the Reference Directions

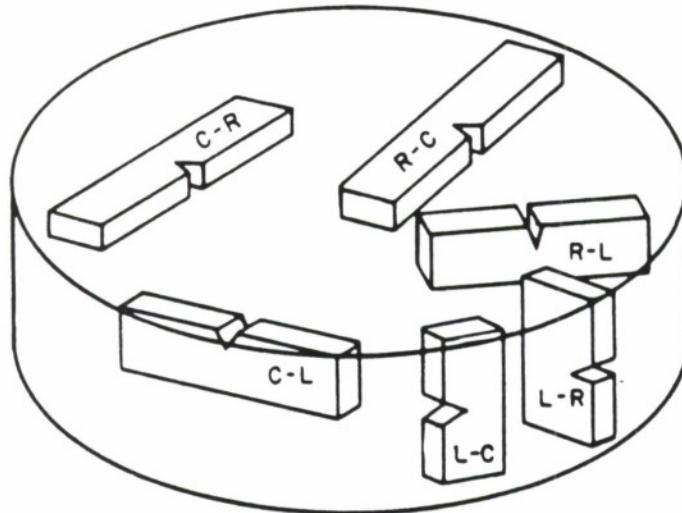


FIG. 8 Crack Plane Orientation Code for Bar and Hollow Cylinder

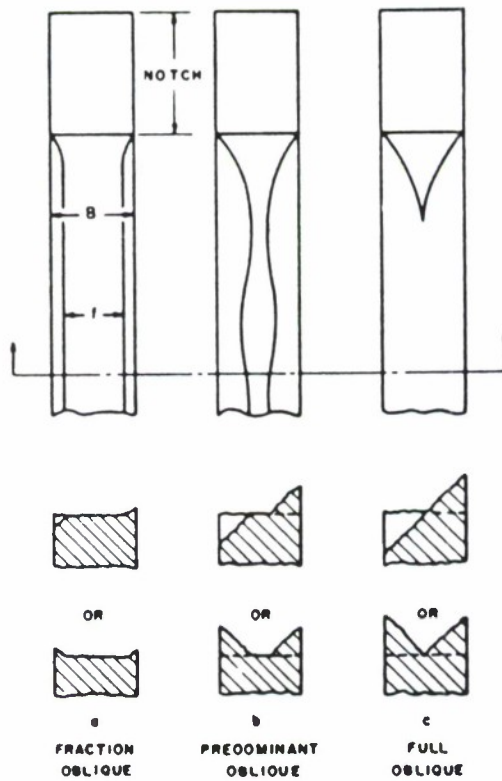




FIG. 9 Common Types of Fracture Appearance



E 399



E_{1C} DATA SHEET
(SAMPLE E)



MATERIAL/FORM _____

SPECIMEN I.D. _____

BEAT TEST _____

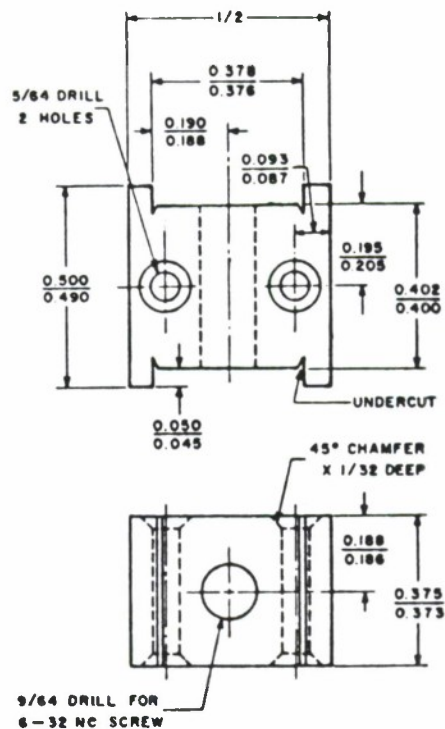
SPECIMEN TYPE _____

DATE ____/____/____

DATE REPORT _____

PARTICULARS	DATA	REF. PARAGRAPH	FRACTURE TEST	DATA	REF. PARAGRAPH
<ul style="list-style-type: none"> Crack Plane Orientation Material 0.25 Offset Yield Strength, σ_{ys}, per E8 Thickness, E Depth (Width), W for - SE(8) for - C(T) for - RC(T) for - 6.6.1.2 (Annex B) Other Shaped Specimens Width, W for Loading Hole Offset, B Outer and Inner Radii, r_1 & r_2 		8.2 7.6.1.1 8.2.1 8.2.2 3.6.1 (Annex 3) 6.6.1 (Annex 6) 6.6.1.2 (Annex B) 5.6.1 (Annex 5) 5.6.1 (Annex 5) 5.6.1 (Annex 5)	<ul style="list-style-type: none"> Crack Lengths - At Center of Crack Front (a_1) At Right of Center (a_2) At Left of Center (a_3) At Right of Surface (a_4) At Left Surface (a_5) Crack Plane Symmetry Loading Rate (inl./min.) Test Temperature Relative Humidity Load-Displacement Record 		8.2.2 8.2.2 8.2.2 8.2.2 8.2.2 8.2.2 8.2.4 8.2 10.2.6 10.2.7 8.4.6.1
FATIGUE PRECRACKING <ul style="list-style-type: none"> $R_{max} < 0.00210 \sigma_{ys}$ (0.00032 σ_{ys}) $R_{min} = 0.6 K_1$ $R_{max} = 0.8 F_{1C}$ at Temperature $R_{max} = 0.8 K_1$ (TT) Crack Lengths - Standard Specimen at Temperature $a = 0.35a$ $R_{max} = 3R$ Cycles for Test 2.55 of "a" 		A2.3.3 A2.3.3 A2.6.1 and A2.6.2 A2.6.4	CALCULATION OF R & K_1 <ul style="list-style-type: none"> $R_{max}/P_0 = 1.1$ $K_1 SE(8)$ $K_1 C(T)$ $K_1 A(T)$ $K_1 RC(T)$ Valid F_{1C} E_{1C} 		9.1.2 3.5.3 (Annex 3) 4.5.3 (Annex 5) 3.5.3 (Annex 3) 6.5.3 (Annex 6) 9.1.1 9.1.3

FIG. 10 Suggested Form of Table for Reporting Information Listed in 10.1 and 10.2



NOTE 1— $\frac{5}{16}$ -in. diameter holes are for strain gage leads.

NOTE 2—Dimensions are in inches.

Metric Equivalents

in	mm	in	mm
$\frac{1}{32}$	0.80	0.195	4.95
0.045	1.14	0.205	5.21
0.050	1.27	0.373	9.47
$\frac{3}{64}$	2.00	0.375	9.52
0.087	2.21	0.376	9.55
0.093	2.36	0.378	9.60
0.125	3.18	0.400	10.16
$\frac{1}{16}$	3.60	0.402	10.21
0.186	4.72	0.490	12.45
0.188	4.78	$\frac{1}{2}$	12.70
0.190	4.83	0.500	12.70

FIG. A1.2 Aluminum-Alloy Spacer Block for Double-Cantilever Displacement Gage

A2. FATIGUE PRECRACKING OF K_{Ic} FRACTURE TOUGHNESS SPECIMENS

A2.1 Introduction

A2.1.1 Experience has shown that it is impractical to obtain a reproducibly sharp, narrow machined notch that will simulate a natural crack well enough to provide a satisfactory K_{Ic} test result. The most effective artifice for this purpose is a narrow notch from which extends a comparatively short fatigue crack, called the precrack. The dimensions of the notch and the precrack, and the sharpness of the precrack, must meet certain conditions which can be

readily met with most engineering materials since the fatigue cracking process can be closely controlled when careful attention is given to the known contributory factors. However, there are some materials that are too brittle to be fatigue cracked since they fracture as soon as the fatigue crack initiates; these are outside the scope of the present test method. The purpose of this annex is to provide guidance on the production of satisfactory fatigue precracks, and to state the associated requirements for a valid K_{Ic} test.

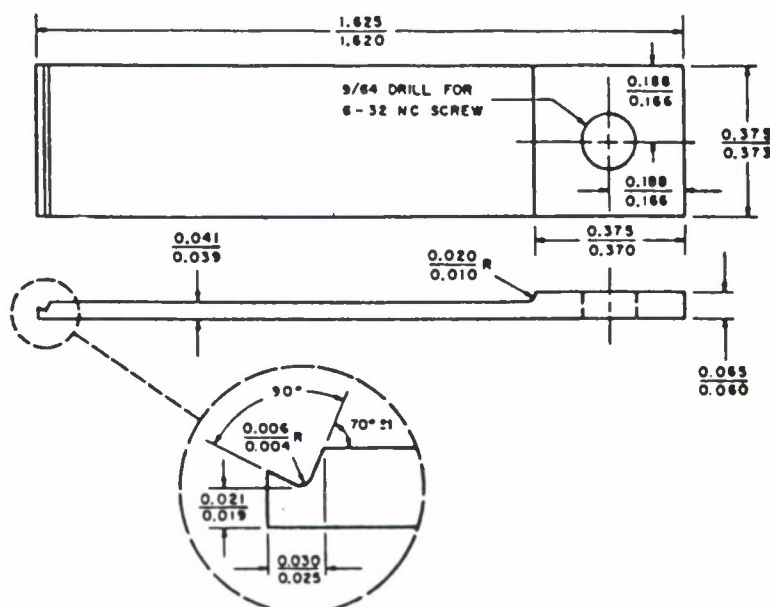
A2.1.2 A fatigue precrack is produced by cycli-

ANNEXES

A1. DESIGN FOR DOUBLE-CANTILEVER DISPLACEMENT GAGE

A1.1 The gage consists of two cantilever beams and a spacer block which are clamped together with a single nut and bolt, as shown in Fig. 1. Electrical-resistance strain gages are cemented to the tension and compression surfaces of each beam, and are connected as a Wheatstone bridge incorporating a suitable balancing resistor. The material for the gage beams should have a high ratio of yield strength to elastic modulus, and titanium alloy 13V-11Cr-3Al in the solution treated condition has been found very satisfactory for this purpose. If a material of different modulus is substituted, the spring constant of the assembly will change correspondingly, but the other characteristics will not be affected. Detailed dimen-

sions for the beams and spacer block are given in Figs. A1.1 and A1.2. For these particular dimensions the linear range (working range) is from 0.15 to 0.30 in. (3.8 to 7.6 mm) and the recommended gage length is from 0.20 to 0.25 in. (5.1 to 6.3 mm). The clip gage can be altered to adapt it to a different gage length by substituting a spacer block of appropriate height. As discussed in 6.3.2 the required precision of the gage corresponds to a maximum deviation of ± 0.0001 in. (0.0025 mm) of the displacement readings from a least-squares-best-fit straight line through the data. Further details concerning design, construction and use of these gages are given in Ref (10).



NOTE—Dimensions are in inches.
Metric Equivalents

in	mm	in	mm
0.004	0.10	0.060	1.52
0.006	0.15	0.065	1.65
0.010	0.25	$\frac{9}{64}$	3.6
0.019	0.48	0.186	4.72
0.020	0.51	0.188	4.78
0.021	0.53	0.370	9.40
0.025	0.64	0.373	9.47
0.030	0.76	0.375	9.52
0.039	0.99	1.620	41.15
0.041	1.04	1.625	41.28

FIG. A1.1 Beams for Double-Cantilever Displacement Gage



ment, as appropriate, shall be reduced so that the terminal value of K_{max} is unlikely to exceed 60 % of the estimated minimum value of K_{Ic} of the material, and also the terminal value of K_{max}/E will not exceed 0.002 in.^{1/2} (0.0032 m^{1/2}). The minimum setting is then adjusted so that the stress ratio is between -1 and +0.1. Fatigue cycling is then continued until the surface traces on both sides of the specimen indicate

that the overall length of notch plus crack will meet the requirements of 7.3.2.1, 7.3.2.2, and Fig. 4 of this test method.

A2.4.4 When fatigue cracking is conducted at a temperature T_1 and testing at a different temperature T_2 , K_{max} must not exceed 0.6 ($\sigma_{YS1}/\sigma_{YS2}$) K_Q , where σ_{YS1} and σ_{YS2} are the yield strengths at the respective temperatures T_1 and T_2 .

A3. SPECIAL REQUIREMENTS FOR THE TESTING OF BEND SPECIMENS

A3.1 Specimen

A3.1.1 The standard bend specimen is a single edge-notched and fatigue cracked beam loaded in three-point bending with a support span, S , nominally equal to four times the width, W . The general proportions of this specimen configuration are shown in Fig. A3.1.

A3.1.2 Alternative specimens may have $1 \leq W/B \leq 4$. These specimens shall also have a nominal support span equal to $4W$.

A3.2 Specimen Preparation

A3.2.1 For generally applicable specifications concerning specimen size and preparation see Section 7.

A3.2.2 It is desirable to fatigue crack the bend specimen in the same fixtures in which it will be tested so that the K calibration is accurately known. However, bend specimens are sometimes cracked in cantilever bending because this method permits ease of reversed loading. If the K calibration for three-point bending is used in cantilever bending, the bending moments for a given K value will be underestimated (7). While fatigue cracking in cantilever bending can yield satisfactory results, it should be emphasized that the crack tip stress field can be distorted and the fatigue crack orientation changed by excessive clamping forces.

A3.3 Apparatus

A3.3.1 *Bend Test Fixture*—The general principles of the bend test fixture are illustrated in Fig. A3.2. This fixture is designed to minimize frictional effects by allowing the support rollers to rotate and move apart slightly as the specimen is loaded, thus permitting rolling contact. Thus, the support rollers are allowed limited motion along plane surfaces parallel to the notched side of the specimen, but are initially positively positioned against stops that set the span length and are held in place by low-tension springs (such as rubber bands).

A3.3.2 *Displacement Gage*—For generally applicable details concerning the displacement gage see 6.3. For the bend specimen the displacements will be essentially independent of the gage length up to a gage length of $W/2$.

A3.4 Procedure

A3.4.1 *Measurement*—For a bend specimen measure the width (depth), W , and the crack length, a , from the notched side of the specimen to the opposite side and to the crack front, respectively.

A3.4.1.1 For general requirements concerning specimen measurement see 8.2.

A3.4.2 *Bend Specimen Testing*—Set up the test fixture so that the line of action of the applied load shall pass midway between the support roll centers within 1 % of the distance between these centers (for example, within 0.04 in. (1.0 mm) for a 4-in. (100-mm) span). Measure the span to within 0.5 % of nominal length. Locate the specimen with the crack tip midway between the rolls to within 1 % of the span, and square to the roll axes within 2°. Seat the displacement gage on the knife edges to maintain registry between knife edges and gage grooves. In the case of attachable knife edges, seat the gage before the knife edge positioning screws are tightened.

A3.4.2.1 Load the specimen at a rate such that the rate of increase of stress intensity is within the range 30 to 150 ksi·in.^{1/2}/min (0.55 to 2.75 MPa·m^{1/2}/s), corresponding to a loading rate for the standard ($B = 0.5W$) 1-in. (25.4-mm) thick specimen between 4000 and 20 000 lbf/min (0.30 to 1.5 kN/s).

A3.4.3 For details concerning recording of the test record see 8.4.

A3.5 Calculations

A3.5.1 *Interpretation of Test Record*—For general requirements and procedures in interpretation of the test record see 9.1.

A3.5.2 *Validity Requirements*—For a description of the validity requirements in terms of limitations on P_{max}/P_Q and the specimen size requirements, see 9.1.2 through 9.1.3.

A3.5.3 *Calculation of K_Q* —For the bend specimen calculate K_Q in units of ksi·in.^{1/2} (MPa·m^{1/2}) as follows (Note A3.1):

$$K_Q = (P_Q S / BW^{3/2}) \cdot f(a/W)$$

where:

$$f(a/W) = \frac{3(a/W)^{1/2} [1.99 - (a/W)(1 - a/W) \times (2.15 - 3.93a/W + 2.7a^2/W^2)]}{2(1 + 2a/W)(1 - a/W)^{3/2}}$$

where:

P_Q = load as determined in 9.1.1, klbf (kN),
 B = specimen thickness as determined in 8.2.1, in. (cm),

S = span as determined in A3.4.2, in. (cm).

W = specimen depth (width) as determined in A3.4.1, in. (cm), and

a = crack length as determined in 8.2.2, in. (cm).

To facilitate calculation of K_Q , values of $f(a/W)$ are tabulated in the following table for specific values of a/W .



cally loading the notched specimen with a ratio of minimum to maximum stress between -1 and $+0.1$ for a number of cycles usually between about 10^4 and 10^6 depending on specimen size, notch preparation, and stress intensity level. The maximum stress intensity in the terminal (2.5 %) stage of fatigue crack growth must not exceed 60 % of the K_{Ic} value of the material. Some fraction of the total number of cycles required to produce the fatigue precrack is consumed in initiation of the crack at the notch root; the remainder account for growth of the crack to the required length. If the total number of cycles is excessive, the reason is usually that the number of cycles required for initiation is excessive rather than that the subsequent rate of crack growth is low. There are several ways of promoting early crack initiation: (1) by providing a very sharp notch tip; (2) by using a chevron notch (Fig. 4); (3) by statically preloading the specimen in such a way that the notch tip is compressed in a direction normal to the intended crack plane but without allowing the specimen strength ratio (see 9.1.5) to be less than -1 ; (4) by using a negative fatigue load ratio, for a given maximum fatigue load, the more negative the load ratio, the earlier crack initiation is likely to occur.

A2.2 Equipment

A2.2.1 The equipment for fatigue cracking shall be such that the stress distribution is uniform through the specimen thickness; otherwise the crack will not grow uniformly. The stress distribution shall also be symmetrical about the plane of the prospective crack; otherwise the crack will deviate unduly from that plane and the test result will be significantly affected (7).

A2.2.2 The K calibration for the specimen, as loaded by the equipment, shall be known with an error of not more than 5 %. The K calibration is the relation of the stress intensity factor K to either the load or to some prescribed displacement and the specimen dimensions (1). The fixtures recommended in the test method (see appropriate annex) are also suitable for fatigue cracking, and K calibrations for specimens loaded through these fixtures are given in the annexes of this test method. If different fixtures are used, the appropriate K calibration should be determined experimentally with these fixtures (7). The advantage of experimental K calibration, as compared with numerical methods of analysis, is that accurate modeling of the boundary conditions with the actual fixtures is assured. It is important to bear in mind that if the fatigue cycle involves reversal of load, the K calibration can be very sensitive to the distribution of clamping forces necessary to grip the specimen.

A2.3 Specimen Requirements

A2.3.1 The fatigue precracking shall be conducted with the specimen fully heat treated to the condition in which it is to be tested.

A2.3.2 The combination of starter notch and fatigue precrack must conform to the requirements shown in Fig. 4. The nominal crack length is equal to $0.50W$ and is the total length of the starter notch slot plus fatigue crack. To facilitate fatigue precrack-

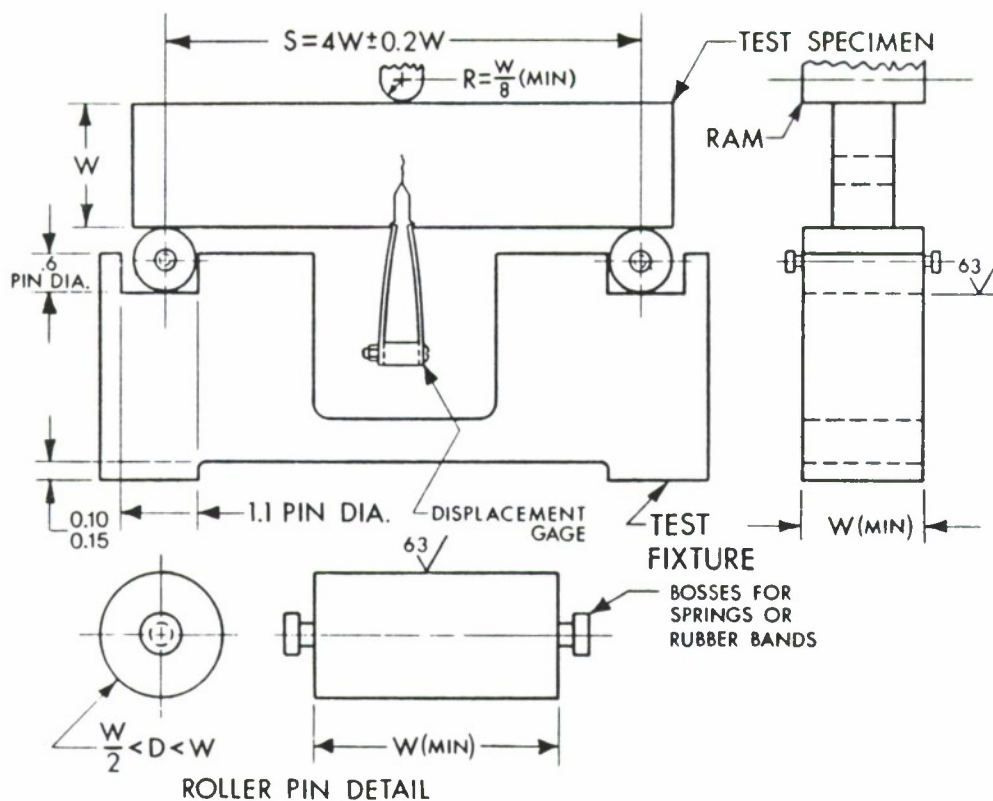
ing at a low level of stress intensity, the notch root radius of a straight-across notch should be no more than 0.003 in. (0.08 mm). If a chevron notch is used (Fig. 4), the notch root radius can be as much as 0.01 in. (0.25 mm) because of the compound stress intensification at the point of the chevron. Early crack initiation can also be promoted by precompression of the notch tip region, as stated in A2.1.2.

A2.3.3 It is advisable to mark two pencil lines on each side of the specimen normal to the anticipated paths of the surface traces of the fatigue crack. The line most distant from the notch tip should indicate the minimum required length of fatigue crack, and the other the terminal part of that length equal to not less than 2.5 % of the overall length of notch plus fatigue crack, that is $0.0125W$. During the final stage of fatigue crack extension, for at least this distance, the ratio of maximum stress intensity of the fatigue cycle to the Young's modulus of the material, K_{max}/E shall not exceed $0.002 \text{ in.}^{1/2}$ ($0.00032 \text{ m}^{1/2}$). Furthermore, K_{max} must not exceed 60 % of the K_Q value determined in the subsequent test if K_Q is to qualify as a valid K_{Ic} result.

A2.4 Precracking Procedure

A2.4.1 Fatigue precracking can be conducted under either load control or displacement control provided that the appropriate K calibration is known with requisite accuracy for the specimen and fixture (A2.2.1). If the load cycle is maintained constant, the maximum K and the K range will increase with crack length; if the displacement cycle is maintained constant, the reverse will happen. The initial value of the maximum fatigue load or displacement should be calculated from the K calibration and the specimen and notch dimensions. It is suggested that this load be selected so that the maximum stress intensity factor in the initial portion of the fatigue cycle does not exceed 80 % of the estimated K_{Ic} value of the material. Higher K values may result in undesirably high crack growth rates. The minimum is then selected so that the stress ratio is between -1 and $+0.1$. The more negative the stress ratio, the faster the fatigue precrack will be completed, but this advantage is offset by the need for more elaborate fixtures than are required when the stress ratio is positive.

A2.4.2 The specimen shall be accurately located in the loading fixture and secured as required so that the boundary conditions correspond to the applicable K calibration. Fatigue cycling is then begun, usually with a sinusoidal waveform and near to the highest practical frequency. There is no known marked frequency effect on fatigue precrack formation up to at least 100 Hz in the absence of adverse environments. The specimen should be carefully monitored until crack initiation is observed on one side. If crack initiation is not observed on the other side before appreciable growth is observed on the first, then fatigue cycling should be stopped to try to determine the cause and remedy for the unsymmetrical behavior. Sometimes, simply turning the specimen around in relation to the fixture will solve the problem. When the most advanced crack trace has almost reached the first scribed line corresponding to 97.5 % of the final crack length, the maximum load or displace-



NOTE 1—Roller pins and specimen contact surface of loading ram must be parallel to each other within $0.002 W$.
 NOTE 2—0.10 in. = 2.54 mm, 0.15 in. = 3.81 mm.

FIG. A3.2 Bend Test Fixture Design

A4. SPECIAL REQUIREMENTS FOR THE TESTING OF COMPACT SPECIMENS

A4.1 Specimen

A4.1.1 The standard compact specimen is a single edge-notched and fatigue cracked plate loaded in tension. The general proportions of this specimen configuration are shown in Fig. A4.1.

A4.1.2 Alternative specimens may have $2 \leq W/B \leq 4$ but with no change in other proportions.

A4.2 Specimen Preparation

A4.2.1 For generally applicable specifications concerning specimen size and preparation see Section 7.

A4.3 Apparatus

A4.3.1 *Tension Testing Clevis*—A loading clevis suitable for testing compact specimens is shown in Fig. A4.2. Both ends of the specimen are held in such a clevis and loaded through pins, in order to allow rotation of the specimen during testing. In order to provide rolling contact between the loading pins and

the clevis holes, these holes are provided with small flats on the loading surfaces (4). Other clevis designs may be used if it can be demonstrated that they will accomplish the same result as the design shown.

A4.3.1.1 The critical tolerances and suggested proportions of the clevis and pins are given in Fig. A4.2. These proportions are based on specimens having $W/B = 2$ for $B > 0.5$ in. (12.7 mm) and $W/B = 4$ for $B \leq 0.5$ in. (12.7 mm). If a 280 000-psi (1930-MPa) yield strength maraging steel is used for the clevis and pins, adequate strength will be obtained for testing the specimen sizes and σ_{YS}/E ratios given in 7.1.3. If lower-strength grip material is used, or if substantially larger specimens are required at a given σ_{YS}/E ratio than those shown in 7.1.3, then heavier grips will be required. As indicated in Fig. A4.2 the clevis corners may be cut off sufficiently to accommodate seating of the clip gage in specimens less than 0.375 in. (9.5 mm) thick.

A4.3.1.2 Careful attention should be given to achieving as good alignment as possible through

Bend Specimens			
a/W	$f(a/W)$	a/W	$f(a/W)$
0.450	2.29	0.500	2.66
0.455	2.32	0.505	2.70
0.460	2.35	0.510	2.75
0.465	2.39	0.515	2.79
0.470	2.43	0.520	2.84
0.475	2.46	0.525	2.89
0.480	2.50	0.530	2.94
0.485	2.54	0.535	2.99
0.490	2.58	0.540	3.04
0.495	2.62	0.545	3.09
		0.550	3.14

NOTE A3.1—The expression in A3.5.3 is considered to be accurate within $\pm 0.5\%$ over the entire range of a/W from 0 to 1 for an $S/W = 4$ (12).

A3.5.4 Calculation of R_{ab} —For the bend specimen calculate the specimen strength ratio (which is dimensionless and has the same value in any consistent system of units):

$$\rightarrow R_{ab} = \frac{6P_{\max}W}{B(W-a)^2\sigma_{YS}}$$

where:

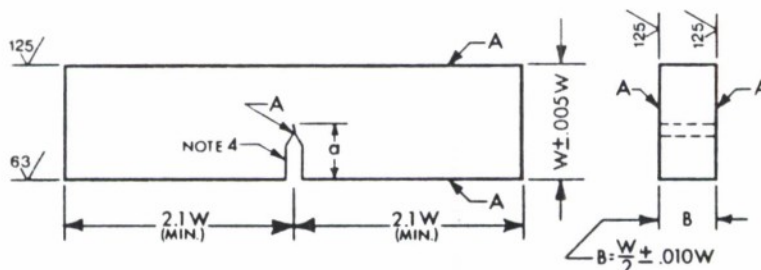
P_{\max} = maximum load that the specimen was able to sustain.

B = thickness of specimen as determined in 8.2.1.

W = width (depth) of specimen, as determined in A3.4.1.

a = crack length as determined in 8.2.2, and

σ_{YS} = yield strength in tension (offset = 0.2 %) (see Methods E 8).



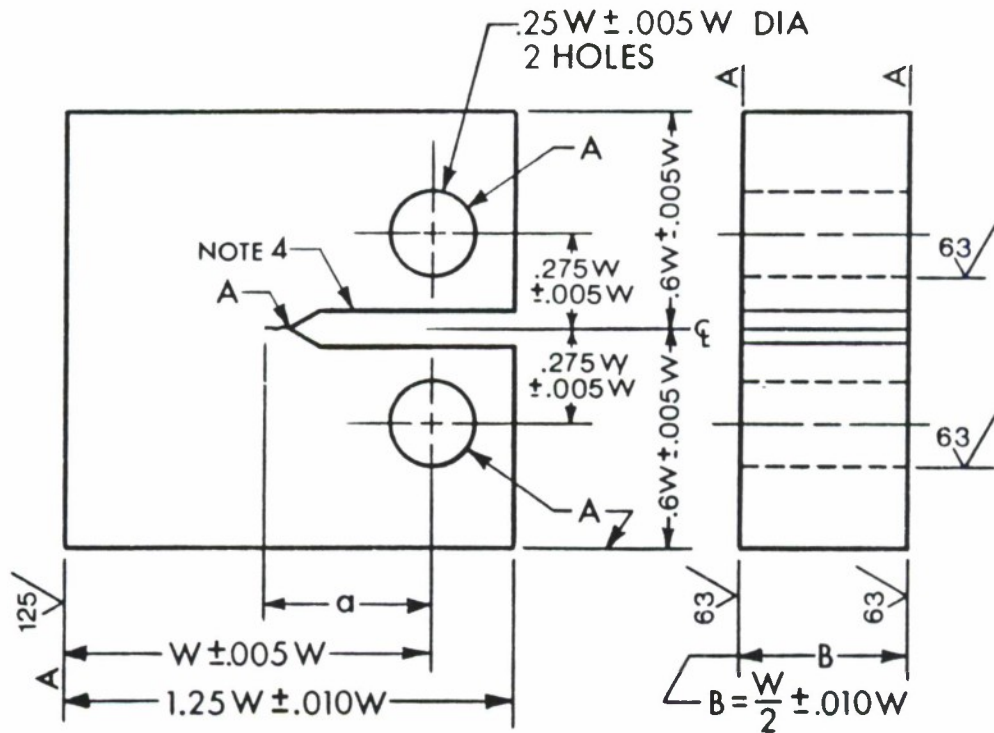
NOTE 1—A surfaces shall be perpendicular and parallel as applicable within 0.001 W TIR.

NOTE 2—Crack starter notch shall be perpendicular to specimen surfaces to within $\pm 2^\circ$.

NOTE 3—Integral or attachable knife edges for clip gage attachment may be used (see Figs. 2 and 3).

NOTE 4—For starter notch and fatigue crack configurations see Fig. 4.

FIG. A3.1 Bend Specimen SE (B)—Standard Proportions and Tolerances



NOTE 1—A surfaces shall be perpendicular and parallel as applicable to within 0.002 W TIR.

NOTE 2—The intersection of the crack starter notch tips with the two specimen surfaces shall be equally distant from the top and bottom edges of the specimen within 0.005 W .

NOTE 3—Integral or attachable knife edges for clip gage attachment to the crack mouth may be used (see Fig. 2 and 3).

NOTE 4—For starter notch and fatigue crack configuration see Fig. 4.

FIG. A4.1 Compact Specimen C (T) Standard Proportions and Tolerances

careful machining of all auxiliary gripping fixtures.

A4.3.2 Displacement Gage—For generally applicable details concerning the displacement gage see 6.3. For the compact specimen the displacements will be essentially independent of the gage length up to 1.2 W .

A4.4 Procedure

A4.4.1 Measurement—For a compact specimen measure the width, W , and the crack length, a , from the plane of the centerline of the loading holes (the notched edge is a convenient reference line but the distance from the centerline of the holes to the notched edge must be subtracted to determine W and a). Measure the width, W , to the nearest 0.001 in. (0.025 mm) or 0.1 %, whichever is larger, at not less than three positions near the notch location, and record the average value.

A4.4.1.1 For general requirements concerning specimen measurement see 8.2.

A4.4.2 Compact Specimen Testing—When assembling the loading train (clevises and their attachments to the tensile machine) care should be taken to minimize eccentricity of loading due to misalignments external to the clevises. To obtain satisfactory alignment keep the centerline of the upper and lower loading rods coincident within 0.03 in. (0.76 mm) during the test and center the specimen with respect to the clevis opening within 0.03 in. (0.76 mm).

A4.4.2.1 Load the compact specimen at such a rate that the rate of increase of stress intensity is within the range 30 to 150 ksi·in.^{1/2}/min (0.55 to 2.75 MPa·m^{1/2}/s) corresponding to a loading rate for a standard ($W/B = 2$) 1-in. thick specimen 4500 and 22 500 lbf/min (0.34 to 1.7 kN/s).

A4.4.2.2 For details concerning recording of the test record see 8.4.

A4.5 Calculations

A4.5.1 For general requirements and procedures in interpretation of the test record see 9.1.

A4.5.2 For a description of the validity requirements in terms of limitations on P_{max}/P_Q and the specimen size requirements see 9.1.2 through 9.1.3.

A4.5.3 Calculation of K_Q —For the compact specimen calculate K_Q in units of ksi·in.^{1/2} (MPa·m^{1/2}) from the following expression (Note A4.1)

$$K_Q = (P_Q/BW^{1/2}) \cdot f(a/W)$$

where:

$$f(a/W) = \frac{(2 + a/W)(0.886 + 4.64a/W - 13.32a^2/W^2 + 14.72a^3/W^3 - 5.6a^4/W^4)}{(1 - a/W)^{3/2}}$$

where:

P_Q = load as determined in 9.1.1, klbf (kN),

B = specimen thickness as determined in 8.2.1, in. (cm),

W = specimen width, as determined in A4.4.1, in. (cm), and

a = crack length as determined in 8.2.2 and A4.4.1, in. (cm).

To facilitate calculation of K_Q , values of $f(a/W)$ are tabulated below for specific values of a/W .

Compact Specimens			
a/W	$f(a/W)$	a/W	$f(a/W)$
0.450	8.34	0.500	9.66
0.455	8.46	0.505	9.81
0.460	8.58	0.510	9.96
0.465	8.70	0.515	10.12
0.470	8.83	0.520	10.29
0.475	8.96	0.525	10.45
0.480	9.09	0.530	10.63
0.485	9.23	0.535	10.80
0.490	9.37	0.540	10.98
0.495	9.51	0.545	11.17
		0.550	11.36

NOTE A4.1—The expression in A4.5.3 is considered to be accurate within $\pm 0.5\%$ over the range of a/W from 0.2 to 1 (12) (13).

4.5.4 Calculation of R_{sc} —For the compact specimen calculate the specimen strength ratio (which is dimensionless and has the same value in any consistent system of units):

$$R_{sc} = \frac{2P_{max}(2W + a)}{B(W - a)^2\sigma_{YS}}$$

where:

P_{max} = maximum load that the specimen was able to sustain,

B = thickness of specimen as determined in 8.2.1,

W = width of the specimen as determined in A4.4.1,

a = crack length as determined in 8.2.2 and A4.4.1, and

σ_{YS} = yield strength in tension (offset = 0.2 %) (see Methods E 8).

concerning specimen size and preparation see Section 7.

A5.3 Apparatus

A5.3.1 Tension Testing Clevis—A loading clevis suitable for testing arc-shaped specimens is shown in Fig. A5.2. Both ends of the specimen are held in such a clevis and loaded through pins, in order to allow rotation of the specimen during testing. In order to provide rolling contact between the loading pins and the clevis holes, these holes are provided with small flats on the loading surface (4). Other clevis designs may be used if it can be demonstrated that they will accomplish the same result as the design shown.

A5.3.1.1 The critical tolerances and suggested proportions of the clevis and pins are given in A5.2. These proportions are based on specimens having $W/B = 2$ for $B > 0.5$ in. (12.7 mm) and $W/B = 4$ for $B \leq 0.5$ in. (12.7 mm). If a 280 000-psi (1930-MPa) yield strength maraging steel is used for the clevis and pins, adequate strength will be obtained for testing the specimen sizes and σ_{YS}/E ratios given in 7.1.3. If lower-strength grip material is used, or if substantially larger specimens are required at a given σ_{YS}/E ratio than those shown in 7.1.3, then heavier grips will be required. As indicated in Fig. A5.2, the clevis corners may be cut off sufficiently to accommodate seating of the clip gage in specimens less than 0.375 in. (9.5 mm) thick.

A5.3.1.2 Careful attention should be given to achieving as good alignment as possible through careful machining of all auxiliary gripping fixtures.

A5.3.2 Displacement Gage—For generally applicable details concerning the displacement gage see 6.3.

A5.3.2.1 An alternative means of measuring the displacement is allowed for the arc-shaped specimen with $X/W = 0.5$. Conical center-punch-type indentations are provided on the inner surface of the C-shaped specimen at mid-thickness and in the plane of the center line of the loading holes as shown in Fig. A5.1a. The load-point displacement of the specimen is measured at these points using a displacement gage fitted with points and meeting the requirements described in 6.4.1.

A5.3.2.2 The displacements will be essentially independent of the gage length for the arc-shaped specimen provided the gage length is equal to or less than $W/2$.

A5.4 Procedure

A5.4.1 Measurement—Before testing an arc-shaped specimen measure $(r_1 - r_2)$ to the nearest 0.001 in. (0.025 mm) or to 0.1 %, whichever is greater at mid-thickness positions on both sides of and immediately adjacent to the crack starter notch mouth. Record the average of these two readings as W . Also measure $(r_1 - r_2)$ at four positions, two as close as possible to the loading holes and two at approximately one-half the circumferential distance between the loading holes and the crack plane. If any of these four measurements differ from W by more than 10 % the specimen should be discarded or reworked. Next,

measure to the nearest 0.001 in. (0.025 mm) or to 0.1 %, whichever is greater, the distance between the loading hole centers and the outside surface of the specimen at the notch plane. This measurement should be made on both sides of the specimen by referencing the loading holes. Subtract W from the average of these two measurements and record the result as X . Measure within 5 % the outer radius, r_2 , if this is not possible, determine the average value of r_2 as follows (see Note A5.1): Measure within 5 % the length, L , of the cord of the outer surface, which cord passes through the loading hole centers (see Fig. A5.3). Using this measurement, calculate

$$r_2 = \frac{L^2}{8(W + X)} + \frac{(W + X)}{2}$$

Then $r_1/r_2 = 1 - W/r_2$.

NOTE A5.1—A 10 % variation of the ratio r_1/r_2 will affect the value of the stress intensity factor by 1 % or less, providing that the relative crack length a/W is not less than 0.3. However, the stress analysis is based on the assumption that the specimens are to be cut from stock of uniform, axisymmetric cross section. If inspection shows that the stock deviates from axisymmetry by more than 10 %, it should be reworked to within this tolerance.

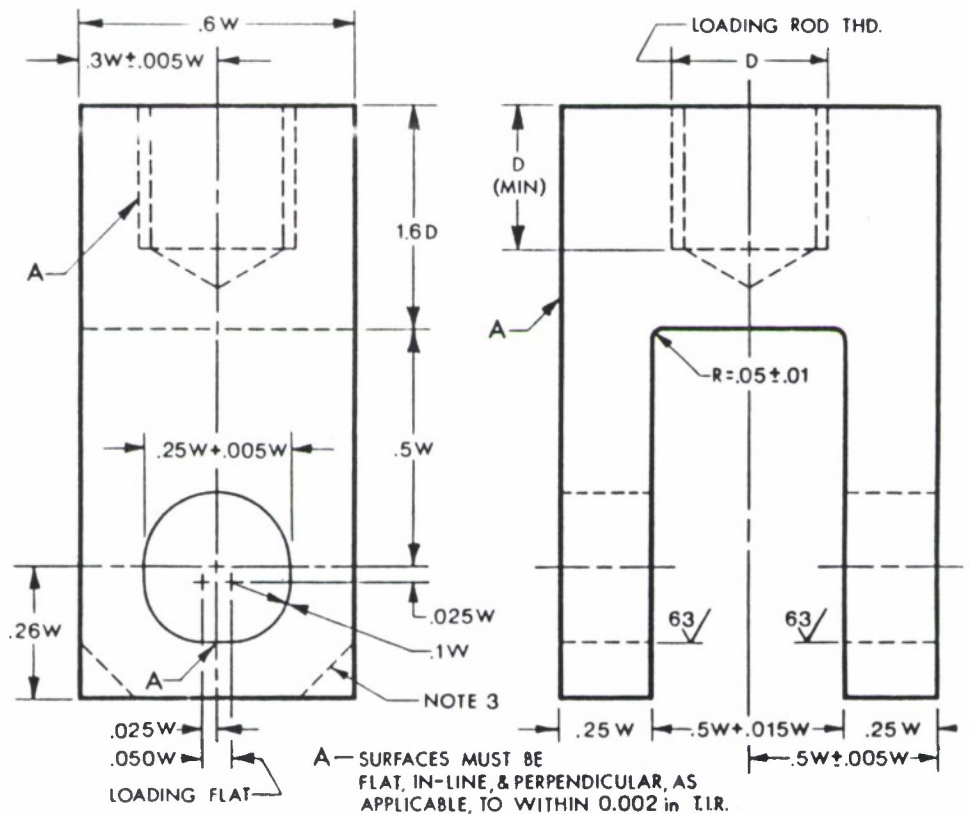
A5.4.1.1 After fracture measure the crack length in accordance with 8.2.2 but a special procedure is necessary for the arc-shaped specimen due to its curvature. Thus, a length measurement, m , made from a reference point adjacent to the crack mouth to a point on the crack front will be greater than the corresponding distance from the virtual point of intersection between the crack plane and the inside circumference of the specimen (see Fig. A5.3). The error, e , may be computed from the following expression:

$$e = r_1 - \left[r_1^2 - \frac{g^2}{4} \right]^{1/2}$$

where g is the distance across the crack mouth at the reference points for measurement of the crack length. It should be noted that g may be equal to N (Fig. 4) or larger than N if machined knife edges are used to hold the clip gage (for example, $g = 0.25$ in. (2.5 mm) as in Fig. 2). If the relative error $e/m < 0.01$, then record m as the crack length; otherwise e should be subtracted from m and the result recorded as the crack length.

A5.4.2 Arc-Shaped Specimen Testing—When assembling the loading train (clevises and their attachments to the tension machine) care should be taken to minimize eccentricity of loading due to misalignments external to the clevises. To obtain satisfactory alignment keep the centerline of the upper and lower loading rods coincident within 0.03 in. (0.76 mm) during the test and center the specimen with respect to the clevis opening within 0.03 in. (0.76 mm).

A5.4.2.1 Load the arc-shaped specimen at such a rate that the rate of increase of stress intensity is within the range 30 to 150 ksi · in.^{1/2}/min (0.55 to 2.75 MPa · m^{1/2}/s). The corresponding loading rates for a standard ($W/B = 2$) 1-in. thick specimen are: (1) for



NOTE 1—Pin diameter = $0.24 W (+0.000 W/-0.005 W)$. For specimens with $\sigma_{YS} > 200$ ksi (1379 MPa) the holes in the specimen and in the clevis may be $0.3 W (+0.005 W/-0.000 W)$ and the pin diameter $0.288 W (+0.000 W/-0.005 W)$.

NOTE 2—0.002 in. = 0.051 mm.

NOTE 3—Corners of the clevis may be removed if necessary to accommodate the clip gage.

FIG. A4.2 Tension Testing Clevis Design

A5. SPECIAL REQUIREMENTS FOR THE TESTING OF THE ARC-SHAPED SPECIMEN

A5.1 Specimen

A5.1.1 The arc-shaped specimen is a single edge-notched and fatigue cracked ring segment loaded in tension. The general proportions of two designs of the standard arc-shaped specimen are shown in Fig. A5.1. The value of the radius ratio r_1/r_2 is not specified, so that specimens can be taken from any cylindrical geometry. However, it should be noted that specimens with $r_1/r_2 = 0$ (that is, from a solid cylinder) do not make the best possible use of the test material because the definition of W was chosen to accommodate hollow cylinders. The disk-shaped specimen should be used for tests on solid cylinders (see Annex A6).

A5.1.2 The arc-shaped specimen is intended to measure the fracture toughness so that the normal to the crack plane is in the circumferential direction and the direction of crack propagation is in the radial

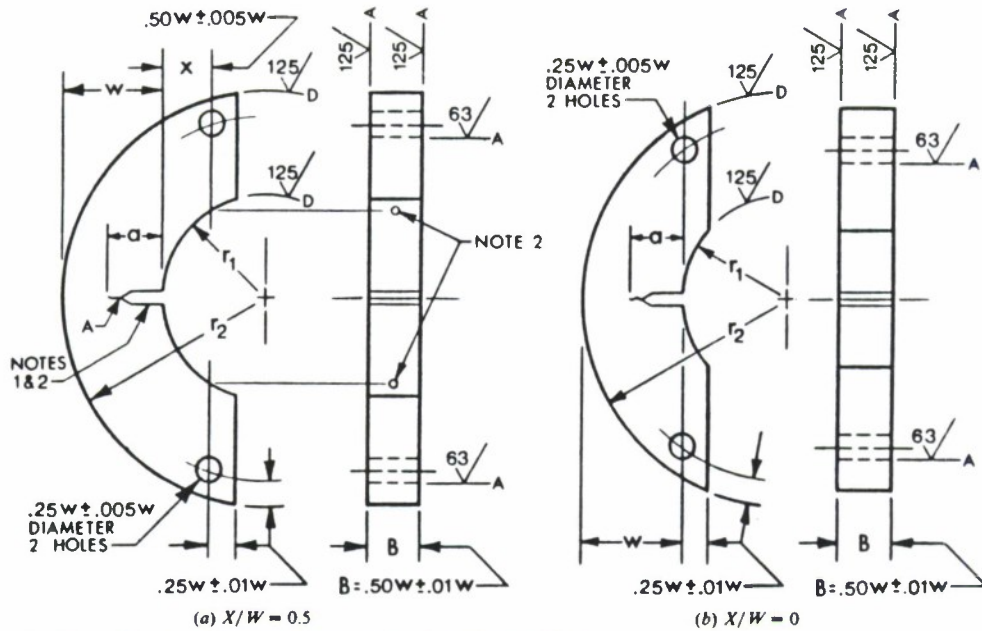
direction. This is the $C-R$ orientation as defined in 9.2.2. For other orientations, a bend (Annex A3) or a compact (Annex A4) specimen should be used.

A5.1.3 The arc-shaped specimen with $X/W = 0.5$ (Fig. A5.1a) represents a half ring segment. The specimen with $X/W = 0$ (Fig. A5.1b) represents the smallest specimen of this configuration that can be cut from a ring.

A5.1.4 Alternative specimens may have $2 \leq W/B \leq 4$ but with no change in other proportions. The use of alternative specimen proportions for the arc-shaped specimen can be advantageous because in many cases it is possible to test ring segments with no machining of the inner and outer radii, that is, with no change in W .

A5.2 Specimen Preparation

A5.2.1 For generally applicable specifications



NOTE 1—For starter notch and fatigue crack configurations see Fig. 4.

NOTE 2—Alternative displacement gage reference points (see A5.4.1.1 for calculation of (a)).

NOTE 3—Axis of holes to be tangent to inner radius within $0.005W$.

NOTE 4— A surfaces to be perpendicular and parallel as applicable to within $0.002W$ TIR. D surfaces to be perpendicular or parallel as applicable to A surfaces to within $0.02W$ TIR (see A5.4.1).

FIG. A5.1 Arc-Shaped Specimen Designs A (T) Standard Proportions and Tolerances



the specimen with an $X/W = 0.5$ between 2800 and 14 000 lbf/min (0.2 to 1.0 kN/s) and (2) for the specimen with an $X/W = 0$ between 4500 and 22 500 lbf/min (0.34 to 1.7 kN/s).

A5.4.2.2 For details concerning recording of the test record see 8.4.

A5.5 Calculations

A5.5.1 For general requirements and procedures in interpretation of the test record see 9.1.

A5.5.2 For a description of the validity requirements in terms of limitations on P_{max}/P_Q and the specimen size requirements see 9.1.2 through 9.1.3.

A5.5.3 Calculation of K_Q —For the arc-shaped specimen calculate K_Q in units of ksi·in.^{1/2} (MPa·m^{1/2}) from the following expression (Note A5.2):

$$K_Q = (P_Q/BW^{1/2})[3X/W + 1.9 + 1.1a/W] \times [1 + 0.25(1 - a/W)^2(1 - r_1/r_2)]f(a/W) \quad (11)$$

where

$$f(a/W) = [(a/W)^{1/2}/(1 - a/W)^{3/2}] \times [3.74 - 6.30a/W + 6.32(a/W)^2 - 2.43(a/W)^3]$$

where:

P_Q = load as determined in 9.1.1, klf (kN),

B = specimen thickness as determined in 8.2.1, in. (cm),

X = loading hole offset as determined in A5.4.1, in. (cm),

W = specimen width as determined in A5.4.1, in. (cm),

a = crack length as determined in 8.2.2 and A5.4.1.1, in. (cm), and

r_1/r_2 = ratio of inner to outer radii as determined in A5.4.1.

To facilitate calculation of K_Q , values of $f(a/W)$ are tabulated in the following table for specific values of a/W :

a/W	$f(a/W)$	a/W	$f(a/W)$
0.450	3.23	0.500	3.73
0.455	3.27	0.505	3.79
0.460	3.32	0.510	3.85
0.465	3.37	0.515	3.91
0.470	3.42	0.520	3.97
0.475	3.47	0.525	4.03
0.480	3.52	0.530	4.10
0.485	3.57	0.535	4.17
0.490	3.62	0.540	4.24
0.495	3.68	0.545	4.31
...	...	0.550	4.38

NOTE A5.2—The accuracy of the expression in A5.5.3 for all values of r_1/r_2 is considered to be as follows: (1) $\pm 1\%$ for $0.45 \leq a/W \leq 0.55$ and X/W of 0 or 0.5, (2) $\pm 1.5\%$ for $0.2 \leq a/W \leq 1$ and X/W of 0 or 0.5, and (3) $\pm 3\%$ for $0.2 \leq a/W \leq 1$ and $0 \leq X/W \leq 1$ (14).

A5.5.4 Calculation of R_{sa} —For the arc-shaped specimen calculate the specimen strength ratio (which is dimensionless and has the same value in any consistent system of units) as follows:

$$R_{sa} = \frac{2P_{max}(3X + 2W + a)}{B(W - a)^2\sigma_{YS}}$$

where:

P_{max} = maximum load that the specimen was able to sustain,

B = thickness of the specimen as determined in 8.2.1,

X = loading hole offset as determined in A5.4.1,

W = width of the specimen as determined in A5.4.1,

a = crack length as determined in 8.2.2 and A5.4.1.1, and

σ_{YS} = yield strength in tension (offset = 0.2%) (see Methods E 8).

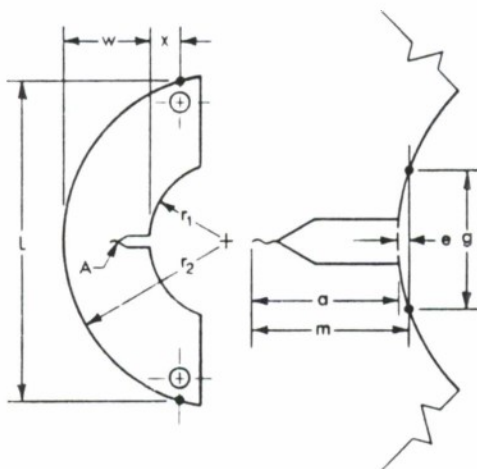


FIG. A5.3 Measurement of Outer Radius (r_2) and Crack Length for the Arc-Shaped Specimen (see A5.4.1)

A6. SPECIAL REQUIREMENTS FOR THE TESTING OF THE DISK-SHAPED COMPACT SPECIMEN

A6.1 Specimen

A6.1.1 The standard disk-shaped compact specimen is a single edge-notched and fatigue cracked disk segment loaded in tension (16). The general proportions of this specimen configuration are shown in Fig. A6.1.

A6.1.2 Alternative specimens may have $2 < W/B < 4$ but with no change in other proportions.

A6.2 Specimen Preparation

A6.2.1 For generally applicable specifications concerning specimen size and preparation see Section 7.

A6.3 Apparatus

A6.3.1 *Tension Testing Clevis*—A loading clevis suitable for testing disk-shaped compact specimens is shown in Fig. A6.2. Both ends of the specimen are held in such a clevis and loaded through pins in order to allow rotation of the specimen during testing. In order to provide rolling contact between the loading pins and clevis holes, these holes are provided with small flats on the loading surfaces (4). Other clevis designs may be used if it can be demonstrated that they will accomplish the same result as the design shown.

A6.3.1.1 The critical tolerances and suggested proportions of the clevis and pins are given in Fig. A6.2. These proportions are based on specimens having $W/B = 2$ for $B > 0.5$ in. (12.7 mm) and $W/B = 4$ for $B \leq 0.5$ in. (12.7 mm). If a 280 000-psi (1930-MPa) yield strength maraging steel is used for the clevis and pins, adequate strength will be obtained for testing the specimen sizes and σ_{YS}/E ratios given in 7.1.3. If lower-strength grip material is used, or if substantially larger specimens are required at a given

σ_{YS}/E ratio than those shown in 7.1.3, then heavier grips will be required. As indicated in Fig. A6.2 the clevis corners may be cut off sufficiently to accommodate seating of the clip gage in specimens less than 0.375 in. (9.5 mm) thick.

A6.3.1.2 Careful attention should be given to achieving as good alignment as possible through careful machining of all auxiliary gripping fixtures.

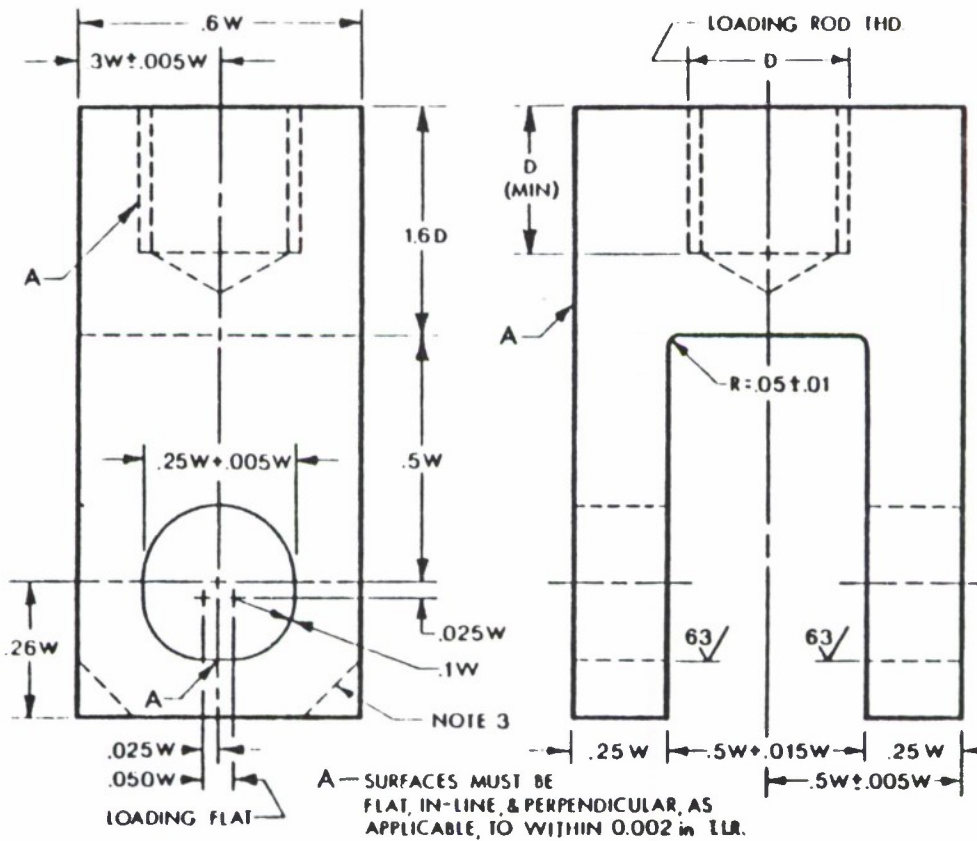
A6.3.2 *Displacement Gage*—For generally applicable details concerning the displacement gage see 6.3. For the disk-shaped compact specimen the displacements will be essentially independent of the gage length up to 0.55 W .

A6.4 Procedure

A6.4.1 *Measurement*—The analysis assumes the specimen was machined from a circular blank and therefore measurements of circularity as well as width, W , and crack length, a , must be made for this specimen.

A6.4.1.1 The specimen blank should be checked for circularity before specimen machining. Measure the radius at eight equally spaced points around the circumference of the specimen blank. One of these points should lie in the intended notch plane. Average these readings to obtain the radius, r . If any measurement differs from r by more than 5 %, machine the blank to the required circularity. Otherwise, $D = 2r = 1.35 W$.

A6.4.1.2 Measure the width, W , and the crack length, a , from the plane of the centerline of the loading holes (the notched edge is a convenient reference line but the distance from the centerline of the holes to the notched edge must be subtracted to determine W and a). Measure the depth, W , to the nearest 0.001 in. (0.025 mm) or 0.1 %, whichever is



NOTE 1—Pin diameter = $0.24 W (+0.000 W/-0.005 W)$. For specimens with $\sigma_{ys} > 200$ ksi (1379 MPa) the holes in the specimen and in the clevis may be $0.3 W (+0.005 W/-0.000 W)$ and the pin diameter $0.288 W (+0.000 W/-0.005 W)$.

NOTE 2—0.002 in. = 0.051 mm.

NOTE 3—Corners of the clevis may be removed if necessary to accommodate the clip gage.

FIG. A5.2 Tension Testing Clevis Design

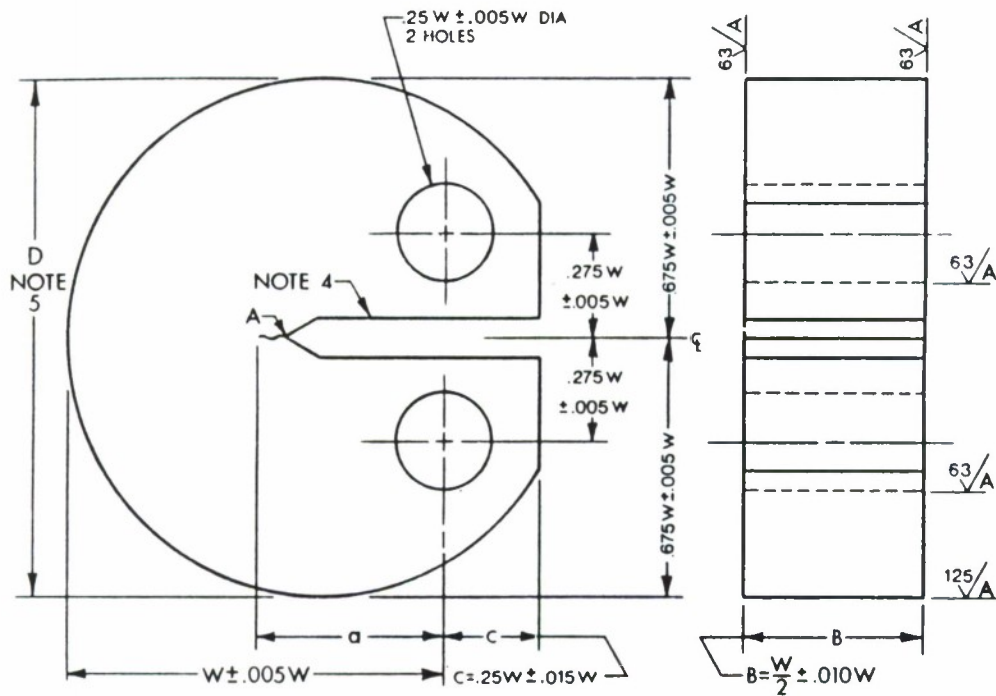


FIG. A6.1 Disk-Shaped Compact Specimen DC(T) Standard Proportions and Tolerances



larger, at not less than three positions near the notch location, and record the average value.

A6.4.1.3 For general requirements concerning specimen measurement see 8.2.

A6.4.2 *Disk-Shaped Compact Specimen Testing*—When assembling the loading train (clevises and their attachments to the tension machine) care should be taken to minimize eccentricity of loading due to misalignments external to the clevises. To obtain satisfactory alignment keep the centerline of the upper and lower loading rods coincident within 0.03 in. (0.76 mm) during the test and center the specimen with respect to the clevis opening within 0.03 in. (0.76 mm).

A6.4.2.1 Load the disk-shaped compact specimen at such a rate that the rate of increase of stress intensity is within the range 30 to 150 ksi·in.^{1/2}/min (0.55 to 2.75 MPa·m^{1/2}/s), corresponding to a loading rate for a standard ($W/B = 2$) 1-in. thick specimen of 4 500 and 22 500 lbf (0.34 to 1.7 kN/s), respectively.

A6.4.2.2 For details concerning recording of the test record see 8.4.

A6.5 Calculations

A6.5.1 For general requirements and procedures in interpretation of the test record see 9.1.

A6.5.2 For a description of validity requirements in terms of limitations on P_{max}/P_Q and the specimen size requirements see 9.1.2 and 9.1.3.

A6.5.3 *Calculation of K_Q* —For the disk-shaped compact specimen calculate K_Q in units of ksi·in.^{1/2} (MPa·m^{1/2}) from the following expression (Note A6.1)

$$K_Q = (P_Q/BW^{1/2})f(a/W)$$

where:

$$f(a/W) = \frac{(2 + a/W)(0.76 + 4.8a/W - 11.58(a/W)^2 + 11.43(a/W)^3 - 4.08(a/W)^4)}{(1 - a/W)^{3/2}}$$

where:

P_Q = load as determined in 9.1.1, klf (kN),

B = specimen thickness as determined in 8.2.1, in. (cm),

W = specimen width as determined in A6.4.1.2, in. (cm), and

a = crack length as determined in 8.2.2 and A6.4.1.2, in. (cm).

To facilitate calculation of K_Q , values of $f(a/W)$ are tabulated in the following table for specific values of a/W :

a/W	$f(a/W)$	a/W	$f(a/W)$
0.450	8.71	0.500	10.17
0.455	8.84	0.505	10.34
0.460	8.97	0.510	10.51
0.465	9.11	0.515	10.68
0.470	9.25	0.520	10.86
0.475	9.40	0.525	11.05
0.480	9.55	0.530	11.24
0.485	9.70	0.535	11.43
0.490	9.85	0.540	11.63
0.495	10.01	0.545	11.83
		0.550	12.04

NOTE A6.1—The expression in A6.5.3 is considered accurate to within $\pm 0.3\%$ over the range of a/W from 0.2 to 1.0 (19).

A6.5.4 *Calculation of R_{dc}* —For the disk-shaped compact specimen calculate the specimen strength ratio (which is dimensionless and has the same value in any consistent set of units) as follows:

$$R_{dc} = \frac{2P_{max}(2W + a)}{B(W - a)^2\sigma_{YS}}$$

where:

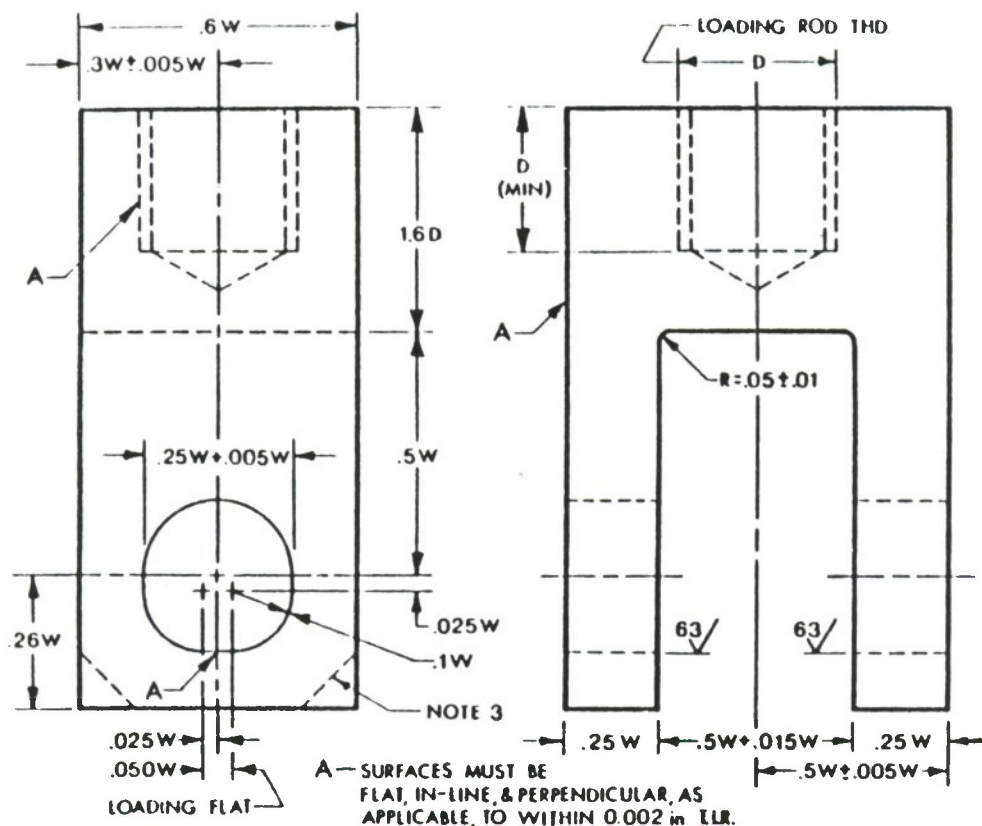
P_{max} = maximum load that the specimen was able to sustain,

B = thickness of the specimen as determined in 8.2.1,

W = specimen width as determined in A6.4.1.2,

a = crack length as determined in 8.2.2 and A6.4.1.2, and

σ_{YS} = yield strength in tension (offset = 0.2 %) (see Methods E 8).



NOTE 1—Pin diameter = $0.24 W (+0.000 W/-0.005 W)$. For specimens with $\sigma_{YS} > 200$ ksi (1379 MPa) the holes in the specimen and in the clevis may be $0.3 W (+0.005 W/-0.000 W)$ and the pin diameter $0.288 W (+0.000 W/-0.005 W)$.

NOTE 2—0.002 in. = 0.051 mm.

NOTE 3—Corners of the clevis may be removed if necessary to accommodate the clip gage.

FIG. A6.2 Tension Testing Clevis Design

REFERENCES

- (1) Brown, W. F., Jr., and Srawley, J. E., "Plane Strain Crack Toughness Testing of High Strength Metallic Materials," *ASTM STP 410*, Am. Soc. Testing Mats., 1966.
- (2) Srawley, J. E., "Plane Strain Fracture Toughness," *Fracture*, Vol 4, Ch. 2, p. 45-68.
- (3) "Fracture Toughness Testing and Its Applications," *ASTM STP 381*, Am. Soc. Testing Mats., April 1965.
- (4) Jones, M. H., Bubsey, R. T., and Brown, W. F., Jr., "Clevis Design for Compact Tension Specimens Used in K_{IC} Testing," *Materials Research and Standards*, Am. Soc. Testing Mats., Vol 9, No. 5, May 1969.
- (5) Wessel, E. T., "State of the Art of the WOL Specimen for K_{IC} Fracture Toughness Testing," *Engineering Fracture Mechanics*, Vol 1, No. 1, January 1968.
- (6) Srawley, J. E., Jones, M. H., and Brown, W. F., Jr., "Determination of Plane Strain Fracture Toughness," *Materials Research and Standards*, Am. Soc. Testing Mats., Vol 7, No. 6, June 1967, p. 262.
- (7) Fisher, D. M., and Repko, A. J., "Note on Inclination of Fatigue Cracks in Plane Strain Fracture Toughness Test Specimens," *Materials Research and Standards*, Am. Soc. Testing Mats., Vol 9, No. 4, April 1969.
- (8) Heyer, R. H., and McCabe, D. E., "Evaluation of a Test Method for Plane-Strain Fracture Toughness Using a Bend Specimen," *ASTM STP 463*, Am. Soc. Testing Mats., 1970, p. 22.
- (9) McCabe, D. E., "Evaluation of the Compact Tension Specimen for Determining Plane-Strain Fracture Toughness of High Strength Materials," *Journal of Materials*, Vol 7, No. 4,



- December 1972, p. 449.
- (10) Fisher, D. M., Bubsey, R. T., and Srawley, J. E., "Design and Use of a Displacement Gage for Crack Extension Measurements," *NASA TN-D-3724*, Nat. Aeronautics and Space Administration, 1966.
- (11) Goode, R. J., "Identification of Fracture Plane Orientation," *Materials Research and Standards*, Am. Soc. Testing Mats., Vol 12, No. 9, September 1972.
- (12) Srawley, J. E., "Wide Range Stress Intensity Factor Expressions for ASTM E 399 Standard Fracture Toughness Specimens," *International Journal of Fracture Mechanics*, Vol 12, June 1976, p. 475.
- (13) Newman, J. C., "Stress Analysis of Compact Specimens Including the Effects of Pin Loading," *ASTM STP 560*, Am. Soc. Testing Mats., 1974, p. 105.
- (14) Kapp, J. A., Newman, J. C., Jr., and Underwood, J. H., "A Wide Range Stress Intensity Factor Expression for the C-Shaped Specimen," *Journal of Testing and Evaluation*, Vol 8, No. 6, November 1980, pp. 314-317.
- (15) Jones, M. H., and Brown, W. F., Jr., "The Influence of Crack Length and Thickness in Plane Strain Fracture Toughness Tests," *ASTM STP 463*, Am. Soc. Testing Mats., 1970, p. 63.
- (16) Underwood, J. H., Newman, J. C., Jr., and Seeley, R. R., "A Proposed Standard Round Compact Specimen for Plane Strain Fracture Toughness Testing," *Journal of Testing and Evaluation*, Vol 8, No. 6, November 1980, pp. 308-313.
- (17) McCabe, D. E., "Evaluation of the Compact Tension Specimen for Plane Strain Fracture Toughness of High Strength Materials," *Journal of Materials*, Vol 7, No. 4, December 1972, p. 449.
- (18) Underwood, J. H., and Kendall, D. P., "Cooperative Plane Strain Fracture Toughness Tests with C-Shaped Specimens," *Journal of Testing and Evaluation*, Vol 6, No. 5, September 1978, p. 296.
- (19) Newman, J. C., Jr., "Stress Intensity Factors and Crack Opening Displacements for Round Compact Specimens," *NASA TM 80174*, Langley Research Center, October 1979.

The American Society for Testing and Materials takes no position respecting the validity of any patent rights asserted in connection with any item mentioned in this standard. Users of this standard are expressly advised that determination of the validity of any such patent rights, and the risk of infringement of such rights, are entirely their own responsibility.

This standard is subject to revision at any time by the responsible technical committee and must be reviewed every five years and if not revised, either reapproved or withdrawn. Your comments are invited either for revision of this standard or for additional standards and should be addressed to ASTM Headquarters. Your comments will receive careful consideration at a meeting of the responsible technical committee, which you may attend. If you feel that your comments have not received a fair hearing you should make your views known to the ASTM Committee on Standards, 1916 Race St., Philadelphia, Pa. 19103, which will schedule a further hearing regarding your comments. Failing satisfaction there, you may appeal to the ASTM Board of Directors.



Designation: E 561 - 81

AMERICAN SOCIETY FOR TESTING AND MATERIALS

1916 Race St., Philadelphia, Pa. 19103

Reprinted from the Annual Book of ASTM Standards, Copyright ASTM
If not listed in the current combined index, will appear in the next edition.

Standard Practice for R-CURVE DETERMINATION¹

This standard is issued under the fixed designation E 561; the number immediately following the designation indicates the year of original adoption or, in the case of revision, the year of last revision. A number in parentheses indicates the year of last reapproval.

1. Scope

1.1 This practice covers the determination of resistance to fracturing of metallic materials by *R*-curves using either the center-cracked tension panel (CCT), the compact specimen (CS), or the crack-line-wedge-loaded specimen (CLWL), to deliver crack-extension force to the material. An *R*-curve is a continuous record of toughness development in terms of K_R plotted against crack extension in the material as a crack is driven under a continuously increased stress intensity factor, *K*.

1.2 Materials that can be tested for *R*-curve development are not limited by strength, thickness, or toughness, so long as specimens are of sufficient size to remain predominantly elastic throughout the duration of the test.

1.3 Specimens of standard proportions are required, but size is variable, to be adjusted for yield strength and toughness of the materials.

1.4 Only three of the many possible specimen types that could be used to develop *R*-curves are covered in this recommended practice.

2. Applicable Documents

2.1 ASTM Standards:

E 338 Sharp-Notch Tension Testing of High-Strength Sheet Materials²

E 399 Test for Plane-Strain Fracture Toughness of Metallic Materials²

E 616 Terminology Relating to Fracture Testing²

3. Summary of Practice

3.1 During slow-stable fracturing, the developing crack growth resistance, K_R , is equal to the crack-extension force, *K* (Note 1), applied to the specimen. The crack is driven forward

by increments of increased load or displacement. Measurements are made at each increment for calculation of *K* values which are individual data points lying on the *R*-curve for the material.

NOTE 1—Extension force may be expressed in terms of *G* if desired through the following conversion: $G = K^2/E$. The use of *K* is presently preferred.

3.2 The crack starter is a low-stress-level fatigue crack.

3.3 Methods of measuring crack growth and of making plastic-zone corrections to the physical crack length are prescribed. Expressions for the calculation of crack-extension force are shown.

4. Significance

4.1 *R*-curves characterize the resistance to fracture of materials during incremental slow-stable crack extension and result from growth of the plastic zone as the crack extends from a sharp notch. They provide a record of the toughness development as a crack is driven stably under increasing crack-extension forces. They are dependent upon specimen thickness, temperature, and strain rate.

4.2 For an untested geometry, the *R*-curve can be matched with the crack-extension force curves to estimate the load necessary to cause unstable crack propagation. (See Fig. 1 (1)³.) In

¹ This practice is under the jurisdiction of ASTM Committee E-24 on Fracture Testing, and is the direct responsibility of Subcommittee E24.01 on Fracture Mechanics Test Methods.

Current edition approved April 24, 1981. Published August 1981. Originally published as a proposed recommended practice in 1974. Last previous edition E 561 - 80.

² Annual Book of ASTM Standards, Part 10.

³ The boldface numbers in parentheses refer to the list of references appended to this practice.

making this estimate, R -curves are regarded as though they are independent of starting crack length, a_0 , and the specimen configuration in which they are developed. They appear to be a function of crack extension, Δa , only (2). To predict crack instability in a component, the R -curve may be positioned as in Fig. 1 so that the origin coincides with the assumed initial crack length, a_0 . Crack-extension force curves for a given configuration can be generated by assuming applied loads or stresses and calculating crack-extension force, K , as a function of crack length using the appropriate expression for K of the configuration. The unique curve that develops tangency with the R -curve defines the critical load or stress that will cause onset of unstable fracturing.

4.3 If the K -gradient (slope of the crack-extension force curve) of the specimen chosen to develop an R -curve has negative characteristics (Note 2), as in the crack-line-wedge-loaded specimen of this method, it may be possible to drive the crack until a maximum or plateau toughness level is reached (3, 4). When a specimen with positive K -gradient characteristics (Note 3) is used, the extent of the R -curve which can be developed is terminated when the crack becomes unstable.

NOTE 2—Fixed displacement in crack-line-loaded specimens results in a decrease of K with crack extension.

NOTE 3—With load control, K usually increases with crack extension.

5. Terminology

5.1 Definitions:

5.1.1 *crack size, a (L)*—a lineal measure of a principal planar dimension of a crack. This measure is commonly used in the calculation of quantities descriptive of the stress and displacement fields, and is often also termed crack length.

NOTE 4—In practice the value of a is obtained from procedures for measurement of physical crack size, a_p , original crack size, a_o , and effective crack size, a_e , as appropriate to the situation being considered.

5.1.1.1 *physical crack size, a_p (L)*—the distance from a reference position to the observed crack front. This distance may represent an average of several measurements along the crack front. The reference position depends on the specimen form, and it is normally taken to be either the boundary, the load line, or the

centerline of a specimen or plate.

5.1.1.2 *original crack size, a_o (L)*—the physical crack size at the start of testing.

5.1.1.3 *effective crack size, a_e (L)*—the physical crack size augmented for the effects of crack-tip plastic deformation.

NOTE 5—Sometimes the effective crack size, a_e , is calculated from a measured value of a physical crack size, a_p , plus a calculated value of a plastic-zone adjustment, r_Y . A preferred method for calculation of a_e compares compliance from the secant of a load-deflection trace with the elastic compliance from a calibration for the type of specimen.

5.1.2 *plastic-zone adjustment, r_Y (L)*—an addition to the physical crack size to account for plastic, crack-tip deformation enclosed by a linear-elastic stress field.

NOTE 6—Commonly the plastic-zone adjustment is given by:

$$r_Y = \frac{1}{2\pi} \frac{K^2}{\sigma_Y^2}, \text{ for plane-stress mode I, and}$$

$$r_Y = \frac{\alpha}{2\pi} \frac{K^2}{\sigma_Y^2}, \text{ for plane-strain mode I,}$$

where $\alpha \approx 1/2$ to $1/4$ and σ_Y is the effective yield strength.

In this method, plane-stress mode I is assumed.

5.1.3 *crack extension, Δa (L)*—an increase in crack size.

NOTE 7—For example, Δa_p or Δa_e is the difference between the crack size, either a_p (physical crack size) or a_e (effective crack size), and a_o (original crack size).

5.1.4 *stress-intensity factor, K , K_1 , K_2 , K_3 (FL^{-3/2})*—the magnitude of the ideal-crack-tip stress field (a stress-field singularity) for a particular mode in a homogeneous, linear-elastic body.

NOTE 8—Values of K for modes I, 2, and 3 are given by:

$$K_1 = \lim_{r \rightarrow 0} [\sigma_y (2\pi r)^{1/2}],$$

$$K_2 = \lim_{r \rightarrow 0} [\tau_{xy} (2\pi r)^{1/2}], \text{ and}$$

$$K_3 = \lim_{r \rightarrow 0} [\tau_{yz} (2\pi r)^{1/2}].$$

where r = a distance directly forward from the crack tip to a location where the significant stress is calculated.

DISCUSSION—In this practice mode I is assumed.

5.1.5 *crack-extension resistance, K_R (FL^{-3/2}), and G_R or J_R (FL⁻¹)*—a measure of the resistance to crack extension expressed in terms of the stress-intensity factor, K , the crack-exten-

sion force, G , or values of J derived using the J -integral concept.

NOTE 9—See definition of R -curve.

5.1.6 R -curve—a plot of crack-extension resistance as a function of crack extension.

NOTE 10—For specimens discussed in Practice E 561, influence in in-plane geometry appears to be negligible, but R -curves normally depend upon specimen thickness and, for some materials, upon temperature and strain rate.

5.1.7 crack displacement (L)—the separation vector between two points (on the surfaces of a deformed crack) that were coincident on the surfaces of an ideal crack in the undeformed condition.

DISCUSSION—In this practice, displacement, v , is the distance that a chosen measurement point on the specimen displaces normal to the crack plane. Total displacement as measured by clip gages or other devices spanning the crack is defined as $2v$. Measurement points on CLWL and CS specimens are identified as locations $V1$ and $V2$.

5.2 Description of Terms Specific to this Method:

5.2.1 plane-stress fracture toughness, K_{IC} —in Practice E 561, the value of K_{IC} at the instability condition determined from the tangency between the R -curve and the critical crack-extension force curve of the specimen.

NOTE 11—See the discussion of plane-strain fracture toughness in Terminology E 616.

5.2.2 fixed load or fixed displacement crack-extension force curves—curves obtained from a fracture mechanics analysis for the test configuration; assuming a fixed applied load or displacement and generating a curve of K versus the effective crack size as the independent variable.

6. Apparatus

6.1 Grips and Fixtures for CCT Specimens—In the center-cracked tension tests, the grip fixtures are designed to develop uniform load distribution on the specimen. To ensure uniform stress entering the crack plane, the length of the specimen between the innermost loading pins shall be at least two specimen widths, $2W$. For panels wider than 12 in. (305 mm), multiple-pin grips are mandatory and the requirement is relaxed to $1.5W$. A typical grip arrangement shown in Fig. 2 has proven useful. Pin or

gimbal connections are located between the grips and loading machine to aid the symmetry of loading. If extra-heavy-gage ultra-high-strength materials are to be tested, the suitability of the grip arrangement may be checked using the *AISC Steel Construction Manual*.

6.2 Grips and Fixtures for Compact Specimens—The grips and fixtures described in Method E 399 are recommended for R -curve testing where CS-type specimens are loaded in tension.

6.3 Fixtures for Crack-Line-Wedge-Loading (CLWL):

6.3.1 Where wedge loading is used, a low-taper-angle wedge with a polished finish and split-pin arrangement shown in Fig. 3 is used. Sketches of a segmented split-pin system which has proved effective for maintaining the load line independent of rotation of the specimen arms are provided in Fig. 4. It has been found convenient to use a wedge whose included angle is 3 deg. With proper lubrication and system alignment a mechanical advantage of five can be expected. Thus, a loading machine producing $\frac{1}{5}$ the maximum expected test load will be adequate. The wedge must be long enough to develop the maximum expected crack-opening displacement. The maximum required stroke can be calculated from the maximum expected displacement $2v$, using the $EB2v/P$ values found in Table 2, the maximum expected K level in the test, and the wedge angle.

6.3.2 The wedge-load blocks which drive the load sectors are constrained on top (not shown) and bottom to restrict motion to a plane parallel to the plane of the specimen. This allows the load to be applied or released conveniently without driving the load blocks and sectors out of the hole in the specimen. The wedge-load blocks are designed so that line contact exists between the wedge-load block and the load sector at a point that falls on the load line of the specimen. This enables the load sectors to rotate as the wedge is driven and the original load line is maintained. Any air- or oil-hardening tool steel will be suitable for making the wedge and wedge-load blocks. A maraging 300-grade steel should be used for the load sectors. The diameter of the sectors shall be slightly smaller (nominally $\frac{1}{4}$ in. (0.79 mm)) than the diameter of the drilled hole in the specimen.

6.4 Face Plates to Prevent Sheet Buckling—Buckling may develop in unsupported speci-

mens depending upon the sheet thickness, material toughness, crack length, and specimen size. Buckling seriously affects the validity of a K analysis and is particularly troublesome when using compliance techniques to determine effective crack length. It is therefore required that rigid face plates be affixed to the CCT, CS, and CLWL specimens in critical regions. A procedure for the detection of buckling using autographic records is described in 8.6.

6.4.1 For the CCT specimen, the buckling restraints shall be attached to the central portion of the specimen. The plates shall be so designed to prevent sheet kinking about the crack plane and sheet wrinkling along the specimen width.

6.4.2 For CS and CLWL specimens, the portion of the specimen arms and back edge which are in compression should be restrained from buckling. For sheet specimens it is convenient to use a base plate and cover plate with ports cut in the cover plate at appropriate locations for attaching clip gages and for crack length observations.

6.4.3 Lubrication shall be provided between the face plates and specimen. Care shall be taken to keep lubricants out of the crack to avoid possible crack acceleration due to aggressive attack. Sheet TFE-fluorocarbon or heavy oils or both can be used. The initial clamping forces between opposing plates need not be excessive, but of the order of a few pounds.

6.5 *Displacement Gages*—Displacement gages are used to accurately measure the crack-opening displacement across the crack at a preselected location and span. In testing small CLWL and CS specimens, the gage recommended in Method E 399 may have a sufficient linear working range to be used. However, in testing larger specimens where W is larger than 5 in. (127 mm), displacements may be of such a magnitude that gages with greater working ranges of the type shown in Fig. 5 are needed. The use of point contacts eliminates error in the readings from the hinge-type rotation of CS and CLWL specimens. The precision of all types of gages shall be checked in accordance with the calibration procedure outlined in 6.4.1 of Method E 399. In addition, absolute accuracy within 2 % over the working range of the gage is required for use with compliance mea-

surements. The gages shall be recalibrated periodically.

6.5.1 A recommended gage for use with CCT panels with a No. 13 drilled hole at the midpoint of the crack is shown in Fig. 6 (6), and a detail of components is shown in Fig. 6a. Proper construction techniques and required electronic procedures are specified in Method E 399.

6.5.2 Other types of gages used over different gage spans are equally acceptable provided the precision and accuracy requirements are retained. The conventional clip gage of Method E 399 may be used with screw attachments spanning the crack at a chosen interval, $2Y$. In CCT tests, it is necessary to be cautious in choosing the proper compliance calibration curve to go with such arrangements because displacement is a function of Y/W .

6.6 *Optical Equipment*—If the material being tested is sufficiently thin so that the crack-tip contour does not vary significantly from surface to midthickness, crack growth can be followed by surface observations using optical equipment. If load is sustained at given increments so that the crack stabilizes, crack length can be determined within 0.01 in. (0.2 mm) using a 30 to 50-power traveling-stage microscope. A movie camera recording system may be useful. A common technique is to record simultaneously load and crack growth using two synchronized cameras.

6.7 *Other Equipment*—Other methods of measuring crack length are available, such as eddy-current probes, which are most useful with nonferrous material, or electrical-resistance measurements, where the extension of the crack is determined from electrical potential differences.

7. Specimen Configuration, Dimensions, and Preparation

7.1 *Specimen Size*—In order for the K analysis to be valid, the specimen ligaments in the plane of the crack must be predominantly elastic at all values of applied load.

7.2 For the CCT panel, the net section stress based on the physical crack size must be less than the yield strength of the material. The CCT panel width, W , is optional provided the requirement of 7.1 is observed. The needed width to be below material yield may be estimated from the maximum expected plastic-



zone size, r_Y (see 9.1.4), which is directly proportional to the square of the material toughness-to-yield strength ratio. As a guide, a specimen $27r_Y$ wide and $\frac{1}{2}$ notched is expected to fail at a net section stress equal to the yield strength (7). It therefore is desirable to have an estimate of the maximum K expected in the test before designing the specimen. As an aid, the following table lists minimum recommended CCT sizes for assumed K_{\max} -to-yield strength ratios.

K_{\max}/σ_Y , in. ^{1/2} (mm ^{1/2})	Width, in. (mm)	$2a_0$, in. (mm)	Length, in. (mm) ^a
0.5(0.80)	3.0(76)	1.0(25)	9(229) ^b
1.0(1.6)	6.0(152)	2.0(51)	12(305)
1.5(2.4)	12.0(305)	4.0(102)	24(610)
2.0(3.2)	20.0(508)	6.7(170)	30(762)
3.0(4.8)	48.0(1219)	16.0(406)	72(1829)

^a Specimen length between grips of CCT specimens is nominally $2W$ with W less than or equal to 12 in. (305 mm), and $1.5W$ for all W greater than 12 in.

^b Pin-loaded specimen of Method E 338.

7.3 The recommended CS specimen is shown in Fig. 7a. Crack-opening displacement is measured at a point $0.1576W \pm 0.0006W$ in advance of the center line of the loading pins. Alternative location of the gage is permitted but displacement values must be linearly extrapolated to $0.1576W$ in order to use the values given in Table 2 for compliance measurement. Span of the gage is not critical so long as it is less than $W/4$.

7.4 The recommended CLWL specimen is shown in Fig. 7b. Hole size is proportioned according to specimen size. Some small amount of specimen brinelling at the hole can be tolerated. Clip gage placement is restricted to $0.1576W \pm 0.0006W$ in front and $0.303W \pm 0.0006W$ behind the load line. Recommended gage span varies with specimen size as shown in the figure.

7.5 In order for a result to be considered valid for CS and CLWL specimens in accordance with this recommended practice, it is required that the remaining uncracked ligament at the end of the test be at least equal to $4/\pi (K_{\max}/\sigma_Y)^2$ where K_{\max} is the maximum K level in a test and σ_Y is the 0.2 % offset yield strength of the material. The initial crack length in CS and CLWL specimens shall be between 0.35 to 0.45 times specimen width.

7.6 *Starting Notch*—The machined starter slot for any of the recommended specimens may be made by electrical-discharge machin-

ing, end milling, or saw cutting.

7.6.1 For the CCT specimen, the machined notch shall be 30 to 35 % of W and shall be centered with respect to specimen width within $0.002W$. It is advisable to have root radii at the ends of the slots of 0.003 in. (0.08 mm) or less to facilitate fatigue cracking. The starter slot must be extended by fatigue cracks not less than 0.05 in. (1.3 mm) in length (see Note 12). The slot must lie within an envelope described by Fig. 8.

7.6.2 For the CS specimen, Fig. 9 shows the allowable notch types and envelope sizes. The machined slots must be extended by fatigue cracks not less than 0.05 in. (1.3 mm) in length.

NOTE 12—Fatigue cracks may be omitted only if it can be shown that the machined notch root radius effectively simulates the sharpness of a fatigue starter crack.

7.7 In fatigue cracking, the minimum-to-maximum load ratio can be chosen through experience. In CCT specimens, the maximum stress in the net section shall not be greater than 50 % of the yield stress. In CS and CLWL specimens, the maximum load in fatigue shall not develop strength ratios greater than 0.5 as calculated in accordance with 9.1.7 of Method E 399. Typically, maximum nominal stresses in fatigue cracking should be between 10 to 40 % of material yield strength.

8. Procedure

8.1 *Measurements*—Measure material thickness, B , to ± 1 % of B at four locations near the crack plane. Measure specimen width, W , accurate to ± 0.5 % of W .

8.2 *Number of Tests*—Replicate R -curves can be expected to vary as do other properties in mechanical tests such as Charpy-V energies or tensile properties. A curve plotted from a single determination may be a smoothly increasing function of crack extension, giving the impression that the single determination is an accurate representation. This is not necessarily so; make at least one additional confirming test.

8.3 *Loading Procedure*—Load the CCT, CS, and CLWL specimens incrementally, allowing time between steps for the crack to stabilize before measuring load and crack length (see Note 13). Cracks stabilize in most materials within seconds of stopping the loading. However, when stopping near an instability condition, the crack may take several minutes to stabilize, depending upon the stiffness of the

loading frame and other factors.

NOTE 13—If autographic instrumentation is used, it is permitted to monitor load versus crack extension continuously under monotonic loading. Load rate must be slow enough so as not to introduce strain rate effects into the R -curve. Static K_{IH} cannot be determined when the crack is steadily creeping or accelerating at or near instability.

8.3.1 *Number of Data Points*—While R -curves can be developed with as few as four or five data points, ten to fifteen give improved confidence, and tougher materials usually require more data points.

8.4 *Physical Crack-Length Measurement*—Measure the physical crack length accurately to 0.01 in. (0.2 mm) at each step using suitable measuring devices described in 6.6 and 6.7. Physical crack length can also be measured with compliance techniques by partial unloading of the specimen after each increment, a technique described in 10.4. Adjust the physical crack length for plastic-zone, r_p , to obtain effective crack length for calculating K .

8.4.1 In CLWL tests where the physical crack length is measured, determine the applied load or K from the relationship of Table 2 using an r_p adjustment to crack length to enter the table. Since r_p is a function of K , an iteration procedure may be necessary.

8.5 *Effective Crack-Length Measurement*—Compliance measurements, $2v/P$, made during the loading of specimens, can be used to determine effective crack length, a_e , directly. The crack is automatically plastic-zone corrected and these values can be used directly in the expressions for K .

8.5.1 Effective crack length can be determined directly in CLWL specimens using a double compliance technique (Note 14). By determining the displacements at two different locations, V_1 and V_2 , along the crack line, as shown in Fig. 7b, an effective crack length-to-width ratio, a_e/W , can be found from the displacement ratio $2v_1/2v_2$ using Table 1. It is convenient to plot autographically $2v_1$ versus $2v_2$ on an X - Y recorder at 100 \times and 200 \times , respectively. The load, P , can be calculated using a_e and displacement at V_1 in conventional compliance relationships appearing in Table 2. In continuous X - Y plots, the wedge direction or load can be reversed at appropriate intervals to determine return slope $2\Delta v_1/2\Delta v_2$, which corresponds to physical crack length, using Table 1. In wedge systems, use a restrain-

ing jig to prevent withdrawal of the split pins along with the wedge.

NOTE 14—It is optional to use double compliance on CS specimens. The procedure is identical to that prescribed for CLWL testing, and effective crack lengths predicted should be identical to those predicted by single compliance. However, use the compliance relationships for CS loading as is noted in Tables 1 and 2.

8.6 *Detection of Buckling*—If compliance instrumentation is used, it is possible to determine when the specimen has developed undesirable buckling. The detection technique involves periodic partial unloading of the specimen as is shown schematically in Figs. 10 and 11. The initial part of the test record should have a linear portion which can be substantially retraced upon partial unloading. Likewise, should buckling or friction problems develop at some later stage in the test, the unloading and reloading slopes will tend to diverge. If the slopes differ by more than 2% or if one or both have no linear range, then buckling or friction is present which is sufficient to cause significant error in compliance indicated crack lengths. Added confidence can be obtained by comparing the crack lengths predicted from return slopes, to physical crack length indicated with other more direct measurement methods.

8.7 Difficulties in the interpretation of test records will be encountered if the specimens are not flat prior to testing and if the plates contain regions of residual stress that are not negligible on a thickness average basis.

8.8 *CCT Specimen Testing*—Carefully align the specimens in the testing machine to eliminate eccentricity of loading. Misalignment can result in uncontrolled or spurious stress distribution in the specimen, which could be troublesome, particularly if compliance measurements are used to determine effective crack length. Fixtures for measuring crack growth may be affixed to the specimen after applying a light preload. Starting crack length in a CCT specimen is nominally 30 to 35% of W , as established in 7.6.1. Measure this to the nearest 0.01 in. (0.2 mm).

8.9 *CS and CLWL Testing*—Starting crack length in a CS and CLWL specimen is nominally 35 to 45% of W , as set forth in 7.5. The stress distribution in these crack-line-loaded types of specimens is such that the crack could deviate away from the original notch direction

as the crack is driven (8). This is usually observed in materials that have appreciable anisotropy of toughness and where the crack is driven in the tougher direction. Accuracy of the elastic displacement relationships decreases with deviation from the crack line; discard the data at deviation angles greater than 10° .

9. Calculation and Interpretation

9.1 To develop an *R*-curve, generate and use crack length and load data to calculate K_R .

9.1.1 For the center-cracked tension specimen use either of the two following and equally appropriate expressions:

$$K_R = (P/WB) \sqrt{a} \cdot [1.77 - 0.177 (2a/W) + 1.77 (2a/W)^2]$$

or

$$K_R = (P/WB) (\pi a \sec (\pi a/W))^{1/2}$$

where:

P = applied load,

B = material thickness,

W = width of specimen, and

a = plastic-zone corrected half-crack length.

9.1.2 For the CS and CLWL specimens, determine K_R as follows:

$$K_R = (P/B\sqrt{W}) \times f(a/W)$$

where:

$$f(a/W) = [(2 + a/W)/(1 - a/W)^{3/2}] [0.886 + 4.64 (a/W) - 13.32 (a/W)^2 + 14.72 (a/W)^3 - 5.6 (a/W)^4]$$

Valid for any $a/W \geq 0.35$

a = plastic-zone corrected crack length measured from load line, and

W = specimen width measured from the load line.

9.1.3 Alternatively, values appearing in Table 2 may be used to calculate K_R .

9.1.4 The crack length used in the expressions of 9.1.1 and 9.1.2 is the effective crack length, which is the total physical crack length plus a correction for plastic zone, r_Y . Correct physically measured crack lengths as follows:

$$a_e = (a + \Delta a + r_Y)$$

where:

a_e = starting half-crack length in a CCT test or crack length in CS and CLWL tests,

Δa = physical crack growth at one crack tip, and

r_Y = plastic-zone adjustment

$$r_Y = (1/2\pi)(K_R^2/\sigma_Y^2)$$

9.1.5 The expression of 9.1.4 for r_Y is most

accurate for high-strength materials of yield strength-to-density ratios above 700 000 psi/lb·in.⁻³ (174 kPa/kg·m⁻³). Lower-strength, high-toughness materials require increasing reliance on compliance methods to correct for plastic-zone effects.

10. Compliance Methods

10.1 *Determination of Effective Crack Length*—The compliance technique uses elastic-spring characteristics of the specimen calibrated over varied crack lengths (9). A calibration curve may be developed experimentally by elastically loading specimens of varied crack sizes and determining the elastic reciprocal spring constant or reciprocal slope of load versus displacement record. Normalize these reciprocal slopes for material thickness and elastic modulus and plot against crack length-to-specimen width ratio. An analytically developed expression for the compliance of the CCT specimen, which can be used instead of an experimentally developed curve (10) is as follows:

$$\frac{E[2v]}{\sigma W} = 2((\pi a/W)/\sin(\pi a/W))^{1/2} \left\{ \frac{2W}{\pi Y} \cosh^{-1} \left(\frac{\cosh \pi Y/W}{\cos \pi a/W} \right) - \frac{1 + \mu}{\left[1 + \left(\frac{\sin \pi a/W}{\sinh \pi Y/W} \right)^2 \right]^{1/2} + \mu} \right\} Y/W$$

(valid for $0.2 < \frac{2a}{W} < 0.8$; $\frac{Y}{W} \leq 0.5$)

where:

E = Young's modulus,

$2v$ = center-opening displacement at center hole,

σ = gross stress, P/BW ,

P = load,

B = sheet thickness,

W = sheet width,

Y = half span of gage,

a = effective half-crack length, and

μ = Poisson's ratio.

10.2 The compliance calibration curve for a 16-in. (405-mm) wide CCT panel using near-zero gage span is presented in Fig. 12. Note that the accompanying analytical curve for compliance was developed for a specific gage half-span-to-specimen width ratio, Y/W .

10.3 In testing to develop an *R*-curve, the test record of load versus clip-gage displace-

ment for the CCT and CS test, or the $2v_1$ versus $2v_2$ record for the CLWL test, will have an initial linear portion, the slope of which should correspond to the starting crack length in the specimen.

10.3.1 In CCT and CS tests, compare the crack length predicted from the initial slope of the test record to the initial crack length. If they differ by more than $0.003W$, treat the initial slope and actual crack length as a single compliance calibration point and vertically adjust the position of the compliance calibration curve to pass through this point using an overlay having the calibration curve shape. Alternatively, this operation may be done arithmetically. Determine all subsequent crack lengths from this transposed curve.

10.3.2 To develop an R -curve for either a CCT or a CS test, draw secants to the test curve from the origin to arbitrarily selected points on the test record (load versus displacement) as shown in Fig. 13. The reciprocal slopes of these secants correspond to effective crack lengths at their points of intersection with the test record. Normalize the reciprocal slopes for elastic modulus and material thickness and enter the calibration record to determine a_e/W .

10.4 In CCT and CS tests, partial unloading at any given point in the test will result in a return slope different from the secant discussed in 10.3.2. The unloading slopes correspond to the physical crack length. This load reversal shall be only enough to establish the return slope accurately from which the physical crack length can be determined. Should the test record not return linearly immediately upon unloading, factors other than material behavior are influencing the test record and return slope measurements should be suspect.

10.5 In a CLWL test record (11), the initial

linear relationship between displacements at locations V_1 and V_2 corresponds to the starting physical crack length in the specimen, and should be accurate within $0.005W$. The V_1/V_2 double compliance calibration curve cannot be shifted as with the CCT and CS specimen single compliance relationships. Despite possible error in prediction of initial crack length, a_0 , the ability to determine increments of crack growth should remain unimpaired. However, if the starting crack length is in error by more than 3% of a_0 , the data shall be discarded and the test equipment checked for conformance to the requirements of this recommended practice. Increments of crack growth are indicated by subtracting the compliance-indicated initial crack length from the crack lengths determined in succeeding increments.

10.6 Calculate K_R in accordance with expressions in 9.1.1 or 9.1.2 using compliance-determined effective crack lengths.

11. Report

11.1 The report shall include the following:

- 11.1.1 Type and size of specimen used,
- 11.1.2 Crack propagation direction (see Method E 399 for coding system),
- 11.1.3 Material thickness,
- 11.1.4 Yield strength,
- 11.1.5 Fatigue precracking data, and
- 11.1.6 Percent oblique fracture (of value as supplementary information only).

11.2 The R -curve may be plotted in terms of either physical or effective crack extension. The legend shall contain the following information: (a) the method of plastic-zone adjustment to the physical crack length, and (b) whether the abscissa is given in terms of physical or effective crack extension. Instability predictions can be made only from effective crack-extension plots.

REFERENCES

- (1) Srawley, J. E., and Brown, W. F., "Fracture Toughness Testing," *Symposium on Fracture Toughness Testing and Its Applications*, ASTM STP 381, Am. Soc. Testing Mats., 1965, pp. 133-198.
- (2) Kraft, J. M., Sullivan, A. M., and Boyle, R. W., "Effect of Dimensions on Fast Fracture Instability of Notched Sheets," *Proceedings of the Crack Propagation Symposium*, College of Aeronautics, Cranfield, England, Vol. 1, 1961, pp. 8-26.
- (3) Heyer, R. H., and McCabe, D. E., "Plane-Stress Fracture Toughness Testing Using a Crack-Line-Loaded Specimen," *Engineering Fracture Mechanics*, EFMEA, Vol. 4, pp. 393-412.
- (4) Heyer, R. H., and McCabe, D. E., "Crack Growth Resistance in Plane-Stress Fracture Testing," *Engineering Fracture Mechanics*, EFMEA, Vol. 4, pp. 413-430.
- (5) Paris, P. C., and Sih, G. C., "Stress Analysis of Cracks," *Symposium on Fracture Toughness Testing and Its Applications*, ASTM STP 381,

- Am. Soc. Testing Mats., 1965, pp. 30-83.
- (6) Sullivan, A. M., and Freed, C. N., "The Influence of Geometric Variables on K_{IC} Values for Two Thin Sheet Aluminum Alloys," *NRL Report 7270*, NRLRA, National Research Laboratory, June 17, 1972.
- (7) Feddersen, C. E., "Evaluation and Prediction of the Residual Strength of Center Cracked Tension Panels," *Damage Tolerance in Aircraft Structures, ASTM STP 486*, Am. Soc. Testing Mats., 1971, pp. 50-78.
- (8) Cotterell, B., "On Fracture Path Stability in the Compact Tension Test," *International Journal of Fracture Mechanics, IJFMA*, Vol 6, 1970, pp. 189-192.
- (9) Boyle, R. W., "Crack Growth in Notched Sheet Specimens," *Materials Research and Standards, MTRSA*, Am. Soc. Testing Mats., Vol 2, No. 8, 1962.
- (10) Eftis, J., and Liebowitz, H., "On the Modified Westergaard Equation for Certain Plane Crack Problems," *International Journal of Fracture Mechanics, IJFMA*, Vol 4, December 1972.
- (11) *Fracture Toughness Evaluation by R-Curve Methods, ASTM STP 527*, Am. Soc. Testing Mats., 1973.
- (12) Newman, J. C., "Crack-Opening Displacements in Center-Crack, Compact, and Crack-Line Wedge Loaded Specimens," *NASA TN D-8268*, July 1976.

TABLE 1 Double Compliance Elastic Calibration Curve—CS and CLWL Specimens (12)

NOTE—Applicable only to the V_1 and V_2 locations shown in Fig. 7(a) and 7(b).

$2V_1/2V_2^A$			$2V_1/2V_2^A$			$2V_1/2V_2^A$			$2V_1/2V_2^A$		
a/w	CLWL	CS	a/w	CLWL	CS	a/w	CLWL	CS	a/w	CLWL	CS
0.350	4.74	5.56	0.415	3.27	3.67	0.480	2.72	2.96	0.545	2.42	2.56
0.355	4.54	5.25	0.420	3.22	3.59	0.485	2.70	2.92	0.550	2.40	2.53
0.360	4.36	5.00	0.425	3.16	3.53	0.490	2.67	2.88	0.555	2.38	2.50
0.365	4.24	4.78	0.430	3.11	3.46	0.495	2.64	2.85	0.560	2.36	2.48
0.370	4.09	4.62	0.435	3.06	3.39	0.500	2.62	2.81	0.565	2.34	2.46
0.375	3.97	4.47	0.440	3.02	3.33	0.505	2.59	2.78	0.570	2.32	2.44
0.380	3.85	4.33	0.445	2.97	3.27	0.510	2.57	2.74	0.575	2.31	2.42
0.385	3.74	4.22	0.450	2.93	3.22	0.515	2.54	2.71	0.580	2.29	2.40
0.390	3.64	4.11	0.455	2.89	3.17	0.520	2.52	2.68	0.585	2.27	2.38
0.395	3.55	4.01	0.460	2.85	3.13	0.525	2.50	2.66	0.590	2.25	2.36
0.400	3.47	3.91	0.465	2.82	3.08	0.530	2.48	2.63	0.595	2.24	2.35
0.405	3.39	3.82	0.470	2.79	3.04	0.535	2.46	2.60	0.600	2.23	2.33
0.410	3.33	3.75	0.475	2.76	3.00	0.540	2.44	2.58			

^A $2V_1/2V_2$ is moderately affected by clip gage span with less than $\pm 2\%$ error introduced by using 0.8-in. (20.3-mm) span instead of measurements on the crack line.

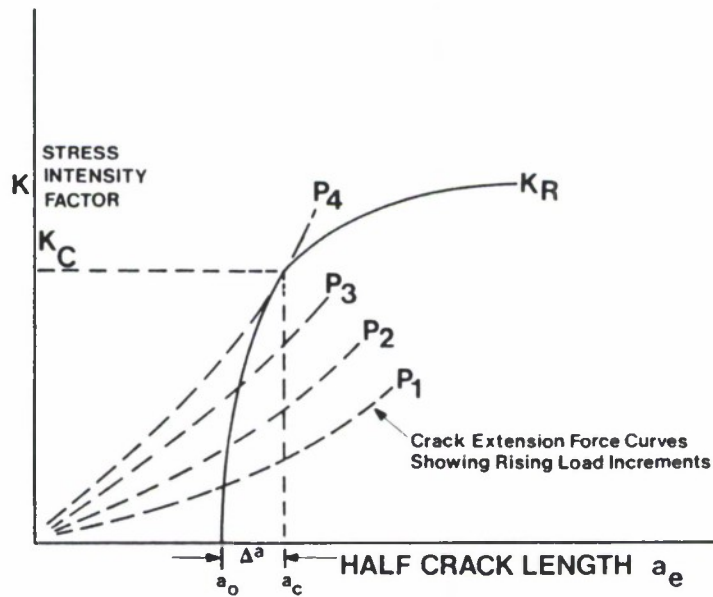


FIG. 1 Schematic Representation of *R*-Curve and Crack-Extension Force Curves Superposed on One Plot

TABLE 2 Dimensionless Stress Intensity Factors and Compliance in Plane Stress for the Recommended CS and CLWL Specimens

NOTE— $H/w = 0.6$.
 Vl at $0.1576W$

a/w	$KBW^{1/2}/P$	$EB2v1/P$		a/w	$KBW^{1/2}/P$	$EB2v1/P$	
		CLWL	CS			CLWL	CS
0.350	6.392	22.83	25.82	0.480	9.093	41.52	44.31
0.355	6.475	23.35	26.33	0.485	9.230	42.52	45.30
0.360	6.558	23.88	26.85	0.490	9.369	43.55	46.33
0.365	6.644	24.43	27.38	0.495	9.512	44.61	47.38
0.370	6.730	24.99	27.94	0.500	9.659	45.70	48.48
0.375	6.818	25.57	28.50	0.505	9.810	46.83	49.60
0.380	6.906	26.16	29.08	0.510	9.964	47.99	50.76
0.385	6.998	26.76	29.68	0.515	10.123	49.18	51.95
0.390	7.090	27.38	30.29	0.520	10.286	50.42	53.19
0.395	7.183	28.02	30.91	0.525	10.453	51.70	54.47
0.400	7.279	28.67	31.55	0.530	10.625	53.02	55.78
0.405	7.376	29.33	32.21	0.535	10.802	54.38	57.15
0.410	7.475	30.01	32.88	0.540	10.984	55.79	58.56
0.415	7.576	30.71	33.57	0.545	11.172	57.24	60.01
0.420	7.678	31.42	34.27	0.550	11.364	58.75	61.52
0.425	7.783	32.15	34.99	0.555	11.563	60.31	63.08
0.430	7.890	32.90	35.73	0.560	11.767	61.92	64.70
0.435	7.999	33.67	36.49	0.565	11.978	63.60	66.37
0.440	8.110	34.45	37.27	0.570	12.1955	65.32	68.10
0.445	8.223	35.25	38.07	0.575	12.420	67.12	69.89
0.450	8.340	36.08	38.89	0.580	12.651	68.97	71.74
0.455	8.458	36.93	39.73	0.585	12.890	70.89	73.66
0.460	8.580	37.80	40.60	0.590	13.136	72.88	75.65
0.465	8.704	38.69	41.49	0.595	13.391	74.94	77.72
0.470	8.830	39.61	42.40	0.600	13.654	77.07	79.85
0.475	8.960	40.55	43.34				

Polynomial expressions fit to the above compliance values are:

Compact Specimen: $EB2v1/P = 103.8 - 930.4(a/w) + 3610(a/w)^2 - 5930.5(a/w)^3 + 3979(a/w)^4$.

CLWL: $EB2v1/P = 101.9 - 948.9(a/w) + 3691.5(a/w)^2 - 6064.0(a/w)^3 + 4054(a/w)^4$.

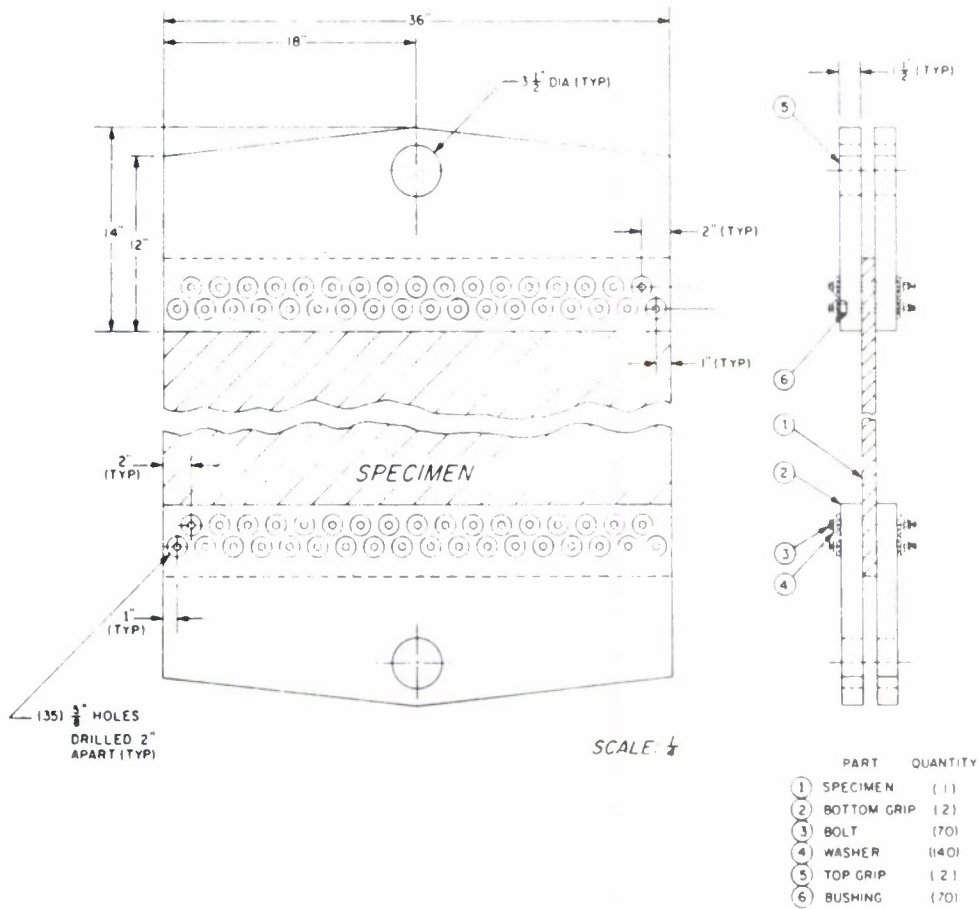


FIG. 2 Center-Cracked Tension Panel Test Setup

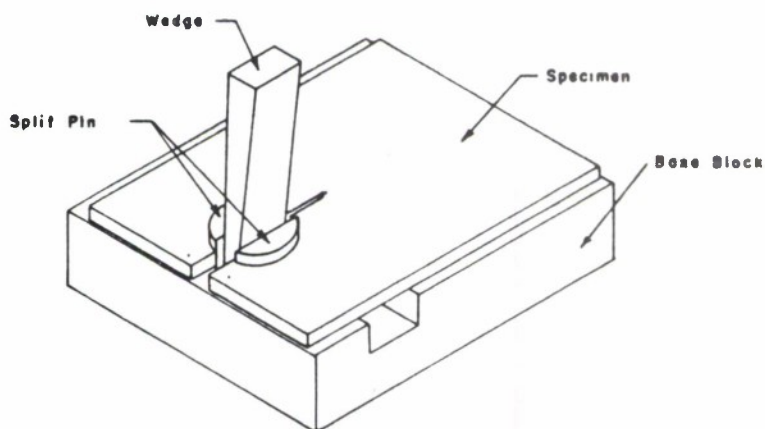


FIG. 3 Crack-Line-Loaded Specimen with Displacement-Controlled Wedge Loading

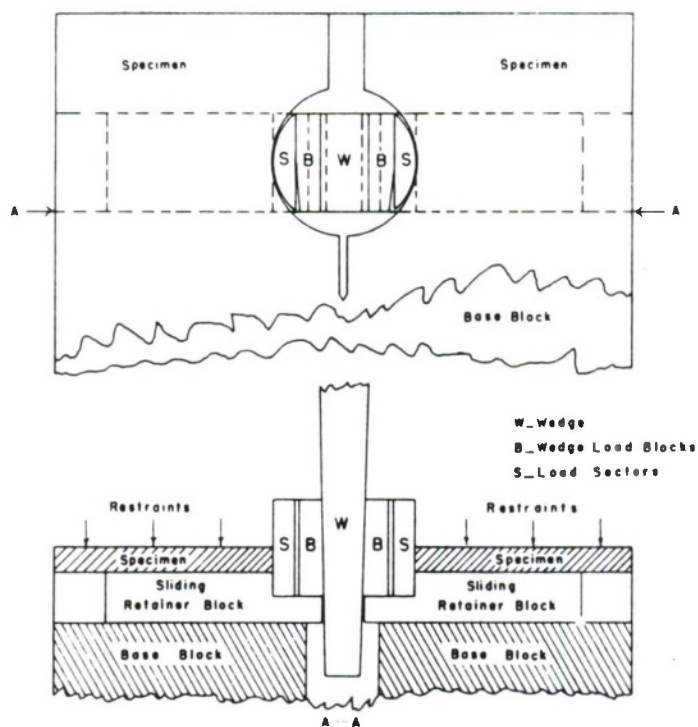


FIG. 4 Detail of Special Wedge and Split-Pin Setup Designed to Prevent Load-Line Shift

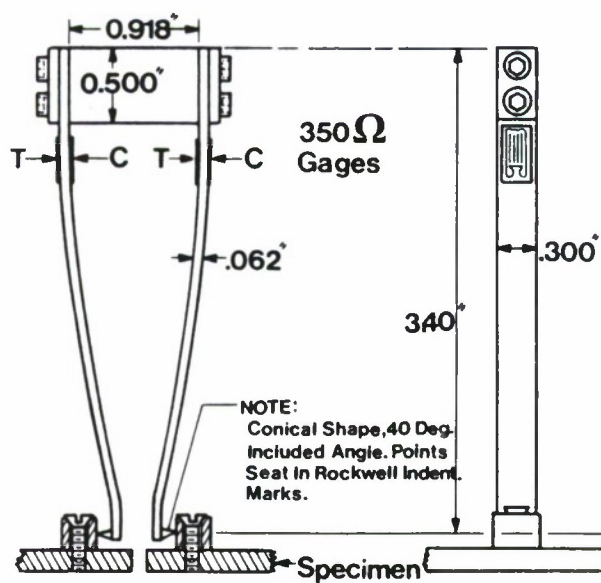


FIG. 5 Enlarged Clip Gage for Double Compliance Work

ASTM E 561

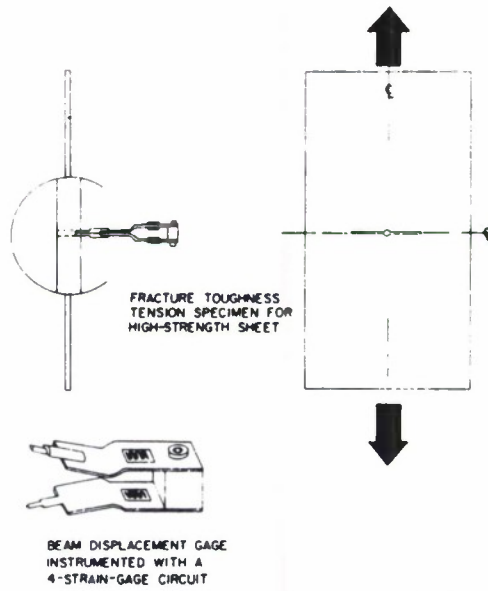


FIG. 6 Clip Gage for Use with Center-Cracked Tension Panels



FIG. 6A Detail Drawings of CCT-Type Clip Gage

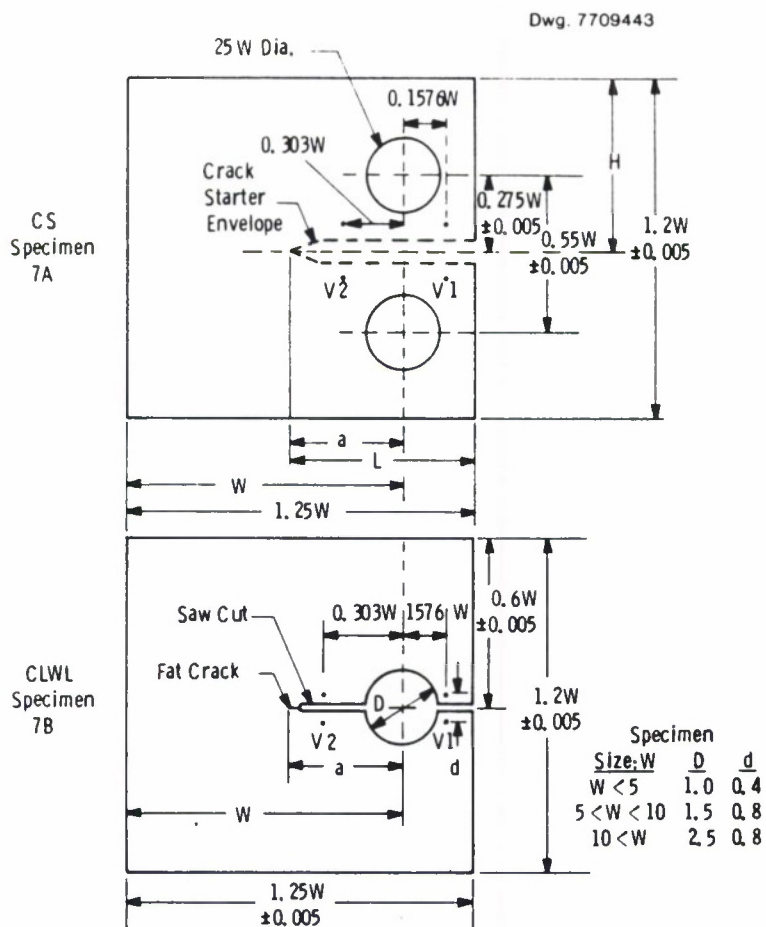


FIG. 7 Compact and Crack-Line-Wedge-Loaded Specimens

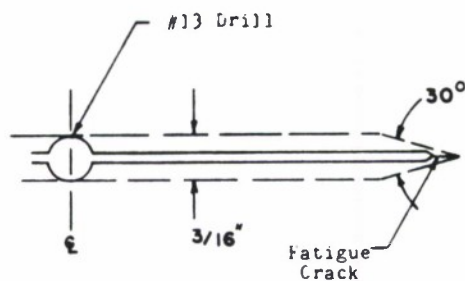


FIG. 8 Enlarged View of the Right Half of the Permitted Notch Envelope in CCT Panels

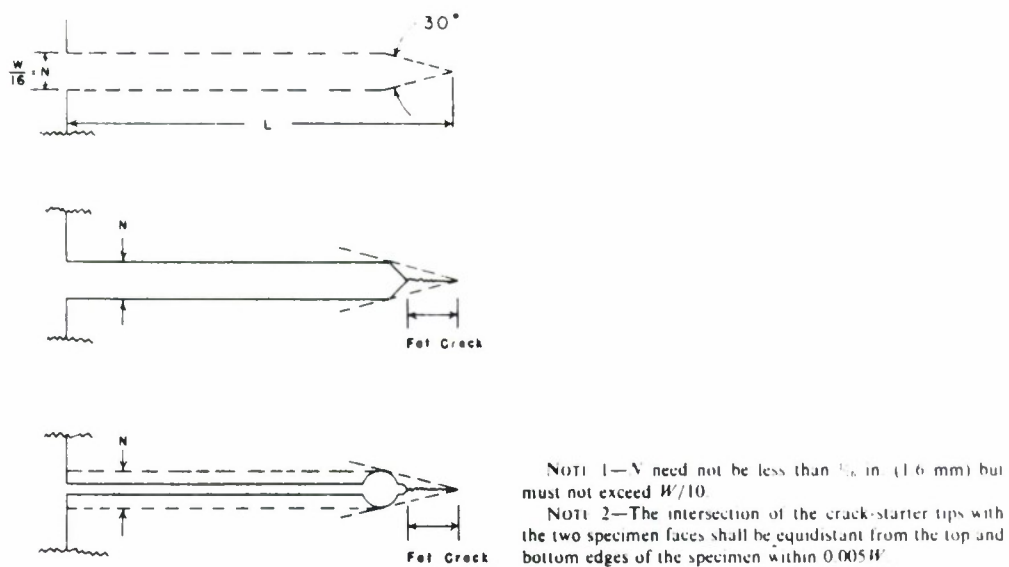


FIG. 9 Envelope for Crack-Starters Notches and Examples of Notches Extended with Fatigue Cracks

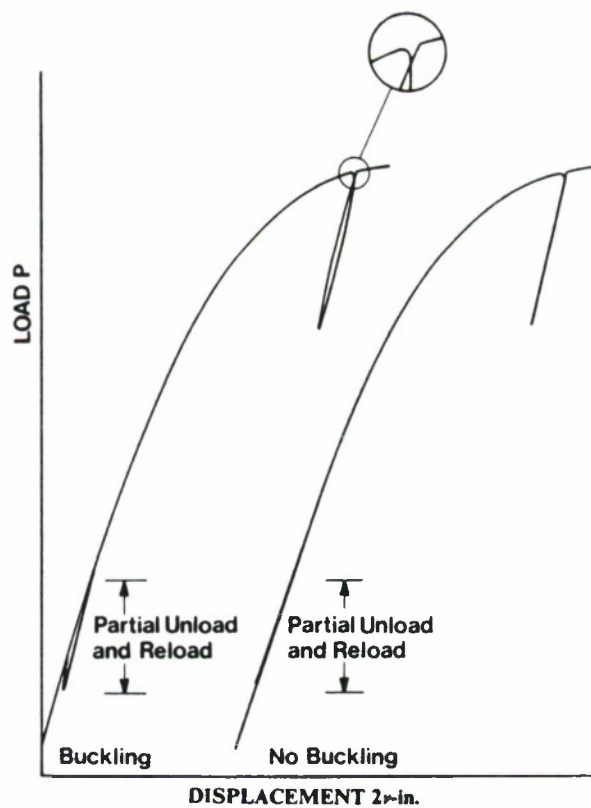


FIG. 10 Detection of Buckling from Compliance Test Records of CCT and CS Specimens

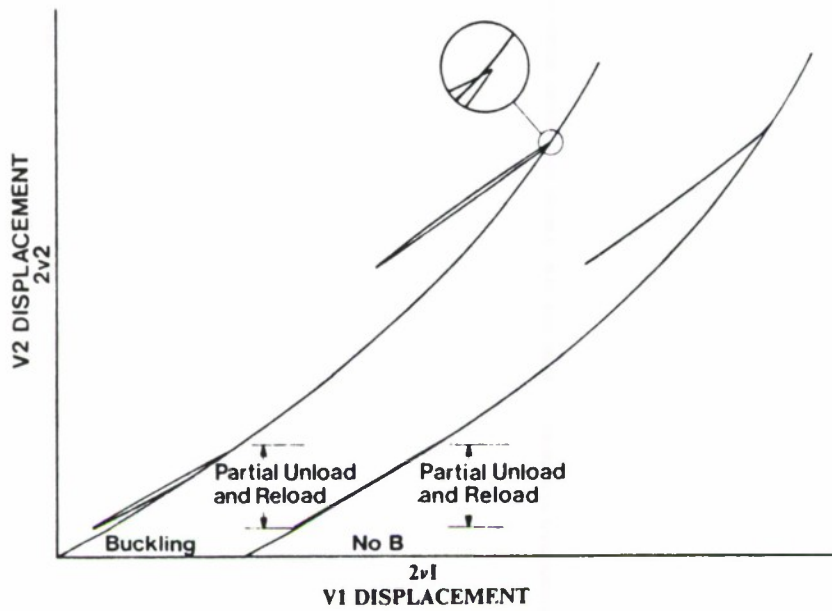
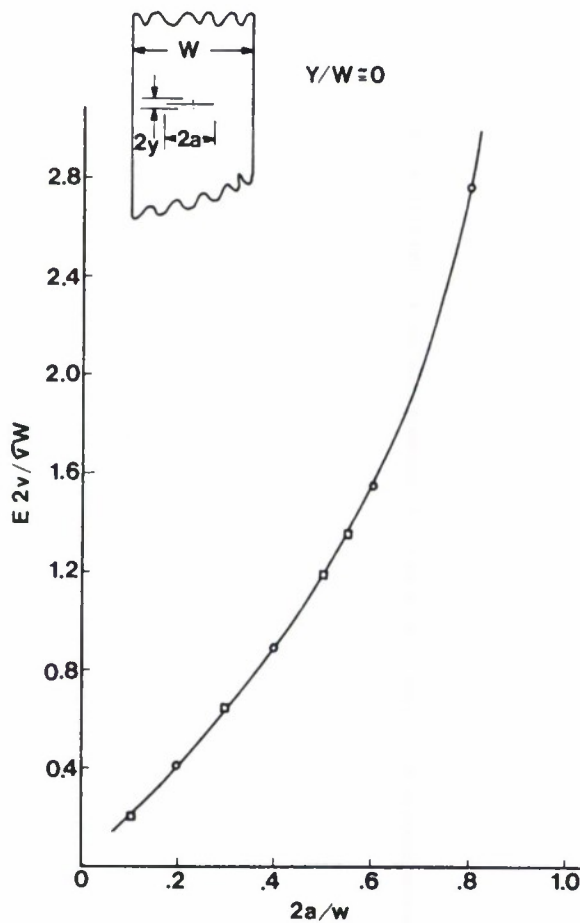


FIG. 11 Detection of Buckling from Double Compliance Test Records of CLWL Specimens



- Boundary Value Collocation.
- Finite Element

FIG. 12 Compliance Calibration Curve for a 16-in. (405-mm) Wide Center Notched Panel with Near Zero Gage Span

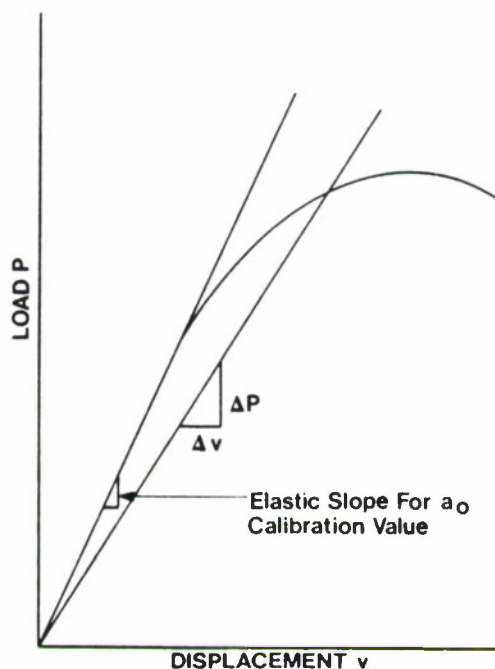


FIG. 13 Schematic Test Record for CCT or CS Specimens

The American Society for Testing and Materials takes no position respecting the validity of any patent rights asserted in connection with any item mentioned in this standard. Users of this standard are expressly advised that determination of the validity of any such patent rights, and the risk of infringement of such rights, is entirely their own responsibility.

This standard is subject to revision at any time by the responsible technical committee and must be reviewed every five years and if not revised, either reapproved or withdrawn. Your comments are invited either for revision of this standard or for additional standards and should be addressed to ASTM Headquarters. Your comments will receive careful consideration at a meeting of the responsible technical committee, which you may attend. If you feel that your comments have not received a fair hearing you should make your views known to the ASTM Committee on Standards, 1916 Race St., Philadelphia, Pa. 19103, which will schedule a further hearing regarding your comments. Failing satisfaction there, you may appeal to the ASTM Board of Directors.



Designation: E 647 - 81

AMERICAN SOCIETY FOR TESTING AND MATERIALS
1916 Race St., Philadelphia, Pa. 19103

Reprinted from the Annual Book of ASTM Standards, Copyright ASTM
If not listed in the current combined index, will appear in the next edition.

Standard Test Method for CONSTANT-LOAD-AMPLITUDE FATIGUE CRACK GROWTH RATES ABOVE 10^{-8} m/CYCLE¹

This standard is issued under the fixed designation E 647; the number immediately following the designation indicates the year of original adoption or, in the case of revision, the year of last revision. A number in parentheses indicates the year of last reapproval.

1. Scope

1.1 This method² covers the determination of constant-load-amplitude fatigue crack growth rate above 10^{-8} m/cycle, using either compact type (CT) or center-cracked-tension (CCT) specimens.³ Results are expressed in terms of the crack-tip stress intensity range, defined by the theory of linear elasticity.

1.2 Materials that can be tested by this method are not limited by thicknesses or by strength so long as specimens are of sufficient thickness to preclude buckling and of sufficient planar size to remain predominantly elastic during testing.

1.3 A range of specimen sizes with proportional planar dimensions is provided, but size is variable to be adjusted for yield strength and applied load. Specimen thickness may be varied independent of planar size.

1.4 Specimen configurations other than those contained in this method may be used provided that well-established stress intensity calibrations are available and that specimens are of sufficient size to remain predominantly elastic during testing.

2. Applicable Documents

2.1 ASTM Standards:

E 4 Load Verification of Testing Machines⁴

E 8 Tension Testing of Metallic Materials⁵

E 337 Test for Relative Humidity by Wet- and Dry-Bulb Psychrometer⁶

E 338 Sharp-Notch Tension Testing of High-Strength Sheet Materials⁷

E 399 Test for Plane-Strain Fracture Toughness of Metallic Materials⁷

E 467 Recommended Practice for Verification of Constant Amplitude Dynamic Loads in an Axial Load Fatigue Testing Machine⁷

E 561 Recommended Practice for R-Curve Determination⁷

3. Summary of Method

3.1 The method involves constant-load-amplitude cyclic loading of notched specimens that have been acceptably precracked in fatigue. Crack length is measured, either visually or by an equivalent method, as a function of elapsed cycles and these data are subjected to numerical analysis to establish the rate of crack growth. Crack growth rates are expressed as a function of the stress intensity factor range, ΔK , which is calculated from expressions based on linear elastic stress analysis.

4. Significance

4.1 Fatigue crack growth rate expressed as a function of crack-tip stress intensity range,

¹ This method is under the jurisdiction of ASTM Committee E-24 on Fracture Testing, and is the direct responsibility of Subcommittee E24.04 on Subcritical Crack Growth.

Current edition approved April 24, 1981. Published July 1981. Originally published as E 647 - 78T. Last previous edition E 647 - 78T.

² For additional information on this method, see RR: E 24 - 1001. Available from ASTM Headquarters, 1916 Race St., Philadelphia, Pa. 19103.

³ Determination of fatigue crack growth rates below 10^{-8} m/cycle requires specialized testing considerations. Test procedures for this growth rate regime are being formulated within by ASTM Subcommittee E24.04 on Subcritical Crack Growth.

⁴ Annual Book of ASTM Standards, Parts 10, 14, 32, 35, and 41.

⁵ Annual Book of ASTM Standards, Parts 6, 7, and 10.

⁶ Annual Book of ASTM Standards, Parts 20, 26, 32, and 41.

⁷ Annual Book of ASTM Standards, Part 10.

da/dN versus ΔK , characterizes a material's resistance to stable crack extension under cyclic loading. Background information on the rationale for employing linear elastic fracture mechanics to analyze fatigue crack growth rate data is given in Refs (1) and (2).⁸

4.1.1 In innocuous (inert) environments, constant-amplitude fatigue crack growth rates above 10^{-8} m/cycle are primarily a function of ΔK and the load ratio, R , or K_{max} and R (Note 1). Temperature and aggressive environments can significantly affect da/dN versus ΔK , and in many cases accentuate R -effects and also introduce effects of other loading variables, such as cyclic frequency and waveform. Attention needs to be given to the proper selection and control of these variables in research studies and in the generation of design data.

NOTE 1— ΔK , K_{max} , and R are not independent of each other. Specification of any two of these variables is sufficient to define the loading condition. It is customary to specify one of the stress intensity parameters (ΔK or K_{max}) along with the load ratio, R .

4.1.2 Expressing da/dN as a function of ΔK provides results that are independent of planar geometry, thus enabling the exchange and comparison of data obtained from a variety of specimen configurations and loading conditions. Moreover, this feature enables da/dN versus ΔK data to be utilized in the design and evaluation of engineering structures.

4.1.3 Fatigue crack growth rate data are not always geometry-independent in the strict sense since thickness effects sometimes occur. However, data on the influence of thickness on fatigue crack growth rate is mixed. Fatigue crack growth rates over a wide range of ΔK have been reported to either increase, decrease, or remain unaffected as specimen thickness is increased. Thickness effects can also interact with other variables such as environment and heat treatment. In addition, materials may exhibit thickness effects only over the terminal range of da/dN versus ΔK , which is associated with either nominal yielding (Note 2) or a K_{max} -controlled instability. The potential influence of specimen thickness should be considered when generating data for research or design.

NOTE 2—This condition will be avoided in tests that conform to the specimen size requirements of 7.2.

4.2 This method can serve the following purposes:

4.2.1 To establish the influence of fatigue crack growth on the life of components subjected to cyclic loading, provided data are generated under representative conditions and combined with appropriate fracture toughness data (for example, see Method E 399), defect characterization data, and stress analysis information (for example, see Refs (3) and (4)).

NOTE 3—Fatigue crack growth can be significantly influenced by load history. During variable amplitude loading, crack growth rates can be either enhanced or retarded (relative to steady-state, constant-amplitude growth rates at a given ΔK) depending on the specific loading sequence. This complicating factor needs to be considered in using constant-amplitude growth rate data to analyze variable amplitude fatigue problems (for example, see Ref (5)).

4.2.2 To establish material selection criteria and nondestructive inspection requirements for quality assurance.

4.2.3 To establish, in quantitative terms, the individual and combined effects of metallurgical, fabrication, environmental, and loading variables on fatigue crack growth.

5. Definitions

5.1 *crack length, a [L]*—in fatigue, the physical crack size used to determine the crack growth rate and the stress-intensity factor. For the CT specimen, a is measured from the line connecting the bearing points of load application, for the CCT specimen, a is measured from the perpendicular bisector of the central crack.

5.2 *cycle—in fatigue*, one complete sequence of values of applied load that is repeated periodically in fatigue. The symbol N represents the number of cycles.

5.2.1 *maximum load, P_{max} [F]*—in fatigue, the greatest algebraic value of applied load in a fatigue cycle. Tensile loads are considered positive and compressive loads negative.

5.2.2 *minimum load, P_{min} [F]*—in fatigue, the least algebraic value of applied load in a fatigue cycle.

5.2.3 *load range, ΔP [F]*—in fatigue, the algebraic difference between the maximum and minimum loads in a fatigue cycle.

5.2.4 *load ratio (also called stress ratio), R* —

⁸ The boldface numbers in parentheses refer to the list of references appended to this method.

in fatigue, the algebraic ratio of the minimum to maximum load in a fatigue cycle, that is, $R = P_{\min}/P_{\max}$.

5.3 *fatigue crack growth rate, da/dN* , [L]—the rate of crack extension caused by constant-amplitude fatigue loading, expressed in terms of crack extension per cycle of fatigue.

5.4 *stress-intensity calibration, K calibration*—a mathematical expression, based on pirical or analytical results, that relates the stress intensity factor to load and crack length for a specific specimen planar geometry.

5.5 *stress-intensity factor, K , K_1 , K_2 , K_3* [$FL^{-3/2}$]—the magnitude of the ideal-crack-tip stress field, a stress-field singularity, for a particular mode in a homogeneous, linear-elastic body.

NOTE 4—Values of K for the modes 1, 2, and 3 are given by:

$$K_1 = \text{Limit}_{r \rightarrow 0} [\sigma_r(2\pi r)^{1/2}]$$

$$K_2 = \text{Limit}_{r \rightarrow 0} [\tau_{xy}(2\pi r)^{1/2}], \text{ and}$$

$$K_3 = \text{Limit}_{r \rightarrow 0} [\tau_{yz}(2\pi r)^{1/2}].$$

where r = a distance directly forward from the crack tip to a location where the significant stress is calculated.

Discussion—In this method, Mode 1 is assumed.

5.5.1 *maximum stress-intensity factor, K_{\max}* [$FL^{-3/2}$]—the maximum value of the stress-intensity factor in a fatigue cycle. This value corresponds to P_{\max} .

5.5.2 *minimum stress-intensity factor, K_{\min}* [$FL^{-3/2}$]—in fatigue, the minimum value of the stress-intensity factor in a cycle. This value corresponds to P_{\min} when $R > 0$ and is taken to be zero when $R \leq 0$.

5.6 *stress-intensity factor range, ΔK* [$FL^{-3/2}$]—in fatigue, the variation in the stress-intensity factor in a cycle, that is, $K_{\max} - K_{\min}$.

NOTE 5—The loading variables R , ΔK , and K_{\max} are related such that specifying any two uniquely defines the third according to the following relationship: $\Delta K = (1 - R)K_{\max}$ for $R \geq 0$ and $\Delta K = K_{\max}$ for $R \leq 0$.

NOTE 6—These operational stress-intensity factor definitions do not include local crack-tip effects; for example, crack closure, residual stress, and blunting.

6. Apparatus

6.1 *Grips and Fixtures for CT Specimen*—A clevis and pin assembly (Fig. 3) is used at both the top and bottom of the specimen to allow in-plane rotation as the specimen is loaded. This specimen and loading arrange-

ment is to be used for tension-tension loading only.

6.1.1 Suggested proportions and critical tolerances of the clevis and pin are given (Fig. 3) in terms of either the specimen width, W , or the specimen thickness, B , since these dimensions may be varied independently within certain limits.

6.1.2 The pin-to-hole clearances are designed to minimize friction, thereby eliminating unacceptable end-movements that would invalidate the specimen K -calibration provided herein. The use of a lubricant (for example, MoS_2) on the loading pins is also recommended to minimize friction.

6.1.3 Using a 1000-MPa (~ 150 ksi) yield-strength alloy (for example, AISI 4340 steel) for the clevis and pins provides adequate strength and resistance to galling and fatigue.

6.2 *Grips and Fixtures for CCT Specimens*—The type of grips and fixtures to be used with the CCT specimens will depend on the specimen width, W (defined in Fig. 2), and the loading conditions (that is, either tension-tension or tension-compression loading). The minimum required specimen gage length varies with the type of gripping and is specified so that a uniform stress distribution is developed in the specimen gage length during testing. For testing of thin sheets, constraining plates may be necessary to minimize specimen buckling (see Recommended Practice E 561 for recommendations on buckling constraints).

6.2.1 For tension-tension loading of specimens with $W \leq 75$ mm (3 in.), a clevis and single pin arrangement is suitable for gripping provided that the specimen gage length (that is, the distance between loading pins) is at least $2W$ (Fig. 2). For this arrangement it is also helpful to either use brass shims between the pin and specimen or to lubricate the pin to prevent fretting-fatigue cracks from initiating at the specimen loading hole. Additional measures that may be taken to prevent cracking at the pinhole include attaching reinforcement plates to the specimen (for example, see Method E 338) or employing a "dog-bone" type specimen design. In either case, the gage length shall be defined as the uniform section and shall be at least $1.7W$.

6.2.2 For tension-tension loading of specimens with $W \geq 75$ mm (3 in.), a clevis with

multiple bolts is recommended (for example, see Recommended Practice E 561). In this arrangement, the loads are applied more uniformly; thus, the minimum specimen gage length (that is, the distance between the innermost rows of bolt holes) is relaxed to $1.5W$.

6.2.3 The CCT specimen may also be gripped using a clamping device instead of the above arrangements. This type of gripping is necessary for tension-compression loading. An example of a specific bolt and keyway design for clamping CCT specimens is given in Fig. 4. In addition, various hydraulic and mechanical-wedge systems that supply adequate clamping forces are commercially available and may be used. The minimum gage length requirement for clamped specimens is relaxed to $1.2W$.

6.3 *Alignment of Grips*—It is important that attention be given to achieving good alignment in the load train through careful machining of all gripping fixtures. For tension-tension loading, pin or gimbal connections between the grips and the load frame are recommended to achieve loading symmetry. For tension-compression loading, the length of the load train (including the hydraulic actuator) should be minimized and rigid, non-rotating joints should be employed to reduce lateral motion in the load train.

7. Specimen Configuration, Size, and Preparation

7.1 *Standard Specimens*—The geometry of standard CT and CCT specimens is given in Figs. 1 and 2, respectively. The specific geometry of CCT specimens depends on the method of gripping as specified in 6.2. Notch and precracking details for both specimens are given in Fig. 5. The CT specimen is not recommended for tension-compression testing because of uncertainties introduced into the K -calibration.

7.1.1 It is required that the machined notch, a_n , in the CT specimen be at least $0.2W$ in length so that the K -calibration is not influenced by small variations in the location and dimensions of the loading-pin holes.

7.1.2 The machined notch, $2a_n$, in the CCT specimen shall be centered with respect to the specimen centerline to within $\pm 0.001W$. The length of the machine notch in

the CCT specimen will be determined by practical machining considerations and is not restricted by limitations in the K -calibration.

NOTE 7—It is recommended that $2a_n$ be at least $0.2W$ when using the compliance method to monitor crack extension in the CCT specimen so that accurate crack length determinations can be obtained.

7.1.3 For both specimens, the thickness, B , and width, W , may be varied independently within the following limits, which are based on specimen buckling and through-thickness-crack-curvature considerations:

7.1.3.1 For CT specimens it is recommended that thickness be within the range $W/20 \leq B \leq W/4$. Specimens having thicknesses up to and including $W/2$ may also be employed; however, data from these specimens will often require through-thickness crack-curvature corrections (9.1). In addition, difficulties may be encountered in meeting the through-thickness crack straightness requirements of 8.3.2 and 8.6.4.

7.1.3.2 Using the above rationale, the recommended upper limit on thickness in CCT specimens is $W/8$, although $W/4$ may also be employed. The minimum thickness necessary to avoid excessive lateral deflections or buckling in CCT specimens is sensitive to specimen gage length, grip alignment, and load ratio, R . It is recommended that strain gage information be obtained for the particular specimen geometry and loading condition of interest and that bending strains not exceed 5 % of the nominal strain.

7.2 *Specimen Size*—In order for results to be valid according to this method, it is required that the specimen be predominantly elastic at all values of applied load. The minimum in-plane specimen sizes to meet this requirement are based primarily on empirical results and are specific to specimen configuration (6).

7.2.1 For the CT specimen it is required that the uncracked ligament, $W - a$, be equal to or greater than $(4/\pi)(K_{\max}/\sigma_{YS})^2$, where σ_{YS} is the 0.2 % offset yield strength of the test material (measured by Methods E 8) at the temperature for which fatigue crack growth rate data are to be obtained.

7.2.2 For the CCT specimen it is required that the nominal stress in the uncracked ligament, given by the following:

$$\sigma_y = \frac{P_{\max}}{BW \left(1 - \frac{2a}{W} \right)}$$

be less than σ_{ys} .

NOTE 8—The above criteria are likely to be restrictive, that is, they may require overly large specimen sizes for materials that exhibit a high degree of strain hardening (for example, annealed low-alloy ferritic steels, annealed austenitic stainless steels, etc.). Currently, there are insufficient data on these materials to formulate easily calculable size requirements that are analogous to those given above. However, data from specimens smaller than those allowed by 7.2 may be validated by demonstrating that da/dN versus ΔK results are equivalent to results from larger specimens that meet the requirements of 7.2. Supplementary information on the extent of plastic deformation encountered in any given test specimen can be obtained by measuring specimen deflections as described in Appendix X2.

7.2.3 Figure 6 gives the limiting K_{\max} values, designated $K_{\max L}$, which are defined by the above specimen size criteria. This information is expressed in dimensionless form so that the curves can be used to calculate either: (1) the value of $K_{\max L}$ for a given combination of specimen size, W , and material yield strength, σ_{ys} , or (2) the minimum specimen size required to obtain valid data up to a desired K_{\max} value for a given material strength level. (However, it should be noted that the desired K_{\max} value cannot be achieved if it is greater than the K value for unstable fracture.) All values of $K_{\max}/(\sigma_{ys}\sqrt{W})$ that fall below the respective curves for the two specimens satisfy the specimen size requirements of this method.

7.3 *Notch Preparation*—The machined notch for either of the standard specimens may be made by electrical-discharge machining (EDM), milling, broaching, or sawcutting. The following notch preparation procedures are suggested to facilitate fatigue precracking in various materials:

7.3.1 *EDM*— $\rho < 0.010$ in. (ρ = notch root radius), high-strength steels ($\sigma_{ys} \geq 170$ ksi), titanium and aluminum alloys.

7.3.2 *Mill or Broach*— $\rho \leq 0.003$ in., low or medium-strength steels ($\sigma_{ys} \leq 170$ ksi), aluminum alloys.

7.3.3 *Grind*— $\rho \leq 0.010$ in., low or medium-strength steels.

7.3.4 *Mill or Broach*— $\rho \leq 0.010$ in., aluminum alloys.

7.3.5 *Sawcut*—Aluminum alloys.

7.3.6 Examples of various machined-notch geometries and associated precracking requirements are given in Fig. 5 (see 8.3).

8. Procedure

8.1 *Number of Tests*—Variability in da/dN data at a given ΔK may vary by a factor of 2 (7). It is a good practice to conduct replicate tests; when this is impractical, tests should be planned such that regions of overlapping da/dN versus ΔK data are obtained. Since confidence in inferences drawn from the data increases with the number of tests, the desired number of tests will depend on the end use of the data.

8.2 *Specimen Measurements*—The specimen dimensions shall be within the tolerances given in Figs. 1 and 2.

8.3 *Fatigue Precracking*—Conduct fatigue precracking with the specimen fully heat treated to the condition in which it is to be tested. The precracking equipment shall be such that the load distribution is symmetrical with respect to the machine notch and K_{\max} during precracking is controlled to within $\pm 5\%$. Any convenient loading frequency that enables the required load accuracy to be achieved can be used for precracking. The machined notch plus the precrack must lie within the envelope, shown in Fig. 5, that has as its apex the end of the fatigue precrack. In addition, the fatigue precrack shall be not less than $0.1B$ or h , whichever is greater (Fig. 5).

8.3.1 The final K_{\max} during precracking shall not exceed the initial K_{\max} for which test data are to be obtained. If necessary, loads corresponding to higher K_{\max} values may be used to initiate cracking at the machined notch. In this event, the load range shall be stepped-down to meet the above requirement. Furthermore, it is suggested that the reduction in P_{\max} for any of these steps be no greater than 20% and that measurable crack extension occur before proceeding to the next step. To avert transient effects in the test data, apply the load range in each step over a crack length increment of at least $(3/\pi)(K'_{\max}/\sigma_{ys})^2$, where K'_{\max} is the terminal value of K_{\max} from the previous load-step. If P_{\min}/P_{\max} during precracking differs from that used during testing, see the precautions described in 8.5.1.

8.3.2 Measure the fatigue precrack length

from the tip of the machined notch to the crack tip on the front and back surfaces of the specimen to within 0.10 mm (0.004 in.) or 0.002 W , whichever is greater. Measure both cracks, front and back, in the CCT specimens. If any two crack length measurements vary by more than 0.025 W or by more than 0.25 B , whichever is less, the precracking operation is not suitable and subsequent testing would be invalid under this method. If a fatigue crack departs more than ± 5 deg from the plane of symmetry the specimen is not suitable for subsequent testing. In either case, check for potential problems in alignment of the loading system or details of the machined notch, or both, before continuing to precrack to satisfy the above requirements.

8.4 Test Equipment—The equipment for fatigue testing shall be such that the load distribution is symmetrical to the specimen notch.

8.4.1 Verify the load cell in the test machine in accordance with Method E 4 and Recommended Practice E 467. Conduct testing such that ΔP and P_{\max} are controlled to within $\pm 2\%$ throughout the test.

8.4.2 An accurate digital device is required for counting elapsed cycles. A timer is a desirable supplement to the counter and provides a check on the counter. Multiplication factors (for example, $\times 10$ or $\times 100$) should not be used on counting devices when obtaining data at growth rates above 10^{-5} m/cycle since they can introduce significant errors in the growth rate determination.

8.5 General Test Procedure—It is preferred that each specimen be tested at a constant ΔP and a fixed set of loading variables. However, this may not be feasible when it is necessary to generate a wide range of information with a limited number of specimens. When loading variables are changed during a test, potential problems arise from several types of transient phenomenon. The following test procedures should be followed to minimize or eliminate transient effects.

8.5.1 If load range is to be incrementally varied it should be done such that P_{\max} is increased rather than decreased to preclude retardation of growth rates caused by overload effects; retardation being a more pronounced effect than accelerated crack growth associated with incremental increase in P_{\max} .

Transient growth rates are also known to result from changes in P_{\min} or R . Sufficient crack extension should be allowed following changes in load to enable the growth rate to establish a steady-state value. The amount of crack growth that is required depends on the magnitude of load change and on the material.

8.5.2 When environmental effects are present, changes in load level, test frequency, or waveform can result in transient growth rates. Sufficient crack extension should be allowed between changes in these loading variables to enable the growth rate to achieve a steady-state value.

8.5.3 Transient growth rates can also occur, in the absence of loading variable changes, due to long-duration test interruptions, for example, during work stoppages. In this case, data should be discarded if the growth rates following an interruption are less than those before the interruption.

8.6 Measurement of Crack Length—Make fatigue crack length measurements as a function of elapsed cycles by means of a visual, or equivalent, technique capable of resolving crack extensions of 0.10 mm (0.004 in.), or 0.002 W , whichever is greater. For visual measurements, polishing the test area of the specimen and using indirect lighting aid in the resolution of the crack tip. It is recommended that, prior to testing, reference marks be applied to the test specimen at predetermined locations along the direction of cracking. Crack length can then be measured using a low power (20 to 50 \times) traveling microscope. Using the reference marks eliminates potential errors due to accidental movement of the traveling microscope. If precision photographic grids or polyester scales are attached to the specimen, crack length can be determined directly with any magnifying device that gives the required resolution. It is preferred that measurements be made without interrupting the test.

8.6.1 When tests are interrupted to make crack length measurements, the interruption time should be minimized (for example, less than 10 min) since transient growth rates can result from interruptions of long duration. A static load not exceeding the maximum load applied during the fatigue test, may be applied during measurement interruptions in order to

enhance the resolution of the crack-tip provision that it does not cause static-load crack extension or creep deformation.

8.6.2 Make crack length measurements at intervals such that da/dN data are nearly evenly distributed with respect to ΔK . The following measurement intervals are recommended according to specimen type:

8.6.2.1 *CT Specimen:*

$$\Delta a \leq 0.02W \text{ for } 0.25 \leq a/W \leq 0.60$$

$$\Delta a \leq 0.01W \text{ for } a/W \geq 0.60$$

8.6.2.2 *CCT Specimen:*

$$\Delta a \leq 0.03W \text{ for } 2a/W < 0.60$$

$$\Delta a \leq 0.02W \text{ for } 2a/W > 0.60$$

8.6.2.3 In any case, the minimum Δa shall be 0.25 mm (0.01 in.) or ten times the crack length measurement precision, whichever is greater.

NOTE 9—The crack length measurement precision is herein defined as the standard deviation on the mean value of crack length determined for a set of replicate measurements.

8.6.3 If crack length is monitored visually the following procedure applies. For specimens with $B/W \leq 0.15$, the crack length measurements need only be made on one side of the specimen. For specimens with $B/W \geq 0.15$, make measurements on both the front and back sides of the specimen and use the average value of these measurements (two values for the CT specimen; four values for the CCT specimen) in subsequent calculations.

8.6.4 If at any point in the test the average through-thickness fatigue crack departs more than ± 5 deg from the plane of symmetry of the specimen, the data are invalid according to the method. In addition, data are invalid where any two crack lengths at a given number of cycles differ by more than $0.025W$ or $0.25B$, whichever is less.

9. Calculations and Interpretation of Results

9.1 *Crack Curvature Correction*—After completion of testing, examine the fracture surfaces, preferably at two locations (for example, at the precrack and terminal fatigue crack lengths), to determine the extent of through-thickness crack curvature (commonly termed "crack tunneling"). If a crack contour is visible, calculate a five point, through-thickness average crack length in accordance with

paragraph 8.2.3 of Method E 399. The difference between the average through-thickness crack length and the corresponding crack length recorded during the test (for example, if visual measurements were obtained this might be the average of the surface crack length measurements) is the crack curvature correction.

9.1.1 If the crack curvature correction results in a greater than 5 % difference in calculated stress intensity factor at any crack length, then employ this correction when analyzing the recorded test data.

9.1.2 If the magnitude of the crack curvature correction either increases or decreases with crack length, use a linear interpolation to correct intermediate data points. Determine this linear correction from two distinct crack contours separated by a minimum spacing of $0.25W$ or B , whichever is greater. When there is no systematic variation of crack curvature with crack length, employ a uniform correction determined from an average of the crack contour measurements.

9.1.3 When employing a crack length monitoring technique other than visual, a crack curvature correction is generally incorporated in the calibration of the technique. However, since the magnitude of the correction will probably depend on specimen thickness, the above correction procedures may also be necessary.

9.2 *Determination of Crack Growth Rate*—Determine the rate of fatigue crack growth from the crack length versus elapsed cycles data (a versus N). Recommended methods are provided in Appendix X1.

NOTE 10—Both recommended methods for processing a versus N data are known to give the same average da/dN response. However, the secant method often results in increased scatter in da/dN relative to the incremental polynomial method, since the latter numerically "smooths" the data (7, 8). This apparent difference in variability introduced by the two methods needs to be considered, especially in utilizing da/dN versus ΔK data in design.

9.3 *Determination of Stress Intensity Range, ΔK* —Use the crack length values of 9.1 and Appendix X1 to calculate the stress intensity range corresponding to a given crack growth rate from the following expressions:

9.3.1 For the CT specimen calculate ΔK as follows:

$$\Delta K = \frac{\Delta P}{B\sqrt{W}} \frac{(2 + \alpha)}{(1 - \alpha)^{3/2}} (0.886 + 4.64\alpha - 13.32\alpha^2 + 14.72\alpha^3 - 5.6\alpha^4)$$

where $\alpha = a/W$; expression valid for $a/W \geq 0.2$ (9, 10).

9.3.2 For the CCT specimen calculate ΔK consistent with the definitions of 5.5; that is:

$$\begin{aligned} \Delta P &= P_{\max} - P_{\min} & \text{for } R > 0 \\ \Delta P &= P_{\max} & \text{for } R \leq 0 \end{aligned}$$

in the following expression (11):

$$\Delta K = \frac{\Delta P}{B} \sqrt{\frac{\pi \alpha}{2W} \sec \frac{\pi \alpha}{2}}$$

where $\alpha = 2a/W$; expression valid for $2a/W < 0.95$.

NOTE 11—Implicit in the above expressions are the assumptions that the test material is linear-elastic, isotropic, and homogeneous.

9.3.3 Check for violation of the specimen size requirement by calculating $K_{\max L}$ (see 7.2 and Fig. 6). Data are considered invalid according to this method when $K_{\max} > K_{\max L}$.

10. Report

10.1 The report shall include the following information:

10.1.1 Specimen type, including thickness, B , and width, W . Figures of the specific CCT specimen design and grips used, and a figure if a specimen type not described in this method is used shall be provided.

10.1.2 Description of the test machine and equipment used to measure crack length and the precision with which crack length measurements were made.

10.1.3 Test material characterization in terms of heat treatment, chemical composition, and mechanical properties (include at least the 0.2 % offset yield strength and either elongation or reduction in area measured in accordance with Methods E 8). Product size and form (for example, sheet, plate, forging, etc.) shall also be identified.

10.1.4 The crack plane orientation according to the code given in Method E 399. In addition, if the specimen is removed from a large product form, its location with respect to the parent product shall be given.

10.1.5 The terminal values of ΔK , R , and crack length from fatigue precracking. If pre-crack loads were stepped-down, the procedure employed shall be stated and the amount of crack extension at the final load level shall

be given.

10.1.6 Test loading variables, including ΔP , R , cyclic frequency, and cyclic waveform.

10.1.7 Environmental variables, including temperature, chemical composition, pH (for liquids), and pressure (for gases and vacuum). For tests in air, the relative humidity as determined by Method E 337 shall be reported. For tests in "inert" reference environments, such as dry argon, estimates of residual levels of water and oxygen in the test environment (generally this differs from the analysis of residual impurities in the gas supply cylinder) shall be given. Nominal values for all of the above environmental variables, as well as maximum deviations throughout the duration of testing, shall be reported. Also, the material employed in the chamber used to contain the environment and steps taken to eliminate chemical/electrochemical reactions between the specimen-environment system and the chamber shall be described.

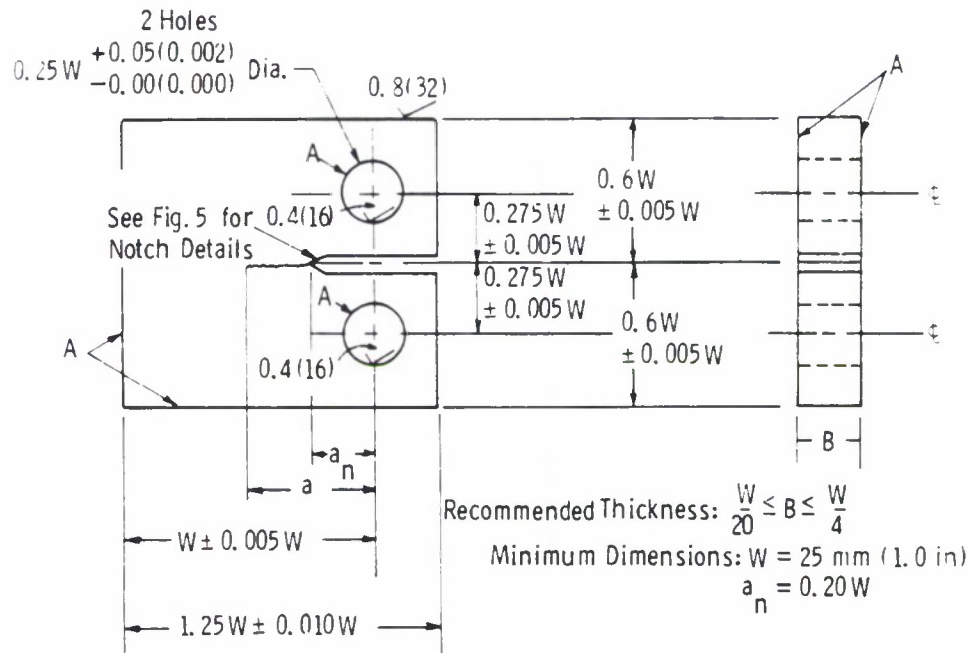
10.1.8 Analysis methods applied to the data, including the technique used to convert a versus N to da/dN , specific procedure used to correct for crack curvature, and magnitude of crack curvature correction.

10.1.9 The specimen K -calibration and size criterion to ensure predominantly elastic behavior (for specimens not described in this method).

10.1.10 da/dN as a function of ΔK shall be plotted. (It is recommended that the independent variable, ΔK , be plotted on the abscissa and the dependent variable, da/dN , on the ordinate. Log-log coordinates are commonly used. For optimum data comparisons, the size of the ΔK -log cycles should be two to three times larger than da/dN -log cycles.) All data that violate the size requirements of 7.2 and Appendix X2 shall be identified.

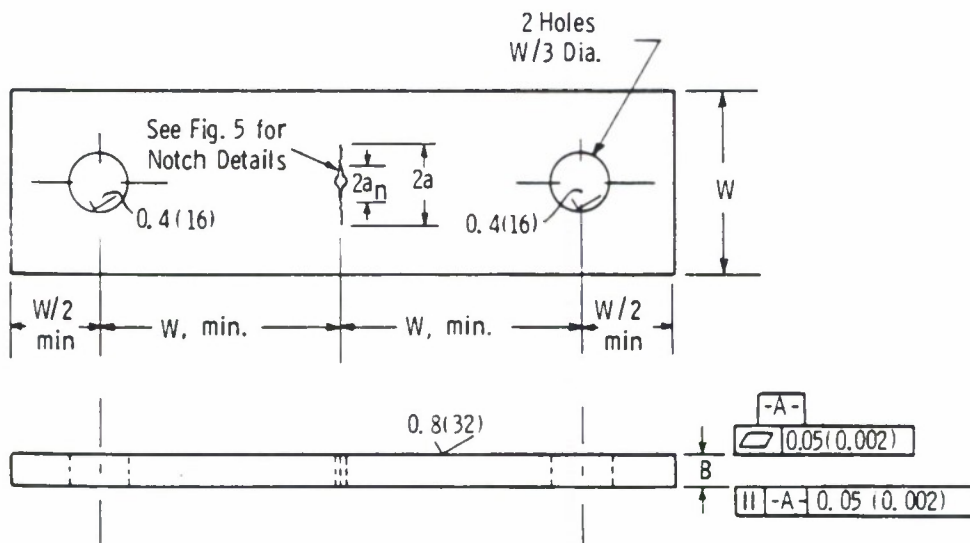
10.1.11 Description of any occurrences that appear to be related to anomalous data (for example, transients following test interruptions or changes in loading variables).

10.1.12 It is desirable, but not required, to tabulate test results. When using this method of presentation, the following information shall be tabulated for each test: a , N , ΔK , da/dN , and, where applicable, the test variables of 10.1.3, 10.1.6, and 10.1.7. Also, all data determined from tests on specimens that violate the size requirements of 7.2 and Appendix X2 shall be identified.



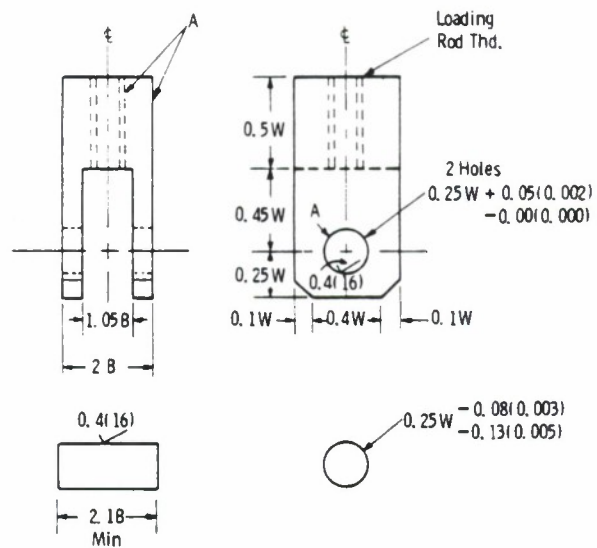
NOTE 1 — Dimensions are in millimetres (inches).
 NOTE 2 — A-surfaces shall be perpendicular and parallel as applicable to within $0.002W$, TIR.
 NOTE 3 — The intersection of the tips of the machined notch (a_n) with the specimen faces shall be equally distant from the top and bottom edges of the specimen to within $0.0005W$.

FIG. 1 Standard Compact-Type (CT) Specimen for Fatigue Crack Growth Rate Testing



NOTE 1 — Dimensions are in millimetres (inches).
 NOTE 2 — The machined notch ($2a_n$) shall be centered to within $\pm 0.001W$.
 FIG. 2 Standard Center-Cracked-Tension (CCT) Specimen for Fatigue Crack Growth Rate Testing when $W \leq 75 \text{ mm (3 in.)}$

ASTM E 647



NOTE 1 — Dimensions are in millimetres (inches).

NOTE 2 — A-surfaces shall be perpendicular and parallel as applicable to within 0.05 mm (0.002 in.), TIR.

FIG. 3 Clevis and Pin Assembly for Gripping CT Specimens

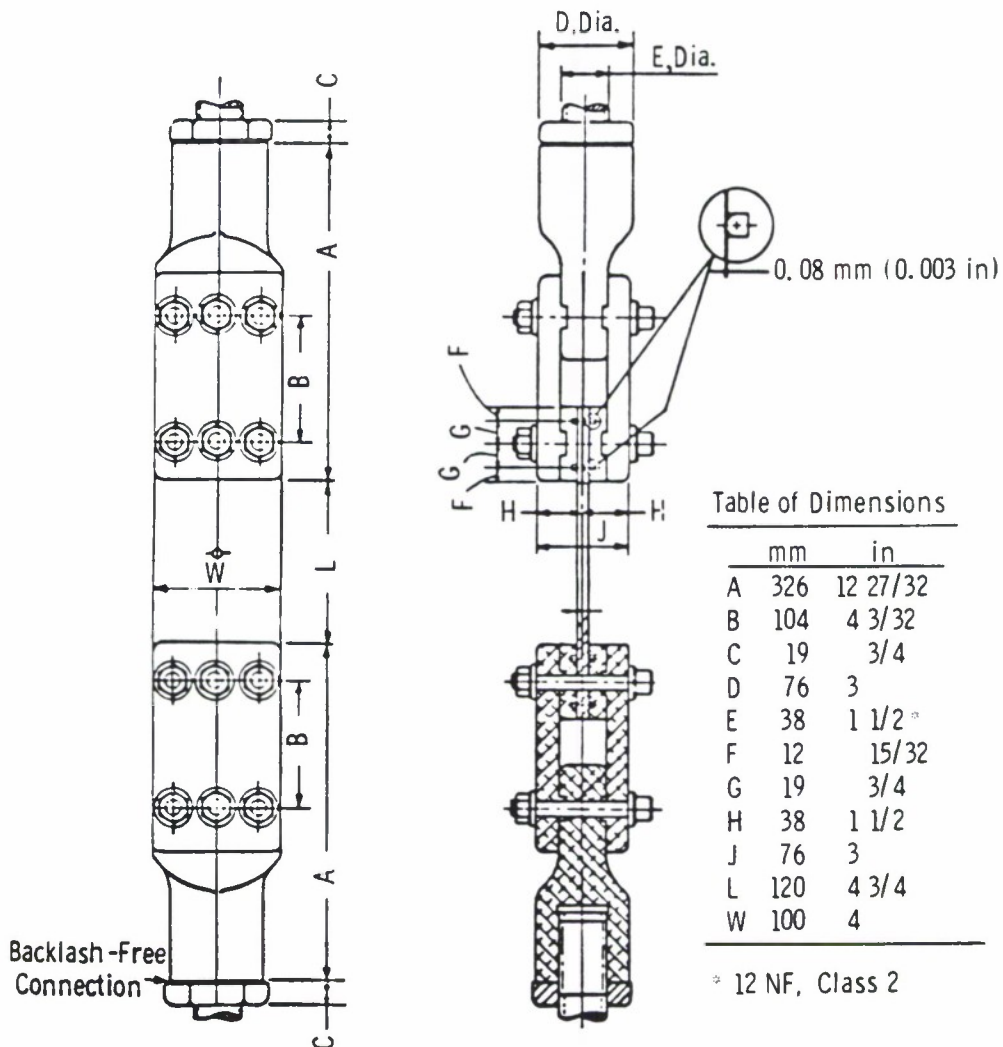


FIG. 4 Example of Bolt and Keyway Assembly for Gripping 100-mm (4-in.) wide CCT Specimen

APPENDIXES

X1. RECOMMENDED DATA REDUCTION TECHNIQUES

X1.1 Secant Method

X1.1.1 The secant or point-to-point technique for computing the crack growth rate simply involves calculating the slope of the straight line connecting two adjacent data points on the a versus N curve. It is more formally expressed as follows:

$$(da/dN)_a = \frac{a_{i+1} - a_i}{N_{i+1} - N_i} \quad (X1)$$

Since the computed da/dN is an average rate over the $(a_{i+1} - a_i)$ increment, the average crack length, $\bar{a} = 1/2(a_{i+1} + a_i)$, is normally used to calculate ΔK .

X1.2 Incremental Polynomial Method

X1.2.1 This method for computing da/dN involves fitting a second-order polynomial (parabola) to sets of $(2n + 1)$ successive data points, where n is usually 1, 2, 3, or 4. The form of the equation for the local fit is as follows:

$$\hat{a}_i = b_0 + b_1 \left(\frac{N_i - C_1}{C_2} \right) + b_2 \left(\frac{N_i - C_1}{C_2} \right)^2 \quad (X2)$$

where:

$$-1 \leq \left(\frac{N_i - C_1}{C_2} \right) \leq +1$$

and b_0 , b_1 , and b_2 are the regression parameters that are determined by the least squares method (that is, minimization of the square of the deviations between observed and fitted values of crack length) over the range $a_{i-n} \leq a \leq a_{i+n}$. The value \hat{a}_i is the fitted value of crack length at N_i . The parameters $C_1 = 1/2(N_{i-n} + N_{i+n})$ and $C_2 = 1/2(N_{i+n} - N_{i-n})$ are used to scale the input data, thus avoiding numerical difficulties in determining the regression parameters. The rate of crack growth at N_i is obtained from the derivative of the above parabola, which is

given by the following expression:

$$(da/dN)_{\hat{a}_i} = \frac{b_1}{C_2} + 2b_2(N_i - C_1)/C_2^2 \quad (X3)$$

The value of ΔK associated with this da/dN value is computed using the fitted crack length, \hat{a}_i , corresponding to N_i .

X1.2.2 A Fortran computer program that utilizes the above scheme for $n = 3$, that is, 7 successive data points, is given in Table X1.1 (see Note X1.1). This program uses the specimen K -calibrations given in 9.3 and also checks the data against the size requirements given in 7.2.

NOTE X1.1 It should be noted that the basic regression equations that are used to calculate da/dN can also be solved on a programmable calculator; thus large electronic computer facilities are not required to use this technique.

X1.2.3 An example of the output from the program is given in Table X1.2. Information on the specimen, loading variables, and environment are listed in the output along with tabulated values of the raw data and processed data. $A(\text{MEAS.})$ and $A(\text{REG.})$ are values of total crack length obtained from measurement and from the regression equation (Eq X2), respectively. The goodness of fit of this equation is given by the multiple correlation coefficient, MCC (note that $\text{MCC} = 1$ represents a perfect fit). Values of $\text{DELK} (\Delta K)$ and $\text{DA/DN} (da/dN)$ are given in the same units as the input variables (for the example problem these are $\text{ksi}/\text{in.}$ and $\text{in.}/\text{cycle}$, respectively). Values of da/dN that violate the specimen size requirement appear with an asterisk and note as shown in Table X1.2 for the final nine data points.

X1.2.4 The definition of input variables for the program and formats for these inputs are given in Table X1.3.

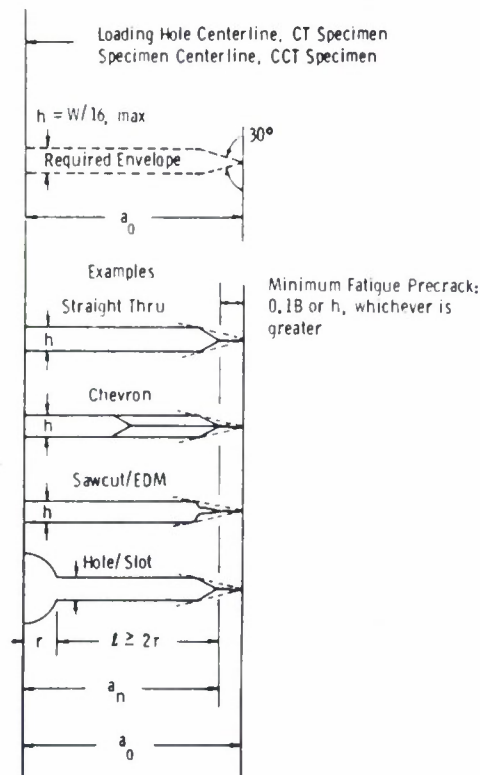


FIG. 5 Notch Details and Minimum Fatigue Precracking Requirements

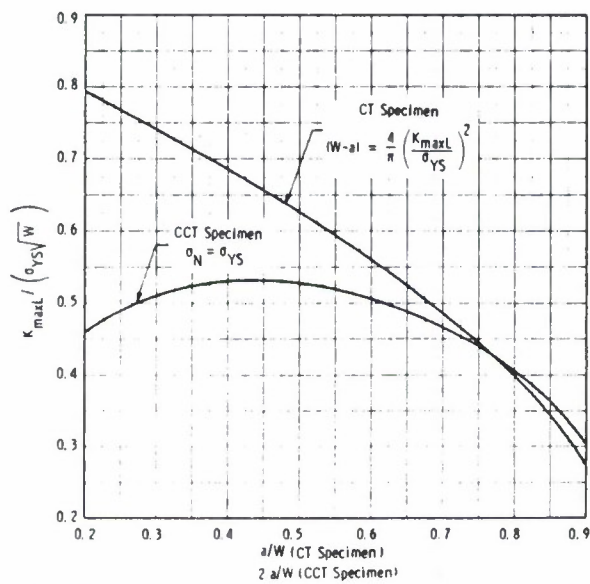


FIG. 6 Normalized Size Requirements for Standard Fatigue Crack Growth Specimens

U1 F. X1.1 Fortran Computer Program for Data Reduction by the Seven Point Incremental Polynomial Technique

```

DIMENSION A(200),N(200),EE(3),DADN(200),DELK(200),IO(7)
OIMEUSION A(10),N(10)
REAL N
N=1
INTEGER NN
NN=1
INTEGER TYPE
TYPE=1
10 FORMAT(A6,5H SPECIMEN,5X,2H6=-,F6.3,5H IN. ,5X,2H7=-,F6.3,5H IN.
,5X,3H8=-,F6.3,5H IN. ,5X,2H9=-,F6.3,5H IN. ,5X,2H10=-,F6.3,5H IN.
15 FORMAT(1H1,5H SEVEN POINT INCREMENTAL POLYNOMIAL METHOD FOR DETERMI
NATION OF )
17 FORMAT(1H1,5H )
20 FORMAT(1H1,5H )
22 FORMAT(1H1,5H )
24 FORMAT(1H1,5H )
26 FORMAT(1H1,5H )
28 FORMAT(1H1,5H )
30 FORMAT(1H1,5H )
32 FORMAT(1H1,5H )
34 FORMAT(1H1,5H )
36 FORMAT(1H1,5H )
38 FORMAT(1H1,5H )
40 FORMAT(1H1,5H )
42 FORMAT(1H1,5H )
44 FORMAT(1H1,5H )
46 FORMAT(1H1,5H )
48 FORMAT(1H1,5H )
50 FORMAT(1H1,5H )
52 FORMAT(1H1,5H )
54 FORMAT(1H1,5H )
56 FORMAT(1H1,5H )
58 FORMAT(1H1,5H )
60 FORMAT(1H1,5H )
62 FORMAT(1H1,5H )
64 FORMAT(1H1,5H )
66 FORMAT(1H1,5H )
68 FORMAT(1H1,5H )
70 FORMAT(1H1,5H )
72 FORMAT(1H1,5H )
74 FORMAT(1H1,5H )
76 FORMAT(1H1,5H )
78 FORMAT(1H1,5H )
80 FORMAT(1H1,5H )
82 FORMAT(1H1,5H )
84 FORMAT(1H1,5H )
86 FORMAT(1H1,5H )
88 FORMAT(1H1,5H )
90 FORMAT(1H1,5H )
92 FORMAT(1H1,5H )
94 FORMAT(1H1,5H )
96 FORMAT(1H1,5H )
98 FORMAT(1H1,5H )
100 FORMAT(1H1,5H )
102 FORMAT(1H1,5H )
104 FORMAT(1H1,5H )
106 FORMAT(1H1,5H )
108 FORMAT(1H1,5H )
110 FORMAT(1H1,5H )
112 FORMAT(1H1,5H )
114 FORMAT(1H1,5H )
116 FORMAT(1H1,5H )
118 FORMAT(1H1,5H )
120 FORMAT(1H1,5H )
122 FORMAT(1H1,5H )
124 FORMAT(1H1,5H )
126 FORMAT(1H1,5H )
128 FORMAT(1H1,5H )
130 FORMAT(1H1,5H )
132 FORMAT(1H1,5H )
134 FORMAT(1H1,5H )
136 FORMAT(1H1,5H )
138 FORMAT(1H1,5H )
140 FORMAT(1H1,5H )
142 FORMAT(1H1,5H )
144 FORMAT(1H1,5H )
146 FORMAT(1H1,5H )
148 FORMAT(1H1,5H )
150 FORMAT(1H1,5H )
152 FORMAT(1H1,5H )
154 FORMAT(1H1,5H )
156 FORMAT(1H1,5H )
158 FORMAT(1H1,5H )
160 FORMAT(1H1,5H )
162 FORMAT(1H1,5H )
164 FORMAT(1H1,5H )
166 FORMAT(1H1,5H )
168 FORMAT(1H1,5H )
170 FORMAT(1H1,5H )
172 FORMAT(1H1,5H )
174 FORMAT(1H1,5H )
176 FORMAT(1H1,5H )
178 FORMAT(1H1,5H )
180 FORMAT(1H1,5H )
182 FORMAT(1H1,5H )
184 FORMAT(1H1,5H )
186 FORMAT(1H1,5H )
188 FORMAT(1H1,5H )
190 FORMAT(1H1,5H )
192 FORMAT(1H1,5H )
194 FORMAT(1H1,5H )
196 FORMAT(1H1,5H )
198 FORMAT(1H1,5H )
200 FORMAT(1H1,5H )

```

TABLE X1.1 Continued

```

00 70 J=1,7
X= (NN(I)-C1)/C2
Y= (NN(I)-C1)/C2
X2= (X+X)
X3= (X2+X)
X4= (X3+X)
X5= (X4+X)
X6= (X5+X)
X7= (X6+X)
X8= (X7+X)
X9= (X8+X)
X10= (X9+X)
X11= (X10+X)
X12= (X11+X)
X13= (X12+X)
X14= (X13+X)
X15= (X14+X)
X16= (X15+X)
X17= (X16+X)
X18= (X17+X)
X19= (X18+X)
X20= (X19+X)
X21= (X20+X)
X22= (X21+X)
X23= (X22+X)
X24= (X23+X)
X25= (X24+X)
X26= (X25+X)
X27= (X26+X)
X28= (X27+X)
X29= (X28+X)
X30= (X29+X)
X31= (X30+X)
X32= (X31+X)
X33= (X32+X)
X34= (X33+X)
X35= (X34+X)
X36= (X35+X)
X37= (X36+X)
X38= (X37+X)
X39= (X38+X)
X40= (X39+X)
X41= (X40+X)
X42= (X41+X)
X43= (X42+X)
X44= (X43+X)
X45= (X44+X)
X46= (X45+X)
X47= (X46+X)
X48= (X47+X)
X49= (X48+X)
X50= (X49+X)
X51= (X50+X)
X52= (X51+X)
X53= (X52+X)
X54= (X53+X)
X55= (X54+X)
X56= (X55+X)
X57= (X56+X)
X58= (X57+X)
X59= (X58+X)
X60= (X59+X)
X61= (X60+X)
X62= (X61+X)
X63= (X62+X)
X64= (X63+X)
X65= (X64+X)
X66= (X65+X)
X67= (X66+X)
X68= (X67+X)
X69= (X68+X)
X70= (X69+X)
X71= (X70+X)
X72= (X71+X)
X73= (X72+X)
X74= (X73+X)
X75= (X74+X)
X76= (X75+X)
X77= (X76+X)
X78= (X77+X)
X79= (X78+X)
X80= (X79+X)
X81= (X80+X)
X82= (X81+X)
X83= (X82+X)
X84= (X83+X)
X85= (X84+X)
X86= (X85+X)
X87= (X86+X)
X88= (X87+X)
X89= (X88+X)
X90= (X89+X)
X91= (X90+X)
X92= (X91+X)
X93= (X92+X)
X94= (X93+X)
X95= (X94+X)
X96= (X95+X)
X97= (X96+X)
X98= (X97+X)
X99= (X98+X)
X100= (X99+X)
X101= (X100+X)
X102= (X101+X)
X103= (X102+X)
X104= (X103+X)
X105= (X104+X)
X106= (X105+X)
X107= (X106+X)
X108= (X107+X)
X109= (X108+X)
X110= (X109+X)
X111= (X110+X)
X112= (X111+X)
X113= (X112+X)
X114= (X113+X)
X115= (X114+X)
X116= (X115+X)
X117= (X116+X)
X118= (X117+X)
X119= (X118+X)
X120= (X119+X)
X121= (X120+X)
X122= (X121+X)
X123= (X122+X)
X124= (X123+X)
X125= (X124+X)
X126= (X125+X)
X127= (X126+X)
X128= (X127+X)
X129= (X128+X)
X130= (X129+X)
X131= (X130+X)
X132= (X131+X)
X133= (X132+X)
X134= (X133+X)
X135= (X134+X)
X136= (X135+X)
X137= (X136+X)
X138= (X137+X)
X139= (X138+X)
X140= (X139+X)
X141= (X140+X)
X142= (X141+X)
X143= (X142+X)
X144= (X143+X)
X145= (X144+X)
X146= (X145+X)
X147= (X146+X)
X148= (X147+X)
X149= (X148+X)
X150= (X149+X)
X151= (X150+X)
X152= (X151+X)
X153= (X152+X)
X154= (X153+X)
X155= (X154+X)
X156= (X155+X)
X157= (X156+X)
X158= (X157+X)
X159= (X158+X)
X160= (X159+X)
X161= (X160+X)
X162= (X161+X)
X163= (X162+X)
X164= (X163+X)
X165= (X164+X)
X166= (X165+X)
X167= (X166+X)
X168= (X167+X)
X169= (X168+X)
X170= (X169+X)
X171= (X170+X)
X172= (X171+X)
X173= (X172+X)
X174= (X173+X)
X175= (X174+X)
X176= (X175+X)
X177= (X176+X)
X178= (X177+X)
X179= (X178+X)
X180= (X179+X)
X181= (X180+X)
X182= (X181+X)
X183= (X182+X)
X184= (X183+X)
X185= (X184+X)
X186= (X185+X)
X187= (X186+X)
X188= (X187+X)
X189= (X188+X)
X190= (X189+X)
X191= (X190+X)
X192= (X191+X)
X193= (X192+X)
X194= (X193+X)
X195= (X194+X)
X196= (X195+X)
X197= (X196+X)
X198= (X197+X)
X199= (X198+X)
X200= (X199+X)

```

TABLE X1.2 Example Output from Incremental Polynomial Computer Program

SEVEN POINT INCREMENTAL POLYNOMIAL METHOD FOR DETERMINING CA/ON

```

SPEC. NO. 1UN-9
CT SPECIMEN
MACHINE 4.000KIPS PHASE 5.000KIPS W= 2.000 IN. AN= .500 IN.
TEMP.= 75.F ENVIRONMENT= AIR TEST FREQ= .100HZ.
OBS.NO. CYCLES A(MEAS.) A(REQ.) M.C.C.
NO. POINTS = 37

```

[illegible]

* - DATA VIOLATE SPECIMEN SIZE REQUIREMENTS

TABLE X1.3 Definition of Input Variables for Fortran Program

Input Card	Program Line	Fortran Code	Variable Definition	Card Columns
1	28	ID(1)	Specimen identification, for example specimen number, heat number, material	1-40*
	28	NPTS	Number of paired (a , N) data points	40-46*
	26	TYPE	TYPE = 1 for CT specimen TYPE = 2 for CCT specimen	47-52*
2	29	PMIN	Minimum load, P_{min} , in kips	1-6°
	29	PMAX	Maximum load, P_{max} , in kips	7-12°
	29	F	Test frequency	13-18°
	29	B	Specimen thickness, B	19-24°
	29	W	Specimen width, W	25-30°
	29	AM	Machine notch length, a_n	31-36°
3	31	ENV	Test environment	1-6°
	31	TEM	Test temperature, °F	7-11°
	31	YS	0.2 % yield stress of specimen	12-19°
	31	KIND	Specimen type, that is, CT or CCT	20-25°
4, 5, 6, etc.	32	A(1)	Crack length, a , measured from machine notch, a_n	A(1) 1-6° N(1) 7-15°
	32	N(1)	Elapsed cycles, N	A(2) 16-21° N(2) 22-30° A(3) 31-36° N(3) 37-45° A(4) 46-51° N(4) 52-60°
				4 paired (a , N) data points per card
				A(5) 1-6° N(5) 7-15° etc.
				next card

Key
 * alphanumeric
 ° integer, entered to far right of available columns
 ° use decimal point

X2. RECOMMENDED PROCEDURE FOR SPECIMENS VIOLATING SECTION 7.2

X2.1 This appendix presents a recommended empirical procedure for use when test specimens do not meet the size requirements of 7.2 (Note X2.1). This procedure is of the greatest utility for low-strength materials, especially those exhibiting much monotonic strain-hardening. Currently, there are insufficient data on these materials to formulate an easily calculable size requirement that would be analogous to those specified in 7.2. For this reason, it is recommended that specimen deflections be measured during testing in order to provide quantitative information on the extent of plastic deformation in the specimen.

NOTE X2.1 — The purpose of the size requirements of 7.2 is to limit the extent of plastic deformation during testing so that results can be analyzed using linear-elastic theory.

X2.2 During a constant-load-amplitude fatigue crack growth test with commonly used specimen geometries, the specimen load-deflection behavior is influenced by plastic deformation as illustrated in Fig. X2.1. As the fatigue crack grows from length a_1 to a_3 , the mean specimen deflection, as well as the compliance (that is, the inverse slope of the curves in Fig. X2.1), increase in a manner predictable from linear-elastic theory. However, as the fatigue crack continues to grow, the mean specimen deflection can eventually become larger than the elastically calculated mean deflection. This difference is due to a plastic deflection, $V_{plastic}$, which is

depicted for crack length a_4 in Fig. X2.1.

X2.3 The plasticity phenomenon described above develops and increases continuously as the fatigue crack grows. This development is illustrated in Fig. X2.2 where both the measured and elastically calculated deflections, corresponding to minimum and maximum load are given. The increasingly larger plastic deflection causes the measured deflections, V_{min} and V_{max} , to become increasingly larger than the elastically calculated deflections, V_{min}^e and V_{max}^e . However, for any given crack length the measured and elastically calculated deflection ranges remain approximately equal (Fig. X2.2) since the cyclic plasticity remains small (Fig. X2.1).

X2.4 Although the cyclic plasticity remains small, it would appear necessary to limit $V_{plastic}$. Limited data on A533-B steel (12) indicate that crack growth rates can be properly analyzed using linear elastic theory provided:

$$V_{plastic} \leq V_{max}^e \quad (X4)$$

This condition can be more conveniently expressed in terms of directly measurable quantities by using the following relationships, which are consistent with Fig. X2.2. Equation X4 is equivalent to

$$V_{max} \leq 2V_{max}^e \quad (X5)$$

and

$$\Delta V = V_{max} - V_{min} = V_{max}^e - V_{min}^e \quad (X6)$$

thus

$$V_{\max}^e = \frac{\Delta V}{1 - R} \quad (X7)$$

combining Eqs X5 and X7 yields:

$$V_{\max} \leq \frac{2 \Delta V}{1 - R} \quad (X8)$$

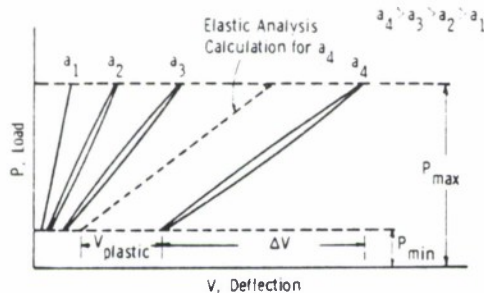


FIG. X2.1 Effect of Plastic Deformation on Specimen Load-Deflection Behavior During Fatigue Crack Growth Rate Testing at Constant-Load-Amplitude

X2.5 When it is necessary to generate data using specimens that do not meet the size criteria of Section 7.2, it is suggested that specimen deflections be measured and that data that violate Eq X8 be so labeled. Information of this type will provide data to further test Eq X8 and will hopefully lead to the formulation of an easily calculable size requirement that would be appropriate for all materials.

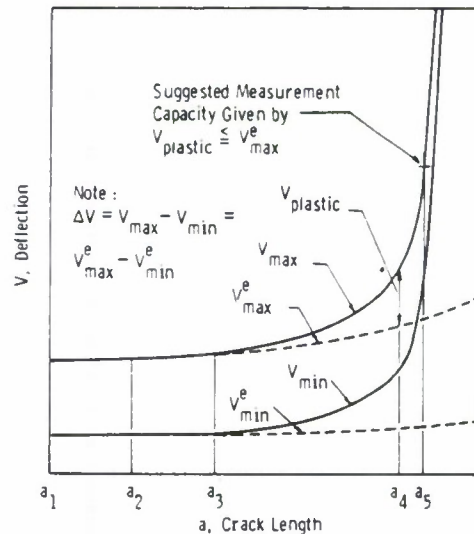


FIG. X2.2 Suggested Specimen Measurement Capacity Based on Comparison of Measured (Elastic Plus Plastic) and Elastic Deflections During a Constant-Load-Amplitude Fatigue Crack Growth Rate Test

REFERENCES

- (1) Paris, P., and Erdogan, F., "A Critical Analysis of Crack Propagation Laws," *Journal of Basic Engineering*, Series D of the Transactions of the ASME, JBAEA, December 1963, pp. 528-534.
- (2) Paris, P. C., "The Fracture Mechanics Approach to Fatigue," *Proceedings of the Tenth Sagamore Army Materials Research Conference*, Syracuse University Press, 1964, pp. 107-132.
- (3) Clark, Jr., W. G., "Fracture Mechanics in Fatigue," *Experimental Mechanics*, EXMCA, September 1971, pp. 1-8.
- (4) Hoepfner, D. W., and Krupp, W. E., "Prediction of Component Life by Application of Fatigue Crack Growth Knowledge," *Engineering Fracture Mechanics*, EFMEA, Vol 6, 1974, pp. 47-70.
- (5) *Fatigue Crack Growth Under Spectrum Loads*, ASTM STP 595, Am. Soc. Testing Mats., 1976.
- (6) Hudak, Jr., S. J., Saxena, A., Bucci, R. J., and Malcolm, R. C., "Development of Standard Methods of Testing and Analyzing Fatigue Crack Growth Rate Data—Final Report," AFML TR 78-40.
- (7) Clark, Jr., W. G., and Hudak, Jr., S. J., "Variability in Fatigue Crack Growth Rate Testing," *Journal of Testing and Evaluation*, JTEVA, Vol 3, No. 6, 1975, pp. 454-476.
- (8) Clark, Jr., W. G., and Hudak, Jr., S. J., "The Analysis of Fatigue Crack Growth Rate Data," to be published in *Proceedings of the 22nd Sagamore Army Materials Research Conference on Application of Fracture Mechanics to Design*.
- (9) Newman, Jr., J. C., "Stress Analysis of the Compact Specimen Including the Effects of Pile Loading," *Fracture Analysis*, ASTM STP 560, Am. Soc. Testing Mats., 1974, pp. 105-121.
- (10) Srawley, J. E., "Wide Range Stress Intensity Factor Expressions for ASTM Method E 399 Standard Fracture Toughness Specimens," *International Journal of Fracture*, Vol 12, June 1976, pp. 475-476.
- (11) Feddersen, C. E., "Discussion in Plane-Strain

ASTM E 647

- Crack Toughness Testing of Metallic Materials," ASTM STP 410, Am. Soc. Testing Mats., 1976, pp. 77-79.
- (12) Dowling, N. E., "Fatigue Crack Growth Rate Testing at High Stress Intensities," ASTM STP 631, Am. Soc. Testing Mats., 1977, pp. 139-158.

The American Society for Testing and Materials takes no position respecting the validity of any patent rights asserted in connection with any item mentioned in this standard. Users of this standard are expressly advised that determination of the validity of any such patent rights, and the risk of infringement of such rights, is entirely their own responsibility.

This standard is subject to revision at any time by the responsible technical committee and must be reviewed every five years and if not revised, either reapproved or withdrawn. Your comments are invited either for revision of this standard or for additional standards and should be addressed to ASTM Headquarters. Your comments will receive careful consideration at a meeting of the responsible technical committee, which you may attend. If you feel that your comments have not received a fair hearing you should make your views known to the ASTM Committee on Standards, 1916 Race St., Philadelphia, Pa. 19103, which will schedule a further hearing regarding your comments. Failing satisfaction there, you may appeal to the ASTM Board of Directors.